PHILIPS TECHNICAL REVIEW

13649-18

N. V. PHILIPS' GLOEILAMPENFABRIEKEN

Bibl. Nat. Lab.

31 DEC. 1959

VOLUME 20

1958/1959

PHILIPS TECHNICAL REVIEW

A publication of the Research Laboratories of N.V. Philips' Gloeilampenfabrieken, Eindhoven, Netherlands. Twelve issues per year and an average of 32 pages per issue. The Review is published in four editions: English, Dutch, French and German, all identical in contents.

Editors

S. Gradstein, Editor-in-chief
D. M. Duinker, Deputy editor
M. Beun
C. M. Hargreaves
J. W. Miltenburg

All rights reserved by N.V. Philips' Gloeilampenfabrieken, Eindhoven, Netherlands. Articles may be reproduced in whole or in part, provided that the editors are first notified and that the source "Philips Technical Review" is mentioned in full. Photographs and drawings for this purpose are available on request.

Correspondence regarding subscriptions should be addressed to the distributors mentioned on the back cover of this issue.

CONTENTS

VOLUME 20, 1958/1959

LIGHT

	Page
The "Electronic Poem" performed in the Philips pavilion at the 1958 Brussels World Fair, A. The light effects, by L. C. Kalff	37
The life of ballasts for gas-discharge lamps, by T. Hehenkamp, I. Transformers and chokes	59
II. Capacitors	162
Radio interference from fluorescent lamps, by H. J. J. van Boort, M. Klerk and A. A. Kruithof	135
*Automatic recording of luminous intensity diagrams, by W. Bähler	288
Transistor D.C. converters for fluorescent-lamp power supplies, by T. Hehenkamp and J. J. Wilting	362

TELECOMMUNICATIONS

	Page
Noise, by K. S. Knol	50
*A noise diode for ultra-high frequencies, by H. Groendijk	108
Printed wiring in radio sets, by R. van Beek and W. W. Boelens	113
The junction transistor as a network element at low frequencies, III. Stabilization of the operating point, in particular with regard to temperature changes, by J. P. Beijersbergen, M. Beun and J. te Winkel	122
Radio interference from fluorescent lamps, by H. J. J. van Boort, M. Klerk and A. A. Kruithof	135
The EC 59, a transmitting triode with 10 W output at 4000 Mc/s, by V. V. Schwab and J. G. van Wijngaarden	225
Precision variable capacitors, by A. A. Turnbull	234
Electron emission of materials for electron tubes, by G. A. Espersen and J. W. Rogers	269
Transmitting valves for use in industry, by E. G. Dorgelo	299
*Colour television in medical teaching, by W. A. Holm and F. H. J. van der Poel	327
*The port of Rotterdam radar system, by B. H. G. Prins and J. M. G. Seppen	349

SOUND

	Page
The "Electronic Poem" performed in the Philips pavilion at the 1958 Brussels World Fair, B. The sound effects, by W. Tak	43
Modern acoustical engineering, I. General principles, by D. Kleis	309

X-RAYS AND NUCLEAR PHYSICS

	Page
*A simple and compact arrangement for measuring the β-activity of weak radioactive samples, by K. van Duuren	170
The scintillation counter, by J. A. W. van der Does de Bye	209
Signal-to-noise ratio and dead time of a scintillation counter, by J. A. W. van der Does de Bye	263
Distant-focus X-ray tubes, by A. H. G. Kuntke	291
An apparatus for cinefluorography with an 11-inch X-ray image intensifier, by J. J. C. Hardenberg	331

*) Articles marked with an asterisk are brief reports.

MEASURING EQUIPMENT

*An experimental pyrometer using a phototransistor and designed for radio-tube inspection, by F.H.R. Almer and P.G. van Zanten 89

*A noise diode for ultra-high frequencies, by H. Groendijk 108

The production and measurement of ultra-high vacua, by A. Venema and M. Bandringa . . 145

*A simple and compact arrangement for measuring the β-activity of weak radioactive samples, by K. van Duuren 170

The scintillation counter, by J. A. W. van der Does de Bye 209

*A method of measuring the resistivity and Hall coefficient on lamellae of arbitrary shape, by L. J. van der Pauw 220

Signal-to-noise ratio and dead time of a scintillation counter, by J. A. W. van der Does de Bye 263

*Automatic recording of luminous intensity diagrams, by W. Bähler 288

*The use of thermistors in the ebullioscopic determination of molecular weights, by J. G. van Pelt 357

MATERIALS AND THEIR RESEARCH

Lattice imperfections in crystals, studied on alkali halides, by Y. Haven 69

*An apparatus for testing the solderability of wire, by J. A. ten Duis 158

*A method of measuring the resistivity and Hall coefficient on lamellae of arbitrary shape, by L. J. van der Pauw 220

*Topotactically crystal-oriented ferromagnetics, by F. K. Lotgering 354

*The use of thermistors in the ebullioscopic determination of molecular weights, by J. G. van Pelt. 357

MISCELLANEOUS

The Philips pavilion at the 1958 Brussels World Fair 1

I. The architectural design of Le Corbusier and Xenakis, after Y. Xenakis . . 2

II. The hyperbolic-paraboloidal shell and its mechanical properties, by C. G. J. Vreedenburgh 9

III. Model tests for proving the construction of the pavilion, by A. L. Bouma and F. K. Ligtenberg 17

IV. Construction of the pavilion in prestressed concrete, by H. C. Duyster . 27

The "Electronic Poem" performed in the Philips pavilion at the 1958 Brussels World Fair,

A. The light effects, by L. C. Kalff 37

B. The sound effects, by W. Tak 43

C. The electronic control system, by S. L. de Bruin 45

The life of ballasts for gas-discharge lamps, by T. Hehenkamp,

I. Transformers and chokes 59

II. Capacitors 162

Science and industry, by H. B. G. Casimir . . 85

*Enclosed welding of rail sections, by G. Zoethout 94

An experimental induction-heating generator using hydrogen thyratrons, by H. L. van der Horst and P. H. G. van Vlodrop 101

The production and measurement of ultra-high vacua, by A. Venema and M. Bandringa 145

A small air fractionating column used with a gas refrigerating machine for producing liquid nitrogen, by J. van der Ster and J. W. L. Köhler 177

*Influence of the Peltier effect in resistance welding, by T. C. Balder 188

A fast method of reading magnetic-core memories, by H. J. Heijn and N. C. de Troye 193

The Philips hot-gas engine with rhombic drive mechanism, by R. J. Meijer 245

Photo-resistors made of compressed and sintered cadmium sulphide, by N. A. de Gier, W. van Gool and J. G. van Santen 277

*) Articles marked with an asterisk are brief reports.

VOLUME 20, 1958/59, No. 1 pp. 1-36 Published 20th September 1958

Philips Technical Review

DEALING WITH TECHNICAL PROBLEMS
RELATING TO THE PRODUCTS, PROCESSES AND INVESTIGATIONS OF
THE PHILIPS INDUSTRIES

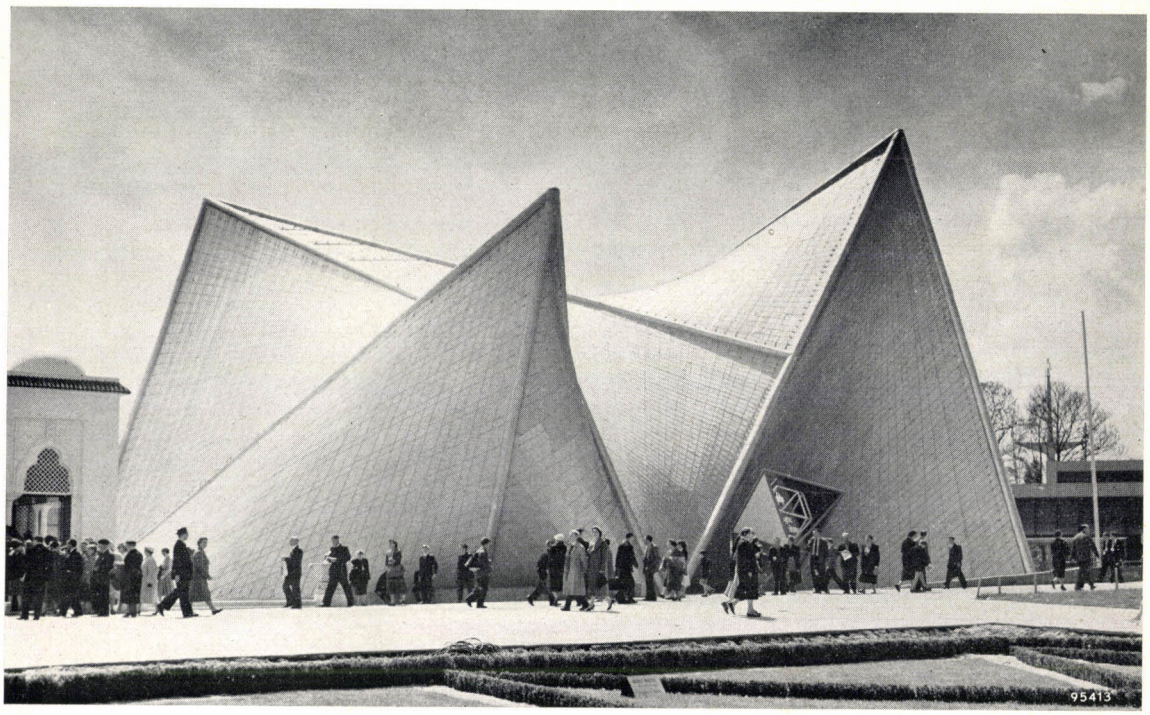

Photo Hans de Boer

THE PHILIPS PAVILION AT THE 1958 BRUSSELS WORLD FAIR

I. THE ARCHITECTURAL DESIGN OF LE CORBUSIER AND XENAKIS
II. THE HYPERBOLIC-PARABOLOIDAL SHELL AND ITS MECHANICAL PROPERTIES
III. MODEL TESTS FOR PROVING THE CONSTRUCTION OF THE PAVILION
IV. CONSTRUCTION OF THE PAVILION IN PRESTRESSED CONCRETE

061.41(493.2):725.91

At the Brussels World Fair, near the Dutch section, Philips have had their own pavilion built. Visitors to the pavilion are entertained to a "spectacle in light and sound", the object of which is to demonstrate the capabilities of modern technology in some of Philips' major fields of endeavour — illuminating engineering, electro-acoustics, electronics and automatic control techniques — and also to give an impression of the way in which these technical facilities may in the future be turned to artistic ends. The basic conception was propounded by Mr. L. C. Kalff, Arts Director of Philips, and the architect Le Corbusier was commissioned to give effect to it. The latter wished not only to design the building but also wrote the scenario for the spectacle, which he has entitled "An Electronic Poem". The music for the spectacle was composed by Edgar Varèse. Completely automatic performances of the spectacle are now being given scores of times a day, controlled by a magnetic tape with fifteen command tracks.

A later article in this Review will be devoted to the performance, *which is produced by film projectors, lamps and hundreds of*

loudspeakers, and to the technical devices and methods used. The articles in the present issue are devoted to the pavilion itself. From the outset this pavilion, designed by Le Corbusier and his collaborator Y. Xenakis, has aroused considerable interest in the world of architecture because of its extraordinary conception and advanced design as a shell structure. The building is entirely composed of shells having the form of hyperbolic paraboloids. The method of construction in prestressed concrete, proposed and translated into reality by Dr. H. C. Duyster, director of the contracting firm N.V. "Strabed" and a specialist in this field, is remarkable for its originality and elegance. Before plunging into this adventure — as Mr. Duyster himself put it — N.V. "Strabed" approached Professor C. G. J. Vreedenburgh of the Delft Technische Hogeschool for advice concerning the stresses that might occur in the shells when loaded by their own weight, and by wind and snow loads. To satisfy N.V. Strabed as to the feasibility of the proposed scheme of construction and supply data for the actual structure, tests on scale models were made by Mr. A. L. Bouma and Mr. F. K. Ligtenberg in the "T.N.O." Institute at Rijswijk (Netherlands) and the Stevin Laboratory at Delft.

These aspects are treated in the four articles printed in this issue: the architect's conception, the mechanical principles, the model tests and the actual construction of the building.

As regards the first article it should be mentioned that Y. Xenakis, the architect largely responsible for designing the shape of the pavilion, has placed at our disposal a description of the way in which the architectural design of the building was evolved. In our opinion, however, there was little point in attempting to render the author's French text faithfully into English or other languages, for translation would do less than justice to the eloquence of the artist's highly individual style and risk distorting the sentiments of the original. It was therefore decided to confine the English rendering of his article to a reproduction of the factual contents *).

The second article in this series also calls for some comment. Although Professor Vreedenburgh has kindly taken great pains to make the train of thought in his text as comprehensible as possible to the readers of this Review, we cannot disguise the fact that many readers will perhaps have difficulty in following the details of his article, lying as it does far outside the range of subjects normally dealt with in these pages. On the other hand, the article should be of particular interest to the specialist, since it provides for the first time in published form certain formulae and results concerning hyperbolic-paraboloidal shells which can be turned to practical architectural use.

*) For those readers who would like to have a copy of the original French text, reprints will be available of the article published in the French edition of this Review.

I. THE ARCHITECTURAL DESIGN OF LE CORBUSIER AND XENAKIS

after Y. XENAKIS †).

061.41(493.2):725.91

A report is given below of the ideas embodied in the architectural conception of the Philips pavilion and of the various stages through which the design passed before the pavilion acquired its final shape. This report is an authorized shortened version of an article by Y. Xenakis, who also provided the drawings illustrating the evolution of the design. These drawings are the main feature of the article.

When Le Corbusier, in the beginning of 1956, agreed to undertake the design of the Philips pavilion, he had in mind a structure to enclose a space of unconventional form and to be materialized by casting cement on a metal-gauze framework suspended from scaffolding. The structure would have a roof and surfaces on which pictures, colours and film scenes could be projected for performing a spectacle in light and sound — a so-titled "Electronic Poem". In October 1956, Y. Xenakis, under the direction of Le Corbusier, entered upon a detailed study of the project [1]). The result was a design based entirely on the use of *ruled surfaces*.

This result, to which artistic intuition as well as practical considerations contributed, will be elucidated in the following pages.

†) Paris, 35 rue de Sèvres.

The first design

The *ground-plan* of the pavilion was fairly simply established, being dictated by the requirements for the performance of the "Electronic Poem". Each performance was to last 8 to 10 minutes and to be attended by some 600 or 700 persons, uniformly distributed over the whole floor surface of the pavilion. A space of more or less circular plan was therefore needed, with an area of 400 or 500 m² and with two large "spouts" as entrance and exit channels.

[1]) A brief account of this study has already been published: Y. Xenakis, Le Corbusier's "Elektronisches Gedicht" und der Philips Pavillon, Gravesaner Blätter 3, 47-54, 1957 (No. 9).

In order to be able to produce various fantastic effects, locally changing colours, shifts of light and shade, etc. in the projection of pictures or colour slides, the enclosing walls (or at least part of them) had to be *curved* surfaces, so that they would receive the light from divergent angles. All uniformity was to be avoided, even the uniformity of curvature found in spherical and cylindrical vaults. This led to the idea of having surfaces with differing radii of curvature. Such surfaces also seemed suitable for meeting the *acoustic* requirements. To allow complete freedom for creating a wide variety of spatial impressions with the aid of loudspeakers, the aim was to avoid as far as possible the uncontrolled acoustic contributions due to reflections from the walls and which are audible either as isolated echos or as reverberation. It is known that parallel flat walls are dangerous in this respect, because of repeated reflections; parts of spherical surfaces are equally inappropriate, since they can give rise to localized echos.

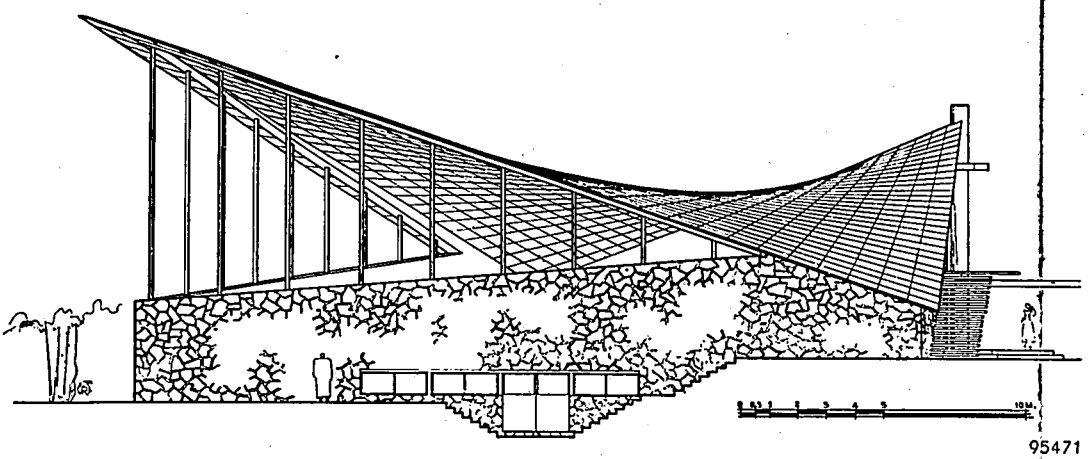

Fig. 1. The church Notre Dame de la Solitude at Coyoacan, Mexico, having a concrete shell roof in the form of a hyperbolic paraboloid, designed by the architect Felix Candela. (Illustration from: F. Candela, Les voûtes minces et l'espace architectural, L'architecture d'aujourd'hui **27**, 22-27, March 1956.)

Having turned his thoughts to surfaces with widely varying radii of curvature, Xenakis was led naturally to consider saddle surfaces, and in particular the *ruled surfaces* that come into this category. Through the work of Laffaille and other pioneers in this field, the architect was familiar with simple ruled surfaces, such as the hyperbolic paraboloid and the conoid. The conoid is obtained by letting a straight line (a generator) slide along two non-intersecting lines (directrixes), one a straight line and the other an arbitrary curve, such that it remains parallel to a given plane. The hyperbolic paraboloid (hypar) is also produced by moving a straight line such that it always remains parallel to a given plane, but in this case it slides along two skew straight lines (rectilinear directrixes). The static stress distribution in a shell having the form of a hyperbolic paraboloid can, to a certain extent, be calculated: such a shell is found to possess remarkable properties of strength and stability (see article II in this series). Moreover, these surfaces produced by straight lines readily lend themselves to construction in straight wooden beams or in concrete (see article IV). These attractive properties have led to an increasing use of such shell structures in various countries, particularly for roof constructions (*fig. 1*).

The Philips pavilion offered the architect a unique opportunity to build a structure entirely from these ruled surfaces, and in this way to create a homogeneous three-dimensional envelope in the sense that the three dimensions would each really play an independent role, as opposed to conventional architecture in which, usually, the form of the ground-plan is still manifest in every section of the building high above the ground.

The working-out of this novel architectural idea, however, was necessarily a process involving artistic intuition and a feeling for form rather than a question of reasoning. The series of sketches, *figs. 2-10*, allow the architect to show how he arrived at his first design.

This design (fig. 10) contains a conoid E, a surface consisting mainly of two conoids A and D, two hyperbolic paraboloids K and G, a connecting cone

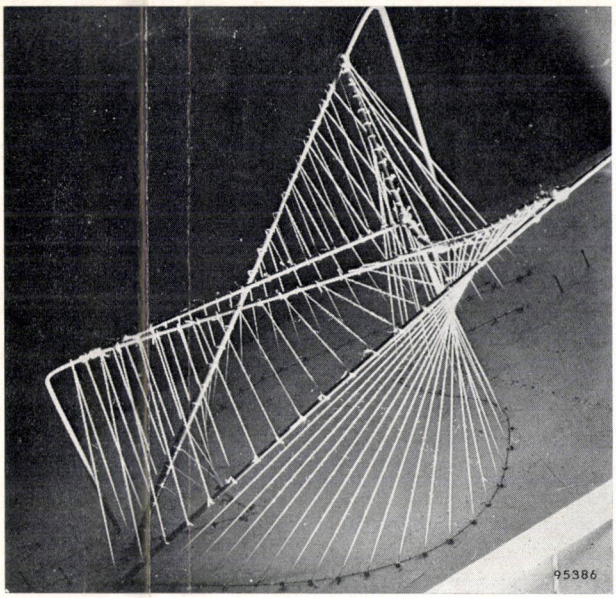

Photo Lucien Hervé

Fig. 11. The first model. The "stomach" is set out on the base of the model; the strings indicate the ruled surfaces. The intersections of the ruled surfaces are represented by spokes of piano wire. Their bent-over ends have no structural significance.

L and two open triangles as entrance and exit. The two peaks, produced from the oblique straight lines arising out of one of the channels (fig. 6) are counterbalanced by a third peak projecting above this channel.

Fig. 11 shows a model of the first design. The ribs in which the surfaces intersect are formed in this model by spokes of piano wire, the bent ends being anchored in a wooden base. The surfaces are produced by spanning strings between the ribs.

The second design

At this stage, engineers of a Parisian firm of contractors were consulted by the architects regarding the system of construction.

With a view to soundproofing, Philips had specified a wall weight of 120 kg/m^2 (concrete or cement about 5 cm thick). There was therefore no question of building the pavilion in the form of a tent, whether or not with metal-reinforced "canvas". The engineers consulted believed that in these circumstances the pavilion would have to be constructed on a fairly heavy metal skeleton, after the manner of the wire spokes in the model and with supporting stanchions corresponding to the vertical bent wires in the model. At all events they thought it desirable to change from conoids to hyperbolic paraboloids so as to make it possible to specify more easily the exact curvature of all surfaces and simplify the calculation of static stresses as well as the work of erection.

This advice was accepted by Le Corbusier and Xenakis, especially since they themselves felt that the first design had certain aesthetic weaknesses which in any case called for modification.

Xenakis set about converting the surfaces by experiment. His method was simple: he used two straight metal spokes joined by a system of elastic strings fixed at equidistant points along each spoke. The strings formed the ruling lines of a hypar, whose geometry was determined by the distance between the spokes, the angle between them and the positioning of two arbitrary strings. Other variables determine the position of the hypar with respect to ground level. To select each of the pavilion surfaces the architect had to proceed by trial and error, simultaneously varying all the above variables; as soon as he found a satisfactory form for a particular surface, he immediately put it down on paper in the form of an orthogonal projection [2]). For this purpose it is sufficient to give horizontal and vertical projections showing the positions of the two spokes and of two pairs of corresponding points thereon (e.g. the end points of the two outermost strings on the spokes; see *figs. 12* and *13*). This done, *all* pairs of corresponding points are fixed, each pair defining a ruling line. The points at which the ruling lines meet the horizontal plane give the intersection of this plane with the part of the hypar surface involved (*fig. 14*). This intersection can be part of a hyperbola or of a parabola (this is the case when one of the spokes is *below* the horizontal plane), or it can be a straight line (one of the spokes lies *in* the horizontal plane), or, in special cases, it can be a single point. There are also some hypar shells in the design, of which the part of the surface used does not touch the ground at all.

The first step in revising the original design was to change the position in space of the three peaks so as to obtain more harmonious proportions. The difference between the second and third peak had to be accentuated, and the middle cone *L* widened. The architect now fixed the height of the peaks at 21 m, 13 m, and 18 m respectively. He then proceeded, by alternately experimenting with the spoke and string model and drawing the surfaces found, to establish the hyperbolic paraboloidal surfaces that both gave an aesthetically satisfying form and yielded intersections with the ground level which were as much as possible in keeping with the original ground-plan.

---

[2]) It is clear that it would hardly be convenient to define the hypar surfaces in terms of the numerical values of the coefficients in the appropriate equation of the surface (see II).

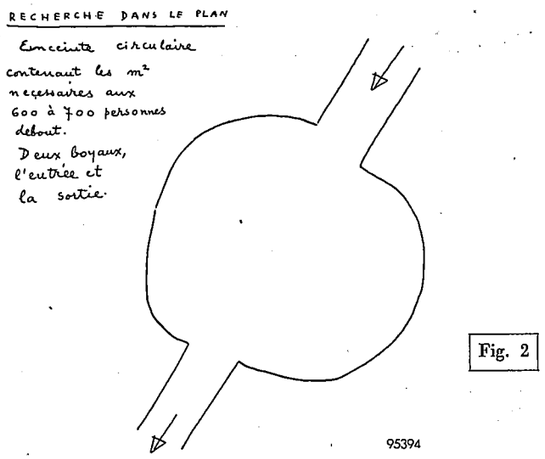

Fig. 2

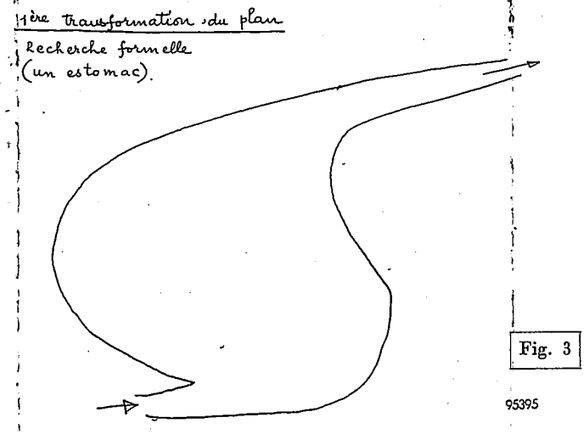

Fig. 3

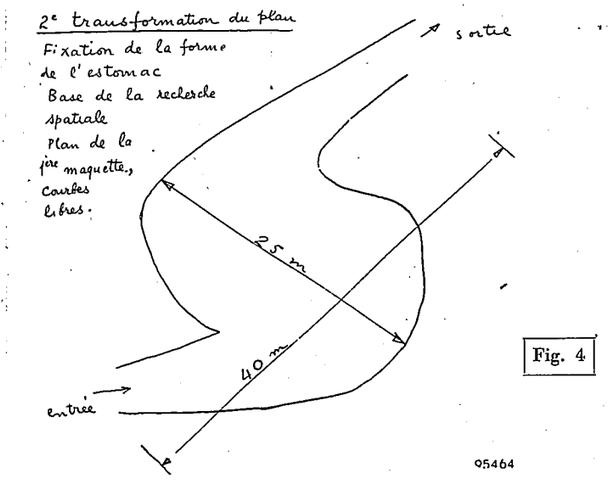

Fig. 4

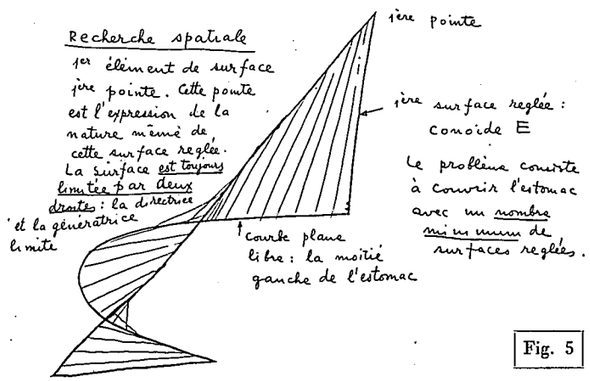

Fig. 5

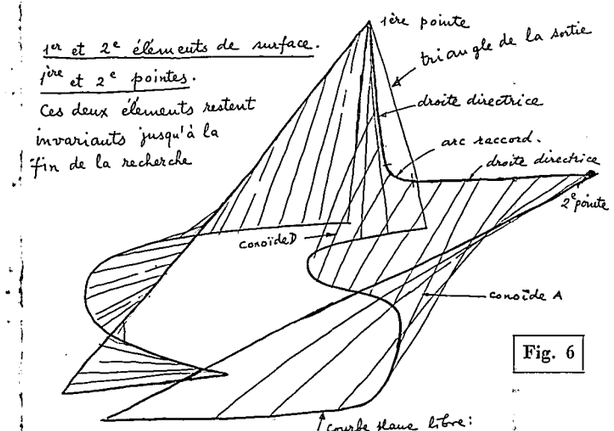

Fig. 6

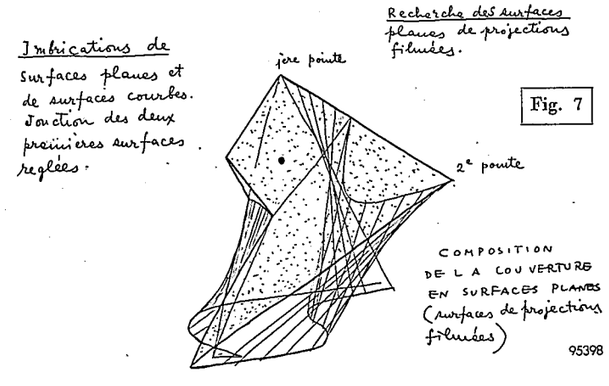

Fig. 7

Parce postulat impliqué dans ces surfaces reglées, toute la plastique du Pavillon sera conditionnée. C'est pour cela que les pointes et leur équilibre plastique sont soulignés dans cet exposé.

95396

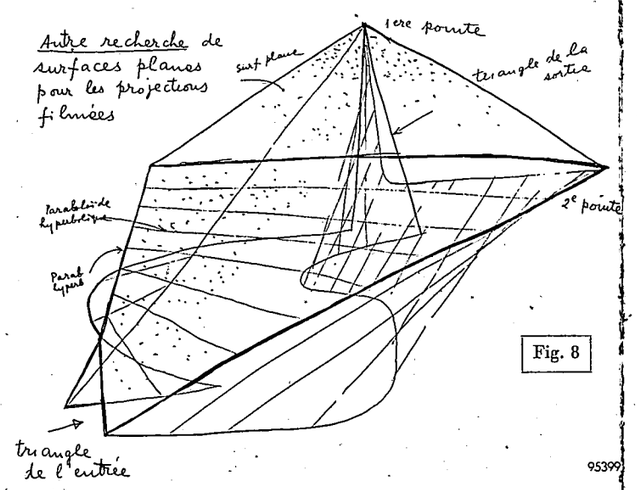

Fig. 8

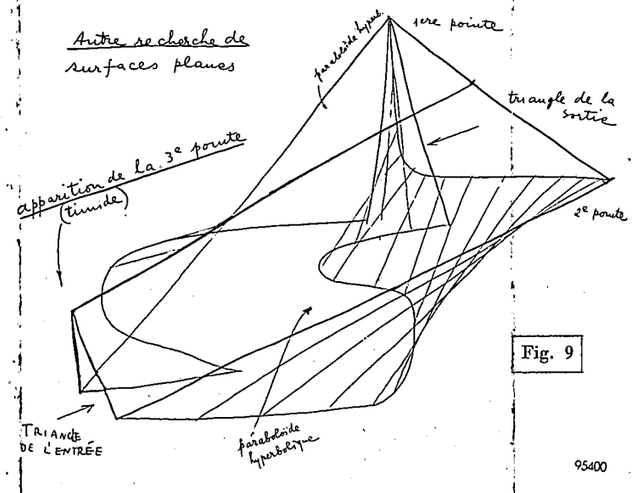

Fig. 9

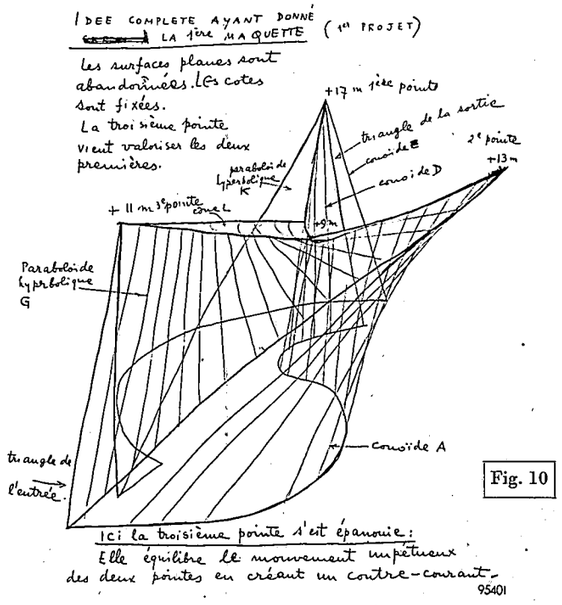

Fig. 10

Figs. 2-4. Development of the ground-plan.

Fig. 2. Circular space with two "spouts" as entrance and exit channels.

Fig. 3. Further development of the plan form; partly from its shape and partly because of its function, the architect refers to it succinctly as "l'estomac".

Fig. 4. The ground-plan forming the basis of the first design.

Figs. 5-10. Stages in the development of the first design.

Fig. 5. Ground profile of the *left half* of the "stomach". The intention was to build over the ground-plan a shell composed of as few ruled surfaces as possible. A conoid (E) is constructed through the ground profile curve; this wall is bounded by two straight lines, viz. the straight directrix (rising from the left extremity of the ground profile) and the outermost ruling line (passing through the right extremity of the ground profile). This produces the first "peak" of the pavilion.

Fig. 6. A ruled surface, but consisting of *two* conoids, A and D, is also laid through the curve bounding the *right half* of the "stomach". The straight directrix of D passes through the first peak, and the outermost ruling line at this side forms with that of E a triangular exit. The straight directrix of A passes through a second peak and is joined by an arc to that of D.

This basic form is that used in the first design and was retained, with some modifications, in the final structure. The main problem of the design was to establish an aesthetic balance between the two peaks.

Fig. 7. Attempt to close the space between the two ruled surfaces of the first design by flat surfaces (which might serve as projection walls).

Fig. 8. Another attempt. Above the entrance channel a small triangular opening is formed, flanked by two hyperbolic paraboloids (later denoted by G and K), and the whole is covered with a horizontal top surface.

Fig. 9. Elaboration of fig. 8. The third peak begins tentatively to take shape.

Fig. 10. The first design completed (see also the first model, fig. 11). There are no longer any flat surfaces. The third peak is fully developed and creates, with its opposing sweep, a counterbalance for the first two peaks. The heights of the three peaks have been established. The third peak and the small arc connecting the straight directrixes of conoids A and D (see fig. 6) form, respectively, the apex and the base of a part of a cone L.

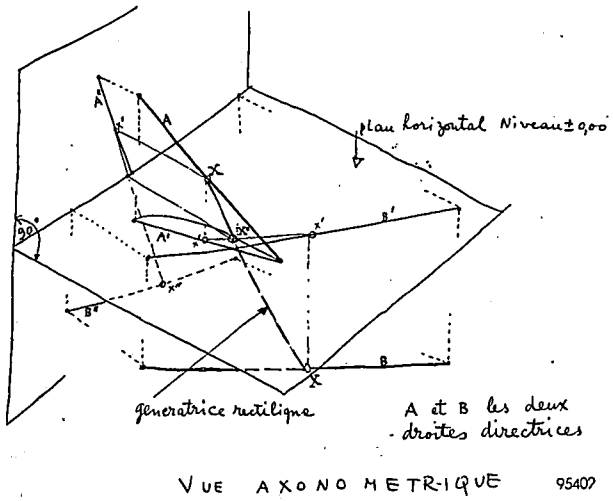

Fig. 12

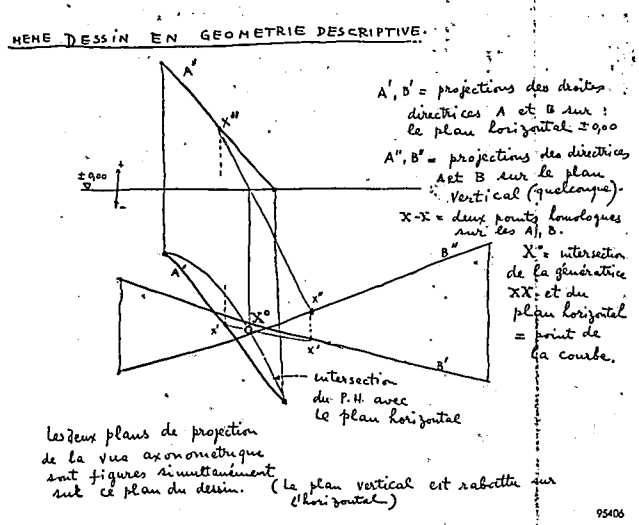

Fig. 13

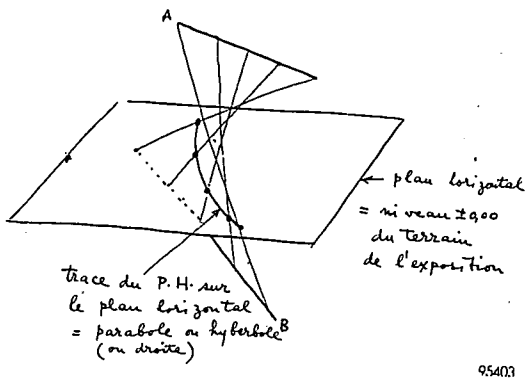

Fig. 14

Fig. 12. Isometric drawing to indicate how the orthogonal projection (fig. 13) of a hyperbolic paraboloid may be constructed. The two directrixes A, B are projected on to a horizontal plane (A', B') and on to a vertical plane (A'', B''); two pairs of points, viz. the end points of A and B, and their corresponding projections are shown.

Fig. 13. Horizontal and vertical projections of the directrixes of a hyperbolic paraboloid from fig. 12. Also shown are the projections $X'X'$ and $X''X''$ of an arbitrary generator line connecting two corresponding points X, X on the directrixes. This generator passes through the horizontal plane at point X^0.

Fig. 14. The intersection of a hyperbolic paraboloid with the horizontal plane is constructed from the points at which a series of generator lines intersect this plane.

By December 1956 the second design had been completely worked out in this way and set down on paper (*figs. 15* and *16*). From this design a new model was made (*fig. 17*).

Comparing the second with the first design, we see that the hypars G and K (which form the most important surfaces for the projection of pictures) have been retained, but the cone L has been widened and the conoids A, E and D changed into five hypars A, E and B, N, D. In addition, two new hypars C and F appear. Surface F, which abuts on E, provides the necessary space for certain installations (air-conditioning plant, toilets, control room) and for the extensive equipment needed for automatically performing, several times an hour, the spectacle of light and sound.

Final modifications

Most of the contracting firms approached by Philips at this stage of the design had only more or less conventional schemes of construction to propose, which were conspicuously out of keeping with the revolutionary style of the structure. Double-walled shells were suggested, having a total thickness of

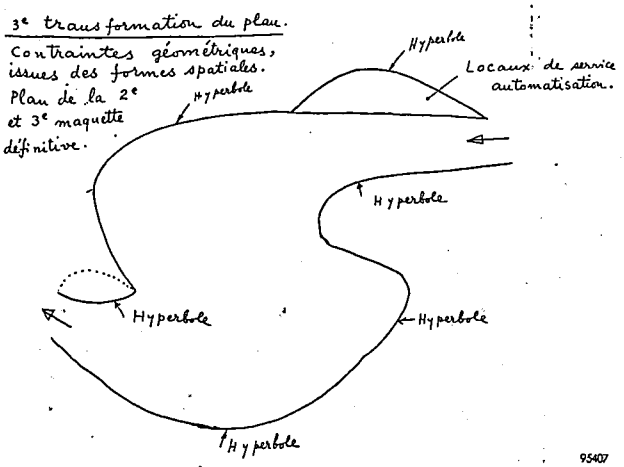

Fig. 15. Revised ground-plan for the second (and definitive) design. The bounding curves are now composed of parts of hyperbolae (for practical reasons the entrance and exit were interchanged with respect to the first design).

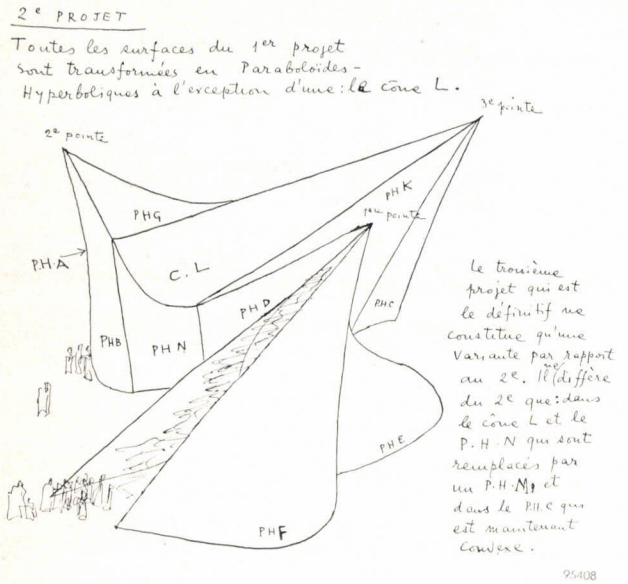

Fig. 16. The second design. All surfaces of the first design, except cone L, have now been converted into hyperbolic paraboloids, and two new hyperbolic paraboloids (F and C) have been introduced. Compared with fig. 10, the design is seen here from the opposite side, as can be seen from cone L, the apex of which appears top right in this sketch. The first peak is here in the foreground.

80 cm and made of wood, metal or plaster carried by fairly complex skeleton structures. The only proposal that was really in unison with the architect's intentions, while being at the same time reasonable in price, came from the Belgian contracting firm N.V. "Strabed", directed by Dr. H. C. Duyster. Mr. Duyster's plan was to build the pavilion as a shell structure of prestressed concrete 5 cm thick, which would be largely self-supporting, i.e. only a few stanchions would be used merely to give the walls some additional support. The intention was to follow closely the form of the second design, with only one minor modification. The latter arose from a misunderstanding of the architect's drawing, in which the hyperbolic paraboloids that did not touch the ground were indicated only summarily, leading Mr. Duyster to interpret the cone L and the hypar N (fig. 16) as parts of a single hypar (denoted M below). In fact, this simplification improved the geometrical purity of the structure. The elegant method by which Mr. Duyster proposed to construct the ruled surfaces of the pavilion in concrete is described in the fourth article of this series.

Finally, another modification was decided on, which, though a minor one in its effect on the strength of the structure, was of the utmost importance as regards the overall architectural effect. The design still envisaged supporting stanchions, one of which was actually inside the enclosed space, and as such was a nuisance. The architect Xenakis now proposed a slight change in the new hypar M and in B in order to make it possible to dispense with the stanchions entirely. The reasoning was that the edge members (ribs) at the relevant shell intersections ought to be able to take over, at least for the greater part, the supporting function of the stanchions.

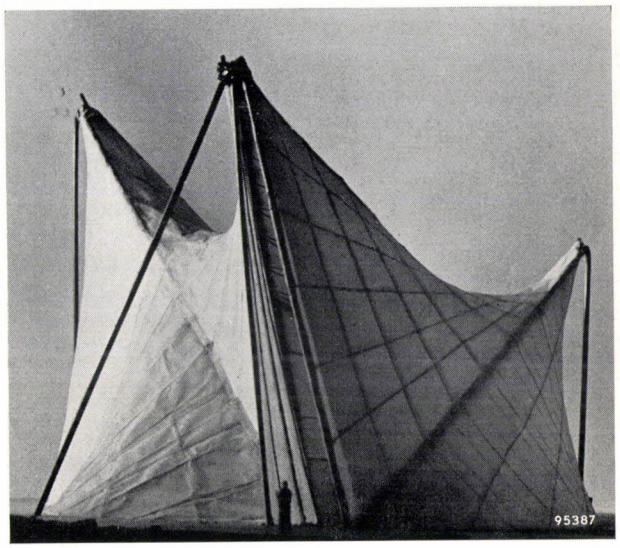

Photo Lucien Hervé

Fig. 17. Second model, seen from the side which now forms the entrance; the third peak is in the foreground.

The model tests (see article III) confirmed that in the design so modified the stanchions were superfluous. The structure was thus made entirely self-supporting, that is to say it no longer contained supporting elements that were not embodied in

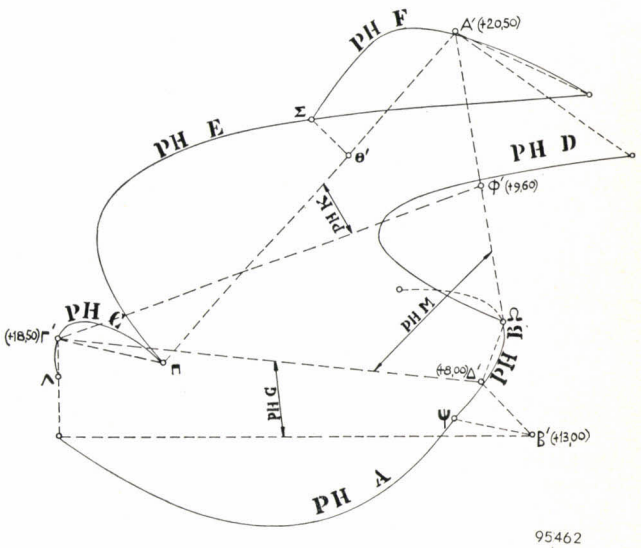

Fig. 18. General plan of the final design (enlarged from fig. 19).

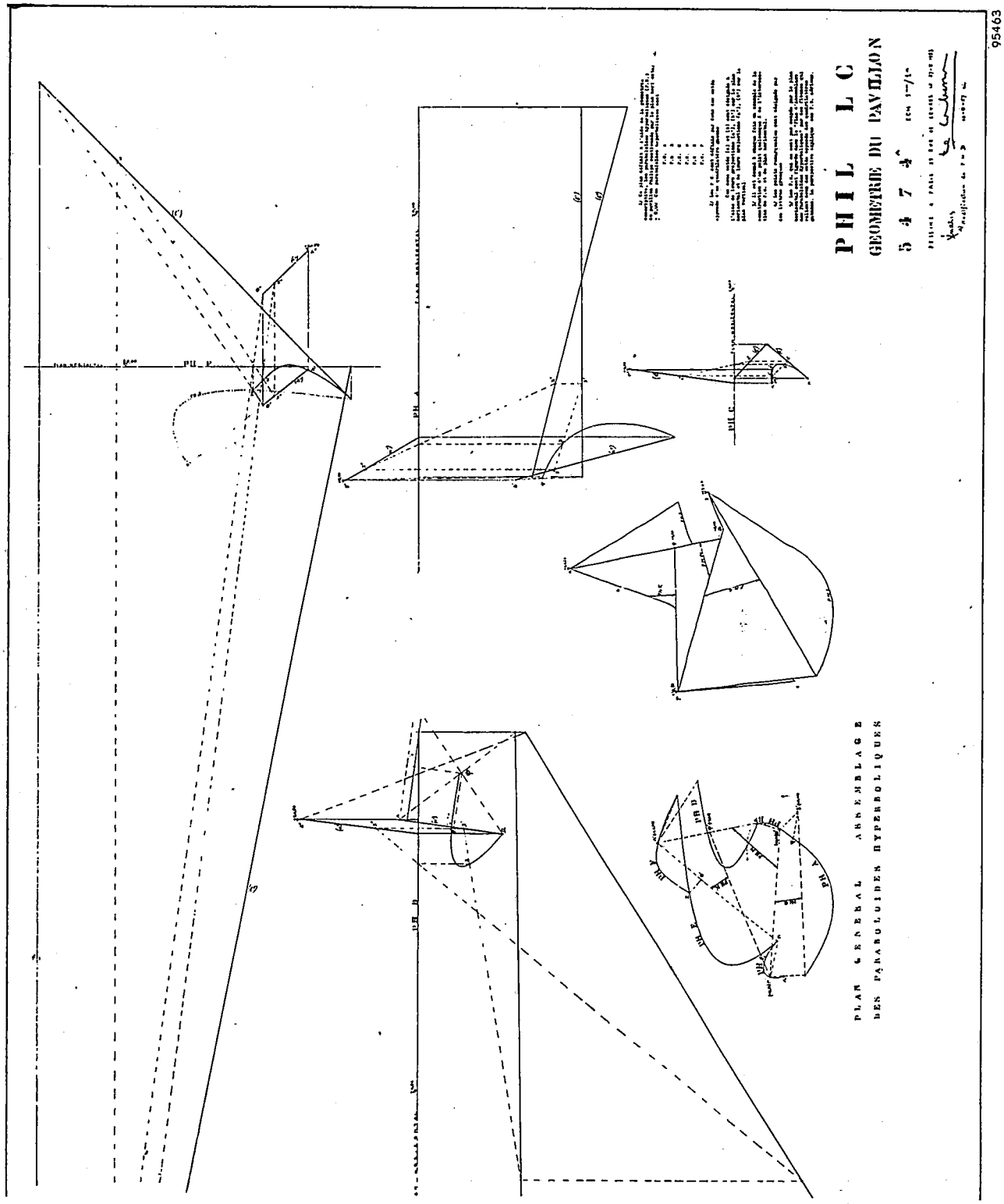

Fig. 19. Part of the scale drawing 1 : 200 of the wall surfaces of the definitive design, signed by the architects Le Corbusier and Xenakis.

the wall surfaces. To strengthen the third peak, which slopes at a very oblique angle, the hypar *C* was made convex at its foot instead of concave, and finally the two triangular openings were partly closed with extra hypars abutting on the existing ones. In this way the definitive form of the pavilion was arrived at, as illustrated in the plans of *figs. 18* and *19*.

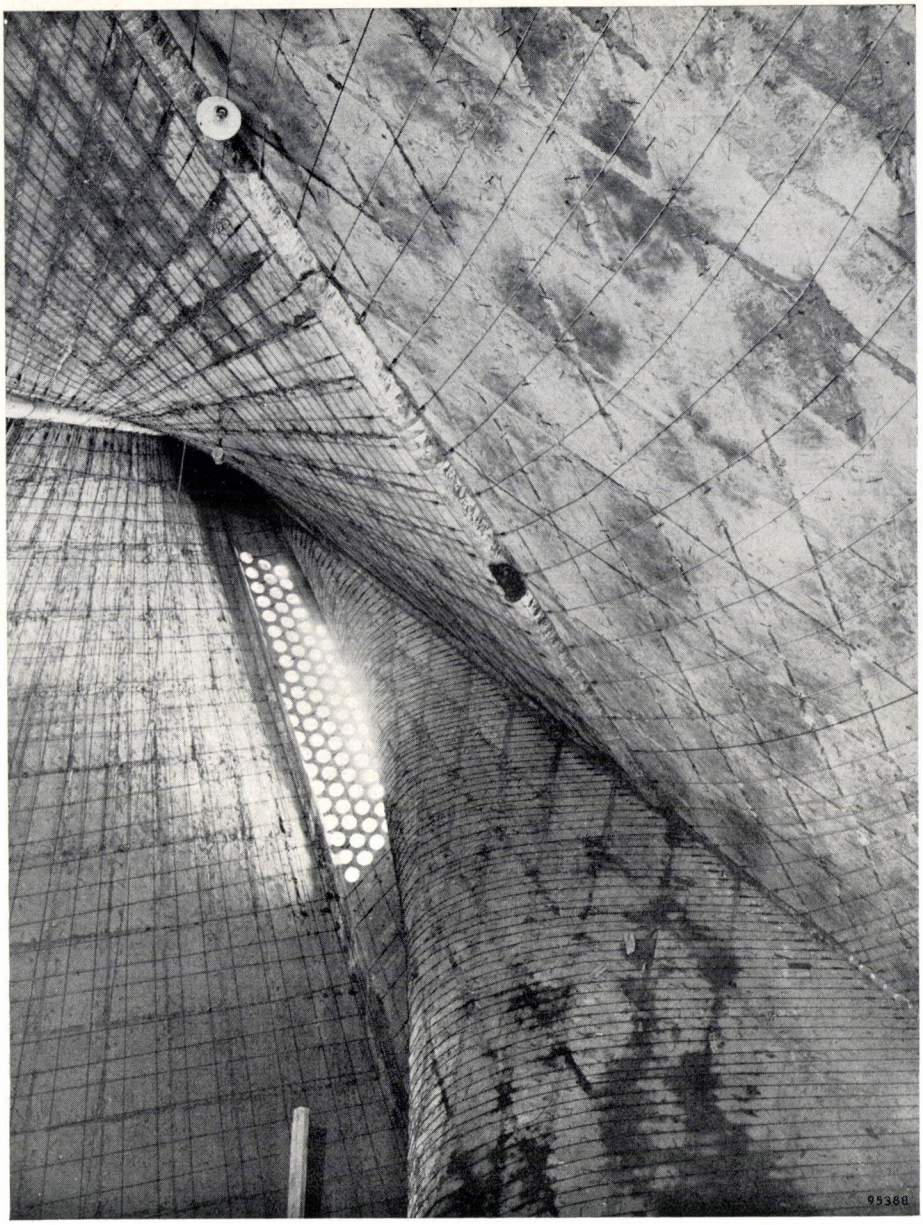

Fig. 20. Photograph of part of the interior of the pavilion. The prestressing wires on the concrete, which enhance the plastic form of the structure, are unfortunately concealed in the finished pavilion by a surfacing required for the projection of colours and pictures.

Fig. 20 shows a photograph of the interior made before the concrete's prestressing wires were concealed by the internal surfacing. This photograph and the title photograph (and also fig. 12 in IV) give an impression of the remarkable plastic figuration of the building.

II. THE HYPERBOLIC-PARABOLOIDAL SHELL AND ITS MECHANICAL PROPERTIES

by C. G. J. VREEDENBURGH *).

624.023.744:061.41(493.2):725.91

It was about the year 1935 that Laffaille and Aimond published the first studies on the distribution of forces in "hypar" shells, i.e. thin-walled structures having the form of hyperbolic paraboloids [1][2]).

Shells of spherical and cylindrical form have been used for many years but practical interest in the hypar shell dates only from the last ten years. It would seem that saddle surfaces (surfaces having opposite curvatures along different directions) such as these did not find much acceptance because they seemed to defy architectural conventions. Moreover it was thought that hypar shells would be more costly to build than shells of the normal spherical and cylindrical shapes.

Views on this subject have now changed considerably. Partly through the pioneering work of Candela in the U.S.A. [3]) and of Hruban in Czechoslovakia [4]), it became realized that hypar shells not only possess great strength and stability but also lend themselves readily to a synthesis of striking architectural forms in keeping with various tendencies in modern art. The design of Le Corbusier and Xenakis for the Philips pavilion in Brussels which, as described in the first article of this series, is entirely based on hyperbolic paraboloids, has certainly shown that hypar shells can be used for creating the most spectacular architectural fantasies. Furthermore, as regards their actual construction, it is now recognized that hyperbolic paraboloids, because of the two systems of straight lines inherent in them [5]), are particularly well adapted to construction in wood as well as in reinforced or prestressed concrete.

The hypar shell, then, has made its entry into architecture and is being used in many countries and for various kinds of building. However, owing to the relative novelty of this structural form and the greater geometrical intricacy of saddle surfaces, the contractor presented with such an assignment will often be unwilling to rely entirely on experience already available and on his own intuition, but will enlist the aid of a scientific analysis of the expected mechanical behaviour of the structure. It thus came about that, towards the end of January 1957, we were approached by the contracting firm "Strabed" for advice concerning the building of the Philips pavilion.

Now it is simply not possible to calculate exactly the states of stress that can arise in such an exceedingly complicated structure of shells and ribs (the latter at the intersections of the shells). On the basis of theoretical considerations alone we were therefore only able to provide Messrs. Strabed with positive advice of a general nature regarding the feasibility of the architects' design and of the proposed method of building; in order to give a definite answer to certain specific questions recourse was necessary, partly because of the limited time available, to experimental stress analysis, using a model. These tests, which were performed at Rijswijk and Delft (Netherlands) by A.L. Bouma and F. K. Ligtenberg, are described in the third article of this series. Nevertheless it will perhaps be useful to show the interested reader how far it is possible to go with a calculation of the general states of stress in hyperbolic-paraboloidal shells, and to describe the nature of the difficulties which, in intricate cases, oblige one to resort to supplementary tests on a model.

The geometry of the hypar shell

To understand the distribution of forces in a hypar shell it is first necessary to recall some facts about its geometry.

With respect to a rectangular system of axes *Oxyz* (see *fig. 1*), the equation for a hyperbolic paraboloid may be written in the form:

$$z = \frac{x^2}{2r_1} - \frac{y^2}{2r_2}, \quad \ldots\ldots \quad (1)$$

---

*) Professor of applied mechanics, Technische Hogeschool, Delft.

[1]) B. Laffaille, Mémoire sur l'étude générale des surfaces gauches minces, Mém. Assoc. Int. Ponts et Charpentes **3**, 295-332, 1935.

[2]) F. Aimond, Etude statique des voiles minces en paraboloïde hyperbolique, Mém. Assoc. Int. Ponts et Charpentes **4**, 1-112, 1936.

[3]) F. Candela, Structural applications of hyperbolic paraboloidal shells, J. Amer. Concrete Inst., Title No. 51-20, January 1955, pp. 397-415.

[4]) K. Hruban, Obecné řešení žlabových skořepin (The general theory of saddle-surface shells), Institute of Technology Brno, 1953.

[5]) See the third and fourth article of this series. A recent example of a large hypar shell consisting of glued wooden sections is the roof construction of the Information Centre in the Place de Brouckère, Brussels.

where O is the apex of the surface, Oz its axis, and xOz and yOz are planes of symmetry which intersect the hyperbolic paraboloid in the parabolae p_1 and p_2 respectively. The quantities r_1 and r_2 are the radii of curvature of the parabolae p_1 and p_2 at the apex O.

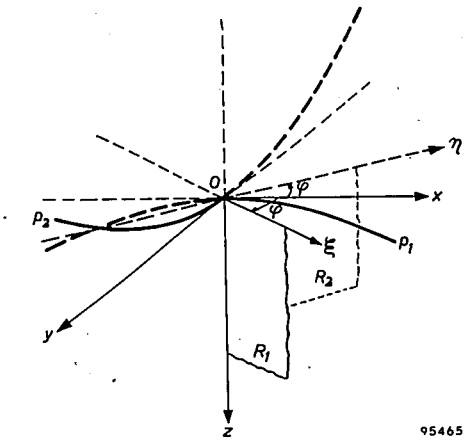

Fig. 1. Geometrical definition of the hyperbolic paraboloid. O = apex; Oz = axis; xOz and yOz are the planes of symmetry; ξOz and ηOz are the directrix planes (R_1 and R_2), to which the two sets of rulings on the surface run parallel.

The plane xOy intersects the surface in the straight lines $O\xi$ and $O\eta$. The axis Ox is the bisector of the angle 2φ between these lines. It can be shown, from (1), that

$$\tan \varphi = \frac{\sqrt{r_2}}{\sqrt{r_1}}. \quad \ldots\ldots \quad (2)$$

With respect to the system of axes $O\xi\eta z$ (the axes $O\xi$ and $O\eta$ are not, in the general case, perpendicular to each other) the equation for the hypar is:

$$z = k\xi\eta \sin 2\varphi, \quad \ldots\ldots \quad (3)$$

where

$$k = \frac{1}{\sqrt{r_1 r_2}}. \quad \ldots\ldots \quad (4)$$

The two planes passing respectively through the axis Oz and the lines $O\xi$ and $O\eta$ are the directrix planes R_1 and R_2 of the hypar. From eq. (3) it can be seen that all planes parallel to R_1 cut the surface in straight lines, likewise all planes parallel to R_2. The hyperbolic paraboloid thus contains two systems of straight lines (rulings). The lines of each system all run parallel to the corresponding directrix plane, but their slope varies with their distance from that plane (see *fig. 2a*).

If we consider a part of the surface of a hypar shell, bounded by two straight lines AB and CD of the one set of rulings and two straight lines AC and BD of the other set (see fig. 2*b*), we see at once that a hyperbolic paraboloid is also obtained when a straight line (e.g. AC), which intersects two skew straight lines (AB and CD), slides along the latter two lines, while remaining parallel to a given plane (in this case the directrix plane to which AC and BD are parallel).

Describing now a parallelogram on two adjoining lines (e.g. AB and AC) of the above figure, the fourth corner of the parallelogram being E, the line DE will run parallel to the axis of the hyperbolic paraboloid and is termed the *linear distortion* v of the hypar surface $ABDC$.

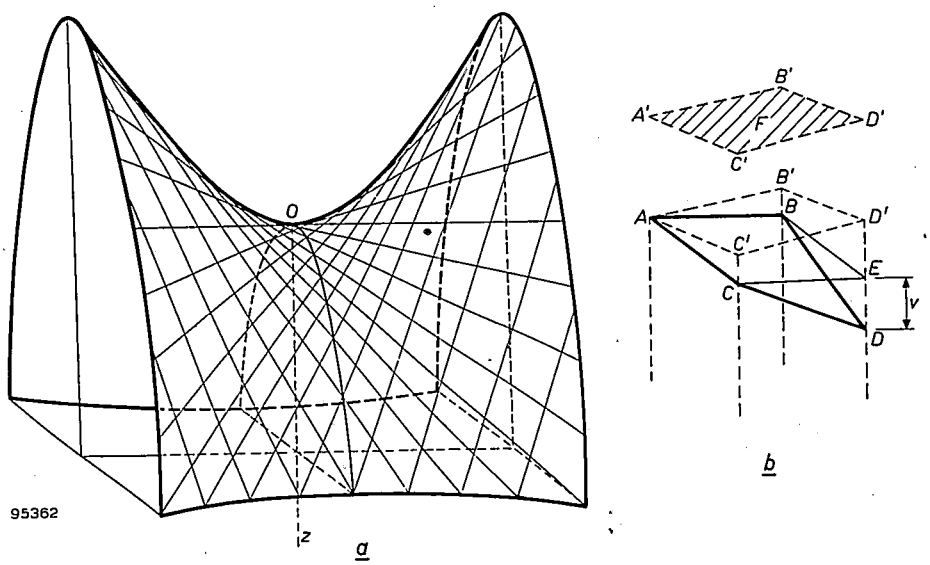

Fig. 2. *a*) Hyperbolic paraboloid showing the two sets of ruling lines. O = apex, Oz = axis. *b*) Part of a hyperbolic paraboloid bounded by four rulings AB, CD, AC, BD. The "linear distortion" is v, the specific distortion is $v/F = k = 1/\sqrt{r_1 r_2}$.

If we project the surface $ABDC$ on to a plane perpendicular to the axial direction DE, and if the area of this projection (parallelogram $A'B'D'C'$) is F, we call the ratio v/F the specific distortion, this being identical with k of formula (4) and constant for all parts of the hypar shell, bounded by four ruling lines. In practice the quantity k is usually determined by calculating the specific distortion.

Finally, the hyperbolic paraboloid can also be regarded as a translation surface. For this purpose let us revert to fig. 1. All planes parallel to the plane of symmetry xOz cut the surface, according to eq. (1), in parabolae which are congruent with p_1, while all planes parallel to the plane of symmetry yOz give intersecting curves congruent with the parabola p_2. We can therefore also imagine the hyperbolic paraboloid as produced by displacing parabola p_2 parallel to itself, its apex gliding along p_1, or by the parallel displacement of parabola p_1, its apex gliding along p_2.

The plane $z = +c$ intersects the hypar, according to eq. (1), in a hyperbola. Projecting this onto the plane xOy, the lines $O\xi$ and $O\eta$ are the asymptotes of this hyperbola, and Ox and Oy its real and imaginary axes respectively. For the plane $z = -c$, the projected intersecting curve is again a hyperbola, again with $O\xi$ and $O\eta$ as asymptotes, but with Ox as its imaginary axis and Oy as its real axis.

In the special case that $\varphi = 45°$ ($O\xi$ and $O\eta$ then being perpendicular to each other) the above intersecting curves are rectangular hyperbolae and the surface is then called a rectangular hyperbolic paraboloid.

If we take an arbitrary hypar and project a number of contour hyperbolae and a number of ruling lines onto the plane xOy, we obtain a diagram such as that of *fig. 3*.

For the sake of completeness we should mention the one-shell hyperboloid, which also contains two systems of ruling lines. These lines, however, are no longer parallel to two directrix planes, but parallel to the generators of a conic surface, the latter being the asymptotic cone of the hyperboloid. A consequence of this fact is that it is much more difficult to calculate the distribution of forces in a hyperboloidal shell than in a hyperbolic-paraboloidal shell.

The membrane theory of the hypar shell

Forces lying in the median surface of a plate or shell are known as membrane forces. (The median surface is defined as the locus of the mid-points of the thickness everywhere in the plate or shell.) Unlike a flat plate, a curved shell is able to take a load perpendicular to its surface in the form of membrane forces. When a shell is allowed to deform freely under a given set of forces, a good approximation to the actual distribution of forces is obtained by assuming that exclusively membrane forces are acting. This is plausible since for a statically possible stress distribution in which no bending or torsion takes place (i.e. a quasi-two-dimensional stress distribution) the deformation energy of a shell structure is approximately a minimum. The usual procedure, therefore, is to begin by calculating the distribution of forces in the hypar shell in accordance with the membrane theory, and subsequently to apply corrections to allow for stress disturbances at the edges of the shell, where the deformations resulting from the membrane stresses are *not* able to take place freely. In the Philips pavilion, for example, at the intersection of each pair of hyperbolic-paraboloidal surfaces, the surfaces are rigidly joined by a rib. The condition here is that the deformations of the rib must be the same as those of the abutting edges of the shells. This gives rise to stresses near the edges, so-called edge disturbances, which we shall consider presently.

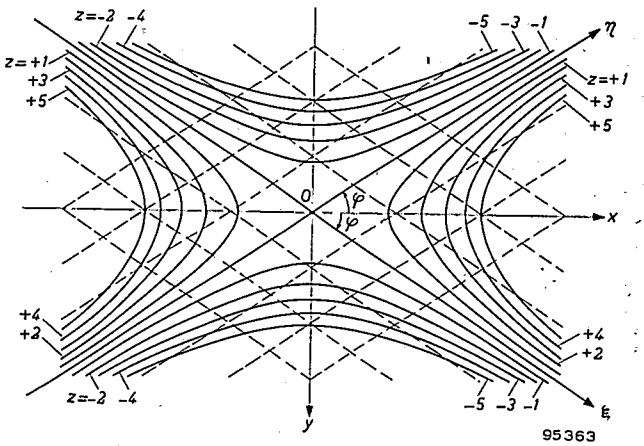

Fig. 3. Projection on the plane xOy of contour lines (hyperbolae) and ruling lines (dashed) of a hyperbolic paraboloid.

The differential equations for the membrane state of stress can best be derived by considering the equilibrium in the directions ξ, η and z of a loaded element. For this purpose we consider a small element of the shell bounded by four neighbouring ruling lines which, when projected on to the horizontal plane $\xi O\eta$, form an elementary parallelogram of sides $d\xi$ and $d\eta$ (see *fig. 4*). The components of the applied load per unit projected horizontal area of the shell in the directions $O\xi$, $O\eta$ and Oz are denoted p_ξ, p_η and p_z respectively. The oblique membrane forces per unit length (called shell forces, analogous to stresses in the more general case of solid bodies) in the shell element are denoted n_ξ, n_η and ϑ.

The projected shell-forces are:

$$\left.\begin{aligned} \bar{n}_\xi &= n_\xi \frac{\cos\alpha}{\cos\beta}, \\ \bar{n}_\eta &= n_\eta \frac{\cos\beta}{\cos\alpha}, \\ \bar{\vartheta} &= \vartheta. \end{aligned}\right\} \quad \ldots\ldots \quad (5)$$

The equilibrium conditions in the ξ, η and z directions yield the following equations:

$$\left.\begin{aligned} &\frac{\partial \bar{n}_\xi}{\partial \xi} + \frac{\partial \vartheta}{\partial \eta} + p_\xi \sin 2\varphi = 0, \\ &\frac{\partial \bar{n}_\eta}{\partial \eta} + \frac{\partial \vartheta}{\partial \xi} + p_\eta \sin 2\varphi = 0, \\ &2\vartheta \frac{\partial^2 z}{\partial \xi\, \partial \eta} + \left(p_z - p_\xi \frac{\partial z}{\partial \xi} - p_\eta \frac{\partial z}{\partial \eta}\right) \sin 2\varphi = 0. \end{aligned}\right\} \quad (6)$$

The expression between brackets is the z-component $\bar{p}_z$ of the net load at the point of the shell under consideration when the latter is resolved into two components, one ($\bar{p}_z$) in the z direction and the other in the tangent plane; the third equation of (6) can therefore also be written:

$$2\vartheta \frac{\partial^2 z}{\partial \xi\, \partial \eta} + \bar{p}_z \sin 2\varphi = 0. \quad \ldots \quad (7)$$

A very simple solution is found when the applied load in the z direction per unit horizontal area of the hypar shell is everywhere constant ($= \bar{g}$, say), while $p_\xi = p_\eta = 0$. From eq. (3) we derive the purely geometrical relation

$$\frac{\partial^2 z}{\partial \xi\, \partial \eta} = k \sin 2\varphi.$$

For the case $\bar{p}_z = \bar{g}$, eq. (7) thus gives

$$\vartheta = -\frac{\bar{g}}{2k} = \text{constant}. \quad \ldots\ldots \quad (8)$$

We see from this formula that the shell force ϑ is inversely proportional to k. In connection with (4) it is therefore advantageous to make the radii of curvature r_1 and r_2 as small as possible. The more pronounced is the curvature of the shell, the more favourable is the stress distribution.

If the shell is bounded by ruling lines, and if the membrane forces n_ξ and n_η at the boundaries may be assumed to be zero (non-rigid edge members), it follows from the first two equations of (6) that these forces are zero at all points of the shell.

A load uniformly distributed per unit horizontal area is therefore transmitted by a hypar shell of vertical axis and constant thickness to the edge members in the form of constant shear stresses along the rulings. The shell is then for practical purposes a structure of *equal strength*, which means that if at one point of the shell the stress reaches its maximum permissible value, it will do so at all points. Since in that case the strength of the material is fully exploited everywhere, it is evident that a structure of equal strength requires a minimum of material.

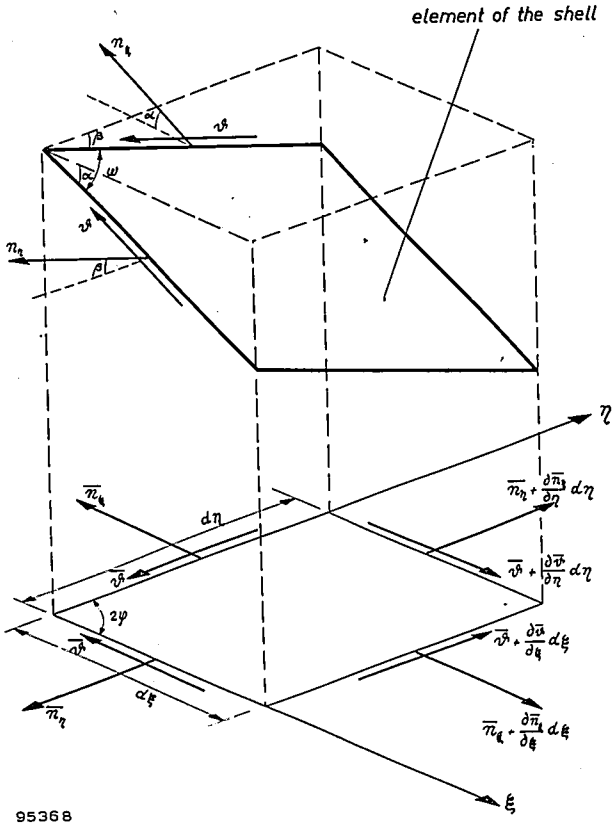

Fig. 4. Equilibrium of a shell element, introducing the oblique shell-forces projected onto the $\xi\eta$ plane. Shell-forces are the forces per unit length of the shell; the components in the median plane of the membrane are generally denoted by n and ϑ. A shell-force divided by the thickness of the shell evidently represents a stress (force per unit area).

The above is further illustrated in *fig. 5*, which depicts a simple shell consisting of four quadrants, each constituting a part of a rectangular hyperbolic paraboloid with edge members. As indicated in one of the quadrants by dashed lines, there are two sets of parabolae on the surface, a set with the convex side upwards and another set with the concave side upwards. The former are in compression and the latter in tension. The load on the shell is now borne for one half by the compression parabolae and for the other half by the tension parabolae. If we consider a point on an edge member where a tension and a compression parabola meet, we see that the reactions of both together produce a shear force along the edge member, so that the latter

N.V. PHILIPS' GLOEILAMPENFABRIEKEN

are not loaded perpendicularly to their axes. The same manner of force-transmission also takes place in non-rectangular hypar shells. This explains why the load in the case of the Philips pavilion is transmitted largely in the form of compressive forces along the ribs to the foundations and why the vertical stanchions originally envisaged for the support of the ribs could eventually be dispensed with.

The distribution of forces as described here applies only to a load uniformly distributed per unit horizontal area, as for example a load of snow of constant (vertical) thickness.

For the dead weight of the shell, the simple distribution of forces holds only approximately. If this weight be g per unit area of the shell, then the shell-force for a shell with a vertical axis (fig. 1) is:

$$\vartheta = -\frac{g}{2k}\sqrt{\Phi}, \quad \ldots\ldots \quad (9)$$

where

$$\Phi = 1 + k^2(\xi^2 + \eta^2 - 2\xi\eta\cos 2\varphi). \quad (10)$$

If the normals to the shell surface do not make large angles with the axis ($\leqslant 15°$), we can put Φ equal to unity. Furthermore we find:

$$\left.\begin{aligned} \bar{n}_\xi &= -\frac{g}{2k}\cos 2\varphi\sqrt{\Phi} + \\ &\quad + \tfrac{1}{2}g\eta\sin^2 2\varphi \ln[\sqrt{\Phi} + k\xi - k\eta\cos 2\varphi] + \mathrm{f}_1(\eta), \\ \bar{n}_\eta &= -\frac{g}{2k}\cos 2\varphi\sqrt{\Phi} + \\ &\quad + \tfrac{1}{2}g\xi\sin^2 2\varphi \ln[\sqrt{\Phi} + k\eta - k\xi\cos 2\varphi] + \mathrm{f}_2(\xi). \end{aligned}\right\} \quad \ldots\ldots \quad (11)$$

The integration functions $\mathrm{f}_1(\eta)$ and $\mathrm{f}_2(\xi)$ must be determined from the boundary conditions.

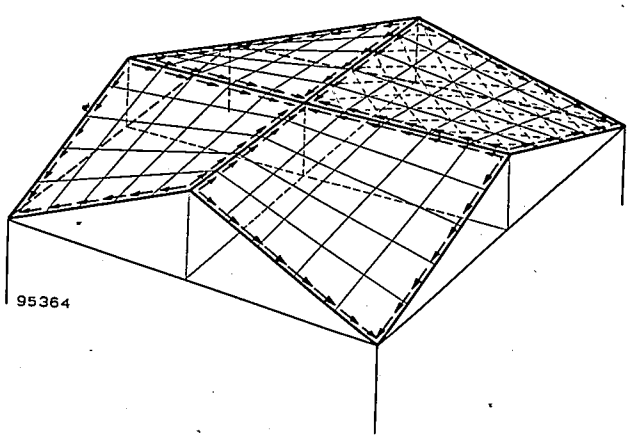

Fig. 5. System of four rectangular hypar shells, loaded uniformly per unit horizontal area. The arrows indicate the shear forces transmitted to the rigid edge members.

In this way we can also calculate the membrane forces for a constant load w per unit area of shell directed everywhere normally to the shell. Such a load is often assumed to represent a *wind* load. We then find:

$$\vartheta = -\frac{w\Phi}{2k}; \quad \ldots\ldots \quad (12)$$

$$\left.\begin{aligned} \bar{n}_\xi &= wk(2\xi\eta - \xi^2\cos 2\varphi) + \mathrm{f}_3(\eta), \\ \bar{n}_\eta &= wk(2\xi\eta - \eta^2\cos 2\varphi) + \mathrm{f}_4(\xi). \end{aligned}\right\} \quad \ldots \quad (13)$$

From the above formulae we see that, as opposed to a snow load, the shell-forces ϑ are no longer constant under a dead weight or wind load, and that the shell forces n now begin to enter into account.

Having calculated the projected shell-forces $\bar{n}_\xi$ and $\bar{n}_\eta$, the actual shell-forces n_ξ and n_η are also known, from equations (5). It should be noted here that (see fig. 4):

$$\left.\begin{aligned} \cos\alpha &= \frac{1}{\sqrt{1 + (\partial z/\partial\xi)^2}}, \\ \cos\beta &= \frac{1}{\sqrt{1 + (\partial z/\partial\eta)^2}}. \end{aligned}\right\} \quad \ldots \quad (14)$$

Finally, in order to judge the strength of the structure, we must determine from the actual shell-forces the *principal shell-forces* [6]) in magnitude and direction for a number of characteristic points of the shell. For this purpose we must know the angle ω between the ruling lines (see fig. 4) at the point under consideration. This is given by the formula:

$$\cos\omega = \frac{(\partial z/\partial\xi)(\partial z/\partial\eta) + \cos 2\varphi}{\sqrt{[1 + (\partial z/\partial\xi)^2]\,[1 + (\partial z/\partial\eta)^2]}}. \quad (15)$$

Since we are concerned here with *oblique* shell-forces, or stresses, it is necessary to modify somewhat the conventional *Mohr circle* construction. *Fig. 6a* shows the conventional construction, for a plane state of stress; such a diagram enables us to determine graphically the direction and magnitude of the principal stresses σ_1 and σ_2, from the normal stresses σ_x and σ_y and the shear stress τ, acting in two mutually perpendicular plane elements (both perpendicular to the stress-free plane). The modified construction is shown in fig. 6*b*; this enables us to determine the direction and magnitude of the principal shell-forces n_1 and n_2 from the oblique shell-forces n_ξ, n_η and ϑ, acting in two plane elements

[6]) Defined analogously to the principal stresses in the case of a plane state of stress, i.e. as the shell-forces in those planes in which there are no shear forces but only normal forces (these are, incidentally, the largest and smallest shell-forces at the point in question).

which make an acute angle ω with each other [7]).

Further, one can construct in the median surface of the shell two sets of curves such that the tangents at each point of intersection represent the directions of the principal shell-forces n_1 and n_2 in that point. These curves are then the principal shell-force "trajectories"; these are sometimes called the principal *stress* trajectories, since the shell stresses are simply the shell-forces divided by the shell thickness.

If prestressed concrete is to be used, one of the questions arising concerns the minimum tensile forces that should be applied in the cables (laid in the direction of the ruling lines); in other words, what are the minimum compressive shell-forces that must be superimposed in the ξ and η directions on the existing stress distribution in order to prevent the occurrence of a tensile stress in any plane element through the point concerned? The graphical solution of this problem is shown in fig. 6*c*.

[7]) C. G. J. Vreedenburgh, Hyperbolic Paraboloidal Shells, collected and edited by W. Grijm, Central Ctte., Studiebelangen, Delft 1954, pp. 17-26.

Edge disturbances

As remarked in the foregoing, the shell in the proximity of a stiff edge cannot freely undergo the deformations arising from the membrane state of

Fig. 6. *a*) Mohr's construction for a plane state of stress. The construction gives the principal stresses σ_1 and σ_2 at any given point when the normal stresses σ_x and σ_y and the shear stress τ in two mutually perpendicular plane elements at that point are known. By plotting σ_x and σ_y on the horizontal axis and τ on the vertical axis, we find the points R_x and R_y. The circle through R_x and R_y, with the centre M on the σ axis, yields the points σ_1 and σ_2. The distances $O\sigma_1$ and $O\sigma_2$ give the magnitude of the principal stresses, their directions being given by $R_y\sigma_1$ and $R_y\sigma_2$, respectively.

b) Modification of Mohr's construction, adapted for the stresses (or, since a membrane state of stress is involved, the shell forces n_ξ and n_η, see fig. 4) in the direction of the ruling lines passing through a point of the hypar. The plane elements in which these forces act are *not* mutually perpendicular, but make an angle ω with each other. Plotting n_ξ and n_η on an axis set at an angle ω with the ϑ axis, and drawing two lines of length ϑ through these points, parallel to the ϑ axis, yields R_ξ and R_η. The circle through R_ξ and R_η with centre M on the relevant n axis yields the points n_1 and n_2. The distances On_1 and On_2 give the magnitude of the principal shell-forces, acting respectively in the directions $R_\eta n_1$ and $R_\eta n_2$.

c) In order to obtain a state of stress entirely free of tensile stresses, Mohr's stress circle must be displaced by external forces in such a way that it comes to lie entirely to the left of the ϑ axis. This can be achieved by means of prestressing cables, applied in the direction of the ruling lines of the hypar; the prestressing shell-forces (compressive forces), directed along n_ξ and n_η, must then be set out from the points n_ξ and n_η on the same oblique axis towards the left.

The *minimum* prestressing is obtained when the circle is tangent to the ϑ axis and when at the same time the new points R_ξ' and R_η', which lie on the same oblique line as R_ξ and R_η, are made to coincide; the circle is then also tangent to this oblique line (at point R'). The centre M' of the circle is therefore found on the line bisecting the angle between the oblique line and the ϑ axis. The figure shows that the prestressing must cause the compressive shell-forces $n_\xi + \vartheta$ and $n_\eta + \vartheta$ (giving the point $n_\xi' = n_\eta'$) and that the state of stress is then converted into a linear compressive stress with a principal shell force On_3 (the other principal stress being zero); On_3 acts in the direction $R'n_3$, i.e. in the direction of the above-mentioned bisector.

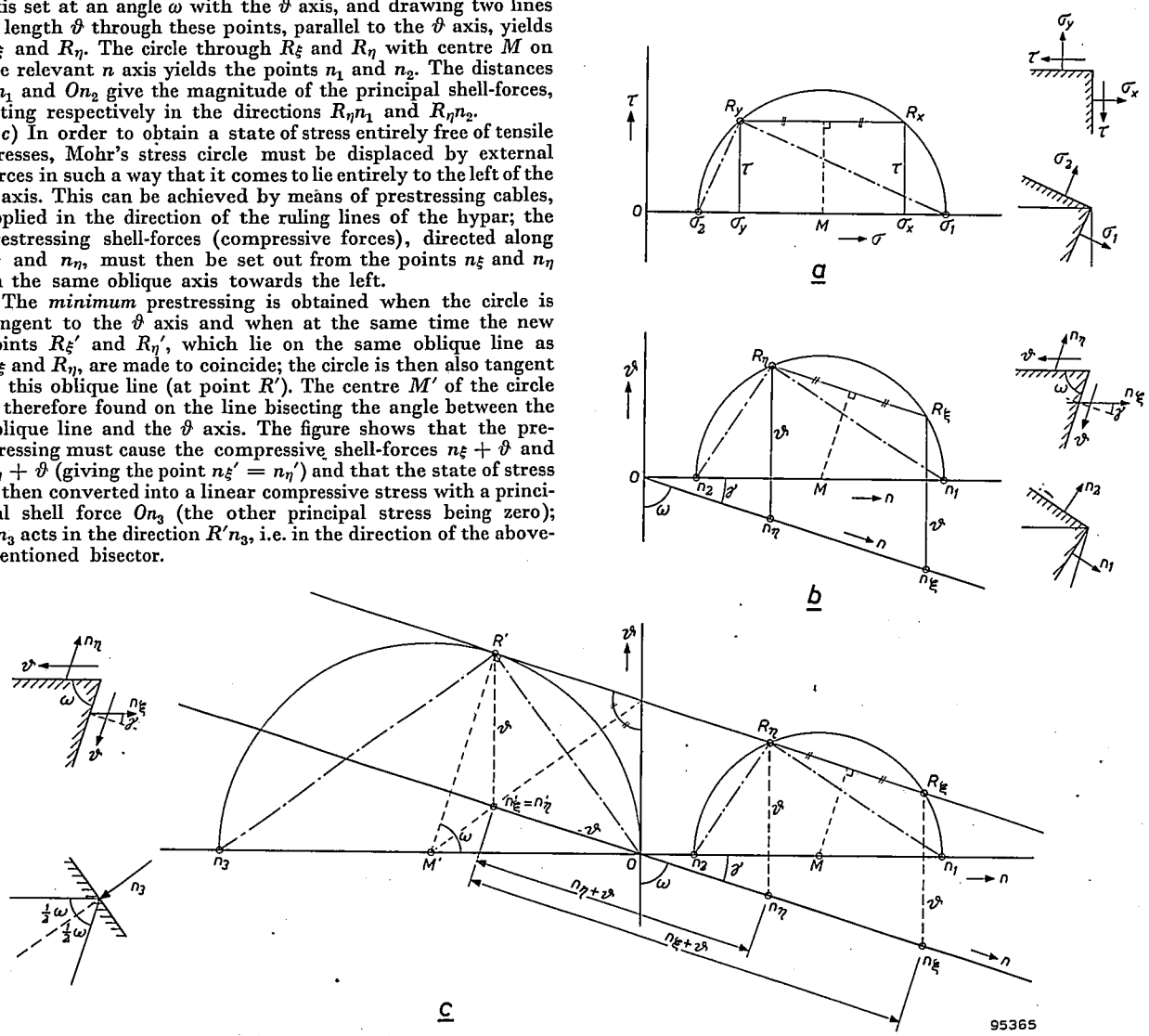

stress. If we imagine for a moment the edge member to be separated from the shell, so that the deformations can take place unhindered, it is clear that the edge of the shell and the edge member will no longer be a precise fit. A fit is only possible when the edge member exerts forces and moments on the edge of the shell (normal, shear and transverse forces, and bending and torsional moments) and the shell exerts opposite forces and moments on the edge member such that the extra deformations enable a perfect fit to be obtained. The calculation of these edge disturbances, which must be superimposed on the membrane state of stress, is one of the most difficult problems of shell theory.

If we approximate to the hyperbolic-paraboloidal shell in a small region by a translation surface of circles of radii r_1 and r_2, then, for small curvatures, the following (tetra-harmonic) differential equation for the edge disturbances is approximately valid:

$$\nabla^8 w = -\frac{D}{K}(1-\nu^2)\left[\frac{1}{r_2^2}\frac{\partial^4 w}{\partial x^4} - \frac{2}{r_1 r_2}\frac{\partial^4 w}{\partial x^2 \partial y^2} + \frac{1}{r_1^2}\frac{\partial^4 w}{\partial y^4}\right], \quad (16)$$

where

w = displacement of a shell point in the direction of the normal,

$$\nabla^2 = \frac{\partial^2}{\partial x^2} + \frac{\partial^2}{\partial y^2}, \quad D = \frac{E\delta}{1-\nu^2}, \quad K = \frac{E\delta^3}{12(1-\nu^2)},$$

δ = shell thickness,

E = modulus of elasticity and

ν = Poisson's ratio.

The quantities D and K represent the tensile and bending stiffness respectively of the shell.

If w is known, we can then find the entire distribution of forces. We find that the disturbances originating from the edge points always consist of the superposition of two spatially periodic waveforms; in many cases both waveforms are rapidly "damped", so that at some distance from the edge members little of the edge disturbance is perceptible.

Partly because a calculation based on equation (16) is extremely complicated, and indeed, not feasible in the case of such intricate boundary conditions as exist in the Philips pavilion, the following approximate calculation of the order of magnitude of the edge disturbances in hypar shells seems to be entirely adequate for practical purposes. The method adopted is based on the fact that, so far as bending phenomena are concerned, a shell can be compared with a plate supported on an elastic foundation. Thus if we imagine a strip of the hypar shell perpendicular to an edge member, this strip will behave to a first approximation as a beam supported on an elastic foundation. If the local principal curvatures [8]) of the hypar shell at the edge point in question be k_1 and k_2, then the coefficient of reaction (foundation modulus) for the equivalent beam on an elastic foundation is approximately:

$$c = E\delta(k_1^2 + k_2^2). \quad (17)$$

(The coefficient of reaction of an elastic foundation is the reaction per unit area when the deflection is equal to unity. The larger c, the greater the rigidity of the foundation.)

It is now possible by simple means to calculate the variation of the edge disturbance, which is in this case determined solely by the bending moment m and the transverse force q, both per unit length of the shell. It is found that the behaviour of the edge disturbances can be described in terms of a "wavelength" and a "damping", both of which are determined by a characteristic length:

$$\lambda = \frac{0.76\sqrt{\delta}}{\sqrt[4]{k_1^2 + k_2^2}}. \quad (18)$$

At a distance of about $3.5\,\lambda$ from the edge, the edge disturbance can be assumed to be negligible. From (18) we see that the zones of appreciable edge disturbance are smaller the thinner the shell and the larger the principal curvatures (i.e. the smaller the principal radii of curvature).

If the load on the shell perpendicular to its surface is equal to p, and if we assume that the shell is clamped perfectly rigidly to the edge member, the edge-disturbance moment m and the edge-disturbance shear force q, both per unit length of shell, will vary with the distance x from the edge as illustrated in *fig. 7*. From the formulae given in the figures it can be seen that each edge-disturbance has the form of a single damped "wave", which can be regarded as the resultant of the two waveforms which satisfy equation (16). The damping is stronger the smaller the characteristic length λ. In the case considered, assuming perfect clamping at the edge, the negative clamping shell-moment is:

$$m_0 = \tfrac{1}{2} p \lambda^2, \quad (19)$$

and the support reaction per unit length (= the shell shear force at the clamping position) is:

$$q_0 = p\lambda. \quad (20)$$

If the shell is hinged to the edge, the support reaction becomes:

$$q_0 = \tfrac{1}{2} p \lambda, \quad (21)$$

[8]) In a hyperbolic paraboloid the principal directions of curvature at a given point coincide with the bisectors of the acute angle formed by the two rulings passing through that point, and its supplement.

and the maximum (positive) shell-moment, occurring at a distance of 0.785λ from the edge member, is:

$$m = 0.16\, p\lambda^2. \quad \ldots\ldots \quad (22)$$

If the edge member itself can undergo deformation, the influence of this deformation can also, if necessary, be taken into account.

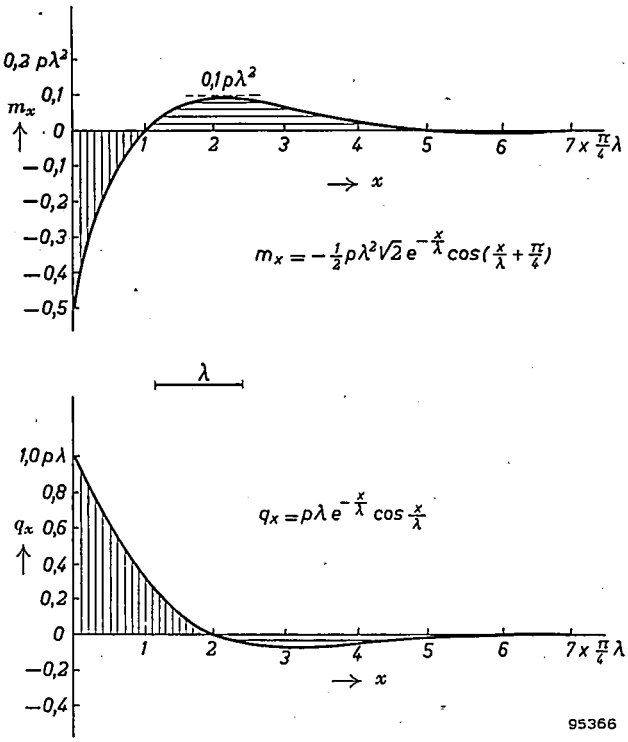

Fig. 7. Curves showing the edge disturbances m (bending moment per unit length of shell) and q (transverse force per unit length of shell) as a function of the distance x from the edge, when the shell is clamped in a perfectly rigid edge member. λ is the characteristic length. At a distance $x = 3.5\lambda = 4.5\ (\pi/4)\lambda$ from the edge, the edge-disturbance waveform is practically damped out.

With the aid of formulae (19) and (22) it is possible to determine the order of magnitude of the edge-disturbance moments for any arbitrary shell. If these moments become unduly large, the shell must be strengthened at the relevant position. In the case of reinforced concrete shells it is sufficient in many cases to add extra steel. Otherwise the shell will have to be made thicker.

With formulae (20) and (21) we can calculate what fraction of the total shell load is transmitted to the edge members by *bending*. Evidently the remaining part is borne by the shell in the form of membrane forces.

The formulae given here, and in particular formula (8), formed the basis for the theoretical determination of the distribution of forces to be expected in the Philips pavilion, and for the provisional dimensioning of the ribs and shell walls, also for the purposes of the model tests.

It may be noted here in passing that the usefulness of formula (19) was recently demonstrated experimentally in the Stevin laboratory at Delft, in the course of tests on a large reinforced concrete model of a hyperbolic-paraboloidal shell as in fig. 5.

Stability against buckling and second-order buckling

It is known that doubly-curved shells are much more stable against buckling than cylindrical ones. For estimating the buckling load p_k of a hyperbolic-paraboloidal shell, i.e. the load perpendicular to the shell surface under which the shell is about to buckle, we can apply Wansleben's theory [9]). We then find:

$$p_k = \frac{2E\delta^2}{\sqrt{3(1-\nu^2)}}\, k_1 k_2, \quad \ldots \quad (23)$$

where k_1 and k_2 respresent the absolute values of the principal curvatures at the point in question.

When $k_1 = k_2$, eq. (23) transforms into Zoelly's formula for a spherical shell. For a more rigorous calculation of the buckling load of a rectangular hyperbolic-paraboloidal shell the reader may be referred to a paper by Ralston [10]).

From formula (23) it can be seen that the buckling load increases, that is to say the danger of buckling decreases, proportionately as the curvatures increase. In the case of the Philips pavilion it was therefore primarily necessary to concentrate on the stability of those parts where the curvatures were very slight. As appears from formula (23), however, the danger of a shell buckling can be substantially reduced by increasing the thickness of the shell. In any case, in applying this formula, a large safety factor must be introduced to allow also for the possible presence of errors in the shape of the shell.

It is not an easy matter to determine theoretically the stability of shells, particularly when, apart from buckling phenomena, second-order buckling ("oil-canning") is to be taken into account. The latter phenomenon consists of the shell suddenly adopting a new position of equilibrium, involving displacements of finite magnitude. The conventiona- theory, which assumes only infinitely small deformal tions, is no longer applicable, and must be replaced by a second-order theory. As regards the danger of second-order buckling, which is more serious than the danger of buckling, it seems to us that the

[9]) K. Girkmann, Flächentragwerke, Springer Vienna, 4th ed., 1956, pp. 516-529.

[10]) A. Ralston, On the problem of buckling of a hyperbolic paraboloidal shell loaded by its own weight, J. Math. Phys. 35, 53-59, 1956.

hyperbolic-paraboloidal shell will be less vulnerable, owing to the saddle form, than the spherical shell. Although this has not yet been proved theoretically, our conjecture is nevertheless confirmed to some extent by the very high stability of hypar shells, as observed in the model tests on the Philips pavilion which are described in the third article in this series.

III. MODEL TESTS FOR PROVING THE CONSTRUCTION OF THE PAVILION

by A. L. BOUMA *) and F. K. LIGTENBERG **).

624.023.744:061.41(493.2):725.91

When the contracting firm "Strabed" approached Professor Vreedenburgh at the end of January 1957 for advice on the building of Philips pavilion, the first question was whether the design of Le Corbusier and Xenakis was indeed realizable as a shell structure of reinforced concrete. The plan of the contractors "Strabed" was to use concrete, 5 cm thick, for making the walls, which were designed as hyperbolic paraboloids, these shell walls to be reinforced in their lines of intersection by cylindrical ribs 40 cm thick.

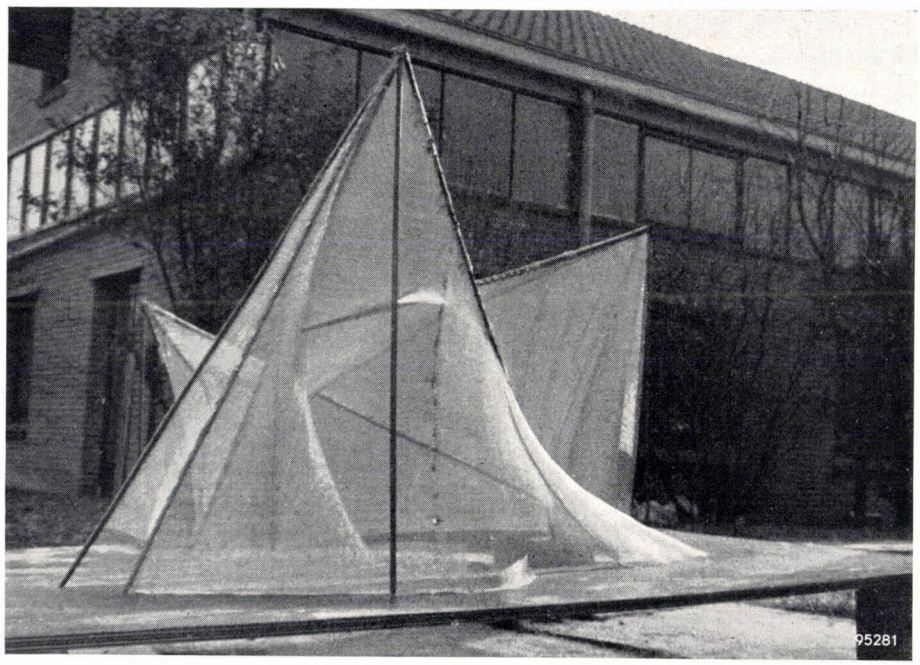

Fig. 1. Framework of tubes and wire-gauze for making the plaster model of Philips pavilion, scale 1 : 25 (T.N.O. Institute, Rijswijk, Netherlands).

In the previous article of this series it was explained that the stresses in hyperbolic-paraboloidal ("hypar") shells can readily be calculated if a membrane state of stress can be assumed. This will only be the case, however, if certain boundary conditions are satisfied. In a structure of such intricate shape as the pavilion under discussion, these boundary conditions are *not* fulfilled in many of the shells, giving rise to much more complex states of stress which are scarcely amenable to exact mathematical analysis. To answer the above question, the obvious procedure was therefore to perform tests on scale models, and to introduce calculations merely for supplementing the experimental results.

For this purpose the Netherlands Institute T.N.O. for Building Materials and Building Constructions prepared a model, scale 1 : 25, consisting of plaster of Paris on a wire-gauze framework (*fig. 1*). Owing to the term fixed for the decision by Messrs Strabed, little more than a week was available for carrying out this investigation, and the results could not

*) Institute T.N.O. for Building Materials and Building Constructions, Rijswijk, Netherlands.
**) Formerly of the Stevin Laboratory, Department of Civil Engineering, Delft Technische Hogeschool.

therefore be considered as any more than a guide. The tests led to the conclusion that, with some minor modifications, the design was feasible.

After Philips had awarded the contract for building the pavilion to Strabed, the investigation was continued more extensively. The object was to get some idea of the stresses occurring in the ribs and walls, in order to determine exactly certain dimensions and the amount of prestressing needed, particularly since the architect had meanwhile altered his design in some respects (see I). The most important of these alterations were also introduced in the model. Furthermore, an attempt was made, by applying overloads, to assess the stability of the structure. In this investigation the structure was regarded as being seamless (monolithic).

In fact the contractors Strabed did not intend to build the pavilion as a monolithic structure. They planned to form the shell surfaces from precast slabs which, after all the surfaces had been built up, were to be prestressed by means of high-tensile steel wires disposed on the inside surfaces of the building. Naturally this method of construction introduced additional problems, and it was therefore desirable to investigate these problems, and in particular the effect of the prestressing, on a new model. To this end a 1:10 scale model was built in the Stevin Laboratory of the Department of Civil Engineering at the Delft Technische Hogeschool. The model, consisting of two adjoining shell surfaces, omitted all details of the design but otherwise simulated as realistically as possible the proposed method of construction (*fig. 2*).

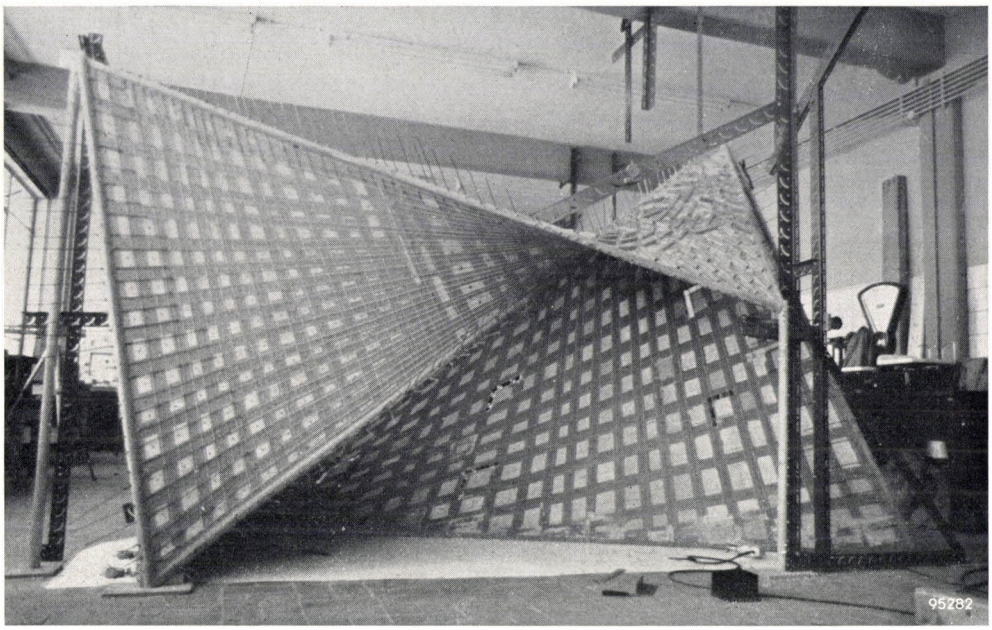

Fig. 2. The 1 : 10 scale model for investigating the system of construction planned by Messrs Strabed (Stevin laboratory, Technische Hogeschool, Delft).

Model tests, general remarks [1])

If model tests are to faithfully simulate the behaviour of a structure subjected to an increasing load up to the moment of collapse, the model must be a perfect scaled-down facsimile of the original and be made of the same material. Phenomena such as crack formation, yielding and rupture will then occur at places analogous to where they would occur in reality and under stresses identical with those associated with the corresponding phenomena in the actual structure.

Since a stress has the dimensions of load per unit area (kg/cm^2), the loads per unit area of the model must be the same as those for the actual structure. If the scale of the model is $1 : n$, the following rules are applicable:

Stresses (kg/cm^2)	1/1
Forces per unit length (kg/cm)	$1/n$
Forces (kg)	$1/n^2$
Moments per unit length (kg)	$1/n^2$
Strains (specific deformations, $\varepsilon = \Delta l/l = \sigma/E$)	1/1

It is by no means always possible, however, to make a model of the same material as the actual

[1]) See J. B. Wilbur and C. H. Norris, Structural model analysis, Chapter 15 in Handbook of experimental stress analysis, edited by M. Hetényi, Wiley, New York 1950.

structure. In the case of the Philips pavilion, for example, it was not practicable to make the 2 mm thick model walls of concrete. One must look then around for another material which is suitable. That presents no particular difficulties if one wishes to investigate the behaviour of the structure merely in the elastic region: one can measure strains (specific deformations) and determine from these the stresses occurring. In that case it is sufficient if the material of the model is elastic within an adequately large range of deformations and satisfies Hooke's law. The material will not, generally speaking, possess the same modulus of elasticity as that of the actual structure. The stresses being equal, the specific deformation in the model is inversely proportional to the modulus of elasticity.

If only the *stress distribution* is of interest, it is no longer necessary to adhere to the rule that the stresses in the model should be equal to those in reality. Stresses can be chosen that are readily measurable on the model material, and the latter (which may, for example, be steel) may then in fact be better suited to experimental investigation than the actual material (e.g. concrete). If the load per unit area of the model is larger, for example, than it will be in reality, the local stresses measured in the model are everywhere also proportionately larger than those that will occur in practice.

The *buckling load* is proportional to the modulus of elasticity of the material. This means that the buckling load of the actual structure is equal to the ratio of the respective moduli of elasticity times the load at which the model begins to show signs of buckling.

In some cases it is also possible to depart from the actual structure by adopting different *relative dimensions* for certain parts of the model, thereby simplifying the building of the model. One must then know, however, which parameters are important for the behaviour of the structure (such as for instance the area of the cross-section or the second moment of area), and for these the true values must be maintained.

A further complication arises if either the material of the actual structure or the model material is not *homogeneous*. This was the case with the plaster model, and we shall go into this in more detail.

Tests on the plaster model

As already mentioned, the first model was made of plaster of Paris on a framework of wire-gauze, the scale being 1 : 25 (fig. 1). The average thickness of the walls was 2.1 mm. The ribs (edge members) were steel tubes with a diameter averaging 8.4 mm and a thickness of 0.7 mm. The tubes were slightly thickened by plaster.

The tensile strength of plaster of Paris is rather higher than that of concrete, and as a material it obeys Hooke's law fairly well. The finished model, a structure of plaster and steel, could therefore be regarded as behaving elastically and in accordance with Hooke's law, so that the *strains* measured on this model could be interpreted with fair accuracy as *stresses*.

For applying the loads a large loading frame was built, by means of which the forces exerted by weights were conveyed via lever systems to the surfaces of the model (*fig. 3*). Measurements were made with the model subjected to:

a) loading by its own weight;
b) a vertical load on a single, fairly horizontal surface, to investigate the effect of a snow load;
c) wind pressure on the surfaces separately, enabling the effect of wind pressure on the windward side and wind suction on the lee-side to be ascertained for two wind directions.

The most unfavourable combined loads of deadweight with snow or wind produced the extreme stresses, moments and forces in the structure.

For measuring horizontal and vertical displacements, altogether 40 displacement dial-gauges, accurate to within 0.01 mm, were placed at various positions on the ribs. The strains were measured with strain gauges, a total of 40 being used for the first tentative tests, and 130 for the subsequent detailed investigation (*fig. 4*). In the latter investigation four strain gauges per measuring point were fixed to the surfaces, two on the outside, often at right-angles to each other, and two parallel to these on the inside. In this way it was possible to determine the force and the moment to which the cross-section concerned was subjected. Two, and where possible three, strain gauges per measuring point were fixed to the ribs.

Since the material of the model was not homogeneous (wire-gauze and plaster), it was not possible to deduce directly the stresses in the actual construction by multiplying the measured strains by the modulus of elasticity of the model material. The following procedure was therefore adopted for interpreting the strain measurements.

Suppose that at a certain point of the model wall the strains ε_1 and ε_2 were measured on the inside and outside surfaces. In the case of a *homogeneous* material, with modulus of elasticity E, the corresponding stresses are then:

$$\sigma_1 = E\varepsilon_1 \quad \text{and} \quad \sigma_2 = E\varepsilon_2$$

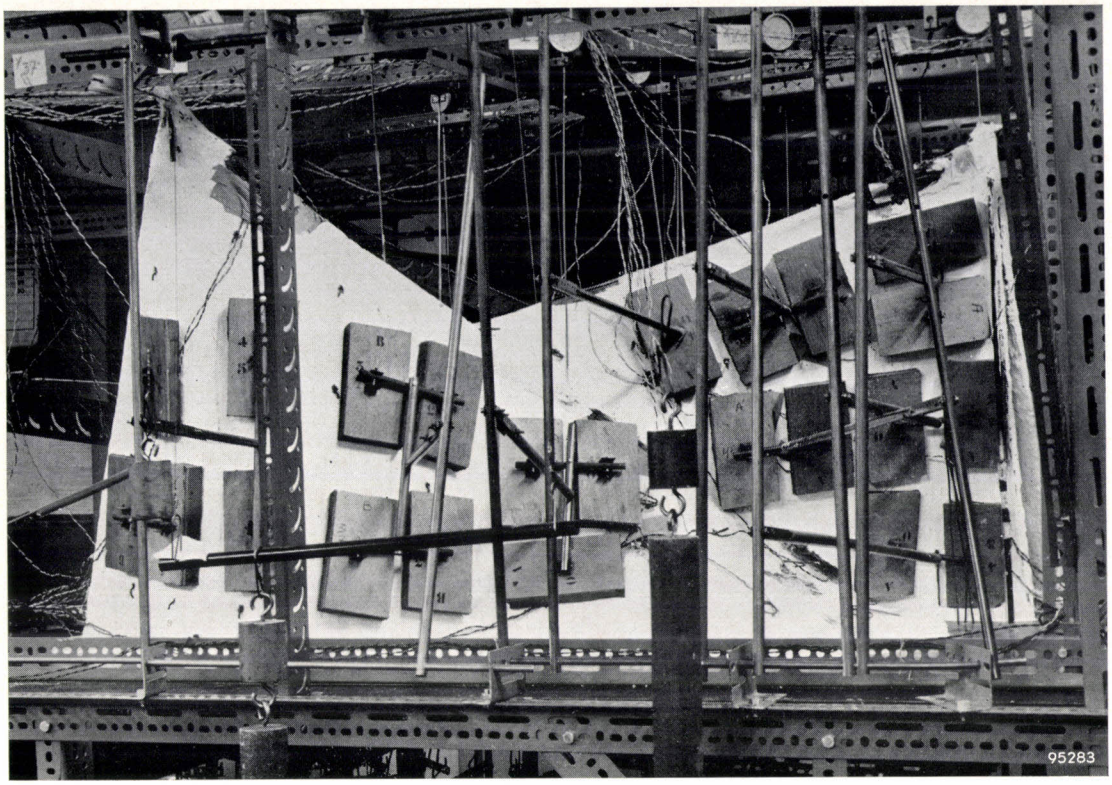

Fig. 3. Plaster model with the lever system for simulating wind loads.

Fig. 4. Equipment used for measurements on the plaster model. A series of displacement dial-gauges are mounted on angle struts and connected via long rods to the model (shown more clearly in fig. 3 above). A large number of strain gauges are fixed to the shell surfaces and the ribs for determining the stresses (whence the elaborate wiring). Some of the indicating instruments are visible in the foreground.

(the influence of the transverse contraction being here neglected). The cross-section, of thickness t, must now transmit per unit length a normal force

$$N = \frac{\sigma_1 + \sigma_2}{2} t,$$

and, introducing I, the second moment of area, a bending moment

$$M = (\sigma_1 - \sigma_2)\, I/t.$$

Introducing the *tensile stiffness* $D = Et$ and the *bending (flexural) stiffness* $K = EI$ of the cross-section, we may write:

$$\left.\begin{aligned} N &= D\,\frac{\varepsilon_1 + \varepsilon_2}{2}, \\ M &= K\,\frac{\varepsilon_1 - \varepsilon_2}{t}. \end{aligned}\right\} \quad \ldots\ldots \quad (1)$$

These relations now apply equally well to a *non-homogeneous* material. Since all the data were not available for calculating the tensile stiffness D and the bending stiffness K of the non-homogeneous material used, these quantities were determined for the model by combining a calculation with a number of simple measurements. For this purpose several test plates of the same construction as the walls of the model were subjected to a purely tensile load and to a bending load. The values found were $D = 40\,000$ kg/cm and $K = 70$ kg cm, the wall thickness being $t = 2.1$ mm. From the strains measured on the model, the forces and the moments per unit length, N and M, were calculated with the aid of formulae (1), and by applying the model rules it was then possible to find N and M in the actual structure (N being n times, and M being n^2 times larger than in the model).

An entirely analogous procedure was adopted for the ribs. From the measured strains the strain ε_z was determined in the centre of gravity of a cross-section. The normal force in the cross-section is then:

$$P = B\varepsilon_z,$$

where B is the tensile stiffness. This was again found experimentally on a number of test rods. According to the model rules the normal force P in the actual structure is n^2 times larger.

Once the tensile stiffness, for example, has been determined for the wall material, one can find with the aid of the formula $D = E't$ an "equivalent modulus of elasticity" E' for an imaginary, equally thick but homogeneous wall with the same D. The value found was $E' = 2\times10^5$ kg/cm^2, and analogously, by representing the bending stiffness by $K = E''I$, E'' was found to be 10^5 kg/cm^2. These moduli of elasticity are thus lower than those for the actual structure of concrete, for which E can be put as 3×10^5 kg/cm^2. The same can also be done for the ribs. With the aid of these equivalent moduli of elasticity the measured strains can also be directly interpreted as stresses in the case of the ribs.

The test programme was carried out completely both on the original design and on the modified design. The original envisaged a number of stanchions for supporting the three peaks. The forces in these stanchions were found to be generally slight. In the modified design it was assumed that the function of these stanchions could safely be taken over by the neighbouring oblique ribs. It was in fact found that the omission of the stanchions had very little influence on the stresses in the model, and therefore this modification of the design was accepted.

The stresses in the walls were found on the whole to be by no means negligible, sometimes exceeding 20 kg/cm^2 and in one instance reaching a maximum of 40 kg/cm^2. This applied particularly to the large vertical surfaces. Johansen's yield line theory offers a reliable method of determining the ultimate load of transversely-loaded flat plates [2]). This theory was accordingly applied to several very flat wall sections to gain some idea of their collapse load.

The extreme values of the forces in the ribs (both tensile and compressive) were found to be about 30 tons, while the extreme values of the stresses — partly caused by bending — amounted to -60 kg/cm^2 and $+80$ kg/cm^2.

After the question as to the feasibility of the structure had been answered by the preliminary measurements, Strabed was able to determine broadly the required amount of prestressing on the basis of the stresses found in the surfaces and ribs.

The interpretation of the measured strains naturally involved various uncertainties. Owing to variations in the thickness of walls and ribs it was impossible to be certain that the actual stress, or force or moment, had been found for all cases. Moreover, as far as the walls were concerned, it was not known exactly where and in what direction the maximum force or the maximum moment occurred,

[2]) R. Hognestad, Yield line theory for the ultimate flexural strength of reinforced concrete slabs, J. Amer. Concrete Inst., March 1953.
P. Lebelle, Calculs "à rupture" des hourdis et plaques en béton armé, Ann. Inst. Tech. Bâtiments et Trav. publ., No. 85, Jan. 1955.

and as regards the ribs it was not known at what points the extreme values of the stresses appeared. The measurements were therefore made at more or less arbitrary points, and it was impossible to check whether the greatest stresses had in fact been observed. The distribution of forces will also have been influenced somewhat by the fact that the ratios of the tensile stiffness and bending stiffness in the walls and ribs of the model were not entirely in accordance with those in reality. Nevertheless the results gave reason to assume that the measurements carried out at the points chosen provided a reasonable idea of the distribution of forces arising under dead-weight, and with wind and snow loads.

The Belgian building authorities had laid down that the building must be able to withstand loading by its own weight plus a double wind load (150 kg/m^2) with complete safety. The model was accordingly subjected to this load, and finally to a load of 1.5 times its own weight and a slightly higher wind load. Even under these conditions no particular effects were noted. In view of the fact that the buckling load is proportional to the modulus of elasticity, this meant that a monolithic structure of a homogeneous material obeying Hooke's law and possessing a modulus of elasticity equal to that of concrete (at least 300 000 kg/cm^2) would be able to withstand a load almost 3 times higher than the above loads. It must be said at once, however, that concrete is not homogeneous and elastic, nor does it obey Hooke's law. Phenomena such as crack formation, plastic yield and creep in concrete can appreciably reduce the safe strength of the building.

The interpretation of the above results on the plaster model in relation to a concrete structure thus left some matters open to doubt. The formation of cracks, however, can be prevented by prestressing. Moreover the system of construction plays an important part, as will be shown in the following.

Investigation of the system of construction on a plywood model

The investigation described in the foregoing was based on the assumption that the Philips pavilion was a monolithic shell structure, the stiffness of the surfaces being approximately identical in all parts. It was the intention of Strabed, however, to build up the shell surfaces from precast slabs, which were first to be erected at the site on scaffolding and then pressed together by prestressing wires. Additional problems were created by these plans, the more so because it was intended to arrange the prestressing wires on the inside of the building only.

The theory was that the prestressing force, although apparently eccentrically applied by the wires inside the building, would nevertheless be effectively exerted centrally in the shell surfaces. The prestressing wires exert on a rib the forces V_1 and V_2, which can be combined to form a resultant R (*fig. 5a*). This resultant R can be resolved

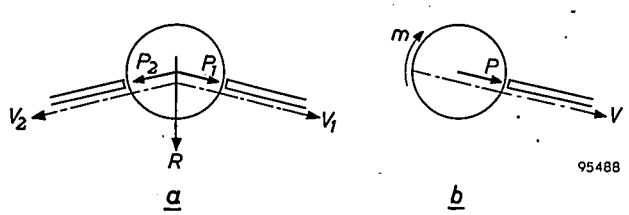

Fig. 5. Forces in a rib, viewed in cross-section.
a) Rib with two abutting shells. By means of prestressing wires, fixed to the inside surface of each shell, forces V_1 and V_2 are exerted on the rib. The resultant R of these forces can be resolved into almost centrally exerted compressive forces P_1 and P_2, by which the shells are prestressed.
b) Rib with only one abutting shell. Here, too, a compressive force P can be made to act centrally on the shell by introducing, besides the force V of the prestressing wires, a torsional prestressing of moment m, in the rib.

into forces P_1 and P_2 which the rib exerts on the shell surfaces abutting on it. As appears from fig. 5*a*, R can be so resolved as to cause the compressive forces P_1 and P_2 to appear practically centrally in the wall surfaces. By allowing a certain freedom in the magnitude of the prestressing forces it is also possible to adjust the orientation of P_1 and P_2.

If only one shell surface abuts on a rib, *torsional prestressing* can be introduced into the rib (see article IV) to produce a moment m of opposite sign, so that the prestressing force V in this case too is effectively exerted as a central compressive force P in the shell surface (see fig. 5*b*). Such a torsional prestressing may, of course, also be usefully applied when two shell surfaces abut on the rib.

Where the shell surfaces meet the ground, a special substructure, which is later rigidly fixed to the foundation beam, can be arranged to supply a moment, whereby here too the prestressing force V is exerted as a central compressive force P in the shell surface.

A structure when prestressed will undergo deformations. If these deformations are opposed by, say, a relatively stiff or fixed section, it becomes a particularly complicated matter to ascertain the effect of the prestressing. A large proportion of the prestressing forces will be lost in this stiff or fixed section and will not be exerted where they are required. For this reason it was thought necessary

to arrange that the substructure could move freely during the prestressing of the shell surfaces.

It was decided to investigate the effect of the movable substructure during the prestressing of the shell on a separate model. The model could also be used to ascertain whether the prestressing in the shell surface did in fact act centrally as postulated above, and whether the pattern of stresses set up in the walls corresponded to that of the stresses in the prestressing wires on the surface of the wall. If the latter was not everywhere the case, there would be a risk of buckling in those parts where the internal (compressive) force per unit length in the cross-section was appreciably larger than the external (tensile) force.

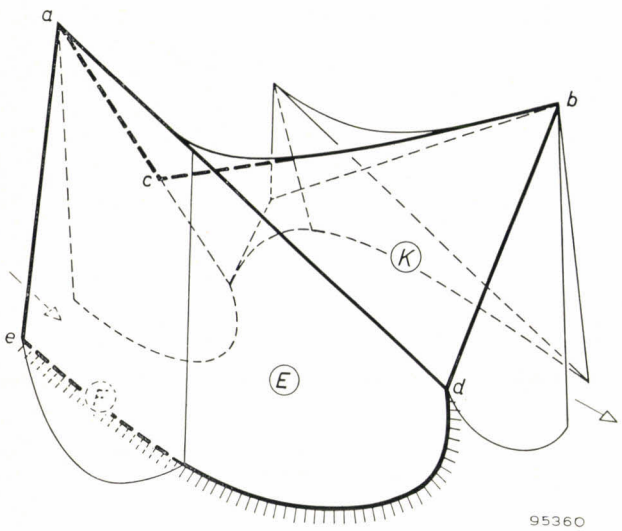

Fig. 6. Sketch of the Philips pavilion, indicating the surfaces E and K from which the plywood model was built (cf. fig. 18 in I). E is bounded by the straight lines ae and ad and the hyperbola ed; K is bounded by the twisted "quadrangle" $acbd$. The model was supported by vertical stanchions under points a, b and c.

From the plaster model a reasonable idea had already been gained as to the behaviour of the structure as a whole. Since the above-mentioned problems concerned details connected with the system of construction, it was sufficient to build a model of only a *part* of the Philips pavilion. The areas selected were those marked E and K in *fig. 6* (see also fig. 18 in I). All details, such as the windows permitting a view into the equipment room, the interior floors and canopies, and in particular the exterior shell surface F meeting E almost in the middle, were omitted. It was expected that all the shell surfaces in the actual Philips pavilion would be subject to more favourable conditions than the two surfaces investigated, which contained *inter alia* a very high, almost entirely flat section; hence

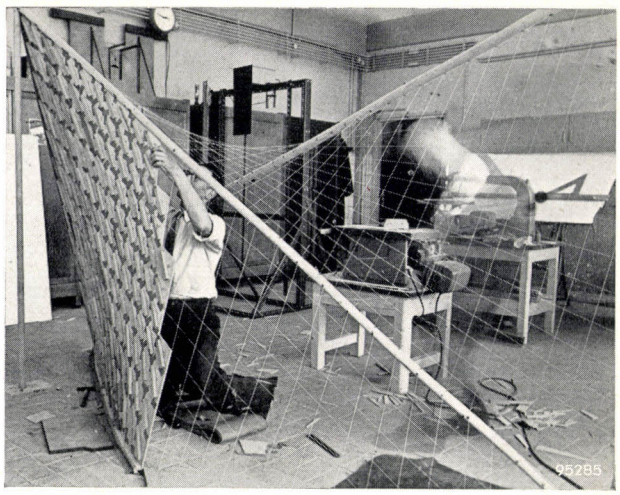

Fig. 7. The plywood model in course of construction. In a manner similar to that to be used in the actual erection, the slabs are fitted together on wire "scaffolding", the wires being spanned between the previously erected ribs in accordance with rulings of the hyperbolic-paraboloidal shells.

any difficulties attaching to the system of construction should come to light readily in the investigation of these two surfaces.

To simulate closely the system of construction the model was built on a large scale (1 : 10). The shell sections were made of plywood slabs (3-ply), each of which was bent, by means of a rigid attachment, to the appropriate saddle shape and finished to ensure an accurate fit (*figs. 7, 8* and *9*). Each slab had an area of approximately 100 cm², so that many hundreds of slabs, and a great deal of work, were needed to build a model 2 m high and 3 m long. A realistic prestressing system was created fairly simply by using prestretched nylon thread for the prestressing wires.

Since the modulus of elasticity of the plywood used was 165 000 kg/cm², i.e. about half that of concrete, the prestressing and the loads were kept

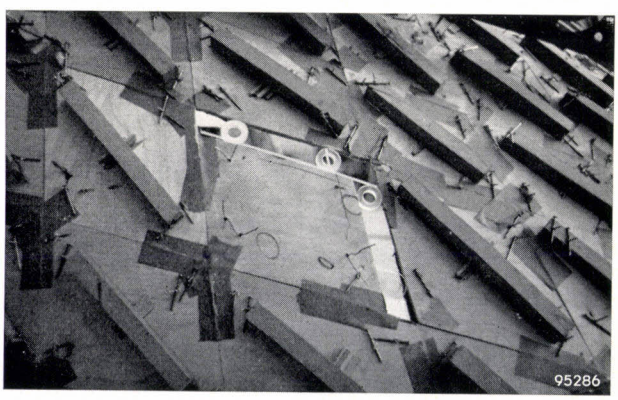

Fig. 8. Detail of a wall of the plywood model, illustrating the bending of each plywood slab to fit a certain part of a saddle surface. In the centre of the photograph is a photo-elastic measuring element.

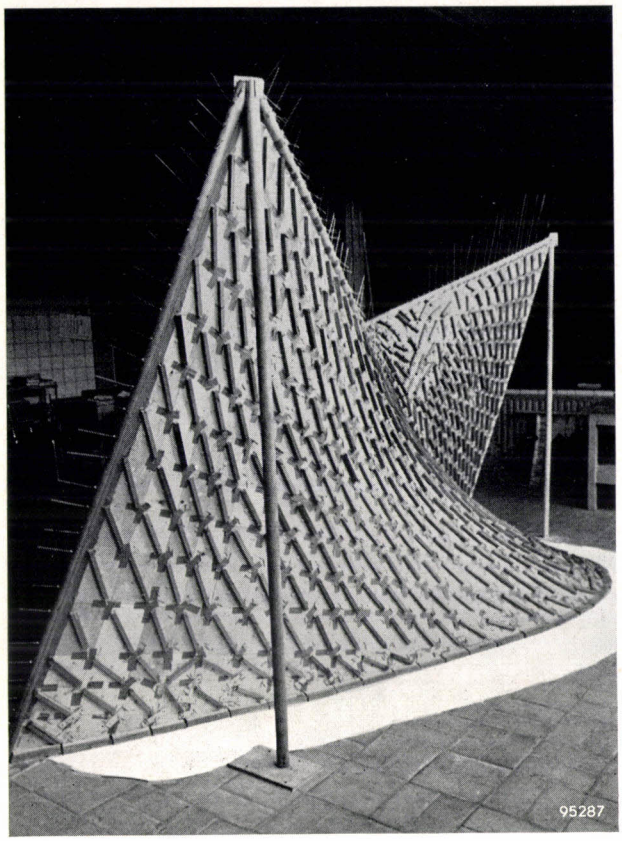

Fig. 9. The complete plywood model.

to half their actual values. Under these conditions, according to the model rules discussed at the beginning of this article, the occurrence of buckling phenomena and rupture (in the joints) in the model should correspond to the manner of their occurrence in the actual structure. The deformations were reproduced on a scale of about 1 : 10.

It was evident that, even without many measurements, a model of this kind would provide considerable insight into the behaviour of the structure during the process of prestressing. Consequently, fewer measurements were carried out than on the plaster model, the emphasis being laid on visual observation of how the model behaved under diverse circumstances.

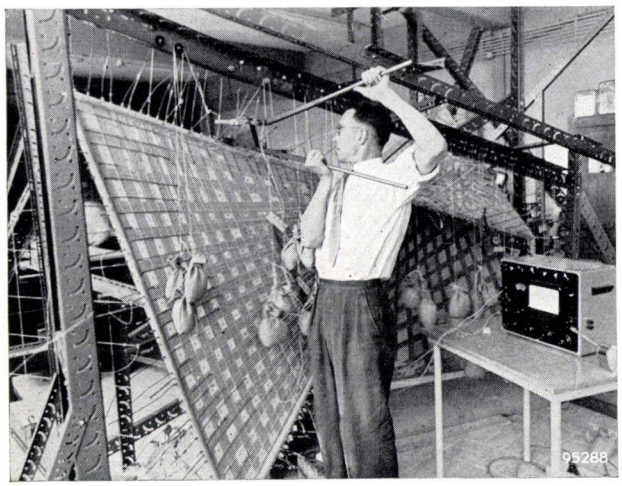

Fig. 10. Prestressing the plywood model.

The plywood slabs from which the model was built up were temporarily held together by strips of adhesive tape (fig. 8). This structure was then uniformly prestressed (*fig. 10*). At first it was found that those ribs of the model which were free on one side were eccentrically twisted by the prestressing, and buckling occurred in a part of the steep upright surface. To prevent this happening it was necessary, as described above with reference to fig. 5*b*, to exert torsional moments on these ribs equal in magnitude to those which would result from the prestressing of the abutting surface (not present in the model). These torsional moments were produced by fixing a large number of spokes at right angles to the ribs, (see also fig. 9) and by arranging for forces to act on the ends of these spokes in directions perpendicular to both the ribs and the spokes. The forces were exerted by wires passing over pulleys and to which weights were suspended (*fig. 11*). This improvement having been introduced, the prestressing was able to be applied without difficulties.

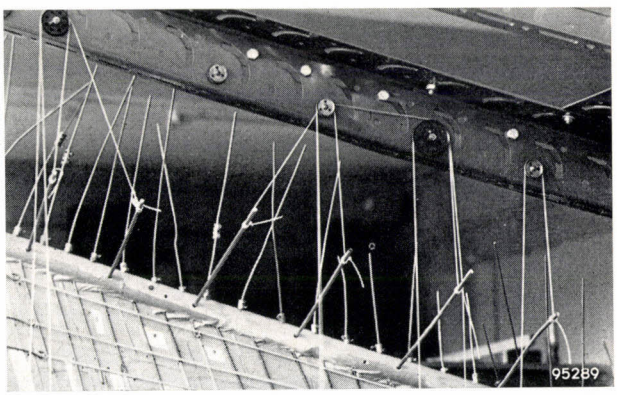

Fig. 11. In the free ribs (to which no second hyperbolic-paraboloidal surface abuts in the model), spokes are fitted by means of which moments can be applied to the ribs (see fig. 5*b*) to oppose the torsional moment exerted by the prestressing wires. This is done by exerting transverse forces on the spokes by wires passing over pulleys and from which sandbags are suspended (see also fig. 10).

The result of this test was entirely satisfactory. The effect of the prestressing was indeed found to be as expected, and the movable substructure also came up to expectations.

Although the model dit not exactly simulate the actual structure as far as the action of forces due to loading are concerned, it was nevertheless thought worth while to investigate the effect of subjecting the model to a load corresponding to its own weight plus wind. Loading due to dead-weight was hitherto

absent, because the weight of the plywood slabs amounted to only about 1/25 of the dead-weight per unit area of the actual structure, whereas it was necessary, owing to the lower modulus of elasticity of the model, to apply *half* the actual dead-weight per unit area. This was done by slowly and uniformly applying increasing numbers of sandbags to the two wall surfaces (*fig. 12*).

though the appearance of such a phenomenon was to some extent a warning signal.

Following this phenomenon the load was removed from the model. Not until the load had been removed in the upper surface *K* did the model return to its original state, from which it was concluded that the reaction forces in the surface supporting this surface had been in part responsible for the

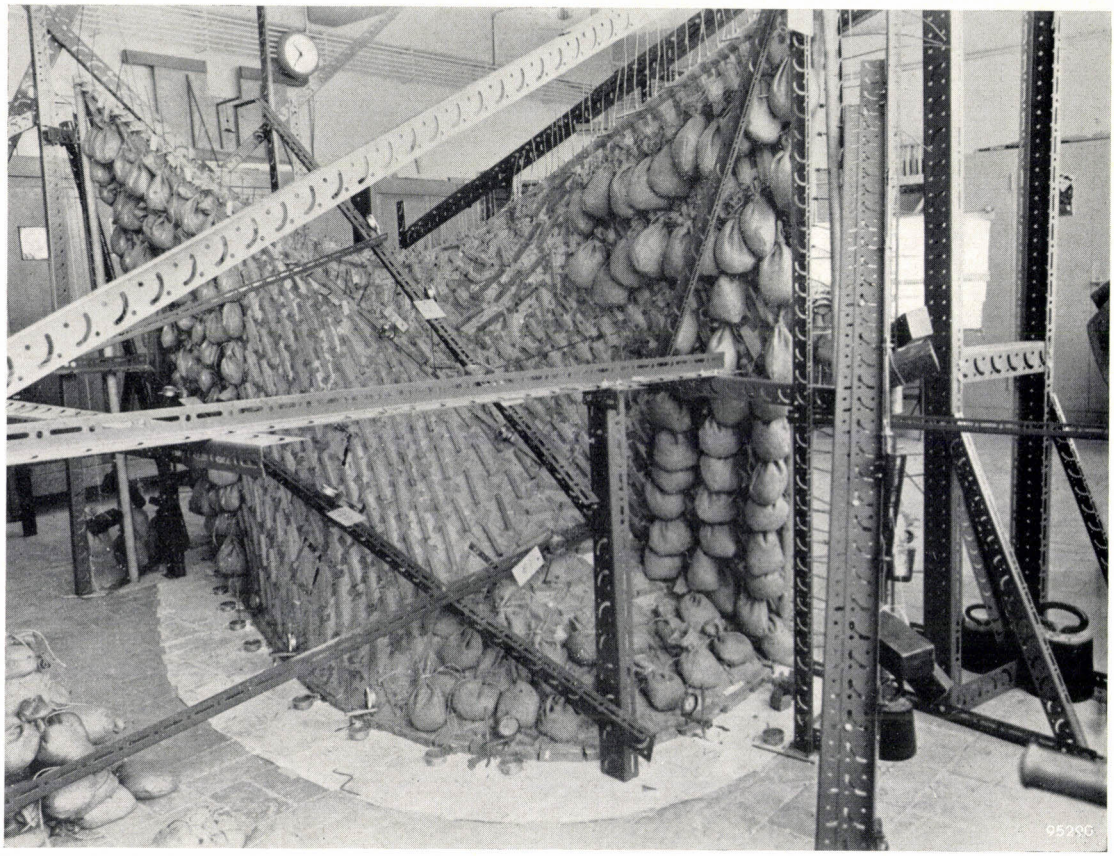

Fig. 12. The plywood model during the application of a load corresponding to the dead-weight of the structure.

When the load had almost reached its full value (corresponding to 0.9 of the dead-weight), the lower surface *E* suddenly began to buckle along an almost horizontal joint in the flat upright section of the wall close to the ground. This buckling was quite unexpected. Originally it was thought that the almost horizontal section of the same surface would be much more dangerous and for this reason the steep part of the wall had been built up much more simply in the model than it was to be in the actual pavilion. In particular, as stated above, the exterior wall surface *F* abutting at this position had been omitted (see fig. 6). It was not, therefore, necessarily correct to conclude from this buckling that the actual pavilion would not be able to carry its own weight, phenomenon. Owing to the absence of the abutting surfaces, the upper surface *K* will have acted more as a thick plate than as a shell, that is to say the state of stress comprised not solely forces and reactions lying in the surface itself (membrane state of stress) but also bending moments and reactions perpendicular to the plane.

The area that had buckled was subsequently stiffened with two ribs in order, among other things, to simulate the effect of the adjoining surface *F*; this produced a stiffness more in accordance with that of the actual structure. It was now found that, when loaded by its own weight and even by very heavy wind loads on both sides, the structure was well able to stand up to all the forces applied (*fig. 13*).

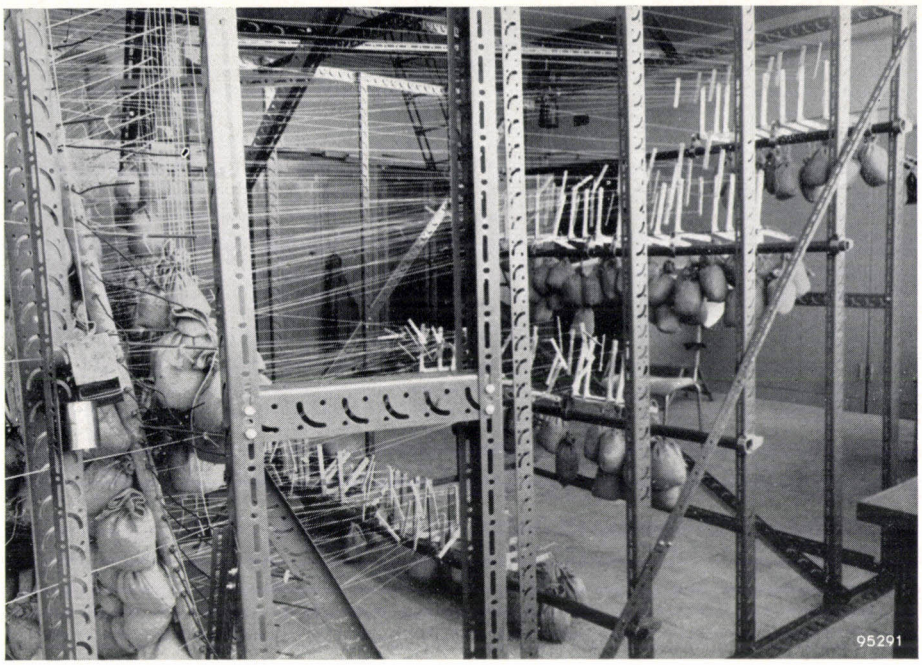

Fig. 13. Arrangement for applying a wind load (tensile load from sandbags hung over pulleys).

Finally, the model was overloaded by allowing several persons to climb on to it (up to about 1.5 × the dead-weight). Although this represented extremely heavy loading, the model was still capable of withstanding shocks and wind loads, so that it may be said to have passed this test very satisfactorily (*fig. 14*).

This result, then, promised well for the actual pavilion, although the original buckling when the model was loaded by its own weight suggested possible dangers. In this respect, however, the jointing of the slabs is of essential importance, and this was impossible to simulate entirely realistically in the model.

Fig. 14. The plywood model severely overloaded.

It seemed desirable to carry out additional tests in order to investigate more closely the buckling stability of a shell surface composed of slabs. This could not be done, however, owing to lack of time. After consultation with Le Corbusier, Philips decided that it would be preferable to apply prestressing wires also on the outside of the building. It seemed to us that this would sufficiently strengthen the coherence of the surfaces and the erection of the Philips pavilion could therefore be started with full confidence in the outcome.

IV. CONSTRUCTION OF THE PAVILION IN PRESTRESSED CONCRETE

by H. C. DUYSTER *). 624.023.744:061.41(493.2):725.91

When the Philips concern asked us to submit a proposal on how the pavilion designed by Le Corbusier and Xenakis might be built, our thoughts turned at once in the direction of self-supporting concrete shells, which would be no thicker than the minimum of 5 cm specified for reasons of soundproofing by the acoustic engineers. In the design submitted to us (see article I, figs. 15-19) the walls were composed of hyperbolic paraboloids, or of surfaces that could readily be transformed into hyperbolic paraboloids, and from experience gained in various projects as well as from theoretical considerations (in part quite new) [1]), we were aware of the outstanding qualities of strength and stability possessed by shells formed as hyperbolic paraboloids ("hypar" shells). Even without detailed analysis we were able to arrive at an idea of the forces and deformations that would occur in the structure as designed, so that we were in a position with the help of elementary calculations, to estimate the strength that would be required at the various points.

We shall not go into the subsequent developments — the more exact calculations by Professor Vreedenburgh, the modification of the first design by Xenakis, the structural tests carried out on scale models, etc. — all these having been sufficiently treated in the preceding articles in this issue (I, II and III). We shall confine ourselves here to questions concerned with the construction of the building in prestressed concrete [2]).

Why prestressing?

It will perhaps be useful first of all to recapitulate briefly the idea underlying the prestressing of concrete. Concrete can safely withstand very considerable compressive stresses — up to 150 kg/cm² in the case of good quality concrete (i.e. made of good materials and carefully manufactured). It is much less capable, however, of withstanding tensile stresses. In order to use concrete in structures where tensile stresses will occur, one of two courses can be adopted: 1) The concrete can be *reinforced*, the reinforcement consisting of steel rods around which the concrete is cast, leading to firm internal adhesion: these rods take up the tension (*fig. 1*). 2) The concrete can be *prestressed*, by means of steel wires which are fixed to both ends of a concrete constructional element; when the wires are tensioned a compressive stress is produced in the concrete, and with appropriate dimensioning the resultant stresses even when the element is loaded will everywhere be *compressive* stresses (*fig. 2*).

Having decided on concrete as the material eminently suitable for giving shape to the ideas embodied by Le Corbusier and Xenakis in their design, we were thus left with the choice between reinforced and prestressed concrete.

Now, for shells as thin as these, reinforced concrete is not an attractive proposition. To make good, homogeneous concrete in the form of such thin layers and for such large and often steep walls as in the present structure, is in itself extremely difficult. When reinforcement is present the difficulties become well-nigh prohibitive. There are thus objections to the *principle* of reinforced concrete. With prestressed concrete, on the other hand, there are no such inherent difficulties: the prestressing wires can be applied not inside the concrete but on its surface, if desired. In fact, the *shape* of the walls of the Philips pavilion lent itself exceptionally well to this treatment owing to the fact that hyperbolic paraboloids may be generated by straight lines, a property possessed in common with ruled surfaces in general; this made it possible to apply all or most of the prestressing wires such that they would run *straight*. This would make it easier to introduce the appropriate prestresses in the material.

*) "Strabed": Société de Travaux en Béton et Dragages, 11 rue Gineste, Brussels.

1) See article II, and the literature there referred to.

2) The most important details of the work have already been described: see H. C. Duyster, Cement **9**, 447-450, 1957 (No. 11-12).

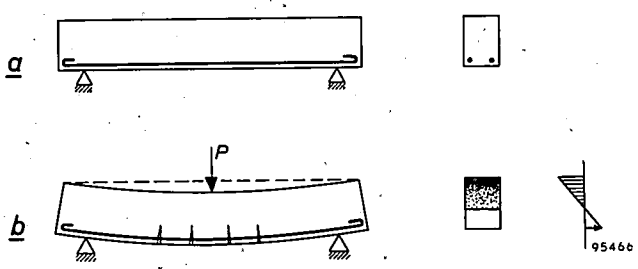

Fig. 1. Principle of reinforced concrete.
a) Beam with steel reinforcement, in unloaded state (deadweight disregarded).
b) Beam subjected to a load *P*. The stippling in the transverse section indicates the occurrence of an axial compressive stress in the concrete. Hair cracks appear in the concrete at the lower surface of the beam, and the steel reinforcement comes under tensile stress. On the extreme right is shown the vertical distribution of the axial stresses (compression towards the left, tension — in the reinforcement — towards the right).

Though the choice necessarily fell on prestressed concrete for the practical reason mentioned, it is important to note that prestressed concrete is, in fact, an intrinsically better solution of the problem than reinforced concrete. The reasons for this are as follows (see also article II).

In a hyperbolic-paraboloidal shell, a load uniformly distributed over its surface (parallel to the hypar axis) is transmitted to the edge members in such a way that, to a first approximation, normal forces alone arise in these members. The shell is then left with purely membrane stresses, which is the most favourable state from the standpoint of strength. The edge members carry the load as a normal force down to the points of support on the foundation.

In reality the picture is not quite as simple as this, differences being introduced mainly as a result of deformations in the structure. Although primarily the shell ought to be able to transmit the load solely by membrane stresses, deformation gives rise to secondary (bending) stresses, and the trajectories of the principal stresses are distorted. These effects are also discussed at greater length in article II. The flatter the shell the more the stress-distribution differs from that of a membrane state of stress. Usually a very localized but pronounced deviation is found near the edge members, for the deformations of the latter are of a different order of magnitude and vary along the edges otherwise than in the thin shell itself.

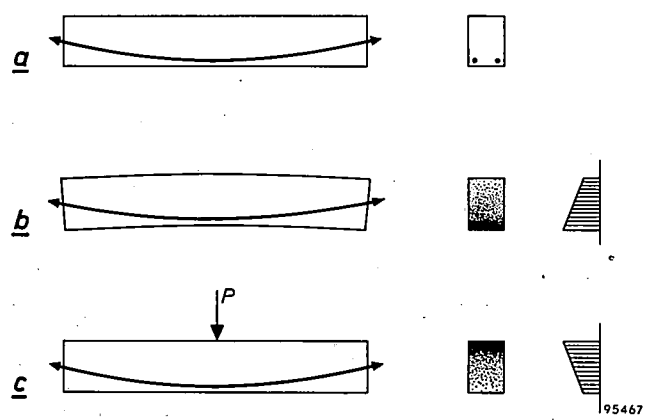

Fig. 2. Principle of prestressed concrete.
a) Beam with prestressing wires, in unloaded state. The wires run through parabolic channels through the concrete.
b) Beam after prestressing, still unloaded. The beam is deformed; compressive stresses appear in the concrete, distributed as shown by the stippling in the transverse section and the graph on the right.
c) Prestressed beam under a load *P*. The stress distribution changes but nowhere do tensile stresses occur in the concrete.

By appropriate prestressing of both the shell and the edge members it is possible to limit the disparities in deformation that are responsible for the occurrence of often relatively large secondary stresses. It will be more economical, then, to construct the shell in prestressed concrete than in reinforced concrete, for the prestressed shell can take up the load mainly with membrane stresses and hence approaches a true "shell" construction, whereas in a shell of reinforced concrete the secondary stresses produced by deformation will generally predominate: it may therefore require much greater wall thicknesses and possibly even additional strengthening with supports.

Two other advantages of prestressing must be mentioned:

a) Of practical, though not vital importance is the fact that, owing to the elimination of tensile stresses in the concrete, the hairline cracks often occurring in concrete structures are entirely avoided. As a result, less stringent demands can be made on the waterproofing of the shells. This is particularly convenient, since to provide the unusually-shaped shells with conventional roofing would be a highly difficult if not impracticable operation.

b) A most essential feature of prestressing, and perhaps the *sine qua non* for the building of the Philips pavilion, is that it enabled us to form the shell surfaces from *precast slabs*. We shall deal with this in more detail.

Construction of the hypar shells from precast concrete slabs

It would have been very difficult, even without reinforcement, to cast the thin and, in many cases, strongly twisted shells of the pavilion *in situ* by means of wooden shuttering. The most experienced workers in concrete would scarcely have been equal to the task, especially when such high demands are made on the quality of the concrete work. Even before "Strabed" was awarded the contract,

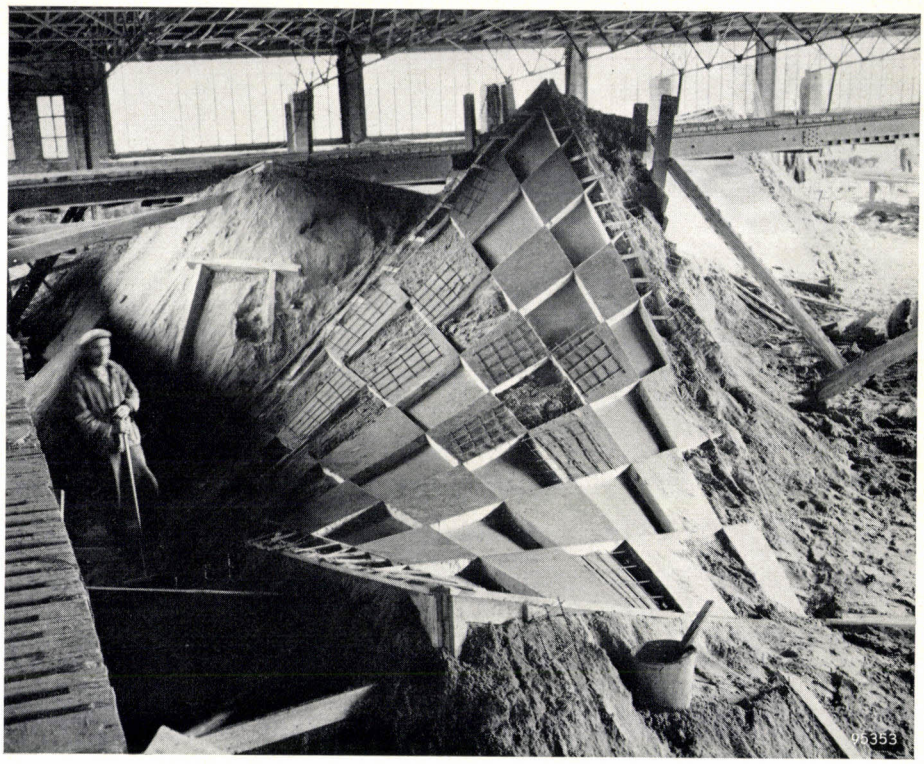

Fig. 3. Concrete slabs being cast on a sand-bed to form a part of a hyperbolic-paraboloidal shell. The mound of sand, containing a certain proportion of loam, is levelled off with a plank sliding over two edges, after the limiting rulings of the shell section have been defined by four planks. The sand is coated with a thin skin of cement. By positioning slats of wood 1 cm thick along the ruling lines the entire surface of the section is divided into lozenge-shaped moulds, of approximately 1 m², into which the concrete is cast to produce slabs 5 cm thick (a light reinforcement mesh is introduced to prevent breakage during transport to the site). The checker-board structure visible on the photograph is due to the system of first casting the "black" squares, the slats being prevented from giving by rods driven into the sand; subsequently, when this concrete is set, the rods are removed and the "white" squares are cast.

we had therefore devised the plan to form each hypar shell from sections which could be cast in open sand-bed moulds. This system of "prefabrication" also offered the advantage that it could be carried out under cover and hence independent of weather conditions; for this purpose a shed stood at our disposal some kilometres from the building site. The extent to which each shell had to be subdivided depended in the first place on the available height in the shed and on the permissible steepness of the slopes of the sand bed (shuttering would again have been necessary if the slopes were too steep). What was even more important was that the cast sections should be easy to handle and transport. With this in mind the size of the precast slabs was fixed at about 1 m². One sand bed was formed for each shell section consisting of a few dozen slabs.

At the site the slabs were fitted together in a manner which will be described, and the joints filled with mortar (the operation thus being a rather odd kind of brick-laying process).

This slab-wise construction of each shell was, of course, only possible owing to subsequent prestressing of the entire structure: the bond between adjacent slabs is even less able to withstand tension than the concrete itself, but thanks to appropriate prestressing no tensile stresses can ever occur anywhere in the walls. The effect of prestressing is to make the entire structure, including the ribs, behave as if it had been cast as one whole.

The prefabrication process brings out even more clearly than the considerations in the previous section how remarkably well the hyperbolic-paraboloidal shell is adapted to construction in prestressed concrete. The sand beds on which the lozenge-shaped concrete slabs were to be cast — each slab individually moulded as part of a particular hyperbolic paraboloid — were very easily made by delineating them, following the ruling lines, with straight planks of wood, and then levelling them off (*fig. 3*). Particular care was needed, however, in setting out the ruling lines along the edges and the curved lower boundary of a shell, as well as in carrying over the corresponding angles from one section of the shell to the next. This would naturally have been simpler if we had been able to make *all* slabs of each shell on one sand bed, but this was not possible for the reasons given (surface steepness, shed height). Following the directions of the ruling lines, slats of wood 1 cm thick were fitted on the sand bed and the slabs cast between them. With a view to transport from the shed to the site, the slabs were provided with a light reinforcement mesh.

We must return at this point to the remarks made at the beginning of this article concerning the choice between reinforced and prestressed concrete. The artifice of prefabricating the hyperbolic-paraboloidal shells in small elements without shuttering brings reinforced concrete into the picture again — as we have just seen — as a reinforcement mesh to facilitate transport. It might seem, then, that in spite of what was said earlier, the shell walls could be made of reinforced

Fig. 4. The 40 cm thick cylindrical ribs were cast *in situ* in "shuttering" erected on scaffolding.

concrete. The reinforcement of the slabs is of no help, however, for *forming* the large walls, for there is no possibility whatsoever of joining up the reinforcement of adjacent precast slabs in such a way that it would keep the concrete free from tensile stresses with the whole structure loaded.

The edge members fitted at the intersections of each pair of hyperbolic-paraboloidal shells are cylindrical concrete ribs 40 cm in diameter. They were cast *in situ* in shuttering on a framework of wooden struts and stays (*fig. 4*) while the more than 2000 slabs were being cast in the shed. It was rational to make the ribs cylindrical, because the shells "turn" about the ribs; with any other shape it would have been troublesome to join the shells to the ribs. Nor would there have been any sense in providing the ribs with any but a circular cross-section, for their purpose was after all to take substantially normal forces and therefore no particular flexural stiffness was required of them.

After the ribs had been cast, further wooden scaffolding was erected, of which the outer-surface beams followed the ruling lines of the hyperbolic-

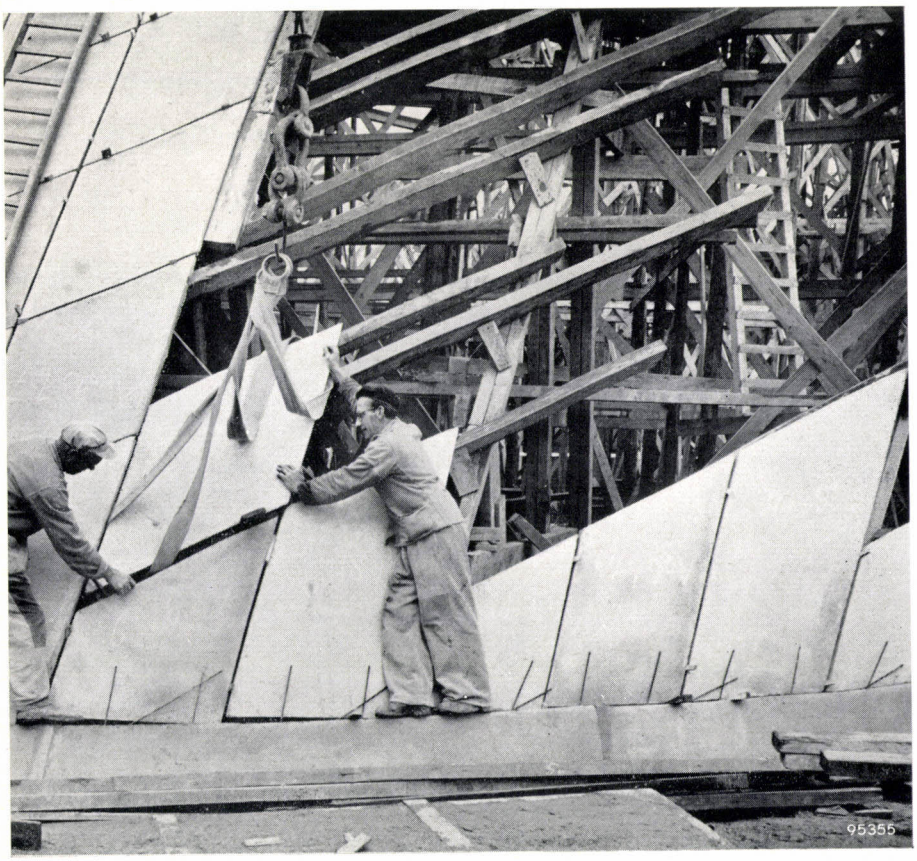

Fig. 5. The precast slabs, only 5 cm thick, were placed in position and mortared on scaffolding incorporating wooden beams along the ruling lines of the shells.

paraboloidal surfaces. The slabs were then placed in position on the scaffolding and provisionally held in place (*fig. 5*). The 1 cm wide joints between the slabs having been filled, the entire structure was prestressed, after which the scaffolding was removed and the finishing touches put to the shell surfaces.

Closer consideration of the prestressing of the shells and ribs

The requisite prestresses in the shells were derived from the results of the model tests performed in the T.N.O. Institute (see III, sub-section entitled "Tests on the plaster model"). The loads allowed for were the dead-weight of the structure together with the sound-proofing, a snow load, and a wind load of 75 kg/m² from various directions.

The necessary prestresses were to be introduced in the shells by systems of 7 mm steel wires laid over the surface and post-tensioned, each wire being capable of taking a maximum tensile force of about 3300 kg. Assuming that the forces so introduced in a shell would everywhere act centrally (i.e. in the median plane of the shell) and would follow the direction of the wires, it was possible to write down the formulae giving the principal stresses produced at each point by the applied forces, as well as the stresses produced along the joints between the slabs and perpendicular thereto. In this way we could ascertain the number and position of the prestressing wires needed.

The assumption just mentioned seems justified in the case of hyperbolic-paraboloidal shells, where the prestressing wires can follow straight lines, always provided, however, that two conditions are satisfied, viz. the wires must be disposed with reasonable uniformity over the shell surface, and the shell must be capable of freely undergoing deformation during the application of the prestresses. The latter condition called for special measures at

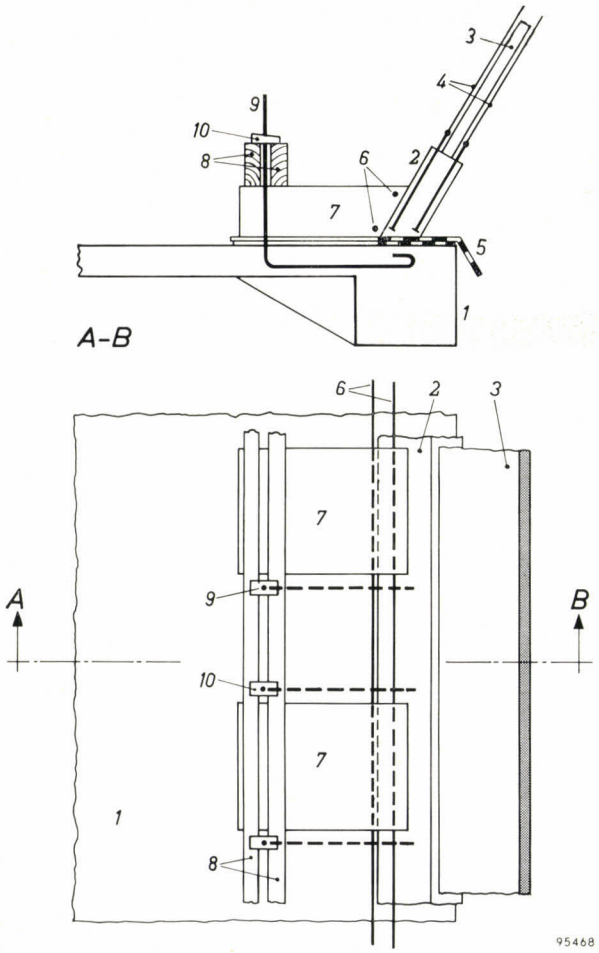

a

b

Fig. 6. *a*) In order for the prestressing to be completely effective, the bottom edge of a shell must be able to move a few cm (without canting, i.e. changing its inclination) over the foundation, during the prestressing process. For this purpose two layers of bituminous felt *5* are introduced between the foundation *1* and the substructure *2* against which the shell *3* is pulled tight by prestressing wires *4*. The substructure itself is prestressed by wires *6* running along the perimeter. Canting is prevented by tail blocks *7* cast on to the edge beam and anchored to the foundation. Anchorage is effected by means of temporary wooden beams *8*, which are fixed by clamps *10* to flexible rods *9* cast into the foundation between the tail blocks.

b) Substructure with tail blocks. In order to fix the whole structure to the foundation, the space between the tail blocks is filled with concrete after the shells have been erected and prestressed (hence after the deformation has taken place). The reinforcement for this concrete filling (not shown in fig. *a*) can be seen between the blocks.

It may be pointed out that the tail blocks were in all cases *inside* the building. In the part of the building shown here, the wall bends outwards. It may also be pointed out that as the substructure can slide only horizontally and any rotational movement is completely prevented, any eccentrically-acting prestress is made to act centrally in the shell: the bending moment will be taken up by the foundation, leaving none in the shell (see III, fig. 5*b*).

various points, particularly as regards the shells resting on the foundation; the substructure of these shells was initially separated from the foundation by two layers of bituminous felt (which also served later for waterproofing the building from the surrounding water channel); this permitted relative movement between substructure and foundation until after prestressing was completed, when the whole structure was joined to the foundation by the addition of concrete (*fig. 6*). Without this measure some of the prestressing forces would have been taken up by the foundations and the stresses introduced in the shell would certainly not have had the right direction. The tests carried out on the plywood model, described in III, showed that this construction functioned as required and, in general, that the above assumption was justified in our case: the fact that no buckling occurred at any part of the model (modified as described, p. 25) during prestressing provided the assurance that the transmitted forces substantially followed the direction of the wires.

In accordance with the original plan the wires in these prestressing tests were applied to only one side of the shell surfaces (corresponding to the inside of the building). Further tests were needed to ascertain whether the shell surfaces would have sufficient stability against buckling when subjected to external loads, but owing to lack of time it was decided with Le Corbusier's approval to apply prestressing wires to the outside surfaces as well (see *fig. 7*). This simplified the problem appreciably.

The wires mainly followed the ruling lines of the hyperbolic-paraboloidal surfaces, but in the case of some shells whose rulings intersected at very sharp angles it was necessary also to apply wires that followed the bisectors of the obtuse angle between the ruling lines. These wires formed the exception in that they followed a curved path.

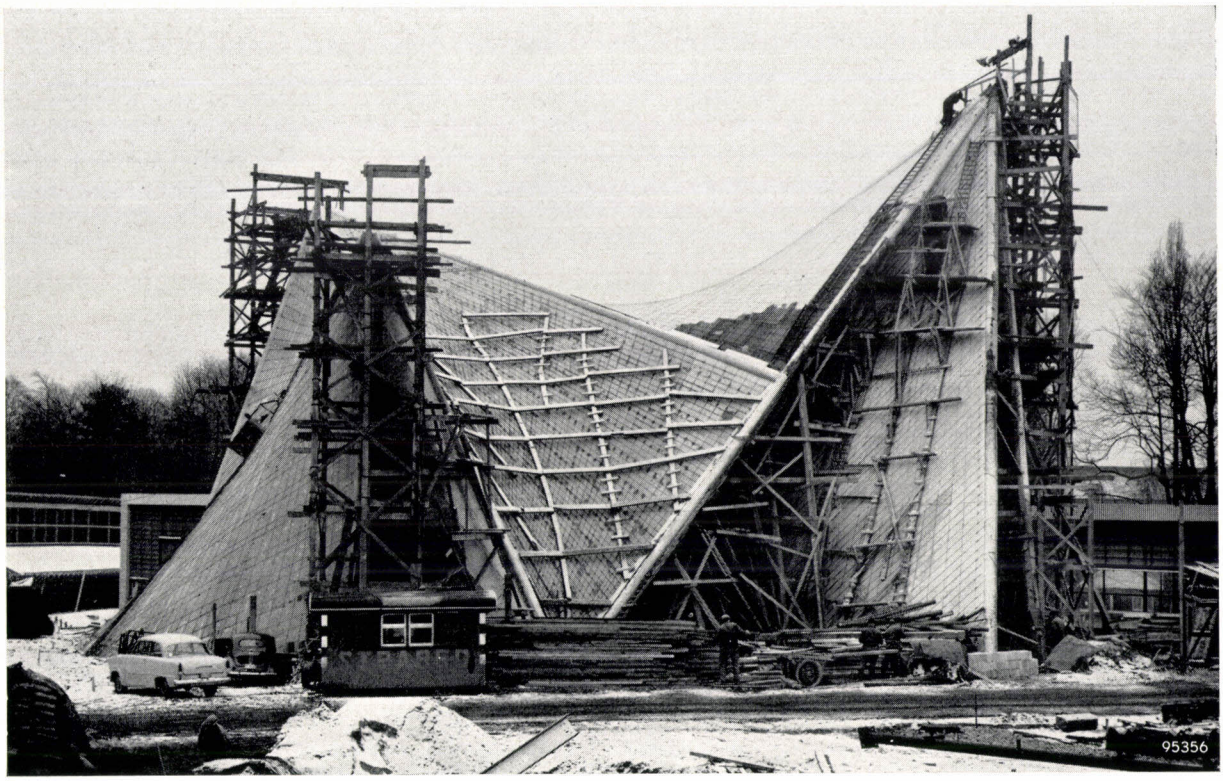

Fig. 7. The pavilion shortly before completion, showing the numerous prestressing wires of high-tensile steel which are applied to both surfaces of the shells. Each wire is 7 mm thick and is tensioned with a force of 3300 kg.

The ribs were also prestressed, in three distinct ways. Firstly, *compressive* prestresses had to be produced by straight wires so that the ribs could take up the tensile stresses measured in the model tests. Secondly, some ribs had to be given a *bending* prestress, by means of wires following a parabolic path in a plane through the axis (cf. fig. 2). This was necessary in particular in the case of two ribs at the entrance and exit, to each of which only one almost flat shell abuts. Thirdly, *torsional* prestresses were introduced in a number of ribs to counteract

the torsional moments imparted to them by the prestressed abutting shells. Although the concrete of the ribs was capable of taking up these torsional moments, it was desirable to eliminate them to ensure centralized prestresses in the shells (see III, fig. 5*b*). As far as we know, this is the first application of torsional prestressing in concrete.

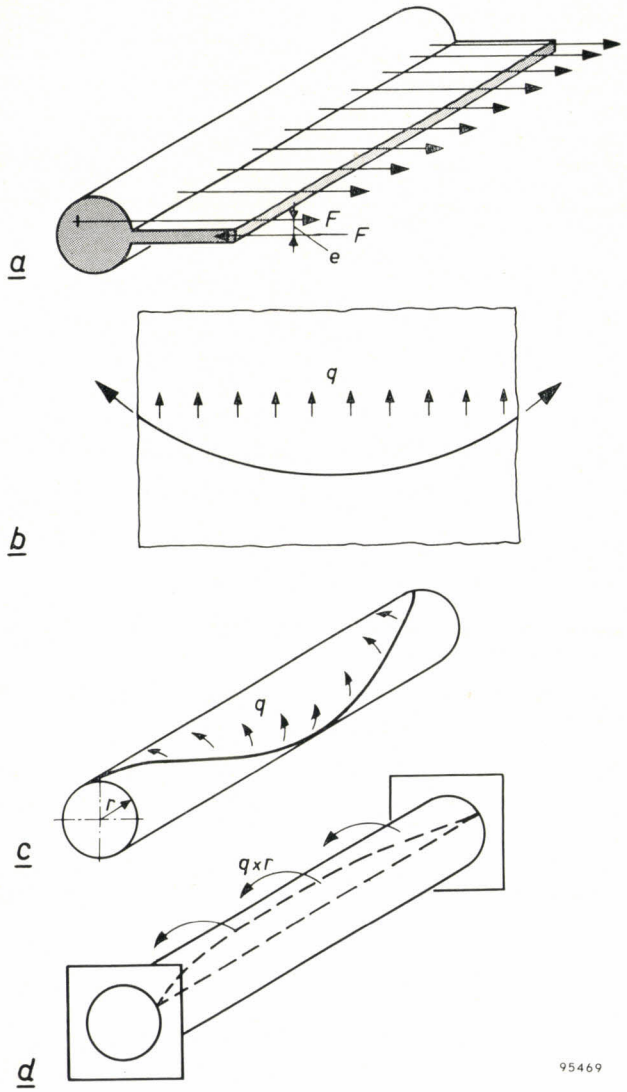

Fig. 8. At places where the prestressing forces (F kg/m, i.e. kg per linear meter) do not act centrally through the shell, (*a*), the rib is loaded by a torsional moment ($F \times e$ kg.m/m), which give rise to bending moments in the shell. These can be eliminated by introducing a torsional prestressing in the rib. For this purpose it is necessary to tension wires along a path that would be parabolic on the surface of the rib. This may be explained as follows. Consider first a plane on which a parabolically curved wire is fixed as shown in (*b*). When the wire is tensioned, the plane is loaded by a uniformly distributed force q kg/m. If this imaginary plane is now wrapped around a cylinder (*c*), the latter is loaded by a uniformly distributed torsional moment $q \times r$ kg.m/m when the wire is tensioned. When q is given the proper value, this moment will exactly compensate for the distortion caused by a uniformly distributed torsional moment $F \times e$ (cf. *a* and *d*). (The parts of the structure to which the ends of the beam are connected and in which the prestressing wire is anchored, e.g. the foundation and the junction with other ribs, are naturally subjected in this process to a torsional load, owing to the reactions to the tensile forces of the wire.)

Fig. 9. Prestressing wires for a rib, mounted before making the shuttering and casting the concrete. This particular rib was fitted only with wires for producing torsional prestressing (eight wires running on the circumference of a cylinder, 35 cm in diameter, formed by a series of iron hoops). The 9 mm wires look thicker here since they have been coated with a preparation to prevent bonding with the concrete.

The torsional prestressing wires were disposed helically round the axis of the ribs (*figs. 8* and *9*). Like the wires for producing the compressive and bending prestresses, they were fixed in position before the shuttering for the ribs was made. All wires (9 mm thick) were coated with a special preparation to prevent bonding with the concrete cast around them and to reduce friction losses when the wires were tensioned.

The contraction which a rib undergoes as a result of compressive prestressing is greater than the deformation, measured along the rib, suffered by the abutting shell under its own prestressing. If shell and rib were first to be joined firmly together and then prestressed, the difference in deformation would once again give rise to extra stresses in the shell. To avoid this, most of the ribs were partly prestressed before the shell was mounted, in such a way that when the final prestressing was applied the deformations then occurring in rib and shell were to all practical purposes equal.

Methods of prestressing

All wires were tensioned by a method devised and currently used successfully by Strabed. The main feature of this method is the possibility of tensioning wires between anchorings fitted to the structure in advance. With the traditional methods it would have been necessary to pull the wires through openings across the ribs, and this — apart from aesthetic objections — would have presented very considerable difficulties in the case of those beams where several wall surfaces meet at small relative angles.

In the method used, anchoring wires are cast into the ribs and into the substructure of the shells at ground level. Each of these wires is threaded through a small steel anchor plate and is crimped at each end. The prestressing wires are coupled to the anchoring wires by special sleeves (*fig. 10*), so designed that no slip can occur during this fixing process.

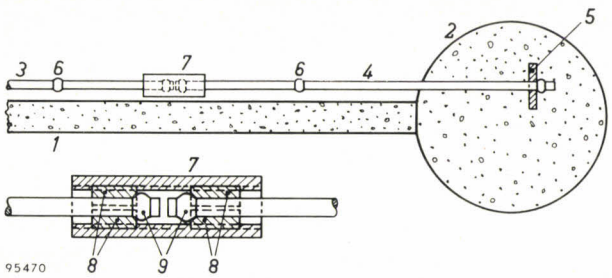

Fig. 10. The "Strabed" system for mounting prestressing wires. *1* = shell, *2* = rib (not shown in exactly the right proportions), *3* = prestressing wire. The anchoring wire *4* with anchorage plate *5* is fixed in the rib during fabrication of the latter. The wires are tensioned with a special jack which grips the crimps (*6*) in the prestressing wire and anchoring wire. The tensioned wire is clamped tight in an internally threaded coupling sleeve *7*, by screwing two split annulus pieces *8* against the crimped ends *9*.

This is particularly important for short wires which were necessarily relatively numerous in the pavilion. The wires are tensioned with a special jack designed by Strabed; this grips the wires from the side. The amount of tensioning applied can be read accurately from a dynamometer fitted to the jack (*fig. 11*).

As may be seen in fig. 11, it is possible, with this Strabed method, to lay the wires very close to the walls to be prestressed (in the Philips pavilion, only 2 to 3 cm from the shells). This is useful in order to be able to introduce the prestresses centrally in the shells, and moreover it is convenient for constructional reasons, since each prestressing wire must be fixed at regular points to the wall.

All the exterior surfaces of the pavilion, including the prestressing wires, were given a coating of special waterproof paint. To this base a final coating of aluminium paint was applied. *Fig. 12* shows the finished pavilion from the entrance end.

In view of the fact that pictures were to be projected on the interior walls, the prestressing wires on the inside shell surfaces were concealed by a sound-absorbent layer of asbestos felting.

Concluding remarks

The erection of exhibition buildings usually involves having to work against time, especially when the building departs so radically from classical concepts as the present one. The marks of haste are bound to be present in the finished structure; this need not be objectionable, however, since a temporary structure can be measured against different standards. Because of this circumstance we were able to experiment with an entirely new system of construction for the Philips pavilion, a system which we would otherwise probably not have dared to embark upon but which in this case was remarkably consistent with the ideas of the patron — N.V. Philips — and of the responsible architect — Le Corbusier. The Belgian Inspectorate of Works (Séco: Bureau de contrôle pour la Sécurité de la Construction en Belgique), by acting expeditiously

Fig. 11. Tensioning a prestressing wire with the "Strabed" jack. The tensioning force is read on a dynamometer.

Photo Hans de Boer

Fig. 12. The finished pavilion, seen from the entrance end.

and offering constructive criticism, also did a great deal to help make the experiment succeed. We were therefore able to use this unique opportunity to gather information and experience which, under normal circumstances, would only have been obtained in the face of much opposition and after a much longer period.

In a number of countries wide and varied use has already been made of shells composed of saddle surfaces, such as the hyperbolic-paraboloidal shell. They have been introduced, for example, as roofs for large halls. We are convinced that their construction in prestressed concrete, whether or not combined with prefabrication, offers yet more

interesting and wider possibilities. The Philips pavilion constitutes proof that such shells can be pieced together to form very intricate structures that serve both as roof and wall. Architects may find it rewarding to exploit the possibilities thus revealed.

Summary I-IV

Based on an idea of L. C. Kalff, the Philips pavilion was designed and equipped for automatic performances of a spectacle in light and sound, a so-titled "Electronic Poem", the scenario of which was written by Le Corbusier and the music composed by Edgar Varèse. The architectural design was undertaken by Y. Xenakis under the direction of Le Corbusier. Visual, acoustical and architectural considerations led to the pavilion being built up entirely from ruled surfaces, viz. hyperbolic paraboloids. In article I, an authorized shortened version of the original French text, the evolution of the first design, which also contained conoids, is illustrated by a series of original sketches by the architect. A description is then given of the semi-experimental, semi-geometrical method by which the surfaces of the first design were completely converted into hyperbolic paraboloids (second design). As a result of this conversion it was found possible to adopt the scheme of construction proposed by the contracting firm "Strabed", which was to build the pavilion as a self-supporting shell in prestressed concrete 5 cm thick.

The excellent mechanical properties of shells shaped as hyperbolic paraboloids (hypars) which made this scheme of construction possible, are discussed in general terms in the second article. After recapitulating the most important geometrical properties of the hyperbolic paraboloid, the author gives a concise explanation of the membrane theory of the hypar shell. The differential equations for the state of stress have an extremely simple solution in the case of a uniaxial, uniform load applied parallel to the axis of the shell; the shell is then found to be a structure of equal strength. The author also gives formulae for somewhat more complex loads, which are of importance under practical conditions, and describes a simple graphical method of determining the principal shell forces and the prestressing forces required in order to avoid in the shell any tensile stresses (which concrete cannot withstand). Finally edge disturbances are considered that occur when the boundary conditions are such as to prevent the existence of a purely membrane state of stress. Some details are given of the stability of hypar shells against buckling and second-order buckling.

The theory gives a general idea of the behaviour of hypar shells, and allows solutions to be found to certain detail problems; but a complete calculation of the mechanical properties of such a complex structure as the Philips pavilion is out of the question. For this purpose model tests were required, and these are described in article III. In accordance with the architects' design, a 1 : 25 scale model was made of the pavilion in plaster of Paris on a framework of wire-gauze, steel tubes simulating the ribs of the structure. The states of stress produced in the model under different loads (dead-weight, wind, etc.) were investigated with a large number of strain gauges and displacement gauges. The conclusion was that a structure of 5 cm thick concrete with 40 cm thick ribs would be sufficiently strong. In a second model 1 : 10, two of the hypar shells were built up from several hundreds of appropriately shaped plywood slabs. These shells were prestressed, and the results observed proved the feasibility of the proposed system of construction, using precast concrete slabs and prestressing wires anchored in the ribs.

This scheme of construction, proposed and translated into reality by the firm "Strabed", is described at some length in the fourth article. The consideration underlying this scheme of construction was that the irregular and steeply twisted shells of the pavilion, which Strabed decided to keep as thin as possible (subject to the minimum of 5 cm dictated by acoustic insulation demands) could not be made by casting concrete *in situ* in shuttering. The hypar shells were therefore built up from more than 2000 slabs, each about 1 m², which were cast in open sand-bed moulds, built to the required shape. The slabs were subsequently erected on site on scaffolding, and pulled tight by steel wires. This construction is also mechanically favourable in that with suitable prestressing of shells and edge members (ribs) the structure can be brought approximately into a membrane state of stress. The precasting and assembly of the slabs were greatly simplified by the fact that the walls were ruled surfaces. The prestressing wires (applied on both surfaces of the walls) followed, as a rule, the ruling lines of the hyperbolic paraboloids. The wires were tensioned using a system devised by Strabed. The special feature of this system is that the anchorings for the wires are fitted to the structure in advance; this apparently minor detail had an important bearing on the successful erection of the pavilion. In addition to compressive and bending prestressing, some ribs were given torsional prestressing, partly to compensate for the torsional moments exerted on the ribs by abutting shells, and partly to introduce the prestressing forces centrally in the shells. This is thought to be the first application of torsional prestressing to concrete.

VOLUME 20, 1958/59, No. 2/3 pp. 37-84 Published 23rd October 1958

Philips Technical Review

DEALING WITH TECHNICAL PROBLEMS
RELATING TO THE PRODUCTS, PROCESSES AND INVESTIGATIONS OF
THE PHILIPS INDUSTRIES

THE "ELECTRONIC POEM" PERFORMED IN THE PHILIPS PAVILION AT THE 1958 BRUSSELS WORLD FAIR

A. THE LIGHT EFFECTS, by L. C. KALFF

B. THE SOUND EFFECTS, by W. TAK

C. THE ELECTRONIC CONTROL SYSTEM, by S. L. de BRUIN.

628.973:534.86:621.316.7.076.7:789.983

In its pavilion at the 1958 Brussels World Fair Philips has broken with tradition, in that its products are not put on display as is customary at other exhibitions and trade fairs, but are symbolized, as it were, by a novel synthesis of light and sound — Le Corbusier's "Poème Electronique". Among those who collaborated with Le Corbusier in achieving this synthesis were the composer Varèse, the film producer Agostini and the technical specialists contributing to this article. The creation of this "Electronic Poem" called for elaborate lighting and electro-acoustical equipment; moreover, since it is performed and repeated almost entirely automatically, an intricate, largely electronic, control system was needed.

A. THE LIGHT EFFECTS

by L. C. KALFF.

Philips is represented at the Brussels World Fair by a pavilion designed by Le Corbusier and Xenakis. The highly unusual architecture of the pavilion is described in a series of articles published in the previous issue of this journal[1]). In the present article we shall be concerned with what takes place inside the structure. Here the public is shown how science and technology have created an instrument which provides the artist with a novel form of expression using light and sound effects. Audiences of some five hundred at a time see a performance of the "Electronic Poem" by Le Corbusier and his collaborators. On the curved walls the audience sees a continuously shifting play of projected pictures and colours. These are accompanied by sound effects which, by means of electro-acoustical tricks, join in creating the illusion of movement.

In this "Electronic Poem", Le Corbusier has attempted to express his view that our increasingly mechanized civilization is striving towards a new harmony. The scenario consists of seven parts, which are entitled:

Genesis.
Spirit and matter.
From darkness to dawn.
Man-made gods.
How time moulds civilization
Harmony.
To all mankind.

[1]) The Philips pavilion at the 1958 Brussels World Fair,
I. Y. Xenakis, The architectural design by Le Corbusier and Xenakis,
II. C. G. J. Vreedenburgh, The hyperbolic paraboloidal shell and its mechanical properties,
III. A. L. Bouma and F. K. Ligtenberg, Model tests for proving the construction of the pavilion,
IV. H. C. Duyster, Construction of the pavilion in prestressed concrete,
Philips tech. Rev. **20**, 1-36, 1958/59 (No. 1).

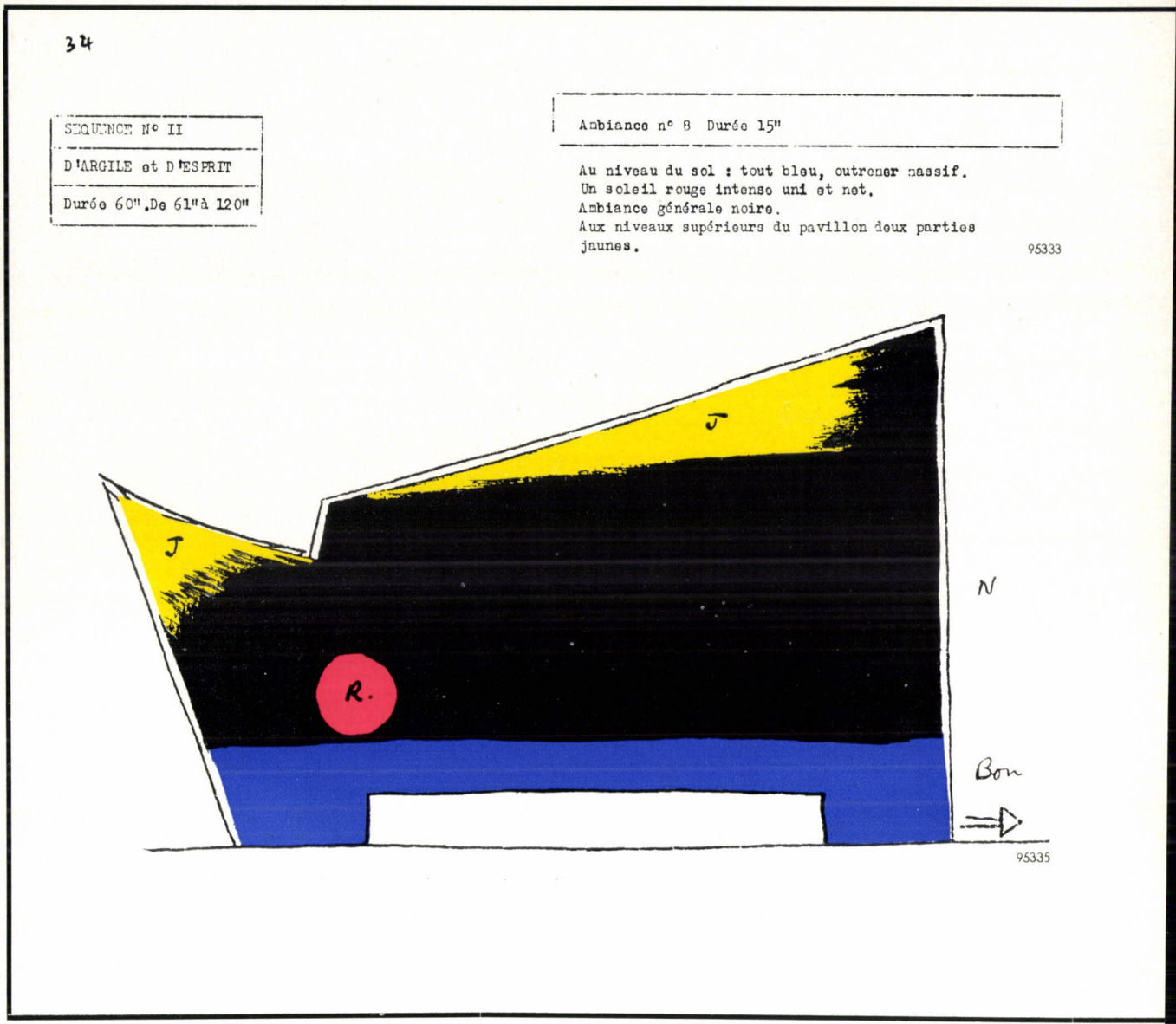

Fig. 1. Two pages of the scenario of Le Corbusier's "Electronic Poem". The page on the left indicates the colours of the "ambiances" in a given time interval; that on the right gives a time schedule, specifying the details of "écrans" and "tritrous".

Le Corbusier's scenario specifies what should be seen from second to second throughout the entire spectacle, which lasts 480 seconds. Two pages of the scenario are reproduced in *fig. 1*.

Le Corbusier distinguishes the following light effects:

1) "*Ambiances*", which are illuminated surfaces intended to conjure up a particular atmosphere. They are produced by projecting coloured light on to the pavilion walls; long bands of colour accentuate the peculiar shape of the building.
2) "*Volumes*", i.e. two figures suspended in space, the one a female figure, the other a space structure of metal tubes, and both treated with fluorescent paint. When irradiated with ultraviolet, the one "volume" glows red, the other greenish blue.
3) "*Ecrans*": these are large areas of the wall on which are projected black-and-white pictures of human beings, animals and all kinds of objects (*fig. 2*). The presence at the same time of "ambiances" makes the black of the projections appear coloured.
4) "*Tritrous*". At certain parts of the wall around the "écrans", brilliantly coloured beams of light or figures in black and white are occasionally projected. This is done by means of a film strip each frame of which is entirely opaque except for three holes ("trois trous") in which the colours or figures are introduced.

35

Sec	Volumes		Ecrans			Sec	Tritons	Paroles
	Mat	Fon	Notes	Vision	Référence			
81				Les quatre savants	T.113	81	Les quatre savants dans les trous éclairés en couleur bleu et rouge.	
82						82		
83						83		
84			Toutes ces têtes seront animées, c'est-à-dire qu'il faut à tout prix éviter la monotonie et la lenteur. Cela doit être vivant	Tête de nègre Congo	T.114	84		
85				Tête de nègre Maori	T.116	85		
86				Tête de nègre Mayogo	T.117	86		
87				Tête de fille Mangbetu	T.118	87		
88				Courbet: femme couchée FAU 227	D.121	88	Les tritrous en couleur bleu et rouge.	
89				Art Attique MAL 49	D;124	89		
90				Art Sumérien MAL 11	D.125	90		
91				Egypte MAL 68	D.128	91		
92				Dame D'Écho MAZ 94	D.130	92		
93				Art Sumérien MAL 11	D.125	93		
94				César MAL 171	D.133	94		
95				Art Celtique MAL 212	D.135	95		

7533a

5) A red sun, a moon, stars and clouds can also be staged.

The technical arrangements made for producing these effects are relatively simple compared with the electro-acoustical equipment and the control system. Nevertheless the realization of the light effects presented certain difficulties. The greatest difficulty arose from the fact that the films and colours were to be projected from opposite sides of the enclosure simultaneously. This entailed a considerable amount of diffusely reflected light, which threatened to spoil the contrasts and the colour effects.

The problem was solved by 1) using the lowest practicable luminous intensities, so that not too much of the auditorium would be seen, 2) avoiding the use of large white surfaces, and 3) choosing suitable combinations of colours. Complementary colours, additively mixed, yield white or at least colours that are less saturated, that is to say less striking. The answer to that was to use only non-complementary colours, such as green and blue, red and yellow, violet and red.

These measures demanded close cooperation between Le Corbusier and film-producer Agostini in regard to the prescribed pictures, and between the illumination engineers, whose task it was to decide on the kinds of light-sources and colour filters to be used. These questions were largely settled at the last moment by experiment in the pavilion itself.

The choice fell on the following light-sources:

a) Four large cinema-projectors, two of them for the pictures and two for the "tritrous". The "tritrous" beams are directed on to the required places by means of mirrors fixed at the appropriate angles. Synchronism between the projectors is assured by means of magslips.

b) Four projection lanterns, each with a 3 kW in-

Fig. 2. An "écran" (picture projected on the wall). The small rectangles are loudspeakers, of which there are 350 in the pavilion.

candescent lamp and a large rotary disc fitted with eight slides or colour filters for the "ambiances". Servo motors rotate the disc into the required position.

c) Two projection lanterns as under *b*) for producing cloud effects.

d) Two projection lanterns each with a 1 kW incandescent lamp, for projecting a sun and a moon.

e) Six spotlights, each with a 500 W incandescent lamp, for projecting the colour "ambiances" onto the walls.

f) Four reflectors, each fitted with a 125 W high-pressure mercury-vapour lamp whose bulb trans-

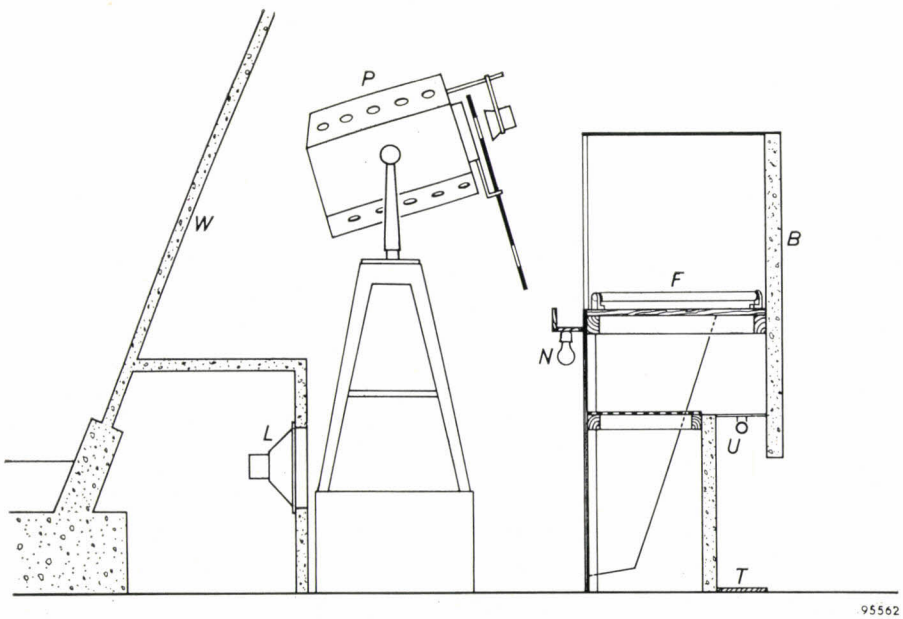

Fig. 3. Vertical section through the space behind the balustrade. *W* concrete wall of pavilion. *L* low-note loudspeaker in one wall of closed concrete cabinet. *P* projection lantern. *F* white and coloured fluorescent lamps. *N* lamp for emergency lighting. *U* tubular ultraviolet lamp for exciting floor-tiles *T* into fluorescence. *B* balustrade.

mits ultra-violet but hardly any visible light. Two of them excite red fluorescence on the female figure, the other two greenish-blue fluorescence on the space structure.

g) Fifty "stars", formed by incandescent 5 W (40 W), in white, red, yellow, green and blue. These lamps are used to light the entire auditorium or, with reduced luminous flux, to create the illusion of a bright horizon. The lamps are accordingly mounted behind a six feet high balustrade which follows the contour of the floor (see vertical section in *fig. 3* and plan in *fig. 4*). The projectors are also mounted behind this balustrade (*fig. 5*).

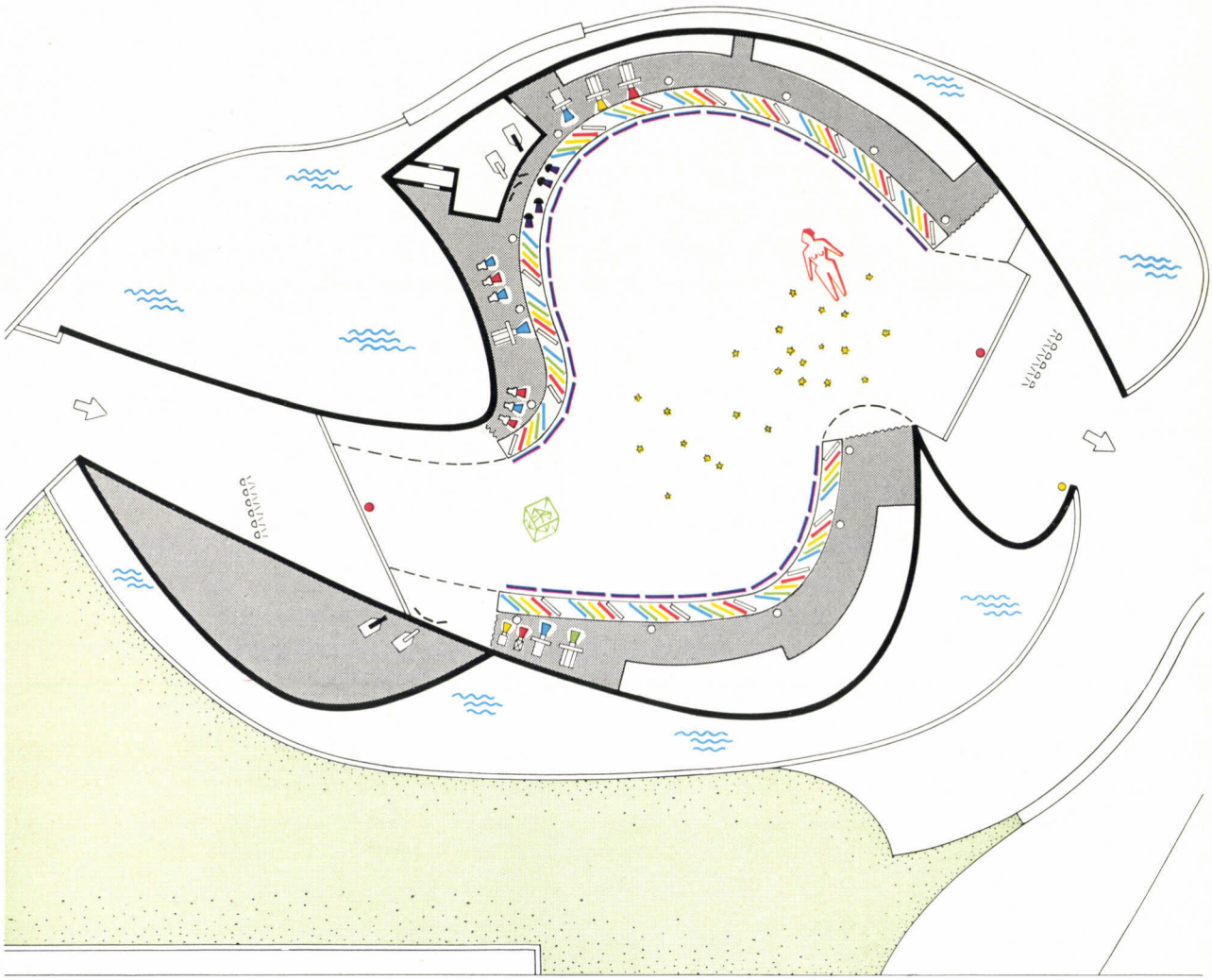

Film projector (for "écrans")
Film projector (for "tritrous")
Projector (for "ambiances")
Projector (clouds)
Projector (sun)
Projector (moon)
Spotlight (coloured patches)
U-V source ("volumes")
Filament lamps (stars)
Fluorescent lamps ("TL" M), white and coloured
U.V. source (floor-tiles)
Emergency lighting (white)
Emergency lighting (red)
Panic lighting
Mirrors for directing "tritrous" beams
Yellow fluorescent lamps ("TL" M) in exit porch.

Fig. 4. Plan of the Philips pavilion with schematic indication of the light-sources.

bulbs scattered over the upper surface of the walls. A twinkling effect is produced by switching the bulbs on and off irregularly (by means of telephone selectors).

h) Forty groups of five fluorescent "TL"M lamps

The brightness of the fluorescent lamps behind the

balustrade is controlled by means of thyratrons [2]). The thyratron control-pulses are phase-shifted by the intermediary of potentiometers driven by servo motors. The latter are in turn driven by control signals recorded on a magnetic tape. Further particulars of the control system — which comprises a great deal more — are given in the last part of this article.

Fig. 5. Glimpse behind the balustrade. Some of the variously coloured fluorescent lamps can be seen and, behind them, an array of projection lanterns with filters for the "ambiances". Above, on the wall, a number of high-note loudspeakers. Bottom right a low-note loudspeaker.

The above projection and lighting installations serve exclusively for producing the light effects required for the performance of the spectacle. We shall now touch on the arrangements made for *utility lighting* in the pavilion (see fig. 4).

First, the regulation safety lighting is run on a 60 V battery and consists of two red incandescent lamps, burning continuously above the entrance and exit, and of several white bulbs that light up automatically in the event of a mains failure. To meet the contingency of panic amongst the audience, emergency lighting can be switched on from the control desk. Furthermore, bluish-white fluorescent tiles are fitted in the floor around the whole length of the balustrade to prevent people knocking themselves upon entering the darkened pavilion. The tiles are excited into fluorescence by 45 tubular ultra-violet lamps of 40 W. In addition, six 40 W "TL" lamps concealed above the entrance on the outside produce a decorative effect at night, particularly since they are yellow fluorescing and hence provide a striking contrast to the blue mercury-vapour light which floods the exterior of the pavilion (16 high-pressure mercury-vapour lamps, each of 250 W).

[2]) K. W. Hess and F. H. de Jong, Controlling the luminous intensity of fluorescent lamps with the aid of relay valves, Philips tech. Rev. **12**, 83-93, 1950/51.

B. THE SOUND EFFECTS

by W. TAK.

Acoustical science has long been familiar with various effects that influence our perception of sound. Reverberation and echo are the best known of these phenomena. Without the agency of visual perception, they provide us with an impression, learnt by experience, of our surroundings. Reverberation and echo can also be created artificially, and in such a way that the listeners' acoustical impression of their surroundings is made to differ appreciably from their visual impression [3]). This discrepancy between seeing and hearing can evoke in an audience the sensation of experiencing something startingly unexpected. With such possibilities electro-acoustics may well contribute something to the development of music.

Equally remarkable effects can be obtained with the technique of stereophony [4]): sounds are heard to issue from a direction where there is no sound-source, and by means of purely electrical manipulations the impression of a moving sound-source is created without there being, in fact, any movement of the source.

These effects were in mind when, at the end of 1956, we discussed with Le Corbusier the sound effects for his "Electronic Poem". The listeners were to have the illusion that various sound-sources were in motion around them, rising and falling, coming together and moving apart again, and moreover the space in which this took place was to seem at one instant to be narrow and "dry", and at another to seem like a cathedral.

At that stage of the plans the music which Edgar Varèse was to compose was still quite literally music of the future. All that was known was that it would be mainly *electronic music,* in the connotation given to the term in recent years; that is to say, music whose actual composition is based on the use of electronic devices. As explained in an earlier article in this Review, electronic devices can be employed to produce entirely novel musical sounds [5]). Although we were as yet unaware of the composer's wishes in the matter, we were certain that stereophony and artificial reverberation would turn out to be important elements of the "Electronic Poem". That was enough to enable us to plan in advance the general scheme of the requisite equipment.

It was our opinion that the simultaneous perception of three sound patterns issuing from or travelling in different directions would constitute a completely new experience. For this reason we decided there and then to develop and build apparatus that would be capable of reproducing the composition via three independent channels. We calculated that it would be possible to achieve the required electro-acoustical effects with the aid of a three-track magnetic tape. Each of the three playback heads would feed, via amplifiers, numerous loudspeakers. On another magnetic tape, having a large number of tracks, control signals would be recorded, some for determining which loudspeakers should be on at each moment, and others for controlling the light effects.

When these preparations were far enough advanced, Varèse came to Eindhoven to "produce" his composition with our cooperation. For this purpose a specially equipped studio was provided. In composing, Varèse concentrated primarily on the character of the tonal pattern, and for the most part left us to decide on the "intonation" (the distribution of the sound over the loudspeakers, i.e. the spatial effect). The composition is characterized by an extraordinary wealth of sounds, the realization of which often involved considerable difficulties [6]). The deficiency of language in this field, the lack of words to express what is intended, was keenly felt. Varèse frequently indicated his wishes by such expressions as "more nasal", "less biting", "more rasping", and it was our job to meet his wishes as well as possible by means of filters, mixers and frequency-shifting circuits. To define the necessary operations we had to resort repeatedly to onomatopœic words, such as "wow wow", "poowhip" "tick tock", "whoop" and "choochah". It should be mentioned, incidentally, that the recording was not limited to electronically produced signals but also included "concrete" sounds picked up by the microphone, for example piano chords, chimes of bells, choral and solo singing, drum beats and workshop noises, which, after electrical treatment (with filters, etc), were also recorded on tape.

[3]) Improving the acoustic properties of a hall by "stereo reverberation" (R. Vermeulen, Philips tech. Rev. **17**, 258-266, 1955/56) is also based on bringing about a difference between the "acoustic" environment and the real one. In this case, however, the difference should be such that the listeners are unaware of it.

[4]) See, for example Philips tech. Rev. **17**, 173 *et seq.*, 1955/56.

[5]) H. Badings and J. W. de Bruyn, Electronic music, Philips tech. Rev. **19**, 191-201, 1957/58 (No. 6).

[6]) We are greatly indebted to Mr J. W. de Bruyn for solving many of these difficulties.

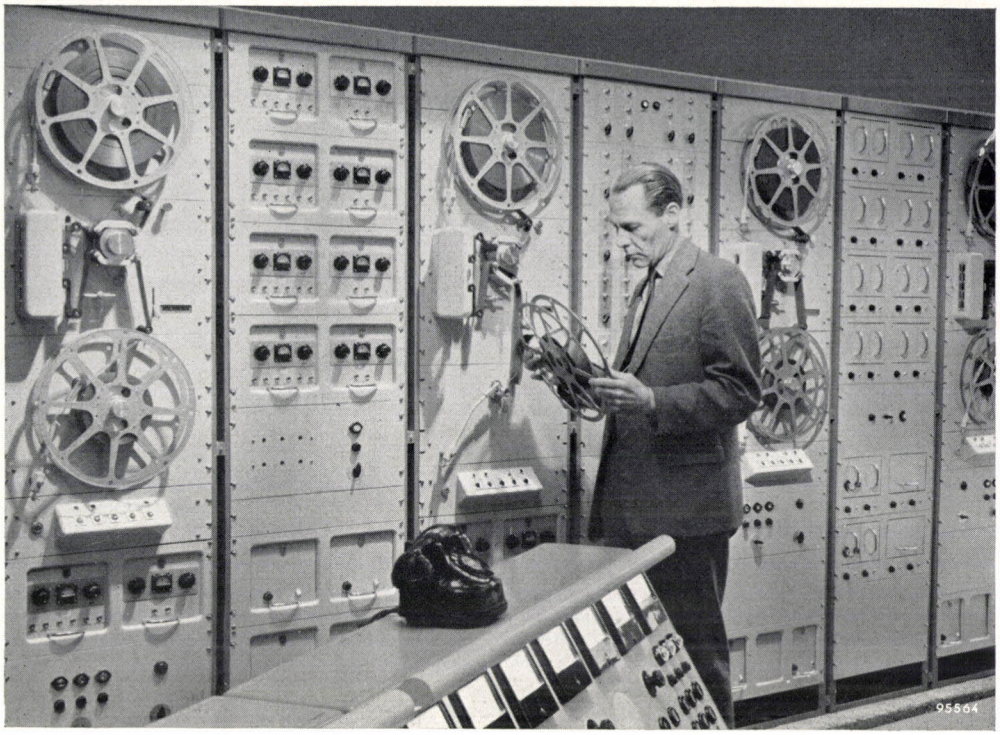

Fig. 6. Special playback machines for the 3-track tape carrying the electronic music by Varèse, and for the 15-track control tape. Two of the four machines are used for each performance.

The recording on the three-track tape was made so as to leave tracks *II* and *III* specifically for reverberation and stereophonic effects. For the purposes of stereophony, compact groups of loudspeakers would be necessary, e.g. one group above the entrance and another above the exit. However, it was not to be expected that everyone in the audience (the pavilion accommodates about 500) would receive a distinct stereophonic impression unless other, more dispersed, groups of loudspeakers were introduced, and the individual loudspeakers switched on and off successively in such a way that the sound-source would describe, as it were, set paths. This system of "sound routes" (*routes de son*) was therefore adopted and has proved successful.

After the composition had been completely built up on the three-track tape, a start could be made on working out a "control score". On a second magnetic tape — containing no fewer than 15 tracks — the control signals were recorded which were to assure the required distribution of the composition over the various loudspeakers. This was work calling for the most scrupulous accuracy, for every control signal had to appear or disappear at precisely the right moment. Further particulars of the control system are given in the next section.

Finally, a few words about the electro-acoustical equipment installed in the pavilion.

Both the sound tape and the control tape have the same width (35 mm) and the same perforation as normal cinematographic film. The perforation is important with a view to the synchronous running of the two tapes. Each tape is scanned separately in a special magnetic playback machine (one with 3 and the other with 15 playback heads) and driven by a rapid-starting synchronous motor. With the exception of the loudspeakers, the entire installation is duplicated, which means that there are four playback machines in the control room (*fig. 6*).

There are altogether 350 loudspeakers. Twenty-five are low-note loudspeakers fitted in one of the walls of the otherwise completely enclosed concrete cabinets [7]) behind the balustrade (see figs. 3 and 5). The efficiency of these loudspeakers is particularly high (20%). The other loudspeakers (efficiency 5%) are mounted partly in compact groups (above the entrance and exit) and partly in dispersed groups (figs. 2 and 5), for example in "sound routes" along the shell ribs and horizontally. Over a complex relay system the loudspeakers are fed from 20 amplifiers, each with an output of 120 W. Six of the amplifiers derive their input signal from sound track *I*, eight from track *II* and six from track *III*. By means of special signals the inputs of the various amplifier groups can be interchanged, allowing a free choice of the path along which a certain sound is to be reproduced.

[7]) See Philips tech. Rev. **18**, 310 *et seq.*, 1956/57.

N. V. PHILIPS' GLOEILAMPENFABRIEKEN

C. THE ELECTRONIC CONTROL SYSTEM

by S. L. de BRUIN.

As mentioned in the foregoing, the light and sound effects of the "Electronic Poem" are controlled by signals recorded on a magnetic tape. A simplified block diagram of the installation is shown in *fig. 7*. The control desks from which the duplicated installation is operated can be seen in *fig. 8*.

On *each* of the 15 tracks on the control tape, twelve control signals can be recorded, each with a fixed amplitude and a fixed frequency which differs from one signal channel to another. There are thus altogether $15 \times 12 = 180$ control channels available. The lowest frequency is 900 c/s (this fairly high value was chosen to exclude the risk of interference from hum), and the highest is 10 500 c/s. Neighbouring frequencies stand in a ratio of 1 : 1.25 to each other.

Each of the 15 playback heads delivers an output of 12 superimposed signals which is split into its components by selective amplifiers. These consist of two amplifying stages with tuned-circuit coupling and a relay. The relay closes only when the input signal in the first stage has the frequency to which the circuit is tuned. *Fig. 9* shows one of the consoles accommodating 48 of the total of 180 selective amplifiers.

Certain control channels are reserved for the light effects. Via some of these channels servo motors can be set in operation which rotate the required colour-filter or slide in front of the lens of the projection lanterns. Other channels control the thyratrons, which regulate the luminous flux of certain

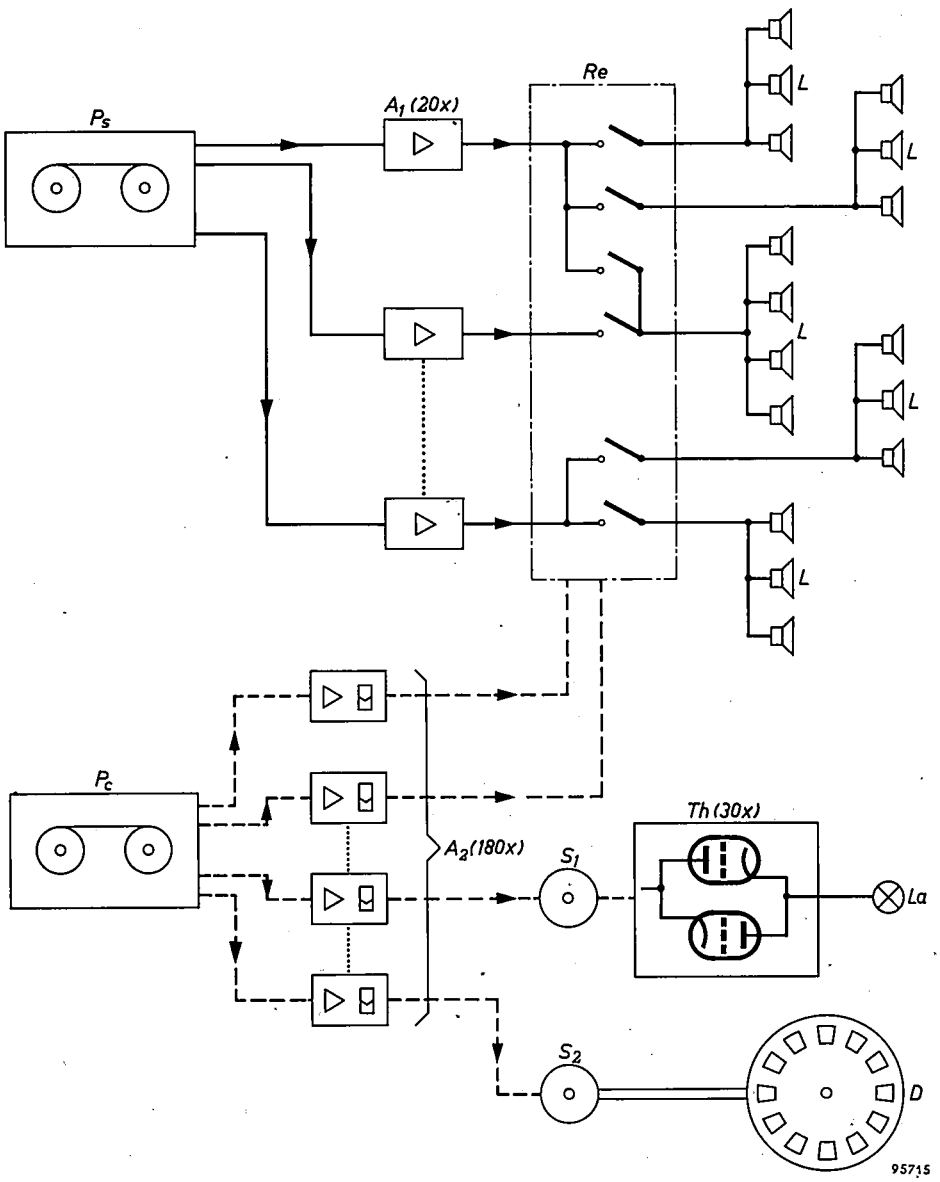

Fig. 7. Simplified diagram illustrating the principle of the installation for performing the "Electronic Poem". P_s playback machine with 3-track sound tape. A_1 amplifiers (20 in all) with 120 W power output. *Re* relays. *L* loudspeakers (350 in all). P_c playback machine wiht 15-track tape on which the control signals, with different frequencies, are recorded. A_2 selective control-signal amplifiers (180 in all); some of these control the loudspeaker relays *Re*, others the groups of servo motors S_1 and S_2. The motors S_1 change the phase of the ignition pulses in the thyratron control-devices *Th* (30 in all), thereby varying the luminous flux of the lamps *La*. The servo motors S_2 rotate discs *D* which contain slides or colour filters.

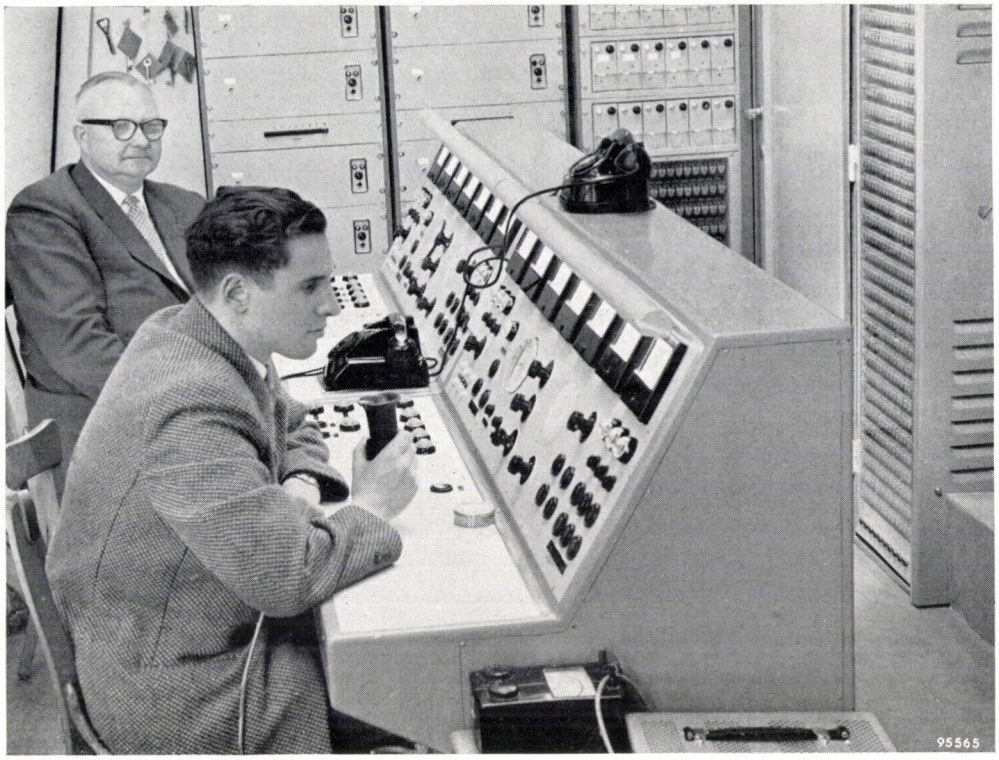

Fig. 8. The two identical control desks.

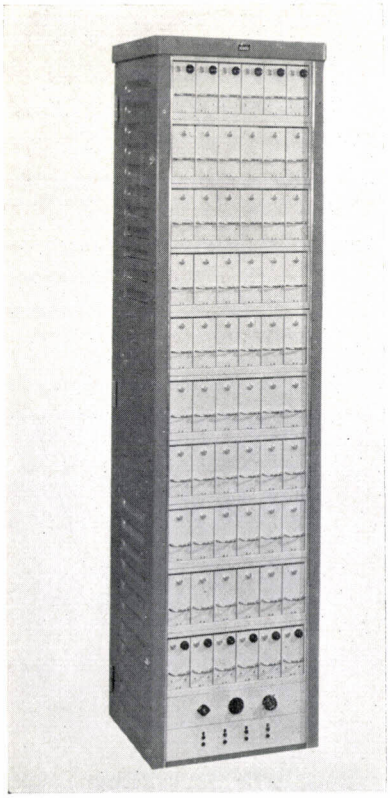

Fig. 9. Rack containing 48 of the 180 selective control-signal amplifiers.

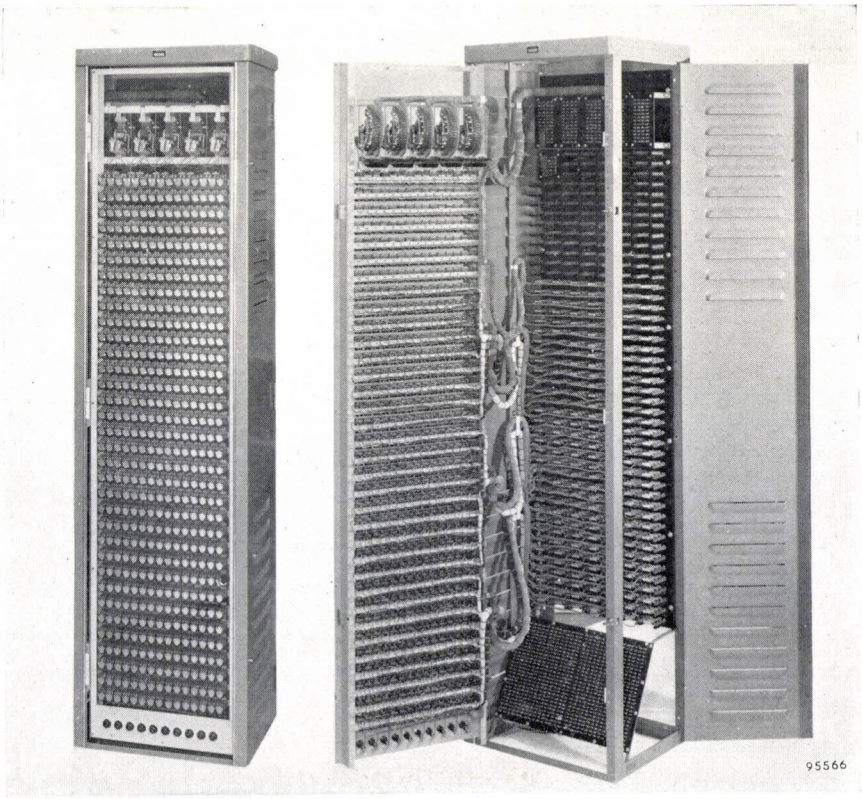

a *b*

Fig. 10. Rack housing the loudspeaker relay system (*Re* in fig. 7), *a*) closed, *b*) opened. In *b*) can be seen the contact fields at which the loudspeakers and the amplifier outputs terminate. The five rotary selectors for the "sound routes" are visible at the top of the rack.

light-sources [2]). This is also done by the intermediary of servo motors. In this case they turn potentiometers that vary the direct current through saturable reactors, thereby shifting the phase of the voltage pulses that ignite the thyratrons and hence changing the average thyratron current. Two thyratrons connected in anti-parallel are circuited in series with the light-source to be regulated. There are altogether 30 of these thyratron regulators.

The remaining control channels are used for the sound effects. They ensure that only those loudspeakers that are required are switched on at any given moment. The switching on and off of groups of loudspeakers is effected by relays (*Re* in fig. 7). A photograph of the relay rack is shown in *fig. 10a*. An interior view is seen in fig. 10*b*. The oblique panel below contains two fields of contacts; on the one field the amplifier outputs terminate, on the other the loudspeakers. Connections between any required loudspeakers and amplifiers (a maximum of 12 loudspeakers to one amplifier) are made or broken by the relays. These receive their energizing current via the contacts of the relays in the selective control-signal amplifiers.

The substantial number of relays needed for all this would have had to be very much larger if use had not been made of a circuit employing rectifier elements. The principle is illustrated in *fig. 11* for three relays, but the circuit can be built for any number. Suppose that, with relays A, B and C, we wish at one instant to energize only A, at another instant both A and B, and sometimes A, B and C together. The first can be done by raising point *1* to a certain positive potential; A then closes and

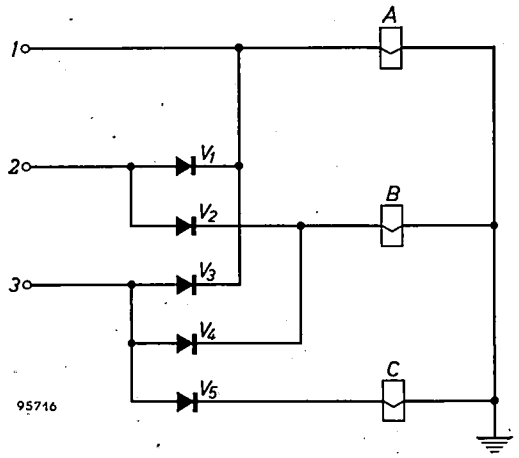

Fig. 11. Circuit with three relays, A, B and C, and rectifiers $V_1 \ldots V_5$. A positive potential applied to points *1*, *2* or *3* energizes respectively relay A, relays A and B, or relays A, B and C.

rectifiers V_1 and V_3 prevent current from reaching B and C. To energize both A and B, point *2* is given a positive potential, and rectifiers V_3 and V_4 prevent relay C from being energized. All three relays are actuated by giving a positive potential to point *3*. Without the rectifiers, additional relays would be necessary, the contacts of which would make or break connections between the coils of A, B and C.

Reference was made above to the system of "sound routes" with which the illusion of a moving sound-source is created. This effect is produced by switching on first, say, only the loudspeakers $L_{121} \ldots L_{125}$ (arbitrary numbering), a moment later $L_{122} \ldots L_{126}$, then $L_{123} \ldots L_{127}$, and so on, ending with, say, $L_{141} \ldots L_{145}$ (*fig. 12*). The rapid switching from one set of loudspeakers to another is

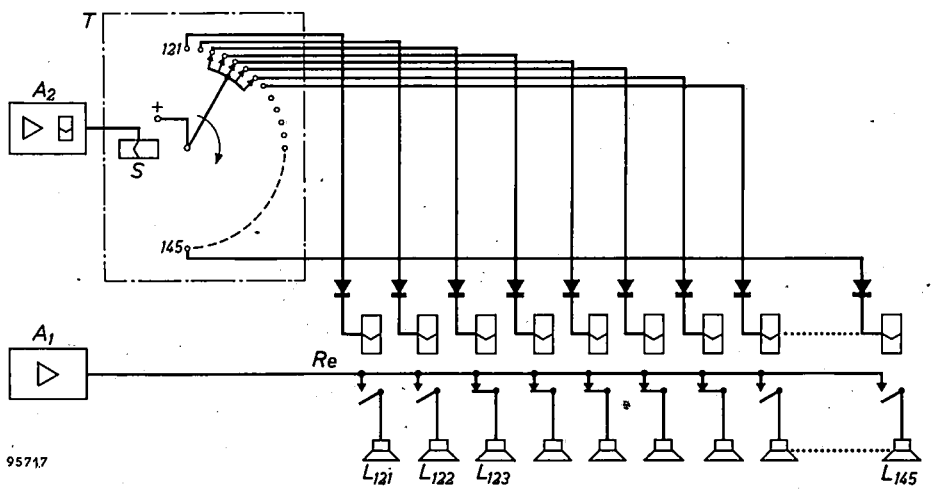

Fig. 12. Diagram of a "sound route", formed by loudspeakers $L_{121} \ldots L_{145}$, which are fed from one of the power amplifiers A_1 via relay *Re*. The solenoid S of a uniselector T is energized by pulses from one of the control-signal amplifiers A_2 (see fig. 7). Five loudspeakers are always in operation at one time. At each selector step, one loudspeaker is switched in and another switched out.

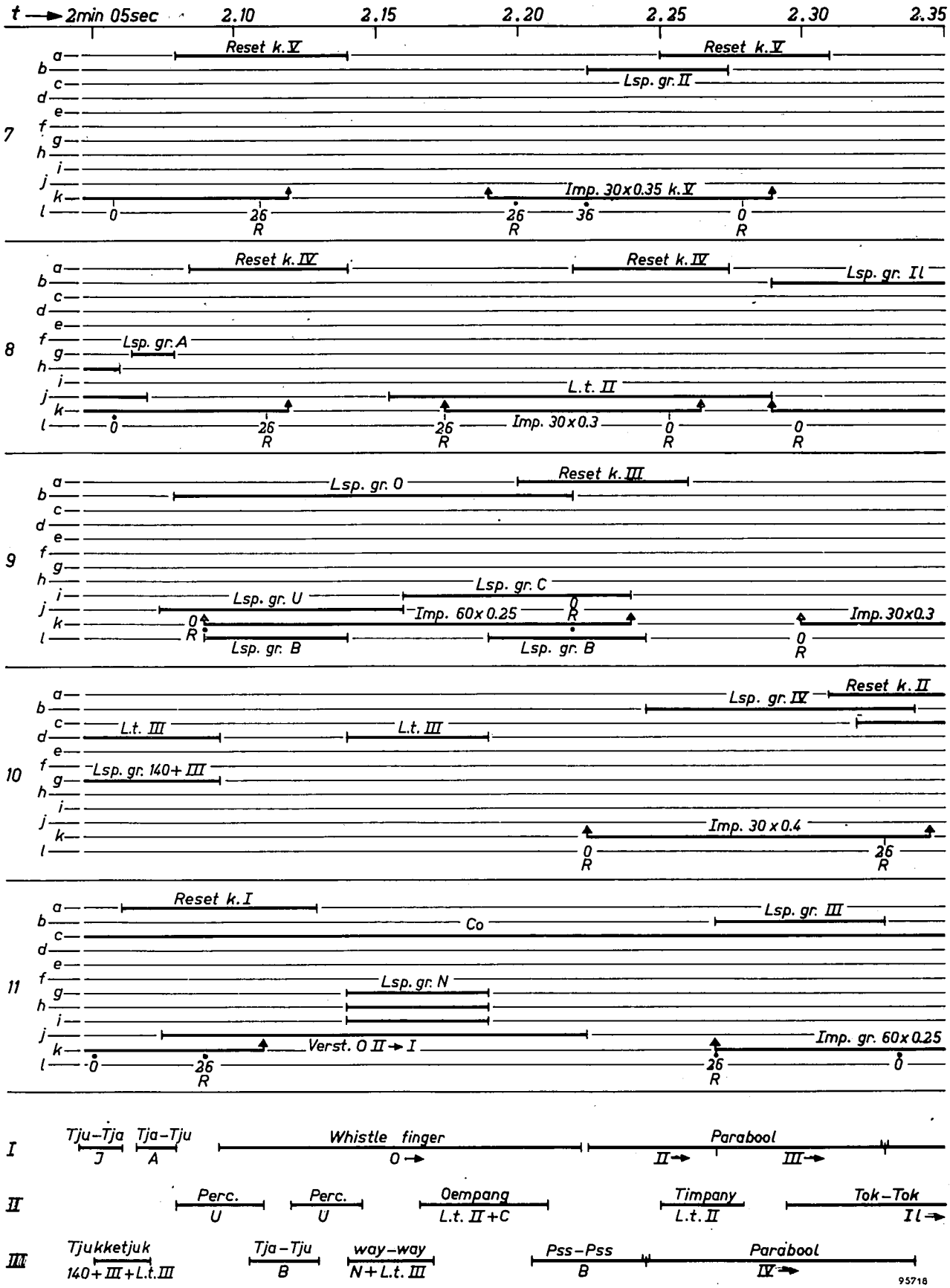
t → 2min 05sec
2.10
2.15
2.20
2.25
2.30
2.35
Reset k.V
Lsp. gr.II
Imp. 30x0.35 k.V
Reset k.IV
Lsp. gr. Il
Lsp. gr.A
L.t. II
Imp. 30x0.3
Lsp. gr. 0
Reset k.III
Lsp. gr. U
Lsp. gr. C
Imp. 60x0.25
Lsp. gr. B
Imp. 30x0.3
Lsp. gr. IV
Reset k.II
L.t. III
Lsp. gr. 140+ III
Imp. 30 x 0.4
Reset k.I
Co
Lsp. gr. III
Lsp. gr. N
Verst. O II → I
Imp. gr. 60x0.25
I
Tju-Tja
J
Tja-Tju
A
Whistle finger
O →
Parabool
II →
III →
II
Perc.
U
Perc.
U
Oempang
L.t. II+C
Timpany
L.t. II
Tok-Tok
Il →
III
Tjukketjuk
140+III+L.t.III
Tja-Tju
B
way-way
N+L.t. III
Pss-Pss
B
Parabool
IV →
95718

Fig. 13

Fig. 13. Schematic representation of the recorded sounds and associated control signals in the time interval from 2 min 05 sec to 2 min 35 sec.

Below: the sounds recorded on the three tracks *I*, *II* and *III*. Above: the control signals present on tracks *7*, *8*, *9*, *10* and *11* of the 15-track tape. The twelve frequency channels of each track are marked *a* . . . *l*.

In order, for example, to reproduce over loudspeaker group *A* the sound "tja-tju" recorded on track *I*, a control signal appears at the right moment in channel *8g* and switches *A* on and off again. In the same way a control signal in channel *9j* ensures that the two percussion sounds on track *II* are reproduced over loudspeaker group *U*.

The sound entitled "whistle finger" on track *I* is to be reproduced by the loudspeakers forming the "sound route" *O*. First, then, there must be a control signal in channel *9b* for ensuring that group *O* will be available during the required time. As a rule this group reproduces sounds from track *II*. "Whistle finger", however, is on track *I*, so that a control signal is needed which will switch over the input of the amplifier for group *O* from track *II* to track *I* at the appropriate moment; this signal appears in channel *11j*. When the above two signals are present, a train of 60 pulses (at a frequency of 4 per second) begins in channel *9k* and these pulses cause one of the rotary selectors (*III*) to make a full revolution. This results in the functioning of "sound route" *O*. The selector must now be returned to its starting position, and this is done by the signal "*reset k III*" in channel *9a*. To ensure that the selector returns exactly to its starting position, even if it has covered too few steps, the number of pulses in channel *9k* is made somewhat larger than the number of selector positions (60 pulses, 52 positions). The simultaneous presence of these pulses and the reset signal prevents the selector from rotating beyond its starting position.

Reset signals also appear in channels *7a*, *8a*, *10a* and *11a* for returning selectors *V*, *IV*, *II* and *I* to their starting positions.

The control signals marked *L.t. II* and *L.t. III* cause the low-note loudspeakers (which form one group) to reproduce sound from tracks *II* and *III*, respectively.

effected by selectors as used in automatic telephone exchanges (*T* in fig. 12). These are operated by signals on the control tape which consist of short pulses with a maximum repetition frequency of 10 per second. The selectors are visible at the top of the rack shown in fig. 10*a* and *b*.

If the loudspeakers of the group concerned are disposed around the auditorium, "circulating sound" is produced by letting the selectors rotate completely several times. Special control signals return the selectors to their starting position after the completion of a "sound route".

Fig. 13 shows a diagrammatic representation of the sound with the associated control signals. The sounds on the three tracks during the interval represented are indicated below, while above can be seen the control signals required for these sounds to be reproduced via the appropriate loudspeakers. Some of the signals are explained in the caption; further details would exceed the scope of this article.

The "Electronic Poem" lasts eight minutes. Each performance is preceded by an introduction in English, French and Dutch, which takes two minutes. Some twenty performances are given daily, alternately via the two installations, which amounts to many thousands of performances throughout the exhibition.

Summary. In the Philips pavilion at the Brussels World Fair performances are given of Le Corbusier's "Electronic Poem", which is a combination of light effects and electronic music involving extensive technical provisions.

The equipment for the light effects includes four large cinema projectors, eight projection lanterns, six spotlights, six ultraviolet lamps, fifty electric bulbs representing stars, and several hundreds of tubular fluorescent lamps in various colours. The luminous flux of most of these light-sources is variable by means of 30 thyratron control circuits.

The electro-acoustical installation comprises a special playback machine with a three-track perforated magnetic tape on which is recorded a composition by Edgar Varèse, 20 amplifiers each with an output of 120 W, 350 loudspeakers and an elaborate switching system with relays and telephone selectors.

The electronic control system employs a second playback machine, which scans a 15-track perforated magnetic tape. Twelve control signals differing in frequency are recorded on each track, so that 180 channels are available for controlling the light-and-sound effects in accordance with the scenario. Both playback machines are duplicated, with a view to providing a reserve as well as ensuring continuous performances.

NOISE

A GENERAL SURVEY

by K. S. KNOL *).

621.396.82

*In this inaugural address as Professor of electronics at the Eindhoven Technische Hogeschool on 17th December 1957, Dr. K. S. Knol reviewed the advances made in understanding the phenomena which give rise to reception disturbances in telecommunication engineering, and which are collectively called "noise". Among the aspects touched on were noise control and some applications of our present-day knowledge in pure scientific research and in industry. With Professor Knol's kind consent and cooperation we print below the principal contents of his address **), supplemented by a bibliography and some illustrations.*

When we try to tune our radio set to a far-distant or weak station we sometimes find that the programme does not come clearly and distinctly through the loudspeaker, but is drowned by crackling and hissing sounds. Particularly characteristic of such sounds are those heard from a frequency-modulated receiver when it is not exactly tuned in. Usually they disappear when the set is tuned to a powerful enough station.

Owners of a television set who attempt to watch a programme from a transmitter which is not within the range necessary to ensure good reception will be familiar with a sight on their screen more resembling a snowstorm than the scene transmitted from the studio.

Both phenomena — hissing and crackling from the loudspeaker and "snow" on the television screen — have the same causes, and in technical parlance the phenomena as well as the causes are collectively termed "noise".

Unattractive as the phenomena may be, the study of noise and with it the search for means of approaching as closely as possible to the natural limit to the amplification of signals, present the research worker with many fascinating problems.

The first problem that arises in this connection is: does the noise originate from inside or outside the receiver? The answer is that both may be the case. We shall first, very briefly, consider noise originating outside the receiver, that is to say noise caused by interfering signals which enter the set either via the aerial or through the cables of the electric mains. Next we shall deal in greater detail with the phenomena causing noise inside the set and which, generally speaking, set a limit to the useful sensitivity of the receiver.

External sources of noise

Interfering signals from outside the set can come from near and afar. Those from nearby may originate in electrical equipment, such as motors, gas-discharge lamps, high-frequency heating apparatus and the ignition systems of cars and other vehicles in which electrical discharges occur. Such interference is known as "man-made noise", and can be suppressed at source.

Another kind of disturbance is to be sought somewhat farther from home, but is still very terrestrial in origin. A thunderstorm within a few miles of the receiver produces, with each lightning flash, a momentary crackling in the loudspeaker. This, however, is not classed as noise. The innumerable discharges from the electrical storms that rage almost without abatement around the earth, and particularly in the tropics, cause continuous crackling interference having the character of rustling. This interference is noticeable particularly on waves that are generally longer than about 10 metres, and which reach the set after travelling a very great distance via multiple reflections between the ionosphere and the earth's surface.

The third kind of noise that can penetrate our receivers from outside is extra-terrestrial in origin, coming to us from outer space: it is called "cosmic noise". Its study has led in latter years to the growth of an entirely new branch of science, radio-astronomy [1]), the rapid progress in which has made it a most valuable complement to classical astronomy. Recent results have supplemented in many respects the astronomer's picture of the cosmos. It should be noted, though, that the radiation predicted by Van de Hulst [2]) — the 21 cm line of hydrogen — which has thrown much light on the structure of the

*) Professor at the recently founded Technische Hogeschool, Eindhoven; formerly with the Philips Research Laboratories, Eindhoven.

**) The full text of the address (in Dutch) has been published by J. B. Wolters, Groningen-Djakarta.

galactic system in particular, cannot readily be classed as noise. The narrow bandwidth of this radiation makes it possible to demonstrate its presence in cosmic noise. It is so weak, however, that it cannot be distinguished from the noise of the receiver other than by special means, and its investigation is therefore primarily a noise problem. It would exceed the scope of this survey to go any deeper into this interesting object.

Internal sources of noise

Thermal noise

The study of the electrical fluctuation phenomena which, quite independent of outside phenomena, give rise to noise in the receiver, is relatively young, dating only from the beginning of this century. Before that time the electrical methods of observation were not sufficiently advanced to demonstrate these phenomena.

A continuous irregular movement of very small particles in a liquid had, however, already been noticed in 1827 by the English botanist Brown. A satisfactory explanation of this Brownian movement, as it is called, was not forthcoming until much later. It was found to be due to the thermal agitation of the liquid molecules, which collide with the larger particles, visible under a microscope, and so cause their random movement. In 1906 Einstein and, working independently, Smoluchowski, succeeded in calculating the mean-square velocity of a particle in random thermal movement [3]), and found it to be proportional to the absolute temperature. Another significant step forward was taken when Smoluchowski predicted in 1912 that Brownian movement could cause spontaneous deflections of a galvanometer coil [4]). It was not until 1925 that such deflections could be actually demonstrated. In that year Moll and Burger reported a method of making an extremely sensitive galvanometer with the aid of a "thermo-relay" [5]). Their galvanometer was in fact so sensitive that it showed spontaneous deflections. They attributed these to microseismic disturbances. Ising [6]) was able to show, however, that these fluctuations could be largely explained by Smoluchowski's theoretical predictions.

It is evident that spontaneous and completely random movements of a galvanometer coil, small though they may be, must set a limit to the useful sensitivity which a galvanometer can be given.

In 1912 there also appeared the still quoted thesis by De Haas-Lorentz [7]) in which she studied, among other things, the effect of the thermal agitation of electrons in electrical networks, thereby continuing a line of investigation already started by Einstein.

In 1928 Nyquist and Johnson demonstrated that the thermal agitation of the electrons in resistors used in amplifiers of electrical signals also set a limit to the useful sensitivity of the amplifiers [8]). Using the laws of thermodynamics, Nyquist calculated the mean-square noise voltage, in a small frequency interval, occurring across a resistor. He found that this, too, was proportional to the absolute temperature T, and also to the value R of the resistance and the width Δf of the frequency interval, but *independent* of the frequency:

$$\overline{v^2} = 4kTR\Delta f,$$

k being Boltzmann's constant.

This result was subsequently confirmed from several quarters. In 1939, for example, Bakker and Heller [9]) calculated the noise current in a wire short-circuiting a resistance, by summing the effect of the movements of all electrons in the resistance, thereby obtaining a result analogous to that of Nyquist.

In all these calculations it is assumed that the resistance is carrying no current, the only consideration being the thermal agitation of the electrons, i.e. thermal noise.

Shot effect

Another kind of fluctuation phenomena occurs when, although there is a continuous current of particles, the particles do not behave like a column of well-disciplined troops, marching in step, but move in more random fashion. We might compare the situation with a downpour of hailstones; if we were to count the number of hailstones falling on a given area in a given time, and we repeated the count at different intervals, we should find that the totals were not identical, but fluctuated around a certain average. The same applies, for example, to the electrons travelling from cathode to anode in a thermionic valve, or to the number of quanta impinging per unit area in an X-ray image intensifier. These fluctuations also give rise to noise. Schottky, who first discovered this kind of noise in 1918 [10]), called it "Schroteffekt" and in the English-speaking countries it has become known as "shot effect".

Schottky worked out a formula for the noise current in a saturated diode, showing that the mean square of the noise current, $\overline{i^2}$, is proportional to the direct current I_s through the diode, to the electronic charge e and to the frequency interval Δf, but again independent of the frequency itself. This brings out very clearly the corpuscular character of the electron current. Schottky's formula made it possible to determine from noise measurements the charge of a

single electron; this was the first instance of the use of noise measurements as an aid to physical research. The first attempt to measure the elementary charge in this way was made by Hartmann [11]), but the result was not satisfactory. For that reason Johnson [12]) checked Schottky's calculations and found that somewhere a factor of 2 had been forgotten. The corrected formula was

$$\bar{i}^2 = 2eI_s\Delta f,$$

but this was not entirely consonant with Hartmann's results. Later the measurements were performed with greater accuracy and results obtained for e that agreed with the values found by other means.

The saturated diode, for which Schottky devised his formula, is nowadays still in daily use as a noise standard in many laboratories (*fig. 1*).

It is a fortunate fact that in most cases the noise in thermionic valves turns out to be a lot less than that in a saturated diode. In the case of valves operating in the space-charge region, where a potential minimum occurs in front of the cathode, the noise current in the anode circuit is found to be greatly diminished. Calculations of the noise current under such conditions have been made by Schottky, Spenke, Rack and North [13]), and others.

Other causes of noise in thermionic valves

In more complicated valves — for example those with more than one grid, such as tetrodes, pentodes and hexodes — a further cause of noise can be the fluctuations due to the division of the electron current between two positive electrodes (partition noise) [14]). The chance factor involved in the number of electrons striking or missing an electrode gives rise to fluctuations in the current to these electrodes.

In valves with secondary-emission electrodes an additional noise current is caused by random fluctuations in the number of secondary electrons liberated per primary electron [15]).

Noise in semiconductors

What we have so far discussed really applies only to thermionic valves that are not operated at extreme frequencies. In the electronic devices based on semiconductors, such as the crystal detectors of early radio sets and the transistors of to-day, we might also, very broadly, distinguish between thermal noise and shot effect for a certain "intermediate" band of frequencies, i.e. frequencies that are not too high and not too low. This frequency band, however, is not the same as for thermionic valves, which is hardly surprising since in semiconductors the flow of current is primarily a diffusion process at room temperature, the charge-carriers having a much lower velocity than in thermionic valves. Consequently the transit-times of the charge-carriers in semiconductors are a great deal longer and transit-time effects therefore play a part at much lower frequencies. In the case of recently-developed transistors, however, whereby use is made of an internal accelerating field, the influence of transit-time effects can be shifted to much higher frequencies.

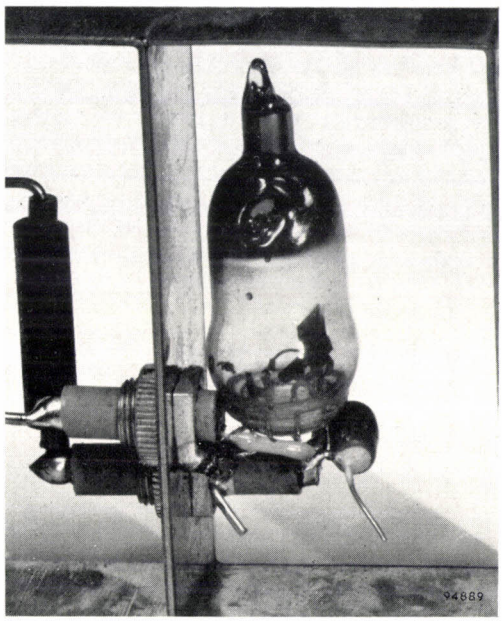

Fig. 1. A modern standard noise-diode, as described in a forthcoming article by H. Groendijk in Philips tech. Rev. **20**, 108-110, 1958/59 (No. 4).

Before dealing with the subject of transit-time effects, let us turn briefly to another and highly important type of noise, which plays a significant part in both thermionic valves and semiconductors, and which appears at very low frequencies.

Noise at very low frequencies

At very low frequencies the noise of thermionic valves and semiconductors is found to become strikingly high. In this case the mean-square noise current in a narrow frequency interval is usually inversely proportional to the frequency:

$$\bar{i}^2 \propto \frac{1}{f}.$$

The first types of point-contact transistors showed this kind of noise to a particularly marked degree.

In 1926 Schottky published a theory of this noise effect in thermionic valves [16]), which was not, however, capable of explaining all the phenomena. Schottky assumed the occurrence on the cathode of

emission centres which, for a certain time, their lifetime, emit a strong current. On the basis of a certain specific lifetime, he calculated the noise spectrum and found that at very low frequencies $\overline{i^2}$ should be constant, while at high frequencies it should decrease in approximately inverse proportion to the square of the frequency:

$$\overline{i^2} = \text{const.}\ (f \text{ low}),$$

$$\overline{i^2} \propto \frac{1}{f^2} \qquad (f \text{ high}).$$

The transition between these two regions would be expected to be at a frequency for which the period of the oscillation is of the same order of magnitude as the life of an emission centre. In practice it has almost invariably been found that $\overline{i^2}$ is still about inversely proportional to f down to extremely low frequencies. The same applies to semiconductors and resistors made of very thin films of metal or carbon through which a current is passed. In fact Rollin and Templeton have shown [17]) that with a resistor of such a kind this noise spectrum extends to frequencies of the order of 10^{-4} c/s, i.e. about 1 cycle per hour (*fig. 2*).

From Schottky's theory also followed a law for the suppression of this noise by the space charge. Measurements proved, however, that the noise suppression was quite different from that predicted by Schottky, and therefore the theory of emission centres had to be abandoned.

It seems likely that variable processes must play some part in cases where the noise is dependent on frequency. A mechanism depending on a single-valued lifetime evidently cannot give an adequate explanation of the spectrum found. It might be possible, however, to explain it by a superposition of processes of widely divergent lifetimes. Recently the existence of such many-valued lifetimes has been demonstrated in the case of energy states on the surface of germanium, by means having nothing to do with noise measurements. For this reason there is a tendency at present to assume that the spectrum in question is caused by a modulation process due to energy states of this nature. Spectra are also found, incidentally, which differ in varying degrees from the type in which $\overline{i^2}$ is inversely proportional to the frequency.

At all events, the nature of this low-frequency noise is extremely complex and manifests itself in dissimilar ways with different materials. Van der Ziel and co-workers have latterly done important work on low-frequency noise in thermionic valves [18]). One particularly interesting result is that their noise measurements have provided indications supporting the pore-conduction mechanism, postulated by Loosjes and Vink [19]), in the oxide cathode. This is a striking example of how noise investigations can be used to gain an insight into other physical phenomena.

Noise at very high frequencies

The causes of noise that dominate at low frequencies have scarcely any influence at very high frequencies. At extremely high frequencies one would even expect a decrease in the thermal noise, as a result of the effects of the quantized nature of the electromagnetic field. At normal ambient temperatures the wavelengths at which quantum effects become noticeable are so short — a few hundredths of a millimetre — that there seems no likelihood at present of their assuming any practical importance. Nevertheless, it should be possible to demonstrate these effects in the laboratory, where the means are available for producing extremely low temperatures and the necessary high frequencies in the microwave region. One would like to see cooperation to this end between specialists in microwave and low-temperature techniques.

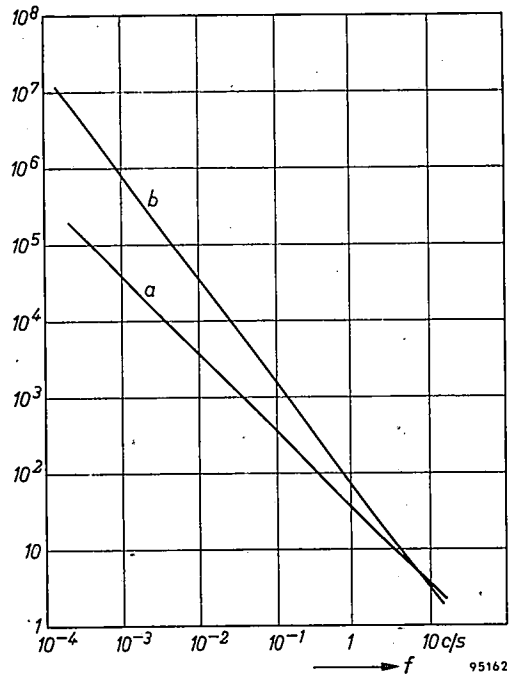

Fig. 2. Relative value of the mean-square noise current per unit bandwidth, as measured at very low frequencies by Rollin and Templeton [17]). For curve *a*, measured on carbon resistors, $i^2/\Delta f$ is inversely proportional to the frequency f; for curve *b*, measured on a germanium wire of 10 kΩ resistance, it is inversely proportional to $f^{1.35}$.

Noise phenomena are, however, noticeably influenced at high frequencies by the electron *transit-*

time effects to which we have already referred. This is manifested in two ways:

1) changes take place in the shot-effect noise current, already present at low frequencies;
2) phenomena appear that are not perceived at low frequencies.

To ascertain the effect of electron transit-times on the noise also present at low frequencies, let us consider a diode having a potential minimum due to space charge. No theory yet exists that accounts in all details for the fluctuations in the anode current for such a case. That being so, one has to resort to an idealized model, assuming that in or just beyond the potential minimum an electron beam emerges with a certain average speed, and that the density and velocity of the electrons show fluctuations around their mean values. But if we try to calculate these fluctuations and their mutual correlation in the potential minimum, we come up against a theoretical problem of considerable difficulty. One might indeed expect, at first sight, that the fluctuations in the number of electrons passing the potential minimum would be related to the fluctuations in the mean velocity of the electrons. However, when we go deeper into the matter we find that with the existing theories it is impossible to demonstrate any correlation. For this reason most investigators take the view that none exists. A mathematical approach has recently been published by Tien *et al.* [20]) in America, who have studied a much more intricate model. With the aid of a modern computer they have attempted to calculate the paths and the behaviour of numerous relatively small mutually-interacting groups of random numbers of electrons emitted successively by the cathode at identical, very short intervals. As can easily be imagined, this was a task of intimidating proportions. The result of the calculations was extraordinarily interesting as regards the expected noise behaviour of travelling-wave tubes, but it yielded no correlation between density and velocity fluctuations.

On the basis of the density and velocity fluctuations in the potential minimum as derived from the theory applicable to low frequencies, one can calculate with the aid of the existing transit-time theories the fluctuations at a position farther on in the beam or in the external circuit. Mention should be made here of the important work by Cutler and Quate [21]), who have shown that the noise in such electron tubes exhibits maxima and minima along the beam (*fig. 3*). Their work led to the development of low-noise travelling-wave tubes.

In simple diodes and triodes the transit-times are usually not long enough to allow the formation of waves. The gradually evolved theory, as finally formulated by Llewellyn and Peterson [22]), is sufficient in their case.

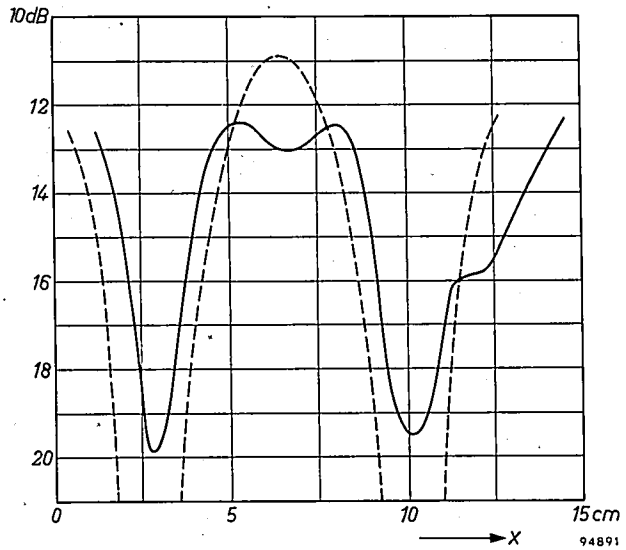

Fig. 3. Mean-square noise current in the electron beam of a travelling-wave tube, as a function of distance x from the anode (after Cutler and Quate [21])). On the ordinate is plotted the number of decibels below the level of the shot effect. The solid curve represents measured values, the broken curve calculated values. Maxima and minima appear along the length of the beam.

Among the phenomena that only become perceptible at high frequencies are *total-emission noise* and *induced grid noise* [23]). The first is due to the many electrons that return to the cathode without having reached the potential minimum. Practically all emitted electrons are involved in this process, hence the name total-emission noise. They make, as it were, brief excursions into the space between the cathode and the next electrode, and then pass directly back to the cathode. Each electron induces in the cathode circuit two equal but opposite tiny current pulses, which are only slightly displaced in time. The noise current so induced in the cathode circuit is therefore noticeable only at extremely high frequencies.

Induced grid noise is due to the fact that every electron travelling from cathode to anode via a grid induces in the grid circuit two almost identical and opposite current pulses, again slightly displaced in time. At high frequencies the pulses of all electrons together give rise to a perceptible noise current in the grid circuit. Since this current owes its existence to the electron current through the valve, there should be complete correlation with the noise current in the anode circuit; it should therefore provide us with a means of reducing the anode noise-current.

Strutt and Van der Ziel have indicated how such a noise reduction might be accomplished [24]). Unfortunately experiments show that the correlation between induced grid noise and anode noise-current is not as was expected. Various laboratories are working on the problems still to be solved in this connection, the frequencies involved ranging from several hundreds to several thousands of megacycles.

The noise characteristics of radio receivers

Now that we are familiar with some of the causes of noise in the elements of a receiver of electromagnetic waves, let us see how we should define the sensitivity of a receiver in the light of these considerations. For clear undisturbed reception of a radio or television programme, the ratio of the signal power to the noise power of the sound or picture is obviously important; it is referred to simply as signal-to-noise ratio.

Together with the signal the aerial also receives noise, the amount of which may vary according to the aerial system. To provide a basis of comparison it is assumed that the noise received corresponds to the thermal noise produced at room temperature in a normal resistance equal to the radiation resistance of the aerial.

To characterize the noise behaviour of a receiver, Friis [25]) introduced the term "noise factor", which denotes the noise-to-signal ratio — i.e. the reciprocal of the signal-to-noise ratio — at the output of the amplifier divided by that of the aerial. This definition, seemingly simple and unambiguous, must nevertheless be used with caution in practice. The reason is that the most favourable noise factor is usually obtained not when the amplification is maximum, but when the aerial is matched to the first amplifier valve, without the transmission of energy being a maximum.

The radio designer intent on building a receiver of optimum sensitivity must of course strive to keep the noise factor as small as possible. To this end he needs data from the valve manufacturer that will enable him to design a circuit which, with due regard to other requirements, such as the desired bandwidth, etc., will have the lowest possible noise factor. At the same time he wants valves that produce little noise.

The valve manufacturer, then, knows what is required of him. The demand for valve data can be readily complied with. There are various methods of specifying the noise characteristics of an amplifier valve, transistor or crystal diode without entering directly into their mode of operation. We shall mention here a very simple method first proposed by Becking [26]). He showed that the contribution to the noise of a fourpole can be fully described by imagining that a noise-voltage source and a noise-current source, which may be correlated, are connected at the input of the fourpole, which itself is thought of as being noise-free. The noise behaviour of the fourpole can then be defined in terms of four easily measured quantities, knowledge of which makes it possible to calculate the noise factor of each input circuit and, conversely, to find that circuit which gives the lowest noise factor. This is sufficient for the radio designer's needs.

The man engaged on valve research, however, is not content with the measurements of noise characteristics alone, but wishes to correlate their values with the physical phenomena inside the valve. This presents various problems that add greatly to the interest of noise investigations. We have already touched on the problem of the fluctuations in the velocity and density of the electrons in the potential minimum, and on the imperfect correlation between induced grid noise and anode noise. For total-emission noise, too, there exists as yet no theory capable of explaining the experiments quantitatively, while as regards semiconductors there are still many unknown factors to be resolved, which are essentially analogous to those of valves.

In every individual case we can try to ascertain the minimum noise factor attainable. The results will vary widely in different frequency bands. The value 1 can never be reached, for this would mean that the amplifier made no contribution to the noise. This, of course, represents the unattainable ideal. In many cases there is no need to make great efforts to reduce the amplifier noise since the noise received by the aerial on normal broadcast wavebands is so high that there is little point in making the receiver very sensitive. For short-wave and television reception, on the other hand, the noise factor can still be usefully reduced, while as regards radar and microwave links for telephony and television, noise remains a stumbling block.

On centimetric waves the lowest noise factors have so far been achieved with travelling-wave tubes. A very low noise factor is difficult to obtain with a triode because of the high level of grid noise and because of the limited noise suppression at present attainable owing to certain still not entirely explained sources of noise in triodes. Efforts are now being made, by further refining an already extremely refined technique and by adopting measures derived from deeper theoretical considerations, to fabricate triodes having a very low noise factor.

The lowest possible noise factor is of paramount importance in equipment used for measuring cosmic noise [1]). For this purpose there is a constant demand for valves and other components of lower inherent noise. One might think in this connection of using a very low-temperature gas or solid, in view of the great reduction of the contribution due to thermal noise at low temperatures. Various possibilities are being studied at the present time. It is quite conceivable, for example, that semiconductors might be made having low-temperature characteristics analogous to those of silicon and germanium at room temperatures.

An extraordinarily interesting development has been taking place in recent years, principally in America, whence the news of "microwave amplification by stimulated emission of radiation", abbreviated to "maser", was disclosed to a surprised world some years ago. The first publication on the maser (*fig. 4*) came in 1955 from Townes and co-workers [27]), who had been working on a gas. About a year later Bloembergen demonstrated that the same principle was applicable to solids [28]). Reports from Russia, too, indicate that similar principles are being applied there with success.

From calculations which seem to be reliable and from preliminary measurements, it appears that very low noise factors are to be achieved by the maser principle. Its application to solids calls for extremely low temperatures. Masers involve rather extensive set-ups, so that it does not look as if they will be put to general use for the time being. For special purposes, however, such as the measurement of cosmic noise, it is possible that the maser will find practical application in the not too distant future [29]).

It is gratifying that a new development of such significance, springing from pure scientific research, should immediately arouse universal interest and give rise to active investigations in laboratories all over the world.

Noise research in the study of physical processes

We have hitherto been discussing noise chiefly as something that limits the sensitivity of receivers, that is to say, regarding it from the standpoint of radio and valve designers. In passing we have referred to the results of noise research as an aid to the understanding of certain physical processes, but in most cases we have been concerned with noise studied as an end in itself. Quite often, however, noise research can be used as a *means* of studying physical processes. We have already mentioned radio-astronomy, the determination of the elementary charge and pore-conduction in the oxide cathode. We can also include under this head the work of Van Vliet [30]), who has been able to draw some important conclusions on electron transitions in single crystals of cadmium sulphide.

Another example is Dahlke's application of noise research for investigating the emission properties of cathodes [31]). This line of investigation is of considerable importance to the factory laboratory, showing as it has done that the effect of inadequate emission from the oxide cathode can be demonstrated much more clearly by noise measurements than by measuring, say, the valve characteristic. Many other such examples might be enumerated.

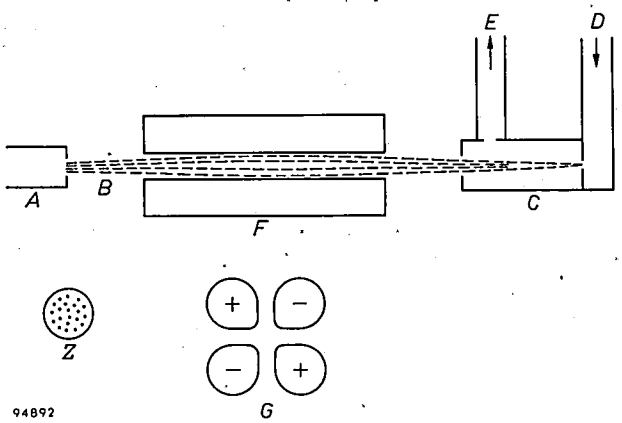

Fig. 4. Simplified diagram of a "maser" arrangement ("*micro*-wave *a*mplification by *s*timulated *e*mission of *r*adiation"; see, for example, W. H. Culver, The maser, Science **126**, 810-814, 1957). A beam B of NH_3 molecules emerges from a source A via numerous fine channels (end view Z). F is an electrostatic electrode system (transverse section G) which selectively focuses the molecules present, causing those in the upper energy-level of a certain transition to converge at C. C is a cavity resonator in which these molecules, in their transition to the lower level, give up energy to microwaves of suitable frequency fed in through waveguide D ("stimulated emission"). E is a waveguide which conveys the thus amplified microwaves to the detector. The entire process takes place in a vacuum. There is good reason to expect that this principle will make it possible to achieve very low noise factors.

Conclusion

To sum up we can say that there are three distinct groups of investigators concerned, each in their own way, with the study of noise.

The first group comprises the fundamental scientists; some, preceded by such famous men as Einstein, Smoluchowski, Zernike, Ornstein, Uhlenbeck and many others, are concerned with noise in the development of physical theory, while others use noise as a means for testing new theories experimentally or to throw light on unexplained phenomena. Until the processes taking place can be explained in physical terms it is not possible to

indicate the means of effectively combating the effects of noise.

The second group, comprising the valve manufacturers, attempts to apply the theoretical findings of the first group to the practical purpose of improving and modifying valve designs. In this way the manufacturers are enabled to supply data on the noise characteristicts of their products.

The third group, that of the radio designers, puts to use the data provided by the valve manufacturers; this of course has long been the practice as regards other valve properties such as operating characteristics, capacitances, etc. Here, too, valve theory has always been left to the valve manufacturers. Armed with the valve data, the radio designer is enabled to design his circuits so that they comply as well as possible with the requirements.

In many cases noise still represents a stumbling block to the radio designer. In radio broadcasting, radar, and some other fields of telecommunications the obstacle can to some extent be circumvented by making the signal stronger, that is to say by building more powerful transmitters, but of course there is always a limit to what can be done in this direction.

Nevertheless it may reasonably be expected that close cooperation between the above three groups, concerned in their different ways with the investigation of noise, will provide the radio listeners and television viewers of the future with a more and more perfect reception.

LITERATURE

1) See e.g. C. A. Muller, A receiver for the radio waves from interstellar hydrogen, Philips tech. Rev. **17**, 305-315 and 351-361, 1955/56.
2) H. C. van de Hulst, Ned. T. Natuurk. **11**, 210, 1945.
3) A. Einstein, Ann. Physik (4) **19**, 371, 1906.
M. von Smoluchowski, Ann. Physik (4) **21**, 756, 1906.
4) M. von Smoluchowski, Phys. Z. **13**, 1069, 1912.
5) W. J. H. Moll and H. C. Burger, Phil. Mag. (6) **50**, 626, 1925.
6) G. Ising, Phil. Mag. (7) **1**, 827, 1926.
7) G. L. de Haas-Lorentz, thesis Leiden, 1912; German edition: Die Brownsche Bewegung und einige verwandte Erscheinungen, Vieweg & Sohn, Brunswick 1913.
8) H. Nyquist, Phys. Rev. (2) **32**, 110, 1928.
J. B. Johnson, Phys. Rev. (2) **32**, 97, 1928.
9) C. J. Bakker and G. Heller, Physica **6**, 262, 1939.
10) W. Schottky, Ann. Physik (4) **57**, 541, 1918.
11) C. A. Hartmann, Ann. Physik (4) **65**, 51, 1921.
12) J. B. Johnson, Ann. Physik (4) **67**, 154, 1922.
13) W. Schottky, Wiss. Veröffentl. Siemens-Werken **16**, No. 2, 1, 1937.
E. Spenke, idem **16**, No. 2, 19, 1937.
A. J. Rack, Bell Syst. tech. J. **17**, 592, 1938.
D. O. North, R. C. A. Rev. **4**, 441, 1940 and **5**, 106, 1941.
14) See e.g. Philips tech. Rev. **2**, 332, 1937 and [32]), p. 105 et seq.
15) See e.g. M. Ziegler, Physica **3**, 1 and 307, 1936, and [32]), p. 112 et seq.
16) W. Schottky, Phys. Rev. (2) **28**, 74, 1926.
17) B.V. Rollin and I. M. Templeton, Proc. Phys. Soc. **B 66**, 259, 1953 and **B 67**, 271, 1954.
18) Communication from A. van der Ziel (unpublished).
19) R. Loosjes and H. J. Vink, Philips Res. Repts **4**, 449, 1949.
20) P. K. Tien, Proc. Inst. Radio Engrs. **44**, 938, 1956.
P. K. Tien and J. Moshman, J. appl. Phys. **27**, 1067, 1956.
21) C. C. Cutler and C. F. Quate, Phys. Rev. **80**, 875, 1950.
22) F. B. Llewellyn and L. C. Peterson, Proc. Inst. Radio Engrs. **32**, 144, 1944.
23) See e.g. G. Diemer and K. S. Knol, The noise of electronic valves at very high frequencies, I. The diode, II. The triode, Philips tech. Rev. **14**, 153-164 (especially p. 162) and 236-244, 1952/53, and [32]), p. 130 et seq. and 139 et seq.
24) M. J. O. Strutt and A. van der Ziel, Physica **8**, 1, 1941; **9**, 1003, 1942; **10**, 823, 1943.
25) H. T. Friis, Proc. Inst. Radio Engrs. **32**, 419 and 729, 1944.
26) A. G. T. Becking, H. Groendijk and K. S. Knol, Philips Res. Repts. **10**, 349, 1955.
27) J. P. Gordon, H. J. Zeiger and C. H. Townes, Phys. Rev. **99**, 1264, 1955.
28) N. Bloembergen, Phys. Rev. **104**, 324, 1956.
29) A "maser" for 21 cm has been in operation in the laboratory of Harvard University since 7th December 1957.
30) K. M. van Vliet, Current fluctuations in semiconductors and photoconductors, thesis Vrije Universiteit Amsterdam, 1956.
31) W. Dahlke, Nachr.techn. Fachber. No. 2, p. 56, 1955.
32) A. van der Ziel, Noise, Prentice-Hall, New York 1954.

Summary. The article substantially reproduces the address delivered by the author on the occasion of his inauguration as Professor of electronics at the Technische Hogeschool, Eindhoven. A survey is given of the phenomena, collectively termed "noise", which cause interference in e.g. radio and television reception. After touching briefly on the noise due to phenomena outside the receiver (man-made noise, atmospherics, cosmic noise), the author discusses at greater length the various forms of noise arising inside the receiver, e.g. thermal noise, shot-effect, partition noise and secondary-emission noise, the noise appearing at very low frequencies and noise phenomena at very high frequencies (quantum noise and transit-time effects). He then discusses the influence of noise on the useful sensitivity of receivers, and concludes with a reference to the application of noise investigations in scientific research and industry.

AUTOMATIC SORTING OF GLASS TUBING

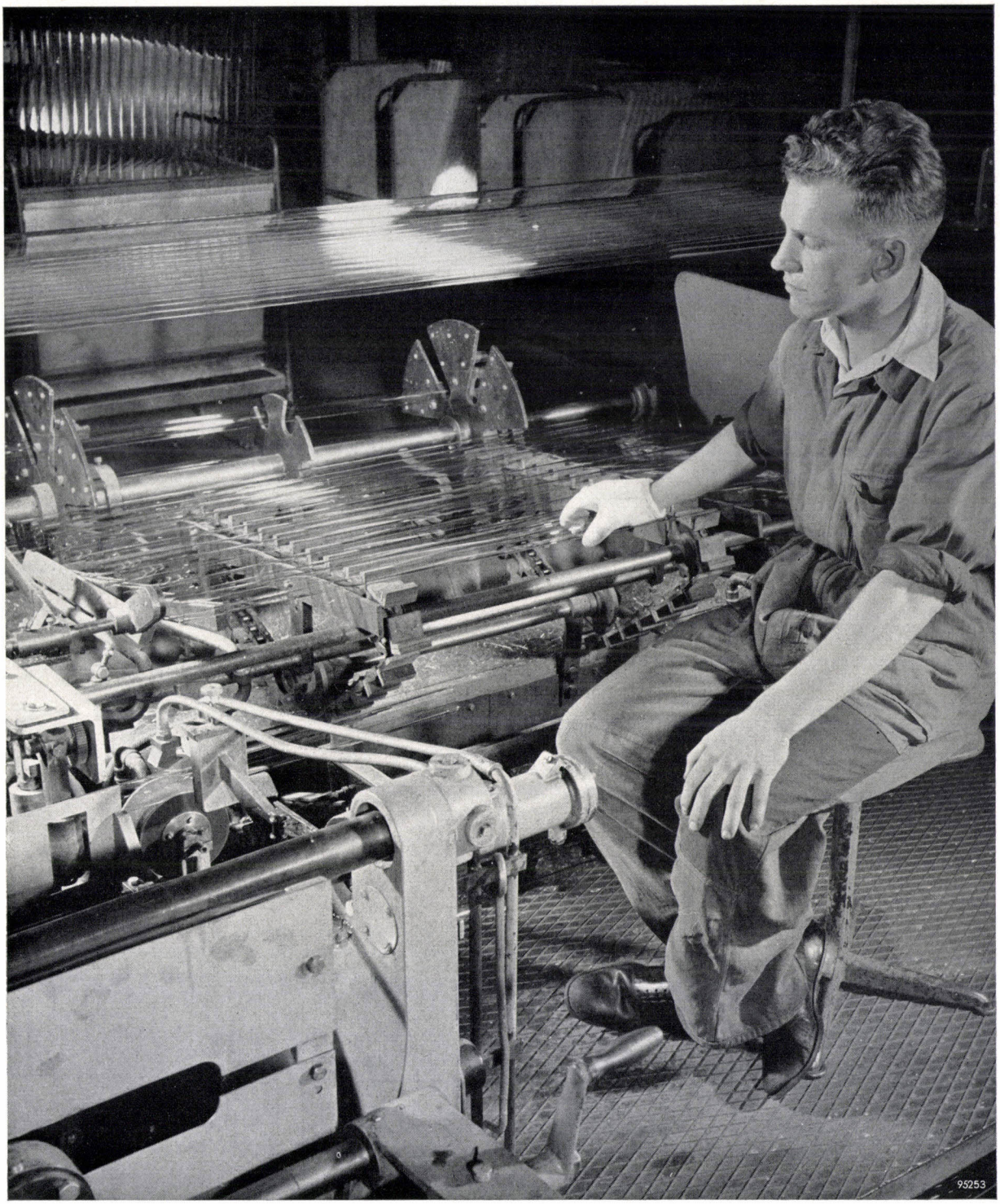

The machine shown here, in the Philips glass works at Roosendaal (Holland), is situated at the end of the glass tube drawing line. The glass tubing is fed from left to right (foreground) and automatically cut to a certain length. The moving belt transports these lengths towards the background in the photograph, where they are sorted according to diameter by rotating slotted discs. The tubing is used for the manufacture of fluorescent lamps.

THE LIFE OF BALLASTS FOR GAS-DISCHARGE LAMPS

I. TRANSFORMERS AND CHOKES

by T. HEHENKAMP. 621.327.032.43:621.314.2:621.318.42

Ballasts for gas-discharge lamps are among the articles that are required to give long service — e.g. twenty years — and to be low in price. This means that the designer must choose the insulating materials with care and ensure that they are operated at the highest temperature compatible with a reasonably long useful life. For these purposes life tests are necessary and, having regard to the long periods involved, the tests must be suitably accelerated. It is also highly important that the official regulations with which ballasts are required to comply should not hamper the development of cheaper apparatus of high quality by laying down unnecessarily low maximum temperatures.

A ballast generally consists of a choke or a transformer, often combined with a capacitor. Part I of this article is concerned with transformers and chokes. Capacitors will be dealt with in Part II, to be published later.

Factors that determine the life of a transformer

The life of a transformer (under which we include chokes for the purposes of this article) is taken to mean the time during which the transformer can operate before the insulation of the windings breaks down under the electrical field to which it is subjected. This time is determined by two quantities: the initial "reserve" of insulating strength and the rate at which this reserve falls to the zero value at which the insulation breaks down.

The reserve of the insulation depends on the *quality* of the insulating material used, on the *quantities* of these materials, and on the *manner in which they are processed.* The initial reserve can easily be ascertained by subjecting the insulation to voltages that are a multiple of those to which it will be subjected during operation. On the other hand, the rate at which the quality of the insulation deteriorates during operation — the aging rate — is much more difficult to ascertain. The following factors may be involved:

1) the electric field-strength in the insulation;
2) the mechanical load exerted on the insulating material;
3) climatic conditions;
4) the temperature of the insulating material.

In the case of transformers for gas-discharge lamps the first two factors are of subordinate importance, for these transformers are used at moderate voltages (except in neon installations, which are not considered here) and low power. Under these conditions ionization does not occur in the insulating material, and therefore the effect of the electrical field-strength on the aging rate is negligible. Because of the low power and the absence of moving parts, the mechanical forces acting on the insulation are small and hence make hardly any contribution to the deterioration of the insulation during the greater part of the life of the transformer. Only when the insulation has undergone considerable structural deterioration is the breakdown accelerated by mechanical forces (we shall return to this subject later).

Climatic influences — apart from ambient temperature — affect transformers for gas-discharge lamps only in exceptional cases. Against moisture and mould it is the usual practice to mount the ballasts in closed boxes and, if necessary, to surround the ballast with a filler.

The temperature of the insulating material thus remains by far the most important factor determining the rate of deterioration. This is true not only of transformers for gas-discharge lamps but also of a large group of other transformers. It is therefore hardly surprising that a great deal of research has been carried out with the object of learning more about the influence of temperature on the rate of aging of insulating materials.

It was long believed that a critical temperature existed which set the boundary between a negligibly slow and a fast aging rate. In about 1930, however, Montsinger [1]) demonstrated that aging occurs at any temperature. His experiments showed that a temperature-dependence exists which can be represented by the equation

$$L = A\, e^{-BT}, \quad \ldots\ldots \quad (1)$$

where L is the life, T the temperature of the insulation, and A and B are material constants. Represented graphically, with temperature on a linear scale and life on a logarithmic scale, this formula

[1]) V. M. Montsinger, Loading transformers by temperature, J. Amer. Inst. Electr. Engrs. **49**, 293-297, 1930.

yields a straight line (*fig. 1*). The constant B determines the angle which the line makes with the T axis. Montsinger found for B a value corresponding to a halving of the life for each 8 °C rise in temperature.

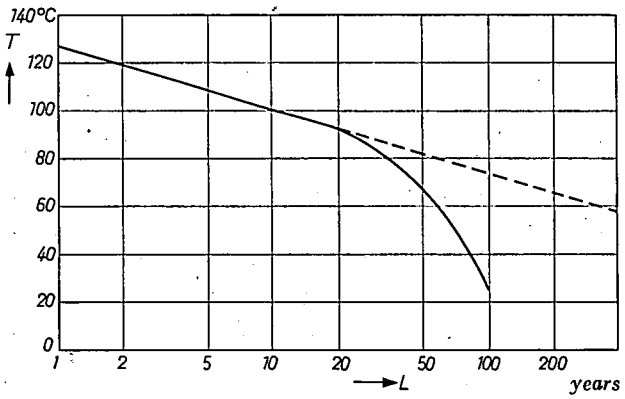

Fig. 1. Effect of the temperature T on the life L of organic insulating material in oil (graph taken from the article quoted under [1]). The straight line corresponds to equation (1), the full line giving the results of tests, and the broken portion being an extrapolation to lower temperatures. Montsinger has suggested that the curve probably deviates from a straight line at low temperatures as shown for $L > 20$ years.

From later investigations [2]) it appeared that the rise in temperature, corresponding to a halving of the life, varies somewhat, approximately from 7 to 10 °C. This variation is probably attributable in part to differences in the materials tested, but they are in any case also due to the fact that not all the tests were made in the same temperature range, the value of B being dependent to some extent on temperature.

On the basis of chemical considerations, Büssing [3]), and later Dakin [4]) arrived at a different formula, of the form

$$L = C\, e^{D/T}, \quad \ldots\ldots \quad (2)$$

where C and D are again material constants and T is the absolute temperature of the insulation. Eq. (2) implies that the life curves plotted in a graph will be straight if L is plotted logarithmically and $1/T$ on a linear scale. In many cases this formula does in fact represent the results of life tests very satisfactorily, as illustrated by the example in *fig. 2*.

If this relation between temperature and life were valid in all cases, the investigation of the various materials and of the products manufactured with them would be a simple matter, for a test at two temperatures would be sufficient to enable one to predict the life at any given temperature. Unfortunately, certain discrepancies occur, so that it is necessary to carry out life tests at a larger number of temperatures. This calls for much more extensive investigations. Another complication is that life tests on finished products are not always possible, for practical or economic reasons. One can therefore either examine the materials individually, or perform tests on simplified "models" of the products. We shall return to these alternatives later.

Choice of temperature range

Whichever method one adopts, it is very important to choose with care the temperature range in which tests are to be carried out.

It is tempting to choose a high temperature range, because of the quick results obtained in this way. The highest temperature at which tests are still possible is determined by the time needed by the product under investigation to reach this temperature. While the product is warming up, there will already be some aging of the insulation, but it is difficult to ascertain to what extent this takes place. For this reason the temperature chosen must be such that the life test is long compared with the time needed for the product to reach temperature equilibrium. In the case of small transformers this leads to a minimum time of several days.

The lowest test-temperature is decided by the accuracy one wishes to achieve in extrapolating the life curve to the normal working temperature. In view of the often wide spread in the measurements,

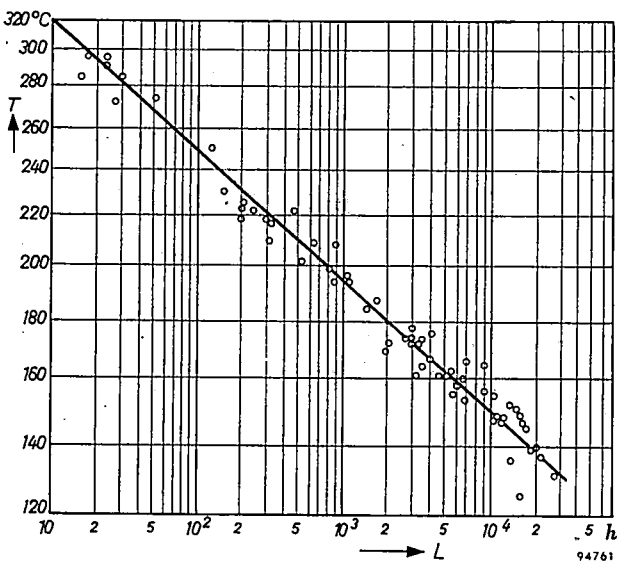

Fig. 2. Effect of the temperature T on the life L of impregnated asbestos paper (taken from article quoted under [11]). The line corresponds to eq. (2).

[2]) See e.g. G. L. Moses, Westinghouse Engr. **5**, 106, 1945.
[3]) W. Büssing, Beiträge zum Lebensdauergesetz elektrischer Maschinen, Arch. Elektrotechn. **36**, 333-361, 1942.
[4]) T. W. Dakin, Electrical insulation deterioration treated as a chemical rate phenomenon, Trans. Amer. Inst. Electr. Engrs. **67**, 113-122, 1948.

the lowest temperature should preferably not be much higher than the working temperature. Many transformers are required to give good service for some ten or twenty years. During this time they are usually not continuously under full load, but are loaded alternately or intermittently. The insulation, then, is subjected to the highest temperature only for a part of the time. For this reason a life of ten years under continuous full load is sufficient in most cases to ensure that, under practical conditions, the transformer will function efficiently for scores of years. In order to be able to extrapolate the results of accelerated life tests with reasonable accuracy to a time of ten years, the longest tests should be carried out at a temperature such that they last about two years.

To sum up, it can be said that the highest and the lowest temperature at which the tests are performed must be such as to correspond to lives of several days and several years respectively.

Life tests on component materials and on models

Among the various approaches to the problem of life tests are tests on the insulating materials themselves and tests on simplified or small-scale models of the transformers concerned. As will be shown below, however, this kind of testing does not generally lead to the required results.

Tests on insulating materials

It would offer considerable advantages if we were able to rely alone on life tests of the insulating materials themselves: the aging and loading of these materials to the breakdown limit requires much simpler equipment and is less expensive than the testing of complete transformers. Testing the material itself, however, is only of limited value, for two reasons. Firstly, there is the difficulty of ascertaining that property of the material which determines its useful life, and secondly it is often difficult to decide on the extent to which this property may deteriorate before the life test can be regarded as ended.

With insulating paper, for example, one can investigate in what way properties such as the breakdown voltage, tensile strength, bending strength, the dimensions (shrinkage) etc. change with time at various temperatures. According to Montsinger [1]) the mechanical properties are decisive, whereas Stewart and Whitman [5]) maintain that the electrical properties are of primary importance (at least in the case of transformers cooled by air or, in general, by a gas). Our own experiments indicate that the electrical properties are decisive if the insulation is loaded almost up to the breakdown limit, but that at the more common lower electrical loads (nominal voltage lower than about 1/3 of the breakdown voltage) the mechanical properties are of paramount importance.

If we know in a given case which property is the most important, there remains the problem of fixing the criterion for the end of the useful life. But even if this too is known, the difficulties are not yet over, for in practice the insulating material in transformers has so deteriorated towards the end of its life that it can no longer be handled. This greatly increases the experimental difficulties.

We shall illustrate these difficulties by some examples.

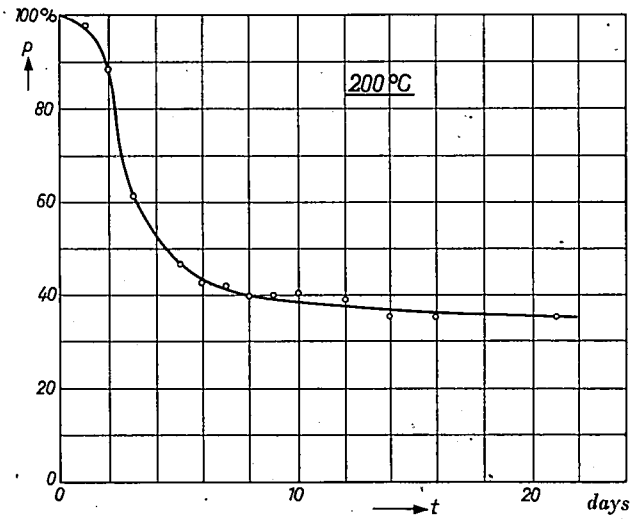

Fig. 3. Relative breakdown voltage p (alternating voltage, 50 c/s) of non-impregnated insulation cardboard 0.5 mm thick, as a function of the time t of exposure to air at 200 °C.

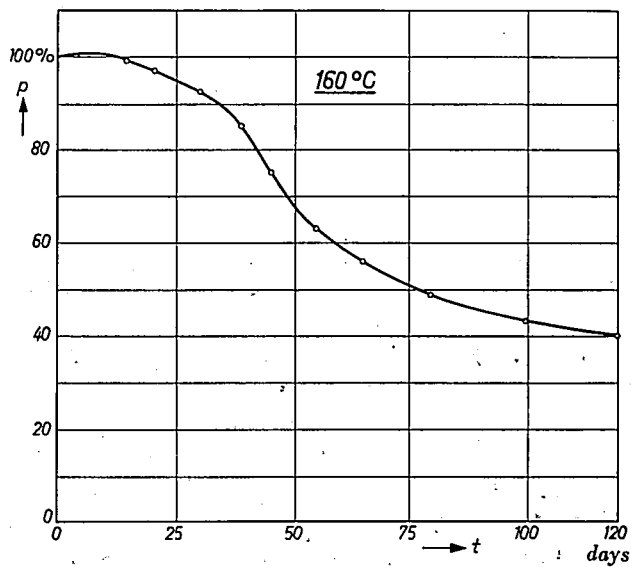

Fig. 4. As fig. 3, but in air at 160 °C.

[5]) H. C. Stewart and L. C. Whitman, Aging characteristics of dry-type transformer insulation at high temperature, Trans. Amer. Inst. Electr. Engrs. **67**, 1600-1607, 1948.

The curve in *fig. 3* shows how the breakdown voltage of non-impregnated insulation cardboard depends upon the aging time, the test being in air at 200 °C. After about ten days the breakdown voltage has fallen to 40% of its initial value. The mechanical properties have so deteriorated by that time as to make further measurements difficult. Only with a number of precautions was it possible to extend the test to 20 days. Even after this time, however, the breakdown voltage still has a value which would be completely safe in the majority of transformers.

Fig. 4 shows the results of a similar test, but now at 160 °C. Here again it was found very difficult to continue the test when the breakdown voltage had fallen below 40% of its initial value.

In *fig. 5* the data from fig. 3 and fig. 4 are compared:

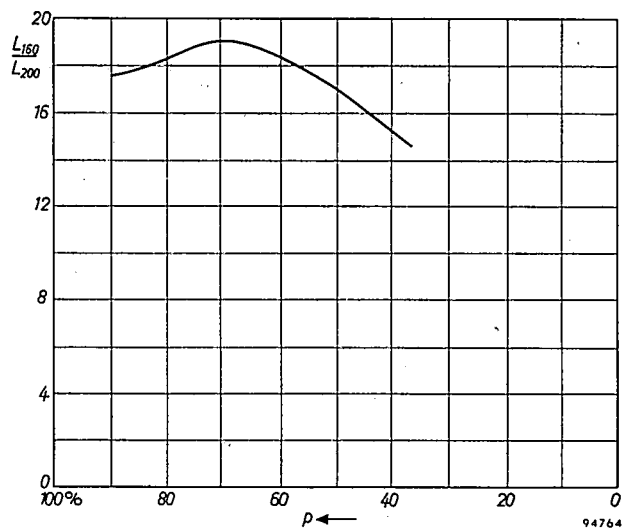

Fig. 5. The ratio of the times after which the breakdown voltage of the material in figs. 4 and 3, at 160 °C and 200 °C respectively, have fallen to the fraction p, as a function of p.

the time L_{160} in which, at 160 °C, the breakdown voltage falls to a fraction p of its initial value is divided by the time L_{200} needed for the same drop at 200 °C, and the ratio L_{160}/L_{200} is shown as a function of p. It can be seen that this ratio is by no means independent of p. This makes extrapolation of the curve to, say, $p = 10\%$, a hazardous matter.

As a second example we mention tests with "enamelled wire" (copper wire coated with an insulating lacquer). Loops of this wire were first examined for weak spots in the insulation by immersing them in a salt-water bath (*fig. 6*) and subjecting the insulation to 300 V alternating voltage. After those loops had been removed that were unable to withstand this load, the others were aged in an oven. At certain intervals they were removed from the oven in groups of ten, and subjected to a

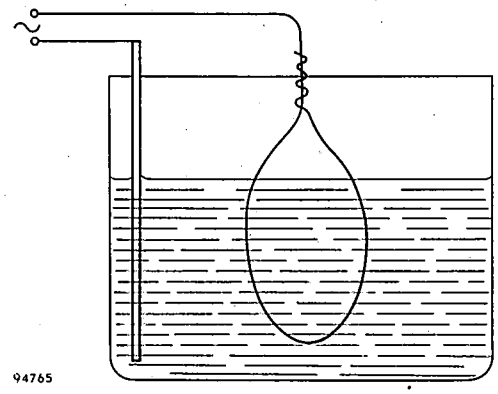

Fig. 6. Set-up to measure the breakdown voltage of the insulation on the copper wire to which figs. 7, 8 and 9 refer. Wires, bent to form a loop, are immersed in a salt-water bath and loaded to breakdown by a slowly increasing alternating voltage.

breakdown-voltage test in the water bath. *Fig. 7* and *fig. 8* show the values of breakdown voltage found as functions of the aging time in air at 200 °C and 160 °C respectively. Here, too, the ratio of the times in which a certain drop in breakdown voltage occurs at each of these temperatures is not constant (*fig. 9*).

Our third example concerns the *weight* of the insulating paper. The loss of weight is an easily ascertainable criterion for the degree of deterioration, even when the material has already lost its structural integrity. *Fig. 10* shows the ratio of the times in which, at 160 and 200 °C, the weight decreases to a fraction p of its initial value, plotted as a function of p. The form of the resultant curve differs from that in both fig. 5 and fig. 9.

The examples given and the results of many other tests have made it clear that it is necessary to know exactly what property of the material determines its useful life and at what load with respect to this property the material breaks down under practical conditions. To determine the slope of the life curve reliably (fig. 2), one must subject the material during the life test to the same load to which it would be subjected in actual operation. If we choose both the load and the permissible degree of breakdown in a relatively arbitrary manner, an entirely different slope may be found, and also the position of the curve with respect to the life axis may be quite wrong.

Having regard also to the considerable spread often found in measurements on materials, we see that it is extremely risky to draw from such tests general conclusions on the life curve of the finished product, and that the accuracy of such conclusions can often be the subject of dispute [3] [6]. These tests

[6] J. J. Smith and J. A. Scott, Temperature aging characteristics of class A insulation, Trans. Amer. Inst. Electr. Engrs. **58**, 435-444, 1939.

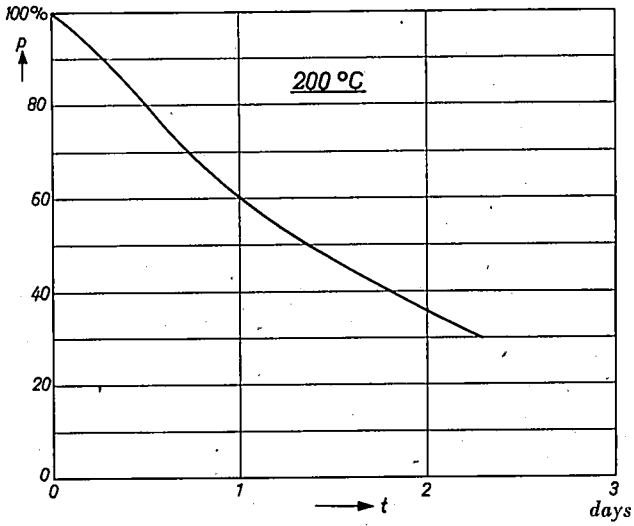

Fig. 7. Relative breakdown voltage p (A.C., 50 c/s) of 0.4 mm thick copper wire insulated with lacquer, as a function of the time t of exposure to air at 200 °C.

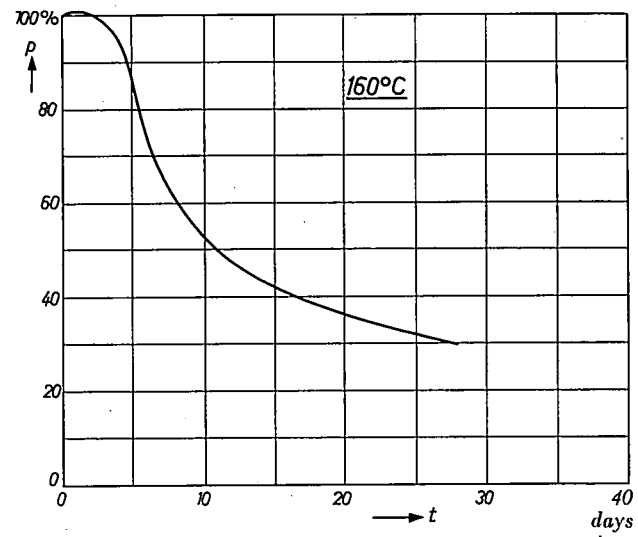

Fig. 8. As fig. 7, but in air at 160 °C.

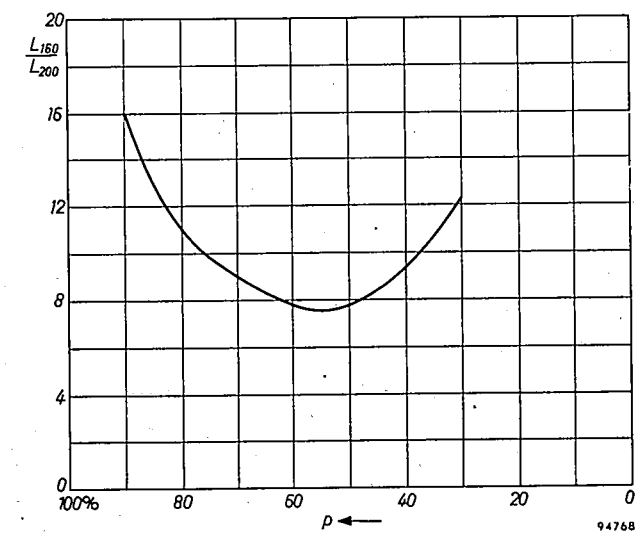

Fig. 9. The ratio of the times after which the breakdown voltage of the copper wires in figs. 8 and 7, at 160 °C and 200 °C respectively, have fallen to the fraction p, as a function of p.

can, however, give a rough impression of the performance that may reasonably be expected from the tested material when incorporated in the transformers. The final appraisal of the serviceability of the product, however, calls for more effective tests.

Model tests

Since, as we have seen, tests on individual insulating materials do not yield adequate results, while tests on complete transformers are often too costly, the solution sometimes adopted is to carry out the tests on a cheaper (often smaller) "model" of the transformer. The processing of the insulating material used and its loading in the model must correspond as closely as possible to the situation in the actual transformer. As regards loading, this can cause difficulties, since the conditions in models will generally be different from those in the actual transformer. The electrical load can usually be imitated quite well, but the mechanical load not so easily: the forces acting on the windings as a result of electric currents and electric fields may have quite different magnitudes in the model. One method of achieving a better approach to the conditions of the actual transformer is to cause the model to vibrate

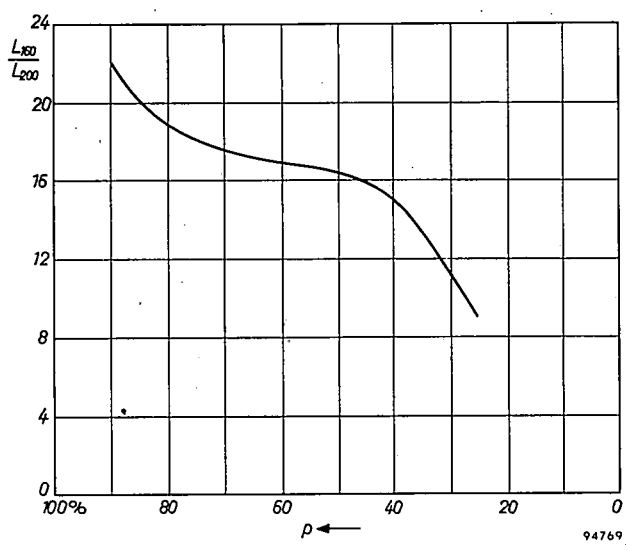

Fig. 10. The ratio of the times after which the weight of the insulating paper, at 160 °C and 200 °C respectively, have diminished to the fraction p, as a function of p.

with the appropriate amplitude and frequency [7]). Another method is to construct only the coils and just for the purpose of testing to make them into complete transformers by placing them over a core [8]). Without measures of this nature, the results

[7]) R. E. Whipple, Aging characteristics of electrical insulation, N.R.L. Report 3708, July 1950.

[8]) J. A. Scott and B. H. Thompson, Temperature-aging tests on class-A-insulated fractional-horsepower motor stators, Trans. Amer. Inst. Electr. Engrs. **61**, 499-501, 1942.

of the tests can be very misleading, as will be illustrated by the following series of experiments.

Large numbers of test models were made to simulate chokes for fluorescent lamps; their construction is illustrated in *fig. 11*. The first four

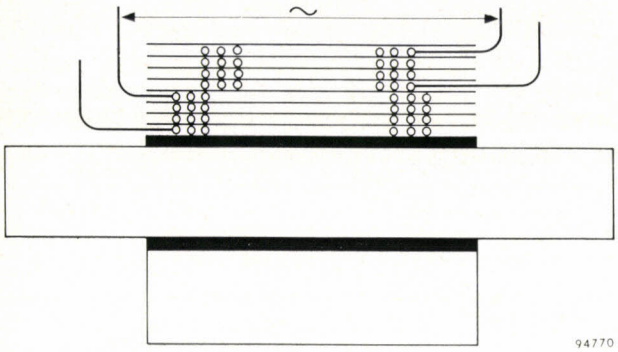

Fig. 11. Cross-section of coils for model tests. On a hollow cylindrical former of insulating material two sets of four layers of "enamelled" copper wire are wound, with intervening layers of insulating paper. The insulation between the fourth and the fifth layer was tested for breakdown. A straight iron core was inserted in the former to prevent deformation.

layers of turns are electrically insulated from the next four layers. The insulation between these groups of layers consists of lacquer + insulating paper + lacquer. The breakdown voltage of this insulation can accordingly be determined without current flowing through the windings, thus avoiding the forces which the current would otherwise occasion. The coils were supported by the core which incorporates a mounting strip (*fig. 12*), and treated

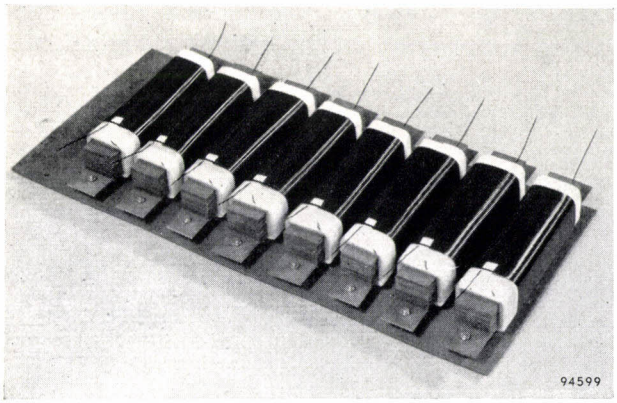

Fig. 12. Choke "models" which were life-tested under conditions of electrical loading only.

with extreme care. Thus, as opposed to the situation with the real chokes in ballasts, the loading of the models was almost exclusively electrical.

The results of the breakdown tests after various aging periods at 200 °C are shown in *fig. 13*. Three regions can be distinguished: in the first region the breakdown voltage drops very rapidly and there is a wide spread in the measurements; in the second region the breakdown voltage is almost constant and the spread small, and in the third region there is again a drop in breakdown voltage and a wider spread.

In the first region the insulation deteriorates not only electrically but also in its mechanical properties and in thickness, but it still remains intact. At this stage, then, we can speak of breakdown in the insulating material itself (*fig. 14*).

With continued aging the paper insulation begins to crack, which can give rise to paths for direct flash-over from one winding to another. The breakdown voltage is then determined largely by the distance to be bridged, hence by the thickness of the insulation beside a crack. This thickness decreases only very slowly with time, so that there is very

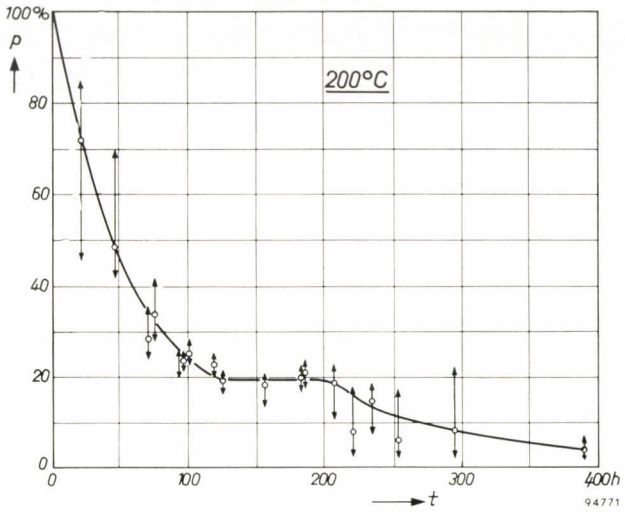

Fig. 13. Relative breakdown voltage p of the insulation between two layers, as a function of the aging time t in air at 200 °C.

little falling-off in the breakdown voltage for some considerable time (the "second region" in fig. 13). As the deterioration continues, the number of cracks shows a marked increase, the insulation disintegrates into ever smaller parts and is finally reduced to shreds. In this third region — as opposed to the others — mechanical forces have a considerable effect on the insulation, for vibrations and shocks accelerate the disintegration process. The time during which the tests can be continued is therefore partly dependent on the care exercised when handling the chokes. The sharp drop in the relative value of the breakdown voltage at 200 hours is presumed to be due to mechanical damage caused when removing the chokes from the oven for testing.

Corresponding tests at 160 °C yielded results as shown in *fig. 15*. Here, too, the first two stages can be distinguished: the third had not yet been reached after 200 days. If, as in figs. 5, 9 and 10, we again

plot as a function of p the ratio of the times in which at 160 and 200 °C, respectively, the breakdown voltage drops to a fraction p, we obtain a curve as shown in *fig. 16*. Here too, instead of a straight horizontal line we have a curve that allows no more than a rough extrapolation to a small value of p. Thus, tests on models also involve the difficulty of

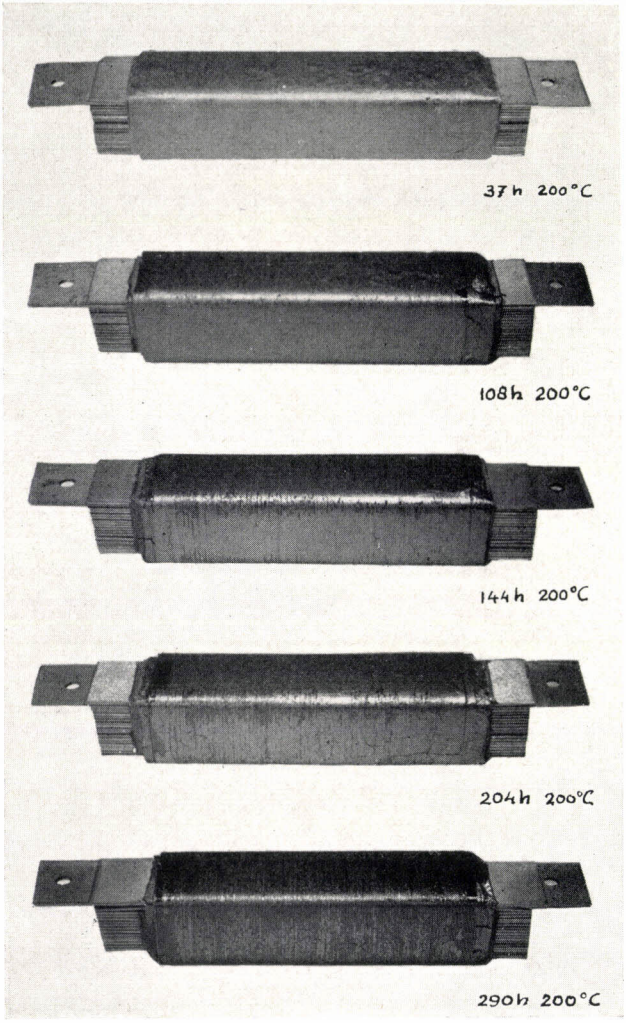

Fig. 14. Choke "models" as in fig. 12 after aging at 200 °C for 37, 108, 144, 204 and 290 hours respectively. The four outside layers have been removed to show the insulation between the fourth and fifth layer, which was that electrically tested. As aging continues, the number of cracks increases and finally the insulation disintegrates.

accurately imitating the conditions of practical operation. In order to compare different insulating systems by means of tests on models it is therefore not enough to carry out all tests under the *same* conditions, but the conditions themselves must be the *right* ones [9]).

[9]) L. J. Berberich and T. W. Dakin, Insulation, March 1956, p. 21.

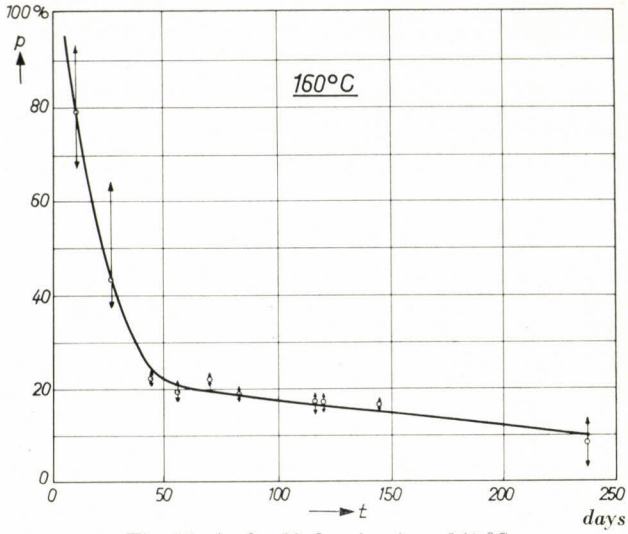

Fig. 15. As fig. 13, but in air at 160 °C.

Life tests on complete products

The foregoing makes it obvious that, if it is at all economically justified, the life tests should be carried out on complete products. The economic objections are not serious if only small transformers are concerned, such as those of ballasts for gas-discharge lamps.

To make the temperature of the insulation higher than normal, one can either increase the heat generated in the transformer itself, or apply heat externally by placing the transformer in an oven. In the following we shall give an example of both methods. In the first the heat generated in the transformer is increased by raising the current density in the windings (the test chokes were wound with thinner wire for this purpose). The second example refers to chokes that were left, unloaded, in an oven and switched on only for a short time once a day.

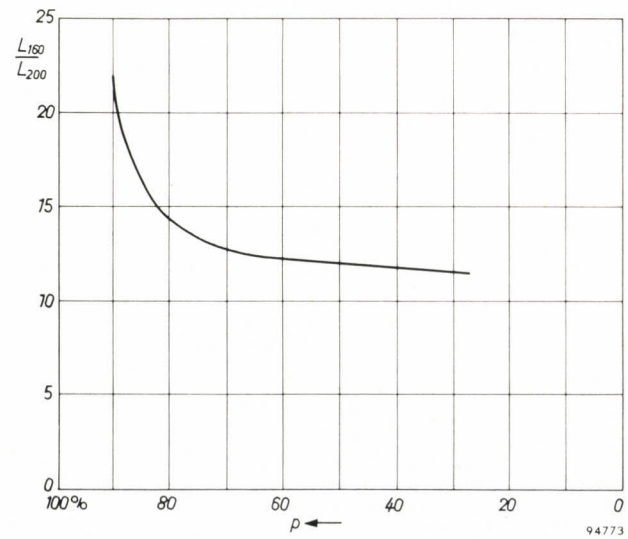

Fig. 16. The ratio of the times after which the breakdown voltage of the insulations in figs. 15 and 13, at 160 °C and 200 °C respectively, have fallen to the fraction p, as a function of p.

Other methods of increasing the current density are:

1) To raise the supply voltage. The drawbacks of this are that, owing to the strong magnetic saturation of the core, the current becomes very dependent on voltage fluctuations, and that the mechanical forces become abnormally large.
2) To introduce air-gaps in the core, or to enlarge the air-gaps. In this case, also, the forces acting on the insulation will not be of the correct magnitude.

These drawbacks are avoided by heating the chokes in an oven. In the design of conventional ovens, however, allowance is not generally made for any heat developed in the object itself, and this heat can so adversely affect the internal temperature distribution as to make the temperature control inaccurate. These difficulties can be overcome by not loading the transformers while they are in the oven (or loaded only for short times, with long intervals in between).

Tests at excess current densities

In order to study the behaviour of the insulating material used at the time in Philips ballasts for fluorescent lamps, forty chokes were constructed in 1949 which differed in only two respects from the normal types used for 40 W, 220 V (50 c/s) fluorescent lamps. In the first place the impregnation with asphalt compound was omitted in order later to be able to investigate separately the influence of different methods of impregnation. In the second place the forty chokes were divided into five groups, each being wound with wire of a different thickness. As a result of the five current densities so obtained, the insulation, which normally reached about 90 °C, now reached temperatures from 100 to 270 °C, thereby giving the desired accelerated aging. Owing to the small diameter of the coils there was no internal temperature-gradient worth mentioning. The temperature of the insulation was ascertained from the increase in the resistance of the winding and from the ambient temperature.

All 40 chokes were connected to 220 V (50 c/s), i.e. to the normal loading voltage when the fluorescent lamp is still short-circuited by its starter. At irregular intervals the installation was switched on and off in order to reproduce the switching transients occurring in actual operation.

The results of these tests are collected in *fig. 17*. It can be seen that they are in good agreement with the life formula (2). After 28 months the tests had to be ended owing to a defect in the test equipment which damaged the 8 chokes that were still under test. The measurements cover lifetimes in the ratio 1 : 400; extrapolation to 10 years is therefore readily possible.

According to fig. 17 the life of the choke at 160 °C is only about 6 times as long as at 200 °C, a fact which had not emerged from any of the tests on individual materials or on models. This again underlines the limited value of the latter tests.

Tests on unloaded chokes in ovens

In 1956 the tests described with reference to fig. 17 were recommenced. Large numbers of chokes were constructed — again chokes for 40 W, 220 V (50 c/s) fluorescent lamps — but of the design as

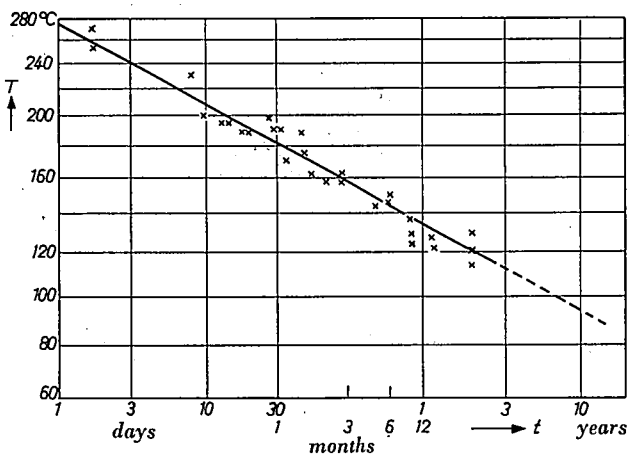

Fig. 17. The life L of non-impregnated chokes for 40 W 220 V (50 c/s) fluorescent lamps as a function of the insulation temperature T. The various temperatures were obtained by running the chokes at different current densities.

used nowadays. They were cast in the appropriate boxes with a filling material based on a polyester resin [10]) and so made into a finished product.

The insulation was raised to the testing temperatures by placing the chokes unloaded, in groups of ten, in ovens. Each group was daily connected for one to two minutes to 220 V (50 c/s) by means of a rapidly switching contact. The closing of this contact produces initial current surges about four times as high as the normal operating current; when the contact opens, voltage surges appear which are about seven times as high as the operating voltage. These loads so far exceed the severest conditions encountered in practice, both in magnitude and in duration, that in our opinion the absence of the much lower operating voltage while in the oven has scarcely any influence.

The results hitherto obtained yield points lying on a straight line (*fig. 18*) which runs parallel to the life curve of fig. 17. Owing to the better insulating materials and to the polyester-resin filling, the life of the choke at each temperature has increased more than eight-fold.

Life under practical conditions

In figs. 17 and 18 the life of the choke is the time at the end of which half of the original number of coils is still intact. Extrapolation to the temperature

[10]) T. Hehenkamp, Philips tech. Rev. **18**, 280, 1956/57.

commonly occurring in practice thus provides the time at which, at that temperature, an average of 50% of the chokes will be defective. To the user, however, this information is not so interesting; he is more interested in the time during which he can expect no serious faults to occur in his installation. To ascertain this time one must know the spread in the life of the chokes, i.e. the reject curve. Although some predictions can be made from the results of the tests described, reliable figures can only be obtained after investigating much larger numbers.

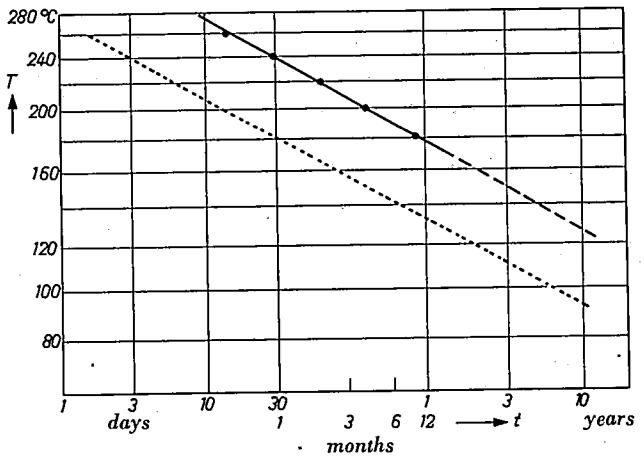

Fig. 18. The life L of chokes for 40 W, 220 V (50 c/s) fluorescent lamps (boxed, with polyester-base filler) as a function of the temperature T of the insulation. The various temperatures were obtained by heating in ovens. The life curve from fig. 17 is shown for comparison (broken line).

This is done at Philips by regularly subjecting samples from the ballasts manufactured for fluorescent lamps, sodium lamps and HPL lamps (high-pressure mercury-vapour lamps with fluorescent outer envelopes) to a life test. As long as the design is not radically modified, it is sufficient to perform this test at only one temperature. This was fixed some years ago at 180 °C.

During the years 1953 to 1956 almost 1000 of such sample tests were carried out. They showed that in 30 days — according to fig. 17 the time in which 50% failures occur at 180 °C — about 3% of the ballasts became defective. It can be concluded from this that the life curve in fig. 17 denotes the times after which about 3% of the ballasts in an installation will become defective. With such a chance of failure an installation gradually becomes due for replacement.

The corresponding figures are not yet accurately known for the ballasts with polyester filling which were recently put into production. It is expected that their life will be at least twice as long.

From these data the permissible temperature of the insulating material can be determined for any installation. For this purpose it is only necessary to know how many years the installation must operate reliably and how many hours it will be in operation during that time. An ordinary lighting installation, for example, will be required to operate for an average of 8 hours per day for 20 years. Since the temperature of the insulation does not reach its final value until about two hours after switching on, these first two hours need hardly be taken into account. As far as aging is concerned, therefore, one may reckon with an average of six hours per day, giving a total aging time of $\frac{6}{24} \times 20 = 5$ years continuous operation.

Ballasts as made in recent years have a life of 5 years continuous operation when the temperature of the insulation is 105 °C. At an ambient temperature of 35 °C this means, therefore, a rise of 70 °C in the temperature of the insulation. When the measurement is performed (as is the usual practice) at a supply voltage 10% higher than the normal mains voltage, the temperature in this measurement may without harm rise to about 80 to 90 °C; most official specifications, however, unnecessarily prescribe a temperature rise of only 70 °C.

In special cases a higher temperature may be permissible, or a lower temperature necessary. The first case arises when a much shorter life is acceptable, for example with show-window lighting which, for advertising reasons, will in many cases be replaced after a few years. On the other hand the temperature of the insulation must remain below a lower maximum value if the lighting is kept on for a longer average time per 24 hours than is assumed above, the same life being required of the installation.

The same conditions apply to the latest ballasts with polyester filling, except that the temperature of the insulation can always be 10 °C higher (i.e. 90 to 100 °C above the ambient temperature at 10% over-voltage).

Classification of insulating materials

For many years now it has been the practice in national and international specifications to classify the various insulating materials, and to lay down a maximum permissible temperature for each class.

It will be evident from the foregoing that a classification of insulating materials into, say, four or six categories, each with a maximum permissible temperature, can be little more than arbitrary. After all, there are many possibilities of appreciably improving the insulation of a transformer, thereby prolonging its life, without the necessity of using a material of a higher category. Some examples will make this clear.

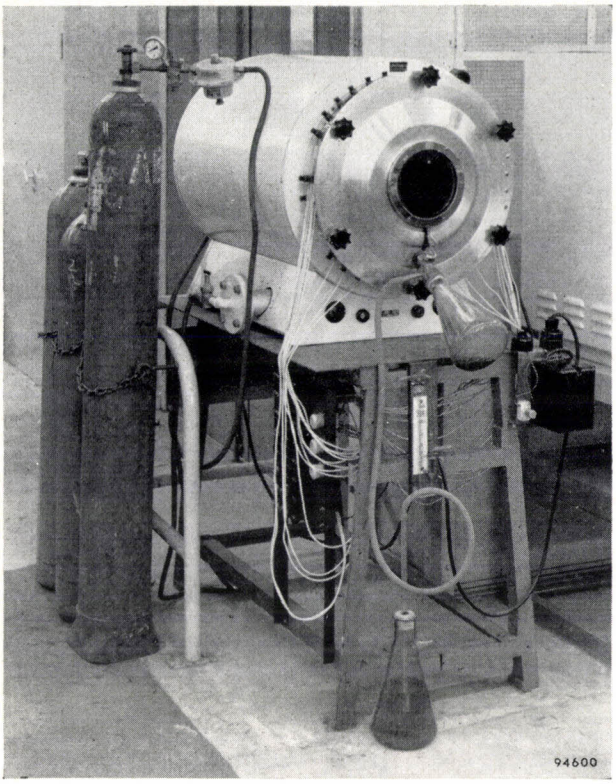

Fig. 19. Oven for life-testing transformers in an oxygen-free atmosphere.

In ballasts for gas-discharge lamps frequent use is made of copper wire insulated by a coating of lacquer ("enamelled" wire). This wire comes into a certain insulation category, but the quality of the lacquer coating varies considerably in practice, giving rise to differences in life. There are also synthetic wire-insulating materials of higher quality than good oil-based lacquers. Some specifications take these into account by permitting a somewhat higher temperature for a synthetic insulating material. This is not without its dangers, however, for some kinds are not even as good as oil-based lacquers of mediocre quality.

Another factor of influence can be the filling material which may be used to seal off the coils. It is known that the processes of deterioration are not so rapid if there is no exposure to oxygen [11]).

[11]) H. C. Stewart, L. C. Whitman and A. L. Scheideler, Aging evaluation of dry-type transformer insulating systems, Trans. Amer. Inst. Electr. Engrs. **72-III**, 267-276, 1953.

Exclusion of air by means of a filling material will therefore increase the life of the insulation, provided of course that the filler does not itself take part in any reaction which offsets the favourable effect. Whether the latter is the case can be ascertained by testing the equipment in an oxygen-free atmosphere with and without filler; an oven used for this purpose is shown in *fig. 19*. Such tests show that unsuitable filling materials shorten the life of the equipment.

In view of the fact that new insulating materials regularly appear on the market, opening up new possibilities, it is plain that classification must go very far indeed if the designer is not to be needlessly hampered in developing an optimum product.

For products that are small and cheap enough to justify life tests the classification should therefore be taken as a rough guide, after which the really permissible temperature should be determined by means of accelerated life tests. A recommendation to this effect has already been made by Stewart [11]). In the latest German specifications for ballasts [12]) this procedure has in fact been adopted [13]).

For larger and more costly transformers it will probably be possible to obtain satisfactory results by tests on models, although the necessary caution will have to be observed in view of their limited reliability.

[12]) VDE 0712, Part 2, April 1957.

[13]) C. H. Sturm, Zur Neuausgabe von VDE 0712 „Zubehör für Leuchtstofflampen", Elektrotechn. Z. **A78**, 363, 1957 (No. 10).

Summary. The life of a transformer (or choke) is the time the transformer can operate before the insulation breaks down. This time is determined by the "reserve" of insulating strength initially present, and by the rate at which this reserve decreases. The reserve depends on the quality, quantity and processing of the insulating materials employed. In the case of transformers and chokes for the ballasts of gas-discharge lamps, the rate of aging is determined primarily by the temperature of the insulation. Life tests can be accelerated by performing them at higher temperatures, e.g. by running at excess current densities or placing the product in an oven. The range of temperatures for such tests should be such that the shortest life amounts to a few days and the longest to a few years. Tests on the insulating materials themselves or on models have only limited value; for this reason, if at all economically justified, the tests should be carried out on the complete product.

LATTICE IMPERFECTIONS IN CRYSTALS, STUDIED ON ALKALI HALIDES

by Y. HAVEN.

548.7:537.311.3

Many properties of solids, including such technically important ones such as electrical conductivity and dielectric losses, cannot be explained on the basis of a purely periodic structure of the crystal lattice. The observed phenomena have therefore come to be attributed to certain deviations from exact periodicity — that is to say, to lattice imperfections. The effects of lattice imperfections on the behaviour of solids can very conveniently be studied on crystals of the alkali halides, since these substances can easily be obtained in a pure state and since in their case the phenomena are often less complicated than in other cases. In this article some results of investigations on these crystals are given, with particular reference to the dielectric properties of an alkali halide (NaCl) in which certain lattice imperfections can be produced by introducing an alkaline-earth halide ($CaCl_2$).

Lattice imperfections in crystals

Since the discovery by Von Laue, Friedrich and Knipping (1912) of X-ray diffraction in crystals and the investigation of this phenomeon by Von Laue, Bragg and many others, a great deal of work has been carried out on the spatial arrangement of the atoms in crystalline solids. It was found that the atoms in the crystal (for convenience we shall often speak of atoms even though ions are concerned) form a three-dimensional network or "lattice" and that the atoms are arranged periodically in the lattice. This is entirely in agreement with the conjecture of Bravais some fifty years earlier concerning the structure of crystals.

It subsequently appeared, however, that many phenomena exhibited by solids could not be explained on the basis of a purely periodic structure of the crystal lattice. Frequently these phenomena are closely related to those properties that are put to use for various technical purposes, especially in electrical engineering and the electronics industry. These are the properties that determine the electrical behaviour of the solid, such as electrical conductivity and dielectric losses. But there are other properties, too, such as mechanical strength, light-absorption, luminescence and certain details of crystal growth, that cannot be quantitatively explained on the assumption of a purely periodic structure. Many of the observed properties of crystals have therefore come to be attributed to certain deviations from periodicity, collectively known as lattice imperfections. Some considerations on the role of lattice imperfections in solid state phenomena were given in an earlier article published in this journal [1]).

The deviations from periodicity, whose existence was initially postulated purely hypothetically, are of many kinds. We shall discuss some of them briefly following the general lines of a survey given by Seitz [2]).

Vacancies. This term is used to designate an empty lattice site, that is, the absence of an atom at a position where, according to the crystal periodicity, there should be an atom.

Interstitial atoms. An atom is referred to as an interstitialcy when it occupies a site lying between the normal lattice sites of the crystal.

Foreign atoms. Foreign substances can be added as "impurities" to a crystal of a given compound. If the substances are distributed atomically in the crystal (thus not locally segregated) the effect will be that atoms are present in the crystal lattice which are foreign to it. These foreign atoms may occupy normal lattice sites (by substitution) or they may be in interstitial sites.

Vacancies, interstitialcies and foreign atoms have an important bearing on the phenomena to be discussed in this article.

Free electrons, electron holes, colour centres, excitons. If an electron is added to a (neutral) crystal lattice, a positive ion of the lattice is entirely or partly neutralized. In general, however, the position of the electron is not fixed, but can change from one ion to another. This, too, can be regarded as a (mobile) lattice imperfection.

Such an added electron may, for example, originate from a foreign atom ("donor") which gives up an electron to the lattice. There are also foreign atoms that deprive the lattice of an electron ("acceptors") This leaves behind a "hole" in the electron distribution, which means to say that one of the ions is then short of an electron. This state, too, provided the temperature is high enough, can shift

[1]) G. W. Rathenau, Imperfections in matter, Philips tech. Rev. **15**, 105-113, 1953/54.

[2]) F. Seitz, contribution in the book: Imperfections in nearly perfect crystals, Wiley, New York 1952, p. 3.

from ion to ion throughout the lattice. At low temperatures, however, one must rather think of the electron hole as localized; in KCl at —200 °C, for example, the hole is bound to two neighbouring Cl ions, giving rise to a Cl_2^- ion [3]).

An electron and an electron hole can also be simultaneously produced by an atom of the original lattice. The pair can then be regarded as a non-localized ionized state.

When a crystal contains yet other lattice imperfections, a certain interaction will arise between the electron and one of these imperfections, e.g. a vacancy. Sometimes the electron may then be trapped. Such an electron, owing to the selective light absorption it causes, is called a *colour centre*.

There also exist excited states of the lattice, in which one of the ions is at a higher energy level, but in which the excess energy is smaller than the energy needed for the formation of a free electron plus an electron hole. If this disturbance is free to wander throughout the lattice it is called an *exciton*.

Some other lattice imperfections are the following.

Grain boundaries. A polycrystalline solid is built op of more or less distinct crystals separated by what are known as "grain boundaries". At these boundaries there is an abrupt change in the orientation of the crystal axes, so that the periodicity is interrupted at these positions, quite apart from the degree of perfection of the crystal grains themselves.

The smaller the crystals the more numerous are the disturbances due to grain boundaries. In the extreme case the crystals are so small that the volume occupied by the affected areas is of the same order of magnitude or greater than that of the unaffected areas. The substance is then called amorphous. A familiar example is glass [4]).

Dislocations. Dislocations are linear lattice defects. A simple form of dislocation can be visualized by thinking of a lattice plane as pushed some way into the crystal, between the other lattice planes (like a snippet of paper inserted between the pages of a book). Near the edge of this interposed lattice plane the crystal is severely deformed. If foreign atoms are present in the crystal, they show a preference to settle at such regions of marked deformation.

Dislocations go a long way towards explaining many properties of metals [5]). In non-metallic substances, too, the occurrence of dislocations must also be borne in mind.

Phonons. Finally, lattice imperfections can also be caused by sound waves passing through a crystal. The deformation thereby caused moves progressively through the lattice at the speed of sound. The sound energy can be thought of as concentrated in a relatively small region (wave packet) which is termed a "phonon" (a term analogous to "photon", a packet of electromagnetic energy).

The thermal agitation of the atoms also represents a disturbance of the lattice. This may be regarded as a swarm of phonons moving through the crystal like the molecules of a gas.

It need hardly be said that, if several of these lattice imperfections are combined, they may give rise to complicated phenomena not easy to disentangle. For this reason the aim in studying lattice imperfections and their effect on various properties is to confine oneself as far as possible to cases in which it may be assumed that only one particular type of imperfection is predominant.

Such cases can often be produced artificially by taking a very pure material and subjecting it to a treatment designed to give rise to a specific imperfection. This treatment may, for example, consist in incorporating as an impurity a small quantity of another pure substance. Several investigators have adopted this method sucessfully with the alkali halides, which in very many respects lend themselves particularly well to investigations of this kind. Not only can these compounds be prepared in a pure state by relatively simple means, but they also have the advantage of possessing a simple crystal structure (monovalent ions). Since, moreover, the ionic character of these compounds is very pronounced, it is possible, in view of the fact that the attractive forces between the ions follow Coulomb's law, to compute the interaction between the particles without involving excessively complicated mathematics.

There are certain other advantages attached to the use of the alkali halides. In the first place they are transparent, which makes it easy, for example, to observe their spectral transmission. In coloured crystals, for example, the position of the absorption bands in the spectrum can be determined. In some cases particular imperfections, such as dislocations, can be made visible under the microscope by such artifices as the introduction of metal that nucleates at the lattice imperfections [6]). A further advantage of alkali halides is that various heat treatments, required in the investigations, can be carried out at relatively low temperatures.

Admittedly, information is obtained in this way on only one category of compounds and on relatively few kinds of lattice imperfections, but if detailed knowledge is thereby obtained this can serve as a point of departure for understanding, at least quali-

[3]) T. G. Castner and W. Känzig, Phys. Chem. Solids **3**, 178, 1957 (No. 3-4).

[4]) It should be mentioned in passing that the structure of glass can be described in another way, i.e. according to the now generally accepted theory of Si-O networks (Zachariasen); see e.g. J. M. Stevels, Philips tech. Rev. **13**, 293, 1951/52.

[5]) H. G. van Bueren, Lattice imperfections and plastic deformation in metals, Philips tech. Rev. **15**, 246-257 and 286-295, 1953/54.

[6]) S. Amelinckx, Phil. Mag. (8) **1**, 269, 1956.

tatively, the part played by lattice imperfections in more complicated compounds.

In the following we shall discuss some investigations on alkali halides concerned with the relation between certain lattice imperfections and electrical properties, in particular dielectric losses.

Crystal structure and lattice imperfections in alkali halides

We shall first deal at some length with several kinds of lattice imperfections postulated in alkali halides, and indicate the reasons for concluding that these imperfections exist.

The alkali halides crystallize in the cubic system, and mostly have the so-called sodium chloride structure [7]). Each alkali ion is surrounded in the ideal lattice by six halogen ions, and each halogen ion by six alkali ions.

An ideal alkali halide crystal composed of ions is theoretically a perfect insulator. In reality, however, conduction, viz. ionic conduction, is found to occur, particularly at high temperatures. This can only mean that numbers of ions depart from their prescribed positions in the lattice. One can imagine that an ion occupies an interstitial lattice site and changes its position in the crystal as an interstitial ion. However, if an ion moves to an interstitial site, it must leave behind an unoccupied site or vacancy. Frenkel remarked as early as 1926 that such vacancies must also give rise to ionic conduction, for a neighbouring ion can occupy the vacancy and in its turn leave an unoccupied site behind. The vacancy then moves through the lattice.

This kind of lattice imperfection (called a Frenkel defect) obeys the rule that electric neutrality of the crystal must always be maintained, for in a region which contains interstitial ions together with the vacancies associated with them, there is no change in the nett electrical charge.

It cannot be said *a priori* which of the two types of ion form the interstitial atoms. Fundamentally there are two possibilities:

1) positive ion on interstitial site + positive-ion vacancy.

2) negative ion on interstitial site + negative-ion vacancy.

Another combination of lattice imperfections is conceivable which also preserves electric neutrality. One can imagine that a positive ion in a certain site in the lattice is removed from the crystal and a negative ion from another site is removed from the crystal. This results in vacancies, neutrality being preserved without it being necessary to assume the presence of interstitialcies. The possibility of this kind of imperfection was first put forward by Schottky (1930).

One can also imagine a situation in which somewhere in the lattice a positive interstitial ion comes into the neighbourhood of a negative interstitial ion.

These considerations give two new possibilities:

3) positive-ion vacancy + negative-ion vacancy (Schottky defect),

4) positive interstitial ion + negative interstitial ion.

There are thus four possibilities to be taken into account in the explanation of ionic conduction in pure alkaline halides. It need not be assumed, however, that these four imperfections will be present at the same time. It has been found, for example, that many aspects of this conduction can be accounted for by assuming that only Schottky defects occur in pure alkaline halides.

Other forms of imperfection are possible when, as already mentioned, an impurity is artificially introduced, e.g. when a small quantity of a divalent metal is incorporated in the monovalent alkaline halide. If, for example, a small quantity of $CaCl_2$ is added to NaCl, the Ca^{2+} ions will be absorbed in the lattice and occupy the sites of Na^+ ions. If nothing else happened at the same time, the effect of this would be to upset the electric neutrality. One can assume that the charge disturbance is compensated by Cl^- ions simultaneously occupying interstitial sites. It is also possible, however, that the Cl^- ions occupy only their proper lattice sites, but that somewhere an Na^+ ion is missing. Our list of lattice imperfections can thus be extended to include:

5) divalent positive ion + negative interstitial ion,

6) divalent positive ion + positive-ion vacancy.

Which of these two imperfections occur in reality will appear in the following.

Ionic conduction and dielectric losses in NaCl doped with $CaCl_2$

The investigations about to be described refer to the case just mentioned in which small quantities of $CaCl_2$ (of the order of 0.01 atomic per cent) were added to NaCl crystals. According to the foregoing, each Ca^{2+} ion must be associated either with *a*) an interstitial Cl^- ion or *b*) an Na^+ vacancy. Conductivity measurements [8]) had already indicated that the second possibility was more favourable, and this

[7]) The compounds CsCl, CsBr and CsI have a different, although also cubic, structure.

[8]) See e.g. H. W. Etzel and R. J. Maurer, J. chem. Phys. **18**, 1003, 1950.

was confirmed by accurate examinations of the density of mixed crystals by Pick and Weber [9]). They found that mixed crystals of KCl-$CaCl_2$ do not increase in density with increasing $CaCl_2$ content, as one would expect if an interstitial Cl ion accompanied each Ca ion added. They found, on the contrary, that the density decreased with increasing $CaCl_2$ content, pointing to the creation of vacancies.

What now is the situation with regard to ionic conduction? We have already seen that vacancies can change their position owing to an ion occupying the vacant site and thus leaving its own site vacant. In occupying a vacant site a positive ion moves on the average in the direction of the field, while the vacancy moves in precisely the opposite direction. The Na vacancies therefore behavé as if they were negatively charged particles.

If β is the mobility of the vacancy (ratio of the mean velocity $\bar{v}$ to the field strength E), n the concentration of the vacancies (ratio of the number of vacancies to the volume of the crystal) and e the "charge" of the vacancy (= electronic charge), the conductivity is given by

$$\gamma = n\,e\,\beta, \quad \ldots\ldots\ldots \quad (1)$$

since, for a field E, the current density is $ne\bar{v}$, which is $ne\beta E$.

If an alternating electric field be applied, the current will then no longer lead the field by 90°, as does the pure displacement current in an ideal insulator, but instead leads the field by an angle $<90°$ owing to the conduction which gives a component in phase with the field. As a result a certain amount of energy is dissipated in the medium in every current cycle, in other words dielectric losses occur.

For an alternating field $E = E_m \exp(j\omega t)$ we can at once write down the mean displacement $\bar{x}$ of a vacancy, for

$$\bar{v} = \frac{d\bar{x}}{dt} = \beta E = \beta E_m \exp(j\omega t). \quad \ldots \quad (2)$$

Hence

$$\bar{x} = \frac{B}{j\omega} E_m \exp(j\omega t) = -j\frac{\beta}{\omega} E. \quad \ldots \quad (3)$$

The dielectric displacement $D = \varepsilon E$, where ε is the dielectric constant, is given by

$$D = \varepsilon_1 E + ne\bar{x} = \varepsilon_1 E - j\frac{\gamma}{\omega} E. \quad \ldots \quad (4)$$

The term $\varepsilon_1 E$ is the contribution from the "medium" *per se*, i.e. the dielectric displacement in the ideal crystal (without vacancies). The dielectric constant ε is now:

$$\varepsilon = \frac{D}{E} = \varepsilon_1 - j\frac{\gamma}{\omega}, \quad \ldots\ldots \quad (5)$$

in which the imaginary term, γ/ω, determines the dielectric losses.

May we now assume that n is equal to the concentration of the added Ca ions? That would mean that all vacancies were able to move freely. We have seen, however, that an Na vacancy behaves like a negative particle. Owing to its double charge, the Ca ion exhibits a local excess of positive charge. The vacancy will therefore be attracted by the Ca ion and will tend to occupy the site of one of the twelve Na ions surrounding the Ca ion. The vacancy is then still at liberty to occupy any arbitrary one of the twelve sites, but it will not readily be able to break away from the Ca ion, at least not at low temperatures. This situation is illustrated in *fig. 1*, in which A represents a Ca ion, B a vacancy bound to this ion and C a free vacancy. It is reasonable to assume that at room temperature, considerable numbers of vacancies are bound to Ca ions and therefore can no longer participate in the conduction. The chief problem now is to determine the ratio between the number of free and the number of bound vacancies. Closer examination of this problem leads to interesting theoretical conclusions, which we shall deal with here in some detail.

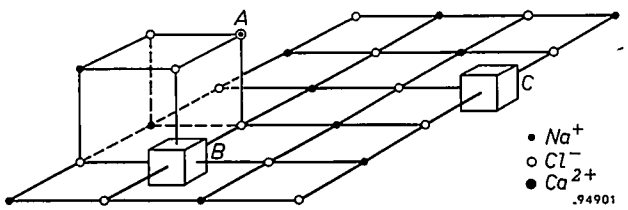

Fig. 1. Part of an NaCl lattice with an incorporated Ca^{2+} ion (A). B represents an Na vacancy bound to Ca^{2+} and C a free vacancy.

The Ca ion with a vacancy bound to it behaves like a "dipole" that can be aligned in a constant electric field. This alignment does not take place immediately after a field is applied but only after a certain delay. We may assume, as Debye did in the case of dipoles in liquids, that the total electrical dipole moment changes according to a time function

$$1 - \exp(-t/\tau).$$

The symbol τ represents a relaxation time, which is a measure of the "friction" to which the dipole is subjected in the "medium". The greater this friction, the greater is τ. Regarded atomically, τ is

[9]) H. Pick and H. Weber, Z. Phys. **128**, 409, 1950.

proportional to the average time that an Na ion must wait before it has an opportunity to move to an adjacent bound vacancy, in the absence of an external field [10]). When an alternating field is applied, the dipoles will change their orientation periodically under the influence of this field. In the first place this affects the dielectric constant of the crystal. The orientation of the dipoles will not, however, be in phase with the alternating field, but will lag in phase. Thus there will again be an imaginary contribution to the dielectric constant, giving rise to dielectric losses.

For the dielectric constant ε of a medium showing dielectric losses we can write:

$$\varepsilon = \varepsilon' - \mathrm{j}\varepsilon'', \quad \ldots\ldots \quad (7)$$

in which ε' and ε'' are both positive. According to the work of Debye

$$\varepsilon' = \varepsilon_1 + \frac{a}{1+\omega^2\tau^2}, \quad \ldots\ldots \quad (8)$$

$$\varepsilon'' = \frac{\gamma(0)}{\omega} + \frac{a\omega\tau}{1+\omega^2\tau^2}, \quad \ldots \quad (9)$$

$$\gamma = \varepsilon''\omega = \gamma\,(0) + \frac{a\omega^2\tau}{1+\omega^2\tau^2}, \quad \ldots \quad (10)$$

where γ is now the A.C. conductivity, and

$$\gamma(0) = n_{\mathrm{v}}\, e\, \beta \quad \ldots\ldots \quad (10a)$$

is the D.C. conductivity, earlier denoted γ (conductivity at zero frequency), which is attritbuable to free vacancies, having a concentration n_{v}.

The constant a is proportional to the concentration n_{d} of the dipoles (bound vacancies). According to Debye's theory,

$$a = \frac{n_{\mathrm{d}}\, p^2}{3kT}, \quad \ldots\ldots \quad (11)$$

where k is Boltzmann's constant and p the dipole moment. If d is the Na-Na distance in the lattice and hence the distance between a Ca ion and a neighbouring Na vacancy, we have

$$p = e\, d. \quad \ldots\ldots \quad (12)$$

Equations (8), (9) and (10) can each in themselves serve to define the dielectric behaviour of the crystal. We can also introduce the loss angle δ, whose tangent

$$\tan\delta = \frac{\varepsilon''}{\varepsilon'} \approx \frac{\gamma(0)}{\varepsilon_1\omega} + \frac{a}{\varepsilon_1}\frac{\omega\tau}{1+\omega^2\tau^2}. \quad \ldots \quad (13)$$

The ω-dependent term of ε' (2nd term in (8)) is here neglected, which is permissible because in the present case $a/\varepsilon_1 \ll 1$. Since ε_1 is a constant, we have that $\tan\delta$ is, to a first approximation, proportional to ε''.

In *fig. 2* the theoretical variation of $\tan\delta$ as a function of $f = \omega/2\pi$ is plotted in a double logarithmic graph. The contributions of the two terms of (13) are also plotted separately. The first term, which is due to the free vacancies, is a straight line with a slope of 45°; the second term, which represents the effect of the dipoles is a symmetrical curve. The maximum of this latter term occurs when $\omega\tau = 1$, so that $\omega_{\max} = 2\pi f_{\max} = 1/\tau$.

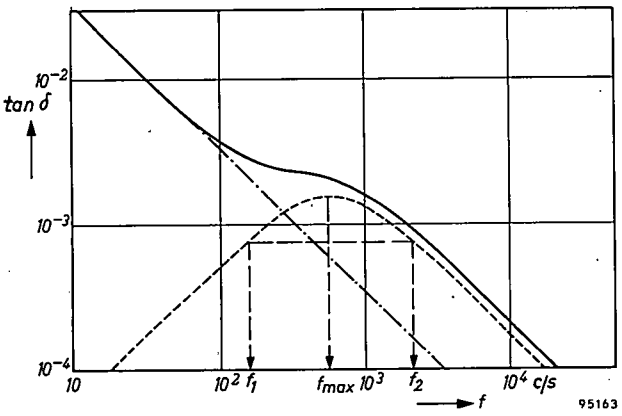

Fig. 2. Theoretical curve of $\tan\delta$ for a crystal exhibiting conduction by free vacancies and dipoles. The dot-dash line represents the contribution of the free vacancies, and the dashed line that of the dipoles. The latter curve is symmetrical with respect to $f_{\max}$, the frequency of the maximum. At f_1 and f_2 the ordinate is half of that of the maximum; $\log f_2/f_1$ is then a measure of the width of the maximum which is theoretically 1.14.

We shall now inquire into how far the behaviour of the mixed crystals of NaCl-$CaCl_2$ is consonant with the theory outlined above. For this purpose, we refer to *fig. 3* in which the measured value of $\tan\delta$ is plotted in a double logarithmic graph as a function of f, the frequency [11]).

We see that $\tan\delta$ does in fact exhibit the expected behaviour as soon as a small quantity of $CaCl_2$ is added to NaCl, whereas in the case of pure NaCl (bottom curve in fig. 3) no such behaviour is observed. It can also be seen that the losses increase with increasing $CaCl_2$ content.

If we compare the curves for 0.03 and 0.14 at. % $CaCl_2$, we see that the inflexion in the curves shifts upwards but *not* sideways as the concentration increases. This lends weight to the assumption

[10]) For the calculation of τ see: Y. Haven and J. H. van Santen, Dielectric relaxation of lattice defects in crystals, Suppl. Nuovo Cimento **7**, 605-611, 1958 (No. 2).

[11]) Y. Haven, Dielectric losses of sodium chloride crystals, J. chem. Phys. **21**, 171-172, 1953. See also Y. Haven, Diëlektrische verliezen van kristallen, Chem. Weekbl. **51**, 15-20, 1955.

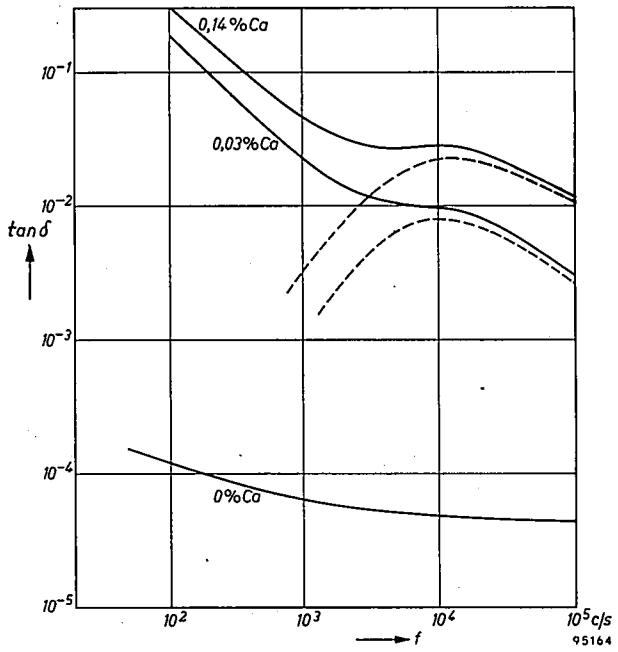

Fig. 3. Measured curves of tan δ in NaCl and in mixed crystals of NaCl-$CaCl_2$. The ratio Ca/Na is given as atoms per cent.

that the inflexion in the curve is due to dipoles. This assumption is also borne out by the fact that the width of the curve representing the dipole contribution (see caption, fig. 2) is more or less in agreement with the width theoretically expected. The width found was 1.2 to 1.3 times the value expected. This is presumably attributable to subsidiary effects neglected in the simplified theory.

Fig. 4 shows the behaviour of the losses as a function of temperature for a specific $CaCl_2$ content. The maximum of the broken curve (dipole contributions) shifts to the right, i.e. to higher frequencies with increasing temperature. Since $\omega_{max} = 1/\tau$, this means that τ decreases with rising temperature, that is, that the rotational mobility of the dipole increases, as was to be expected. The height of the maximum (determined by the value of a, and hence that of n_d) also rises slightly. We shall return to this effect later. On the basis of the picture outlined above the sum of the concentration n_v of the free vacancies and the concentration n_d of the dipoles is equal to the concentration n_{Ca} of the Ca ions added to the crystal:

$$n_v + n_d = n_{Ca}.$$

It can be shown that we can reasonably assume this to be the case at moderately high temperatures (~1000 °K). In that case n_v and n_d can, in principle, be determined from the chemical equilibrium:

$$\text{free } Ca^{2+} + \text{free Na vacancy} \rightleftarrows Ca^{2+} + \text{bound vacancy}.$$

In this reaction we can apply the law of mass action:

$$\frac{n_{\text{free}Ca} \times n_v}{n_d} \approx \frac{n_v^2}{n_d} = K, \quad \ldots \quad (14)$$

where K is the equilibrium constant (dependent on the temperature) for the reaction, given by

$$\ln K = C - \frac{q}{kT}, \quad \ldots \quad (15)$$

in which q is the "dissociation energy" per dipole and C is again a constant, related to the Ca concentration. Hence with increasing temperature, K increases also. For $T = 1000$ °K we estimate $n_v/(n_v + n_d) = n_v/n_{Ca} \approx 0.8$, showing that at this temperature most of the vacancies are free vacancies.

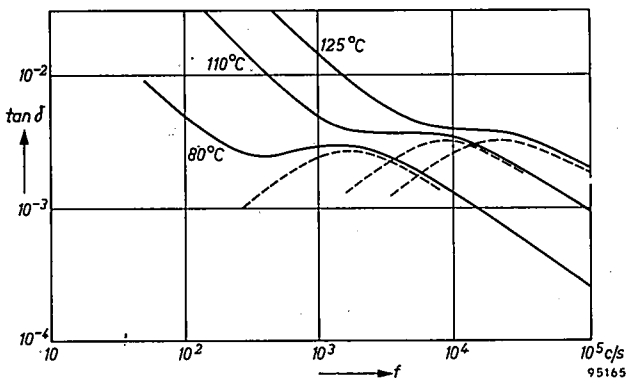

Fig. 4. Curves of tan δ against frequency f in a mixed crystal of NaCl-$CaCl_2$ at different temperatures. The broken lines represent the dipole contributions.

Putting $n_{Ca}/K = z$ and introducing the "degree of dissociation" $a = n_v/n_{Ca}$, we may write equation (14) in the form

$$\frac{a^2 z}{1-a} = 1. \quad \ldots \quad (14a)$$

This leads to

$$\frac{n_v}{K} = az = -\tfrac{1}{2} + \sqrt{z + \tfrac{1}{4}}, \quad \ldots \quad (16)$$

and

$$\frac{n_d}{K} = (1-a)z = z + \tfrac{1}{2} - \sqrt{z + \tfrac{1}{4}}. \quad \ldots \quad (17)$$

In the case of (16), we see that $az \approx z$ when $z \ll \frac{1}{4}$, and $az \approx \sqrt{z}$ when $z \gg \frac{1}{4}$. For (17) we have $(1-a)z \approx z^2$ when $z \ll \frac{1}{4}$ and $(1-a)z \approx z$ when $z \gg \frac{1}{4}$. Both functions are shown in *fig. 5*. This figure also shows the curve of a as a function of z. For $z \ll \frac{1}{4}$, $a \approx 1 - z$, and for $z \gg \frac{1}{4}$, $a \approx 1/\sqrt{z}$. As $z \to \infty$ the value of a slowly approaches zero. From this we see that at high temperature (large K) and not too large n_{Ca}, the value of a approaches unity and hence $n_v \approx n_{Ca}$. The dissociation is then practically complete. At low temperature (small K) and large n_{Ca} we find $1 - a \approx 1$ or $n_v/n_{Ca} \approx 0$, and hence $n_d \approx n_{Ca}$, which means that there is almost complete associaton.

Having estimated in this way the value of n_v (strict accuracy being neither necessary nor possible), we can now derive from the D.C. conductivity $\gamma(0) = n_v e \beta$ the mobility β of the free vacancies. Clearly, β, like $\gamma(0)$, is very dependent on temperature.

At the low temperatures, e.g. about 100 °C, at which our experiments were performed, one is no longer so certain whether the above-mentioned condition $n_v + n_d = n_{Ca}$ is satisfied or whether the equilibrium discussed gives a true picture of the

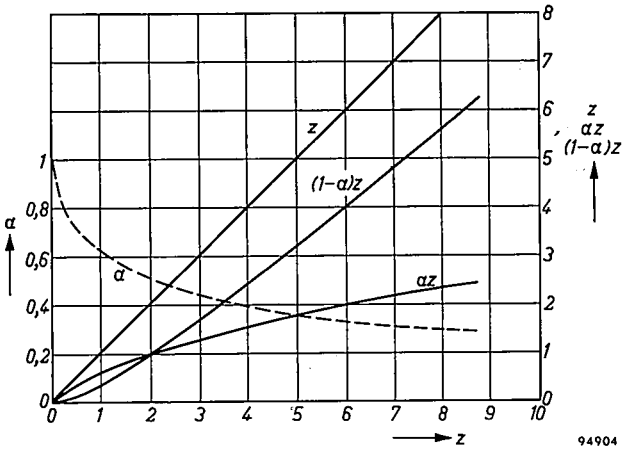

Fig. 5. Graph of αz, $(1-\alpha)z$ and α as a function of $z = n_{Ca}/K$, to illustrate the chemical dissociation equilibrium $\alpha^2 n_{Ca}/(1-\alpha) = K$ (see eq. 14a).

situation in the crystal. One can then, however, acquire information about n_v and n_d independently.

On the assumption that equation (11) is correct, we can determine n_d from the value of α, i.e. from the tan δ curve.

As regards n_v, we earlier calculated its value (approximately) at high temperatures from equations (14) and (15) and derived the values of β from the measured values of $\gamma(0)$ at those temperatures; now at low temperatures we can conversely derive n_v from the value of $\gamma(0)$ measured at these low temperatures. This value is, of course, found by extrapolating $\omega \tan\delta$ to $\omega = 0$. To find n_v, however, we must also know the value of β at low temperatures. Now, at high temperatures, the relation between β and T can be represented by an empirical formula of the form:

$$\beta = \frac{A}{T} \exp\left(-\frac{B}{T}\right). \quad \ldots\ldots \quad (18)$$

The value of β at low temperatures can thus be estimated by extrapolating the curve corresponding to (18) to the temperatures in question.

No more than a rough estimate is obtained in this way: the values of A and B reported by various investigators show quite considerable disparities, indicating that extrapolation to low temperatures involves a rather high degree of uncertainty. In *Table I* are given the values of A and B as found by different investigators, and also the corresponding values of β (in units of (m/s)/(V/m) = m²/Vs) for $T = 1000$ °K and 383 °K.

Table I. Values of A and B in (18) as estimated by various investigators, and the associated values of β at 1000 °K and 383 °K [12]). The symbol ν represents the average frequency (derived from β) at which Na^+ ions jump to free vacancies (at 383 °K).

Investigator	A	B	β (m²/Vs)		ν
			1000 °K	383 °K	
Etzel-Maurer	1.96	9860	10.5×10^{-8}	3.4×10^{-14}	3.5×10^{3}
Lidiard	2.12	9750	12.8	5.2	5
Bean	0.46	9050	5.5	7.1	7
Haven	0.225	8360	5.2	20	21

It can be seen that at 1000 °K the values of β differ by a factor of about 2, and at 383 °K by a factor of about 6.

In *Table II* second column, are set out the number of free Na vacancies per Na^+ ion (n_v/n_{Na}) calculated from the author's measurements of $\gamma(0)$ and β, as a function of the total number of Ca^{2+} ions per Na^+ ion (n_{Ca}/n_{Na}) given in the first column. The fourth column gives the number of dipoles (n_d/n_{Na}) calculated from the dielectric losses.

Table II. Number of free and bound vacancies per Na^+ ion (2nd and 4th columns) in mixed crystals of NaCl-$CaCl_2$, as a function of the total number of Ca^{2+} ions per Na^+ ion. The figures in the third and fifth columns indicate the vacancies as a fraction of Ca^{2+}.

n_{Ca}/n_{Na}	Free Na vacancies (n_v)		Bound Na vac. (n_d)	
	n_v/n_{Na}	n_v/n_{Ca}	n_d/n_{Na}	n_d/n_{Ca}
0.6×10^{-4}	0.003×10^{-4}	0.005	0.08×10^{-4}	0.13
1.0	0.016	0.016	0.16	0.16
1.7	0.028	0.016	0.60	0.35
2.5	0.043	0.017	0.9	0.36
3.6	0.07	0.019	1.5	0.42
5.2	0.11	0.021	3.2	0.62
9	0.13	0.014	3.0	0.33
17	0.19	0.011	6.2	0.36
27	0.3	0.011	6.7	0.25

In *fig. 6* the values of n_v/n_{Na} and n_d/n_{Na} from Table II are plotted against n_{Ca}/n_{Na}. The values of n_v/n_{Na} have been multiplied by 10, partly for reasons of clarity in the graph and partly to allow for a possibility that the values of β used in our calculation might have been too large (see author's value Table I). The sum $n_d/n_{Na} + 10\, n_v/n_{Na}$ is plotted as the broken curve. It may reasonably be assumed that this curve represents an upper limit to the values of $(n_v + n_d)/n_{Na}$.

[12]) Y. Haven, Concentration and association of lattice defects in NaCl, Rep. Conf. on defects in crystalline solids (Bristol 1954), 1955, pp. 261-272.

If the situation is completely in accord with the equilibrium ($n_v + n_d = n_{Ca}$) assumed above, we should find for $(n_v + n_d)/n_{Na}$ a 45° line. We see that, for $n_{Ca}/n_{Na} \leqslant 5\times10^{-4}$, the values found remain 20 to 40% below that line; at higher concentrations the deviation is still greater, for the values are roughly constant.

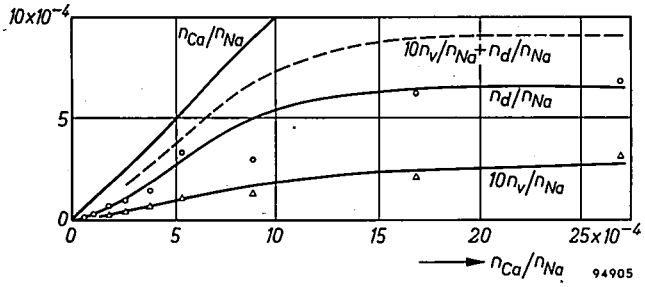

Fig. 6. Values, taken from Table II, of n_d/n_{Na} and n_v/n_{Na} (the latter $\times 10$) plotted against n_{Ca}/n_{Na}. These curves should be compared with the theoretical curves in fig. 5. The substantially horizontal parts of the curves at high Ca concentrations indicates segregation of $CaCl_2$.

The substantially constant values found at Ca^{2+} concentrations greater than about 10^{-3} is probably because, at these concentrations, the solubility limit of $CaCl_2$ in solid NaCl is exceeded, in which case the surplus $CaCl_2$ is precipitated. In analogous cases, e.g. in NaCl to which $PbCl_2$ or $CdCl_2$ had been added, it has been possible to observe this precipitation in that the formerly transparent crystal becomes turbid (a milky clouded appearance due to the different refractive indices of $PbCl_2$ and $CdCl_2$).

Confining our attention to the smaller concentrations ($n_{Ca}/n_{Na} < 5\times10^{-4}$), it would be very agreeable if we were able to compare the form of the n_v and n_d curves with the theoretical curves of fig. 5. This is not readily possible, however, partly because of the uncertain value of n_v and partly because the value of the reaction constant K at low temperature is not accurately known.

The fact that the values found for n_v and n_d are smaller than corresponds to $n_v + n_d = n_{Ca}$ does not in itself prove that the equilibrium that we assume with some justification at high temperatures is no longer valid at low temperatures. It is quite conceivable that the real values of n_v and n_d are larger than the values derived from observations. As regards n_d it may well be that a smaller value for the dipole moment p should be inserted in (11) than the value ed from (12): it is possible that the Ca ions in their holes are slightly attracted towards the Na vacancies, so that the length of the dipole becomes smaller than d. If we do not assume that the too low values derived for n_v and n_d are entirely attributable to such an effect, we must necessarily conclude that yet other combinations of Ca^{2+} ions and vacancies are possible at low temperatures, i.e. more complex configurations which do not contribute to the dielectric losses. The increase in $(\tan\delta)_{max}$ with increasing temperature, to which reference has already been made (fig. 4), might point to this: at higher temperatures the more complex configurations become dissociated.

In this connection it should be pointed out that the above conjecture that the Ca^{2+}-vacancy spacing is less than the normal Na^+-Na^+ spacing d might conceivably go so far that the spacing becomes $\frac{1}{2}d$. In that case the Ca^{2+} ion is interstitially positioned between two Cl^- ions, as illustrated in *fig. 7*. One can also regard this as a $CaCl_2$ molecule that has replaced two NaCl molecules, with the result that two vacancies are created, one on each side of the Ca ion. Such a configuration would have zero dipole moment.

It is also conceivable that more complex configurations exist which do have a dipole moment, and hence also contribute to the losses, but for which the relaxation time τ differs from that applicable to the simple dipoles, so that ω_{max} (fig. 2) has a different value. In fact some loss-curves measured at low temperatures give indications of extra maxima outside the principal maximum caused by the dipoles.

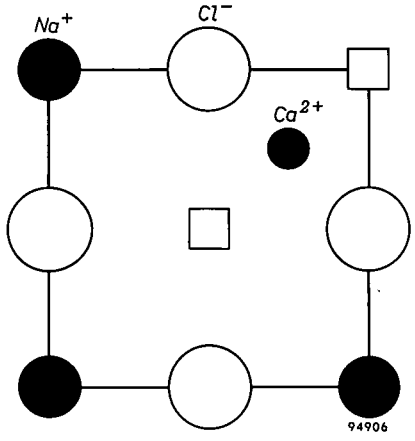

Fig. 7. Possible interstitial position of a Ca^{2+} ion between two Cl^- ions. The squares represent Na vacancies. This configuration has zero dipole moment.

Finally it should be mentioned that in silver halides, e.g. in mixed crystals of AgBr-$CdBr_2$, dipole concentrations n_d have been found that are substantially lower than the concentration of foreign ions, namely about 60% lower (on the assumption that the dipole moment is given by ed [13]).

[13]) J. Teltow and G. Wilke, Naturwiss. **41**, 423, 1954.

The mechanism of the movement of vacancies

As we have seen above, ionic conduction takes place both in pure NaCl and in mixed crystals of NaCl and $CaCl_2$ owing to Na ions moving to neighbouring vacancies and in their turn leaving a vacant site behind. With AC conduction in NaCl-$CaCl_2$ the vacancies that are bound to Ca ions also contribute to the conduction; the Na ion that fills such vacancies then becomes one of the positive neighbours of the Ca ion.

The question now arises in what way an Na ion, whether "free" or "bound" moves through the lattice to an Na vacancy. At all events the Na ion has to force its way between the surrounding Cl ions, that is to say it must cross a potential barrier. To do so it requires a certain activation energy which it can draw from the thermal agitation.

An Na ion is surrounded in the crystal lattice by six Cl ions which form the corners of an octahedron, as illustrated in perspective by *fig. 8*. The Cl ions *A* and *B* lie in a plane parallel to the plane of the drawing (a (110) lattice-plane, diagonal plane of the cubic unit cell), and the ions *C*, *D*, *E* and *F* lie in front and behind this plane at distance of $\frac{1}{2}$Cl-Cl. Two extra Cl ions are shown, namely *G* and *H*, also in the first-named plane.

At *K* there is an Na ion and at *L* a vacancy. The Na ion can move to the vacancy in a straight line via point *1* (midway between *C* and *D* in the 110 plane), or, as shown by the broken line, via points *2* (midway between three Cl ions) and *3* (midway between four tetrahedral Cl ions), or again it can follow a path somewhere between these extremes, for example via point *4*, which lies just as far from the Na ion *M* as does point *K*. In considering which of these paths is most probable, we must take into account mainly the following contributions to the potential energy:

1) Coulomb energy,
2) polarization energy, and
3) repulsion energy.

It has not yet proved possible to calculate the absolute height of the potential barrier for the various paths, but the above-mentioned measurements of dielectric losses and the electrical conductivity permit some qualitative statements to be made.

We are interested in the first place in the difference between the jump to a free vacancy and the jump to a bound vacancy. The most important factor here is the repulsion which the jumping Na ion suffers from the extra positive charge of Ca^{2+}, i.e. the difference in the Coulomb energy contribution in consequence of the presence of Ca^{2+}.

At *M* in the figure an Na ion is shown that also lies at a distance of $\frac{1}{2}$Cl-Cl or $\frac{1}{2}$Na-Na in front of the plane of the drawing. We now imagine this ion to be substituted by Ca^{2+}. This gives a Coulomb contribution to the potential energy amounting, for the points indicated in the figure, to:

K or *L*	*1*	*2*	*3*	*4*
3.592	4.165	3.326	3.064	3.592 eV

Movement of the Na ion in from *K* (or *L*) to the positions *1*, *2*, *3* or *4* thus involves the following changes (due to Coulomb interaction *alone*) in the required activation energies:

1	*2*	*3*	*4*
+0.57	−0.27	−0.53	0 eV

The actual net change in potential energy is probably smaller, since the polarization energy has a compensating effect, but we may safely assume that, owing to the presence of the Ca, the already difficult path via *1* becomes even more difficult, and that via *2* and *3* easier.

This is more or less in agreement with what we may conclude from the observations about the jump frequencies. The jump frequency of Na^+ to a bound vacancy at 110 °C can be calculated as 40×10^3 per sec. On the other hand the value of the jump frequency ν to a *free* vacancy can be derived from

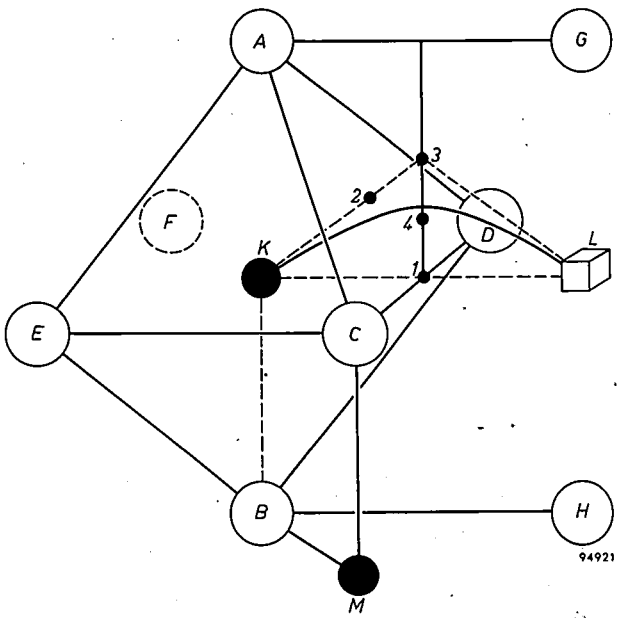

Fig. 8. Perspective sketch of a part of an NaCl crystal, with a (110) plane (diagonal plane of cube) parallel to the plane of the drawing. *A* ... *H* represent Cl ions, *K* an Na ion, *L* a vacancy, *M* an Na ion that can be replaced by a Ca ion. The possible paths of an Na ion are indicated (via *1*, via *2* and *3*, and between *3* and *4*).

the quantity β [14]). The values found, varying from 3.5×10^3 to 21×10^3 per sec, are given in Table I.

Comparison of the above values for the jump frequencies, incomplete as they may be, indicate that the potential barrier is somewhat lowered in the presence of a Ca^{2+} ion. It is reasonable to assume that the most favourable path for the Na^+ ion is a bent path passing, for example, between points *3* and *4* in the figure. This applies both for the jump to a free and to a bound vacancy, for we cannot expect the route to be greatly altered by the presence of Ca^{2+}.

Ionic conduction in silver-halide crystals

In connection with the results discussed above, we shall now briefly mention some particulars concerning silver-halides. Since these are also monovalent compounds one might be inclined at first sight to believe that conduction takes place in these crystals in the same way as in the alkaline halides, namely by means of free vacancies (Schottky defects). In fact, results resembling those for alkaline halides are obtained when a Cd halide is added as an impurity to Ag halides. An Ag^+ ion is then replaced by Cd^{2+} giving rise to Ag^+ vacancies, which cause conduction. In the pure halides AgCl and AgBr, however, there is evidently a preference for a different kind of lattice imperfection, viz. Frenkel defects, whereby Ag vacancies are associated with interstitial Ag ions (case 1 of the section dealing with lattice imperfections in alkaline halides). In this case, too, of course, the vacancies can cause conduction. However, the interstitial atoms also contribute to the conduction, and since these are approximately four times as mobile as the vacancies, conduction in the pure compounds is mainly due to the interstitial atoms.

Conduction due to interstitial atoms is an indirect effect. One must assume that an interstitial atom displaces a regular lattice atom and occupies its site, and that the displaced atom is driven to an interstitial site, from which the process can be repeated.

The latter conclusion was drawn by comparing the diffusion constant of Ag ions in the crystal with its contribution to the ionic conductivity.

Colour centres in mixed crystals of NaCl-$CaCl_2$

Finally, returning to the mixed crystals of NaCl-$CaCl_2$ which we have already considered in some detail, we shall now consider what happens in these crystals when, besides the existing vacancies, other lattice imperfections, namely colour centres, are present.

When a pure alkali-halide crystal is heated in the vapour of its alkali metal, e.g. an NaCl crystal in Na vapour or a KCl crystal in K vapour, the originally clear crystal is seen to become coloured. KCl, for instance, turns purple and exhibits in its absorption spectrum an absorption band in the green.

In accordance with a conjecture of J. H. de Boer dating back to 1935, it is assumed that a K atom attaches itself as an ion to the crystal and unites with a Cl ion diffusing out of the lattice. The electron of the K atom moves to the vacancy left by the departure of the Cl ion. This electron, which gives rise to the absorption band, is called a colour centre (*F* centre) [15]). It has been uncertain, however, whether the electron occupies the middle of a vacancy (Mott) or whether it unites more or less with the positive ions surrounding the vacancy (De Boer) The greater likelihood of the latter view has been confirmed, among other things, by investigations of the paramagnetic resonance of *F* centres in alkali-halide crystals [16]).

Colour centres can also be brought about in the crystal at high temperatures when electrolytic conduction takes place under a strong electric field. The electrons that must enter the lattice in order to form the colour centres originate in this case directly from the negative electrode.

When the above-discussed mixed crystals of NaCl and $CaCl_2$ are heated in Na vapour, not only are colour centres formed, but the divalent Ca ions (Ca^{2+}) may be reduced to monovalent ions (Ca^+). Further to what has been said above on pure alkali halides, one can regard this as a process in which electrons are introduced into the crystal, some of which do not move to a Cl vacancy but attach themselves to a Ca^{2+} ion. It should be noted, however, that most of the electrons find a place in the Cl vacancies and so give rise to the usual colour centres. Large numbers of monovalent Ca^+ ions are only obtained when the crystal, treated as described, is irradiated at lower temperatures by light in the absorption band of the colour centres. This might be explained on the following basis. Irradiation in the *F* band raises the electron in the vacancy to a higher energy level; as a result the electron is able to break its bond with the vacancy, and thereafter

[14]) The jump frequencies of the bound and free vacancies themselves are respectively 4 and 12 times higher, in view of the number of Na^+ neighbours present in each case.

[15]) See e.g. E. J. W. Verwey, Electronic conductivity of non-metallic materials, Philips tech. Rev. **9**, 46-53, 1947/48.

[16]) See e.g. J. S. van Wieringen, Paramagnetic resonance, Philips tech. Rev. **19**, 301-313, 1957/58 (No. 11).

to move more or less freely through the lattice. If in so doing its meets a Ca^{2+} ion, it enters into union with it.

This phenomenon can be demonstrated very elegantly in the analogous case of KCl to which $SrCl_2$ has been added. Here, too, F centres are chiefly formed (by heating in K vapour) as a result of which the crystal, as before, turns purple. After cooling, the crystal is irradiated with green light, whereby the colour changes to red and a new absorption band in blue is formed, pointing to a somewhat stronger bond. This absorption is attributable to the formation of Sr^+ ions, which can be regarded as a complex of Sr^{2+} + electron situated in the lattice.

The phenomenon of divalent ions being reduced to monovalent ions has some connection with the phenomenon of "controlled" valency [17]). In the case described above we were concerned with divalent ions incorporated in a lattice of monovalent ions. Now let us see what happens when, conversely, monovalent ions are incorporated in a lattice of divalent ions, e.g. Li_2O added to NiO. One might imagine that here, too, electric neutrality would be preserved by the occurrence of vacancies, viz. O vacancies. It is found in this case, however, to be energetically favourable if, for each incorporated Li^+ ion, an Ni^{2+} ion is simultaneously oxidized to Ni^{3+}. The lattice imperfections occurring here thus consist in the substitution of two Ni^{2+} ions by a monovalent and a trivalent ion.

The causes of the differing behaviour of the two kinds of mixed crystals, NaCl-$CaCl_2$ and NiO-Li_2O can be described in the following way. The electron that reduces the Ca^{2+} ion to Ca^+ is admittedly bound somewhat more strongly to the Ca^{2+} ion than in an F centre, but the very large number of possible ways in which the second case, the combination Ca^{2+} + Na vacancy + F centre, may be realized compared with the first case, $Ca^{2+} + e \rightarrow Ca^+$, swings the balance in favour of the second case ("entropy gain" prevails over "energy gain"). The energy gain in the bound with Ca^{2+} is particularly small in this case owing to the loss of polarization energy during the formation of the bond.

In the NiO-Li_2O system, on the other hand, it is advantageous for an electron to be withdrawn from Ni^{2+}, because the polarization energy here contributes positively to the process, and moreover a comparison of the probability of occurrence of $2Li^+ + 2Ni^{3+}$ with that of $2Li^+$ + O vacancy shows that the entropy gain in the former process is larger.

Concluding remarks

The investigations described in the foregoing have led to a quantitative insight into a number of phenomena which must be attributed to the presence of lattice imperfections in crystals of alkali halides and in silver halides. The investigations have in the first place increased our knowledge of the behaviour of these relatively simple compounds, but their principal importance lies in the fact that they point the way to the explanation of the behaviour of more complex crystals, for which alkali and silver halides can serve as a "model". Compound lattice imperfections in certain crystals, interesting perhaps because of their technical importance, can make their influence felt in extremely complicated ways. Any attempt to analyse this influence must necessarily be preceded by careful verification of the role played by the various lattice imperfections in more elementary compounds such as the alkali halides.

Summary. After an introductory discussion of crystal structure and lattice imperfections in general, the author deals more in detail with the situation in alkaline halides, both in the pure state (Frenkel and Schottky defects) and after the introduction of impurities consisting of a halide of a divalent metal. Ionic conduction and dielectric losses in mixed crystals of NaCl-$CaCl_2$ are dealt with at some length with reference to measurements of dielectric loss angle tan δ as a function of frequency. It is shown that Na^+ vacancies occur in these processes, some of these vacancies being free and others associating with Ca^{2+} ions to form dipoles. The degree of association of these dipoles is determined at higher temperatures, and possibly also at lower temperatures, by a simple chemical equilibrium. For the purpose of a quantitative agreement with the theory of this equilibrium, however, it is necessary to assume that the dipole strength may be smaller than the obvious value ed (where e is the electronic charge and d the Na-Na spacing in the lattice). It is also possible that at low temperatures there exist, besides the dipoles, more complex configurations which make no contribution, or at least very little, to the dielectric losses. After a discussion of the mechanism of ionic conduction and the path of the Na^+ ion in the lattice, the behaviour of silver halides is compared with that of alkali halides. Finally, some attention is given to the behaviour of NaCl-$CaCl_2$ when heated in Na vapour (formation of colour centres and reduction of Ca^{2+} to Ca^+).

[17]) E. J. W. Verwey and F. A. Kröger, New views on oxidic semi-conductors and zinc-sulphide phosphors, Philips tech. Rev. **13**, 90-95, 1951/52.

ABSTRACTS OF RECENT SCIENTIFIC PUBLICATIONS BY THE STAFF OF N.V. PHILIPS' GLOEILAMPENFABRIEKEN

Reprints of these papers not marked with an asterisk * can be obtained free of charge upon application to the Philips Research Laboratory, Eindhoven, Netherlands.

2544: P. C. van der Willigen: De invloed van waterstof op de kwaliteit van de las (De metallurgie van het lassen van staal, Lassymposium 1957, Ned. Ver. voor Lastechniek, The Hague, pp. 24-29). (The effect of hydrogen on the quality of the weld; in Dutch.)

Although the embrittling of steel by hydrogen has been known for over a century, it is only since world war II that the unfavourable influence of hydrogen on the arc welding of steel is understood. Hydrogen is one of the causes of porosity in the weld, of microcracks in quenched weld-metal and of weld-metal cracking and underbead-cracking in low-alloy steel. A number of experiments which give an idea of the typical behaviour of hydrogen in steel are reviewed. Welding experiments on the influence of hydrogen are described, showing clearly that the danger of hydrogen, still doubted by some, is indeed very real. An attempt is made to contribute to an understanding of the phenomena.

2545: G. Diemer, G. J. van Gurp and H. J. G. Meyer: The nature of the edge emission in CdS (Physica **23**, 987-988, 1957, No. 10).

Letter presenting experimental evidence in confirmation and extension of an earlier view that CdS emission bands in the region of 5100-5500 Å are due to recombination of electrons and holes via impurity centres.

2546: N. W. H. Addink: A note on the determination of the Avogadro number (pp. 221-223 of supplement No. 1 to Nuovo Cimento **6**, series X, 1957).

Note on the small deviations in the values of Avogadro's number found by different experimental methods. The following are among the causes of the deviations: crystal imperfections and errors in density measurements, especially for small crystals. From measurements on KCl crystals prepared from the melt it is suggested that these crystals are left with $\sim 2 \times 10^{-4}$ frozen-in vacancies per cm^3, which agrees satisfactorily with the number derived from conductivity measurements ($1{:}2 \times 10^{-4}$ per cm^3).

2547: G. Meijer: The influence of light quality on the flowering response of *Salvia accidentalis* (Acta bot. neerl. **6**, 395-406, 1957, No. 4).

Salvia accidentalis is an obligate short-day plant. However, flower initiation may occur after a long-day treatment, depending on light intensity and the colour of the main light period. In *Salvia occidentalis* as in *Hyoscyamus niger* the effect of a long-day treatment is influenced by at least two different photoreactions.

2548: G. Meijer and R. van der Veen: Wavelength-dependence of photoperiodic responses (Acta bot. neerl. **6**, 429-433, 1957, No. 4).

It has been shown in several plants that the effect of a short-day treatment does not depend on the light quality of the main light period. However, to obtain a long-day effect by interrupting the long-night period with a red or green irradiation, it is shown that for certain plant species a special blue-light requirement for the main light period exists.

2549: P. Massini: Photosynthetic phosphorylation as an explanation for induction phenomena in photosynthesis (Acta bot. neerl. **6**, 434-444, 1957, No. 4).

The initial uptake of CO_2 by photosynthetically active tissue after the transition from dark to light is investigated. It is suggested that this phenomenon is caused by a shift in the *p*H of the cell medium toward alkalinity which is due to the formation of energy-rich phosphates in the light.

2550: J. H. Stuy: Herstel van beschadiging door straling bij micro-organismen (Chem. Weekblad **53**, 621-625, 1957, No. 47). (Recovery of micro-organisms from radiation damage; in Dutch.)

A short survey is given of the radiation killing of micro-organisms and the subsequent reactivation phenomena. A possible connection between these phenomena is discussed.

2551: J. B. de Boer: Blendung beim nächtlichen Strassenverkehr (Zentralblatt Verkehrs-Medizin, Verkehrs-Psych. angr. Geb. **3**, 185-203, 1957, No. 4). (Glare in road traffic at night; in German.)

The night driver is troubled by the glare of two kinds of light sources, headlights and lanterns for public lighting. Glare from these sources may be either disability glare or discomfort glare. Visibility tests have shown the former to be absent if the latter is kept within satisfactory limits. Further tests have allowed quantitative conclusions to be arrived at with regard to the permissible degree of discomfort glare due to public lighting. Limitation of glare to this degree, while maintaining an adequate luminance of the road surface necessary for sufficient visibility, requires more light. This is made justifiable, however, by the efficient means nowadays available for lighting roads. On roads thus lit, drivers should use side lights only, as dipped headlights, however well they work, cause considerable discomfort from glare. Good lighting for roads carrying dense traffic can therefore only be obtained from fixed sources. The influence of colour on discomfort glare is briefly discussed.

2552: A. H. Boerdijk: Apparatus for routine refraction measurements of layers of lacquers with digital reading (Rev. sci. Instr. **28**, 840-841, 1957, No. 10).

Brief description of an instrument for the rapid measurement of the refractive index of thin layers, based on measurements of the Brewster angle. The range is $n = 1.3$ to $n = 1.8$, and the accuracy is to the third decimal place.

2553: L. M. Nijland and L. J. van der Pauw: The effect of heat treatment on the bulk lifetime of excess charge carriers in silicon (J. Electron. Control **3**, 391-395, 1957, No. 4).

In a recent paper G. Bemski (1956) described the decrease of the bulk lifetime of excess charge carriers in silicon found when silicon samples were quenched from temperatures lower than 550 °C to room temperature, and the complete or partial restoration of the original lifetime when the samples were annealed in the same range of temperatures. The authors have studied the effects of heat treatment of silicon in the range between room temperature and 1250 °C. It was found that bulk lifetime both in p- and n-type crystals made by the floating-zone method and of n-type crystals made by the Czochralski technique might be increased by annealing at temperatures between about 300 C° and 700 °C. Annealing at temperatures higher than about 700 °C decreased lifetime both in p- and n-type crystals. In all cases the samples were relatively slowly cooled. The mechanism of these changes in lifetime is not well understood.

2554: J. A. Kok and M. M. G. Corbey: Dipoles and electric breakdown (Appl. sci. Res. **B 6**, 449-455, 1957, No. 6).

It is shown that breakdown of insulating or dielectric material may be caused either by polarizable particles or permanent dipoles. Induced dipoles as well as permanent dipoles may gather at a place of maximum stress and form a bridge. Bridges consisting of permanent dipoles may cause the gap between the valence energy band and the conduction energy band to be filled by impurity or imperfection levels. The low ionization potentials of electrons attached to permanent dipoles may facilitate breakdown. An attempt is made to reconcile Crowe's results with the authors'.

2555: F. L. H. M. Stumpers: Information theory and international radio organizations (IRE Trans. on Information Theory **IT-3**, 85, 1957, No. 2).

Guest editorial (to the above Transactions) on the applications of information theory in radio communication.

2556: J. A. Kok: Doorslagverschijnselen in vloeibare isolatoren (Ingenieur **69**, E179-E181, 13 Dec. 1957). (Electrical breakdown of liquid insulators; in Dutch.)

The electrical breakdown strength of insulating oil depends on the size of foreign particles, which may form bridges in a place of maximum electric stress (see No. **2507** of these Abstracts). A theoretical relation has been derived and verified with colloid suspensions of particles of known radius. Mineral oils may deteriorate if the particles unite by the process of flocculation, the occurrence of which depends on the relative magnitudes of the attractive London-Van der Waals forces acting between the particles and the repulsive forces between their ion atmospheres. The possibility of using a mineral oil as an insulator depends on the existence of an upper limit of the size of particle complexes due to the rapid fall-off of the L.-v. d. W. forces at diameters exceeding 500 Å.

2557: J. Meltzer: Insektizide und akarizide Wirksamkeit von 2,4,5,4′-Tetrachlor-Diphenyl-Sulphon (Tedion) (Z. ang. Entomologie **41**, 58-63, 1957, No. 1). (Insecticidal and acaricidal activity of 2,4,5,4′-tetrachlorodiphenyl sulphonide (Tedion); in German.)

Tedion does not have contact poisonous activity on insects. *Musca domestica L.*, *Sitophilus granarius L.* and *Ephestia kuehniella Zell.* are not killed by contact in treated Petri dishes. *Aphis fabea Scop.* and larvae of *Leptinotarsa decemlineata Say.* and *Diataraxia oleracea L.* were not killed by contact with, or feeding on plants dipped into Tedion emulsions. *Aphis mellifica L.* is not affected by Tedion as a contact poison, applied in as high a dosage as 16 g/m². *Drosophila melanogaster* has been bred in media containing 10-100 ppm of Tedion without influence on development and number of hatched flies. Two successive generations of *Ephestia kuehniella Zell.* have been bred on rolled oats, treated with 1-100 ppm of Tedion. No influence on time of development nor on percentage of hatching was noted. A feeding experiment with addition of 500-62 500 ppm of Tedion to honey-sugar paste shows that Tedion does not affect the bee. Eggs of *Tetranychus urticae Koch* could be killed by emulsions of the extracts made from the digestive tract of the treated bees, but were not affected by an extract of the control bees. Tedion appears to be a highly specific acaricide which is safe for man and animal, and which does not affect predator and parasite insects and bees.

2558: J. Meltzer: Penetratie en werkingsduur van enkele spintoviciden (Meded. Landbouwhogesch. Opzoekingsstat. Gent **22**, 457-464, 1957, No. 3). (Penetration and residual action of some red-spider ovicides; in Dutch.)

Of the four red-spider ovicides chlorobenside, Tedion, p-chlorophenyl-p-chlorobenzene sulphonate and p-chlorophenyl benzene sulphonate, the last one is the fastest to penetrate through the treated leaves, but also the fastest to loose activity. Only Tedion remains highly active two weeks after the treatment. The oral uptake of Tedion by the females and the larvae plays an important role in its action.

2559*: M. van Tol: Automatische regeling van kernreactoren (Chapter, pp. 87-101, in the book: Ontwikkelingen in de moderne regeltechniek, Verslag T.W.O. Kon. Inst. Ingenieurs, Utrecht 1957). (Automatic control of nuclear reactors; in Dutch.)

This paper deals with the automatic control of small nuclear reactors where temperature variations are unimportant. As an example, the automatic control of the reactor shown at the exhibition "Het Atoom" in Amsterdam, 1957, is discussed in some detail. (See also Philips tech. Rev. **19**, 245-257 and 273-285, 1957/58, Nos. 9 and 10.)

R 332: W. Ch. van Geel, C. A. Pistorius, and B. C. Bouma: Luminescence of the oxide layer on aluminium during and after its formation by electrolytic oxidation (Philips Res. Repts. **12**, 465-490, 1957, No. 6).

Report on measurements of the luminescence occurring with an anodically deposited oxide layer on aluminium (a brief description was given in J. Phys. Radium **17**, 714-717, 1956; No. **2426** of these Abstracts). During the formation of the oxide layer a pronounced luminescence appears. When the field strength in the layer is kept constant, the luminescence L is found to increase with the thickness d according to $L = a(e^{bd} - 1)$. At constant layer thickness, L is found to be proportional to the current I, so that $L = \beta I(e^{bd} - 1)$. The authors assume that during the formation — the current then being partly an electronic current — the collisions with the ions liberate electrons, which in turn, by excitation of the ions of foreign metals, cause the luminescence. With the formed layer, the small leakage current causes a weak luminescence. An alternating voltage of sinusoidal or rectangular shape gives a flash of luminescence at every reversal of the polarity. The intensity of this flash is found to decrease as a function of time. This is the reason why, if an alternating voltage is applied, the curve of L as a function of I or of V describes a loop. The cathode flash is explained by assuming that the layer contains traps, which are filled with electrons as soon as the Al becomes the cathode. During this process electrons recombine with the ions of foreign metals contained in the lattice. The process is of short duration. As soon as the Al becomes positive the anode flash occurs, which is considered to be the rest of the cathode flash.

R 333: P. B. Braun: The crystal structures of a new group of ferromagnetic compounds (Philips Res. Repts. **12**, 491-548, 1957, No. 6).

In this thesis (Amsterdam, December 1956) the crystal structures of four new compounds are described, the study of which has contributed in an essential way the the development of the hexagonal ferromagnetic iron compounds known as ferroxplana

(see Philips tech. Rev. **18**, 145-154, 1956/57, No. 6). The new compounds are: **W** = $Ba\,Fe_2^{II}\,Fe_{16}^{III}\,O_{27}$, **X** = $Ba_2\,Fe_2^{II}\,Fe_{28}^{III}\,O_{46}$, **Y** = $Ba_2\,Zn_2^{II}Fe_{12}^{III}\,O_{22}$ and **Z** = $Ba_3\,Co_2^{II}\,Fe_{24}^{III}\,O_{41}$; the chemical formulae of two of them were found simultaneously with the structure. The structures of the new compounds and the magnetoplumbite structure are mutually related. Oxygen and barium atoms together form a slightly expanded close-packed arrangement, with the barium atoms in certain selected positions, and the smaller ions in certain of the holes between the large ones. In all of these structures, "plates", either four or six oxygen layers thick, can be distinguished, which have very nearly the spinel structure. The relations between the structures are discussed from two different points of view. In the appendix a specially developed machine is described for the automatic summation of Fourier series with 60 cosine- and 60 sine-terms.

R 334: L. J. van der Pauw: A method of measuring specific resistivity and Hall effect of discs of arbitrary shape (Philips Res. Repts. **13**, 1-9, 1958, No. 1).

A method of measuring specific resistivity and Hall effect of flat samples of arbitrary shape is presented. The method is based upon a theorem which holds for a flat sample of arbitrary shape if the contacts are sufficiently small and located at the circumference of the sample. Furthermore, the sample must be singly connected, i.e., it should not have isolated holes.

R 335: H. G. Beljers: Determination of the gyromagnetic ratio and the magnetic resonance damping coefficient of ferrites (Philips Res. Repts. **13**, 10-16, 1958, No. 1).

Resonance experiments are described on polycrystalline ferrite spheres in a microwave cavity with a linearly polarized magnetic field. Fundamental quantities, like the g-factor and the damping coefficient of the ferrite, are derived from the measurements. The damping coefficient can be calculated either from a line-width measurement or from the maximum amount of absorption in the ferrite at resonance. For a few samples reasonably corresponding results by the two methods are given.

R 336: P. Penning: Precipitation of nickel and copper from supersaturated solutions in germanium (Philips Res. Repts. **13**, 17-36, 1958, No. 1).

During the anneal of germanium samples supersaturated with nickel, unidentified acceptors with a low activation energy are observed, besides the acceptor levels arising from substitutional nickel atoms. Their density increases rapidly in the beginning of the anneal and reaches a value comparable to the density of nickel atoms originally present in the sample. In spite of this, the total density of acceptors ionized at room temperature remains approximately constant. Upon further annealing, the density of acceptors associated with substitutional nickel atoms and the density of the unidentified acceptors decrease exponentially with the same time constant. To explain this, a theory is put forward in which the new acceptors are assumed to be associated with vacancies left behind in the lattice when a substitutional Ni-atom jumps to an interstitial site. The interstitial Ni-atoms diffuse rapidly to nuclei of precipitation. The ratio between the densities of substitutional Ni-atoms and vacancies reaches a constant value K during the first period of anneal. According to the theory, the rate of precipitation as observed in the second part of the anneal depends on the rate of removal of vacancies, thus making it structure-sensitive, and on the value of K. A similar process is proposed for the precipitation of copper in germanium. The value of K for copper appears to be larger than for nickel. The vacancy acceptor level is found to be located at 0.02 eV from the valence band. The presence of a high density of vacancies during the precipitation of one of the two elements, copper or nickel, greatly facilitates the penetration of substitutional atoms of the other element into the sample. It is shown that concentrations much larger than the saturation concentration may be obtained. Several secondary effects of this interaction between copper and nickel are observed. The results are in good agreement with the theory. Finally it is shown how this rapid penetration of substitutional atoms in the presence of vacancies may have influenced the experimental results of other authors.

R 337: S. Duinker: General properties of frequency-converting networks (Philips Res. Repts. **13**, 37-78, 1958, No. 1).

In this thesis (Delft, June 1957; see also **R 339**, some general properties of frequency-converting networks (i.e. networks used for the purpose of modulation, mixing, detection, etc.) are analysed. These networks generally contain non-linear elements. Properties of elements satisfying the condition of "local passivity" are analysed. It is assumed

that the fundamental state, resulting from the presence of energy sources, is subjected to a small disturbance. The first-order perturbational equations are linear differential equations with time-dependent coefficients which satisfy the reciprocity condition. These equations are further analysed, assuming a periodic fundamental and perturbational state and after the introduction of complex quantities. The network equations can then be represented with the aid of infinite matrices. The effect on the matrix equations is investigated of the shifting of the time origin, of the interchanging of the role of the signal frequency and a frequency generated by conversion, of a symmetric fundamentals tate and of the presence of linear impedances. After introducing the notions of "fictitious" meshes and ports it is shown that the equivalent circuit of a conversion network includes network elements that are not physically realizable and even may be active. An energy theorem for purely-reactive conversion networks is derived and the possibility of instabilities, the conversion gain, and the condition for the absence of reaction on the signal source are discussed. The simplification of the matrix equations resulting from a balanced configuration of elements is discussed with the aid of some examples.

R 338: P. Penning: Generation of imperfections in germanium crystals by thermal strain (Philips Res. Repts. **13**, 79-97, 1958, No. 1).

Thermal strain is induced in a crystal if it is heated inhomogeneously. These strains can be so large that either plastic flow or cracking may take place. Both effects have been observed in crystals quenched from high temperature. In the case of plastic flow the distribution of dislocations, as revealed by etching, shows marked characteristics, dependent on the manner of quenching and the orientation of the crystal. It is shown that these characteristics can be explained very well if it is assumed that the amount of plastic flow is directly proportional to the elastic strain induced by the non-uniform temperature. During the growth of a crystal from a melt, thermal strain may also very well be present in the crystal. The main sources of these strains are indicated and their influence on the perfection of the growing crystal are discussed. Secondary effects of plastic flow due to thermal strain in grown crystals and quenched samples, such as residual stresses and the freezing-in of defects, are discussed briefly. See also Philips tech. Rev. **19**, 357-364, 1957/58 (No. 12).

VOLUME 20, 1958/59, No. 4 pp. 85-112 Published 30th October 1958

Philips Technical Review

DEALING WITH TECHNICAL PROBLEMS
RELATING TO THE PRODUCTS, PROCESSES AND INVESTIGATIONS OF
THE PHILIPS INDUSTRIES

SCIENCE AND INDUSTRY

by H. B. G. CASIMIR.

001.658:37

During the Golden Anniversary of the State of Oklahoma, on June 17, 1957, an international symposium was organized at Oklahoma City under the general heading: science, industry and education. A number of the foremost leaders of research institutions from different countries were invited to give their views on problems related to this general theme. The following article is a slightly abridged version of the address delivered by Prof. H. B. G. Casimir, director of the Philips Laboratories and member of the board of directors of the Philips Industries.

The subject of the relations of science, industry and education is an extensive one about which a lot can be said and has been said, and it would be useless if I tried once more to survey the whole field. I shall therefore concentrate on three statements of which I trust that they are sufficiently controversial to form a contribution to discussions on this subject.

The first one relates to laboratory administration and runs as follows: in an industrial research laboratory it is impossible to relate research products budgetwise to industrial and commercial projects. Any attempt at operating a laboratory on a budget system will either be detrimental to research itself or it will lead to a mild form of cheating which makes the whole system illusory.

My second statement is that although industry is for its future dependent on fundamental research, very few fundamental results have come, will come or should come out of an industrial research laboratory.

My third statement: it is wrong to regard education and research as two distinct and separate tasks of a University.

Before proceeding any further I should make it clear what I understand by the words fundamental research, research, development and so on.

I shall describe what one might call the spectrum of research. At one end of the spectrum there is Fundamental Research with very heavy capital *F* and capital *R*. I should like to define this as research dealing with entirely new phenomena connected with basically and philosophically new principles in the description of nature. It is easy to give examples: the work of Faraday and Maxwell on the electromagnetic field, the work of Boltzmann and Gibbs on the kinetic explanation of thermodynamic phenomena, Einstein's theory of relativity, Bohr's quantum theory of the atom and the new quantum mechanics of Heisenberg, Schrödinger and Dirac belong clearly to this category. Next comes fundamental research with a more modest *f* and *r*. The aim is still the understanding of nature, but it is dealing with fields in which the basic principles are well understood. Work on molecular spectra, solid-state physics, electromagnetic diffraction, hydrodynamics would come in this group.

My next category is target-research. The method of working, the scientific approach is still the same, but now one has a definite technical target in mind: one is for instance no longer working on fluorescence in general, but is trying to find a substance which under electron bombardment gives a good output of red light with a more or less specified delay-time. In the engineering field a similar type of work is what I like to call project-research, but what is also frequently covered by the words advanced development. By this I understand work aimed at realizing a concrete technical object but with the qualification that it is still uncertain to what extent the thing we have in mind is possible. The first people who started to build electron microscopes knew almost nothing about the potential possibilities of this instrument; for those who came later in the field it was evident that an electron microscope could be

built, but it was impossible to tell beforehand what resolving power would be obtained with a reasonable amount of work. At present, unless we go to the very furthest limits of resolving power, it is almost possible to lay down specifications beforehand and to make a reasonable estimate of the cost of this development in time, manpower and facilities. This I consider characteristic of development, the possibility to estimate more or less accurately what is required to make a prototype of more or less specified characteristics. I have twice inserted more or less; this is not very elegant phrasing, but anyone who has had to do with the administration of research and development will agree that it is a necessary precaution.

Next in my list appear factory-engineering and trouble-shooting, activities that are related to development, but that often also give rise to problems of target-research. In our own organization the end of the spectrum is application-research, the work on specific applications of our own products. This would comprise such things as illumination-engineering, the art of adapting public address systems to existing buildings or the adaptation of a high-frequency furnace to a special industrial process. As I said before, this application-research has in our firm a somewhat separate position because of the nature of its relations with industrial and commercial activities, but from a more scientific and technical point of view it is a combination of the former types.

Perhaps the word spectrum is not too badly chosen for there is in reality a continuous transition and just as it is difficult in the solar spectrum to tell whether a certain colour is a bluish green or a greenish blue, one may differ in opinion about whether a certain type of work is target-research or development, and so on.

In our organization each industrial division is responsible for its own development, factory engineering and application work, whereas fundamental research, target-research and project-research or advanced development are carried out in our central research laboratory. I believe that this division has been found useful by all organizations that are dealing with a wide and diversified range of products. The basic principles underlying a simple radio receiver and a modern radar installation are not too different, but there is such a tremendous difference in style of technical realization that it is hard to imagine a central research and development organization able to cope competently with the development work for both the one and the other.

If you remember my definitions, you will notice that the work of our factory laboratories begins where results are reasonably certain and where costs can be predicted. The work in the research laboratories may be equally practical or applied in character, but there is always this distinction that there is a much higher degree of uncertainty and this leads directly to my first statement. In the case of factory development it is reasonable to ask whether the cost of developing a product can be earned back by sales of that product. Development costs of a specified product are part of the cost price of that product. It is impossible to make a similar breakdown of the expenses of a research laboratory: some of the work may not lead anywhere — much of it will later turn out to be useful in fields vastly different from those envisaged when the work was started. We originally studied ferromagnetic ferrites for a special application in carrier telephony: many years later we found that the bulk of our production goes into television receivers. From a long-range point of view our work on ferromagnetism has been succesful and profitable but if our nascent carrier telephony department had had to bear the initial expenses it would have been killed right at the start.

But, you will ask, why should the cheating come in? The reason is that the total budget of a research laboratory is determined fairly accurately by the number of scientific workers: if in a given field of research and a given country you want to have a laboratory where a number of research workers can work efficiently and are adequately provided with technical assistance, workshops and so on, then the cost per research worker will always come out the same. Further, a research institution should aim at continuity of staff, for it is an exception that a man, however competent he may be, does valuable work during his first half year or so in new surroundings, and some of the best research workers become productive only after several years. A slow and continuous flow of people is all right, but one should try to avoid discontinuous expansions or reductions.

The art of running a laboratory on a budget system consists therefore in splitting a sum total that is known beforehand into a number of separate items in such a way that those in charge of appropriations will fall for it. If I had to do this in my own institution I would start arguing in the following way: we have a fairly large group working on fluorescence. It is useful to both our lampworks and our cathode-ray tube factory. On the other hand some fairly abstract mathematical work on electron optics is being done, for which it is hard to find a suitable place on the budget.

Should the latter fact induce us to discontinue this work, which we think in the long run may prove quite useful? Better place it under the general heading of cathode-ray tubes, which sounds reasonable, and in order not too overload the budget for this division, put the whole fluorescence research on the budget for the lighting division, which is less crammed. And so on. It is this kind of artificial splitting and combining which I had in mind when I spoke of a mild form of cheating. Fortunately in our company we have done away with this system altogether. The research laboratories as a whole are each year allotted a lump sum calculated in such a way that it provides reasonable working conditions for the number of people employed and leaves room for slow expansion. Only in the case of large capital investments, new buildings, etc., do we apply for an additional budget. Of course we have to keep an eye on expenses, but no reference is ever made to a budget for a specific project. The notion of such a budget simply does not exist.

In my dictionary of English slang I find "Dutch reckoning" defined as a lump account without particulars. I am proud of being a Dutchman, so you can hardly be surprised that I consider this type of reckoning ideally suited to the needs of a research laboratory. So much about my first statement.

My second statement was that industry depends on the results of fundamental research — and here I mean to say Fundamental Research with capitals — but that such results do not come out of industrial laboratories. History gives ample evidence for this. Electrical engineering could not even be imagined without the pioneering work of Faraday and of Maxwell whose work in those days was entirely outside the scope of existing industries. There would be no radio without the work of Maxwell and Hertz, but it did not occur to the electrical industries of those days to do the work by which Hertz justly became famous. Speaking and working about electrons was almost anathema to the electrical engineer at the turn of the century, but today an evergrowing industry is based on the very notion of electrons. No company interested in power plants could dream that the work of the Curies, Rutherford and others would eventually lead to a new source of power. An industry may take a long range point of view, it may encourage fundamental research, it may not require results of immediate practical value, but it cannot be expected to work on basic principles and phenomena for which even our most vivid imagination cannot foresee whether, or in what field, they will find applications. Today at the very front of science, physicists are working on elementary particles, on concepts like parity, on the relations between mesons and nuclear forces. No one can foresee to what this will lead. No industry laboratory could be expected to do cosmic-ray work on a large scale or to be the first to build at its own cost a cosmotron, and yet if we deny the possibility of future applications we are probably just as short-sighted as the power engineer early in the century who derided electrons. The places for Fundamental Research are the University laboratories.

Here someone might interrupt me and object: What about the transistor? Now first of all let me say that the transistor is not only an extremely important and useful device that will have a far reaching influence on the whole field of electronics, but that the research that led to the transistor is a very beautiful piece of work indeed, combining well planned and yet imaginative experiments with a penetrating and elegant theoretical analysis. So it is not a question of grapes being sour: on the contrary they are very sweet; and though they may have been a little bit too high for us to pick, all the electronic industries got a generous helping after the picking. And yet I think the transistor is a good example for my thesis. So allow me to go into technical details for a moment and let me review the basic thoughts that play a role in the transistor.

First of all the idea of electrons, a notion connected especially with the theoretical work of my countryman Lorentz and the experiments of J. J. Thomson. Next the statistical theory of matter and its relation to thermodynamics (Maxwell, Boltzmann, Gibbs). The application of such methods to the motion of electrons led, in the hands of Lorentz and of Niels Bohr in his little known thesis, to important results. But there remained a number of very puzzling questions: How it is possible that the conduction electrons do not contribute appreciably to the specific heat; how can we imagine that an electron can move freely through a metal; and how is it possible that the sign of the so-called Hall effect is sometimes as if the current through a metal were carried by positive carriers, although we know that electrons are negatively charged? The solution of these riddles required entirely new notions.

The first was solved by the Fermi-Dirac statistics, a modification of classical statistical theory, brought about firstly by a recognition of the existence of quantum states and secondly by the Pauli exclusion principle. The application of Fermi-Dirac statistics to the motion of the electrons in a metal was worked out by Sommerfeld and turned out to be a great improvement. The solution of the second problem is due to Bloch and Peierls after some preliminary

and more qualitative work of Houston. It is based on new quantum mechanics where electrons are described by waves, a theory connected with the names of de Broglie and Schrödinger. It is found that these electron waves are free to move in a perfectly periodic field of force and the analysis of such waves by Brillouin and others led to the notion of electron bands. The third riddle was solved by Peierls; he was the first to introduce the notion of a hole in a filled electron band and to show that it behaves as it it were a positive electron. From then on the problems became less fundamental, but the essential ideas about semiconductors were still mainly the result of University work. Now the one new principle that was added by the Bell people to existing notions was the idea that electrons can persist for some time in p-type germanium, that is, germanium containing such impurities that the conduction is due to the motion of holes; similarly injected holes can persist for some time in n-type germanium. This is both an important experimental fact and an interesting theoretical idea, but from a philosophical point of view it is certainly not on a par with the great new ideas of quantum mechanics. The work on transistors is essentially a brilliant and novel application of known principles, that would be a beautiful piece of physical research anyway, but happens to be of great technical consequence too.

Once more, the fundamental notions that are required by industry are coming from the universities.

I would add the following. The rise of an industry depends on leadership that recognizes among other things the necessity of research. But when it comes to fundamental research we are again faced with the same situation on a different level. For the future of a single industry it is essential that it be broad-minded with respect to its own research; for the community as a whole and for the future of all its industries, it is essential to support also the most abstract type of fundamental work. Industrial laboratories are part of a far-seeing policy of industrialists. Wise statesmanship of the leaders of a nation will result in sponsorship of academic research.

Why then my third statement? Why is it wrong to say that Universities have not only an educational task but should *also* carry out research? Because this way of looking at things shows a basic misunderstanding of the nature of a University. It is the task of a University to live a scientific life and to initiate a younger generation in this way of thinking. This initiation requires instruction in certain techniques, but these are only means to a goal. There is only one form of real higher education and that does not consist in listening to lectures, in performing classroom experiments or in solving textbook problems: it consists in struggling on the borderline of knowledge, with the unknown and the unexpected, under the guidance of an inspired and inspiring teacher.

I have discussed, in the foregoing, one or two aspects of the relations between science and industry. I have emphasized the importance of industrial research for industry and of academic research for industrial research. But that is not the whole story. Although our technical civilization is the result of a joining of forces of philosophical inquisitiveness and industrial zeal, our desire to understand nature is not only justified by its practical importance. It corresponds to a noble urge of the human race that is also an aim in itself. Even the most die-hard materialist feels dimly that the mathematician dealing with an impressive edifice of abstractions and the astronomer probing the structure of the universe are doing valuable things and are in some way contributing to the richness of human experience.

There enters some of this even in a simple piece of applied research. To feel that one's work is not only of practical use but has also inherent value and beauty, is one of the things that make life worth living. We research people should count ourselves fortunate beings.

AN EXPERIMENTAL PYROMETER USING A PHOTOTRANSISTOR AND DESIGNED FOR RADIO-TUBE INSPECTION

536.52:621.383:621.314.7:621.385.1

In radio-tube manufacture it is important to be able to measure the temperature of various parts of finished tubes while they are in operation. Sometimes it is desired to perform a large number of such measurements in a short time.

Often it is clearly out of the question to use an instrument that has to be placed in contact with the object (such as a thermometer or thermocouple); recourse must therefore be had to one that works at a distance, i.e. that responds to the radiation from the object whose temperature is to be measured.

The optical pyrometer is the instrument most commonly used for this purpose. In this, an image of the surface being investigated is formed in the plane of the filament of a small incandescent lamp. The lamp current is adjusted to a value such that the eye is no longer able to distinguish the incandescent filament from its background. The temperature of the object can be derived from the value of the lamp current.

The method can of course be employed only where the object radiates light. The lowest temperature that can be measured thus lies round about 630 °C [1]). The temperature of the cathode of a vacuum tube (~700 °C) [1]) can thus be determined by this method. For accuracy in the measurement of such low temperatures, however, it is necessary to work in a dark room. Also the work is tiring to the eyes. It is only possible to carry out a large number of measurements in a short time if experienced observers are available who are accustomed to the work [2]). It is quite impossible, with the optical pyrometer, to investigate those parts of a radio tube whose normal working temperatures are lower than that of the cathode.

This state of affairs has prompted the search for a method in which an objective radiation detector would take the place of the human eye, the need for experienced observers thus being done away with, and which would moreover allow the range of measurement to be extended to lower temperatures.

It has been found that these requirements can be satisfied by making use of a transistor that is sensitive to radiant energy (Philips type OCP 71 germanium phototransistor). A diagram of a pyrometer equipped with one of these transistors is shown in *fig. 1*. (This pyrometer was built for experimental purposes only; it is not marketed.) The optical system is constructed largely from a single-lens miniature reflex camera: the lens [3]) of the camera (L) throws a full-sized image of the object under investigation (O) on to a diaphragm (D). The light-sensitive region of the transistor is located immediately behind the opening in the diaphragm. This opening has a diameter of only 0.6 mm. Since the image is of the same size as the object, the transistor "sees" a circular patch of the latter that is likewise only 0.6 mm across; consequently this pyrometer can be used to make spot measurements of temperature over quite small objects, such as the electrodes of radio tubes [4]). The location of the spot under measurement is found by turning mirror AM into position AM'. The object — illuminated by the normal ambient light in the room — then appears on the ground-glass screen G. D', a mark on the screen, indicates the spot that is being "seen" by the transistor [5]).

The beam from the object is chopped at a frequency of 175 c/s by a rotating perforated disc (C). Consequently the current through the transistor exhibits an A.C. component of 175 c/s whose amplitude is a measure of the incident radiation density. The ripple signal is fed into a narrow-bandwidth amplifier selective to frequencies in the vicinity of 175 c/s. The amplifier output is indicated on a meter. By chopping the beam and using a selective amplifier, the meter-reading is determined almost solely by the incident radiation and is independent, or practically so, of random fluctuations in the transis-

[1]) These values are *apparent temperatures* determined with an optical pyrometer calibrated with a black body, usually called the "brightness temperatures", see below, small print.

[2]) Results obtained by inexperienced observers exhibit a standard deviation that is generally greater than 5 °C; with experienced observers the standard deviation is 1 °C.

[3]) Relative aperture 1 : 2.9; f = 50 mm.

[4]) Lead-sulphide photo-cells and certain other photoconductors are also very sensitive in the infra-red and are often used as the detector element in radiation pyrometers. PbS cells are, however, unsuitable for our purpose for the following reasons: *a*) Their high sensitivity is obtained only for radiation of a considerable range of wavelengths, extending far into the infra-red; measurements of temperatures through glass (e.g. through the envelope of a radio valve) would therefore involve working with far less than the optimum sensitivity. Also the imaging of the object by means of lenses would give rise to complications. *b*) The sensitivity per unit area of the PbS cell is much less than that of the phototransistor.

[5]) During assembly of the pyrometer, account must be taken of the chromatic aberration of the optical system: the infra-red radiation, where the transistor is at its most sensitive, is brought to focus somewhat further from the lens than visible light.

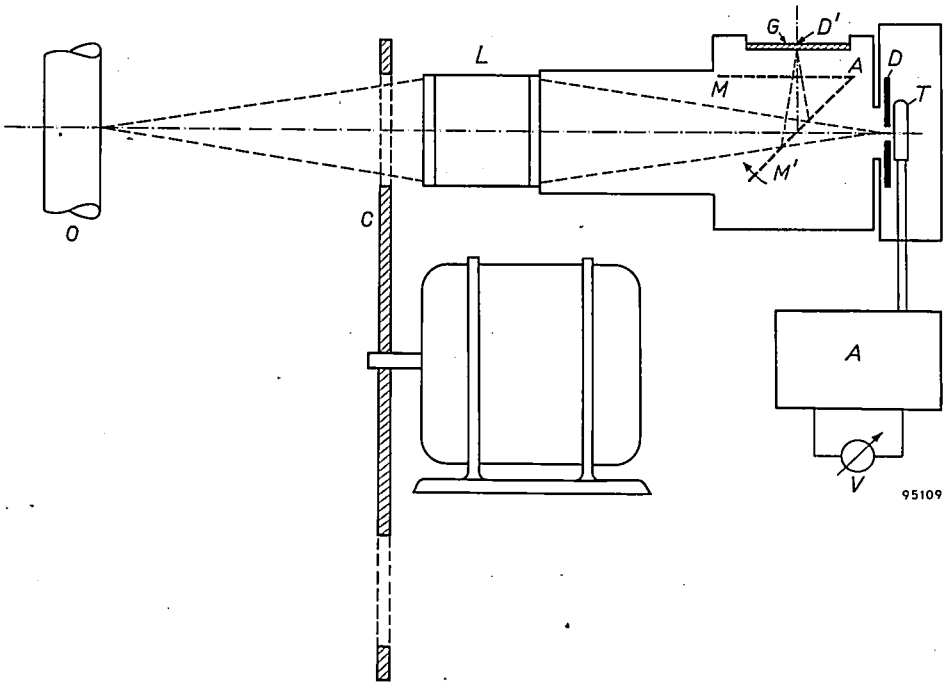

Fig. 1. Schematic diagram of radiation pyrometer based on phototransistor. A full-sized image of the object O (the anode of a radio tube, for example) is projected by the lens system L on to diaphragm D, behind which is the phototransistor T. The perforated disc C, mounted on the spindle of a synchronous motor, chops the beam at a rate of 175 times per second. With the mirror AM placed in position AM', the instrument can be aligned so that the point whose temperature it is desired to measure forms an image coinciding with mark D' on ground-glass screen G. Variations in the transistor current are converted into voltage variations: components with a frequency of 175 c/s pass through the selective linear amplifier A. The output voltage, after being rectified, is measured by means of meter V.

tor current [6]). Also, the amplifier design is such that fluctuations in its supply voltage have little effect. The selective amplifier is also responsible for a considerable improvement in the signal-to-noise ratio; noise frequencies lying outside the

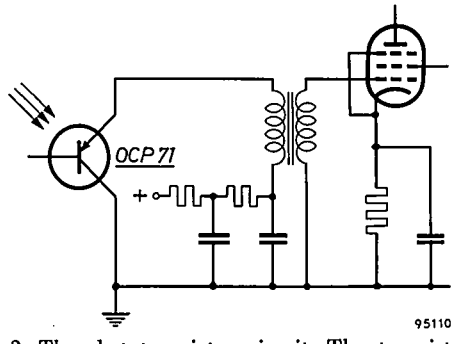

Fig. 2. The phototransistor circuit. The transistor output is transformer-coupled to the first tube of the amplifier.

pass-band are eliminated. Amongst other things, this has an important bearing on the question of extending the range of measurable temperatures, for the signal-to-noise ratio sets a lower limit to this range. For the present apparatus the lower limit is at an *apparent temperature* of about 200 °C (see below, small print). A high signal-to-noise ratio is obtained not only by reducing noise but also by having the strongest possible signal; this means that the relative aperture of the optical system should be large. The uncertainty (standard deviation) in the measurement of temperature with this apparatus is approximately 1 °C, and is thus about the same as that involved in measurements with the optical pyrometer by experienced observers.

Fig. 2 shows the transistor circuit and the manner in which variations in the current through the transistor are converted into variations in the grid voltage of the first tube of the amplifier just referred to. The variations in grid voltage are proportional to those in the transistor current, the factor of proportionality being equal to the product of the input impedance of the transformer at a frequency of 175 c/s (700 kΩ) and the transformation ratio. Transformer coupling is favourable from the standpoint of signal-to-noise ratio, the mean noise voltage across an impedance (within a given frequency interval) being proportional to its D.C. resistance (which is only 20 kΩ for both windings of the transformer). The second and third stages of the amplifier are selective (their resonance frequencies being 169

[6]) Fluctuations in the transistor current may be due to stray light falling on to the transistor and, in particular, to changes in its temperature. It is possible, in principle, to reduce such effects by using a bridge circuit comprising two selected transistors with matched properties.

and 181 c/s respectively; both have a quality factor Q of 17). In this way a frequency-response curve is obtained that is almost horizontal between 170 and 180 c/s and drops steeply outside these two frequencies (*fig. 3*). The output stage (which is not selective) is connected to a precision milliammeter (with an accuracy of 0.5%) via a transformer and a full-wave rectifier consisting of four germanium diodes. The reading given by the meter is proportional to the amplitude of the variations in the transistor current. An attenuator inserted between the first and second stages of the amplifier allows the amplification to be attenuated in six steps down to a factor of 1000. Under conditions of maximum amplification, full-scale deflection of the meter needle corresponds to a 3 μV variation in the grid voltage of the first tube. The linearity of the amplifier is excellent. The amplification factor varies by less than 1% for different signal strengths. The mean noise (and interference) voltage on the grid of the first tube is approximately 0.2 μV.

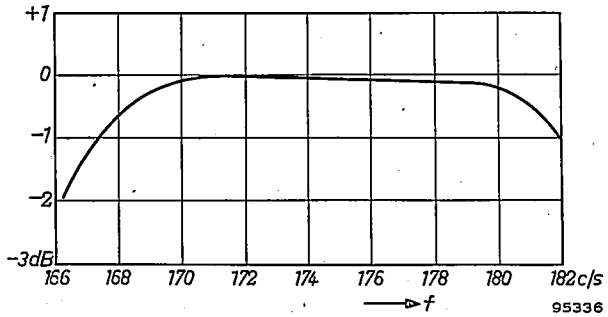

Fig. 3. The frequency response curve of the amplifier. Between 170 and 180 c/s the amplification varies by less than 0.3 dB; beyond 165 c/s and 183 c/s, amplification falls off by more than 3 dB.

Since the current through a transistor depends on its temperature, the phototransistor used in this apparatus is mounted in an aluminium block through which water from the mains supply is circulated. In this way the temperature of the transistor is reduced and stabilized at approx. 16 °C. Lowering the temperature has a favourable effect on the signal-to-noise ratio.

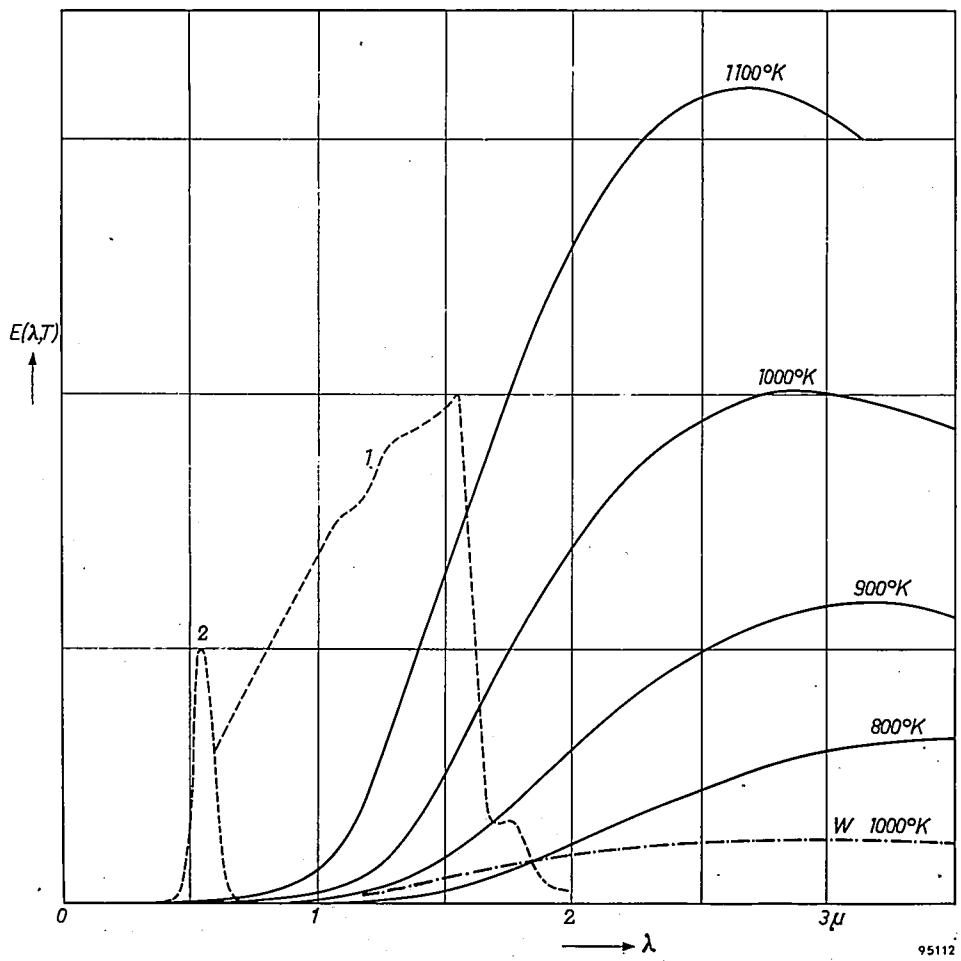

Fig. 4. Spectral energy distribution of the radiation from a black body at 800, 900, 1000 and 1100 °K (fully-drawn curves). The $E(\lambda,T)$ curve for a tungsten source at 1000 °K (chain-dotted line) is shown for the purpose of comparison. Dotted line *1* represents the spectral sensitivity of the OCP 71 transistor in arbitrary units; dotted line *2* is the sensitivity curve of the human eye, also in arbitrary units.

To reduce the risk of electrical leakage from the transistor, it is coated with a thin skin of a water-repellent resin prior to mounting, by treatment with dimethyldichlorosilane, $(CH_3)_2Cl_2Si$.

The conditions under which the new pyrometer is used may be illustrated with the help of *fig. 4*. The fully-drawn curves in this figure are those of the spectral energy distribution $E(\lambda,T)$ of radiation from a black body at various temperatures T between 800 °K and 1100 °K. Dotted line *1* indicates the spectral sensitivity of the transistor on an arbitrary scale; the peak of the curve occurs at 1.55 μ. Dotted line *2* is the sensitivity curve of the human eye, which of course governs measurements made with the optical pyrometer. The figure shows that the new pyrometer is sensitive to a wider band than the optical instrument, being able to detect wavelengths as long as 2 μ. Thus its sensitive range is not limited, as that of the optical pyrometer is, to the extreme tail of the energy spectrum from bodies at about 1000 °K; the new instrument is sensitive to wavelengths at which the radiation density is considerably higher.

In accordance with the usual practice, the pyrometer is calibrated with the aid of a black body, each meter-reading being correlated with a certain temperature. A source of radiation other than a black body that gives rise to the same meter-reading as a black body at a temperature Z may be said to have an apparent temperature of Z; its true temperature T is higher. If, with this instrument, it is to be possible to determine the true temperature from the apparent temperature, further calibration has to be undertaken; this involves measuring the temperature of the object in some other manner, with a thermocouple, for example. For some materials it is almost impossible to measure the true temperature, and in such cases one must make do with measurement of the apparent temperature; knowledge of this does in fact suffice for the solution of many problems in radio-tube manufacture.

In principle, the familiar formulae of radiation pyrometry might be employed for deriving the true temperature T from the apparent temperature Z. The relationship between T and Z becomes comparatively simple if the pyrometer satisfies two conditions: *a*) that it is sensitive only to radiation falling within so narrow a wavelength interval that it can be regarded as monochromatic, and *b*) that this wavelength is short compared with the wavelength of the peak of the radiated spectrum.

The energy distribution of the radiation emitted by a black body is given by Planck's formula. However, for $\lambda T \ll C_2$ (where $C_2 = hc/k = 1.438 \times 10^{-2}$ m.°K, the second constant in Planck's formula), i.e. for the shorter wavelengths of the emitted spectrum (condition *b* above), Planck's formula may be replaced by the simpler formula of Wien:

$$E(\lambda,T) = 2\,C_1\lambda^{-5}\,e^{-C_2/\lambda T}. \quad \ldots\ldots \quad (1)$$

The transistor is, in fact, not sensitive to wavelengths longer than 2 μ, which is a short wavelength in comparison with $\lambda = C_2/T$ for bodies at the temperatures that interest us, viz. 1000 °K ($C_2/1000 \approx 14\ \mu$). Under these circumstances, Wien's formula deviates, in fact, less than 0.1% from Planck's formula.

The requirement of monochromatic radiation (condition *a* above) arises from the fact that the bodies whose temperatures are to be measured are, in general, selective emitters, i.e. non-black bodies whose emissivity varies with the wavelength. If we consider only the radiation within a given small wavelength interval $d\lambda$, a non-black body emitting the same energy as a black body (at another temperature) may be said to have an apparent temperature Z numerically equal to the true temperature of the black body; the true temperature T of the non-black body is of course higher. This may be expressed by equating the energies emitted:

$$E(\lambda,Z)d\lambda = e(\lambda,T)d\lambda, \quad \ldots\ldots \quad (2)$$

where e represents the energy distribution function for the non-black body.

From the definition of the emissivity $\varepsilon(\lambda,T) = e(\lambda,T)/E(\lambda,T)$, we re-write (3) as:

$$E(\lambda,Z) = E(\lambda,T)\,.\,\varepsilon(\lambda,T). \quad \ldots\ldots \quad (3)$$

If, then, our pyrometer responds only to monochromatic radiation, within a specified interval $d\lambda$, at which the emissivity ε is known, the true temperature T of a body can be calculated from the apparent temperature Z which is measured on the black-body calibrated pyrometer. If ε does not vary too rapidly with wavelength, the true temperature could be calculated with reasonable accuracy even when the pyrometer responds to a small range of wavelengths. (This is indeed the case in the optical pyrometer.) The relationship between T and Z is now given by substituting (1) in (3). The fact that we may use Wien's formula (1) in the present circumstances makes this relation very simple:

$$\frac{1}{Z} = \frac{1}{T} - \frac{\lambda}{C_2}\log\varepsilon(\lambda,T). \quad \ldots\ldots \quad (4)$$

Experiments show that for temperatures between 500 °K and 1000 °K the new pyrometer behaves as if it were indeed responsive only to radiation of a single wavelength. *Fig. 5* shows the response of the pyrometer to radiation from a black body, plotted logarithmically in arbitrary units against the reciprocal of the absolute temperature. The values fall almost exactly on a straight line: this implies response to a single wavelength (take logs of equation (1); the equation then represents a straight line if λ is constant). The slope of the line in fig. 5 corresponds to a wavelength of 1.51 μ.

Having shown that conditions *a*) and *b*) are both satisfied, we might now expect that we could apply (4) to obtain the true temperatures of bodies from the measured apparent temperatures. Unfortunately, however, (4) can rarely be applied in practice owing to the lack of reliable data on the emissivities of many of the materials used in electron-tube manufacture.

Of course, if the true temperature of an object has been measured by some other method, it is quite possible to proceed in the reverse direction and to determine ε from the pyrometer response. This is, of course, the usual procedure. The response curve appropriate to nickel appears in fig. 5 as a dotted line. This curve likewise proves to be straight and, moreover, to be parallel to that for the black body. From the vertical distance between these straight lines the value

of ε can be calculated (see definition of ε, above). Its value, which is independent of temperature (the lines being parallel), is found to be 0.22.

The disparity between the true and the apparent temperatures is a good deal greater with the transistor pyrometer than it is with the optical instrument [7]). For nickel at a temperature of 797 °C, the disparities are 139 °C and 45 °C respectively.

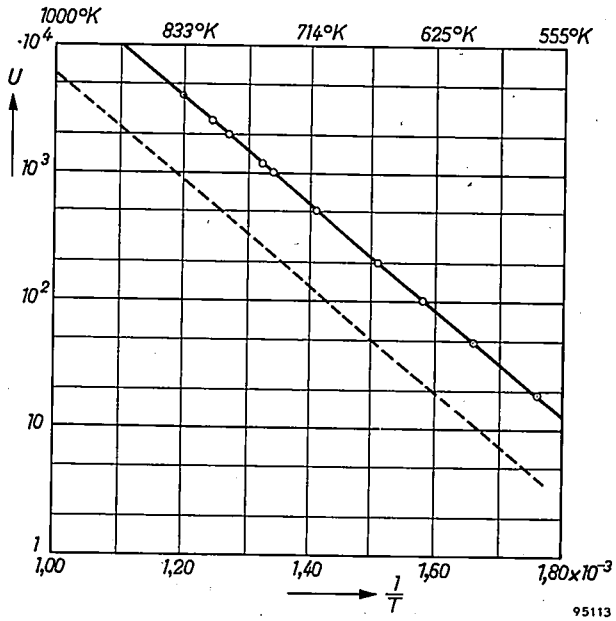

Fig. 5. The logarithm of U, the response of the pyrometer (in arbitrary units), as a function of the reciprocal of the absolute temperature. The fully-drawn curve refers to a black body, the dotted one to a nickel source. Both curves are straight; moreover, they are parallel.

[7]) From (4) it can be shown that, for any given temperature, this disparity is approximately proportional to λ. In the measurement of temperature of metals, the effect is generally reinforced by a fall-off in the spectral emissivity of the metal at the longer wavelengths.

It is particularly convenient, from the practical standpoint, that the transistor is insensitive to radiation of wavelengths longer than about 2 μ. It is possible, in consequence, to measure the temperatures of electrodes of finished radio tubes without corrections having to be made on account of radiation absorbed by the glass envelope; the amount of absorption in glass of this thickness only becomes significant for wavelengths longer than 2 μ. On the other hand, of course, the instrument cannot be used for measuring the temperature of the envelope itself. Reflection from the surface of the glass does, however, have to be taken into account. The simplest way of doing so is to carry out the calibration procedures referred to above with reference objects that are likewise behind glass.

As already stated, the lowest measurable temperature is determined by the signal-to-noise ratio. In an instrument now being constructed, in which the system of lenses is replaced by a mirror with a very large aperture, the signal-to-noise ratio will be considerably higher and the range of measurement will consequently extend to even lower temperatures. In addition, the rotating disc in this instrument will be inserted between the optical system and the transistor, close to the diaphragm. This will allow the size of the disc and the mechanical power unit to be considerably reduced, so that it will be possible to combine them with the camera in one assembly. By virtue of this the new instrument will be a portable one.

F. H. R. ALMER and P. G. van ZANTEN.

ENCLOSED WELDING OF RAIL SECTIONS

621.791.75:625.143

One very well-known practical consequence of thermal expansion is that enough space has to be left between the rails of the permanent way to allow them to expand to the anticipated maximum without any danger of buckling. Now the railway authorities would be glad enough to do away with these gaps between rails, for their elimination would result in an immense saving in maintenance on the track and rolling stock. It has been estimated that no less than 80% of maintenance costs are attributable to jolts set up as trains pass over the gaps. The reduction of jolting and noise would also mean more comfort for the passenger. However, the danger of buckling has always made the gaps a necessary evil.

In recent years there has been a change for the better in this respect, thanks to improvements that have been made in most countries in the manner of laying the rails. Rails are now fixed more firmly to the sleepers, the distance between sleepers has been reduced, and the gravel metalling has been improved. These improvements have reduced the risk of buckling to such an extent that it has become unnecessary to leave gaps between sections of rail.

For fullest advantage to be taken of this fact, the ends of the sections should be welded together. Until a few years ago, however, no satisfactory method existed that could be employed for doing so *in situ*. Non-electric methods, such as thermite welding, do not in general give very good results. In arc-welding, one comes up against the difficulty that the greater part of the weld has to be made between vertical faces, namely the cross-sections of the web and head of the rail. This means that only a moderate welding current can be used, otherwise the filler metal will run away before it has time to solidify. Making the weld is therefore a slow job. Worse still, on account of the low current value too little heat is communicated to the parent steel on either side of the weld, which therefore cools quickly, becoming very hard and brittle in places owing to its high carbon content. The only electrical method of satisfactorily welding rails was resistance welding. That method cannot of course be employed on the track. It is in fact employed sometimes in railway workshops, but the overall length of the welded sections is restricted by the need to transport them on a string of flats wagons. A total length of 60 yards — 200 yards in exceptional cases — is not usually exceeded; and the problem of joining the welded sections together still has to be solved.

It became clear that the whole question was of more than local interest when, in quick succession, inquiries reached Philips Welding Department from four railway companies in different countries. We believe we have found the answer to their problem in the shape of an arc-welding method that was in process of development when the inquiries were made. For reasons that will become clear in a moment, we refer to the method as "enclosed" welding.

The investigations that eventually led to the enclosed welding method were undertaken in the following circumstances.

Metallurgical research had established that hydrogen was frequently the cause of unsatisfactory results in arc-welding by the normal method. Fairly large quantities of that element are present in the deposits from normal welding electrodes, such as mineral-coated and rutile electrodes. *Basic* types of electrode coatings ("low-hydrogen electrodes") have brought about a big improvement in this respect [1]).

A characteristic difference between basic (or low-hydrogen) and non-basic electrodes becomes apparent when molten steel and liquid slag are present in equilibrium. Where non-basic electrodes have been used, the steel may contain slag inclusions and the slag itself may be free from metal (*fig. 1a*);

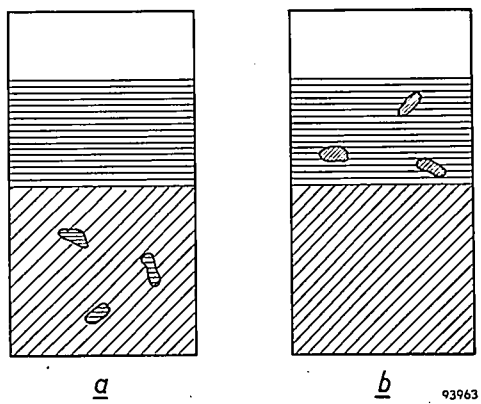

Fig. 1. Diagrams to show equilibrium states of molten steel and liquid slag when (*a*) non-basic electrodes have been used, (*b*) when basic electrodes have been used. In case (*a*) it is possible for slag to be present in the steel, but not for steel to be present in the slag; precisely the opposite applies in case (*b*).

when basic electrodes are employed, however, the weld steel is *slag-free*, although drops of metal may be present in the slag (fig. 1*b*). (It may be observed that the question as to which of the two states will result is not merely a matter of specific gravities.) It was clear that this particular property of basic

[1]) J. D. Fast, Philips tech. Rev. 14, 96, 1952/53.

electrodes, which plays no part in ordinary welding, might assume a practical importance: even when working with a large weld-pool, it would be possible to obtain a deposit essentially free from the macroscopic slag inclusions that do a great deal to weaken a weld.

Our investigations, referred to above, were directed toward finding a practical way of exploiting this fact. After a series of tests, we arrived at the arrangement shown in *fig. 2* for making a *vertical* butt weld.

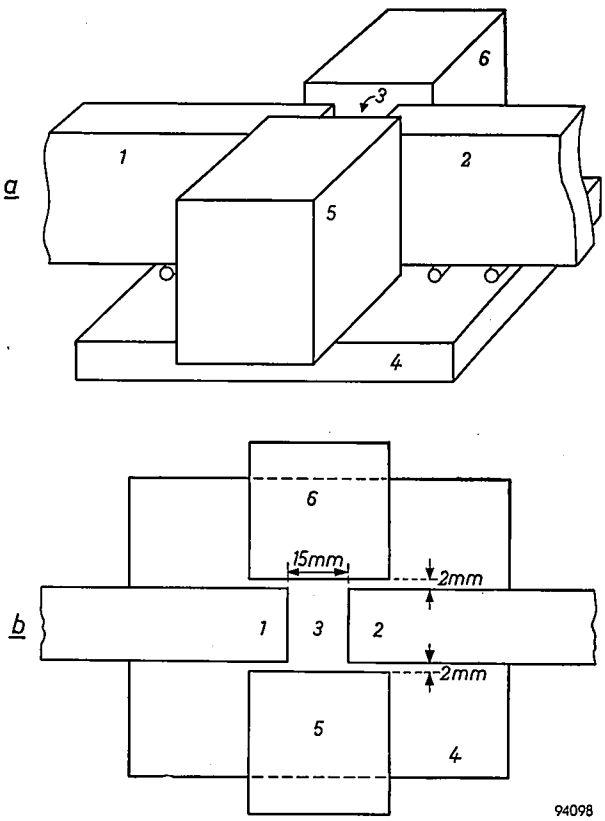

Fig. 2. Arrangement for enclosed welding of two steel bars *1* and *2*. The enclosure consists of a base-plate *4* and blocks *5* and *6*, all of copper. Welding is carried out inside the compartment *3*. The clearances through which the slag runs out are visible in the plan view.

Two steel bars *1* and *2* to be welded together, are arranged vertically with a gap *3* of about 15 mm between their edges. The bottom of the gap is closed by a copper base-plate *4*, and its sides are blocked by copper blocks *5* and *6*. A basic welding electrode is introduced into the compartment *3* thus formed, and the arc is struck against the lower part of one of the bar ends. A thick electrode (5 to 8 mm) and a correspondingly heavy welding current (250 A to 450 A alternating current) is preferably employed. A large pool of molten steel, with liquid slag on top of it, is now formed in the compartment. Since narrow clearances (2 mm) have been left between the workpieces and the copper blocks and base-plate — see view from above in fig. 2 — the thin liquid slag runs out through these openings, but the steel remains. The function of base-plate *4* and blocks *5* and *6* is rather similar to that of the moulds ("shuttering") used for concrete structures — they form a temporary enclosure for the concrete while it is setting.

These tests confirmed that, when basic electrodes are used, the deposited steel will be free of macroscopic inclusions if only it has remained molten for a long enough time. That condition appears to be satisfied by the arrangement shown in fig. 2, providing halts for electrode changing are of very short duration (when large cross-sections are being welded, dozens of electrodes are necessary for the one job). There is a big difference between enclosed welding and normal welding in layers: in the former the whole weld actually constitutes a single layer; in the latter case, thin layers up to the required number are deposited one on top of the other. As a result of this, and as a consequence, too, of the heavier welding current, the amount of heat applied per unit length of an enclosure-welded joint is about seven times as much as that applied per unit length and per layer in normal welding. In enclosed welding the parent steel facing the weld cools so slowly that no appreciable hardening takes place in the transition (heat-affected) zone. A second consequence of the rapid heating rate is that the work proceeds quickly. The components of the enclosure can be used over and over again, for hundreds of jobs. All that is necessary is now and again to regrind those faces that have roughened with use.

Although the process looked promising, it was found that even low-hydrogen electrodes still contained too much hydrogen for enclosed welding. The difficulty is that the high column of molten steel prevents the escape of the hydrogen [2]) which must be removed as the temperature drops. The enclosed welding of vertical and almost vertical joints only became a complete success once a special ("extra low-hydrogen") electrode had been developed. To prevent these new electrodes (Philips 56 R) absorbing moisture in transit or during storage they are supplied only in airtight tins.

The manner of welding rail sections end-to-end can be divined from the simple arrangement in fig. 2. However, the shape of the rail cross-section calls for enclosure components that are more elaborate then those for flat plates. *Figs. 3a* and *b* show the components required and their positioning. Welding of rail sections begins at the foot of the rail. Here a

[2]) P. C. van der Willigen, De metallurgie van het lassen van staal, Lassymposium Utrecht 1957, page 25 (in Dutch).

difficulty arises that always gives trouble when massive objects are to be welded: the bulk of the rail remains cold, and hence initially the parent steel in the vicinity of the weld cools quickly, thereby becoming brittle. The difficulty may be overcome by delaying the cooling process. A simple way of doing so is to heat the foot with an oxyacetylene flame prior to welding, raising its temperature to about 400 °C. *Fig. 4a* shows the enclosure in position: foot and web of the rails have already been welded, and the welding of the head can now begin. The completed weld may be seen in fig. 4*b*.

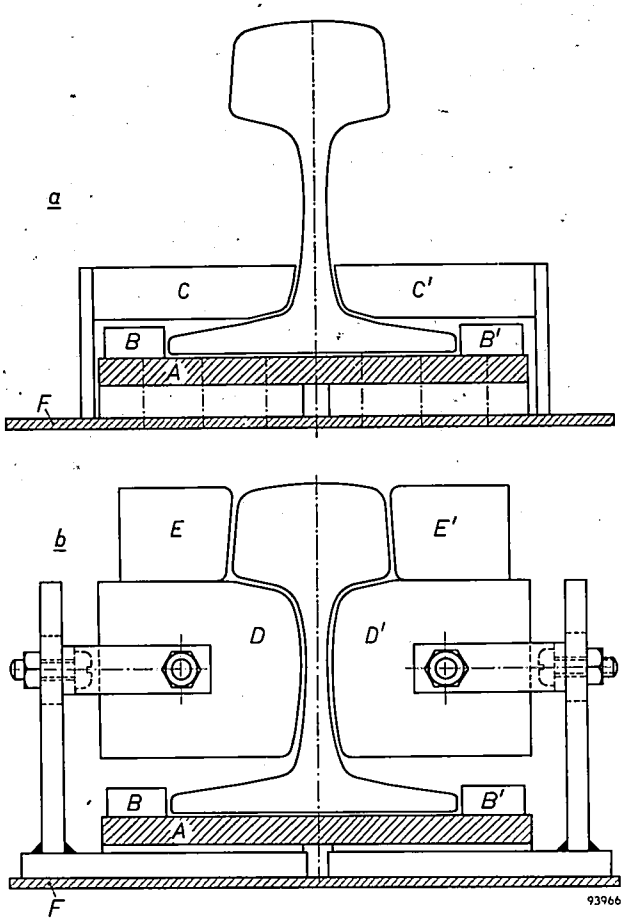

Fig. 3. Enclosure for welding rail sections. *a*) With the base-plate *A* and small blocks *B* and *B'* in position, the foot is welded. Blocks *C* and *C'* are then added and the lower part of the web is welded. *b*) Blocks *C* and *C'* are replaced by large blocks *D* and *D'*, and the welding of the web is completed. Adding blocks *E* and *E'* allows the head to be welded. Base-plate *A* and blocks *B* ... *E'* are of copper. *F* is a steel plate on which rest the clamps for blocks *D* and *D'*.

Important advantages of enclosed welding are that no preparative machining and but little finishing are required and that, as already stated, it is a quick method. (Providing the gap in the rails is of the right size, the weld can be made and finished off within half an hour.) Further practical details are given in an article [3]) that has appeared elsewhere. Suitable enclosures can equally well be designed for other cross-sections; among the enclosures designed, there is one for rods of circular section such as used for the reinforcement of concrete.

A new welding method cannot be recommended unless both laboratory investigation and practical tests have proved its soundness. As regards the former, the Philips Laboratory at Eindhoven has made photographs of etched sections and radiographs of numerous specimens of enclosed welds. These testify to the absence of macroscopic inclusions (*fig. 5*). In addition, the Vickers-Lips hardness meter, which is ideally suited to the purpose [4]), has been used to determine local variations in hardness in the weld itself, in the transition zones and at places beyond that part of the rail affected by the welding operation. Hardness curves obtained in this way are shown in *fig. 6*, from which it may be seen that the value of 300 VPN 10 [5]) — which is still quite acceptable — is nowhere exceeded.

A great variety of methods are used by railway engineers in various countries for testing the mechanical endurance of rails. All such tests have been carried out by outside organisations, since Philips does not possess the appropriate equipment. *Pulsation tests* and *tup tests* are the most important kinds.

Pulsation tests, the purpose of which is to determine fatigue strength, have been conducted by the Netherlands Railways and British Railways, by T.N.O. [6]) Delft (on behalf of Kloos and Sons' Workshops at Kinderdijk, Holland) and also at the Munich Technische Hochschule (on behalf of the Bamag Works at Butzbach, Germany). In these tests the operative quantity is P, the tensile stress in the outermost fibre of the foot of the rail. A stress P is caused to oscillate between a low minimum value P_{min} (e.g. one or two kg/mm^2) and a gradually increasing maximum value P_{max}. The fatigue strength is taken to be the value of P_{max} at which fracture just fails to occur after say 1 000 000 pulsations have been passed (however, the number of pulsations to which the test piece is subjected may be as high as 3×10^6, 5×10^6 or even 10×10^6). As always, finish-machining and polishing the weld has a good effect on the test results, since this removes surface irregularities at which fracture is

[3]) G. Zoethout, Het bekist lassen van spoorstaven, Lastechniek **23**, 274-277, November 1957 (in Dutch).
[4]) H. T. Schaap, Hardheidsmeters en hun bruikbaarheid voor het onderzoeken van de overgangszones van lasnaden, Lastechniek **18**, 27-33, 1952 (in Dutch).
[5]) VPN = Vickers' pyramid number. The figure 10 signifies that the measurement was made with a force of 10 kg.
[6]) Dutch National Council for Industrial Research.

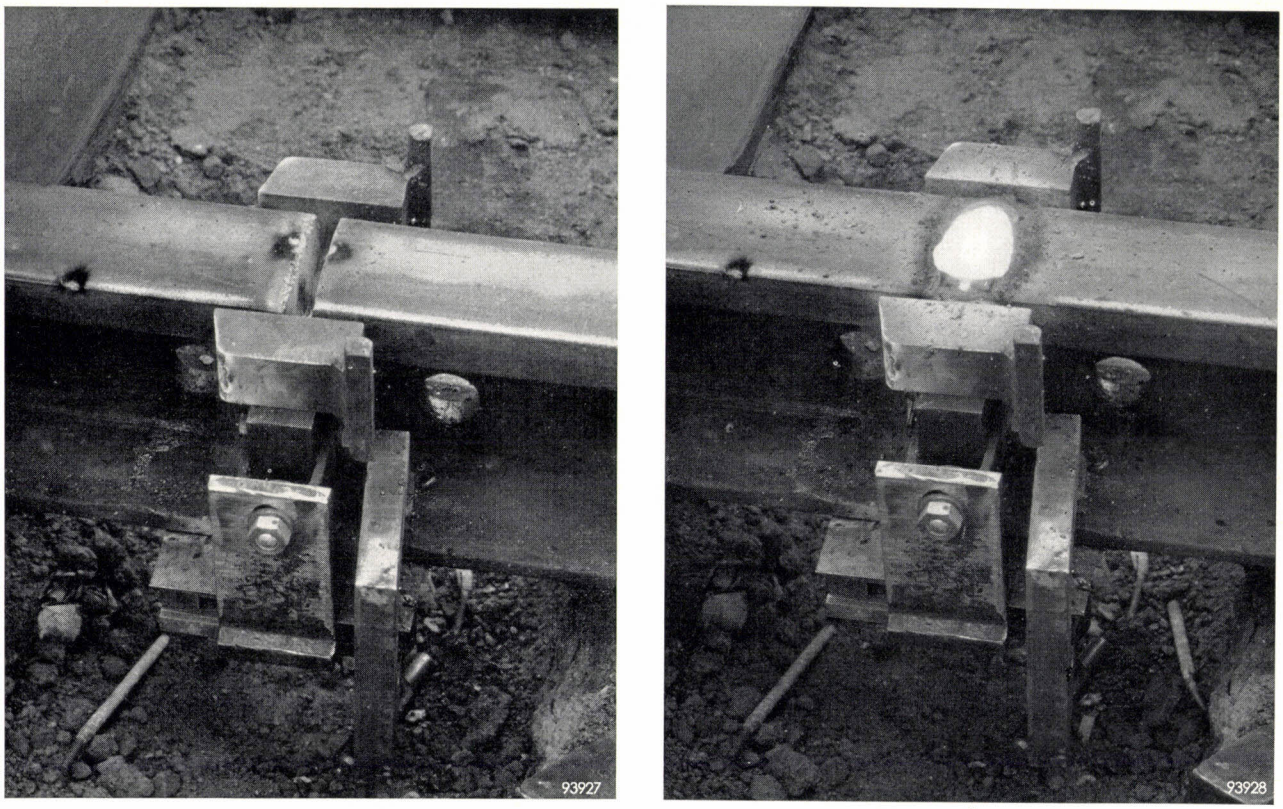

a *b*

Fig. 4. Enclosed welding of rail sections. *a*) Foot and web have already been welded, and the welding of the head can now begin. *b*) The completed weld.

liable to nucleate. In tests by the Netherlands Railways, and in tests by British Railways, in which only the underside of the foot had been so finish-machined, the welds were found to have fatigue strengths approximately half that of the unwelded rail. Fatigue strengths but little inferior to that of the rail itself were found for the finished and polished specimens used for experiments at T.N.O. and Munich. For practical purposes it is recommended that at least the foot, the tread and the inside edge of the head should be finished and polished.

The Netherlands Railways have carried out so-called four-point bend tests, as illustrated in *fig.* 7. To prevent the rough surface of the weld prejudicing the reproducibility of the result, the load was applied a few centimetres on either side of the joint. Typical results appear in *Table I*; a mean fatigue strength of 19 kg/mm^2 was found for these specimens.

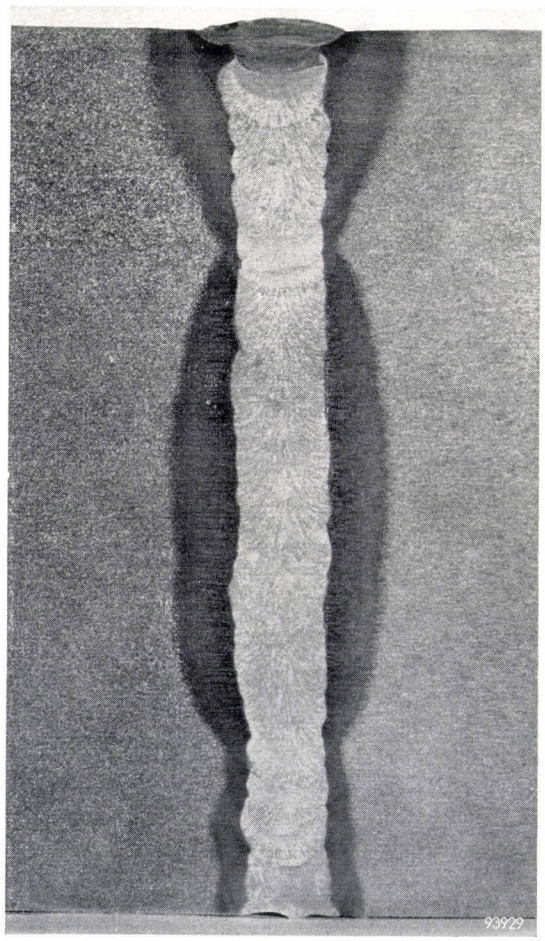

Fig. 5. Photograph of the etched cross-section of a weld made by the enclosed method between two rail sections (0.8 × actual size). No macroscopic slag inclusions are present. The dark regions on either side of the weld are the transition (heat-affected) zones.

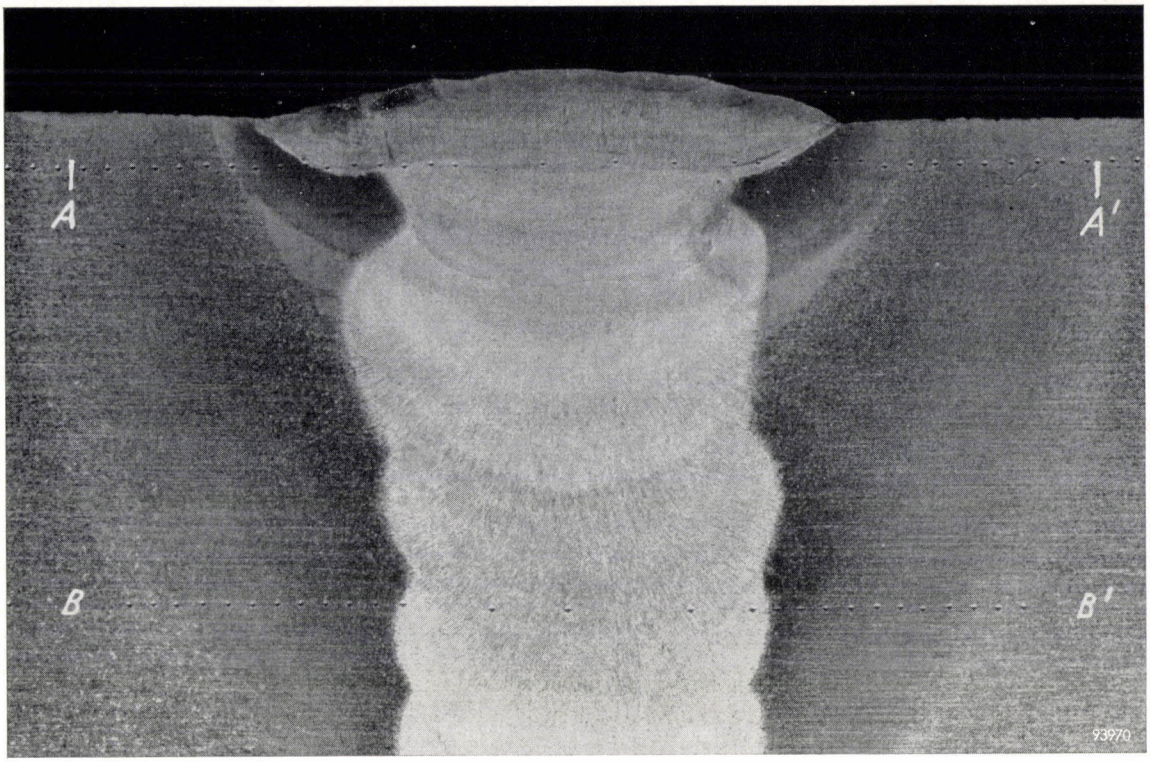

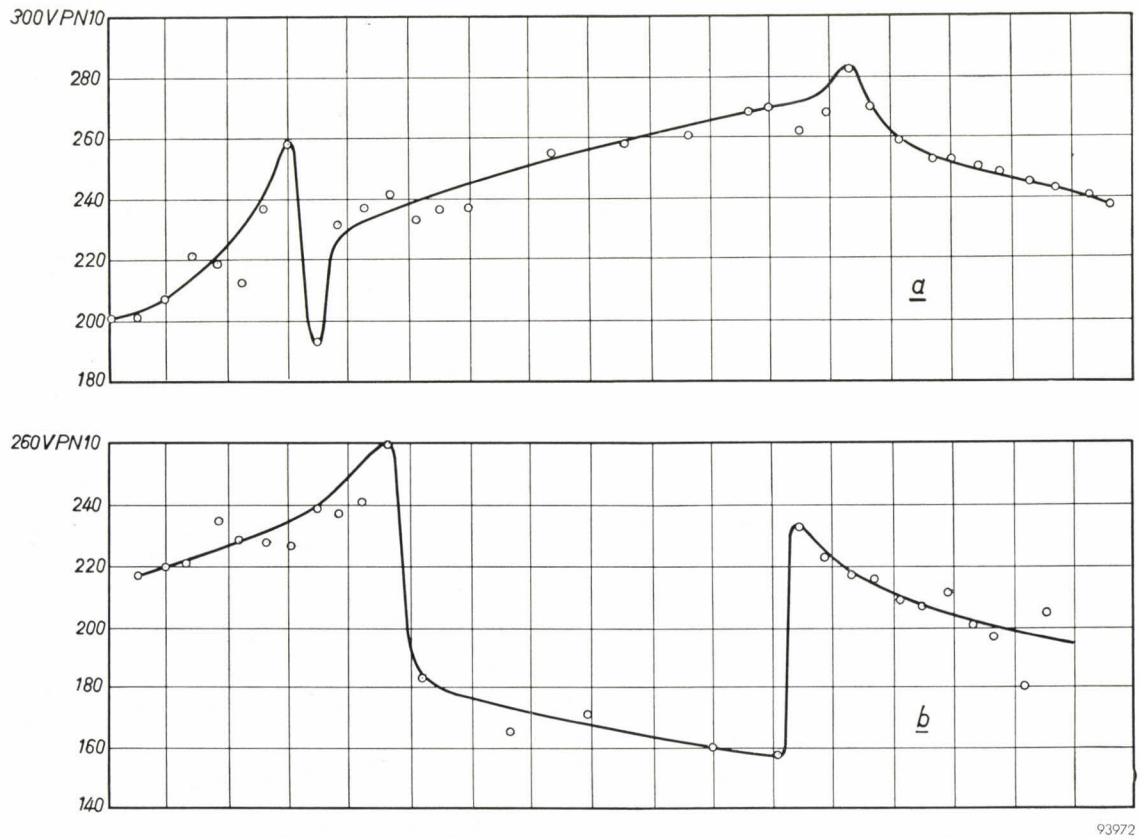

Fig. 6. The photograph shows a detail of the head of the weld appearing in fig. 5 (3.2× actual size). A row of indentations made by the Vickers-Lips hardness meter may be seen between A and A'. The hardness values determined from the indentations and expressed in Vickers units are plotted in curve a. Curve b corresponds to the indentations B-B'. All values occurring in the curves are well below 300 VPN 10 [5]).

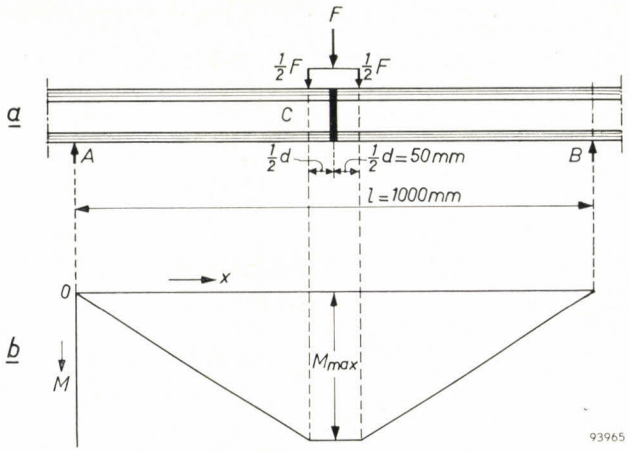

Fig. 7. Four-point bend test on enclosure-welded railway sections, as conducted by the Netherlands Railways. *a*) The specimen of welded rail *C* rests on supports *A* and *B* (distance apart $l = 1$ m) with the weld in the middle. A pulsating force $\frac{1}{2}F$ is applied at two points a distance of $\frac{1}{2}d = 50$ mm on either side of the weld; the weld has not been finished or polished, but at the points where the forces are applied the steel has its original smooth surface. *b*) Bending moment M as a function of length x along the specimen. Between the points of application of the load the bending moment has a uniform maximum value of $M_{max} = \frac{1}{4}F(l-d)$.

Tests on behalf of British Railways, carried out in the Derby laboratory of the British Transport Commission, gave comparable results.

Table II contains the results of tests on two finished and polished weld samples. The tests were carried out at the Institute for Rail and Road Construction of Munich Technische Hochschule, under the direction of Prof. Meier. The results agree fairly well with those of corresponding tests done by T.N.O., in which small rods cut out of the foot of the weld sample constituted the test objects.

Tup tests have been conducted by the railway authorities in England (British Railways) and France (S.N.C.F.).

The British Railways tests, carried out in their laboratory at Redbridge, consisted in allowing a tup of $1\frac{1}{4}$ tons (1270 kg) to fall on the weld from a height that was progressively increased by 6 inches until fracture occurred. The distance between the two supports on which the test object rested was 1.20 m, and the rails weighed about 54 kg per metre. Eight out of ten welds fractured at 5.33 ton.metres, the remaining two at 7.00 ton.metres.

In their laboratory at Moulin-Neuf, the S.N.C.F. carried out six tup tests whereby a tup of 1000 kg

Table I. Results of pulsation tests carried out by the Netherlands Railways on six welds between rail sections, only the foot of the weld having been finish-machined. The rails weighed 46 kg per metre. $P_{min} = 2$ kg/mm².

P_{max}, kg/mm²	Number of pulsations	Result
17	2 700 000	No fracture
18	2 760 000	No fracture
19	3 160 000	No fracture
20	2 170 000	Fracture
20	2 430 000	Fracture
20	3 200 000	Fracture

Table II. Pulsation tests carried out by Munich Technische Hochschule on two samples of finished and polished welds between rail sections weighing 49 kg/m. $P_{min} = 1$ kg/mm².

Sample	P_{max}, kg/mm²	Number of pulsations	Result
1	22	2 000 000	No fracture
	24	2 000 000	No fracture
	26	2 000 000	No fracture
	28	2 000 000	No fracture
	30	2 000 000	No fracture
	31.5	2 000 000	No fracture
	32.5	983 000	Fracture
		Total 12 983 000	
2	25	5 000 000	No fracture
	28	5 000 000	No fracture
	31	3 900 000	No fracture
		Total 13 900 000	

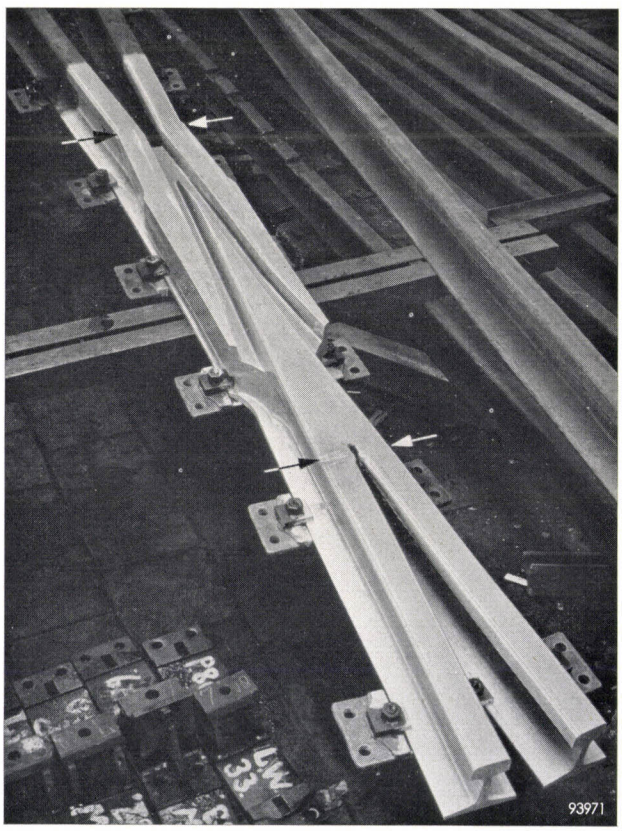

Fig. 8. Switchpoints, welded at both ends to normal rail sections. The joints are indicated by arrows. The section between the welds is milled out of a single steel block ("monoblock" construction).

was dropped on the weld from a height of 6 m and the work done in causing fracture was recorded automatically. Here the distance between the supports was 0.70 m and the rails were of the U33 type. The results obtained were 4.37, 3.21, 3.165, 4.83, 1.51 and 5.23 ton.metres. (They cannot be compared with the English results on account of the quite different conditions under which the tests were performed.)

We may conclude with some notes on the actual employment of enclosed welding on the railways. The workshops of Kloos en Zonen at Kinderdijk, to which reference has already been made, were the first to put the enclosed welding of rail sections into practice: some 90 switchpoints of the so-called "monoblock" type were welded to normal lengths of rail (*fig. 8*). These are now in use in the marshalling yard of the IJmuiden Blast Furnaces. Since then, welding by the new method has been done on a large scale in a number of other shunting yards in the Netherlands (Rotterdam and Eindhoven) and Belgium (Beringen). Having had good results with enclosed welding in a shunting yard near Toten, British Railways are now using the process on both branch and main lines. A number of gangs are proceeding with this work daily, and have already made thousands of welds.

G. ZOETHOUT.

AN EXPERIMENTAL INDUCTION-HEATING GENERATOR USING HYDROGEN THYRATRONS

by H. L. van der HORST and P. H. G. van VLODROP. 621.385.38:621.365.5

Hydrogen thyratrons, originally developed for the generation of modulating pulses for radar magnetrons, can also be used with advantage in induction-heating generators. As described below, the circuit is a modern version of the time-honoured spark-gap oscillator used in the early years of radio telegraphy.

The method of heating electrically conductive materials by inducing a current in them is widely used in industry. Its general advantage is that the heat can be applied very rapidly. In various heat treatments, for example surface hardening, a particular advantage is that the supply of heat can be accurately controlled and localized, and the fact that the method is very clean is of importance in melting processes. The object to be inductively heated is placed in the "work" coil, which is connected via a transformer to a generator, as represented schematically in *fig. 1*.

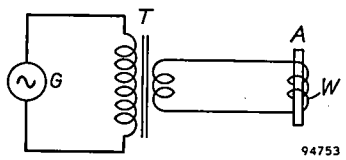

Fig. 1. Induction heating of a workpiece *A*. *W* work coil, *T* transformer, *G* generator.

With an eye to efficiency the choice of frequency is important. In an earlier article in this Review [1]) it was shown that a certain minimum frequency f_{min} is needed to ensure that the workpiece receives a large proportion of the power supplied to the work coil. The minimum frequency is higher the smaller the size, conductivity and permeability of the workpiece. Sizes, in particular, vary very widely; f_{min} lies in the region of the mains frequency only when the size of the workpiece corresponds to a quantity of the order of 1000 tons. In the majority of cases the quantities are smaller, and therefore a generator of higher frequency is needed to ensure a reasonable efficiency.

For workpieces ranging in weight from some hundreds to a few kilograms, *rotary converters* are suitable generators. They are designed for a fixed frequency not higher than about 10^4 c/s, and for power outputs up to about 1000 kW. Smaller objects are preferably heated at higher frequencies (10^4 to 10^7 c/s), generated by transmitting tubes. With the advance of transmitting-tube technique it is now possible to make electronic generators of 500 kW. They are used, among other things, for the preparation of alloys.

For the sake of completeness, and especially having regard to what follows, we must mention an older type of high-frequency generator, namely the spark-gap oscillator, in general use several decades ago in radio telegraphy. Here the charge built up in a capacitor discharges periodically via a spark gap through an oscillatory circuit, thereby producing in this circuit a damped oscillation.

In 1947 experiments were started in the Philips Laboratory at Eindhoven with the object of giving the spark-gap oscillator a new lease of life by substituting one or more senditrons for the spark gap. (Senditrons are rectifying tubes containing a mercury-pool cathode and a capacitative igniter electrode [2]).) Such an oscillator would have the advantage of a higher efficiency than an oscillator with a transmitting tube. It was found, however, that higher frequencies could be obtained with a certain type of thyratron (rectifying tubes with hot cathode, control grid and gas filling), namely the *hydrogen thyratron* developed for modulating magnetrons in radar transmitters. A thyratron of this type is shown in *fig. 2*. Hydrogen is used as the gas filling because it has the shortest de-ionization time. This property accounts for the fairly high frequencies (up to 10 kc/s) that can be generated with these thyratrons in the circuit described below. Owing to their higher arc voltage and the presence of a hot cathode, their efficiency is somewhat lower than that of senditrons, but still so much better than with transmitting tubes that no forced cooling with water

[1]) E. C. Witsenburg, Heating by high-frequency fields, I. Induction heating, Philips tech. Rev. **11**, 165-175, 1949/50.

[2]) T. Douma, A new method for converting D.C. energy into high-frequency A.C. energy with a high efficiency, specially intended for high-frequency induction heating, Communication News **10**, 52-68 and 69-82, 1949.

or air is required. This is an important practical advantage.

A generator with an oscillating vacuum tube and subject to variable load conditions, as is the case in induction heating, is liable to be overloaded unless

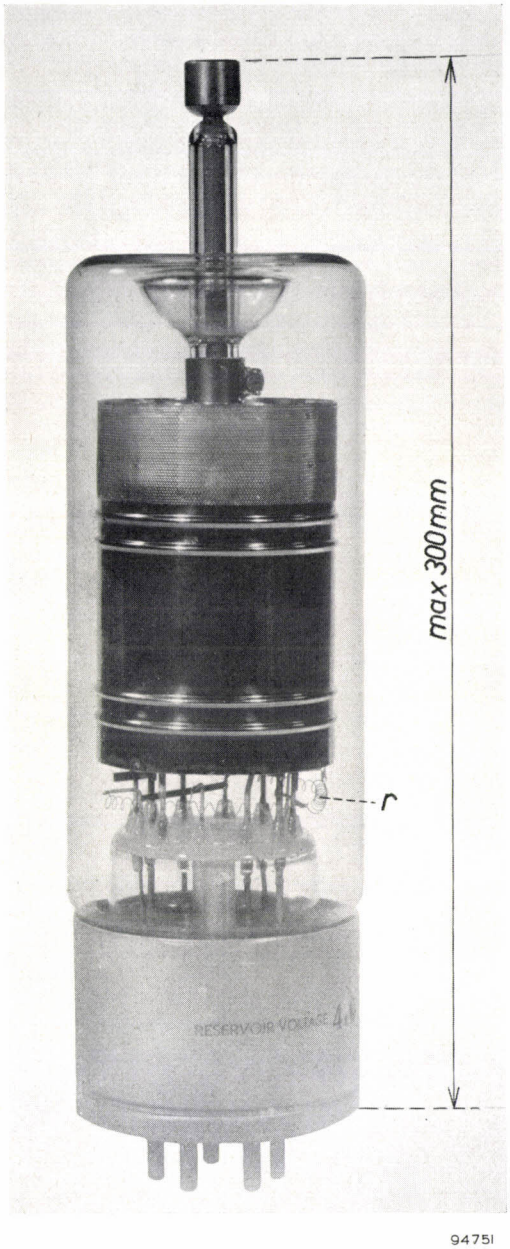

Fig. 2. Philips hydrogen thyratron type 5949. Max. peak anode voltage: 25 kV in both forward and inverse directions. Max. peak anode current: 500 A. Max. mean anode current: 0.5 A. The tube contains a hydrogen replenisher r in the form of a separate filament. As long as this is cold, practically all the hydrogen is adsorbed on its surface. The correct hydrogen pressure is established when this filament is connected across the prescribed voltage.

safety measures are adopted, or at least a certain degree of skill exercised in operation. The generator described here excites damped oscillations, the damping varying with the load. The changes in damping are put to use for controlling the thyratrons in such a way as to render other precautions superfluous. This makes the generator very easy to operate.

The circuit diagram is shown in its simplest form in *fig. 3*. The circuit works as follows. During the time that the thyratron *Th* is not conducting, the polyphase rectifier R (voltage V_0) charges the capacitor C_1, via a choke L_3, to a voltage that may be higher than V_0 (maximum $2V_0$); C_1 cannot, of course, loose any charge through the rectifier. Next, *Th* is ignited by a pulse on its control grid, so that C_1 can now discharge through the current-limiting choke L_1 and the thyratron into capacitor C_2. The transformer T provides the coupling with the work

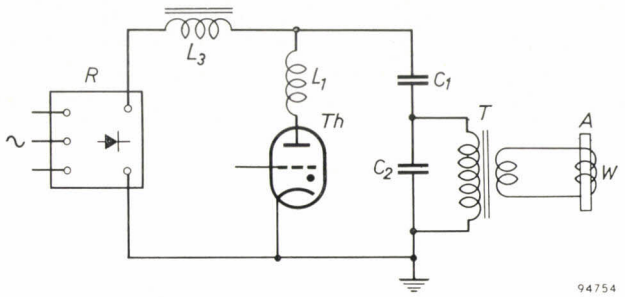

Fig. 3. Simplified diagram of an induction-heating generator with a hydrogen thyratron. Capacitor C_1 is charged up via choke L_3 by rectifier R (thyratron *Th* not yet conductive). When *Th* fires, C_1 discharges through the current-limiting choke L_1 and *Th* into capacitor C_2, which, with the self-inductance equivalent to the loaded transformer T, constitutes an oscillatory circuit. A damped oscillation then takes place in this circuit. W work coil, A workpiece.

coil W, which contains the workpiece A. We can regard T as equivalent to a certain self-inductance L_2 and a resistance, and these, together with the capacitor C_2, constitute an oscillatory circuit. Since the self-inductance L_1 is a mere fraction of L_2, the capacitor C_1 discharges very rapidly into C_2. This excites the circuit L_2-C_2, which produces a damped oscillation. Meanwhile the thyratron has become non-conducting. The voltage on C_1 gradually rises again, and as soon as C_1 is once more sufficiently charged, the cycle can again be repeated by the next pulse on the grid of *Th*. Numerous variants of this circuit are possible. The advantage of the one described is that the thyratron cathode and one side of the rectifier and transformer can be connected to earth, which is no mean consideration in view of the high tension used ($V_0 = 10$ kV).

In order for the circuit to function as described, it must comply with several conditions, which we shall now review very generally.

A closer analysis of the circuit [3]) reveals that it turns mainly on two parameters: the capacitance ratio C_1/C_2 and the self-inductance ratio L_1/L_2. The capacitance ratio influences the voltage v_{th} across the thyratron. In *fig. 4a, b* and *c* the variation of v_{th}/V_0 with time is shown for $C_1/C_2 = \frac{1}{2}$, 1 and 2, respectively, for the case of $L_2 \gg L_1$. It can be seen that v_{th} exceeds $2V_0$ neither in the forward nor in the inverse direction only when $C_1/C_2 = 1$; in that case, then, the thyratron is used to the best advantage as far as the voltage is concerned. In practice, however, the most favourable situation obtains at a somewhat smaller value of C_1/C_2, e.g. at $C_1/C_2 \approx 0.75$. The reason is that L_2, although larger than L_1, is in practice not many times larger (fig. 4 applies only to $L_2 \gg L_1$).

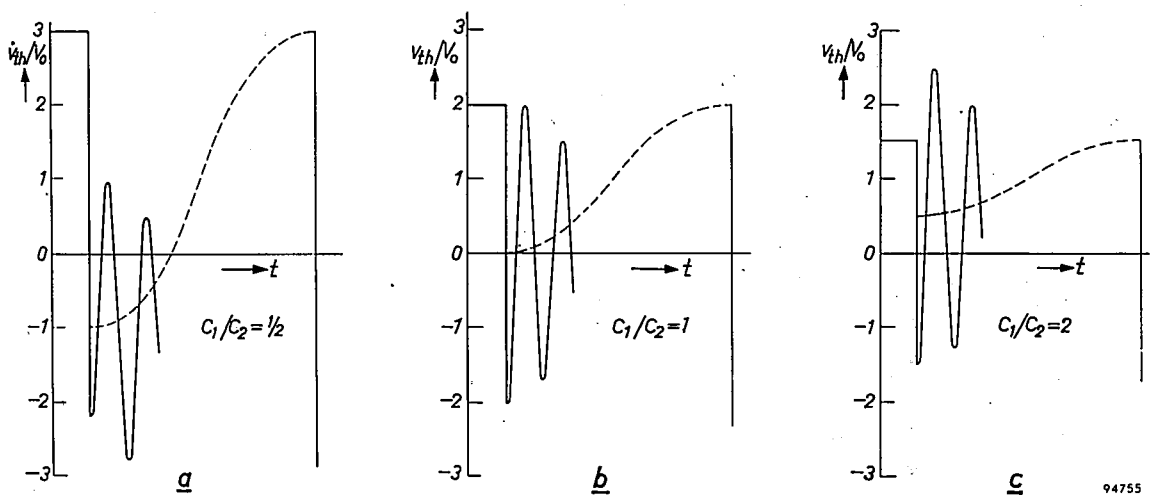

Fig. 4. v_{th}/V_0 as a function of time t for various values of C_1/C_2, in the case where $L_2 \gg L_1$. Only when $C_1/C_2 = 1$ does v_{th} remain less than $2V_0$ in *both* the forward and inverse directions.

For efficient operation it is essential that the thyratron should automatically become non-conducting in every cycle. The discharge current from C_1 flows through the series circuit made up of L_1, the thyratron and the parallel circuit L_2-C_2. In order to ensure automatic extinction of the thyratron the values given to the elements in this circuit must be such as to allow the current to drop to zero. Whether this can happen depends mainly on the self-inductance ratio L_1/L_2. In the article quoted under [2]) it was shown that when $C_1 \gg C_2$ (and neglecting the circuit resistance) the condition for the current to return to zero is: $L_1/L_2 \leqq 0.217$. Where $C_1 \approx C_2$ (see above), L_1/L_2 must still remain below a certain maximum value, but in that case the maximum is higher, e.g. 0.35.

[3]) See Electronic Applications **18**, 57-67, 1957/58 (No. 2).

The self-inductance L_1 is one of the parameters determining the time needed for C_1 to discharge into C_2. To keep this time as short as possible, the value of L_1 should be as low as practicable. It should not, however, be lower than a certain minimum, as otherwise the current through the thyratron would exceed the maximum permissible peak rating. We can roughly estimate the minimum value of L_1 by neglecting the parallel circuit L_2, and disregarding the voltage drop in the thyratron (about 150 V) with respect to the voltage V_{C1} (e.g. 15 kV) to which the capacitor C_1 was charged. In this approximation the circuit consists only of the series capacitances C_1 and C_2 (equivalent to a single capacitance $C' = C_1C_2/(C_1 + C_2)$), and the self-inductance L_1. The current flowing through this circuit reaches a peak value

$$\hat{I}_a = \frac{V_{C1}}{\sqrt{\frac{L_1}{C'}}},$$

hence

$$L_1 = \left(\frac{V_{C1}}{\hat{I}_a}\right)^2 \frac{C_1C_2}{C_1 + C_2}.$$

With a type 5949 thyratron the maximum permissible value of $\hat{I}_a$ is 500 A. In practice, however, it is found that L_1 must be several times larger than appears from the last equation, as otherwise, immediately after extinction of the thyratron, the residual ionization would be so strong, and the negative potential on the anode would rise so rapidly, as to give rise to backfire.

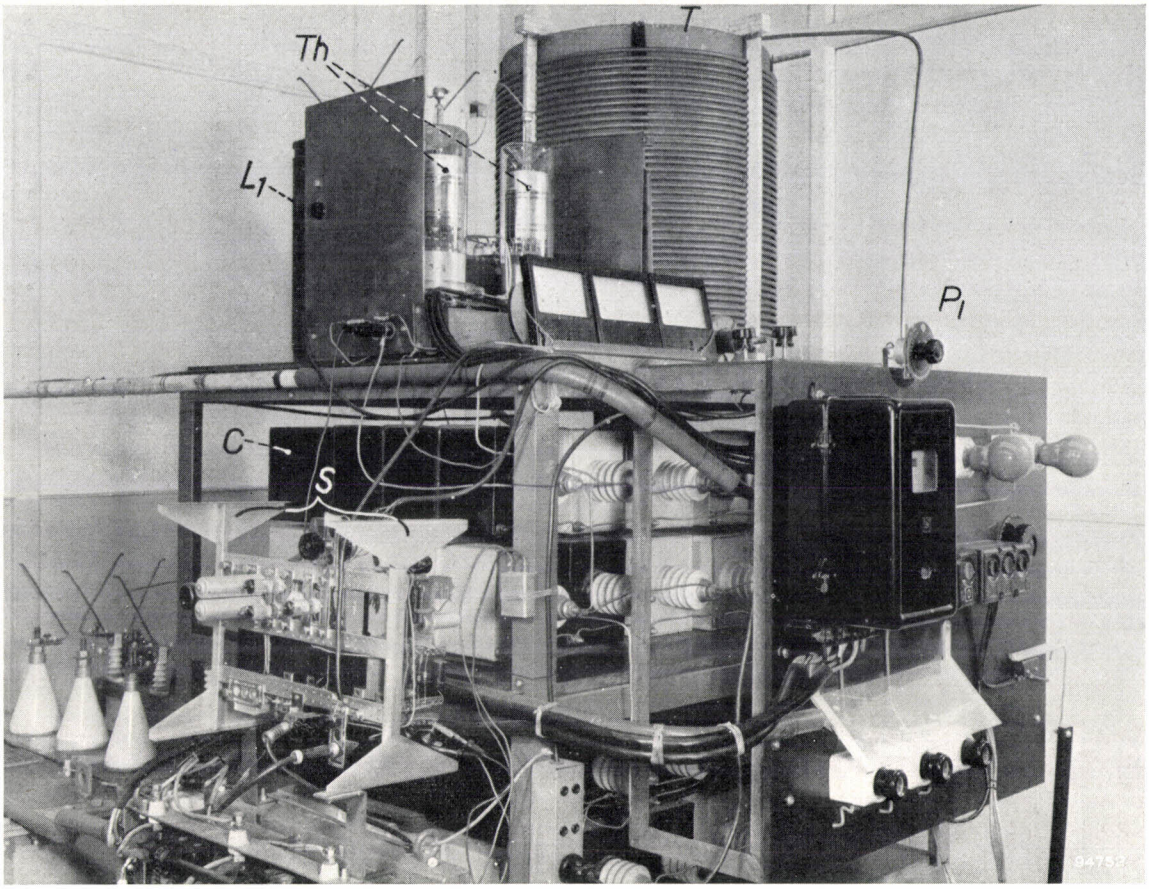

Fig. 5. Experimental set-up of an induction-heating generator containing two hydrogen thyratrons 5949 (*Th*) connected in parallel. L_1 is one of the chokes in series with the thyratrons. At C are the capacitors C_1 and C_2 (fig. 3). T transformer (see fig. 6). S control circuit (see fig. 7). P_1 power-control potentiometer.

The frequency f_0 at which the circuit L_2-C_2 oscillates is

$$f_0 = \frac{1}{2\pi\sqrt{L_2C_2}}.$$

The use of hydrogen as the gas filling in the thyratron permits working with frequencies f_0 as high as 10 000 c/s. This gives the following relation between L_2 and C_2:

$$L_2C_2 = \frac{1}{4\pi^2\times 10^8} \text{ henry} \times \text{farad}.$$

The foregoing considerations are a guide to the correct choice of C_1, C_2, L_1 and L_2.

There remains the self-inductance L_3 of the choke through which C_1 is charged (fig. 3). If the value of L_3 is too low, the thyratron, once it is ignited, will continue to carry current, resulting in a short-circuit across the rectifier. If L_3 is too large, it may happen in certain circumstances that C_1 will be charged to too high a voltage, so high that the thyratron can no longer be kept non-conducting. We have found by experiment that these two limiting values of L_3 are not very far apart.

In the present experimental set-up, shown in *fig. 5*, two thyratrons type 5949 are connected in parallel. In order to ensure that both tubes strike, a choke having a self-inductance $2L_1$ is connected in series with each tube; these two chokes replace the single choke L_1. The complete circuit is then made up of: $C_1 = 0.35$ μF, $C_2 = 0.48$ μF, $L_1 = 175$ μH (i.e. 350 μH in series with each tube), $L_2 = 525$ μH, $L_3 = 0.29$ H, $f_0 = 10$ kc/s and $V_0 = 10$ kV.

In an induction heater using an oscillating transmitting tube, the latter must always be kept matched to its load; this may be done by adjusting a capacitor and/or the coupling of the high-frequency transformer. This is not necessary with a generator working on hydrogen thyratrons, which simplifies operation. Moreover it permits the use of a low-loss transformer having a fixed and very tight coupling, the design of which is sketched in *fig. 6*.

For the experimental installation just outlined the *overall efficiency* has been determined, i.e. the

ratio of the power P_2 developed in a given workpiece to the power P_1 which the rectifier draws from the mains (hence including the losses in the rectifier, in the transformer and in the work coil). For measuring P_2 a workpiece was used consisting of concentric steel cylinders, between which water was passed. P_2 was derived from the rate of flow of the water and its rise in temperature. The overall efficiency found was $P_2/P_1 = 5400$ W/8490 W $= 63.4\%$. It is probable that this figure could be raised to about 70% by improving the circuit design.

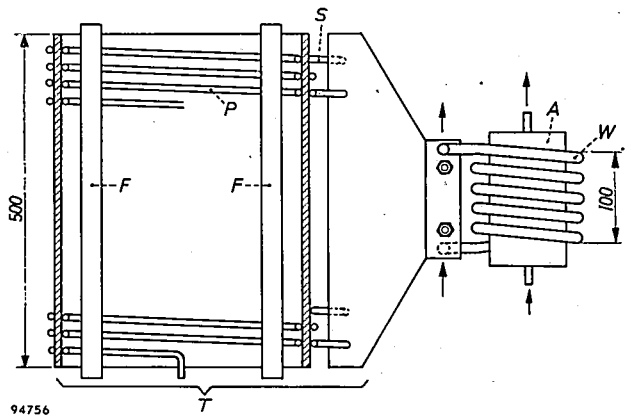

Fig. 6. Cross-section of transformer T. The primary P and the secondary S have an equal number of equally thick turns but those of S are interconnected so as to form a number of parallel-connected coils each of two turns. A very tight coupling is obtained by winding the primary concentrically inside the secondary and locating each primary turn exactly opposite to a secondary turn (see figure), and by the use of a "core" of 36 rods of ferroxcube F. The work coil W can, where necessary, be water-cooled. A is the workpiece, here also provided with water cooling for the purpose of determining the power developed. Dimensions in mm.

An important factor is the number of times C_1 discharges per second into C_2, i.e. the repetition frequency f_r of the pulses that ignite the thyratron. By regulating f_r it is a simple matter to vary the power between wide limits. The circuit for generating these pulses is shown in *fig. 7*. Section A contains a capacitor C_3 which is charged by a direct-voltage source via a resistor R_1. In parallel with C_3 is a (small) thyratron Th_1, which is initially kept non-conducting by negatively biasing the grid with a voltage from a potentiometer P_1. As C_3 charges up, the potential of point Q rises and the grid voltage becomes less negative until, at a given value, Th_1 strikes. Thereupon C_3 discharges through Th_1 during which process the cathode of Th_1 momentarily assumes a high potential, and this pulse ignites thyratron Th_2 in section B of the circuit. The energy accumulated in a lumped delay line L_5-C_5-L_6-C_6 now discharges via Th_2, giving rise to a rectangular pulse of constant duration (2 μsec) on the cathode resistance R_5 (the pulse duration is twice the transmission time along the delay line). These pulses are suitable for igniting the hydrogen thyratrons. Their steep trailing edge is conducive to rapid de-ionization. The repetition frequency f_r can be varied with P_1 (see also fig. 5) which controls the negative grid

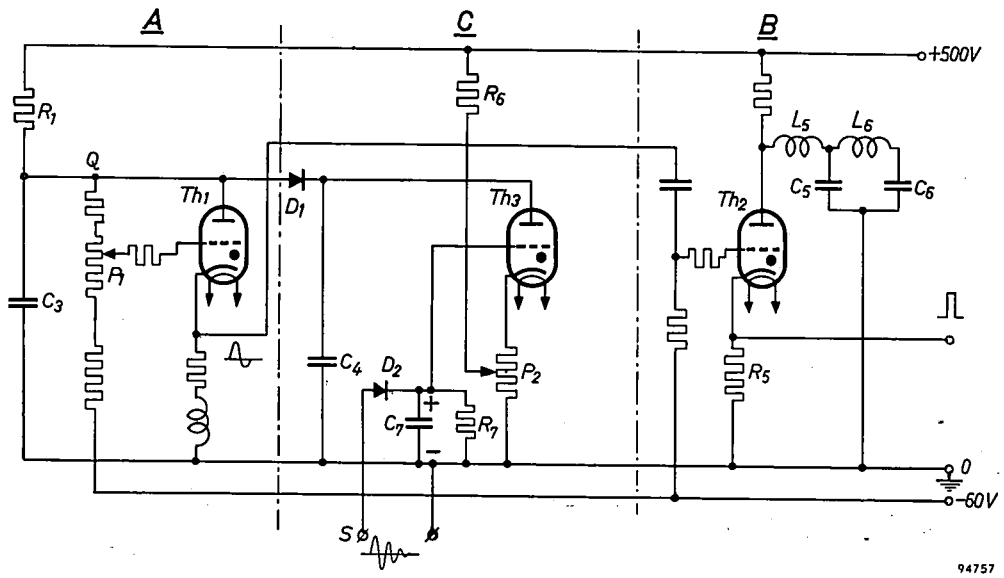

Fig. 7. Control circuit. In section A auxiliary pulses are generated which produce in section B the pulses for igniting the hydrogen thyratrons. Section C serves for automatically reducing the repetition frequency when the damping decreases (e.g. when the work is removed from the work coil). Th_1, Th_2 and Th_3 are low-power rare-gas thyratrons (type PL 5727, "Special Quality"). The repetition frequency is varied with potentiometer P_1. L_5-C_5-L_6-C_6 constitutes a delay line (pulse-forming network). For further explanation see text.

bias on Th_1. The higher f_r the larger is the mean anode current through the hydrogen thyratrons, the maximum permissible value of which is 0.5 A for each tube of type 5949. This sets an upper limit to f_r; in the present set-up it is about 250 c/s.

Not only is it possible in this way to control the power with a small potentiometer, but the power can also be automatically reduced when the work-piece is removed from the work coil. Section C in fig. 7 is used for this purpose. A capacitor C_4 and a thyratron Th_3 are connected, via a metal rectifier D_1, in parallel with capacitor C_3. The current flowing through resistor R_6 and through the lower part of potentiometer P_2 produces across P_2 a voltage which, as negative grid bias, normally keeps thyratron Th_3 non-conductive. Capacitor C_4 charges up via D_1 to the highest voltage reached by C_3, and retains this charge, the latter being prevented by D_1 from returning from C_4 to C_3. Thus, once it is charged up, C_4 performs no function until it has discharged through Th_3. When that happens it is effectively in parallel with C_3 and the time constant in section A increases from R_1C_3 to $R_1(C_3 + C_4)$; consequently the repetition frequency f_r drops correspondingly — e.g. to 1 pulse per second — and the power likewise. The ignition of Th_3 that initiates this process is triggered by the damping of the oscillatory circuit (T-C_2, fig. 3). For this purpose an auxiliary coil is fitted to the transformer T and connected between point S and earth as shown in fig. 7. From the damped alternating voltage induced in this coil a direct voltage is set up, via rectifier D_2, across R_7-C_7, this voltage constituting a positive component of the grid bias on tube Th_3. The voltages and the time constant R_7C_7 are such that, with normal (i.e. strong) damping, this direct voltage is insufficient to ignite Th_3, but quite sufficient when the damping is weak, for example when the work coil is unloaded. The repetition frequency thus drops suddenly to a low value as soon as the damping falls below a predetermined minimum, which is set by means of potentiometer P_2.

Apart from the rapid discontinuous control of f_r as just described, automatic continuous control is also possible. The need for this arises when f_r becomes so high, or the damping so low, that when the hydrogen thyratron is again ignited, the previous oscillation still has an appreciable amplitude. The power then varies noticeably with the phase of the ignition with respect to the remaining oscillation. Unwanted voltage build-up across the oscillatory circuit is prevented by arranging for the tube to fire at an instant (*fig. 8*) that corresponds to a negative peak of the remaining oscillatory voltage across the thyratron. This synchronization is obtained by a small extension to section A in fig. 7, namely by adding to the exponentially rising grid bias of Th_1, a small damped alternating voltage which is again

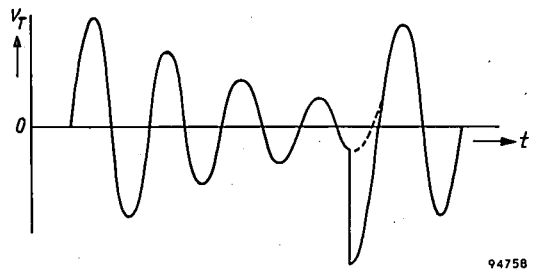

Fig. 8. Damped voltage waveform v_T across the oscillatory circuit. Re-ignition of the thyratron at a negative peak of v_T (i.e. negative with respect to earth) prevents unwanted voltage build-up across the oscillatory circuit.

drawn from an auxiliary coil on the transformer. The resultant form of the grid voltage is then as shown in *fig. 9*. It can be seen from this that the ignition will take place near a peak of the ripple voltage. It is also clear, however, that the moment of ignition will depend somewhat on the damping: if, for example, the damping becomes weaker, the amplitude of the oscillating voltage component on the grid at the end of each period $1/f_r$ retains a larger value, and consequently the tube will fire somewhat earlier, f_r will be higher and the power greater. There are cases in which this effect is favourable (e.g. when an iron object reaches the Curie point, which, in view of the sharp decrease in permeability, makes an increase in the supplied power desirable) and there

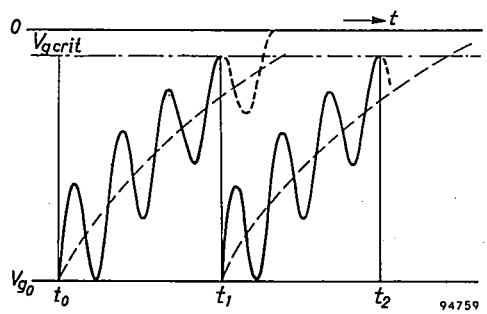

Fig. 9. Broken line: the exponentially rising grid voltage on Th_1 in fig. 7. V_{g0} negative bias. For synchronizing the ignition a damped alternating component is superimposed on the exponentially rising grid voltage. The critical grid voltage $V_{g\,crit}$ is then exceeded near a peak of the alternating voltage, so that the tube fires at $t = t_1, t_2$, etc.

are also cases in which it is unfavourable. In the first category there is a need to intensify the said effect, and in the other category to compensate or even over-compensate it. Both can quite easily be done by including in the grid circuit of Th_1 (fig. 7) a direct voltage which, again, depends on the damped

alternating voltage and which is obtained by rectifying the latter, exactly as described for thyratron Th_3. With the one polarity of this direct voltage the effect is intensified, and with the other it is attenuated or even reversed. In this way f_r can be made to vary continuously — and in the manner desired — with the damping.

With this incomplete discussion of the possibilities offered by control of the thyratrons, we have tried to show that the new generator can be designed in such a way as to dispense with the need for intricate safety measures and special operating skill. Against the limitation of the frequency to 10 kc/s there are also the advantages, already referred to, that the tubes require no forced cooling and that the efficiency is higher.

Summary. With a circuit similar in principle to the spark-gap oscillator used in the early days of radiotelegraphy, but in which the spark-gap is replaced by a hydrogen thyratron, damped oscillations can be generated with a frequency of up to 10 kc/s. Such frequencies are suitable for induction heating. The power can be controlled by varying the repetition frequency of the pulses that ignite the thyratron. A description is given of a control circuit for generating these pulses and for automatically varying the frequency and power. Since variations in the workpiece call for no change in capacitance or coupling, the generator is easier to operate than types employing transmitting tubes. Other advantages compared with the latter type of generator are that the thyratron requires no forced cooling and that the efficiency is higher.

A NOISE DIODE FOR ULTRA-HIGH FREQUENCIES

621.385.2.029.63:621.317.34

The lower limit to the strength of the input signal that an amplifier can effectively amplify is determined by the noise added to the signal by the amplifier itself from its own valves and resistors. This contribution can be measured by connecting the amplifier to a noise source producing a noise signal of known strength (noise standard) [1]).

A commonly used noise standard is a saturated diode. The noise power produced by such a diode is proportional to the average number of electrons moving per second from cathode to anode, and hence proportional to the direct current flowing through the valve [2]).

If a diode of this type is to be used for noise measurements at very high frequencies, two main difficulties are encountered: 1) The finite transit time of the electrons begins to play a part, causing a reduction in noise current. 2) Between the actual noise source, which is situated between the electrodes of the diode and operates as a current source of infinite internal resistance, and the amplifier to be examined, is a network formed by the self-inductances and capacitances of the lead-in wires of the electrodes. The effect of this network becomes more and more strongly felt as the frequency rises. It is very difficult to make a quantitative estimate of the effect of these stray impedances.

The latter difficulty in particular soon becomes apparent at increasing frequency. If such a diode is to be used at very high frequencies, these stray impedances should be kept as low as possible. In the noise diode K81A, which was introduced a few years ago [3]), anode and cathode are fitted low down on the lead-in pins close to the glass base of the tube, making it possible to use this valve at frequecies up to 300 Mc/s.

We have now built a diode of extremely small dimensions that can operate at considerably higher frequencies. This noise diode (made only for experimental purposes), bearing the laboratory designation 10P, employs the same envelope and base as used for sub-miniature valves [4]); see *fig. 1*.

The anode is a cylinder with a length of 4 mm and an internal diameter of 1 mm. The directly heated cathode is a 0.1 mm diameter tungsten wire strung in the axis of the anode. At an anode voltage of 100 V the diode operates well within the saturation region. The maximum permissible anode dissipation being 2 W (anode current 20 mA), the noise

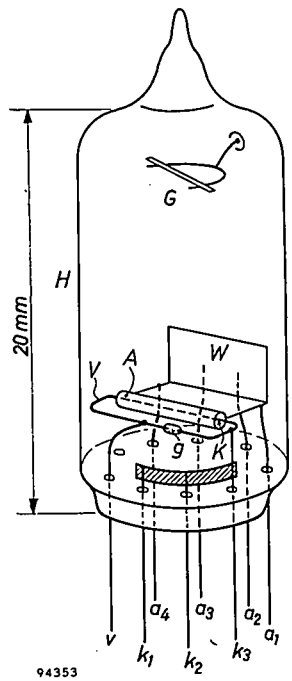

Fig. 1. Construction of a noise diode for very high frequencies (laboratory designation 10P). *H* envelope (sub-miniature valve); *A* anode; *K* filament with tensioning spring *V*; *W* cooling fin attached to the anode; *g* glass bead for insulation; a_1, a_2, a_3, a_4 anode lead-ins; k_1, k_2, k_3 cathode lead-ins; *v* return lead for filament current; *G* getter holder, sealed in the glass envelope.

output is amply sufficient for measuring noise factors [2]). To keep the self-inductance of the lead-in wires as low as possible, the anode is mounted on four lead-in wires which are joined outside the tube, whilst one end of the filament is similarly connected to three lead-in wires (the other end, fixed to a tensioning spring, has only a single lead-in, being the filament-current return lead). To keep the electrode capacitances small, the getter holder is mounted quite separately in the envelope wall at the other end of the valve. The external parts of the lead-in wires are silver-plated, so that the desired connections can be readily soldered at a very short distance (approx. 2 mm) from the valve base.

If the cathode and anode connections were joined, a series resonant circuit consisting of the capacitance of the diode and the self-inductances of the lead-in

[1]) See e.g. F. L. H. M. Stumpers and N. van Hurck, An automatic noise-figure indicator, Philips tech. Rev. **18**, 141-144, 1956/57.

[2]) See e.g. G. Diemer and K. S. Knol, The noise of electronic valves at very high frequencies, I. The diode, Philips tech. Rev. **14**, 153-164, 1952/53.
A. van der Ziel, Noise, Prentice-Hall, New York 1954, page 63 ff.

[3]) This valve is nearly identical to the noise diode 10M mentioned in the article quoted in [2]), p. 155.

[4]) Cf. B. A. Cant, Problems in the construction of small radio valves, Philips tech. Rev. **18**, 217-222, 1956/57.

N.V. PHILIPS' GLOEILAMPENFABRIEKEN

wires would be formed having a resonance frequency f_0. In the evaluation of the noise factor of an amplifier connected to the diode, these stray impedances manifest themselves, at a frequency f, as a correction factor $\{1 - (f/f_0)^2\}^{-2}$. The uncertainty in determining f_0, however, renders this correction inaccurate as soon as f is no longer small with respect to f_0. For the new noise diode 10P, f_0 is found to be roughly 3500 Mc/s; at 1000 Mc/s, therefore, the correction factor does not amount to more than 18%. As a result of the very small dimensions, the reduction of the noise current due to the transit time of the electrons is as little as 3% at 1000 Mc/s. The sub-miniature noise diode 10P can therefore be effectively employed for noise measurements at frequencies up to 1000 Mc/s, i.e. well within the U.H.F. region.

We shall now consider some of the various ways in which the diode can be connected in circuit as a noise generator.

In the circuit of *figs. 2a* and *b* the noise current of the diode produces across the lumped resistance R a certain (calculable) noise voltage, which acts as the input voltage for the amplifier under test. The direct-current circuit and the high-frequency circuit are separated by the lumped capacitances C_1 and C_2. Since, however, C_1 and C_2 possess a fairly high stray self-induction (which reduces the above-mentioned resonance frequency), this circuit does not utilize the valuable properties of the valve 10P to full advantage.

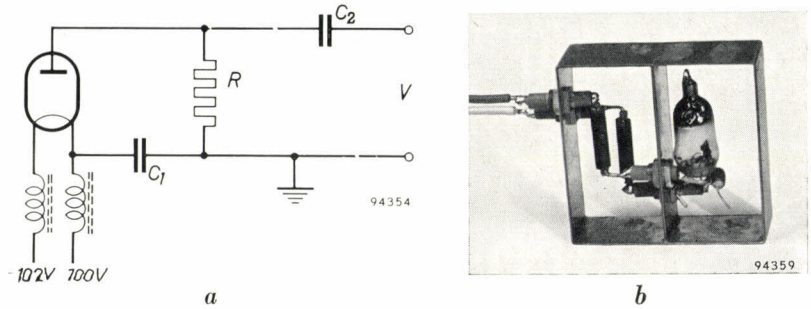

a *b*

Fig. 2. The noise diode 10P in a circuit with lumped elements. The input terminals of the amplifier under test are connected at V.

More satisfactory are the arrangements shown in *figs. 3* and *4*, employing a Lecher system and a coaxial line respectively [5]). In the circuit of fig. 3*a* a noise voltage of known value is produced across the resistor R'. The amplifier to be examined is connected across R' via a Lecher line A of any desired

[5]) The arrangement with the Lecher system has been designed and worked out by J. Stolk, that with the coaxial transmission line by N. van Hurck.

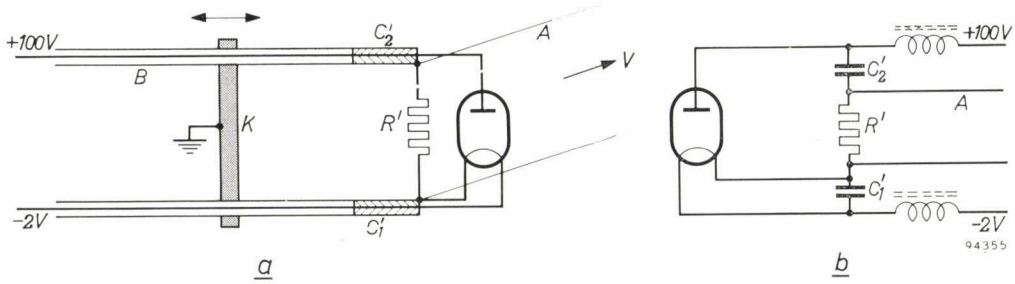

a b

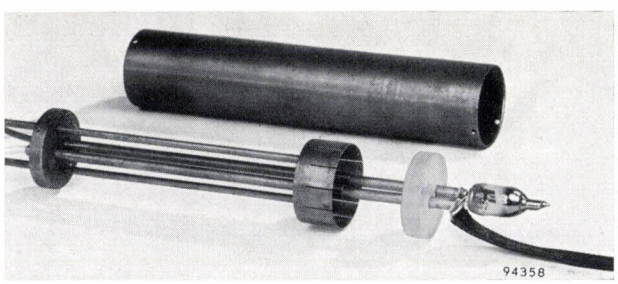

c

Fig. 3. *a*) Circuit diagram, *b*) equivalent circuit, *c*) photograph of a set-up with the noise diode 10P in a Lecher system. The amplifier under test is connected at V via a Lecher transmission line A of any desired length. By adjusting the shorting bridge K on the Lecher line B the valve capacitance is locally tuned away (i.e. compensated at the terminals of the resistor R'). In the equivalent circuit (*b*) the shorting bridge is omitted.

length. The separation from the direct-current circuit is here achieved by the capacitances C_1' and C_2' (see the equivalent circuit in fig. 3*b*), which consist in practice of ceramic tubes inside the hollow conductors of the Lecher line *B*. The influence of the overall valve capacitance (including C_1' and C_2') slight influence on the position to which the shorting bridge has to be set to obtain the desired resonance.

Similar considerations apply to the arrangement with a coaxial transmission line, figs. 4*a* and *b*. At the right the transmission line is connected to the amplifier, whose input impedance is made equal

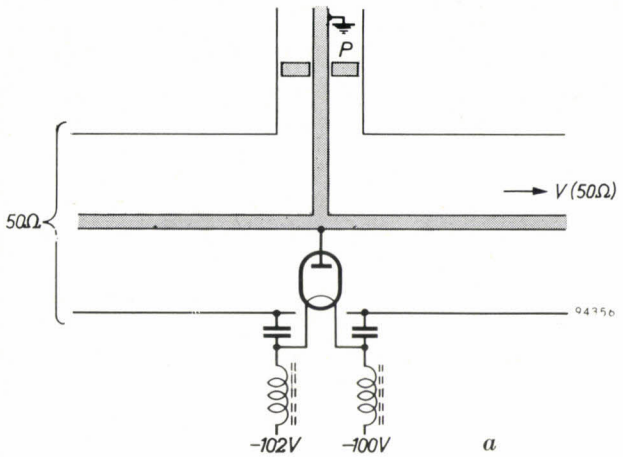

a

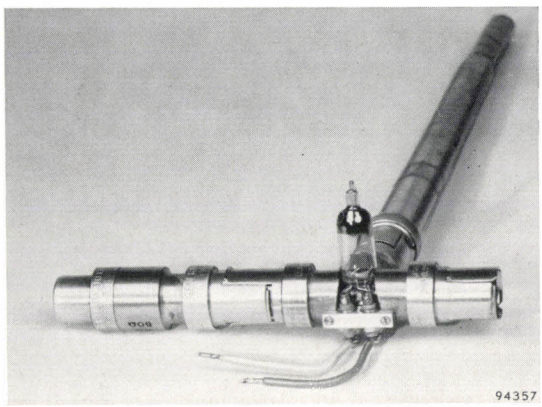

b

Fig. 4. The noise diode 10P in a coaxial transmission line arrangement. Here the disturbance of the field caused by the diode itself is locally tuned away by means of the shorting piston *P*.

upon the noise voltage across R' is completely compensated by an appropriate adjustment of the shorting bridge *K* across this Lecher line: effectively, R' is shunted with a self-inductance whose reactance is exactly equal and opposite to that of the valve capacitance [6]). The stray self-inductances of C_1' and C_2' have no disturbing effect, since they merely contribute to the distributed self-inductance of the transmission line *B*: their presence merely has a to the characteristic impedance of the coaxial line (50 Ω); at the left the line is terminated with an impedance of the same value. Under these conditions the noise power supplied by the diode to the amplifier can be readily evaluated. It is true that the presence of the diode and the necessary aperture in the exterior conductor cause some disturbance of the field, so that the line is no longer perfectly matched, but the influence of this disturbance can be locally tuned away by means of a shorting piston as shown in the diagram.

H. GROENDIJK.

[6]) See e.g.: J. C. van den Hoogenband and J. Stolk, Reflection and impedance measurements by means of a long transmission line, Philips tech. Rev. **16**, 309-320, 1954/55.

ABSTRACTS OF RECENT SCIENTIFIC PUBLICATIONS BY THE STAFF OF N.V. PHILIPS' GLOEILAMPENFABRIEKEN

Reprints of these papers not marked with an asterisk * can be obtained free of charge upon application to Philips Electrical Ltd., Century House, Shaftesbury Avenue, London W.C. 2.

2560: J. A. Hartveld: Moderne Fahrzeugbeleuchtung mit Fluoreszenzlampen (Elektrizitätsverwertung **32**, 213-224, 1957, No. 6-7). (Modern vehicle lighting with fluorescent lamps; in German, with comprehensive abstracts in English and French.)

General article on the various types of fluorescent lamps used in vehicles with accumulator or mains power supplies. For low-voltage (24 V) accumulators, rotary mercury jet inverters in conjunction with transformers offer the most efficient means of obtaining a suitable running voltage. An efficiency of 42 lumens/watt can be achieved for 40 W "TL" lamps. For 72 V accumulators, short 15 W "TL" C lamps can be fed directly, giving 30 lumens/watt. For 110 V supplies the 20 W "TL" C lamp has been developed. When power is available from the overhead lines or conductor rails, the supply may be D.C., 550 V, 600 V, 1500 V or 3000 V, or A.C., 15 000 V $16\frac{2}{3}$ c/s, or 25 000 V 50 c/s. For D.C. supplies the "TL" R lamp has been developed. For 25 000 V 50 c/s the "TL" S lamp is suitable after transformation of the supply. Owing to flicker, fluorescent lamps cannot be fed directly from $16\frac{2}{3}$ c/s supplies; in this case accumulators are used, or a separate D.C. generator. (See also Philips tech. Rev. **18**, 11-18, 1956/57.)

2561: F. K. Lotgering and E. W. Gorter: Solid solutions between ferromagnetic and antiferromagnetic compounds with NiAs structure (Phys. Chem. Solids **3**, 238-249, 1957, No. 3-4).

Several solid-solution series with NiAs structure have been prepared between a ferromagnetic ($x = 0$) and an antiferromagnetic ($x = 1$), viz. (*a*) $CrTe_{1-x}Se_x$, (*b*) $Mn_{1-x}Cr_xSb$ and (*c*) $CrTe_{1-x}Sb_x$. The system $Cr_{1-x}Mn_xTe$ shows a miscibility gap. Saturation magnetizations have been measured between 20 °K and the Curie temperatures, and susceptibilities between the Curie temperatures and 850-1100 °K. In (*b*) and (*c*) the Curie and Néel temperatures decrease on addition of the other component, but do not simultaneously drop to zero. Notably in (*b*), compositions occur for which a Néel temperature is present above a Curie temperature. The saturation magnetization decreases with x in both systems, but in a different way. The magnetic properties found can be accounted for by assuming that the dominant exchange interaction is not a direct M-M interaction, but a superexchange interaction via the metalloid atom X, via the largest of the three angles M-X-M that occur for nearest neighbours M-X. These interactions are supposed to be strong and positive for Mn-Sb-Mn and Cr-Te-Cr configurations, strong and negative for Cr-Sb-Cr and weak for Mn-Sb-Cr configurations.

2562: G. Brouwer and S. van der Meer: A network analog of a statically loaded two-dimensional frame (Proc. Soc. Exper. Stress Anal. **15**, No. 1, 35-42, 1957).

With certain restrictions, a two-dimensional structure of rods may be represented by an electric circuit model consisting of resistor networks and feedback amplifiers. The mechanical quantities, such as loads, shearing forces, bending moments and deflections correspond to currents and potentials of the electrical model. The design of intricate frameworks can be carried out rapidly by means of an analog computor of the type discussed in this paper. A generalization to three-dimensional cases is possible.

2563: J. D. Fast: Einfluss der Gase beim Lichtbogenschweissen von Stahl (Schweissen und Schneiden **9**, 512-517, 1957, No. 12). (Effects of gases on the arc welding of steel; in German.)

The questions discussed in this paper include: interaction between gas and liquid weld-metal, the formation of blowholes, the detrimental effects of gases in the weld-metal, and aging phenomena and brittleness caused by gases.

2564: P. C. van der Willigen: Einfluss von Wasserstoff auf die Eigenschaften der Schweisse (Schweissen und Schneiden **9**, 517-521, 1957, No. 12). (Effects of hydrogen on the properties of welds; in German.)

This paper discusses the question of supersaturation with hydrogen, the formation of micro-cracks and macro-cracks, and the occurrence of fish-eyes.

2565: J. A. M. Dikhoff: Temperaturbestimmungen im Gleichstromkohlebogen (Proc. Colloquium Spectroscopicum Internationale VI, Amsterdam, 1956, published 1957 as an extra

volume of Spectrochimica Acta and as a book by Pergamon Press, pp. 162-167). (Determination of temperature in D.C. carbon arcs; in German.)

Temperatures in carbon arcs have been determined by means of the intensity ratio between various spectral lines of zinc. A description is given of specially prepared electrodes permitting a steady supply of a small quantity of zinc during arcing. The result obtained for the centre of the arc, according to Addink's method, is a temperature of about 6100 °K. Apart from alkali metals, the evaporating materials affect this temperature only slightly. The results of temperature measurements in carbon arcs with argon or with argon + oxygen as discharge gas are also given and compared with the results published by Schöntag.

2566: N. W. H. Addink: Temperature measurements with reference to spectrochemical analyses (Proc. Colloquium Spectroscopicum Internationale VI, Amsterdam, 1956, published 1957 as an extra volume of Spectrochimica Acta and as a book by Pergamon Press, pp. 168-178).

It has been found that in the D.C. carbon arc there exists a relation between the ionization potential (V_i) of an element to be analysed and the ratio K/Q (K is the element concentration establishing a unit-intensity value of a spectral line of the element, which is excited in the constant-temperature D.C. carbon arc ($T = 6100$ °K), whilst Q means the same, except the excitation temperature is ~6700 °K). It is shown that the elements can be divided roughly into two groups: those which are mainly excited in the column ($V_i \geqslant 7.5$ V) and those which are excited in the mantle of the arc ($V_i \leqslant 7$ V). A comparison with arcs described by other investigators is given. The knowledge of various temperatures has led to an improvement of the analysis carried out with these D.C. arcs. In an added supplement the lower limits of detection determined by various authors are compared.

2567: J. Ugelstad and J. de Jonge: A kinetical investigation of the reaction between amides and formaldehyde (Rec. Trav. chim. Pays-Bas **76**, 919-945, 1957, No. 11).

This paper deals with the kinetic measurement of the reaction between formaldehyde and the amides of carboxylic acids or urea. It is shown that the formation of a methylol amide proceeds by a bimolecular reaction, while its decomposition is a monomolecular reaction. The reactions are catalysed by H_3O^+ and OH^- ions and show general acid catalysis. General base catalysis was found in the urea-formaldehyde system, but could not be detected in reactions of formaldehyde with amides of carboxylic acids. A mechanism for the reactions of formaldehyde with amides in general (including urea) is proposed. In strongly alkaline solution the rates of decomposition of methylol amides were found to be independent of the hydroxyl-ion concentration. The acid dissociation constants of some methylol amides have values of about 10^{-14} moles.l^{-1} at 0 °C. The equilibrium constants of several amide-formaldehyde systems have roughly the same value (about 22 l.mole^{-1} at 25 °C), independent of pH (range pH = 2-12). The rates of the reactions between formaldehyde and the various amides differ markedly. The relative rates found in alkaline solution are discussed.

VOLUME 20, 1958/59, No. 5 pp. 113-144 Published 22nd November 1958

Philips Technical Review

DEALING WITH TECHNICAL PROBLEMS
RELATING TO THE PRODUCTS, PROCESSES AND INVESTIGATIONS OF
THE PHILIPS INDUSTRIES

PRINTED WIRING IN RADIO SETS

by R. van BEEK and W. W. BOELENS.

621.396.62.049.75

*The manufacture of most mass-produced articles is highly mechanized, that is to say the conveyance of components and product, the assembly of the components and other operations call for little manpower. This is the situation — to confine ourselves to the radio industry — in the fabrication of thermionic valves *). The assembly of radio sets, on the other hand, was relatively little mechanized until a few years ago, although it had long been done on the conveyor belt and wide use made of electrically driven screwdrivers and similar tools. The mounting of components, the wiring and the soldering of the connections, however, were almost entirely manual operations. This state of affairs has undergone a radical change since the introduction of "printed wiring", which is increasingly coming into use in radio and television sets.*

The assembly of a radio chassis comprises the following operations:

1) mounting and fixing the components;
2) wiring up the circuit;
3) soldering the connection points;
4) electrical trimming;
5) testing the complete assembly.

The mechanization of the wiring operation had already been thought of before the war. The idea was to apply to a sheet of insulating material a pattern of conducting connections arranged in accordance with the circuit required. One method of doing this was based on the use of insulating sheets covered on one side with copper foil; the wiring pattern was imprinted on the foil with protective paint, after which the uncovered copper was etched away. The result was termed "printed wiring", and this term has been retained to cover other processes subsequently developed.

Advantages and disadvantages of printed wiring

The development of printed wiring processes received a marked impetus during the last world war, particularly in the United States. The reasons were shortage of labour, rising wages and the need for speedy production of all kinds of electronic apparatus. Frequently such equipment was more complicated than pre-war radio sets and the production runs were relatively small. The latter two circumstances militated against the system of manual wiring, for with every new set put into production mistakes in connections are bound to be made in the beginning, especially when the circuits are intricate. In the long run a stage is normally reached where the number of mistakes is acceptably low, but when the production run is fairly small it is scarcely possible to reach that stage. In this respect printed wiring offers a considerable improvement.

Another advantage of printed wiring is that all points to be soldered lie approximately in the same plane. This makes a form of mechanical soldering possible — *dip-soldering*. We shall return to this later.

From the standpoint of pure radio engineering, printed wiring as against conventional wiring has disadvantages as well as advantages, although they are only of secondary importance. The differences are concerned with 1) the material of the mounting

*) See, for example, G. Alma and F. Prakke, A new series of small radio valves, Philips tech. Rev. **8**, 289-295, 1946. An example relating to TV tubes will be found in: A. H. Edens, A method of sealing the window and cone of television picture-tubes, Philips tech. Rev. **19**, 318-323, 1957/58 (No. 11).

plate (ordinarily metal but insulating material in the case of printed wiring), 2) the material between the connections (air in the one case and solid insulating material in the other) and 3) the configuration of the wiring (in three dimensions and in two dimensions respectively).

Since printed wiring is applied to a sheet of insulating material, the screening effect of a metal chassis is lacking. A favourable point, however, is that the capacitances with respect to earth are smaller. Also there is the advantage of well-defined earth leads (in contrast with the erratic paths through a metal plate) but against this there is the draw-back of their somewhat higher impedance.

The solid insulating material of a printed circuit makes the capacitances between the connections a little higher, but this can be remedied by applying screening strips. Moisture can cause some conduction along the surface, and this must be taken into account when designing the wiring layout.

The two-dimensional configuration of the wiring as opposed to the conventional three-dimensional configuration also has its good and bad aspects, as tabulated below.

Conventional wiring (three dimensions)	*Printed wiring* (two dimensions)
All critical connections can be short, because they can cross each other.	Some critical connections are always fairly long, having to pass around others.
Capacitances are low mutually and with respect to the chassis, but vary considerably from one set to another	Mutual capacitances are somewhat higher, but very constant from one set to another. Compensations can be introduced in the wiring itself.
Wiring has small surface area but circuit not immediately traceable. Electrical contacts for trimming purposes not always easy to make.	Surface area necessarily about twice as large, but circuit arrangement very distinct and neat. All points readily accessible.

Long connections in printed wiring can sometimes be avoided by using bridging pieces known as jumpers. These are ordinary bent copper wires mounted in the same manner as components, e.g. resistors. Certain components can also often be mounted in such a way that they act as a "bridge".

An important point to consider is the introduction of modifications, as is frequently necessary in the case of a set newly put into production. In sets with orthodox wiring it is usually a simple matter to add a small component or to replace a component by another of different dimensions. With printed wiring, however, this usually involves considerable difficulties.

Printed wiring was first employed at Philips in 1955 in a small model radiogramophone and shortly afterwards in radio sets of the family "B2X67 U". It then gradually came into use in other types of set, and also in television receivers. In the latter not merely the connections but coils, too, are printed so that here is a case of "printed *circuits*".

Fabrication of printed wiring panels

Within the scope of this article we cannot deal in detail with the various processes by which printed wiring panels are fabricated (an insulating sheet carrying printed wiring is called a panel). We shall only sketch the broad outlines of the way in which these panels are made for a simple type of radio receiver. We shall then follow the further progress of these panels in the production process.

After the wiring layout has been drawn, exactly as required, it is transferred photochemically to a silk screen. The screen is normally permeable to a certain type of resin, but is made non-permeable by the transferred pattern which corresponds to the conducting parts of the circuit under production. The resin is now applied via the silk screen to both sides of a nickel plate, which has previously been very thinly copper-plated. The wiring pattern is thus transferred to this plate; at the "conducting" parts the copper remains bare, whilst the "non-conducting" parts are covered by the resin. The plate is then once again immersed in a copper-plating bath and the copper — which deposits only on the uncovered parts of the base — is allowed to grow to the required thickness (usually slightly thicker than the coating of resin). This being done, the plate is rinsed and then immersed in an adhesive.

Ten sheets of paper, impregnated with a synthetic resin, are now placed one above the other in a press; on top of these is placed the adhesive-coated plate and this is in turn surmounted by ten more sheets of impregnated paper (*fig. 1*). This assemblage is heated during the pressing operation and each stack of paper is "baked" into a single sheet of paper-reinforced plastic. Owing to the adhesive the copper wiring adheres more strongly to the plastic sheet than does the thin copper layer to the nickel. A parting can thus easily be effected at this latter boundary surface, leaving 1) the nickel plate, which can be used again, and 2) two aggregates, each consisting of a sheet of plastic with the deposited system of wiring on it, surmounted by a thin layer of cop-

per. After etching away the thin layer of copper we have two plastic sheets carrying the printed wiring. The thickness of the wiring is about 0.002″ ($\frac{1}{20}$ mm), the width and spacing round about $\frac{1}{16}$″ (1 to $1\frac{1}{2}$ mm).

Manufacture of a radio receiver with printed wiring

To illustrate the process of manufacturing radio receivers with printed wiring panels we shall describe the fabrication of type B2X67 U sets, which have been in production for some years now. These sets are of simple design, having either one or two wavebands and no power transformer.

The simpler model has only one waveband, viz:

Either medium waveband (with "ferroceptor"),
or 16-62 m (with plate aerial),
or 24-94 m (with plate aerial).

It has no tone control.

The more elaborate model has two wavebands:

either medium wave and long wave (with one "ferroceptor"),
or medium wave and 16-62 m (with "ferroceptor" and plate aerial),
or medium wave and 24-94 m (with "ferroceptor" and plate aerial),
or 13-42 m and 41-135 m (with plate aerial only).

This model has a tone control.

Both types can be adapted for a mains voltage (AC or DC), of either 110-127 V or 220 V.

The various models differ considerably in their high-frequency stages; hence each would require a different pattern of printed wiring. This is avoided by mounting the high-frequency stages on a conventional chassis, which allows room for the maximum number of components that may be required. The rest of the sets (beginning with the mixer stage) is standard and is constructed entirely with printed wiring (*fig. 2a* and *b*). Because of the larger surface area needed for the printed wiring, the cabinet for this set is somewhat bigger than it would otherwise have been.

As can be seen in fig. 2*b*, the conductors broaden out at the places where they have to make contact with a component. At each such position there is a hole in the panel. The connecting leads or lugs of the components are pushed through the holes, cut and bent, and are then together dip-soldered to the wiring.

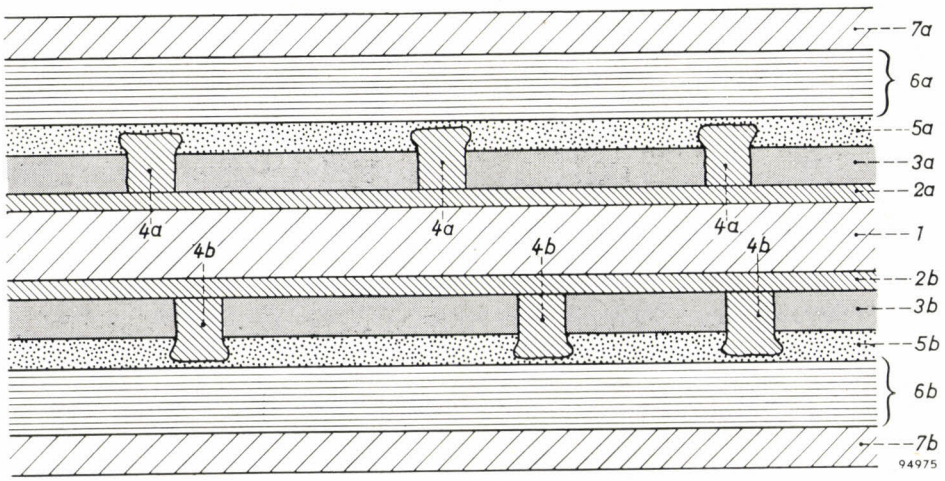

Fig. 1. Schematic cross-section of the stack from which the printed-wiring panels are pressed (not to scale). *1* nickel plate, coated on both sides with a very thin layer of copper *2a-2b*. *3a-3b* coating of non-permeable resin. *4a-4b* electro-deposited copper, which forms the wiring. *5a-5b* adhesive. *6a-6b* stacks of ten sheets each of impregnated paper. *7a-7b* steel platens. After the pressing operation, the two stacks are parted at the boundaries *1-2a* and *1-2b*, between the nickel and copper.

The obvious method of making the holes in the panel is to punch them. However, if an arbitrary pattern of holes of varying sizes is to be punched in the panel, with a different pattern for each type of set, many costly dies would be needed. If, on the other hand, it is possible to use holes of a standard size disposed in a standard grid, a universal stamping tool can be made which can serve for producing any desired combination of holes. There is a tendency nowadays to use holes of $\frac{1}{20}$″ diameter disposed at the intersections of a standard grid of $\frac{1}{10}$″ (2.54 mm) pitch (the holes only being at those intersections where they are needed). A standard grid of this kind imposes certain requirements on the uniformity of the connections of the components used. Various components, such as carbon resistors, paper and

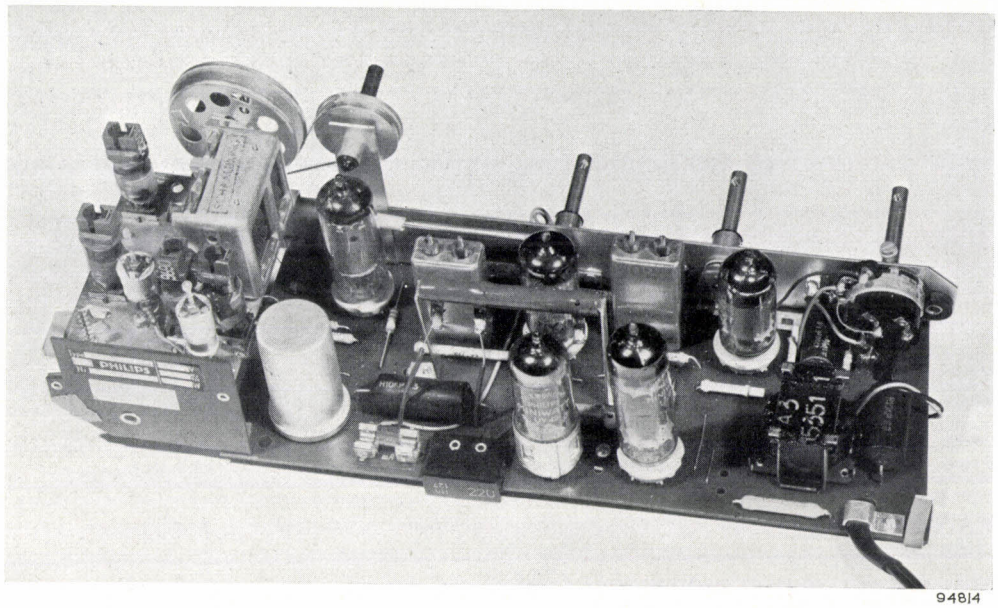

a

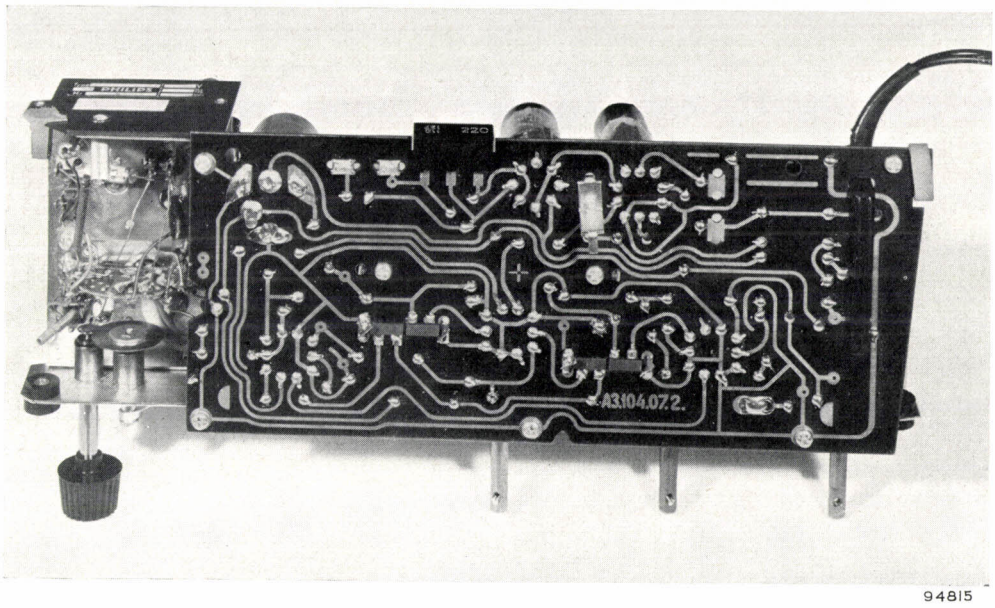

b

Fig. 2. Chassis of type B2X67 U radio receiver: *a*) rear top view, *b*) view from underneath. To the left of the photos is the small conventional chassis carrying the radio-frequency section; the rest of the assembly is the printed wiring panel with its components and valves.

ceramic capacitors, output transformers and some recently developed valve holders, already meet these requirements; others, electrolytic capacitors for instance, do not as yet. The latter, while not precluding the use of printed wiring, call for extra tools both for punching the non-standard holes and for fixing the particular components.

The fabrication of the type of set illustrated in fig. 2 comprises the following operations:

1) mounting of components on the panel,
2) dip-soldering,
3) assembling the high-frequency section (chassis with conventional wiring)
4) mounting this chassis to the panel,
5) electrical trimming,
6) mounting in the cabinet, reception test and packing.

Mounting of components on the panel

After the panels have been thoroughly cleaned, dried and sprayed with soldering flux (*fig. 3*), the components are mounted in the following order:

a) components with long connecting leads,
b) valve holders,
c) components with "twist" lugs.

a) *Components with connecting leads* include ceramic and paper capacitors and resistors. Jumper wires also come into this category. Before these components are mounted they are subjected to a preparatory operation, which consists in placing 50 or 100 of them in a row on a jig and bending the leads over the jig with a simple tool (*fig. 4*), such that the centre-to-centre distance of the leads is a multiple of $\frac{1}{10}''$. The component is then ready to mount on the panel, its two leads being inserted through appropriate holes in the grid pattern. The use of this standard grid limits the number of bending jigs needed.

Racks containing the prepared components are placed within the operative's reach on benches embodying two types of special cutting and bending machines (*fig. 5a*). The first machine is used only for "*thin*" components, such as carbon resistors, ceramic capacitors and jumper wires, and the second only for "*thick*" components, such as paper capacitors. This division into thin and thick components avoids the difficulties that would be involved in exerting simultaneous pressure on both types close together.

The operative places a panel into the machine with the printed wiring facing downwards and inserts the components with their bent connecting leads in the appropriate holes. A pressure pad holds panel and components in position while the machine is operated to cut off the ends of the wires to the required length and bend them over, thereby fixing the components firmly to the panel. The process can be followed with the aid of *fig. 6*. The panel *M* (fig. 6*a*) lies on a bronze friction-plate *W*, under which are situated successively a bending plate *B*, a cutter *K* (both of hard steel), and a bronze-clad steel base-plate *S*. The leads inserted through the

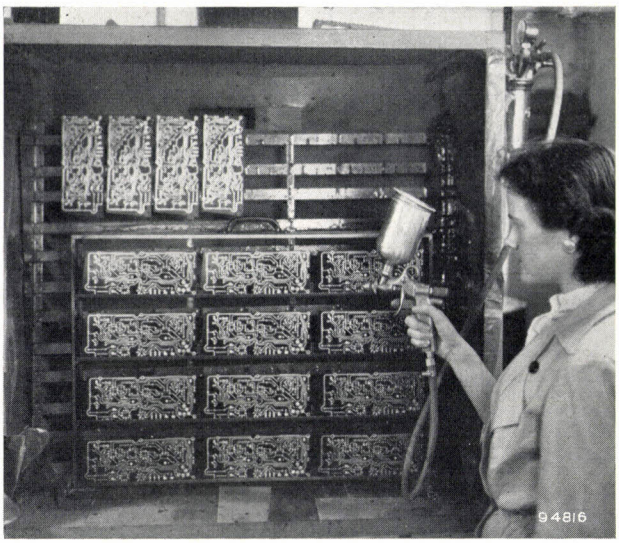

Fig. 3. Spraying soldering flux on the printed wiring.

Fig. 4. Preparation of "thin" components having connecting leads. The leads of 50 or 100 components in a row are simultaneously bent over a jig so that they fit into the holes in the panel.

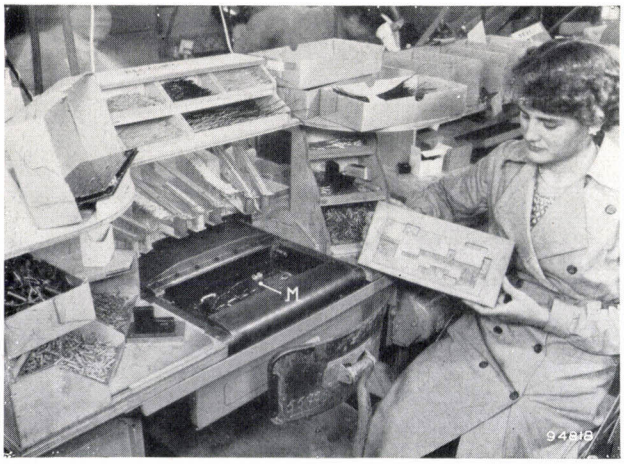

a

b

Fig. 5. Cutting and bending machine. *a*) A panel *M* is placed in the machine and the "thin" components inserted in the panel. *b*) The cover plate is closed, after which the machine automatically cuts and bends the connecting leads.

holes in the panel pass through corresponding holes in plates *W*, *B*, *K* and *S*. Once all thin components are in position, the operative places the pressure pad over them (fig. 5*a*) and slides forward the cover plate (fig. 5*b*). The closing of the cover plate initiates the following train of events:

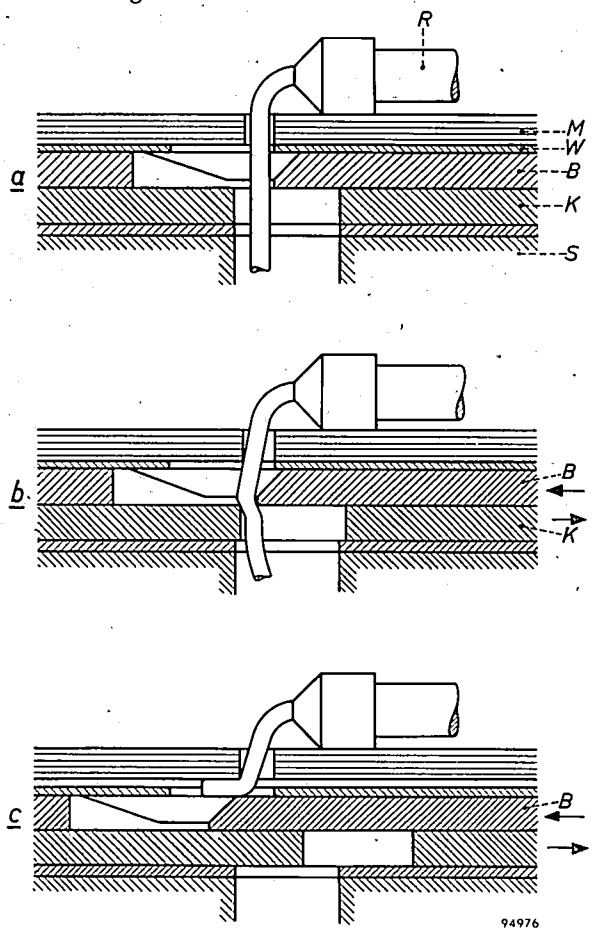

Fig. 6. Cross-section of part of the cutting and bending machine. *a*) Starting position. *M* panel with a component *R* (carbon resistor). *W* friction plate. *B* bending plate. *K* cutter. *S* support plate surfaced with bronze.
b) The bending plate moves to the left, the cutter to the right; the left connecting lead of resistor *R* is cut to length.
c) The bending plate has moved farther to the left, bending the lead over against the panel. The right connecting lead is treated in the same way by further movements of the two plates.

1) Air under pressure enters the cover plate, the underside of which consists of a rubber diaphragm. The pressure pad is thus pressed down to hold the components firmly in position.
2) As soon as the air pressure reaches a certain value, eccentrics set the cutter and the bending plate in motion. As illustrated in fig. 6*a-c*, this causes the leads to be cut off to the right length and bent over so that the components sit tight.
3) The air pressure in the cover plate is released.

The operative now slides the cover plate open, removes the pressure pad and lifts out the panel complete with the thin components.

Among the thick components, whose turn it is to be subjected to the same operations in the second machine, is the output transformer. This has no connecting leads, but short connecting lugs which fit into the grid and are merely bent over in the machine.

The cutting and bending machine is designed to handle a total of 30 components at one time. A larger number of different components could hardly be arranged within reach of the operative. Also the forces involved in the simultaneous cutting and bending of so many leads would become excessive.

The wires connecting the panel to an external component (to the loudspeaker for example) cannot be fixed in the cutting and bending machine, for a straight single wire with one end bent over would fall out of the panel. These wires are bent as shown in *fig. 7* underneath the panel by means of a hand-tool, and so prevented from falling out.

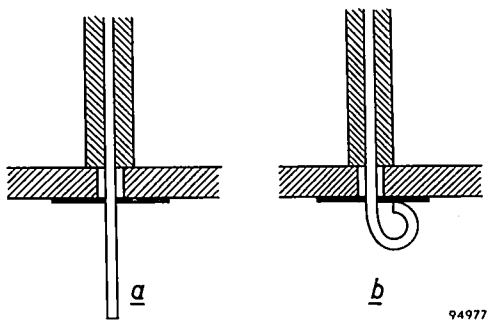

Fig. 7. Method of fixing a wire required to connect a point of the printed wiring to a component outside the chassis (e.g. the loudspeaker).
a) The bared end of the wire is pushed through a hole in the assembly plate.
b) The end is curled over to prevent the wire from falling out. Good electrical contact is effected by dip-soldering.

b) *The valve holders.* A "Noval" base (nine pins at nine corners of a regular decagon, the tenth corner being left open), which is used for many radio valves, does not fit the standard grid of printed wiring panels. For this reason a special valve holder has been designed (*fig. 8*), the contact sockets of which are provided with lugs (*3*) arranged to fit in the grid. Protective pads of foam plastic are placed over the lugs when the valve holders are made, to prevent possible damage during transport to the set assembly department.

The valve holders are fixed to the panel with a hand press which simultaneously bends the nine lugs outwards (fig. 8). The press is shown in *fig. 9*.

c) *Components with "twist" lugs.* The I.F. band-pass filters and electrolytic capacitors have so-called

"twist" lugs, the lugs being pushed through slits in the panel and twisted 60° by a special tool, in the case of the I.F. filters. The capacitor lugs are too short for mechanical twisting and are therefore twisted manually with a pair of pliers.

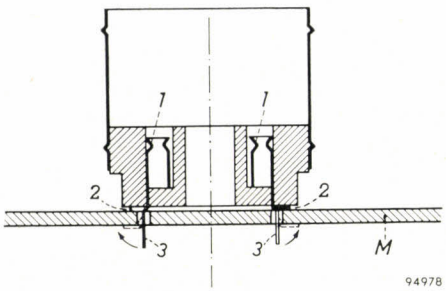

Fig. 8. Holder for valves with "Noval" base. Each contact socket *1* has a split lug. Parts *2* of the lugs are bent round to keep the sockets firmly in the holder. Parts *3* are bent so that they will fit into the standard grid pattern of the panel *M*. To fix the holder to the panel, the nine lugs *3* are simultaneously bent outwards (see arrows) by a special tool mounted in a hand press.

Dip-soldering

After the panels have once again been sprayed with flux, the electrical connections are soldered. This is done in a bath containing molten solder, the level and temperature of which are automatically kept constant. The panel, printed wiring downwards, is placed on a jig which exposes only those regions where soldering has to take place (*fig. 10*); the oxide film is brushed from the surface of the molten solder and a safety grill is then closed. The soldering cycle now proceeds mechanically: the jig descends until the underside of the panel just rests on the surface of the solder, and ascends again after a certain time. The panel is kept in vibration both during the dipping process, to ensure good wetting by the solder, and during the ascent, to prevent the formation of unduly large blobs of solder which might establish unwanted connections. Temperature and dipping time are so chosen as to ensure soldered joints of very high quality without allowing the panel to get too hot.

After the connections have been soldered, the valves are fitted in their holders and the assembled panel inspected.

The sequence of operations in the assembly of the panel as described can be seen in the plan in *fig. 11*. The plan also includes the final stages of the process, which we shall now touch on briefly.

Final stages of assembly

The radio-frequency section of the type B2X67 U receivers consists essentially of a few coils and the variable capacitors, together with trimming capa-

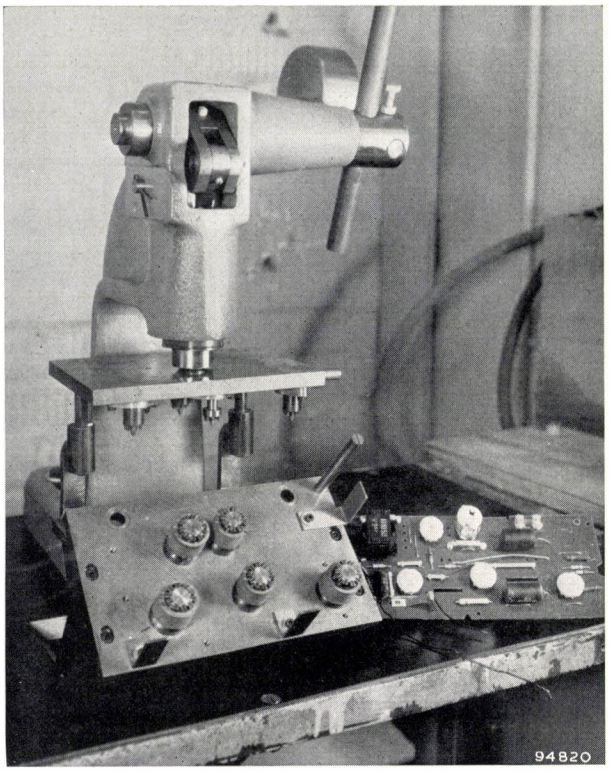

Fig. 9. Hand press for fixing the valve holders to the panels. Foreground, left: lower plate with dies for five valveholders. The upper, punch plate is seen mounted in the press. The dies on the lower plate bend the nine contact lugs outwards (see fig. 8). Right: panel with components, including the five valve holders.

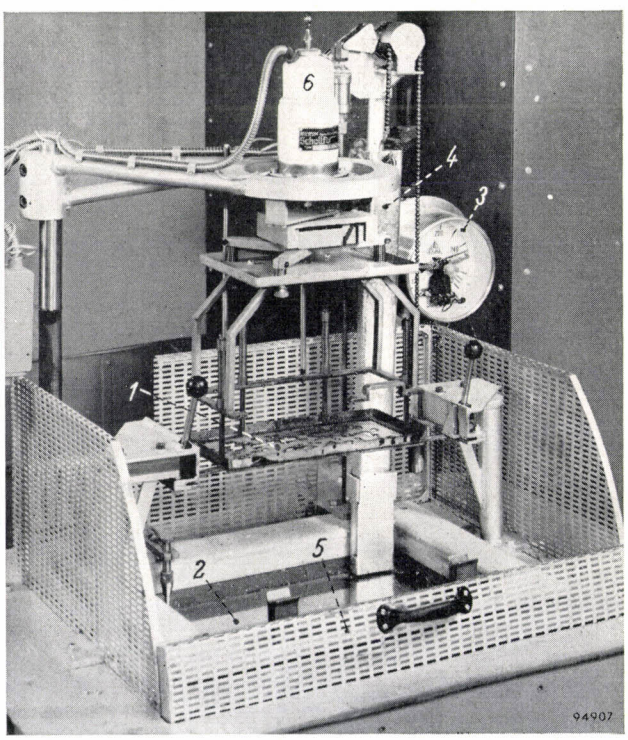

Fig. 10. Dip-soldering machine. The panel, printed wiring downwards, is placed on a jig *1*, which shields the parts not to be soldered. *2* bath with molten solder, the temperature and level of which are automatically kept constant. *3* thermometer. *4* bar of solder. *5* safety grill which, when closed, starts the soldering cycle. *6* vibrator, which keeps the panel in vibration during and after soldering.

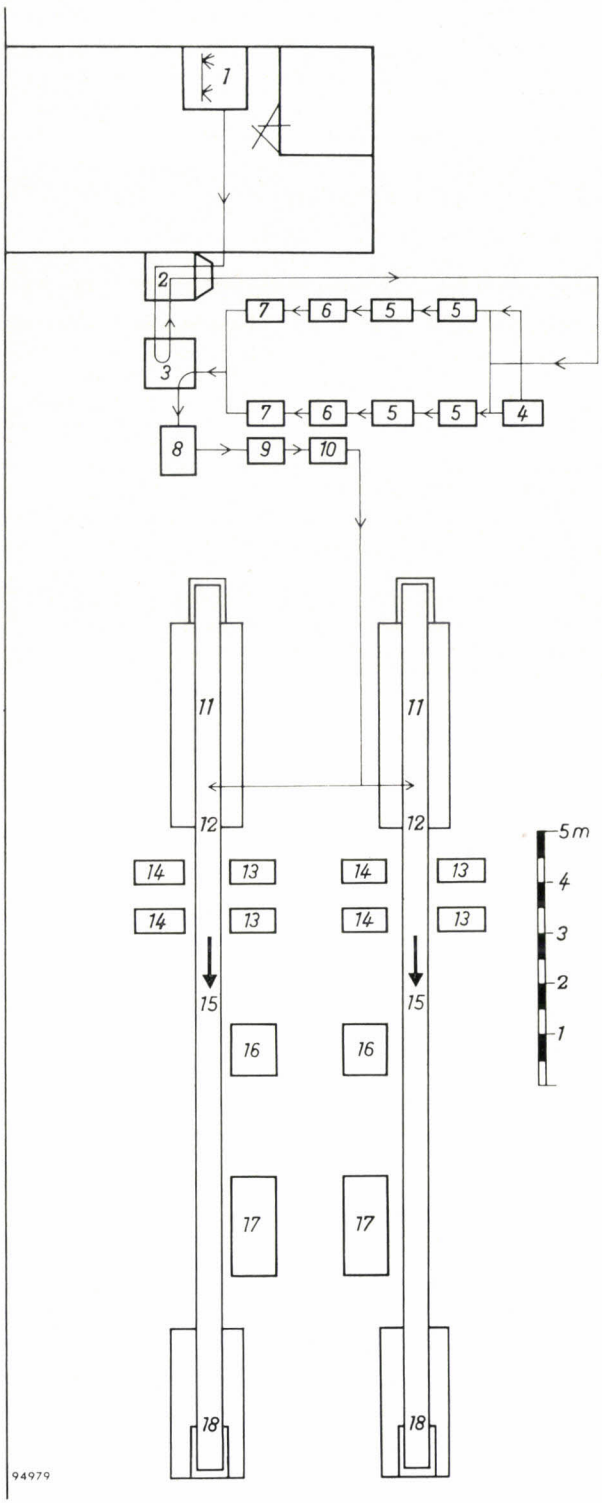

Fig. 11. Plan of assembly department for radio sets incorporating printed wiring. *1* cleaning the printed panels. *2* drying. *3* spraying of soldering flux. *4* preparation of small components. *5* cutting and bending machines. *6* mounting of valve holders. *7* mounting of I.F. band-pass filters and electrolytic capacitors. *8* dip-soldering. *9* insertion of valves. *10* inspection. *11* assembly of R.F. section (metal chassis with conventional wiring) on conveyor belt. *12* mounting of R.F. chassis to printed-wiring panel. *13* trimming. *14* testing and inspection. *15* mounting in cabinets. *16* H.T. test. *17* reception test (R.F. signal modulated with music applied to aerial terminal) in sound-proof cubicle. *18* packing.

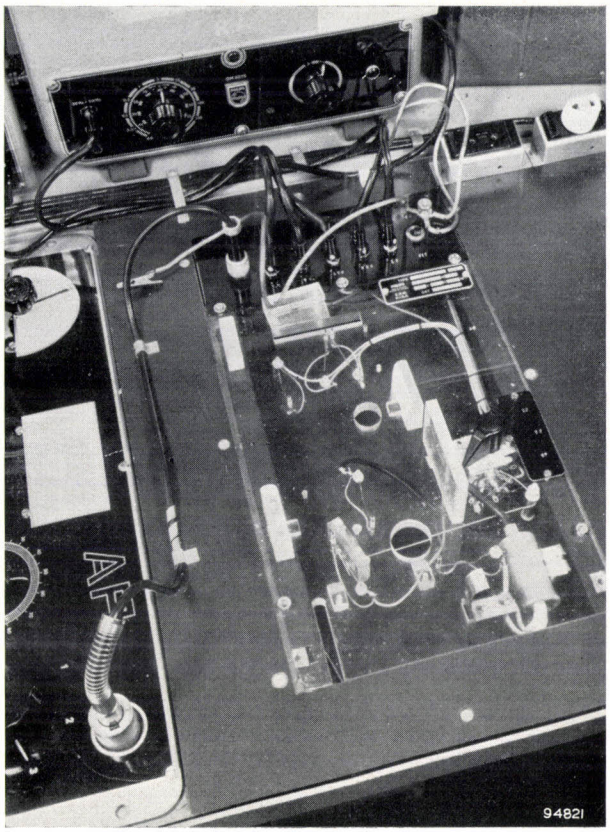

a

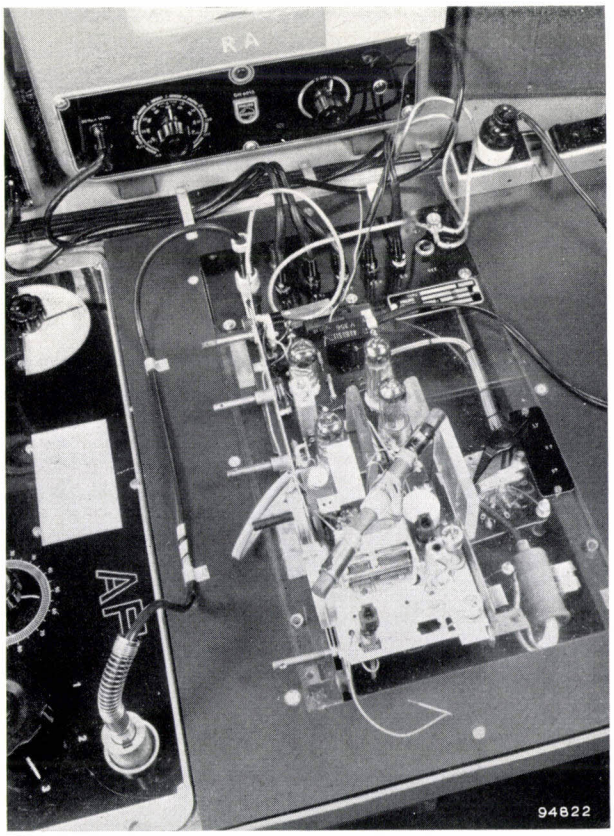

b

Fig. 12. Test bench for trimming (*13* in fig. 11). *a*) Without chassis. *b*) With chassis in position. The necessary contacts with the printed wiring are made by spring-loaded pins.

citors and the wave-change switch. These components are mounted and wired up in the conventional way on a metal chassis As indicated in fig. 11 (*11*) this is done on a conveyor belt. At the end of the line (at *12*), the chassis complete with components is fixed and connected to the completed printed wiring panel to form a single assembly.

In the trimming operations (*13*) which now follow, advantage is derived from the fact that printed wiring lies in one plane, making every point readily accessible. When the chassis is placed in position on a special test bench, spring-loaded pins make the necessary contacts at various points of the printed wiring for test purposes (*fig. 12*). Another advantage of printed wiring is that trimming at this stage is required only for the radio-frequency section (the coil and the trimmer capacitor in the aerial circuit and in the oscillator circuit). Because of the reproducible capacitance between the connections on the printed wiring panel the band-pass filters can be adjusted in advance, i.e. during manufacture of these components, and no further adjustments are needed.

The concluding stages — mounting the chassis in the cabinets, the reception test (R.F. signal modulated with music applied to aerial terminal) and packing — are no different from those for receivers constructed by orthodox methods and will therefore not be discussed here. It is worth noting, however, that the factory bay housing the printed wiring section (*1 . . . 10* in fig. 11) is particularly small compared with the section handling the more conventional assembly work (*11 . . . 18*) and employs relatively few personnel.

Summary. Attempts to mechanize the wiring operations in electronic apparatus have led to the development of "printed wiring". Advantages of this process from the standpoint of organization are that it saves factory space and personnel and practically eliminates the wiring faults which are inevitably made with conventional wiring in the early stages of the production run of a new radio set. From the standpoint of pure radio engineering, printed wiring has both advantages and disadvantages, although these are of only minor significance.

The authors describe briefly the fabrication of printed wiring panels for Philips radio receivers and discuss the manufacture of a simple receiver (type B2X67 U) in which these panels are used.

THE JUNCTION TRANSISTOR AS A NETWORK ELEMENT AT LOW FREQUENCIES

III. STABILIZATION OF THE OPERATING POINT, IN PARTICULAR WITH REGARD TO TEMPERATURE CHANGES

by J. P. BEIJERSBERGEN, M. BEUN and J. te WINKEL.

621.375.4

This, the third and last article on the transistor as a network element at low frequencies, is addressed particularly to readers who are familiar with electronic tubes and who desire to know how the problem of stabilizing the D.C. operating point of a transistor differs from the corresponding problem with valve circuits. The early part of the article is accordingly devoted to explaining how differences between transistors and tubes give rise to differences in circuitry. Here, as in the rest of the article, full use is made of graphical methods. Except in the appendix, formulae relating to the physics of the transistor are not invoked.

The network that (together with the properties of the transistor) determines the D.C. operating point of a transistor calls for much more attention from the designer than is the case for tube circuits. If the properties of the transistor (or the tube) change, that is to say, if the characteristics become changed in shape or are displaced, there is a change in the D.C. operating point. One consequence of this may be that the transistor (or tube) can no longer deliver a signal of the required amplitude; indeed, the output current may be reduced to zero or driven out of the linear range. *Fig. 1* illustrates a case that may arise in transistor practice. A D.C. network is assumed to have properties such that *1)* I_B, the base current, is maintained at a constant value of -50 μA which is independent of the transistor properties (this implying that the transistor is biased by a constant current supply to the base) and *2)* the operating point Q lies somewhere along the straight line AB. The D.C. operating point is at Q or Q' according as the I_E-V_C characteristic for $I_B = -50$ μA is represented by the fully-drawn or the broken curve. The maximum amplitude of the A.C. voltage on the output is considerably less in the latter case than it is in the former.

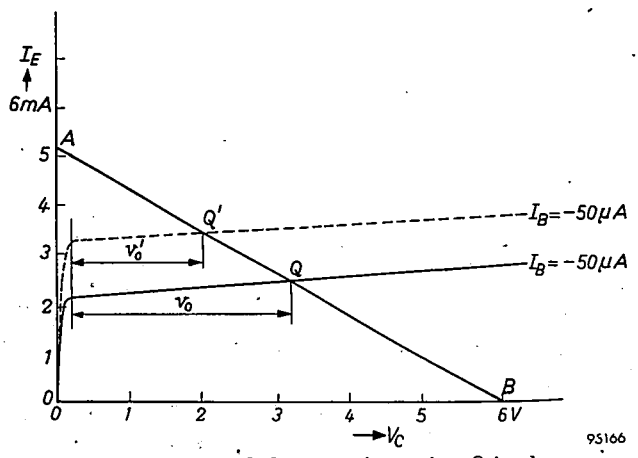

Fig. 1. Displacement of the operating point Q in the output graph of a transistor, in consequence of a change in the transistor characteristics. It is assumed that the characteristic appropriate to a constant base current of $I_B = -50$ μA moves from the position indicated by the fully-drawn curve to that indicated by the broken-line curve, the shift occurring on account of a rise in temperature, for example, or because the transistor has been exchanged for another individual. If the biasing network responsible for setting the operating point has properties such that the base current maintains the value -50 μA and such that the operating point is forced to remain on line AB, then the point will move from Q to Q'. As a result, the maximum amplitude of the signal voltage across the output will fall from v_o to v_o'.

A change of temperature may be regarded as the primary cause of the shift of transistor characteristics. With the OC 71, a shift such as that assumed in fig. 1, whereby the emitter current I_E rises from 2.5 mA to 3.5 mA, may result from a temperature change as small as from 25 °C to 40 °C. In the second place, the characteristics of two individuals of the same type of transistor may differ considerably. For example, at the same temperature of 25 °C, the emitter current for $I_B = -50$ μA might be 1.75 mA in one OC 71 and 3.75 mA in another individual of the same type.

Generally, it will not be permissible for such large changes to take place in the emitter current. An account of the measures that may be taken to counteract such changes and an analysis of the influence exercised by ambient temperatures will make up the greater part of the article. It is not necessary, for the purpose of the article, to know the physical mechanism underlying the large effect of ambient temperature on the functioning of a transistor, and we shall therefore make no reference to it. It may, however, be pointed out that it is impossible to manufacture transistors that are wholly insusceptible to temperature changes. The underlying cause of temperature effects in semiconductors is the considerable increase with temperature in the equilibrium concentrations of the minority charge-

N.V. PHILIPS' GLOEILAMPENFABRIEKEN

carriers. Those interested will find a more detailed explanation in the appendix. For the benefit of readers familiar with tube circuits, we shall constantly note points of difference from or similarity to electronic tubes, particularly in the earlier part of the article.

Stabilization of tube and transistor circuits

With tubes the situation is much less complicated than it is with transistors, and for this there are two main reasons. The first is that the ambient temperature has practically no effect on tube characteristics, while it has a considerable effect on those of transistors. The second reason is that, providing there is no flow of grid current, the characteristics of tubes at low frequencies can be displayed by a family of curves drawn in one graph; two graphs are required for displaying transistor characteristics [1]). Accordingly, with transistors, we must take account of shifts affecting the characteristics in *both* graphs.

The operating point P of the tube in the circuit of *fig. 2a* lies on a vertical straight line $V_g = E_g =$ constant in the I_a-V_g graph (*fig. 3a*). The "dynamic" I_a-V_g characteristic, which takes account of the fact that V_a decreases as I_a increases (in consequence of R_a), also appears in this graph. The dynamic characteristic can be derived, in the usual way, from the family of static I_a-V_g characteristics (V_a as running parameter). If for some reason or other — the replacement of the tube, for example, or a change in the anode voltage — this characteristic shifts from position *1* to position *2*, the anode current will change by an amount ΔI_a. The commonly employed circuit shown in fig. 2*b* is a better one, for in this case (see fig. 3*a*) the operating point lies on a straight line passing through the origin (the tangent of the angle it makes with the ordinate is proportional to R_k), and the change in the anode current is only $\Delta I_a'$. As compared with the circuit of fig. 2*a*, therefore, that of fig. 2*b* offers a certain stabilization of the anode current against displacement of the I_a-V_g characteristic. The degree of stabilization can be improved by inserting a separate voltage source E_g' in the grid lead (figs. 2*c* and 3*a*) with the positive terminal to the grid, and by giving R_k' a correspondingly larger value. This is only done in special cases in tube circuits.

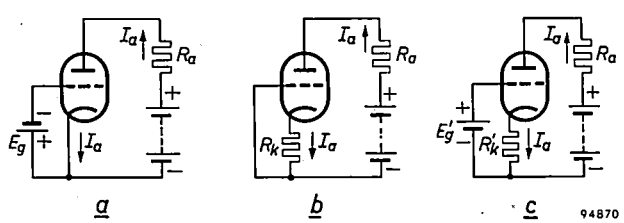

Fig. 2. *a*) Tube circuit in which the grid is biased with a constant direct voltage E_g.
b) Here the grid bias is obtained by means of the voltage drop across cathode resistor R_k. As compared to (*a*), this circuit provides a certain degree of stabilization of the anode current (see fig. 3*a*).
c) Stabilization of the anode current can be improved by putting a battery E_g' in the grid lead, the polarities being as shown; a larger cathode resistor R_k' can then be used. Alternatively, the battery may be inserted in the cathode lead.

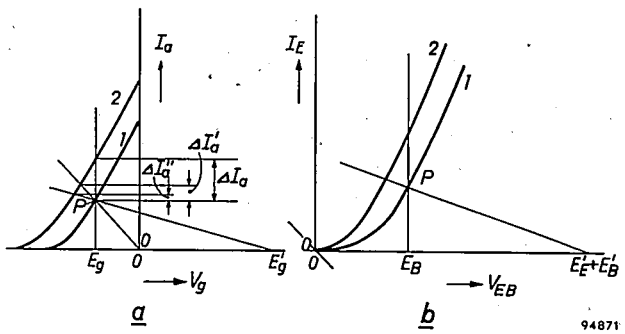

Fig. 3. *a*) Stabilization of a tube anode current. If curve *1* represents the appropriate I_a-V_g characteristic, then for a certain constant direct voltage E_g on the grid (as in fig. 2*a*), the operating point will be located at P. If the characteristic shifts into position *2*, I_a will change by an amount ΔI_a. With the circuits shown in figs. 2*b* and 2*c*, the operating point lies on a straight line passing through the origin or through point E_g', respectively. Displacement of the characteristic from *1* to *2* results in grid current changes of only $\Delta I_a'$ and $\Delta I_a''$.
b) The corresponding graph for a transistor. The characteristics lie on the other side of the ordinate; in consequence of this, the operating point of a transistor in a circuit having a resistor only in the emitter lead (fig. 4*b*) would be at the origin. Such a circuit is therefore useless.

For a meaningful comparison between transistors and tubes the emitter must be regarded as answering to the cathode, the base to the grid, and the collector to the anode. Correlating the electrodes in this fashion is justified by the fact that in a transistor $V_{BC} \approx V_{EC}$ and, if sign be disregarded, $I_E \approx I_C$ [2]). Accordingly, we shall make no distinction between V_{BC} and V_{EC} in what follows, but refer only to V_C, calling it the collector voltage. Similarly, we shall refer only to I_E, which we shall simply call the transistor current, without any further qualifica-

[1]) This is discussed in detail in the first of this series of articles; J. P. Beijersbergen, M. Beun and J. te Winkel, The junction transistor as a network element at low frequencies, I. Characteristics and *h* parameters, Philips tech. Rev. **19**, 15-27, 1957/58, particularly pp. 15-16. This article will hereinafter be referred to as I. The graphs discussed in the article (page 18) ought strictly to have a third axis with a scale of temperatures. The curved lines appropriate to given parameter values would then become curved planes.

[2]) See I, page 16, for a more detailed explanation. At this juncture we would remind the reader of the conventions regarding signs. Currents are denoted as positive when their direction is towards the transistor; as regards voltages, a positive value signifies that the electrode denoted by the first suffix letter has a higher potential than the electrode denoted by the second suffix.

tion. I_E may be taken to stand for either the emitter or the collector current [3]). The transistor characteristic corresponding to fig. 3*a* is thus the (dynamic) I_E-V_{EB} characteristic (shown in fig. 3*b*; it can be derived from the static I_E-V_{EB} characteristics having V_C as their running parameter). The reader will notice straight away that the curve lies on the side of the ordinate opposite to that of the tube characteristics in fig. 3*a*; this is a further difference between the transistor and the tube that has not so far been mentioned [4]).

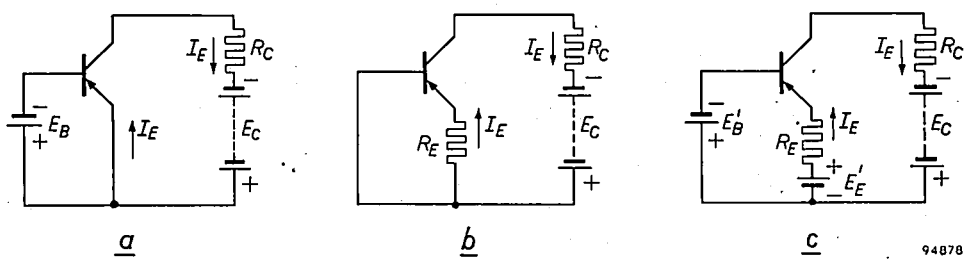

Fig. 4. *a*), *b*) and *c*) are transistor circuits analogous to the tube circuits appearing in figs. 2*a*, *b* and *c*. The circuit (*b*) with only a resistance R_E in the emitter lead and no voltage source between emitter and base is useless, since the operating-point current is zero (see fig. 3*b*).

The transistor circuits analogous to those of figs. 2*a*, *b* and *c* appear in *figs.* 4*a*, *b* and *c*. For a circuit as that of fig. 4*b*, having only a resistor in the emitter lead — and no voltage source between emitter and base — the operating point lies on a straight line passing through the origin. It will be evident from fig. 3*b* that such a circuit cannot be employed for transistors: I_E would be zero. However, a resistance may well be inserted in the emitter lead provided that a voltage source is inserted between base and emitter (fig. 4*c*). The voltage source may be placed either in the base or in the emitter lead, and in fig. 4*c* one has been included in both leads in order to show that there is no preference. It will be seen from the graph in fig. 3*b* that, compared with fig. 4*a*, the circuit of fig. 4*c* offers a certain degree of stabilization of I_E against displacement of the I_E-V_{EB} characteristic.

Fig. 5 shows I_E-V_{EB} characteristics drawn with the transistor temperature t_j (suffix j stands for "junction") as the running parameter. A general rule is that the characteristic moves about 2.2 mV to the left for every °C rise in temperature [5]). The graph makes it clear that it is a mistake to bias a transistor with a voltage source located between base and emitter (as in fig. 4*a*): as the operating point now runs on the vertical line $V_{EB} = E_B$, a quite small temperature rise is enough to cause a considerable increase in the transistor current.

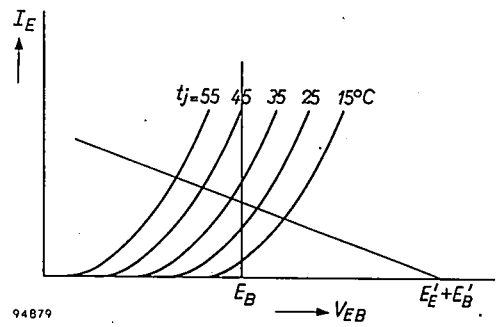

Fig. 5. I_E-V_{EB} transistor characteristics with t_j, the temperature of the transistor crystal, as the running parameter. The characteristic moves about 2.2 mV to the left for every °C rise in t_j. Keeping the base voltage E_B constant (fig. 4*a*) restricts the operating point to the vertical line, which thus results in a rapid increase of I_E with t_j; this, then, is an unsatisfactory way of biasing a transistor.

There is a second way of stabilizing I_E against displacement of the I_E-V_{EB} characteristic, this being by leaving out the resistor in the emitter lead (R_E) and putting one in the base lead (R_B). We then have *fig. 6*. An analogous case does not arise with tubes, for the grid current is zero.

In order to investigate the functioning of this circuit we must consider the relation between I_E and I_B. From now on, therefore, the second graph, that in which I_E is plotted against I_B, will come into the picture (see *fig. 7*). Applying Kirchhoff's

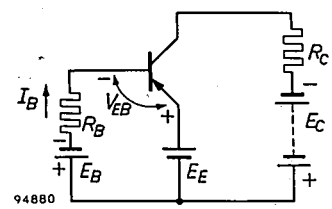

Fig. 6. A second method of rendering the transistor current I_E less sensitive (than it is in fig. 4*a*) to displacement of the I_E-V_{EB} characteristic is to place a resistor R_B in the base lead instead of R_E in the emitter lead (as in fig. 4*c*).

[3]) Without saying so, we have been assuming that the transistor is of the *P-N-P* type. In this type of transistor the emitter current is positive and the collector current is negative. Choosing the symbol I_E thus does away with unnecessary minus signs. The collector voltage V_C is identified with V_{EC} and V_{BC} (and not with V_{CE} and V_{CB}) for the same reason.

[4]) The difference might also be formulated as follows: in a transistor the potential of the base has a value intermediate between the collector and emitter potentials; in a tube the potential of the grid is not only lower than the anode potential — it is slightly lower even than that of the cathode.

[5]) See appendix.

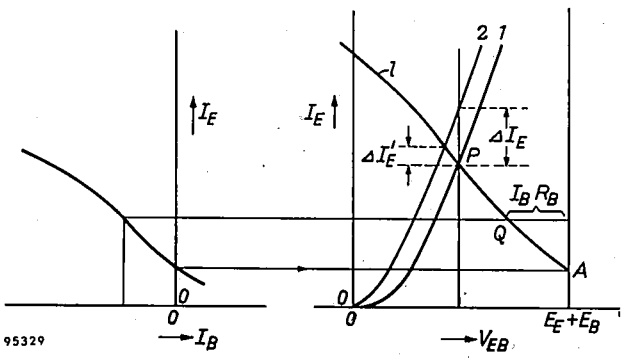

Fig. 7. Location of the operating point P in the I_E-V_{EB} graph for a circuit having a resistor R_B in the base lead (fig. 6). Curve l is constructed by plotting it point by point, use being made of the I_E-I_B graph on the left; P is the point where l intersects the appropriate I_E-V_{EB} characteristic. If this characteristic shifts from position 1 to position 2, V_{EB} being kept constant (fig. 4*a*), the current increases by an amount ΔI_E; the effect of resistor R_B is to reduce this increase to $\Delta I_E'$.

second law to the mesh formed by the emitter and base leads in fig. 6, we find that

$$V_{EB} = E_E + E_B + I_B R_B. \quad . \quad . \quad . \quad (1)$$

From the dynamic I_E-I_B characteristic a value of I_B is found that corresponds to some arbitrary value of I_E. (This characteristic too can be derived from the static characteristics, viz. those having V_C as the running parameter.) $I_B R_B$ can then be worked out, whereupon V_{EB} is determined from (1). In this way a point Q in the I_E-V_{EB} graph is obtained (see fig. 7; note that the I_B value associated with point Q is negative). The plotting of a series of such points allows a curve l to be drawn, which represents the locus of the operating point. The curve must, of course, pass through the point A corresponding to $I_B = 0$. It is evident that a high value of R_B and an appropriately large value of $E_E + E_B$ make l more horizontal and therefore provide good stabilization of I_E against displacement of the I_E-V_{EB} characteristic.

We shall now simplify matters by adopting a straight-line approximation to the I_E-I_B characteristic. The equation of the linearized characteristic is

$$I_E = -I_{CE0} - \alpha_{FE} I_B, \quad . \quad . \quad . \quad (2)$$

in which $-I_{CE0}$ is the intercept on the I_E axis (*fig. 8*) and α_{FE} is the current amplification factor, assumed to be constant, in the common-emitter configuration [6]). Curve l now becomes a straight line through A.

[6]) The symbols employed in this article are those proposed by the Institute of Radio Engineers; see Proc. Inst. Rad. Engrs. 44, 934-937, 1956.

The symbols I_{c0}' and α' are frequently employed in place of I_{CE0} and α_{FE} respectively. Since we are concerned here with dynamic characteristics, it is not entirely correct to use α_{FE}, the static current amplification factor, in equation (2). In doing so we neglect the difference between the static and dynamic characteristics.

The susceptibility of I_E to displacement of the I_E-V_{EB} characteristic diminishes as the value of R_B is increased, but at the same time there is an increase in the susceptibility to displacement of the I_E-I_B characteristic. This can be confirmed by studying fig. 8. We render I_E fully insusceptible to displacement of the I_E-V_{EB} characteristic by employing base *current* biasing, which implies that I_B is independent of the transistor. The value of I_E associated with this particular value of I_B is fixed by the appropriate I_E-I_B characteristic; thus the I_E-V_{EB} characteristic has ceased to play any part. On the other hand, the susceptibility of I_E to displacement of the I_E-I_B characteristic is now at a maximum. The shift that this characteristic may undergo is considerable. For the OC 71 transistor, an I_{CE0} of —150 μA is normal at 25 °C, but it may amount to —325 μA in some individuals. The current amplification α_{FE} given by the OC 71 may vary between 35 and 75. I_{CE0} is heavily dependent on temperature too; it is a fairly general rule for germanium transistors that the I_{CE0} value doubles with every 7 °C temperature rise (see the appendix).

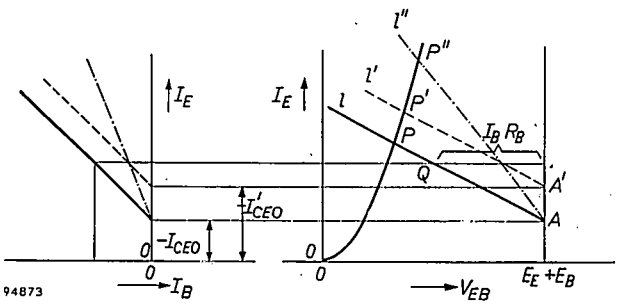

Fig. 8. The same as fig. 7, but here a straight line has been taken as an approximation to the I_E-I_B characteristic. In consequence curve l also becomes a straight line. A is a point on l, and therefore, to be able to draw this straight line, one need only determine one other point Q. If $-I_{CE0}$ (the transistor current at $I_B = 0$) increases, assuming the value $-I'_{CE0}$ say, I_E will also increase; l will shift to l' and P to P'. The operating point also shifts if the slope of the I_E-I_B characteristic alters (e.g. to the position of the chain-dotted line) — in other words, if the current amplification factor alters; line l becomes line l'' and P becomes P''. The result is again a change in the value of I_E.

The circuit of *fig. 9a* represents a case of almost pure base current biasing. Here E_B and E_C are zero. The collector voltage is provided by E_E, which therefore has to be large compared to V_{EB}. Hence E_E is approximately equal to $I_B R_B$. Having decided the value I_B is to have, we can thus determine R_B. I_B will now maintain the value chosen for it, irrespective of temperature or the properties of the individual transistor. The circuit is usually drawn in the form shown in fig. 9*b*. It was this circuit that we had in mind when giving the example

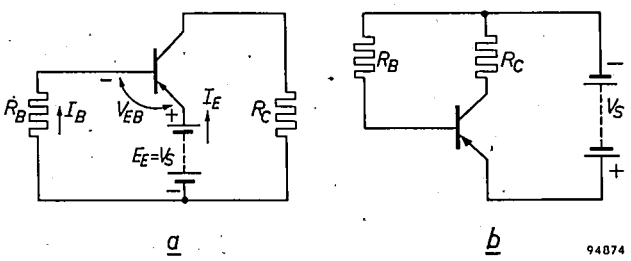

Fig. 9. *a*) A transistor circuit representing a case of almost pure base current biasing. The transistor current is insensitive to displacement of the I_E-V_{EB} characteristic, but highly sensitive to displacement of the I_E-I_B characteristic. Exactly the opposite applies in the circuit of fig. 4*a* (which has voltage biasing between emitter and base).
b) The same circuit as (*a*) but drawn in a more conventional form.

of operating-point shift illustrated in fig. 1. Of course, a really pure case of base current biasing only arises if E_E and R_B are made infinitely large, their ratio being kept constant.

Summarizing, one may say that having a *voltage* source between emitter and base ($R_B = 0$) renders I_E insusceptible to displacement of the I_E-I_B characteristic, but results in maximum susceptibility to displacement of the I_E-V_{EB} characteristic; with a base *current* biasing ($R_B = \infty$) it is just the reverse. It may be asked which of the two extreme methods is the better. From theoretical considerations (see appendix) it follows that, if the transistor is initially biased such that I_B is zero, the transistor current I_E increases with temperature at about the same rate for both types of biasing. However, as the initial value of I_B is made more and more negative, I_E thereby becoming ever greater, base current biasing becomes more favourable than voltage biasing between emitter and base. It will be seen from *fig. 10* that on the whole these inferences hold good in practice. This explains why in discussions of the stabilization of the transistor current it is usually implicit that base current biasing is employed, this being regarded as the standard case, as it were.

It is also possible to determine the operating-point value of the transistor current in the general case, in a circuit including both R_E and R_B (*fig. 11a*). Applying once again Kirchhoff's second law to the mesh formed by the emitter and base leads, now in fig. 11*a*, we find that

$$V_{EB} = E_E + E_B - I_E R_E + I_B R_B . \quad . \quad . \quad (3)$$

In order to find curve *l* in the I_E-V_{EB} graph, we assume a certain value for I_E, read the corresponding value of I_B from the I_E-I_B characteristic and proceed to plot $I_B R_B$, starting not from the vertical line $V_{EB} = E_E + E_B$, but from the oblique line

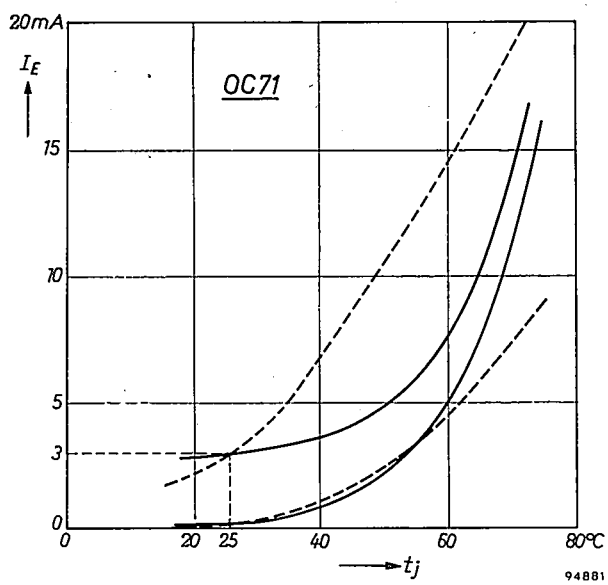

Fig. 10. The transistor current I_E as a function of transistor temperature t_j. The fully-drawn curves are curves for constant base current I_B; the lower one is valid for $I_B = 0$, the upper one for that value of I_B that, at $t_j = 25$ °C, gives a transistor current $I_E = 3$ mA. The broken curves are curves of constant voltage V_{EB} between emitter and base; the lower and upper ones respectively hold for those values of V_{EB} that, at $t_j = 25$ °C, correspond to $I_B = 0$ and to $I_E = 3$ mA.

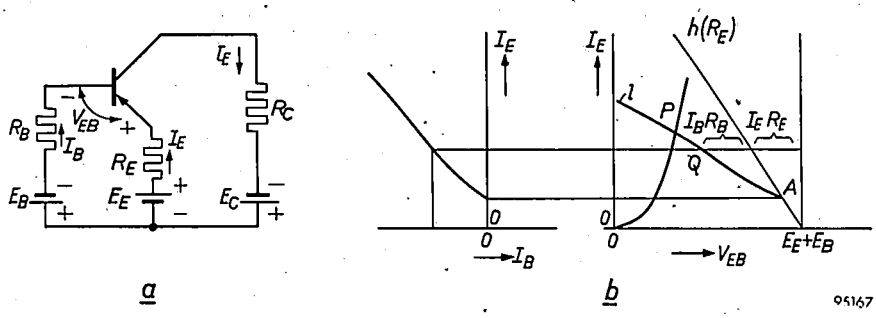

Fig. 11. (*a*) A transistor circuit with resistors and batteries in the base, emitter and collector leads.
(*b*) Graphical determination of the operating point *P* for circuit (*a*). The only difference from the procedure illustrated in fig. 7 is that, in order to find *l*, one measures the distance $I_B R_B$ not from the vertical line $V_{EB} = E_E + E_B$, but from the line $h(R_E)$, the equation of which is $V_{EB} = E_E + E_B - I_E R_E$. If the I_E-I_B characteristic is taken to be a straight line, curve *l* will likewise be straight.

$V_{EB} = E_E + E_B - I_E R_E$ (fig. 11*b*). This new datum line passes through point $E_E + E_B$ on the V_{EB} axis and lies at an angle to the vertical whose tangent is proportional to R_E. (From now on we shall refer to it as $h(R_E)$.) Here too, if the I_E-I_B characteristic is taken to be a straight line, l will also be straight [7]).

Definition of the D.C. operating point

Of the six variables, viz. three currents (I_E, I_C and I_B) and three voltages (V_{EB}, V_{BC} and V_{CE}) that are associated with a transistor, not more than two can be allotted desired values at a given temperature. The values of the other four quantities are fixed by the two that have been chosen. All this is explained in I on page 15. Similarly, it will generally only be possible to keep two of the said variables constant despite changes in the transistor properties, such as arise on account of temperature changes or because the original transistor has been exchanged for another individual; the values of the other four will usually alter. If therefore it is to be possible to say that two transistors have the same D.C. operating point or that the point remains steady when the temperature changes, one must first decide which two variables are going to be taken to define the operating point. By ignoring the distinction between I_E and $-I_C$ and between V_{EC} and V_{BC}, we have already reduced the number of variables to four, namely to I_E, V_C, I_B and V_{EB}. Of these, we shall select I_E and V_C to characterize the D.C. operating point. There are good reasons for so doing. In the first place, of course, I_E and V_C are the coordinates of the output characteristics for all three of the fundamental configurations, viz. the common-emitter, common-base and common-collector configurations (see I, page 18); the position of the operating point in these graphs determines the range throughout which the transistor can be fully driven (see fig. 1, for example). In the second place, the product $I_E \times V_C$ represents, with fair accuracy, the total amount of power dissipated in the transistor. Hence stabilizing I_E and V_C will ensure that the dissipated power remains within narrow limits, and will remove the danger of the transistor temperature rising too much above ambient temperatures. This matter will be discussed in more detail in the following section. In the third place, the A.C. properties of a given transistor are only slightly dependent on temperature if I_E and V_C are kept constant [8]).

[7]) This graphical method of determining I_E as a function of t_j was brought to our attention by D. A. Munnik and P. Varekamp, members of the laboratory staff at the Philips Semiconductor Factory at Nijmegen.

Thermal equilibrium

As already stated, the power P_C dissipated in the transistor is approximately equal to $I_E \times V_C$. In a state of thermal equilibrium, the temperature t_j of the transistor crystal will, of course, always exceed the ambient temperature t_{amb} by an amount such that P_C is equal to P_{amb}, the power being transferred from the transistor to its surroundings in the form of heat. A fair approximation for the heat thus transferred away per second is

$$P_{amb} = (t_j - t_{amb})/K, \quad \ldots \quad (4)$$

where K is a constant which is the thermal resistance (or reciprocal heat-transfer coefficient), and is mainly dependent on the mechanical design of the transistor and on the manner in which it is mounted on the chassis (i.e., K depends on the thermal contact between the crystal and its surroundings). Data relating to the thermal resistance are supplied by the manufacturer for each type of transistor [9]). From (4) we see that P_{amb}, plotted as a function of t_j for given values of t_{amb} and K, gives a straight line; see *fig. 12*.

The properties of the transistor being dependent on t_j, P_C will be some function of t_j which, depending on the circuit and on the transistor itself, may

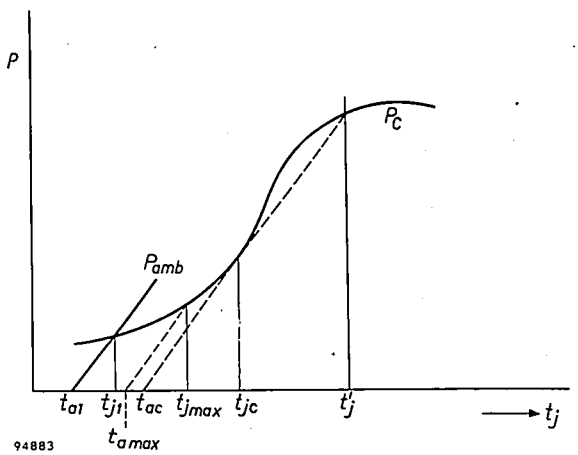

Fig. 12. The power P_C dissipated in a transistor is a function of t_j, the temperature of the transistor crystal. The shape of the function depends on the parameters of the transistor circuit. The power P_{amb}, transferred from the transistor to its surroundings, is proportional to the difference between t_j and the ambient temperature t_{amb}. Provided thermal equilibrium exists, at an ambient temperature of t_{a1} the transistor temperature will be t_{j1}. As t_{amb} increases, the straight line representing P_{amb} moves to the right. If P_C has the shape indicated here, once t_{amb} attains the value t_{ac} the transistor will not remain at t_{jc} but will assume the temperature t'_j (temperature "run-away").

[8]) See, for example, J. P. Beijersbergen, M. Beun and J. te Winkel, The junction transistor as a network element at low frequencies, II. Equivalent circuits and dependence of the h parameters on operating point, Philips tech. Rev. **19**, 98-105, 1957/58, particularly Table III and formulae (4) and (5). This article will hereinafter be referred to as II.

[9]) If the transistor is fitted with a cooling fin, its thermal resistance depends to some extent on the ambient temperature.

for example have the form arbitrarily assumed in fig. 12. It is clear that the transistor will only be in thermal equilibrium when its temperature has attained a value t_{j1} at which $P_C = P_{amb}$. The state of equilibrium will be stable, for if t_j rises higher than t_{j1}, P_{amb} will exceed P_C, with the result that t_j decreases; if on the other hand t_j falls below t_{j1}, P_{amb} will be less than P_C, with the result that t_j increases until it attains the value t_{j1}.

As the ambient temperature rises, the straight line P_{amb} is displaced to the right, maintaining the same slope. If in this way it becomes tangential to the curve at a point of increasing slope (broken line, when $t_{amb} = t_{ac}$), the transistor temperature will rise considerably, reaching the value t_j' (temperature "run-away").

The curve of P_C cannot go on rising indefinitely. This is in any case evident from the fact that the D.C. source is unable to supply unlimited power. Usually P_C exhibits a maximum, as has been assumed in fig. 12. It may easily happen, however, that the transistor breaks down before this maximum is attained.

The manufacturer generally indicates a maximum permissible value of transistor temperature ($t_{j\,max}$) because it is impossible to give any guarantee regarding the life of the transistor if it is operated above this temperature. In the assumed case illustrated in fig. 12, the circuit in question can only be employed at ambient temperatures below $t_{a\,max}$. In other cases the circuit might be such as to give the P_C curve a quite different shape, in which t_{jc} occurred at a value lower than $t_{j\,max}$; the ambient temperature would then have to remain below t_{ac} (the intercept of the tangent).

At any given value of t_j, $P_C - P_{amb}$ represents the amount of heat that becomes available each second to raise the temperature of the transistor crystal. Of course, if $P_C - P_{amb}$ is negative, it represents the amount of heat withdrawn from the crystal each second, in which case t_j drops. A state of equilibrium will be attained all the quicker the more rapidly the curves P_C and P_{amb} approach each other. It is not impossible for the two curves to be almost coincident over a considerable range of temperatures in the region of their (stable) point of intersection. If this is so, it will take a long time for equilibrium to be attained; moreover, a slight change in t_{amb} will cause the transistor to start creeping towards a new and distant equilibrium temperature. The new equilibrium temperature may well be higher than $t_{j\,max}$.

We shall now describe how the curve of P_C for a given circuit can be determined, given the transistor characteristics.

Determination of I_E, V_C and P_C as functions of t_j

The D.C. circuits discussed in this article can all be reduced to the fundamental D.C. circuit that appears in fig. 11*a*. One of the three e.m.f.'s shown in the diagram can, of course be left out without diminishing the generality. The reason why the three are shown is to make it convenient to compare an actual practical circuit with this fundamental one.

If the I_E-I_B and I_E-V_{EB} characteristics for a given value of t_j are available, the corresponding I_E can be determined by the graphical method illustrated in fig. 11*b*. If families of these characteristics, corresponding to a set of t_j values, are available, it is possible to determine I_E as a function of t_j. The following formula (Kirchhoff's second law, applied to the mesh formed by the emitter and collector leads in fig. 11*a*) can then be used for calculating V_C for each I_E value:

$$V_C = E_E + E_C - (R_E + R_C)I_E. \quad . \quad . \quad (5)$$

We can now plot V_C as a function of t_j; P_C can also be so plotted, since $P_C = I_E \times V_C$. If K is also known, P_{amb} can also be plotted (eq. 4). We thus have a graph similar to fig. 12 from which we can find out how the circuit will behave as the ambient temperature changes.

As observed earlier in this article, it is the *dynamic* characteristics that should really be used; these take account of the fact that I_E depends on V_C. However, satisfactory results are generally obtained by the use of the static characteristics, valid for constant V_C.

This amounts to making use of straight lines parallel to the V_C axis as approximations to the I_E-V_C characteristics having I_B as the running parameter, as also to those having V_{EB} as the running parameter. The main implication of these approximations is that the *Early effect* is being neglected (see II, page 104).

The required characteristics — those drawn in fig. 11*b* — can be determined by measurement, the transistor being placed in a thermostatted enclosure. It is advisable to have the collector voltage low (e.g. 2 V) for the purpose of these measurements, in order to keep down the power dissipated in the transistor, so that the transistor crystal remains at the temperature of the thermostat.

If the necessary equipment is not available, one may proceed as follows. The manufacturer supplies I_E-I_B and I_E-V_{EB} characteristics for one temperature (usually $t_j = 25$ °C); alternatively the curves can be worked out from the data supplied. The corresponding curves for other t_j values can be obtained with the aid of two rules that have already been given in the course of this article:

1) The I_E-V_{EB} curve moves about 2.2 mV to the left for every °C rise in t_j.
2) The I_E-I_B curve moves upwards by about 10% for every °C rise in t_j (I_E doubling with every 7 °C).

An explanation of these rules will be found in the appendix.

Simplified method

The method just described is proper to an exact analysis of the thermal behaviour of a given transistor in a given circuit, but it is rather involved.

It has already been observed that l becomes a straight line if it be assumed that α_{FE} is independent

of I_E. If it be further assumed that α_{FE} is independent of temperature, the I_E-I_B characteristics having t_j as the running parameter become parallel straight lines, and so do the l curves. There is then no need to draw the I_E-I_B characteristics. All that is necessary is to plot a value $-I_{CE0}(t_{j1})$ on the I_E axis, whence we find the corresponding point $A(t_{j1})$ on the $h(R_E)$ line (*fig. 13*). A second point

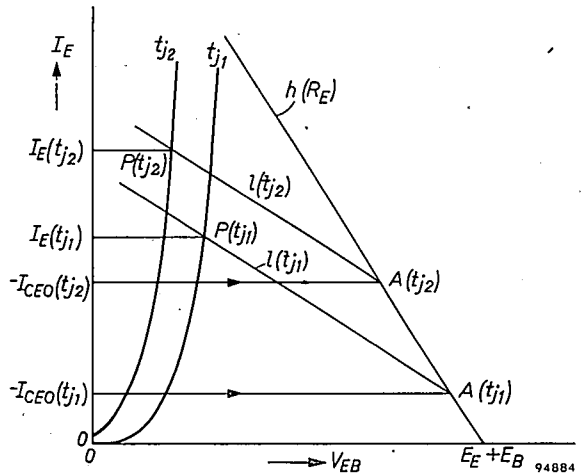

Fig. 13. If α_{FE}, the current amplification factor, is assumed to be independent of I_E and t_j, the l curves become parallel straight lines. It is an easy matter to find the points A at which they intersect with straight line $h(R_E)$, and hence to determine the operating point P for various values of t_j.

can be determined with the aid of α_{FE} (the value of which, of course, has to be known) and equation (2). Taking another value of t_j, say t_{j2}, one proceeds in the same manner to find $A(t_{j2})$, subsequently drawing a line $l(t_{j2})$ parallel to $l(t_{j1})$ through point $A(t_{j2})$.

This procedure is quite satisfactory in cases where I_E does not exceed a few milliamperes. Where currents are higher, the fact that α_{FE} decreases must be taken into account. The current amplification factor of an average OC 72, for example, falls off from 70 to 50 as I_E increases from 10 mA to 80 mA. Usually this kind of information is included in the manufacturer's data. The meaning of α_{FE} in such data is $\alpha_{FE} = \{I_E - (-I_{CE0})\}/I_B$. Often the symbol $\overline{\alpha'}$ is used to denote this quantity.

Design of a circuit to meet a specified thermal stability

The circuit in *fig. 14a* is one that is very commonly employed. If the supply (of e.m.f. V_S) has a negligible internal resistance, it will be found by applying Thévenin's theorem [10]) that fig. 14*a*, as seen by the transistor, is equivalent to fig. 14*c*. This in its turn is equivalent to fig. 11*a* provided E_E in that figure is taken to be zero and R_B and E_B have the following relationship to the resistances in the circuit of fig. 14*b*:

$$R_B = \frac{R_1 R_2}{R_1 + R_2}, \quad \ldots\ldots (6)$$

$$E_B = V_S \frac{R_1}{R_1 + R_2}. \quad \ldots\ldots (7)$$

We shall now discuss the case of a circuit that is required to have a certain specified thermal stability: we shall suppose that it has already been decided what the D.C. operating point shall be at a certain ambient temperature (V_{C1}, I_{E1} at t_{amb1}), and that it is not permissible for the current to rise higher than I_{E2} at a certain higher ambient temperature t_{amb2}. If V_S, the voltage of the supply source, is given, then

$$R_E + R_C = (V_S - V_{C1})/I_{E1}. \quad \ldots (8)$$

We shall assume that R_C is known, and hence we shall be able to work out R_E. The powers dissipated in the transistor at the two ambient temperatures of t_{amb1} and t_{amb2} are $P_{C1} = I_{E1} \times V_{C1}$ and $P_{C2} = I_{E2} \times V_{C2}$, respectively. V_{C2}, the operating-point voltage at t_{amb2}, is worked out from (8), the suffixes therein being changed from 1 to 2. For a state of thermal equilibrium to exist, P_C must be equal to P_{amb}; t_{j1} and t_{j2}, the temperatures the transistor

[10]) Thévenin's theorem implies that it is permissible to replace the part of the network to the left of the broken line (fig. 14*b*) by an e.m.f. in series with a resistance. The e.m.f. is equal to the open-circuit voltage across the terminals located on the broken line; the resistance is that measured between these terminals when V_S is short-circuited.

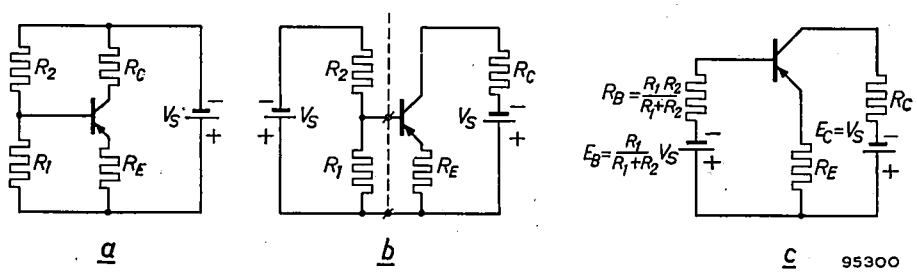

Fig. 14. *a*) A direct-current circuit frequently employed in transistor practice. If the internal resistance of the battery (of e.m.f. = V_S) is negligible, then, seen from the transistor, (*a*) is equivalent to (*b*). Application of Thévenin's theorem [10]) to the portion on the left of the dotted line results in the transformation of (*b*) into (*c*), the circuit thereby being reduced to that in fig. 11*a*.

will have when the temperatures of its surroundings are t_{amb1} and t_{amb2}, can therefore be worked out from (4). V_{EB1} and I_{B1}, the values associated with the combination of t_{j1} with I_{E1}, are taken from the curves appropriate to the transistor temperature t_{j1}. Insertion of these values and that of R_E in (3) gives us an equation involving two unknowns, $E_E + E_B$ and R_B. A second equation is obtained by proceeding in the same manner but by taking the combination of t_{j2} with I_{E2}. From the two equations R_B and E_B can be calculated ($E_E = 0$). Finally, in (6) and (7) we have two further equations that allow us to work out the values of resistors R_1 and R_2. This completes the dimensioning of the circuit.

The foregoing implies the use of the *static* I_E-I_B and I_E-V_{EB} characteristics. Sometimes a more exact procedure, based on the *dynamic* characteristics, is desirable. The data supplied by the manufacturer are generally sufficient to allow the static characteristic (with V_C as the parameter) to be derived for one temperature (usually $t_j = 25$ °C). Once $R_E + R_C$ has been worked out from (8), it is possible to construct the dynamic characteristics for this same temperature of $t_j = 25$ °C. The two rules given earlier on page 128 can equally well be applied to these dynamic characteristics, in order to get some idea of their position at other temperatures.

Spread in properties. An example of stabilized design

It was stated in the earlier part of the article that different individuals of the same transistor type may exhibit a considerable divergence in their properties. If a transistor-equipped device is to be produced in quantity, and if it is desired to avoid the need to bias each transistor individually, then allowance must be made for this spread in properties. We shall explain how this is done by working through a simple example; the design will also allow for changes in ambient temperature.

Our example concerns an OC 71 in the driver stage of an amplifier. The circuit of which the OC 71 forms part is as shown in *fig. 15a*. From the A.C. point of view, the transistor is in the common-emitter configuration (fig. 15*b*). The performance

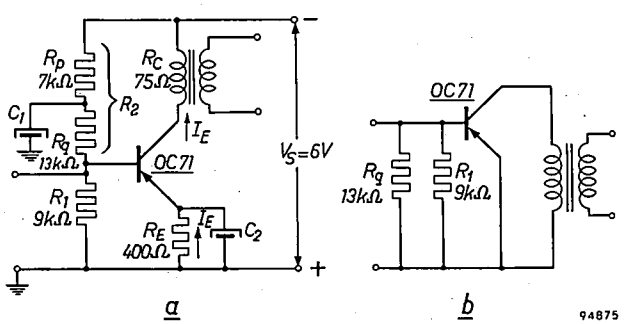

Fig. 15. *a*) Circuit for a type OC 71 transistor in the driver stage of an amplifier. By way of illustration, the values of the various resistors are worked out in the text in conformity with an assumed set of requirements.
b) A.C. circuit corresponding to (*a*).

required of the output stage necessitates that the OC 71 of the driver stage should deliver a signal voltage of 3.8 V peak, and a signal current of 2.7 mA peak, at its output. Assuming a knee voltage of $V_C = 0.3$ V, we see that the operating point in the I_E-V_C graph (*fig. 16*) will have to remain on

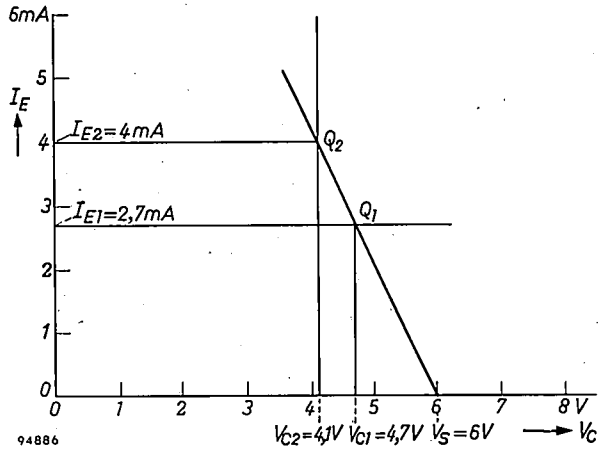

Fig. 16. With regard to the operating point of the transistor in the circuit of fig. 15, it is required that I_E shall remain between 2.7 mA and 4 mA and that V_C shall not drop below 4.1 V. The supply voltage $V_S = 6$ V is given, thus fixing the direct-current load line Q_1Q_2.

the right of the vertical line $V_C = 3.8 + 0.3 = 4.1$ V and above the horizontal line $I_E = 2.7$ mA. The D.C. resistance of the primary winding of the transformer coupling the driver stage to the output stage is $R_C = 75\ \Omega$. The supply voltage is $V_S = 6$ V. It is desired that the transistor current I_E shall not rise higher than 4 mA, since the D.C. magnetization of the transformer would then be excessive. This limitation fixes the D.C. load line in fig. 16. From its slope we find that $R_E + R_C = 475\ \Omega$. Since $R_C = 75\ \Omega$, we have $R_E = 400\ \Omega$. The voltage and current values appropriate to operating point Q_1 are $V_{C1} = 4.7$ V and $I_{E1} = 2.7$ mA. The power then dissipated is $P_{C1} = 4.7 \times 2.7 = 12.7$ mW. For an OC 71 mounted so as to allow the free access of air, K has a value of 0.4 °C/mW. When the transistor is operating at Q_1, therefore, the crystal temperature t_j is $12.7 \times 0.4 \approx 5$ °C higher than the ambient temperature. Proceeding in a similar way, we find that at Q_2 the crystal temperature is nearly 7 °C higher than the ambient temperature. It is required that the amplifier may be used at ambient temperatures between 15 °C and 45 °C; in other words, the operating point must keep within Q_1 to Q_2 at these ambient temperatures. Now, a low value of I_E is favoured by a low temperature and low values of α_{FE} and $-I_{CE0}$; on the other hand, a high temperature and high values of α_{FE} and $-I_{CE0}$ tend to result in high I_E values. (It will be seen

in a moment that this is so.) In *fig. 17* I_E-V_{EB} characteristics have been drawn that are appropriate to the lowest and highest values of t_j, namely to $t_{j1} = 15 + 5 = 20$ °C and $t_{j2} = 45 + 7 = 52$ °C. I_E-I_B characteristics for these t_j values appear on the left-hand side of the figure. The $t_{j1} = 20$ °C characteristic is that for minimum values of α_{FE} and $-I_{CE0}$ (the latter being taken to be zero); and low I_{CE0} and α_{FE} values combine to keep I_E low, whereas a high temperature and high I_{CE0} and α_{FE} values have the opposite effects. That this is so can easily be confirmed from fig. 17: as α_{FE} increases, the $l(t_j)$ lines turn clockwise about their points of intersection with $h(R_E)$ — these being the points marked A in fig. 13 — and I_E increases. (But this is not entirely obvious, as may be seen

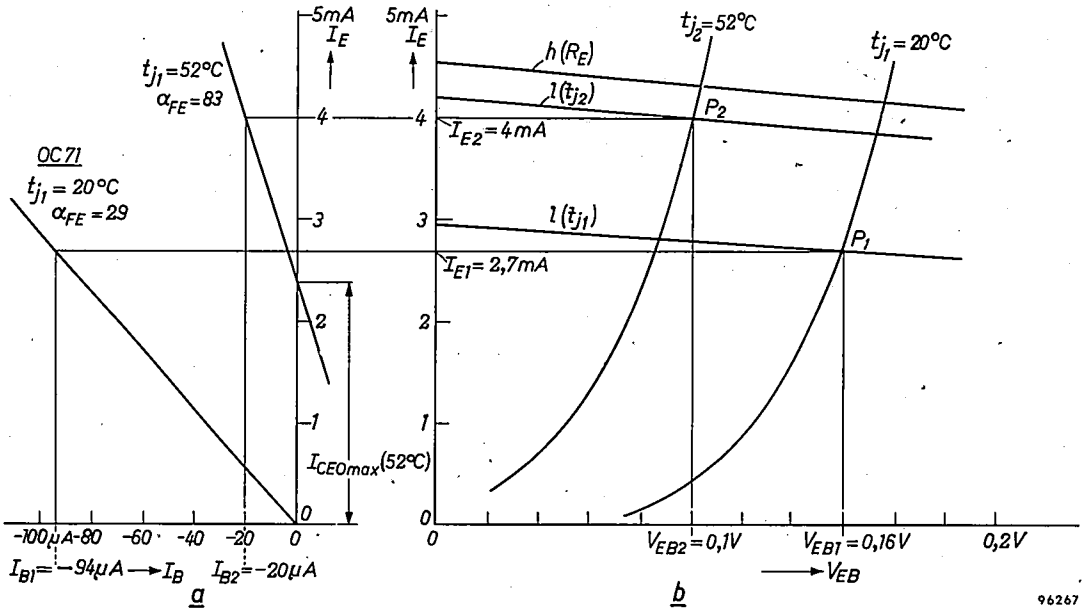

Fig. 17. I_E-V_{EB} characteristics (on the right) and I_E-I_B characteristics (on the left) for an OC 71 at transistor temperatures of $t_{j1} = 20$ °C and $t_{j2} = 52$ °C. The I_E-I_B characteristic for 20 °C is appropriate to an individual transistor whose I_{CE0} and α_{FE} are the lowest occurring in the spread of values; that for 52 °C applies to an individual whose I_{CE0} and α_{FE} are the highest occurring. This graph is used to work out the circuit of fig. 15.

the $t_{j2} = 52$ °C characteristic is that for maximum values of α_{FE} and $-I_{CE0}$. Straight lines have been drawn as approximations to the true I_E-I_B characteristics; they are not parallel, however, on account of the difference in the α_{FE} values. Fig. 17 gives us the following information: $V_{EB1} = 0.16$ V; $V_{EB2} = 0.1$ V; $I_{B1} = -94$ μA; $I_{B2} = -20$ μA. Determining R_B and E_B with the aid of (3) in the manner already described (page 130) we find that $R_B = 6.2$ kΩ and $E_B = 1.83$ V. We now determine R_1 and R_2 with the aid of (6) and (7), and find that $R_1 \approx 9$ kΩ and $R_2 \approx 20$ kΩ.

The lines $h(R_E)$, $l(t_{j1})$ and $l(t_{j2})$ are also drawn in fig. 17. They are not necessary for the calculation, but give a general impression of the situation. In the first place they show that, with the scales used in the figure, the point E_B on the abscissa and the points A_1 and A_2, where $h(R_E)$ intersects $l(t_{j1})$ and $l(t_{j2})$ respectively, lie well outside the graph. It was for this reason that formula (3) was used for determining E_B and R_B and that no attempt was made to arrive at them by geometrical construction.

Secondly, it was stated that a low temperature from *fig. 18*. Here A is on the left of the appropriate I_E-V_{EB} characteristic and, as a result, I_E decreases instead of increasing as α_{FE} increases.)

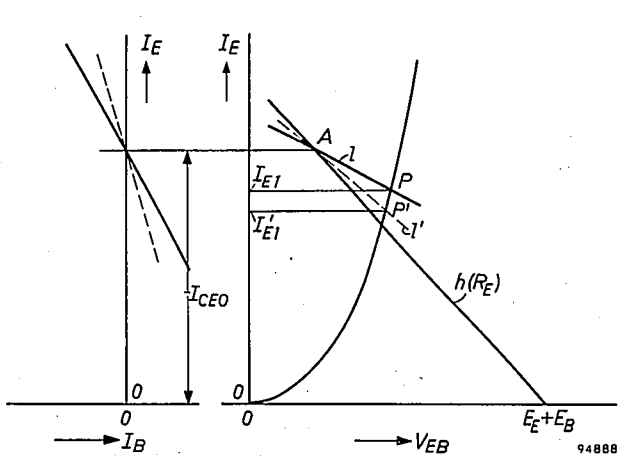

Fig. 18. Demonstration of the fact that it is possible for an increase in α_{FE} to be associated with a fall-off in I_E; this occurs when point A lies on the left of the appropriate I_E-V_{EB} characteristic. As α_{FE} increases, the I_E-I_B characteristic rotates, moving clockwise from a position such as that of the fully-drawn line to one such as that shown by the dotted line. Line l turns about A in the same sense, moving into position l'. The current decreases from I_{E1} to I_{E1}'.

In the third place, fig. 17 reveals that shifting the I_E-V_{EB} characteristic to the right also tends to keep I_E down. This suggests that, to allow for the spread in this characteristic, we ought to have used the curve furthest to the right for $t_j = 20$ °C and that furthest to the left for $t_j = 52$ °C. However, another glance at the figure will make it clear that the position of the I_E-V_{EB} characteristic has relatively little effect on the value of I_E. We may therefore conclude that our use here of the I_E-V_{EB} characteristics proper to an average transistor will not give rise to any grave error. There are, however, cases in which the position of the I_E-V_{EB} characteristics exercises a considerable influence — particularly where the transistor is a high-power type and heavier currents occur, in consequence of which the calculations arrive at much lower values for the resistors R_E and R_B.

Resistor R_2 (see fig. 15*a*) is split into resistors R_p and R_q, and the point between them is earthed for alternating current via capacitor C_1. The object is to prevent the alternating voltages that arise across the internal resistance of the supply source (a quantity that has so far been disregarded) from reaching the input side of the transistor. It will be seen from fig. 15*b* that, from the alternating current point of view, R_1 and R_q are in parallel across the input of the transistor. The value of R_q might be 13 kΩ, say; the resistance of R_1 and R_q combined would then be 5.7 kΩ. The OC 71 has an input resistance of approximately 1 kΩ. In such a case, where no large currents are involved it is preferable to have the OC 71 driven by a current [11]) rather than a voltage signal, in order to keep down distortion; it is therefore desirable that the resistance across its input should be rather higher than 5.7 kΩ; the combined value might be 10 kΩ, for example. This would mean using larger denominations for resistors R_1 and R_2. This we may do, provided there is no objection to I_{E_2} rising above 4 mA. Alternatively, one might try a different transformer ratio, such that Q_1 changes its position. We shall not go beyond this point. Our only reason for mentioning the complications is to show that it is often only after a certain amount of repeated recalculation that an acceptable compromise is arrived at and that all the requirements, which are often conflicting, are to some extent reconciled.

Use of a temperature-dependent resistor

Sometimes the element employed for R_1 is a resistor whose value decreases as its temperature rises — a thermistor [12]) for example, or a germanium diode. The result of so doing is that E_B and R_B fall off with rising temperatures and the stabilization of I_E may be improved in consequence. Given R_2 one can calculate, for each value of t_j, what values R_1 must have in order that the transistor current shall keep to the prescribed value. In order to do this, the corresponding values of V_{EB} and I_B are determined from the characteristics for the junction temperatures t_j in question. Formulae (3), (6) and (7) supply three equations involving the three unknowns E_B, R_B and R_1. In this manner R_1 is determined as a function of t_j. Since I_E is now constant, V_C and P_C are constant too; therefore the difference between the transistor temperature and that of its surroundings is constant and, if K is given, this difference is known. If we assume that the temperature of resistor R_1 is always the same as the ambient temperature, we can say how R_1 should vary as function of the ambient temperature in order that I_E shall remain constant. A resistor or combination of resistors can now be sought which, exhibiting the desired type of dependence on temperature with reasonable precision [13]), can satisfactorily be employed for R_1. Once such a resistor or combination of resistors has been found, there will no longer be any need for the design to take account of the most unfavourable combination of temperature changes and at the same time to allow for shifts of characteristics due to spread. This gives one a wider margin for dealing with other requirements that the circuit has to satisfy.

Appendix: Physical background to temperature effects in transistors

The main reason for the profound effect of temperature on the behaviour of transistors is that, in semiconductors, the equilibrium concentrations of the minority charge-carriers are rapidly changing functions of the temperature. If there is equilibrium between the processes of generation and recombination [14]), the product of the hole concentrations (p) and electron concentrations (n) in a semiconductor is given by

$$p_0 n_0 = K(T). \quad \ldots\ldots\ldots \quad (9)$$

The suffix 0 after p and n denotes that *equilibrium* concentrations are involved. $K(T)$ is an equilibrium constant such as is always involved in reversible reactions in physical chemistry. Here the reversible reaction is constituted by the generation of electrons and holes and their recombination. $K(T)$ is roughly proportional to $\exp(-V_g q/kT)$, where V_g represents the gap in eV between the valence and the conduction bands. Accordingly, qV_g is the energy required to liberate an electron, a hole being generated at the same time. Now, in an N region in a semiconductor, the electron concentration is virtually equal to the excess of donors over acceptors. The n_0 of such a region is therefore independent of temperature. In accordance with (9), therefore, p_0 must increase in proportion with $K(T)$, and hence in proportion with $\exp(-V_g q/kT)$. Conversely, in a P region it is n_0 that is proportional to $\exp(-V_g q/kT)$.

In order to make clear the influence that the equilibrium concentrations have on the properties of a transistor, we shall make recourse to the simple theory of the transistor dealt with

[11]) See for example I, page 20, left column.

[12]) E. J. W. Verwey, P. W. Haaijman and F. C. Romeijn, Semiconductors with large negative temperature coefficient of resistance, Philips tech. Rev. **9**, 239-248, 1947/48.

[13]) A practical example may be found in C. Huber and J. Rodrigues de Miranda, A transistor pre-amplifier for the magnetodynamic pick-up, Philips tech. Rev. **18**, 238-242, 1956/57.

[14]) See for example J. C. van Vessem, The theory and construction of germanium diodes, Philips tech. Rev. **16**, 213-224, 1954/55, especially pp. 214 and 215.

in an earlier article in this periodical [15]). *Fig. 19* shows how the concentrations of minority charge-carriers are distributed inside a *P-N-P* transistor. In the junction planes *3* and *4* these minority concentrations are kept at zero by a potential difference of a few volts, applied in the reverse direction across the *P-N* junction between collector and base. Across the *P-N* junction between emitter and base a small voltage $V_{EB'}$ (approx. 0.1 V) is applied in the forward direction, and this keeps the minority concentrations in cross-sections *1* and *2* at values of $n_E(1)$ and $p_B(2)$, which are given by

$$n_E(1) = n_{E0} \exp(qV_{EB'}/kT), \quad . \quad . \quad . \quad . \quad (10a)$$

$$p_B(2) = p_{B0} \exp(qV_{EB'}/kT). \quad . \quad . \quad . \quad . \quad (10b)$$

n_{E0} and p_{B0} are the equilibrium concentrations of the minority charge-carriers in emitter and base respectively. Here the potential difference between emitter and base is allotted the symbol $V_{EB'}$. The prime sign indicates that the symbol refers to the voltage between the junction planes *1* and *2*; this voltage is not the same as the voltage V_{EB} between the emitter and base *electrodes* because the base current, in passing through the transistor crystal, has to overcome what is termed the internal base resistance $R_{BB'}$ [16]).

The gradient of the hole concentration in the base, and hence also the diffusion current of these holes, is proportional to $p_B(2)$. According to the simple theory as put forward in the article already referred to [15]), this diffusion current represents almost the whole of the transistor current I_E [17]). Now V_g is approximately 0.75 V for germanium, and hence p_{B0} is proportional to $\exp(-0.75\ q/kT)$. This in combination with (*10b*) gives us the following expression for the transistor current

$$I_E = C \exp[(-0.75 + V_{EB'})q/kT]. \quad . \quad . \quad . \quad (11)$$

C is a constant [18]) that evidently represents the current that would flow at a $V_{EB'}$ of 0.75 V if the simple theory continued to hold good with such large differences of potential across the junction [19]). Equation (11) shows that the I_E-$V_{EB'}$ characteristics having T as the running parameter are a family of exponential curves, all of which pass through point $I_E = C$, $V_{EB'} = 0.75$ V. If I_E is plotted logarithmically these characteristics become straight lines passing through the said point (*fig. 20*).

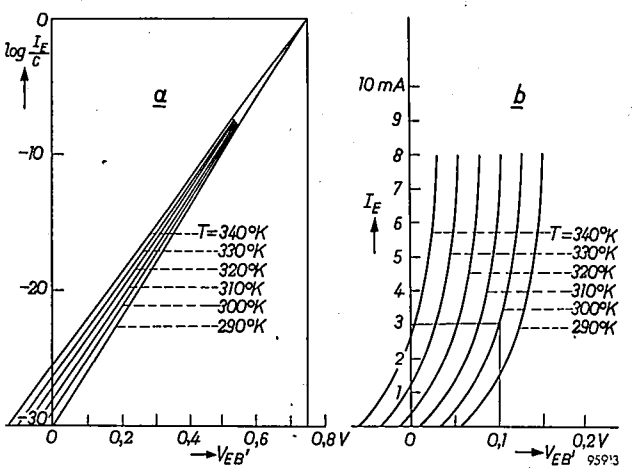

Fig. 20. Theoretical I_E-$V_{EB'}$ characteristics for a germanium transistor, with temperature as parameter. They are exponential in form (*b*) and they all meet at a point at which $V_{EB'} = 0.75$ V. This may be seen in graph (*a*), in which I_E is plotted logarithmically.

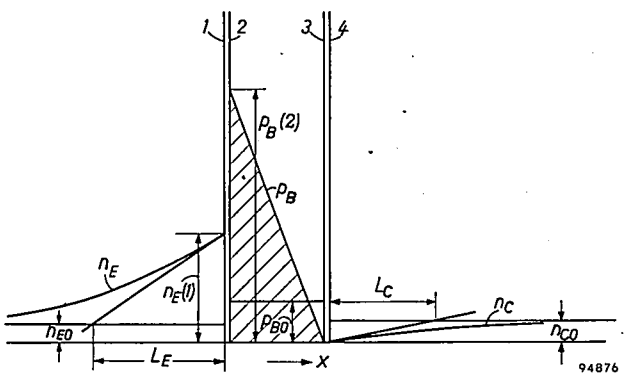

Fig. 19. Concentrations of minority charge-carriers as a function of position inside a *P-N-P* transistor; n_E are electrons in the emitter, n_C are electrons in the collector and p_B are holes in the base. The *equilibrium* concentrations of the minority charge-carriers in emitter, base and collector are n_{E0}, p_{B0} and n_{C0} respectively. The concentration gradients of the electrons in cross-sections *1* and *4* are $(n_E(1)-n_{E0})/L_E$ and n_{C0}/L_C respectively, L_E and L_C being the diffusion lengths in emitter and collector.

Equation (11) can be rewritten in the form:

$$V_{EB'} = -\left(\frac{k}{q} \ln \frac{C}{I_E}\right) T + 0.75. \quad . \quad . \quad . \quad . \quad (12)$$

It will be seen from this that if the current I_E is maintained at a constant value (say I_{E_1}) when T changes, $V_{EB'}$ will decrease by a constant amount of $(k/q) \ln (C/I_{E_1})$ per degree rise of temperature. If therefore a family of I_E-$V_{EB'}$ characteristics is drawn for a set of T values with the same interval (say 10 °K) between them, the curves will intersect a horizontal line $I_E = I_{E_1}$ at equal intervals of 10 $(k/q) \ln (C/I_{E_1})$. The value of $(k/q) \ln (C/I_{E_1})$ for a given I_{E_1} cannot be calculated directly, since C is unknown. However, if I_{E_1} is adjusted to a value such that $V_{EB'}$ is approximately 0.1 V at room temperature ($T \approx 300$ °K), then it follows from (12) that $(k/q) \ln (C/I_{E_1}) = (0.75 - 0.1)/300 = 2.2 \times 10^{-3}$ V/°C. Thus we may conclude that the I_E-$V_{EB'}$ characteristic moves about 2.2 mV to the left for every °C rise in temperature. This is the first of the two rules given on page 128.

A complication arises on account of the internal base resistance $R_{BB'}$, which we have already had occasion to refer to in this appendix. The effect of $R_{BB'}$ is to make the I_E-V_{EB} characteristics rise less steeply than pure exponential functions; nevertheless their displacement per °C temperature rise remains the same. If the I_E-V_{EB} characteristic is only available for one temperature — a case that often arises in practice — good approximations to the true characteristics for other temperatures can be obtained by assuming that the entire curve moves to the left at the rate of about 2.2 mV/°C. With heavier operating-point currents, such as those in high-power transistors under Class *A* operation, the curve may move a good deal less, e.g. 2 mV/°C at $I_E \approx 0.5$ A and only 1 mV/°C at $I_E \approx 1$ A. Fig. 20*a* shows that this effect might have been anticipated on theoretical grounds. However, there are other effects, not discussed here, which also play a part.

15) F. H. Stieltjes and L. J. Tummers, Simple theory of the junction transistor, Philips tech. Rev. **17**, 233-246, 1955/56.

16) See II, page 103.

17) In actual fact, as the transistor current increases, the portion for which the electric field is responsible starts to become significant; see for example F. H. Stieltjes and L. J. Tummers, Behaviour of the transistor at high current densities, Philips tech. Rev. **18**, 61-68, 1956/57, especially pp. 64 and 65.

18) C also exhibits some dependence on temperature, one reason being that the diffusion constant of the holes is temperature-dependent to some extent. However, so long as $V_{EB'}$ and T have practical values, this dependence is drowned by the effect T exercises on I_E via the exponential function.

19) The failure of the theory in these circumstances is discussed in the article cited in footnote 17).

In order to sketch in the background to the behaviour of the I_E-I_B characteristic, we may draw up a balance sheet for the electrons in the base region; the number entering it must be equal to the number leaving it plus the excess electrons undergoing recombination (i.e. the number of free electrons that are lost each second owing to recombination with holes in the base, minus the number gained in consequence of generation).

We shall make use of fig. 19 in drawing up our balance sheet. Electrons arrive in the base from the collector, the number thus gained each second being proportional to the concentration gradient in cross-section *4*. In its turn, this gradient is proportional to n_{C_0}, and hence to $\exp(-V_g q/kT)$. This, then, is the quantity to which the rate of arrival from the collector is proportional. The base current I_B is responsible for electron removal at the rate of I_B/q electrons per sec. Electrons are also transferred to the emitter, the number removed each second being proportional to the concentration gradient in cross-section *1*. In its turn, this gradient is proportional to $n_E(1)-n_{E_0}$ and hence — in accordance with (10*a*) — to $n_{E_0}[\exp(qV_{EB'}/kT)-1]$. It is generally permissible to neglect the term -1 in the square brackets. Since n_{E_0} is proportional to $\exp(-V_g q/kT)$, we see that the rate at which electrons are transferred to the emitter is proportional to $\exp[(-V_g + V_{EB'})q/kT]$. The final item in our account is the loss due to excess recombination over generation. This is proportional to the area of the hatched triangle of fig. 19 [20]) and hence to $p_B(2)$. But $p_B(2)$, like $n_E(1)$, is proportional to $\exp[(-V_g + V_{EB'})q/kT]$, and hence the loss due to excess recombination is also proportional to this expression. We now have the following for the rates at which electrons are gained and lost by the base:

Gain from collector	$\propto \exp(-V_g q/kT)$	electrons/sec,
Loss via I_B	$= I_B/q$	„ „ ,
Loss to emitter	$\propto \exp[(-V_g+V_{EB'})q/kT]$	„ „ ,
Recombination excess	$\propto \exp[(-V_g+V_{EB'})q/kT]$	„ „ .

This balance sheet of electron gain and loss gives us the following equation, in which the a's are constants of proportionality:

$$a_1\exp(-V_g/kT)-(1/q)I_B-(a_2+a_3)\exp[(-V_g+V_{EB'})q/kT] = 0. \quad (13)$$

By eliminating $\exp(-V_g + V_{EB'})q/kT$ from (11) and (13) and solving for I_E, we find that

$$I_E = \frac{-C}{q(a_2+a_3)} I_B + \frac{Ca_1}{a_2+a_3}\exp(-V_g q/kT). \quad (14)$$

This expression indicates that the I_E-I_B characteristic is a straight line that intersects the I_E axis at a value of I_E that is proportional to $\exp(-V_g q/kT)$. By differentiating with respect to T, we find that the intercept (which represents $-I_{CE_0}$, cf. formula (2)) lengthens by $100\ V_g q/kT^2$ per cent per degree of temperature. Since $V_g = 0.75$ V, $q = 1.6\times10^{-19}$ coulomb and $k = 1.38\times10^{-23}$ J per degree, the increase, in the region of room temperature ($T \approx 300$ °K), is about 10% per °C, i.e. the intercept doubles with every 7 °C. This is the second of the rules given on page 128.

Finally, let us compare I_E as function of T in the two cases of base current supply and voltage supply between base and emitter (see page 126 and fig. 10). By differentiating (14) and (11) with respect to T, we obtain the slopes of the curves for I_B = constant and $V_{EB'}$ = constant, respectively:

$$\left(\frac{\partial I_E}{\partial T}\right)_{I_B} = \frac{0.75\,q}{kT^2}(-I_{CE_0}),$$

$$\left(\frac{\partial I_E}{\partial T}\right)_{V_{EB'}} = \frac{(0.75-V_{EB'})}{kT^2} I_E.$$

If we start from a point in the I_E-t_j plane at which $I_B = 0$, I_E is equal to $-I_{CE_0}$ and, since $V_{EB'} \ll 0.75$, the slopes of the curves for I_B = constant and for $V_{EB'}$ = constant are about the same. Hence they more or less coincide. If however we start from a point at which $I_E \gg -I_{CE_0}$, then

$$\left(\frac{\partial I_E}{\partial T}\right)_{V_{EB'}} \gg \left(\frac{\partial I_E}{\partial T}\right)_{I_B},$$

i.e. the curve for $V_{EB'}$ = constant rises much more steeply. In these circumstances, therefore, a base current supply is better than a voltage supply between base and emitter.

Instead of germanium, silicon is sometimes used for making transistors. V_g for silicon is higher than for germanium, being about 1.1 V instead of 0.75 V. In silicon, therefore, the effect of temperature on the equilibrium concentrations of the minority charge-carriers is even greater than it is in germanium. The I_E-V_{EB} characteristics of silicon transistors do in fact shift further per °C than those of germanium transistors. A calculation shows that, if $V_{EB'} = 0.1$ V, the displacement of the silicon transistor characteristic at room temperature will be $(1.1-0.1)/300 = 0.0033$ V/°C = 3.3 mV/°C. The percentage rise in $-I_{CE_0}$ is also higher, being about 14.5% as against 10% per °C. Nevertheless, displacement of the I_E-I_B characteristics is more troublesome with germanium than with silicon transistors, because the value of $-I_{CE_0}$ at room temperature is much smaller for the latter than for the former.

Summary. The biasing arrangements of a transistor, i.e. the network which determines the D.C. operating point, have a considerable bearing on the way I_E, the transistor current (which may be taken to mean the emitter or the collector current, as preferred), reacts to changes in temperature or to replacement of the transistor. The transistor current is sensitive to such changes on account of (1) displacement of the I_E-V_{EB} characteristic (V_{EB} being the potential difference between emitter and base) and (2) displacement of the I_E-I_B characteristic (I_B being the base current). These characteristics undergo displacement both when the temperature changes and when the existing transistor is replaced by another. With tubes, there is only one characteristic to be dealt with, namely the I_a-V_g characteristic, and since this is not affected by temperature changes, the situation is a good deal less complicated than that arising with transistors. Points of similarity and difference between transistors and tubes are noted throughout the article.

In a circuit biased by a *voltage* source between base and emitter, I_E is insensitive to displacement of the I_E-I_B characteristic but, on the other hand, highly sensitive to displacement of the I_E-V_{EB} characteristic. This is explained with the help of graphs. One can lessen the susceptibility of I_E to these changes by inserting a resistor R_E in the emitter lead or, alternatively, by inserting a resistor R_B in the base lead. However, the latter method renders I_E sensitive to displacement of the I_E-I_B characteristic. Raising the value of R_b to infinity (which results in base *current* biasing) renders I_E insensitive to displacement of the I_E-V_{EB} characteristic, but very sensitive to displacement of the I_E-I_B characteristic. Normally a combination of resistors R_E and R_B is employed.

In consequence of their sensitivity to temperature changes, the thermal equilibrium of transistors with their surroundings is of importance. The question of thermal equilibrium is investigated graphically. It is explained how a slight rise in ambient temperature can result in a large increase in transistor temperature (temperature "run-away"). A graphical method for analysing the behaviour of a given transistor in a given circuit is then discussed. The converse problem is also dealt with — the dimensioning (with the aid of graphs) of a circuit for a given transistor so as to satisfy certain requirements regarding thermal stability. The procedure is illustrated by the working out of an example; the circuit in question has in addition to allow for spread in the properties of different individuals of the same transistor type. Finally, the authors indicate how the sensitivity of I_E to temperature changes can be very largely compensated by including a resistor with a negative temperature coefficient in the circuit.

The physical background of the effect of temperature on transistor behaviour is treated in an appendix.

[20]) See the article cited in footnote [15]), page 240.

RADIO INTERFERENCE FROM FLUORESCENT LAMPS

by H. J. J. van BOORT, M. KLERK and A. A. KRUITHOF.

621.396.82:621.327.534.15

Radio reception, particularly of weak stations in the medium-wave band, is sometimes subject to interference from high-frequency oscillations generated in fluorescent lamps and entering the receiver via the mains. Quantitative information on this irregular phenomenon is obtained with a standard test arrangement, the results being analysed statistically. The authors describe an investigation on this basis into the strength of the interference penetrating into the mains with various types of lamps and ballasts. They indicate what they believe to be the cause of the interference and discuss some methods of reducing its penetration into the mains.

Capricious occurrence of the interference

It has been found that some fluorescent lighting installations interfere with radio reception. The interference is strikingly unpredictable in its occurrence, it being almost impossible to say beforehand whether it will arise with a given installation or not [1]). As a rule the radio interference caused by the lamps constitutes a nuisance only at frequencies below about 1500 kc/s. It is hardly ever troublesome on the short-wave bands and quite inappreciable in frequency-modulation and television reception.

In this article we shall be concerned only with the long and medium waves, which are the most important regions affected by this form of interference. We shall investigate the reason for the irregular nature of the phenomenon and show how this irregularity can be largely eliminated for the purpose of measurements. Some quantitative and qualitative data on the origin of the interference will be given and methods indicated for reducing it.

The two causes of the irregularity

The irregular nature of the radio interference generated by fluorescent lamps has two entirely distinct causes. Firstly the oscillations produced in the lamp can fluctuate considerably in strength, and secondly the oscillations can be transmitted to the receiver in different ways, resulting in substantial variations in the coupling between the lamp and the receiver. We shall first consider the coupling between lamp and receiver and then describe a standardized method of measurement which, by eliminating the variation in coupling, gives a direct impression of the variations in the strength of the oscillations generated in the lamp.

Transmission of oscillations to the receiver

An article dealing at some length with the ways in which interference can enter a radio receiver was published in this journal as long ago as 1938 [2]). A brief recapitulation is given below of the contents of that article insofar as they are relevant to the present considerations.

The high-frequency oscillations produced in a fluorescent lamp can be transmitted along two different paths to a radio receiver: *a*) directly from the lamp to the aerial, and *b*) via the electric mains. The interference reaching the receiver by the direct path is noticeable only when the distance between the effective part of the aerial and the lamp is less than 2 to 3 metres. Since it should normally be possible when installing the receiver to make this distance larger (e.g. by using a screened lead-in cable) the direct lamp-to-aerial transmission of oscillations is left out of account in the standardized method of measurement. The transmission of interference via the mains involves capacitances which are generally disregarded in the more usual considerations of an electric-light mains, but which are by no means negligible where high-frequency oscillations are concerned. To illustrate the manner in which such oscillations are propagated from the lamp to the receiver via the electric-light mains, *fig. 1* shows schematically the principal paths through which high-frequency currents can flow [3]). In this diagram p and q represent the two mains conductors, and C_N, C_{N1} and C_{N2} the capacitances between these conductors mutually and with respect to earth. The fluorescent lamp L has a capacitance C_L with respect to earth. The capacitance of the coil of the ballast choke S is represented by C_S. The usual

[1]) A not inconsiderable proportion of the interference experienced is due to unreliable contacts in the electrical installation. Such interference is easy to remedy and is not dealt with in this article.

[2]) L. Blok, Radio interference, Philips tech. Rev. 3, 235-240, 1938.

[3]) See also H. J. J. van Boort and M. Klerk, High-frequency oscillations in low-pressure mercury arcs, Appl. sci. Res. **B5**, 69-74, 1955.

suppressor capacitor C_0 is shunted across the glow-discharge starter G.

The part of the figure bounded by a broken line represents a small part of the receiver circuit. Of the power transformer only the primary and the filament-current windings are shown. The latter is coupled to the mains conductors via the capacitances C_{T1} and C_{T2} between the windings. The aerial A has capacitances C_A, C_{A1} and C_{A2} with respect to earth and to the mains conductors.

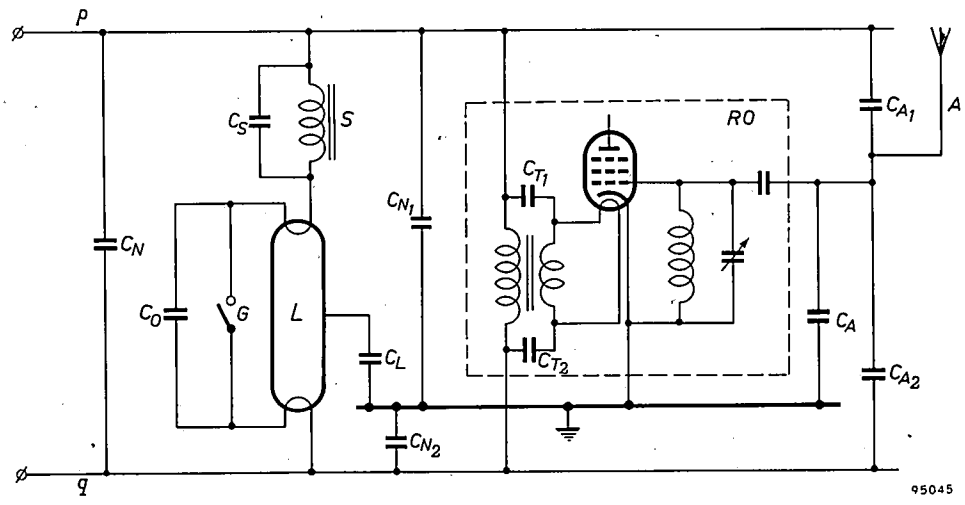

Fig. 1. Diagram of the principal circuit paths along which high-frequency electrical oscillations from a fluorescent lamp can enter a radio set via the mains conductors p and q. L lamp, G starter, C_0 suppressor capacitor, C_L capacitance between lamp and earth, S ballast choke, C_S self-capacitance of choke, C_N capacitance between mains conductors, C_{N1} and C_{N2} capacitances between mains conductors and earth, A aerial, C_A capacitance between aerial and earth, C_{A1} and C_{A2} capacitances between mains conductors and aerial, RO input stage of radio receiver, C_{T1} and C_{T2} capacitances via which the filament-current winding of the power transformer is coupled to the two mains conductors.

It can be seen from this diagram that high-frequency oscillations can penetrate from the mains into the receiver in two ways, namely via the aerial and via the capacitances of the power transformer. In most practical cases the interference entering through the aerial is predominant.

When two voltages V_p and V_q of a given frequency are present on the mains conductors p and q, and these voltages differ both in amplitude and phase, each voltage can be resolved into two components, viz.

1) a component $+\frac{1}{2}V_1$ (for V_p) or $-\frac{1}{2}V_1$ (for V_q) consisting of voltages of equal amplitudes and opposite phase between the conductors and earth; V_1 is called the *symmetrical* component;

2) a component V_2, consisting of voltages of equal amplitudes and the same phase between the conductors and earth, called the *asymmetrical* component.

This is illustrated by vector diagrams in *fig. 2*.

In the following we shall consider the symmetrical and asymmetrical components of the interfering voltage separately.

Fig. 3 shows schematically the capacitances from fig. 1 over which the high-frequency oscillations from the lamp can reach the aerial. The symmetrical and asymmetrical components of the high-frequency voltages on the lamp electrodes are denoted by V_1* and V_2*. They produce on the mains conductors p and q the symmetrical and asymmetrical voltages

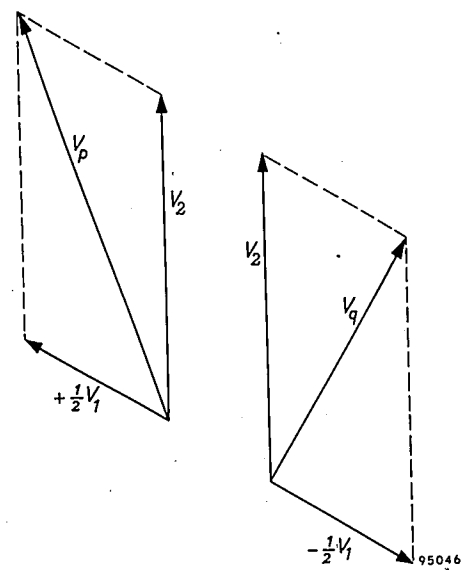

Fig. 2. The two alternating voltages, V_p and V_q, between the mains conductors and earth, resolved into a symmetrical component V_1 and an asymmetrical component V_2.

V_1 and V_2 respectively. Since the circuit, generally speaking, is not symmetrical with respect to earth, V_1 is not exclusively caused by V_1^*, nor V_2 by V_2^*, but V_1 and V_2 are both influenced by V_1^* *and* V_2^*. In most cases, however, V_1^* is the main origin of V_1, and V_2^* of V_2.

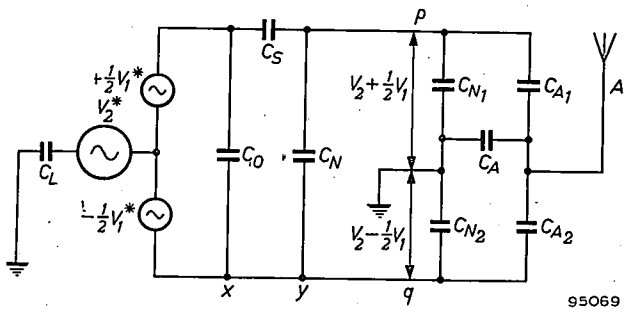

Fig. 3. Schematic representation of the circuit elements via which high-frequency oscillations from a fluorescent lamp can be propagated to the aerial. V_1^* and V_2^* represent the symmetrical and the asymmetrical components of the high-frequency voltages at the lamp electrodes. V_1 and V_2 are the corresponding high-frequency voltages on the mains conductors. The other letters have the same meaning as in fig. 1.

From fig. 3 we see that the symmetrical voltage component V_1 acts on a bridge circuit consisting of the capacitances C_{N1}, C_{N2}, C_{A1} and C_{A2}. If the bridge is balanced, i.e. if the condition $C_{A1}C_{N2} = C_{A2}C_{N1}$ is satisfied, the voltage V_1 will not cause any voltage to appear between the aerial and earth terminals. Although this condition is never exactly fulfilled, it is probable nevertheless that it has the effect of greatly reducing the influence of the symmetrical component of the interference voltage.

The current produced by V_2^* flows through C_L to earth and returns to the lamp along two principal paths, viz. via C_{N2} and via the series arrangement of C_{N1} and C_S. It is obvious that, as regards the asymmetrical component V_2, it is not possible to achieve any marked reduction of the interfering voltage on the aerial terminals by balancing the bridge circuit on the right of fig. 3.

Concerning the penetration of interference into the receiver through the power transformer, it should be noted that several receiver elements are capacitively coupled to the two mains-conductors via the transformer. (In fig. 1 this is indicated for the filament winding by the capacitances C_{T1} and C_{T2}. Analagous capacitances are, of course, present in other windings of the transformer.) Consequently it is possible that here, too, the symmetrical component of the interfering voltage will not, or only very weakly, enter the receiver; for the asymmetrical component, there is again little chance of balancing out the interference voltages.

In practice all the capacitances in figs. 1 and 3 can have very divergent values, which means that the strength of the coupling between lamp and aerial is subject to considerable variation.

Measurement of the interference voltage

The Commission Internationale Spéciale des Perturbations Radiophoniques (C.I.S.P.R.) has standardized a method of measuring the symmetrical and asymmetrical voltage components introduced into the mains conductors by a source of interference. The circuit used is as shown in *fig. 4*. The interference source (in our case the fluorescent lamp) connected to terminals L is fed from the mains network N via chokes S_1 and S_2. The interference current flows from L through the capacitors C_1 and C_2 and through the parallel branches of resistors. The values of the resistors are such that, for not too low frequencies, the impedance between the two mains conductors, and the impedance of both together with respect to earth, amount to 150 ohms.

The symmetrical component of the interference voltage is measured between terminals A_1 and A_2, and the asymmetrical component between B_1 and B_2. The measurements are performed with a standard test receiver of the super-heterodyne type. The input side, which is electrically symmetrical with respect to earth, contains an attenuator composed of resistors. The bandwidth of the intermediate-frequency section of the receiver is 10 kc/s. The output signal of the I.F. section is measured with a voltmeter, the response of which is made to simulate approximately the sensitivity of the human ear to crackling and hissing noises. [4])

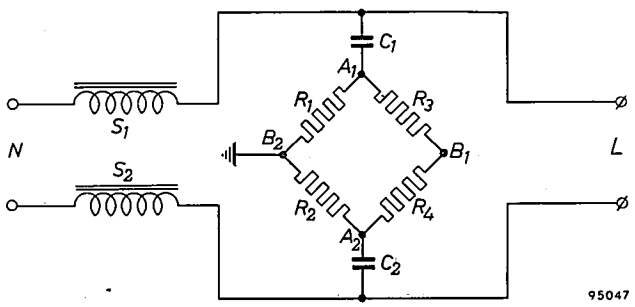

Fig. 4. Diagram of the circuit standardized by the C.I.S.P.R. for measuring the high-frequency oscillations transmitted by an interference source to the mains conductors. N mains, L interference source (fluorescent lamp with ballast), S_1 and S_2 isolating chokes, C_1 and C_2 coupling capacitors, capacitance 0.1 μF, R_1 and R_2 resistors of 300 Ω, R_3 and R_4 resistors of 100 Ω. The symmetrical component is measured between points A_1 and A_2, the asymmetrical between B_1 and B_2 (earth).

[4]) This meter can be regarded as a peak voltmeter, but one which does not record voltage surges of very short duration or very small repetition frequency. This is achieved by a suitable choice of the capacitors and resistors and of the inertia of the meter.

With this set-up, then, it is possible to measure the two components of the interference voltage produced in the mains conductors by any interference source. Since in this arrangement the coupling between the interference source and the test receiver is fixed, the variation occurring in practice in the coupling between source and receiver is eliminated. The results of the measurements therefore provide information only on the voltage produced by an interference source, and do not directly reveal the nuisance it causes in a particular case. If measurements on diverse lamps disclose differences in the strength of the interference, these differences must stem from the lamps themselves.

Results of measurements on "TL" 40 W lamps

The most comprehensive interference measurements have been made on 40 W tubular ("TL") fluorescent lamps. The ballast consisted of a choke which, for the purposes of the following, we shall refer to as type I. The suppressor capacitor used (C_0 in fig. 1) had a capacitance of 0.01 μF. We shall first discuss the results of these tests; later on we shall indicate in how far the interference level differs from the values given here when other types of ballasts and lamps are used.

Altogether more than 800 "TL" 40 W lamps were investigated. They were obtained by daily setting aside, during a period of six months, a few lamps from normal production runs [5]). Before measurement the lamps were given two burn-in periods, each of 24 hours. Since the discharge sets in only at that end of each coiled filament electrode which is nearest to the mains, the lamps were reversed during the burning-in process so that the arc burnt equally long on both ends of the electrodes.

The measurements of the interference voltages were carried out at seven frequencies, viz. two in the long waveband, three in the medium wavebands and two in the transitional range in between. The frequencies are specified in *Table I*. No measurements were made in the short-wave bands, on which fluorescent lamps cause little or no interference.

The results of the measurements were similarly frequency-dependent in each of the three frequency ranges for all lamps; for this reason, only the mean values per frequency range are given in the Table. The results tabulated show first the mean values, S and A respectively of the symmetrical and asymmetrical components of the interference voltage, both measured in decibels with respect to 1 μV at the terminals of the test receiver. To give an impression of the variation about these mean values, the table also contains the standard deviation σ of both components [6]). Another important quantity is the level of the interference voltage which is not exceeded by "almost all" the lamps. If we take "almost all" to be 99% and if the results show a normal distribution around the mean, it can easily be shown that this quantity is equal to the larger of the two components, S, plus 2.3 σ. This value is given in column M. Conversely, there is of course a value of the symmetrical component that is exceeded by "almost all" the lamps, and that is equal to S minus 2.3 σ. In a batch of about 100 lamps we can therefore expect a spread of 4.6 σ in both components, and from the data in the Table we thus calculate the spread for each frequency range as 14, 18 and 23 dB, respectively. Furthermore, experience has shown that every lamp during its useful life can exhibit variations in its interference voltage of the same magnitude as found with a group of lamps all of the same age. The interference can both rise and fall during the life of a lamp, so that the average value in a large group remains much the same. Since there is a possibility that a lamp which initially causes little interference may later generate a great deal, one must always reckon with the maximum value M mentioned in Table I.

Table I. Mean values of the symmetrical component S and of the asymmetrical component A of the interference voltage, measured with the C.I.S.P.R. test equipment. Both components are given in decibels above 1 μV. σ is the standard deviation and $M = S + 2.3\ \sigma$.

Frequency range	Measuring frequencies	S	A	σ	M
Long waveband	160 and 240 kc/s	52	38	3.1	59
Transitional region	350 and 550 kc/s	50	40	3.8	59
Medium waveband	750, 1000 and 1400 kc/s	42	33	4.9	53

What level of interference is a nuisance?

It is evident that the nuisance experienced from a given level of interference voltages will be greater the weaker or more distant the station to which the receiver is tuned. In many countries the requirement, based on experience, is that both components of the interference voltage, measured with the C.I.S.P.R. test equipment, should be lower than 1 mV, i.e. less than 60 dB above 1 μV.

[5]) No systematic discrepancies were found between the production batches involved.

[6]) Since the ratio between the two components in each of the three frequency ranges is almost constant, this standard deviation holds for both components.

In special cases it may be desirable to specify more stringent requirements, particularly for the reception of extremely weak stations, in laboratories where highly sensitive apparatus is in use, or where the impedances of the electric light mains have very unfavourable values, such as to prevent the partial compensation, described above, of the symmetrical component of the interfering voltage.

As we have seen, the value 60 dB is only very rarely exceeded in the case of "TL" 40 W lamps with a type I choke.

In order to discover whether the interference could be further reduced by making modifications in the lamp itself or in the circuit, it was desirable to ascertain at what point in the gas discharge the origin of the interference should be sought, and in what way the interference is connected with the mechanism of the discharge.

Origin of the interference in the lamp

For the purpose of locating the exact region in a lamp where the high-frequency oscillations arise, the lamp under investigation was fed via an isolating transformer, which made it possible to earth the circuit at any point. Also used for the investigation was a semi-circular metal strip, which we shall henceforth refer to as an "aerial probe" [7]). This was fitted round the lamp and could be moved to and fro. The interference voltage picked up by this probe was passed to a C.I.S.P.R. test receiver, the I.F. signal of which was applied to the vertical deflection plates of an oscilloscope. The horizontal deflection of the oscilloscope was synchronized with the mains voltage.

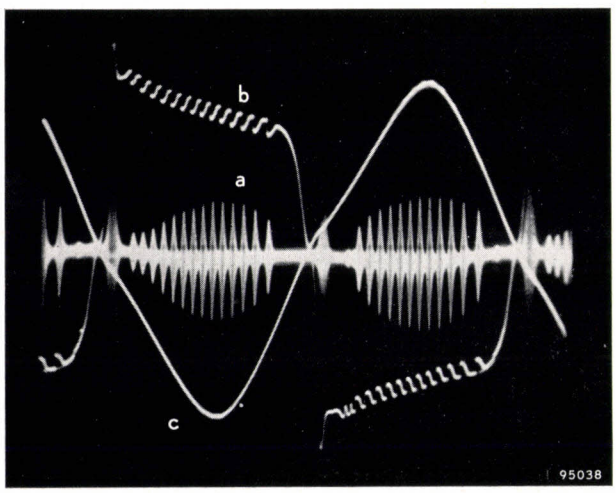

Fig. 5. Oscillograms of the interference voltage (a), the lamp voltage (b) and the current (c). The lamp circuit was not earthed. The aerial probe was fitted midway along the lamp, and the C.I.S.P.R. test receiver tuned to 300 kc/s.

Fig. 5 shows the waveform (marked a) which appears on the oscilloscope screen when the lamp circuit is not earthed, the aerial probe placed midway along the lamp and the test receiver tuned to 300 kc/s. The figure also shows the voltage (b) across the lamp, and the current (c). It can be seen that the high-frequency voltage a is very strong at the beginning of each half-cycle, just when the voltage across the lamp reaches the ignition potential. We shall call this part the *ignition interference*. Thereafter the interference voltage shows a number of peaks near the middle of each half-cycle. In many cases a strongish peak appears at the end of each half cycle (not visible in fig. 5); this we shall call the *extinction interference*. Usually the extinction interference is weaker than the ignition interference.

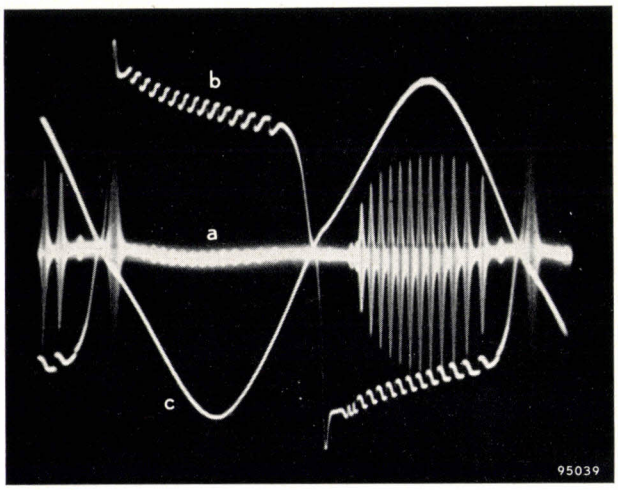

Fig. 6. As fig. 5, but now with one of the electrodes earthed and the probe placed near this electrode.

If we now earth one of the lamp electrodes and move the probe near that electrode, the waveform obtained on the oscilloscope screen is as shown in *fig. 6*. Obviously this waveform exhibits primarily that part of the oscillations which originates in the proximity of the earthed electrode, for the interference generated here gives rise to the full voltage over the small part of the discharge lying between the probe and the earthed electrode. Interference originating at the other electrode or at other positions in the lamp gives rise to only a small voltage over the same small part of the discharge.

From the absence in fig. 6, compared with fig. 5, of exactly half the oscillations, it can be concluded that the interference originates near the electrodes.

[7]) This investigation was begun round about 1942 by C. J. D. M. Verhagen, now professor of applied physics at Delft. See also the article quoted under [3]).

If we examine the polarity of the lamp we find that ignition and extinction oscillations are generated during the half-cycle in which the electrode concerned is the cathode. We shall therefore designate both as *cathode interference*. The oscillations in the middle of the half cycle arise when the electrode concerned is the anode, and these we shall refer to as *anode interference* [8]).

The fact that both kinds of interference originate near the electrodes can be confirmed by other experiments. If the electrode where the aerial probe is positioned be heated by an additional current, the waveform of the cathode interference is found to be affected. A magnet brought close to the same electrode affects the waveform of the anode interference. The same experiments when carried out at the other end of the lamp produce no change in the oscillogram.

Tests with a movable probe mounted *inside* the lamp close to an electrode, demonstrated that the source of the cathode interference must be located at no more than a few millimetres away from that turn (or the two turns) of the coiled electrode where the discharge takes hold.

Further investigation showed that the cathode interference is chiefly made up of components with frequencies higher than about 350 kc/s, while the anode interference contains mainly components with frequencies lower than 250 kc/s. This is the reason that it was possible, for the statistical analysis of the results, to divide the entire frequency range into three parts according to the behaviour of the lamps. In the medium waveband the cathode interference predominates, in the long wavebands the anode interference, while in the transitional region now the one and now the other predominates.

Closer investigation of the cathode interference

The cathode interference, in view of its predominance in the important medium waveband, was subjected to a closer investigation, involving both the electrical and the optical phenomena occurring in a lamp.

In order to study the *electrical* phenomena the output signal of the I.F. section of a C.I.S.P.R. test receiver was again applied to the vertical deflection plates of an oscilloscope. For the horizontal deflection, use was now made of an extended time-base, enabling a small part of each cycle to be displayed over the whole breadth of the screen.

The *optical* phenomena can only be observed in lamps whose envelopes have not been provided with a fluorescent layer, for this layer scatters the light of the discharge to such an extent that the spatial distribution of the latter cannot be observed. Moreover, the inertia of the fluorescence phenomenon makes it impossible to observe rapid changes.

Two methods were adopted for studying the optical phenomena in a discharge lamp. In the first a photo-multiplier tube was mounted close to one of the electrodes and its output voltage applied to an oscilloscope. In the second the area around an electrode was observed through a narrow slit in a disc which was made to revolve synchronously with the mains frequency (*fig.* 7) [9]). It was possible

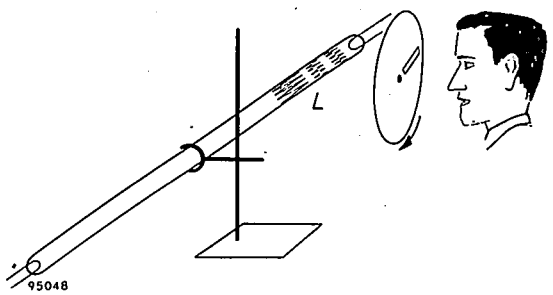

Fig. 7. Observation of the lamp L through a revolving disc T. Since the disc revolves in synchronism with the mains frequency, the observer views the discharge for a short instant of fixed phase during each cycle.

to vary the instant of the cycle at which the discharge was observed. In this way the observer was able to examine the discharge near an electrode for a very short time during each cycle. Owing to the inertia of the eye, however, no variations taking place *during* the instant of observation were perceptible. The photo-multiplier tube, on the other hand, has an almost instantaneous response to the total luminous flux emitted near the electrode under examination, and therefore provides a more detailed picture of the luminous intensity as a function of time.

Fig. 8 shows two oscillograms obtained with the aid of the aerial probe, the C.I.S.P.R. test receiver and the extended time-base. The middle waveform represents the ignition interference, the top and bottom waveforms the lamp voltage and current, respectively. Making allowance for a slight phase-shift in the equipment, one can conclude from these oscillograms that the ignition interference occurs at the moment when the voltage, after having passed

[8]) Similar interference was found by H. L. Steele, Illum. Engng. **49**, 349, 1954, and by C. Matsuda, Y. Otami and R. Itadani, Mem. Fac. Engng. Kyoto **19**, 25-49, 1957.

[9]) See also: J. W. Culp, Noise in gaseous discharge lamps, Illum. Engng. **47**, 37-46, 1952.

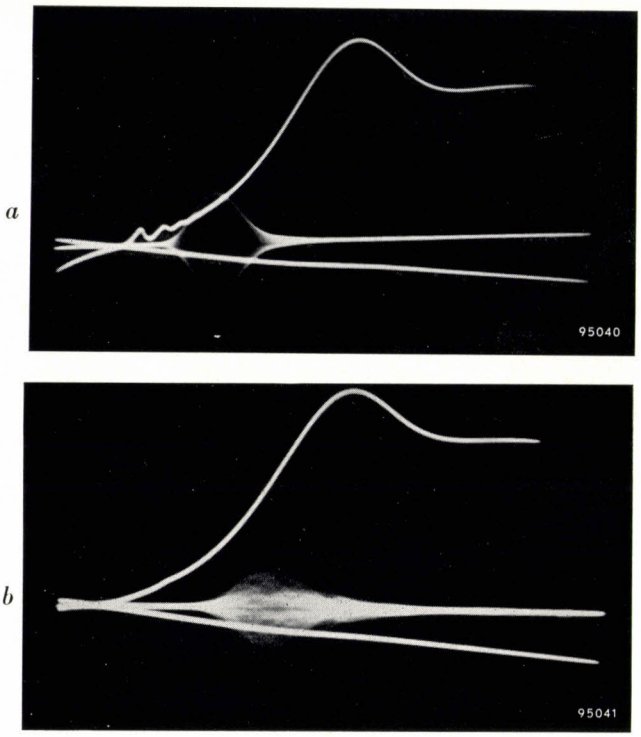

Fig. 8. Oscillograms of the ignition interference, recorded with the aid of an extended time-base. Upper waveform: lamp voltage. Middle waveform: interference voltage picked up in the test receiver via the aerial probe. A small phase shift occurs in the apparatus, so that the middle curve should be thought of as shifted about 4 mm to the left. Lower waveform: current. In *a* the interference consists of regular oscillations (stationary waveform envelope), in *b* of irregular oscillations.

through zero, again rises to about 14 V. It can also be seen that this interference can occur in two ways, sometimes as a regular oscillation with a stationary envelope, which also manifests itself in the voltage waveform, as in fig. 8*a*, but usually as an irregular oscillation (fig. 8*b*), in which case only a very faint kink is perceptible in the voltage waveform at the beginning of the oscillation. Analogous phenomena are observed in the case of extinction interference.

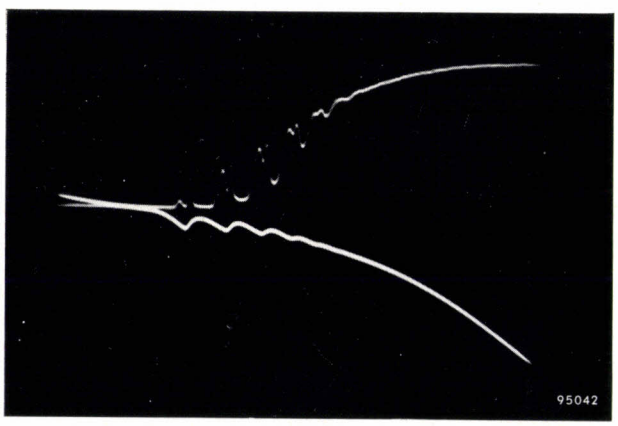

Fig. 9. Oscillograms of the ignition interference with regular oscillations, recorded on expanded time base. Upper waveform: luminous intensity, recorded with photomultiplier tube. Lower waveform: lamp voltage.

The regular oscillations are found to have a frequency of some tens of kc/s. They are non-sinusoidal, so that harmonics are encountered at higher frequencies, but in the medium waveband these harmonics are quite weak. With the photo-multiplier tube the regular oscillations can also be very clearly observed in the light of the discharge. *Fig. 9* shows an oscillogram (upper waveform) obtained in this way. As can clearly be seen, every maximum in the luminous intensity is really a double peak. In this case one observes through the revolving disc a luminosity that entirely surrounds the electrode (*fig. 10a*).

The strongest interference in the medium waveband is caused by lamps generating irregular cathode oscillations (fig. 8*b*). The frequency of these oscillations lies in the region of some hundreds of kc/s. Their amplitude is hardly affected by the external circuit. Through the revolving disc the luminosity is observed to occur at some distance from the electrode early on in the cycle (fig. 10*b*) and only later in the cycle surrounds the electrode entirely.

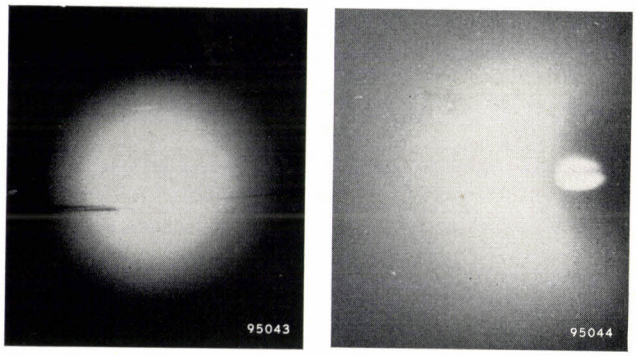

a *b*

Fig. 10. *a*) Luminosity near the cathode during ignition interference with regular oscillations. The glowing cathode is in the middle of the luminous area (but not visible owing to overexposure of the photo).
b) The same during ignition interference with irregular oscillations. The glowing cathode is visible on the right of the discharge.

The irregular oscillations can also be generated in a lamp operating on direct voltage. To achieve this, the discharge current must be smaller than the (temperature-dependent) cathode saturation current. Plainly, in an A.C. discharge this state occurs at the beginning and end of each half cycle in which the electrode concerned is the cathode, for owing to the thermal inertia of the electrodes the saturation current at the beginning and end of each cathodic half-cycle is still fairly high, in spite of the fact that heating chiefly takes place about midway through each half cycle. Since the lamp current gradually rises and falls, the state favouring

the generation of irregular oscillations will occur twice per cycle for each electrode.

The phenomena described suggest that the irregular oscillations may be regarded as oscillations of positive ions in the potential minimum which occurs in front of the cathode while the discharge current is lower than the saturation current of the cathode.

Since a high saturation current is necessarily associated with the cathode condition needed to ensure that the lamp has an adequate life, it is not likely that the level of the oscillations generated in the lamp can be appreciably lowered without impairing the desired properties of the cathode. When it is required to reduce the radio interference caused by the lamps, it is therefore necessary to find means of preventing the oscillations from entering the electric mains.

Means of suppressing the interference

It should be noted first of all that the choke in the ballast and the capacitor C_0 in fig. 1 should both be regarded as means of reducing the interference. The self-capacitance C_S of the choke constitutes the largest impedance in the principal path for the symmetrical component (see fig. 3). This is confirmed by the fact that when a capacitor is shunted across the choke the symmetrical component shows a marked increase. With a capacitor of 1250 pF the respective increases in the long-wave, transitional and medium-wave bands were found to be 16 dB, 12 dB and 5 dB. By splitting the choke into two parts, and including one of these parts in each of the leads of the lamp it is possible to reduce the symmetrical component. The reduction obtained in a specific case was 12 dB. This component can be reduced by about 20 dB, if the choke be wound according to a special system which leaves both halves with a particularly low self-capacitance.

In the circuit path for the asymmetrical component the largest impedance is usually the capacitance C_L between the lamp and earth (see fig. 3). Increasing this capacitance by earthing the fixture on which the lamp is mounted, or by earthing a metal fixture around the lamp, is found to increase the asymmetrical component by 12 and 20 dB respectively. If there is a choke in each of the two leads to the lamp, the impedances represented by the self-capacitance of these chokes also affect the asymmetrical component. (In that case a capacitor C_S is inserted in the lead between points x and y in fig. 3, so that the impedance in this branch is increased.) In this way we were able to reduce the asymmetrical component by 4 dB. With a low-capacitance system of winding the reduction amounted to 14 dB. The impedance between the lamp and the mains can be further increased by introducing low-capacitance high-frequency chokes in the two leads to the lamp. With chokes having a self-capacitance of only 15 pF it was possible to reduce the asymmetrical component by about 18 dB. Often, however, the leads from the choke to the lamp run parallel with the mains conductors, which means that the high-frequency chokes are bypassed by capacitances which can be much larger than their own self-capacitance. In such cases nothing is gained by using these chokes.

The suppressor capacitor C_0 reduces both components of the interference voltage, but just as with C_S, its effect is greater on the symmetrical component. If C_0 is removed, the symmetrical component increases by about 20 dB and the asymmetrical component by about 10 dB. Increasing C_0 from 10 000 to 20 000 pF causes a drop of 5 dB in the symmetrical and 2 dB in the asymmetrical component.

A simple method of further suppressing the interference is to use a so-called delta filter, consisting of three capacitors connected as shown in *fig. 11*.

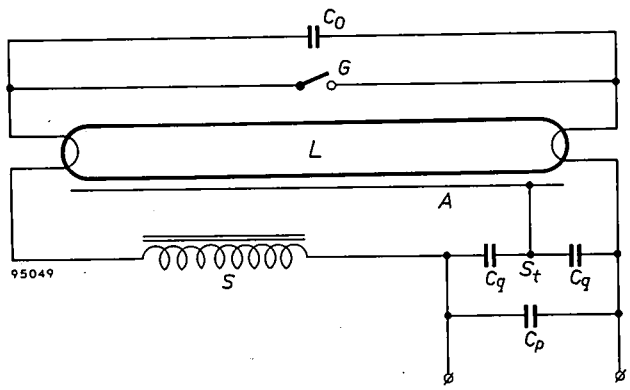

Fig. 11. Fluorescent lamp with series-connected choke and delta filter. L lamp, G glow-discharge starter, C_0 suppressor capacitor, S choke. The delta filter consists of three capacitors: $C_p = 0.2\ \mu F$ and $C_q = 2500$ pF. The star point St is connected to the fixture A. The fixture must not be earthed.

The capacitor C_p, of 0.2 μF, is connected between the two mains conductors, hence in parallel with C_N (see fig. 3). This results in a drastic drop, about 35 dB, in the symmetrical component. The remaining magnitude of this component is roughly inversely proportional to C_p [10]).

The mains conductors are connected via the two capacitors C_q to the fixture A. To eliminate the

[10]) It should be noted that the shunt capacitor which can be used to improve the power factor cos φ, also causes, like C_p, a marked drop in the symmetrical component.

possibility of receiving an electric shock from the fixture, the capacitance of each must not exceed 2500 pF. They influence almost exclusively the asymmetrical component, the more so the better the lamp is shielded by the fixture.

In *Table II* some figures are given of the reduction in the asymmetrical component brought about by the use of a delta filter. Column 1 gives the reduction in dB in the earlier-mentioned three frequency ranges when the lamp was mounted at a distance of 2 cm from a metal fixture with a breadth of 3.5 cm. The fixture was connected to the star point *St* of the filter (see fig. 11). Column 2 gives the reduction obtained after a metal cover had been fixed above the lamp.

Table II. Reduction, in dB, obtained in the asymmetrical interference component by the use of a delta filter. Column 1: "TL" lamp mounted on metal fixture. Column 2: after fixing a metal cover above the lamp, mounted on fixture.

Frequency range	1	2
Long waveband	10	22
Transitional region	6	15
Medium waveband	4	17

It appears from this table that a metal shield at one side of the lamp, combined with a delta filter, causes appreciable suppression of the interference. The same degree of suppression is achieved when, instead of a metal cover, metal louvres are fixed underneath the lamp, again connected to the starpoint *St*. An advantage of using a delta filter is that no earth lead is necessary. In many cases it is not possible to install a good earth lead, and in other cases the lead would have to be so long that it would itself act as a coupling element with the receiver aerial. If a good, short earth lead is available, it may then be beneficial to connect the starpoint of the delta filter to it, but *not* the fixture, for that would mean an increase in C_L (see fig. 3).

Other ballasts and other „TL" lamps

The investigation described in this article has been carried outover a period of some years. The choke referred to as type I, and which was used for the experiments hitherto discussed, was of a kind manufactured up to about 1951. Tests were subsequently carried out with a later version (type II, known as "Alfo" ballasts [11]), manufactured up to about 1956, in which the filler used between core, coil and casing was crinkled aluminium foil. Finally, interference measurements were also made with the latest ballasts (type III), containing a filler on a polyester-resin base [11]).

Since the question obviously arose whether the interference might perhaps enter the mains conductors to a different extent when other types of ballast were used, tests were also made on "TL" 40 W lamps with capacitative ballasts, consisting of a choke and capacitor in series. These ballasts are employed in large installations to improve the power factor.

Although far fewer tests were carried out in this investigation than in the experiments discussed in the foregoing, they were enough to provide a general picture of the level of interference arising with the diverse lamps and ballasts.

The averages of the results of these tests for the three frequency regions are given in *Table III*, together with the corresponding figures for type I, taken from Table I, for comparison.

The spread in the results for a large number of lamps is independent of the ballast, so that the values of the standard deviation σ, given in Table I, also apply to the other ballasts.

We see from Table III that in the important medium-wave bands the larger component of the interference voltage is smaller for the choke ballasts types II and III and the capacitative ballast than for the choke of type I.

Table III. Average values *S* and *A* of the symmetrical and asymmetrical components, respectively, of the interference voltage using different ballasts, viz. chokes of types I, II and III and a capacitative ballast, with a "TL" 40 W lamp. Both components are given in dB above 1 μV.

Frequency range	Type I		Type II		Type III		Cap.	
	S	*A*	*S*	*A*	*S*	*A*	*S*	*A*
Long waveband	52	38	52	38	47	43	49	35
Transitional region	50	40	44	37	40	41	45	38
Medium waveband	42	33	34	30	33	34	37	33

In many cases an inductive and a capacitative ballast are combined to form what is called a "duo-ballast". The interference from two "TL" 40 W lamps with a duo ballast is found to be no greater than that from one lamp.

If two "TL" 20 W lamps connected in series be substituted for one "TL" 40 W lamp, no change is found in the asymmetrical component, but the symmetrical component increases by about 2.5 dB; it increases by twice this amount when four 20 W lamps are substituted for the two 40 W lamps used with a duo-ballast. Longer lamps and lamps of higher current generally cause somewhat stronger

[11]) Th. Hehenkamp, Small ballasts for fluorescent lamps, Philips tech. Rev. **18**, 279-281, 1956/57.

interference, whereas shorter lamps and lamps of lower current cause somewhat less; the differences, however, are not very large.

Table IV gives the average results of tests performed on two other types of lamp, viz. "TL" M lamps with the appropriate ballast [12]) and "TL" S lamps in series with an incandescent lamp [13]).

Table IV. Mean values of the symmetrical component S and the asymmetric component A of the interference voltage from "TL" M and "TL" S lamps. Both components are expressed in dB above 1 μV.

Frequency range	"TL" M		"TL" S	
	S	A	S	A
Long waveband	42	44	80	53
Transitional region	40	42	78	55
Medium waveband	30	32	70	48

It can be seen that with the "TL" M lamps the asymmetrical component is slightly larger than the symmetrical. Both are well below the specified limit of 60 dB.

In the case of "TL" S lamps in series with an incandescent lamp, both components are much larger than with the lamps discussed in the foregoing. We see that the symmetrical component is considerably in excess of 60 dB. Two reasons can be indicated for this higher level of interference:

a) Since there is no choke in the lamp circuit, the current in "TL" S lamps is subject to more abrupt variations, causing both components at all frequencies to increase by about 8 dB above those in a circuit with a choke ballast.

b) The suppressor capacitor C_0 (see fig. 1) is not generally used with "TL" S lamps in series with an incandescent lamp. This results in an increase of 20 dB in the symmetrical and 7 dB in the asymmetrical component of the interference voltage.

In order to keep the interference from "TL" S lamps below the usual 60 dB limit it is essential to use a delta filter. This reduces the symmetrical component by 31 dB, resulting in a level somewhat lower than that of a "TL" 40 W lamp with choke and suppressor capacitor. The asymmetrical component is only slightly reduced by a delta filter when no shielding fixture is used; nevertheless this component is then just small enough to make the cases in which the 60 dB limit is exceeded a rare occurrence. If necessary the symmetrical component can be further reduced by increasing the capacitance C_p of the delta filter, and the asymmetrical component can be lowered by electrical screening by a metal fitting.

The interference from "TL" S lamps operated with a ballast containing a choke and suppressor capacitor is, of course, no greater than from a normal "TL" lamp with the same ballast (see Table III).

Summary. The radio interference from fluorescent lighting installations is a capricious phenomenon. The irregularity is due to the marked variations in the strength of the interference source and of the coupling between the lamp and the receiver. The interference enters the receiver principally via the electric-light mains and the aerial. A test arrangement standardized by the C.I.S.P.R. is used for measuring the symmetrical and asymmetrical components of the interfering voltage induced in the mains conductors by a fluorescent lamp with ballast. The usual upper limit specified for both components is 1 mV, i.e. 60 dB above 1 μV. It is found that this limit is appreciably exceeded only with "TL" S lamps when series-connected with an incandescent lamp and with no suppressor capacitor (in the absence of any special measures of suppression).

The interference source is located in the vicinity of the lamp electrodes. The strongest interfering voltage is generated near an electrode during that part of each cycle in which it functions as cathode. The cause of the interference is considered to be oscillations of positive ions in the potential minimum which occurs in front of the cathode when the discharge current is smaller than the temperature-dependent saturation current of the cathode. Means of reducing the interference penetrating into the mains conductors are: splitting the choke into two parts, using low-capacitance chokes, electric shielding of the lamp and using a three-capacitor delta filter. With the latter the interference from "TL" S lamps in series with incandescent lamps can also be kept below the permissible limit.

[12]) W. Elenbaas and Th. Hehenkamp, A new fluorescent lamp in a starterless circuit, Philips tech. Rev. **17**, 288-293, 1955/56.

[13]) W. Elenbaas and T. Holmes, An instant-starting fluorescent lamp in series with an incandescent lamp, Philips tech. Rev. **12**, 129-135, 1950/51.

VOLUME 20, 1958/59, No. 6 pp. 145-176 Published 8th December 1958

Philips Technical Review

DEALING WITH TECHNICAL PROBLEMS
RELATING TO THE PRODUCTS, PROCESSES AND INVESTIGATIONS OF
THE PHILIPS INDUSTRIES

THE PRODUCTION AND MEASUREMENT OF ULTRA-HIGH VACUA

by A. VENEMA and M. BANDRINGA.

621.51:531.788.74

In order to produce ultra high vacua (i.e. pressures lower than 10^{-7} mm Hg) it was the practice until recently to work with a closed system and to use in the last phase of the pumping process some form of "internal pump", e.g. a getter, an ionization gauge or both. The article below shows that it is also possible to attain vacua considerably better than 10^{-7} mm Hg with a normal mercury diffusion pump, which has the advantage of a considerably greater pumping speed. The mercury diffusion pump must, for this purpose, form part of a specially designed vacuum system.

Recent years have seen a marked growth of interest in ultra-high vacuum technique. The reason is that the extremely low pressures offer interesting possibilities for the investigation of surface properties, e.g. for measuring contact potentials and studying adsorption phenomena. Only when the pressure of the ambient gas atmosphere is sufficiently low can a completely clean surface remain clean for a time long enough to allow experiments to be carried out on it. At a pressure of 10^{-7} mm Hg a clean surface may be completely covered by a monolayer in a matter of 10 seconds; even at this low pressure the number of molecules from the gas atmosphere incident per second on one cm^2 at room temperature is still 4×10^{13}. A reduction of the pressure by, say, a factor of 1000 increases the time available for experiments by the same factor.

A few years ago it was thought that pressures in the range of 10^{-7} to 10^{-10} mm Hg could hardly be reached. A pressure of 10^{-7} mm Hg was regarded as particularly low, and the fact that it was not possible to reach lower pressures was attributed to incomplete mastery of pumping technique. In 1947, however, Nottingham [1]) pointed out that the measuring instrument used in this pressure range, the ionization gauge, might not be capable of giving a true reading of such extremely low pressures. This investigator suggested that every ionization gauge has a certain minimum indication which depends on the design of the gauge; with the instruments used at that time this indication corresponded to a pressure of 10^{-7} to 10^{-8} mm Hg. In 1950 and 1951, manometer designs were proposed by Bayard and Alpert [2]), by Lander [3]) and by Metson [4]), which offered an appreciable extension of the measuring range. In 1953 and 1954 Alpert [5]) and Alpert and Buritz [6]) described in two detailed articles a technique by which it was possible to produce and reliably measure vacua in the range from 10^{-9} to 10^{-10} mm Hg.

In the present article we shall describe a pumping system by means of which pressures in the range from 10^{-10} to 10^{-12} mm Hg can be achieved, as well as an ionization gauge for measuring these pressures. First, however, we shall deal with the problem of lowering the minimum reading of an ionization gauge (and hence the smallest measurable pressure) after which we shall discuss Alpert's method of producing a pressure of 10^{-10} mm Hg, and mention some general aspects of the pumping process at extremely low pressures. From these aspects we shall derive the principles on which the design of our pumping system is based.

[1]) W. B. Nottingham, information communicated to D. Alpert (see [5])).

[2]) R. T. Bayard and D. Alpert, Rev. sci. Instr. **21**, 571, 1950.
[3]) J. J. Lander, Rev. sci. Instr. **21**, 672, 1950.
[4]) G. H. Metson, Brit. J. appl. Phys. **2**, 46, 1951.
[5]) D. Alpert, J. appl. Phys. **24**, 860, 1953.
[6]) D. Alpert and R. S. Buritz, J. appl. Phys. **25**, 202, 1954.

Ionization gauges for ultra-high vacua

In the pressure range with which we are concerned the only possible measuring instrument is the ionization gauge. The normal design consists of a cathode (usually a tungsten filament) situated in the middle of the electrode system, surrounded coaxially by the anode, in the form of a cylindrical wire helix, and the ion collector, also in the form of a helix; see *fig. 1*. In some cases an additional electrode is

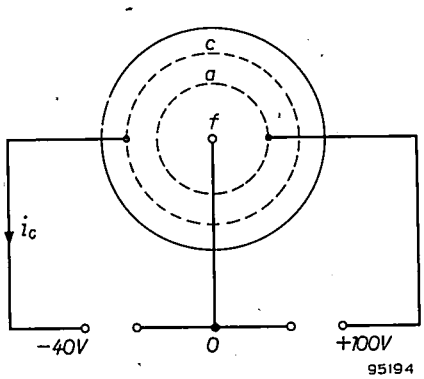

Fig. 1. Principle of the ionization gauge. The electrons emitted by cathode *f* are accelerated in the field between *f* and the anode *a* (the latter in the form of a cylindrical wire helix) giving them a kinetic energy high enough to enable them to ionize gas molecules. The electrons finally arrive at *a*. The positive ions formed in the space between *a* and the collector *c* (of the same form as the anode) move to the collector. Within a certain pressure range, the current i_c in the collector circuit is proportional to the pressure.

introduced between cathode and anode for the purpose of stabilizing the electron current [7]). The instrument functions as follows. The electrons emitted by the cathode are accelerated in the field between cathode and anode until their kinetic energy is high enough for them to be capable of ionizing gas molecules. The ions formed in the space between cathode and anode play no part in the measurement; the positive ions, however, which are formed in the space between anode and collector, are attracted towards the collector, which is at a lower potential than the anode. The resultant current flowing in the collector resistance is proportional, over a wide range of pressures, to the number of molecules present per unit volume, and is hence proportional to the pressure. This proportionality is lost, however, when pressures in the region of 10^{-8} mm Hg are reached. In fact, the current appears to be unable to drop below a specific value no matter how low the pressure may be.

What is the cause of this residual reading? Nottingham [1]) assumed that the residual current is not due to positive ions impinging on the collector, but to photoelectrons liberated from the collector as a result of soft X-rays which are generated when electrons from the cathode strike the anode. In order to be able to measure pressures lower than about 10^{-8} mm Hg it is therefore necessary to reduce this "X-ray effect". Gauges in which this has been achieved are reported in the publications [2]), [3]) and [4]) mentioned above. The instrument built by Bayard and Alpert [2]) is the simplest in design and therefore most commonly used. In this type of ionization gauge the ion collector is a thin wire mounted centrally in the cylindrical anode. The cathode is outside the anode. The sensitivity with this electrode arrangement is about the same as with the old design but there is now substantially less electron emission from the ion collector. In this way the "X-ray limit" is shifted to a pressure which is 100-1000 times smaller than in the old version. The ionization gauge which we have built, and which will be described in this article, is also of the type with central collector.

Alpert's method of producing extremely low pressures

The technique described by Alpert [5]) for obtaining reliable vacua in the range of 10^{-10} mm Hg is based on a property common to every ionization gauge and which, depending on the circumstances, may be either an advantage or a disadvantage. This is the property of the gauge to adsorb gas more or less permanently on the glass envelope and on certain electrodes. In most cases the glass envelope of the gauge acquires a charge such that positive ions are attracted to the glass where they are neutralized and sorbed as molecules. The same can happen on the electrodes when the latter have the appropriate potential. At an electron current smaller than about 0.01 mA this pumping action is usually slight, but it is quite pronounced if the electron current is 0.1 mA or more. Its effect on pressure measurements can be distorting in view of the fact that the ion gauge must as a rule be connected to the vessel via a tube. Between the ends of this tube a noticeable difference in pressure can arise, and the gauge reading is then no longer a direct measure of the pressure in the vessel. The pumping action of the ion gauge can, however, also be turned to advantage for the purpose of cleaning up the small amounts of gas which, even after careful outgassing of walls and components, may still be liberated inside the system. By this means the pressure can be reduced to a low value and maintained at that value.

[7]) An instrument of this type was described earlier in this Review by E. Bouwmeester and N. Warmoltz: Philips tech. Rev. **17**, 121, 1955/56; see also Appl. sci. Res. **B 2**, 273, 1951.

The pump system developed by Alpert on this principle consists of an oil-diffusion pump, capable of reducing the pressure in the system to be evacuated to a value of about 10^{-7} mm Hg, an all-metal valve which isolates the pump from the system, and the ionization gauge. If, after the requisite pressure has been reached, it is required to introduce a certain gas into the system, use can be made of a second metal valve, which connects the system to a reservoir. With the first valve open and the pressure in the system having been reduced to about 10^{-7} mm Hg by the diffusion pump, the entire system is placed in a "bake-out" furnace (with the pump attached, but outside the furnace) and heated for six to eight hours at a temperture of about 450 °C. This having been done, the gauge electrodes are outgassed by electron bombardment. The valve is then closed and the ionization gauge set in operation with an electron current of 10 mA. The pressure is now observed to fall, and within an hour it reaches a value in the range from 10^{-9} to 10^{-10} mm Hg.

Factors governing the lowest attainable pressure

We shall now turn to the principles underlying our pump system, which we shall derive from a general consideration of the pumping process in the range of low and extremely low pressures and from a closer analysis of Alpert's method.

When a vessel is evacuated one generally notices that the pressure at first drops fairly rapidly and then reaches an almost constant value. After some time the pressure is found to drop still further, but much more slowly than in the beginning. To explain this behaviour it must be remembered that the gas removed by the pump is initially present not only in the enclosed space but also adsorbed at the walls and at the surface of the components. The free gas is exhausted fairly quickly, the removal being faster the greater the pumping speed at the exit [8]) and the smaller the volume. The gas adsorbed at the walls and components may now be liberated, and a pressure sets in such that the amount of gas given off is equal to that removed by the pump. A state of quasi-equilibrium arises, i.e. a quasi-stationary state of flow. The rate of release of gas from the walls diminishes very slowly and the pressure likewise. The pressure prevailing in the space after the quasi-stationary state has set in is governed by the amount of gas given off per second and by the pumping speed.

Mathematically, the variation of pressure with time can be described as follows.

Let the temperature be constant and uniform over the whole system. A quantity of gas, i.e. a certain number of molecules, is then entirely determined by the product of pressure and volume. Let Q_A represent the quantity of gas of kind A which is liberated from its bound state per second and Q_B that of gas of kind B, etc. The quantity of gas A with which the pump can deal per second can be described as $S_A p_A$, where S_A is the pumping speed for gas A and p_A the partial pressure of gas A.

If the pump is now connected directly — i.e. using no manifold — to the vessel to be evacuated, then the pressure at the pump mouth is the same as that in the space. The partial pressure p_A will then obey the relation:

$$-V\frac{dp_A}{dt} - S_A p_A + Q_A = 0, \quad \ldots\ldots \quad (1)$$

where V is the volume of the vessel and t the time. For gases B, C and so on, corresponding relations hold. If Q_A changes but slowly with time, and if S_A may be regarded as independent of p_A, the solution of this equation is:

$$p_A = p_{A_0} e^{-\frac{S_A}{V}t} + \frac{Q_A}{S_A}\left(1 - e^{-\frac{S_A}{V}t}\right), \quad \ldots \quad (2)$$

where p_{A_0} is the value of p_A at the time $t = 0$. As long as t is small, i.e. at the beginning of the pumping process, then the first term on the right-hand side is considerably larger than the second, and hence almost entirely governs the value of p_A. The second term indicates the value which the pressure ultimately reaches. Naturally, the time at which the two terms are equal depends on the values of Q_A, S_A, p_{A_0} and V. Corresponding equations again hold for the other gases (B, C, etc.), and the total pressure, when there is no interaction between the gases, is given by:

$$p = p_A + p_B + p_C + \cdots \quad \ldots\ldots \quad (3)$$

Interaction between the gases does not take place, at least not in the evacuated space, since the mean free path at the low pressures we are considering is very long and the number of collisions between the molecules is very small compared with the number of collisions against the walls.

As can be derived directly from equations (2) and (3), the value of p ultimately established in the space is governed by the quantity of gas liberated, Q, and the pumping speed S.

In order to lower the pressure as far as possible it is necessary on the one hand to reduce to a minimum the release of gas in the space, and on the other hand to step up the pumping speed. Disregarding leaks, the release of gas from the walls can be minimized by prolonged baking out at a suitably high temperature and low pressure. Naturally, in a high-vacuum apparatus materials must be avoided that cannot readily be de-gassed, for which reason the materials used are at present limited to metals and glass.

[8]) The pumping speed is the ratio between the quantity of a given gas evacuated per second and the pressure of that gas (measured at the position at which the pumping speed is to be calculated). The pumping speed is usually measured in litres per second. At the inlet aperture of a pump this ratio is constant within a wide range of pressures. Where a mixture of gases is concerned, the above is still valid provided the calculation is made for each component on the basis of its partial pressure.

It cannot be concluded from the above that the pressure in a space in which the release of gas has been reduced to zero can go on falling indefinitely. The pumping speed — we shall assume for a moment that only one type of gas is concerned — does not remain indefinitely constant, but decreases when the pressure has dropped below a certain value, and finally becomes zero. The pressure at which this happens we shall call the limiting pressure for a particular type of gas. The value of this limiting pressure differs from one pump to another. Where a mixture of gases is concerned, as is always the case in practice, the limiting pressure for all components is not reached simultaneously. As soon as the limiting pressure for one of the components is reached, the composition of the gas at that moment begins to change, in the sense that it becomes richer in this component, and so on.

In the light of the above considerations we shall now examine the ionization gauge used as a pump. Its particularly favourable properties are: 1) small wall area and the fact that it can be readily outgassed, enabling the release of gas to be reduced, and 2) the property of still being able to sorb gas even at extremely low pressures. The pumping speed, however, is not so favourable. Alpert [5]) estimates the pumping speed of his arrangement in the case of chemically inert gases — i.e. gases not taken up by the hot cathode — at approximately 0.02 l/sec. The pumping speed for chemically active gases, such as oxygen, is substantially higher; it is the chemically inert gases that determine the lowest attainable pressure.

A circumstance that can be a difficulty in some experiments is that the ionization gauge used as a pump does not *remove* the gas from the system. There is always a possibility that it will again be released from the gauge. If, for example, one wishes to carry out an experiment in a well-defined atmosphere having a pressure of 10^{-8} mm Hg, the maximum one will wish to allow for the partial pressure of foreign gases will be 10^{-10} mm Hg. A high vacuum of this order is first produced by means of the Alpert system, after which the required gas is allowed to flow in from a reservoir at such a rate that, with the ionization gauge pumping the pressure reaches the prescribed value. Proceeding in this way one is still not certain, however, that the composition of the gas will be exactly as hoped for. Since the gas-collecting components of the gauge are subjected to much more intensive ion bombardment after the filler gas is introduced, other gases, earlier taken up, can again be released and thus entirely alter the composition of the gas. This is a well-known phenomenon with the Penning manometer. Of course, one can avoid this effect by switching off the manometer before admitting the gas. In that case, however, the pressure can no longer be measured, and moreover pumping ceases from the moment of switching off.

Another difficulty that can arise is concerned with the diffusion of helium from the atmosphere through the glass envelope of the apparatus. Alpert has very neatly demonstrated that this phenomenon does in fact occur and in some cases governs the lowest obtainable pressure [5]). True, the effect of this diffusion can be limited by an appropriate choice of glass, but when the experiment calls for high wall temperatures, this diffusion can indeed be troublesome. The simplest method of removing this helium is to use a pump having a much greater pumping speed than is possible with an ionization gauge.

A higher pumping speed is also desirable when experiments are to be carried out on surfaces in a very high vacuum without it being possible to minimize the release of gas from the material under investigation. The only way to produce the requisite low pressure in such a case is to use a pump having a high pumping speed.

These considerations led us to set up a pumping arrangement capable of permanently removing the gas from the system and with which relatively high pumping speeds can be achieved, substantially higher than with the ionization gauge. With this arrangement we have achieved pressures which even the improved ionization gauge was unable to measure. It is estimated that the pressure in our experiments was lower than 10^{-12} mm Hg.

The pumping system

Choice and construction of the vacuum pump and accessories

If the object is to build a pumping system having a high pumping speed for all gases, the use of a diffusion pump is the obvious solution. Although the speed of this pump generally decreases with increasing molecular weight of the pumped gas, this effect is not very serious [9]). Diffusion pumps of high pumping speed are easy to make. Another question, however, is whether the pressure at which the pumping speed drops to zero — the earlier mentioned

[9]) The pumping speed varies from one gas to another approximately in proportion to the root of the molecular weight. It should also be recalled that the pumping speed depends on the pressure, so that one cannot state an unqualified value for a given gas or pump.

N.V. PHILIPS' GLOEILAMPENFABRIEKEN

limiting pressure — is adequately low with the diffusion pump. The foregoing has made clear that this limiting pressure need certainly not lie at 10^{-7} mm Hg, as was formerly believed because of misapprehension regarding the residual reading of the ionization gauge; it may indeed be much lower.

The principle of operation of the diffusion pump was described some years ago in an article in this journal [10]). For the purposes of the present article a few points may be recapitulated to clarify the problem with which we are concerned. The operation of this type of pump is based, as the name indicates, on the diffusion of the pumped gas in a stream of vapour. The stream of vapour is produced in the pump by the boiling of a suitable fluid (mercury, oil). In the following we shall speak of gas and vapour in order to distinguish clearly between the two media. The density of the vapour is much greater than that of the pumped gas, and the gas molecules are entrained in the vapour. The vapour is next condensed and the gas, which now has a greater density than at the pump mouth, then passes through a second diffusion stage, where the same process is repeated. One or more other stages may follow, and finally the gas leaves the system via a (mechanical) backing pump. In some cases the diffusion pump contains only one stage. The gas leaves this pump with a lower pressure than in the case of a multi-stage pump; in such a case more stringent requirements are imposed on the backing pump as regards the pumping speed at low pressures.

We shall now consider the factors governing the limiting pressure at the pump mouth and the method of making this pressure as low as possible.

a) The first factor is the pressure of the saturated vapour of the pump fluid used and of the decomposition products resulting from the boiling of this fluid. By interposing liquid nitrogen traps between the pump and the receiver one can greatly reduce the chance of a molecule of these vapours reaching the evacuated vessel. The traps should have the highest possible conductance for the gas stream if the ultimate pumping speed in the vessel is not to be unduly reduced; but it is also necessary to minimize the chance of a vapour molecule passing through a trap. It is not the case, however, that all decomposition products at the temperature of the trap (—196 °C) have such a low vapour pressure as to be harmless. We have confirmed this by a number of qualitative experiments [11]). Measurements with a mass spectrometer have shown that hydrocarbons of low molecular weight arise during the boiling of organic fluids in a pump [12]). For these reasons we decided on mercury as the pump fluid.

b) The second factor is the release of gas from the pump itself — particularly from the part through which the gas passes before entering the diffusion zone — and the release of gas from all components of the system to be pumped. As already mentioned, the release of gas from the components can be reduced by heating the components at low pressure and a sufficiently high temperature. With this in mind we designed our pumping system such that the most critical part of the pump — that which provides the pumping action, in our case the upper section — can be baked out in a furnace. The same applies to the traps.

c) The third factor is the back-diffusion of the gas in the pump against the vapour stream. The effect of back-diffusion can be reduced by minimizing the pressure at the pump outlet. This can easily be done by using a second diffusion pump as backing pump. In our arrangement this second pump can reach a pressure at its mouth of 10^{-7} mm Hg. This also favours the out-gassing of the first pump.

If other effects are negligible, so that the limiting pressure is determined solely by the back-diffusion (assuming, again, only one kind of gas is present) there is a constant ratio in a diffusion pump between the pressure at the pump mouth and that at the outlet. The value of this ratio naturally varies with the speed of the vapour stream and with the nature of the gas. The ratio is highest, i.e. back-diffusion is most troublesome, in the case of light gases. In our pump this ratio is smaller than 10^{-6} for hydrogen, at a moderate vapour speed. With a normal vapour speed, and when pumping heavier gases, this ratio is therefore appreciably smaller.

d) Finally, there is the fact that the pump fluid itself is not entirely gas-free and cannot be made so. When the vapour condenses, a certain fraction of the pumped gas dissolves in the vapour. If the above-mentioned factors *a*), *b*) and *c*) have been reduced to the minimum by carefully calculated measures, it may well be that this particular effect will determine the lowest obtainable pressure. In such a case, the minimum pressure is independent of the backing-vacuum pressure over a relatively wide range [13]).

[10]) F. A. Heyn and J. J. Burgerjon, Philips tech. Rev. **14**, 273-276, 1952/53.

[11]) The decomposition products of the following were investigated: Apiezon A and C, Octoil S and Silicone DC 703. See also: C. Hayashi, J. Phys. Soc. Japan **9**, 287, 1954.

[12]) J. Blears, J. sci. Instr., Suppl. No. 1 (Vacuum Physics), p. 36, 1951.

[13]) N. A. Florescu, Vacuum **4**, 30, 1954.

Fig. 2 shows a cross-section of the diffusion pump designed in these laboratories, which satisfies in particular the requirement mentioned under *b*); a photograph of the pump can be seen in *fig. 3*.

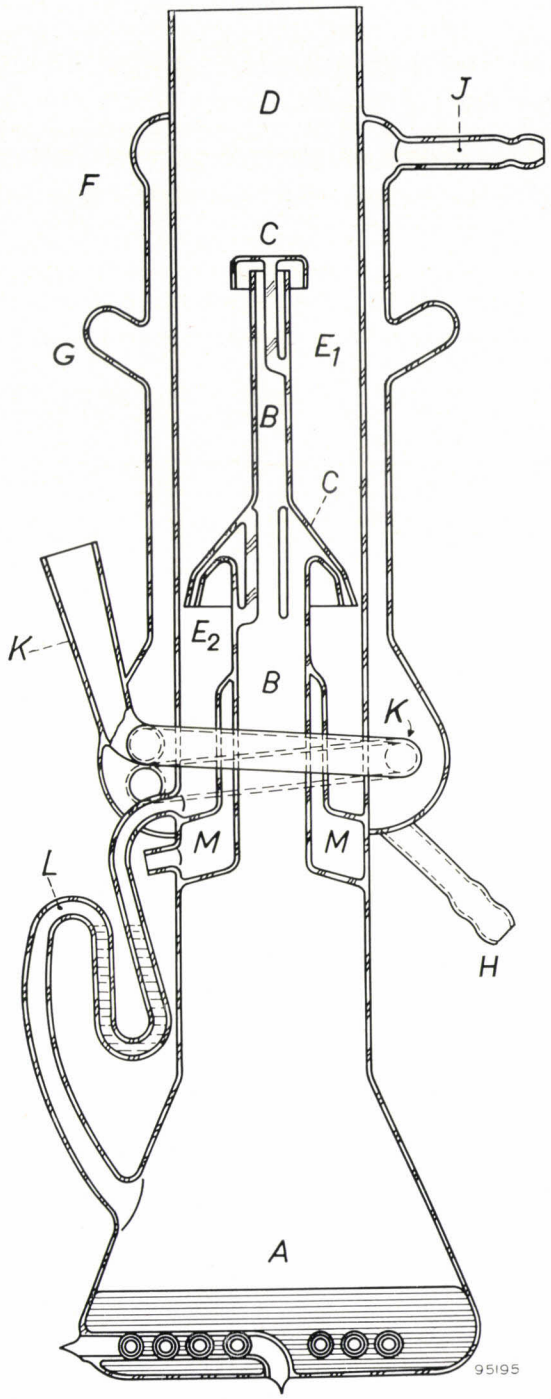

Fig. 2. Cross-section of the glass two-stage mercury diffusion pump. *A* boiler with heater. *B* funnel. *C* nozzles. *D* pump mouth. E_1 and E_2 diffusion space of the two stages. *F* water-cooled jacket with expansion bulge *G*. *H* and *J* inlet and outlet, respectively, for cooling water. *K* pump outlet; to ensure complete condensation of the mercury a fairly long section of the outlet passes through the water-cooled jacket. *L* return tube for condensed mercury; it also functions as valve and manometer. *M* space communicating with the backing-vacuum, and providing heat insulation between boiler and cooler. This insulation limits heat losses and reduces the risk of the glass breaking as a result of thermal stresses.

Fig. 3. The glass two-stage mercury diffusion pump.

It is, as the figures show, a two-stage glass pump. It is so constructed that the part responsible for the pumping action — at least as far as the first stage is concerned — can be outgassed in a furnace. One of the measures adopted to this end was to position the boiler containing the mercury as low as possible. Further particulars are given in the caption to

fig. 2. The pumping speed for nitrogen is 60 l/s over a wide pressure range; the maximum permissible backing-pressure for air, with a heater dissipation of 400 W, is 0.5 mm Hg [14]).

The design of the traps [15]) is illustrated in *fig. 4*. Both the inside and outside walls of the space between the inlet and outlet of the trap can be cooled — with liquid nitrogen, for example. A mercury atom is certain to strike the cold wall at least once during its passage in the trap. Two versions of the traps with different dimensions have been made having conductances for nitrogen of 25 l/s and 15 l/s; a photograph of the first type is shown in *fig. 5*.

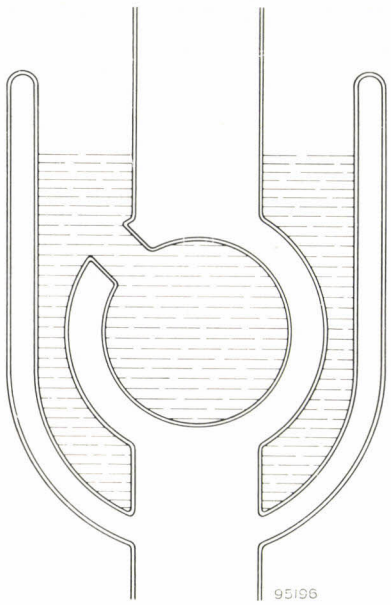

Fig. 4. Schematic cross-section of a liquid nitrogen trap having very high conductance and high condensation efficiency.

Fig. 5. One of the liquid nitrogen traps.

Layout and operation of pumping system

The design of the pumping system was based on the idea that the vessel should be outgassed longest, because at that position the pumping speed is lowest for those gases on which the traps have no effect. *Fig. 6* shows a photograph of the apparatus. The glass diffusion pump passes through a hole in an asbestos-cement table, such that the upper stage of the pump is above the table top. Above the pump are, in succession, the three traps, followed by the vessel and the ionization gauge. Below the table top are mounted a metal mercury-vapour diffusion pump, which acts as backing pump, and a vacuum reservoir. The reservoir is connected to the outlet of the metal pump as soon as the major part of the gas has been pumped out; up to that moment this pump is connected to a rotary-pump. The pressure in the reservoir can rise to about 5 mm Hg without seriously reducing the pumping speed of the metal pump. Also under the table top is the safety equipment responsible for switching off the electric current (both pumps, metal and glass, are electrically heated) if the cooling water pressure drops too low or if the gas pressure rises above a certain value owing to a leak. Also, in this event, a valve between the two diffusion pumps closes automatically.

The part of the installation above the table can be heated to 450 °C. The furnace in which this is done can be moved upwards after use into the position in which it appears in the photograph.

[14]) If the pressure difference between the inlet and outlet of a diffusion pump exceeds a certain value, the pumping speed drops sharply. The value of this reverse pressure is of the order of magnitude of 0.01 to 1 mm Hg. Owing to the use of two stages, the maximum backing pressure of the pump described here is sufficient to enable the pump to be used for "normal" high vacua in combination with merely a rotary backing-pump. For our purpose it has been found that a single-stage pump capable of being outgassed, together with a second diffusion pump, is also suitable.

[15]) Designed in co-operation with J. H. N. van Vucht.

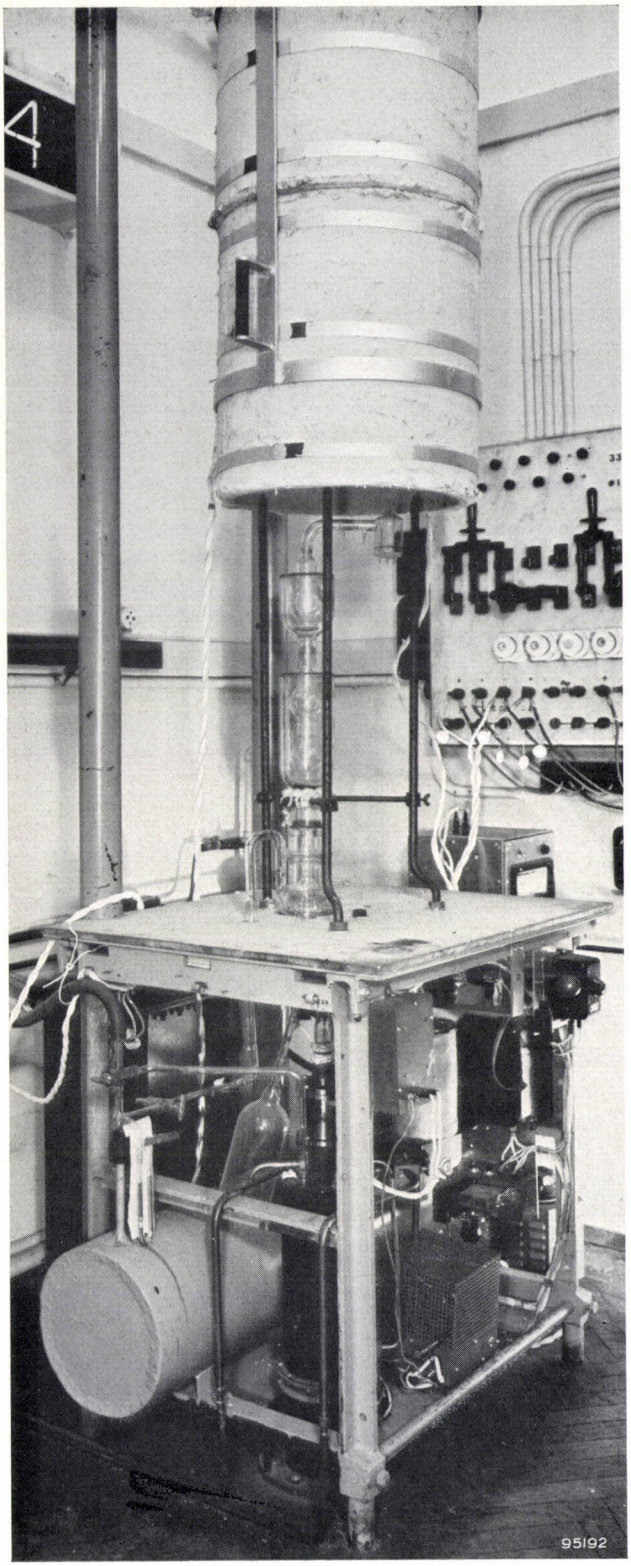

Fig. 6. The pumping system for producing ultra-high vacua. The glass two-stage mercury diffusion pump is partly above and partly below the table top of asbestos-cement. Under the table are the metal diffusion pump for the backing-vacuum, and the vacuum reservoir. Above the glass pump are three traps one above the other, a manifold bent over to the right, to be regarded as the vessel, and connected to it an ionization gauge of special design. The furnace surmounting this system can be lowered to the table top, enabling all parts above the table to be baked out.

With regard to the efficiency of the traps the following may be said. The probability of a mercury atom leaving the cooled surface on which it impinges is not zero. This probability is in fact greater here than in the case of a sealed-off space held at the temperature of liquid nitrogen; the "temperature" of the incident atom is not always equal to that of the wall after a single collision. Furthermore, the density of the mercury vapour at the inlet of the first trap is still great enough for the mean free path of the atoms to be of the order of magnitude of the dimensions of the trap. This means that the mercury atoms undergo here a by no means negligible number of mutual collisions, which enable some of them to pass through the cooler without having come into contact with a wall. In fact, mercury is still to be found at the outlet of the first trap. For this reason it is necessary to have a second trap in series with the first; if the system is to be in operation longer than about 24 hours, a third trap is necessary in order to maintain the pressure in the region of 10^{-11} mm Hg.

Accordingly, measures must also be taken to keep the liquid level in the traps automatically constant. For this purpose we used a device described by Feld and Klein [16]) and illustrated in *fig. 7*. The trap R (here shown only schematically) is filled from a reservoir C by means of a syphon S. The pressure above the boiling fluid in C is regulated by the temperature in an air-filled vessel T. If this temperature rises above a certain value, the pressure in T becomes so high as to cause the mercury in a valve V to close an opening O, causing the pressure in C to rise. Fluid then flows through the syphon, the liquid level in the trap rises and the temperature in T drops. The valve opens again, the pressure above the fluid in C falls and the supply of fluid ceases. This system works very reliably and is simple in design.

The vacuum system is outgassed and set in operation in the following way. Initially the furnace rests on the table top. Everything above the table top is baked out and while this is happening neither the glass pump nor the coolers can function. The system is exhausted with the metal vacuum pump. After this has been in progress for some considerable time, e.g. all night, the furnace is moved up high enough to allow the glass pump to be put into operation. The remainder above the pump is kept at 450 °C. The outgassing process can now be effectively continued owing to the fact that the pressure of all gases in the system (except the mercury vapour) drops sharply as a result of the glass pump coming into operation, the pumping speed now being increased by a factor of 50. After some hours the furnace is moved up still higher to expose the first trap, which is then filled with liquid nitrogen. At intervals of a few hours the other traps are also taken into use.

The components of any experimental object that may be in the vessel are now thoroughly outgassed by heating them to an appreciably higher temperature than the wall of the vessel, which is

[16]) M. Feld and F. S. Klein, J. sci. Instr. **31,** 474, 1954.

still at 450 °C. The arrangement must of course be so designed as to make this possible. At the same time the electrodes of the ionization gauge are subjected to the same treatment. Finally, the latter section is allowed to cool. If only the ionization gauge is connected above the last trap, the pressure in the former will then have fallen to below the lower limit of the measuring range of the gauge, i.e. below about 10^{-12} mm Hg.

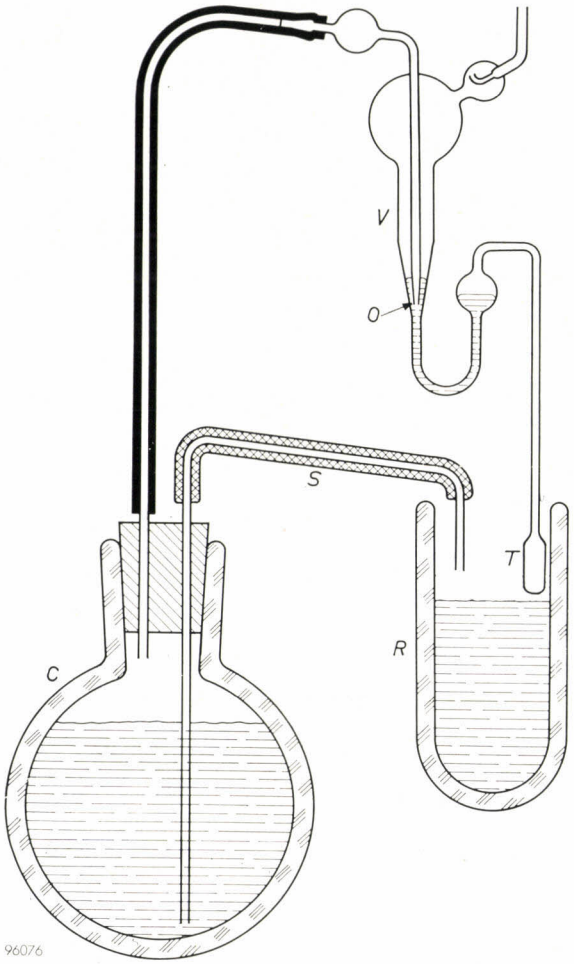

Fig. 7. Apparatus which automatically keeps the liquid nitrogen in a trap at the correct level. In the trap R is situated at the appropriate height a vessel T, which is air-filled and connected to a valve V. If the level of the liquid nitrogen in R falls, the temperature of T rises, the air pressure increases and at a certain moment the mercury in V closes the opening O as shown. The communication between the reservoir C and the atmosphere is now broken. The pressure above the boiling fluid in C rises, and after a short delay the syphon S comes into operation. As soon as the temperature of T drops low enough, owing to the rise in the nitrogen level in R, for O to open again, the syphon ceases to function.

If the experimental object is of such a nature as to prohibit the presence of mercury vapour in the vessel at any stage in the operations, the glass diffusion pump and the first trap cannot be baked out in the furnace. In that event it will be necessary to heat the remaining two traps with the vessel and the gauge for a sufficiently long period. In other respects the outgassing process is the same.

It is obvious that the vertical arrangement described here is only one example out of many possibilities. Other arrangements can be built on the same principle, possibly with more than one furnace.

It may be asked whether the increased pumping speed obtained here (as high as 5-10 l/s in the vessel) is not offset by an increase in the total release of gas from the wall, so that as regards the lowest obtainable pressure there is in fact no improvement compared with the method of pumping with the ionization gauge. In that method, it may be argued, the pumping speed was admittedly low, but at least the gas-releasing surface was small. A quantitative study of this problem (see appendix) has shown that this is not the case and that a quite substantial gain is possible in the degree of vacuum obtainable.

The ionization gauge

In designing the ionization gauge our guiding principles were to produce a gauge having a measuring range with the lowest limit compatible with a simple and robust construction; furthermore the electrodes should be easily outgassed and the gas-release should be as low as possible. *Fig. 8* shows the design finally evolved. To comply with the first

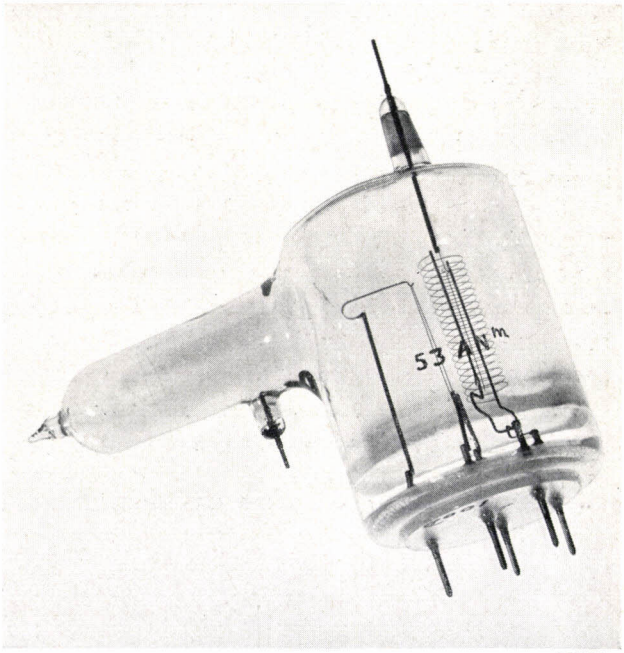

Fig. 8. The ionization gauge. The ion collector is a thin wire mounted inside the anode, the cathode being external to them. To prevent excessive heating of any one part of the wall, the cathode is mounted centrally in the glass tube. The glass wall has a conductive coating.

of the above requirements the electrode configuration is the same as in the instrument by Bayard and Alpert; to ensure minimum gas-release no stabilizer grid is used and moreover the dimensions of the electrodes have been kept fairly small. Although this entails lower sensitivity, we believe that this is more than compensated by the advantages gained. The anode is of molybdenum and consists of a cylindrical helix mounted between two wire supports. The cathode and collector are of tungsten. The power dissipated by the cathode, which is mounted centrally with respect to the glass envelope, is relatively small. Thanks to these measures no part of the tube wall undergoes any appreciable rise in temperature, and the chance of gases being released from the wall as a result of irradiation is very slight. Finally, the inside of the glass wall was made conductive. This proved to be particularly necessary for work with low electron currents. If the wall potential is not fixed it can assume all kinds of values, causing changes in the electron paths and hence altering the sensitivity. It may then happen that at the same pressure two settings of the gauge are possible, characterized by different ion currents. The wall is usually given the same potential as the ion collector [17]).

With the exception of the cathode, the electrodes can best be outgassed by electron bombardment. Not only the anode wires and the ion collector, but also the support wires for the anode can be heated in this way to 1100-1200 °C. A further advantage of this method of heating is that certain impurities on the electrodes, which only have a low vapour pressure even at high temperature, are dissociated under the influence of the fast electrons and rapidly disappear. The power needed to bring the anode and collector up to the required temperature is 15 to 20 W. At an anode voltage of 150 V the contribution of the X-ray effect to the collector current corresponds to a pressure of 5×10^{-11} mm Hg if the collector wire is 25 μ thick, and to 2×10^{-10} mm Hg if the wire is 150 μ thick. The upper limit of the measuring range and the sensitivity are the same as with an instrument of the older design.

The omission of the stabilizer grid calls for certain special measures in the circuitry of the instrument. If one wishes to keep the electron current constant for some time — and this is certainly very desirable during the measurement — it can only be done by automatically regulating the temperature of the cathode, that is to say by making the electron current itself control the filament current. This of course demands additional circuitry, but this is no particular objection, especially since the electronic equipment can be used for different types of gauges (provided they do not differ unduly in their characteristics); also there is a greater chance of having to replace the gauge tube then of replacing the electronic equipment. Moreover, being less complicated in design, this gauge is cheaper than the type with stabilizer grid.

Electrical characteristics

As mentioned in the introduction, the collector current i_c of an ionization gauge consists of two components, that from the positive ions originating from the gas, i_i, and that from the electrons liberated from the anode by X-rays, i_p.

These two components depend in different ways on the electron energy. The relation between i_i and the anode voltage V_a is given by a curve which greatly resembles curves of ionization probability as a function of electron energy. This curve has a flat maximum which, for most cases, lies at approximately 100 V. As regards the second component, Alpert [5]) has pointed out that i_p is proportional to V_a^α, the value of α lying between 1.5 and 2.

The above enables us to understand the form of the curves representing the relation between i_c and V_a shown in *fig. 9*. The various curves hold for different pressures and were obtained with two models of the new ionization gauge having collector wires of 150 μ and 25 μ thickness, respectively.

We shall first consider curves *1* and *2*, which relate to the comparatively high pressure of approximately 10^{-6} mm Hg. Here i_p is negligible compared with i_i, that is to say the curves show, to a good approximation, the above-mentioned relation between i_i and V_a. Turning now to curve *5*, which is the lowest-lying of the curves obtained with the gauge with thick collector wire, we see that, at high V_a in particular, this curve approaches a straight line having a slope of 1.8 (dot-dash line). Evidently the X-ray limit has been reached in this case (i_p being proportional to V_a^α, as stated) and i_i is now negligible. Curve *3* occupies an intermediate position. Curve *4* holds for the same pressure, but was obtained with the other gauge; this curve, however, still exhibits the "i_i character" at this pressure. The X-ray limit of this gauge is seen to correspond with a pressure approximately ten times smaller than that which we found in the case of the gauge with the thick collector wire.

In one of our experiments the gauge with thin wire was used in the above-described pumping system for producing an ultra-high vacuum. At a

[17]) Nottingham (1954 Vacuum Symposium Transactions, Committee on Vacuum Techniques, Boston, Mass. U.S.A. 1955, p. 76) counteracted this effect by introducing an additional electrode surrounding the existing electrode system and situated fairly close to the glass wall. This method, however, increases the quantity of material and also makes the bake-out rather more complicated.

certain moment in the period during which the pressure was still falling slowly, measurements were carried out, the results of which are embodied in curve *6*. The pressure had then already fallen to about 2.5×10^{-11} mm Hg. The measurements carried out when i_c was no longer decreasing are represented by curve 7. This can no longer be distinguished from a straight line corresponding to the X-ray effect; in other words the pressure — which can no longer be derived with any accuracy from these measurements — must have been lower than 10^{-12} mm Hg [18]).

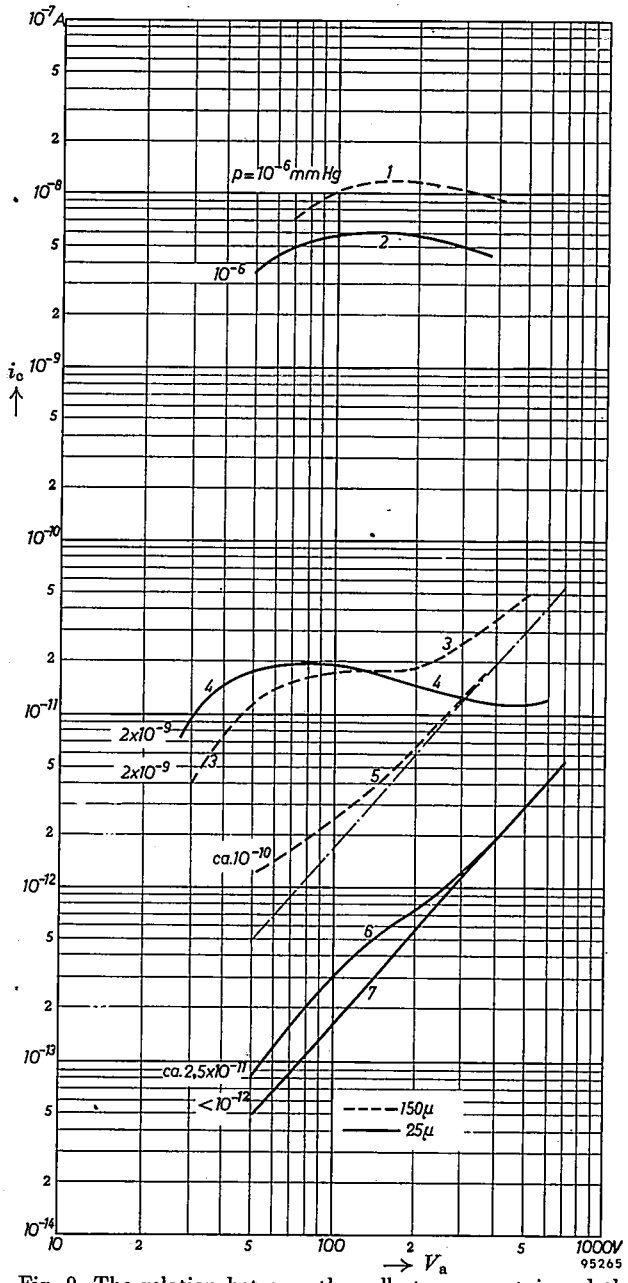

Fig. 9. The relation between the collector current i_c and the anode voltage V_a of the ionization gauge, for two versions of the gauge and at different gas pressures. The dashed curves relate to the gauge having a collector wire 150 μ thick, and the solid curves to the gauge having a collector wire 25 μ thick. At a relatively high pressure $i_c \approx i_i$ (i_i is the ion current), and the curve has approximately the form of an ionization probability curve. At relatively low pressure $i_c \approx i_p$, and the curve is linear (when plotted logarithmically). The slope lies between 1.5 and 2. The measurements were made with an electron current of 1 mA. (Some of these measurements were carried out by S. Garbe and A. Klopfer of the Philips laboratory in Aachen.)

The ion current i_i, from which ultimately the pressure in the gauge must be derived, is proportional to this pressure and also, of course to the number of electrons emitted by the cathode per unit time, that is to say to the electron current i_e. We may write

$$i_i = k\, p\, i_e .$$

The proportionality factor k is dependent on the nature of the gas. This is due to the fact that the chance of ionization being caused by an electron of a certain kinetic energy differs from gas to gas. The factor k is called the sensitivity of the gauge. The sensitivity of this gauge for nitrogen, where p is expressed in mm Hg and where V_a is 150 V, is $k = 11.2$ with the thick collector wire and 7.2 with the other.

This constant is determined in the pressure range from 10^{-3} to 10^{-5} mm Hg by comparing the readings of the ionization gauge with those on a McLeod gauge. In this range i_p is of such subordinate significance that the collector current i_c may be taken as equal to i_i. Alpert [5]) has shown that the value of k found with the type of pressure gauge described here, in this range of pressures, also holds at substantially lower pressures.

We may summarize as follows the advances made in the production and the measurement of ultra high vacua and the methods which have made these advances possible:

1) The X-ray limit of the ionization gauge has been lowered to the range of 10^{-12} mm Hg by using the electrode system designed by Bayard and Alpert and a thin collector wire (25 μ).

2) Pressures less than 10^{-12} mm Hg have been obtained by:

a) using a pump of high pumping speed, viz. a glass mercury-diffusion pump;

b) introducing three liquid nitrogen traps of special construction (maximizing the conductance and the chance of condensation) between pump and receiver;

c) minimizing the gas-releasing surface of the pump system and the material;

[18]) This pressure was calculated on the assumption that the gas concerned was nitrogen. The true composition was unknown, this gas not being a residue of the original gas contained in the vessel (e.g. air) but consisting of molecules liberated from the walls.

d) designing the pumping system such that the first pump as well as the vessel, the gauge and the traps can be outgassed in a bake-out oven (in order to produce a sufficiently low pressure for this purpose, the first pump is not followed directly by a rotary backing pump but by a second diffusion pump);
e) reducing the back-diffusion in the glass pump (a very low backing-vacuum is also necessary for this purpose, again calling for the use of a second diffusion pump).

If it is desired to introduce instruments in the vessel for carrying out experiments, these must be outgassed just as thoroughly as the electrodes of the ion gauge. Their construction must therefore allow of high-frequency heating, for example.

Appendix: Calculation of the pressure distribution in the new pumping system and of the lowest pressure attainable in the ionization gauge.

We shall now derive the formula for the pressure distribution in the pumping system, and with the aid of this formula we shall calculate the lowest pressure obtainable in the ionization gauge. We shall then compare this pressure with that obtainable with an ionization gauge used as a pump. In deriving the said formula we shall disregard, for the sake of simplicity, the special form of the traps employed. We regard the space to be evacuated simply as a cylindrical tube closed at one end and connected at the other end to a pump. We further assume that the gas liberated from the walls is not taken up by the coolers. (This gas may be helium, diffusing from outside through the glass wall, or gas from another source dissolved in the glass. Gases that are indeed retained in the cooler — meaning that their saturation vapour pressure at a temperature of —190 °C is smaller than, say, 10^{-12} mm Hg — can be left out of consideration; the pumping speed for these gases is extremely high.)

The tube schematizing the system is sketched in *fig. 10*. The pump is connected at *O*; the pumping speed is *S*. The radius of the tube is *r* and the length *l*. The *x* axis is the long axis of the tube with its origin at *O*. Our calculation refers to

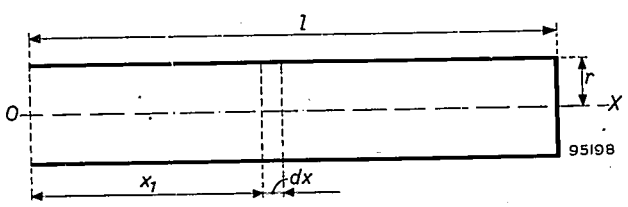

Fig. 10. Calculation of the pressure as a function of position *x* in a tube whose walls give off gas. One end of the tube is sealed and the other (at *O*) is connected to a pump.

only one kind of gas. As soon as the quasi-stationary state has set in, the pressure is entirely governed by the gas production. The gas production per unit time and per unit area we shall denote as *q*.

We consider an annular element of the cylinder wall at a distance x_1 from the pump and having a width d*x*. The gas production per unit time of this surface element is $2\pi rq\mathrm{d}x$. The gas flows partly to the right and partly to the left. In the flow to the right no "loss" occurs, so that the contribution which the element makes to the pressure at all points of higher *x* value is constant. Towards the left, however, the contribution decreases the shorter the distance is to *O*, this being due to the pumping action. In the state of quasi-equilibrium the pump removes just as much gas as the wall produces, that is to say, the contribution from the surface element mentioned to the pressure p_0 at point *O* is

$$\mathrm{d}p_0 = \frac{2\pi rq}{S}\mathrm{d}x. \quad \ldots\ldots\ldots \quad (I)$$

The gas conductance of a tube of length *x* and radius *r* is given, to a good approximation, by the formula:

$$F = \frac{1}{4}\pi r^2 v_a \frac{8r}{3x}, \quad \ldots\ldots\ldots \quad (II)$$

where v_a is the arithmetic mean velocity of the molecules. The formula is better applicable the smaller is r/x.

When a quantity of gas $2\pi rq\mathrm{d}x$ flows through this tube, a pressure difference arises at the ends equal to:

$$\mathrm{d}(p-p_0) = \frac{2\pi rq}{F}\mathrm{d}x = 2\pi rq\,\frac{\frac{3x}{8r}}{\frac{1}{4}\pi r^2 v_a}\mathrm{d}x = 2\pi rq\,\frac{3x}{2\pi r^3 v_a}\mathrm{d}x. \quad (III)$$

We shall now try to find the pressure prevailing at position $x = x_1$ by calculating the contributions successively of a surface element for which $x < x_1$, one for which $x > x_1$, and of the end surface; we denote these contributions p_1, p_2 and p_3 respectively.

The contribution to the pressure at position x_1 in the case of all surface elements for which $x < x_1$ is given by

$$\mathrm{d}p_1 = 2\pi rq\left(\frac{1}{S} + \frac{3x}{2\pi r^3 v_a}\right)\mathrm{d}x. \quad \ldots\ldots \quad (IV)$$

This is obtained by adding equations (I) and (III). The total contribution from these elements together is thus

$$p_1 = 2\pi rq\int_0^{x_1}\left(\frac{1}{S} + \frac{3x}{2\pi r^3 v_a}\right)\mathrm{d}x = q\left\{\frac{2\pi}{S}rx_1 + \frac{3}{2v_a}\frac{x_1^2}{r^2}\right\}. \quad (V)$$

The contribution to the pressure at position $x = x_1$ made by elements in which $x > x_1$, is

$$p_2 = 2\pi rq\int_{x_1}^{l}\left(\frac{1}{S} + \frac{3x_1}{2\pi r^3 v_a}\right)\mathrm{d}x = \quad [19]$$

$$q\left\{\frac{2\pi}{S}r(l-x_1) + \frac{3}{v_a}\frac{x_1(l-x_1)}{r^2}\right\}. \quad \ldots\ldots \quad (VI)$$

The contribution from the end surface is

$$p_3 = \pi r^2 q\left(\frac{1}{S} + \frac{3x_1}{2\pi r^3 v_a}\right) = q\left\{\frac{\pi r^2}{S} + \frac{3}{2v_a}\frac{x_1}{r}\right\}. \quad (VII)$$

Hence, the pressure at position x_1 is

$$p(x_1) = p_1 + p_2 + p_3 = q\left\{\frac{2\pi rl}{S} + \frac{\pi r^2}{S} + \frac{3}{2v_a}\cdot\frac{x_1}{r} + \frac{3}{v_a}\cdot\frac{lx_1}{r^2} - \frac{3}{2v_a}\frac{x_1^2}{r^2}\right\}. \quad (VIII)$$

For $x_1 = l$ we obtain the highest value of pressure:

$$p_l = q\left\{\frac{1}{S}(2\pi rl + \pi r^2) + \frac{3}{2v_a}\cdot\frac{l}{r}\left(1 + \frac{l}{r}\right)\right\}. \quad (IX)$$

[19]) The integrand in this formula differs from that in formula (V) only in that the quantity *x* between brackets is replaced by the constant x_1.

Because of the approximation used, this formula is valid only when l is several times larger than r, and is better applicable the larger is l/r.

In our case l was 60 cm and r was 2.5 cm. We shall now calculate p_l, on the assumption that the gas concerned has approximately the same molecular weight as air. At the same value of q, the pressure in the case of lighter gases is lower. Substitution of the above values for the dimensions and of 60 l/s for the pumping speed yields the result:

$$p_l = 0.039\ q\ .$$

For comparison we shall calculate the pressure that would be obtained with an ionization gauge used as a pump. We put the area of the gas-releasing surface at 300 cm^2. At a pumping speed of 20 cm^3/s we then find $p = 15\ q$, which is higher by a factor of almost 400.

From formula (IX) we can ascertain the manner in which the dimensions of the pumping system can be varied without changing p_l. We must remember in this connection that S is approximately proportional to the square of the diameter of the pump. If we ensure that the ratio between pump and tube diameters remains unchanged when changing the dimensions, then S is also proportional to r^2 and formula (IX) transforms into a function of l/r. In this case, therefore, p_l will not change as long as l/r is kept constant. We find, then, that p_l is approximately invariant when the linear dimensions of tube and pump are changed by the same factor.

Summary. The lowest pressure that can be achieved in a vessel connected to a vacuum pump is determined by the gas liberated from the walls and by the speed of the pump. After the space has been exhausted a quasistationary state of flow sets in, whereby the pump removes just as much gas as the walls produce. The pumping speed is not, however, a constant, but rapidly falls to zero when the pressure approaches a certain limiting value, which differs from one gas to another. It is found that the limiting pressure of a normal mercury-diffusion pump can be lowered to below 10^{-12} mm Hg. The pressure difference between the inlet and outlet of the pump (the backing-pressure) was lower than 10^{-6} mm Hg. A second diffusion pump is used to produce the backing-vacuum. Diffusion pumps, moreover, have a high pumping speed (at pressures well above the limiting pressure). With a pumping system designed in the Philips laboratory at Eindhoven a pressure of less than 10^{-12} mm Hg has been obtained with the aid of a glass two-stage diffusion pump, preceded by a metal diffusion pump for producing the backing-vacuum; this system contains three liquid nitrogen traps between pump and evacuated vessel. The traps prevent the penetration of mercury vapour into the vessel. The pumping system is so designed that the vessel with attached ionization gauge, the traps and the first stage of the glass pump can be outgassed by heating them in an oven to 450 °C. The traps have a very high conductance and condensation efficiency. The pumping speed after the last trap is still 5-10 l/s. The wall area of the space to be evacuated is kept as small as possible. The ionization gauge is of the type with central ion collector (wire 25 μ thick), the design being such that the contribution of the X-ray effect to the collector current corresponds to a pressure of only 5×10^{-11} mm Hg. The anode and the collector can be outgassed by electron bombardment to a temperature of 1200 °C.

AN APPARATUS FOR TESTING THE SOLDERABILITY OF WIRE

621.315.5.001.4:621.791.3

The electrical connections between components in electric apparatus are usually made by soldered joints. These joints, particularly in mass production, must be effected quickly and reliably. To achieve this the solder must rapidly and thoroughly wet the metals to be joined. In order to investigate the conditions to this wetting process, that is to ascertain the "solderability" of the metal parts, an objective criterion is needed. To this end a soldering test is carried out under standardized conditions that closely approach practical conditions.

For the general investigation of solderability wide use is made of what is known as the "spread" test. At Philips this test is performed in the following way. A measured quantity of solder (say 0.2 g) is placed, together with a suitable amount of flux, on a square sample ($30 \times 30 \times 0.3$ mm) of the metal to be soldered. This small plate is then heated by floating it on a bath of molten solder kept at constant temperature. When the solder on the plate melts, it wets part of the surface, the size of the patch wetted depending on the conditions. Approximately 15 seconds after beginning to melt, the solder has usually stopped spreading. The area of the patch wetted after this time is taken as a measure of the solderability under the conditions of the test [1]).

The spread test is well adapted for investigating the conditions favourable for dip-tinning, a process in which metal parts are simply given a thin coating of solder by dipping them in a bath of molten solder. The test does not so readily allow conclusions to be drawn with regard to the *joining* of wires by dip soldering or by soldering-iron work, however. A drawback in this respect is that the spread time of 15 seconds is long compared with the time of about 2 seconds which is common for work with the soldering-iron. An example will make this clear. If, instead of a solution of pure rosin in alcohol, a more active flux be used, consisting of pure rosin with 10% ureum in alcohol, the solder will initially spread faster (see curves *A* and *B* in *fig. 1*). This very favourable effect is not revealed, however, by the results of the test. As seen from the figure, the test indicates the pure rosin to be the better of the two fluxes. The error in the conclusion is still more evident when pure rosin in alcohol is compared with an even more active flux, namely hydrazine-hydrochloride in water (fig. 1, curve *C*). In many cases the spread test also fails to reveal the effect, generally favourable, of a higher soldering temperature. The correlation between practice and the results of such tests is therefore not very good. Attempts have been made to overcome these drawbacks by measuring the wetted area after shorter intervals, while the spreading is still in progress. Apart from photographic methods, which are rather cumbersome, all the methods hitherto proposed have been wanting in accuracy. A further disadvantage of the spread test is the somewhat lengthy procedure of determining numerically the size of the moistened area. What is more, this form of test is obviously far from ideal when the metal to be soldered is in the form of *wire*, which is usually the case in the electronics industry, where the most common components — resistors and capacitors — have wire connections.

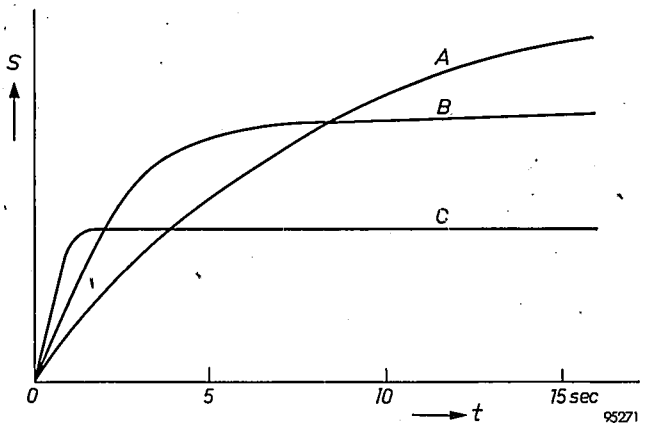

Fig. 1. The area S of a heated metal plate wetted by flowing solder, as a function of time in the "spread" test. The three curves relate to tests in which only the flux was varied: curve *A* refers to pure rosin in alcohol, curve *B* to pure rosin with 10% ureum in alcohol, and curve *C* to hydrazine hydrochloride in water. The area wetted after 15 sec is taken as a measure of the solderability. Interpreting the tests on this basis, the favourable effect of an initially rapid spread is lost.

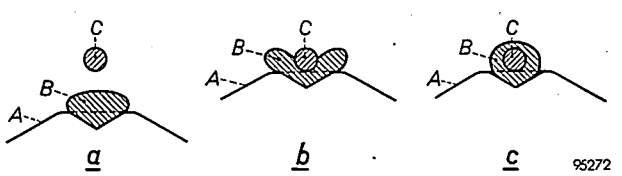

Fig. 2. Principle of the solderability test developed at Philips.
a) In a hollow in the heated soldering block *A* lies a globule of solder *B*, above which is clamped the wire *C* under investigation.
b) The block is raised; the wire splits the globule in two.
c) The two halves meet at the top of the wire and flow together. The time between the splitting and the flowing-together is taken as a measure of the solderability of the wire.

[1]) For other versions of this test see, for example, W. R. Lewis, Notes on soldering, published by the Tin Research Institute, Greenford, Middlesex, England, 1948; also L. Pessel, Symposium on solder, Amer. Soc. Test. Mat., Special technical publication No. 189, p. 159-174, 1956.

With this in mind we have developed a method which is specially adapted for testing the solderability of wire and which avoids the drawbacks described above. The measure of solderability is taken as the time needed for a drop of solder to flow entirely around a wire of the metal under investigation. The principle of the test is illustrated in *fig. 2*. In a small hollow in a block of chromium-plated chrome-nickel steel (the soldering block) a measured quantity of the solder is introduced. The exact quantity is obtained by punching a pellet out of a bar of solder rolled to a certain thickness. The soldering block is electrically heated. When the solder has melted it remains in the hollow in the form of a globule, for solder does not wet chromium. The wire to be investigated is clamped centrally above the globule of solder, having been dipped beforehand in the flux. The soldering block is now raised so that the wire cuts the drop of solder in two. The two halves creep up round the wire at a speed which depends on the conditions. When they come into contact at the top of the wire they flow together with an abrupt movement. The instant at which this happens can be observed very precisely.

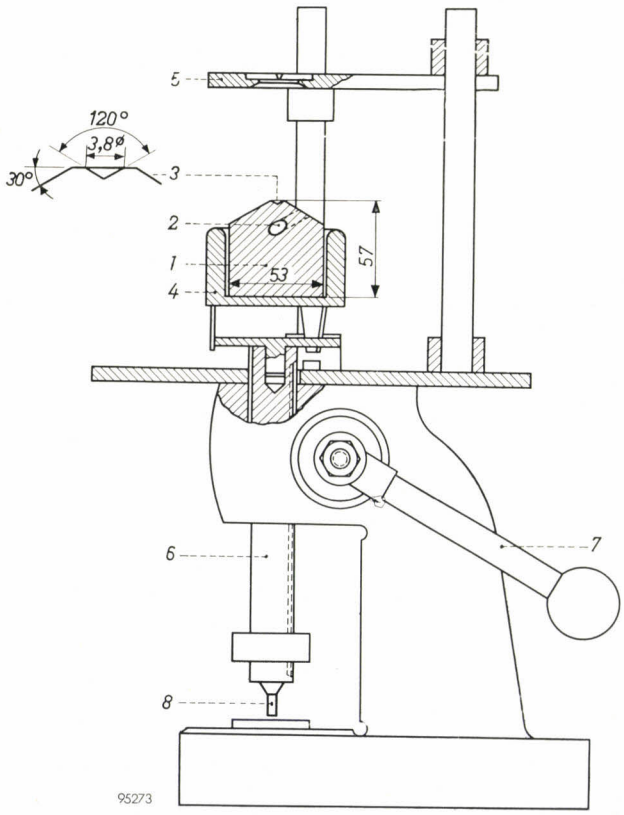

Fig. 3. Schematic cross-section of the apparatus for testing the solderability of wire. *1* soldering block, *2* hole for thermometer, *3* hollow for the drop of solder, *4* heater jacket, *5* wire holder, *6* toothed plunger, *7* lever for raising the soldering block, *8* tool for punching out the solder pellets. The shape and dimensions (mm) of the hollow for the drop of solder are given in the inset sketch.

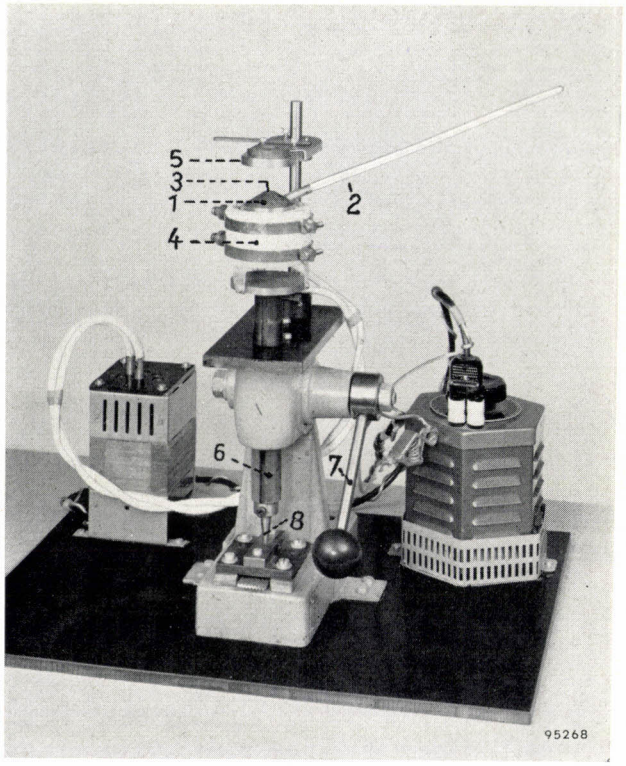

Fig. 4. Photograph of the apparatus for testing the solderability of wire. *2* is the thermometer. Other numbers as in fig. 3.

The time elapsing between the splitting of the globule and the flowing together at the top of the wire is measured with a stopwatch. The shorter this "soldering time", the better the solderability. The results show very good correlation with practice.

The temperature of the globule is measured with a mercury thermometer, inserted in a cavity in the soldering block. The correction to be made for the thermometer reading is ascertained by replacing the solder on the block by salts of known melting point. The construction of the apparatus is illustrated schematically in *fig. 3* and a photograph is shown in *fig. 4*. In *fig. 5a* and *b* can be seen the molten drop of solder immediately before and after the instant it flowed around the wire.

In order that the results obtained with each apparatus should be comparable it is necessary to ensure that they are identical in certain essential points. This applies, for example, to the dimensions of the hollow that holds the globule of solder, for they determine the height of the globule, and a higher globule (for example) will flow more rapidly around the wire (*fig. 6a*). The dimensions of the hollow are given in fig. 3. With these dimensions and with a solder globule of 190 mg, the apparatus is suitable for testing wire of 0.5-1.0 mm diameter. The other dimensions of the soldering block and the material of which it is made influence the supply of

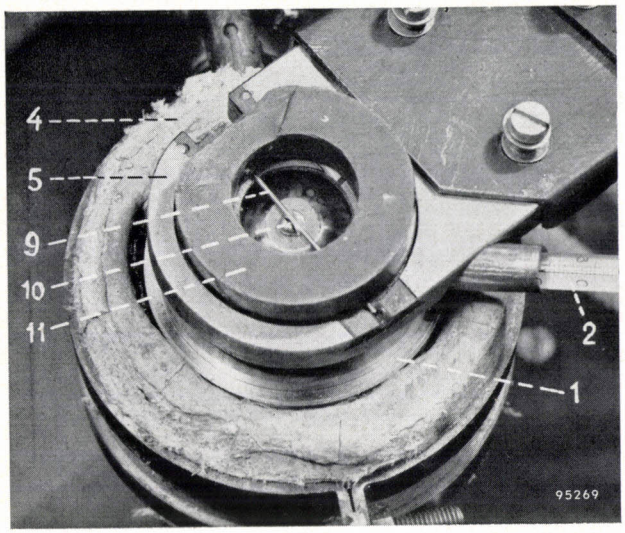

a

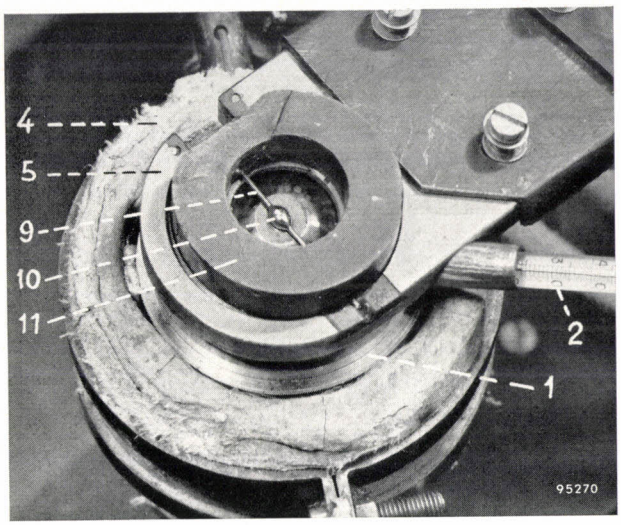

b

Fig. 5. Close-up views of a globule of solder, *a*) split by the wire under test and *b*) after flowing around the wire. *2* thermometer, *9* test wire, *10* globule of solder, *11* ferroxdure magnet for clamping the wire. Other numbers as in fig. 3.

heat to the globule, whilst the length of the wire and the way in which it is clamped affect the dissipation of heat. In these matters too, therefore, individual instruments must be closely identical.

With the test method described, an investigation has been carried out into the influence of various factors on the soldering process, the principal factors being:

1) composition and quantity of the solder;
2) composition and quantity of the flux;
3) composition and surface state of the metal to be soldered;
4) temperature.

The investigation was prompted in particular by the need for greater control of the dip-soldering process as used for printed wiring [2]). In this process all connections between the mounted components and the printed wiring are simultaneously soldered by dipping in a bath of molten solder. In hand soldering, with a soldering-iron, any difficulty in soldering particular wires can usually be overcome by suitable raising the soldering temperature or by applying a more active flux. In the dip-soldering of printed wiring the difficulties are much greater: often the base cannot be subjected to too high a temperature without the printed wiring becoming loose, and there is a considerable risk that a highly active flux may creep and create leakage paths. These considerations impose more stringent requirements on the solderability of the connection wires.

The investigation was designed round certain fixed conditions, one of the variables being changed at a time for each experiment. The fixed conditions were chosen with a view to obtaining a soldering

[2]) See for example R. van Beek and W. W. Boelens, Printed wiring in radio sets, Philips tech. Rev. **20**, 113-121, 1958/59 (No. 5).

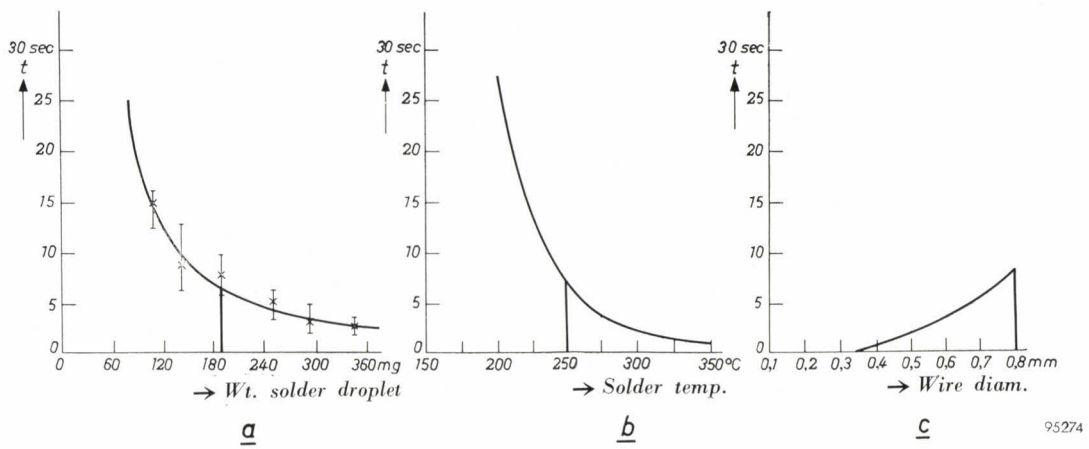

Fig. 6. Influence of (*a*) quantity of solder, (*b*) temperature and (*c*) diameter of wire, on the solderability of the wire. Soldering time *t* is plotted vertically. The points (×) plotted in (*a*) are the averages for 10 experiments; the spread in the observations is also shown.

time that was not so short as to make the influence of favourable factors scarcely perceptible. These conditions were:

Solder: 60% tin, 40% lead; globule quantity 190 mg (22.4 mm^3).

Flux: 40 parts by weight of pure rosin and 60 parts by weight of alcohol, applied to the wire by dipping.

Wire: copper wire of 0.8 mm diameter; degreased successively in trichlorethylene and acetone.

Temperature: 250 °C.

The average "soldering time" under these conditions was about 7 sec.

Very favourable conditions yielded times shorter than 1 second. The effects of variations in the quantity of solder, the temperature and the wire diameter can be seen in fig. 6*a*, *b* and *c*. There is a fairly wide spread in the results, but the averages of ten tests for each measuring point lie reasonably well on the curves. Since each measurement takes little time, it is practicable to make a number of repeat observations under the same conditions.

A slight change in the composition of the solder can cause a marked change in the soldering time. The addition of 1% cadmium or zinc lengthens the soldering time to more than 30 sec. On the other hand, the addition of 1% silver has a slight shortening effect. With solder consisting of pure tin the soldering time is longer than 30 sec.

The experiments on the influence of the solder composition were repeated at a soldering temperature of 300 °C. The soldering times were found to be fairly short and the differences less marked. With printed wiring, however, low-temperature soldering is necessary and in that case the composition of the solder is of importance.

As regards the composition of the flux it was found that the concentration of the pure rosin solution must be at least about 25% if it is to be applied by dipping the wire in it. With rosin concentrations of 20% the soldering time was frequently in excess of 30 sec. Increasing the content from 25% to 40% gives hardly any further improvement. The addition of a quantity of ureum equal to 10% of the quantity by weight of pure rosin reduces the soldering times to less than 1 sec. The same short times are obtained with solutions of the monohydrochloride or dihydrochloride and monohydrobromide or dihydrobromide of hydrazine in water. Owing to their rapid decomposition, the concentration of these four compounds has a definite lower limit. The limiting concentration for the first three lies at about 3% and for the fourth at about 2.5%; at these concentrations soldering times shorter than 0.1 sec as well as longer than 30 sec are found. The best results with zinc chloride are found for an approximately 10% solution in water, the average soldering time then being 1.2 sec.

The composition of the metal to be soldered and the condition of the metal surface are extremely important factors. It is well known that thin coatings of certain metals, e.g. tin, applied by electroplating or by hot-dipping to copper wire can greatly improve the solderability. However, moisture on the surface, and, in particular, heating of the wire (say, 2 hours at 190 °C, as for example in the stove-enamelling of painted parts) can reduce this effect and make the solderability of tinned wire a great deal poorer. Less trouble in these respects is obtained with hot-dipped coatings of tin-lead (50% Sn, 50% Pb) and electroplated layers of tin-zinc (80% Sn, 20% Zn). The spread in the results of temperature and moisture tests is often greater for hot-dipped than for electroplated coatings.

It should be noted that a soldering block of aluminium was used for the investigation described here. Because of its harder wearing properties the chromium-plated chrome-nickel steel block, already mentioned, was later adopted for routine tests.

J. A. ten DUIS.

Icoma 2371

THE LIFE OF BALLASTS FOR GAS-DISCHARGE LAMPS

II. CAPACITORS

by T. HEHENKAMP.

621.319.4:621.327.4

With the spread of lighting by gas-discharge lamps there has been an enormous increase in the use of capacitors, which are used in ballasts with the object, among other things, of improving the power factor. It has therefore become a matter of considerable economic importance to produce capacitors for this purpose which are both long-lived and low-priced. The problems involved are more complicated than in the case of transformers and chokes for lamp ballasts, but they have been so far solved that capacitors fabricated by modern methods can now be used in ballasts without misgivings.

Many ballasts for gas-discharge lamps contain capacitors, the chief purpose of which is to improve the power factor. These capacitors are of the type having a dielectric of impregnated paper and a hermetically sealed casing. The dielectric is impregnated either with a mineral oil (sometimes vaseline) or with a synthetic oil such as chlorodiphenyl.

The life of these capacitors is just as important as that of the transformers or chokes described in Part I of this article [1]). The primary factor governing the life of the latter is the temperature of the insulating material. The life of capacitors, however, is a problem of much greater complexity, for it is influenced not only by insulation temperature but also by the field strength. This is substantially higher than in the transformers and can be as much as 100 to 200 kV/cm (10 to 20 V/μ) [2]). The reason for the use of such high field strengths is that the volume of a capacitor is about inversely proportional to the square of the field strength, so that raising the field strength allows an appreciable reduction of dimensions and price. At field strengths of this order, however, ionization is quite likely to occur in holes in the dielectric. This damages the dielectric material and leads to breakdown.

The influence of temperature on the life of the dielectric in a capacitor is comparable with that found with transformers (see Part I). Although the temperature-rise due to dielectric losses is not considerable, it must be remembered that the capacitors often operate in a high ambient temperature (owing to the proximity of warm transformers and lamps) and that they cannot withstand nearly such high temperatures as transformers. One of the reasons for the latter fact is that the dielectric losses rise steeply with temperature, causing the capacitor to enter into a state of thermal instability [3]).

Thermal stability

If one determines the loss P_1 in a capacitor at constant field strength and varying dielectric temperatures, one finds a curve that rises steeply when a certain temperature region is reached (*1* in *fig. 1*). The dissipation of heat P_2 to the surrounding medium is almost proportional to the dielectric's mean rise in temperature ΔT above the ambient temperature:

$$P_2 = K\,\Delta T.$$

The proportionality constant K depends on certain constructional parameters (such as internal thermal conductivity and surface heat transfer coefficient) and on the external cooling conditions. The internal thermal conductivity causes a temperature gradient in the dielectric, making the temperature in the middle of the capacitor higher than at the walls. In ballast capacitors, however, this temperature gradient is not important and can be disregarded in approximate calculations.

Assuming the capacitor to be continuously loaded at an ambient temperature T_0 we can determine approximately the temperature acquired by the dielectric in the steady state. Through point T_0 on the abscissa of fig. 1 a straight line *2* is drawn which makes an angle α with this axis such that

$$\tan \alpha = \frac{P_2}{\Delta T} = K.$$

[1]) T. Hehenkamp, The life of ballasts for gas-discharge lamps, I. Transformers and chokes, Philips tech. Rev. **20**, 59-68, 1958/59 (No. 2/3).

[2]) The numerical values of field strengths and voltages throughout this article refer to the r.m.s. values.

[3]) J. Coquillion, Condensateurs au papier imprégné de pyralène pour le courant alternatif, Electricité **40**, 237-243, 1956.

In general this line cuts the loss curve *1* at two points. It can be seen that the point of intersection on the right represents an unstable state of equilibrium, while the point on the left is a stable state. As the temperature of the dielectric rises, it will thus settle down to the value T_d corresponding to the left point of intersection.

If the ambient temperature be raised, the straight line will move, maintaining the same slope, to the right. The two points of intersection approach each other and finally coincide to form a single point of contact. In this state

$$\frac{dP_1}{dT} = K.$$

This is the *stability limit*, and it is reached at an ambient temperature T_s. Thermal stability is no longer possible at an ambient temperature higher than this; the capacitor then goes on rising in temperature until it breaks down. Breakdown occurs at, or close to, the hottest part of the dielectric, i.e. in the centre. By switching off the capacitor a few moments before it breaks down and unwinding the paper, one can find the place where the breakdown would have occurred as a darkly discoloured patch caused by overheating (*fig. 2*).

A capacitor of the same type subjected to a different electrical load gives a loss curve differing from *1* in fig. 1, and hence has a different critical ambient temperature T_s. If the field strength be lowered, for example, the losses decrease, which means, according to fig. 1, a higher value of T_s. By plotting the same graph for different field strengths one finds the relation between field strength and T_s. *Fig. 3* shows the result; the line found for this relation is usually straight or slightly curved.

In fig. 3 the region right of the line is unusable: a capacitor loaded in this region would soon break down. Left of the line stability is assured, at least as long as the losses do not increase unduly owing to ageing of the dielectric.

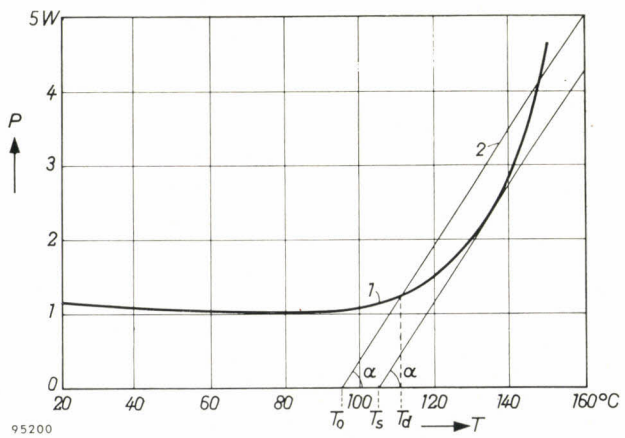

Fig. 1. Curve *1*: Loss P_1 in a 3.8 μF capacitor as a function of the temperature T of the dielectric, at constant field strength (22 V/(μ)²) and constant frequency (50 c/s). The dielectric consists of three layers of paper 8 μ thick, impregnated with pentachlorodiphenyl.

Curves *2*: Graphical construction for finding the equilibrium temperature T_d of the dielectric for an ambient temperature T_0. Through point T_0 on the abscissa a straight line *2* is drawn at an angle $\alpha = \tan^{-1} K$; the line *2* intersects with curve *1* in two points; the left point of intersection corresponds to the temperature T_d. The highest ambient temperature at which a stable state can still be established is the value T_s on the abscissa, which is the point where the line *2* tangential to *1* intersects the T axis.

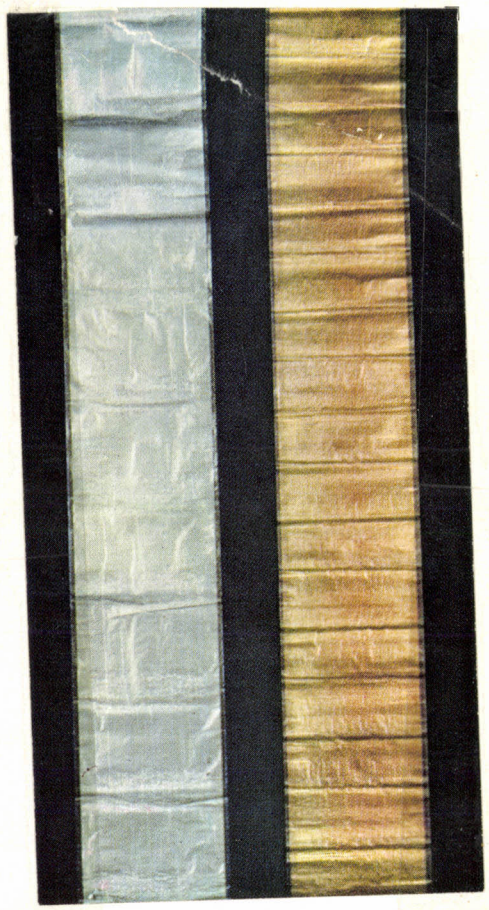

Fig. 2. Two strips of paper unwound from a capacitor which was switched off just before thermal instability would have caused breakdown. Left, a strip from the outside (coldest) layers; right, a strip from the inside (hottest) layers. The right strip has turned brown due to overheating.

The thermal stability limit can also be found by a direct test method. The capacitor, under the appropriate electrical load, is placed in an oven whose temperature is somewhat lower than the value of T_s estimated to correspond to the field-strength selected. Once a state of equilibrium is reached, the oven temperature is raised in small steps, with a pause after each step to allow equilibrium to be re-established. When equilibrium no longer sets in, the oven temperature is then about equal to T_s and the capacitor soon breaks down.

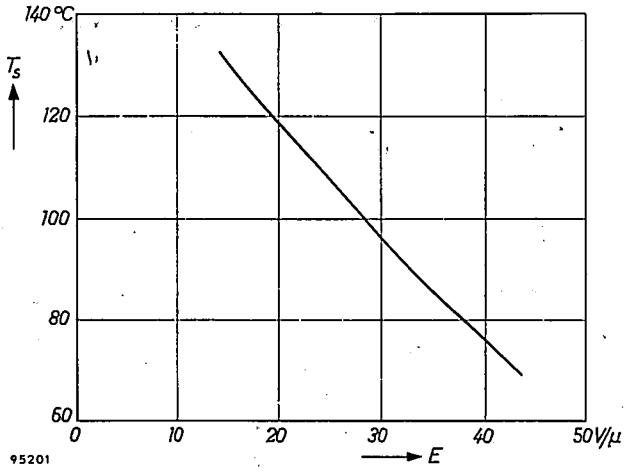

Fig. 3. The ambient temperature T_s at which the limit of stability is reached, as a function of the field strength E. The values of T_s are determined graphically as indicated in fig. 1, for capacitors having a loss curve *1* as in fig. 1.

Life at high temperatures

When a capacitor is loaded with a certain field-strength E at an ambient temperature T_0 which is but little lower than the value of T_s corresponding to E, the capacitor must obviously be expected to have a short life. The reason is that as soon as the dielectric begins to deteriorate under the influence of the electrical and thermal loading, the capacitor will become unstable, owing to the increasing losses, at a lower ambient temperature than was the case in the initial state (*fig. 4*). The difference $T_s - T_0$ (fig. 1) is according to this reasoning a measure of the reserve available in the capacitor. This reserve and the rate at which it drops to zero (the aging rate) determine the life of the capacitor. This is true within a limited temperature range, as appears from life tests at high ambient temperatures.

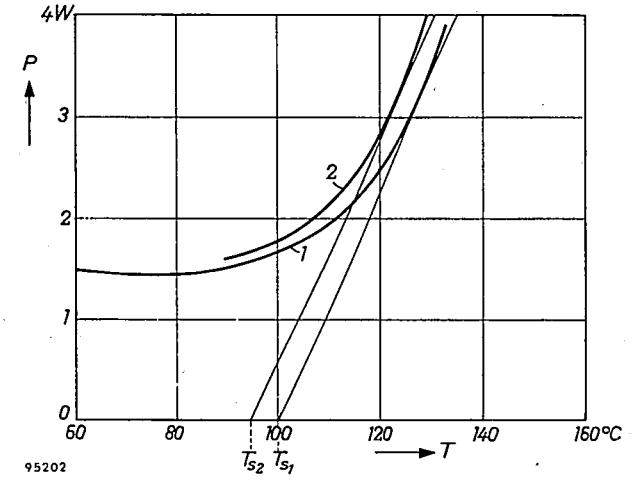

Fig. 4. Loss curve of a 3.8 μF capacitor for a field strength of 25 V/μ and a frequency of 50 c/s, in the initial state (curve *1*) and after 250 hours loading at 25 V/μ and 90 °C (curve *2*). Owing to the aging of the dielectric the stability limit has dropped from $T_{s1} = 100$ °C to $T_{s2} = 95$ °C.

An example is given in *fig. 5*, which represents the results of life tests on capacitors of 4 μF having a 30 μ paper dielectric. When the ambient temperature is lowered the life is found to increase enormously. This suggests that at, say, $T_0 = 40$ °C, the capacitor would have an extremely long life. Such an extrapolation, however, is very dangerous, for this expectation is by no means always borne out in practice. The reason for this is the increase in the degree of ionization at low temperatures, which we shall now discuss.

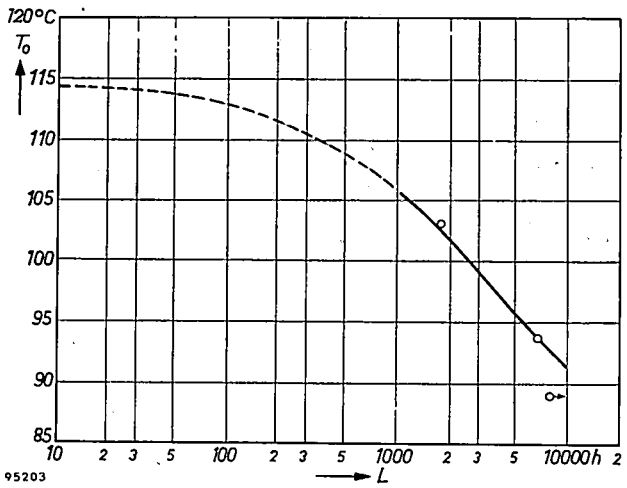

Fig. 5. Ambient temperature T_0 at which capacitors having a dielectric of three layers of paper 10 μ thick, impregnated with vaseline, and under a load $E = 17.5$ V/μ, attain a life L. The stability limit T_s for $E = 17.5$ V/μ lies at 114 °C. At this ambient temperature the capacitor has a life of only a few hours. The test at 89 °C was still not concluded after 8000 hours.

Ionization in the dielectric; life at low temperatures

If there is a gas bubble in the dielectric, a disproportionately large field concentration will occur over it, for the dielectric constant of the gas is only $\frac{1}{4}$ to $\frac{1}{6}$ of that of the impregnated paper. Since the field strength in the paper is already high, the field in the gas can easily reach a value at which ionization can occur (corona) [4]). As a result the dielectric around the gas bubble becomes impaired (*fig. 6a* and *b*). This leads to increased losses (*fig. 7*), while the breakdown potential decreases [5]).

In the greatly simplified case of a uniform field — gas bubble with flat bounding surfaces perpendicular to the electric field and a thickness which is small in proportion to the other dimensions — the field strength at which ionization begins to occur can

[4]) C. de Lange, Pressure condensers, Philips tech. Rev. 4, 254-259, 1939.

[5]) T. W. Liao, Corona and its effects on insulation, Insulation, March 1957, pages 18-21.

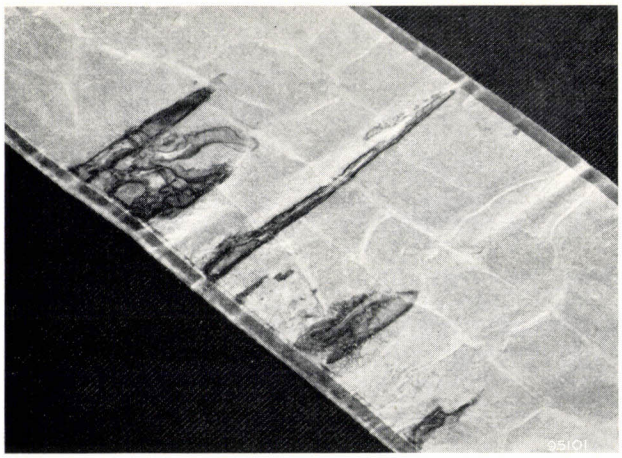

a

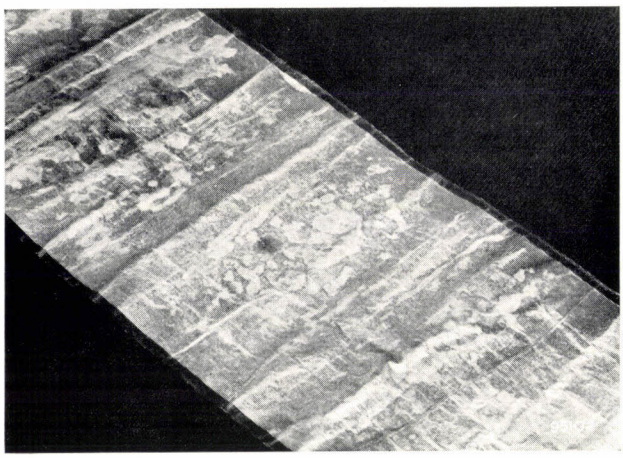

b

Fig. 6. Illustrating how ionization damages a dielectric impregnated (*a*) with pentachlorodiphenyl and (*b*) with vaseline. In (*b*) breakdown has occurred at one of the damaged regions.

be ascertained with the aid of Paschen's law, which is represented graphically for air in *fig. 8*. In reality the conditions are, of course, much more complex. Owing to the irregular structure of the paper fibres and the presence of the impregnating agent, the field strength will vary from one place to another. We may therefore expect no more than a rough correspondence to the case of a uniform field.

For this reason the potential at which ionization begins to occur must be measured in every individual case. Ionization is accompanied by slight irregularities in the current through the capacitor. The presence of ionization can therefore be demonstrated by means of a circuit which amplifies these irregularities and makes them visible on a cathode-ray oscilloscope [6]). A suitable circuit for this purpose is shown in *fig. 9*. The capacitor under investigation C_x is connected to another capacitor C_0 of good quality, not heavily loaded, and two resistors to form a bridge circuit. The one diagonal is fed by a variable alternating voltage in series with a choke L. The latter limits the current in the event of C_x breaking down during the measurement. By almost balancing the bridge the voltage across the other diagonal, in so far as the fundamental and the harmonics are concerned, is made very small. Apart from this small residual voltage there will be another, irregular, voltage present if ionization occurs in the capacitor. The total output voltage of the bridge is amplified, in which process components having frequencies below about 8000 c/s are removed. The result is made visible on an oscilloscope.

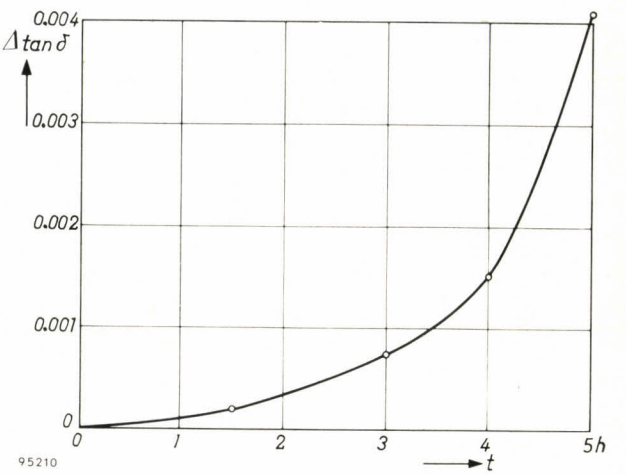

Fig. 7. Increase of loss factor tan δ measured after the dielectric had been loaded under 42 V/μ, at room temperature, for a time t (3.8 μF capacitors having three layers of paper 8 μ thick, impregnated with pentachlorodiphenyl). To minimize the rise in dielectric temperature, the capacitors were loaded continuously for only half-hours at a time, with intermediate cooling. Tan δ was measured at a dielectric temperature of 120 °C to improve the sensitivity of the measurements.

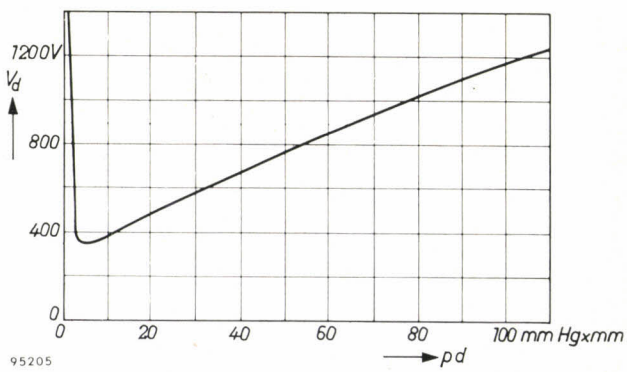

Fig. 8. The Paschen curve for air: breakdown voltage V_d for air in a uniform electrical field, as a function of the product pd of air pressure p (in mm Hg) and the distance d (in mm) between the electrodes.

[6]) R. J. Hopkins, T. R. Walters and M. E. Scoville, Development of corona measurements and their relation to the dielectric strength of capacitors, Trans. Amer. Inst. Electr. Engrs. **70-II**, 1643-1651, 1951.

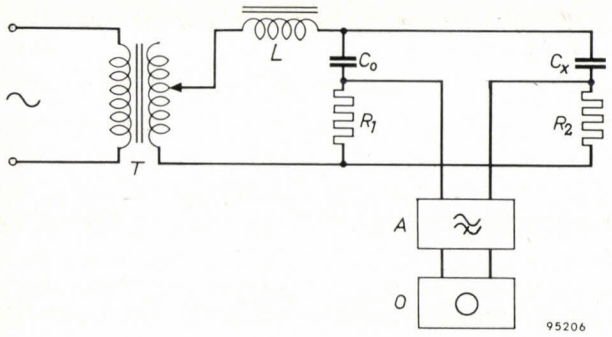

Fig. 9. Circuit for determining the degree of ionization in the dielectric of a capacitor. The test capacitor C_x, a high-quality and low-loaded capacitor C_0 and resistors R_1 and R_2 form a bridge circuit. This is fed from the mains transformer T via choke L. The amplifier A transmits only components having frequencies above about 8000 c/s. O cathode-ray oscilloscope.

Some examples of the oscillograms so obtained are shown in *fig. 10*. The tests were made on non-impregnated capacitors. The dielectric consisted of three layers of paper 8 μ thick. After drying and degassing, the capacitors were filled with air at 1 atm instead of oil, and the cans were then sealed by soldering. After cooling to room temperature the internal pressure was about 500 mm Hg. Since the non-impregnated dielectric contains innumerable gaps between the paper fibres, capacitors of this kind are eminently suitable for demonstrating ionization phenomena.

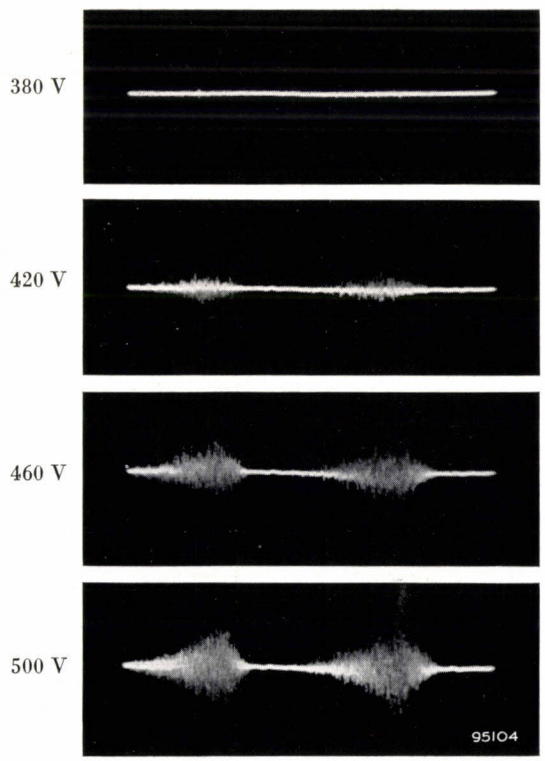

Fig. 10. Oscillograms obtained with the circuit of fig. 9. With 380 V across C_x the first small ionization peaks become visible. As the voltage is raised, the amplitude and number of the peaks increase rapidly.

The total length of the traces shown corresponds to 1/50 sec. The capacitor under investigation had a capacitance of about 2.5 μF and a non-impregnated dielectric consisting of three layers of paper 8 μ thick.

By placing such a capacitor under a bell jar, connected to a vacuum pump, and making a small opening in the can, the potential at which ionization begins can be found at different air pressures. The results are shown in *fig. 11*, curve *1*. Like the curve representing Paschen's law (fig. 8), the curve found in this case shows a minimum; the numerical values, however, differ markedly from those with an arrangement of flat electrodes with only air between them.

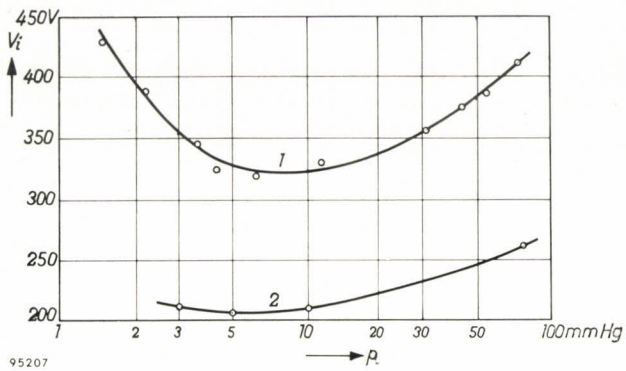

Fig. 11. Curve *1*: voltage V_i at which ionization begins (in the capacitor referred to in fig. 10) as a function of the air pressure p in the capacitor. Curve *2* was measured after the capacitor had been impregnated with a mineral oil (the impregnation being deliberately poor).

By properly impregnating the capacitor, one can make the ionization begin at a higher voltage than in a non-impregnated capacitor. A badly impregnated capacitor, on the other hand, can lead to ionization at a lower voltage, as low in fact as 200 V (fig. 11, curve *2*).

In practice capacitors are impregnated at a high temperature, and the can is sealed at about 80 °C. During cooling to room temperature the pressure in the can decreases as a result of shrinkage of the impregnating fluid. The amount by which the pressure decreases depends on the temperature difference and on constructional details, such as the degree of filling and the stiffness of the can. This explains the unexpected fact (cf. fig. 5) that capacitors which have a reasonably long life at 80 °C and higher, frequently have a very short life at low temperature: the reduced pressure arising at low temperature is conducive to the formation of cavities in the dielectric, which are filled with gas at this low pressure. Considerably more ionization then occurs than at

higher temperatures, with adverse consequences for the life of the capacitor [7]).

Some typical results of life tests are shown in *fig. 12*, which refer to capacitors of the same type as used for the tests of fig. 5. These capacitors, which

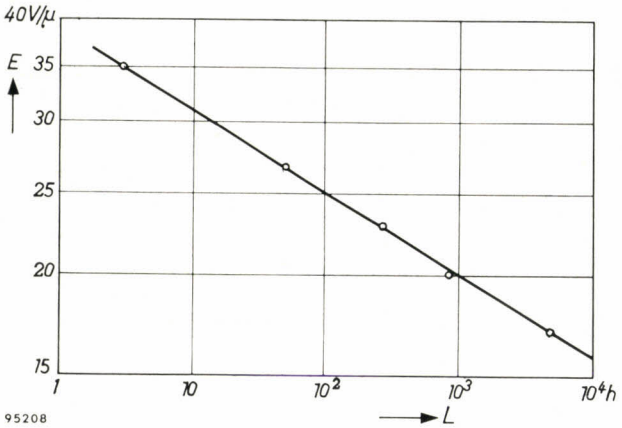

Fig. 12. Field strength E at which capacitors (of the same type as in fig. 5) reach a life L at an ambient temperature of about 25 °C. Each point represents the average of at least 20 individually-tested capacitors.

exhibit fairly heavy ionization, were tested at room temperature at different field strengths. The life is found to be inversely proportional to the tenth power of the field strength. Only at field strengths smaller than about 7 V/μ can the line be expected to level off towards longer life values, because with fields of this order it was no longer possible to detect any ionization.

According to fig. 5 it was to be expected that at 17.5 V/μ and room temperature the life of a capacitor would be far in excess of 10^5 hours (12 years). It can be seen from fig. 12, however, that, owing to ionization, the life is in fact only about 4400 hours.

Tests at periodically varying temperatures

Capacitors for the ballasts of gas-discharge lamps are normally intended to operate at voltages varying from 200 to 600 V. At these voltages the possibility of ionization must always be taken into account. A life test should therefore be carried out at the most unfavourable, i.e. the lowest, operating temperature that can occur. On the other hand, one must also reckon with the highest ambient temperature likely to be encountered. In this case, it is true, there will be less ionization or even none at all, but against this is the fact that the dielectric may deteriorate at high temperature and there is a possibility that thermal instability will set in.

[7]) In the case of high-power capacitors this can be avoided by mounting the capacitor elements in a steel cylinder. After evacuation and impregnation the cylinder is filled with a gas under high pressure (see article [4])). This method is not suitable for low-power capacitors.

A satisfactory method of limiting the number of tests while still making full allowance for the various influences is to vary the temperature periodically. The procedure is as follows. The capacitors to be tested are placed in an oven and the capacitors and the oven are switched on simultaneously. Owing to the dielectric losses and the rising temperature of the oven the capacitors get hot, in a manner corresponding to practical conditions. Some time after temperature equilibrium has been reached, for example after 4 hours, the oven as well as the capacitors are switched off. Since the oven cools much more slowly than a capacitor under practical conditions, a fan is switched on at the same moment in order to accelerate the cooling. The oven and the capacitors are subsequently switched on again, and the process is repeated. A photograph of the apparatus is shown in *fig. 13*. The equipment is suitable for examining capacitors that are intended for indoor lighting installations, and which are therefore not exposed to particularly low temperatures. The upper limit of the alternating oven-temperature can be fixed to correspond to the highest ambient temperature to

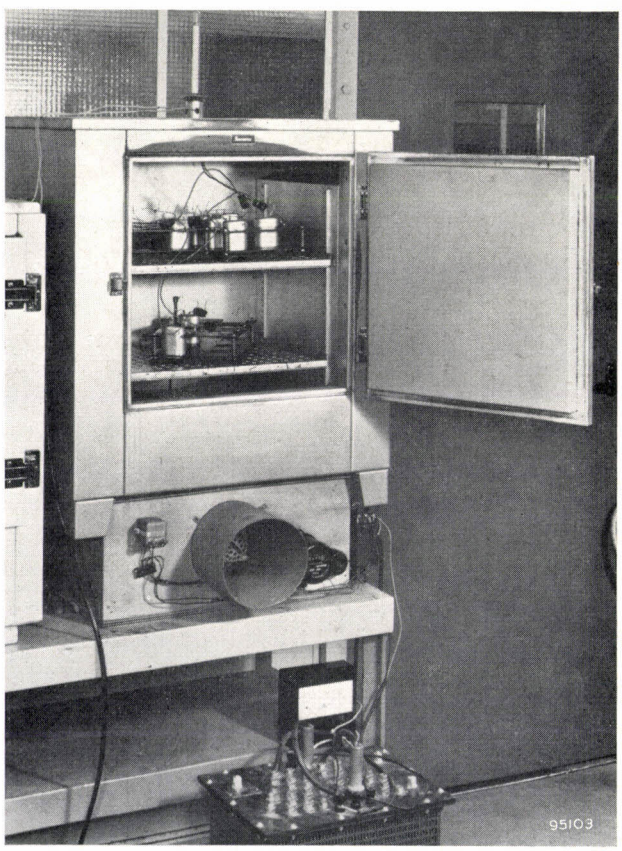

Fig. 13. Apparatus for performing life tests with periodically varying ambient temperature. The capacitors are arranged on racks to ensure that their mutual spacing remains the same in every test. A fan (under the oven) blows air at about 20 °C through the oven during the cooling process.

which the capacitors are likely to be exposed in actual operation (account being taken of the heating effect of lamps and chokes or transformers in the lamp fitting).

Capacitors intended for outdoor installations, for example for road lighting, must also be able to withstand temperatures as low as —20 °C. In this case the lower limit of the temperature range is obtained with a refrigerating system.

To shorten the duration of the test the field strength can be boosted to a value higher than the maximum permissible value under operating conditions. The test can be carried out at several values of field strength, and the life at the normal field strength predicted by extrapolating the results. An example is given in *fig. 14*. This relates to capacitors of the same type as those of fig. 12. They were loaded under electric fields of various values, at temperatures varying from 20 to 80 °C. The points found lie almost on a straight line which runs approximately parallel to the line shown in fig. 12, but is displaced somewhat towards longer life values. This is quite understandable, for condensers of the type in question are most heavily loaded at low temperature. In the test this happens for only a part of the time; the higher temperature prevailing during the remainder of the test caused little damage in this case, so that a longer life was found than would have been the case at a constantly low temperature.

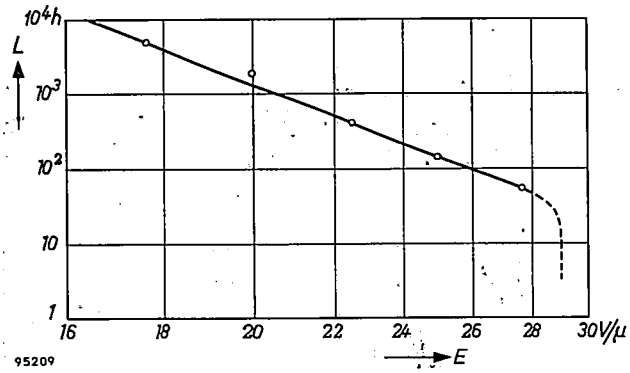

Fig. 14. Life L of capacitors (the same type as in figs. 5 and 12) in an alternating-temperature test as a function of field strength E. The temperature limits were 20 and 80 °C. Each point represents the average for 18 capacitors.
At $E \approx 29$ V/μ the capacitors enter into the unstable region during the warm part of the cycle. At this point the life curve may therefore be expected to bend over to very short life values.

High-voltage breakdown tests

The high-voltage test is a familiar and quick method of examining capacitors, and one which is found in many inspection specifications. The test is sometimes carried out with direct voltage, sometimes with alternating voltage.

In the first case only the breakdown potential is determined, or at least whether this voltage is higher than a specific value. It provides no information whatsoever on the much more important properties of the dielectric, such as the power factor, the likelihood of ionization and the dependence of the aging of the dielectric on temperature.

The test with alternating voltage seems to be more useful in that dielectric losses and ionization are not entirely neglected. During the short duration of the test, however (usually one minute), the capacitor does not become hot enough to allow thermal instability, which is almost certainly present, to be detected. Nor does the ionization have any opportunity to cause perceptible damage.

Neither of these tests, therefore, discloses more than the capacitor's ability to withstand peak voltages of short duration (and the same applies to the surge-voltage tests specified in some countries). Nothing can be concluded from these about the life of the capacitor under practical conditions. It is a simple matter, for example, to make a capacitor capable of withstanding a high test voltage but which, in actual operation, will not have a long life. All that is necessary for this purpose is to build up the dielectric from, say, four layers of paper 7.5 μ thick, and to choose a type of paper and impregnating agent having high losses which rise steeply with temperature. Because of the division into four layers there is very little chance that weak spots in the paper will overlap. It is therefore readily possible to attain a breakdown voltage of 6000 V, which is 15 times the value of a reasonable operating voltage for a dielectric with a total thickness of 30 μ. At quite a low ambient temperature, however, the capacitor will no longer be thermally stable. If one modifies the design by taking two layers of paper 15 μ thick, the breakdown voltage will drop to about 3000 V, but if the paper and impregnating agent are of good quality one will now have a capacitor with much greater thermal stability and a longer life.

In order, therefore, to properly assess the life of capacitors it is necessary to subject them to life tests under conditions of reasonable field strength overload — e.g. not exceeding 1.5 to 2 times the normal field strength — and to vary the temperature periodically between limits equal to those which will be encountered in practice.

If capacitors for lamp ballasts are developed and tested in this way, their life will not be inferior to that of transformers and chokes. The view still

widely held that the capacitor is the weakest link in the chain may once have been justified, but nowadays it need by no means be so.

Summary. In ballasts for gas-discharge lamps capacitors are often used with the object, among other things, of improving the power factor. The life of these condensers depends not only on temperature (as in the case of transformers and chokes) but also on the field strength.

Associated with the fact that the dielectric losses increase sharply with temperature is the danger of thermal instability: if the ambient temperature exceeds a certain critical value (the stability limit) a stable temperature state is no longer attained and the capacitor soons breaks down.

The higher the ambient temperature the quicker the dielectric's reserve of insulation is exhausted — analogous to what is found with the insulation of transformers. This suggests that the capacitor should have an extremely long useful life at low ambient temperature. However, the lower pressure obtaining in sealed capacitor cans increases the chance of gas bubbles forming in the dielectric and of ionization occurring in these bubbles. This ionization causes the dielectric to age very rapidly. The author discusses a method of demonstrating the presence of ionization.

The familiar high-voltage breakdown test merely discloses whether the breakdown potential exceeds a certain value, and provides no information on the expected life of the capacitor. An efficient method of life testing is to load the capacitors with a field strength 1.5 to 2 times higher than normal, while at the same time periodically varying the ambient temperature between the extreme values to which the capacitors might be exposed in actual operation.

ANNEALING TELEVISION PICTURE-TUBE BULBS

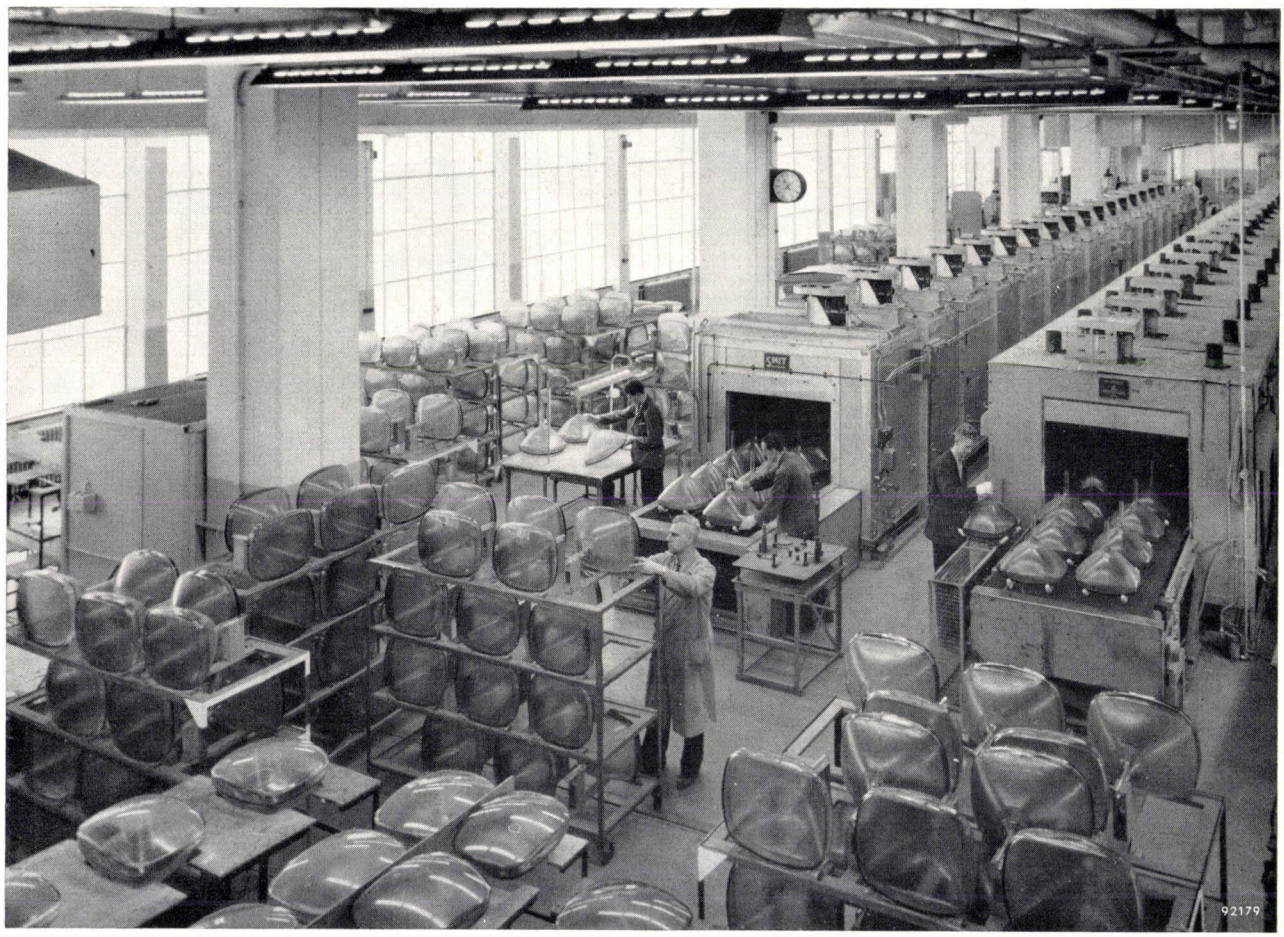

The bulb of a television picture-tube is made up of three parts: the conical body, the cylindrical neck and the window. When these parts are fused together, stresses are set up in the glass. To relieve these stresses the bulbs are placed on a conveyer belt which passes them through a tunnel annealing oven. The above photograph, taken in the new television tube factory in Eindhoven, shows this process in operation.

A SIMPLE AND COMPACT ARRANGEMENT FOR MEASURING THE β-ACTIVITY OF WEAK RADIOACTIVE SAMPLES

621.387.4:539.16.08

In recent years greatly increased importance has been attached to the measurement of very weak radiations, particularly in connection with the radioactive contamination of the atmosphere, rainwater, foodstuffs and the waste water from medical, radiochemical and nuclear-physics laboratories. For all such purposes, detectors are required that combine extreme sensitivity with the utmost reliability.

In the majority of cases the aim is to monitor the beta activity, for example of the hazardous isotope Sr^{90}. The Geiger counter tube with end-window, such as the Philips types 18505 and 18506, is still the most commonly used beta detector, because of its high sensitivity to beta rays, its great stability, and the simplicity of the auxiliary equipment [1]).

Among the most important factors governing the lower limit of detection are the *background counts* of the detector. The background count is the number of discharges in the tube per unit time caused by any agency other than that which is to be detected. They are caused, *inter alia*, by:

1) gamma radiation originating from the surroundings, e.g. from neighbouring radioactive preparations, natural radioactivity of building materials (in which the isotope K^{40}, for instance, is often present), or from the air (which may carry radon or disintegration products of radon);
2) mesons of cosmic radiation;
3) beta and gamma radiation originating from impurities in the materials of which the counter tube is made.

The interference from neighbouring gamma radiation can be eliminated by shielding. Obviously, the shielding materials must themselves contain no radioactive impurities, particularly that part of the shielding in the immediate vicinity of the counter tube. Lead has generally too much radioactive contamination for the purpose. Iron is more satisfactory, but best of all is mercury, because it can readily be purified. Reasonable shielding is possible with a mercury shield of, say, 3 cm thickness, enclosed in a 15 cm thick iron shield; the mercury then absorbs the radiation from the radioactive impurities in the iron.

Owing to the very great penetrating power of mesons, other means must be sought of overcoming this source of error. Hitherto it has been customary to surround the counter tube with a number of *guard counters*, which are so disposed that every meson triggering the central counter necessarily triggers one or more guard counters also. The circuit operates on the anti-coincidence principle, that is to say a count from the central tube is recorded only when none of the guard counters are simultaneously triggered.

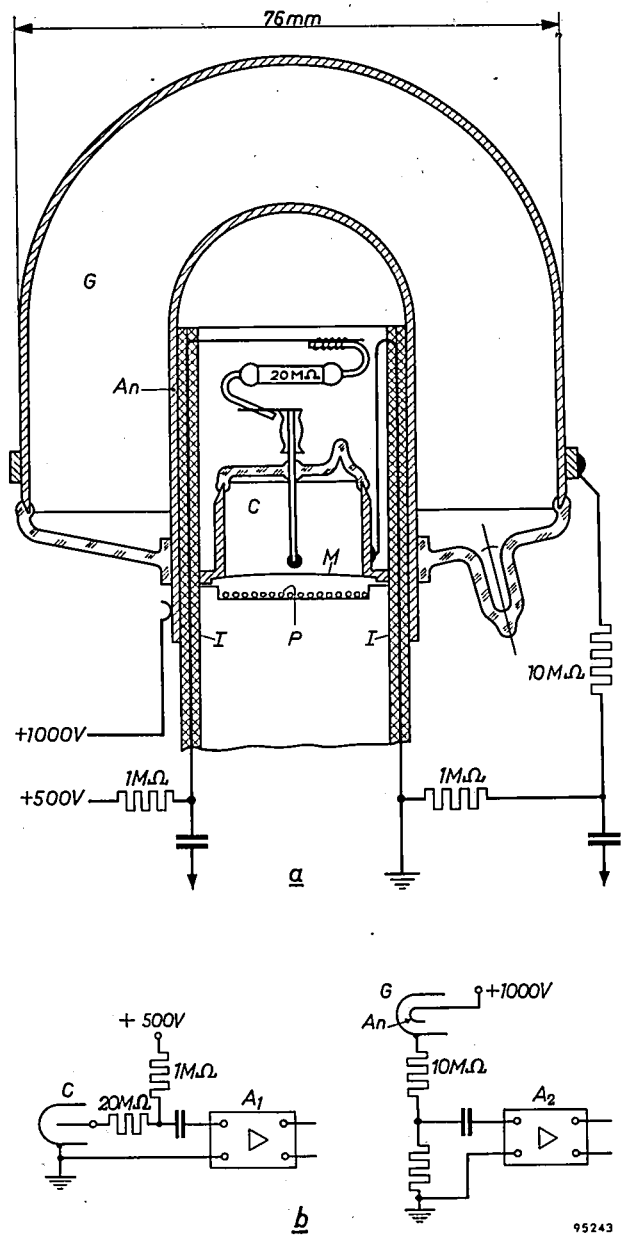

Fig. 1. *a*) Cross-section and *b*) circuit of a guard counter *G* with hollow anode *An*, in which is situated the central beta counter *C* (with mica window *M*). *I* insulation. *P* radioactive sample. A_1 and A_2 amplifiers.

[1]) See N. Warmoltz, Geiger-Müller counters, Philips tech. Rev. 13, 282-292, 1951/52.

N.V. PHILIPS' GLOEILAMPENFABRIEKEN

Such an arrangement, consisting of 10 to 15 counter tubes, is naturally fairly voluminous. If it is surrounded by a 3 cm shield of mercury plus a 15 cm shield of iron to screen it from gamma radiation, the aggregate equipment weighs something like 2000 kg, which is too cumbersome in many cases.

Fig. 1 illustrates an arrangement of counter tubes using a new type of guard counter. The two electrodes of the guard counter are concentric hemispheres to which coaxial cylinders are connected. The beta counter fits inside the hollow anode of the guard counter. With this arrangement no meson can actuate the inner counter tube without at the same time actuating the exterior counter. In its operation this tube is similar in many respects to the counter tubes described in an earlier publication by the Philips laboratory, Amsterdam [3]). The complete monitoring equipment is shown in *fig. 2* [4]).

The fact of there only being one guard counter offers the following advantages:

1) the smaller size entails a great saving in the weight of the shielding (a saving of more than 1000 kg),
2) the layout and supervision of the equipment are greatly simplified, and
3) the electronic apparatus is simpler.

The central counter tube in fig. 1 is a modified experimental version of type 18505. The main differences are:

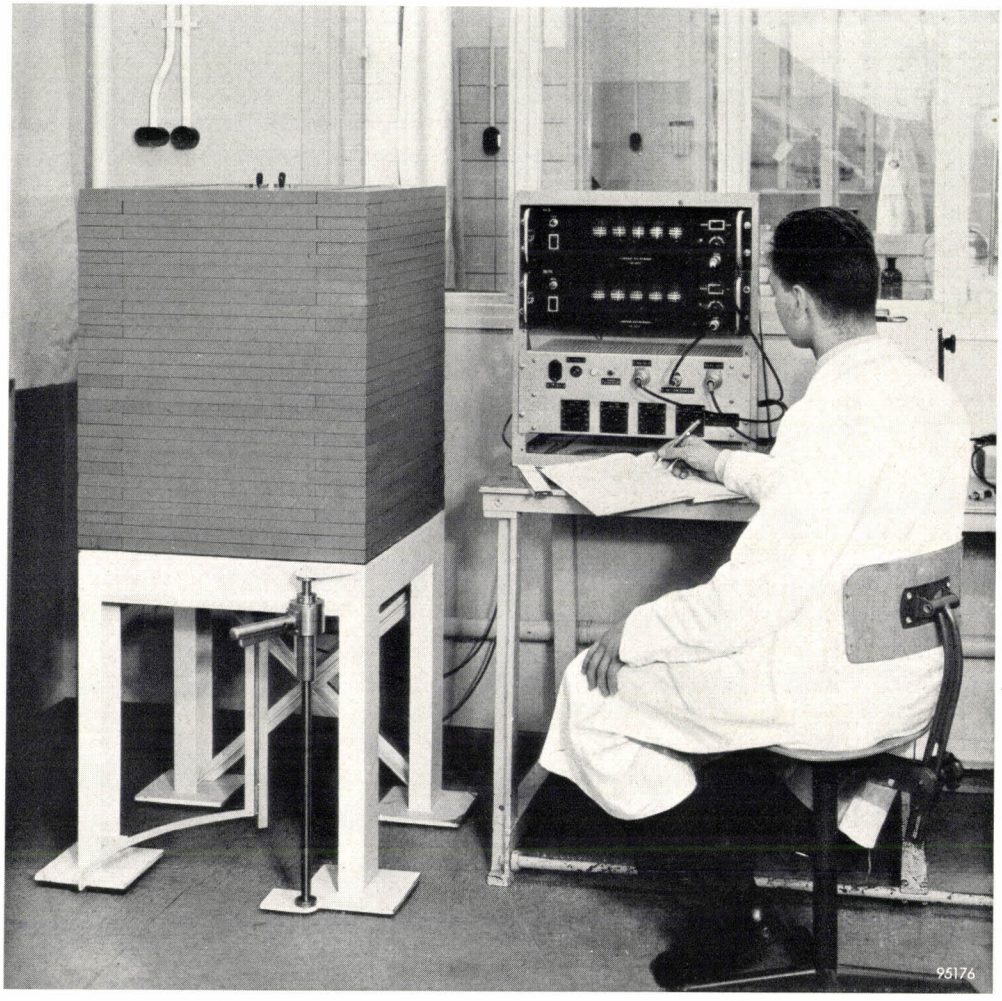

Fig. 2. Complete equipment for measuring weak beta activity. Left, gamma-ray shielding, consisting of 20 cm thick iron blocks surrounding a 2.5 cm thick shield of mercury. The latter surrounds an arrangement of a counter tube and guard counter as illustrated in fig. 1. Right, the amplifiers in an anti-coincidence arrangement, on top of which are mounted two scalers, each composed of five decimal counter tubes type E1T [2]). The number of counts before and after meson correction can be read directly from the tubes in the front panel.

[2]) Philips tech. Rev. **14**, 313, 1952/53.

[3]) J. Hermsen, A. M. J. Jaspers, P. Kraayeveld and K. van Duuren, New Geiger tube designs, hollow anode and parallel plate counters, Proc. International conference on the peaceful uses of atomic energy, Geneva 1955 (published by United Nations, New York 1956), part 14, pages 275-276.

[4]) A more detailed description of this measuring arrangement was given by K. van Duuren, W. K. Hofker and J. Hermsen at the 1958 Geneva Conference (to be published as contribution P. 2343 in the Proceedings of this conference).

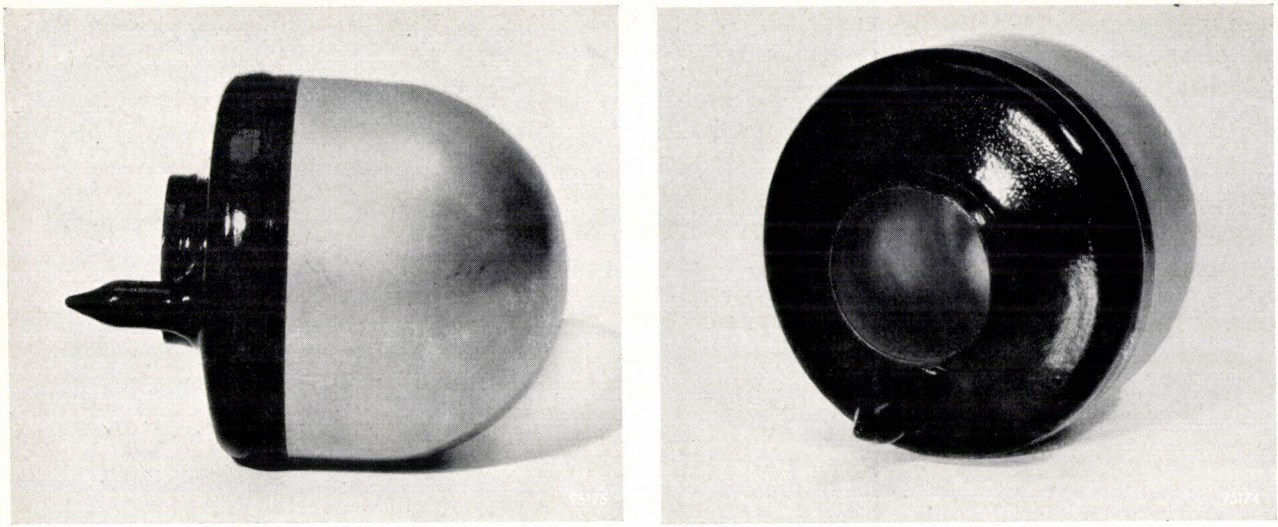

Fig. 3. Guard counter as in fig. 1.

a) the length has been cut down to 1/3 of the original length, to reduce the tube's sensitivity to gamma radiation;
b) the materials used have been carefully chosen to keep the contribution made by the tube wall to the background counts as low as possible.

In a particular case the background counts of the counter tube inside the guard counter were reduced to 0.7 per minute, as compared with the 20 background counts recorded in the same laboratory with a normal counter tube, type 18505, having the same sensitivity to beta rays but without shielding.

Photographs of the guard counter tube are shown in *fig. 3*.

K. van DUUREN *).

*) Philips laboratory (Synchrocyclotron), Amsterdam.

ABSTRACTS OF RECENT SCIENTIFIC PUBLICATIONS BY THE STAFF OF N.V. PHILIPS' GLOEILAMPENFABRIEKEN

Reprints of these papers not marked with an asterisk * can be obtained free of charge upon application to the Philips Research Laboratory, Eindhoven, Netherlands.

2568*: H. Bremmer: Comparaison des fluctuations de l'amplitude et de la phase des champs engendrés par diffusion (champs de turbulence) (Onde électr. **37**, 498-500, May 1957; in French).

This article deals with the statistical theory of fading phenomena, in particular with respect to the propagation by scattering of microwaves. The fading occurring at large distances (far beyond the horizon) is compared with that within the horizon. In both these cases special attention is paid to the difference in fading rate for the amplitude and that for the phase. These two fading rates differ at large distances; for short-distance scattering they are equal as far as the approximations used here are concerned.

2569*: N. Warmoltz and H. A. M. de Grefte: Spectromètre de masse pour détection des fuites, fonctionnant avec un mélange à faible teneur en hélium (Le Vide **12**, 202-207, 1957, No. 69; in French).

A mass spectrometer leak detector of the Nier type with a radius of curvature of 5 cm is described using an electron multiplier for measuring the ion current. In this manner the sensitivity is increased so far that one can use as probe gas for leak testing a mixture containing only 1% of helium. The apparatus can also be used as an analyser for masses up to about 50.

2570: J. P. M. Gieles: The measurement of group delay in triode amplifiers at 4000 Mc/s (Onde électr. **37**, 781-788, October 1957).

In microwave repeaters for long distance links using frequency modulation, not only the amplitude characteristic but also the phase characteristic is extremely important. The latter can be described in terms of the group delay, which should be as constant as possible over the transmission band

desired. The total delay variation admissible for colour television could perhaps be as low as 50 mμs. For direct UHF links equipped with EC 56, this results in a variation of less than 0.1 mμs per stage if the distortion is cumulative, so that a very high accuracy in the measurement of the group delay is necessary. Measurements are performed in a closed loop that is made to oscillate by the amplifier under test. The loop also contains a precision phase shifter. A simple formula can be derived, expressing the total group delay of the loop in terms of the frequency shift resulting from an introduced phase shift. The frequency shift can be measured very accurately by a beat-tone procedure. The results have an accuracy of about 0.1 mμs and indicate that the triode is indeed capable of fulfilling the severe requirements. Finally, some remarks are made concerning level to phase conversion.

2571: J. Links, J. E. Rombouts and P. Keulen: The "bulging factor", a fungistatic antibiotic produced by a streptomyces strain, with evidence of an active water-excreting mechanism in fungi (J. gen. Microbiol. **17**, 596-601, 1957, No. 3).

The "bulging factor", a new antibiotic with a chemical nature related to streptothricin, is produced by a Streptomyces strain and was isolated as reineckate and picrate. A study on its mode of action resulted in the development of a plate technique for assaying bulging factor activity. Evidence is presented in support of a theory about the existence of an active water-excreting mechanism in fungi susceptible to the bulging factor.

2572*: G. Ahsmann: On the impedance of the anode-fall region of a glow discharge in the noble gases (Rendiconti Terzo Congresso internazionale sui fenomeni d'ionizzazione nei gas, Venice 11-15 June 1957, Fondazione "Giorgio Cini", Società Italiana di Fisica, Milan 1957, pp. 19-25).

The complex impedance of glow discharges was measured in a discharge tube fitted with adjustable electrodes. As the electrode distance is increased the impedance is initially independent of the distance; however when the distance is so great that an anode fall begins to develop, the impedance in a given frequency region increases rapidly. The cause of this increase lies in the anode fall layer and in the Faraday dark space. An equivalent circuit is given for the anode region of the discharge when an anode fall is present.

2572a*: J. A. Kok: Mechanism and properties of various types of electrical discharges in gas-filled triodes (Rendiconti Terzo Congresso internazionale sui fenomeni d'ionizzazione nei gas, Venice 11-15 June 1957, Fondazione "Giorgio Cini", Società Italiana di Fisica, Milan 1957, pp. 548-557).

A report on the work described here has also appeared in Appl. sci. Res. **B5**, 445-553, 1956 and **B6**, 207-221, 1956; see these abstracts Nos. **2368** and **2445**.

2572b*: W. Verwey: Probe measurement of electron temperature in the positive column of a rare-gas discharge and correlation with microwave noise (Rendiconti Terzo Congresso internazionale sui fenomeni d'ionizzazione nei gas, Venice 11-15 June 1957, Fondazione "Giorgio Cini", Società Italiana di Fisica, Milan 1957, pp. 1115-1130).

The Langmuir probe is a very useful tool for the determination of electron temperatures in the positive column of gas discharges. Its reliability however, is subject to some doubt, especially at high current densities and comparatively high gas pressures. This article describes measurements with the probe on rare-gas discharge tubes at pressure up to 20 mm Hg, and for current densities of 0.04 A/cm². These tubes were developed as standard noise sources for the cm waveband. The electron temperatures measured with the probe are found to be in good agreement with those determined from noise measurements. In the probe measurements special attention was paid to the effect of the work function of the probe material.

2572c*: N. Warmoltz and H. J. J. van Boort: A flash tube for colour photography of the human retina (Rendiconti Terzo Congresso internazionale sui fenomeni d'ionizzazione nei gas, Venice 11-15 June 1957, Fondazione "Giorgio Cini", Società Italiana di Fisica, Milan 1957, pp. 1131-1134).

Short description of a method of making colour photographs of the human retina for diagnostic purposes. A special electronic flash tube has been developed that has a very high brightness (peak value $\sim 1.5 \times 10^6$ cd/cm² (9× brighter than the sun) and a flash duration of 3.5 msec. With this very short exposure (which is sufficient because of the high brightness) sharper photographs are possible than with the usual carbon arc. A 6000 μF condensor charged to 500 V dissipates an energy of 750 joules in the lamp. See also Philips tech. Rev. **15**, 342-346, 1953/54.

2573: J. Smit: The spontaneous Hall effect in ferromagnetics, II (Physica **24**, 39-51, 1958, No. 1).

It is shown that the spontaneous part of the Hall effect arising from the spontaneous magnetization is caused by skew scattering of the magnetized conduction electrons (in this case the 3d-electrons) due to their transverse polarization induced by spin-orbit interaction, which acts as an impact parameter in the collision process. The problem could be approximately solved for scattering on an impurity atom by converting it into that of the scattering on a vortex-like perturbing centre. The order of magnitude of the calculated Hall angle agrees with the experimental one ($\approx 10^{-2}$). It is shown quite generally that for lattice vibration scattering the Hall effect should be proportional to the square of the resistivity, as has been found experimentally for pure iron and nickel.

2574: U. Enz: Time-dependent constricted hysteresis loops in a single crystal of manganese ferrous ferrite (Physica **24**, 68-70, 1958, No. 1).

The time-dependence of the initial permeability (i.e. disaccommodation) is measured on a single-crystal toroid of manganese ferrous ferrite. This effect is as high as 95% of the value immediately after demagnetization of the ring. It is shown that disaccommodation is a time-dependent blocking of domain walls. The blocked walls cause constricted minor hysteresis loops, characterized by a critical magnetic field which is necessary to overcome the blocking force. The constriction is time-dependent.

A 2: E. Kauer and A. Rabenau: Über den Bandabstand von Galliumnitrid und Aluminiumnitrid (Z. Naturf. **12a**, 942-943, 1957, No. 11). (On the band structure of gallium nitride and aluminium nitride; in German.)

Note on the determination of the energy difference between the conduction band and the valency band in polycrystalline gallium nitride and aluminium nitride, by means of measurements of the diffuse reflection as a function of the wavelength of the incident radiation. The (room-temperature) values found are: for gallium nitride 3.2 eV and for aluminium nitride >5 eV.

A 3: A. Rabenau and P. Eckerlin: Die K_2NiF_4-Struktur beim La_2NiO_4 (Acta cryst. **11**, 304-306, 1958, No. 4). (The K_2NiF_4 structure in La_2NiO_4; in German.)

Report of an X-ray diffraction investigation into the structure of La_2NiO_4 using Debye-Scherrer photographs and Cu Kα radiation. It is found that La_2NiO_4 has a structure related to the perovskite structure already found in K_2NiF_4 and studied by Balz and Plieth. The lattice constants of the tetragonal La_2NiO_4 were found to be: $a = 3.855 \pm 0.001$ Å and $c = 12.652 \pm 0.003$ Å. The K_2NiF_4 structure is also exhibited in La_2CoO_4, but here it was orthorhombically deformed. The lattice constants are: $a = 5.539$ Å, $b = 12.66$ Å, $c = 5.482$ Å.

A 4: K. Jost and G. Schiefer: Die Auswertung von Vierpol- und Materialmessungen mit dem logarithmischen Leitungsdiagramm (Archiv elektr. Übertragung **12**, 295-300, 1958, No. 7). (The analysis and evaluation of 4-pole and material measurements with the aid of the logarithmic transmission-line chart; in German.)

A method is described that allows the quadripole parameters, and in particular the material constants μ, ε, tan δ_μ and tan δ_ε to be measured with the aid of a coaxial slotted line. The numerical evaluation is greatly simplified by the adoption of a logarithmic transmission-line chart whose curves of constant VSWR and constant node displacement l/λ simultaneously represent curves of the function $\ln \tanh (a + jb)$ for constant a and b.

R 339: S. Duinker: General properties of frequency-converting networks (Philips Res. Repts. **13**, 101-148, 1958, No. 2).

Continuation of **R 337**.

R 340: H. L. Spier and W. L. Wanmaker: Influence of additives on particle size of tungsten powder prepared by reduction with hydrogen from tungsten trioxide (Philips Res. Repts. **13**, 149-156, 1958, No. 2).

An investigation is carried out into the reduction with hydrogen of tungstic acid and tungsten trioxide doped with various additives. It is shown that the addition of potassium silicate and potassium silicotungstate results in a marked growth of the tungsten particles, while other additives as calcium nitrate or magnesium sulphate tend to give a small particle size. From the behaviour of the pure potassium silicotungstates during reduction, an explanation of the observed phenomena is proposed.

R 341: W. van Gool: Fluorescence and photoconduction of silver-activated cadmium sulphide (Philips Res. Repts. **13**, 157-166, 1958, No. 2).

Several Ag-activated CdS phosphors are described, with Ga or Cl as coactivator. The fluorescence at low temperature shows two bands with maxima at

6200 Å and 7300 Å. High Ag concentration and low coactivator concentration promote the short-wave emission. Phosphors with equal concentrations of activator and coactivator show only the long-wave emission. Optimal photoconduction and low dark-current are only found with an activator-coactivator ratio slightly greater than unity. A series of mixed crystals (Zn,Cd)S activated with Ag shows clearly the relation between 6200 Å emission in CdS and a 3880 Å emission in ZnS and also between the 7300 Å band in CdS and the normal blue Ag band at 4350 Å in ZnS. The behaviour of the Ag bands in CdS is quite similar to those of Cu in ZnS. These results show that the conclusions drawn by Lambe and Klick regarding the position of the impurity level responsible for the 6200 Å Ag emission in CdS cannot be applied to the normal blue Ag emission in ZnS-Ag. These results led to an improvement of the properties of a red colour-television phosphor.

R 342: J. Bloem: Discussion of some optical and electrical properties of Cu_2O (Philips Res. Repts. **13**, 167-193, 1958, No. 2).

From known optical and electrical data on Cu_2O a band scheme is constructed for this semiconductor. The equilibria between the solid constituents and a vapour containing oxygen are calculated. From these data the conductivity and the concentrations of the various defect centres can be evaluated for Cu_2O at high temperatures in equilibrium with an applied partial pressure of oxygen. The results are shown to be in good agreement with experiment. The optical and electrical properties after quenching, however, do not correspond to the model mentioned above. If association between defects is considered during the cooling process, the optical properties can be explained. As to the Hall-effect data, the occurrence of chemisorption of oxygen during quenching must also be taken into account, especially if well-conducting surface layers are formed, which appears to be the case at the lower oxygen pressures preferently, whereas at high oxygen pressures conduction through the bulk of the crystallites prevails. The intermediate region of mixed conduction is characterized by a very low effective mobility.

R 343: K. M. Adams: On the synthesis of three-terminal networks composed of two kinds of elements (Philips Res. Repts. **13**, 201-264, 1958, No. 3).

In this thesis (Delft, 1957) the synthesis of series-parallel LC three-terminal networks is investigated. A set of necessary and sufficient conditions and a method of realization of all sets of series-parallel LC three-terminal network functions from the zeroth to the sixth degree are given. Some of these conditions are essentially new, that is, independent of any previously derived conditions. They are necessary for the synthesis of series-parallel LC three-terminal networks, but it is not known whether they are also necessary for the synthesis of three-terminal networks of arbitrary structure. In principle, it is possible to apply the method to functions of higher degree than the sixth, but the amount of computation required increases in general very rapidly with the degree.

R 344: W. Ch. van Geel, C. A. Pistorius and P. Winkel: Photo effects with anodic oxide layers on tantalum and aluminium (Philips Res. Repts. **13**, 265-276, 1958, No. 3).

This article deals with the photoelectric properties of the system $Ta\text{-}Ta_2O_5$-electrolyte during irradiation with ultraviolet light. The electrolyte has also been replaced by a transparent layer of a metal or a semi-conductor. When the system is short-circuited, a photo-current (i_0) is produced which is proportional to the intensity of irradiation. With a high external resistance a photo-e.m.f. V appears which shows considerable inertia as a function of the time t and which can be written as $V = V_{max}(1-e^{-kt})$. It appears that k is proportional to the intensity of irradiation. The value of k decreases with increasing thickness d of the layer. After correcting for this change of k, which is probably due to absorption, we find that $i_0 d =$ constant. An attempt is made to explain the observed phenomena by assuming that the work function $Ta\text{-}Ta_2O_5$ is smaller than the work function electrolyte-Ta_2O_5.

R 345: P. Winkel, C. A. Pistorius and W. Ch. van Geel: On the relation between current and field during anodic oxidation (Philips Res. Repts. **13**, 277-295, 1958, No. 3).

Starting from the assumption that an anodic oxide layer on metals like Al and Ta has an amorphous structure, a relation between field and current during anodic oxidation is derived. It appears that this relation is somewhat different from the exponential one usually derived in literature (Verwey, Mott). With the new relation, it is possible to explain the various results obtained with the experiments presented in this paper. Probably it may explain the rather different numerical results mentioned in literature in the same way. The consequences of the amorphous structure on a more detailed picture

of the oxidation process have also been calculated. The results point to a frequency dependence of one of the parameters as was actually observed in the experiments. The observed agreement between theory and experiments has made it possible to calculate approximately the parameters introduced in this theory.

R 346: C. Z. van Doorn: Quantum efficiency of *F*-centre fluorescence in KCl (Philips Res. Repts. **13**, 296-300, 1958, No. 3).

The quantum efficiency of *F*-centre fluorescence at 77 °K in X-ray and additively coloured KCl has been measured using an integrating sphere. Values of up to 91% have been found, depending on the concentration of *F* and *M* centres.

R 347: A. van Weel: Analysis of diode-detector circuits for signals with asymmetrical sidebands (Philips Res. Repts. **13**, 301-326, 1958, No. 4).

A theoretical analysis is given of a diode detector stage for a modulated signal with asymmetrical sidebands of which the carrier is detuned with respect to the resonance frequency of the I.F. circuit. The equivalent circuit is found to be a three-port consisting of the impedances for upper- and lower-sideband frequencies and video frequency in series. Measurements show different overall characteristics in the case of equal positive or negative detuning of the carrier frequency; this effect is caused by the asymmetrical shape of the diode-current peak.

R 348: K. F. Niessen: Non-magnetic ions in an antiferromagnetic (Philips Res. Repts. **13**, 327-334, 1958, No. 4).

An experimental method is described for determining the distribution of a relatively small number of foreign non-magnetic ions between the two sub-lattices of an antiferromagnetic, in which they replace the same number of original magnetic ions. The influence of the foreign ions on several measurable quantitites is investigated. This influence can be used to determine some specific constants of the antiferromagnetic. In the anisotropy energy besides the usual terms an interaction term between the two sub-lattices is taken into account. Use is made of the spontaneous magnetization, the parallel and perpendicular susceptibilities, the critical field strength and the antiferromagnetic resonance.

R 349: H. J. Oskam: Microwave investigation of disintegrating gaseous discharge plasmas (Philips Res. Repts. **13**, 335-400, 1958, No. 4).

The disappearance of electrons from an isothermal disintegrating gaseous discharge plasma is investigated both theoretically and experimentally by considering the shift of the resonance frequency of a microwave cavity enclosing the plasma. The first few sections discuss theoretically such items as (1) the complex conductivity of a plasma at high frequencies, (2) the influence of the various loss processes on the shape of the electron density – time curve, (3) the connection between the conductivity of the plasma and the properties of the cavity for various types of cavity. In measuring the frequency shift as a function of time, it proves to be necessary to limit the power of the probing signal (frequency $\approx$ 10000 Mc/s) to a few microwatts. The construction and preparation of the gas containers and the measurements are presented. The disappearance process of the electrons from the plasma in helium is found to be ambipolar diffusion even at a pressure of 25 mm Hg. The mobility of the He_2^+ ions in helium at standard density is $\mu_0(He_2^+) = 17.3 \pm 0.7$ cm/s per volt/cm. In the neon afterglow, however, the electrons disappear at a pressure of 20 mm Hg by dissociative recombination with Ne_2^+ ions ($\alpha \approx 2.5 \times 10^{-7}$ cm^3/s). An admixture of rare-gas atoms with a lower ionization potential than that of the main gas is found to have a great effect on the disappearance of the electrons. The afterglow is studied in the binary gas mixtures of helium with a small concentration of neon, argon, or krypton, and also in neon-argon and neon-krypton mixtures. Measurements in these mixtures all show the production of a considerable number of atomic ions of the admixture, even at very low concentrations of the latter. The process concerned in helium-neon is a charge-transfer process between a He_2^+ ion and a neon atom; the relevant cross-section is found to be $Q_{ce} \approx 1.5 \times 10^{-15}$ cm^2. In the other mixtures the atomic ions are produced by the Penning effect and possibly by the above type of charge-transfer process, which cannot be separated in the present experiment. In all gas mixtures the atomic ions are found to be converted into molecular ions by three-body collisions with an atom of the main gas and an atom of the admixture. The probability of this conversion process proves to depend strongly on the difference between the ionization potential of the main gas and that of the admixed atoms, and is found highest in helium-neon. Moreover, the measurements suggest the conversion of Ne^+ ions into $(HeNe)^+$ ions by a three-body collision with two helium atoms.

VOLUME 20, 1958/59, No. 7 pp. 177-208 Published 10th February 1959

Philips Technical Review

DEALING WITH TECHNICAL PROBLEMS
RELATING TO THE PRODUCTS, PROCESSES AND INVESTIGATIONS OF
THE PHILIPS INDUSTRIES

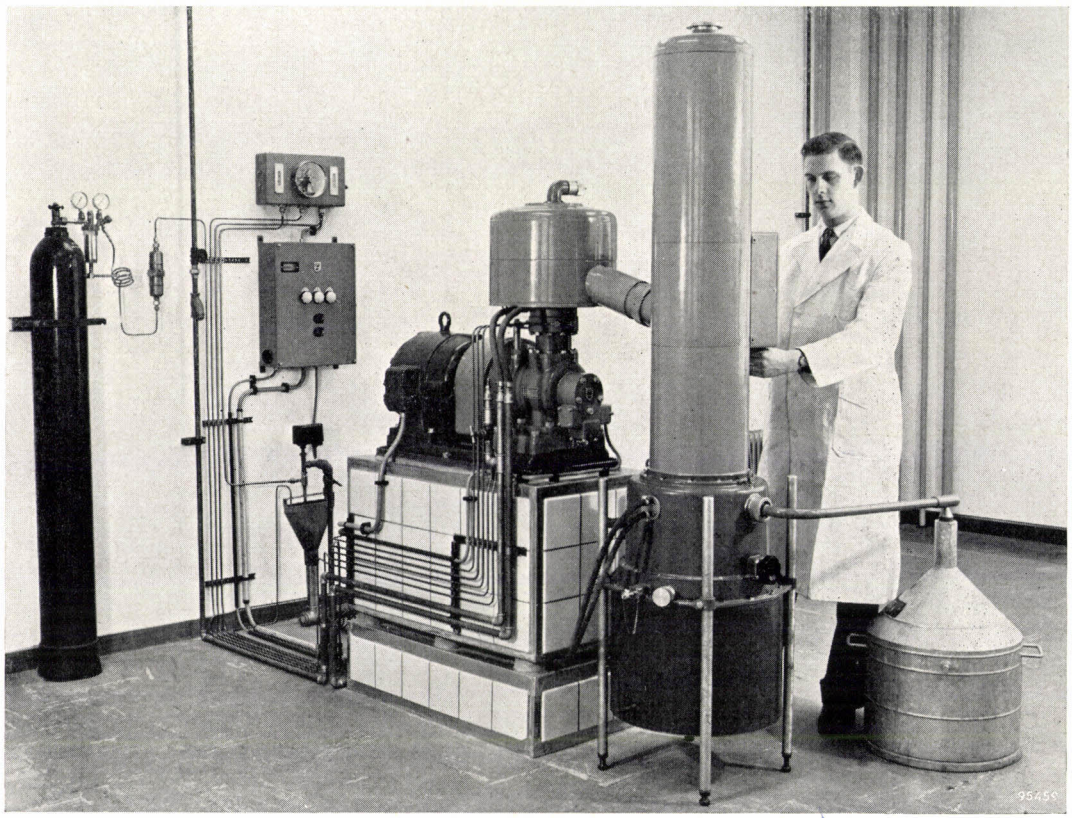

A SMALL AIR FRACTIONATING COLUMN USED WITH A GAS REFRIGERATING MACHINE FOR PRODUCING LIQUID NITROGEN

by J. van der STER and J. W. L. KÖHLER.

621.573.049.2:546.17-14

The advent of the gas refrigerating machine has made it possible to build a simple and economically working installation for producing pure liquid nitrogen from atmospheric air. The article below describes the operation and construction of such an installation which has been developed in the Philips laboratories, Eindhoven, and is now on the market.

Recent years have seen a marked increase in the use of liquid air and liquid nitrogen in laboratories and in industry. These extremely cold liquids, whose respective temperatures are about —194 °C and —196 °C, are used primarily for purposes of cooling. They find application, for example, in vacuum technique (absorption of residual gases at low temperature), in research on the properties of solids at low temperatures, for the shrink-fitting of precision components and for the "freezing-in" of a state of chemical equilibrium.

Moderate amounts of liquid air can be made

simply and cheaply with the gas refrigerating machine [1]). When working with liquid air, however, certain precautions are necessary, for it can be dangerous if brought into contact with inflammable substances. For this reason, and also when the temperature of a cooling bath is to be kept very constant, it is often preferable to use liquid nitrogen. Liquid nitrogen can, of course, be produced by condensing nitrogen from a cylinder with the aid of a gas refrigerating machine, but this calls for a regular and considerable supply of cylinders if continuous production is required.

The installation which is the subject of this article produces liquid nitrogen from atmospheric air. The installation, which is fully automatic, consists essentially of a gas refrigerating machine and a fractionating column, and delivers 4 to 5 litres of liquid nitrogen per hour. It differs from other air-fractionating plants in that it does not involve compression of the air. In consequence the installation is light and simple in design and moreover small.

Before describing the installation, we shall deal briefly with the physical principles of the separation of gases and consider the construction and operation of a fractionating column.

Separation of the components of the gas mixtures

Physical principles

If we determine, at constant pressure, the boiling point of some mixtures of, say, liquid oxygen and nitrogen, and the dew point of some vapour mixtures (i.e. the temperature at which condensation occurs upon cooling), we find that the boiling point of a given liquid mixture does not coincide with the dew point of a vapour mixture of the same composition; the dew point is always higher than the boiling point. In a phase diagram, showing temperature versus composition (T, x diagram, *fig. 1*), the dew points corresponding to the various compositions together form the *vapour curve* V and the boiling points the *liquid curve* L. At the extreme left and extreme right of the diagram, where the concentration of one of the components is 100%, the two curves meet at a point, the ordinate of which gives the boiling point of this compound.

It can be seen from the diagram that when a liquid and a vapour are in equilibrium, i.e. when they have the same pressure and temperature, the vapour in our example contains more nitrogen than the liquid (denoted in fig. 1, e.g. by points D and C). On the other hand, when a boiling liquid and a saturated vapour of the same composition are brought together (points B and A, respectively) the liquid, as already mentioned, is colder than the vapour. The vapour, then, will tend to condense

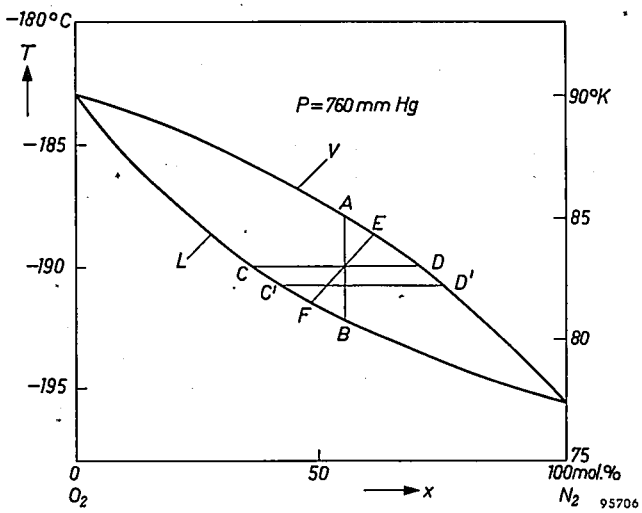

Fig. 1. Phase diagram for mixtures of oxygen and nitrogen under a pressure of 1 atm. The percentage of nitrogen is set out along the abscissa (x) and the temperature (T) on the ordinate. The curve V indicates the variation of the dew point, curve L the variation of the boiling point. The dew point of a vapour of a given composition is always higher than the boiling point of a liquid with the same composition. Starting from a quantity of boiling liquid and a quantity of *warmer* (saturated) vapour, a state of equilibrium is always reached (liquid and vapour temperatures equal) whereby the vapour is enriched in nitrogen and the liquid in oxygen.

on the surface of the liquid. The oxygen will show the greater tendency to do so, since pure oxygen condenses at a temperature 13 °C higher than pure nitrogen. The result is that, when equilibrium is reached, the vapour has become richer in nitrogen and the liquid richer in oxygen. The final state arrived at, for example either C and D or C' and D', depends on the relative proportions of liquid and vapour originally brought together. Similarly, a state of equilibrium, say C-D, can be reached starting from vapour and liquid mixtures of unequal composition, denoted for example by E and F.

Accordingly, when the system changes to a state of equilibrium from a non-equilibrium state in which the vapour is warmer than the liquid, the vapour always becomes richer in nitrogen and the liquid richer in oxygen. This phenomenon can be utilized for separating a mixture into its components. In practice a fractionating column is used for this purpose.

[1]) For a description of the principles and construction of the gas refrigerating machine, see J. W. L. Köhler and C. O. Jonkers, Philips tech. Rev. 16, 69-78 and 105-115, 1954/55.

Construction and operation of a fractionating column

A fractionating (or "rectifying") column is essentially a vertical tube containing a number of horizontal baffle plates and in which a certain temperature gradient is maintained (cold above and warm below). A stream of liquid flows from top to bottom and a vapour stream from bottom to top.

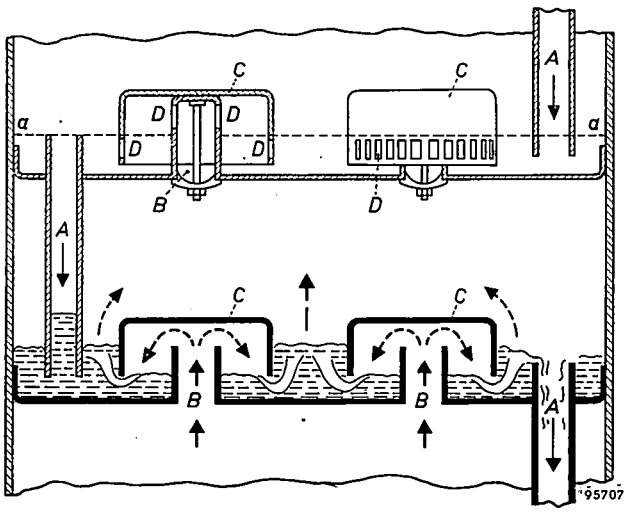

Fig. 2. Schematic representation of part of an air fractionating column, showing two baffle plates. The sketch of the upper plate gives an idea of the geometry and construction of one of the many possible forms; the lower sketch illustrates the passage of vapour and liquid through the plate. *A* overflow pipes, *B* vapour inlet, *C* bubble cap, *D* openings through which vapour passes, *a-a* level of liquid if no vapour should pass through.

Both streams pass the plates, which are designed to establish intimate contact between liquid and vapour. When they leave a plate, liquid and vapour are accordingly in equilibrium, whether or not they were so before arriving at the plate (*fig. 2*).

Fig. 3a represents schematically part of such a fractionating column. The dashed lines *p*, *q* and *r* are three plates. The arrows indicate the flow of liquid and vapour to and from the plates. Fig. 3*b* shows a phase diagram in which the points denoted by letters represent the composition and temperature of the liquid or vapour mixtures denoted by the same letters in fig. 3*a*. Since a temperature gradient prevails in the column, the liquid (*E*) flowing down to the plate *q* has a somewhat lower temperature than the vapour (*N*) that reaches this plate from below. Upon leaving the plate they are in equilibrium, i.e. in fig. 3*b* the points *E* and *N* have moved to *F* and *O*, respectively. The vapour continues upwards to plate *p*, where it is again enriched in the more volatile component (point *P*), while the liquid is enriched at plate *r* in the less volatile component (point *G*). Thus, as the vapour rises, the point on the vapour line in fig. 3*b* shifts increasingly towards the right. Finally it reaches approximately the point K_N, which means that at the top of the column the vapour consists almost entirely of the more volatile component.

The vapour mixture to be fractionated enters the column about half-way up, having been cooled beforehand to approximately the temperature prevailing at that position. It then undergoes the process described, whereby its components are separated. The more volatile component leaves the column at the top (the top product) and the other component (the bottom product) leaves at the base.

In small columns a filling of an appropriate packing material is often used instead of baffle plates. Like the plates, the packing is required to establish intimate contact between vapour and liquid; in other words, vapour and liquid must remain uniformly distributed over the surface of the packing, which should be large per unit volume. If large columns are filled with such packing, there is a tendency for the liquid to stream down one side, which adversely affects the column's efficiency. To avoid the latter phenomenon ,and for various other reasons, large columns are almost invariably equipped with plates.

In order to maintain the flow of liquid, part of the top product is condensed and returned to the column as "reflux". For the column to function properly, the ratio between the reflux and the fraction of the top product taken off must exceed a certain minimum value. We shall return to this subject presently. Similar considerations apply to the bottom product: part is tapped off and part ascends again as vapour.

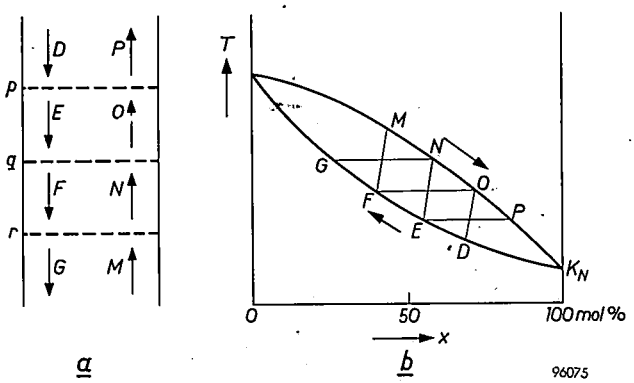

Fig. 3. Separation of a gas mixture. *a*) Schematic diagram of part of a fractionating column containing three plates (*p*, *q* and *r*). When a temperature gradient exists in the column (cold above, warm below), the descending liquid and the ascending vapour undergo a change in composition every time they pass a plate.
b) Phase diagram. The points denoted by capital letters represent the properties (T, x) of the vapour or liquid at the positions denoted by the same letters in fig. 3*a*. The liquid becomes increasingly richer in the less volatile component, and the vapour increasingly richer in the other ($x = 100\%$).

For the condensation of the top product it is clearly necessary to absorb the heat dissipated, while to evaporate the bottom product heat must be supplied. Given the mixture to be fractionated, i.e. given the temperatures prevailing at the top and bottom of the column, it is the designer's task to ensure that dissipation and supply of heat take place in the most economical manner. If the column temperature is above room temperature, as it is in the fractional distillation of crude oils, the cooling can usually be effected with mains water and the heating with steam. The problem is then simple. In the fractionation of air, which takes place at about —190 °C (the temperature must be —183 °C at the bottom of the column and —196 °C at the top) the way in which the requisite refrigeration and heat transfer are achieved governs the efficiency and simplicity of the installation.

The physics of this heat engineering problem may be further examined with the help of *fig. 4*. The figure represents schematically a fractionating column K, with a condenser T at the top, which produces the reflux, and a boiler B at the bottom, in which a part of the bottom product is vaporized to maintain the ascending vapour stream. The temperatures of condenser and boiler are respectively T_T and T_B, where $T_T < T_B$. The mixture enters the column at M, and its components, P_T and P_B, leave the column at T and B, respectively. To condense the reflux, it is necessary in the stationary state for a heat flow Q_T to leave the condenser, and in order to vaporize part of the bottom product a heat flow Q_B must be supplied to the boiler.

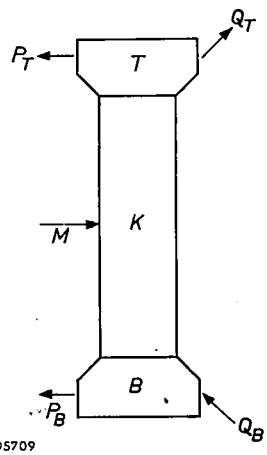

Fig. 4. Supply and withdrawal of heat in an air fractionating installation. K column, B reboiler, T condenser. The mixture to be fractionated enters at M. P_T top product (mol/sec), P_B bottom product (mol/sec), Q_B heat supplied to B (J/sec), Q_T heat withdrawn at T (J/sec).

If the air entering the column and P_T and P_B leaving it are all in the saturated gaseous state, then to a first approximation $Q_T = Q_B$. Thus, the fractionation of a gas mixture requires the existence of a heat flow only in the column itself, i.e. in that part of the installation shown in fig. 4. To maintain this heat flow, external plant is needed for conveying per second an amount of heat Q_T ($\approx Q_B$) from T to B, that is from a colder to a warmer point. Energy must of course be supplied to the plant for the purpose (second law of thermodynamics).

If the top product is to be tapped off in liquid form, the absorbtion of heat Q_T must be increased by the latent heat of condensation of the top product. Similarly, if the bottom product is to be tapped off in liquid form, the latent heat of condensation of P_B must be subtracted from the heat Q_B fed to B.

In air fractionating installations, ingenious but intricate methods of vapour condensation and liquid evaporation have hitherto been employed for supplying heat to B and withdrawing heat from T. The medium is the air itself or one of its fractionated components, and therefore the air must be compressed [2]).

Principle of the new installation for producing liquid nitrogen

With reference to *fig. 5* we shall now discuss the underlying principle of the new installation, the application of which first became possible with the advent of the gas refrigerating machine. Element A in the figure is the gas refrigeration machine, element B the fractionating column and element C a heat exchanger, which also serves as a water and CO_2 trap. Air (*1*) is fed into the system and liquid nitrogen (*2*) and gaseous (impure) oxygen (*3*) are extracted. The air feed is pre-cooled in the heat exchanger C by the oxygen exhausted from the column; it is also partly dried in C. By heat exchange with the liquid oxygen at the base of the column the air is further cooled and at the same time the residual water vapour and carbon dioxide are removed. The air then enters the fractionating column at a suitable point between top and bottom.

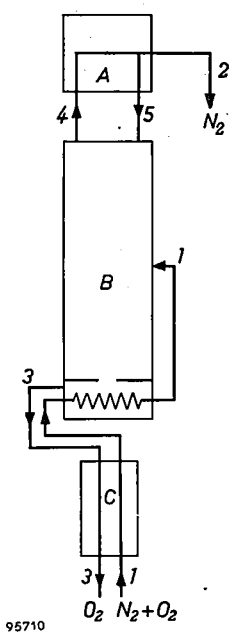

Fig. 5. Block-diagram of liquid-nitrogen installation. A gas refrigerating machine, B fractionating column, C heat exchanger (also water and CO_2 trap). The oxygen evaporating at the bottom of B (the reboiler) leaves the installation via C (*3*), where it cools the incoming air (*1*) and thereby attains room temperature itself. The air is further cooled in the reboiler and enters the column part way up. Saturated nitrogen vapour (*4*) leaves the column at the top and is condensed by the refrigerating machine. Part of the condensate is tapped off (*2*) and part is returned to the column as reflux (*5*).

[2]) This subject is treated at length in Handbuch der Kältetechnik, Part 8, Springer, Berlin 1957, and in M. Ruhemann, The separation of gases, Oxford University Press, 1949. See also: H. C. A. Holleman, Philips tech. Rev. 4, 128-135, 1939.

The virtually pure nitrogen vapour leaving the column (*4*) is condensed by the gas refrigerating machine. Part of this condensate is returned to the column as reflux (*5*) and the remainder is taken off as product (*2*). Cooling of the air at the base of the column (termed the "reboiler") causes the evaporation of liquid oxygen. Part of this vapour is returned to the column, and the remainder is blown out via *C*.

It will be noted that, whilst the column delivers nitrogen vapour at the top and liquid oxygen at the bottom, the products extracted from the installation are *liquid* nitrogen — the required product — and oxygen *gas*. If the liquid oxygen were to be tapped off at the base, it would not be possible to utilize its stored "cold" for cooling the air feed. The consequence would be a drop in the production of liquid nitrogen. This is at once apparent when it is remembered that the machine's refrigerating capacity is constant, and also that the "cold" now leaves the installation only in the form of liquid products. The extraction of liquid oxygen is thus not impossible. However, the production of liquid oxygen is only about a quarter of the liquid nitrogen production; it is unlikely that this production ratio will be just that required by the user.

In the next section we shall examine the way in which the reflux ratio is affected by the design of the system described above.

Before the installation can function it must first be cooled to the working temperature which, as we have seen, is between —196 °C and —183 °C. For this purpose, air is fed directly to the gas refrigerating machine via another water and CO_2 trap [3]. The liquid air so produced flows to the column and cools its interior by evaporation.

Reflux ratio; theoretical considerations

We shall first calculate the minimum reflux necessary for a gas fractionating column to function properly. We base the calculation on the equilibrium mass transfer in the part of the column lying between the inlet point and the top.

This part of a column is represented by the diagram in *fig. 6*. The arrows indicate the liquid and vapour flows, the dashed lines the plates immediately above and below the inlet. The letters between brackets represent the concentration of the lighter — i.e. the more volatile — component.

[3]) In the starting period the air cannot follow the normal path via the heat exchanger and the reboiler. At this stage these elements are not yet cooled and therefore trap no water or carbon dioxide, so that stoppages might be caused elsewhere in the installation.

The mixed feed (air) enters the column, in the form of a saturated vapour, at the rate of F mol per second. We let z_F denote the concentration of the lighter component in the feed (in our case the nitrogen content). Of the condensed top product (concentration z_T), T mol per second is tapped off and L mol per second returned to the column. For the sake of simplicity we assume that there is no heat transfer between the column itself and the surrounding medium, and further that the latent heat of evaporation is the same for both components. In this case the descending flow of liquid is uniform though not, of course, constant in composition, over the whole height of the column. Counter to this flow of liquid there is a vapour stream of $(V—F)$ mol per sec below the inlet and V mol per sec above.

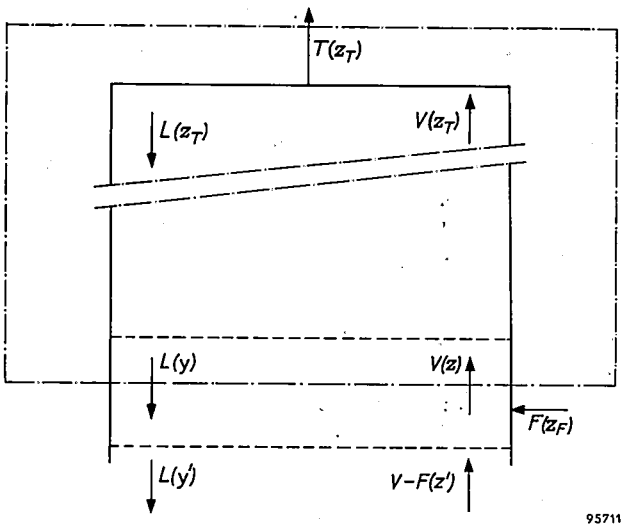

Fig. 6. Mass balance of part of a column situated between the inlet and the top, assuming that both components have the same latent heat of evaporation. The rates of vapour and liquid flow are accordingly constant over the whole height of the column (V and L mol/s). The mixture to be fractionated enters at the rate of F mol per second; the vapour flow below the inlet is $V—F$. The flow of the extracted top product is T. The dashed lines represent the baffle plates immediately above and below the inlet. The concentration of the volatile component, which changes from plate to plate, is indicated between brackets.

In the stationary state there can be no accumulation of either of the components, that is to say as much of each component enters the outlines part in fig. 6 as leaves it. For the more volatile component this yields the relation: $T \times z_T = V \times z - L \times y$, and for both components together: $T = V - L$. From these relations we can calculate the reflux ratio r, which is of course equal to L/T. We find:

$$r = \frac{z_T - z}{z - y} \quad \ldots\ldots\ldots \quad (1)$$

In the state of equilibrium the vapour issuing

from the plate just under the inlet has acquired the same concentration as the mixture entering the column. Hence z is equal to z_F, and the formula for the reflux ratio becomes:

$$r = \frac{z_T - z_F}{z_F - y} \quad \ldots\ldots \quad (2)$$

A similar consideration tells us more about the value of y and leads to the minimum condition for r. In a working column the vapour when ascending must become increasingly richer, and the liquid when descending increasingly poorer, in the lighter component; in other words, y must be greater than y' (see fig. 6). But the concentration y' applies to the liquid issuing from the plate immediately below the inlet, and this liquid is in equilibrium with the vapour of concentration z_F. The value of y', then, is a fixed quantity and for a given z_F can be read from the phase diagram (cf. fig. 1). We shall call this value y_{ZF}. The column can only function properly, i.e. deliver a top product of concentration z_T, provided that y is greater than y_{ZF}, that is provided r is greater than the value r_0 given by the equation:

$$r_0 = \frac{z_T - z_F}{z_F - y_{ZF}} \quad \ldots\ldots \quad (3)$$

For producing pure nitrogen ($z_T = 1.00$) by air fractionation ($z_F = 0.78$), the value of r_0 according to equation (3) is 0.7. Exact calculation, taking account of the exact values of the molar latent heat of evaporation, yields a value of 0.8 for r_0 [4]). This means that, in order to extract one mol of nitrogen, at least 0.8 mol of liquid N_2 must be returned to the column as reflux. Thus, for every litre of liquid extracted, at least 1.8 litres must be condensed.

The appropriate value of r in a given case, that is to say, the amount by which r must exceed r_0, depends on the length of the column (the condition $r > r_0$ having been derived from the condition $y > y'$). If r approaches r_0, then y approaches y', which means that the gain in concentration per baffle approaches zero. Where $r = r_0$, the fractionation would therefore require an infinite number of plaves. In practice, excess reflux is always employed in order to keep the size of the column within reasonable limits.

[4]) W. H. Keesom, Rapports et Communications No. 17, 6e Congrès International du Froid, Buenos Aires 1932, p. 136; or, Comm. Kamerlingh Onnes Lab. Univ. Leiden **19**, 1929/31, Suppl. No. 69. Further ibid. **20**, 1931/33, Suppl. No. 72a, and W. H. Keesom and W. Tuyn, ibid. **20**, 1931/33, Suppl. No. 72b.

The reflux ratio in the new installation

With an installation operating on the principle illustrated in fig. 5, the value of r cannot be freely chosen; on the contrary, r is a fixed quantity. In order to examine the factors that here govern the reflux ratio in the new installation and to ascertain the value of r, we shall draw up a heat balance, on the basis of the block diagram in *fig. 7*. The elements *A*, *B* and *C* represent, as in fig. 5, the gas refrigerating machine, the column and the heat exchanger, respectively.

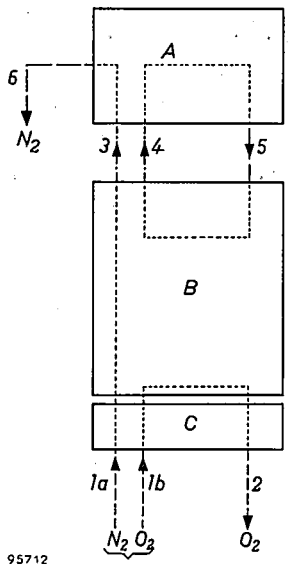

Fig. 7. Heat balance of the installation. *A* gas refrigerating machine, *B* column, *C* heat exchanger, *1* inflowing air (*1a* nitrogen, *1b* oxygen), *2* expelled oxygen; flows *1b* and *2* compensate each other thermally. Flow *1a* is of the same magnitude as flows *3*, = *6*, which represent the tapped-off fraction of the top product; this flow supplies 6190 joules per mol. Flow *4* is the fraction of the top product used as reflux after condensation. Flows *4* and *5* can be regarded as a circulating quantity of nitrogen of constant temperature, which withdraws from the column 5600 joules per mol (the latent heat of evaporation of nitrogen).

Air at room temperature (*1a* and *1b*) enters the installation, oxygen of the same temperature (*2*) and liquid (boiling) nitrogen (*6*) leave it. The ingoing and outgoing amounts of oxygen are equal; the same is true of the nitrogen. The oxygen from the air going in (*1b*) and the oxygen exhausted (*2*) thermally cancel out and may therefore be disregarded for the purposes of the heat balance. The nitrogen that will ultimately leave the installation as product is initially at room temperature, but leaves the column as saturated vapour at —196 °C (*3*). This cooling involves the dissipation of 6390 joules per mol. Finally, we consider the fraction of the top product that is not tapped off (*4*) and the reflux (*5*). The streams (*4*) and (*5*) together form a closed circuit in which nitrogen, possessing the purity of the top product, circulates. During a complete circulation this nitrogen does not change in temperature. It is, however, continuously condensed in *A* and again evaporated in *B*. As a result, 5600 joules per mol reflux are withdrawn from *B*. Since 1 mol extracted product corresponds to r mol reflux, this means that 5600 r joules are taken from the column per mol product. In the state of thermal equilibrium this energy is exactly equal to the above 6390 joules,

and therefore the value of the reflux ratio r is 1.14.

This value is appreciably higher than the minimum reflux ratio r_0, which, as we have seen, is about 0.8.

The foregoing considerations show that with an air fractionating installation operating on the principle described in fig. 5 the equilibrium value of r is fully determined by the thermal properties of the top product, which in our case is nitrogen. As will be recalled, the value of r_0 is governed not only by the requisite purity of the top product but also by the composition of the mixture to be fractionated and by the shape of the phase diagram. It may very well be that for some gas mixtures the equilibrium value of r is smaller than r_0. The system described — which has proved eminently suitable for an air fractionating installation required to deliver liquid nitrogen — is thus not universally applicable. For instance, an analogous system cannot be used for producing pure liquid oxygen from air.

Regulation of the column

It is most important that a small installation like the one under discussion should be simple to operate. The only deliberate control operations in the present case are limited to starting up the installation; thereafter the control is fully automatic. Regulation is necessary for the flow of the air feed, the flow of the oxygen waste product, and also the division of the condensate (the liquid nitrogen) into reflux and extracted product.

The flow of the air feed is maintained by the subatmospheric pressure produced in the installation owing to the condensation of the saturated nitrogen vapour, measures having been taken (see below) to make it impossible for the air to enter the column except via the entry port. The air is therefore sucked into the column in the right amount, without the need for a regulating device. Regulating devices are, however, necessary in the other cases and these will now be discussed with reference to *fig. 8*. This figure shows in diagrammatic form the column (*1*), the reboiler (*2*) and the various means of regulation; for the sake of clarity, most other components of the installation are omitted.

Removal of oxygen

Since a certain negative pressure prevails in the column, the oxygen cannot simply be blown out if the column and reboiler are in direct communication. In order nevertheless to allow this straightforward method of removal to be adopted, the installation is in the first place so designed that the liquid from the column can only enter the reboiler through the standpipe (*3*). In the second place the fraction of the vaporized oxygen flowing back to the column can only enter the column through pipe (*4*) which contains an adjustable flow resistance in the form of a valve (of comparatively wide through-way, however). The latter is adjusted in such a way that the pressure drop across it causes the pressure in the reboiler to rise above that of the atmosphere. The oxygen is then automatically blown out.

The gauge pressure in the reboiler is proportional to the amount of oxygen that evaporates, and this

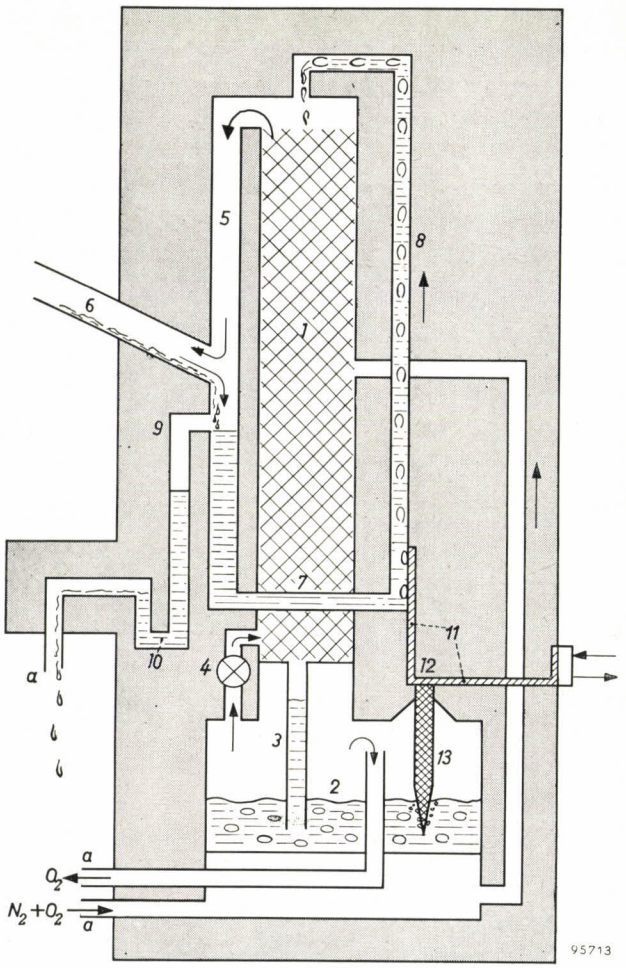

Fig. 8. Regulation of the column. The liquid from the column *1* can only reach the reboiler *2* via the standpipe *3*. The evaporating oxygen in *2* returns partly to the column via the valve *4*. This is so adjusted that the pressure in *2* is slightly higher than atmospheric pressure, so that oxygen vapour is blown off. The saturated nitrogen vapour leaving the column at the top enters the refrigerating machine via tubes *5* and *6*; after having been condensed, it flows back through *6* into the lower part of tube *5*. The latter forms the high-density arm of a vapour-bubble pump (*5*, *7*, *8*), which pumps the reflux to the top; tube *8* is heated by means of a copper strip *11* to which a finger *13* is fixed. The tip of the finger reaches into the liquid in the reboiler. If the reflux is excessive, the level in *2* rises, and the pin withdraws more heat from strip *11*, thereby slowing down the pumping action. The product is extracted via the overflow *9* and the trap *10*.

is roughly proportional to the amount of air sucked in, for it is this air that supplies the heat needed to evaporate the liquid in the reboiler. A variation in the quantity of incoming air therefore automatically gives rise to an approximately equal (relative) change in the quantity of oxygen exhausted; in other words, the ratio between these two quantities remains nearly constant. Since air contains 78% nitrogen, at least 22% of the gas mixture sucked in must be exhausted [5]). The valve is so adjusted that 25 to 32% is exhausted, which means that the vapour so removed consists partly of nitrogen. Thus, for a given production of liquid nitrogen, more air is sucked in than would be the case if exactly 22% were exhausted. It might be thought that this would entail some loss of energy and adversely affect the efficiency of the installation. This is not so, however, the reasons being that the air is not compressed (hence there is no loss due to the work of compression) and that the waste product is again raised to room temperature. Accordingly, fairly coarse adjustment of the valve is permissible, which simplifies operation.

The solution described has proved entirely satisfactory, even in the face of *wide* variations in the capacity of the refrigerating machine, in the humidity of the air and in the accumulation of deposits in the heat exchanger.

Division of liquid nitrogen into product and reflux

In reality the refrigerating machine is not above the column, as might be suggested by fig. 5, but at the side of it, and therefore the reflux has to be pumped up to the top of the column. This is done by means of a *vapour-bubble pump*, which is essentially merely a U-shaped tube partly filled with liquid. In one limb of the pump — the "riser" tube — the liquid is "diluted" with vapour bubbles. The specific gravity of the contents of this tube is thereby reduced, causing the liquid level to rise. The vapour bubbles are produced by evaporating the liquid to be pumped. For this purpose heat is applied to the base of the riser tube [6]).

In fig. 8 the pump is composed of tubes *5*, *7* and *8*. The riser tube is heated by means of a copper strip *11*, one end of which is fixed to tube *8* near the bottom, while mains water flows over the other end. The system functions as follows. The vapour leaving the top of the column flows to the gas refrigerating machine through the upper part of tube *5* and through tube *6*. The condensate runs back down tube *6* and passes into the lower part of tube *5*. The level of the liquid in the latter tube is in principle determined by the height of tube *8*, and by the concentration of bubbles in the liquid in this tube. At a given bubble concentration this level exactly coincides with the overflow outlet *9*. If the bubble concentration is greater, this level is not reached and all liquid nitrogen emanating from *6* is returned to the column as reflux. If the bubble concentration is less, part of the condensate leaves the installation via *9* and the trap *10*.

The use of a vapour-bubble pump makes it possible to divide the condensate into product and reflux simply and automatically by the expedient of regulating the heat supply. The heating strip *11* is so designed as to conduct slightly too much heat to the riser tube. Fixed to this strip at point *12* is a copper "finger" *13* which passes through the cover of the reboiler into the liquid oxygen. The position of point *12* is so chosen that its temperature is higher than that of the liquid oxygen when the liquid level in the reboiler is below the tip of the finger. If the reflux is excessive the level in the reboiler rises. As a result the temperature of point *12* drops and less heat is conducted to the pump. The latter then pumps up less liquid, and the reflux accordingly decreases until equilibrium is reached. The shape of the finger is such that the system cannot go into oscillation. Good thermal insulation is, of course, provided between the finger and the cover of the reboiler.

Another great advantage of using a vapour-bubble pump and the system of regulation just described is that no moving parts are involved.

Starting-up the installation

During the starting period, the gas refrigerating machine sucks in ambient air directly, as already mentioned. The openings marked *a* in fig. 8 are then closed. The liquefied air flows via tube *6* to the column, where it evaporates. Air then flows back through *6* to the condenser of the machine, where it is again liquefied, passes again to the column, and so on. This means that only a very limited amount of air (about 1 m^3) need be sucked in from outside for cooling the installation, thus allowing the water and CO_2 trap on the refrigerating machine to be kept small in size.

After some time the liquid in the reboiler rises to a level high enough to bring pin *13* into play,

---

[5]) This 22% is composed of 21% oxygen and 1% argon. Since there is little difference between the thermal properties of these gases, the argon behaves in this installation in the same way as the oxygen.

[6]) The bubble pump widely used in the oil industry is based on the same principle, but in this case the "dilution" is effected with a gas which is forced through a nozzle or a porous plug into the liquid.

whereupon the vapour-bubble pump forces less liquid up the tube. The level of liquid in tube *5*, which can be read from a meter, then rises also. One can now switch over to the normal situation. The final step is to adjust the valve *4* to the appropriate setting, by consulting the meters that indicate the quantities of air and oxygen respectively sucked in and blown out per second. The starting period lasts altogether about $1^1/_2$ hours.

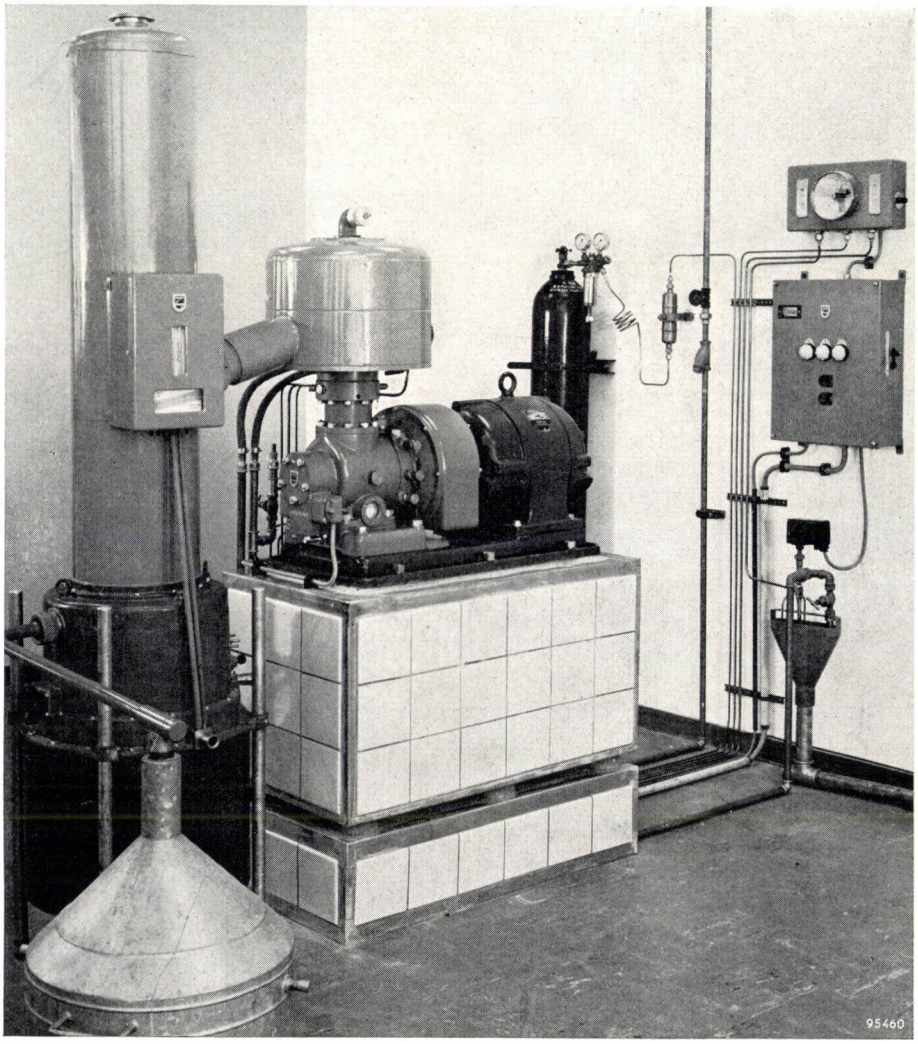

Fig. 9. The Philips liquid-nitrogen installation type PW 7050. Left, the air fractionating column which forms a single unit with the water and CO_2 trap mounted at the base. Centre, the gas refrigerating machine, on which is mounted (under the same hood) the condenser and a second water and CO_2 trap; the latter functions during the starting period. The instrument panel mounted on the column jacket contains meters for reading the flow of incoming air, the flow of expelled oxygen and the level of liquid in the high-density arm of the reflux pump. The installation delivers 4 to 5 litres of liquid nitrogen per hour with a power consumption of 6 kW and can operate continuously for a week. The entire installation covers a floor area of only 0.50×2.00 m.

Technical details and performance

As we have seen, the actual lay-out of the installation differs from that shown diagrammatically in fig. 5 in that the refrigerating machine is mounted at the side of the column instead of on top of it (see *fig. 9* and title photograph).

This layout has the virtue of making all components of the installation readily accessible and it also allows easy decoupling of column and refrigerating machine. A convenient feature of this construction is that, by removing the column from the refrigerating machine and fitting the latter with another condenser, one has a simple installation for producing liquid air. Similarly, by reversing the procedure, one can easily convert a liquid air installation into an installation for producing liquid nitrogen from atmospheric air.

When the installation is working, the temperature

of the column is extremely low, and since heat losses must be avoided as far as possible, the actual column is sheathed in a thick layer of insulating material. What can be seen in fig. 8 is only the jacket around this insulation. The insulating material used is silica-aerogel, a powdered substance with especially favourable properties in that it has very low thermal conductance and can be poured, making it a simple matter to fill up the space reserved for insulation.

The actual column is a tube, 4.5 cm in diameter and 90 cm in length, which is filled to the top with a packing material. The packing consists of small pieces of wire gauze bent into a saddle shape (see *fig. 10*). At the top, and at the air inlet, distributors ensure uniform distribution of the liquid.

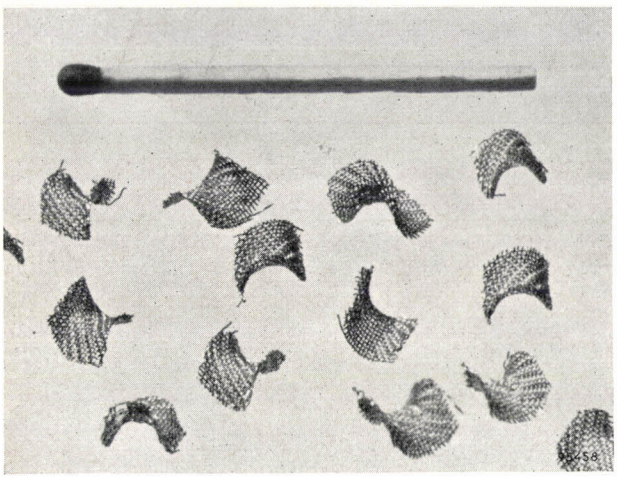

Fig. 10. The saddle-shaped pieces of metal gauze forming the packing in the fractionating column.

We shall not deal with the constructional details of the heat exchanger, in which the expelled oxygen cools the indrawn air, and which also functions as a water and CO_2 trap [7]). It will suffice to mention that it combines a very high heat and mass transfer with a very low resistance to flow; moreover, it takes a long time before the channels become blocked with ice and snow. The installation can accordingly be operated continuously for a full working week, and defrosted at the week end. The ice and snow separator mounted on the refrigerating machine and which functions during the starting period, as described above, is of the same type.

The installation consumes a power of 6 kW. Performance data and dimensions are given in *Table I*.

[7]) This will be described in due course in a separate article.

Table I. Particulars of the complete installation PW 7050 for making liquid nitrogen.

Production	4 to 5 litres per hour
Purity	better than 99.5%
Power consumption	6 kW
Specific power	1.2-1.5 kWh per litre
Total production in one working period	500-1000 litres *)
Height	2 metres
Floor area	0.5 × 2 metres
Total weight	400 kg (approx.)

*) Dependent on the air humidity.

Comparison with other systems

Since the fractionation of air takes place at an extremely low temperature, the most important feature of an installation for producing liquid nitrogen or oxygen from air is, as we have seen, the way in which the low temperature is produced and the requisite flow of heat achieved. The system is of course always designed so that the energy required, other than that for the refrigeration, is kept to a minimum. The systems hitherto employed are on the whole rather complex [8]). One feature they have in common is that the air is compressed before being fed to the fractionating column.

For the liquefaction of gases, particularly in small installations, use is often made of the Joule-Kelvin effect. The gas is first highly compressed and then expanded at low temperature through a porous plug or throttle valve. The gas is thereby cooled and partly condensed. For producing liquid air or nitrogen the compression required is generally in the region of 200 atm, and more air is processed per mol product than in the system described in this article. Another method, used more especially in large installations, is to let a compressed cold gas expand adiabatically (isentropically) by causing it to perform external work on the piston of an expansion chamber or on the rotor of a turbine. Other conditions being equal, the refrigeration with this method is greater than with that employing the Joule-Kelvin effect, less compression being necessary.

The gas refrigerating machine also involves the compression and expansion of a gas. This is done, however, not with the air to be fractionated but with hydrogen or helium in a closed system [9]). Several advantages accrue from not compressing the

[8]) See note [2]).

[9]) In this respect the installation corresponds to the one earlier described for producing liquid air with the gas refrigerating machine, in which the air to be liquefied is not compressed either.

air feed itself. In the first place, it dispenses with the need for expansion valves. the small orifices of which may freeze up, and secondly there are no moving parts to get ice-bound at low temperature. The absence of moving parts also precludes oil contamination of air and product. Furthermore, since the installation is not required to compress large quantities of air, its construction is relatively light. The fact, then, that the air is not compressed contributes in large measure to the simplicity and reliability of the installation.

Summary. In the Philips laboratories an installation has been developed for the economic production of liquid nitrogen from atmospheric air on a moderate scale (e.g. for laboratory purposes). The installation, which consumes 6 kW, delivers 4 to 5 litres of liquid nitrogen per hour with a purity of 99,5%. It consists essentially of an air fractionating column and a gas refrigerating machine (as described earlier in this Review) to produce the necessary low temperature.

The air is pre-cooled in a heat-exchanger by the oxygen expelled as waste product, and further cooled by liquid oxygen contained in a reboiler at the base of the column. It then enters the column as a virtually saturated vapour at a point some way up. The column is an insulated tube 4.5 cm in diameter and 90 cm in height, which is filled with small saddle-shaped pieces of wire-gauze and in which liquid flows from top to bottom and vapour from bottom to top. The liquid in descending becomes increasingly richer in oxygen and contains but little nitrogen when it enters the reboiler at the base. The ascending vapour increasingly richer in nitrogen and leaves the column at the top as almost pure nitrogen. This top product, as it is called, is condensed by the gas refrigerating machine; part of the condensate is extracted as product and part returned to the top of the column as reflux, thus maintaining the downward flow of liquid essential to the functioning of the column. Since the reflux governs the heat transfer from the column to the refrigerating machine, its value is fixed. The thermal properties of nitrogen, which determine this value, are such that the minimum reflux needed for fractionating is amply exceeded. For practical reasons the refrigerating machine is mounted at the side instead of at the top of the column. This makes it necessary to pump the reflux, which is done by means of a "vapour-bubble" pump. Regulation of this pump, and of the exhaust of the waste product, is fully automatic. The column contains no moving parts that could freeze up, and stoppages are virtually precluded. The heat exchanger, through which the air is sucked in, also functions as a water and CO_2 trap. The installation can operate continuously for a week. The starting period is about $1^1/_2$ hours.

INFLUENCE OF THE PELTIER EFFECT IN RESISTANCE WELDING

537.322.15:621.791.76

During tests on a spot-welding machine for the fabrication of grids for radio valves, the direction of current flow was found to have a marked influence on the strength of the weld. It will be shown below that this at first sight surprising phenomenon can be explained by assuming it to be due to the Peltier effect.

The situation is illustrated schematically in *fig. 1*. Two molybdenum wires are simultaneously welded crosswise to a thicker nickel wire, over and under

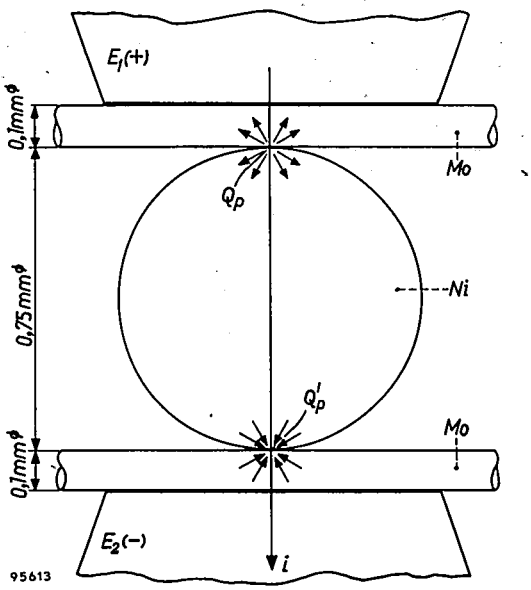

Fig. 1. Sketch of arrangement for spot-welding two molybdenum wires to a nickel wire. If the current i flows from top to bottom in the diagram, an amount of heat Q_P (Peltier heat) is developed at the upper weld and approximately the same amount of heat Q_P' is absorbed at the lower weld. As a result the upper weld has a higher temperature than the lower. E_1 and E_2 are the (copper) electrodes.

the latter. The welding current is supplied by the discharge of a capacitor through the primary coil of the welding transformer; as a function of time it has roughly the form shown in *fig. 2*. The current is effectively unidirectional; in fig. 1, for example, it flows from top to bottom [1]). Thus, in the upper weld it flows from molybdenum to nickel and in the lower weld from nickel to molybdenum. Now, the Peltier effect is the thermo-electric phenomenon that when current flows through a junction of two dissimilar conductors, heat is developed or absorbed at that junction, depending on the direction of the current. Whether Peltier heat will be developed or absorbed can be deduced from the behaviour of the conductors in question when made to form a thermocouple. From *fig. 3* and its caption we see that in the situation of fig. 1, Peltier heat will be generated at the upper weld and absorbed at the lower. The Peltier heat is added to or subtracted from the ohmic heating, as the case may be. According to this reasoning, then, the upper weld develops the higher temperature. It is in fact found that when the current pulse is just high enough to weld the upper wire

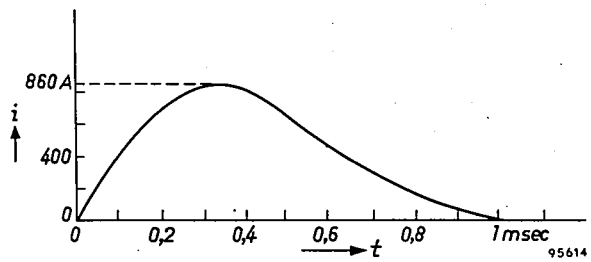

Fig. 2. The welding current-pulse as a function of time.

firmly, the lower weld is not yet properly consolidated. If the current pulse is raised sufficiently to weld the lower wire firmly, the upper wire usually melts through. If the direction of current flow is reversed the same phenomena occur, but now with the roles of the upper and lower wires interchanged.

Although critical adjustment of the current pulse makes it possible to obtain satisfactory welds at both the upper and the lower stations, it takes only a few welds before surface contamination of the electrodes attenuates the pulse enough to prevent a good weld at the lower wire. When the electrodes have been cleaned, a number of good double welds can again be made.

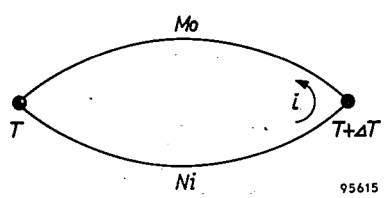

Fig. 3. In a thermocouple formed by Ni and Mo, the current i at the hot junction (temperature $T + \Delta T$) flows from Ni to Mo. The Peltier effect opposes this current flow, i.e. it heats the cold junction (temperature T; heat Q_P is liberated here) and cools the hot junction (where heat Q_P' is absorbed). Thus when a current is driven through an Mo-Ni junction, heating occurs when the current direction is from Mo to Ni.

[1]) The current pulse of opposite polarity, which follows the first sharp peak, transports just as much electric charge, but it is longer drawn out and reaches nothing like the amplitude of the first peak. For this reason it has little importance in the welding process.

In principle, the Peltier effect occurs whenever two dissimilar materials are jointed by resistance welding. The fact that the effect is so unusually pronounced in the case described is partly attributable to its relatively high value at an Ni-Mo junction, but is mainly due to the fine gauge (0.1 mm) of the molybdenum wire used. With such fine wire a relatively slight rise in the heat developed at the welding zone tips the scales between non-adhesion and a melted-through wire.

cient, for which one of the Thomson relations is relevant [2]):

$$P = T\frac{dV}{dT}. \quad \ldots\ldots\ldots \quad (2)$$

T is the temperature of the junction in °K. V is the thermo-electromotive force in a thermocouple formed by the two metals concerned, one junction of which is held at a constant temperature while the other has the temperature T. In *fig. 4a* the

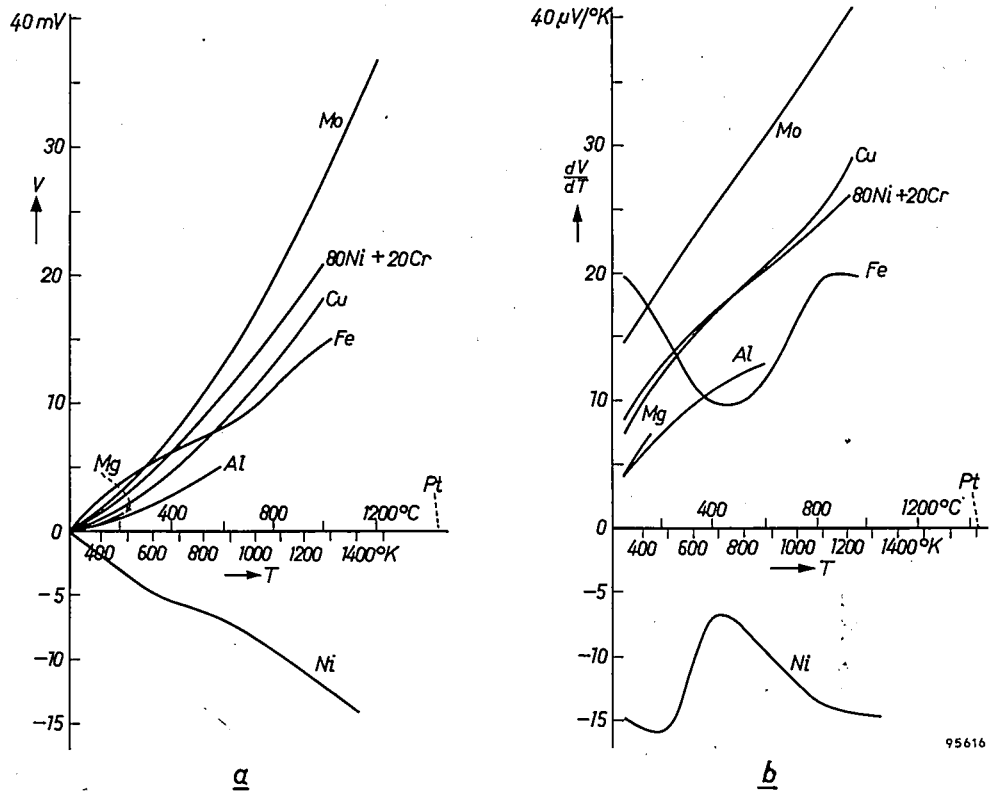

Fig. 4. *a*) Thermo-e.m.f. V of a number of metals, with respect to platinum, as a function of the temperature T of one of the junctions. The other junction is at 273 °K (0 °C). The positive sign means that at the cold junction the thermo-e.m.f. is directed from the metal to the platinum [3]).
b) Values of dV/dT (the so-called thermo-electric power) as a function of T, derived from the curves in (*a*). As a result of the Peltier effect a junction is heated when a current flows from the metal with the higher value of dV/dT to the metal with the lower.

We have already touched on the connection between Peltier heat and the behaviour of a thermocouple made from the contacting metals in question. We shall examine this connection more closely, in order to be in a position to predict whether in a given case the Peltier effect may be expected to influence a weld significantly or not.

Let Q_P be the Peltier heat developed per second, i.e. the Peltier power. This is proportional to the current i through the junction:

$$Q_P = Pi. \quad \ldots\ldots\ldots \quad (1)$$

The proportionality factor P is the Peltier coeffi-

thermo-e.m.f.'s of several metals with respect to platinum are plotted as a function of temperature [3]). The thermo-e.m.f. for any two metals is found from this graph by measuring the vertical distance between the curves for the metals in question From

[2]) See e.g. S. G. Starling, Electricity and magnetism, Longmans, London 1939, 6th edition, pages 210-212. A treatment of Thomson relations, taking account of irreversible processes, will be found in R. C. Tolman and P. C. Fine, On the irreversible production of entropy, Rev. mod. Phys. **20**, 51-77, 1948, in particular pages 70-72.

[3]) The curves are plotted from data given by W. F. Roeser and H. T. Wensel in: Temperature, Report of a symposium held at New York in 1939, Reinhold, New York 1941, pages 1309-1310.

fig. 4*b*, which sets out the derivatives with respect to T of the curves in fig. 4*a*, the values of dV/dT (the so-called thermo-electric power) can be found in the same way for an arbitrary combination of metals. It can be seen from fig. 4*b* that in the case of Fe-Mo, for example, the values of dV/dT are appreciably smaller than for Ni-Mo. This implies that if an iron wire were substituted for the nickel wire in fig. 1, it should be easier to obtain good simultaneous welds of the upper and lower wires.

case of Cu-Mg junctions, give rise to additional heating of the positive electrode and to cooling of the negative electrode. To check this, measurements were made of the thermo-e.m.f. in one of the alloys used in the investigation (*fig. 5*). The results showed that the positive electrode does indeed attain the higher temperature (*fig. 6*).

The observations and considerations discussed above prompted a more comprehensive experimental and theoretical investigation of the influence

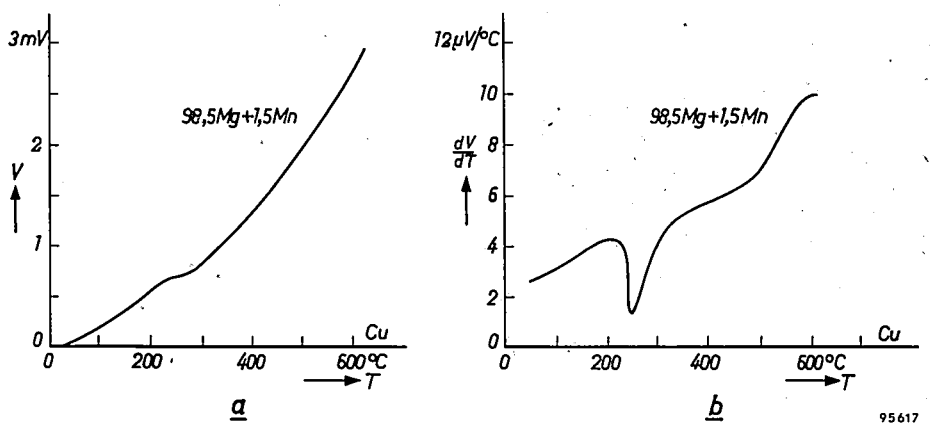

Fig. 5. *a*) Thermo-e.m.f. V of copper with respect to an alloy of Mg with 1.5% Mn plotted against the temperature T; *b*) the derivative of this curve with respect to temperature, again as a function of T.

Such is indeed found to be the case. Even with Fe-Mo the Peltier effect still makes itself felt, for at a certain setting of the current pulse the upper wire is completely welded and the lower one is still loose. However, a slight increase of current is sufficient to weld both wires firmly. The weld cycle can then be repeated thousands of times without it becoming necessary to clean the electrodes and without there being any tendency for the wires to melt through at one side or break away at the other.

The Peltier effect also probably explains why, in spot welding, one electrode tip often deteriorates more rapidly than the other (burning and pick-up; the latter being the transfer of electrode copper to the workpiece, or of material from the workpiece to the electrode.) Hess *et al.* [4]) reported in 1947 a detailed investigation of this phenomenon as observed in the spot welding of magnesium alloy sheet — a case of considerable importance in aircraft construction. They found that when welding with current pulses which were mainly unidirectional the positive electrode suffered more than the negative. If the Peltier effect were the cause it should, in the

of the Peltier effect in resistance welding. This investigation was undertaken in the Philips laboratory at Aachen [5]). The photograph in *fig. 7*, which

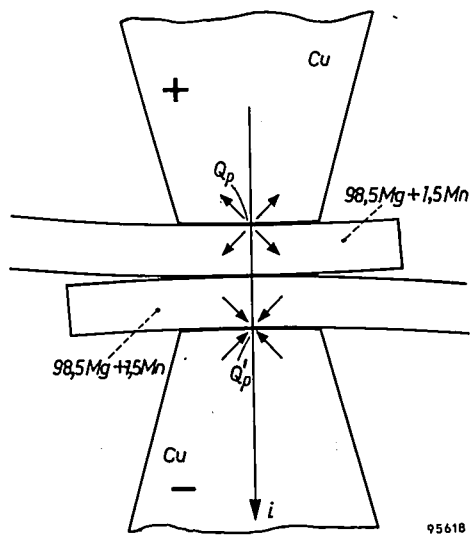

Fig. 6. The Peltier effect may largely explain why in spot-welding one electrode often wears faster than the other. In the welding of Mg sheet, the positive electrode gets hotter, according to fig. 5*b*, and hence deteriorates earlier than the other [4]).

[4]) W. F. Hess, T. B. Cameron and R. A. Wyant, Observations of electrode tip pickup and tip life in the spot welding of magnesium alloy sheet, Welding Journal **26**, Supplement, pp. 433s-442s and 484s, 1947.

[5]) A report on this investigation, by S. Scholz, will shortly be published elsewhere.

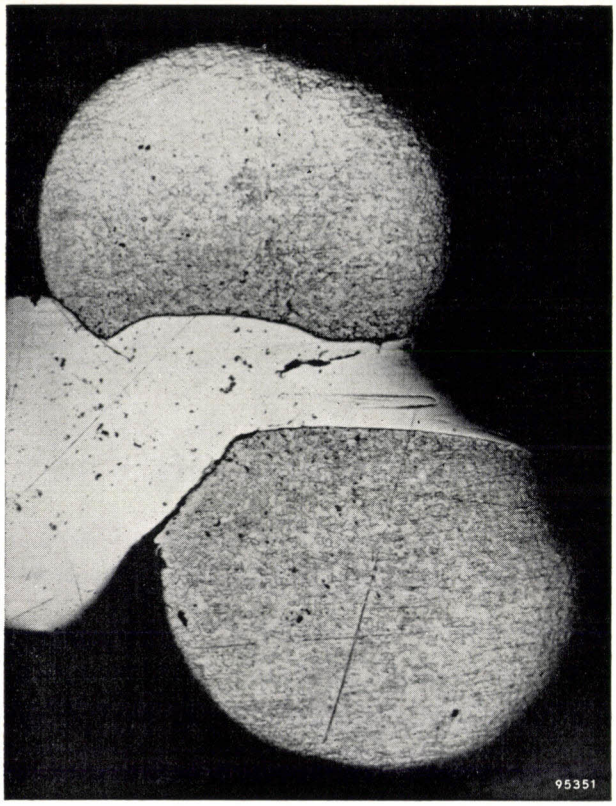

Fig. 7. Cross-section of a weld of two Ni wires on a Ni-Cr wire. Current flows from the top to the bottom wire. In accord with fig. 4*b*, the lower weld has fused farther than the upper. Wire gauge 0.5 mm. This photograph was kindly put at our disposal by S. Scholz of the Philips Laboratory at Aachen.

originates from this source, shows clearly the asymmetry that results from making a double weld such as in fig. 1 when the metal combination shows a large Peltier effect.

Energy involved in the Peltier effect

We shall now make a theoretical estimate of the energy released, or absorbed, in the form of Peltier heat during the welding process. We can then compare this energy with the total energy used for making a weld.

The Peltier heat is given by

$$\int i \times T \frac{\mathrm{d}V}{\mathrm{d}T}\,\mathrm{d}t\,.$$

The integration is carried out over the duration of the welding process; fig. 2 gives i as a function of time t. In *fig. 8*, $\mathrm{d}V/\mathrm{d}T$ is plotted against T for the combination Ni-Mo (the curve is derived from fig. 4*b*). The same figure shows $T(\mathrm{d}V/\mathrm{d}T)$ as a function of T. We assume further that the temperature T of the weld zone varies as a function of time t in the manner shown in *fig. 9*, it being estimated that the maximum temperature remains about 100 °K below the melting point of Ni (approx. 1700 °K). With the aid of fig. 8 we can now plot the Peltier coefficient $P = T(\mathrm{d}V/\mathrm{d}T)$ as a function of t, and also the Peltier power $Q_\mathrm{P} = P \times i$. This is done in fig. 9. The area bounded by the latter curve gives the total Peltier heat, which is found to be 4.2×10^{-2} joule. The capacitor, which contains the

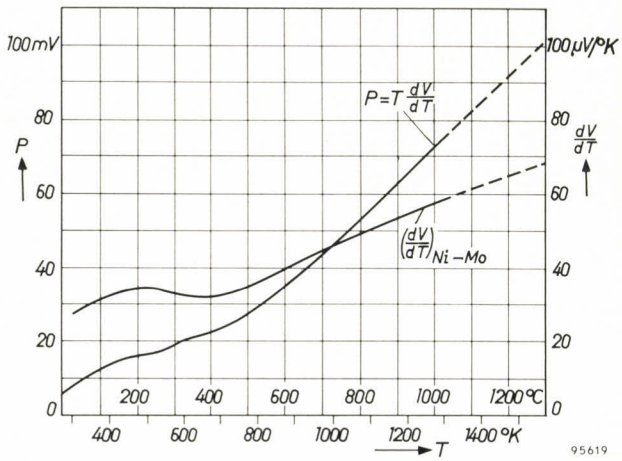

Fig. 8. The thermo-electric power $\mathrm{d}V/\mathrm{d}T$ for the combination Ni-Mo as a function of T (derived from fig. 4*b*), and $T(\mathrm{d}V/\mathrm{d}T)$ as a function of T.

welding energy, has a capacitance C of 6.7×10^{-6} farad and is charged to a voltage V_C of 980 V. The energy released upon discharge is $\frac{1}{2}CV_\mathrm{C}^2 = 3.2$ joule. Estimating that about half of this generates useful heat in the immediate vicinity of both junctions, then 0.8 joule is available per weld. The calculated Peltier heat comes to about 5% of this value. The quantities of heat available for the one weld and for the other thus differ by 10%. This makes it a plausible assumption that the Peltier effect causes a significant discrepancy between the two welds.

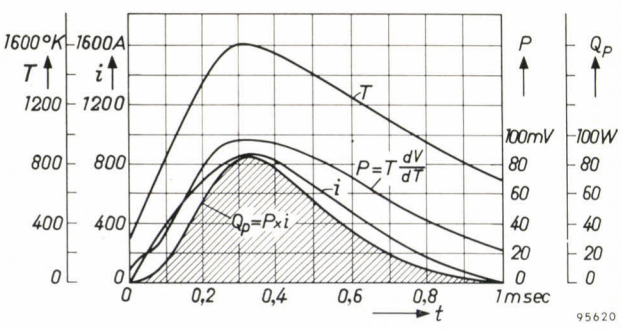

Fig. 9. To calculate the Peltier heat at a junction between Ni and Mo, it is assumed that the temperature T of the welding zone varies as a function of time t in the manner shown. Also plotted as a function of t are the welding current i, the Peltier coefficient $P = T(\mathrm{d}V/\mathrm{d}T)$ and the Peltier power $Q_\mathrm{P} = P \times i$.

The Thomson effect

Finally, a word about the Thomson effect. This is the phenomenon that when an electric current i flows through a wire in which a temperature gradient exists, an amount of heat, in addition to the joule heat, will be developed or absorbed, depending on the direction of the current. The Thomson heat developed, or absorbed, per second in an element dx of such a wire is given by

$$dQ_{Th} = \sigma i \frac{dT}{dx} dx. \quad . \quad . \quad . \quad . \quad (3)$$

The proportionality factor σ, which is the Thomson coefficient, is dependent on the material of the wire and on the temperature.

In our case considerable temperature gradients will arise in the molybdenum wires between the weld zones and the welding electrodes. It is therefore reasonable to ask whether perhaps the Thomson effect too will have any significant influence on the weld. The Thomson coefficients of a number of metals (including Mo) have been measured as a function of temperature by Lander [6]); see *fig. 10*. To be able to say anything about the influence of the Thomson effect we assume that at the moment when the weld has reached its maximum temperature (1600 °K) the temperature of the electrode tip is 600 °K. We assume furthermore that the temperature gradient in an Mo wire is linear from weld to electrode. Near the junction, where the temperature is higher than ~1000 °C, the Thomson coefficient in the Mo wires is negative (see fig. 10). A simple calculation shows that in this part of an Mo wire the Thomson power Q_{Th} at the moment under consideration is about 5 W. From fig. 9 we see that the Peltier power is then about 80 W.

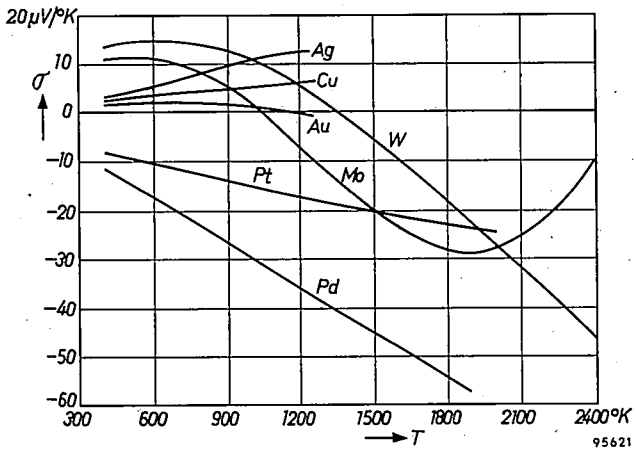

Fig. 10. Thomson coefficients σ for various metals as a function of temperature, after Lander [6]). The sign convention adopted is: a positive value of σ means that heat is developed when the temperature gradient and the electric current are in opposite directions.

The Thomson heating is thus much smaller than the Peltier heating and may be assumed to have no significant influence on the weld. It will have less influence still if thicker wires are welded, for in that case the Thomson heat will not be so concentrated at the junction.

T. C. BALDER.

[6]) J. J. Lander, Measurements of Thomson coefficients for metals at high temperatures and of Peltier coefficients for solid-liquid interfaces of metals, Phys. Rev. **74**, 479-488, 1948.

A FAST METHOD OF READING MAGNETIC-CORE MEMORIES

by H. J. HEIJN and N. C. de TROYE. 621.318.42:621.374.32:681.142

In the operation of a magnetic-core memory, especially as used in electronic computers, the reading of selected cores, the storage of the resultant signals in a buffer register and the restoration to the memory of the extracted information are processes that must be carried out at great speed. Transistors are now proving useful in this respect. After explaining the operation of magnetic-core memories, the article below describes three new circuits. The first employs transistors as intermediate store elements, to provide simple output stages. In the second a transistor is used as a switch to prevent parasitic voltage pulses from blocking the output stages; this appreciably shortens the "cycling time", i.e. the time taken to complete the three processes mentioned. The third circuit serves to stabilize the current pulses needed to read the cores and to restore the information. The operation of this circuit is based on the saturation of a ferrite ring.

For some time now, Philips have been supplying components of varying complexity to manufacturers of electronic computers. In this connection research work is in progress on memory systems which employ magnetic materials having a rectangular hysteresis loop [1]). A description wil be given in this article of such a memory system, as used in an experimental computer built in the Research Laboratories at Eindhoven, where it is now in operation.

A "memory" is a device capable of storing numbers, or other data, and of delivering its information when called upon to do so. The following are some typical applications.

1) *Translating machines.* For translating texts from one language into another. The machine "reads" the words and selects from its memory system the equivalents in the other language, while observing the rules of grammar.

2) *Automatic telephone exchanges.* It is required that the *shortest* connection between two subscribers should be established. This takes a certain amount of time, during which the data for connecting the subscribers must be retained.

3) *Automatic lathes.* A memory device is coupled to a lathe while the turner makes a "master" workpiece. All operations are recorded and stored in the memory device, which is subsequently used to control other lathes for producing duplicates.

4) *Electronic computers.* These machines are capable of performing automatically large numbers of calculations. The programmed sequence of operations, the data and the interim results are "written" into a memory or "store". Clearly, such memories are often extremely complex devices.

[1]) See e.g. H. P. J. Wijn, E. W. Gorter, C. J. Esveldt and P. Geldermans, Conditions for square hysteresis loops in ferrites, Philips tech. Rev. **16**, 49-58, 1954/55.

The binary system

In everyday life numbers are expressed in the decimal system. As the name implies, the base (or radix) of this system is "ten", i.e. it makes use of ten distinct digits from 0 to 9. For a memory device, however, it is more convenient to use the binary number system, which has only the two digits 0 and 1. We shall briefly examine the reasons for this choice.

To explain how a number is represented in a given number system it is useful to distinguish between the *symbol* — meaning the combination of digits — and the *value*, which is the number of units represented by the number. The value follows from the symbol by virtue of the fact that each digital position in the symbol is understood to be a certain power of the base. An example will make this clear. The number represented in the binary system by the symbol 11101 has the numerical value, expressed in the decimal system, of: $1\times2^0 + 0\times2^1 + 1\times2^2 + 1\times2^3 + 1\times2^4 = 29$ (the digits are taken in order from right to left).

A number can be represented in the binary system by a row of similar elements each of which can occur in two distinct states: one of these states is identified with the digit "0" and the other with the digit "1". To do the same in another number system, for example in the 10-based (decimal) or 60-based system, elements are needed that can occur in 10 or 60 distinct states, respectively. If the requirement is to be able to represent numerals up to a given value, fewer elements are needed the larger the base decided on, but the complexity of the elements used increases accordingly. To determine whether the base should be large or small, the product of the number of elements and the number of states per element can be regarded as an indication of the

complexity of the total system of representation. It appears that this product is a minimum when the number e (= 2.718 ...) is taken as the base[2]). The nearest integer to this is 3, but 2 is also near, and moreover many simple elements are known which, disregarding transitional states, are essentially on-off (i.e. two-state) devices. For example, a lamp is either on or off, a relay open or closed, a thermionic valve conducting or non-conducting. For these two reasons, the base 2 is virtually the only one used in memory systems.

A digit in a binary number is known as a "bit", which is an abbreviation of "binary digit". By the capacity of a memory is meant the number of bits it is capable of holding.

Types of memory systems

The last ten years have seen a marked increase in the types of memory in use. It would exceed the scope of this article to discuss them all, but it will be as well to mention some of them before dealing at greater length with the magnetic-core type.

Punched cards

Punched cards can be regarded as memory elements in that they store information by virtue of the presence or absence of holes at given positions. The punched card system is one of the few memory systems that existed before the last war. A complete memory consists of a stack of cards and a machine for reading them. Its capacity can be increased at will by adding to the stack. For data to be obtained from a given card, however, the machine must scan the cards in the stack one by one until it finds the card required. The information on a given card is thus not immediately accessible, but is yielded up only after a certain variable "search time" or "access time".

The magnetic drum

The magnetic drum first came into use as a memory during the last war. It consists of a cylinder which is coated with a magnetic material and rotates about its axis at constant speed. Along the surface of the cylinder are arranged numerous magnetic heads which, as in magnetic sound recording, can locally magnetize the surface of the drum. The surface is divided into large numbers of elements, identified by the number of the head under which they pass and by a system of numbered lines traversing the drum parallel to the axis (*fig. 1*). The sense in which a surface element is magnetized is either the same as or opposite to the sense of rotation. The one sense signifies "0" and the other "1". Each surface element thus offers room for 1 bit. The heads serve both for recording (writing) the information and for detecting (reading) it.

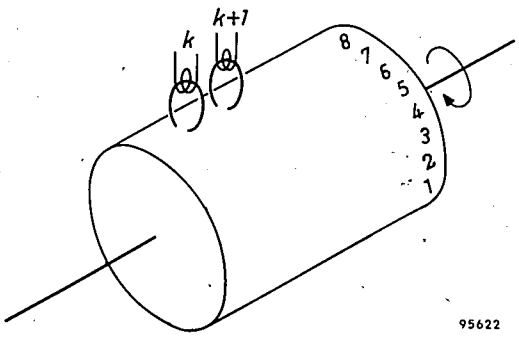

Fig. 1. Schematic representation of a magnetic-drum memory showing the arrangement of the magnetic heads. The surface is divided into elements, each capable of storing one "bit" of information. The position of an element is defined by the number of the magnetic head, k, $k + 1$, ... under which the surface element revolves, and by the number of the parallel line on which the element lies.

The various bits of the same number can be arranged on the same parallel line and simultaneously written or read with all heads. This is called the parallel mode of operation. Another possibility is to arrange the bits of a number so that they pass in succession under one and the same head. This is called the serial mode.

The access time of drum memories amounts on an average to half the time of one revolution.

The information stored in a punched card or magnetic drum memory can be retained indefinitely without the need for special measures to preserve it. This is an advantage over the delay lines and electrostatic memories touched on below. Nor is the information removed by the read-out process, and this distinguishes the punched card and magnetic drum memories favourably from the magnetic core type.

Delay lines

The principle of the delay-line memory is very simple. The information is injected into the line in the form of a pulse train. The pulses travel through the line with a certain velocity, are taken off at the end of the line and returned to the line input via an amplifier which regenerates the original shape and strength of the pulses. Current pulses are used in the case of an electrical delay line. An elastic medium can also be used, however, in which the information is propagated as sound waves (stress

[2]) See, for example, R. K. Richards, Arithmetic operations in digital computers, D. van Nostrand, New York 1955, p. 7.

pulses). A sonic delay-line often consists of a mercury column. The maximum access time in this case is determined by the length of the column and the propagation velocity of sound in mercury.

A drawback attaching to all delay lines is that the regeneration of the pulses calls for complex equipment.

The Williams system

The Williams tube storage system is one of the best known examples of a group of memories in which the information is stored in the form of electric charges (electrostatic memories). In this system the screen of a standard cathode-ray tube is divided into numerous small domains. The electron beam can be directed on to each domain in turn and can write a bit by producing, or not producing, an electric charge.

Like delay lines, electrostatic memories must be provided with a regeneration device, as otherwise the information would leak away.

Magnetic-core memories

In recent years much faster memory systems have been developed which consist of numerous small rings of a ferromagnetic material having a rectangular hysteresis loop [3]). Impetus was given to this development by the advent of ceramic ferromagnetic materials (ferrites [4])), from which very small cores can be made. Ferrites being insulators, there is no difficulty with eddy currents which, when metallic magnetic materials are used, restrict the speed of reading and writing. Examples of the ferrite cores used in the memory circuits dealt with in this article are shown in *fig. 2*.

The induction in a ferromagnetic toroid, which is first driven to saturation and from which the magnetizing field is then removed, can only assume the two values $+B_0$ and $-B_0$ (see *fig. 3*, which shows an idealized loop). If we attach to these two remanent states of magnetization the significance "1" and "0", respectively, we have an element capable of representing one bit, that is, of containing one bit of information. Rectangularity of the hysteresis loop is not necessary in principle, for any shape of hysteresis loop will give rise to two stable states. However, for reasons which will become evident presently, the rectangularity *is* necessary for a practical memory system.

[3]) These systems were devised at about the same time, but independently, by J. A. Rajchman (R.C.A. Rev. **13,** 183-201, 1952) and J. W. Forrester (J. appl. Phys. **22,** 44-48, 1951).

[4]) See Philips tech. Rev. **8,** 353, 1946, **13,** 181, 1951/52 and **14,** 245, 1952/53, and also the article mentioned in [1]).

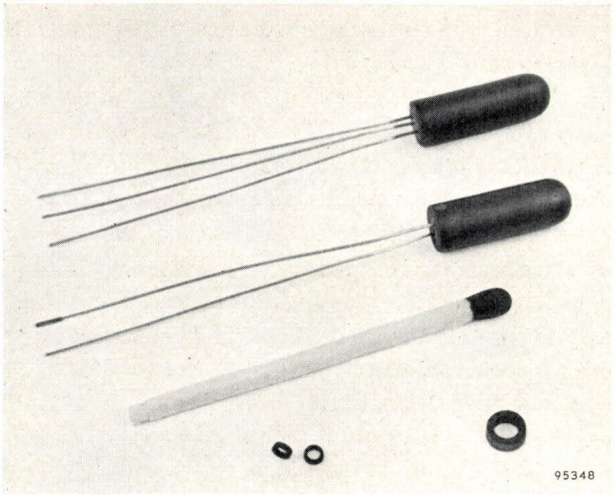

Fig. 2. The basic components of the magnetic-core memory developed at the Philips Laboratories, Eindhoven: a germanium transistor, a germanium diode, rings of ferroxcube 6D3 which serve as memory elements (centre foreground), and a ring of ferroxcube 6E1 as used in a circuit for producing current pulses of stable shape and height.

In order to be able to read the information in a core and if necessary to change it (by reversing the magnetization), the core is threaded with one or more wires through which currents of the requisite magnitude are conducted. The manner in which the wires are threaded through the cores depends on the solution adopted for the selection problem. This requires some explanation.

Since the numbers are often merely a code for information of widely different kinds, they are usually referred to not as numbers but as "words".

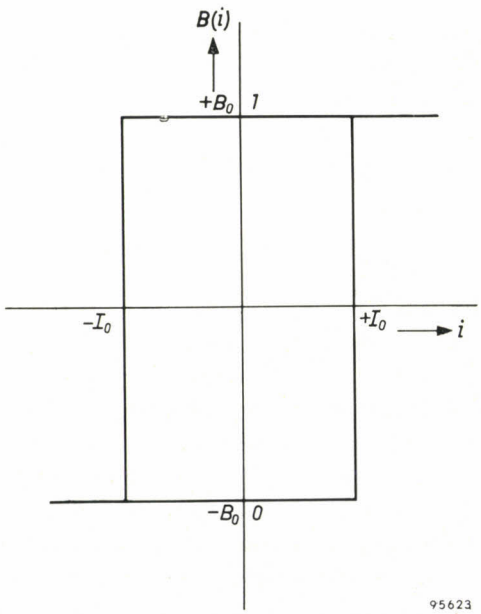

Fig. 3. Idealized rectangular hysteresis loop (induction B as a function of current i) of a magnetic core as used in a memory system. The two states $+B_0$ and $-B_0$ represent respectively the digits "1" and "0".

A word, in order to be stored in the memory, is first recorded in a "buffer register". This is a single series of elements which can be in one of two possible states (flip-flops); a pulse arriving at any flip-flop causes it to jump into its other state. The memory is divided into word registers each of which consists of as many cores as the buffer register contains elements. The word in the buffer register must now be transferred to that particular word register of the memory which has been selected for that word. This is one aspect of the selection problem. The other aspect is how to transfer a word from a given word register of the memory into the buffer register. The registers in the memory are also frequently referred to simply as "words"; a memory may be said to be, for example, a memory of 80 words each of 12 bits, which means that it has 80 word registers each of 12 cores, whilst the buffer register likewise consists of 12 elements.

To give a very simple example, we consider a case where each word consists of one bit, so that the buffer register, too, consists of only one flip-flop. A common wire S_x passes through a number of cores $T_1 \ldots T_i \ldots T_n$, and wires $S_{y1} \ldots S_{yi} \ldots S_{yn}$, respectively, pass through each core separately (*fig. 4*). Let I_0 be the current needed to change the

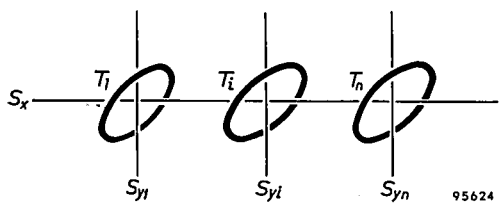

Fig. 4. Magnetic cores with selection wires S_x and S_y. This arrangement constitutes a very simple magnetic-core memory with one bit per word.

magnetization of a core from the one remanent state to the other. We assume that the core material has a rectangular hysteresis loop. To read the contents of core T_i we pass through each of the two wires S_x and S_{yi} a current pulse of magnitude $\frac{1}{2}I_0$ in the negative direction as understood in fig. 3. Only core T_i is then subjected to a field strong enough to reverse its magnetization ($\frac{1}{2}I_0 + \frac{1}{2}I_0$); the other cores receive merely $\frac{1}{2}I_0$. If core T_i was set to the "1" state, its magnetization reverses and this induces an e.m.f. in a third wire (not shown in fig. 4) which threads all cores and is connected to the flip-flop of the buffer register. This wire is the "read" or "information" wire (for brevity, denoted I wire). Owing to the rectangular hysteresis loop of the core material, the magnetization of the cores subjected to $\frac{1}{2}I_0$ remains constant. These cores therefore produce no output in the I wire. The flip-flop having previously been set to the "0" state(i.e. the buffer register having been cleared), the e.m.f. induced in the I wire brings the flip-flop into the "1" state, which thus takes over the information from core T_i. If T_i was originally in the "0" state its magnetization is not reversed and therefore no e.m.f. is induced in the I wire. The flip-flop remains in the "0" state and hence again reads the state of T_i.

Reading the contents of a core evidently amounts to writing an "0" in the core. If the core was in the "1" state it is therefore necessary, if the original information is not to be lost, to restore the "1" after the reading operation. Before discussing a method of thus "regenerating" information, we shall elaborate somewhat on the configuration of fig. 4.

Matrix memories

Fig. 5 shows diagrammatically a collection of cores arranged like the elements of a matrix, hence the name "matrix memory". The matrix in fig. 5 has selection wires in the x and y directions. The cores are situated at the points of intersection. An S_x wire passes through all cores in each row and an S_y wire through all cores in each column. The information wire I is threaded through every core and is again connected with the buffer register flip-flop. Like the single row of cores in fig. 4, the matrix constitutes a memory for words consisting of one bit, and thus the buffer register is again a single flip-flop. Finally, there is another wire threaded through every core — the "inhibit" wire B, whose function will presently be made clear.

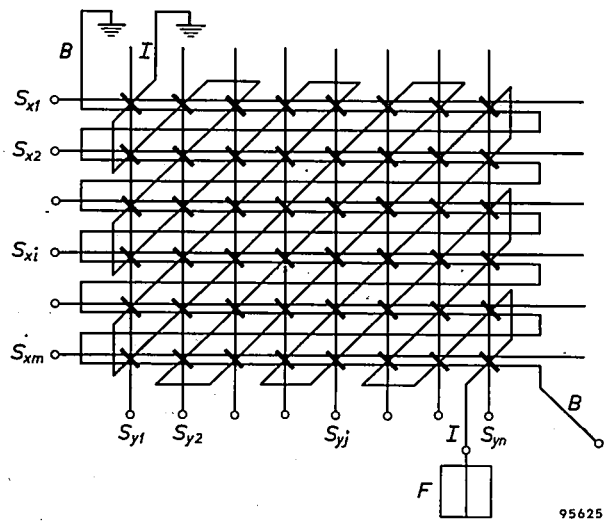

Fig. 5. Extension of the memory in fig. 4 to a matrix arrangement of cores. This register also contains one bit per word. The wires $S_{x1} \ldots S_{xm}$ and $S_{y1} \ldots S_{yn}$ are the selection wires. I is the information wire; this threads every core and is connected to the flip-flop F which constitutes the buffer register. The inhibit wire B also threads every core.

The information is read in the manner discussed with reference to fig. 4: to transfer the contents of core T_{ij} to the buffer register, negative current pulses of magnitude $\frac{1}{2}I_0$ are conducted simultaneously through the selection wires S_{xi} and S_{yj}. This sets the core to the "0" state. To restore the core to its original state, positive pulses of $\frac{1}{2}I_0$ are arranged to pass simultaneously through the wires S_{xi} and S_{yj} immediately after the read-out. If nothing further happens, the core T_{ij} is thereby brought into the "1" state. If this core was in the "1" state before the read-out, the positive pulses thus achieve their object; if it was in the "0" state, however, it must remain in that state. To ensure that such will be the case, a negative current pulse of magnitude $\frac{1}{2}I_0$ is sent through the inhibit wire B at the same time as the positive pulses pass through S_{xi} and S_{yj}. This negative pulse neutralizes one of the positive pulses and prevents core T_{ij} from changing into the "1" state. Whether or not a pulse *is* sent through the inhibit wire is controlled by the flip-flop in the buffer register which took over the information from core T_{ij}.

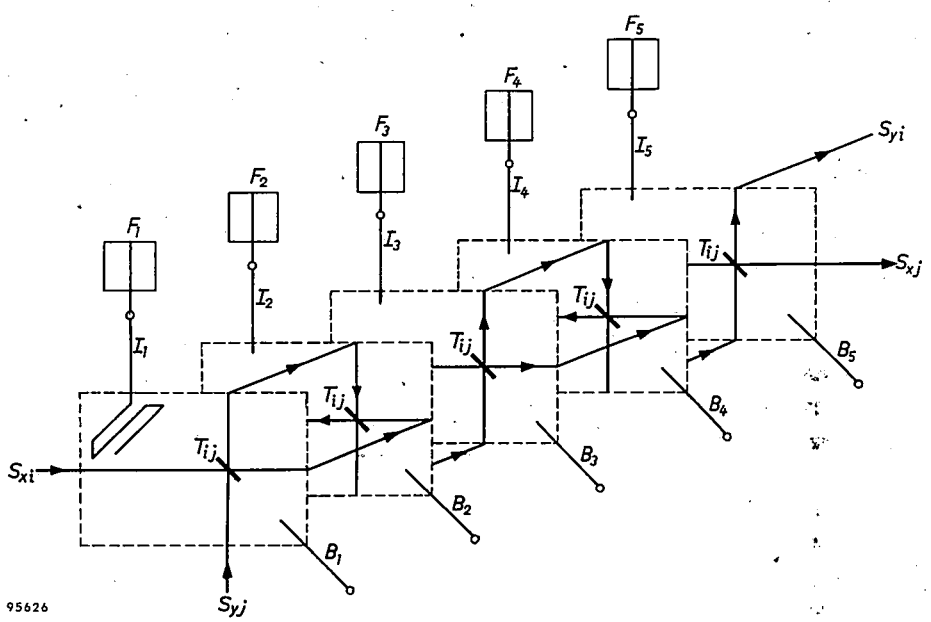

Fig. 6. A magnetic-core memory consisting of 5 matrices as in fig. 5 mounted one behind the other. The selection wires S_x and S_y pass through all five matrices; each matrix, however, has its own information wire I with flip-flop F and its own inhibit wire B, which is driven by this flip-flop.

Fig. 6 goes a step further. It represents a memory containing words of 5 bits [5]). This memory consists of 5 matrices of the kind discussed above. All wires S_{xi} and S_{yj} with the same index i or j are connected in series; each matrix retains, however, its own information wire I and its own inhibit wire B. When currents $-\frac{1}{2}I_0$ are passed through the wires S_{xi} and S_{yj}, the cores T_{ij} are read (brought into state "0") simultaneously in all five matrices, and the e.m.f.'s which may be induced in the information wires $I_1 \ldots I_5$ actuate the five flip-flops of the buffer register which receive the information. To restore the information to the memory the direction of the pulses in the S_{xi} and S_{yj} wires is reversed and at the same time the flip-flops are used to control the five inhibit wires $B_1 \ldots B_5$.

Disturbing pulses

Let us consider one of the five matrices in fig. 6, i.e. a matrix as in fig. 5. We assume that the core T_{ij} is to be read, and that it is in the "1" state, so that its magnetization reverses in the read-out process. Of all the cores in the matrix, only T_{ij} receives a current pulse $-I_0$; of the other cores, $n-1$ on wire S_{xi} and $m-1$ on wire S_{yj} receive $-\frac{1}{2}I_0$, while no current pulse at all passes through the remainder. Since the hysteresis loop is never perfectly rectangular, small flux changes also occur in the $m+n-2$ cores which simultaneously receive $-\frac{1}{2}I_0$ (*fig. 7*). These flux changes produce in the information wire I, threading as it does every core, spurious signals which can form a resultant disturbing pulse of appreciable magnitude. This pulse is smaller the better the loop-rectangularity of the core material, that is to say the more truly horizontal are the top and bottom of the hysteresis

[5]) An arrangement as in fig. 6 was first used by J. A. Rajchman; see the first article mentioned in [3]).

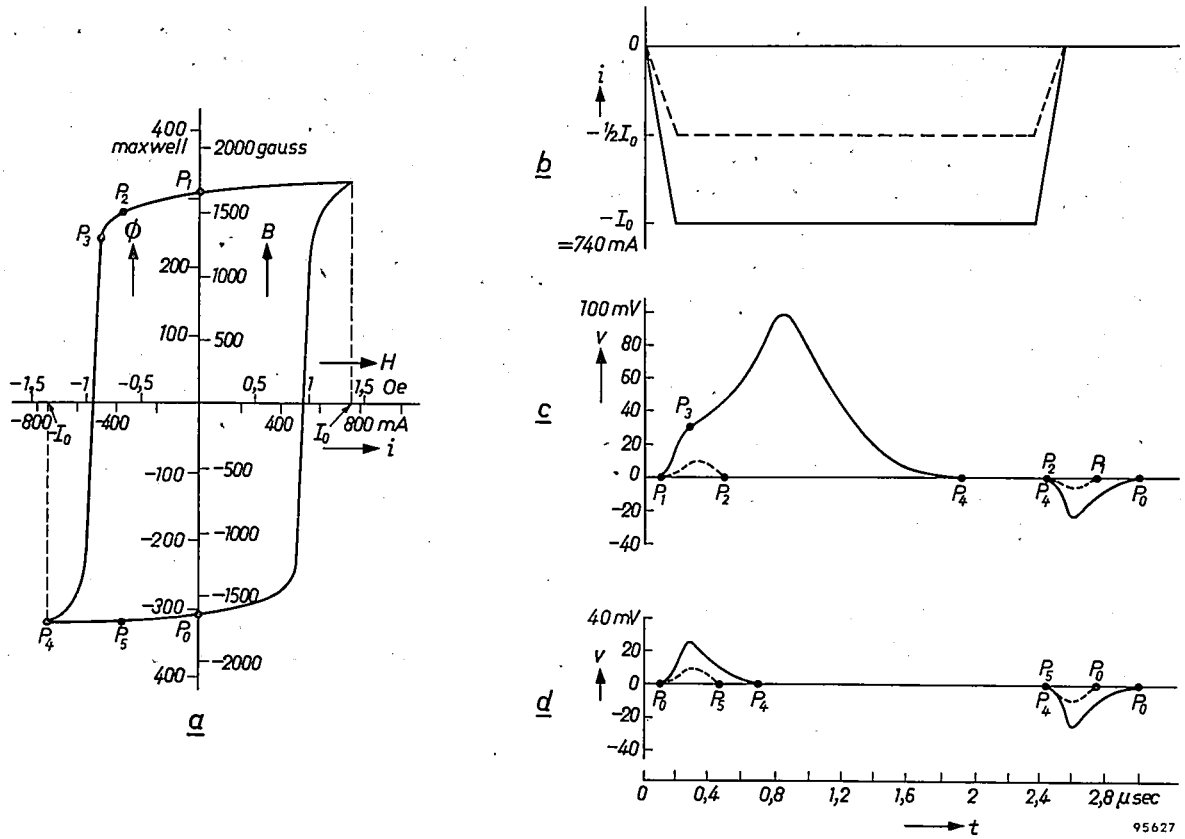

Fig. 7. Hysteresis loop of a core of ferroxcube 6D3 (*a*). If two wires are threaded through the core and a current pulse passes through one of them, a voltage pulse is induced in the other. If the initial state is point P_1 (see *a*), and the current pulse has the form represented by the solid line in (*b*), the point P in (*a*) passes from P_1 via P_3 and P_4 to P_0. Voltage pulses are then induced as shown by the solid curves in (*c*). The letters P on these curves correspond to those in (*a*). When a current pulse is applied with the wave form shown by the dashed line in (*b*), the operating point in (*a*) moves from P_1 to P_2 and back. The corresponding voltage pulses are shown as dashed curves in (*c*). If the initial state of the core was at P_0, voltage pulses appear as shown in (*d*). Of all these voltage pulses, only the large pulse in (*c*) is the useful one; the others are disturbing pulses.

loop. The magnitude of such a pulse is also markedly influenced by the way in which the I wire is threaded through the cores. In fig. 5 this is done in such a way that the I wire threads half the cores on an S_x wire in one direction and the other half in the opposite direction. The same applies to the cores on an S_y wire. With this arrangement the disturbing signals largely neutralize each other. A drawback of this threading system is that the cores are distributed in two equally large groups which deliver useful voltage-pulses of opposite polarity. The output amplifier serving the flip-flop must therefore be able to handle pulses of both polarities, which is an added complication. Moreover, the resultant disturbing pulse can, under certain circumstances, still be large enough to give difficulties.

Since disturbing pulses cannot entirely be avoided in this system, means must be found of rendering them harmless in the final output signal. The total signal appearing at the flip-flop has the waveform shown in *fig. 8*. The first peak p is due to the unwanted signals; its height is, of course, a function of matrix size, being greater the larger are m and n. There are two methods of suppressing the effect of this peak. One method is to integrate the total signal.

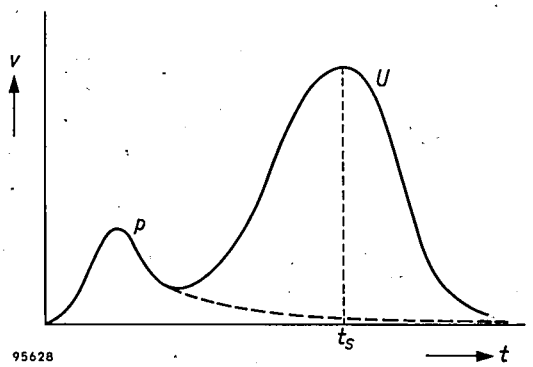

Fig. 8. The total voltage pulse in an I wire on reading a core in a memory as in fig. 5 or 6, when this core is in a "1" state. The voltage peak U induced by the flux reversal is preceded by a disturbing pulse p. The latter is the resultant of the unwanted e.m.f.'s induced by cores situated on the two selection wires which intersect in the selected core. The dashed curve applies when the ring is in a "0" state.

The result of the integration is a signal which is proportional to the area bounded by the curve representing the original signal. The disturbing pulse is of much shorter duration, i.e. much narrower than the pulse caused by a reversal of magnetization, and it therefore contributes little to the integrated signal. The other method makes use of the fact that the disturbing pulse precedes the useful one. If the amplitude of the signal be measured at the moment t_s in fig. 8, a large or small value will be found, depending on whether the selected core was in the state "1" or "0".

But even though the disturbing pulses can be made ineffectual, it is still preferable to avoid them altogether since their suppression involves additional equipment. A memory system has in fact been developed at the Cambridge University Mathematical Laboratory which completely avoids disturbing signals by means of a special method of threading the cores [6]).

The Cambridge system

In the system we have just been considering, the number of two-dimensional matrices equals the number of bits per word, and the number of cores per matrix equals the number of words in the memory. In the Cambridge system all cores are arranged in a single two-dimensional matrix (*fig. 9*). The cores in a column form a word, so that there are as many words as there are columns, and the number of rows is equal to the number of bits per word. We shall now describe how this memory functions.

Reading. A wire which we shall call the A wire (address wire) passes vertically through the cores of each word. To read a word, a negative current-pulse — the reading pulse — with an amplitude equal to or larger than I_0 is sent through the relevant A wire. This ensures that all cores for that word are set to the "0" state. Those cores that were in the "1" state thus undergo a reversal of magnetization and thereby each induce an e.m.f. in the respective information wires, which pass through the cores horizontally. We shall refer to the latter wires as I-R (information-read) wires to distinguish them from the I-W (information-write) wires which are also threaded horizontally through the same cores, and whose function will be discussed presently. The voltage pulses in the I-R wires pass through the output amplifiers Q and actuate the flip-flops F of a buffer register, which, having previously been set to the "0" state, are now changed to the "1" state. The flip-flops that receive no voltage pulse remain unaffected. Plainly, disturbing signals cannot accumulate, for on each I-R wire there is always only one core that receives a current pulse. Another feature that can be of advantage is that in principle there is no limit to the permissible magnitude of the reading pulses in the A wires.

Restoring the information. To return the cores pertaining to the read-out word to their original state, a positive current pulse $\frac{1}{2}I_0$ is sent through the relevant A wire and also through the I-W wires corresponding to the flip-flops which changed to

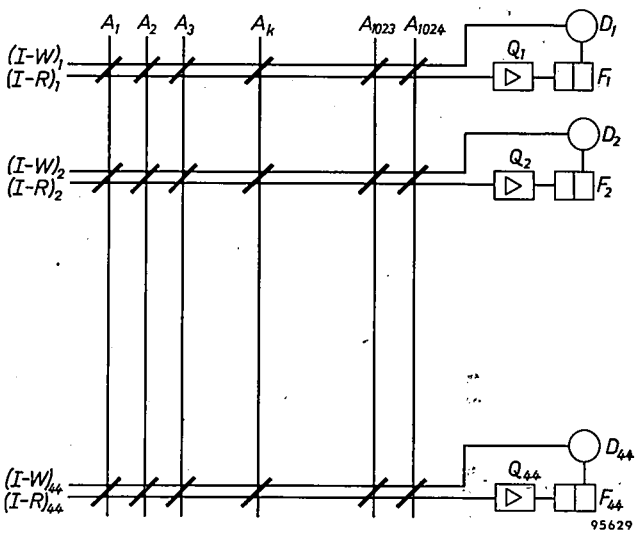

Fig. 9. Simplified diagram of a Cambridge-type memory system. It is assumed that the cores form a matrix of 1024 columns and 44 rows. Each column constitutes one word. Through all the cores of a row are threaded the information wires I-R (for reading) and I-W (for writing). These I wires are connected with the 44 flip-flops F of the buffer register. $Q_1 \ldots Q_{44}$ are the output amplifiers; $D_1 \ldots D_{44}$ are the circuits which supply the current pulses $+\frac{1}{2}I_0$ to the I-W wires for restoring the information after reading. The cores in the columns are threaded by the address wires $A_1 \ldots A_{1024}$, through which current pulses $-I_0$ are passed for reading and half-write pulses $+\frac{1}{2}I_0$ for restoring the information.

"1" in the reading operation. For this purpose the flip-flops in question control the circuits D which supply the requisite pulses. The coincidence of two positive current pulses $\frac{1}{2}I_0$ causes all cores whose magnetization was reversed by the read-out to return to their former state.

In the process as described, the negative reading pulse in an A wire must be equal or greater than I_0, while the sum of the positive half-write pulse in the A wire and that in the I-W wire, required to restore the information, must also be equal to or greater than I_0. The half-write pulses individually, however, and particularly those in the I-W wire, should not exceed $\frac{1}{2}I_0$. Consider, for example, the core $(k, 2)$ in fig. 9 and assume that this is in the "0" state.

[6]) W. Renwick, A magnetic-core matrix store with direct selection using a magnetic-core switch matrix, Proc. Instn. Electr. Engrs. **104 B**, Suppl. No. 7, 436-444, 1957.

In the $(I\text{-}W)_2$ wire a half-write pulse appears every time a word has been read whose second core was in the "1" state. Whenever this happens, core $(k, 2)$ is disturbed. These repeated pulses shift the operating point of core $(k, 2)$ upwards. If the pulses are not larger than about $\frac{1}{2}I_0$, this process soon stops (*fig. 10*); if they are larger than $\frac{1}{2}I_0$, however, the operating point continues to shift upwards and the information in the core is gradually destroyed [7]).

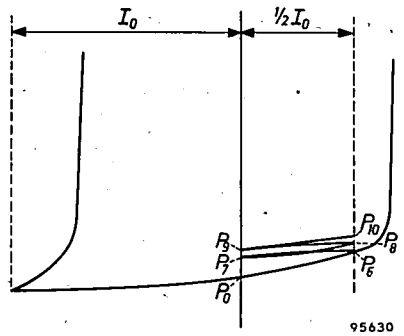

Fig. 10. Displacement of the operating point of a magnetic core as a result of repeated current pulses of magnitude $+\frac{1}{2}I_0$. The operating point lies originally at P_0, corresponding to the "0" state. Under the influence of the first current pulse it moves to P_6, and returns to P_7 upon completion of the pulse. The second pulse brings the operating point via P_8 to P_9. Upon the third and subsequent pulses the operating point continues to move between P_9 and P_{10}. If the magnitude of the current pulses is *greater* than about $\frac{1}{2}I_0$, the operating point continues to shift upwards with successive pulses and the information contained in the core is gradually destroyed.

The half-write pulses in the A wires are less dangerous. In the A_k wire, for example, a half-write pulse appears only after the kth word has been read, and during the reading process all cores of this word (and hence core $(k, 2)$ also) are set to the "0" state. The operating point of core $(k, 2)$ can therefore never shift cumulatively upwards as a result of half-write pulses in the A_k wire. Nevertheless, it is desirable to prevent the half-write pulses in the A wires from causing the critical point P_6 in fig. 10 to be exceeded, and therefore the half-write pulses both in the $I\text{-}W$ and in the A wires should be limited to $\frac{1}{2}I_0$. Since their sum must be at least I_0, they must accordingly be made exactly equal to $\frac{1}{2}I_0$.

We shall now show that the tolerance in these pulses can be widened by applying a *bias current*. Another advantage of a bias current is that it makes it possible for the reading and writing pulses through the A wires to have equal amplitudes.

[7]) See e.g. the article mentioned in [1]), pages 57 and 58, and the first article mentioned in [3]), pages 192 et seq.

The bias current

The bias current is a constant negative current I_p which is passed through an additional wire threaded through all the cores, parallel to the A wires. The bias current I_p is usually $-\frac{1}{3}I_0$. The "0" and "1" states then correspond to the points marked as such in *fig. 11*. To read the word at address k (the word through which the A_k wire passes; fig. 9) it is necessary to pass through the A_k wire a negative current pulse $-G$ which is greater than $\frac{2}{3}I_0$ (see fig. 11). For restoring the information, the positive pulse must not be greater than $(\frac{1}{3} + \frac{1}{2})I_0 = \frac{5}{6}I_0$, if the critical point P_6 on the loop is not to be exceeded. If this pulse is also made equal to G, i.e. equal to the read pulse, then $\frac{2}{3}I_0 < G < \frac{5}{6}I_0$, which gives us a certain tolerance for G. The pulse in the $I\text{-}W$ wire should not exceed $\frac{5}{6}I_0$ either. It is preferable to make G larger than the minimum value, since this increases the speed at which the magnetization of a core reverses, resulting in a higher voltage pulse in the $I\text{-}R$ wire. The pulse in the $I\text{-}W$ wire may then be made correspondingly smaller.

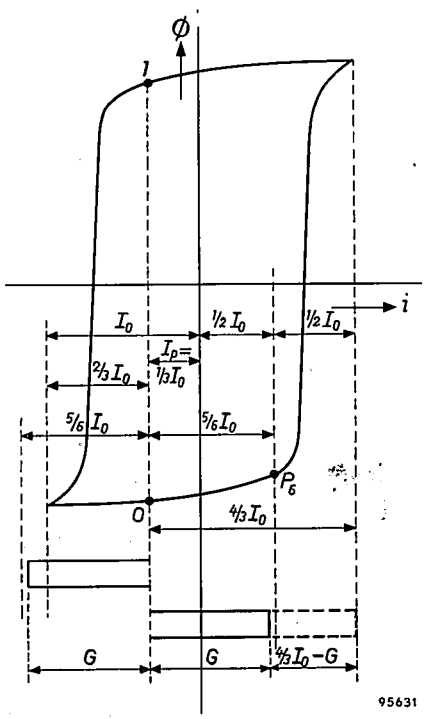

Fig. 11. When the cores are subjected to a constant bias current $I_p = -\frac{1}{3}I_0$, the remanent magnetization states representing "0" and "1" correspond to the operating points marked as such. There is now considerable freedom in the choice of the current-pulse amplitude in the A wires for reading and writing; moreover the pulses can now be made equal in magnitude. For reading (negative pulse) this amplitude G must be greater than $\frac{2}{3}I_0$, but for writing (positive pulse) it must not exceed $\frac{5}{6}I_0$ in order not to pass the point P_6 on the loop (see also fig. 10). The "half"-write pulse through the $I\text{-}W$ wire is represented by a broken line. This is added to the half-write pulse through the A wire.

Cycling time

If special measures are not taken, the cycling time is not particularly short for this type of memory. The cycling time is the minimum time that must lapse before a word can again be read. The fact that it is fairly long is due to the large voltage pulse induced in the *I-R* wire in the writing process (i.e. when restoring the information). The *I-W* and the *I-R* wires together can be regarded as two windings which are magnetically coupled by the commonly threaded cores (i.e. as a transformer). The effective permeability of the cores, which is related to the angle made by the top and bottom edges of the hysteresis loop with the i axis, is appreciably greater than 1. For this reason, an e.m.f. is induced in the *I-R* wire when a current is switched on or off in the *I-W* wire. In the *latter* case, the e.m.f. has the same polarity as that produced when the magnetization in a core reverses from "1" to "0", but is much larger (e.g. 40 times as large). A normal amplifier is blocked for a certain time by a voltage pulse which is many times larger than that for which it is designed. It is thus necessary to wait until the amplifier has recovered. To prevent blocking one must therefore limit the amplitude of this parasitic pulse. One way of doing this is to connect a diode across the input of the amplifier and to arrange for it to become conductive(and so short-circuit the amplifier) when the pulse amplitude attains a certain value. This, however, is scarcely an improvement, for the effect is to spread the pulse over a period which is longer the more the amplitude is limited. (We do not intend to explain this phenomenon here.) The object of shortening the cycling time is thus not achieved in this way. A method which does achieve this object will be discussed presently.

An improved memory system

The memory used in the experimental computer now in operation in the Philips Laboratories at Eindhoven is a further development of the Cambridge system. Its storage capacity is 1024 words of 44 bits. The inside diameter of the cores employed is 1.3 mm and the outside diameter 1.95 mm. Their height is 0.58 mm (fig. 2). They are made of ferroxcube 6D3; their magnetization reverses at a current $I_0 = 740$ mA.

The memory operates on essentially the same principle as the Cambridge system. We shall first consider 44 cores which together form one word (*fig. 12*). The address wire is now divided into an *A-R* (address-read) wire and an *A-W* (address-write) wire. There is also a wire *P* for the bias current, so that three wires pass vertically through the cores forming a word. The *A-R* and *A-W* wires are connected via separate switches to the same current source (not shown in fig. 12). Since the current pulses *G* must flow in opposite directions for reading and writing, these wires, seen from the current source, are threaded in opposite directions through the cores. The bias current is $-\frac{1}{3}I_0$, hence $-\frac{1}{3}\times 740 \approx -250$ mA. The value of *G* must therefore be at least $\frac{2}{3}I_0 \approx 490$ mA, but must remain below $\frac{5}{6}I_0 \approx 615$ mA. In our case *G* is 600 mA; the voltage pulses on the output amplifier are then about twice as high as when *G* is minimum.

The *I-R* and *I-W* wires are combined to form single *I* wires, which perform the functions of both reading and writing. This simplifies the threading

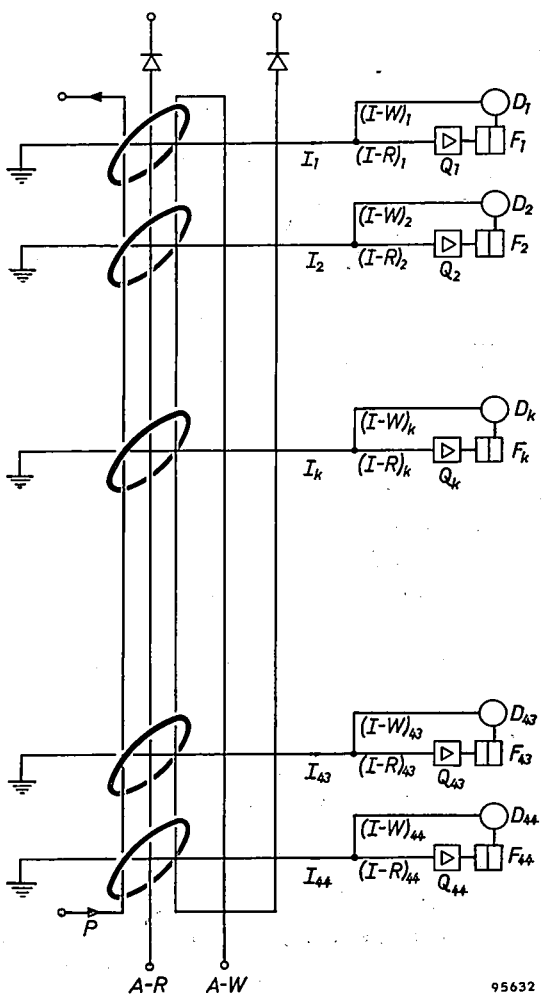

Fig. 12. Arrangement of the cores forming one word in the magnetic-core memory developed at Philips, based on the Cambridge system. The address wire is divided into an *A-R* wire for reading and an *A-W* wire for writing. The *I-R* and *I-W* wires are combined to form single *I* wires, which are used both for reading and writing and branch into two only just before the amplifiers *Q*. These amplifiers operate the flip-flops *F* of the buffer register. The circuits *D* supply the current pulses to the *I* wires for restoring the information; they are controlled by the flip-flops *F*.

of the matrix. Since G exceeds $\frac{2}{3}I_0$ by a certain amount, the writing current through the I wire (for restoring the information) can be made correspondingly smaller, and need amount to only 380 mA.

The cores of 32 words are arranged in matrix form, corresponding to a Cambridge memory system with 32 words. The complete memory consists of 32 of these matrices, mounted vertically and parallel to each other. Thus the memory constitutes a matrix of $32 \times 32 = 1024$ words. The arrangement, seen from above, is shown diagrammatically in *fig. 13a*. Each core in this figure represents the vertical projection of a word consisting of 44 stacked cores. The details are explained in the caption to fig. 13. A part of the memory is shown in *fig. 14*. The way in which the wires are threaded through the cores can be seen in *fig. 15*.

Reading a word and restoring the information

To read the word at the address (i, j) the switches $(T\text{-}R)_i$ and T_j are momentarily closed. A reading pulse then passes through the $(A\text{-}R)_{ij}$ wire and the selected word appears in the buffer register. The diodes in the $A\text{-}W$ wires ensure that no current flows along forbidden paths via these wires. Next, in order to write the information back into the memory, the switches $(T\text{-}W)_i$ and T_j are momentarily closed. A current pulse then passes through the $(A\text{-}W)_{ij}$ wire in a direction opposite to that of the reading pulse. The diodes in the $A\text{-}R$ wires now prevent the current from following any other path. At the same time the flip-flops in the buffer register, which during the reading process have been set to "1", provide the necessary pulses in the I wires.

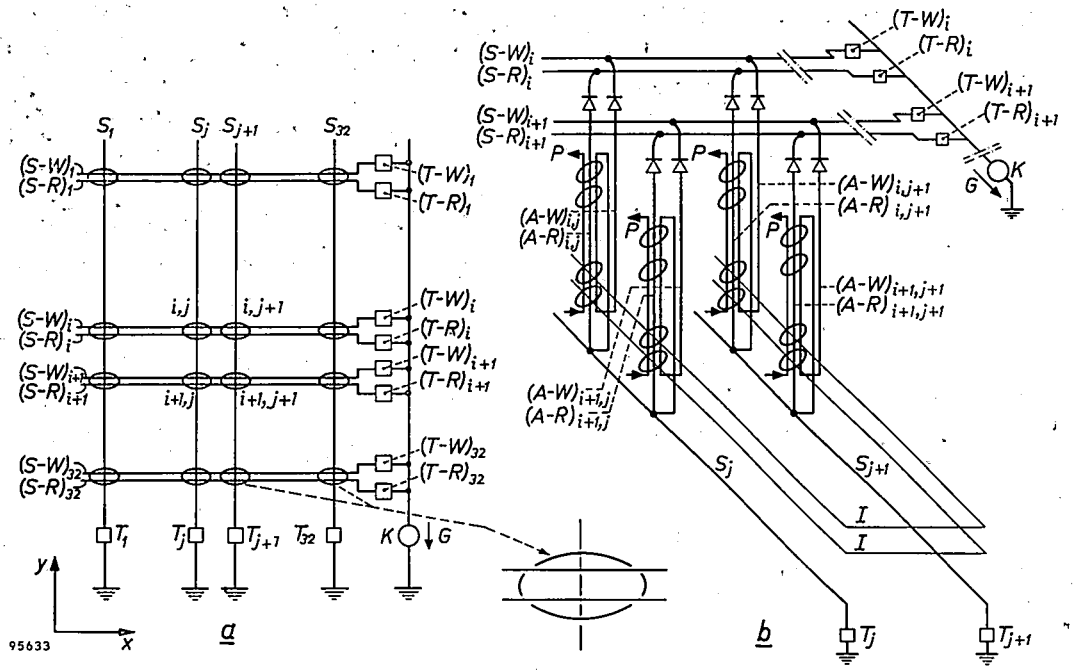

Fig. 13. Principle of the word arrangement in the Philips memory system.
a) Each core drawn represents the vertical projection of 44 cores which together form a word. Through each word (thus downwards in this plan view) are threaded an $A\text{-}R$ wire and an $A\text{-}W$ wire running from the $S\text{-}R$ and $S\text{-}W$ wires threaded in the x-direction at the top of the word, to the S wire threaded in the y-direction at the bottom (see also *b*). All selection wires $S\text{-}R$, $S\text{-}W$ and S possess their own switch, respectively $T\text{-}R$, $T\text{-}W$ and T. When $(T\text{-}R)_i$ and T_j are momentarily closed, the current source K sends a read pulse $-G$ through the word at the address (i, j); when $(T\text{-}W)_i$ and T_j are momentarily closed, the current source sends a write pulse $+G$ through the word. The I wires are not shown in this figure.
b) Perspective drawing of the arrangement of the words at addresses (i, j), $(i + 1, j)$, $(i, j + 1)$ and $(i + 1, j + 1)$. In addition to the parts mentioned in (*a*), two of the 44 I wires are shown here, which terminate at the buffer register (not drawn). It can also be seen how the $A\text{-}R$ and the $A\text{-}W$ wires, seen from the current source K, are threaded in opposite directions through the word cores. The diodes in the $A\text{-}R$ and $A\text{-}W$ wires (visible in the photo in fig. 14) ensure that if, for example, switches $(T\text{-}R)_i$ and T_j are closed, the current cannot take any other path than through the $(A\text{-}R)_{ij}$ wire. The wire marked P is the bias wire, which is threaded through every core in the memory.

N. V. PHILIPS' GLOEILAMPENFABRIEKEN

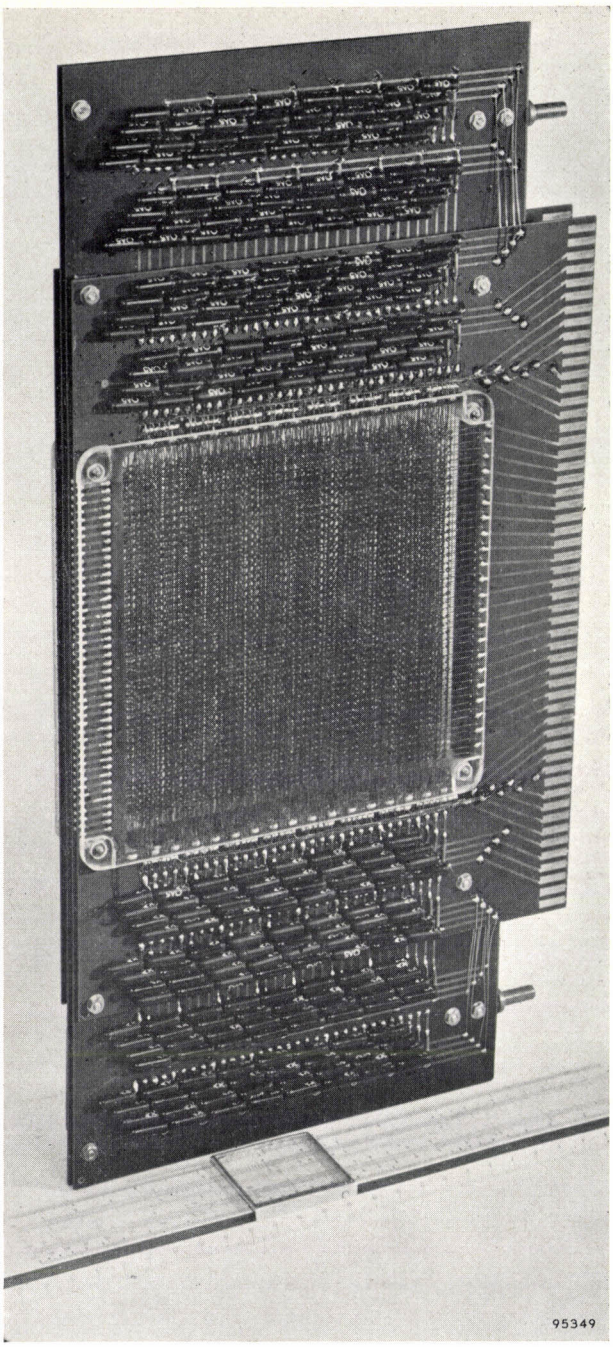

Fig. 14. A part of the Philips memory system. The complete memory consists of four such plug-in units mounted together in a cabinet. The terminal strips seen on the right slide into contact terminals and make the necessary connections with the computer. Use is made of printed wiring [8]). The section shown consists of four matrix groups of 64 columns (the words) each of 44 cores. The complete memory thus has 16 of these matrix groups mounted parallel to each other. This is, however, merely a question of geometric arrangement: electrically the whole memory contains 32 matrices as illustrated in fig. 13. (At the top and bottom can be seen the diodes in the A-R and A-W wires.)

Output amplifiers

The circuits Q in fig. 12, which, in accordance with usage, we call "amplifiers", scarcely deserve this name. Two P-N-P transistors are used, which do not amplify but are used as switches. This application of a transistor depends on the resistance between the emitter and the collector being low when the base current is sufficiently large, and high when the base current is zero.

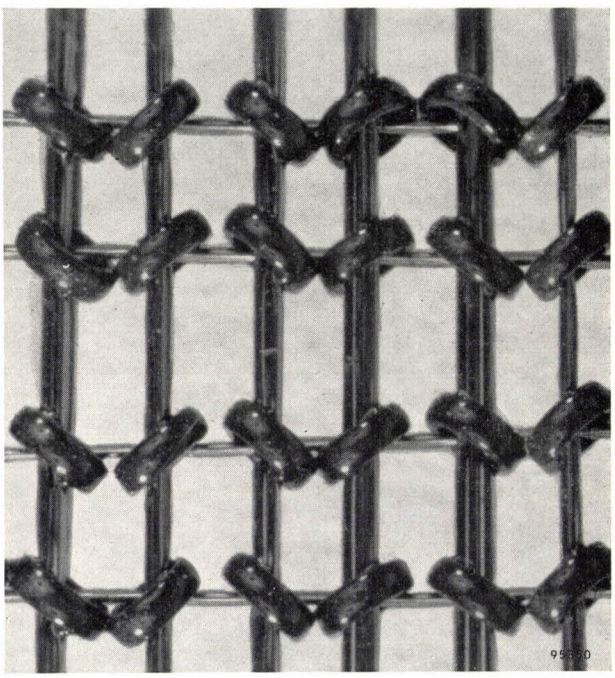

Fig. 15. Detail of the Philips memory, magnified about 7×. It will be seen that four wires are threaded through each core: horizontally the information wire and vertically the two address wires and the bias wire.

The operation of a transistor as a switch may be explained with reference to *fig. 16*. In fig. 16*a* a transistor is shown with a resistor R_E in the emitter lead and a resistor R_C in the collector lead. A current source I_B is included in the base lead and a voltage source (e.m.f. $= V_S$) in the collector lead. The I_C-V_C characteristics are shown in fig. 16*b* [9]), which also shows a load line drawn from point V_S on the V_C axis. The slope of the load line corresponds to the value $R_E + R_C$ (the base current is always small compared with the emitter and collector currents, so that practically the same current I_C flows through R_E and R_C). When $I_B = 0$, the operating point of the transistor is P_1. The collector current is then small and the switch is non-conducting, i.e., open. If, on the other hand, the base current is equal to or greater than I_{B_2}, the operating point is P_2. This results in a high collector current I_{C_2} and the switch is conducting, i.e. closed. The fact that the switch is not an ideal one appears from the small potential difference remaining between emitter and collector. An equivalent mechanical switch is shown in fig. 16*c*.

[8]) See e.g. R. van Beek and W. W. Boelens, Printed wiring in radio sets, Philips tech. Rev. **20**, 113-121, 1958/59, No. 5.

[9]) For a discussion of transistor characteristics, see J. P. Beijersbergen, M. Beun and J. te Winkel, The junction transistor as a network element at low frequencies, I. Characteristics and h parameters, Philips tech. Rev. **19**, 15-27, 1957/58.

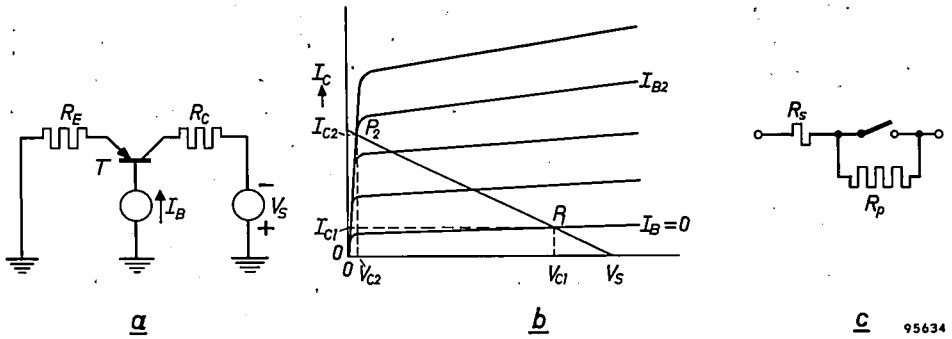

Fig. 16. The transistor as a switch.
a) A transistor T with a resistor R_E in the emitter lead, a resistor R_C and a voltage source V_S in the collector lead and a current source I_B in the base lead.
b) I_C-V_C characteristics with I_B as the running parameter, showing a load line corresponding to the situation in (*a*). When $I_B = 0$, the transistor current is very low (I_{C1}) and the voltage across emitter-collector is high (V_{C1}; switch open). When $I_B > I_{B2}$, the transistor current is high (I_{C2}) and the voltage across it low (V_{C2}; switch closed). The signs of currents and voltages are not specified here.
c) A mechanical switch approximately equivalent to the transistor switch. R_s is a low resistance, R_p a high one.

The circuit diagram of an output amplifier is shown in *fig. 17*. We shall first consider the function of the transistor switch T_2. When, in the reading process, a core undergoes a flux reversal (at which moment the transistor switch T_1 is closed), a voltage pulse appears on the primary of the transformer which will give rise to an open circuit voltage on the secondary of about —6 V. This voltage pulse drives electrons into the base of T_2, thereby producing a base current and

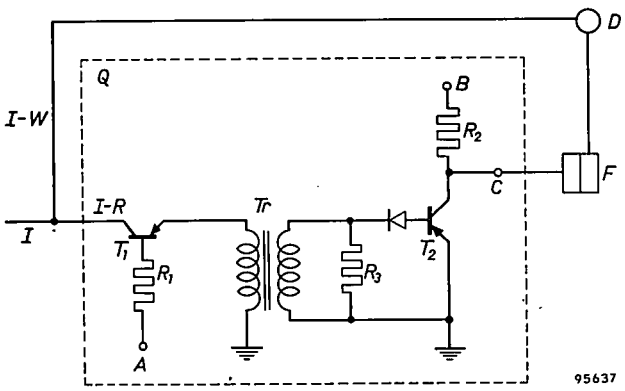

Fig. 17. Circuit diagram of the output amplifiers Q of fig. 12. The transistor T_1 is a switch which makes the connection with the information wire I only at moments when the useful voltage pulses are expected. Parasitic pulses are thus given no opportunity to block the amplifier. Transistor T_2 also acts as a switch, but serves in addition as a temporary storage element, thus making it possible to simplify the circuitry of Q.

making T_2 conducting. Since, however, terminal B is earthed at that moment, the switch is unable to pass current. Now it is a special property of the transistor switch that it remains conducting (closed) as long as there are electrons in the base in excess of the equilibrium concentration. As long as B remains earthed, the excess electrons vanish from the base only by recombination with holes. This takes time, and while it is happening the transistor remains conducting [10]). If during this time a pulse of, say, —10 V is applied to terminal B, terminal C will nevertheless remain at zero potential since it is earthed via T_2 [11]). Care has been taken that the flip-flop connected to C is in the "1" state. (In the present arrangement, clearing of the buffer register involves setting all flip-flops in the "1" state.) The flip-flop therefore remains in the "1" state and represents correctly the state of the read core. If the core is in the "0" state, so that its magnetization is not reversed by the read current, no voltage pulse appears on R_3. Accordingly, no electrons are injected into the base of T_2 and this transistor switch remains non-conducting. When a voltage pulse is now applied to terminal B, terminal C will follow and the flip-flop switches to the "0" state. Here again, then, the state of the flip-flop agrees with the original state of the core.

---

[10]) The existence of this property does not follow from the characteristics in fig. 16*b*, which relate merely to the stationary states. To explain the property it is necessary to consider the phenomena taking place inside the transistor. See e.g. F. H. Stieltjes and L. J. Tummers, Simple theory of the junction transistor, Philips tech. Rev. **17**, 233-246, 1955/56. The property is related to the complex of phenomena comprised under the term "hole storage".

[11]) When a current flows from emitter to collector in a P-N-P transistor, electrons enter the base from the collector and a different number leave the base and go to the emitter (see e.g. Philips tech. Rev. **20**, page 133 et seq.). How long the base remains with excess electrons, i.e. how long the transistor remains conducting after it has been triggered, is therefore no longer dependent solely on the recombination process. Nevertheless, once the transistor *is* conducting it persists in this state for some time.

The function of the diode preceding T_2 is to prevent any positive voltage overshoot over R_3, which might follow the negative pulse, from depriving the base of the injected electrons, in which case switch T_2 would again become non-conducting.

The great advantage of the circuit described is that it provides, with simple means, a certain amount of freedom in choosing the moment at which the pulse is applied to B. This is necessary with the computer in which the memory is used, for the flip-flop is not yet free to take over information exactly at the moment it arrives at the output amplifier. This amplifier now retains the information until the flip-flop has completed its previous task. In this way T_2 serves as an intermediate storage element [12]).

The function of transistor switch T_1 is to ensure a short cycling time. We have already seen that, when a current pulse is passed through the *I-W* wire, a high voltage pulse appears in the *I-R* wire which temporarily blocks the amplifier. This was due to the high mutual inductance between the *I-W* and *I-R* wires. These wires are now combined, but the voltage pulse is still produced as a result of the self-inductance of the *I* wire; since this wire threads 1024 cores, its inductance is high. After the *I* wire has passed through the last core, it splits into an *I-R* and an *I-W* wire again. The *I-R* wire is connected with the collector of transistor T_1, whose emitter is earthed via the primary of transformer *Tr*. During the reading of a word, terminal *A* is held at a negative potential with respect to earth; the voltage supply together with the large resistor R_1 forms a current source which supplies a base current high enough to make the transistor switch T_1 conductive. The voltage pulse which is generated by a core that was in state "1" thus appears unhindered on the primary of transformer *Tr*. (While this takes place, the circuit *D* has a high impedance and cannot therefore disturb the pulse in the *I-R* wire.)

When the circuit *D* sends a current pulse through the *I* wire for the purpose of restoring the information, terminal *A* remains open and the base current of T_1 is therefore zero. The transistor switch is now non-conducting, which means that the *I* wire is virtually isolated from the amplifier. We now have a situation which is exactly the opposite of that discussed on page 201, in which the pulse was limited in amplitude, but automatically increased in duration, by the use of a diode. The pulse is now high, but short in duration. However, since the impedance of T_1 (non-conducting) is very large with respect to the impedance of the transformer, the pulse on the transformer is kept small. The pulse is so small there is now no danger of electrons being injected into the base of transistor T_2, which, as mentioned above, would cause this switch to remain conducting for a while, and make it necessary, before reading the next word, to wait until the electrons had recombined with holes. The use of transistor T_1 allows the cycling time to be reduced from 10 μsec, which is the normal value for magnetic-core memories, to 3 μsec. For practical reasons a cycling time of 4.5 μsec has been chosen. *Fig. 18* shows the timing of the various current and voltage pulses.

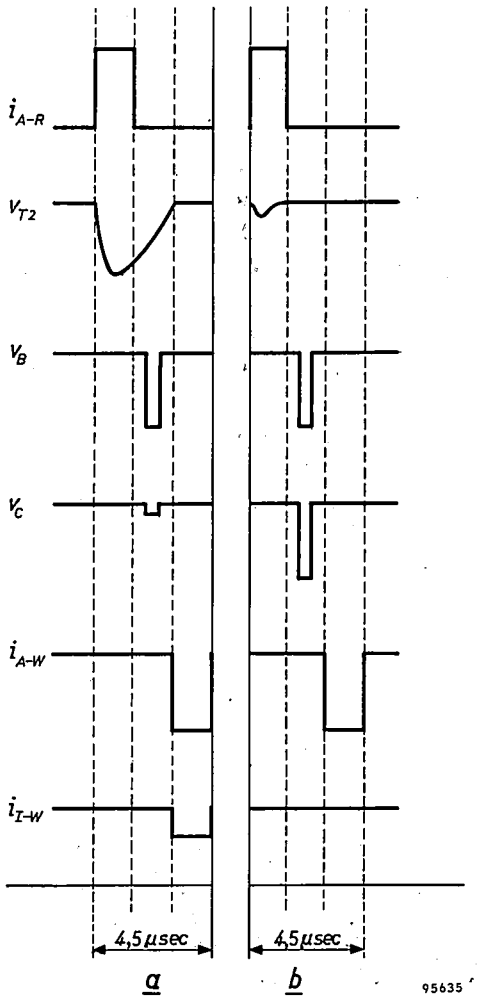

Fig. 18. Timing of the current and voltage pulses over the cycling time (*a*) when reading a core in the "1" state and (*b*) when reading a core in the "0" state. $i_{A\text{-}R}$ read pulse in the *A-R* wire (fig. 12), with amplitude *G* (see fig. 11); v_{T_2} voltage pulse appearing at the base of transistor T_2 (fig. 17); v_B voltage on terminal *B*; v_C voltage on terminal *C*; $i_{A\text{-}W}$ and $i_{I\text{-}W}$ current pulses in the *A-W* and *I* wires for restoring the information. The amplitudes of the latter current pulses are respectively *G* and $\frac{4}{5}I_0 - G$ (see fig. 11).

[12]) The idea of using a transistor as a temporary storage element is due to H. Rodrigues de Miranda (now with the Philips semiconductor factory at Nijmegen, formerly with the Philips Research Laboratories at Eindhoven).

The selector switches

The selector switches T-R, T-W and T in fig. 13 must be closed during carefully defined intervals in order to form the necessary current pulses. Here, too, transistors are used as switches. Since the currents to be switched are too high for a single transistor of the type used, each switch consists of six transistors connected in parallel (*fig. 19*). A resistor is connected in the emitter lead of each transistor. These resistors ensure that the current is uniformly distributed among the six transistors.

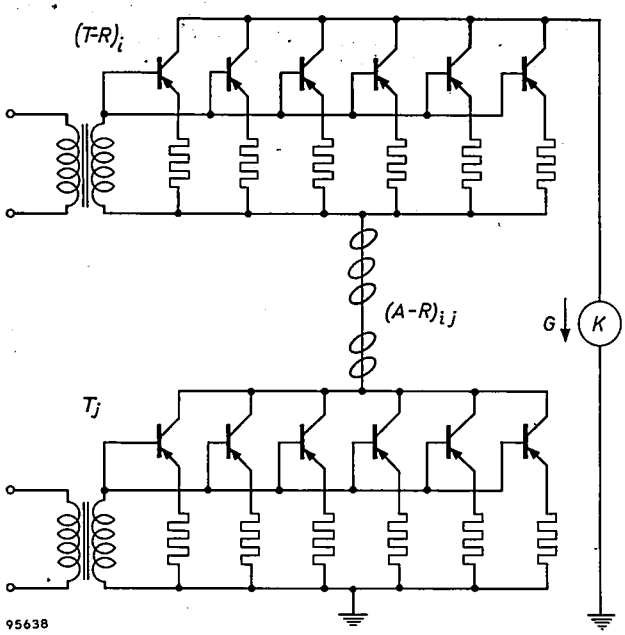

Fig. 19. Two selector switches as in fig. 13, viz. $(T\text{-}R)_i$ and T_j, which when conducting, allow the current source K to send a read pulse $-G$ through the $(A\text{-}R)_{ij}$ wire. The switches consist of six transistors connected in parallel. They are made conducting or non-conducting by current pulses through the primaries of their transformers.

The switches are closed by means of a transformer included in each switch circuit. When a current pulse is passed through the primary, the leading edge induces in the secondary a voltage pulse whose polarity is such that electrons are injected into the transistor bases via the base contacts. As discussed on pp. 203, 204, the transistors are thereby made conducting and the switch closes. The transistors remain conducting until the injected electrons have vanished. The trailing edge of the primary current pulse induces a secondary voltage pulse whose polarity is opposite to that of its predecessor. This pulse withdraws what remains of the injected electrons from the base, so making the switch non-conducting. A switch is thus open during time intervals which exactly coincide with the drive pulses through the primary of its transformer. The incidence and duration of the small drive pulses can be controlled with sufficient accuracy by conventional means. The transistors used are of the high-frequency type; they have very thin base, and a small injection of electrons is sufficient to make them conducting. Only small pulses are thus needed for driving the selector switches.

The current source

As earlier explained (page 202), in order to read the the word from the address (i, j), the switches $(T\text{-}R)_i$ and T_j are momentarily closed. The current source K in fig. 19 (see also fig. 13*a* and *b*) is then connected to earth via the $(A\text{-}R)_{ij}$ wire. This current source must meet certain stringent requirements. Depending on the number of word cores which undergo a flux reversal, an inverse voltage of varying magnitude is induced, but this must not be allowed to have any appreciable effect on the magnitude or shape of the current pulse. An obvious solution is to make up the current source from a voltage source of high e.m.f. in series with an adequately high resistance. In the intervals when no current is being drawn — i.e. when all selector switches are open — the full e.m.f. would then be across the emitter and collector terminals of the transistors. This e.m.f. would be substantially higher than the maximum voltage of 15 V permissible across the transistors. For our purposes, then, another solution must be found.

The current source employed consists of a voltage source connected in series not with an ordinary resistance but with the secondary of a transformer (*fig. 20*). The transformer core consists of a ring of ferroxcube 6E1 ("switch core"). This material also has a rectangular hysteresis loop but its "flux-reversal time" or "switching time" is longer than that of the material 6D3 used for the memory cores [13]).

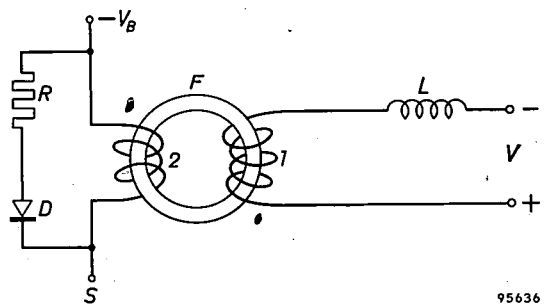

Fig. 20. The current source K of figs. 19 and 13. Through the primary winding *1* of the ferroxcube core F a constant current is passed, supplied by the current source formed by the voltage source V in series with a choke L. The secondary winding *2* is connected at one end to the voltage source $-V_B$ and at the other end S to the selector switches T-R and T-W. The resistor R and the diode D prevent the build-up of a high voltage when the secondary is interrupted.

[13]) See H. van der Heide, H. G. Bruijning and H. P. J. Wijn, Switching time of ferrites with rectangular hysteresis loop, Philips tech. Rev. **18**, 336-346, 1956/57.

A switch core of this kind is included in the photograph of fig. 2. Through the primary winding (*1*, fig. 20) a constant current is passed which is supplied by a source of conventional design — i.e. consisting of a voltage source in series with a choke — and which is powerful enough to keep the current constant notwithstanding the fluctuations on the secondary winding of the transformer. The secondary winding (*2*) is therefore effectively a choke. The primary current is so high as to saturate the ferroxcube core, consequently the self-inductance of the choke is low. If two selector switches are closed (see fig. 19) a secondary current flows which increases rapidly in magnitude owing to the low inductance of the choke. However, the sense of the current through the secondary is such that it attenuates the field produced by the primary current. If the secondary current reaches a value such that the core is no longer saturated, the self-inductance of the choke rapidly increases, and from that moment the secondary current rises only very slowly. After some time, however, this current would nevertheless attain a value capable of saturating the ferroxcube core, but now in the opposite direction. In that case the secondary current would again increase rapidly. The circuit must therefore be designed so that the selector switches open again before this renewed saturation can take place [14]).

When the secondary current is interrupted, the core rapidly returns to its original state of saturation. The flux change to which this gives rise induces in the secondary winding a high voltage pulse of the same polarity as the battery voltage $-V_B$. Measures are needed to prevent this voltage from appearing over the transistors. In the circuit described, this voltage is short-circuited by means of a diode, in series with a resistor, connected in parallel with the secondary winding.

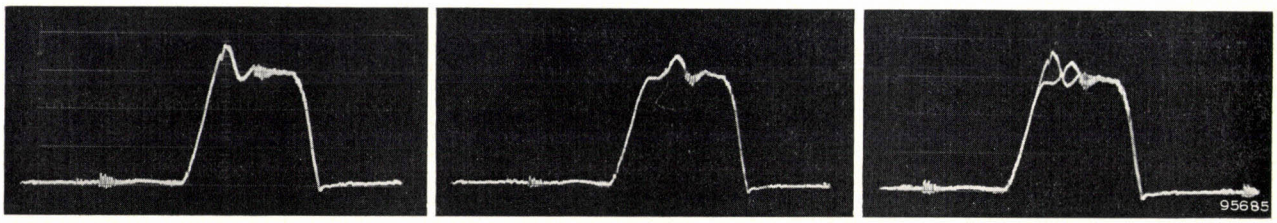

a *b* *c*

Fig. 21. Oscillograms of a current pulse as supplied by the current source in fig. 20, (*a*) when none of the cores undergoes flux reversal, and (*b*) when the magnetization of all cores reverses. The fact that both current pulses are almost identical can be seen by their close coincidence in (*c*), where they are recorded as a single oscillogram.

The efficiency of the circuit is demonstrated by the oscillograms in *fig. 21*, which show the current pulses when none and when all 44 cores of a word undergo a reversal of magnetization.

Summary. The article first reviews various types of memory systems as used in computers and telephone exchanges, etc., namely punched cards, magnetic drums, delay lines, electrostatic memories and magnetic-core memories. The latter are then dealt with at greater length. Their operation depends on the use of large numbers of small rings (cores) of a ferroxcube material having a rectangular hysteresis loop. Wires threaded through the cores conduct the current and voltage pulses required for recording and reading the information. There are various methods of threading the wires. Considerations relating to disturbing pulses, which arise as a result of the imperfect rectangularity of the hysteresis loops, have led to a special system of threading known as the Cambridge system. This system has been further developed at the Philips Research Laboratories in Eindhoven. A version is described which employs cores of ferroxcube 6D3. This memory contains 1024 words of 44 bits; its special feature is its low cycling time, which need be no more than 3 μsec, i.e. about 1/3 of the value hitherto considered as normal in such memories. This is achieved by preventing parasitic pulses from blocking the output amplifiers. When a parasitic pulse arrives, the amplifier inputs are isolated by means of a transistor used as a switch. Each amplifier contains a second transistor, also used as a switch, its use being based on the circumstance that a transistor is capable of storing for a few μsec the information read from the memory. The flip-flops of the buffer register are thus given an opportunity to complete their previous task before taking over the information from the output amplifiers. A further feature is the way in which the current pulses for reading and for restoring the information are stabilized in shape and magnitude, independent of the number of cores whose magnetization is reversed at the same time. For this purpose advantage is taken of the circumstance that the inductance of a choke is greatly diminished when the choke core is saturated.

[14]) The possibility of using a ferrite core in the manner described was suggested by T. Tulp of the Philips Research Laboratories at Eindhoven.

ABSTRACTS OF RECENT SCIENTIFIC PUBLICATIONS BY THE STAFF OF N.V. PHILIPS' GLOEILAMPENFABRIEKEN

Reprints of these papers not marked with an asterisk * can be obtained free of charge upon application to the Philips Research Laboratory, Eindhoven, Netherlands.

2575: G. W. van Oosterhout and C. J. M. Rooijmans: A new superstructure in gamma-ferric oxide (Nature **181**, 44, 4 Jan. 1958).

The structure of γ-Fe_2O_3 has hitherto been considered to be the spinel structure in which Fe^{3+} vacancies — possibly in combination with H^+ ions — are randomly distributed over octahedral sites. Accurate X-ray diffraction has shown that in fact the vacancies are ordered. The unit cell consists of three spinel blocks one above the other ($Fe_{64}O_{96}$) in which the 8 vacancies ($Fe_3O_4 = Fe_{72}O_{96}$) are distributed according to a four-fold screw axis.

2576: J. Verweel: Fysische eigenschappen van ferromagnetische oxydes (Ingenieur **70**, O 7-O 11, 1958, No. 2). (Physical properties of ferromagnetic oxides; in Dutch.)

The physical properties of magnetic materials are briefly described. A review is given of some properties of magnetic oxides. The ferromagnetic resonance phenomenon is explained and shown from measurements of the complex permeability versus frequency of some NiZn ferrites.

2577: L. Seekles, P. Reitsma, T. J. de Man and J. H. G. Wilson: Resultaten van de tijdige intraveneuze toediening van hoge doseringen kristallijn vitamine D_3 in gesolubiliseerde vorm aan rundvee ter voorkoming van melkziekte (T. Diergeneesk. **83**, 125-136, 1958, No. 4). (Results of the timely intravenous injection of large doses of crystalline vitamin D_3 in solubilized form in cattle as a preventative against milk fever; in Dutch.)

Following a survey of the relevant literature, three experiments are described which were carried out with the purpose of investigating the possibility of preventing milk fever in cows by the administration of a massive dose of vitamin D_3. The investigations, in which the University of Utrecht, the Animal Health Service in the Noord-Holland Province, veterinary practitioners in the same province and N.V. Philips-Roxane closely collaborated, were carried out under practical conditions for three consecutive years, during the early months of 1955, 1956 and 1957. All cows used in these investigations, a total of about 150, had suffered from milk fever at least once and were chosen from farms with a history of milk-fever occurrences. The results show that milk fever in cows can be prevented significantly by the timely intravenous injection of 10 million I.U. of crystalline vitamin D_3 in a solubilized form (10 cc "Duphafral" D_3-1000, N.V. Philips-Roxane) administered during a period of from 2 to 8 days prior to parturition.

2578: J. de Boer: Microscopisch onderzoek van de domeinstructuur in polykristallijn bariumtitanaat (Chem. Weekbl. **54**, 137-141, 1958, No. 11). (Microscopic investigation of the domain structure in polycrystalline barium titanate; in Dutch.)

Polished and etched specimens of polycrystalline barium titanate are microscopically examined. No big changes in the domain structure are observed after polarization perpendicular to the surface. From observations on single crystals the conclusion was formed that the domain structure is strongly influenced by mechanical stresses. In Mn_3O_4, which is neither ferromagnetic nor ferroelectric, a twinning pattern analogous to a domain structure can be observed which is due to mechanical stresses alone. It is concluded that in polycrystalline barium titanate the polarization of the domains can be reversed, but 90° rotation is strongly hindered. The maximum attainable polarization is therefore much lower than that of single crystals.

2579: H. G. Bruijning: Some components used in the nanosecond field (Nucl. Instr. **2**, 81-87, 1958, No. 2).

General discussion of some of the properties required of valves, transistors, crystal diodes and transformers for applications involving nanosecond pulses.

2580: A. van der Ziel and A. G. T. Becking: Theory of junction diode and junction transistor noise (Proc. Inst. Electr. Engrs. **46**, 589-594, 1958, No. 3).

A. van der Ziel has given formulae for shot noise in junction diodes and junction transistors for transistors in which 1) all current is carried by one type of carrier, 2) the carrier flow is one-dimensional, 3) the recombination is by volume recombination. These equations are here proved with the help of a corpuscular approach without any significant restrictions except that the individual holes can be treated as independent. The emitter and collector currents are then split into various parts for which the noise spectrum can be obtained by relatively simple reasoning.

VOLUME 20, 1958/59, No. 8 pp. 209-244 Published 23th March 1959

APRIL.

Philips Technical Review

DEALING WITH TECHNICAL PROBLEMS
RELATING TO THE PRODUCTS, PROCESSES AND INVESTIGATIONS OF
THE PHILIPS INDUSTRIES

THE SCINTILLATION COUNTER

by J. A. W. van der DOES de BYE.

621.387.464

The scintillation counter — the most efficient gamma-ray counter now available — is finding ever-increasing application in medicine and industry as well as in physics. In many hospitals, its use in conjunction with radioisotopes ("tracers") has become a part of routine diagnostic practice.

A description is given below of the scintillation counter marketed some time ago by Philips. The article briefly discusses the physical principles underlying the operation of a scintillation counter, and the disturbing effects of inherent noise and background radiation which must be reckoned with both by the designer and by the user of such equipment.

The method of measuring the intensity of high-energy radiation by means of the scintillation effect, i.e. the property of some substances to emit flashes of light when exposed to such radiation, is one of the earliest known to nuclear physics. The method originally consisted in counting the number of scintillations produced by α particles incident on a zinc-sulphide screen; the observer viewed the screen under a magnifying glass or microscope and counted the scintillations visually. With the development of the Geiger-Müller counter in the thirties, which, with electronic scalers, made it possible to count very many more particles (quanta) per second and was moreover suitable for detecting β and γ radiation, the scintillation method fell into disuse. In the last ten years, however, in conjunction with the photomultiplier tube, it has acquired a new lease of life as the *scintillation counter*, which is now an important and widely used monitoring instrument in the fields of nuclear physics and medicine.

The following remarks will serve to define roughly the position of the scintillation counter in relation to the other types of radiation detectors. As is known, the quanta and particles emitted by radioactive substances give rise to *ionization* and *excitation* in their passage through matter. The operation of the hitherto most widely used radiation detectors, viz. the ionization chamber, the proportional counter and the Geiger-Müller counter, is based solely on the ionization effect. These instruments are ideally suited for the detection of charged particles — the Geiger tube counts every charged particle — but not for the detection of gamma rays. Owing to their high penetrating power, there is a considerable chance of the gamma quanta passing right through the detector without causing any ionization, or excitation. In the Geiger counter the chance of an incident γ-quantum being counted is, within a wide energy range, of the order of magnitude of only 1%.

Since the chance of a γ-quantum being absorbed increases with the total mass of the absorbing medium, appreciable improvement in the situation could only be obtained by using instruments containing a substantial quantity of liquid or solid matter as detector. Attempts to construct ionization chambers filled with a liquid or solid proved successful in principle, but failed to lead to instruments that could be produced and used on a large scale [1]). A great step forward was made with the advent of the photomultiplier tube which, being a much more rapid detector than the human eye, made it possible to revert to the old scintillation method, i.e. to a method of detection based not on the accumulation of liberated charges but on the localized luminescence caused in some substances by ionization and excitation. (The ordinary photoelectric cell is also fast, but for other rea-

[1]) A discussion of the properties of various materials that can be used in an ionization chamber of the crystal-counter type is given by F. C. Champion, Progr. nucl. Phys. 3, 159-176, 1953.

sons is unsuitable.) Provided they are optically transparent, scintillating materials of relatively large volume can be used without impairing the detectability of the light flashes, enabling a gamma-ray counter to be built that can count a high percentage of the incident quanta, even of very hard radiations (high quantum counting efficiency).

A scintillator at present commonly used is sodium iodide, activated with a small amount (about 1%) of thallium. For some years now it has been possible to make single crystals of this substance, thus meeting the two requirements of transparency and large mass. The fact that NaI is extremely hygroscopic, however, entails special measures in mounting the crystal.

In regard to its "dead time", i.e. the time which must elapse after a count before the next quantum can be counted, the scintillation counter is far superior to the Geiger counter and is roughly on a par with the proportional counter. The dead time of a scintillation counter [2]) fitted with an NaI(Tl) crystal is at most $2\frac{1}{2}$ μsec. Finally, it is also possible with the scintillation method to measure the *energy* of the incident quanta, that is to say to construct *scintillation spectrometers*.

Its high quantum counting efficiency for gamma rays makes the scintillation counter very suitable for applications involving the use of only small quantities of radioactive material. This is particularly the case where the material is administered to a patient for medical purposes, the object usually being to study the patient's metabolism. The property of some chemical compounds to concentrate in certain tissues may also be exploited; the tissues then become radiation sources and are as such detectable. With a narrow collimator, through which the scintillator "sees" only a small part of the object at a time, the size and shape of such tissues can be determined by scanning the object point by point.

Monitoring for radioactive contamination of the ground and of the human body also involves only slight amounts of radioactive material, and scintillation counters are therefore often employed in equipment for this purpose [3]).

Scintillation counters are sometimes used instead of Geiger counters for the measurements on liquid samples occurring in medical and biological practice. The scintillation counters designed for such work often have a hollowed-out (well-type) crystal into which a test tube fits, so that a very large fraction of the total emitted γ radiation enters the crystal. Moreover, the position of the sample with respect to the crystal is not nearly so critical as when a flat crystal is used.

Many industrial applications are a variant of radiography with X-rays, being similarly based on the locally varying attenuation suffered by a beam of gamma rays in passing through an inhomogeneous body. The non-destructive testing of materials, as for example the detection of flaws in castings and controlling the thickness of sheet metal in a rolling mill, are often carried out with gamma rays, for which purposes the object is scanned with a scintillation counter. Prospecting for uranium ores with a portable scintillation counter is a familiar example of the geological applications.

In the following pages we shall describe the scintillation counter developed and marketed by Philips, and discuss the physical principles underlying its operation. We shall then consider disturbing effects, such as noise and background radiation, and conclude by touching briefly on the properties of scintillating materials other than NaI(Tl), the detecting of radiations other than gamma radiation, and scintillation spectrometry.

Description of the scintillation counter

The scintillating material, in the shape of a cube or cylinder, is mounted with one of its flat faces in good optical contact with the window of a photomultiplier tube, behind which is situated the photocathode. The electrons released from the photocathode by a light flash are attracted to a secondary-emitting electrode (dynode) which is maintained at a certain positive potential (about 150 V) with respect to the cathode. Each electron impinging on this dynode liberates a number of secondary electrons, which in their turn travel to the next dynode, and so on (*fig. 1*). The number of dynodes, i.e. the number of times this process is repeated, is about 10 in most commercially available photomultiplier tubes. This gives a tube gain of between 1 and 10 million times, making it possible to detect scintillations that liberate only one electron from the photocathode.

The current pulses at the output of the photomultiplier give rise to voltage pulses across the anode load. These are passed through a suitably designed amplifier, and the amplified pulses are fed via a *pulse-height discriminator* — a circuit preset to pass only those pulses that exceed a certain

[2]) A forthcoming article in this Review will deal with problems concerning the dead time of a scintillation counter in more detail than is possible here, and will also explain the reasons for the value mentioned above. For the dead time of the proportional counter see P. H. Dowling, C. F. Hendee, T. R. Kohler and W. Parrish, Philips tech. Rev. **18**, 262-275, 1956/57.

[3]) See e.g. A. Nemet, R. B. Stephens and W. A. Bayfield, Philips tech. Rev. **16**, 201-210, 1954/55.

N.V. PHILIPS' GLOEILAMPENFABRIEKEN

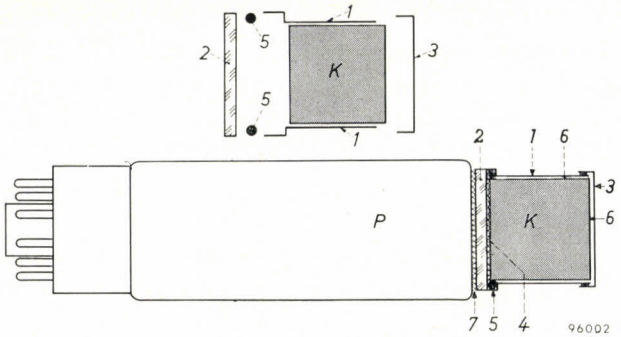

Fig. 1. Example of the way in which an NaI(Tl) crystal (K) can be mounted on the photomultiplier tube (P) in a scintillation counter. The crystal is hermetically sealed in a holder, which completely prevents the penetration of water vapour. *1* aluminium sleeve, *2* glass base, *3* aluminium cap cemented to the sleeve, *4* thin film of transparent viscous fluid, *5* rubber ring, *6* reflecting layer of MgO between aluminium wall and crystal, *7* fluid film as *4*. The two fluid films improve the optical contact between the crystal, the glass base and the tube window. The rubber ring separates the fluid from the MgO, which serves to increase the reflection from the walls.

height — to a scaling circuit. Each stage of the latter divides the number of pulses it receives by a certain factor — in the present instance 10. This is conveniently achieved by the use of decade scaler tubes [4]), from which the number of counted pulses in units, tens, hundreds, etc., can be read directly, each tube delivering one digit of this number. A block diagram of the arrangement is given in *fig. 2*. A photograph of the complete Philips scintillation counting equipment is shown in *fig. 3*. The counter is fitted with an NaI(Tl) crystal, which is mounted together with the multiplier tube (Philips 50 AVP) and the first amplifying stage (cathode-follower circuit) to form a *probe*. The latter is connected by a cable to the rack containing the rest of the equipment. This consists of a power pack which supplies the high tension for the multiplier tube (for 10 dynodes, about 1500 V), a pulse amplifier and a counting unit fitted with decade scaler tubes, which also functions as a fixed-level (non-variable) discriminator. The equipment allows the counting rate, i.e. the average number of quanta detected per unit time, to be determined either from the number of quanta counted within a given time, or from the time taken for the number of counts to reach a pre-set value, e.g. 10 000 [5]).

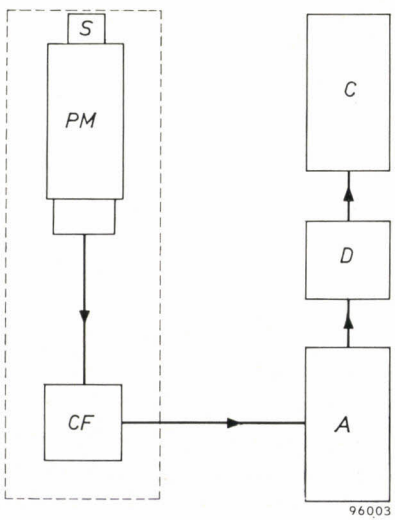

Fig. 2. Block diagram of a scintillation counter layout. S scintillator, PM photomultiplier tube, CF pre-amplifier, A pulse amplifier, D discriminator, C counting unit. Scintillator, photomultiplier tube and pre-amplifier are mounted together in a "probe".

The chance that the counter will register a gamma quantum entering the crystal is about 50% for quanta of 500 keV, 35% for quanta of 1 MeV and 25% for quanta of 2 MeV. In the case of soft gamma and X-ray quanta (10-50 keV) the chance is almost 100%. These values relate to a cylindrical crystal 2.5 cm in diameter and 2 cm in height. Crystals of other dimensions can also be mounted.

Processes occurring in the scintillation material

Before discussing the properties of the scintillation counter, we shall briefly review the processes that occur inside the scintillator. These are of two kinds, the first being the *absorption* of gamma quanta, which takes place in three ways, and the second the *emission of light* (the actual scintillation process).

Absorption of gamma rays

When a beam of mono-energetic gamma quanta passes through a layer of matter of thickness d, the intensity $I(d)$ of the emergent beam is given, as for X-rays, by the formula

$$I(d) = I(0)\, e^{-\varrho\sigma d}, \quad \ldots\ldots \quad (1)$$

where $I(0)$ is the intensity of the incident beam, ϱ the density of the material and σ the mass attenuation coefficient. If the product $\varrho\sigma$ is large, the material is strongly absorbent. The mass attenuation coefficient depends on the chemical composition of the absorber (but *not* on its state of aggregation) and on the energy E_0 of the incident gamma quanta.

The absorption of the gamma quanta may involve three distinct processes: the photo-electric effect, the Compton effect and pair production. The probability of these processes taking place varies

[4]) See e.g. A. J. W. M. van Overbeek, J. L. H. Jonker and K. Rodenhuis, Philips tech. Rev. **14**, 313-326, 1952/53.

[5]) Cf. W. Parrish, Philips tech. Rev. **17**, 206-221, 1955/56.

with E_0, but differently in each case. Each process has its own mass attenuation coefficient, defined respectively as σ_f, σ_c and σ_p; the value of σ is the sum of the three. During these processes the energy of the gamma quantum is either wholly or partly converted into the kinetic energy of one or more electrons. If, then, a beam of mono-energetic gamma quanta is absorbed, the energy spectrum of these electrons is not mono-energetic (monochromatic), but fairly complex and partly continuous.

Since only the total electron energy is important for the scintillation process, we shall assume that we are concerned with a single electron of energy E_0. The photo-electric effect thus produces in the electron energy spectrum a mono-energetic peak [6]). The photo-electric effect makes a large contribution to the absorption when E_0 is smaller than 200 keV; the absorption of soft and moderately hard X-radiation is almost entirely due to this effect. In this case, then, $\sigma \approx \sigma_f$.

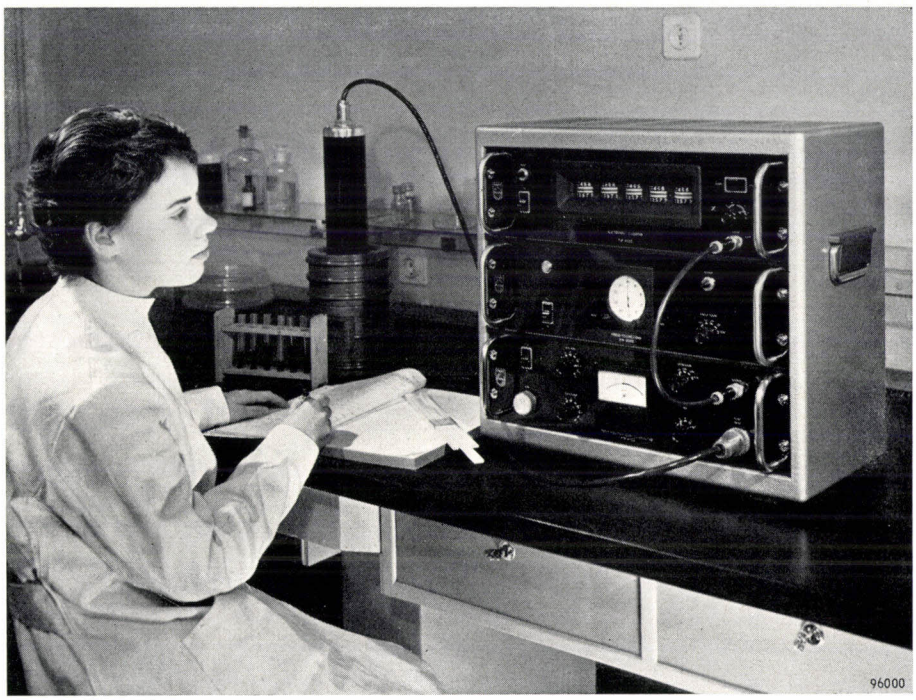

Fig. 3. The Philips scintillation counter in use. The upper part of the probe projects above a lead shield ("castle") at the bottom of which the radioactive specimen is situated. The probe is connected by a cable to the cabinet containing the rest of the electronic equipment. The bottom unit contains on the left the power pack for the photomultiplier tube (and to which a Geiger counter can also be connected) and on the right the pulse amplifier. The top unit contains the counting circuit, which also functions as pulse-height discriminator. The middle panel is fitted with a clock which indicates the time in which the apparatus has counted a pre-determined number of pulses.
The apparatus was developed to the production stage under the direction of Mr. A. Mooy.

In the first of the three processes — the *photo-electric effect* — an electron (usually a K electron) is ejected from its shell by the gamma quantum. The latter is thereby completely absorbed, i.e. the energy of the photo-electron is equal to the gamma energy minus the electron binding energy. When the electron configuration returns to its normal state — which it does in a very short time — the binding energy in question is emitted in the form of X-ray quanta or Auger electrons, or both. Any X-ray quanta emitted are in turn absorbed in their immediate surroundings, so that the quantum energy E_0 is entirely converted into electron kinetic energy.

In the second of the three processes — the *Compton effect* — a γ-quantum collides with an electron to which it transfers only a part E_c of its energy. It then continues on its way in a different direction (scattering) with an energy $E' = E_0 - E_c$. For a given direction of electron and scattered gamma quantum, it is possible to calculate E_c and E' by treating the gamma quantum as a particle having

[6]) In small crystals the X-ray quanta which "carry off" the binding energy E_b may nevertheless escape. In that case a residual "escape peak" is found beside the main photo-electric peak. If E_0 is of the order of 1 MeV or more, then $E_0 \gg E_b$ and the two peaks virtually coincide. This subject is dealt with at greater length on pp. 269-270 of the article quoted in [2]).

a kinetic energy E_0 (and E' after the collision) and a momentum E_0/c (or E'/c), and by applying to the collision process the laws of conservation of energy and momentum. The energy E_c transferred to the electron in this collision may have any value between 0 and $E_0/(1 + E_r/2E_0)$, where E_r is the energy corresponding to the rest mass of an electron, viz. 0.51 MeV. The spectrum of the E_c values is thus continuous, and the larger E_0 the larger the maximum value of E_c/E_0; at $E_0 = 2$ MeV this amounts to 0.80, and at 10 MeV to 0.977. The probability that a certain value of E_c will occur is a function of E_c and of E_0. With increasing E_0 the relatively small values of E_c decrease in significance and the energy spectrum of the Compton electrons acquires more the character of a peak.

There is of course a chance that the scattered gamma quantum will be absorbed. If it is absorbed by the photo-electric effect, this again is a case of the entire energy E_0 being converted into electron kinetic energy; outwardly this is not to be distinguished from the direct occurrence of the photo-electric effect. Naturally, the chance of this happening increases according to the quantity of material used. With increasing scintillator size, therefore, the "photo-electric peak" becomes larger at the expense of the Compton continuum [7]).

The probability of a Compton collision, like the probability of photo-electric absorption, decreases with increasing E_0, but it does so in a much less pronounced way. In an NaI(Tl) crystal the probability of a Compton collision is already greater than that of the photo-electric effect at an E_0 value of 0.5 MeV.

The third process — *pair production* — occurs only when $E_0 \geqq 1.02$ MeV. The chance of this occurring increases with increasing E_0. Where E_0 is of the order of 10 MeV or more, pair production predominates over the other two effects. The process consists in the conversion of a gamma quantum into two particles which are identical except for their sign, namely an electron and a positon. The kinetic energy of the pair is $E_0 - 1.02$ MeV (i.e. E_0 less $2E_r$, the energy equivalent of the rest mass of the created particles). Thus, besides the "photo-peak" in the electron energy spectrum there may be a "pair peak", which is outwardly identical with the photo-peak caused by gamma quanta having an energy $E_0 - 1.02$ MeV. This pair peak is superimposed on the Compton continuum.

The average life of a positon is very short. It unites with an electron and the consequent annihilation of the pair gives rise to the emission of two identical but oppositely directed (conservation of momentum) gamma quanta each having an energy of 0.51 MeV. Generally this annihilation occurs when the positon has lost its kinetic energy; sometimes, however, also when it is in motion.

Naturally there is a certain chance that one or both annihilation quanta will be absorbed in the scintillator. If both are absorbed, then the entire E_0 is again absorbed and the photo-peak becomes larger at the expense of the pair peak. The cases, however, where only one of the annihilation quanta is absorbed give the appearance of a third peak in the electron energy spectrum, its position being exactly midway between the photo-peak (corresponding to the absorption of E_0) and the pair peak (absorption of $E_0 - 1.02$ MeV). In the absorption of gamma quanta by pair production the photo-peak will thus be relatively larger when a scintillator of larger mass is used, just as was the case with the Compton effect.

Fig. 4 shows the variation with E_0 of σ_f, σ_c and σ_p, and of their sum σ, for NaI. *Fig. 5* shows the spectrum of the energies transferred to the electrons in the case of gamma quanta of equal energy (in this case 2 MeV).

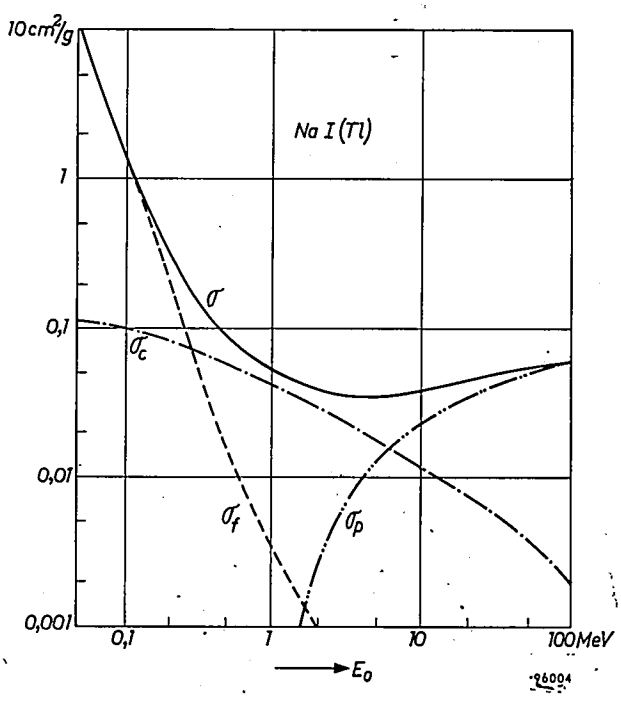

Fig. 4. Absorption of gamma radiation in NaI. The curves show how the contributions of the photo-electric effect (σ_f), the Compton effect (σ_c) and pair production (σ_p) to the mass attenuation coefficient (σ) depend on the quantum energy E_0.

[7]) The name "photo-electric peak" is really not applicable in this case; one should speak rather of a "peak of complete absorption".

The scintillation process

The energy E_1 which the liberated primary electrons have acquired from an incident gamma quantum is given up by these electrons in small amounts to other electrons in their path. After a short time the latter electrons have arrived at discrete energy levels above the ground state [8]). The subsequent events differ slightly from one scintillating material to another, but are essentially as follows. The "packet" of energy, corresponding to the difference in energy of an electron in the excited and in the ground state, is able to move through the scintillating material (i.e. it is transferred from electron to electron). At a certain moment, however, it is held up at some point, especially at places where foreign atoms or ions are situated (e.g. a Tl ion in the NaI crystal, or an impurity of some kind, or a molecule of dissolved substance), or in so-called *traps,* such as dislocations and vacancies. Upon capture in such a centre, a certain proportion of the energy is converted into thermal energy of the material. Depending on the nature of the centre, three things can happen to the remaining energy. In the first place it can be entirely or partly converted into a light quantum (fluorescence). The fluorescence light quanta emitted after absorption of one gamma quantum together constitute the light flash or scintillation. Secondly, de-excitation can take place via a radiationless transition (quenching). Thirdly the centre may possibly be one from which a lower energy level cannot be directly reached (trap). De-excitation may then occur by prior transition, owing to absorption of thermal energy, to a somewhat higher energy level (in the conduction band) from which a fluorescence centre can be reached (phosphorescence). Evidently, the material for a scintillation counter should exhibit a maximum of fluorescence and a minimum of quenching and of phosphorescence. The phosphorescence of NaI(Tl) and of plastic scintillators is low; in liquids it is entirely absent.

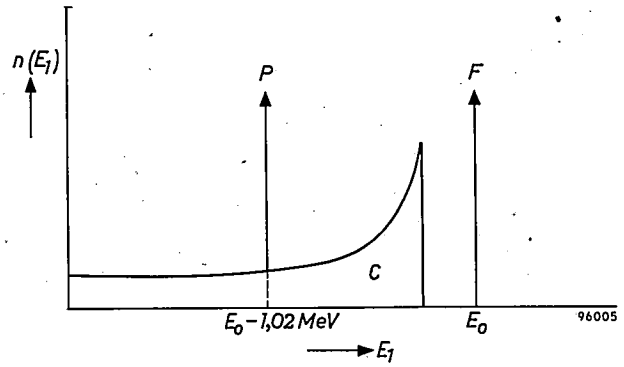

Fig. 5. Spectrum of the total energy E_1 of the primary electrons liberated by gamma quanta of 2 MeV. Note the Compton continuum (C), which is sharply cut off at the maximum Compton energy, and the "line" (F) of still higher energy. The latter is the "photo-electric peak", for which E_1 is equal to E_0, the energy of the detected gamma quanta. If, as in this case, the quantum energy is greater than 1.02 MeV, another "line", the pair peak (P), appears at a position corresponding to an energy $E_0 - 1.02$ MeV.

The number per unit time of the de-excitations by fluorescence is proportional to the number of occupied fluorescence levels (N) and to the number of unoccupied sites in the ground state. If the latter number is large compared with the first, so that it may be regarded as constant, we can write:

$$-\frac{dN}{dt} = \frac{N}{\tau_0}, \quad \ldots\ldots \quad (2)$$

where τ_0 is the average life of an electron in the energy state concerned and t the time. If N_0 is the value of N at $t = 0$, the solution of (2) is:

$$N = N_0 \, e^{-t/\tau_0}. \quad \ldots\ldots \quad (3)$$

The intensity of a scintillation accordingly decreases exponentially with time; the time constant is τ_0.

If the fluorescence light quanta have an average energy E_f — in NaI(Tl) about 3 eV — then the total energy of a single scintillation is $N_0 E_f$. Owing to the quenching process and the radiationless transitions that occur together with the emission of light, this energy is smaller than the total absorbed energy E_1. The ratio η between E_1 and $N_0 E_f$ is called the *luminous efficiency* of the material. For NaI(Tl) the value of η is independent of E_1 and lies between 0.08 and 0.09.

From scintillation to electrical pulse; fluctuation phenomena

The N_0 light quanta that together form a scintillation will obviously not all strike the photocathode in the multiplier tube, nor does each quantum that *does* strike the photocathode produce an electron at the first dynode. The number of such electrons N_1 constitutes a fraction a of N_0. To produce a single effective photo-electron in the multiplier tube an energy E_i is therefore needed; this quantity, which we shall call the "*liberating energy*", is equal to $E_f/a\eta$. Since a, like η, is about 0.08, the value of E_i is approximately 450 eV, i.e. about 15 times larger than in an ionization chamber or proportional counter. A gamma quantum of a given

[8]) Many electrons initially receive more energy than they need to reach one of these levels; they then arrive in a higher continuum of energy levels, called the *conduction band.* While they remain in this band they can move through the crystal under the influence of an electric field. The action of the crystal counter (see [1])) is based on this phenomenon, which is more or less analogous to the ionization of a gas.

energy gives rise to larger pulses the larger is a, that is to say the smaller is E_i. The consequences of this will be discussed in the next section. The value of E_i for NaI(Tl) is independent of the energy of the incident gamma quantum.

The value of a is greater the better the spectral sensitivity of the photocathode matches the spectrum of the scintillations. The dashed line in *fig. 6*

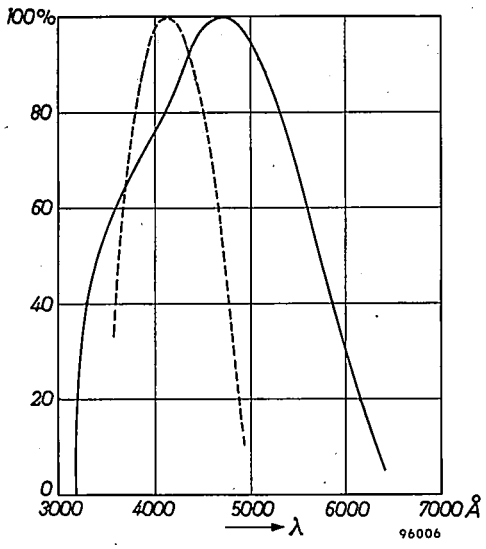

Fig. 6. Spectral intensity distribution of the scintillations in an NaI(Tl) crystal (dashed curve) and spectral sensitivity of the Philips photomultiplier tube 50 AVP. The maxima of both curves are given the value 100%.

represents the spectral energy distribution of scintillations from NaI(Tl). The maximum lies at about 4100 Å, i.e. well in the blue part of the spectrum. The solid curve represents the spectral sensitivity of Philips photomultiplier tube type 50 AVP, which is specially suited for mounting in scintillation counters and is used, for example, in the present equipment.

When gamma quanta of a certain energy strike the scintillating crystal, the total energy E_1 of the electrons liberated by a single gamma quantum is not, as we have seen, of constant magnitude, but shows a complete spectrum of values (fig. 5). Even with constant E_1, however, certain fluctuations occur in the number of light quanta produced, in the fraction of this number that reaches the photocathode, in the number of photo-electrons liberated by a certain number of light quanta — i.e. in a and in η — and in the current gain g of the multiplier tube. One therefore measures at the output of the tube a spectrum of pulse amplitudes which may be regarded as a blurred version of the spectrum of electron energies E_1 (*fig. 7*).

The effect of these fluctuations is best demonstrated by the broadening of the photo-peak ($E_1 = E_0$). The position of this peak, i.e. the mean voltage of the pulses constituting the peak, is determined by the average values of a, η and g, and its width by the spread in these values.

The distribution of the values of N_1, the number of photo-electrons arriving at the first dynode per gamma quantum, can be described by a Gaussian distribution function, provided that $\overline{N_1}$, the mean value of N_1, is not too small. The standard deviation is equal to $\sqrt{\overline{N_1}}$. Frequently the half-height width of the Gaussian curve is taken, which is 2.36 × the standard deviation. The relative value of this measure of distribution is then $2.36/\sqrt{\overline{N_1}}$, and can also be written as $2.36\sqrt{E_0/E_i}$.

The variation of g which, together with the spread in N_1, determines the width of the photo-peak, can only be calculated subject to certain assumptions with regard to the secondary emission. We shall not deal with this here. Experiments have shown that the statistical fluctuations in g have relatively little effect on the blurring of the pulse spectrum.

The blurring of the pulse spectrum in consequence of the fluctuation phenomena described is principally of importance in scintillation spectrometry, which is touched on in the end of this article. It has no direct influence on the counting of the scintillations, and only rarely any indirect influence. In fact the high amplification in the multiplier tube allows pulses generated by a single photo-electron to appear above the noise of the pulse amplifier, even when g may happen to be particularly small.

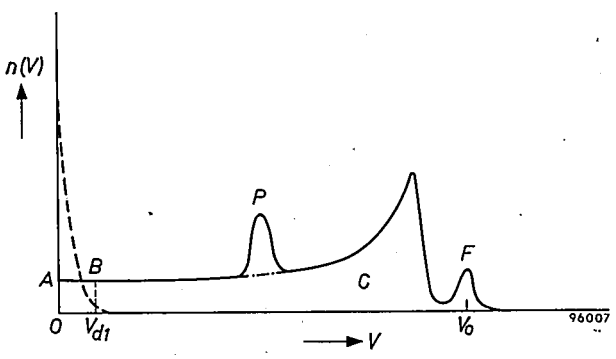

Fig. 7. Spectrum of the amplitude V of the electrical pulses delivered by the photomultiplier tube (solid curve). Owing to fluctuation phenomena in the scintillator and in the multiplier tube, the pulse-height spectrum does not exactly follow that of fig. 5, but is "blurred". The degree of blurring can be judged from the width of the peak F.

The dashed line gives the spectrum of the noise pulses; if the discriminator setting corresponds to a pulse-height V_{d1}, an average of one noise pulse per second is passed. This also suppresses a fraction of the wanted pulses equal to the ratio of the area $OABV_{d1}$ to the total area bounded by the solid curve. The ratio of the areas under the scintillation-pulse curve and the noise-pulse curve is here arbitrarily chosen. It depends on the noise intensity and the strength of the specimen under assay.

Counting the scintillations

Noise

Owing to the continuous energy spectrum of Compton electrons (as shown in fig. 7), there is a distinct possibility of small pulses occurring, even when the energy of the γ-quantum is large. From the conclusion of the last section it might be inferred that all these small pulses would be counted, down to about the voltage corresponding to the liberating energy E_i (about 450 eV). The actual situation, however, is somewhat less favourable owing to the inherent noise in the photomultiplier tube.

This noise is due to the fact that the photocathode emits a certain number of electrons per unit time even in the absence of incident light; these electrons give rise to spurious pulses (of the order of 10 000 per sec). The pulse-height distribution of this noise [9]) is represented by the dashed line in fig. 7. Most noise pulses originate from a single primary electron, only a small number from more than one.

The great majority of the noise pulses are due to the thermionic emission of electrons from the photocathode, which depends on the temperature and on the work function of the cathode material. It is a fortunate circumstance that many scintillating materials emit very strongly in the blue part of the spectrum, and it is therefore not necessary to select cathode materials having a very low work function. The noise pulses caused by thermionic emission all correspond, of course, to a single electron leaving the photocathode (mono-electronic pulses).

The relatively few poly-electronic pulses are presumably caused by residual gas ions colliding against the photocathode.

Two other causes of noise are thermionic and field emission from the dynodes. The first gives rise to pulses which, on an average, are much smaller than the above-mentioned mono-electronic pulses. Field emission can be virtually eliminated by suitably designing the dynode system.

If the enormous number of noise pulses were also counted, it would be practically impossible to use the scintillation counter as a radiation monitor. They can of course be largely eliminated by setting the pulse-height discriminator to a value V_{d1} such that, for example, only one noise pulse is counted per second. This naturally means that a certain fraction of the scintillation pulses will no longer be counted. This fraction can be found by dividing the area $OABV_{d1}$ in fig. 7 by the total area bounded by the curve representing the pulse spectrum. The fraction of uncounted pulses is smaller the larger is V_0 (see fig. 7) in relation to V_{d1}, or in other words, the smaller the liberating energy E_i. Further, a scintillator of larger dimensions is advantageous, in that relatively more gamma quanta then give rise to pulses in the photo-peak F of the spectrum than in the continuum C (fig. 5). The fulfilment of the first requirement, a small E_i value, depends on the following factors.

1) The number of light quanta produced in the scintillator by a colliding electron of a given energy, i.e. the luminous efficiency η. This is determined by the nature of the scintillating material.
2) The fraction of these light quanta that reaches the photocathode. If the scintillator is fully transparent, with one of its faces in good optical contact with the multiplier tube and with its other faces highly reflective, this fraction may closely approach 100%.
3) The chance of these light quanta liberating an electron from the photocathode. This chance, and the fraction mentioned under 2), together determine the value of the factor α introduced at the beginning of the last section.

In modern scintillation counters the undetectable fraction of the total number of scintillations amounts to only a few per cent. Other conditions being equal, the fraction is greater the lower the energy of the incident γ-quanta, for the value of V_0 is then smaller whereas the discriminator threshold is kept fixed at the value V_{d1} [10]).

To ascertain how the discriminator setting V_{d1} which leads to an average count of one noise pulse per second is related to V_0, it would be necessary to determine the value of V_0 and the form of the pulse spectrum. With the ordinary scintillation counting apparatus, however, this is not readily possible.

This object can nevertheless be achieved by plotting a curve of the counting rate versus the voltage (counting characteristic). Using a γ-active sample of constant intensity, the high tension H on the multiplier tube is varied while the discriminator setting V_d remains unchanged. Since the current amplification factor of the multiplier tube depends very closely on H, the variation of H implies a variation of V_0; with increasing H the value of V_0 increases, so that V_d/V_0 decreases. The pulse spectrum is extended but V_d remains constant. At all values of H where V_d is exceeded by a peak in the pulse spectrum (fig. 7), the number of pulses counted per unit time (the ordinate value of the curve) sharply increases.

[9]) By "noise" we refer to all unwanted pulses arising from random processes and which together constitute the "dark current". Spurious pulses associated with the scintillations are therefore not included under this term.

[10]) This relationship is not valid in all circumstances. If E_0 is small (< 100 keV) the continuum C (fig. 7) is of little significance compared with the peak F. This effect again reduces the undetectable fraction.

N.V. PHILIPS' GLOEILAMPENFABRIEKEN

The numbers in *fig. 8* indicate the points of correspondence between the pulse-height spectrum and the counting characteristic, i.e. those abscissa values of the spectrum that are equal to V_d at the various H values. With increasing H the characteristic asymptotically approaches the maximum value (points *7* to *11*), but as soon as V_d is made smaller than V_{d1} (the discriminator threshold at which, for a given H, one noise pulse per second is counted), more and more noise pulses start to be counted and the total count rate again rises sharply with H.

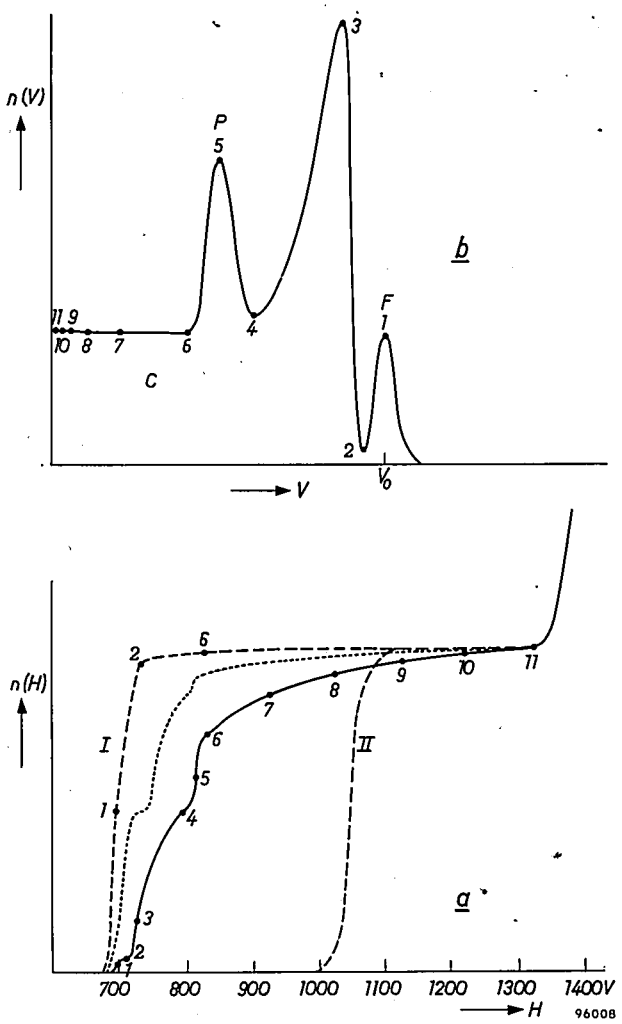

Fig. 8. The counting characteristic (*a*) of a scintillation counter is obtained by varying the voltage H on the photomultiplier tube while keeping the discriminator setting constant. Since the current gain of this tube varies with H (roughly in proportion with the 8th to 10th power of H), the result obtained in this way resembles that which would be obtained by keeping H constant and varying the discriminator setting V_d from the maximum pulse-height to 0. When V_d is exceeded by a peak in the pulse-height spectrum (*b*), the counting rate rises sharply. The numbers indicate the points of correspondence between the two curves. If V_0 is large with respect to V_d (points *7* to *11*), the number of counted pulses no longer varies markedly with H, but approaches the maximum value asymptotically. If H is very high (i.e. if V_0 is relatively *very* large with respect to V_d), more and more noise pulses are counted and the curve again rises steeply. The longer the horizontal part of the curve (the plateau), the better the counter. The solid curve applies to a small crystal, the dotted curve to a larger one and the dashed line *I* to an infinitely large crystal. Curve *II*, which has substantially the same form as curve *I*, applies to radiation of only 100 keV, the other curves to radiation of 2 MeV.

The substantially horizontal part of the counting characteristic is called the *plateau*.

The existence of this plateau — the region in which the count rate is substantially independent of H — naturally favours the accuracy of measurement. With a good-quality scintillation counter, i.e. one in which $V_{d1} \ll V_0$, the plateau is broad, whereas with a poor-quality counter it is narrow, or even absent (i.e. the two steep parts of the curve run immediately one into the other). On the other hand, it should not be forgotten that the shape of the characteristic and the length of the plateau also depend on the energy of the counted γ-quanta (see fig. 8), just as the ratio V_{d1}/V_0 does.

If we know the relation between the maximum pulse-height V_0 and the energy E_0 of the incident γ-quanta, we can calculate directly the equivalent γ energy to which V_{d1} corresponds. In modern scintillation counters this energy (E_{eq}) is 5 to 15 keV. In practice, E_0 varies from 50 to 3000 keV.

Since the ratio E_{eq}/E_0 is directly related to V_{d1}/V_0, the value of E_{eq} can also be regarded as a measure of the quality of the scintillation counter; the smaller is E_{eq}, the more favourable are the noise characteristics. For NaI(Tl), where V_0 is proportional to E_0, the ratios V_{d1}/V_0 and E_{eq}/E_0 are in fact identical, and E_{eq} is proportional to the liberating energy E_i.

The great advantage of secondary-emission amplification, as takes place in the photomultiplier tube, becomes evident if the multiplier tube in the scintillation counter is replaced by an ordinary photo-electric cell with amplifier. The minimum energy which the γ-quanta must then have in order to be counted amounts to several MeV. Pulses originating from quanta of less energy are drowned in the noise of the amplifier.

Other sources of noise in the equipment

Owing to the use of caesium in the fabrication of the multiplier tube (for the photocathode and sometimes also for the dynodes), the tube contains a small amount of caesium vapour. The caesium atoms may be ionized by colliding with electrons, and then move in the electrical field to the cathode. A pulse may therefore be followed a few μsec later (the transit time of the ions) by an "after pulse" [11]). When the voltage on the multiplier tube is high, this effect is by no means negligible and calls for an increase in the discriminator setting.

---

[11]) See C. F. Hendee and W. B. Brown, Philips tech. Rev. **19**, 50-58, 1957/58.

Unwanted pulses are also caused by electrons exciting the anode into luminescence. The light so produced falls on the cathode and gives rise to undesired photo-emission. This effect also increases sharply with the tube voltage and, together with the above after-pulsing effect, determines the maximum permissible value of this voltage.

Background radiation

Whereas the noise pulses originating in the equipment itself can be adequately reduced in number by suitable pulse-height discrimination, tube voltage, etc., this is not the case as regards stray radiation. An ever-present source of such background is cosmic radiation, but natural radioactive substances in the surroundings and radioactive impurities in the counter itself also contribute to the background count.

The number of such quanta and particles incident on the scintillator can be limited by shielding the probe and the radioactive specimen inside a thick-walled lead "castle" (see fig. 3). For a probe containing an NaI(Tl) crystal of some tens of grammes, the background count can be reduced in this way from some scores to as few as 5 pulses per second. This method cannot, of course, be used in measurements on a patient, but an improvement is nevertheless possible with the aid of a lead collimator. This is a cylindrical or conical tube mounted in such a way that the scintillator "sees" only the part or organ of the body under investigation (*fig. 9*). If the background quanta are mainly of lower energy than the quanta to be counted, they can be entirely or largely suppressed by the discriminator. This admittedly reduces the counted fraction of the quanta to be counted, but this may not prove a serious drawback.

However this may be, it is necessary before carrying out any measurement to determine separately the number of background quanta occurring per unit time, and this should be done in conditions closely approaching those under which the measurement is performed. The true intensity of the radiation source is then subsequently found by deducting this background counting rate from the total counting rate.

Accuracy of measurement

Since the emission of radiation quanta or particles by radioactive atomic nuclei is a random phenomenon, the number of pulses (n) counted in a given time shows statistical fluctuations. The root mean square value of the fluctuations (standard deviation) is $\sqrt{\bar{n}}$ where $\bar{n}$ is the average value that would be found for n if the measurement were to be repeated a very large number of times. Two measurements on different specimens thus have the same relative error when they relate to the same number of quanta. To obtain the same relative precision, it is therefore necessary to make a measurement of longer duration on a weakly radioactive specimen than on a strongly radioactive specimen. With the Philips apparatus (fig. 3), this is done automatically, as already described. The "counting strategy" used, however, depends on the nature of the problem.

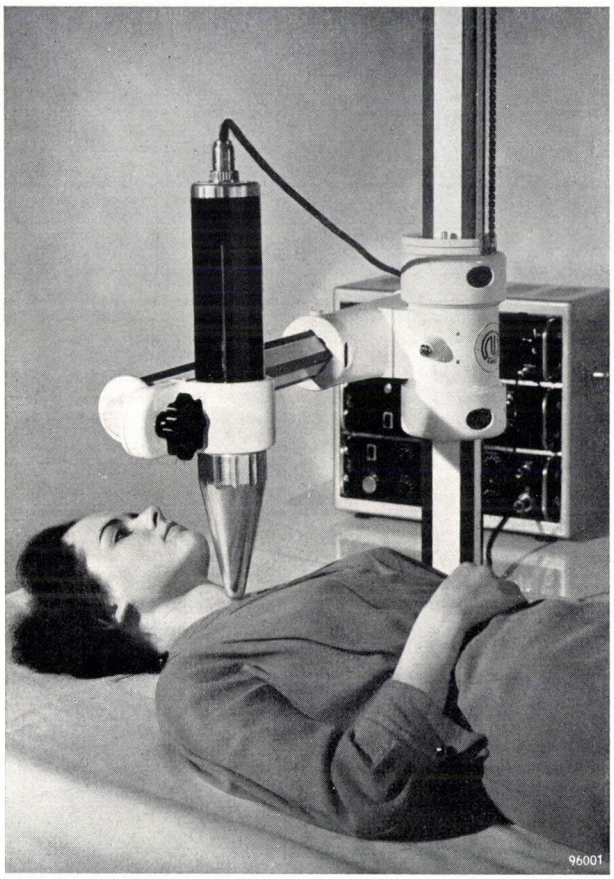

Fig. 9. In order to shield the scintillator from background radiation, the probe may be fitted in a lead collimator. With a very narrow collimator it is possible to chart the shape of an organ in which a radioactive substance has accumulated (see e.g. J. A. W. van der Does de Bye, Nucleonics **14**, No. 11, 128-134, 1956). The photograph shows the set-up for a thyroid-gland examination.

For a treatment of these problems, which are by no means restricted to the scintillation method, the reader is referred to the article mentioned in footnote [5]).

Other scintillating materials and the detection of other radiations

In the foregoing we have been concerned in particular with the detection of γ radiation by a scintillation counter containing an NaI(Tl) crystal as scintillating material. For some measurements, NaI(Tl) has the drawback of a fairly long fluorescence decay constant (0.25 μsec). In some solid, monomer organic crystals the duration of a flash is a factor of 10

smaller (anthracene 3×10^{-8} sec), and is shorter still in plastic scintillators and certain scintillating fluids ($3\text{-}8\times10^{-9}$ sec).

The fluorescence decay constant of the latter substances approaches the spread in the transit time of the electrons in the multiplier tube. For the tubes which are best in this respect the spread is about 1.5×10^{-9} sec (on a transit time of 3×10^{-8} sec). When such "fast" materials are used, this spread partly determines the maximum counting rate, which represents the utmost limit of detection. Obviously, high demands are then made on the response of the associated electronic equipment.

Since α-particles have an extremely short range in a solid (some tens of microns), they can be detected with very thin layers of scintillating material, for example ZnS (activated by Ag) in powdered form. Moreover, since they are as a rule particles of very high energy, no trouble is experienced from unwanted radiation in measurements on an α-radiator. Compared with the detection of β and γ radiations, however, or with neutron detection, discussed below, the monitoring of α radiation is of less frequent occurrence. An example of its application will be found in article [3]).

Like γ-quanta, neutrons cannot be detected directly. Fast neutrons betray their existence by collisions with atomic nuclei, to which they give up part of their energy. The part given up is greater the lighter the excited nucleus, and hence is greatest for the hydrogen nucleus (proton). In this case the spectrum of the energy of collision runs from 0 to the full energy of the neutron (neutrons and protons having approximately the same mass) and has a sharp cut-off at these lower and upper values. Suitable scintillators are therefore organic substances, which are rich in hydrogen. A detectable fraction of neutron collisions, however, calls for a very large mass of material.

Thermal neutrons, which have an energy of about 0.025 eV, can only be detected via a nuclear reaction. For this purpose, lithium or boron is added to the scintillator; after capturing a thermal neutron, these atoms then emit a high-energy α-particle. Use is also made of single crystals of LiI(Sn) or LiI(Eu), but the latter are even more hygroscopic than NaI(Tl). Nuclear reactions in which only hard γ-quanta are emitted (which readily escape from the scintillator), or on which the daughter atoms (which remain in the scintillator) are radioactive, cannot of course be used.

Scintillation spectrometry

The fact that the height of the scintillation pulses varies with the absorbed gamma energy — and is proportional thereto in the case of NaI(Tl) — makes it possible with suitably calibrated apparatus to find the value of E_0 from the recorded pulse-heights. What is of special interest is V_0, the average pulse-height in the photo-peak; in this case the Compton continuum plays no part. Where we are concerned not with monochromatic gamma radiation but with the analysis of a gamma-ray *spectrum*, the presence of the Compton continuum is in fact a hindrance [12]). At high quantum energies, where the photo-peak is relatively small, the pair peak — which is then large — can be helpful, the average pulse-height in that peak being a measure of E_0 — 1.02 MeV.

Since a pulse spectrum is to be recorded, measures are needed to ensure that the measurement is not distorted by large pulses being clipped in the amplifier. The amplification should not be too high: it should be adjusted such that the discriminator threshold (1 noise pulse per sec) lies well below the linearity limit of the amplifier. When the usual type of pulse-height discriminator is used, the spectrum is presented in the form of an integrated pulse-height distribution from which the spectrum must then be derived by differentiation. A pulse-height spectrum can be obtained directly by using a differential discriminator, an instrument designed to pass only those pulses whose amplitudes lie within two close limits. In this way the analysis also gains in accuracy.

Variants of the normal scintillation spectrometer are the Compton and the pair spectrometer. The first of these uses two scintillation probes, which are set up a certain distance apart; coincidences are counted between pulses from the one probe, which is irradiated by the specimen, and pulses from the other, which is subjected solely to scattered gamma quanta with a specific scattering angle. The set-up is such that the γ-quanta measured are those scattered at some angle greater than 90°, for in this region the energy spectrum of the colliding electrons is fairly narrow, making it possible to calculate E_0 with reasonable accuracy from the known scattering angle and the energy transferred to an electron.

The pair spectrometer uses three probes, set up such that the three scintillators lie on a straight line. The middle probe is irradiated and the other two detect annihilation quanta. The pulses are counted in three-fold coincidence and the amplitudes of the pulses from the middle probe are measured. From the "normal" pulse spectrum, then, only the pair peak is selected for each component of the investigated radiation.

The energy resolution of a spectrometer, i.e. the ability to distinguish between γ-quanta of slightly different energy, is naturally better the narrower the photo-electric or pair peak. Here, too, a small value of E_i is desirable.

Summary. As opposed to other instruments for detecting radiations from radioactive substances, the scintillation counter is based not on the accumulation of electrical charges produced by ionizing events, but on the fact that in certain substances a short-lived flash of light (scintillation) occurs upon excitation. The scintillation is detected by means of a photomultiplier tube. Provided the scintillating material is optically transparent, its size can be increased without unduly impairing the detectability of the scintillations. A large detector can therefore be used, consisting of a substance of high density; this results in a satisfactory quantum counting efficiency even for hard gamma rays.

In the Philips scintillation counter, discussed in this article, the pulses delivered by the multiplier tube are passed, via an amplifier and a pulse-height discriminator, to a decade scaling circuit. The pulses vary in amplitude between zero and a maximum value corresponding to the total energy of the gamma quantum. The form of the pulse-height spectrum is determined by the three processes involved in the absorption of gamma quanta, viz. the photoelectric effect, the Compton effect and pair production. The excitation to which this absorption gives rise in the scintillating crystal leads to instantaneous or delayed light emission (fluorescence and phosphorescence) and also to radiationless transitions. In some scintillators, including the widely used NaI(Tl) crystal, the pulse-height is proportional to the absorbed energy. However, since the excitation-scintillation process and the chance of a light quantum striking the photocathode are subject, like the response of the multiplier tube, to fluctuations, the pulse-height spectrum is only a "blurred" version of the true absorption spectrum. In the range of low-amplitude pulses, moreover, detection is hampered by noise pulses originating from the multiplier tube. These can be largely suppressed by an appropriate setting of the discriminator, without which it would be impossible to monitor weakly radioactive specimens. In modern counters this setting corresponds to the maximum height of pulses arising from gamma quanta of 5 to 15 keV.

The counting system in the Philips apparatus is designed to allow the counting rate to be determined either from the number of pulses recorded in a given time or from the time interval taken to accumulate a predetermined number of counts. To suppress background radiation during a measurement, the specimen and the "probe" — which contains the scintillator, the photomultiplier tube and a cathode-follower pre-amplifier valve — are placed in a lead "castle". When the nature of the measurement precludes this form of shielding, a lead collimator may be used. With a very narrow collimator it is possible to chart the shape of a radioactive object (e.g. the thyroid gland of a patient to whom ^{131}I has been administered).

[12]) The gamma-ray spectra of radioactive substances possess roughly 1 to 10 spectral lines. Although this number is small compared with the number of lines usually found in optical spectra, the analysis of a spectrum with 10 lines, particularly when some of them are weak, imposes heavy demands on a scintillation spectrometer.

A METHOD OF MEASURING THE RESISTIVITY AND HALL COEFFICIENT ON LAMELLAE OF ARBITRARY SHAPE

621.317.331:538.632.083

Resistivity and Hall-coefficient measurements at different temperatures play an important part in research on semiconductors, such as germanium and silicon [1]), for it is from these quantities that the mobility and concentration of the charge carriers are found.

Such measurements are commonly carried out with a test bar as illustrated in *fig. 1*. The resistivity is found directly from the potential difference and the distance between the contacts O and P, the current i and the dimensions of the bar. To determine the Hall coefficient the bar is subjected to a magnetic field B applied at right angles to the direction of the current and to the line connecting the diametrically opposite contacts O and Q. From the potential difference thus produced between these latter contacts the Hall coefficient is derived. (The relation between the Hall coefficient and the change in electric potential distribution due to a magnetic field will be explained presently.)

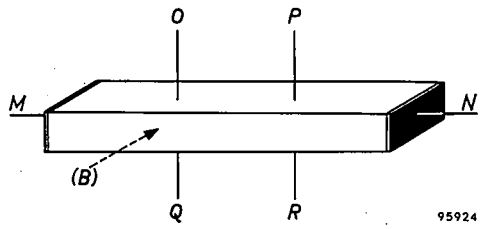

Fig. 1. Classical form of sample used for resistivity and Hall-coefficient measurements. The test bar is provided with current contacts M and N and voltage contacts O, P, Q and R. The fourth voltage contact R serves for check measurements.

In measurements performed at low temperatures — e.g. in liquid nitrogen — point contacts possess resistances of the order of megohms, in consequence of which the voltages cannot be determined with sufficient accuracy. In such cases "bridge-shaped" samples are used as illustrated in *fig. 2*. The voltage and current contacts here have a relatively large surface area, and hence the contact resistances are low.

The methods referred to are based on the fact that the geometry of the sample ensures a simple pattern of virtually parallel current stream-lines. Formulae have been devised to correct for the deviation from parallelism in fig. 2, caused by the finite width of the arms. A drawback of the bridge-shaped sample is that it is rather difficult to make, having to be cut out of the brittle semiconductor material with an ultrasonic tool. There is therefore a considerable risk of breakage, particularly when the arms are made narrow.

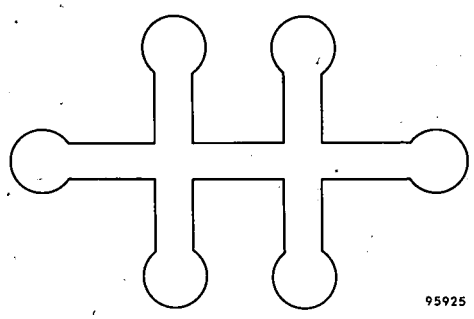

Fig. 2. The bridge-type sample, which is provided with relatively large contact faces to reduce contact resistances. This form is of special importance in measurements at low temperatures.

In the following we shall describe a method of performing resistivity and Hall-coefficient measurements on lamellae of arbitrary shape [2]). The lamella must not, however, contain any (geometrical) holes.

New method of measuring resistivity

We take a flat lamella, completely *free of holes*, and provide it with four *small* contacts, M, N, O and P, at arbitrary places *on the periphery* (*fig. 3*). We apply a current i_{MN} to contact M and take it off at contact N. We measure the potential difference $V_P - V_O$ and define:

$$R_{MN,OP} = \frac{V_P - V_O}{i_{MN}}.$$

Analogously we define:

$$R_{NO,PM} = \frac{V_M - V_P}{i_{NO}}.$$

The new method of measurement is based on the theorem that between $R_{MN,OP}$ and $R_{NO,PM}$ there exists the simple relation:

$$\exp\left(-\frac{\pi d}{\varrho} R_{MN,OP}\right) + \exp\left(-\frac{\pi d}{\varrho} R_{NO,PM}\right) = 1, \quad (1)$$

where d is the thickness of the lamella and ϱ the

[1]) See e.g. C. Kittel, Introduction to solid state physics, 2nd edition, Wiley, New York 1956, Chapter 13, p. 347 et seq.

[2]) L. J. van der Pauw, A method of measuring specific resistivity and Hall effect of discs of arbitrary shape, Philips Res. Repts. **13**, 1-9, 1958 (No. 1).

resistivity of the material. If d and the "resistances" $R_{MN,OP}$ and $R_{NO,PM}$ are known, then (1) yields an equation in which ϱ is the only unknown quantity.

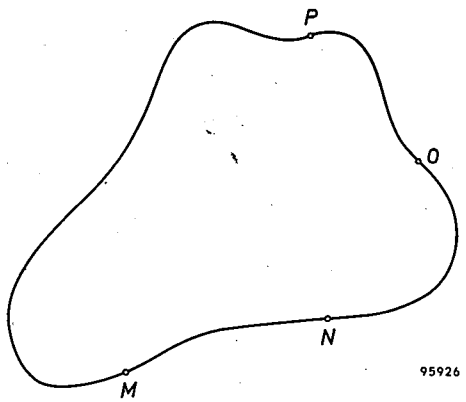

Fig. 3. A flat lamella of arbitrary shape, with four contacts M, N, O and P on the periphery, as used in the new method of measuring resistivity. The Hall coefficient can also be measured on a sample of this kind.

The situation is particularly straightforward if the sample possesses a line of symmetry. In that case, M and O are placed on the line of symmetry, while N and P are disposed symmetrically with respect to this line (*fig. 4*). Then:

$$R_{NO,PM} = R_{MN,OP}, \quad \ldots\ldots \quad (2)$$

which may be seen as follows. From the reciprocity theorem for passive fourpoles, we have quite generally that $R_{NO,PM} = R_{PM,NO}$ (interchange of current and voltage contacts), and it follows from the symmetry that $R_{PM,NO} = R_{MN,OP}$. Hence we arrive at (2); ϱ can then easily be found from (1):

$$\varrho = \frac{\pi d}{\ln 2} R_{MN,OP}. \quad \ldots\ldots \quad (3)$$

In this case a single measurement suffices.

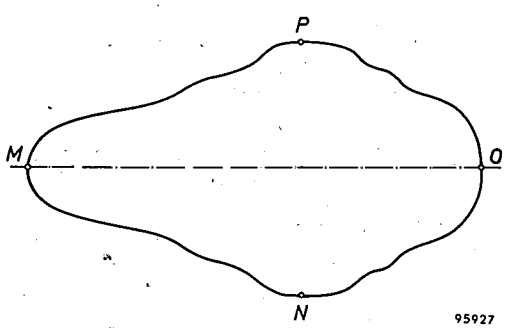

Fig. 4. The resistivity measurement is simplified if the sample has a line of symmetry. If two of the contacts are situated on the line of symmetry and the two others are symmetrically situated with respect to this line, one measurement is sufficient to give the required resistivity.

In the general case it is not possible to express ϱ explicitly in known functions. The solution can, however, be written in the form

$$\varrho = \frac{\pi d}{\ln 2} \frac{R_{MN,OP} + R_{NO,PM}}{2} f, \quad \ldots \quad (4)$$

where f is a factor which is a function only of the ratio $R_{MN,OP}/R_{NO,PM}$, as plotted in *fig. 5*. Thus, to determine ϱ, we first calculate $R_{MN,OP}/R_{NO,PM}$, read from fig. 5 the corresponding value of f and then find ϱ from (4).

Photographs of samples as used for the old and for the new method are shown in *fig. 6*.

The complete proof of the theorem underlying the measurement of ϱ is given in the paper quoted in footnote [2]). The proof consists of two parts. First of all, relation (1) is developed for a special case, the case of a lamella in the form of an infinite half-plane, provided with four contacts at the

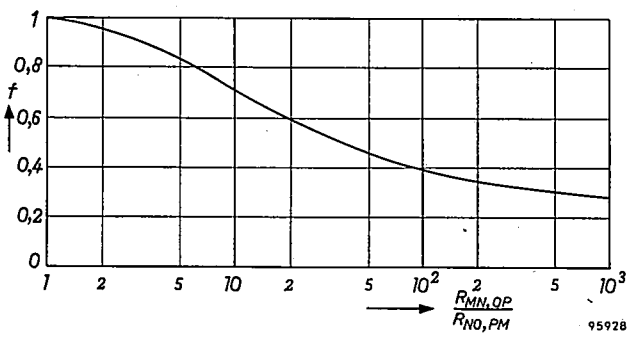

Fig. 5. Between the factor f in formula (4) and the ratio $R_{MN,OP}/R_{NO,PM}$ there exists the relation:

$$\cosh\left\{\frac{(R_{MN,OP}/R_{NO,PM})-1}{(R_{MN,OP}/R_{NO,PM})+1}\frac{\ln 2}{f}\right\} = \tfrac{1}{2}\exp\frac{\ln 2}{f},$$

which is represented here graphically.

periphery. It is then shown that the relation must also apply to a lamella of any shape. This is done by means of conformal mapping of the arbitrarily shaped plate on the infinite half-plane with the aid of complex functions.

We shall consider the first part of the proof in more detail, since it reveals the origin of the exponential functions in (1).

We first consider a lamella which extends to infinity in all directions. To a point M we apply a current $2i$, which flows away from M with radial symmetry into infinity. Let d again be the thickness of the lamella and ϱ the resistivity. Then at a distance r from M the current density is

$$J = 2i/2\pi rd.$$

The field-strength E is radially oriented and according to the generalized form of Ohm's law has the value:

$$E = \varrho J = \varrho i/\pi rd.$$

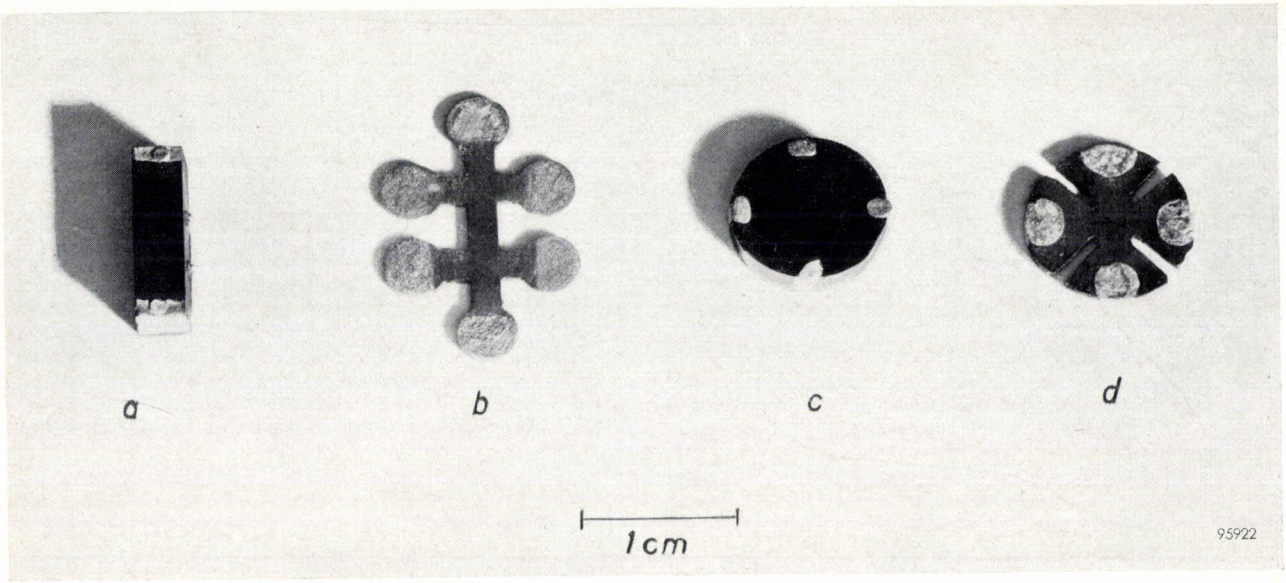

Fig. 6. Some samples of silicon used for resistivity and Hall-coefficient measurements. Samples *a* and *b* correspond respectively to figs. 1 and 2. Measurements on samples *c* and *d* are possible only by the new method. The incisions in sample *d* serve to reduce the error caused by the contacts not being infinitely small.

The potential difference between two points O and P lying on a straight line with M (*fig. 7a*) is:

$$V_P - V_O = \int_P^O E \, \mathrm{d}r = \frac{\varrho i}{\pi d} \int_P^O \frac{\mathrm{d}r}{r} = -\frac{\varrho i}{\pi d} \ln \frac{a+b+c}{a+b}.$$

Since no current flows in the direction perpendicular to the line through M, O and P, the result obtained remains valid if we omit the part of the lamella at one side of this line — yielding a half-plane — and if at the same time we halve the current (fig. 7*b*).

Next we consider the case of *c*) in fig. 7, where a current i now flows *out* from a point N, that again lies on the same straight line with OP, viz. on the edge of the infinite half-plane. We now find:

$$V_P - V_O = +\frac{\varrho i}{\pi d} \ln \frac{b+c}{b}.$$

Superposition of the cases *b*) and *c*) in fig. 7 yields the case *d*), the current i being introduced at M and taken off at N. The value now assumed by $V_P - V_O$ is found by adding together the two previous results. After dividing by i we then find:

$$R_{MN,OP} = \frac{\varrho}{\pi d} \ln \frac{(a+b)\,(b+c)}{(a+b+c)b},$$

or

$$\frac{(a+b+c)b}{(a+b)\,(b+c)} = \exp\left(-\frac{\pi d}{\varrho} R_{MN,OP}\right).$$

Similarly we find:

$$\frac{a\,c}{(a+b)\,(b+c)} = \exp\left(-\frac{\pi d}{\varrho} R_{NO,PM}\right).$$

Addition of the last two equations yields (1).

We shall now explain how formula (4) follows from (1). For simplification we put:

$$\left.\begin{aligned} \pi\, d\, R_{MN,OP} &= x_1, \\ \pi\, d\, R_{NO,PM} &= x_2. \end{aligned}\right\} \quad \ldots\ldots\ldots \quad (5)$$

Formula (1) can then be written:

$$\mathrm{e}^{-\frac{x_1}{\varrho}} + \mathrm{e}^{-\frac{x_2}{\varrho}} = 1. \quad \ldots\ldots\ldots \quad (6)$$

Next we write:

$$x_1 = \tfrac{1}{2}\{(x_1 + x_2) + (x_1 - x_2)\}$$
$$\text{and} \quad x_2 = \tfrac{1}{2}\{(x_1 + x_2) - (x_1 - x_2)\},$$

whereby (6) takes the form:

$$\mathrm{e}^{-\frac{x_1+x_2}{2\varrho}} \left(\mathrm{e}^{-\frac{x_1-x_2}{2\varrho}} + \mathrm{e}^{+\frac{x_1-x_2}{2\varrho}}\right) = 1.$$

This is the same as:

$$\mathrm{e}^{-\frac{x_1+x_2}{2\varrho}} \cosh \frac{x_1 - x_2}{2\varrho} = \tfrac{1}{2}. \quad \ldots\ldots\ldots \quad (7)$$

The exponent of e in (7) is now written as $-(\ln 2)/f$, i.e. we put:

$$\frac{x_1 + x_2}{2\varrho} = \frac{\ln 2}{f}. \quad \ldots\ldots\ldots \quad (8)$$

Formula (7) then becomes:

$$\mathrm{e}^{-\frac{\ln 2}{f}} \cosh\left(\frac{(x_1/x_2) - 1}{(x_1/x_2) + 1} \times \frac{\ln 2}{f}\right) = \tfrac{1}{2}.$$

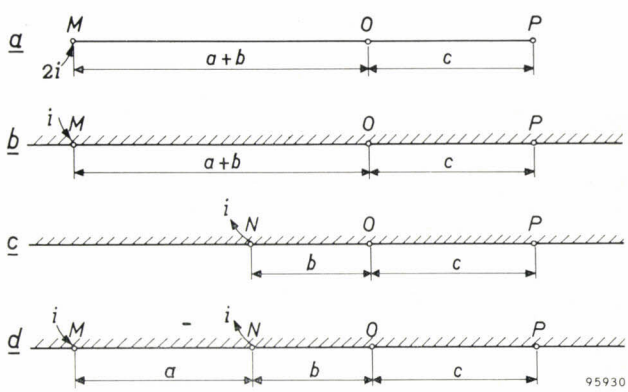

Fig. 7. Illustrating the derivation of formula (1).

This expression represents a relation between f and x_1/x_2, and hence also between f and $R_{MN,OP}/R_{NO,PM}$ (see 5). The relation is shown graphically in fig. 5. By re-writing (8) to give ϱ and substituting for x_1 and x_2 from (5), we find formula (4).

Method of measuring the Hall coefficient

The Hall coefficient, too, can be measured on an arbitrary lamella as in fig. 3. We then apply the current to one of the contacts, say M, and take it off at the contact following the succeeding one, i.e. in our case at O. We measure $R_{MO,NP}$, after which we set up an uniform magnetic induction B at right angles to the surface of the lamella. This changes $R_{MO,NP}$ by an amount $\Delta R_{MO,NP}$. We shall now denote the Hall coefficient R_H and show that it is given by:

$$R_H = \frac{d}{B} \Delta R_{MO,NP}, \quad \ldots . \quad (9)$$

provided that:

a) the contacts are sufficiently small,
b) the contacts are on the periphery,
c) the lamella is of uniform thickness and free of holes.

The validity of formula (9) depends on the distribution of current stream-lines not changing when the magnetic field is applied. With samples of the classical shape of figs. 1 and 2, where the current stream-lines are always parallel to the edges of the sample, there is evidently no change. From the properties of the vector field representing the current density it follows that the same also applies to lamellae of arbitrary shape, provided the above conditions are satisfied [3]).

Under the magnetic induction B, the charge carriers, with charge q, are subjected to a force perpendicular to the stream-lines and perpendicular to the lines of magnetic induction. The magnitude of this force is $F = qvB$, where v is the velocity of the charge carriers. Between v, the concentration n of the charge carriers and the current density J there exists the relation $v = J/nq$. Dividing the force exerted on the charge carriers by their charge q, we see that the effect of the magnetic field is equivalent to an apparent electric field E_H, the Hall electric field, for which we can write [4]):

$$E_H = \frac{1}{nq} J B.$$

[3]) The proof of this statement is also indicated in the paper quoted under [2]).

[4]) This formula is not entirely exact because, apart from their ordered motion with velocity v, the electrons also move randomly owing to thermal agitation. More precise calculation shows, however, that the formula given here is a good approximation.

E_H is proportional to J and to B; the proportionality constant ($= 1/nq$) is called the Hall coefficient R_H.

Since q is known, one can calculate from R_H the concentration n of the charge carriers.

The fact that the current stream-lines are not affected by the magnetic field implies that after application of the magnetic field the electric field is no longer in the same direction as the current stream-lines, but has acquired a transverse component E_t which exactly compensates the apparent Hall electric field E_H (*fig. 8*). The change $\Delta(V_P - V_N)$ in the potential difference between P and N is therefore given by integrating E_t from P over a path orthogonal to the current stream-lines to N' across the lamella (*fig. 9*), and thence along the periphery — i.e. along a stream-line — from N' to N. The last portion of the path makes no contribution to the integral; hence

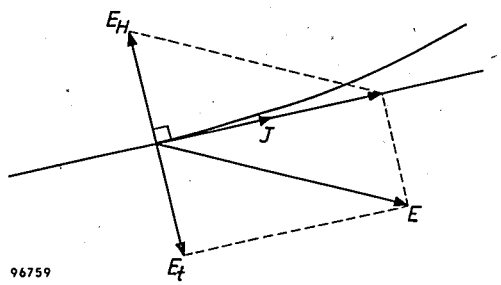

Fig. 8. The resultant of the electrical field-strength E and the Hall field-strength E_H lies in the direction of the current density J. Resolving E in directions perpendicular and parallel to J therefore yields a perpendicular component E_t which in magnitude is equal to E_H.

$$\Delta(V_P - V_N) = \int_P^{N'} E_H \, ds = R_H B \int_P^{N'} J \, ds = R_H B \frac{i_{MO}}{d},$$

where d is again the thickness of the lamella. This expression leads directly to (9).

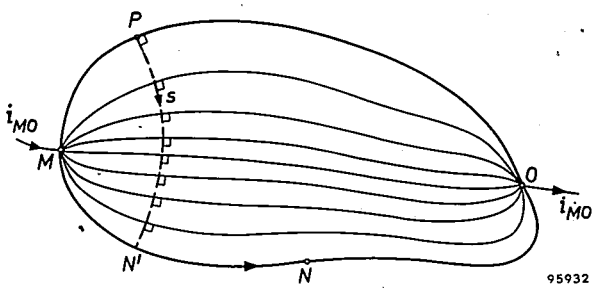

Fig. 9. To calculate by how much the potential difference between points P and N changes when a magnetic field is applied at right-angles to the plane of the sample, the transverse electric field E_t produced by the magnetic field is integrated along the path s which runs from P, orthogonal to the current stream-lines, to N' and thence along the periphery from N' to N.

Estimation of errors

In the foregoing we have assumed the contacts to be "sufficiently" small and to be situated on the periphery. To gain an idea of the error made in the calculations when these conditions are not exactly satisfied, we have worked out the error for three cases. For simplicity we consider a circular disc of diameter D with the contacts mutually 90° apart. We assume further that only one of the contacts is not ideal. The three cases are represented in the adjoining *table*, together with the formulae for the relative errors in the resistivity and the Hall coefficient. The cases are:

a) One of the contacts has a length l along the periphery.

b) One of the contacts has a length l perpendicular to the periphery.

c) One of the contacts, although a point, is situated at a distance l from the periphery.

In practice, none of the contacts will be ideal. To the first approximation the total error is then equal to the sum of the errors per contact.

Table. The relative errors $\Delta\varrho/\varrho$ and $\Delta R_H/R_H$ in the calculated values of the resistivity and the Hall coefficient for a circular disc of diameter D on which one contact P is non-ideal, in the senses indicated in the sketches.

	$\Delta\varrho/\varrho$	$\Delta R_H/R_H$
a 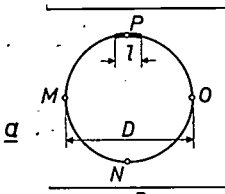	$\approx \frac{-l^2}{16D^2 \ln 2}$	$\approx \frac{-2l}{\pi^2 D}$
b 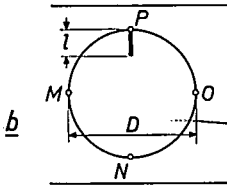	$\approx \frac{-l^2}{4D^2 \ln 2}$	$\approx \frac{-4l}{\pi^2 D}$
c 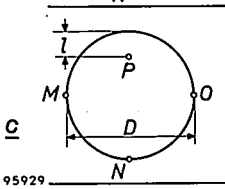	$\approx \frac{-l^2}{2D^2 \ln 2}$	$\approx \frac{-2l}{\pi D}$

95929

The value of the method described here lies in the fact that, in many cases, the material under investigation is already available in the form of small lamellae (e.g. thin discs sawn from a crystal rod); these samples now need no further preparation and can therefore be used for other purposes after the measurement.

If very small contacts are undesirable, having regard to contact resistances in measurements at low temperature, use can be made of "clover-leaf" samples (see fig. 6*d*), the incisions in which substantially reduce the error due to the finite dimensions of the contacts. The clover-leaf sample thus replaces the bridge-type sample (fig. 6*b*) which is used for the same purpose in the classical method. The clover-leaf sample is easier to make than the bridge-type sample and is also less susceptible to breakage.

L. J. van der PAUW.

THE EC 59, A TRANSMITTING TRIODE WITH 10 W OUTPUT AT 4000 Mc/s

by V. V. SCHWAB *) and J. G. van WIJNGAARDEN.

621.385.3.029.64

The versatility of the triode valve stems largely from its wide frequency coverage. Moreover, it operates on low supply voltages and needs no electron-focusing devices. These advantages over microwave tubes of the klystron and travelling-wave type have led to the development of triodes for operation at increasingly higher frequencies. A triode has now been developed in the Philips laboratories which can be used very successfully as a transmitting tube in microwave radio links for relaying telephony and television signals on 7.5 cm waves. Its high power output ensures good communications even under conditions of strong interference.

Introduction

The type EC 59 transmitting triode is one of the most recent fruits of the development work on microwave triodes being carried out in the laboratories of the Philips concern. Following the completion of the disc-seal triodes EC 56 and 57 [1]), intended for operation at 4000 Mc/s, the need was felt for a tube which, at the same frequency, would be capable of delivering a power of 10 to 20 watts with reasonable power gain at a bandwidth of 100 Mc/s. During the relay of television programmes the hitherto available power output of 1.5 W, as delivered by the EC 57 triode, may, under adverse conditions (interference, fading), be too low to produce an acceptable signal-to-noise ratio at the receiving end. To allow for such contingencies, a certain surplus of transmitting power is desirable.

With the EC 59 triode, which is the subject of this article, it is now possible to meet these requirements. In a subsequent article a description will be given of the amplifier designed to operate with this tube.

Theoretical considerations

Fundamentally the EC 59 triode resembles in many respects type EC 57, which was earlier described in this Review. Both tubes are "disc-seal" triodes, characterized by the planar structure and rotational symmetry of their electrode systems.

In a triode the time τ_{kg} taken by an electron to reach the grid is determined by the distance travelled, d_{kg}, and by the mean potential V_0 in the grid plane:

$$\tau_{kg} = \frac{3\,d_{kg}}{\sqrt{2\,\frac{e}{m}\,V_0}} \quad \ldots\ldots\ldots \quad (1)$$

Here e and m are respectively the charge and mass of an electron. For the tube to function properly, this transit time should be small compared with the time T of one cycle of the input signal.

It might appear from (1) that by raising the potential V_0 one could arbitrarily shorten the transit time. According to Child's law [2]), however, the current density J of the emission of the cathode is also governed by V_0 and d_{kg}:

$$J = \frac{4}{9}\,\varepsilon_0 \sqrt{2\,\frac{e}{m}}\,\frac{V_0^{\frac{3}{2}}}{{d_{kg}}^2} \quad \ldots\ldots \quad (2)$$

(ε_0 = dielectric constant of vacuum), and the result of raising V_0 indefinitely would therefore be to saturate the cathode and so drive the tube beyond control. One can get a better idea of the possible ways of reducing τ_{kg} by eliminating V_0 from both equations. One then finds, with d_{kg} in cm and J in ampere/cm^2,

$$\tau_{kg} = 6.7\times10^{-10}\left(\frac{d_{kg}}{J}\right)^{\frac{1}{3}}\text{sec.}$$

At 4000 Mc/s, then, where the period T is 2.5×10^{-10} sec, the relative transit time is:

$$\frac{\tau_{kg}}{T} = 2.68\left(\frac{d_{kg}}{J}\right)^{\frac{1}{3}} \quad \ldots\ldots \quad (3)$$

It can be seen that the relative transit time can be minimized by reducing the distance d_{kg} and also by increasing the current density J. Thus, where the grid-to-cathode distance is made larger in a given case, it is still possible to maintain the same transit time by increasing the current density.

*) Member of the Development Laboratory of Valvo G.m.b.H. Radioröhrenfabrik, Hamburg.

[1]) G. Diemer, K. Rodenhuis and J. G. van Wijngaarden, The EC 57, a disc-seal microwave triode with L cathode, Philips tech. Rev. **18**, 317-324, 1956/57.

[2]) C. D. Child, Phys. Rev. **32**, 492, 1911.

The cathode

In view of the evident advantage of a high current density, the EC 59, like the EC 57, is provided with an L (dispenser) cathode. This is capable of supplying continuously the full saturation current, about 5 A/cm², whereas with an oxide cathode in this type of tube only 300 mA/cm² could be obtained, i.e. only a few % of its saturation current. Moreover, since, with the L cathode, the cathode current need not be so very much smaller than the saturation current, the space-charge potential minimum is flattened and also lies nearer to the emitting surface (see the article cited under [1])). This reduces the loss caused by electrons which, being unable to pass the potential minimum, return to the cathode, and in the process absorb energy from the high-frequency electromagnetic field (total-emission damping). A further advantage of the L cathode is that it is better able to withstand "back heating", a phenomenon discussed later in this article (see section in small print, p. 228). Also, owing to the emitting surface being metallic, it can be made flat and smooth and is not formed by a layer of fairly high resistance as in the case of an oxide cathode.

Considerations concerning the grid-anode space

For a transmitting tube the product of the output power P and the bandwidth B is of primary importance. It is given by the formula [3]):

$$P \times B = \alpha J^2 d_{ga} \frac{C_{ga}}{C_{ga} + C_s} a^2, \quad . \quad . \quad (4)$$

where d_{ga} is the distance between grid and anode, a the radius of the cathode and of the anode (supposed equal), C_{ga} the capacitance between grid and anode in the tube, and C_s the remaining stray capacitance in parallel with C_{ga}; α is a factor allowing for the transit-time effects, the feedback and the dielectric losses in the glass, but is not relevant to the present considerations.

The product of power gain G and bandwidth B, which was discussed in the article cited under [1]), may be written in the somewhat modified form:

$$G \times B = \beta \sigma d_{ga} \frac{C_{ga}}{C_{ga} + C_s}, \quad . \quad . \quad . \quad (5)$$

where σ is the transconductance per unit area of cathode surface (this quantity depends solely on d_{kg} and J); β has a significance similar to that of α in (4).

We see that (4) and (5) contain, respectively, the factors

$$d_{ga}\, a^2 \frac{C_{ga}}{C_{ga} + C_s} \quad \text{and} \quad d_{ga} \frac{C_{ga}}{C_{ga} + C_s},$$

both of which are of a geometric nature. The designer of a transmitting tube sets out to achieve a specific value of the product $P \times B$, so that in this case the first factor is of primary importance. It is found that for a transmitting tube the value of a must be greater than for a receiving tube.

In order to see how the design of the EC 59 is affected by the above considerations, it will be necessary to examine the exact nature of C_{ga} and C_s. In the frequency range in which the tube operates, the output circuit is formed by a resonant cavity having a localized narrower space, where the electric field is concentrated and which is the gap traversed by the electrons ("re-entrant" cavity); see *fig. 1*. The anode surface and the grid plane constitute part of this cavity. This is the essence of the electrode configuration in a disc-seal triode [4]). To a first approximation one can represent

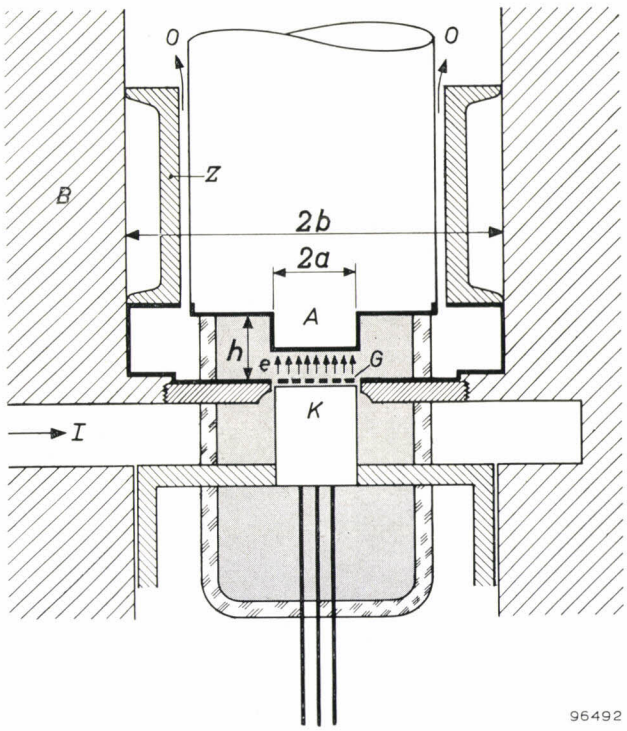

Fig. 1. Schematic diagram of a disc-seal triode, mounted in an amplifier, showing the output resonant cavity (bold lines). A anode, G grid, K cathode, Z tuning piston moving in metal block B. The glass spacer ring between grid and anode divides the resonant cavity into two parts, the inner part being evacuated (evacuated part of tube is shaded). The arrow I indicates the high-frequency energy entering via a waveguide, of which the very small cathode-grid gap forms a part. The small arrows e represent the electrons traversing the electrode space; the alternating electrical field of the resonant cavity is largely concentrated in this space. The two arrows O denote the high-frequency energy leaving the annular output gap (quarter-wave transformer).

[3]) J. G. van Wijngaarden, Onde électrique **36**, 888, 1956.

[4]) It is evident that the output circuit is not formed by the tube alone.

this resonant cavity electrically by a capacitance in parallel with a self-inductance. The capacitance consists partly of the capacitance between the two electrodes (grid and anode), C_{ga}, partly of the capacitance contributed by the sharp edges of these electrodes, and by the capacitance of the two end surfaces. The two latter together constitute C_s. The capacitances C_{ga} and C_s depend in a complex way on the dimensions indicated in the figure. These dimensions are so chosen as to achieve the desired value of the product $P \times B$. This choice is also influenced, however, by the following considerations:

1) The resonant cavity must be tunable to the required frequency.
2) The distance d_{ga} must not be unduly large; otherwise the anode voltage required might become too high, which may result in a drop in efficiency.
3) The distance h between the anode bush and the grid disc (see fig. 1) cannot, for constructional reasons, be reduced *ad libitum*.
4) The product $G \times B$ must have a reasonable value.

Another important factor which limits the possibilities at high frequency is the permissible dissipation of grid and anode. The higher the frequency f at which the cavity is to resonate, the smaller must be the dimensions, the latter being inversely proportional to the frequency for geometrically similar resonant cavities. The surface area of the anode must therefore be inversely proportional to f^2. If we compare tubes of the same power output at different frequencies, we can speak of "equivalence" if the *relative* bandwidth is the same; the required value of the product $P \times B$ for such "equivalent" tubes is thus proportional to the frequency. Since the cavity dimensions vary inversely with the frequency, the factor $d_{ga} a^2 C_{ga}/(C_{ga} + C_s)$ in equation (4) clearly varies according to f^{-3}; hence J^2 must vary according to f^4, i.e. the required J is proportional to f^2. Since the anode (and the cathode) area is proportional to f^{-2}, the total current, and consequently (see (2)) the voltage, too, remain independent of the frequency.

We see, then, that the specific anode dissipation increases with the square of the frequency in the case of "equivalent" tubes. If the materials for anode and grid are suitably chosen, however, the power to be dissipated is not a serious limiting factor in the design of tubes for the range around 4000 Mc/s. The specific anode dissipation in the EC 59 is 780 W/cm², the total dissipation being 125 W. The heat generated is dissipated by a water-cooling system.

Another point of consideration is the glass of the tube envelope which, being in the high-frequency field of the resonant cavity, might be heated to the softening point as a result of dielectric losses. This must obviously be avoided. The calculation for the resonant cavity with $h = 4$ mm shows that a generated power of $P = 1500/f$ (P in watts, f in 10^9 c/s) is permissible in the case of glasses for which $\varepsilon_r \tan \delta \approx 3 \times 10^{-3}$. At 4000 Mc/s this implies a maximum permissible high-frequency power of 400 W. It is clear, therefore, that the heating of the glass imposes no limitations on the design of the EC 59 triode.

Design of the EC 59 tube

The first step in dimensioning the tube was to determine the current density required from the cathode. With the L cathode it was found possible to set the current density J at 1.5 A/cm² (this operating current must of course be lower than the saturation current); at this value the tube can operate at a normal cathode temperature, which is important if it is to have a reasonable life. With a cathode-grid distance $d_{kg} = 0.06$ mm, we then have according to (1): $\tau_{kg} = 1.07 \times 10^{-10}$ sec, which at 4000 Mc/s corresponds approximately to $\tau_{kg}/T = 0.4$. Taking a cathode of diameter $2a = 4.5$ mm, and aiming at a value for $P \times B$ of 2×10^9 watt c/s, we find with the aid of (4):

$$a\, d_{ga} \frac{C_{ga}}{C_{ga} + C_s} = 1.75 \times 10^4 \text{ cm}^2/\mu\text{F}.$$

The value of $C_{ga}/(C_{ga} + C_s)$ was taken as 0.3, which is larger than in the case of the triode EC 57, owing to the larger value of a. The value of $C_{ga}/(C_{ga} + C_s)$ fixes the grid-anode distance, d_{ga}, at 0.3 mm. The other dimensions of the resonant cavity (fig. 1) are then determined: $h = 5.5$ mm and $b = 13$ mm. With these dimensions the resonant frequency is higher than required; by adjusting a piston so as to vary the size of the cavity, the system can be tuned to the correct frequency.

At a grid-cathode distance of 0.06 mm and an anode current density of 1.5 A/cm², the mean potential in the grid plane will be about 7 V, according to equation (2). If we then select the anode voltage (500 V) and the grid bias (−5 V), we arrive at a value of the amplification factor. Since d_{ga} is already fixed, we are left with two variables for achieving this amplification factor; these are the diameter and the pitch of the grid wires. In this connection it must be taken into account that, if the pitch is made much greater than the distance between grid and cathode, the result will be non-uniform emission

("Inselbildung") of the cathode [5]). With regard to grid dissipation, which occurs when a large control signal is applied, it was found desirable to use a grid wire of not too fine a gauge. Having decided on 30 μ wire, it was necessary to choose a pitch of 130 μ in order to obtain the required amplification factor [6]).

Fig. 2 shows a cross-section of the tube thus designed. The table below gives the principal dimensions and electrical data of the EC 59 compared with those of the EC 57.

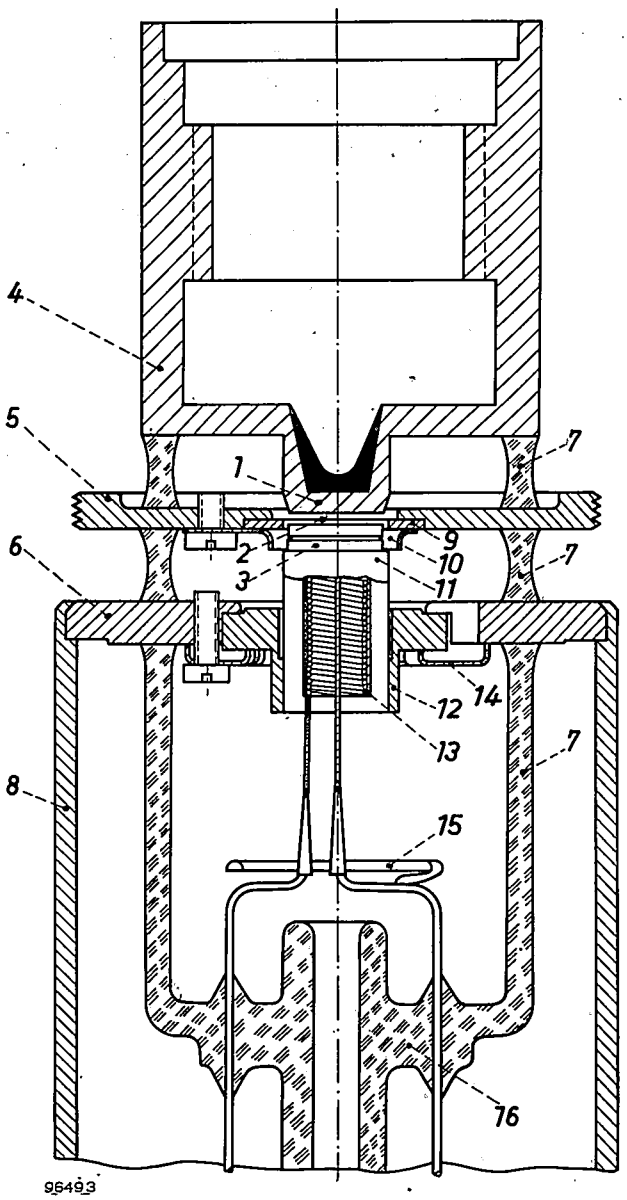

Fig. 2. Cross-section of disc-seal triode EC 59. *1* anode, *2* grid, *3* L cathode, *4* anode bush, *5* grid disc, *6* cathode disc, *7* three glass rings, *8* cathode bush, *9* grid frame, *10* shield, *11* Ta-foil cylinder, *12* cathode holder, *13* filament, *14* spring washer, *15* getter, *16* sintered-glass base.

	EC 57	EC 59
Cathode diameter $2a$	3 mm	4.5 mm
Grid-wire diameter	7.5 μ	30 μ
Pitch of grid wires .	48 μ	130 μ
d_{kg}	40 μ	60 μ
d_{ga}	240 μ	300 μ
J	0.84 A/cm²	1.5 A/cm²
$P \times B$	150 watt Mc/s	1000 watt Mc/s
$G \times B$	1600 Mc/s	1000 Mc/s

We see that with the EC 59 the product $P \times B$ is about 7 times larger than with the EC 57. The product $G \times B$ has dropped to about 60%, but at the required bandwidth of 100 Mc/s the tube still provides a gain of 10× (10 dB).

The above design considerations were based on a formula for the product $P \times B$ derived from the familiar theory applicable to low frequencies [7]). Furthermore, in determining the cathode-grid distance, use is made of the results of transit-time theory for small signals. The transit times in the case of *large* control signals give rise to the following additional effects.

a) In the space between grid and cathode the phenomenon of "back heating" occurs, causing a loss of emission. Owing to their finite transit time, the electrons emitted with a certain

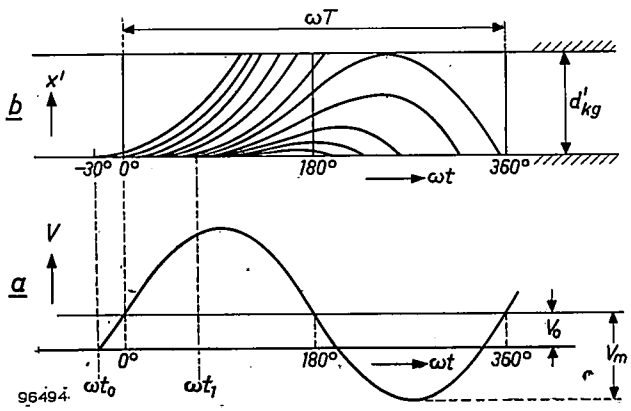

Fig. 3. *a*) Voltage V between grid and cathode (amplitude V_m, grid bias V_0) as a function of phase angle ωt.
b) Position x' between cathode and grid of electrons which have left the cathode at different instants within the duration $T = 2\pi/\omega$ of one cycle, plotted as a function of ωt. The transit time τ_{kg} from cathode to grid is *not* small with respect to T. In each cycle the phase ωt_0 of the first electron is determined by $V = V_0 + V_m \sin \omega t_0 = 0$, whence

$$\omega t_0 = -\sin^{-1}(V_0/V_m).$$

We have here class AB operation (see e.g. F. E. Terman, Electronic and radio engineering, McGraw-Hill, New York 1955, p. 255). The coordinate x' is a *reduced* coordinate, so that the figure is valid for arbitrary values of d_{kg}, V_0 and ω.

[5]) This is due to a non-uniform potential distribution at the grid; immediately opposite the grid wires the field at the cathode may even change sign. The result is a reduction of the active emitting surface of the cathode.

[6]) P. H. J. A. Kleijnen, Philips Res. Repts. **1**, 81, 1946.

[7]) See e.g. J. P. Heyboer, Transmitting valves, Philips Technical Library, 1951.

phase delay ωt_1 after the beginning of each cycle are no longer able to reach the grid, the effective potential in the grid plane having changed sign while the electrons are on their way (see *fig. 3*). These electrons therefore contribute nothing to the release of energy in the space between grid and anode, although they do absorb energy from the control signal, and they return to the cathode with a velocity which, in general, is greater than zero. With high negative grid bias, the phenomenon can assume inadmissible proportions. The best setting is found to be in the region of class B, which constitutes a favourable compromise between amplification and efficiency. (Back heating should not be confused with the phenomenon of total-emission damping, mentioned above.)

b) In a certain part of each cycle the electrons pass through the grid, and the first electrons do so at a greater speed than the later ones. Because of this their arrival on the anode is spread out over a greater part of the cycle than at the grid, resulting in a drop in efficiency.

c) The amplification decreases rapidly with increasing input power. This is due not only to the two phenomena mentioned above, which occur at high frequencies, but also to the fact that, (as at low frequencies), the grid intercepts part of the electrons during its positive period. These electrons, too, therefore contribute nothing to the transfer of energy to the grid-anode space. The grid current to which they give rise does not, however, call for more input power. In the grounded-grid circuit the input power is not affected by the presence of grid current, since the cathode-grid circuit is distinct from the grid-anode circuit [8]).

The mathematical treatment of these effects involves considerable difficulties, and it is therefore not possible to allow for them systematically in a design.

Engineering problems

The shape of the tube (*fig. 4*) is largely determined by the requirements imposed on the anode circuit. As we have seen, the anode-grid space is part of the output cavity of the amplifier in which the tube is incorporated. The electrode system is a planar structure with rotational symmetry. The anode proper is visible in the photograph as a small protrusion below the anode bush. In the amplifier the resonant cavity is further bounded by the cylindrical side walls of the block into which the tube is screwed, by the grid disc, and at the top by a piston; between the piston and the anode bush is an annular gap which forms a $\lambda/4$ transformer, coupling the cavity to the output waveguide. The diameter of the anode bush and of the glass spacer ring between it and the grid disc must be smaller than the dimension $2b$ of the resonant cavity (fig. 1). The diameter of the cathode bush is larger than that of the grid disc, but it should still be small enough to prevent resonance modes of higher order occurring in the high-frequency cathode "choke" [9]). These considerations determine the diameters of the bushes (see figs. 2 and 4).

[8]) See e.g. W. Kleen, Einführung in die Mikrowellen-Elektronik, I. Grundlagen; Hirzel, Stuttgart 1952.

The anode circuit losses must be kept as low as possible. All surfaces should be well polished and be good conductors. The screwed connections between the tube and the different parts of the amplifier should also be mechanically and electrically sound. The anode bush is hollow and open at the top (*fig. 5a*), so that it can be water-cooled. The inside of the bush is threaded, allowing screw attachment of the inner conductor of a coaxial system; the

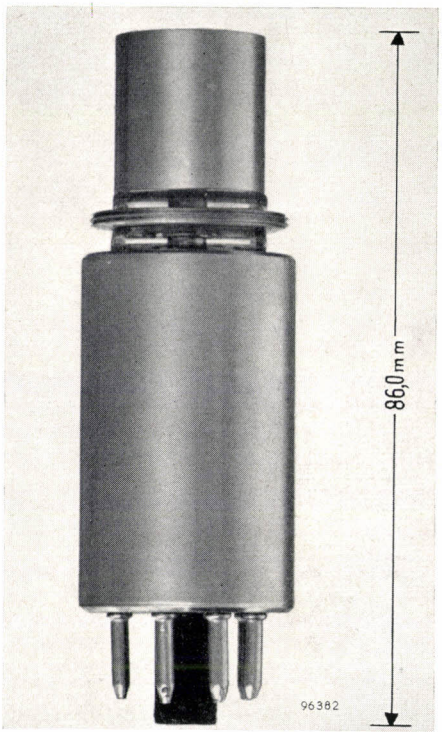

Fig. 4. The disc-seal triode EC 59. From top to bottom: anode bush, grid disc with screw-thread, cathode bush and pins in glass base. Through the glass spacer rings the actual electrodes can be seen.

water-cooling channels run through this inner conductor (see fig. 5*b*). The anode construction adopted allows a certain freedom in the design of this cooling system.

Construction and assembly of the tube

To meet the requirement of good heat conductance, the anode is made of molybdenum provided with gold plating. The grid and cathode discs are made of an alloy of iron, nickel and cobalt ("Vacon 12") and are also gold-plated. The glass used between the electrodes has particularly low dielectric losses. These glass rings, and a glass cylinder underneath the cathode disc, are sealed in a jig

[9]) See e.g. J. P. M. Gieles, A 4000 Mc/s wide-band amplifier using a disc-seal triode, Philips tech. Rev. **19**, 145-156, 1957/58 (No. 5), especially p. 146.

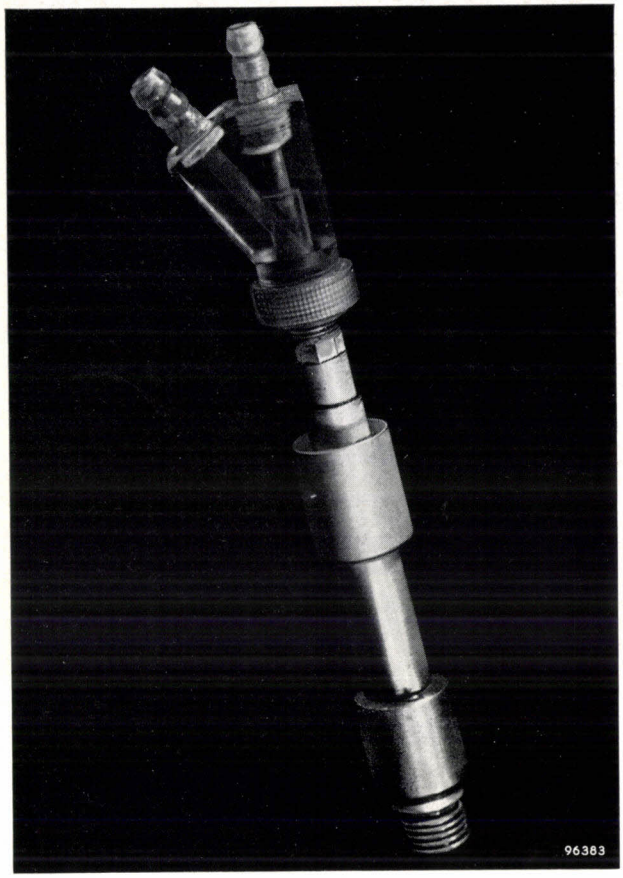

b

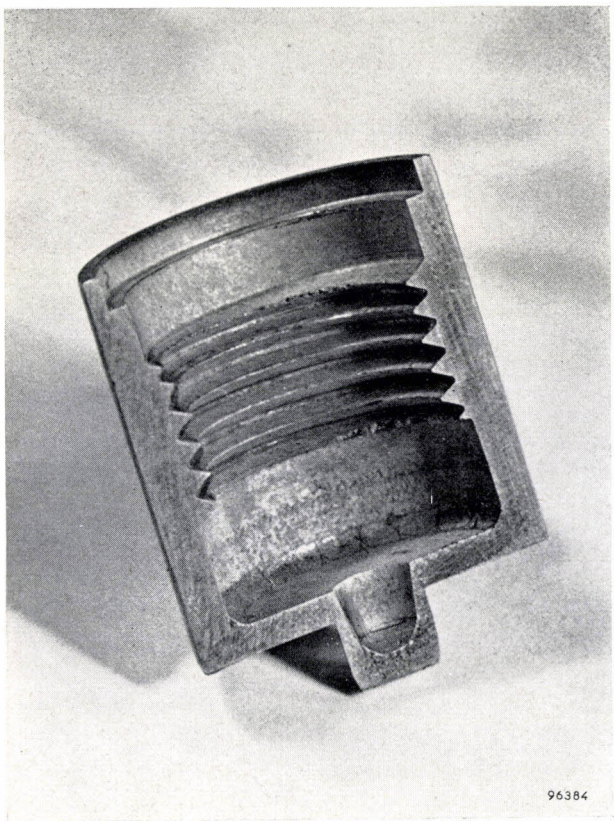

a

Fig. 5. *a*) Cut-away anode bush of the EC 59; *b*) inner conductor of coaxial system which is screwed into the anode bush, and through which the cooling channels pass (this is thus a component of the amplifier).

to the previously enamelled discs. The resultant assembly (*fig. 6a*) is set up on a precision lathe. The anode surface is machined flat, and the seatings are cut for the grid and the cathode holder. The distance between these faces must be very accurately adjusted. This is done by means of dial gauges (see *fig. 7*) mounted on the lathe. On the outside of the tube the thread is cut into the grid disc and the cathode disc is machined to size. All these operations are performed without moving the position of the assembly on the lathe, so that all surfaces are parallel and concentric. The grid is constructed by the method described in an earlier article [1]).

As mentioned, the cathode is of the L type. A molybdenum cylinder with a diametral wall forms two chambers. In the upper (smaller) chamber a tablet of barium-strontium carbonate is inserted, and a flat porous plate of tungsten is welded over the end. The filament is introduced into the lower chamber. A cylinder of tantalum foil (10 μ wall thickness) is fixed around the molybdenum tube and welded to the gold-plated "Vacon" holder. Fig. 6*b* shows the individual components and, on the left, the completely assembled cathode. Note the machined face on the cathode holder which is pressed against the cathode disc, and which determines the grid-cathode distance. To make this face parallel with the cathode surface, the cathode assembly is set up on a lathe via a universal joint. With a highly sensitive dial gauge, adjustments are made until the cathode surface is perpendicular to the axis of rotation. The thrust face of the cathode holder is then machined to produce the exact required distance between the face and the cathode surface. The accurate parallel alignment thus obtained is demonstrated by the fact that only very slight differences are found between the static characteristics of one tube and another.

Like the EC 57, the EC 59 is assembled under a dust cover. After the envelope has been de-burred and cleaned, and the spacings again checked, the grid is fixed to the grid disc by means of screws. The cathode holder is then mounted and pressed against the seating in the cathode disc by a spring-loaded washer. A sintered-glass base with filament and getter (fig. 6*c*) is introduced into the glass cylinder and sealed to the glass, after which the tube is pumped and sealed off. A photograph of the finished tube can be seen in fig. 6*d*. The cathode cylinder is now rimmed onto the cathode disc on a lathe; in this way any possible excentricity is kept within fine limits.

Finally the tube is aged and subjected to static and dynamic tests.

N.V. PHILIPS' GLOEILAMPENFABRIEKEN

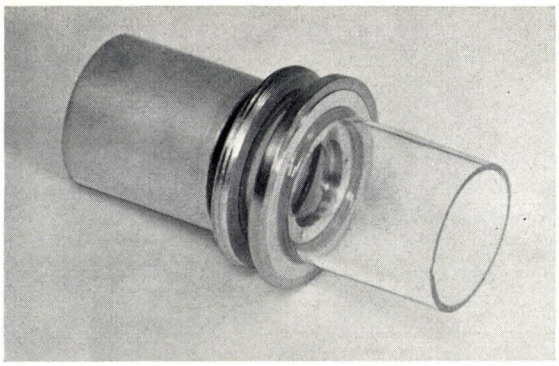

a

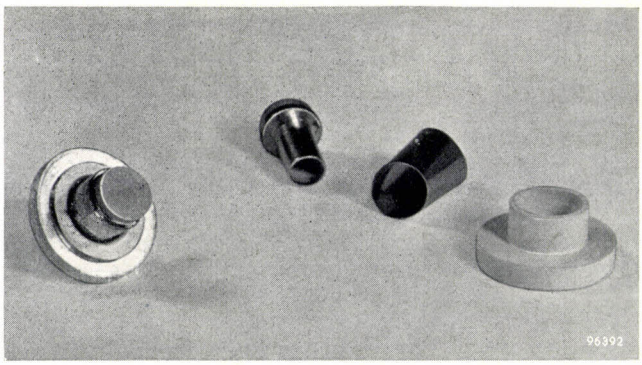

b

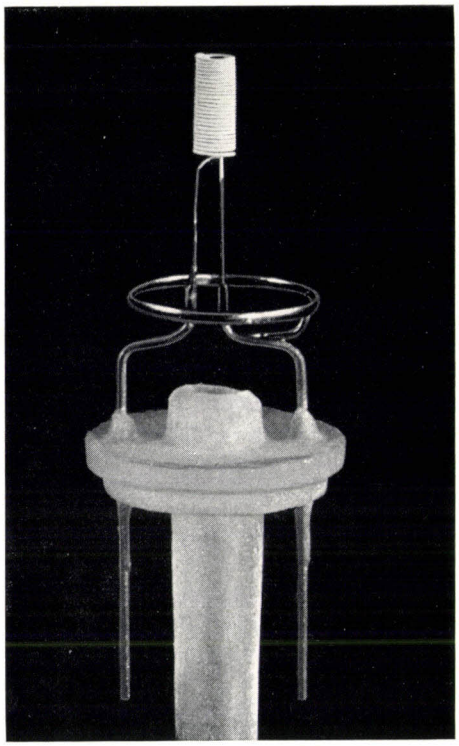

c

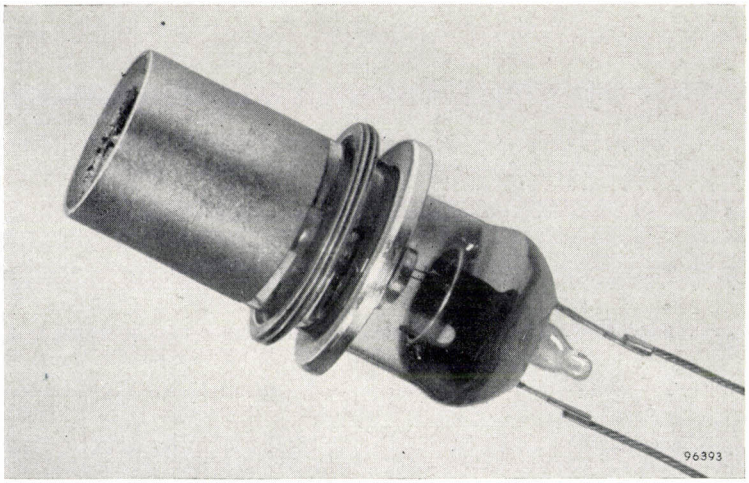

d

Fig. 6. Components of the EC 59 in various stages of fabrication.
a) Anode bush, grid disc and cathode disc sealed to glass.
b) From left to right: assembled cathode, molybdenum cylinder, tantalum-foil cylinder and unmachined cathode holder.
c) Filament and getter ring on sintered-glass base.
d) Grid and cathode mounted, sintered-glass base with filament sealed in, and tube evacuated.

Fig. 8 shows two tubes under static loading, cooling being provided by a closed water-circuit. The water reservoir with radiator and pumping motor are in the foreground. The water in the reservoir is kept at a temperature of about 50 °C. The advantage of this system is that the water is never below room temperature when it enters the cooling system, so that there is no risk of arcing being caused by condensation on the anode bush. Moreover, water at higher temperature has a better coefficient of heat transfer.

The set-up for life testing under dynamic load is shown in *figs. 9* and *10*. The signal from the oscillator (left) passes via an attenuator to the amplifier on the right. The tube is not visible, being completely enclosed in the amplifier block. The output signal is passed via an attenuator to the next amplifier stage. There are thus several amplifiers connected in series, so that with a single oscillator it is possible to test a series of transmitting tubes at the same time. The attenuators are adjusted so that each amplifier can deliver an output of 10 W for an input power of about 1 W.

Another version of this tube is at present being developed in Hamburg, employing *ceramic* instead of glass seals; this tube will be described in a forthcoming article. Furthermore, by slightly modifying the anode design, it has proved possible to cool the EC 59 with *air* instead of water. At an anode dissipation of 115 watts the air-cooling system maintains

Fig. 7.

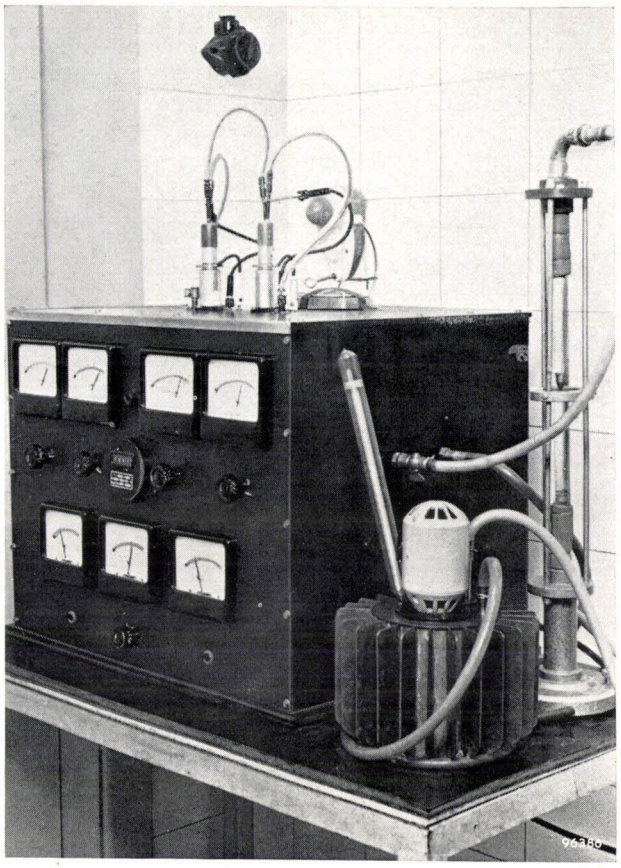

Fig. 8.

Fig. 7. Machining the thrust face in the cathode holder.
Fig. 8. Experimental arrangement for static life-tests, the tubes being cooled by a closed water circuit. Two EC 59 tubes are on the top of the cabinet. Bottom right are the water reservoir with cooling fins, circulation pump and thermometer.

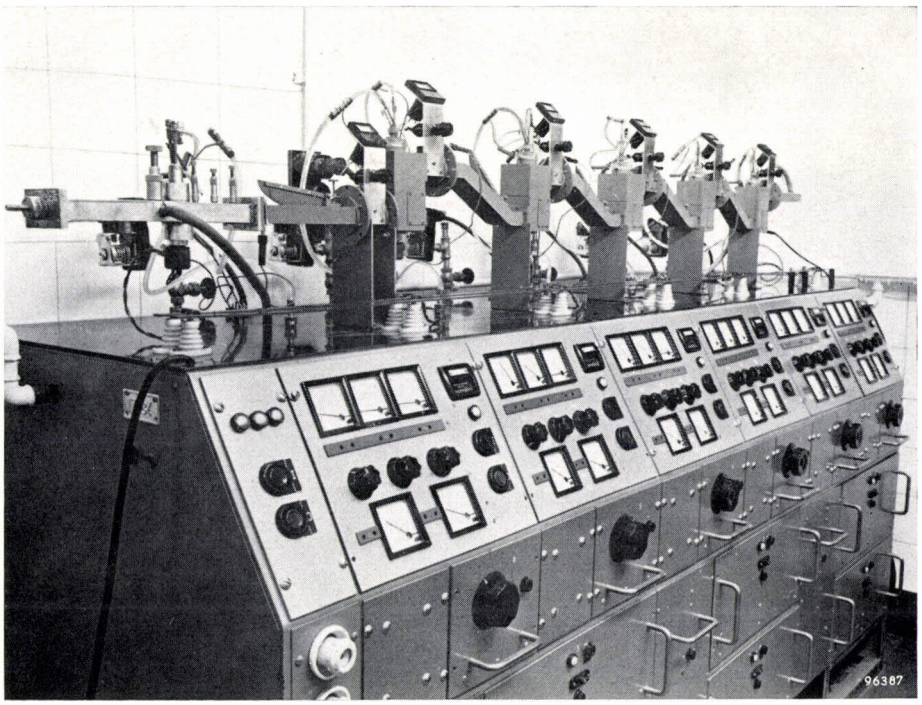

Fig. 9. Arrangement for dynamic life-tests. The tubes operate day and night under the same conditions as in normal use.

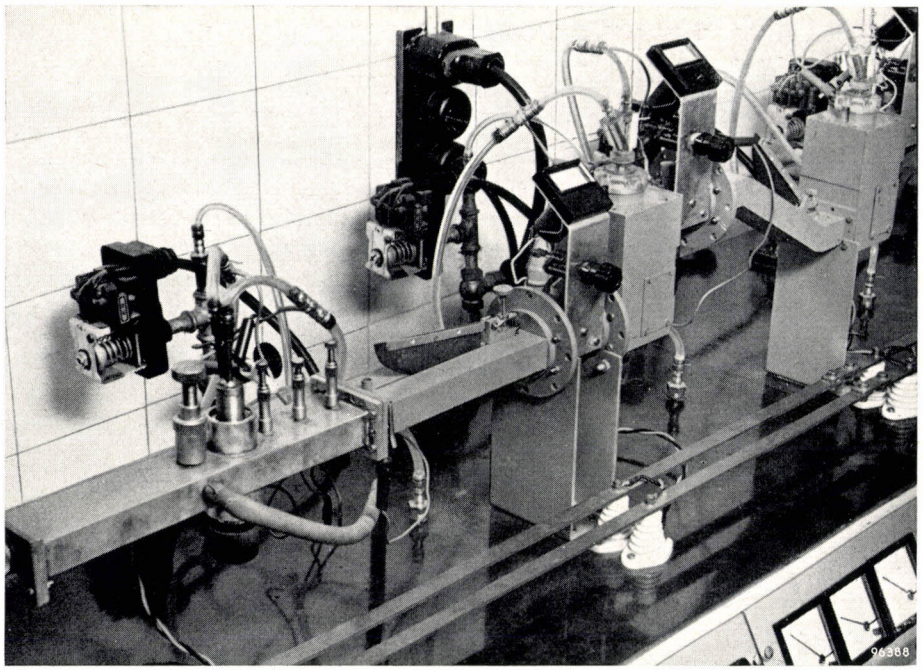

Fig. 10. Detail view of the set-up for dynamic life tests. Left, the oscillator; right, the first two amplifying stages containing type EC 59 tubes.

the temperature of the anode at 120 °C above room temperature at the position of the glass seal. The quantity of air required is then 75 l/min at a pressure of 47 cm water. The cooling method preferred will depend on local conditions.

Summary. In the design of a microwave transmitting triode the fundamental requirement is a relatively short electron transit time in the cathode-grid space. For the tube to operate at very high frequencies, the distance between grid and cathode must therefore be extremely small (some tens of microns) and the cathode current density very high. In these respects the L cathode constitutes an important step forward. At a given current density, the product of bandwidth and output power is mainly determined by the geometry of the tube. A large power-bandwidth product depends, among other things, on minimizing the capacitance between grid and anode. Another important factor is the specific anode dissipation, which rises with increasing frequency. The disc-seal triode EC 59, which is a further development of the earlier described type EC 57, can deliver a high-frequency power of 10 W at 4000 Mc/s over a bandwidth of 100 Mc/s and at a power gain of about 10 dB. The tube is water-cooled (air cooling is also possible). The extremely small clearances between the electrodes are adjusted during fabrication by first sealing the anode bush and the grid and cathode discs in the glass spacer rings and then machining on a precision lathe the seatings into which the actual electrodes are subsequently fitted. In this way the disposition of the electrodes is very accurately fixed. A description is given of the design and fabrication of the tube, and brief mention is made of the cooling system and the method of life testing.

PRECISION VARIABLE CAPACITORS

by A. A. TURNBULL *).

621.319.43

Electronic equipment for military uses is designed for specifications which require components of very high quality. Components must frequently be not only of high accuracy and stability but must also be compact and robust. The article below describes two precision variable capacitors which, although compact, have a performance comparable with laboratory capacitors of considerably larger size.

Two types of precision variable capacitors (*fig. 1*) have been designed at the Mullard Research Laboratories for high grade electronic equipment, meeting stringent specifications as regards their accuracy and stability [1]). One of these capacitors gives a linear frequency law for use in transmitter master-oscillator circuits or in receiver local oscillator circuits. The other is a sine-frequency-law capacitor and was designed primarily for the conversion of radar range and bearing information from polar to cartesian form [2]).

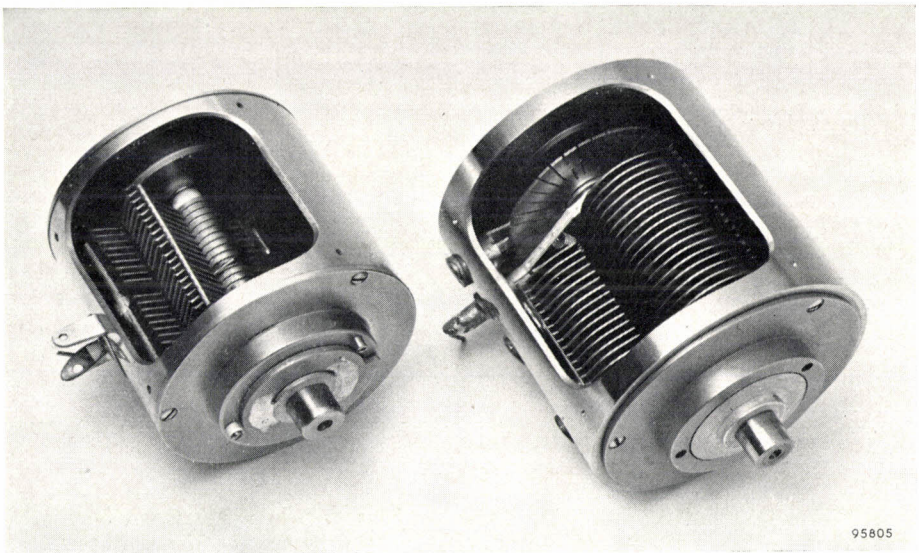

Fig. 1. The two precision capacitors with covers removed. Left, the linear-law capacitor. Right, the sine-law capacitor.

The term stability in connection with these capacitors implies stability over long periods, stability with respect to temperature variations and with respect to vibration. In addition close limits are imposed on any deviation from the relevant frequency law, and the capacitors must also possess a high degree of re-settability. A further requirement is that the capacitors should be sufficiently small to allow their convenient installation in equipment, particularly in compact military equipment. The linear-law capacitor, for example, was originally designed for a specific equipment, in which three of these capacitors were ganged in line. In the layout of this equipment only a limited space was available for the capacitors. Similar considerations also limit the size of the sine-law capacitor.

Some of the features common to both the capacitors may be described, before passing on to the detailed consideration of each type. As stability was the primary consideration in design, structural rigidity is essential. For this reason the capacitors are mounted in a robust cylindrical case with an aperture to permit access to the vanes during assembly. A cover to fit over this aperture is provided for electrical screening and dust protection. A substantially mono-metallic construction is used which avoids stresses being set up due to differential expansions. In certain versions of the linear capaci-

*) Mullard Research Laboratories, Salfords, Surrey, England.

1) A brief description has been published in Brit. Comm. and Electronics **4**, 756-759, 1957.

2) British Patent No. 764 478.

tor one of the rotor vanes is replaced by a bi-metallic vane to increase stability in cases where the equipment is not temperature-regulated. This will be discussed further below.

Mechanical play in the rotors of the two capacitors has been practically eliminated by the use of high-precision angular contact ball-bearings (see below) in which the eccentricity is less than 0.0001 inch. The rotor is mounted in such a way that there is a certain axial and radial load on the bearings; in this way both axial and radial slackness are taken up and no play is possible.

Instability of electrical origin, such as varying surface conductivity or varying dielectric losses in the insulators, is minimized by the use of high-grade ceramic insulators. These support the stator vanes, the rotor vanes being mounted on the earthed rotor assembly.

The temperature coefficient of capacitance is determined largely by the linear temperature coefficient of expansion of the metal used. For both capacitors brass is used for most of the metal parts: this results in a temperature coefficient of capacitance of $+18 \pm 5$ parts per million per °C.

The shape of the vanes differs, of course, in the two capacitors. The shapes required for the linear law and for the sine law were first calculated theoretically. Considerable experimental work was necessary, however, to obtain the correct vane shapes to ensure precise conformity to the ideal curves.

Furthermore, in order that these accurate frequency laws are maintained from one capacitor to another in production, particular care is necessary in the choice of materials for the vanes and in the application of precision techniques for assembly. Stator and rotor vanes are assembled in special jigs, as will be described presently.

Design of the linear law capacitor

The linear-law capacitor is designed for use in oscillator circuits in which a frequency coverage of two to one is required for a capacitance change of about 300 pF. This is obtained in the present design with an angular rotation of 150°. Over this range the capacity conforms to the ideal linear law within $\pm 0.05\%$ in frequency. Furthermore the *rate* of deviation from the ideal law is nowhere greater than 0.02% in frequency per 5° shaft rotation.

The general layout of the linear-law capacitor can be seen from the schematic diagram of *fig. 2*. The stator vane packet is supported on three supports, two being ceramic pillars and the third a glass-metal seal assembly which forms part of the stator terminal. The electrical connection to the rotor assembly is made by a wiper mounted in the centre of the rotor shaft. The use of a central wiper minimizes the self-inductance of the capacitor. The wiper consists of two rhodium-flashed beryllium-copper wires spring-loaded into a locating groove in the shaft. The rhodium plating gives low contact

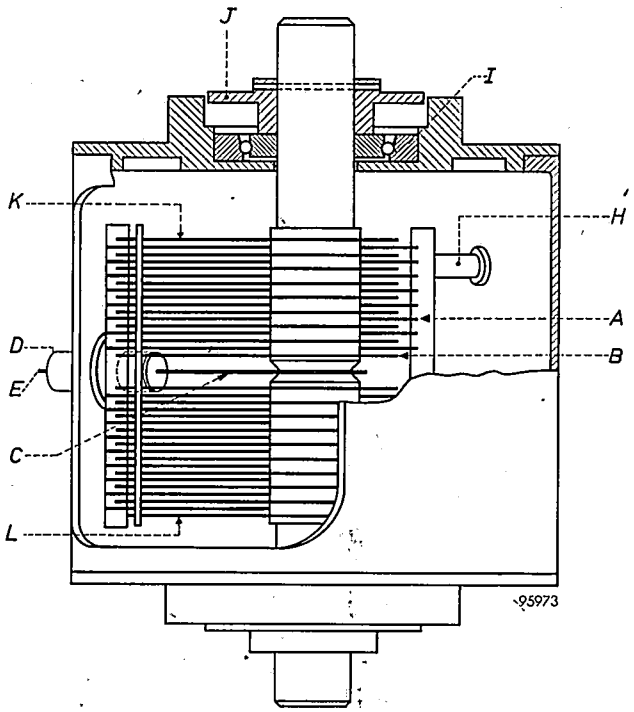

Fig. 2. Simplified cross-section of the linear-law capacitor. *A* stator vanes, *B* rotor vanes, *C* rhodium-plated beryllium-copper wiper wire, *D* stator terminal, *E* rotor terminal, *H* ceramic insulator, *I* angular-contact ball-bearing, *J* bearing thrust collar with locking pin through shaft, *K* trimmer vane, *L* second trimmer vane (uncompensated versions) or bi-metal vane (temperature-compensated versions).

resistance and good wearing properties. The wiper is connected to the central wire of a coaxial connector using "Fluon" (polytetrafluorethylene) insulation. Normally the capacitor is used with the wiper connected to the case, except when special versions are used in which the shaft is insulated from the case with ceramic spacers.

Temperature compensation

For certain applications, for example where it is not practicable to mount the capacitor in temperature-regulated surroundings, it is desirable to provide some measure of temperature compensation. In some models of the linear-law capacitor, therefore, the last vane at one end of the rotor is replaced by a bi-metal vane, which gives the capacitor a temperature coefficient of about —15 parts per million per °C near the maximum capacitance setting. The negative temperature coefficient obtained with this bi-metallic vane reduces short-term

instability of oscillator circuits due to variation in temperature by approximately compensating the normally positive temperature coefficients associated with the coil in the circuit. (With care and using selected materials it is possible to construct coils having a positive temperature coefficient as low as +15 p.p.m./°C.)

The figure of —15 p.p.m./°C for the temperature coefficient of the capacitor refers to the maximum setting of the capacitor. The temperature coefficient near the minimum capacitance settings will not be effective in compensating temperature variations in the coil inductance since, here, the capacitance of the variable capacitor in circuit is a much smaller proportion of the total circuit capacitance. Approximate temperature compensation of the oscillator at the minimum capacitance setting can be effected by placing in parallel with the variable capacitor a fixed capacitor C_p whose temperature coefficient is so chosen that near the minimum setting of the variable capacitance the overall circuit-capacitance temperature coefficient is —15 p.p.m./°C. The overall circuit capacitance then comprises (*fig. 3a*) the minimum capacitance of the variable capacitor C_v, the fixed parallel capacitance C_p, and the stray circuit capacitance C_s. On now rotating the variable-capacitor shaft to near its maximum setting where its temperature coefficient of capacitance is nominally —15 p.p.m./°C, the overall circuit temperature coefficient of capacitance deviates only slightly from —15 p.p.m./°C.

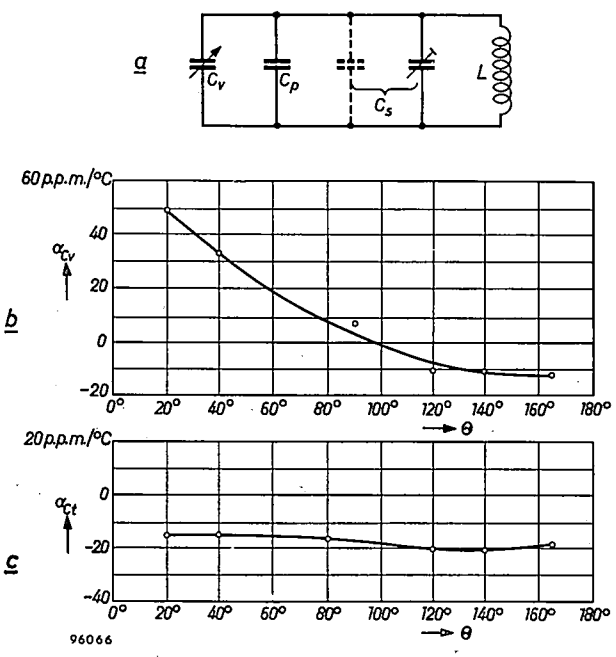

Fig. 3. Temperature compensation of linear-law capacitor. *a*) Tuned circuit consisting of the variable capacitor C_v, a fixed parallel capacitor C_p, the stray circuit-capacitance plus that of a trimmer C_s and a coil L. *b*) Variation of the temperature coefficient α_{C_v} of the variable capacitor with angular setting of the shaft. *c*) Variation of total circuit capacitance α_{C_t} with angular setting of shaft.

In fig. 3*a*, C_v is the capacitance of the variable capacitor, C_s is the stray circuit capacitance plus the capacitance of a trimmer, and C_p is the fixed parallel capacitance, of such a value that the total capacitance in parallel with C_v is $C_p + C_s = 65 \pm 1$ pF. (This value is the parallel capacitance necessary to correct the variable capacitor and thus give precise conformity with the linear frequency law. Adjustment to the precise value between the limits ±1 pF is effected by an empirical method.)

From $f = L^{-1/2} C^{-1/2}/2\pi$ it follows (T = temperature) that:

$$\frac{df}{dT} = \frac{1}{2\pi}\left[-\tfrac{1}{2}L^{-3/2}C^{-1/2}\frac{dL}{dT} - \tfrac{1}{2}L^{-1/2}C^{-3/2}\frac{dC}{dT}\right] =$$
$$= -\tfrac{1}{2}\left[\frac{f}{L}\frac{dL}{dT} + \frac{f}{C}\frac{dC}{dT}\right].$$

If now we let α_f denote the temperature coefficient of frequency f, α_{C_t} the temperature coefficient of the total circuit capacitance C_t and α_L the temperature coefficient of the coil inductance, then

$$\alpha_f \equiv \frac{1}{f}\frac{df}{dT} = -\tfrac{1}{2}(\alpha_L + \alpha_{C_t}).$$

Since α_L is approximately +15 p.p.m./°C, we require that α_{C_t} be approximately —15 p,p,m./°C in order that α_f may be approximately zero. The manner in which the temperature coefficient α_{C_v} of the variable capacitor itself varies with the angular setting of the rotor is shown in fig. 3b. If now the temperature coefficient α_{C_p} of the fixed parallel capacitance is adjusted (see below) such that at, say, the angular setting 20°, the temperature coefficient α_{C_t} of the total circuit capacitance is nominally —15 p.p.m./°C, then α_{C_t} will vary with the angular setting of the rotor as shown in fig. 3*c*.

It can be seen that the maximum value of α_{C_t} is approximately —21 p.p.m./°C. At this point therefore, for α_L equal to +15 p.p.m./°C, α_f would be $-\frac{1}{2}(+15 - 21) = 3$ p.p.m./°C. This simplified outline of the method of temperature compensation, which ignores such factors as possible variations of α_L with frequency, shows that it is possible with sufficient care to effect temperature compensation to within 3 p.p.m./°C over the whole frequency range.

It should be added that figs. 3*b* and *c* refer to a single typical capacitor employing a bi-metallic compensating vane. However (see *Table I* below), there is a spread of ±10 p.p.m./°C in the temperature coefficient as between actual manufactured capacitors, near the maximum capacitance setting. Taking this factor into account it may not always be possible to effect the temperature compensation of an oscillator to within 3 p.p.m./°C but it should always be possible to achieve compensation to within 10 p.p.m./°C (in frequency).

When the required temperature coefficient of C_p has been calculated, one method whereby it may be adjusted to the required value is to make C_p comprise two fixed capacitors in parallel. One of these capacitors would normally be a high-grade silvered-mica capacitor and the other a relativily small-valued capacitor of silvered-ceramic construction. Since silvered-ceramic capacitors with a fairly wide

Table I. Summarized specification for linear-law precision variable capacitor.

Capacitance at 0°	20.0 ± 1 pF
Capacitance variation for 2 : 1 frequency range (for angular swing 26°-176°)	292.8 pF
Conformity to linear law (with optimum parallel capacitance)	± 0.05 % in *frequency*
Self-inductance	0.015 μH
Power factor at maximum capacitance, measured at 1 Mc/s	< 0.00005
Insulation resistance (stator to rotor)	> 1000 MΩ
Breakdown voltage measured at 50 c/s	> 500 V r.m.s.
Torque	< 6 oz.in. [<450 g.cm = 0.044 N.m]
Temperature coefficient near maximum capacitance:	
for uncompensated versions	+ 18 ± 5 p.p.m./°C
for compensated versions	− 15 ± 10 p.p.m./°C
Dimensions:	
overall length	4.4 in.
overall width	3.0 in.

range of known positive or negative temperature coefficients are obtainable, it is usually possible by selecting a suitable capacitor of this type to achieve the correct temperature coefficient of the overall circuit capacitance at the minimum setting (20°) and hence temperature compensation of frequency over the whole range.

Design of the sine-law capacitor

The frequency law of the sine-law capacitor is such that when the capacitor is connected in a suitable oscillatory circuit the oscillator frequency varies sinusoidally about a mean value as the rotor shaft is rotated continuously. This variable frequency may be expressed as:

$$f_\Theta = f_m + f_1 \cos \Theta,$$

where f_Θ is the oscillator frequency for the setting Θ of the shaft and f_m is a fixed frequency. To convert polar coordinates in a radar system to cartesians, which was the use for which this capacitor was originally designed, the capacitor shaft is arranged to rotate in synchronism with the radar aerial direction Θ while the capacitor forms part of the frequency-determining circuit of a variable-frequency oscillator. By beating the sinusoidally frequency-modulated signal $f_\Theta = f_m + f_1 \cos \Theta$ with the signal from a fixed-frequency oscillator of frequency f_m, the resultant difference frequency is $f_1 \cos \Theta$.

If now a suitable gate is opened at the time the radar transmitted pulse sets out, and closed again at the moment the radar echo is received, the number of cycles performed by the oscillator (which can be directly counted) will be proportional to both the range R of the target and also to cos Θ (*fig. 4*).

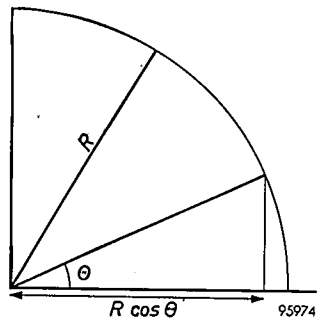

Fig. 4. Conversion of radar data from polar coordinates to cartesians, using the sine-law capacitor to produce a signal of frequency porportional to the cosine of the angular position of the radar aerial. The time interval between transmission of a pulse and reception of its echo is proportional to the range R. Hence for all points at a given range (R, say) this time is the same. Since, however, the frequency of the signal transmitted in any direction Θ is proportional to cos Θ, the number of cycles counted in the above-mentioned time interval is in each case proportional to cos Θ, so that this number of cycles is a measure of the x-coordinate $R \cos \Theta$. A similar arrangement generates the y-coordinate $R \sin \Theta$.

A second variable capacitor ganged 90° out of phase with the first and forming part of a second oscillatory circuit enables $R \sin \Theta$ to be generated.

The design of the sine-law capacitor follows the same general lines as the linear-law capacitor. The main differences are in the vane packets and in the wiper, which now has to stand up to continuous rotation. This capacitor is somewhat larger than the linear-law capacitor. The general layout is shown in *fig. 5*.

As with the linear capacitor, the shape of the vanes was derived theoretically and then the precise profile determined with the aid of experimental data. In this way it is possible to construct capacitors whose capacitance is accurate at all settings to within ±0.02% of the maximum capacitance.

To obtain the conformity to within these close limits, two extra vanes termed the corrector vane and the trimmer vane are added to the rotor and also two small stator vanes termed stator flags are present (their location is shown in fig. 5). *Fig. 6* shows the shape of the vanes. The corrector vane is used to give a coarse correction to the overall capacitance law to within ±0.96 pF for all angular settings. The final correction is made by adjusting the segments of the trimmer vane. This vane has a circular profile with 36 radial slots (see also fig. 1; the corrector vane is behind the trimmer vane in this photograph and is therefore not visible). It will be noted from fig. 6 that all rotor vanes includ-

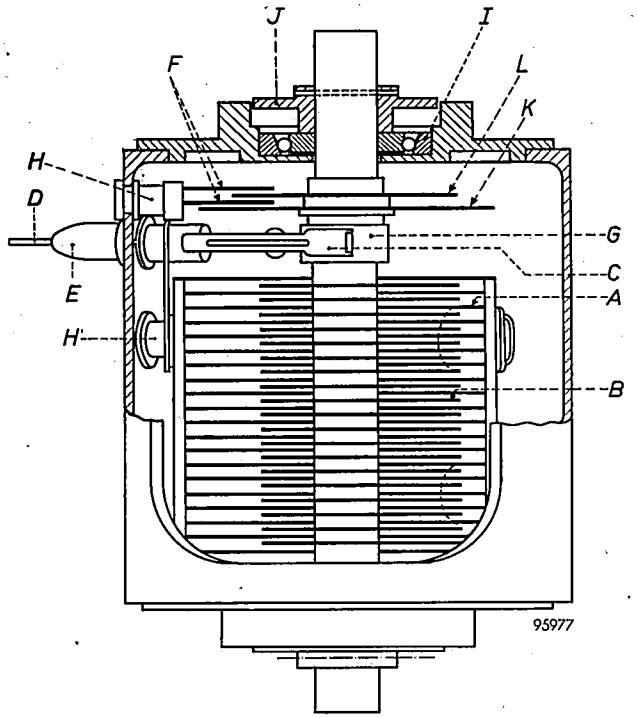

Fig. 5. Simplified drawing showing construction of sine-law capacitor. *A* stator vanes, *B* rotor vanes, *C* silver-graphite wiper brush, *D* stator terminal, *E* rotor terminal, connected to case, *F* stator flags, *G* silver slip ring, *H* ceramic insulators, *I* angular-contact ball-bearing, *J* bearing thrust collar with locking pin through shaft, *K* trimmer vane, *L* corrector vane.

ing the corrector and trimming vanes and the stator vanes are symmetrical about a central line, so that the law of the capacitor obtained as the rotor shaft is rotated from 0° to 360° is symmetrical about 180° (defining 0° to correspond to minimum capacitance).

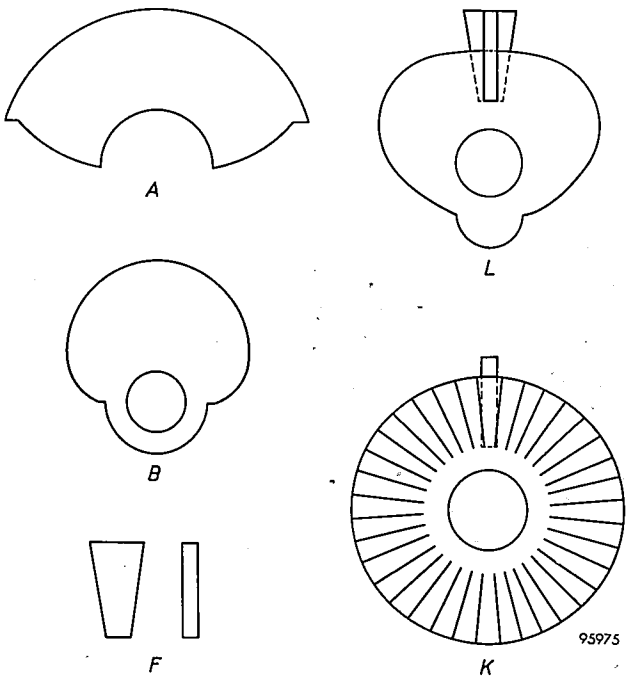

Fig. 6. Profiles of vanes in sine-law capacitor. *A* stator vane, *B* rotor vane, *E* the two stator flags, *L* corrector vane, showing relative positions of stator flags on either side of vane, *K* trimmer vane, showing relative position of the smaller stator flag.

The equipment for which this capacitor was designed provides temperature stabilization for the oscillator components. No bi-metallic temperature-compensating vane is therefore needed, although it is still necessary that the temperature coefficient of the capacitor should be small and held within close limits. In fact the temperature coefficient is held to within $+18 \pm 5$ p.p.m./°C at maximum capacitance (see *Table II*).

Table II. Summarized specification for sine-law precision variable capacitor.

Frequency law	$f_\Theta = f_m + f_1 \cos \Theta$, where $f_m = 500\,000$ c/s and $f_1 = 47\,680$ c/s
Capacitance at 0°	30.5 pF
Capacitance swing 0°-180° (and 180°-360°)	398 pF
Conformity to law	± 0.02 % of *maximum capacitance*
Power factor at maximum capacitance, measured at 1 Mc/s	< 0.0003
Torque	< 3 oz.in. [<225 g.cm = 0.022 N.m]
Temperature coefficient of capacitance	+18±5 p.p.m./°C
Dimensions:	
overall length	5.0 in.
overall width	3.25 in.

The sine capacitor has to be used under conditions of continuous rotation for exceptionally long periods without any significant wiper-bearing wear taking place. The design provides for a shaft rotation at a rate of 10 r.p.m. for not less than 5 million revolutions. To achieve this long life and to give a consistently low contact resistance (approximately 0.001 Ω), the capacitor uses a wiper consisting of silver-graphite brushes bearing on a silver slip ring (see fig. 5).

The stator vane packet is supported from the cylindrical case and insulated from it by four ceramic pillars. A further ceramic pillar supports the two stator flags. The capacitor terminals are coaxial, "Fluon" insulation being used for the stator connector.

Manufacture and assembly

The method of assembling the vanes consists basically of applying precision techniques to a fairly standard procedure. The principle involved is that of assembling the rotor shaft together with the rotor and stator vanes as one unit. The vanes are separated by spacer vanes and accurately jigged in their correct relative positions while the rotor vanes are soldered to the shaft and the tie bars to

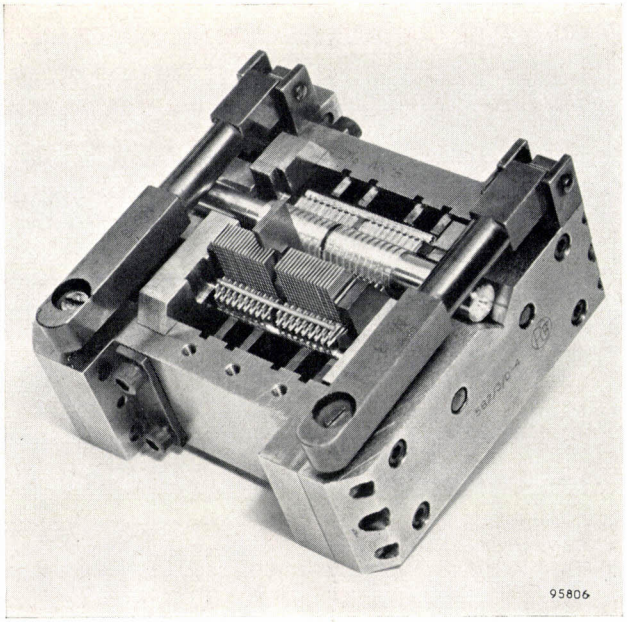

a

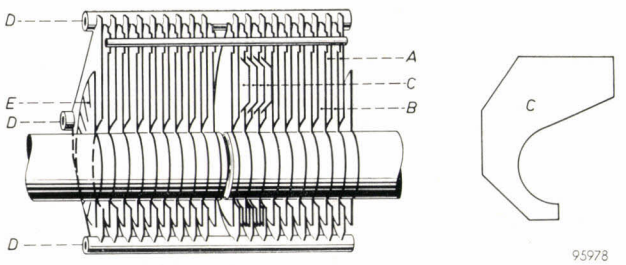

b

Fig. 7. *a*) Assembly jig with stator, rotor and spacer vanes in position. *b*) View of vane packet of linear capacitor after removal from jig. *A* stator vanes, *B* rotor vanes, *C* spacer vanes (only four shown in position, for clarity). *D* stator-vane tie bars, *E* trimmer vane. The shape of the spacer vanes is shown on the right.

the vanes. The jig used for this purpose is shown in *fig. 7a*. The sketch of fig. 7*b* shows a view of the assembly after removal from the jig. This assembly (with the spacer vanes still in position) is now mounted within the capacitor case. This is effected by locating the inner halves of the bearing races on the shaft and loading them on the outer races with a thrust of 40 pounds weight, which is applied to collars that are also located on the shaft and subsequently locked to the shaft with taper pins. At this stage the complete vane packet (i.e. including the stator vanes) is free to rotate with the shaft. The stator vane packet is then fixed to the insulated supports which are mounted on the capacitor case, by soldering the tie bars to the supports. In this manner, throughout the assembly of the capacitor, the accurate relative positioning of the rotor and stator vane packets is maintained. The final operation of removing the spacer vanes permits the shaft to be rotated.

The accuracy of the capacitors is determined to a very large extent by the tolerance on the thickness of the spacer vanes. The brass strip from which the spacer, rotor and stator vanes are blanked undergoes a process during its manufacture when the surface is shaved to yield a very close tolerance on thickness such that there are no greater variations than about 0.0004 inch from the nominal value and no greater variations in thickness over the whole area of any one metre long strip than 0.0001 inch. In order that the average rotor-to-stator spacing should be even more accurately controlled, one half of the spacer vanes used for any one capacitor are made of strip with a thickness error no greater than 0.0002 inch in *excess* of the nominal value while the other half are made from strip with the same error in thickness *less* than the nominal value.

For the linear-law capacitor the method of assembly of the rotor and stator vanes must be such that the resultant law of the capacitor, prior to adjustment by means of the trimmer vane, be within approximately 0.25% in frequency. Only then can the final adjustment by means of the trimmer vane be effected to the required tolerance of $\pm 0.05\%$ in frequency.

Both capacitors are mounted by clamping in a U-shaped cradle, a basic type of which is shown in *fig. 8a*.

A special flexible coupling has been designed for the purpose of ganging the capacitors to each other and to the drive shaft. A collar is attached to each shaft by means of grub screws, each collar being linked to a rigid outer rim by means of a flexible corrugated diaphragm (see fig. 8*b*). With the shafts aligned and set at the correct relative angle, the

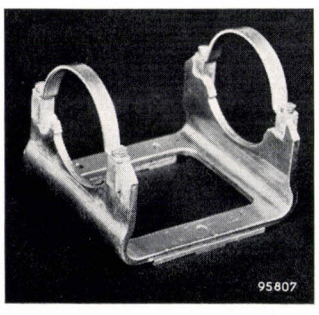

a

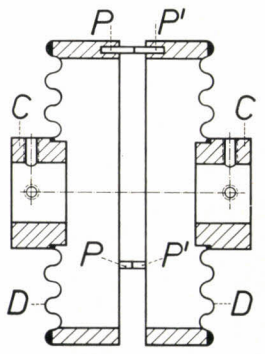

b

Fig. 8. *a*) Basic form of the mounting cradle for the precision capacitors. *b*) Flexible coupling used for ganging the shafts. The collars *C* of each half are locked with grub screws to the two shafts such that, with the shafts at their desired relative orientation, the three pins *P* are approximately aligned with the three pins *P*.′ After the grub screws have been tightened, the shafts are set *precisely* to the correct relative orientation and solder is run over the junctions of the pins. *D* are corrugated metal diaphragms.

two rigid rims are then locked together by running solder between the two sets of three pins. This procedure avoids the slight relative rotation between the two shafts that usually occurs when the grub screws of a coupling are tightened onto the shafts.

Performance and characteristics

The linear-law capacitor

Over a frequency range of 2 : 1 (a capacitance swing of approximately 300 pF), the linear capacitor conforms to the straight-line law to within $\pm 0.05\%$ in frequency as is required. *Fig. 9* is a graph for a typical capacitor showing how the errors vary with the angular setting of the shaft. It can be seen that nowhere do the errors exceed 0.05% in frequency between the angles 18° and 176°. The frequency coverage of 2 : 1 is obtained between the angles 26° and 176° (the same frequency coverage may also be obtained between other pairs of angles,

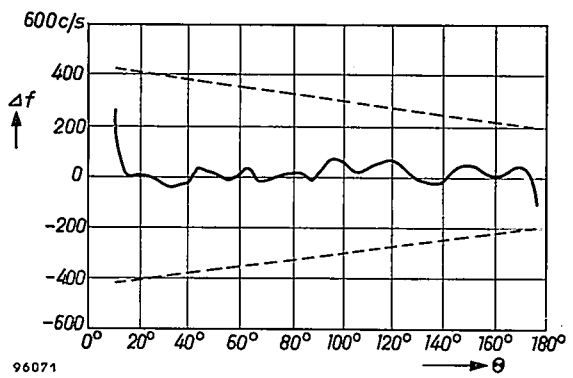

Fig. 9. Typical curve for a linear-law capacitor showing deviations Δf from the straight-line frequency law against angular setting Θ. From 26° to 176° the oscillator frequency passes from 800 kc/s to 400 kc/s. The two oblique dotted lines correspond to frequency errors of $\pm$ 0.05%.

such as 22° and 174° or 18° and 172°). As mentioned above, this performance is obtained when the total capacitance in parallel with the variable capacitors is 65 $\pm$ 1 pF.

The temperature coefficients of capacitance of both versions of this capacitor, i.e., temperature-compensated and non-temperature-compensated, have been given above (see also Table I).

The long-term stability of a number of capacitors has been measured in the laboratory over a period of several years. Periodic measurements of their frequency calibration curves show that these capacitors have a stability of better than $\pm 0.02\%$ in capacitance. Some long-term-stability tests performed by the National Physical Laboratory are shown in *fig. 10a*. The relative humidity at the times of the measurement is shown in fig. 10*b*. The strong correlation between these quantities

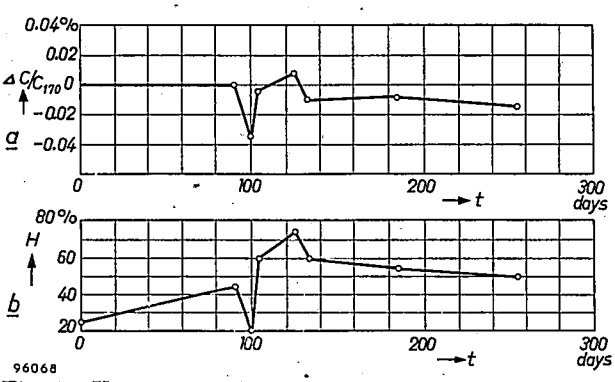

Fig. 10. Uncompensated linear-law capacitor.
a) Variation, over a period of many months, in the *capacitance* swing between the settings 0° and 170°, expressed as a percentage of the capacitance at 170°, measured at 1 kc/s.
b) Corresponding readings of relative humidity H taken at the same times as the measurements of $\Delta C/C_{170}$.

It should be pointed out that these variations in capacitance, which are themselves very small, give rise in practice to much smaller percentage *frequency* variations owing to the presence of a parallel capacitance (fig. 3).

shows that to minimize capacitance variations desirable to use the capacitor under conditions of low relative humidity. This can be achieved fairly easily by raising the temperature of the immediate surroundings slightly above the ambient temperature, or by dessicating the capacitor enclosure.

Vibration tests carried out over the frequency range between 10 c/s and 150 c/s with corresponding accelerations of 0.2*g*-6.8*g* produce only slight changes in capacitance. In all cases the frequency law remains unaltered well within the specified limits of $\pm 0.05\%$.

The sine-law capacitor

The accuracy achieved in the sine-law capacitor is $\pm 0.02\%$ of the capacitance swing. Since the latter is about 400 pF (0°-180°, and 180°-360°), the accuracy of the capacitor is within about ± 0.08 pF for all angular settings. *Fig. 11* is a graph showing the departure from the ideal law for a typical sine-law capacitor. Also shown in this graph are the specification limits in terms of the frequency (equivalent to ± 0.08 pF).

Table II summarizes the properties of this capacitor.

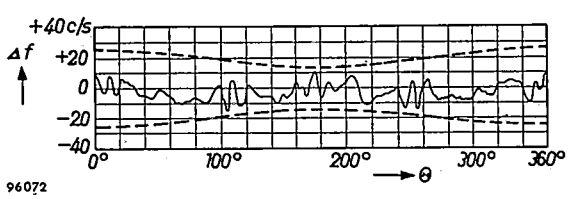

Fig. 11. Deviation Δf in c/s of a typical sine-law capacitor from the ideal sine frequency law, the frequency swing of the oscillator being from 452.32 kc/s to 547.68 kc/s. The dotted lines above and below the curve represent the specification limits (equivalent to ± 0.08 pF).

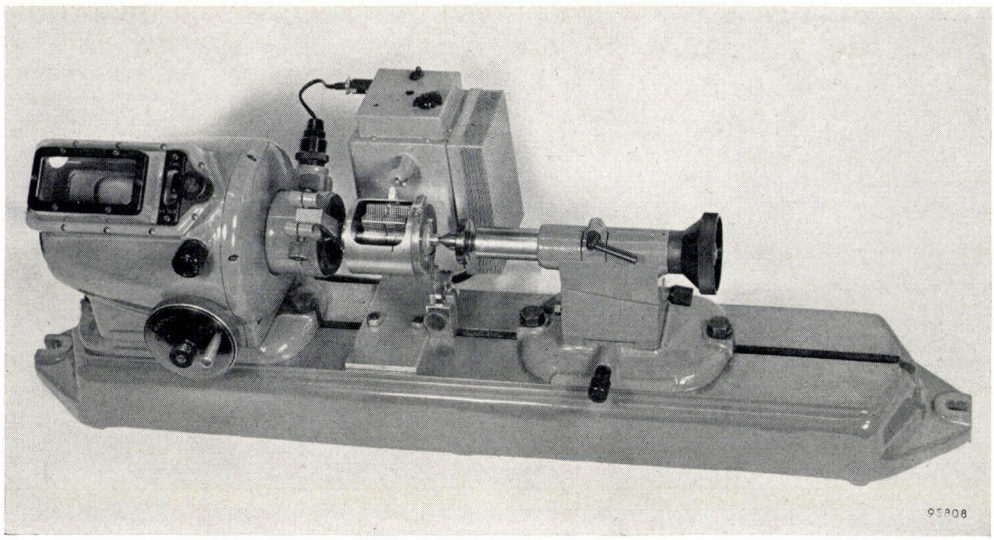

Fig. 12. Precision instrument used for setting angles of the sine-law capacitor. (Optical dividing head by Messrs Precision Grinders Ltd., Mitcham, Surrey, England.)

Measurements have been made to assess the long-term stability of several of these capacitors. These measurements are not easy, however, because of the difficulty in defining the angular position of the shaft of each capacitor. The shaft of this capacitor can rotate continuously, i.e. it has no end stop;

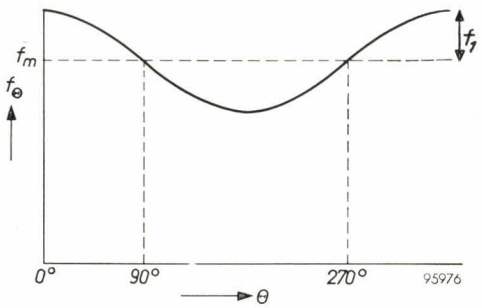

Fig. 13. Indicating the setting of the sine-law capacitor to the two datum positions at 90° and 270° where the oscillator frequency is equal to f_m.

it is therefore much more difficult to set up this capacitor to any datum position. In the absence of a mechanical datum, a method of setting-up by electrical means has to be used. The capacitor is mounted on an instrument whose shaft, coupled to the rotor of the capacitor, can be set to any desired angle with a high degree of precision (to approximately 9 seconds of arc). A photograph of this apparatus is shown in *fig. 12*. The shaft is locked to the instrument and the positions (180° apart) at which the circuit gives the same frequency are found experimentally. (Since the law of the capacitor is $f_\Theta = f_m + f_1 \cos \Theta$, there are two positions of the shaft at 90° and 270°, differing by exactly 180°, which give rise to the same oscillator frequency f_m, see *fig. 13*.) Using these two measured angular positions as the datum angles, measurements show that the instability of the capacitors is not greater than $\pm 0.01\%$ of maximum capacitance over periods of up to three months. Periodic measurements have also been made on two capacitors, while actually installed in their equipment, over a period of some eighteen months. No evidence of instability greater than $\pm 0.02\%$ of maximum capacitance has been found over this period.

Summary. Two precision variable capacitors are described, one giving a straight-line frequency law and the other a sine frequency law. In order to achieve high accuracy and stability, both capacitors have precision bearings and are mounted in rigid cylindrical cases. The vanes are manufactured from brass sheet machined to close tolerances. The linear-law capacitor has a capacitance variation corresponding to 2 : 1 in frequency, for an angular swing of 26° to 176°. The deviation from the straight-line law is never greater than $\pm 0.05\%$ in frequency. The temperature coefficient of capacitance is about +18 parts per million per °C. Special temperature-compensated versions, however, have a temperature coefficient which is equal to −15 p.p.m./°C. The sine-law capacitor is designed so that its shaft can rotate continuously for long periods. Special attention is therefore paid to the wiper contacts which are of silver-graphite, bearing on a silver slip ring. The capacitance swing (from 0°-180° and 180°-360°) is 398 pF. Conformity to the sine law is within $\pm 0.02\%$ of maximum capacitance. The temperature coefficient is +18 p.p.m./°C. One important use of this capacitor is for the conversion of radar data from polar to cartesian form.

ABSTRACTS OF RECENT SCIENTIFIC PUBLICATIONS BY THE STAFF OF N.V. PHILIPS' GLOEILAMPENFABRIEKEN

Reprints of these papers not marked with an asterisk * can be obtained free of charge upon application to the Philips Research Laboratory, Eindhoven, Netherlands.

2581: A. Claassen and L. Bastings: The extraction of ferric chloride with methyl isobutyl ketone and amyl acetate (Z. anal. Chem. **160**, 403-409, 1958, No. 6).

The extraction of iron as ferric chloride in 7 M hydrochloric acid by a mixture of (1+1) or (2+1) methyl isobutyl ketone and amyl acetate is quantitative for macro as well as for micro amounts of iron. The distribution ratio is very high (~4000). With these mixtures no emulsification difficulties are encountered as they are with methyl isobutyl ketone alone. The behaviour of 44 elements in this extraction has been investigated.

2582: H. O. Huisman, A. Smit and J. Meltzer: Investigations on organic insecticides, I. Preparation and insecticidal properties of some substituted polyenamides (Rec. Trav. chim. Pays-Bas **77**, 97-102, 1958, No. 2).

The preparation and insecticidal properties of a number of substituted polyenamides are described in connection with the occurrence of this type of compound in nature.

2583: H. O. Huisman, J. H. Uhlenbroek and J. Meltzer: Investigations on organic insecticides, II. Preparation and acaricidal properties of substituted diphenylsulphones, diphenylsulphides and diphenylsulphoxides (Rec. Trav. chim. Pays-Bas **77**, 103-122, 1958, No. 2).

The preparation and acaricidal properties of a number of variously substituted diphenylsulphones, diphenylsulphides and diphenylsulphoxides are described. A few of them possess strong acaricidal properties. The most outstanding proved to be 2,4,5,4'-tetrachlorodiphenylsulphone — "Tedion V18" — which combines high activity on all stages, except adult spider mites, with total absence of phytocidal side-effects and toxicity for warm-blooded animals.

2584: T. Kralt, H. D. Moed and J. van Dijk: Ionylamines, I. Synthesis of di- and tetrahydro-α- and -β-ionylamines and their spasmolytic action (Rec. Trav. chim. Pays-Bas **77**, 177-195, 1958, No. 3).

The synthesis and properties of amines and quaternary ammonium compounds with the C-skeleton of ionone and C_{18}-ketone are described. The spasmolytic activities of the compounds were determined. The results are discussed and it is concluded that these series of amines show a high musculotropic spasmolytic activity. The relationship between the chemical structure and the spasmolytic activity in these series of amines is fairly clear and regular.

2585: H. D. Moed, T. Kralt and J. van Dijk: Ionylamines, II. Synthesis of tetra- and hexa-hydro-ψ-ionylamines and their spasmolytic action (Rec. Trav. chim. Pays-Bas **77**, 196-208, 1958, No. 3).

The synthesis and properties of amines with the C-skeleton of ψ-ionone are described. The spasmolytic activities of the compounds have been determined. The results are discussed and the conclusions are reached that the ψ-ionylamines form a series of compounds with high musculotropic spasmolytic activity and that in this series there exists a fairly clear and regular relationship between chemical structure and spasmolytic activity.

2586: H. Koopman and J. Daams: Investigations on herbicides, I. 2-(substituted amino)-4,6-dichloro-1,3,5-triazines (Rec. Trav. chim. Pays-Bas **77**, 235-240, 1958, No. 3).

In view of their herbicidal properties a number of 2-(substituted amino)-4,6-dichloro-1,3,5-triazines were synthesized by a method described in the literature. The influence of the side chain on the herbicidal properties was determined. For this reason some derivatives mentioned in the literature were included to compare them with the new compounds in the authors' biological tests.

2587: M. P. Rappoldt, P. Westerhof, K. H. Hanewald and J. A. Keverling Buisman: Investigations on sterols, X. The conversion of ergosterol and pre-ergocalciferol by U.V. light of 254 mμ (Rec. Trav. chim. Pays-Bas **77**, 241-248, 1958, No. 3).

A study is presented of the conversion of ergosterol and pre-ergocalciferol by U.V. light of 254 mμ. From the experiments certain conclusions are drawn regarding the formation of tachysterol$_2$ from ergosterol and on the quantum-efficiency of the interconversion of pre-ergocalciferol and tachysterol$_2$.

2588: H. D. Moed, J. van Dijk and H. Niewind: Synthesis of β-phenylethylamine derivatives, V. Bronchodilators II (Rec. Trav. chim. Pays-Bas **77**, 273-282, 1958, No. 4).

The chemistry is described of three adrenaline-like compounds:

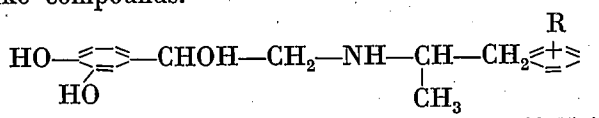

(R = *o*-OH, *m*-OH and *m,p*-$(OH)_2$)

The compounds were examined for their ability to protect guinea pigs from bronchial spasm induced by acethylcholine. The possible influence of the hydroxylated benzene nucleus of the side chain on the drug-receptor combination is discussed.

2589: M. P. Rappoldt, J. A. Keverling Buisman and E. Havinga: Studies on vitamin-D and related compounds, VIII. The photoisomerisations of provitamin-D and its irradiation products (Rec. Trav. chim. Pays-Bas **77**, 327-330, 1958, No. 4).

Results of kinetic investigations and measurements of quantum yields are reported, which cannot be explained by the most simple scheme imaginable for the photochemical interconversions of provitamin-D and its isomers. At least two excited transitory species have to be assumed. More experimental data will be needed before a decision can be made in favour of one or other of the hypothetical, more complicated, pathways.

2590: W. Haidinger: Ein Beitrag zur Kenntnis der brennflecklosen Bogenentladung (Z. Physik **151**, 106-113, 1958, No. 2). (Contribution to the study of arcs without cathode spot; in German.)

For high-pressure xenon discharges with short arcs, it is shown that the transition from an arc with cathode spot to an arc without cathode spot is dependent on the form and emission of the cathode. A special cathode is described for which the transition current under otherwise equal conditions is reduced by about 40%. When this cathode is provided with readily emitting substances, the transition current can be diminished more than 85%. Contrary to earlier experience a re-ignition peak is observed at small currents (low cathode temperature) with this arc.

2591: J. Hornstra: Dislocations in the diamond lattice (Phys. Chem. Solids **5**, 129-141, 1958, No. 1/2).

In this paper several possible structures of dislocations in the diamond lattice are discussed. Special attention is paid to the occurrence of broken bonds in the core of the dislocations and in jogs; for instance, edge-type dislocations can occur in configurations without broken bonds. Jogs can act as a source or sink of interstitials and vacancies; in the diamond lattice this is complicated by the existence of two kinds of atom sites. The most probable types of partial dislocations and the mechanism of their formation from simple dislocations are discussed. In the last section something is said about the occurrence of partial dislocations at twin boundaries and about a line imperfection with zero Burgers vector which may occur at the end of a twin lamella.

2592: J. H. Spaa: A beam-scanned rotating heavy-ice target for high loads (J. sci. Instr. **35**, 175-178, 1958, No. 5).

Of the several possible targets for the $D(d,n)^3He$ reaction the heavy-ice target proves to be the most suitable for outputs of about 10^{10} neutrons per second. Beam scanning in two perpendicular directions combined with rotation of the target is found to be necessary to secure a sufficient life of the ice surface.

2593: F. A. Kröger and H. J. Vink: Relations between the concentrations of imperfections in solids (Phys. Chem. Solids **5**, 208-223, 1958, No. 3).

Imperfect crystals behave statistically like liquid solutions, the crystal being the solvent and the imperfections the solutes. Application of the law of mass action to atomic and electronic reactions taking place in the crystal and between the crystal and the other phases leads to the notion that the concentrations of the various imperfections are interdependent as a result of reactions having partners in common. The consequences of this interdependence are demonstrated by means of a graphical method. Imperfections having opposite effective charges tend to increase each other's concentrations. Foreign atoms are incorporated in a manner dependent both on the energy levels caused by them and on the type of imperfection prevailing in the crystal in the absence of these foreign atoms. In monatomic solids the mechanism of incorporation can be influenced only through the temperature; in compounds it can also be influenced through the partial pressures of the components of the basis crystal. It is shown that the arguments given are valid irrespective of the type of bonding.

2594: G. D. Rieck: Growth and preferred orientations of crystals in tungsten wires (Acta metallurgica **6**, 360-366, 1958, No. 5).

In recrystallized wires of doped tungsten, large crystals have their [421] or [531] axis parallel to the wire axis and small ones tend to keep the original deformation texture [110]. It can be shown that, assuming glide both along ⟨111⟩ and along ⟨100⟩ in the tungsten crystals during drawing, the majority of the crystals attain a [110] texture. However, some crystals which have an orientation near [531] deform on one glide system only. Therefore, during the last stages of drawing, they will tend to turn with respect to neighbouring crystals having a [110] texture. The presence of a dope inhibits the growth of most of the crystals, but least so that of the [531] crystals, as these will have undergone considerable grain boundary slip, resulting in crumbling of the dope skins. Less dope results in more smaller crystals, fewer of which have [531] orientation. The nature of the fragmentation which was already found in the large crystals can be explained on the assumption of tubes or strings of contaminations with blocks and leaks at random places.

2595: J. J. de Jong, J. M. G. Smeets and H. B. Haanstra: Some results of an electron-microscopical study of the metallographic structure of two alloys for permanent magnets (Ticonal G and Ticonal X) (J. appl. Phys. **29**, 297-298, 1958, No. 3).

The microstructures of "Ticonal" G and X in the condition of optimum magnetic properties are studied by the electron microscope using the direct carbon replica. It is argued that a very critical and extensive checking of results is essential in order to arrive at reliable conclusions. Work along these lines demonstrates that *a*) the main structural patterns for "Ticonal" G and X are the same, *b*) the details of the structure of "Ticonal" G and X differ strikingly with respect to texture, width, length-to-width ratio, delineation and intergrowth, and *c*) the influence of the magnetic field during cooling on the structure of "Ticonal" G on a plane // H_u can be shown directly. It cannot yet be decided whether the structure in the optimum condition is a true two-phase structure or a single-phase structure with periodic fluctuations in composition. It is possible that the dimensions revealed by etching do not represent those of the magnetic areas. (Photographs showing the microstructure of "Ticonal" G have appeared in this Review; see Vol. **19**, 11-14, 1957/58.)

2596: A. L. Stuijts and H. P. J. Wijn: Preparation and properties of crystal-oriented ferroxplana samples (J. appl. Phys. **29**, 468-469, 1958, No. 3).

Samples of the hexagonal ferroxplana materials, with a preferential plane for the magnetization, show an increased resonance frequency compared to samples of cubic ferrites with the same permeability. It has been found possible to use the large stiffness for rotation of the magnetization out of the preferential plane, in order to orientate the single crystal particles of a ferroxplana powder in a magnetic field. In this way samples with two different textures have been obtained. In one case the basal planes of the crystals have one direction more or less in common (fan texture); in the other case all basal planes lie more or less parallel to each other (foliate texture). In both cases the permeability is appreciably increased, while the resonance frequency is only slightly decreased. Permeabilities of 56 at 90 Mc/s and 28 at 230 Mc/s, both for $\tan \delta = 0.1$, have been found. This large increase in permeability is caused mainly by an elimination of the effect of the anisotropic permeability of the crystals.

2597: J. Meltzer and F. C. Dietvorst: Action of Tedion on eggs and ovaries of spider mites (T. Pl.ziekten **64**, 104-110, 1958, No. 1).

Eggs of *Tetranychus urticae Koch* of nought to four days of age do not differ in susceptibility to "Tedion". The moment of kill after treatment with "Tedion" is not restricted to a special stage of development. However, most kill occurs between egg stage and nymphochrysalis. "Tedion" affects developing eggs in the ovary of *Tetranychus urticae Koch* after the females have taken up "Tedion" orally. This effect lasts for at least five days after transfer of the females to untreated plants. With CPBS and "Chlorbenside" no complete kill is obtained in this manner, even less than a day after transfer to untreated plants. "Tedion" affects also the developing eggs in the ovary of *Metatetranychus ulmi Koch.* However, in this species the killing effect is lost within two to four days after transfer of the females to untreated plants. "Chlorbenside" acts slightly less in this manner, whereas CPBS is far less active.

VOLUME 20, 1958/59, No. 9 pp. 245-276 Published 8th May 1959

Philips Technical Review

DEALING WITH TECHNICAL PROBLEMS
RELATING TO THE PRODUCTS, PROCESSES AND INVESTIGATIONS OF
THE PHILIPS INDUSTRIES

THE PHILIPS HOT-GAS ENGINE WITH RHOMBIC DRIVE MECHANISM

by R. J. MEIJER.

621.412-231.312

Since the first reports on the Philips hot-gas engine, published in this Review in 1946 and 1947, further research and development on the engine has taken place along two different lines. These investigations have resulted on the one hand in the construction of the cold-gas refrigerating machine, now in production for some years, and on the other hand they have led to the design of a new type of drive mechanism which is of special importance for the hot-gas engine proper (particularly large machines). By the application of this drive mechanism it has been possible to drop the idea of using one piston to perform both power and gas-transfer functions (the "double-acting" principle) and return to the thermodynamically more efficient system of separate power and transfer pistons. In this way and by the incorporation of a number of improvements in the design of regenerator, heater etc., the engine has now been given a form that promises well for future development. Measurements carried out on a 40 H.P. experimental engine built according to the new design have demonstrated that, as far as efficiency and specific power are concerned, the new engine can compete with the best amongst familiar forms of prime mover, besides possessing all the virtues inherent in the hot-gas cycle.

With the help of modern materials and with new knowledge of flow and heat-transfer phenomena, the hot-air or hot-gas cycle, which has been known since the early part of the last century, can be made to take place with high efficiency. This was made clear in a series of articles that appeared in earlier volumes of this Review [1,2,3,4,5]).

Contrary to expectation, development work on the cycle in the Philips laboratories did not in the first place lead to a hot-gas engine, but to a *gas refrigerating machine* — which, in the meantime, has come to occupy an important place in refrigeration practice [4,5]). There are several reasons for the slower development of the *engine*. The principal among these were the practical difficulties encountered when it was tried to apply what was termed the "double-acting" or single-piston principle.

This was indeed an elegant principle. The basic type of hot-gas engine, the Stirling engine, has separate power and transfer pistons, while in our "double-acting" engine one moving body performed the functions of both, this constituting a very considerable mechanical simplification. Moreover, in distinction to the small transfer-piston (or displacer-piston) engines made at the time (which worked very well), the single-piston engines did not require the crankcase to be pressurized. This promised considerable advantages for higher-power engines where a pressure crankcase would necessarily involve large-weight penalties. However, these advantages had to be paid for. In the first place an exceptionally intractable lubrication problem now arose: a piston had to act as a moving gas-tight seal between a hot and a cold space between which a large periodic pressure difference occurs. Also, both thermodynamically and aerodynamically, this type of engine was inferior to the displacer-piston engines, owing to the fact that the volume variations of the hot and cold spaces could no longer be freely chosen as regards their relative magnitude and phase.

With further development it has proved possible to drop the idea of a single "double-acting" piston and to design an engine of the *displacer-piston* type

1) H. Rinia and F. K. du Pré, Air engines, Philips tech. Rev. **8**, 129-136, 1946.
2) H. de Brey, H. Rinia and F. L. van Weenen, Fundamentals for the development of the Philips air engine, Philips tech. Rev. **9**, 97-104, 1947/48.
3) F. L. van Weenen, The construction of the Philips air engine, Philips tech. Rev. **9**, 125-134, 1947/48.
4) J. W. L. Köhler and C. O. Jonkers, Fundamentals of the gas refrigerating machine, Philips tech. Rev. **16**, 69-78, 1954/55.
5) J. W. L. Köhler and C. O. Jonkers, Construction of a gas refrigerating machine, Philips tech. Rev. **16**, 105-115, 1954/55.

which also possesses the feature that the crankcase need not be pressurized. This was made possible by the embodiment of a new kind of drive mechanism. The latter offers the additional advantage that even a one-cylinder engine can be perfectly balanced. Of the various engines built according to this design, a single-cylinder 40 H.P. machine will be described here and some results of measurements of the output and efficiency will be given.

To save the reader the trouble of consulting earlier volumes of this Review, we shall now very briefly recapitulate the principles of the hot-gas engine, restricting ourselves to an engine provided with a displacer piston.

Brief account of the hot-gas cycle

An internal-combustion engine provides a surplus of work in virtue of the compression at low temperature of a certain quantity of air, to which atomized fuel is added either before or after the compression, the subsequent heating of the mixture by rapid combustion, and its expansion at high temperature.

The hot-gas engine is based on the same principle, i.e. the compression at low temperature and expansion at high temperature of a given quantity of gas. The heating takes place, however, in an entirely different manner, the heat being supplied to the gas from outside, through a wall. For this reason the description "external-combustion engine" is appropriate. Owing to the high thermal capacity of the wall, it is not of course possible to heat and cool the gas simply by rapid heating and cooling of the wall. Stirling had realized as far back as 1817, however, that the gas temperature could be made to change periodically by causing a "displacer piston" to transfer the gas back and forth between two spaces, one at a fixed high temperature and the other at a fixed low temperature — see *fig. 1*. If we raise the displacer piston in fig. 1, the gas will flow from the hot space via the heater and cooler ducts into the cold space. If now the displacer piston is moved downwards the gas will return to the hot space along the same path. During the first transfer stroke the gas has to yield up a large quantity of heat; an equal quantity of heat has to be taken up during the second stroke. The *regenerator* shown in fig. 1 is inserted between the heater duct and cooler duct in order to prevent unnecessary wastage of this heat. It is a space filled with porous material to which the hot gas yields heat before entering the cooler; when the gas streams back, it takes up the stored heat again prior to its entry into the heater.

The displacer system, which serves to heat and cool the gas periodically, is combined with a power piston that compresses the gas while it is in the cold space and allows it to expand while in the hot space (all dead spaces in cooler, heater etc. being disregarded). Since compression takes place at a lower temperature than expansion, a surplus of work results. *Fig. 2* shows four phases of the cycle through which the whole system passes if a *discontinuous* movement of power piston and displacer piston is presupposed. The displacements they are assumed to undergo are plotted as functions of time in *fig. 3*; the ordinates in band *E* represent the variation in the volume of the hot space, and those in band *C* the variation in the volume of the cold space. The volume variations are plotted separately in the lower part of the diagram. *Fig. 4* is the p,V diagram of the cycle (V is the total volume of the gas).

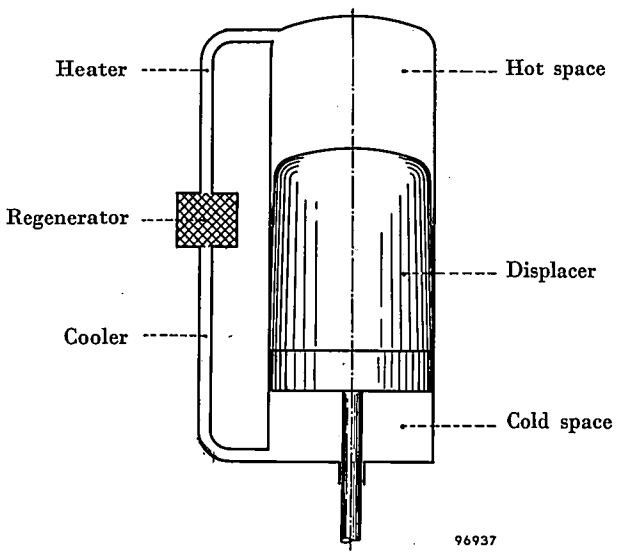

Fig. 1. Principle of the displacer-piston system. Moving this piston up and down causes the gas to be transferred back and forth between the hot and cold spaces, via heater, regenerator and cooler.

In a practical version of the engine the movements of power and displacer pistons must of course be *continuous*, not discontinuous, as they have been assumed to be in these figures; the continuous movements will be obtained with the aid of some kind of crank and connecting rod mechanism. It will not then be possible to distinguish any sharp transitions between the four phases, but this will not alter the principle of the cycle (or detract from its efficiency — see below). The movements of power piston and displacer might now be as indicated in *fig. 5*, in which the volume variations of the cold and hot spaces have again been plotted separately. The only essential condition for obtaining a surplus of work is that the volume variation of the hot space should

N.V. PHILIPS' GLOEILAMPENFABRIEKEN

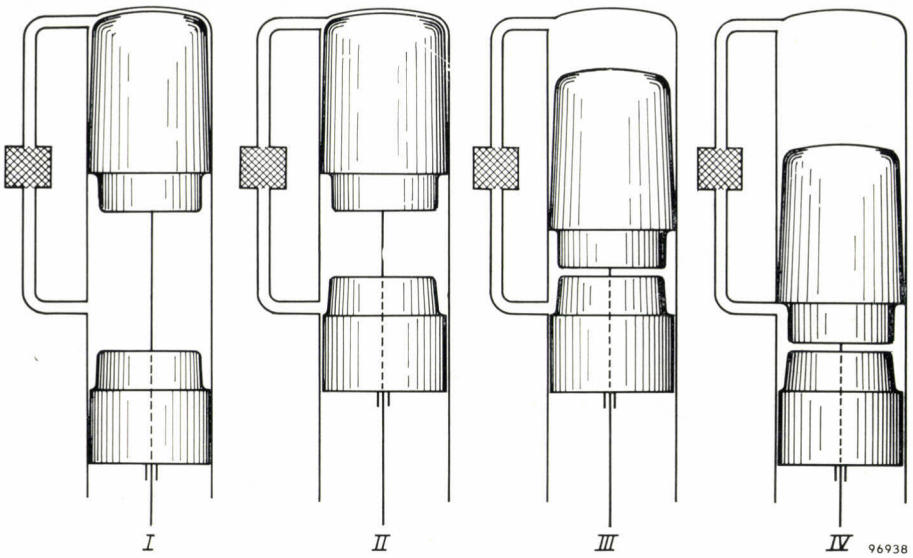

Fig. 2. Diagrams to illustrate the hot-gas cycle. For the sake of clarity the power piston and the displacer piston are supposed to move discontinuously; it is then possible to distinguish four phases that make up the complete cycle.

I Power piston is in lowest, displacer piston in highest position. All the gas is in the cold space.

II The displacer piston is still in the highest position. The power piston has compressed the gas while it is at low temperature.

III The power piston is still in its highest position. The displacer piston has pushed the gas through the cooler, regenerator and heater into the hot space.

IV The hot gas has expanded, and the power and displacer pistons have together returned to the lowest position. While the power piston remains there, the displacer piston will now push the gas through heater, regenerator and cooler into the cold space, whereupon situation *I* will have been restored.

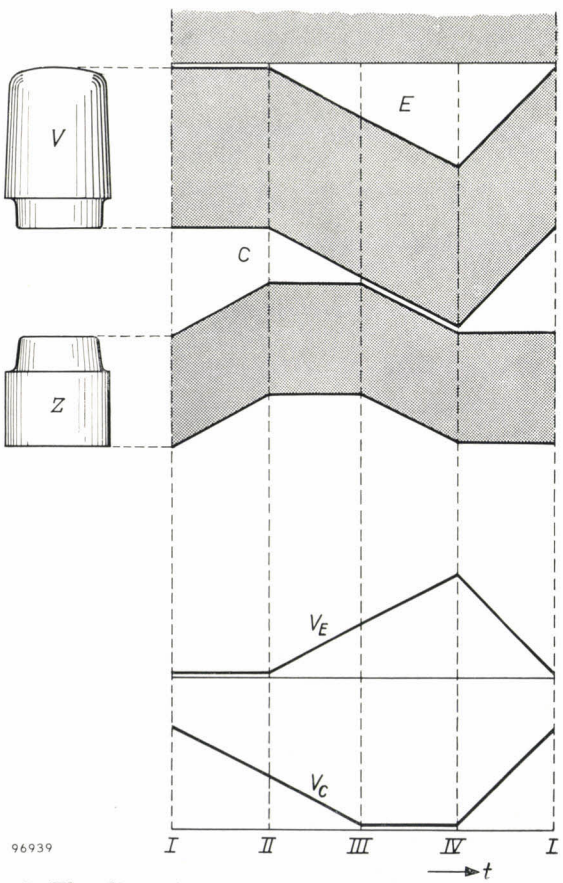

Fig. 3. The discontinuous movements of power piston (Z) and displacer piston (V) assumed in fig. 2, plotted as functions of the time. Band E represents the volume variatons of the hot space, band C those of the cold space. These variations are plotted separately lower in the diagram.

have a phase lead with respect to that of the cold space; this is equivalent to requiring that the appropriate p,V diagram, shown in *fig. 6*, should be traced out in the clockwise direction.

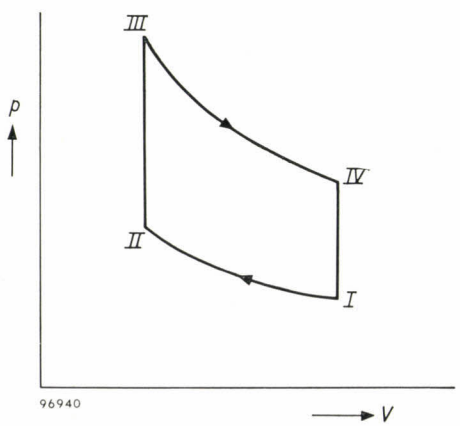

Fig. 4. The p,V diagram of the hot-gas cycle represented by fig. 3.

For the subsequent discussion of specific power and efficiency it will be necessary to recall the more important of the formulae worked out in the articles cited. They are based on the assumption that V_E, the volume of the hot (expansion) space, and V_C, the volume of the cold (compression) space, vary with the crank angle α in a purely sinusoidal fashion:

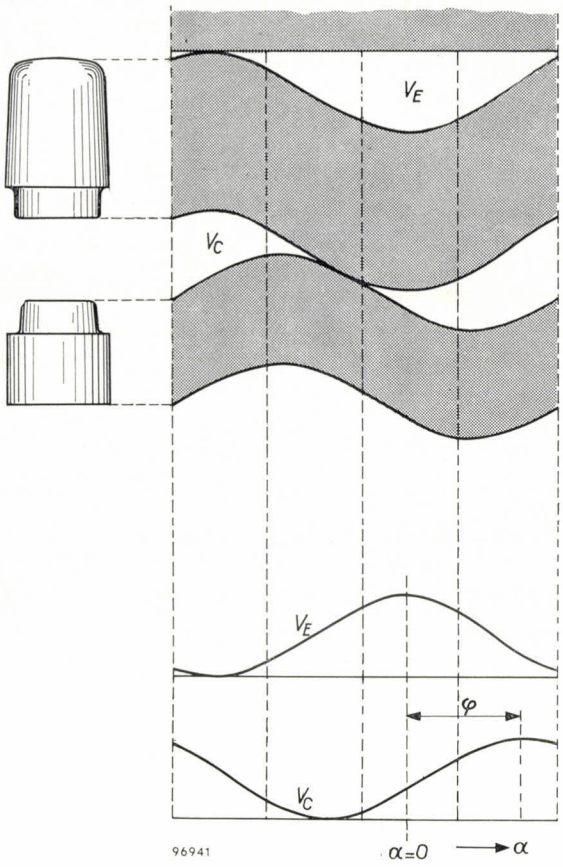

Fig. 5. As for fig. 3, except that now the piston and displacer movements are *continuous* (the abscissa represents the crank angle α). It is no longer possible to distinguish sharp transitions between the phases of the cycle.

$$\left.\begin{aligned} V_E &= \tfrac{1}{2}V_0(1+\cos\alpha), \\ V_C &= \tfrac{1}{2}wV_0[1+\cos(\alpha-\varphi)]. \end{aligned}\right\} \quad . \; . \quad (1)$$

The crank angle α (for constant angular velocity ω, proportional to the time: $\alpha = \omega t$) is measured from the position at which V_E has its maximum value V_0; φ is the phase angle between the volume variations of the hot and cold spaces, and w is the ratio between their maximum volumes. In reality the variations in V_E and V_C will certainly not be purely sinusoidal, but the calculations show that the effect of the higher harmonics can generally be neglected. A further assumption underlies the derivation of the formulae, namely that the cycle is "ideal", characterized by constant gas temperatures T_E and T_C in the hot and cold spaces respectively, and negligible flow and other losses (to which we shall return later on). Another important quantity introduced is the gas temperature ratio,

$$\tau = T_C/T_E \qquad (\tau < 1). \; . \; . \; . \quad (2)$$

The condition that the mass of the working fluid remains constant throughout the cycle now leads to the formula for the pressure p as a function of the crank angle:

$$p = p_{max}\frac{1-\delta}{1+\delta\cos(\alpha-\Theta)}, \quad . \; . \; . \quad (3)$$

in which p_{max} is the maximum pressure occurring during the cycle and

$$\delta = \frac{\sqrt{\tau^2+w^2+2\tau w\cos\varphi}}{\tau+w+2s}, \quad . \; . \; . \quad (4)$$

$$\tan\Theta = \frac{w\sin\varphi}{\tau+w\cos\varphi} \qquad (\Theta < 180^\circ) \; . \quad (5)$$

(s is the relative volume of the "reduced dead space"). From the above we obtain the average pressure,

$$\bar{p} = p_{max}\sqrt{\frac{1-\delta}{1+\delta}}, \; . \; . \; . \; . \; . \quad (6)$$

and the power output

$$P = \tfrac{1}{2}\omega V_0\bar{p}\,(1-\tau)\frac{\delta}{1+\sqrt{1-\delta^2}}\sin\Theta. \; . \; . \quad (7)$$

We are concerned here with a reversible cyclic process in which, in accordance with the "idealized" conditions assumed (isothermal behaviour in cold and hot spaces and 100% efficient regenerator action), the supply of heat takes place at only one temperature T_E and the removal of heat at only one temperature T_C. There is a theorem in thermodynamics which states that under these conditions the efficiency with which heat is converted into work (the thermal efficiency) is that of the Carnot cycle:

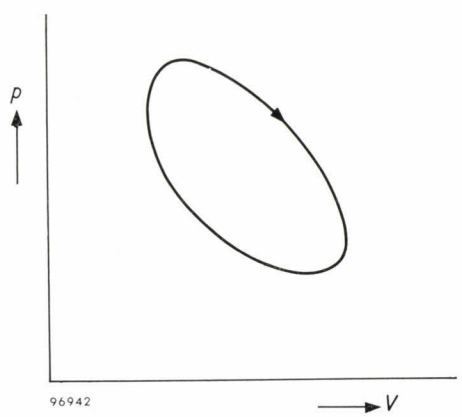

Fig. 6. The p,V diagram of the cycle represented by fig. 5.

$$\eta = \frac{T_E-T_C}{T_E} = 1-\tau. \; . \; . \; . \quad (8)$$

From this we may obtain the quantity of heat supplied per second,

$$q_E = \frac{P}{\eta} = \tfrac{1}{2}\omega V_0\bar{p}\frac{\delta}{1+\sqrt{1-\delta^2}}\sin\Theta. \; . \quad (9)$$

This recapitulation will suffice for our present purposes. We shall now go on to draw certain conclusions which have been essential in deciding the manner in which the cycle must be made to take place in a practical hot-gas engine.

Specific power, losses and overall efficiency

The main considerations governing the design of an engine will in general be to see that its specific power and overall efficiency are as high as possible (consistent, of course, with certain conditions, such as a reasonable working life). The former term refers to the power output per unit volume swept out by the power piston. Overall efficiency is defined as the ratio of work performed per unit time divided by the heat content of the fuel consumed per unit time. These two aims are in some respects contradictory.

We see from formula (7) that the output of a given engine (for which certain values of the parameters w, φ and s have been decided upon) can be stepped up by increasing the mean pressure $\bar{p}$ and the shaft revolutions n (angular velocity ω) and by reducing the ratio τ. A reduction in τ also brings about a direct improvement in the efficiency; formula (8) shows that, theoretically, η is dependent on τ alone. The coolant temperature, which determines T_C, should therefore be made as low as possible, and the temperature T_E at which heat is supplied to the heater element should be made as high as possible, i.e. as high as the properties of the heater wall material (e.g. resistance to creep and oxidation) will permit. To find out the effect on the efficiency, if any, of the other two factors, $\bar{p}$ and n, we shall have to pay attention to the various kinds of *losses*, which are not taken account of the in formulae. The following are the most important [6]).

a) Losses due to mechanical friction in the moving parts.

b) "Adiabatic losses". Within the spaces whose volumes vary, expansion and compression take place more or less adiabatically, not isothermally, with the result that T_{Ea}, the mean temperature in the hot space, will be lower than T_E, the heater temperature and that at which heat is supplied. Similarly, T_{Ca} in the cold space is higher than T_C. Internally, therefore, the engine has a temperature ratio $\tau_a = T_{Ca}/T_{Ea}$ which is greater than the external τ, the implication being a lower efficiency.

c) Fluid friction or flow losses, representing the work done in forcing the gas to flow back and forth through cooler, regenerator and heater.

d) Regenerator losses. Since in practice a regenerator can never be 100% effective, the temperature of the gas leaving it is too high on entry into the cooler and too low on entry into the heater. Thus an additional amount of heat is removed in the cooler, and lost to the engine.

e) Heat-transfer losses at the walls of the elements responsible for heat exchange between the working fluid on the one hand and the coolant and combustion gases on the other. As with the "adiabatic losses", these losses have the consequence that the ratio τ is effectively increased.

f) Flue losses, which are inevitable in any kind of burner. The hot burning gases can yield up heat to the heater body only while their temperature is yet above that of the latter. When they have cooled to this temperature the remaining heat content of the gases will — if no special measures are taken — be lost via the flue. These flue losses can, however, be considerably reduced by further cooling the flue gases by heat exchange with the incoming fresh air, which is consequently preheated.

Now, closer consideration of the influence of $\bar{p}$ and n on the losses shows that the former factor has little effect on their relative magnitude [7]). Hence it is always advantageous to make $\bar{p}$ as high as possible; the experimental engine that will be described below was designed for an average pressure $\bar{p}$ of up to about 100 kg/cm². On the other hand, an increase in the engine speed does affect efficiency adversely, because the *flow losses* increase with n at more than a strictly proportional rate. These losses, however, do not only depend on the engine speed (and, of course, on the dimensioning of the ducts); they differ considerably according to the gas used as the working fluid. Since the hot-gas cycle takes place within a closed system, the designer has a free choice as to the gas so used. We decided on *hydrogen* as the working fluid for the new engine. Owing to its low density, flow losses are not excessive even at considerable engine speeds. Moreover, with hydrogen good heat-transfer characteristics are attainable. In the machine described here the nominal running speed is 1500 r.p.m.

---

[6]) Losses (*a*) to (*e*) inclusive were discussed at rather greater length with reference to the cold-gas refrigerating machine [5]), in which they likewise occur; the losses under (*f*) are of course absent in the refrigerating machine.

[7]) However, the relative magnitude of the losses (*e*) does depend somewhat on the power developed by the engine and therefore also on $\bar{p}$ (and n too): the greater the rate at which it is desired to pass heat through a given area of heat-exchanger wall, the greater will be the temperature drop across the wall, and hence the smaller is the internal temperature difference, i.e. the greater is the ratio τ.

Helium may also be used as the working fluid instead of hydrogen. The overall efficiency is then found to be somewhat lower.

The further details of the engine we shall now proceed to describe are mainly concerned with the new drive mechanism to which reference has already been made, the design of regenerator, heater, cooler and air pre-heater and finally a complete control system for regulating the power of the engine.

The drive mechanism of the displacer-piston machine

Earlier versions

There are various ways of making the power and displacer pistons perform the required movements. *Fig. 7* shows a drive mechanism of a kind that used to be embodied in small hot-gas engines. The power piston is linked to the crankshaft K by a connecting rod (con-rod) D in the normal way; the movement of the displacer is derived from that of the power piston with the aid of the rocker T, which is linked by arm S_1 to the displacer-piston rod V and by arm S_2 to a certain point on the power-piston con-rod. The latter has to be forked in order to leave free passage for the arm S_1 and the displacer-piston rod, which passes centrally through the power piston. A different form of drive mechanism has been adopted for the Philips gas refrigerating machine — see *fig. 8*. There are three cranks in the shaft, and the two outside ones, which lie at the same angle, are linked to the piston by two parallel con-rods; the displacer piston is actuated from the middle crank, which is offset by a certain angle from the other two.

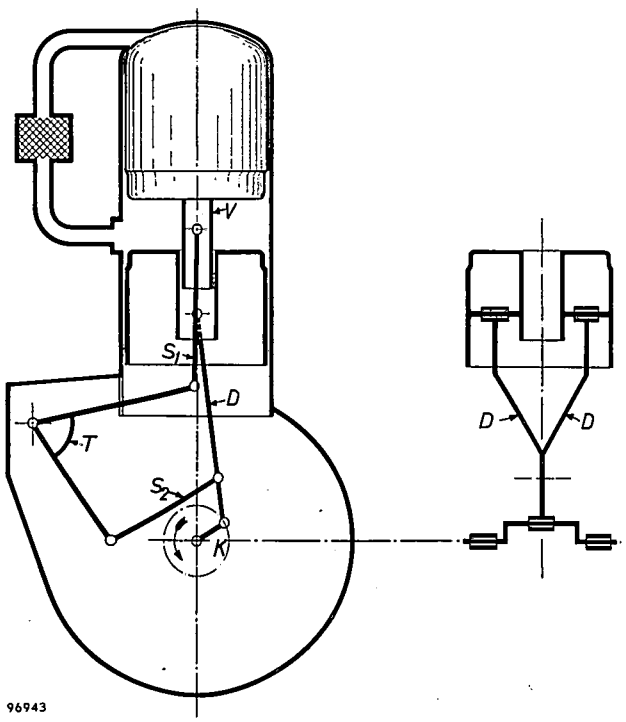

Fig. 7. Drive mechanism of the kind formerly used in small hot-gas engines. D = forked piston con-rod. K = crankshaft. T = rocker linked by arms S_1 and S_2 to the displacer-piston rod V and to a certain point on D.

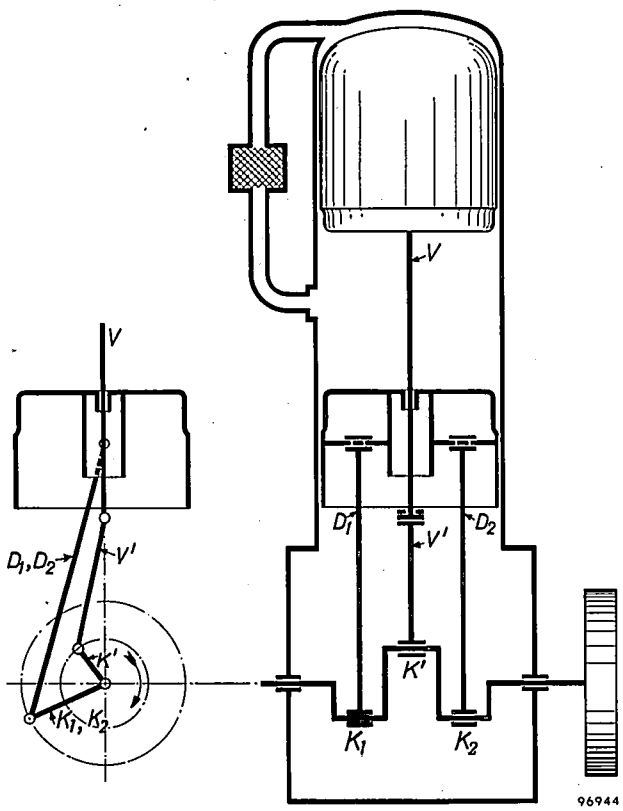

Fig. 8. Drive mechanism used in the gas refrigerating machine. The piston has two parallel con-rods D_1 and D_2 which link it to cranks K_1 and K_2; between the latter is a third crank K', which con-rod V' links to the displacer-piston rod V.

We alluded in the introduction to the drawback of mechanisms such as those of figs. 7 and 8, especially for large engines: the crankcase has to be filled with the working gas under high pressure. This is necessary for two reasons: first, to limit the leakage of gas past the piston; second, to preclude unnecessarily large downward forces on the drive mechanism. In the absence of any compensating pressure (buffer pressure) in the crankcase there is a difference of pressure across the piston fluctuating between p_{min} and p_{max}, the minimum and maximum pressures occurring within the cylinder during the cycle. Introducing a buffer pressure of value p_{min}, for example, reduces the maximum pressure difference across the piston to $p_{max} - p_{min}$.

It is clear that with such a pressurized crankcase considerable weight penalties are involved. Particularly troublesome in large engines, this drawback becomes even more of an embarrassment if it is

desired to operate at very high pressures in order to increase the specific power in the way explained above.

The new drive mechanism (rhombic drive)

The above-mentioned drawbacks do not arise in the new drive, which we now propose to describe. Briefly, it comprises twin cranks and con-rod mechanisms, identical in design and offset from the central axis of the engine; the cranks rotate in opposite senses and are coupled by two gearwheels.

Fig. 9 is a schematic diagram of the system. Fixed to the power piston *1* by way of piston rod *2* is a yoke *3*. One end of the yoke is linked by con-rod *4* to crank *5*, the other end by con-rod *4'* to crank *5'*. The displacer piston is actuated by a precisely similar arrangement: the displacer-piston rod *7*, which passes through the hollow rod *2*, has fixed to it a yoke *8* which is linked to cranks *5* and *5'* by con-rods *9* and *9'* respectively. If *9* and *9'* are given the same length as *4* and *4'*, the two pairs of con-rods will form a rhombus, only the angles of which vary

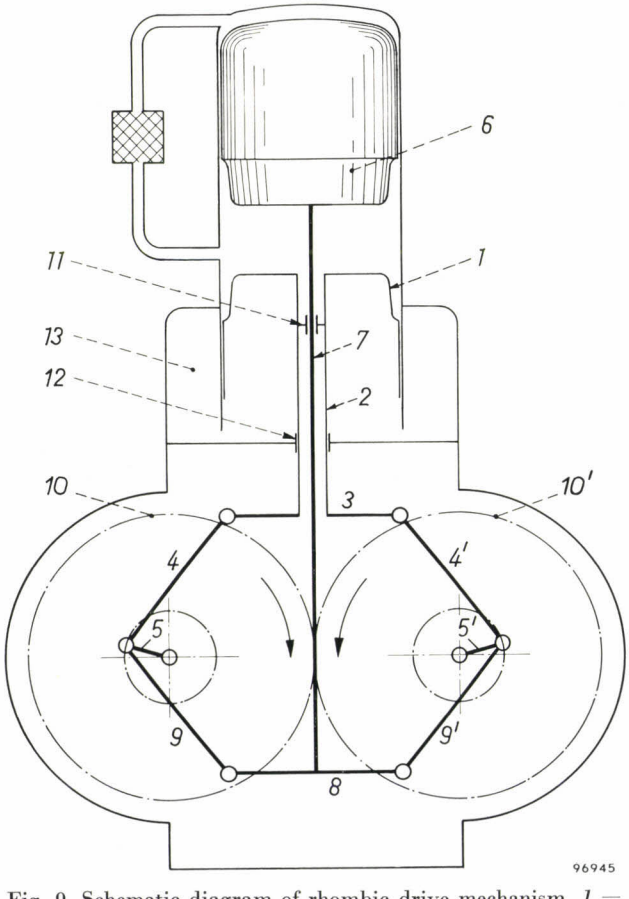

Fig. 9. Schematic diagram of rhombic drive mechanism. *1* = power piston. *6* = displacer piston. *5-5'* = cranks in two shafts rotating in opposite senses and coupled by gears *10-10'*. *4-4'* = con-rods pivoted from ends of yoke *3* fixed to the hollow power-piston rod *2*. *9-9'* = con-rods pivoted from ends of yoke *8* fixed to displacer-piston rod, which runs through the hollow power-piston rod. *11* and *12* = gas-tight stuffing-boxes. *13* = buffer space containing gas at high buffer pressure.

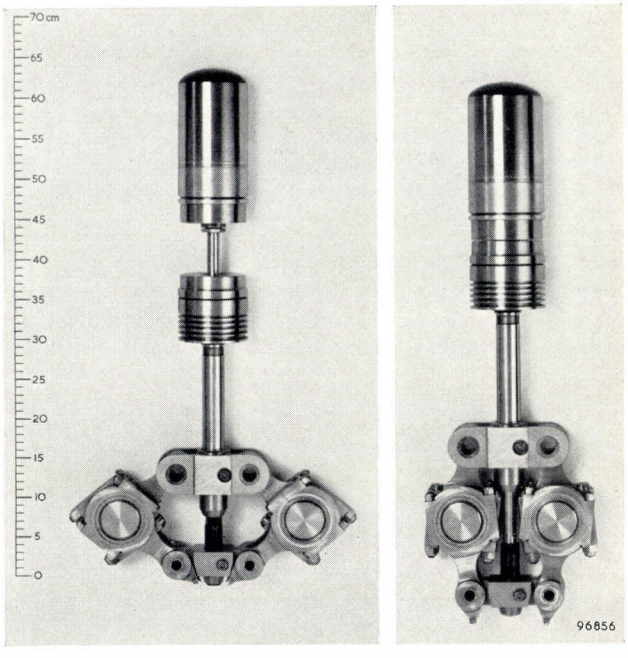

Fig. 10. Model of an actual rhombic drive mechanism, in two positions (cranks and gearwheels not present in this model).

when the system is in motion; it is for that reason that we have adopted the name "rhombic drive". Gearwheels *10-10'* ensure exact symmetry of the system at all times. The two crankshafts being geared together, the entire shaft output can be taken off either.

Fig. 10 shows a practical form of such a crank mechanism. The motion is illustrated by photographing the mechanism in two different positions (the cranks and the gearwheels are absent in this model).

The symmetry of the system and the coaxial arrangement of power-piston and displacer-piston rods make it an easy matter to avoid putting the crankcase under high pressure. The stuffing-box *11* for the displacer-piston rod is inside the hollow power-piston rod. One more seal, namely the stuffing-box round the power-piston rod (*12* in fig. 9), is all that is necessary to form a comparatively small cylindrical chamber *13* under the piston, separate from the crankcase; this "buffer space" can be filled with gas at the desired buffer pressure. The success of this arrangement depends essentially on the fact that the power-piston rod stuffing-box is subject to no lateral thrust, as *the horizontal components of the forces exerted by each pair of con-rods are exactly balanced at each yoke.* (That they do so, and that frictional losses are low in consequence, has the further advantage of enhancing the mechanical efficiency of the system.) The minimum permissible volume of the buffer space is determined

only by the range within which it is desired to limit the pressure variations inside the chamber. In a multi-cylinder engine the buffer chambers can be interconnected; this allows the volume of the individual spaces to be made even smaller.

In principle a space of this kind can be walled off under the piston in engines embodying the crank systems shown in figs. 7 and 8, but it is then necessary to have the rods running in a crosshead guide in order to prevent their gas-tight stuffing-boxes being acted upon by the horizontal components of the connecting-rod forces. This leads to considerable structural complications.

The power piston and displacer movements resulting from the new drive are displayed graphically in *fig. 11*, in the same way as in figs. 3 and 5. It will be seen that if the direction of rotation is as indicated in fig. 9, the volume variation of the hot space

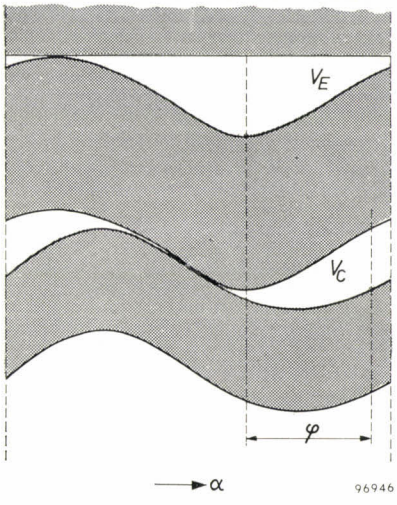

Fig. 11. Curves similar to those in figs. 3 and 5, showing the displacements undergone by the power and displacer pistons in a rhombic drive system such as that of fig. 9.

will have a phase lead with respect to that of the cold space, as is required. The power and displacer pistons do not by any means move in simple harmonic motion, but it is found that a very good version of the Stirling cycle is obtainable. This might seem surprising, for on the face of it the use of the rhombic drive may appear to have restricted the freedom of choice with regard to parameters w and φ (the amplitude ratio and relative phase of the variations in volumes V_E and V_C — see above), which play a large part in the design of a hot-gas engine. However, more exact analysis of the new drive shows that it is in fact possible, by altering the offset of the crankshafts, the proportions of cranks and con-rods and the ratio of power and displacer piston diameters, to vary these parameters over quite a wide range.

The balancing of the drive mechanism

The rhombic drive has the important property of allowing the designer of an engine even with only *one* cylinder to obtain complete dynamic balancing of the forces due to the inertia of moving parts, and of the moments of these forces — "complete" in the sense that the fundamentals *and* all the higher harmonics are balanced. We shall demonstrate this for the simple case where the con-rods are of equal length (as in fig. 9).

The configuration is given in *fig. 12*. On grounds of symmetry it is clear that the sum of all inertial forces acting horizontally is zero at any given instant. The same applies to all inertial-force moments about an axis perpendicular to the plane of the drawing. Hence all we need consider are the inertial forces acting in the vertical direction. We begin by resolving the circular motion of each crankpin T-T' into a vertical and a horizontal component. The vertical movements that the power and displacer pistons make as a result of the *horizontal* movement of the crankpins are equal and opposite because the con-rods are of equal length (symmetrical deformation of the "rhombus"). Hence, if the masses of the two pistons (including the rods etc. attached thereto) are made equal:

$$m_Z = m_V, \quad \ldots\ldots \quad (10)$$

the sum of the vertical inertial forces corresponding to horizontal crankpin movement is always zero. There remain the vertical movements of power and displacer pistons as a result of the *vertical* component of the crankpin movement. These movements are exactly equal and, moreover, identical with the vertical movement of the crankpins. One can therefore imagine the moving mass of the two pistons,

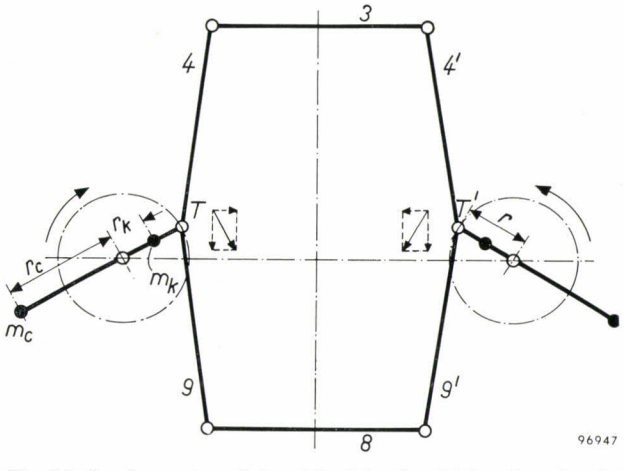

Fig. 12. Configuration of rhombic drive in which yokes *3* and *8* are of equal length, and all four con-rods *4-4'* and *9-9'* are equal. For discussing the inertial forces, the circular motion of crankpins T-T' can be resolved into vertical and horizontal components.

$m_z + m_v$, as localized in the crankpins, $\frac{1}{2}(m_z + m_v)$ in each. By means of two counterweights m_c mounted opposite each crankpin at a suitable radius r_c, vertical inertial forces can be created which exactly balance those of $(m_z + m_v)$ — and this is true even if the rotation of the crankshafts is not exactly uniform.

In fact, the mass and offset of each counterweight are chosen such that the latter also serves to balance the crank and other eccentrically positioned moving parts. If m_k is the effective mass of all these parts, and r_k the distance of their centre of gravity from the crankshaft axis, we have the following condition for balancing:

$$r_c m_c = \tfrac{1}{2} r (m_z + m_v) + r_k m_k . \quad . \quad . \quad (11)$$

From the foregoing it will be clear that the reason why it is possible in this way to balance the inertial forces in a displacer type of engine is that, even for single-cylinder machines, there are *two* reciprocating masses whose movements differ in phase [8]). In order to satisfy the condition $m_z = m_v$ it will generally be necessary to make the masses of the two pistons themselves different. This should not involve any difficulty, for the two bodies have different shapes and different functions and are not interchangeable.

The configuration of fig. 12 is a special case of a much more general form of the new drive. We obtain the more general form by abandoning the restriction that the pairs of connecting rods are equal in length, and by allowing each displacer-piston con-rod to hinge not on the crankpin but about any arbitrary fixed point on the power-piston con-rod (see *fig. 13*). In this general form, which design considerations may render more attractive than the special one of figs. 9 and 11, the power and displacer piston rods continue to move coaxially without the presence of any lateral thrust. This means that the expedient of the buffer chamber with gas under pressure can again be applied without complications. Moreover — and perhaps surprisingly — it can be shown that the inertial forces of the moving parts of the general form of this drive mechanism can be completely balanced as before, provided certain straightforward conditions are fulfilled. We shall state these conditions here without proof. For balancing to be possible the parameters of the mechanism as indicated in fig. 13 must satisfy the equations:

$$\left.\begin{aligned} \Delta e &= 0 , \\ c &= \sqrt{1 - 2\frac{a}{l}\cos\beta + \left(\frac{a}{l}\right)^2} , \\ m_1 - m_4 &+ \frac{a}{l}(m_3 + 2m_4)\cos\beta = 0 . \end{aligned}\right\} \quad . \quad . \quad . \quad (12)$$

The net inertial force can then be completely balanced by fitting counterweights whose positions and masses are given by

$$\gamma = \pi - \tan^{-1} \frac{\frac{a}{l}(m_3 + 2m_4)\sin\beta}{m_1 + m_2 + m_3 + m_4 + \frac{r_k}{r} m_5}$$

and

$$m_6 = \frac{r}{r_c} \sqrt{\left(m_1 + m_2 + m_3 + m_4 + \frac{r_k}{r} m_5\right)^2 + \left\{\frac{a}{l}\left(m_3 + 2m_4\right)\sin\beta\right\}^2} \quad . \quad . \quad . \quad (13)$$

respectively. It will be seen that when a is zero, as it is in the special case first discussed, these conditions transform into the simple ones given earlier.

The particular version of the hot-gas engine with which we shall concern ourselves in this article has the simple form of crank mechanism shown in fig. 9.

In addition to inertia forces, an *alternating moment* acts on the foundation of every piston engine when under load as a consequence of the periodic variation of the torque produced on the shaft. With the rhombic drive mechanism (either the special or the general form) a relatively simple expedient makes it possible to balance out a large part of this alternating moment. It is only necessary to fit two flywheels instead of the usual one, one on each of the two oppositely-rotating crankshafts.

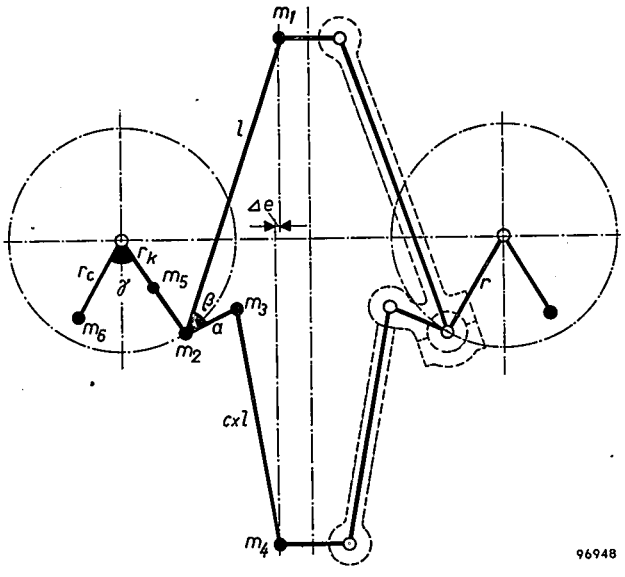

Fig. 13. General form of the new drive. $m_1 \ldots m_6$ are the masses of the moving parts, imagined localized at various points for the purpose of deriving the conditions for the balancing of inertial forces and moments.

Further constructional details of the engine

The general appearance and layout of the experimental engine may be seen in *fig. 14*. *Fig. 15* is a cross-sectional sketch, burner and pre-heater not being shown; for the sake of clarity some of the parts have not been drawn exactly to scale. The notation of the drive mechanism is the same as in preceding diagrams; the counterweights are also shown (*14*).

[8]) It is clear that the rhombic drive could also be used for attaining complete dynamic balancing in internal-combustion engines, but it would probably be a proposition only in engines with at least two cylinders, i.e. in which at least two pistons are in reciprocating motion.

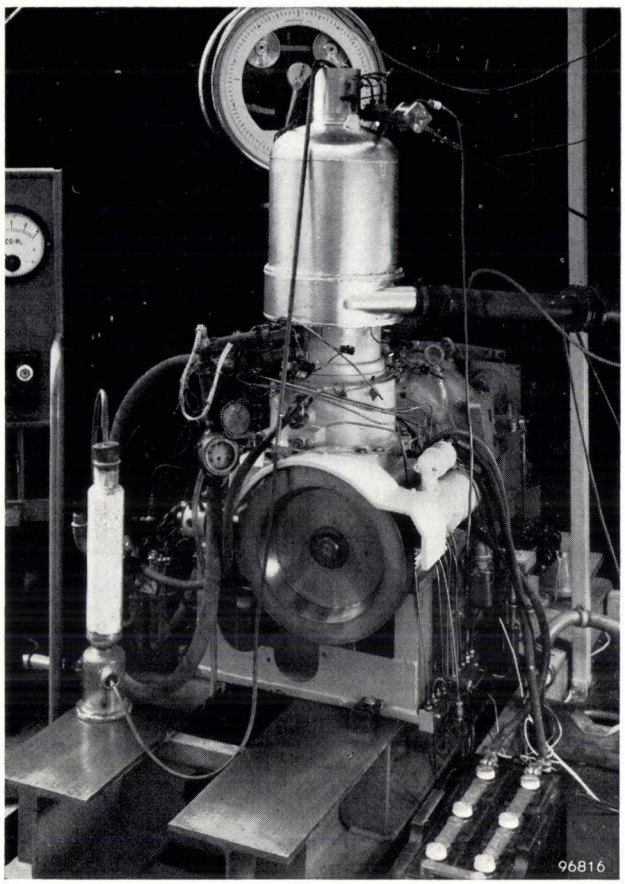

Fig. 14. Experimental model of the Philips hot-gas engine with rhombic drive, in position on the test bench.

As in previous designs described in this Review[3]), the cooler, regenerator and heater all have an annular configuration, and are mounted around the expansion-compression cylinder. This arrangement makes for compactness, and low gas-flow losses. The displacer piston consists of the piston base *6a* and a thermally insulating dome *6b*. The piston base fits like an ordinary piston into the cylinder *16* at the level of the cooler. There is a small clearance between the dome *6b* and the cylinder wall *15* of the hot space, just sufficient that the two never come into contact. Underneath the power piston the buffer chamber *13* can be seen.

The design of the *regenerating casing* has undergone a good deal of modification. In the first version of the experimental engine the regenerator casing was a comparatively flat annular body (*fig. 16*); the cylinder wall *15* formed the inner wall, the outer wall *a* being joined to the cylinder via perforated flange *b*. Considerable stresses were set up in the walls of the casing owing to expansion of the upper side as its temperature rises to the high value T_E, the lower side remaining at the low temperature T_C. Efforts to step up the output of the hot-gas engine were soon brought to a halt by the thermal stresses arising in this way, these becoming excessive especially as the working pressure of the engine was raised. The difficulty has been avoided by dividing up the annular regenerator space into a number of

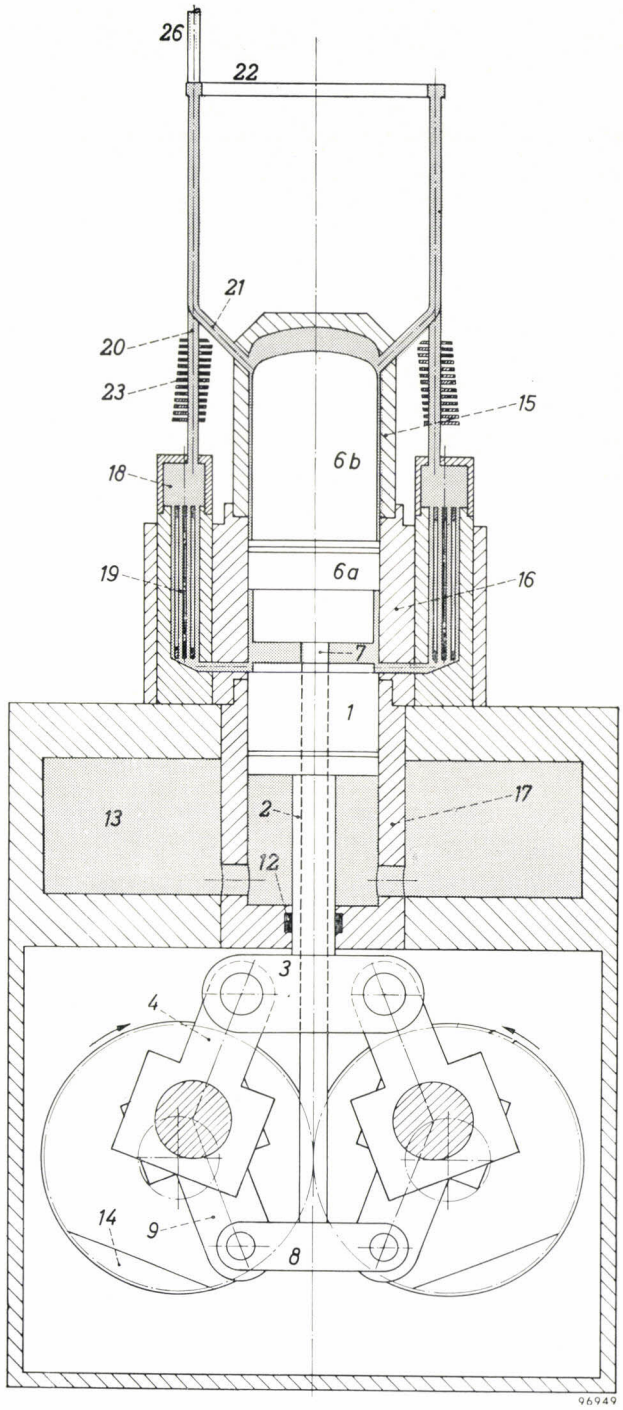

Fig. 15. Cross-section of the engine shown in fig. 14, much simplified and, for the sake of clarity, not entirely drawn to scale. The burner and air pre-heater are absent; they are shown separately in fig. 18. Spaces filled with hydrogen are shaded. *1* = power piston. *6a* and *6b* = displacer piston and insulating dome. *12* = power-piston stuffing-box. *13* = buffer chamber. *14* = counterweights. *15*, *16*, *17* = cylinder in which power piston and displacer piston move. *18* = regenerator compartment. *19* = cooler compartment, *20*, *21*, *22* = heater tubes. *23* = fins. *26* = tube for temperature probe. Other symbols as in fig. 9.

small chambers ("cups") not contiguous with the cylinder wall; see *fig. 17*. Thermal stresses in the regenerator wall then ceased to be a problem. Furthermore, it was now possible to ensure that the lines of principle stress ran substantially straight from the head of the cylinder *15* via the cylinder

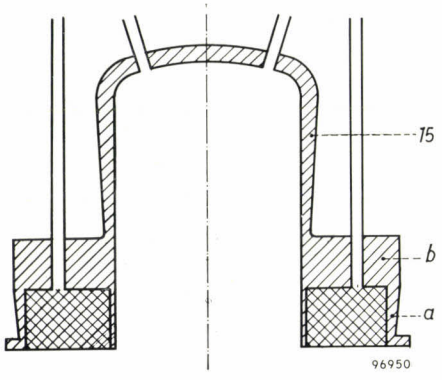

Fig. 16. Earlier design of regenerator compartment, with cylindrical outer wall *a* attached to cylinder wall *15* by means of perforated flange *b*.

wall *16*, *17* to the base of the latter cylinder (see fig. 15). In earlier designs embodying the flange mentioned above, these lines tended to curve outwards, which meant that the flange had to withstand a strong bending moment. The new design allows the whole assembly to be kept comparatively light despite the high maximum pressure of the gas.

The design of the cooler has been adapted to that of the regenerator. The cooler housing *19* contains a number of tubes bunched together in groups (cooler "units"), the end of each unit protruding into one of the regenerator cups. The tubes of each cooler unit are mounted with a *sliding fit* in the cooler housing; in this way the regenerator cups are left free to undergo small longitudinal displacements consequent on the expansion of the heater tubes.

The heater consists of two sets of pipes, *20* and *21*, in close-packed configuration but with small clearances. The hot gases from the burner are blown between these tubes in a direction perpendicular to their length. The tubes of set *20* terminate inside the regenerator cups (see figs. 15 and 17); gas from the regenerator streams upward through these tubes into the annulus *22*, whence it is carried downwards by the tubes of set *21*, which are brazed into the hot end *15* of the cylinder. To improve the heat transfer between the combustion gases and the working gas, a series of fins *23* are brazed to the pipes of set *20*.

The heater is surrounded by the air *pre-heater* (*27* in *fig. 18a*), which functions in the following way. The air necessary for combustion enters the

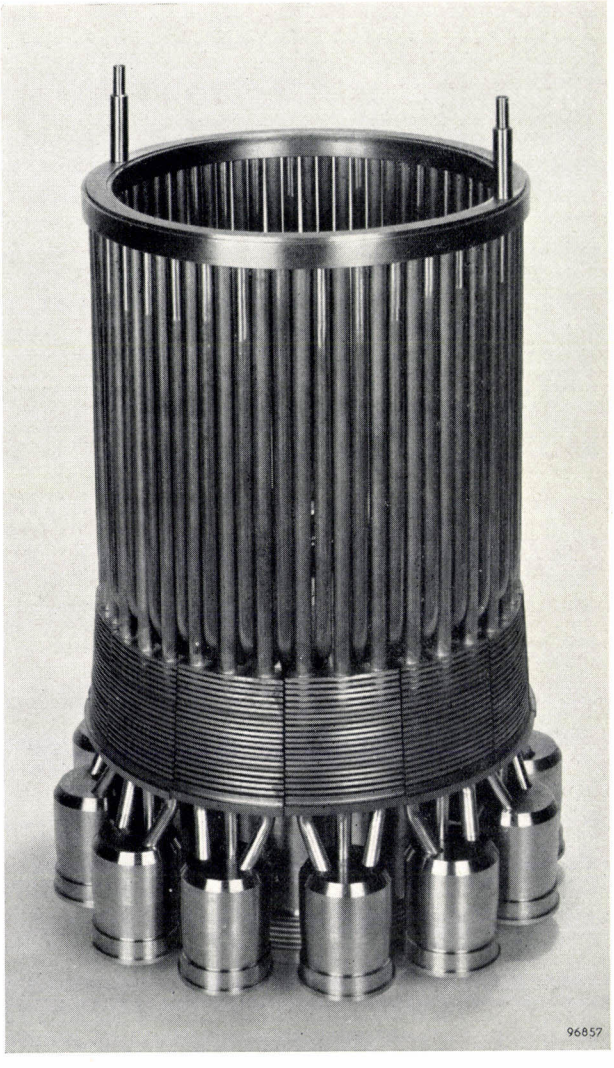

Fig. 17. New design of regenerator compartment and heater. The regenerator (below) is now split up into a series of cups surrounding but not touching the displacer cylinder. The new design solved the thermal-stress problem. It will be seen that three tubes issue from each regenerator cup, their extensions forming the vertical heater tubes that carry the upward-streaming gas. Alternating with these, and connected to them via the annulus at the top, are downward-flow tubes that lead to the head of the cylinder. The lower part of this tube system is fitted with fins in order to improve the heat transfer from the combustion gases to the tubes.

lower end of channels A_1 situated around the outer perimeter of the air pre-heater (fig. 18*b*) and then flows via the spaces A between the spirally curved partitions into the channels A_2 around the inner perimeter and thence, upwards, to the burner. The exhaust gases, which leave the burner with a temperature somewhat higher than that of the heater, enter channels B_1 around the inner perimeter and flow via B, a second set of spiral spaces lying between the A spaces, in a direction opposite to that of the incoming air, to the channels B_2 around the outer perimeter of the air pre-heater. It has proved pos-

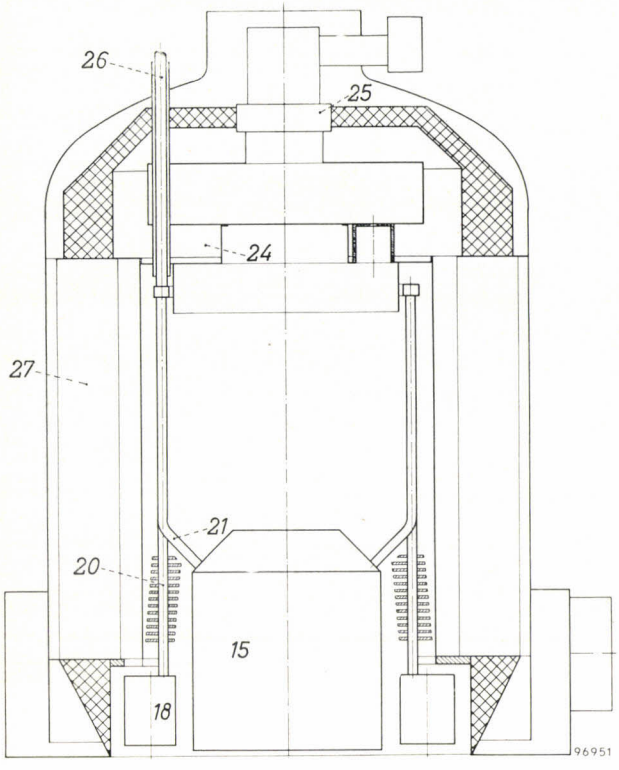

a

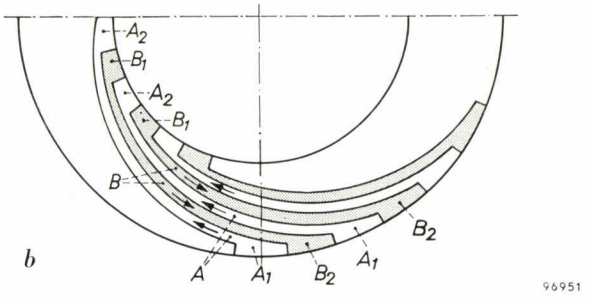

b

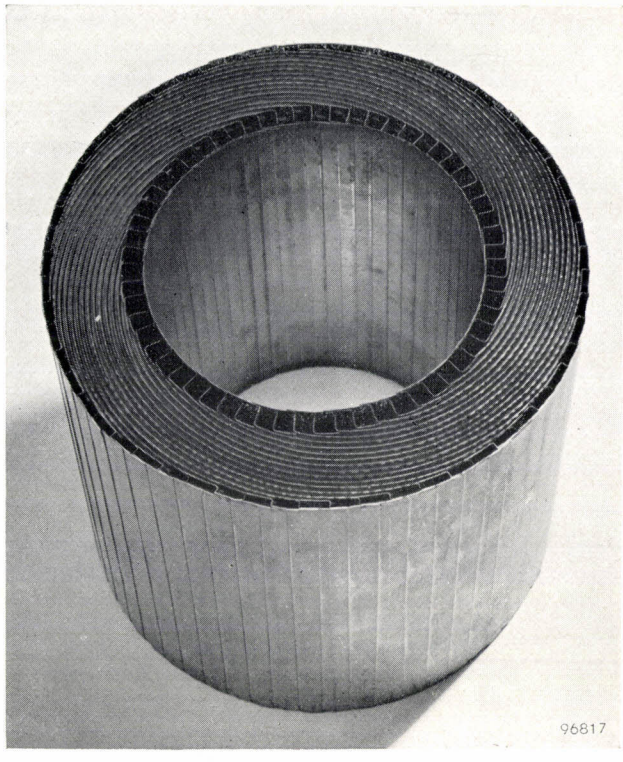

c

Fig. 18. *a*) Cylinder head of engine, surmounted by burner *24*, atomizer *25* and surrounded by air pre-heater *27*. Other symbols as in fig. 15.
b) Cross-section through air pre-heater, showing the narrow A and B spaces which lie between the spirally curved partitions and through which pass, in opposite directions, fresh air for and spent gases from the burner. The air enters via the lower end of the channels A_1 and leaves via the upper end of A_2, both sets of channels running parallel to the cylinder axis. Similarly the burnt gases enter via the lower end of channels B_1 and leave via the upper end of channels B_2, likewise parallel to the cylinder axis.
c) View of air pre-heater, which fits over the heater shown in fig. 17.

sible on this principle to build a very compact pre-heater (fig. 18*c*) with low resistance to air flow. Moreover, the pre-heater "insulates itself"; all the channels around its outer perimeter (A_1 and B_2) are near the ambient temperature.

The *burner* (*24* in fig. 18*a*) is of the "swirl-chamber" type, which can be used in conjunction with a large number of fuels possessing widely differing properties, such as coal gas, propane, butane, kerosene, diesel oil and light fuel oil. If liquid fuels are to be used, the burner is fitted with an atomizer *25*, which sends a fine spray of the liquid into the upper part of the burner.

Regulation of engine output

It will be seen from formula (7) that the power output of the hot-gas engine can be controlled very conveniently by altering $\bar{p}$, the mean pressure of the working gas; changing $\bar{p}$ has no effect on the thermal efficiency (eq. 8) of the engine, provided the cooler and heater temperatures remain unaltered. To fulfil this proviso a separate automatic regulator is required. (The overall efficiency is in fact somewhat affected by a pressure change because, in addition to the effect mentioned under [7]), the absolute magnitude of some — less important — losses remains practically constant; the effect can be deduced from fig. 21 below.)

Accordingly, the control system of the hot-gas engine falls into two parts:

1) A system for admitting gas to and withdrawing it from the engine in order to adjust the pressure to give the output required (i.e. the braking torque), while maintaining the (pre-set) speed of the engine constant.
2) A system for controlling the fuel supply to the burner in such a way that the temperature of the heater remains steady when the power output (and hence the rate at which heat has to be

supplied) is changed. For this purpose, control action is exercised by a thermostat, the temperature-sensitive element of which is inserted, for example, in the stream of gas through one of the heater pipes (through tube *26* in fig. 15; in the heater of fig. 17 two such tubes are incorporated).

The control system for regulating the pressure will be discussed here.

Regulation of the pressure in the engine described here is effected by a set of hydraulically operated valves. A diagram of the system is given in *fig. 19*. The governor *1*, which is driven by the engine shaft, ensures that, at the nominal speed to which the governor causes the oil pressure in pipes *2* and *3* to drop, with the result that valve *9* of the regulator *10* opens up, whereby allowing gas from the cylinder to flow via non-return valve *11* to the inlet of a small auxiliary compressor *12*, whence it passes into the tank *6*. The release of gas from the engine continues until the nominal speed is attained (whereupon valve *9* closes).

As stated above, the buffer space *13* under the piston (see also fig. 15) is filled with gas at a buffer pressure; this pressure must also undergo adjustment in accordance with changes in the load. The engine under discussion has been designed for a buffer pres-

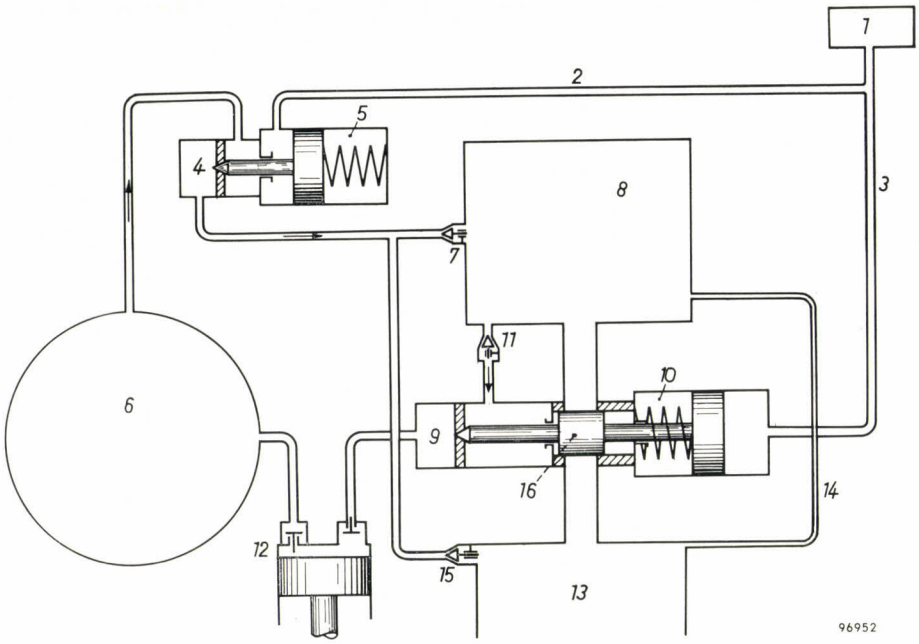

Fig. 19. Hydraulic mechanism for regulating the output of the hot-gas engine. By altering the oil pressure in pipes *2* and *3*, governor *1* controls the operation of valves *4* and *9*. If the engine speed falls below the pre-set value, gas from the tank *6* flows via valves *4* and *7* into the cylinder *8*; if the speed setting is exceeded, gas passes from *8* via valves *11* and *9* and compressor *12* back to *6*. The function of the slide throttle *16*, which connects the cylinder with the buffer space *13*, is to ensure a rapid response when the load is reduced suddenly.

engine has been adjusted to run, a certain oil pressure is maintained in pipes *2* and *3*. If the engine slows down slightly in consequence of an increase in the braking torque, the governor raises the oil pressure in those pipes, with the result that valve *4* in the feed device *5* opens up, and gas from tank *6* passes via feed valve *7* into the space *8* which represents the cylinder of the hot-gas engine. Pressure inside the engine having risen accordingly, its power output increases. The injection of additional gas continues until the engine speed has reverted to the original setting (whereupon valve *4* closes). If the speed increases slightly in consequence of a decrease in the braking torque, the sure equal to $\bar{p}$, the mean pressure in the cylinder. In principle this buffer pressure is obtained automatically, by means of a capillary tube connecting the buffer space with the cylinder. We shall return presently to other provisions made for this purpose.

The auxiliary compressor gives a gas-tank pressure rather higher than the minimum pressure in the cylinder under conditions of full load. For increasing the engine output, therefore, it is possible to inject additional gas via valve *7* until the full power is developed. This adjustment takes place very rapidly. When it is a question of reducing the output, for example from full power, the auxiliary compressor initially performs no function

because gas from the cylinder returns to the tank via valves *11* and *9* under the excess pressure in the cylinder; this continues until the maximum pressure in the cylinder has dropped to the tank-pressure value. This too happens very quickly. If, however, the cylinder pressure is to be lowered still further, then the auxiliary compressor must function, and thereafter it is this that determines the speed of response. If a *sudden* decrease in the load (e.g. sudden removal of the whole braking torque) is not to result in racing of the engine, the compressor required would have to be very large. This difficulty has been overcome by incorporating an additional regulating mechanism. Besides opening and closing valve *9*, regulator *10* actuates a slide throttle *16* which offers the gas a direct path between cylinder and buffer chamber; the escape of gas will be large or small in accordance with the magnitude of the change in the load. It is clear that this gas escape path is equivalent to a leak past the power piston: it causes a certain decrease of the useful power delivered by the engine (which is now indeed associated with a decrease in efficiency; whence the term "loss-regulation", coined for this control). Because the action of the slide throttle has an almost instantaneous effect, a very small auxiliary compressor is adequate [9]).

In consequence of the direct connection between cylinder and buffer space when the power of the engine is being reduced, the buffer pressure likewise adjusts itself almost immediately to the correct value. This quick readjustment is highly desirable, since it limits unnecessary asymmetrical thrust on the drive mechanism. A similar purpose is served by valve *15*. It prevents the buffer pressure lagging too much when output is suddenly *raised* to a much higher value: if the value from which it is raised is so low that the mean pressure in the cylinder is less than the tank pressure, gas from the tank will pass directly into the buffer chamber via valves *4* and *15*.

Engine data and test results

We now give the more important data relating to a single-cylinder hot-gas engine designed and built in Philips Research Laboratories, Eindhoven, along the lines described above.

Cylinder bore	88 mm
Power-piston stroke	60 mm
Nominal engine speed	1500 r.p.m.
Mean piston velocity at 1500 r.p.m.	3 m/sec
Highest permissible value of p_{max}	140 kg/cm² (~140 atm)
Mean pressure $\bar{p}$ corresponding to the above value of p_{max}	105 kg/cm² (~105 atm)
Compression ratio p_{max}/p_{min}	2.0
Nominal cooling-water temperature	15 °C (~60 °F)
Nominal heater temperature	700 °C (~1290 °F)
Working fluid	Hydrogen
Fuel	Light fuel oil

We have already alluded to the advantages of hydrogen as the working fluid; the flow losses are relatively small and good heat transfer is attainable, the efficiency being thereby greatly enhanced. In addition, the speed of response of the engine to changes in the load or controls, which is ultimately determined by the effective cross-sectional areas of ducts and valves in the regulating system, is improved by using a low-density gas.

The results of measurements of the brake horsepower and specific fuel consumption of the engine will now be dealt with. The efficiencies derived from these figures relate to the engine without auxiliary devices [10]) and are based on a fuel of calorific value (low heat value) 10000 kcal/kg (≈18000 B.T.U./lb). The measurements were made at four different pressure levels corresponding to p_{max} values of 50, 80, 110 and 140 kg/cm², and at six different engine speeds for each of these pressure levels, namely at 250, 500, 1000, 1500, 2000 and 2500 r.p.m. *Fig. 20* is a general view of the equipment used for the measurements. In *fig. 21* the measured power and overall efficiency are plotted as functions of the engine speed in r.p.m. It will be noted that a power of up to 40 H.P. can be developed and that the overall efficiency has a maximum value of 38%. In addition, the measured torque is plotted

[9]) In a multi-cylinder engine we arrange for the leakage to take place in a rather different manner: the slide throttle opens a gas path from one cylinder to the next. This is equally effective because neighbouring cylinders must in any case differ in phase. Thus the one throttle provides instantaneous "loss regulation" for two cylinders.

[10]) Apart from the usual pumps and fans for forced oil feed and cooling, the auxiliaries comprise the regulating compressor already mentioned and a blower for the burner. Of all these the latter absorbs the most power, viz. 1 to 2% of the engine output.

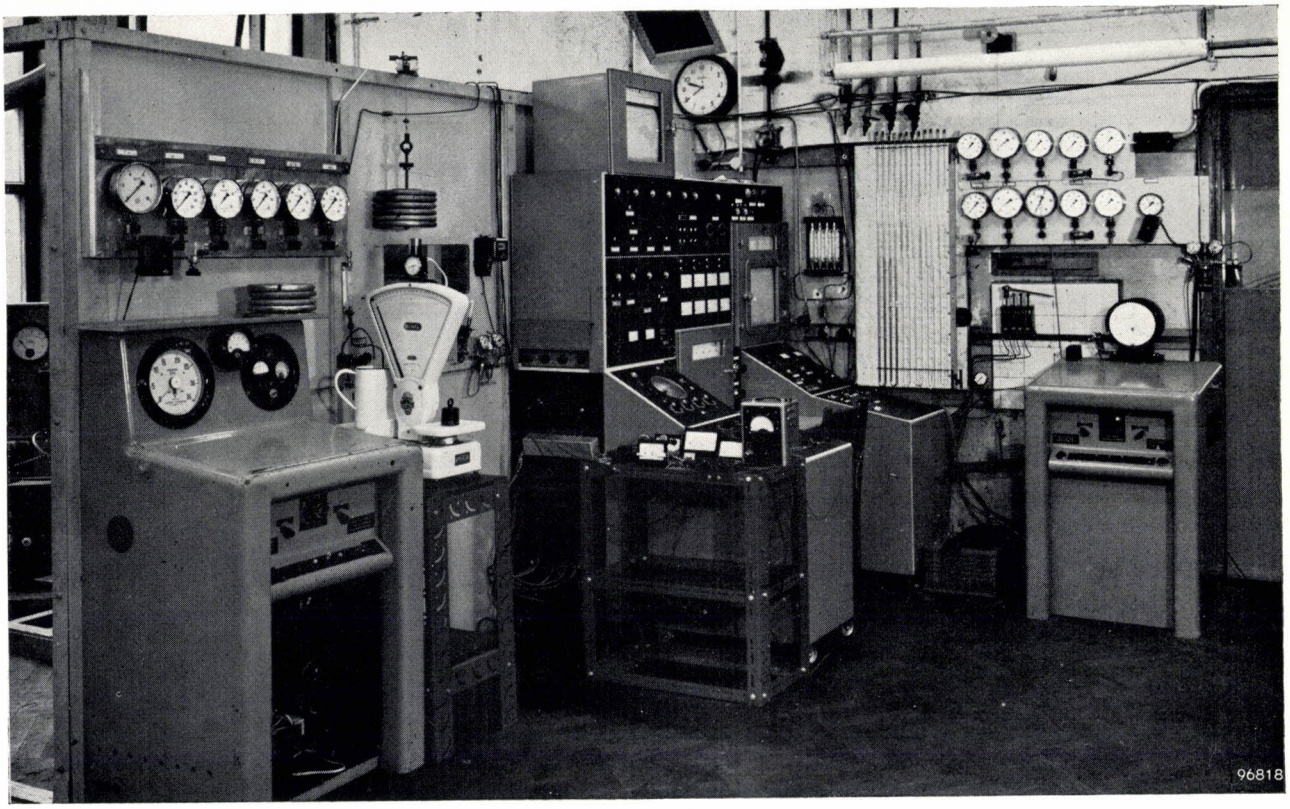

Fig. 20. Equipment used for measuring the torque, shaft power and efficiency of the hot-gas engine under widely differing conditions.

in *fig. 22* for the highest working pressure, for which $p_{max} = 140$ kg/cm². The unusual flexibility of the engine is apparent from the small variation in the torque (11.5 to 15 kg.m or 80 to 110 lb.ft) at greatly different speeds. Equally remarkable is the fact that the overall efficiency varies only slightly over a considerable range of speeds and pressures.

It is the usual practice to display the results of

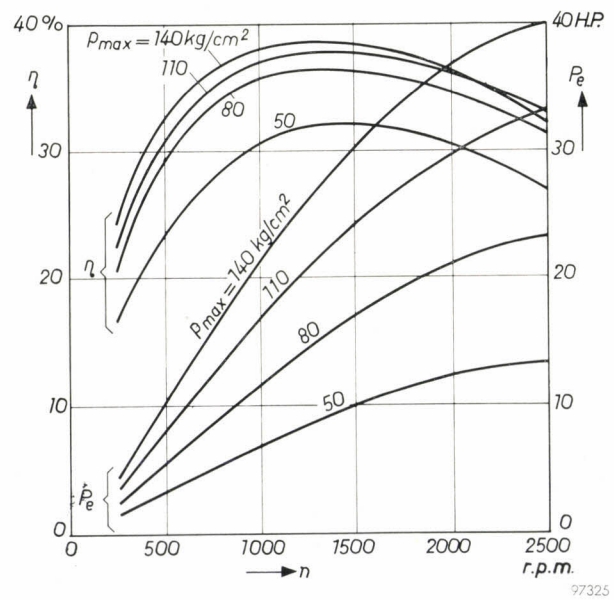

Fig. 21. Measured shaft power P_e and efficiency η of the experimental version of the new Philips hot-gas engine with rhombic drive, plotted as functions of the engine speed for various values of p_{max}.

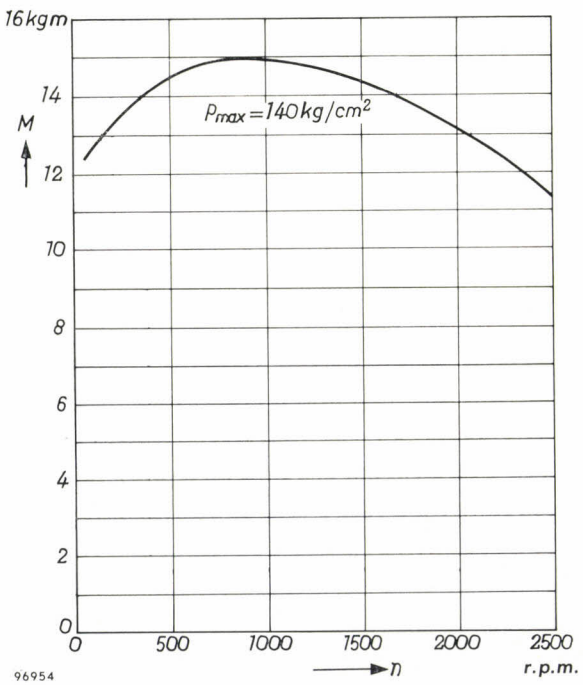

Fig. 22. Measured torque M as a function of the engine speed, for the highest admissible pressure level.

engine tests in a graph such as that of *fig. 23*. Here the coordinates are the engine speed and p_e, the "mean effective pressure" (m.e.p.). This latter is not the mean gas pressure actually occurring in the engine but merely a formal ratio, being defined as the work done by the shaft per revolution divided by the volume swept by the piston; hence the product of p_e and n, the speed in r.p.m., is the specific power output. For a given engine, therefore, every point in the p_e,n diagram corresponds to a definite value of the power developed P_e, and the curves of constant P_e are hyperbolae, in view of the fact that

$$p_e . n \propto P_e . \quad . \quad . \quad . \quad . \quad (14)$$

In such a diagram contours of constant specific fuel consumption (grams of fuel per horsepower-hour, output measured at the shaft) are now drawn.

Fig. 23*a* shows these curves for the experimental engine. The upper boundary to this family of curves, indicated by a broken line, is due to the ceiling on the gas pressure in the cylinder; in the present case the highest permissible pressure is 140 kg/cm², and consequently P_e for a given engine speed cannot exceed the value corresponding to that pressure.

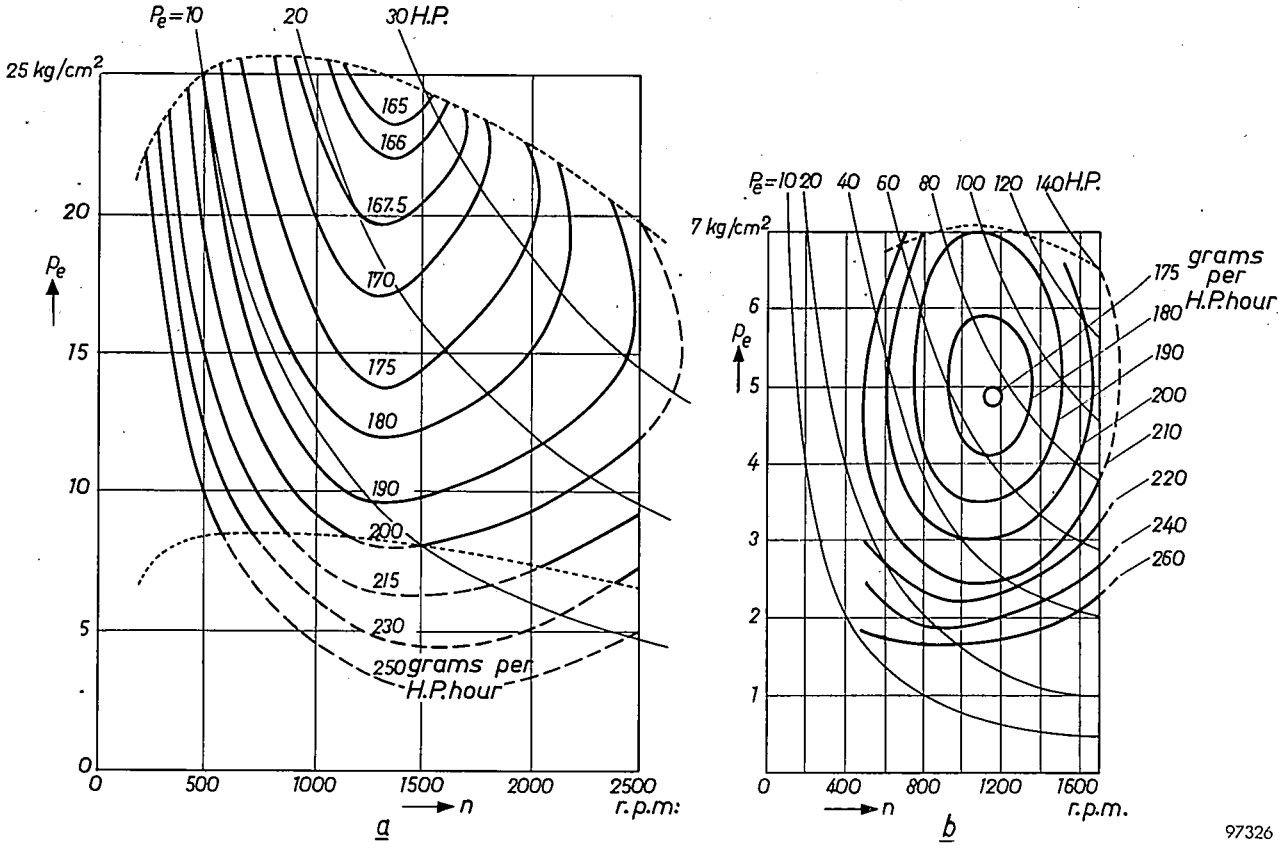

Fig. 23. *a*) Curves of constant specific fuel consumption (in grams of fuel per H.P. hour; for lb per H.P. hour divide by 453) are drawn here in the p_e,n diagram for the hot-gas engine. p_e is the mean effective pressure (m.e.p.) defined as the useful work done by the shaft per revolution divided by the volume swept out by the piston. Accordingly, $p_e . n \propto P_e$, which means that, for a given engine, every point in the diagram corresponds to a definite value of the power P_e and that the curves of constant P_e (lightly drawn in the diagram) are hyperbolae. The broken line representing the upper limit to the measurements corresponds to the pressure ceiling of $p_{max} = 140$ kg/cm² (this curve is derived from the P_e curve for this pressure, given in fig. 21, simply by dividing each ordinate by the corresponding abscissa). The broken line representing the lower limit corresponds to the lowest pressure level at which measurements were made, corresponding to $p_{max} = 50$ kg/cm².
b) p_e,n diagram for a diesel engine (after J. M. Kuijper, Dieselmotoren, Stam, Haarlem 1954, page 81, fig. 52).

(The lower boundary to the curves is not an actual restriction on the engine; it corresponds to the lowest pressure at which measurements were carried out, namely $p_{max} = 50$ kg/cm². The broken-line portions of the curves of constant specific fuel consumption, which lie beneath the lower limit, have been extrapolated.)

The striking thing about the diagram is that the curves do not form complete loops, as they do in the corresponding diagram for a diesel engine, for

example — see fig. 23*b*. This means that the hot-gas engine achieves its highest efficiency at an m.e.p. which lies close to the highest permissible value. This highest permissible value is here not determined by a "smoke-limit" as in a diesel engine, but simply by the strength of the engine casing. In making such a comparison, however, it should be emphasized that *m.e.p. values alone are quite useless* (and so is the specific power output) *as a yardstick for comparing the hot-gas engine with internal-combustion types* from the standpoint of *bulk*. The fundamental differences are too great. A better yardstick is the specific weight, that is, the weight per horsepower.

All the above values were measured with the nominal heater and cooler temperatures given earlier. The effect of changes in these temperatures on output and efficiency may be seen in *figs. 24a* and *b*. The curves given are appropriate to an engine speed of 1500 r.p.m. and a p_{max} of 140 kg/cm².

Finally, *figs. 25a* and *b* are graphs showing the heat balance of the engine plotted as a function of p_e (at $n = 1500$ r.p.m.) and as a function of n (at $p_{max} = 140$ kg/cm²) respectively. The narrowness of the band representing flue losses shows the effectiveness of the air pre-heater: over a large range of n and p_e values the burner has an efficiency of

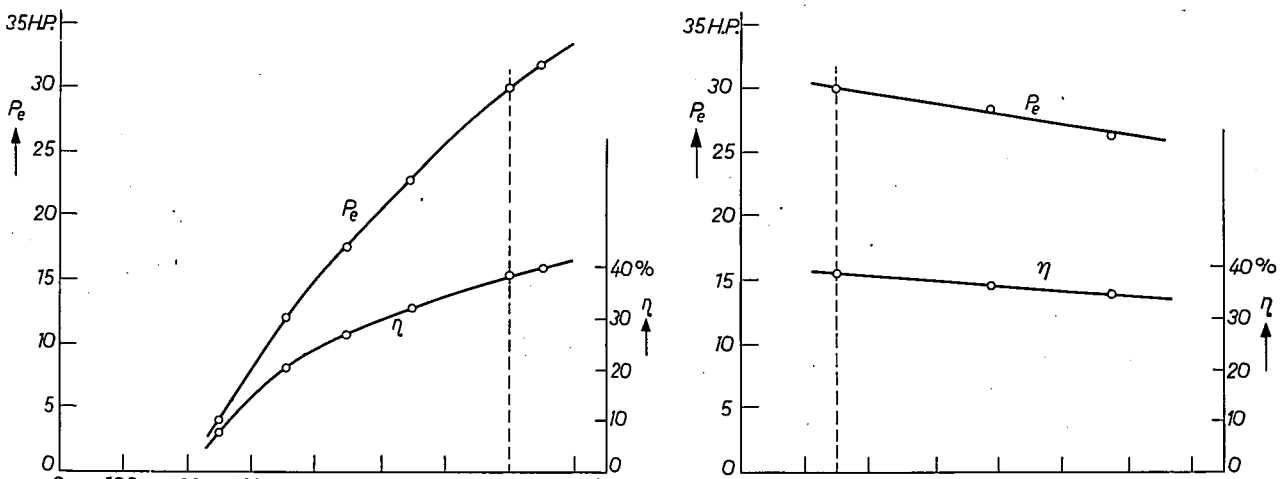

Fig. 24. Shaft power and efficiency of the experimental hot-gas engine as functions of (*a*) the heater temperature and (*b*) the cooler temperature. The curves are those appropriate to an engine speed of 1500 r.p.m. and a p_{max} of 140 kg/cm².

Although few special measures were taken to keep the weight of the present experimental engine low, the specific weight is in fact only 5 kg per H.P. (11 lb per H.P.).

The following are the extreme values found for various quantities.

Maximum shaft output P_e *)	40 H.P.
Maximum mean effective pressure p_e **) . . .	26 kg/cm² (~ 26 atm)
Maximum torque **) .	15 kg.m (~110 lb.ft)
Maximum specific power output*) (H.P. per litre swept volume of piston)	120 H.P./litre
Minimum specific fuel consumption ***) . .	165 grams/H.P.hour (0.36 lb/H.P.hour)

*) Occurs at $n = 2500$ r.p.m. and $p_{max} = 140$ kg/cm².
**) Occurs at $n =$ approx. 800 r.p.m. and $p_{max} = 140$ kg/cm².
***) Occurs at $n =$ approx. 1350 r.p.m. and $p_{max} = 140$ kg/cm².

over 90%. Chief amongst what are shown as "other losses" are those due to mechanical friction. The item may also include losses due to incomplete fuel combustion ("non-detectable" flue losses). One cannot expect these "other losses" to be specified with any great accuracy, but from the good reproducibility of the results, we may reasonably conclude that the mechanical efficiency of this rhombic-drive engine is high.

Concluding remarks

To end with, we may recall here the essential features of the hot-gas engine in general (cf. [2])):

a) Liquid and gaseous fuels of greatly differing properties can be used, little modification of the engine being necessary.

b) Lubricating-oil consumption is low and there is little wear, owing to the absence of corrosive substances and to the relatively low piston velocity.

c) Noise level is very low.

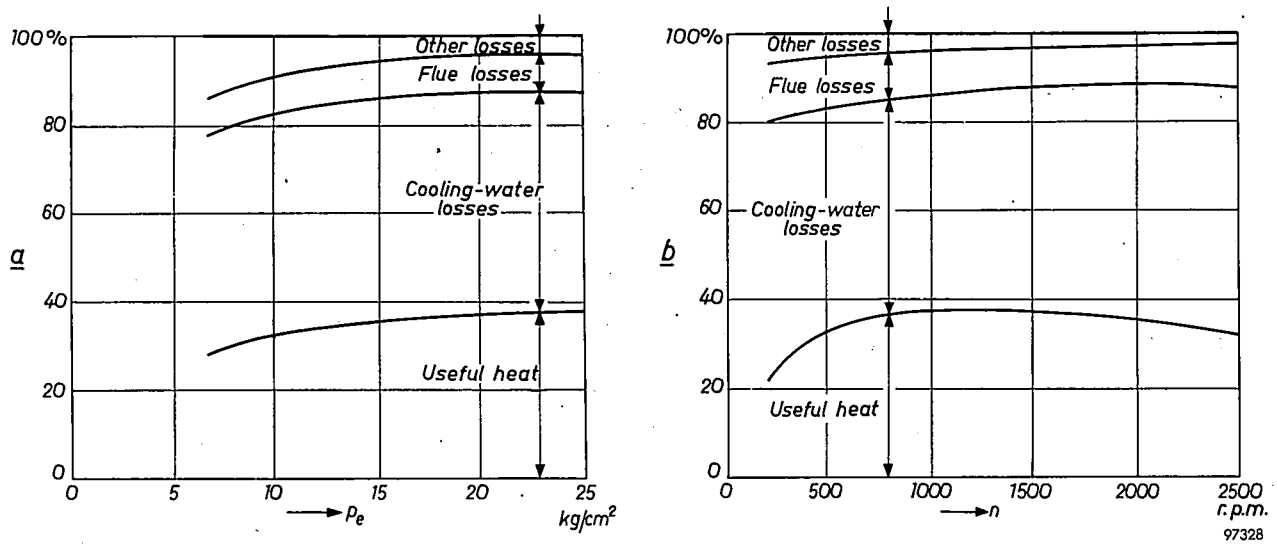

Fig. 25. Heat balance for the experimental hot-gas engine (a) as a function of p_e at n = 1500 r.p.m., and (b) as a function of n at p_{max} = 140 kg/cm².

d) The torque varies only slightly over a large range of engine speeds.

e) The torque variation as a function of the crank angle is relatively small. In this respect a single-cylinder hot-gas engine is comparable with a four-cylinder internal-combustion engine.

In addition to these general features, the experimental engine described here converts heat into mechanical energy with a high efficiency, as the results of our measurements illustrate. Moreover it has been shown that good values of the weight per horsepower are attainable. These favourable qualities are mainly to be attributed to three features of the design: the use of a displacer piston with its attendent aerodynamic and thermodynamic advantages, the use of hydrogen as the working fluid, and the use of high working pressures. A further advantage of the newly developed engine is its freedom from vibration, in consequence of the complete dynamic balancing of the inertial forces of moving parts.

Summary. After a brief recapitulation of the hot-gas cycle as applied to an engine provided with a displacer piston, certain new design features of the Philips hot-gas engine are described. An account is given of a new kind of drive mechanism in which the required power and displacer piston movements are obtained by means of twin crank and con-rod mechanisms offset from the engine axis; the crankshafts are coupled by two gearwheels, and rotate in opposite senses. Where such a system is used, the buffer pressure that is desirable under the power piston can be contained in a relatively small cylindrical buffer chamber — there is no need to pressurize the whole crankcase. The new drive mechanism also permits complete dynamic balancing of the inertial forces of moving parts, even in a single-cylinder engine. Other innovations concern the design of the regenerator compartment, the cooler and the heater: an entirely new approach has cleared up the problem of thermal stress in these components, whose weight can be kept quite low despite the high gas pressure. The pre-heater has also been redesigned, with the result that burner efficiencies of up to 90% are now reached. In addition, a fast-acting system has been developed for regulating the engine output, this being controlled by altering the mean working pressure of the gas in the cylinder.

These various features have been applied in the design and construction of an experimental single-cylinder engine of about 40 H.P., containing hydrogen (helium could also be used) as the working fluid and burning light fuel oil. The highest pressure permissible in the cylinder is 140 kg/cm². The nominal speed of the engine is 1500 r.p.m. Extensive tests on this engine, the results of which are given in the article, show that with the heater temperature at 700 °C it attains an overall efficiency of up to about 38% (engine alone, without auxiliaries). The maximum value of the specific power was found to be 120 H.P. per litre swept volume and the best specific fuel consumption 165 grams (0.36 lb) per H.P. hour. The specific weight of the engine is 5 kg (11 lb) per H.P.

N. V. PHILIPS' GLOEILAMPENFABRIEKEN

SIGNAL-TO-NOISE RATIO AND DEAD TIME OF A SCINTILLATION COUNTER

by J. A. W. van der DOES de BYE.

621.387.464

In a scintillation counter a high ratio between the peak amplitudes of scintillation and noise pulses is obviously desirable. For some applications, moreover, the highest possible counting rate is required. This article discusses the design of the electronic equipment in the light of these considerations and describes how — since the two requirements conflict to a certain extent — a favourable compromise can be achieved in a given case.

In a scintillation counter used for detecting gamma quanta, each absorbed γ-quantum gives rise to an electrical pulse, the height of which may have any value between zero and a certain maximum. A fraction of these pulses will not be passed by the discriminator, the function of which is to transmit only pulses greater than a preset minimum amplitude and so to suppress the majority of the noise pulses. For a given type of scintillator, with given dimensions, this fraction can be smaller the relatively lower is the height of the noise pulses. The ratio between this height and the height of the scintillation pulses can be varied within certain limits by appropriately designing the electronic circuit.

Together with the fluorescence decay constant of the scintillating material, the electronic circuit also governs the minimum value that can reasonably be chosen for the *dead time* of the equipment, i.e. the time during which the counting system cannot react to a new pulse supplied to it. This dead time determines the maximum number of quanta or particles that can be counted per second. In this article we shall examine the influence of the electronic circuit on the two above-mentioned characteristics of a scintillation counter. We shall see that these characteristics cannot be varied entirely independently of each other. The theory shows, however, the means of obtaining, for a given dead time, the most favourable ratio between the amplitudes of scintillation and noise pulses — the *signal-to-noise ratio*. It also shows what sacrifice we must make with regard to the dead time in order to achieve a certain signal-to-noise ratio.

Our calculations will be based on the formulae which describe a scintillation pulse and a noise pulse as a function of time. For deriving the first of these formulae it will be convenient to begin with a brief recapitulation of the way in which the absorption of a γ-quantum in the scintillator gives rise, via the scintillation effect, to the occurrence of a pulse.

Scintillation pulses and noise at the amplifier input

Scintillation pulses

As explained in an earlier article [1]), a γ-quantum incident on the scintillating material gives up its energy E_0 wholly or partly to one or more electrons. These electrons in turn transfer the energy E_1 they have received to other electrons in small portions, giving rise to excitation in the scintillator. Some of the latter electrons in returning to the ground state, cause the emission of light quanta. The light quanta following upon the absorption of one γ-quantum together constitute a scintillation. In a good counter a large fraction of these scintillations can reach the photocathode of the photomultiplier tube. However, by no means all the quanta incident on the photocathode give rise to the emission of a photoelectron capable of entering the dynode system.

It is evident from the above that the average energy E_i which a γ-quantum must transfer to the scintillator in order to cause one useful electron to be emitted by the photocathode is substantially larger than the portions in which the primarily liberated electrons give up their energy. In the most commonly used scintillating material, NaI(Tl), the minimum value of E_i, which we term the *liberating energy*, is about 450 eV, which in this material does not depend on E_1.

Let g be the current gain of the multiplier tube, ε the charge of the electron and t the time, then the form of the current pulse delivered by the tube after the absorption of a γ-quantum, is given by [2]):

[1]) J. A. W. van der Does de Bye, Philips tech. Rev. **20**, 209-219, 1958/59 (No. 8). We shall refer to this article henceforth as I.

[2]) The current and voltage measured at the anode impedance of the multiplier tube will be denoted by i' and V'; the voltage measured at the amplifier output by V.

$$i'(t) = \frac{g\,\varepsilon}{\tau_0}\frac{E_1}{E_i}\,e^{-t/\tau_0}, \quad \ldots\ldots \quad (1)$$

where τ_0 represents the time constant of the decay of the intensity of a scintillation [3]). The fraction E_1/E_i is equal to N, i.e. to the number of electrons liberated from the photocathode that arrive in the dynode system [4]).

This current pulse produces across the anode impedance, consisting of the resistance R_a and the (stray) capacitance C_a in parallel, a voltage pulse of the form:

$$V'(t) = \frac{g\,\varepsilon}{C_a}\frac{E_1}{E_i}\frac{\tau_1}{\tau_0-\tau_1}\left\{e^{-t/\tau_0} - e^{-t/\tau_1}\right\}, \quad \ldots \quad (2)$$

where $\tau_1 = R_aC_a$. The peak value of V', i.e. the pulse height, is:

$$V_m' = \frac{g\,\varepsilon}{C_a}\frac{E_1}{E_i}\left(\frac{\tau_1}{\tau_0}\right)^{\frac{\tau_0}{\tau_0-\tau_1}}. \quad \ldots\ldots \quad (3)$$

This peak value, even with given E_i and g, is evidently not a fixed quantity. An increase in τ_1/τ_0 causes an increase in V_m': for large τ_1/τ_0 the term in τ_0 and τ_1 approaches the value 1, but the pulse duration is then very long, and this is undesirable having regard to the dead time. *Fig. 1* shows the shape of the pulse for various values of τ_1/τ_0. The pulse shapes at the amplifier output are modified by the frequency response of the amplifier connected to the photomultiplier tube. We shall return to this point in the next section.

The noise

The noise, it will be recalled, consists chiefly of pulses arising from the thermionic emission of electrons from the photocathode in the multiplier tube (mono-electronic pulses). They occur at the rate of some thousands to tens of thousands per second. In addition there is a much smaller number of poly-electronic pulses, which are presumably due to the collision of residual-gas ions against the photocathode. These pulses together constitue what is termed the *dark current* of the multiplier tube.

The mono-electronic voltage pulses are of the form:

$$V_r'(t) = \frac{g'\,\varepsilon}{C_a}\,e^{-t/\tau_1}. \quad \ldots\ldots \quad (4)$$

This formula closely resembles that for the scintillation pulses (2), except that it does not, of course, contain τ_0 and that the number of electrons leaving the photocathode per event is here generally equal to unity (for scintillations this number is equal to E_1/E_i; see (2)). The quantity g' is the amplification factor of the multiplier tube, the value of which fluctuates considerably for mono-electronic pulses. The average value of g' is equal to that of the quantity g found in the formulae (1) to (3). The height of the pulse is $g'\varepsilon/C_a$. Owing to the fluctuation of g', this height differs from one pulse to another; the noise shows a relatively broad pulse-height spectrum.

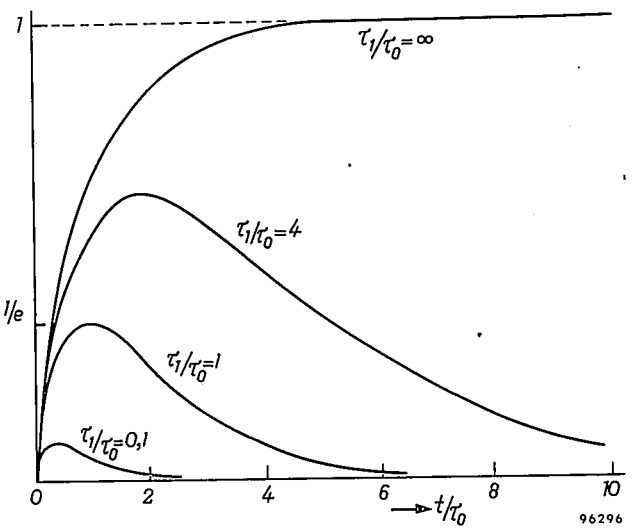

Fig. 1. The shape of scintillation pulses showing their dependence on the ratio between the time constant of the anode circuit of the photomultiplier tube (τ_1) and the decay constant of the scintillation (τ_0). $V'(t)$ (see formula (2)) is plotted on the ordinate (the scale being such that the pulse height is equal to unity for $\tau_1/\tau_0 = \infty$); the abscissa represents the time (in units of τ_0). τ_1/τ_0 must be neither very large nor very small; if it is very large the pulses are too long, while if it is very small difficulties arise which are explained later in this article.

The discriminator level V_{d1} at which, on an average, one noise pulse is passed per second, depends of course on the form of the noise spectrum — which we shall assume to be constant for all cases — and on I_{th}, the number of thermal noise pulses per second [5]). In the formula

$$V_{d1}' = \frac{g\,\varepsilon}{C_a}\,D\,(I_{th}) \quad \ldots\ldots \quad (5)$$

the function $D(I_{th})$ describes the influence which the *form* of the noise spectrum and the *intensity* of the noise exert on V_{d1}'.

[3]) Cf. formula (3) in I. For NaI(Tl) the value of τ_0 is 0.25 μsec.

[4]) The fact that this number differs slightly from pulse to pulse, even with constant E_1, can be disregarded here. The same applies to the fluctuation of g, at least as far as the scintillation pulses are concerned.

[5]) The choice of one noise pulse per second is, of course, somewhat arbitrary. Further details regarding the form of the noise spectrum are given in I and in the appendix to this article.

Scintillation pulses and noise at the amplifier output

If the frequency response of the amplifier were horizontal over the whole frequency range concerned, it would be a simple matter to determine from formulae (3), (4) and (5) the height of the scintillation and noise pulses at the output of the pulse amplifier, as well as the discriminator level at which exactly one noise pulse is counted per second. In that case it would be sufficient merely to multiply these formulae by a constant factor G, the amplification factor. However, in reality the amplifier response is not everywhere horizontal. We shall describe the actual situation by multiplying the factor G by a function φ, which comprises not only the influence of the time constants governing the frequency response of the amplifier but also the effect of τ_1 (the time constant of the anode circuit of the multiplier tube) and τ_0 (the decay constant of the scintillation). This function thus includes all time constants that govern the amplitude of the pulse. The form assumed by φ for scintillation pulses therefore differs from that for noise pulses, since as regards the latter, τ_0 is of no significance: we shall denote the two forms of φ by φ_1 and φ_2 respectively.

Formulae (3) and (5) thus become:

$$V_m = \frac{G g \varepsilon}{C_a} \frac{E_1}{E_i} \varphi_1 \quad . \quad . \quad . \quad . \quad . \quad (6)$$

for the height of the scintillation pulses, and

$$V_{d1} = \frac{G g \varepsilon}{C_a} \varphi_2 D(I_{th}) \quad . \quad . \quad . \quad . \quad (7)$$

for the earlier specified discriminator level.

Let E_{eq} be the value of E_1 at which V_m is equal to V_{d1}. From (6) and (7) we then obtain:

$$E_{eq} = E_i D(I_{th}) \varphi_2/\varphi_1 . \quad . \quad . \quad . \quad . \quad (8)$$

The value of E_{eq} — i.e. the energy of the γ-quanta which, in the case of complete absorption ($E_1 = E_0$), give rise to pulses of a height equal to V_{d1} — is a measure of the signal-to-noise ratio. This ratio is equal to E_0/E_{eq} and hence inversely proportional to E_{eq}.

The effects of E_i, of the thermionic emission and of the time constants on the value of E_{eq} appear separately in eq. (8) [6]). We see that, apart from aiming at low values of E_i and $D(I_{th})$ — as we already know — we must aim at a minimum for φ_2/φ_1.

[6]) The separation of the influences of the dark current and the time constants, as done here, is possible only when the average interval between two pulses (i.e. $1/I_{th}$) is large with respect to the time constants τ_n which determine the pulse duration; in other words, the dimensionless products $I_{th}\tau_n$ must be small. If this is not the case, E_{eq} depends on the values of these products and is larger than follows from eq. (8).

Since the time constants influence not only E_{eq} — and hence the signal-to-noise ratio — but also the dead time of the apparatus, we shall deal with both aspects together in the next section.

Before doing so, however, we must examine rather more closely the nature of φ_1 and φ_2. For this purpose it is necessary to make a certain assumption regarding the frequency response of the pulse amplifier. We shall assume that this has approximately the same shape as the frequency response of the "integrating" network of time constant τ_2, shown on the right of the equivalent circuit in *fig. 2*. The caption to this figure explains the other elements of this diagram, the composition of which is based solely on the mathematical analogy and does not, of course, resemble the actual circuit. For frequencies $f > 1/2\pi\tau_2$ the gain of this network is more than 3 dB smaller than at very low frequencies. Since in our model the lower limit of the range of frequencies passed by the amplifier lies at 0 c/s, the bandwidth of the amplifier is also equal to $1/2\pi\tau_2$.

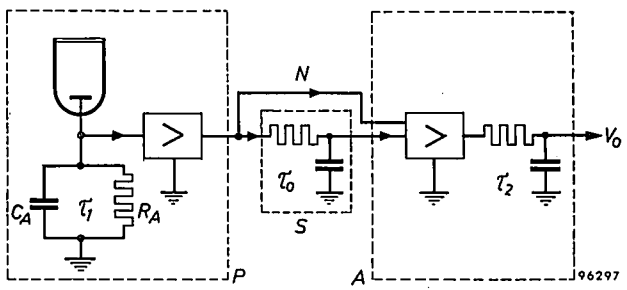

Fig. 2. Equivalent circuit of the counting system: scintillator (S), photomultiplier tube plus anode network (P) and pulse amplifier (A). The two first elements have time constants τ_0 and τ_1, respectively. The frequency response of the amplifier is approximately represented by that of an integrating network of time constant τ_2. The sign > denotes amplification independent of the frequency. The noise is introduced via a separate network N in parallel with S (see formula (4)). The diagram can be justified as follows. Omission of A gives a circuit corresponding to formula (2) for the scintillation pulses at the amplifier input. If S is also omitted, the remainder of the circuit corresponds to formula (4) for the noise pulses.

The form of the functions φ_1 and φ_2

Starting from the assumptions made above, it is possible to write formulae for the scintillation and noise pulses as a function of time. For the scintillation pulses we can write:

$$V(t) = A_1 e^{-t/\tau_0} + A_2 e^{-t/\tau_1} + A_3 e^{-t/\tau_2}, \quad . \quad . \quad (9)$$

and for the noise pulses

$$V_r(t) = B_1 e^{-t/\tau_1} + B_2 e^{-t/\tau_2}. \quad . \quad . \quad . \quad (10)$$

In principle one should be able to find the functions φ_1 and φ_2 by deriving expressions for the height of both types of pulse from (9) and (10). This is

analytically possible for the noise pulses, which are described by only two exponential terms, but not for the scintillation pulses. The way in which φ_1 varies with the different time constants can be found only by numerical calculation. It can, however, be shown that the value of φ_1 — like that of φ_2 — depends solely on the value of the ratios τ_1/τ_0 and τ_2/τ_0. We shall henceforth denote these ratios τ_1' and τ_2', respectively.

It is convenient to represent the numerical results graphically by drawing lines of constant φ in a figure having τ_1' and τ_2' as the coordinates. These lines are thus the loci of all combinations (τ_1', τ_2') leading to the same value of φ. The φ_1 lines were calculated with an electronic computer [7]). *Fig. 3* shows the curves for $\varphi_1 = 0.10$, 0.20, 0.25, 0.30 and 0.368. It is easier to calculate φ_2, since it does not depend on τ_0. A glance at the equivalent circuit of fig. 2 shows that τ_0 and τ_2 play completely analogous parts, that is to say φ_2 depends on τ_1 and τ_2 in the same way as V_m' on τ_1 and τ_0; see formula (3). Just as V_m' was there determined by the ratio τ_1/τ_0, in this case φ_2 is determined by the ratio τ_1/τ_2 (which is equal to τ_1'/τ_2'); in other words, the lines of constant φ_2 in fig. 3 are straight lines through the origin. For large τ_1' and τ_2' the curves $\varphi_1 =$ const. approach asymptotically the straight lines $\varphi_2 =$ const. corresponding to the same value of φ_2 (i.e. $\varphi_1 = \varphi_2$).

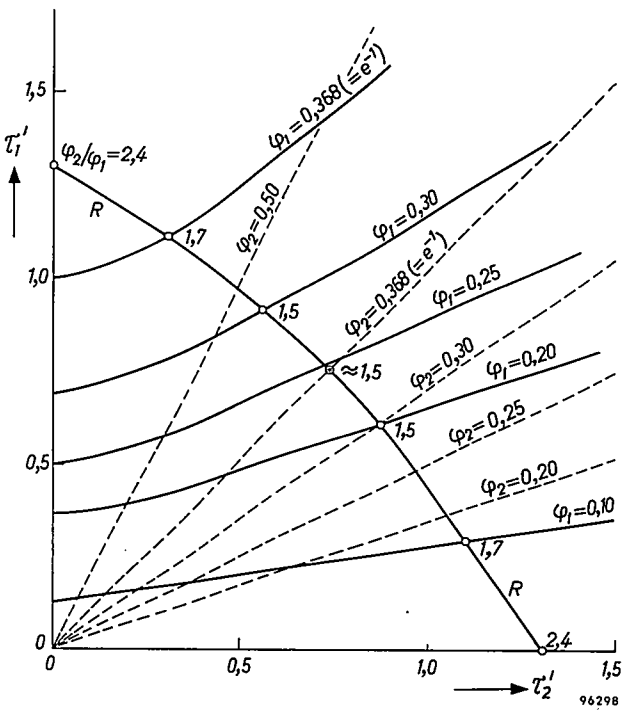

Fig. 3. Graphical determination of the time constants τ_1' and τ_2' with the object of obtaining the most favourable signal-to-noise ratio. With τ_2' on the abscissa and τ_1' on the ordinate, lines of constant φ_1 and φ_2 are drawn (cf. formulae (6) and (7)) from which the value of φ_2/φ_1 can be calculated for any combinaton of τ' values. The lines of constant φ_2 are straight lines through the origin; for large coordinate values each line corresponding to a certain value of φ_1 approaches asymptotically the line of constant φ_2 for which $\varphi_2 = \varphi_1$. Lines of constant pulse duration can also be drawn, e.g. the curve R in the figure refers to a pulse duration of $10\tau_0$. The smallest value of φ_2/φ_1, and hence the most favourable signal-to-noise ratio, is found at points $\tau_1' = \tau_2'$.

[7]) The programming of these calculations was done by A. J. W. Duijvestijn.

Signal-to-noise ratio and dead time as a function of φ_1 and φ_2; bandwidth of pulse amplifier

In every point of fig. 3, i.e. for every combination (τ_1', τ_2'), we now know the values of φ_1 and φ_2 and hence also the value of the ratio φ_2/φ_1. (The latter is always greater than unity.) The problem of the most favourable signal-to-noise ratio can therefore very simply be solved by ascertaining the point of the (τ_1', τ_2') field at which the ratio φ_2/φ_1 is minimum (cf. formula (8)).

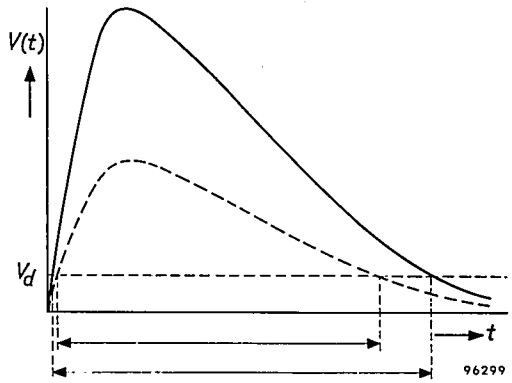

Fig. 4. The pulse duration, i.e. the time during which $V(t)$ is greater than the discriminator level V_d, is not constant but depends on the pulse height.

At the same time, however, the designer must ascertain whether in this case the pulse duration, hence the dead time, also has an acceptable value, and if not, how the time constants must be chosen in order to reach the most favourable compromise.

The pulse duration, which we define for the output pulses as the time during which $V(t)$ is greater than the discriminator level V_d, depends on the form of the pulse, i.e. on all time constants and also on the height of the pulse; see *fig. 4*. Since the dead time of a counter should be constant — a varying dead time would make it impossible in the case of high counting rates to apply a correction for the uncounted pulses [8]) — it may not be determined by the pulse duration. The dead time must accordingly be made at least equal to the maximum possible

[8]) See e.g. Philips tech. Rev. **16**, 360-370, 1954/55 or **17**, 206-221, 1955/56.

value of the pulse duration, i.e. to the duration of the largest pulses [9]). This is done by appropriately designing the electronic circuit of the counter. By "pulse duration" in the following we shall be referring to this maximum value.

At a given τ_0, more than one combination τ_1', τ_2' can lead to a certain pulse duration. The locus of all combinations τ_1', τ_2' leading to the same pulse duration is found to be a curve that is roughly a quadrant about the origin (see fig. 3). It can be shown that this curve (with the same scale of abscissa and ordinate) is symmetrical with respect to the line $\tau_1' = \tau_2'$ (the "diagonal"). The same applies to the variation of φ_2/φ_1 on this curve; the minimum is always on the diagonal. The most favourable solution is therefore to choose $\tau_1' = \tau_2'$. The requisite numerical value of the time constants then depends only on the desired pulse duration.

The curve of constant pulse duration drawn in fig. 3 applies to a pulse duration as defined above, of $10\tau_0$. It can be seen that in this case the minimum value of φ_2/φ_1 is approximately 1.5, and that this value increases the more one moves away along this curve from the diagonal. On the coordinate axes the value has risen to 2.4.

Having decided on the pulse duration and the associated values of τ_1' and τ_2' that lead to a minimum value of φ_2/φ_1, we have then also established E_{eq} (see eq. (8)), the bandwidth of the amplifier (since $2\pi f\tau_2 = 1$) and the pulse heights. For the pulse duration selected above, the corresponding values amount to $\varphi_2/\varphi_1 = 1.5$ (i.e. $E_{eq} = 1.5 \times$ the minimum value [10]), $f = 1$ Mc/s and the pulse height is approximately one quarter of the maximum pulse height ($\varphi_1 \approx 0.25$; see eq. (6)).

Although the frequency response of the pulse amplifier is only approximately represented by a fourpole of time constant τ_2 (fig. 2) — a more detailed representation requires more time constants and therefore involves considerable difficulties — one can nevertheless draw the following conclusions:

1) A large bandwidth with respect to $1/2\pi\tau_0$ results in a low signal-to-noise ratio.
2) A small bandwidth with respect to $1/2\pi\tau_0$ results in a long dead time.

These conclusions are soon arrived at when it is realized that a large bandwidth means a small τ_1' and τ_2'. From fig. 3 it can be seen that φ_2/φ_1 is large for small τ_1' and τ_2', hence E_{eq} is large and the signal-to-noise ratio small. On the other hand, when τ_1' and τ_2' are large, φ_2/φ_1 is approximately equal to unity. This implies a particularly good signal-to-noise ratio, but at the same time the pulse duration, and hence the dead time, is very long (cf. fig. 1).

Choice of pulse duration and dead time

The current pulse from the photomultiplier tube consists of a group of mono-electronic pulses originating from the individual photoelectrons. At the beginning of the current pulses these mono-electronic pulses lie very close together, but in the "tail" the average interval between the moments at which they occur becomes increasingly longer.

If the output pulse duration, determined by the time constants of the apparatus, and the dead time are of the order of magnitude of τ_0 (or smaller), some of the mono-electronic pulses are counted separately. These pulses are indistinguishable from the noise pulses, so that by shortening the pulse duration and the dead time we apparently increase the intensity of the noise. In order to count to more than one "noise" pulse per second in this case, we must therefore raise the discriminator level, which means that a larger fraction of the scintillation pulses will not be counted. The choice of the dead time will accordingly rest on a compromise.

By way of illustration, let us see what the situation is when, as in the example earlier discussed, the pulse duration is made equal to $10\tau_0$. From the formula describing the decay of a scintillation [11]), it follows that the number of photoelectrons occurring after the moment $t = 10\tau_0$ is equal to Ne^{-10}. If the γ-energy absorbed in the scintillator is, say, 3 MeV, this number is approximately equal to one (since N is E_1/E_i, hence in this case about 10^4; $e^{-10} \approx 10^{-4}$). Where the dead time of the counter is also about $10\tau_0$ — i.e. about 2.5 μsec in a counter with an NaI(Tl) scintillator — 10000 scintillations can be counted per second without appreciable correction of the dead time. In our example, then, we also have 10000 "tail pulses", that is to say, the noise intensity is about twice as great. This can be corrected by quite a small increase in the discriminator level (see appendix, eq. (11)).

It is evident from the foregoing that the dead time of a scintillation counter is primarily determined by the nature of the scintillating material. Whatever compromise is chosen, the pulse duration will never be shorter than τ_0; on the contrary, it comes out as a rule at 7 to 10 τ_0. This means that the reso-

[9]) In practice these are pulses produced by γ-quanta of about 3 MeV. Since V_{d1} in modern counters corresponds to an E_{eq} value of 10 keV, these pulses are about 300 times higher than the discriminator level.

[10]) At an E_1 value of 450 eV and a $D(I_{th})$ value of 10 (see appendix), E_{eq} in this case is therefore 6.75 keV (eq. 8).

[11]) See formula (3) in I.

lution of scintillation counters fitted with different scintillating materials can be roughly compared and determined by considering the τ_0 value of the materials in question.

The fact that the dead time of a scintillation counter is almost entirely determined by τ_0 is thus due to a pulse being a group of mono-electronic pulses. If the pulse were a continuous phenomenon, so that no trouble would be experienced from the above-mentioned tail pulses, it would be possible to somewhat reduce τ_1' before the signal-to-noise ratio were as high as that with which we are concerned in the present case. This would, of course, entail more amplification (cf. fig. 1).

Appendix: The form of the noise spectrum

Since little is known theoretically about the statistics of secondary emission, i.e. about the nature of the fluctuations of g', it is not possible to calculate the form of the noise spectrum, nor therefore that of the function $D(I_{th})$. This relation can, however, be deduced from experiments, whereby the number of noise pulses passed per second is plotted against the discriminator level V_d for various values of I_{th}. The results of such a measurement are shown in *fig. 5*. The point at which the curves are intersected by the horizontal line corresponding to $I_d = 1$ yield combinations of D and I_{th} from which the function $D(I_{th})$ can be derived. We find

$$D(I_{th}) \approx 0.9 + 1.25 \log I_{th}. \quad . \quad . \quad . \quad . \quad (11)$$

For $I_{th} = 10^4$ pulses per second, D is thus approximately 6.

When poly-electronic pulses are present in any appreciable numbers, the value found for D is substantially higher (see the dashed line in fig. 5). The number of such pulses need not even be particularly large to produce such an increase. A measurement of the dark current does not therefore give much indication of the discriminator level necessary in order to limit the noise count rate to a certain figure.

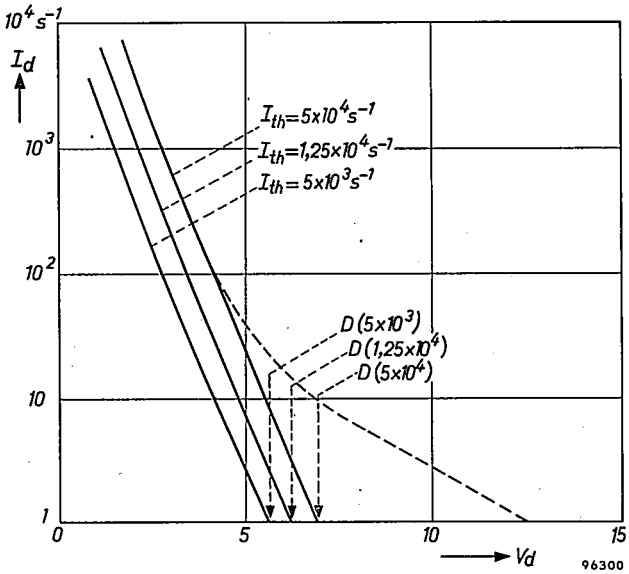

Fig. 5. The relation between the discriminator level at which one noise pulse per second is passed, and the number of (thermionic) noise electrons emitted per second, I_{th}, i.e. the function $D(I_{th})$, can be empirically determined from the points where the horizontal line corresponding to an ordinate value of 1 count per sec intersects the three plotted curves. The latter give the relation between the number of noise pulses passed per second I_d and the discriminator setting V_d, for various values of I_{th}. (The numbers along the V_d axis express the value of V_d in terms of a unit equal to the average noise pulse height.)

Summary. The ratio between the height of scintillation pulses corresponding to a certain absorbed energy and the discriminator level at which no more than (e.g.) one noise pulse per second is counted, the "signal-to-noise" ratio, depends on the decay constant of the scintillation effect (τ_0), on the time constant of the anode circuit of the photomultiplier tube (τ_1) and on the frequency response of the amplifier. If the latter can be approximately represented by only one time constant (τ_2), it is possible to solve, at least numerically, the problem of what combination yields the best signal-to-noise ratio.

The time constants also determine, however, the pulse duration, and hence the dead time of the scintillation counter. The scintillation pulse consists of a group of mono-electronic pulses. To avoid counting too many of these separately in the tail of the scintillation pulse and thereby raising the effective noise level, the pulse duration cannot be made shorter than 7 to 10 τ_0. Having decided on the scintillating material (thus fixing τ_0) and on the pulse duration, one can give the signal-to-noise ratio the largest value possible under these conditions by selecting that combination of τ_1, τ_2 at which $\tau_1 = \tau_2$.

ELECTRON EMISSION OF MATERIALS FOR ELECTRON TUBES

by G. A. ESPERSEN *) and J. W. ROGERS **).

621.385.002:537.581

The characteristics of some electron tubes, especially those operating at high power, are often adversely affected by electron emission from parts of the tube other than the cathode. This unwanted emission depends to a great extent on the material used. Certain components therefore need to be made of materials which, even when hot, emit few electrons. This article describes an investigation of a number of such materials used in the construction of electron tubes.

Introduction

In conventional electron tubes the cathode is always regarded as the sole source of the electron current to the anode. The cathode is made emissive by heating it and the emission density is increased by coating the cathode with a substance possessing a low work function. Emission from other parts [1]) gives a tube characteristics which were not intended by the designer, and as a rule impairs its operation. The parts most likely to be responsible for unwanted thermionic emission are of course those which get very hot during normal duty. This may be expected particularly in high-power tubes, e.g. transmitting tubes. In conventional transmitting tubes the control grid is the worst offender in this respect since, for various reasons, it can acquire a fairly high temperature. The main reasons are:

a) The grid absorbs part of the heat radiated by other electrodes. Naturally the principal source of this heat is the cathode, but the anode is an important source of heat in tubes where the anode is not cooled by air or water.

b) The grid is difficult to cool by conduction.

c) In an operating transmitting tube the grid is generally positive with respect to the cathode for a part of every cycle. During this time the grid is bombarded by electrons from the cathode (i.e. grid current flows), and this bombardment contributes to the heating of the grid.

d) At high frequencies the internal capacitances of the tube generally form part of the circuit capacitances, resulting in appreciable high-frequency currents through the grid wires and hence extra heating.

With regard to grid emission, another unfavourable circumstance is that evaporation products from the cathode can readily collect on the grid surface, thereby substantially lowering its work function. Most important of all, electron emission from the grid has more undesirable effects on the circuit than emission from other electrodes.

Another type of tube in which undesired electron emission may occur are magnetrons. In this case a high temperature and vapour deposits from the cathode on the end caps enclosing the electrode system of the magnetron can also give rise to unwanted thermionic emission.

In the construction of an electron tube two methods are adopted to reduce unwanted emission from certain components:

a) The components are designed and assembled in such a way as to ensure that they are heated as little as possible.

b) The components are made of a material possessing a high work function, even when covered with evaporation products from the cathode [2]).

In connection with the latter point, an investigation was carried out some years ago at Irvington to examine the suitability of various materials for use in the construction of electron tubes [3]). In the present article we shall describe these experiments and the results obtained.

The investigation was made with tubes specially designed for the purpose, and the utmost care was taken to ensure maximum cleanliness of all parts, since even minute contaminations have a very marked effect on the emission characteristics of a material.

Construction and processing of the experimental tubes

For the majority of experiments, tubes of the planar-triode type as represented in *fig. 1* were used.

*) Philips Laboratories, Irvington-on-Hudson, N.Y., U.S.A.
**) Formerly with Philips Laboratories, Irvington.

[1]) Secondary emission, which is usefully employed in some electron tubes, is not considered here.

[2]) A design has been considered whereby the components likely to give rise to unwanted emission become so hot during normal operation that cathode material deposited on them is either absorbed or readily evaporated again. This method, however, is difficult to control.

[3]) See G. A. Espersen and J. W. Rogers, Studies on grid emission, I.R.E. Transactions on Electron Devices **ED 3**, 100-107, 1956.

The anode consisted of a molybdenum cylinder. The cathode had the same dimensions as the anode and was heated by an internal filament. The material under investigation was placed in the form of a loop of 0.010" wire midway between cathode and anode.

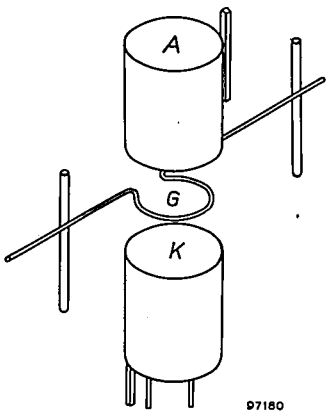

Fig. 1. Schematic representation of the structure of the experimental tubes. *A* anode, *G* "grid", *K* cathode.

The diameter of the loop was 0.085". Because of its position in the electrode system, we shall refer to this loop henceforth as the "grid". In addition to this structure, a getter and also a diode consisting of a tungsten filament and a molybdenum anode, were incorporated in the envelope. The purpose of the latter was to enable the vacuum in the tube to be checked by measuring the work function of the tungsten filament. A bad vacuum increases the work function. Exclusive use was made of tungsten, molybdenum and tantalum for the tube structure, including the stem leads. The grid consisted of the material to be tested. Before assembly, all components were thoroughly cleaned. Careful precautions were taken during assembly to prevent contamination of the components. For example, to avoid copper deposits during the welding of the electrodes, welding tips of tungsten were employed.

During the sealing-in of the electrodes in the glass envelope, care was taken to avoid excessive heating of the triode structure, by simultaneously passing a stream of dry nitrogen through the envelope. The entire tube was baked for one hour at 720 °K while being evacuated. During the pumping process the parts were degassed by heating in the usual way, the getter being glowed below its flashing temperature. The getter was not flashed until about ten minutes after the tube had been sealed off, during which time the tube was "seasoned" at a high temperature. Immediately before sealing-off, and again about a day later, the vacuum in the tube was checked with the aid of the auxiliary diode. If at that time the vacuum was found to have deteriorated, the tube was rejected.

Two types of triode were used, one being a single-ended structure and the other a double-ended structure with the anode and grid terminals brought out at opposite ends of the envelope. In the latter case the leakage path between anode and grid has a higher resistance, and this type of tube was therefore used when the emission current to be measured was less than about 0.2 mA peak.

Methods of measurement

Most of the measurements were made by a method [4]) in which the grid was heated continuously, either by direct conduction or by electron bombardment. Once every $^1/_{60}$ second a negative voltage pulse of 100 microseconds duration was applied to the grid, each pulse producing a sufficiently large potential difference between the grid and the other electrodes to give rise to grid emission currents of saturation value. A plot of grid current versus time is shown in *fig. 2*. The grid emission was measured by determining the amplitude of the current pulses on an oscilloscope.

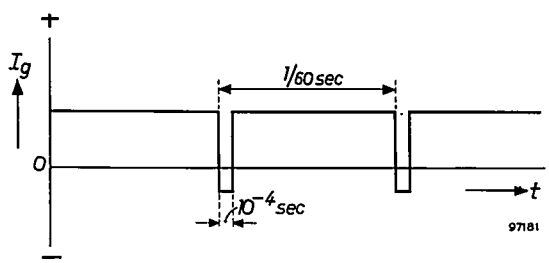

Fig. 2. Grid current I_g versus time t in a grid-emission measurement by the pulse method.

When the emission current was less than about 0.2 mA peak it was necessary to abandon the pulse method because of the sensitivity limitation of the oscilloscope. In such cases a D.C. method was used in which the emission current was measured by a galvanometer, the grid being raised to the required temperature with an auxiliary current (see *fig. 3*). In principle this method is simpler than the pulse measurement. However, it was found desirable to use the D.C. method only when the low value of grid current made it necessary, the reason being that the measurements could be made in a much shorter time by the pulse method, hence with much less chance of the conditions in the tube changing during a test run.

[4]) Developed by R. A. La Plante, Amperex Electronic Company.

The main materials subjected to emission tests were tungsten, molybdenum, gold-plated molybdenum and titanium. Loops were made of these materials as denoted by *G* in fig. 1. Since the extent to which evaporation products collect on these

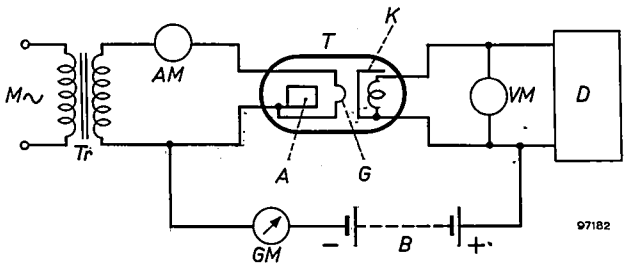

Fig. 3. D.C. method of measuring grid emission. *T* tube under test, *M* mains voltage, *Tr* transformer for heating grid *G*, *D* filament supply, *B* battery, *AM* ammeter, *VM* voltmeter, *GM* galvanometer.

loops depends on the properties of the cathode, three different types of cathode were used in the tubes under test, viz. L cathodes [5]), impregnated cathodes [6]) and oxide cathodes.

Results

During the measurements the L-type and impregnated cathodes were operated at 1275 °K, and the oxide cathodes at 1100 °K, all types having first been run for 100 hours to stabilize their properties. In the course of this "seasoning" the grid remained fairly cold and the evaporation products of the cathode settled in layers on its surface. In many cases these deposits were removed by "glowing" the grid, i.e. by passing a current through it, prior to the measurement. Some measurements were carried out, however, without the grid having first been cleaned after seasoning.

The variation of the grid emission as a function of time is shown for several grid materials in *fig. 4*. In these tests an L cathode was used, operated at 1275 °K. The temperature of the grids was 1200 °K, with the exception of the gold-plated molybdenum grid, which was heated to only 1100 °K, the reason being that above this temperature the gold would evaporate. For the same reason the gold-plated grids, unlike all others, could not be cleaned after seasoning by glowing them as described above.

It appears from fig. 4 that in all cases the grid emission decreases as a function of time and approaches a stable equilibrium value. For tungsten and gold-plated molybdenum, however, the emission

[5]) H. J. Lemmens, M. J. Jansen and R. Loosjes, Philips tech. Rev. **11**, 341-350, 1949/50.
[6]) R. Levi, Philips tech. Rev. **19**, 186-190, 1957/58.

Table I. Final value of the saturation grid emission current for various grid materials when an L cathode operated at 1275 °K was used. (The symbols Mo + Zr or Ca or Mg and Mo + Au indicate molybdenum plated with the second metal; Mn-Ni is an alloy of manganese and nickel.)

Material	Grid temperature (°K)	Grid current (μA)
W	1200	414
Mo	1200	300
Mo+Zr or Ca or Mg	1200	24
Mn-Ni	1200	24
Mo + Au	1100	4.48
Zr	1200	2.24
TiO_2	1200	0.10
Ti	1200	0.0004

rises to a maximum before beginning to drop. The time needed to reach the stable equilibrium value is always short compared with the life of the tube, and in practice therefore it is this final value that is of major importance. The stable equilibrium values for a number of materials are collected in *Table I*. From this table, and also from fig. 4, it can be seen that of all the materials tested, titanium exhibits the lowest emission, both as bright titanium wire and when plated on a core of molybdenum. The emission rises sharply, however, if the titanium is covered with titanium oxide.

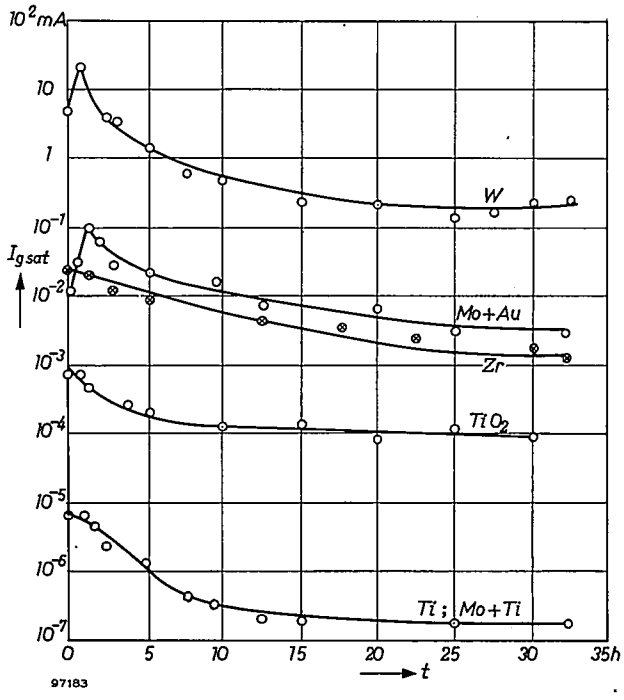

Fig. 4. Saturation grid emission current $I_{g\ sat}$ versus time for various grid materials in an experimental tube fitted with an L cathode. Mo + Au means gold-plated molybdenum, and Mo + Ti titanium-plated molybdenum. Prior to each run the grids, except the Mo + Au grid, were cleaned by heating them for several hours. During the measurements the temperature of the gold-plated grid was 1100 °K and of the others 1200 °K.

To illustrate the influence of the cathode employed, the results are given in *Tables II* and *III* of a series of measurements run with the three types of cathode mentioned above. Table II refers to a tungsten grid and Table III to a gold-plated molybdenum grid. The tables give the initial, maximum and final values of the emission current, together with the time required to reach maximum emission [7]).

Table II. Saturation grid emission current of a tungsten grid at 1200 °K, using three different types of cathode.

Cathode	Cathode temperature (°K)	Grid emission current (mA)			Time required to reach max. value (hours)
		Initial value	Max. value	Final value	
Impregnated	1275	2.0	17	2.6	1.0
L	1275	2.1	50	17	18
Oxide	1100	3.7	54	8.0	25

Table III. Saturation grid emission current of a gold-plated molybdenum grid at 1100 °K, using three different types of cathode.

Cathode	Cathode temperature (°K)	Grid emission current (mA)			Time required to reach max. value (hours)
		Initial value	Max. value	Final value	
Impregnated	1275	0.70	1.1	0.28	2
L	1275	0.21	1.8	0.21	5
Oxide	1100	0.60	2.8	0.21	25

Titanium having been found to have the lowest emission, more comprehensive measurements were carried out on this material [8]). *Fig. 5* shows emission plotted as a function of grid temperature for a grid of pure titanium and for a grid coated with titanium oxide. It is noticeable that oxidation causes a sharp increase in the emission of titanium. At a temperature of 1600 °K the oxide is reduced to titanium and the curve for the oxide therefore falls back to that corresponding to the pure metal. (Experiments performed by V. L. Stout [9]) have shown that the oxygen formed in this process is not liberated but is dissolved in the titanium.)

[7]) The data for the L cathode in Tables II and III are not in agreement with fig. 4. The reason is that the measurements concerned were performed under different conditions. For the data in the tables, the pulsed grid voltage was applied only during the short intervals required for the measurements and not throughout the entire time mentioned in the tables. In the runs whose results are illustrated in fig. 4, the pulsed grid voltage was applied continuously.

[8]) G. A. Espersen, U.S. Patent 2 846 609, 5 August 1958: Non-emissive electrode for electron-discharge device.

[9]) Private communication from Dr. V. L. Stout, General Electric Research Laboratory, Schenectady, N.Y., U.S.A.

In the measurements to which fig. 5 refers, an L cathode was used. After seasoning the cathode at 1500 °K, the evaporation products deposited on the grid were not removed, and this probably explains the remarkable shape of the emission curve for titanium. During the increase of the grid temperature to about 1000 °K, the cathode material deposited on the grid is activated, causing the emission to rise in spite of the fact that above 600 °K there is appreciable evaporation of the barium. With the grid above 1000 °K, however, the deposits on the grid evaporate almost completely, causing a drop in

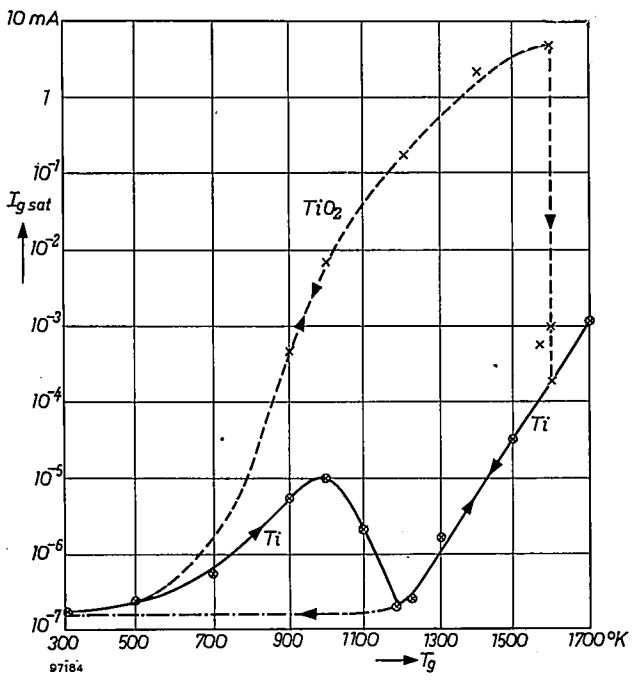

Fig. 5. Saturation grid emission current $I_{g\,sat}$ as a function of grid temperature T_g for bright titanium and for oxidized titanium (tube with L cathode). The cathode evaporation products deposited on the grid were not removed before measurement.

emission, and finally, above 1175 °K, the emission rises again in accordance with the characteristic for pure titanium. This explanation was confirmed by the fact that, when the grid temperature dropped again, the emission underwent no rise below 1175 °K, but showed the values denoted by the dot-dash curve in fig. 5.

The emission from a titanium-plated molybdenum wire was found to be virtually identical with that from a wire consisting entirely of titanium. For molybdenum wire sprayed with titanium powder, however, the emission was several orders of magnitude higher. This was probably due to traces of oxide in the powder used.

Fig. 6 shows how the emission of titanium varies

as a function of time at different temperatures. Prior to these measurements the grid had been exposed for some hours to an L cathode glowing at 1500 °K, during which time it had acquired deposits of cathode material. At the end of each run the grid was cleaned by heating it, after which the cathode was again glowed for some time at 1500 °K. In this way the same conditions were obtained at the beginning of each series of measurements. The

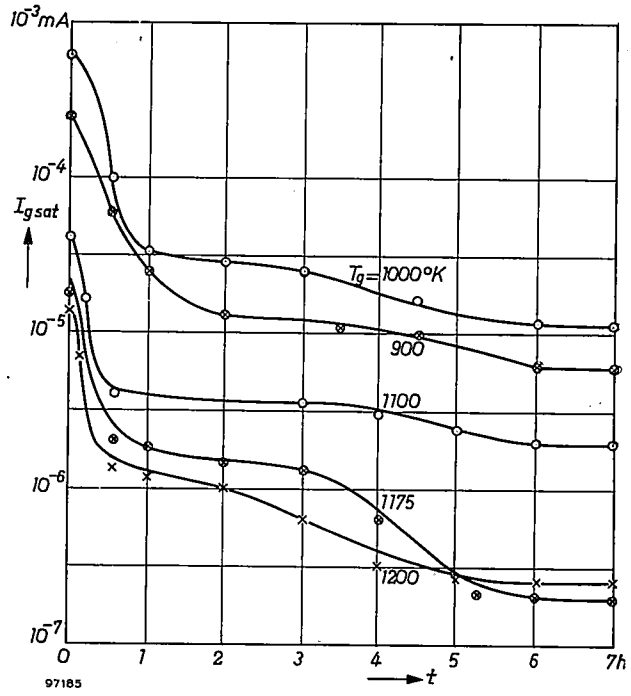

Fig. 6. Saturation grid emission current $I_{g\,sat}$ of titanium grid as a function of time t (hours) for various values of grid temperature T_g (tube with L cathode).

emission characteristic of non-oxidized titanium as a function of temperature, as illustrated in fig. 5, is fully confirmed by the final values indicated by the curves in fig. 6.

Measurements in which evaporation products from the cathode had already settled on the grid beforehand (and were thus not first removed) were also carried out on materials other than titanium. Some results are represented in *fig. 7*, together with the curve for titanium already given in fig. 5. The grid emission characteristics of zirconium and tungsten also show dips. They occur at 1600 °K and 1900 °K, respectively (the latter dip falls outside the figure). The dip is not as great for these materials as for titanium, however. Again, the reason for these minima is believed to be the reduction of barium oxide to barium, which is evaporated from the surface of the grid while the oxygen dissolves in the base material [10]).

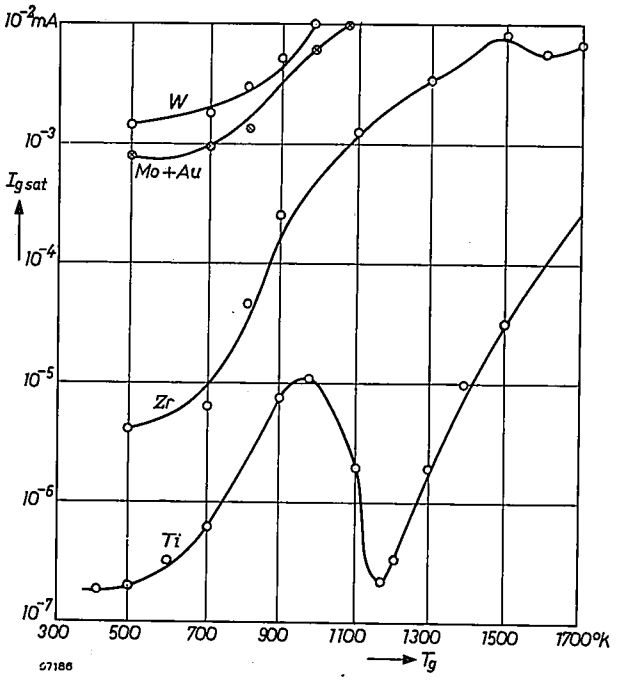

Fig. 7. Saturation grid emission current $I_{g\,sat}$ as a function of grid temperature T_g for various grid materials (tube with L cathode). The cathode evaporation products deposited on the grid were not removed prior to the measurement.

In order to ascertain the rate at which the cathode material deposited on the grid evaporates when it is not continuously supplemented by further evaporation products from the cathode, measurements were carried out with the L cathode kept cold. Prior to each run the grid was exposed, as before, to the evaporation products of the cathode which was glowed at 1500 °K. The results of these measurements for several materials are set out in *Table IV*.

Table IV. Decay of grid emission current for grids of various materials covered with evaporation products of an L cathode. During the measurements the cathode was not heated. (Mo + Au denotes gold-plated molybdenum.)

Grid material	Grid current (mA)		Time required to reach final value (hours)
	Initial value	Final value	
W	39	1.7	28
Mo + Au	9.6×10^{-3}	3×10^{-3}	10
Zr	5.4×10^{-3}	2.2×10^{-3}	6
Ti	0.6×10^{-3}	0.3×10^{-3}	7
TiO_2	2×10^{-3}	0.058×10^{-3}	—

The values tabulated are the initial and final values of the emission current, and the time needed to reach approximately the final value. During the measurements the grid temperature was 1200 °K,

[10]) X-ray diffraction analyses were made to determine whether the barium combined with the titanium instead of evaporating. No titanates were found.

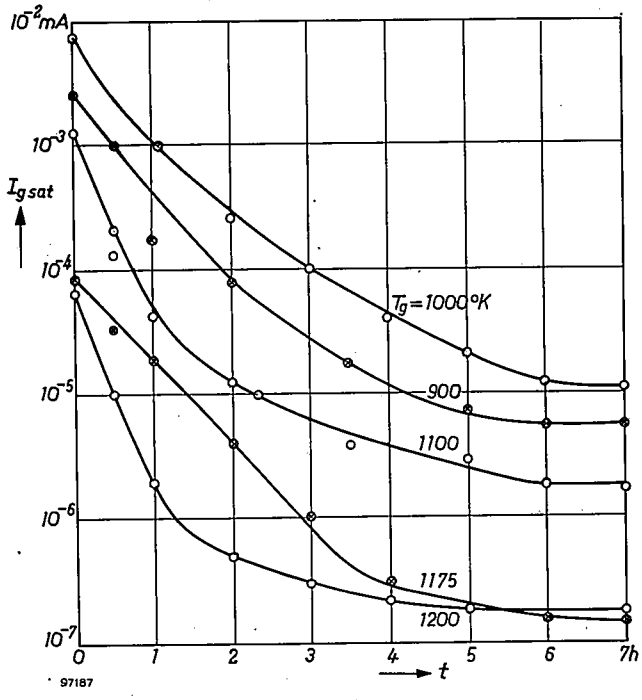

Fig. 8. Saturation grid emission current $I_{g,sat}$ of titanium grid as a function of time t (hours) for various values of grid temperature T_g. During the measurement the cathode was kept cold.

with the exception of the gold-plated molybdenum grid which, for the reasons already given, was heated to only 1100 °K. For titanium the measurements were repeated at various other temperatures. The results of these tests are represented in *fig. 8*. Prior to each run the grid was exposed for 16 hours to the cathode at 1500 °K, so that the starting conditions can again be regarded as equal for all curves. From fig. 8 it can be seen that in all cases the cathode deposits on the grid have evaporated after a few hours.

Summary. The operation of certain types of vacuum tube is often seriously affected by thermionic emission from parts of the tube exposed to the evaporation products of the cathode. The extent to which this unwanted emission occurs depends partly on the materials used. With this in mind, an investigation was made into the emissive properties of various materials widely used in the construction of electron tubes. Special tubes were built for this purpose, care being taken to ensure that all parts were scrupulously clean. To simulate practical operating conditions, the cathode evaporation products were allowed to form deposits on the grid. Measurements were also carried out at different operating temperatures. Three types of cathode were used, viz. impregnated cathodes, L cathodes and oxide cathodes. Of all materials tested, clean titanium was found to have the lowest emission. It shows a much greater emission, however, if coated with titanium oxide.

ABSTRACTS OF RECENT SCIENTIFIC PUBLICATIONS BY THE STAFF OF N.V. PHILIPS' GLOEILAMPENFABRIEKEN

Reprints of these papers not marked with an asterisk * can be obtained free of charge upon application to the Philips Research Laboratory, Eindhoven, Netherlands.

2598: T. J. de Man, J. R. Roborgh and E. J. ten Ham: Effect of the method of administering massive doses of vitamin A on the liver storage in rats (T. Diergeneesk. **83**, 380-387, 1958, No. 10).

Experiments with rats showed a better liver storage of vitamin A when this vitamin was given orally as a massive dose from an aqueous dispersion than when applied in the same way from an oily solution. Only a very small percentage of the vitamin A from an oily solution, administered intramuscularly, was stored while under the same conditions from an aqueous dispersion about 60% could be recovered in the liver. The liver storage from an aqueous dispersion of vitamin A, given intravenously, proved to be about 70% of the applied dose. The vitamin A content of a liver depot in rats decreased but slowly in 1-1.5 month, indicating that a liver depot of a sufficiently high level is able to supply the necessary amounts of vitamin A to the animal for a considerable length of time.

2599: F. W. de Vrijer: The choice of chrominance signals in the N.T.S.C. system with a view to the differential sensitivity of the human eye to colour (Acta electronica **2**, 103-109, 1957/58, No. 1/2).

In an N.T.S.C.-type colour-television system the phase of the subcarrier determines to a first approximation the hue, and the amplitude of the subcarrier relative to the value of the luminance signal determines the saturation of the reproduced colour in a colour-receiver. Colour deviations will occur in case of noise in the chrominance channel and in case of phase errors of the receiver subcarrier reference oscillator. These phase errors may be caused by noise or otherwise. The sensitivity of the signal to these effects is influenced by the particular choice of chrominance signals transmitted. In order to make an optimum choice, the differential sensitivity of the human eye to colour has to be taken into account. In this paper known data on hue tolerances are used to calculate the sensitivity to phase errors in the N.T.S.C. system. Experiments were performed with an actual colour-television system to get more exact numerical data. These data are used to calculate the optimum choice of chrominance signals with respect to subcarrier phase errors. This optimum choice turns out to be not very much different from the actual N.T.S.C. system. The paper concludes with some remarks on the sensitivity to noise in the chrominance channel of the N.T.S.C. signal.

2600: L. Heijne: The lead-oxide vidicon (Acta electronica **2**, 124-131, 1957/58, No. 1/2).

A description is given of an experimental photoconductive television pick-up tube, using an evaporated layer of lead monoxide. The layer is microcrystalline. The most important properties of the tube are: *a*) negligible dark current (approx. 0.003 μA); *b*) high sensitivity (100-200 μA/lm); *c*) approximately linear light-transfer characteristic; *d*) fast response also at low light levels. The sensitivity is maximum in the blue or green parts of the spectrum depending on the thickness of the photoconductive layer. The decay of the signal after a sudden interruption of the light is primarily determined by the discharging mechanism of the scanning beam, and not by inherent inertia of the photoconductor itself. At high illumination levels the photocurrent may become saturated as a result of progressive target discharge. At short wavelengths space-charge in the interior of the photoconductor may also limit the signal current. The influence of target thickness on decay, gamma and spectral response is discussed in detail.

2601: H. A. Klasens and A. Bril: Phosphors for colour television (Acta electronica **2**, 143-152, 1957/58, No. 1/2).

When selecting the most suitable phosphors for tricolour tubes and projection tubes for colour television, the following points have to be considered: *a*) The colour reproduction. *b*) The overall efficiency. *c*) The picture quality. To obtain the best colour reproduction, the chromaticity coordinates should be as near as possible to the corners of the chromaticity diagram. For the calculation of the lumen output of the screen a white colour with chromaticities $x = 0.310$ and $y = 0.316$ (illuminant C) was chosen, since most objects have rather unsaturated colours. It is shown that the choice of the red phosphor mainly determines the luminous properties of

the screen and that a compromise has to be found between colour reproduction and light output. The ideal red phosphor should have a narrow emission band with a sharp cut-off towards shorter wavelengths near 6100 Å. Stray electrons and misalignment of the primary electron beam cause some colour distortion and loss of contrast in tricolour tubes. The picture quality can be improved by reducing the efficiencies of the green and blue phosphors. Such a phosphor compensation may furthermore improve the gamma match in three-gun tubes. Phosphors for flying-spot tubes are briefly discussed.

2602: J. C. Francken and R. R. Bathelt: Measurement and evaluation of colour purity in colour tubes (Acta electronica **2**, 153-158, 1957/58, No. 1/2).

Purity of the separate colour fields in colour tubes is one of the requirements for achieving good colour rendition. After a short survey of possible causes of deterioration of the primary colour and of the known methods for measuring chromaticity, a colorimeter is described, especially designed for use with colour tubes. The instrument is based on the principle of visual additive mixing of three light sources. As such three special cathode-ray tubes are used, fitted with the same phosphors as are used in colour tubes. A rapid evaluation of colour purity is thus possible, as well as a quantitative computation of chromaticity coordinates. The accuracy of the method is greatest in the vicinity of the primaries, a property that suits the purpose. Examples of measurements on actual tubes are given. For routine testing of tubes, in cases where reject limits have already been established, an objective method using coloured filters in combination with a photomultiplier is easier and faster. A short description is given of the combinations used for colour-tube testing.

2603: E. F. de Haan and H. Zimmer: Postfocussing colour tubes (Acta electronica **2**, 189-193, 1957/58, No. 1/2).

A colour tube, using a focussing mask, is discussed. The holes in the mask are slits of a special form in order to obtain postfocussing action with a low voltage ratio between mask and screen. A transparency of 60% has been obtained for the mask. It is found that a spherical mask with these slits is easy to construct and therefore it is possible to use a normal envelope with a spherical inner face. Moreover, it is possible to deposit the phosphors by the married-parts method. The phosphor lines have a critical determined width in order to obtain better contrast.

2604: J. Haantjes: Physical aspects of coding systems used in colour television (Acta electronica **2**, 320-326, 1957/58, No. 1/2).

This paper deals with several physical and physiological phenomena playing a role in the viewing of television images. The influence of these phenomena in the choice of an appropriate signal carrying the essential information in an effective way is discussed. This problem cannot yet be considered as completely solved as it still forms the subject of many investigations. The choice of an adequate colour-television system raises again problems of the same nature. The properties of the human eye with regard to the observation of colour and colour detail are dealt with. Besides factors of a physical nature other factors of technical and economic importance have to be taken into account in the choice of a colour transmission system. After discussion of some proposed methods the opinion is expressed that under the circumstances a system on the principle of that adopted in the U.S.A could also be introduced in Europe. The paper ends with a report of the work done in the Philips Research Laboratory at Eindhoven with regard to the adaptation of the N.T.S.C. system to the existing 625 line monochrome standard.

2605: J. E. Rombouts and A. Kaars Sijpesteijn: The chemotherapeutic effect of pyridine-2-thiol-*N*-oxide and some of its derivatives on certain plant diseases (Ann. appl. Biol. **46**, 30-36, 1958, No. 1).

Limited systemic protection of broad bean against *Botrytis fabae* and of cucumber against *Cladosporium cucumerinum* has been observed as a result of the application of pyridine-2-thiol-*N*-oxide and its carboxymethyl derivative. Apparently this protection is, to some extent, the result of translocation of the chemicals in the plants. It was found that the vapour phase of pyridine-2-thiol-*N*-oxide plays an additional role in the chemotherapeutic activity. There is no evidence that the copper chelate of pyridine-2-thiol-*N*-oxide is translocatable in plants. Root applications of these three compounds had no chemotherapeutic effect.

2606: C. J. Bouwkamp: A simple method of calculating electrostatic capacity (Physica **24**, 538-542, 1958, No. 6).

Attention is drawn to a simple theorem enabling the evaluation of the electrostatic capacity of certain conductors in free space such as a system of two spheres in contact with each other and a "ring without hole".

VOLUME 20, 1958/59, No. 10 pp. 277-308 Published 29th July 1959
N.V. PHILIPS' GLOEILAMPENFABRIEKEN

Philips Technical Review

DEALING WITH TECHNICAL PROBLEMS
RELATING TO THE PRODUCTS, PROCESSES AND INVESTIGATIONS OF
THE PHILIPS INDUSTRIES

PHOTO-RESISTORS MADE OF COMPRESSED AND SINTERED CADMIUM SULPHIDE

by N. A. de GIER, W. van GOOL and J. G. van SANTEN.

621.383.4

Research into the solid state has led, especially in recent years, to a number of new electronic devices, which have rapidly found a variety of practical applications. The germanium diode and the transistor, to give two examples, have assumed great importance in a very short space of time. Another recent development, which is likely to find wide application, is the cadmium sulphide photoconductive cell (photo-resistor).

The article which follows describes how these photo-resistors can be produced on an industrial scale and discusses some of their many possible applications.

Introduction

For a considerable number of years science and industry have been making use of devices capable of converting light into electrical signals. The oldest of these is the familiar *vacuum photocell.* This is an evacuated glass envelope containing a sensitive layer (the photocathode) from which electrons are freed by the action of light (photo-electric emission), and an anode which stands at a higher potential (about 100 V) and towards which the freed electrons move. The anode current is equal to the current constituted by the electrons released from the photocathode. The sensitivity of this type of photocell is approximately 10^{-8} amperes per lux; with normal intensities of illumination, therefore, the output signal has to be amplified considerably before it can be conveniently measured or used for some practical purpose.

A current several times greater than that of the liberated photo-electrons can be obtained from a cell of this kind by filling the envelope with a suitable gas. The photo-electrons traversing the field between the cathode and anode ionize the gas, so providing a current amplification. The higher the anode voltage, the greater is the amplification obtained in this way; but the voltage across the cell must, of course, remain well below the breakdown value.

The *photomultiplier* is a refined version of the vacuum-type photocell. One to ten millionfold amplification takes place in this tube by virtue of secondary electron emission from auxiliary electrodes (dynodes). Accordingly, the sensitivity of photocells of this type is as high as $\sim$ 0.1 ampere/lux, but they have the disadvantage of requiring a voltage between 1000 and 2000 V. Nevertheless, in certain applications amplification by secondary emission is a much more attractive proposition than the use of ordinary amplifying tubes.

The vacuum-type photocell and the photomultiplier distinguish themselves from all other types by virtue of their extraordinarily fast response, for they can handle periodic signals with frequencies up to 100 Mc/s. The gas-filled photocell is much less fast, being unable to cope with frequencies above 10 kc/s. The spectral region to which these three types of photocell are sensitive is determined by the nature of the cathode material. Only for a few materials is the long-wavelength limit (the so-called "red limit") in the long-wave half of the visible range or in the infra-red [1]).

[1]) More about the vacuum and gas-filled types of photocell may be found in Philips tech. Rev. **2**, 13-17, 1937 and **4**, 48-55, 1939. For the photomultiplier see Vol. **16**, 250-257, 1954/55.

A general account of the photo-electric effect and of photocells and their applications may be found in V.K. Zworykin and E.G. Ramberg, Photoelectricity and its application, John Wiley, New York 1949, or H. and A. Simon, Der lichtelektrische Effekt und seine Anwendungen, Springer, Berlin 1958.

More recently photocells have been developed whose action is based on the *internal* photo-electric effect occurring in certain solids which in darkness are poor conductors. Electrodes are fitted to a disc or block of a substance of this kind: depending on the nature of these electrodes we get a *photo-conductive cell* or *photo-resistor*, i.e. a device whose electrical conductivity varies with the intensity of the incident light, or a *photo-voltaic cell*, which is a device across which differences of electrical potential arise when light falls upon it. In the last few decades selenium photocells of the latter type (barrier-layer cells) have come into use on a considerable scale. One well-known application is in the photo-electric exposure meters used in photography. Photo-voltaic cells are more sluggish than the vacuum type, being unable to handle frequencies above 2 kc/s, but they are ten times as sensitive [2]). The spectral sensitivity curve of the selenium photo-voltaic cell exhibits a peak at approximately 6000 Å, which lies at about the centre of the visible spectrum.

Selenium photo-resistors have never found large-scale application. The *germanium point-contact diode*, the *germanium photo-transistor* and other devices that have been developed during the last ten years have proved to be more useful. Because their sensitive surfaces have a very small area, their sensitivity as defined above, in amperes/lux — their *lux* sensitivity — is on the low side; they do however have a high *lumen* sensitivity, i.e. a sensitivity measured in amperes/lumen. The photo-transistor is sensitive not only to the visible range but also to wavelengths well inside the infra-red band (to about 2 μ) [3]). Photo-resistors made of *cadmium sulphide* can have even higher lumen sensitivities. The photo-resistors made by Philips, which contain a sensitive layer of compressed and sintered cadmium sulphide, have a lumen sensitivity approaching that of the photomultiplier. Their lux sensitivity is also very high, being exceeded only by that of the photomultiplier.

To give an idea of the sensitivity of these cells, it may be mentioned that when exposed to an intensity of illumination of 1000 to 10 000 lux, their resistance is of the order of only 100 Ω. Their dark resistance is of the order of 100 MΩ. It is thus possible to control a relay by means of a simple arrangement consisting of relay and cell in series with a voltage supply.

It may be useful, to prevent any misunderstanding, to say something more about the two measures of sensitivity for photocells and photo-resistors. The lux sensitivity (in A/lux) may be worked out from the lumen sensitivity (in A/lumen) by multiplying the latter by the area (in m^2) of the sensitive surface of the cell or resistor. Of course, when stating the sensitivity of a photo-resistor in either of these units it is necessary to state also the applied voltage to which the sensitivity applies. The advantage of using the two measures of the sensitivity lies in the field of comparisons between photo-resistors and other kinds of photocell.

Before discussing the method of production of the light-sensitive material for the new photo-resistors, we shall give a brief account of the phenomenon of photoconductivity as it occurs in CdS and other substances. From this it will be evident which property is the best suited for characterizing the merits of a photoconductive substance, and how the optimum form of a cell based on that substance may be decided upon.

The phenomenon of photoconductivity in CdS

In a non-conductive solid all electrons are bound to the ions or atoms which go to make up the crystal lattice; free electrons such as exist in metals are absent or present only in very small numbers. This also applies to photoconductive substances like CdS, insofar at least as they are not exposed to radiation. When radiation falls on the crystal the energy of the radiation is absorbed by the lattice. Very briefly, a number of electrons then become more or less free, so that the substance ceases to be an insulator and becomes a conductor. We shall now determine the quantities governing the conductivity of a piece of crystalline photoconductive substance, and find out how its conductivity depends on them.

We shall denote by F the number of light quanta absorbed per cm^3 and per second, and by τ the average time elapsing before an electron is recaptured by an ion or atom that has lost one of its own electrons (τ is the "mean life time" of the free electron). Assuming that every absorbed light quantum liberates one electron, we can say that in equilibrium the number of free electrons present per cm^3 will be [4])

$$n = \tau F. \quad \ldots\ldots \quad (1)$$

[2]) When the electrodes of a photo-voltaic cell are joined, a current flows which, provided the resistance of the external circuit is small ($< 10\ \Omega$), is independent of this resistance and proportional to the intensity of illumination. In this case the sensitivity can thus again be expressed in amperes per lux. Cf. Philips tech. Rev. **8**, 65-71, 1946.

[3]) One application in which sensitivity to infra-red is of particular importance is the transistor pyrometer described in Philips tech. Rev. **20**, 89-93, 1958/59 (No. 4).

[4]) Expression (1) is not based on any theory concerning the freeing or absorption of electrons but is a perfectly general statistical law.

If two electrodes are affixed to the CdS crystal and a voltage applied to it, the free electrons will move at a velocity v which is proportional to the field strength E in the crystal:

$$v = \mu E. \quad . \quad . \quad . \quad . \quad . \quad . \quad . \quad (2)$$

The factor of proportionality μ is termed the *mobility* of the electrons. Using (1) and (2), the current density J, which is *nev*, can be written as

$$J = nev = \mu\tau eEF \quad . \quad . \quad . \quad . \quad . \quad (3)$$

(e is the charge on the electron).

If the crystal has the shape of a rectangular slab of width l, thickness t and length d (see *fig. 1*; d is the distance between the electrodes), and if a voltage V is applied to it, then $E = V/d$. If Q light quanta strike the crystal per second and each of them liberates an electron, the (mean) value of F will be Q/ldt. The current through the crystal will accordingly be

$$i = Jlt = \mu\tau e \frac{V}{d} \frac{Q}{dlt} lt = \frac{\mu\tau eV}{d^2} Q. \quad . \quad . \quad (4)$$

With electrodes of suitable material, properly connected to the crystal material, electrons will be able to enter the crystal from the cathode and to leave it by way of the anode. It will thus be possible for a current of the above magnitude to flow permanently, and the crystal will constitute a practical photo-resistor. To obtain a high sensitivity, the product $\mu\tau$ (see eq. 4) must have a high value; in addition the distance between the electrodes must be kept small. We see that the lumen sensitivity — i.e. the ratio between i and Q, apart from a constant factor — will be independent of the area of the surface exposed to light. That being so, the lux sensitivity will be exactly proportional to that area. It is also plain that the current will increase in direct proportion to the applied voltage. If the highest possible sensitivity is desired, therefore, the voltage across the crystal should be high.

In deriving (3) it was tacitly assumed that when current flows through the crystal the charges are carried by electrons only. In some substances it is possible for the empty places left by liberated electrons in the ions (or atoms) to move, and so to contribute to the total current flowing. In CdS, however, the mobility of these "holes" is negligibly small compared with that of the electrons. No further assumptions were involved in the derivation of (3). It is therefore valid for all photoconductors in which electron conduction is predominant.

Consider now the magnitude of the current through the crystal as given by (4), measured in electronic charges per second, and compare this rate of flow with the number of electrons (Q) released per second. We see that the former is $\mu\tau V/d^2$ times greater than the rate of release. This "amplification factor" may have values of the order of 10^3 to 10^4. Enigmatic at first sight, the fact that in equilibrium it is possible for more electrons to leave the crystal than are liberated by the incident light becomes understandable when it is realized that there is nothing to stop free electrons entering from the negative electrode. It may therefore happen that an electron released inside the crystal passes round the circuit many times before it is recaptured. In the absence of radiation, however — in other words, when no free electrons have arisen inside the crystal and passed out of it via the anode — it is impossible for a large number of electrons to enter the crystal from the cathode, their passage being impeded by a space-charge effect.

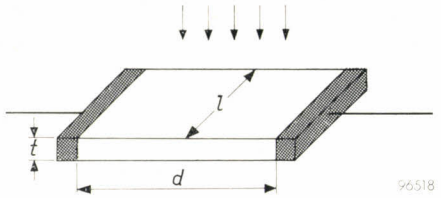

Fig. 1. The diagram represents a slab of photoconductive material fitted with two electrodes a distance d apart. The area exposed to radiation is $l \times d$.

The use of CdS as photoconductive material

Although it has been known for many years that it is possible in a group of CdS crystals to find individuals that exhibit an exceptionally high photosensitivity, the use of the compound for the large-scale production of photo-resistors has only recently become a practical proposition. For example, if a number of CdS single crystals are made by the Frerichs method [5]), large differences are found not only in the shape and dark resistance of individual crystals but also in their photosensitivity, which is considerable in some and poor or even nil in others. It is true that good crystals can be picked out, but the Frerichs method is not suitable for the production of photo-resistor material on a large scale.

During recent years research has been carried out on CdS and related compounds (e.g. cadmium selenide and cadmium telluride) in many quarters, and this has revealed that photoconductivity only occurs in CdS when certain impurities known as activators are present; other impurities act as inhibitors. The activators include the elements Cu, Ag, Cl and Ga [6]). Iron is an inhibitor, and must not be present in concentrations greater than one atom per million Cd atoms. The endeavour must therefore be to make

[5]) R. Frerichs, Phys. Rev. **72**, 594, 1947. In this method cadmium vapour is caused to react at 800 °C to 1000 °C with H_2S in a quartz tube through which a slow stream of H_2S and hydrogen is passed. The vapour is produced by heating metallic cadmium in the "upstream" portion of the tube. The CdS crystals form in the colder, "downstream", portion of the tube.

[6]) Only the first two are essential for the absorption of radiant energy. The usefulness of the other two lies in the fact that they cause the Cu or Ag or both to take up the proper positions in the crystal lattice.

cadmium sulphide crystals in which suitable impurities are present, and to do so by a process that allows the concentrations of the activators to be conveniently controlled. Such a process has now been developed. A precipitate of CdS is first prepared by passing hydrogen sulphide through a solution of a Cd salt. This provides very pure CdS in the form of an extremely fine powder, the size of the grains being 0.1 μ or less. To this powder are added the activators — copper and gallium in the case of the photo-resistors discussed in this article. The powder is then subjected to a temperature between 700 °C and 900 °C. This heat treatment, which lasts several hours, results in the formation of much larger grains (10 to 100 μ), in which the added activating material is uniformly distributed and which exhibit a high degree of photosensitivity.

To produce a homogeneous coherent material from this powder, having a photosensitivity little inferior to that of the grains, the following process has been developed in the Philips Research Laboratories. It proved quite practicable to compress the powder into tablets without using a binder. The filling factor of the compressed powder is approximately 90%, which is a very high figure compared with other substances and which can only be explained by the fact that the grains are to some extent plastic. The pressing operation gives rise to imperfections in the crystal lattice, and these tend to reduce the photosensitivity of the material very considerably. However, unlike the inhibiting impurities, the lattice imperfections can be considerably reduced or modified, this being done by a second heat treatment. Careful consideration must be given to the temperature to which the compressed powder is to be heated, the duration of the treatment, and the atmosphere in which it is carried out. In the course of this treatment the grains coagulate in such a way that finally a material is obtained which is fairly strong mechanically, besides possessing a high degree of photosensitivity. However, it is still possible to recognize the grains in the structure of the material; see *fig. 2*.

Heat treatment enhances the photosensitivity of the material, partly because it largely removes the lattice irregularities and partly because it improves contact between the grains. The dark resistance, which is less dependent on the intergranular contact resistance, is not seriously affected by the heat treatment. Needless to say, the chance of impurities being introduced into the material in the press must be carefully guarded against. The risk of contamination is reduced to a minimum by making the punch and die of suitable material and giving them a particularly fine finish.

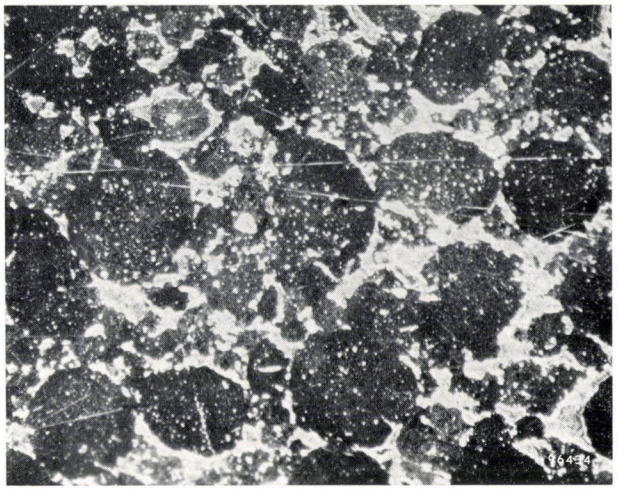

Fig. 2. Cross-section through a piece of compressed and sintered cadmium sulphide. Separate grains can still be discerned. Magnification approx. 150×.

If the properties of the material produced in this manner are compared with those of one in which coherence has been obtained by adding a binder, a striking difference is found in regard to photoconductivity: the effective value of the product $\mu\tau$ is considerably greater for the compressed and sintered material than for the other kind.

Certain further observations may be made with regard to the dosage of the additives. It has been found that there must be a very definite (constant) ratio between the copper and gallium concentrations. Too much Cu reduces the photosensitivity of the material, while a relatively high Ga concentration results in a low dark resistance. The higher the concentrations in which additives are present, the more serious are the effects of departures from the correct proportions. On the other hand it is desirable to add activators in fairly high concentrations so that these may be large in comparison with those of the impurities already present. This is the only way of making sure of getting a product whose properties are reasonably constant. All in all, there is not much freedom with regard to the choice of these concentrations.

The ORP 30 and ORP 90 photo-resistors

Fig. 3 shows two photo-resistors made of compressed and sintered cadmium sulphide. Both consist of a glass envelope (having the sole purpose of protecting the contents) inside which is a plate of photoconductive material 0.8 mm thick; coated on one side are metal film electrodes in the form of two interlocking combs; see *fig. 4*. The use of electrodes of this shape satisfies two conditions for high sensitivity, namely that the sensitive area should be large and the distance between the electrodes small — see formula (4). The "teeth" of the combs are 1 mm apart. The electrodes are formed on the plate by applying a mask to it and depositing upon it a suitable material (Cu, Ag, Al or Au) evaporated in a

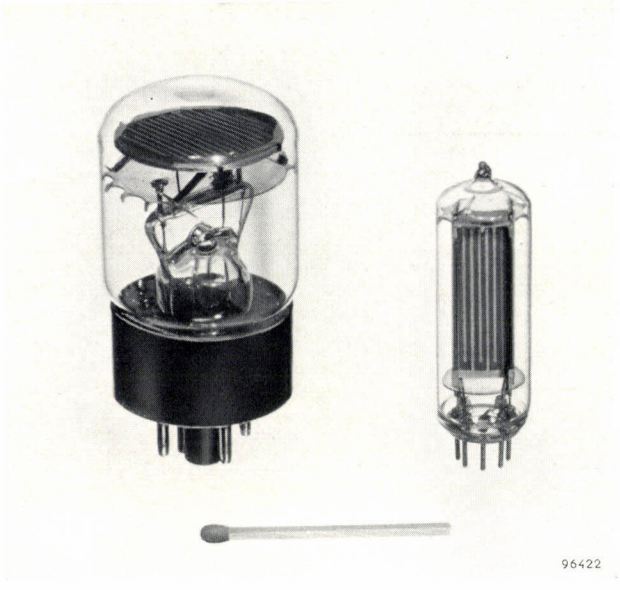

Fig. 3. CdS photo-resistors of type ORP 30 (left) and ORP 90 (right), developed by the Electronic Tubes Division of Philips.

vacuum. As equation (4) shows, the sensitivity of the resistor increases with the voltage across it. The highest voltage permissible is determined by the clearance between the electrodes. It will be noted that in the ORP 90 the CdS plate is mounted parallel to the axis of the tube, whereas the plate in the ORP 30 is perpendicular to the tube axis. The former tube is designed to respond to light striking its side, the latter to light coming from above. The ORP 90 has the same sort of base as a 7-pin miniature tube and is therefore uniform in this respect with the 90 CV and 90 CG photocells.

Measurements have provided the following information about the properties of the sensitive layer in these photo-resistors.

a) *Sensitivity*. The product $\mu\tau$ has been found to have an average value of 0.5 cm^2/V [7]).

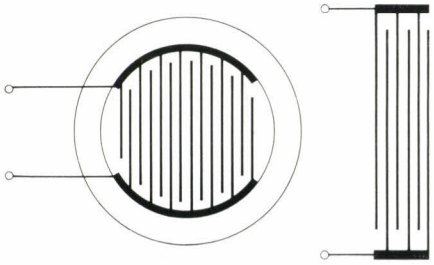

Fig. 4. Diagram showing the shape of the electrodes in the ORP 30 (left) and ORP 90 (right) CdS photo-resistors. This form of electrode makes it possible to combine the advantages of a large area of sensitive surface and a small clearance between the electrodes.

[7]) In single crystals of activated CdS, higher $\mu\tau$ values are found, of the order of 10 cm^2/V; for layers made of powder containing a binder, the highest $\mu\tau$ values are between 0.01 and 0.1 cm^2/V.

b) *Spectral sensitivity* (*fig. 5*). The resistors are sensitive throughout almost the whole of the visible range and a good way into the infra-red band. Their sensitivity peak occurs round about 6800 Å.

c) *Current-voltage relation*. The variation of the current through the resistor with applied voltage is roughly linear. The voltage exponent (see *fig. 6*) is between 1.05 and 1.10, which implies that Ohm's law is approximately obeyed. (This is not so for materials containing a binder, the current through these varying with a voltage exponent between 3 and 4.)

d) *Relation between current and illumination*. This relation is also roughly linear, the exponent being about 0.85 (*fig. 7*).

e) *Effect of temperature*. Temperature has very little effect, as may be seen in *fig. 8*: a rise from 0 °C to 40 °C causes the current to fall off by only 10%. In this respect the performance of cadmium sulphide photo-resistors is particularly good compared with that of other types.

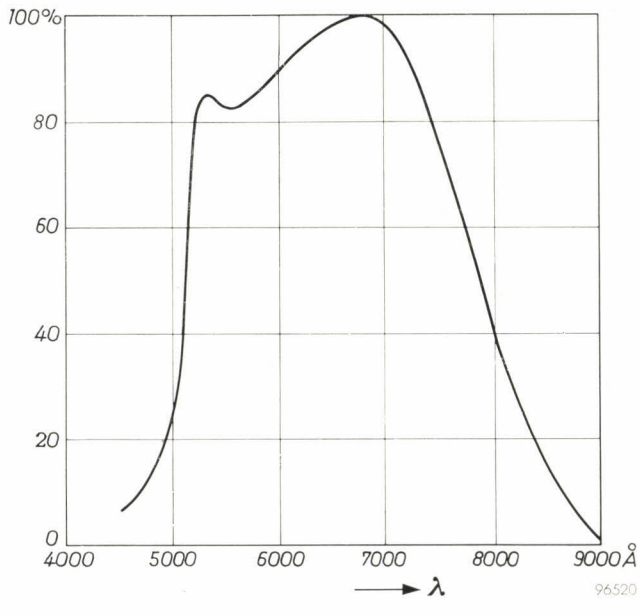

Fig. 5. Spectral sensitivity curve of photo-resistors made of compressed and sintered CdS. This material retains its high sensitivity well into the infra-red. The sensitivity peak occurs in the red part of the spectrum.

f) *Speed of response* (*fig. 9*). The photo-resistors are unable to follow rapid changes in the intensity of illumination. However, the more intense the illumination, the more quickly they react. After the tube has been exposed to 100 lux, the current decays to half-strength within 5 milliseconds; but after exposure to 0.1 lux, the current takes 0.25 s to decay to its half-value.

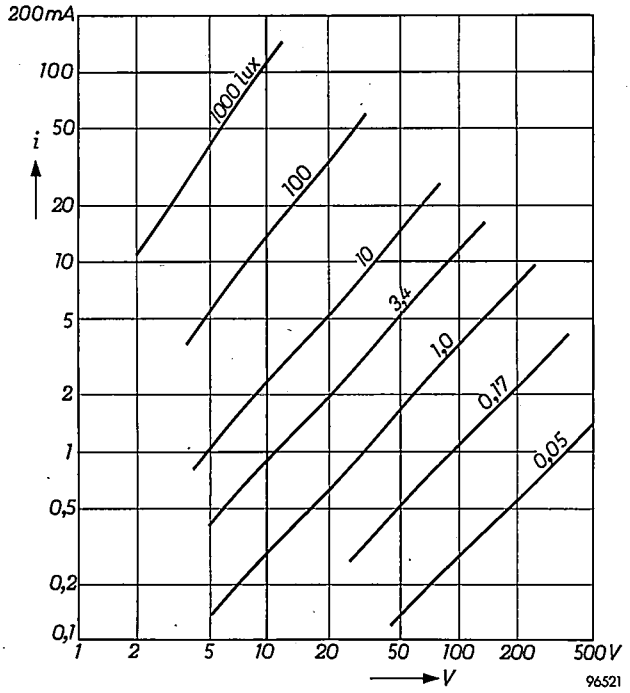

Fig. 6. Curves of current i versus voltage V, as obtained from measurements carried out on an ORP 90 photo-resistor exposed to various intensities of illumination. The current-voltage relation can be expressed by $i = \text{const.} \times V^{\alpha}$, i.e. the relation between $\log i$ and $\log V$ is linear. Since the value of α is close to unity (about the same for all the curves), the relation between i and V is practically linear, in other words pressed and sintered CdS roughly obeys Ohm's law (at a given illumination).

g) *Dark resistance.* The resistance of the ORP 30 in the dark exceeds 10^7 Ω, that of the ORP 90 exceeds 10^8 Ω.

A number of characteristic quantities relating to the new photo-resistors are summarized in *Table I*, to enable the properties of these devices to be conveniently compared with those of other types. Sensitivity is indicated both in amperes per lumen (S) and in amperes per lux (H). As already pointed out, the ratio between the two sensitivity values is equal to the area (A) of the sensitive surface.

Inserting the above-mentioned value of 0.5 cm²/V for $\mu\tau$, 2×10^{16} for the number of quanta absorbed per lumen, and 1.6×10^{-19} coulomb for the charge on the electron, we obtain the following sensitivity values for CdS resistors:

$$S = 1.6\times10^{-3}\,\frac{V}{d^2}\ \text{ampere/lumen} \quad . \quad . \quad . \quad (5)$$

and

$$H = 1.6\times10^{-7}\,\frac{AV}{d^2}\ \text{ampere/lux}. \quad . \quad . \quad . \quad (6)$$

In the above formulae V is expressed in volts, d in cm and A in cm².

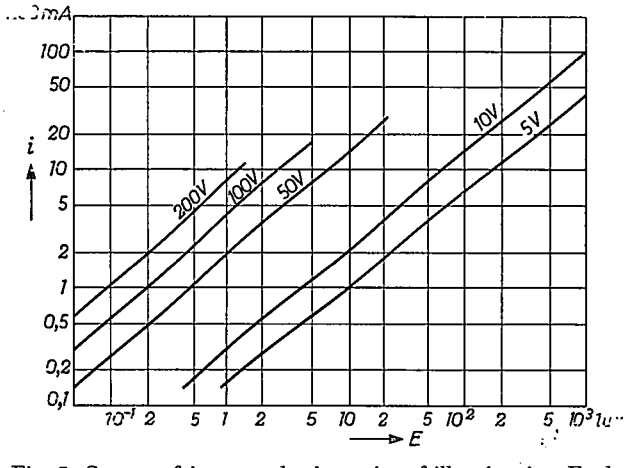

Fig. 7. Curves of i versus the intensity of illumination E, obtained from measurements carried out on the ORP 90 with various voltages applied to the cell. This relation too is an exponential function with a power close to unity; that is to say, i is roughly proportional to the illumination as well as to the applied voltage.

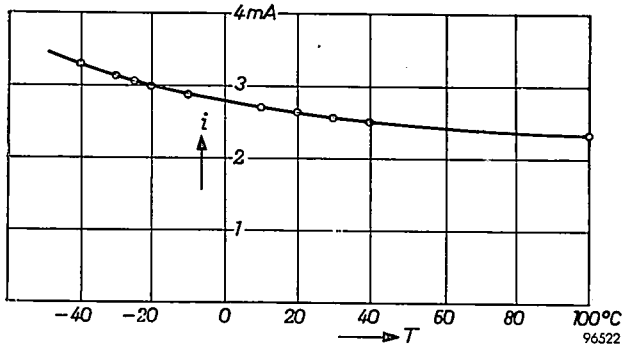

Fig. 8. The photoconductivity of resistors made of compressed and sintered CdS is but little dependent on temperature. The graph shows how the current i through an ORP 90 cell varies with the temperature T, for an illumination of 10 lux and a voltage across the cell of 10 V.

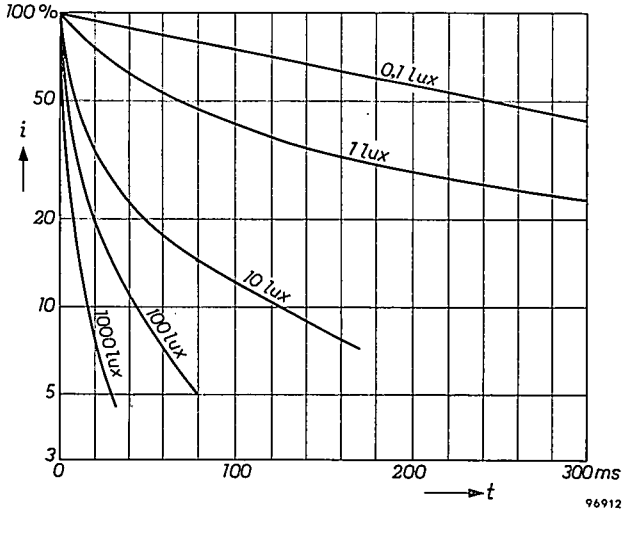

Fig. 9. Some idea of the inertia of CdS photo-resistors may be obtained by measuring how the current (i) changes with time (t) subsequent to removal of the incident light. The shape of the decay curve is found to depend on the intensity of illumination to which the cell was exposed immediately before. When the prior illumination was very intense, the current falls off very quickly to a small proportion of its original value; the decay is much slower where the intensity was low.

Table I. Comparison between the properties of various photosensitive devices. The sensitivity values express the response to radiation from a tungsten-ribbon lamp with a colour temperature of 2800 °C. The last four columns indicate respectively: N the number of quanta absorbed per lumen, I_{max} the highest permissible value of the current, Q_{max} the highest permissible power and f_{max} the highest frequency of fluctuations in the intensity of illumination to which the device can respond.

Type of cell or resistor	S (A/lumen)	A (cm^2)	H (10^{-4} A/lux)	N (10^{16} qu/lumen)	I_{max}	Q_{max}	f_{max}
90 AV: vacuum-type photocell	0.00005	4	0.0002	1	10 μA	—	100 Mc/s
90 AG: gas-filled photocell	0.00013	4	0.0005	1	10 μA	—	10 kc/s
50 AVP: photomultiplier	500	8	4000	1	100 mA	—	100 Mc/s
Selenium photo-voltaic cell	0.0005	10	0.005	1	—	50 μW/lumen	2 kc/s
OAP 12: photo-diode	0.05	0.01	0.0005	20	—	0.12 W	50 kc/s
OCP 71: photo-transistor	0.3	0.07	0.02	20	—	0.10 W	750 kc/s
ORP 30: CdS photo-resistor (at 100 V)	16	2.5	40	2	—	1.2 W	3 c/s for 30 lux 1 c/s for 4 lux

Applications of CdS photo-resistors

Vacuum and gas-filled photocells can usefully be replaced by CdS photo-resistors in any application where sensitivity is important but speed of response is less so. The great advantage of CdS photo-resistors in such applications is that they can be connected directly to a relay; amplifiers and thyratrons are not required. The resulting simplifications in circuitry are considerable.

These applications of the CdS photo-resistor are not new in principle, but there is a further group of applications of the device in which it cannot be replaced by vacuum or other types of photocell. We shall now go on to discuss one or two examples from each of these groups.

An example of the first group of applications is flame monitoring in automatic oil-heating installations, for which purpose type ORP 90 is generally used. The flame is "seen" by a photocell that is usually located in the air intake duct. The oil is ignited electrically, by a spark igniter of one kind or another. If the oil has not ignited by a certain time after the oil cock has been opened and the igniter excited, the monitoring system automatically cuts off the oil supply and causes an alarm signal to be given. If, on the other hand, ignition takes place promptly, after a brief delay the monitoring system switches off the ignition arrangement. If the flame should go out the oil supply is again cut off and an alarm signal given.

The "crackle-free potentiometer" is an entirely new application. Most potentiometers in common use are resistors with a movable tapping, and the changes in output voltage resulting from movement of the sliding contact are not completely continuous. Consequently crackling arises while the slide is in motion. Such phenomena may be objectionable in certain kinds of electronic equipment — in particular, in measuring instruments, amplifiers and radio and television receivers. A crackle-free potentiometer circuit can be made by putting a fixed resistor in series with a CdS photo-resistor. Changes in the luminous flux incident on the photo-resistor cause its resistance and hence the voltage across its electrodes to change (*fig. 10*). The luminous flux can be

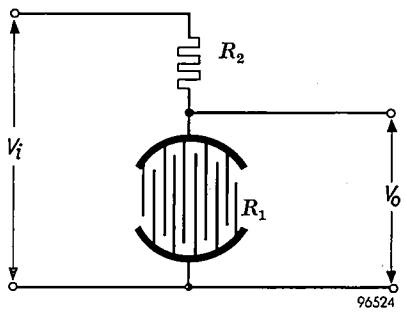

Fig. 10. Crackle-free potentiometer circuit, consisting of a fixed resistor R_2 and a photo-resistor R_1. An increase in the illumination causes a decrease in the resistance of R_1, and hence in the voltage V_o tapped off across R_1. If a resistor of about 2 MΩ be used for R_2, the potentiometer is suitable as a volume control in a radio receiver.

altered by changing the current flowing through the filament of an incandescent lamp; the thermal inertia of the filament precludes abrupt changes in the light emission, so that no crackling arises [8]). A crackle-free potentiometer satisfying the requirements of the volume control in an ordinary radio receiver can be obtained by combining a CdS photo-resistor, which must have a dark resistance

[8]) Alternatively, the intensity of illumination can be regulated mechanically, for example by moving or turning one of two diaphragms mounted close together. If the intensity of illumination is required to increase logarithmically as a function of the angle turned through, say, by a factor of 10 000, the diaphragm will have to have a special shape. Such an arrangement will be crackle-free provided the mechanical finish of the diaphragms is good.

of at least 10 MΩ, with a fixed resistor having a value of about 2 MΩ. While the photo-resistor is not exposed to light, the voltage tapped off is 10/12ths or a good 80% of the voltage across both resistors. Exposed to an illumination of 10 000 lux, the photo-resistor only offers a resistance of about 200 Ω, so interference from other light in the vicinity. Over part of its range, the output voltage of the simple potentiometer shown in fig. 10 increases exponentially with the resistance of the control rheostat in the lamp circuit (*fig. 12*).

By making CdS photo-resistors with more than two

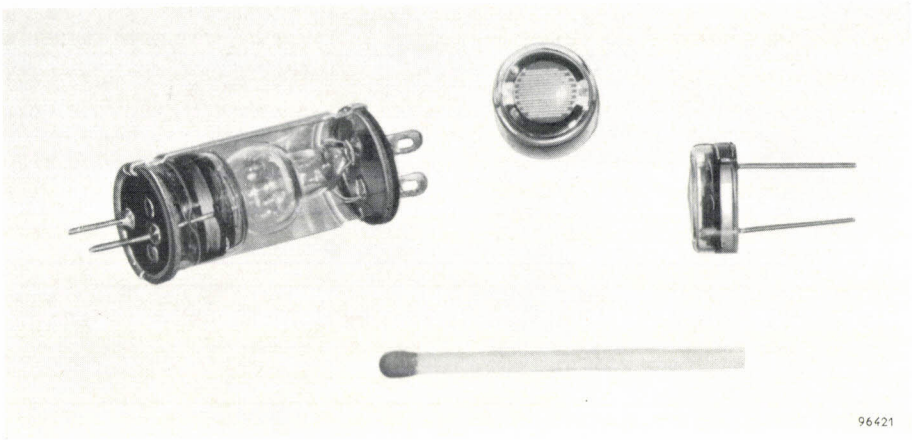

Fig. 11. If the illumination of a CdS photo-resistor forming part of a crackle-free potentiometer is to be controlled by varying the current flowing through an electric bulb, it is worth while to combine photo-resistor and bulb in one unit enclosed in a light-tight envelope. The photograph shows a device of this kind (the envelope has been partly cut away) developed by the Industrial Components and Materials Division of Philips. Two views of the CdS photo-resistor used in this device are also shown. Provided it is run at the rated voltage of 6.3 V, the bulb has a very long life.

that the tapped voltage now falls to 1/10 000 of the supplied voltage. It is therefore possible for the voltage tapped by the potentiometer to vary by a factor of nearly 10 000, although the overall resistance of the potentiometer never falls below 2 MΩ.

The relation between the current and voltage in photo-resistors made of compressed and sintered CdS is almost linear (fig. 6), i.e. these devices roughly obey Ohm's law; hence their resistance is practically independent of the applied voltage, and the distortion introduced by the photo-resistor potentiometer as in fig. 10 is only very slight. The distortion is not more than 0.2% for an output voltage of 0.2 V. Since the volume control of a radio receiver is located at the *input* of the audio-frequency amplifier, the output voltage does not in practice attain this value and the amount of distortion arising in the volume control is therefore negligible. If the CdS photo-resistor in the circuit of fig. 10 were replaced by some other cell not obeying Ohm's law, the resulting circuit would be crackle-free, it is true, but quite useless for a radio receiver.

Fig. 11 shows a device in which a small CdS photo-resistor is combined with a miniature electric lamp to form a unit ideally suited to radio and television sets. It is enclosed in a light-tight tube to obviate

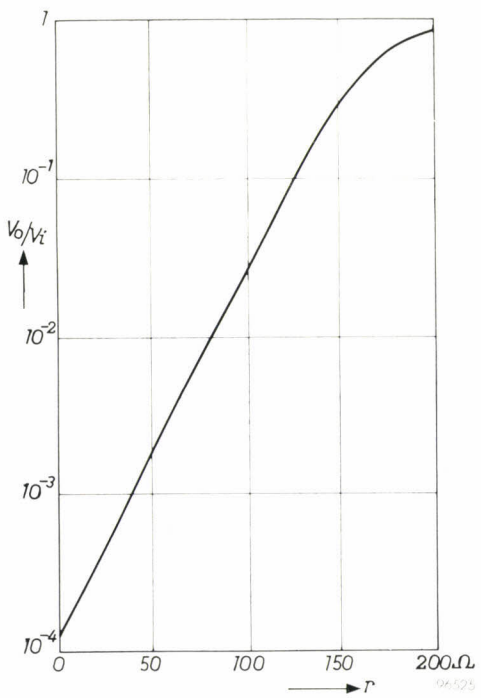

Fig. 12. The tapped voltage V_o (expressed as a fraction of the total voltage V_i) of a crackle-free potentiometer (CdS photo-resistor as in fig. 11 plus 2 MΩ fixed resistor) as a function of r, the resistance of the control rheostat in the circuit supplying the electric bulb. In the range where the tapped voltage is 10% of the total voltage or less, the relation between V_o/V_i and r is logarithmic. The lamp supply voltage was 6.3 V.

N.V. PHILIPS' GLOEILAMPENFABRIEKEN

electrodes it is possible to design circuits to give so-called *physiological volume control* [9]). When its output voltage is small, a volume control of this kind attenuates low-frequency sounds to a less extent than high-frequency ones, the purpose served

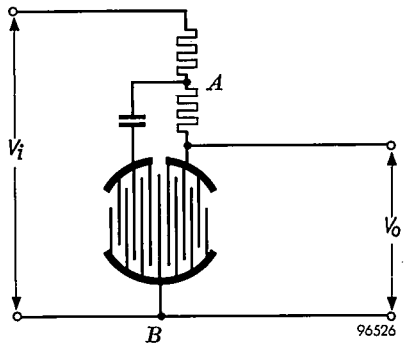

Fig. 13. Illustrating the principle of a "physiological" volume control embodying a photoconductive cell. The cell used in this circuit must have more than two electrodes (in this case it has three). As the intensity of illumination increases, the output voltage for low frequencies falls off less sharply than that for high frequencies.

being to stop the former becoming inaudible before the latter do as the output voltage is decreased. The principle of the circuit is shown in *fig. 13*. When the two variable resistors (the two parts of the photo-resistor) have a high resistance, the branch containing the capacitor plays little part, the other branch exercising the main control function. When the variable resistors have a low resistance (because strong light is falling on the photocell), the *A-B* section of the potentiometer, owing to the presence of the capacitor, offers considerably more impedance to low frequencies than to high; in other words the output voltage — at a given illumination a constant

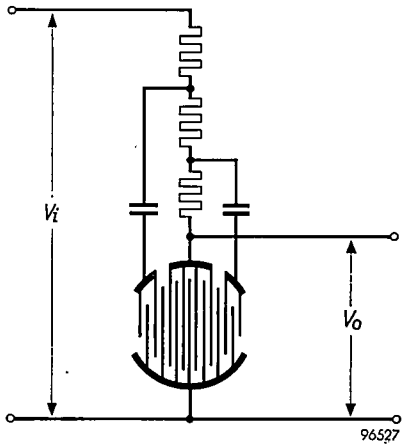

Fig. 14. Practical form of "physiological" volume control. The photo-resistor used here has four electrodes.

[9]) A brief account of a type of circuit normally used for this purpose (embodying a carbon potentiometer) is given in Philips tech. Rev. **19**, 47, 1957/58, and is shown on the extreme left of fig. 8, on page 46.

proportion, independent of frequency, of the voltage between *A* and *B* — represents a higher proportion of the input voltage for low frequencies than it does for high. The circuit of fig. 13 does not produce the desired effect to a sufficiently pronounced degree: the ratio of the output voltages for 100 and 1000 c/s is not greater than 3 or 4, whereas the ratio required is 10 to 20. In practice, therefore, a rather more complicated circuit is used; see *fig. 14*. Its frequency characteristics are given in *fig. 15*.

It might well be asked whether difficulties may not arise from the use of alternating current for supplying the lamp. The luminous flux may be expected to show some fluctuation (at double the mains frequency) and the voltage from the output of the photo-resistor potentiometer will exhibit

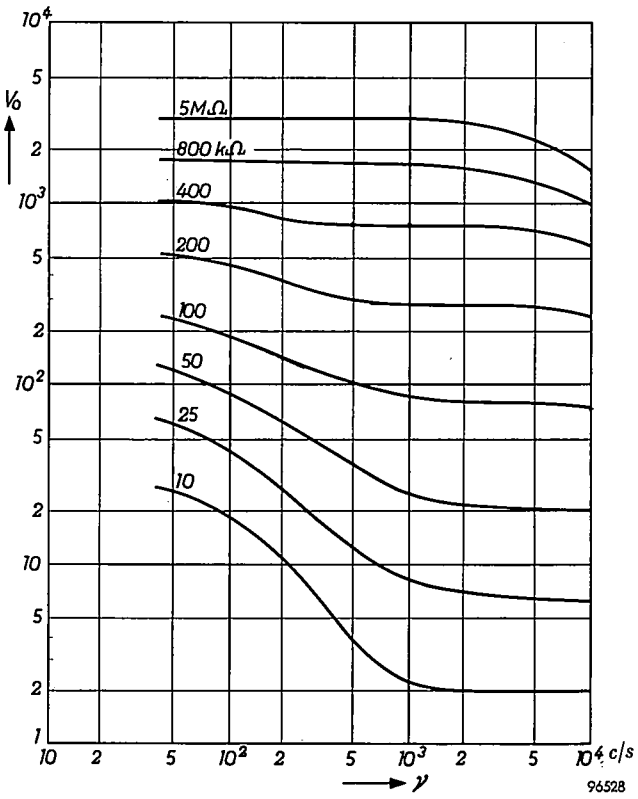

Fig. 15. Frequency characteristics of the circuit of fig. 14, each curve being appropriate to a different value of photocell resistance. When the resistance of the cell is high, the output voltage (V_o) is more or less independent of frequency over the range 50 c/s to 5000 c/s; when the cell resistance is low, V_o is almost 10 times as high for 50 c/s as for 1000 c/s.

corresponding amplitude variations. It has been found that the 100 c/s modulation of the sound signal is inaudible provided its depth does not exceed 3%. The results of measurements are given in *fig. 16* and from these it is clear that, for the normal resistance values of the photo-resistor shown in fig. 14, the modulation depth will be very much less than 3%

(being 0.1% at 150 kΩ and 0.3% at 50 kΩ). Ordinarily, therefore, the ripple is quite inaudible. Only when the resistance of the cell (and thus the voltage across it) is very low, is the 3% limit slightly exceeded.

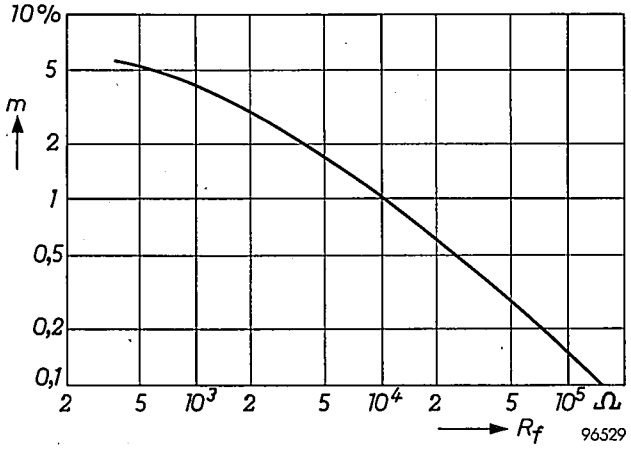

Fig. 16. Supplying the lamp in the circuit of fig. 14 with alternating current gives rise to modulation having twice the mains frequency; the depth m of this modulation decreases as the cell resistance R_f increases. The modulation remains inaudible ($m < 3\%$) so long as the cell resistance exceeds 2000 Ω, as it normally does.

We have already seen that the conductivity of the resistor does not immediately drop to its minimum value when the incident light is removed (fig. 9), that is to say, the conductivity does not alter instantaneously in response to changes in illumination. Consequently a certain inertia is associated with the operation of a volume control of the kind described above. However, the response is quite fast enough for the purposes of a volume control.

Potentiometers embodying CdS resistors have advantages over and above freedom from crackle. There is no need for the control rheostat to be mounted in the immediate vicinity of the photo-resistor plus lamp, and each can therefore be given whatever location is most convenient. In the case of a volume control for an ordinary wireless set, the potentiometer unit can be placed close to the detector diode [10]), while the control rheostat is given a position such that it is within easy reach of the listener. One can even go so far as to enclose the rheostat in a separate box connected to the set by a few yards of cable — a simple way of providing remote control.

Between the CdS photo-conductor and the filament of the bulb there is no electrical contact whatsoever, and this form of remote control can therefore be employed in equipment in which the CdS resistor is in a high-potential part of a circuit; the control circuit can be kept at earth potential by supplying the bulb from a separate transformer or transformer winding.

Remote control with the aid of a CdS photo-resistor is suitable for all kinds of other applications. Amongst these mention may be made of the adjustment of brightness and contrast in television receivers and the control of volume in stereophonic sound reproduction.

A third application of the CdS photo-resistor is in a simple circuit for stabilizing an alternating voltage. The secondary of the transformer in this circuit (*fig. 17*) supplies both a potentiometer chain, of which a CdS photo-resistor forms part, and a small lamp that shines on the photo-resistor. If the voltage across the secondary should rise on account of an increase in the input voltage, the bulb will shine more brightly, so lowering the resistance of the CdS photo-resistor and reducing the proportion of the secondary voltage that appears at the output. With suitable resistance values, increases in the secondary voltage can be exactly compensated by the decrease in the output voltage, so that over a large range the latter is independent of the input. No current can however be taken from the output of this stabilized voltage supply.

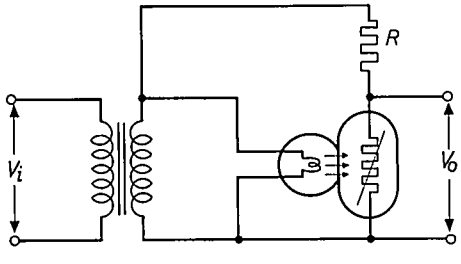

V_i	V_o
260V	2,51V
220V	2,50V
170V	2,51V
130V	2,51V
120V	2,49V
80V	2,15V

Fig. 17. Circuit incorporating a photo-resistor for stabilizing an alternating voltage. Over a large range of input voltages (V_i) the output voltage (V_o) hardly varies at all when no current is taken.

In conclusion we shall name one or two other possible applications, some of which are not new, it is true, except in the sense that the embodiment of a CdS photo-resistor simplifies the circuitry. Because the cells exhibit maximum sensitivity to red light, and are sensitive to infra-red with wavelengths up to 0.9 μ, they are particularly suitable for employment in fire-alarm systems. They can also be employed for the detection of smoke, for switching street lighting on and off automatically, for dimming the headlamps of cars automatically (the photo-resistor only needs a low voltage such as that already available in a car), for automatically adapting the contrast and brightness of a television image to the

[10]) With regard to the use of a diode as detector, and the associated volume-control arrangement, see for example M. Mandl, Handbook of basic circuits, Macmillan, New York 1956, A3 and A5, or F. E. Terman, Radio Engineers Handbook, McGraw-Hill, New York 1943, page 641.

room lighting level — here advantage is taken of the fact that the current through the cell is proportional to the illumination — and so on. We may add that, in those applications where some system or other has to be switched on or off, it is not always necessary to have the photo-resistor controlling a relay; in some cases the cell itself can be used as a switch.

To sum up, it may be said that CdS photo-resistors have already found application in many fields and that the future will prove their usefulness in many others, this in virtue of their great sensitivity to light, their low supply voltage, their high load capacity and their insensitivity to temperature changes.

Summary. Cadmium sulphide photo-resistors, highly sensitive to light, can now be manufactured on an industrial scale. The basic material is very pure powdered CdS (grain size 0.1 μ); to this certain substances containing copper and gallium are added, the mixture being subjected to a heat treatment. The result is a coarse powder made up of grains measuring 10 to 100 μ, in which the additives are now uniformly distributed; this is compressed into plates of the desired shape. Lattice defects created by the pressing process (and which reduce the photosensitivity of the substance) are largely removed or modified in a second heat treatment, which causes the grains to cohere. Photo-resistors made of this material have a sensitivity (A/lux) approaching that of the photomultiplier, far exceeding that of other types of photocell, and varying little with temperature. CdS photo-resistors can be used to operate relays directly. The potential applications of the device are legion. Established applications include flame monitoring and the construction of crackle-free potentiometers which can be remote-controlled.

AUTOMATIC RECORDING OF LUMINOUS INTENSITY DIAGRAMS

621.317.39-52:535.247.4

The purpose of the instrument described here is to automatically record the luminance pattern of beamed light sources.

The luminance pattern is formed of contours of equal luminous intensity, known as isocandela curves, drawn on graph paper. In principle, the curves are obtained in the following manner.

The light source to be measured is mounted in such a way that it can be turned about two axes at right angles to each other; the angles through which it turns on these axes (its azimuth and elevation, for example) serve as coordinates to define the alignment of the lamp. A calibrated photocell is fixed a suitable distance away from the light source. As the latter turns, therefore, the photocell scans through all directions in the cone of light emitted. A certain value of the luminous intensity is now chosen. When the source points in a direction such that the illumination of the photocell corresponds precisely to the chosen luminous-intensity value, the coordinates defining the alignment of the source will then determine one point on the relevant isocandela curve. Other points on the same curve are found by turning the source on its two axes such that the illumination of the photocell remains constant.

The procedure normally employed hitherto consists in finding, by trial and error, a sufficient number of such points for each luminous-intensity value to allow the appropriate isocandela curve

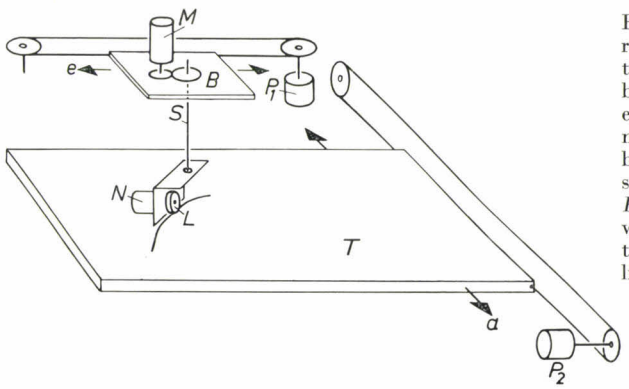

96657

Fig. 1. Diagram and photograph of the recorder portion of the instrument. T is the recording table and B the carriage, both being free to move at right angles to each other on guide-rails. T and B are moved by the wheel L, which is driven by a small motor N. Servo-motor M steers L via rod S. Potentiometers P_2 and P_1 control separate positional servos which communicate the displacement of table and carriage to the mounting of the light source under measurement.

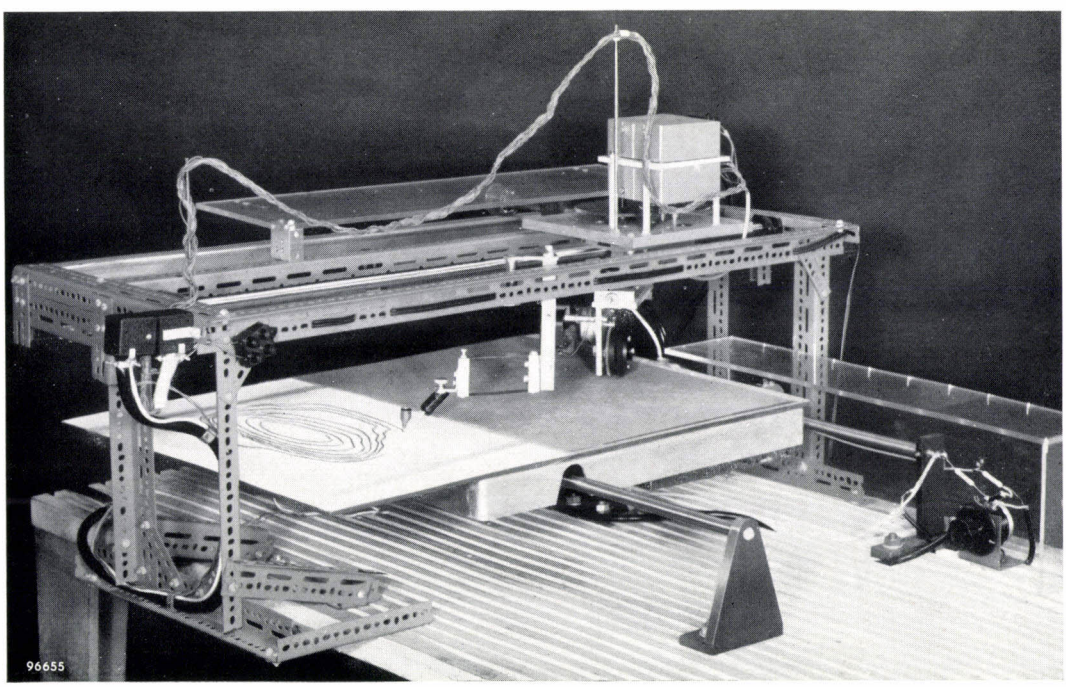

96655

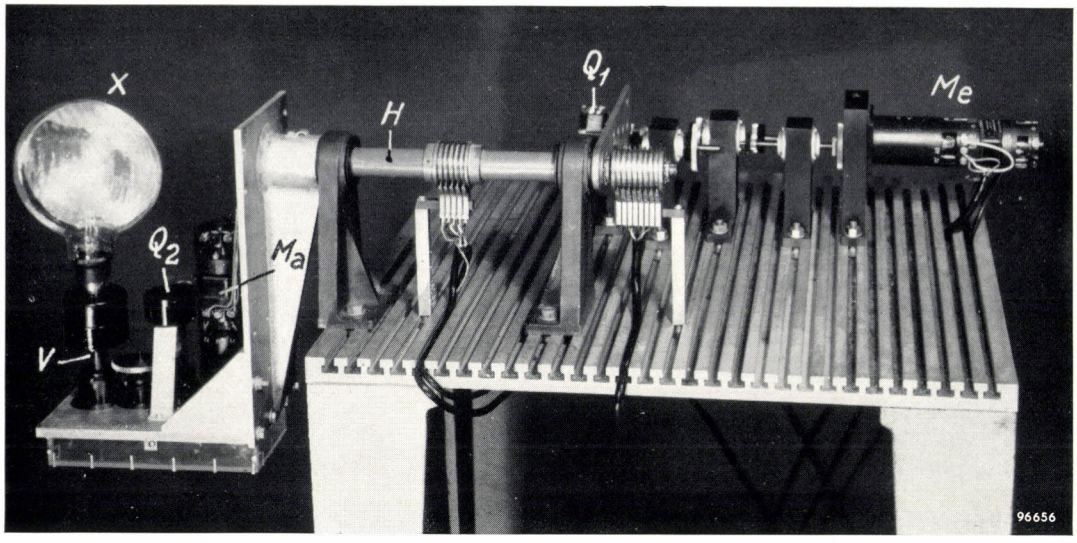

Fig. 2. Light-source holder and actuating mechanism. Servo-motors M_a and M_e turn the source about the vertical shaft V and the horizontal shaft H respectively. M_a and M_e are controlled by P_2 and P_1 (shown in fig. 1) by means of the balancing potentiometers Q_2 and Q_1 respectively.

to be drawn manually with reasonable accuracy. This is clearly a time-consuming business, particularly if the number of curves required is large; moreover, a curve drawn thus will only coincide exactly with the true isocandela curve at the points actually measured.

The isocandela-diagram recorder developed in the Philips Research Laboratories for the Photometric Laboratory of our lamp factories is open to neither of these disadvantages. In this instrument the light source moves *automatically* and in such a way that, within a specified margin of error, the illumination of the photocell always remains at the same, pre-set value. Briefly, the design and functioning of the instrument are as follows.

The current from the photocell is compared with a reference current, the resulting difference signal being used to control a servo-motor (M in *fig. 1*). In the absence of a difference signal, i.e. when the intensity of illumination of the photocell has the pre-set value, the servo-motor remains unenergized. When the illumination is too high, the shaft of the motor turns in one sense; when it is too low, the shaft turns in the opposite direction. The rotation of the shaft is transmitted via a reduction gear to steering rod S. This carries a holder in which are suspended a drive wheel L and its motor N. Both the recording table T and the servo-motor carriage B can move freely at right angles to each other on guide-rails. They are moved by the drive wheel as a result of the friction between the latter and the recording table. Each movement is communicated to the mounting of the light source under measurement by positional servo systems (here in the form of slide-wire potentiometers controlling servo-motors). The two shafts about which the light source turns are driven by the servo-motors (M_a and M_e in *fig. 2*) of the two servo systems. At any instant, therefore, the light source is always pointed in a direction (azimuth and elevation) corresponding to the position of table and carriage.

For the purpose of tracing an isocandela curve the drive-wheel motor N is supplied with a constant current, with the result that the drive wheel has a constant peripheral velocity. This velocity resolves itself into movements of carriage B and registration table T, each running along its respective guide-rails. If at any instant the intensity of illumination on the photocell has the pre-set value, no current passes through the servo-motor that actuates steering rod S; in consequence of this the path of the drive wheel is straight with respect to the table — that is to say, table and carriage move in such a way that the wheel traces a straight line on the table. The movements of carriage and table alter the alignment of the light source, and if as a result of this the intensity of illumination of the photocell undergoes a change, then the drive wheel ceases to run straight; at any given instant, the current flowing through servo-motor M has a value such that the steering rod and drive wheel are turned to left or right in accordance with the shape of the isocandela curve being determined. The intensity of illumination of the photocell is thereby restored to its original value, and in virtue of this continuous correction the steering rod is always "on course". A stylus fixed to the servo-motor carriage maps out the curve on graph paper fixed on the recording table. (Since all points on the

carriage generate curves of identical size and shape with respect to the table except for a constant displacement, it is possible to fix the stylus to any convenient point on the carriage.)

A set of isocandela curves obtained in this manner appears in *fig. 3*. As will be clear from the above description and from this example, it is possible with the new instrument to trace curves forming closed loops — the luminance curves of beamed light sources are almost all of this form. The use of the instrument represents a very great saving of time compared with plotting and drawing the curves by hand.

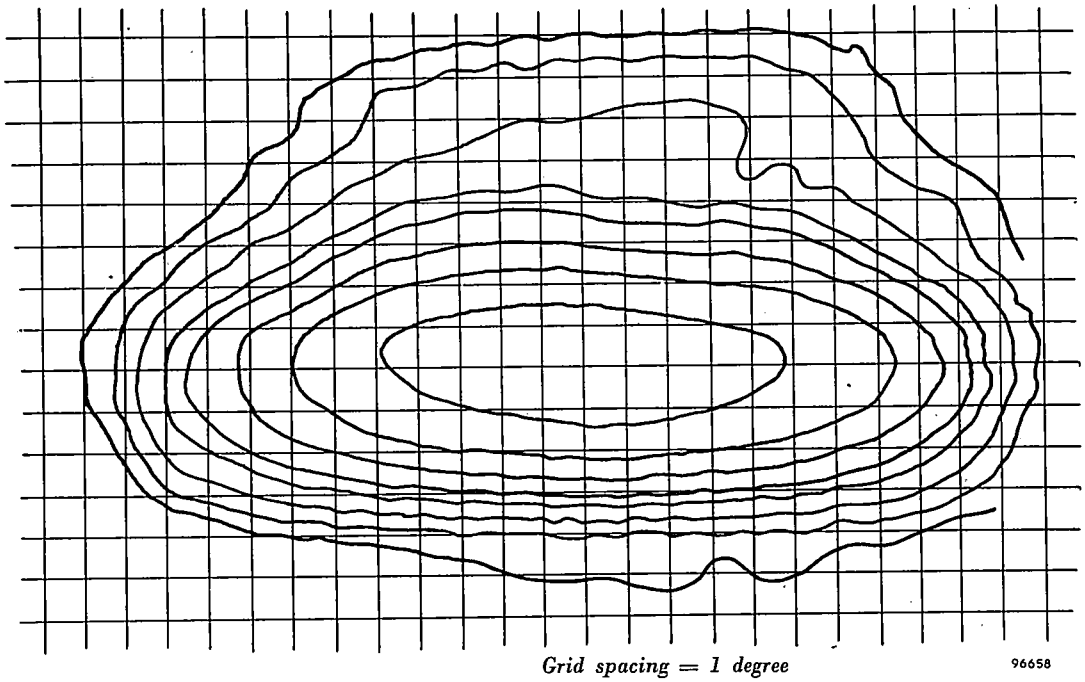

Fig. 3. Isocandela curves recorded by the instrument described in the text. The curves refer to the lamp — a projector for airfield beaconing — shown in the holder in fig. 2.

In passing, it may be observed that, combined with suitable measuring and scanning apparatus, the recorder portion of the apparatus (the part in fig. 1) can be used for the automatic tracing of all kinds of other "iso" curves, such as the curves of equal potential in an electrolytic-tank model, for example.

The designing of the instrument involved various interesting problems mainly concerned with stability of the movement. Inspection of the differential equation describing the behaviour of the system shows that from the viewpoint of stability the point of contact of the drive wheel L should not, as might be supposed, be placed directly in line with steering rod S (see fig. 1); instead, it should have a small off-set d from the axis of rod S. Good results are obtained by satisfying the condition

$$\frac{d}{v} \approx \sqrt{kv},$$

in which v is the constant peripheral velocity of the drive wheel, referred to above, and k is a coefficient related to the loop gain of the servo system. This condition and a number of constructional details will be discussed at greater length in a fuller description of the instrument that will appear in these pages in due course.

W. BÄHLER.

DISTANT-FOCUS X-RAY TUBES

by A. H. G. KUNTKE *).

621.386.1:537.533.3

There exists a comprehensive literature of theoretical and experimental investigations concerning the focusing of the electron beam in cathode-ray tubes, but little has yet been published on the analogous problem in X-ray tubes. The article below is a contribution to this subject. It describes a development the results of which have been applied for some years now by C. H. F. Müller A.G. and by Philips. Although this development refers to a special case, the considerations discussed here are perhaps of more general interest.

The focusing problem in cathode-ray tubes and X-ray tubes

X-ray images being shadow images, the smallest possible source of radiation and the most uniform possible brightness are necessary to produce sharp definition. The electrons emitted by the cathode in an X-ray tube, and which, upon striking the anode, give up their energy largely in heat and partly in the generation of X-rays, must therefore converge on the anode to a focus of a certain specified size. Upon arrival at this focus the electrons should be as uniformly distributed as possible. (Their density may, however, permissibly be somewhat greater at the edges, where the heat is more readily dissipated; otherwise, with an entirely uniform electron distribution, all parts of the anode material would not reach the rated maximum temperature.)

The problem of focusing an electron beam is more familiar in connection with cathode-ray tubes. In such tubes the electrons are accelerated by a constant voltage. Focusing problems arise because of the long trajectories which the electrons must describe before impinging on the fluorescent screen, and because the beam current is variable. In addition, there is the deflection of the beam to consider. To obtain the required narrow beam in these tubes, use is made of systems with auxiliary electrodes operated at different potential, some adjustable [1]); in some cases, too, focusing magnetic fields are used [2]).

With an X-ray tube it is necessary — without affecting the size of the focus — to be able to vary not only the beam current but also, as a rule, the accelerating voltage. For example, the current in diagnostic tubes must be capable of being varied by a factor of 500 and the voltage by a factor of 5. Normally, however, the electrons in X-ray tubes have only a short distance to travel from cathode to target, e.g. 10 to 20 mm, or, in the case of tubes operated at 200 or 300 kV, up to 50 or 100 mm. For normal X-ray tubes, therefore, a much simpler focusing system suffices than for cathode-ray tubes: the focusing system consists merely of a metal cathode block provided on the side facing the anode with a round, cup-shaped or oblong recess. Fitted inside this recess is an appropriately shaped filament, electrically connected with the cathode block. The cathode block and the anode constitute an electron-optical system of only two electrodes (*fig. 1*), the focusing properties of which are determined mainly by the shape of the cathode assembly. In practice, such a system is very desirable, since the voltages for the X-ray tube, which is enclosed in an earthed shield, have to be led in through high-tension cables, and a two-electrode system requires the fewest cables.

There is another reason why a two-electrode system is unsuitable for television picture-tubes and other cathode-ray tubes, namely the necessity for inertialess control of the beam current, with the accelerating voltage kept constant. For this purpose an extra electrode is used in the form of a circular or cylindrical diaphragm, to which a control voltage is applied for modulating the beam current. In general, then, only a fraction of the available electron emission is used; the filament operates in the space-charge region. In the case of X-ray tubes, inertialess control of the tube current is not necessary; on the other hand not merely the current but the voltage, too, must be capable of adjustment, and both independently of each other. For this reason the cathode in X-ray tubes is generally operated at saturation emission [3]). The current is

*) C. H. F. Müller A.G., Hamburg.

[1]) For one of the most recent developments in this field, see J. C. Francken, J. de Gier and W. F. Nienhuis, A pentode gun for television picture-tubes, Philips tech. Rev. **18**, 73-81, 1956/57.

[2]) See e.g. J. A. Verhoef, The focusing of television picture-tubes with ferroxdure magnets, Philips tech. Rev. **15**, 214-220, 1953/54.

[3]) Exceptions to this are certain small, special equipments for which control of the voltage is deemed unnecessary; see e.g. Philips tech. Rev. **6**, 229, 1941, and **10**, 224 et seq., 1948/49. It should be noted that variation of the current by means of a control voltage slightly alters the position of the beam cross-over and hence the size of the focus.

then adjusted to the required value by regulating the cathode temperature (filament current control).

In the case of certain types of X-ray tube used for therapeutic purposes and for the industrial examination of materials, the situation is somewhat different from that in normal X-ray tubes in that the electrons do *not* describe such short trajectories as described above. The focus in their case is formed at the end of a long, hollow rod, which can be introduced into body cavities for irradiating deep-seated lesions, or into boilers, pipes, etc. for taking radiographs of not readily accessible parts. In such X-ray tubes the electrons must travel through the hollow rod as a narrow beam, in some cases a distance of 700 mm or more. Good focusing is necessary here not only to obtain sharply defined shadow images and to make efficient use of the tube output, but also to prevent the undesirable generation of heat and X-rays at places such as the rod wall and the diaphragms.

Where such long trajectories are required of the electrons, the simple two-electrode system does not seem at first sight very promising. In the past magnetic means of focusing have therefore been resorted to in certain special cases [4]) and also for series-produced X-ray tubes with "rod anodes". Use was made of small permanent magnets or a focusing coil, which were slid over the rod anode and acted as a lens for converging the divergent electron beam. Any variation in tube voltage then calls for an adjustment of the magnetic field, i.e. of the magnetic lens, in order to keep the beam properly focused, and this is an undesirable complication. The difficulty is aggravated if the tube operates on a pulsating voltage, since the magnetic field must also be pulsated in the correct phase.

If we look more closely into the electron optics of the two-electrode system, however, we find that it is certainly possible (within certain limits, of course) to produce long and narrow electron beams with this system. We shall briefly review here the considerations that have led to this conclusion, and describe a number of X-ray tubes whose design, completed some years ago, is based on the principles evolved [5]).

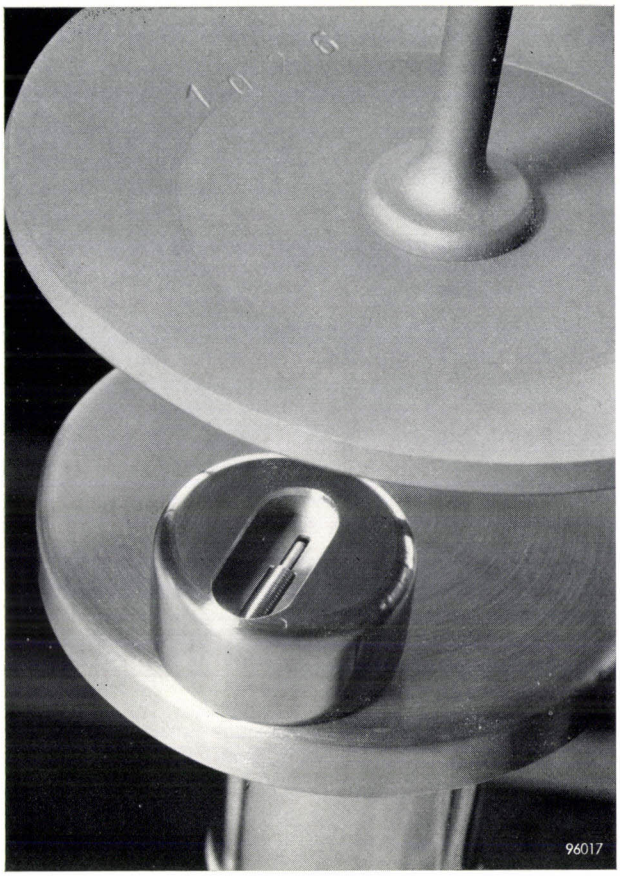

Fig. 1. Electrode system of an X-ray tube with rotating anode (the tungsten disc in the upper part of the photograph) and a double focus. This is a simple two-electrode system. The cathode here has two separate cylindrical filaments, the smaller one producing an extremely narrow line focus (width 0.3 mm).

Electron-optical considerations

We base our considerations on the above-mentioned fundamental fact that the filament in an X-ray tube is operated in the saturation region, so that all emitted electrons contribute to the formation of the focus. The cathode required is therefore the classical, directly heated type, consisting of a coiled or spiralized tungsten wire. Oxide cathodes are quite unsuited for our purpose since, having regard to their life under continuous loading, they cannot be allowed to deliver more than $^1/_{100}$ of their saturation current. Other types of cathode, such as the L type, are excluded because of barium evaporation, amongst other things. We thus arrive at a cathode system which, in its simplest form, is as shown in *fig. 2*. The system contains a closely coiled filament, which can be treated to a first approximation as a simple cylinder, situated in a slot in the cathode block. The cylindrical shape corresponds to a line focus, as required for most X-ray tubes. Disregarding the boundary effects at the ends of the cylinder, we can regard the potential field between cathode and anode as purely two-dimen-

[4]) See e.g. J. H. van der Tuuk, A million-volt X-ray tube, Philips tech. Rev. **4**, 153-161, 1939; W. Hondius Boldingh and W. J. Oosterkamp, A 400 kilovolt installation for X-ray therapy, Philips tech. Rev. **8**, 105-110, 1946.

[5]) The writer read a paper on this subject to the International Congress on X-rays at Copenhagen in 1953, which has since appeared in the journal published by C. H. F. Müller A.G., "Röntgenstrahlen; Geschichte und Gegenwart", 1956. The most important results and their application in endotherapy tubes are described briefly in Philips tech. Rev. **13**, 77 et seq., 1951/52.

sional. This is represented in fig. 2 by equipotential lines (lines of intersection of equipotential surfaces with the plane of the drawing). The paths described by the electrons emitted from the filament can be most simply determined by experiment with a rubber membrane model of the potential field, on which small balls are rolled [6]). Some characteristic trajectories found in this way are also shown in fig. 2. If we look at the situation at some distance from the cathode, we see that there are three principal beams, one originating from the foremost the beam. If the target surface is situated at this position, the desired focus with an approximately uniform distribution of electron bombardment and of X-ray emission is obtained. Since the equipotential surfaces in this region are virtually parallel and have a constant gradient, the potential pattern is not essentially altered if the target is introduced here slightly above or below the point indicated by the arrow. However, both above and below this region the electron density is non-uniform and will not produce a good focus. By proportionately

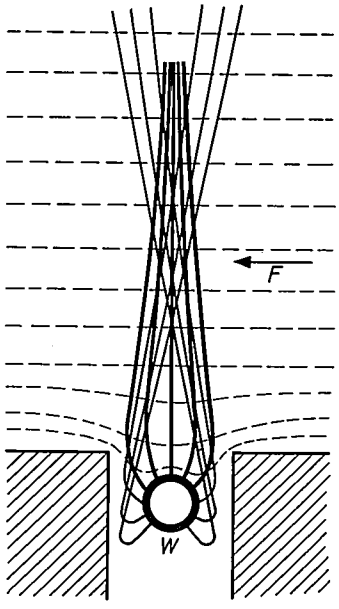

Fig. 2.

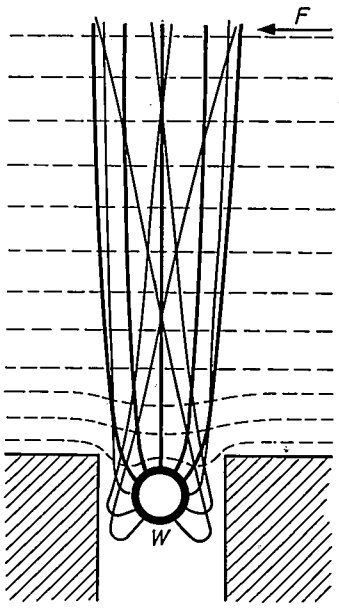

Fig. 3.

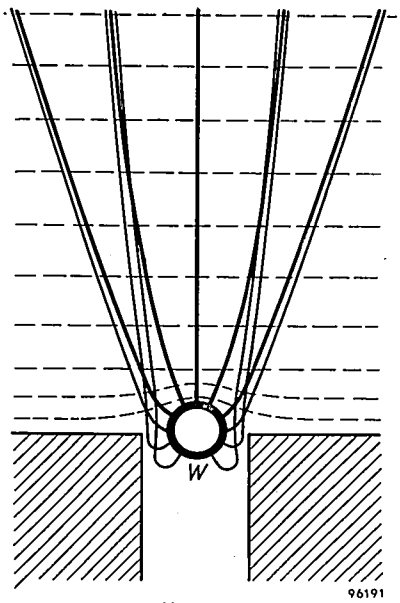

Fig. 4.

Fig. 2. Basic form of cathode system (cylindrical filament W in a slot), shown in cross-section. The dashed lines are equipotential lines, determined by the electrolytic-tank method. The thickly drawn lines are electron paths, found by experiment with a rubber membrane analogue. The focus is produced at F.

The filament is regarded here and subsequently as a simple cylinder. To a first approximation the electron emission between the turns of the coiled wire can be disregarded.

Fig. 3. As in fig. 2, but with the filament moved up nearer to the mouth of the slot.

Fig. 4. As in figs. 2 and 3, but with the filament moved up further still. No focus is now produced in the anode space.

third of the filament and two from the two thirds at the rear of the filament. The rays of each of the two latter beams are reflected from the sides of the slot and cross each other. In the region at the height of the arrow the distribution of the electrons is approximately uniform over the cross-section of changing all distances and also the dimensions of the cathode slot and filament, the focus obtained can be given the requisite size.

If the filament is moved somewhat towards the top of the slot, as shown in *fig. 3*, the three electron beams run more parallel and the region of uniform electron density is shifted farther outwards. At the same time, however, the total cross-section of the beam at that point is widened, so that this simple measure does not achieve the object, which is to produce the same focus at a greater distance. With continued displacement of the filament upwards we finally reach a situation where, as shown in *fig. 4*,

[6]) See P. H. J. A. Kleijnen, The motion of an electron in two-dimensional electrostatic fields, Philips tech. Rev. 2, 338-345, 1937.

The rubber membrane has been used for investigating the cathode system of X-ray tubes also by A. R. Lang and D. A. G. Broad, Electron optics of X-rays tubes and the design of unbiased sharply-focusing cathodes, Brit. J. appl. Phys. 7, 221-226, 1956. No long-distance focusing is involved here, however.

there is no longer any region in the anode space in which all three beams intersect each other. Even with this situation, however, focusing is still possible if the cathode system is given a somewhat more complicated shape while retaining a two-electrode structure. An additional, broader recess, or cup, fixed to the front of the original cathode system of slot and filament modifies the potential field near the cathode in the manner shown in *fig. 5*.

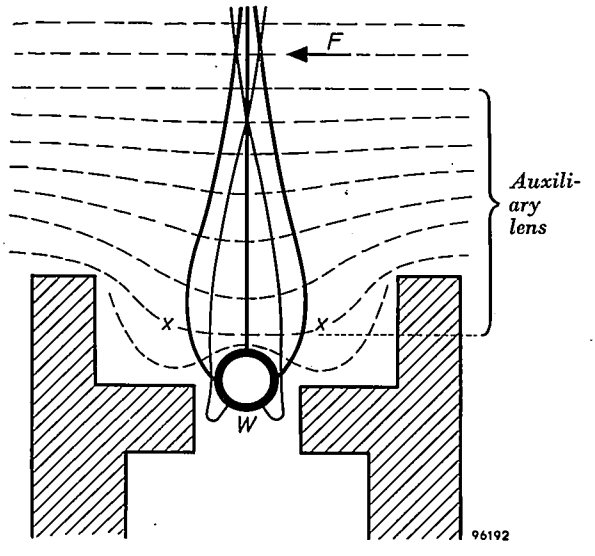

Fig. 5. By introducing a cathode cup in front of the configuration in fig. 4 an "auxiliary lens" is formed (extending from the substantially flat equipotential surface x-x upward; see brace), which again produces a focus, but now at a greater distance from the cathode.

As the illustrated electron trajectories show, a focus is again obtained which is now at a greater distance from the cathode.

Since the addition of such a cathode cup increases the number of design parameters by two at least (depth and breadth of the cup), it is now virtually impracticable to investigate all the possibilities by experiment, or by calculation. Nevertheless, it is possible by simple reasoning to gain enough insight to provide guidance on the design of practical systems.

In the close proximity of the filament, thought of as a cylinder, the equipotential surfaces closely follow the curvature of the cylinder. At the level of the mouth of the cup, however, they will evidently have the opposite curvature, so that between them there will always be an equipotential surface which will be flat within a certain range. Clearly, the potential field between this "flat" equipotential surface and the anode may be regarded as constituting an electrostatic lens (accelerating lens) situated in front of the electron-optical system of filament and slot. This auxiliary lens can be characterized by two parameters, namely by the power of the lens and the distance to the filament-slot system. It would seem at first sight difficult to say anything about the focusing brought about by the two electron-optical systems in combination, because of the complex situation near the filament. However, if the electron trajectories as far as the flat equipotential surface, where the auxiliary lens begins, have been determined by experiment with the rubber membrane analogue, we can for the present purpose replace the electron trajectories simply by their tangents at the points where they intersect this equipotential surface (*fig. 6*). We need then no longer be concerned with the complicated situation near the filament. These tangents can be constructed with satisfactory accuracy, since, as can be seen in fig. 6, the electron trajectories are not very strongly curved at the places where they cross the flat equipotential surface.

If the tangents of all electron trajectories be traced backwards (fig. 6), we see that these "virtual

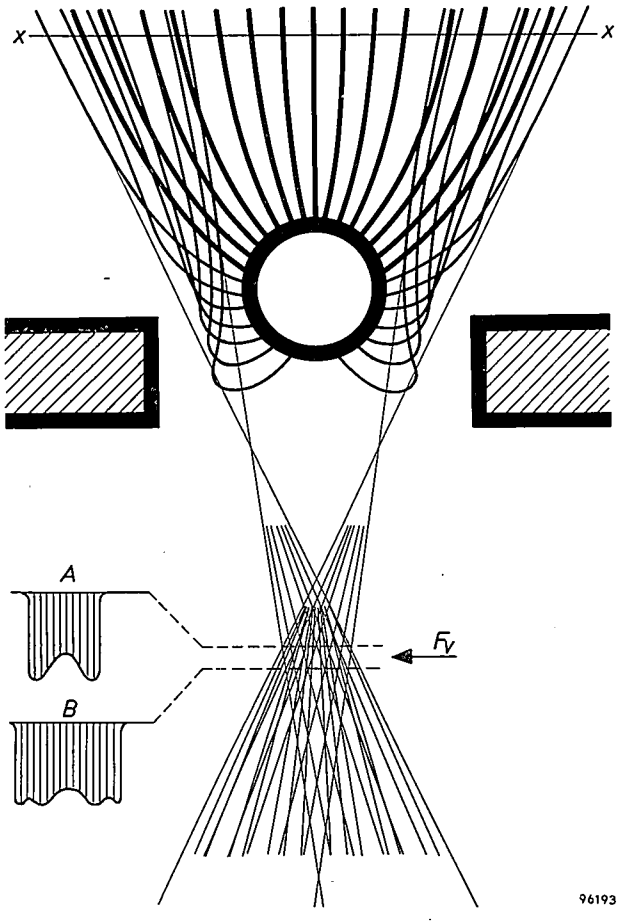

Fig. 6. The "virtual object" F_V, projected by the auxiliary lens, is constructed by producing back the tangents of the experimentally found electron trajectories at the points of intersection with the plane x-x. The figure shows the distribution of electron density in the cross-sections A and B of the pencil of tangents behind the cathode.

paths" (which the electrons can be imagined to describe in the total absence of any field in the entire space behind the flat equipotential surface) again form our three beams, but now they intersect in a minimum cross-section *behind* the filament at the plane A. This zone of intersection may be regarded as a virtual image of the filament, produced by the filament-slot electron-optical system. (It is not actually a true virtual image, for in every "image" point there converge rays from *different* points of the filament.) We must now design our auxiliary lens so as to obtain on the target a focus that is the real image, approximately free from aberration, of the plane A, or possibly of the plane B, where the intersecting tangents are rather more uniformly distributed (see the "electron density" distribution in these planes as sketched in the figure). The virtual electron distribution in plane A — or in plane B if the auxiliary lens be so adjusted — acts as the virtual object [7]).

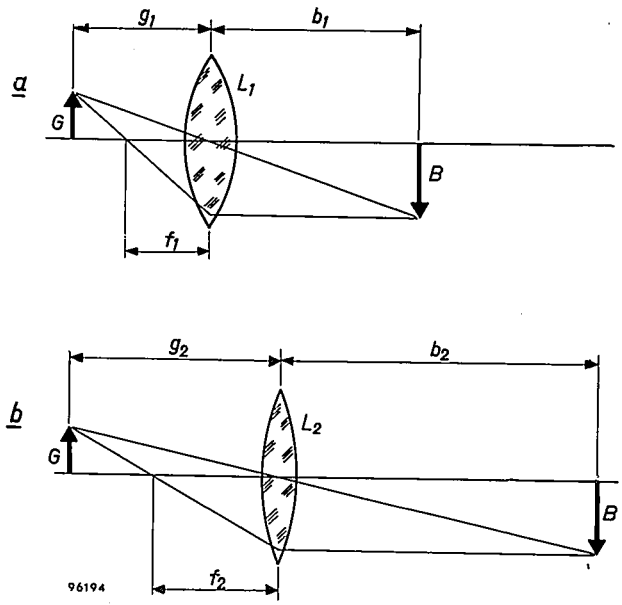

Fig. 7. Optical analogy.
a) A slightly magnified image B of the object G, situated at a distance g_1 from the thin lens L_1 (focal length f_1) is produced at a distance b_1.
b) To produce a k times more distant but no larger image of the same object, a weaker lens is required (focal length $f_2 = kf_1$) which must be situated at a distance k times greater than g_1 from G.

[7]) The combined action of the two parts of the potential field must of course lead to a result which is independent of the equipotential surface one may choose as the boundary. Provided image aberrations may be disregarded, tangents can in fact be constructed for any given boundary plane, but any other choice than that described here may reduce the accuracy and make it more difficult to define the "auxiliary lens". See also the part of this section in small print.

It should be noted that, for the case of a *point source* in fig. 6, it can be demonstrated by a simple calculation that *in the paraxial approximation* the tangents constructed on the electron trajectories, where they intersect an arbitrary plane perpendicular to the axis, all intersect exactly in one point on the axis behind the point source.

What we must do to solve the problem posed at the outset, i.e. to produce a small focus at a long distance from the cathode, can now be inferred from the optical analogy. Taking the virtual object and its position as given, we need an auxiliary lens of *low power* and situated at a *long distance* from the object (see *fig. 7a* and *b*). In our case this implies the use of a cathode cup of considerable diameter and depth. Since we have two geometrical parameters available, it is fairly evident that the flat equipotential surface can be made to remain at approximately the same place; in this way we satisfy the condition that the virtual object and its position should not be significantly affected by the change in the dimensions of the cup. On the other hand, the shaping of the filament and its immediate surroundings still makes it possible within certain limits to exert some influence on the virtual object to be imaged by the auxiliary lens, both as to its position

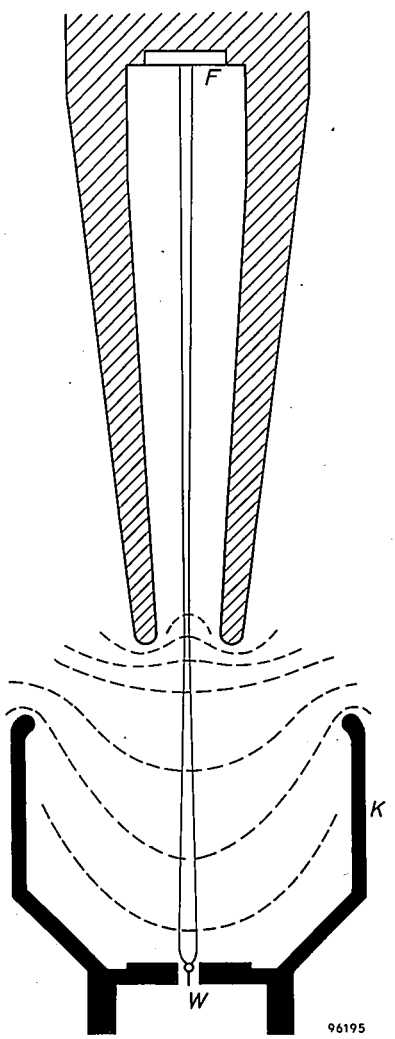

Fig. 8. Simplified cross-section of the electrode system of a distant-focus X-ray tube. W filament, K cathode cup, F focus. Some of the equipotential surfaces and electron paths are shown.

and size and as to the distribution of the electron density. In this way, and by suitably dimensioning the cup, varying requirements can be fulfilled with regard to the size and distance of the focus, and to the distribution of the load on the focus.

Depending on the requisite distance of the focus, the dimensions of the cathode cup can be quite considerable. *Fig. 8* shows schematically the electrode system in one of the distant-focus X-ray tubes which we have developed on this principle and which are all characterized by their exceptionally large cathode cup. The focus of this tube is situated on the end of the tubular anode. The figure also shows the electron beam and a number of equipotential surfaces. The electrode system illustrated is that of the industrial X-ray tube shown in fig. 12, in which a 0.4 mm focus is produced, with the electrons travelling a distance of 200 mm.

The optical analogy should not be applied without reservation, since both the "auxiliary lens" and the filament-slot lens in the X-ray tube are entirely different in a certain respect from optical lenses: the rays move in a space of continuously changing refractive index, corresponding to the continuously increasing velocity of the electrons on their way to the target. Because we have chosen the "flat" equipotential surface, however, for dividing up the field into two lenses, we have a virtual object at a fairly considerable distance from the auxiliary lens, and the image (the focus) is also produced, as intended, at a considerable distance away. The variation in the refractive index is thus compressed in a relatively limited space. Hence the accelerating potential field can reasonably be taken as equivalent to a thin lens. On the other hand, a given lens has a longer focal length in a medium the higher the refractive index of that medium. In the anode space this index is much higher than in the cathode space (owing to the greater velocity of the electrons), and therefore in this case the discrepancy between the electron-optical case and the optical case works in favour of the former when long focal lengths are required.

However this may be, as a heuristic principle the optical analogy has served well, as is demonstrated by the successful design of a range of distant-focus X-ray tubes.

Some practical types of distant-focus X-ray tubes

Fig. 9 shows an endotherapy tube the construction of which was described some years ago in this journal (see article [5])). The tube has an extended anode in the form of a hollow rod having an inside diameter of only 9 mm, the target of gold-plated copper being mounted at the end. The electrons travel a total distance of 250 mm to the target; for reasons of heat dissipation the focus diameter is fairly large, being 6 mm. Because of the small inside diameter of the rod-anode its overall thickness, including a cooling-water jacket, is no more than 15 mm, which makes the tube eminently suitable for the kind of irradiation required in gynaecological treatments.

The tube shown in *fig. 10* is a special type designed for industrial radiography; it operates on 150 kV with earthed anode. The long, tubular anode makes it possible to introduce the source of radiation up to a depth of about 65 cm into narrow pipes, boilers or other hollow bodies. The tube has a round focus, so that the rays emerge with rotational

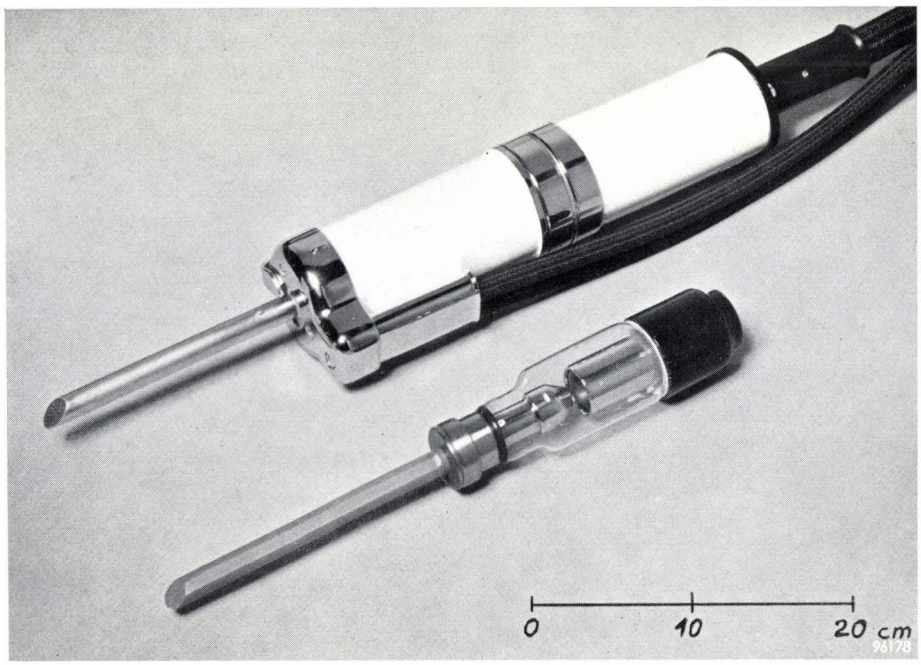

Fig. 9. Rod-anode X-ray tube for endotherapy (irradiation of body cavities). The electrons describe a trajectory of about 250 mm from the filament to the target at the end of the tubular anode.

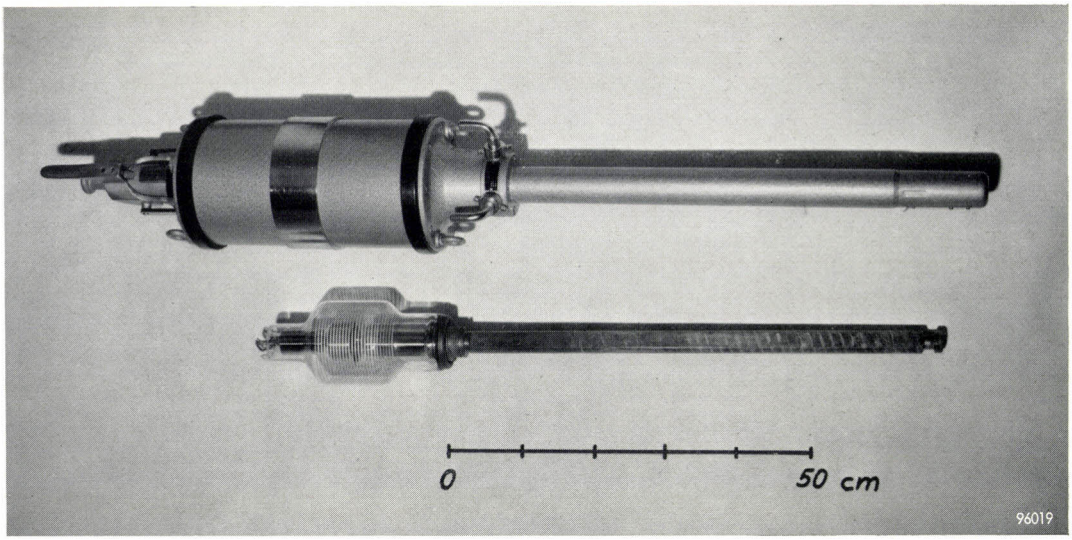

Fig. 10. A 150 kV earthed-anode X-ray tube for the examination of materials. At the end of the rod-anode a round focus of 5 mm diameter is produced; electron trajectory 800 mm long.

symmetry. When an X-ray film is placed around the part of a pipe to be examined, a single exposure suffices to obtain a radiograph of the whole 360° periphery of the pipe wall. The electrons in this tube have a trajectory of 800 mm and the focus produced at the end of the rod-anode is only 5 mm in diameter. The cathode cup in this tube has a large diameter as may be seen in the photograph. To produce the round focus required for the applications envisaged, the filament is not of cylindrical form but is wound to form a segment of a sphere (see *fig. 11*). A cylindrical shield is fitted close to the filament to prevent a halo being produced around the focus by electrons escaping backwards. As appears from fig. 11, the virtual object of this system is again the region where the tangents of the electron trajectories, projected backwards, intersect. The general situation, particularly as regards the function of the accelerating lens, corresponds entirely to that already discussed.

It can also be seen from fig. 11 that the smallest obtainable cross-section of the beam formed by the projected tangents is determined by the filament structure, since the latter governs the directions in

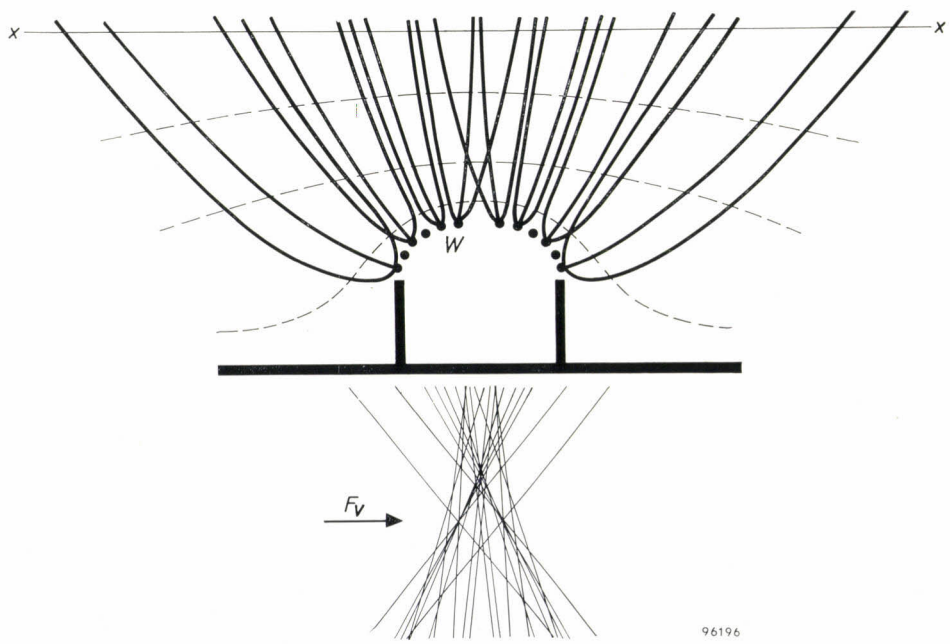

Fig. 11. The filament W of the tube shown in fig. 10 is wound to form a segment of a sphere. With an "auxiliary lens" of suitable power, taken as beginning at the plane x-x, the narrowest cross-section F_V of the pencil of tangents to the electron trajectories is projected as the focal spot on the target.

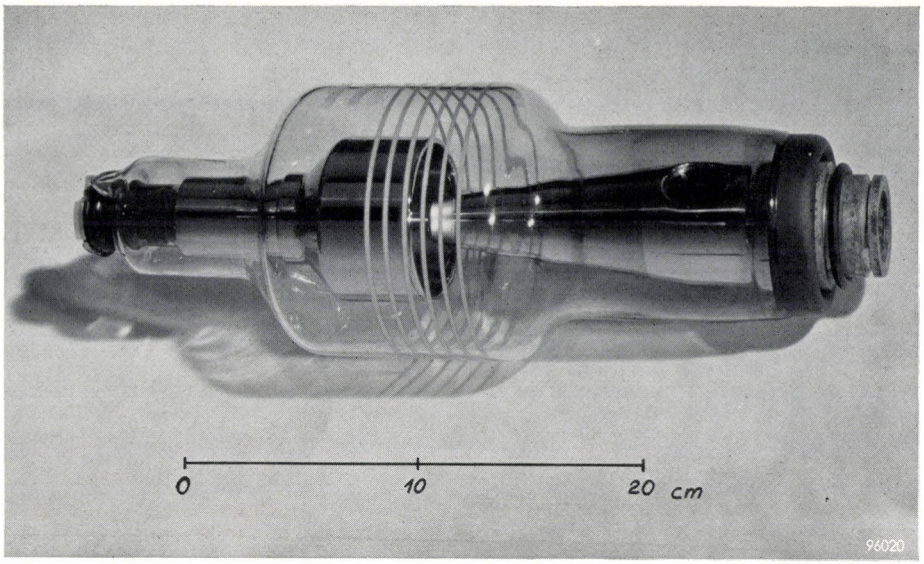

Fig. 12. Industrial X-ray tube with double focus. Electron trajectory 200 mm long; widths of the two line foci, 2.5 and 0.4 mm.

which the electrons are emitted. With a smooth cathode surface it should be possible in principle to reduce this cross-section considerably, and hence the focus too. However, the fact that X-ray tubes operate in the saturation region of the cathode makes it desirable to use tungsten filament wire, and for a cathode of tungsten wire there are only two constructions stable enough for practical purposes, viz. the helix and the flat spiral.

It may be remarked at this point that, although in the cathode systems so far described an accelerating lens produces an image of a virtual object lying *behind* the cathode, it is also possible in principle for the virtual object to lie *in front of* the cathode. For a line focus, the filament would then have to be mounted deeper inside the cathode slot in the system shown in fig. 2; for a round focus as in fig. 11 the spherical segment would have to be inverted, so that its concave side faces the target. Furthermore, the accelerating lens would have to be shifted correspondingly forwards, which can be done by making the cathode cup quite a lot deeper. In general this has the drawback, however, of resulting in a very low field-strength at the cathode. With heavy currents and low voltages the tube then no longer operates in the saturation region but in the space-charge region, one consequence of which is that the tube current and voltage have an undesirable effect on the dimensions of the focus.

Within the permissible range of currents and voltages, this drawback does not attach to systems in which the virtual object is *behind* the cathode, and therefore such systems are to be preferred.

In fig. 10 a number of parallel bands can be seen encircling the glass envelope. These are thin, equally spaced layers of metal applied to the inside wall of the envelope. Their purpose is to ensure that charges built up on the glass, which are unavoidable with the high tensions involved, will not alter the rotational symmetry of the potential field in the tube. There is thus no risk of the focus being shifted by radial potential differences. Evidently, a tube with the long electron trajectories here employed is particularly sensitive to such shifts. The metal rings have the further advantage of evening-out the potential drop in the axial direction, thereby precluding the occurrence of excessively steep potential gradients anywhere on the glass envelope.

Finally, *fig. 12* shows a double-focus X-ray tube, again intended for industrial radiography. The two foci, either of which can be used according to requirements, are line foci with widths of 2.5 and 0.4 mm. Although the electron trajectories are here only 200 mm, the production of the very small focus of 0.4 mm called for a large cathode cup, as can be seen in the photograph and also in the cross-section given in fig. 8.

Summary. Whereas the electron beam in cathode-ray tubes is focused by means of several electrodes or with the aid of magnetic fields, a two-electrode system is normally sufficient for focusing the electrons in an X-ray tube. This article shows that a two-electrode system still serves where the electrons have to describe long trajectories, as in rod-anode X-ray tubes. For this purpose a cup-shaped body is fixed in front of the normal cathode system, basically a coiled filament situated in a slot in the cathode block. The cup has the same potential as the cathode. This arrangement constitutes an "auxiliary lens". The electrons from the filament can be imagined to originate from a virtual object behind the cathode (or in front, with certain electrode configurations), i.e. a virtual "image" produced by the slot-filament electron-optical system and having a fairly uniform electron distribution. The auxiliary lens produces an image of this virtual object on the target. The position, size and electron density distribution of the virtual object depend on the design of the cathode system; these parameters have been obtained from experiments, for a series of cases, using a rubber membrane analogue. From the optical analogy of the problem it can be concluded that a distant focus calls for an auxiliary lens of low power, i.e. a wide and deep cathode cup. Various types of X-ray tube have been designed on this principle and are briefly described in this article. In one of these tubes a focus of 5 mm diameter is produced at the end of a tubular anode on a target 800 mm from the filament.

TRANSMITTING VALVES FOR USE IN INDUSTRY

by E. G. DORGELO.

621.385.3

*Thermionic valves used for generating or amplifying high-frequency oscillations of considerable power are traditionally called transmitting valves. They are still referred to as such even where there is no question of transmitting, as when the oscillations are turned to use in industry or for therapeutic purposes. Examples of such applications are R.F. induction and dielectric heating (the latter also in the form of diathermy). In recent years, too, the generation of ultrasonic oscillations has come into prominence in techniques such as the ultrasonic cleaning of liquids and surfaces, ultrasonic soldering, ultrasonic machining, etc. *). In many of these "industrial" applications, as opposed to the use of transmitting valves in actual transmitters, the valves may be subjected to highly varying loads and to rougher handling. These differences have led to the development of special valves designed to meet the electrical and mechanical demands imposed by industrial applications.*

Transmitting valves operating in telecommunication transmitters are in general subjected to a constant electrical load. This makes optimum matching possible between the valve and the circuit to which the power is delivered.

The situation is entirely different as regards transmitting valves used in industrial equipment, such as generators for R.F. induction or dielectric heating (diathermy is an example of the latter) or ultrasonic generators. The resistance R_a as seen by the valve [1]) is far from constant in such cases, and in consequence both the power delivered by the valve and the power dissipated in it are subject to considerable variations. Investigations in Philips Transmitting Valve Applications Laboratory have shown that in the welding of plastics by dielectric heating, R_a varied in a particular case by a factor 2.5, while variations by a factor 3 occurred in the inductive heating of iron.

The aim is generally to minimize the variations in output power by an appropriate choice of circuitry and valve characteristics. As regards the power dissipated in the valve, maximum values are laid down which must not be exceeded. Apart from the inconstancy of R_a, fluctuations in the mains voltage also enter into consideration, since these can sometimes cause both the anode supply voltage and the heater voltage to differ appreciably from the rated values.

These types of valve thus operate under much less favourable conditions in industry than in telecommunication transmitters. In the past, attempts have been made to meet this difficulty by adopting a larger type of valve than the power required really calls for. For example, if a 1 kW generator is fitted with a transmitting valve capable of delivering 3 kW, there is a reasonable chance that this valve will never be overloaded as a result of load and mains variations. On the whole, however, this does not constitute any improvement with respect to the variation of the output power.

A more fundamental approach to the problem of "industrial" transmitting valves has given rise to two lines of investigation:

a) a theoretical study of the manner in which the operating point of the valve is shifted as a result of variations in R_a, and

b) a technological investigation aimed at producing electrode materials whose properties will remain constant under changing temperatures and which can be subjected to heavy electrical and mechanical loading.

The theoretical investigation has been dealt with at length elsewhere [2]). We shall give here a brief summary of the conclusions arrived at before dealing in more detail with the technological aspects.

Effect of varying load resistance on the operating point of the valve

Industrial triodes operate in an oscillator circuit as a rule with automatic biasing, which means that during each oscillation cycle the grid voltage is momentarily positive with respect to the cathode; the resultant grid current flows through a resistor R_g (*fig. 1*), producing across this resistor a voltage which, smoothed by a capacitor C_g, constitutes the negative grid voltage V_{g0} for the valve.

*) See e.g. E. A. Neppiras and R. D. Foskett, Ultrasonic machining, Philips tech. Rev. **18**, 325-334 and 368-379, 1956/57, and the literature therein referred to.

[1]) By definition, R_a is the real part of V_{a1}/I_{a1}, where V_{a1} and I_{a1} are the complex fundamental components of the anode voltage and anode current, respectively.

[2]) Output and load resistance of oscillating triodes in RF heating generators, Electronic Appl. **18**, 19-26, 1957/58 (No. 1).

A favourable property of this circuit is that V_{g0} is not constant but changes with varying R_a in such a way as to oppose changes in the output power P_o. In many cases, however, this compensating effect is far from adequate. One of the results of the above-mentioned theoretical investigation has been to

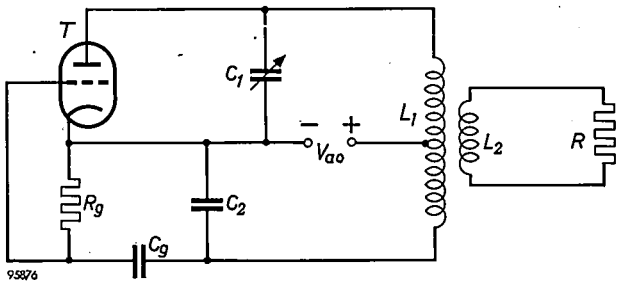

Fig. 1. Oscillator circuit with automatic biasing. T triode. L_1-C_1 tuned circuit. L_2 secondary coil, loaded with a resistance R. V_{a0} anode high-tension. C_2 decoupling capacitor. R_g grid resistance across which the grid current pulses produce a negative grid voltage, which is smoothed by capacitor C_g.

fraction of the electrons emitted by the cathode. Owing to secondary emission from the grid, however, the actual grid current is smaller than the intercepted fraction of the cathode current [3]). The extent to which secondary emission occurs therefore affects the shape of the grid current characteristics and accordingly influences also the optimum value of μ.

Until quite recently, grids were used consisting entirely of one metal only (tungsten, molybdenum, tantalum), having as a rule a fairly high secondary emission. The most favourable value of μ was then 30 to 40. To suppress thermionic emission, modern grids are coated with substances possessing a high work function; their secondary emission too is then low in most cases. As explained in the article under [2]), P_o depends least on R_a when a grid of this kind is combined with an amplification factor of approximately 20.

If μ be given the optimum value, there is the

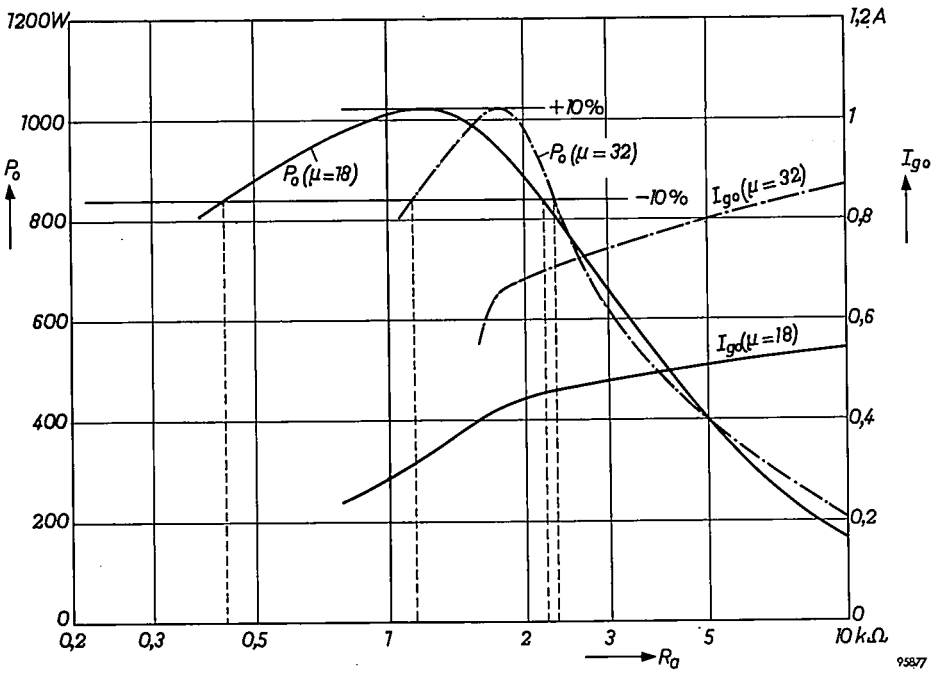

Fig. 2. Output power P_o and mean grid current I_{g0} of an oscillating transmitting triode as a function of the load resistance R_a for two similar valves, both with a grid showing low secondary emission. Dot-dash curves: valve with $\mu = 32$; solid curves: valve with $\mu = 18$. To keep P_o constant to within 10%, R_a should be kept within the limits 1100-2350 ohms (ratio 1 : 2.1) for the valve with $\mu = 32$, whereas R_a may vary from 430 to 2200 ohms (ratio 1 : 5.1) for the valve with $\mu = 18$. Another advantage of the low μ is that the grid current remains much lower at high values of R_a.

show that the value of the amplification factor μ of the triode has an important influence in this respect, P_o having been found to depend least on R_a when μ has a certain optimum value. The magnitude of this optimum value of μ depends solely on the shape of the grid current characteristics.

The grid current is due to the grid intercepting a

further incidental advantage that the power dissipated in the grid varies relatively little with R_a.

The influence of μ can be seen for a given case from *fig. 2*, which shows the output power P_o and

[3]) E. G. Dorgelo, Gitterprobleme bei Sendetrioden in Schaltungen der industriellen Elektronik, Funk-Technik **12**, 528 et seq., 1957 (No. 15).

the average grid current I_{g0} as functions of R_a for two similar valves, both with low secondary grid emission but with $\mu = 32$ in the one valve and with $\mu = 18$ in the other. Given a permissible variation of $\pm 10\%$ in P_o, then R_a in the valve with $\mu = 32$ may vary only from 1100 to 2350 ohms; in the valve with $\mu = 18$ it may vary from 430 to 2200 ohms; these variations in R_a are in the ratio of 1 : 2.1 and 1 : 5.1, respectively. Moreover, it can be seen that at extremely high values of R_a (no-load operation) the grid current rises far less in the valve with $\mu = 18$ than in the valve with $\mu = 32$.

The considerations outlined above have led to a new range of transmitting-type valves specially designed for industrial use. These valves combine low secondary grid emission with a fairly small value of μ. It is due to this combination that variations in R_a, such as occur in industrial applications, give rise to much smaller changes in the output power than was the case with the types of valve formerly used, which possessed heavy secondary grid emission and a high amplification factor.

Technological aspects of the new valves

The cathode

After comparison of the different types of cathodes now available, the choice fell on the thoriated tungsten cathode for the new range of industrial transmitting valves. Although much higher peak emissions can be obtained with oxide cathodes, and even higher with dispenser cathodes [4]), there is no need for such high emissions in transmitting valves used for industrial purposes. A general drawback of oxide cathodes in high-power valves is the relatively low temperature of the cathode, which lies between 1000 and 1200 °K. The surrounding electrodes may also reach temperatures of this order and so may cause excessive back-heating of the cathode. This makes oxide cathodes unsuitable for valves of the type described here.

Another drawback of oxide cathodes and also of dispenser cathodes in such valves is the fairly heavy evaporation of the alkaline-earth metal (barium) contained in the cathode material. If this metal settles on the grid, the grid itself becomes emissive, particularly when it is heavily loaded and therefore hot. Grid emission can disturb the operation of the oscillator and shorten the life of the valve. This can be prevented to some extent by plating the grid, for example with gold, but at the high temperatures reached by the grid, such a coating very soon evaporates.

Thoriated tungsten, on the other hand, has considerable advantages as a cathode material in valves of the type here discussed [5]). In the first place, the operating temperature of a thoriated tungsten cathode (about 2000 °K) is so much higher than that of the surrounding electrodes as to make back-heating negligible. In the second place, the evaporation of thorium (and tungsten) at 2000 °K is very low compared with the evaporation of barium from an oxide or dispenser cathode.

The grid

Even a very small amount of thorium deposited on the grid would give rise to troublesome thermionic emission. To avoid this, the grid in the range of valves concerned is made of so-called K material. This is a newly developed material with particularly favourable properties, including a high work function even when thorium has settled on it. The surface is rough, which is conducive to good heat radiation. A grid of K material can withstand a continuous load of 25 W/cm^2; the thermionic emission thereby, with thorium deposited on the grid, is only about 1 μA/cm^2, and this value undergoes scarcely any change after thousands of hours of operation [6]).

The ultimate loading of K material — i.e. the loading at which the grid is immediately destroyed — is many times higher than its normal load. For example, for one of the new valves, the triode TB 5/2500, the normal grid input power is between 40 and 70 W; the permissible maximum is 120 W [7]), but real difficulties arise only in the region of 500 W.

For comparison, we may quote some figures for grids of molybdenum wire with a coating of platinum (the material generally used to suppress thermionic grid emission): at a normal loading of 10 W/cm^2 the emission is approximately 2 μA/cm^2 and the maximum permissible loading is only 15 W/cm^2.

The anode

The new range of tubes includes types whose anodes dissipate sufficient heat by radiation alone, as well as types requiring additional cooling with air or water.

[4]) A. Venema, R. C. Hughes, P. P. Coppola and R. Levi, Dispenser cathodes, Philips tech. Rev. **19**, 177-190, 1957/58 (No. 6).

[5]) Cf. P. J. Papenhuijzen, A transmitting triode for frequencies up to 900 Mc/s, Philips tech. Rev. **19**, 118-128, 1957/58 (No. 4).

[6]) See fig. 9 and the related text in the article quoted under [5]).

[7]) The data for Philips transmitting valves nowadays no longer give the maximum grid input power, but the maximum value of the mean grid current, the reason being that the user can measure the current but not the power.

The valves cooled by heat radiation have an anode consisting of a thick-walled block of graphite. Sintered onto the surface of the graphite is a coating of zirconium powder, which improves the heat radiation and has good gettering properties. The heat capacity of the anode is high enough to permit heavy intermittent overloading [8]). The permissible anode dissipation of the TB 5/2500, for example, is 800 W in continuous operation, whereas it may be 1200 W when operated 5 sec on and 5 sec off, and 1500 W at 1 sec on and 4 sec off.

The types with water or air cooling have a copper anode which forms part of the envelope. In the case of air cooling the anode is brazed to a copper cooling-fin assembly. In such cases a solder having a fairly low melting point used to be employed (cadmium, tin, lead or an alloy of these metals). In the new valves an alloy of copper and silver is used, the melting point of which is so high as to exclude the possibility of the solder being melted through overloading of the valve.

The metal anodes are very thick-walled, so that their heat capacity is also high enough to permit considerable overloads during intermittent operation. A further advantage of the thick wall is that so-called "hot-spots", resulting from non-uniform electron bombardment over the anode surface, are prevented.

Mechanical aspects of electrodes and envelope

Since there is a risk of the valves being roughly handled in industrial applications, efforts were made in designing the new range of valves to increase their mechanical strength.

In transmitting valves with a thoriated tungsten cathode the cathode has always been a weak point. Not only is it easily broken by shocks, but it is also frequently subject to a slow progressive deformation which may lead in the long run to short-circuiting between cathode and grid. This is particularly the case when the cathode is frequently switched on and off.

Extensive tests have revealed that this deformation can be reduced to negligible proportions by using a sufficiently thick filament and keeping the temperature on the low side. In the new valves the filament is 1 mm thick, which is twice as thick as in comparable valves of the older type. The filament wire is "carbonized" in the usual way, i.e. glowed in a hydrocarbon gas or vapour. This turns the surface of the filament into a layer of tungsten carbide, which allows the emission to remain for longer periods above a certain limit than would otherwise be the case. In the new valves the carbide layer has about the same thickness as in the old types. In order to obtain sufficient emission at the reduced temperature (see above), the filament power in relation to the maximum anode current required has been chosen rather on the high side.

Further improvement is obtained by using wire of a different composition and crystal structure, both of which are kept under careful control. After being switched on and off many thousands of times, these new cathodes exhibit no deformation of any significance.

Fluctuations in the filament voltage of from −10% to +5% of the rated value do not appear to have any adverse effect on the operation or life of the valve. This fortunate circumstance is probably due to the fact that with the thick filament the volume (and hence the reserve of thorium) is relatively large in proportion to the surface of the wire, from which the thorium evaporates.

A further step in the direction of shockproof valves has been taken by adopting relatively large spacings between the electrodes, particularly between cathode and grid. Two years ago in another place a plea was put forward for small interelectrode spacings in industrial valves [9]). The reason advanced at the time, namely increased transconductance resulting in reduced grid input power, is certainly correct from an electrical point of view. We believe, however, that this would greatly increase the danger of short-circuits arising from vibrations and shocks, and that a high "grid safety factor" can better be achieved by combining relatively large interelectrode spacings with a grid material capable of withstanding very heavy loads. In the latter respect, K material is particularly favourable.

K material also has the property of being ductile and therefore not easily broken. Furthermore, after intermittent operation of the filament, it shows practically no tendency to deformation. In *fig. 3* radiographs can be seen of a molybdenum wire grid with platinum coating (*a*) and of a grid of K material (*b*). After only six hours intermittent loading at 350 W the first shows distinct deformation, whereas the second has not been significantly deformed after a thousand hours at the same input.

A vulnerable part of the radiation-cooled valves is the glass envelope. The new valves of this type have an envelope which, while it may not look very elegant, has proved to be very strong and possesses

[8]) Intermittent use of oscillator tubes in RF heating generators, Electronic Appl. **18**, 41-47, 1957/58 (No. 2).

[9]) W. J. Pohl, The design and operation of high-power triodes for radio-frequency heating, Proc. Instn. Electr. Engrs. **104 B**, 410-416, 1957 (No. 16).

N.V. PHILIPS' GLOEILAMPENFABRIEKEN

a fairly uniform temperature distribution, so that the stresses in the glass are low.

Random samples of the valves are tested on their mechanical strength by the impact of a heavy hammer with a rubber-faced head against the valve envelope, the valve being freely suspended as shown in *fig. 4*. The moment of inertia, the various dimensions and the type of rubber are in accordance with American military specifications [10]). The requirement is that the impact of the hammer, given a specific initial amplitude, should cause no contact, even though momentary, between the electrodes. The initial amplitude at which no contact occurs in the case of the TB 5/2500, for example, is 40° to 45°; the maximum acceleration is then about 30 times that of gravity.

In all valves of the new range the lead-ins pass through a thick-walled section of pressed hard-glass. The cups are made from kovar (an alloy of iron, cobalt and nickel); they are conical in shape and hence so rugged that even when the pins are forcibly bent no perceptible movement of the electrodes occurs.

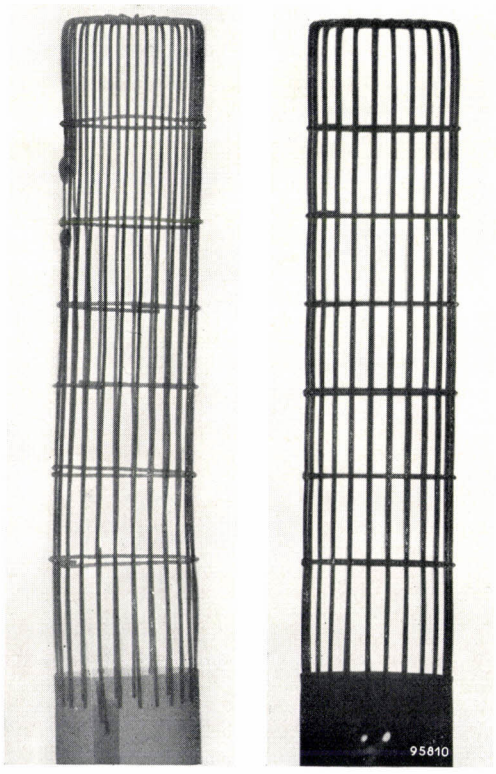

a *b*

Fig. 3. Radiographs of two grids after intermittent loading at 350 W. *a*) Grid of molybdenum wire with platinum coating, after 6 hours intermittent loading. *b*) Grid of K material, after 1000 hours at the same load.

[10]) Military standard test methods for electronic and electric component parts, Section Mil-E-1B, p. 43.

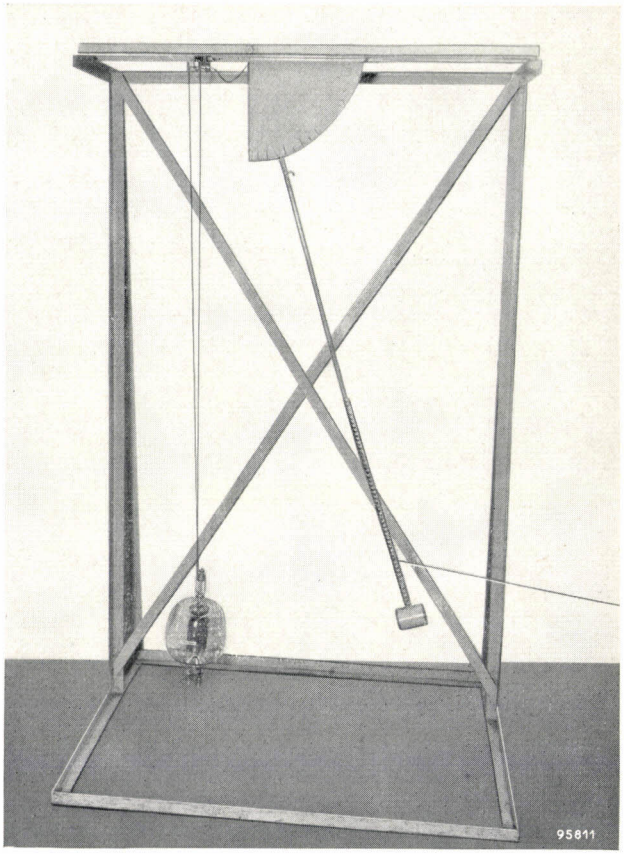

Fig. 4. Device for mechanically testing transmitting valves. The (rubber-covered) hammer is given a specific initial amplitude for each type of valve and then allowed to swing and strike the freely suspended valve. The impact should cause no contact, even momentary, between the electrodes. The valve undergoes an acceleration about 30 times that of gravity.

Life tests

To give an idea of the method of investigating the life of the valves, we shall describe here the switching cycle of the life tests carried out on type TB 5/2500.

The valve is operated at the maximum permissible frequency (50 Mc/s) and at the maximum permissible anode voltage (5 kV) [11]). The filament voltage is stabilized and is periodically made 10% lower and 5% higher than the rated value. The load resistance (incandescent lamps) is so chosen as to ensure maximum power consumption. The full load is periodically switched on and off. Immediately after the load is switched out, the grid input rises rapidly to higher values. Owing to the large heat capacity of the anode, the latter cools off only very slowly. This means that both grid and anode have their maximum temperature each time the load is suddenly switched out. This method was chosen deliberately to make the life tests as heavy as

[11]) Since this article was written, the maximum permissible anode voltage has been increased to 6 kV for this type.

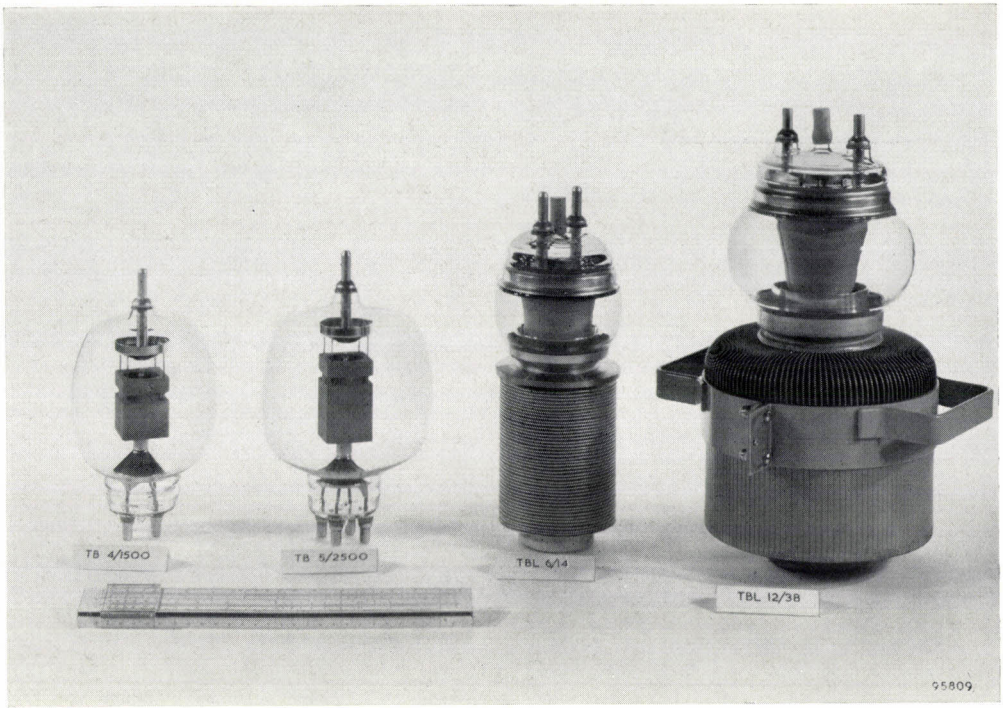

Fig. 5. The range of industrial transmitting valves. From left to right: the two glass types TB 4/1500 and TB 5/2500, and the two metal types TBL 6/14 and TBL 12/38 (air-cooled). Water-cooled versions of the metal-type valves are also made (TBW 6/14 and TBW 12/38).

possible. Moreover, every now and then the entire circuit is suddenly switched on and off at the mains.

The moments at which these switching operations take place are selected such that each combination of states occurs once every two days. Before the test has begun, and after 1, 10, 100, 1000, 2000 hours, and so on, the electrical characteristics of the valve are measured. Among other things, the grid emission is measured at a grid input power of 200 W, which is three to five times higher than the normal value. The grid-emission values found are less than 300 μA, even after many thousands of hours.

Principal data of the new valves

The new range of industrial valves consists at present of four types (*fig. 5*): types TB 4/1500 and TB 5/2500 operate at 50 Mc/s max., and types TB 6/14 and TB 12/38 at 30 Mc/s max. A fifth type for generating about 10 kW is still in development. The principal technical data are given in the *table*.

All these valves have been specially designed to operate under fluctuating loads. The minimum value of the load resistance R_a is determined by the maximum permissible anode dissipation. The maximum value of R_a in the case of conventional transmitting valves is limited by the maximum grid loading, but it is here unlimited. The permissible grid input power for the new valves is so high as to completely exclude difficulties on this score.

Principal technical data of the new range of industrial valves.

Output power of generator kW	Valve type	Max. anode dissipation		Max. anode H.T.	Max. power delivered by valve
		Continuous kW	Intermittent kW	kV	kW
1-1.5	TB 4/1500	0.5	1.0	6	1.7
2-2.5	TB 5/2500	0.8	1.5	6	2.7
~ 10	TBL 6/14 *)	10	15	8	14
	TBW 6/14 *)	15	15	8	14
~ 30	TBL 12/38 *)	15	25	13	39
	TBW 12/38 *)	25	25	13	39

*) L = air cooling, W = water cooling.

Summary. The increasing use of transmitting-type valves in industry (for R.F. induction and dielectric heating, ultrasonic generators) has created a demand for valves capable of withstanding severe load variations and rough handling. To meet this demand, a new range of valves has been developed: types TB 4/1500 and TB 5/2500 for operation at 50 Mc/s max., and types TB 6/14 and TB 12/38 for operation at 30 Mc/s max.; a fifth type is in course of development. The valves have a very thick thoriated tungsten cathode of new composition and modified crystal structure, a grid of K material (characterized by low thermionic and secondary emission, and good ductility) and an anode possessing a high heat capacity. The solution of the problem of grid loading has been sought not in reducing the grid input power (which would require a high transconductance and hence small cathode-to-grid spacings) but rather in using a grid of a material able to withstand heavy electrical loading (K material) in conjunction with a relatively large cathode-to-grid spacing. Moreover, the amplification factor μ has been given the optimum value. The result is that with load-resistance variations by a factor 3 the power delivered by the new valves changes by no more than $\pm 10\%$. The permissible grid input power is so high as to prevent it ever constituting a limitation.

MANUFACTURE OF TELEVISION PICTURE TUBES

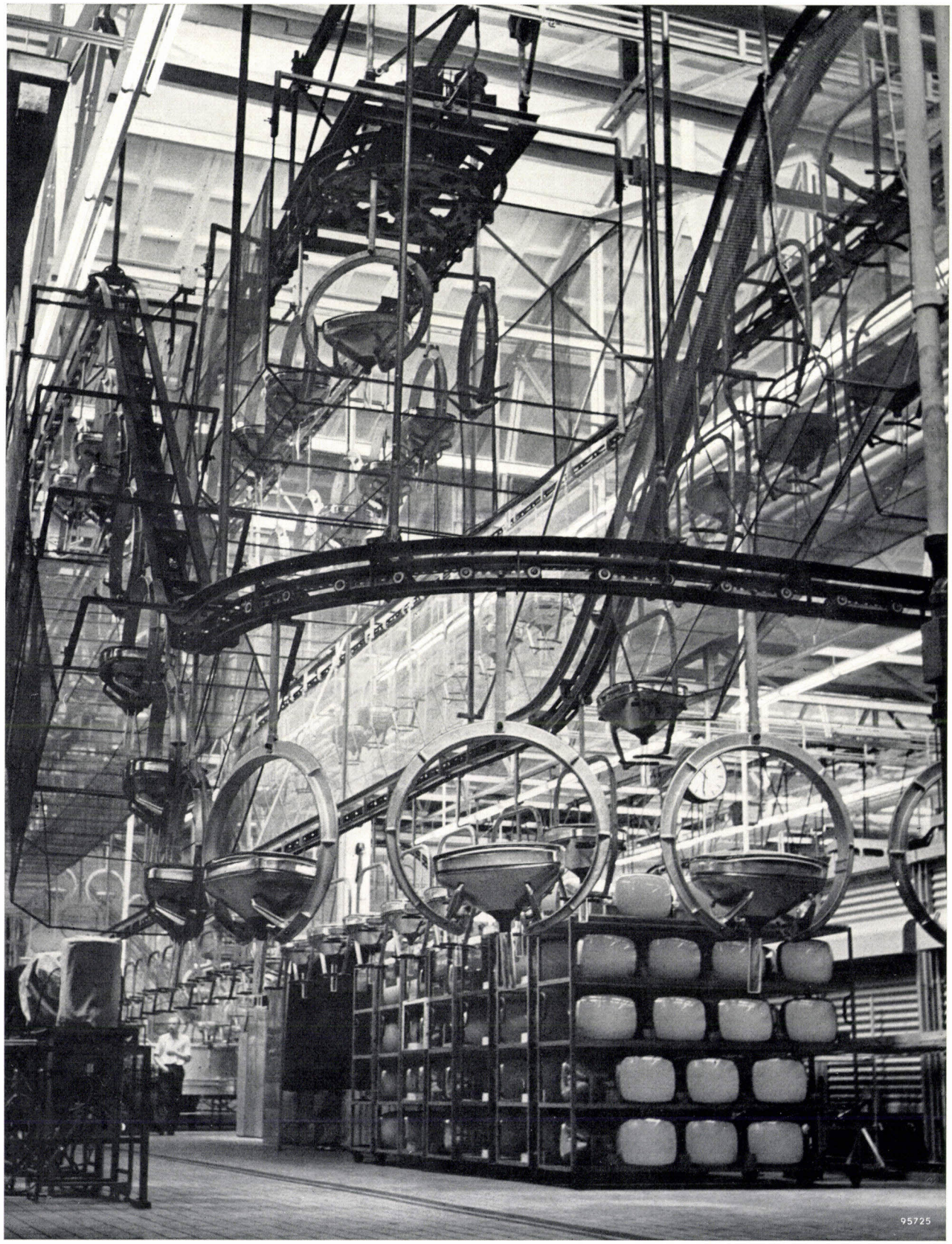

Transport system for 21 inch picture-tubes
in the television tube factory of Valvo G.m.b.H., Achen.

ABSTRACTS OF RECENT SCIENTIFIC PUBLICATIONS BY THE STAFF OF N.V. PHILIPS' GLOEILAMPENFABRIEKEN

Reprints of these papers not marked with an asterisk * can be obtained free of charge upon application to the Philips Research Laboratory, Eindhoven, Netherlands.

2607: P. J. W. Jochems, O. W. Memelink and L. J. Tummers: Construction and electrical properties of a germanium alloy-diffused transistor (Proc. Inst. Rad. Engrs. **46**, 1161-1165, 1958, No. 6).

The fabrication of high-frequency transistors by the alloy-diffusion method is described. A group of transistors was subjected to an extensive series of measurements in order to establish an equivalent circuit characterizing the transistor for small A.C. amplitudes at a fixed D.C. bias. The resulting "physical" T equivalent circuit is valid up to at least 25 Mc/s. The different circuit elements are discussed with respect to their physical background. A translation from the T circuit into the electrically more convenient Π circuit is also presented.

2608: G. H. Jonker: Ferrimagnetic iron oxide compounds with hexagonal crystal structures (XVIe Congrès int. Chim. pure et appl., Paris 18-24 July 1957, Sect. Chim. min., Birkhäuser Verlag, Basel 1958, pp. 117-123).

Short review describing the discovery and the systematic chemical and crystallographic investigation of hexagonal ferrimagnetic compounds of the ternary system BaO-MeO-Fe_2O_3 (Me represents a small divalent metal atom). See also Philips tech. Rev. **18**, 145-154, 1956/57.

2609: F. A. Kröger and H. J. Vink: The incorporation of foreign atoms in crystalline solids (Halbleiter und Phosphore, International Colloquium Garmisch-Partenkirchen 1956, edited by M. Schön and H. Welker, published by Vieweg & Sohn, Brunswick 1958, pp. 17-34).

In this paper it is shown how the concentrations of the various native atomic and electronic imperfections and those due to the foreign atom depend on each other and on the composition of the gas phase. Various ways of incorporation of the foreign atom are described. The properties of the crystal due to the foreign atom and to the native atomic and electronic imperfections depend on the way of incorporation. A number of examples are given to illustrate the various possibilities. A new nomenclature for describing centres in crystals is proposed (see also these Abstracts No. **2593**).

A 5: E. Kauer and A. Rabenau: Zur Kenntnis des Halbleiterverhaltens der Chalkogenide des Aluminiums, Galliums und Indiums (Z. Naturf. **13a**, 531-536, 1958, No. 7). (Studies of the semiconducting behaviour of the chalcogenides of aluminium, gallium and indium; in German.)

Optical measurements show that all chalcogenides of aluminium, gallium and indium of the type $A_2^{III}B_3^{VI}$ have semiconducting properties. The band gap and its temperature dependence are given and compared with the results of other authors. The increase of the band gap with decreasing atomic number and increasing ionic character agrees with the accepted binding rules which, in the case of the chalcogenides investigated here, show a wide independence of the lattice structure.

R 350: H. J. Oskam: Microwave investigation of disintegrating gaseous discharge plasmas (Philips Res. Repts. **13**, 401-457, 1958, No. 5).

Continuation of **R 349.**

R 351: G. Diemer, G. J. van Gurp and W. Hoogenstraaten: Analysis of mixed ambipolar and exciton diffusion in CdS crystals (Philips Res. Repts. **13**, 458-484, 1958, No. 5).

A detailed discussion is given of the experimental conditions under which photodiffusion experiments were performed. An analysis is made of various effects interfering with the interpretation of experimental curves in terms of mixed ambipolar and exciton diffusion and especially the influence of fluorescent light has been studied. The requirements a crystal has to fulfil in order that the exciton diffusion is not drowned in the interfering effects are discussed. For one extensively-studied sample fulfilling these requirements it could be shown that exciton diffusion very probably does play a part (diffusion length $l_{De} \approx 3$ mm at room temperature). Finally, the velocity of propagation for the exciton diffusion in this crystal is discussed.

R 352: O. W. Memelink: The deplistor, a semiconductor switching device (Philips Res. Repts. **13**, 485-488, 1958, No. 5).

A device on near-intrinsic germanium is described which makes use of the depletion region surrounding

an alloy contact biased in the reverse direction. Appropriate circuit conditions allow the deplistor to be used as a switching element with a negative differential resistance.

R 353: P. Winkel and D. G. de Groot: Impedance of dielectric layers (Philips Res. Repts. **13**, 489-498, 1958, No. 5).

It is shown that, according to a theory on amorphous dielectrics as given earlier by Gevers and Du Pré, a correlation must exist between the real and the imaginary component of the impedances of a dielectric layer. This correlation has, in fact, been observed with the dielectric layers formed by the anodic oxidation of Al and Ta, which are known to be amorphous. New data on these layers are presented. They reveal no indication that these layers have any strongly asymmetric structure, as has been suggested in the literature in connection with experiments on niobium oxide. Moreover, the experimental results with aluminium-oxide layers, containing some boehmite, can only be explained by the present theory.

R 354: P. Winkel and B. Verkerk: On the mechanism of electrolytic rectification (Philips Res. Repts. **13**, 501-505, 1958, No. 6).

Various experimental facts point to the conclusion that electrolytic rectification is to be considered as a process taking place uniformly across the surface layer.

R 355: B. Verkerk, P. Winkel and D. G. de Groot: On the mechanism of anodic oxidation of tantalum (Philips Res. Repts. **13**, 506-508, 1958, No. 6).

The mechanism of ionic transport during the anodic oxidation of tantalum is studied. A thin layer of radioactive tantalum is applied to a tantalum sheet. After oxidation the oxide layer is dissolved in successive stages and the activity distribution is measured. It is shown that the transport of Ta ions is governed neither by a pure vacancy mechanism, nor by a pure interstitial process.

R 356: F. L. H. M. Stumpers: The spectrum of limited gaussian noise (Philips Res. Repts. **13**, 509-514, 1958, No. 6).

The energy spectrum of the output of a non-linear device with an input of gaussian noise can be expressed directly in terms of the Laplace transform of its characteristic and of convolutions of the input bandpass form. The expression is derived and the result applied to several forms of limiter characteristic. The same method can be applied if a carrier signal is also present. The amplitude of the carrier wave after limiting and the energy spectrum of the output noise are also calculated.

R 357: W. Hoogenstraaten: Electron traps in zinc-sulphide phosphors (Philips Res. Repts. **13**, 515-693, 1958, No. 6).

In this thesis (Amsterdam, February 1958) an attempt is made to clarify the chemical and physical nature of electron traps in zinc-sulphide phosphors. These traps are thought to be responsible for the possibility of energy storage in phosphors, leading to a long temperature-dependent afterglow of the fluorescence and to the phenomena of thermoluminescence. First, the phenomenological theory of the kinetic electron processes, based on the energy-level model, is discussed. It appears that the best method for studying traps and their depths is that of the thermal glow curve, of which the theory is discussed. By means of this method, a number of phosphors based on ZnS and on mixed crystals of ZnS with CdS or ZnSe, activated by Cu, Ag or Au and doped with various other elements, are studied. It is found that the following impurities or lattice defects give rise to traps, of which the thermal depths (in eV) have been estimated: Cl (0.25); Br (0.26); Al (0.25); Sc (0.34); Ga (0.42); In (0.50); Co (0.52); Ni ($\geqslant$0.58); O (0.59); V_S^+ (0.27); $(V_S^+)_2$ (0.44) and $(Cd)_x$ (0.53). The depths of these traps are nearly independent of the kind of activator. The introduction of both Cd and Se into the matrix generally causes a shift to lower temperatures of the characteristic glow peaks indicating a diminishing of the trap depths. Further, the incorporation of Cd leads to a new glow peak, which is attributed to traps caused by associated Cd atoms. The absolute light sums of various phosphors were measured and are found to amount to only 0.01 - 0.08 quantum per activator or trap atom. Furthermore, it is observed that the light sum of ZnS-Cu-Co phosphors decays slowly even at 77 °K. Both phenomena are explained by a direct recombination of trapped electrons with excited activator centres by a quantum-mechanical tunnelling process. In a theoretical section, the energy states and other properties of various types of centres are discussed on the basis of the so-called effective-mass equation. The perturbation of the discrete energy levels by interaction with neighbouring centres is shown to provide a qualitative explanation for the trap-depth distribution as has been found from a more detailed study of apparently simple glow peaks. A theoretical treatment of the spontaneous transition between occupied traps and

empty centres is attempted and leads to results in fair agreement with the decay experiments at low temperatures.

R 358: K. Helmers: On a simple model for impurity band conduction (Philips Res. Repts. **14**, 1-10, 1959, No. 1).

The influence of the randomness in impurity-centre positions on impurity band conduction can be studied using a crude model (stochastic resistance network). Further simplification of the model leads to the stochastic resistance chain, the statistical theory of which is developed. Typical one-dimensional effects appear at small impurity-centre concentrations.

R 359: G. Diemer, G. J. van Gurp and W. Hoogenstraaten: Analysis of mixed ambipolar and exciton diffusion in CdS crystals (Philips Res. Repts. **14**, 11-28, 1959, No. 1).

Continuation of **R 351**.

R 360: S. Duinker: Traditors, a new class of non-energic non-linear network elements (Philips Res. Repts. **14**, 29-51, 1959, No, 1).

The network elements resistor, inductor, capacitor, transformer and gyrator form a complete set within the domain of constant, passive, linear networks. In this paper an attempt is made to find an extension of this set of elements so as to make possible the synthesis of constant, passive, but locally active, non-linear networks. The analysis is based on the Lagrangian dynamical equations. It is found that a class of multiport elements can be defined, for which the name *traditors* has been coined, which are characterized by the property that at any instant the total power delivered to them is equal to zero. The open port and the closed port, the transformer and the gyrator can be considered as belonging to this class and as being the only linear members. Besides the latter it is probably necessary to introduce only one other type of the class, namely, one with three ports, to synthesize the whole class. Arbitrary non-linear inductors and capacitors are shown to be equivalent to combinations of traditors and linear reactors. Equivalent circuits for sets of non-linearly insulated conductors and sets of non-linearly coupled coils can also be obtained. Traditors are shown to be locally active elements. In many cases the introduction of traditors yields network equations that cannot be solved explicitly. No definite answer can as yet be given to the question of physical realizability of these elements.

R 361: J. te Winkel: Transmission-line analogue of a drift transistor (Philips Res. Repts. **14**, 52-64, 1959, No. 1).

A transmission line that is governed by the same differential equations as a drift transistor is discussed. It provides a relatively simple way of deriving the base transport parameters and the small-signal equivalent circuit of the transistor, without solving the differential equations explicitly.

R 362: J. Haantjes and G. J. Lubben: Errors of magnetic deflection, II (Philips Res. Repts. **14**, 65-97, 1959, No. 1).

This paper deals with some practical deflection-coil design considerations proceeding from an earlier study. First, formulae are derived for the field in the case of a single-wire deflection coil. Subsequently some simplified equations for the deflection errors are derived, assuming the deflection field to be constant inside the coil and zero outside the coil. Using these approximations as design formulae, it is shown that in general a different kind of coil shape is necessary in order to avoid each particular kind of error. Finally the convergence errors in some kinds of colour-picture tubes are discussed, viz. the shadow-mask tube and a tube with post acceleration with the three guns positioned in one plane. It is shown that it is possible to design a deflection coil for the last-mentioned tube in such a way that no dynamic convergence is necessary.

R 363: H. J. Oskam: Showing the presence of very small percentages of neon in helium (Philips Res. Repts. **14**, 98-100, 1959, No. 1).

Measurements of the afterglow in helium and in helium with 1.7×10^{-6} and 10^{-5} per cent neon are presented. The observed influence of the admixed neon atoms on the afterglow curve is consistent with the value of the cross-section of He_2^+ ions for a recently-found charge-transfer reaction with neon atoms.

Now available:

G. W. van Santen, Mechanical vibration (second, revised edition, pp. 310, 220 figures; Philips Technical Library, Eindhoven 1958).

This book, which first appeared in English in 1953, has been revised and supplemented where necessary with recent information (e.g. on vibration amplitudes in rotating machines, vibration measuring instruments, etc.). Also a number of errors which had crept into the first edition have been corrected.

VOLUME 20, 1958/59, No. 11 pp. 309-348 Published 21st September 1959

Philips Technical Review

DEALING WITH TECHNICAL PROBLEMS
RELATING TO THE PRODUCTS, PROCESSES AND INVESTIGATIONS OF
THE PHILIPS INDUSTRIES

MODERN ACOUSTICAL ENGINEERING

I. GENERAL PRINCIPLES

by D. KLEIS.

534.86:534.84:621.395.623.8

*The electrical reproduction of music and speech has been raised to such a high standard in recent years that even practised and critical listeners are scarcely able to distinguish between the reproduction and the original. This was a condition that had to be fulfilled before electro-acoustical methods could be applied to improve the acoustic deficiencies of auditoriums. In this connection it was noted three years ago in this Review as an important milestone in the development of electro-acoustics that leading musicians not only permit microphones and loudspeakers and all that goes with them in the concert hall, but actually welcome their help in making the hall more "playable" *). Since this was written "loudspeakers and all that goes with them" have come into use in numerous concert halls and theatres, including such renowned ones as the Scala in Milan, and the Théâtre National Populaire in the Palais de Chaillot, Paris. It has even happened that performances in acoustically poor halls have been made conditional upon such an installation being in operation.*

In part I of his paper, printed here, the author deals with the principles of acoustic installations both for the amplification of sound and the improvement and control of auditorium acoustics. Some practical installations will be described at greater length in part II.

Electro-acoustical engineering has made great strides in recent years. There have been marked improvements in microphones, amplifiers and loudspeakers, whilst magnetic recording, long-playing gramophone records and frequency modulation have provided novel and better means of recording and transmitting sound. As a result it is now possible to reproduce both music and speech in their original spectrum of frequencies, with virtually their full dynamic range and without troublesome noise. This implies that the equipment used must not only be of high quality, but must also be suitably adapted to its purpose and be operated by properly trained personnel. In practice, when the reproduction is not perfect, it is all too often due to shortcomings in one of these requirements.

The spectrum and the dynamic range, however important, are not the only factors governing the total impression received from the reproduced sound. Where grouped voices or musical instruments are concerned, their spatial configuration plays a considerable part. With *stereophonic reproduction*, employing two or more separate sound channels, full justice can be done to the movement of actors across a stage, the lay-out of an orchestra, etc. [1]). The impression created is far more lifelike than if only one sound channel were used, no matter how good its quality. It has been demonstrated that even critical listeners are scarcely able to distinguish, if at all, between "live" music and its stereophonic reproduction in the same hall [2]).

Modern electro-acoustical devices make it possible not only to unobtrusively reinforce speech or music in the performance of a play or opera (e.g. in a large auditorium or in the open air), but even to relay the speech or music entirely by means of a stereophonic installation without the audience being aware of it. The way now lies open to liberate performances from the restrictions imposed by the size and fitments of the stage. The actions thus

*) Philips tech. Rev. 17, 265, 1955/56.

[1]) See Philips tech. Rev. 17, 173 et seq., 1955/56, and the literature referred to there.

[2]) R. Vermeulen, A comparison between reproduced and "live" music, Philips tech. Rev. 17, 171-177, 1955/56.

become much more natural and the audience gets a greater sense of participation. This can best be illustrated with some examples.

In plays and operas an actor who is not a musician often has to appear to be playing a musical instrument. He then mimes the actions whilst the actual music emanates from the orchestral pit or from the wings. The audience is usually only too well aware of this artifice either because the sound comes from the wrong direction or because its quality or timbre is not what was expected. However, if the music is played into concealed microphones and the stereophonic sound "image" arranged to move with the actor, the illusion can be well-nigh perfect. A variant of this method is to record the music stereophonically beforehand and to play it back during the performance, letting the actor follow the sound image.

To produce certain effects in operas it is sometimes necessary to have musicians or a chorus concealed in or behind the wings. Quite apart from the unsuitable acoustics of the wings for such a purpose, it is in any case impracticable on a small stage, and even on a large stage the musicians and choristers can hinder the exits and entrances of the other artists. It is much better to make a tape recording of the choral or instrumental music and to play back the tape during the performance. Moreover, electro-acoustical techniques make it possible, if desired, to create the illusion of a much larger chorus. For musical instruments or off-stage sound effects the loudspeakers can be installed in the wings. Such sound effects as footsteps, the roar of cannons, a thunderstorm and rain can be far more impressive when they are played back from a carefully recorded tape than when they have to be created afresh for every performance with acoustically ill-adapted equipment of limited scope.

Another great advantage of producing sound effects electro-acoustically is that the effects need not be confined to the area of the stage. Crowd noises for example, can be made to surround the audience, clarion calls to sound from the back of the hall, thunder and rain to be heard from above. The same sounds can also be made to move through the auditorium stereophonically. With "panoramic sound" and "travelling sound", as these techniques are called, very striking effects can be achieved. The audience is caught up in the action and is given the sensation of participating in it.

These examples should suffice to show how much a stage performance can gain in scope and forms of expression from the support of a good electro-acoustical installation.

So far our remarks have been confined to stage and orchestral performances and to the support lent to them by electro-acoustical techniques. The impression made by a performance, however, is not determined solely by the programme and the method of rendering it, but also to a considerable extent by the acoustics of the auditorium. A speech and a play lose much if they are heard in a hall where reverberations mar intelligibility, whereas an orchestral work played in a hall where the reverberation is excessively damped lacks the fine full tone it acquires in a properly designed concert hall. The high quality of modern sound-reproduction now makes it possible to use electro-acoustical techniques for improving the acoustic properties of halls. There are widespread needs in this respect. There are still many halls in use whose acoustics are quite unsuitable for their purpose. Structural alterations may in some cases provide a solution, but this is not always possible because of the architectural or historic value of the building; moreover it will generally be very much more costly and take longer than installing the electro-acoustical equipment necessary to effect the improvement. There need be no aesthetic objections to the presence of microphones and loudspeakers, since they can be unobtrusively mounted and often completely concealed.

More frequently it happens that the same hall is required to serve for performances of widely different kinds, e.g. for plays, operas, orchestral concerts, etc., each of which make their own demands on the acoustics of the auditorium. This is especially the case in small towns where it is financially out of the question to run a theatre as well as a concert hall. But even in large towns the problem of conflicting acoustic requirements is certainly not unknown; as will appear in part II of this article, there are opera houses that also serve for the performance of symphony concerts, and theatres where organ recitals are given, and so on. The acoustics of such auditoriums should obviously be variable. The non-electrical means available — for example, reversible wall panels which are acoustically hard on one side and sound-absorbent on the other — are costly and in any case never produce really satisfactory results. Electro-acoustically, on the other hand, the acoustics of an auditorium can be varied very much more simply, quickly and efficiently, making it possible to create the acoustic conditions most suited to a wide variety of purposes.

A system of variable acoustics offers particular advantages for the performance of plays and operas, in that it allows the acoustics to be adapted at any

given moment to the scene being enacted. During a church scene, for example, the auditorium can be given the acoustic properties of a large church. The audience then not only sees the spectacle on the stage but receives the suggestion that it is itself seated in the church depicted.

In the hands of a good producer this system can provide a perfect synthesis of the illusions created by the play, the decor, the lighting and the sound. As a result the audience can share as never before in the action on the stage, and the performance itself is freed from the restrictions normally imposed by the stage and the auditorium. To this end trained operators are required who can manipulate the apparatus expertly to call forth the effects sought by the producer. During the performance the operators must of course adhere strictly to the scenario as established by the producer during the rehearsals.

In halls whose acoustic properties are unsuitable for musical performances the musicians cannot properly appraise their own playing nor can they hear sufficiently that of their fellow members of the orchestra. Electro-acoustics can effect a considerable improvement in both respects. The result is a "more playable" hall and a better orchestral performance. This is certainly no less important than improving the acoustics of the hall itself.

Installations for improving auditorium acoustics but which are not intended for producing sound effects may often be very large and technically elaborate but their operation should be simple enough to be entrusted to the technicians normally employed in the building. The operations should not entail more than switching the apparatus on and off, routine checking and setting a selector switch to a position corresponding to the type of performance (stage play, opera, chamber music, symphony concert, organ recital). The task of adapting the technical devices to the nature of the hall and to the requirements of the theatre — a task calling for a great deal of skill and experience — rests with the installation engineers.

The Philips Theatre in Eindhoven and the "Gebouw voor Kunsten en Wetenschappen" at the Hague were the first theatres to be provided with an installation designed to make the acoustics suitable for concerts [3]). Since then Philips have brought out theatrical installations of much wider scope, which serve for controlling the acoustics of the auditorium both for music and speech, and also for producing sound effects. Among the buildings thus equipped are the Scala in Milan, the Palais de Chaillot in Paris and the Grand Auditorium built for the 1958 World Fair in Brussels. These installations further make numerous provisions for the members of the public outside the auditorium, for the artists and for the technical staff of the theatre. Details of the installations will be described in part II of this article.

In the part about to follow we shall discuss the acoustical and technical principes of sound installations. These principles apply not only to systems for the complete control of auditorium acoustics in theatres but equally to the far more numerous systems whose aim is more modest, for example installations for making speech intelligible in churches and auditoriums, and for relaying and reinforcing speech and music in stadiums and at open-air meetings, etc. As an example of an elaborate public address system we shall discuss in part II the installation in the "Volkswagen" factory at Wolfsburg.

First of all some general comments. The guiding principle when using electro-acoustical techniques to support a performance or to control the acoustics of an auditorium should be that the electro-acoustical nature of the sound must never be obtrusive. Whether it be a simple speech-reinforcement system or a complex theatrical installation, electro-acoustics achieves its highest success when the acoustical excellence of a performance is attributed to the performance itself and to the acoustics of the auditorium. One prerequisite is that the electro-acoustical equipment employed should be of the highest quality. It is equally necessary, however, to take account of the properties of hearing (the last link in the chain from sound generation to sound perception) and of the laws of auditorium acoustics. We shall therefore preface our discussion of acoustical engineering proper with a brief treatment of these two subjects.

Some properties of hearing

Pitch and loudness

The subjective properties *pitch* and *loudness* are logarithmically related to the physical quantities frequency and intensity of the sound. This logarithmic relation forms the basis for expressing these physical quantities in terms of octaves and decibels [4]). Loudness is not solely determined by the intensity of the sound, however, but also by its frequency. This characteristic of hearing can be expressed in so-called *equal loudness contours*. An equal loudness

[3]) R. Vermeulen, Stereo-reverberation, Philips tech. Rev. 17, 258-266, 1955/56.

[4]) R. Vermeulen, Octaves and decibels, Philips tech. Rev. 2, 47-56, 1937.

contour is a curve of sound intensity (dB) as a function of frequency (*fig. 1*) whereby all points on the curve are of equal loudness (phons). At low frequencies the contours are virtually horizontal when the sound intensity is high, but show a marked slope when the intensity is low. This indicates that the timbre of reproduced speech or music will depend on the volume with which it is reproduced. The ear is highly sensitive to such variations in timbre, and therefore correct adjustment of the volume is essential to the lifelike reproduction of sound [5]). In practice this rule is all too frequently violated, usually by the volume control being turned up too high. The inevitable result is an unnatural timbre, owing to the accentuated loudness of the low notes. Moreover, the sound is not made more but less intelligible because the loud low notes mask the high notes necessary for intelligibility. This sometimes leads to unjustifiable complaints about installations which are not themselves at fault but are wrongly operated.

In cases where the loudness has to exceed the natural level, owing for example to ambient noise, the low notes should be appropriately attenuated in order to restore the balance between low and high notes. Conversely, where the loudness must be lower than the natural level — e.g. when playing orchestral music in a small room — the low notes should be correspondingly boosted ("low note compensation").

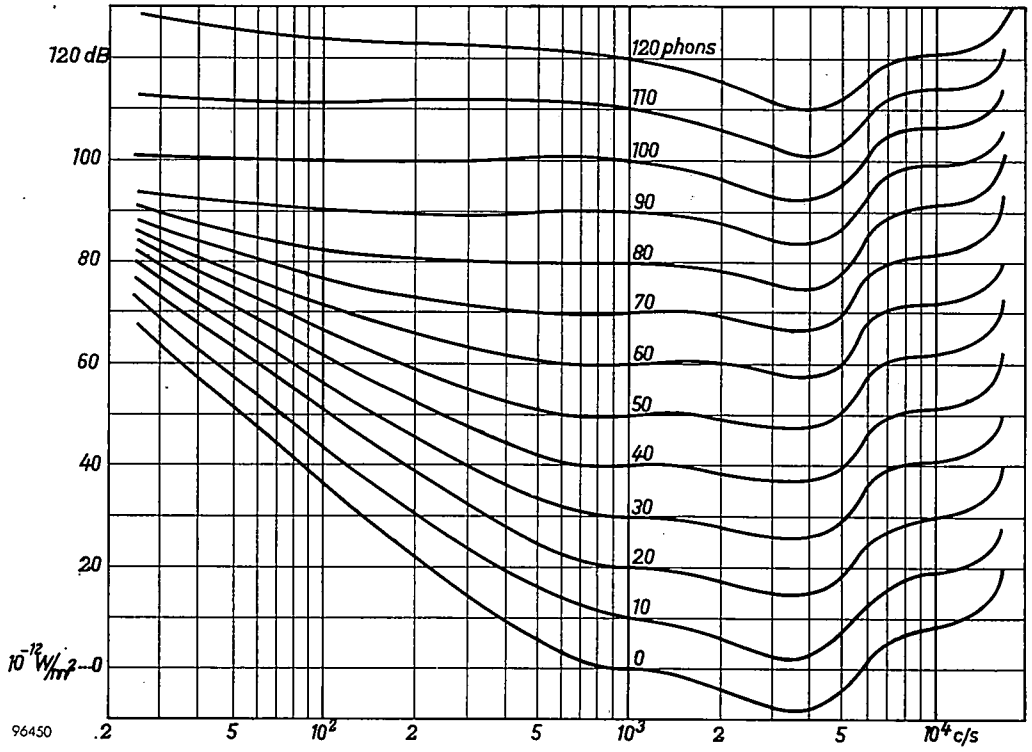

Fig. 1. Equal loudness contours, i.e. curves of sound intensity (in dB above 10^{-12} W/m²) for constant loudness level (in phons) as a function of frequency. The contour at 0 phon is the threshold of hearing. At low frequencies the contours run roughly horizontal when the sound level is high, but slope sharply when the level is low. (After H. Fletcher and W. A. Munson, J. Acoust. Soc. Amer. 5, 82, 1933.)

Binaural location

Another important auditory property is the ability to hear the direction from which a sound comes. We shall first consider the case of an observer listening to a sound source in the open air. The sound from a source which is mounted at head-height outside the plane of symmetry of the head is not received equivalently by both ears. The ear turned more towards the source receives the sound earlier and in greater intensity than the other ear which the sound reaches only after bending around the head. The more lateral the position of the source with respect to the ears the more will the sounds reaching the two ears differ in time of arrival and in intensity. Binaural location depends primarily on the *intensity* differences, especially in the high notes since these are strongly screened by the head, whereas the low notes are less screened and reach both ears with almost equal loudness. The direction of low notes thus cannot be judged precisely. In a

[5]) In the comparative experiments discussed in article [2]) particular care was therefore taken to ensure that the reproduced music was just as loud as the live music.

N.V. PHILIPS' GLOEILAMPENFABRIEKEN

stereophonic system, therefore, the notes below 300 c/s are sometimes not reproduced via two channels but via one only, so that only one bass loudspeaker is required.

In an enclosed space the ears are virtually unable to locate the sound if it consists of a sustained note. The ears are then at different positions in a standing wave pattern and so perceive marked differences that have nothing to do with the direction of the sound source. On the other hand, if the sound is suddenly switched on, its location is easily determined since the first sound to reach the ears already reveals the direction from which it came before the pattern of standing waves is built up. Sounds with frequent transients (speech, percussion instruments) are thus most readily located by the ears.

So far we have considered directions in the horizontal plane at ear height. The elevation of a sound source is much more difficult to detect aurally, inasmuch as it is perceived indirectly through slight unconscious movements of the head [6]). Visual indications can strongly influence the aural perception of elevation. As cinema projection screens got bigger and wider the need was felt for some means of making the sound move horizontally with the visible source on the screen, but never vertically, because of the difficulty of perceiving elevation.

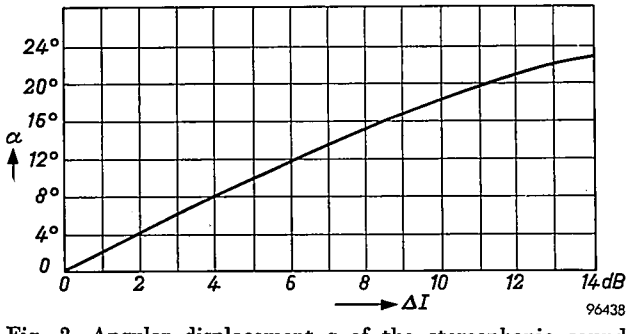

Fig. 2. Angular displacement α of the stereophonic sound image from its midway position as a function of the difference in intensity ΔI between the two loudspeakers.

Binaural hearing, then, makes it possible to locate the direction of a single sound source and to perceive the spatial distribution of a number of sound sources (auditory perspective). The latter gives orchestral music a certain transparency, in that the ears can distinguish spatially between the instruments. This is not possible monaurally, nor if the music is heard reproduced via a single channel.

Stereophony

When two loudspeakers are set up a certain distance apart and reproduce simultaneously the same sound with equal intensity, a listener at the same distance from both loudspeakers does not hear two sound sources but only one, and this virtual "sound image" is located midway between the two loudspeakers. If one of the loudspeakers radiates the sound earlier or louder than the other, the sound image is perceived to be closer to the first loudspeaker. A lead in time of three millise-

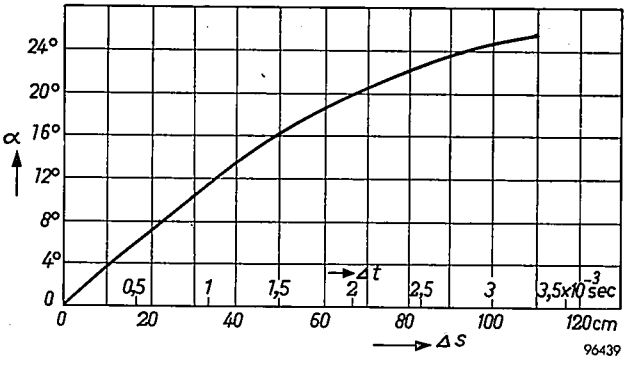

Fig. 3. Angular displacement α of the stereophonic sound image from its midway position as a function of the time difference Δt between the sound from the two loudspeakers. (Δs is the corresponding difference in the distance travelled by the two contributions.)

conds or an intensity preponderance of 15 dB shifts the sound image fully to the first loudspeaker; smaller differences in time and intensity produce, independently and additively, proportionally smaller displacements; see *fig. 2* and *fig. 3* [7]). Displacements due to a time difference can be corrected by applying a certain intensity difference; in *fig. 4* it is shown that an intensity difference of 5 dB corresponds to a time difference of 1 millisecond.

The auditory property causing two sounds to merge into a single sound image, whose location within the limits mentioned is determined by the differences in the time of arrival and intensity of the two sounds, constitutes the basis of stereo-

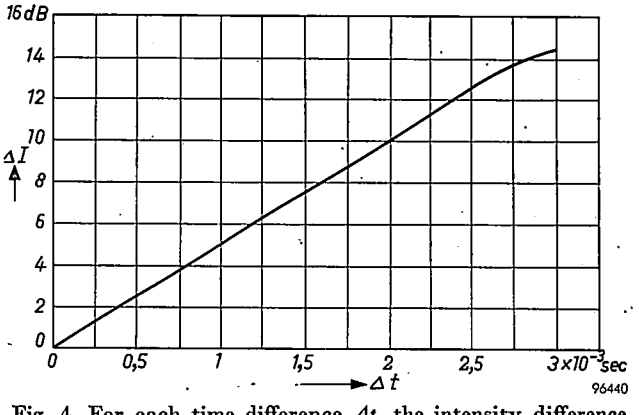

Fig. 4. For each time difference Δt, the intensity difference ΔI is plotted which causes the same angular displacement of the stereophonic sound image.

[6]) K. de Boer, A remarkable phenomenon with stereophonic sound reproduction, Philips tech. Rev. **9**, 8-13, 1947.

[7]) K. de Boer, Stereophonic sound reproduction, Philips tech. Rev. **5**, 107-114, 1940.

phonic reproduction. With a suitable arrangement of two microphones connected via separate channels to two loudspeakers (*fig. 5*) the sound sources in front of the microphones are imaged between the loudspeakers. In this way the sound image of speech or music can be arranged to lie at an arbitrary position between the loudspeakers. Moreover the sound image can be shifted by introducing from a control desk appropriate time or intensity differences, or both, between the signals in both channels. This is a familiar technique in film studios for making films with more than one sound track, and is known by the name of "pan potting" ("panoramic potentiometer control").

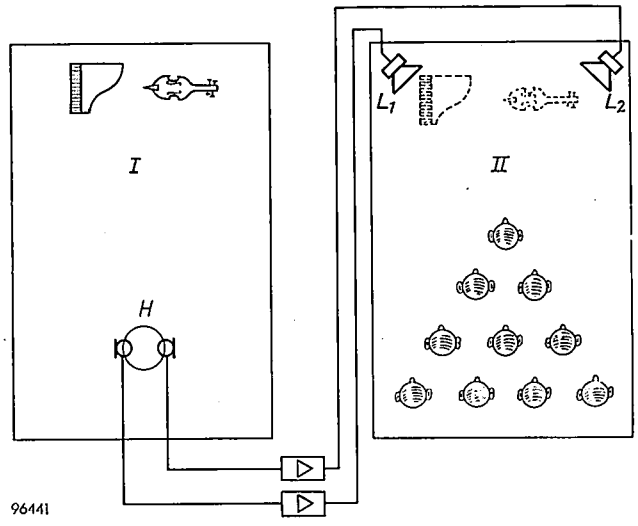

Fig. 5. Stereophonic transmission of music. The microphones on an artificial head *H* in room *I* are connected via separate channels to loudspeakers L_1 and L_2 in auditorium *II*, where the audience receives stereophonically an impression of the spatial disposition of the musical instruments.

If the listener is not equidistant from the two loudspeakers the result is an additional time difference due to the difference in distance. Consequently the stereophonic sound image shifts towards the loudspeaker nearer to the listener. In a large part of an auditorium this displacement can be kept within reasonable bounds by suitably disposing and directing the loudspeakers (we shall return to the latter point presently). By these means it is possible to produce intensity differences that depend so much upon the position of the listener as to compensate largely for the effect of the differences in distance.

Where sound from two loudspeakers reaches the listener with a time difference of more than 3 milliseconds, the sound is heard to be issuing from that loudspeaker whose sound was first received; even if the intensity from the other loudspeaker is increased, the sound image can no longer be displaced. For such a listener, the stereophonic character of the reproduction is absent. Where the time difference is about 20 milliseconds the delayed loudspeaker can be made 10 dB louder than the other before the listener is aware that sound is issuing from it at all. Nevertheless, the delayed loudspeaker does influence the quality of the sound, which is thereby made not only louder but also fuller in tone.

Where the time difference is greater than 50 milliseconds, the sound last to arrive is heard separately as a disturbing echo, unless it is 10 or more decibels weaker than the preceding sound.

The fact that sound arriving with a delay of about 3 to 50 milliseconds is aurally merged with the preceding sound, and is also heard to issue from the direction of the preceding sound, can be utilized for electrical sound-reinforcement in order to amplify speech, for example, by up to 10 dB, in such a way that the listeners are not aware of the electroacoustical aids employed. They hear the sound apparently coming from the speaker, even though the loudspeaker sound comes from a different direction.

The above auditory properties make directional hearing possible in an auditorium spite of the fact that most of the sound reaches the listeners after reflection from the walls, hence from directions other than that of the sound source. The reflected sound waves travel a circuitous path through the auditorium and thus always reach the listeners later than the sound waves travelling directly from the source. The delays suffered by reflected sound in a large hall, particularly after multiple reflections from the walls, far exceed the above-mentioned time difference of 50 milliseconds, which corresponds to a distance of about 17 metres. Nevertheless, in a hall with good acoustic properties the reflections are not heard separately but together as a reverberation. The ear distinguishes individual reflections only where they stand out above the general level of sound and are also delayed by at least 50 milliseconds. If they are part, however, of a succession of reflections each following within 50 milliseconds of each other, they are not heard individually.

To recapitulate, then, there are three cases to be distinguished in the reproduction of sound via two loudspeakers:

1) Where the sounds follow within 3 milliseconds of each other, they merge to form a single stereophonic sound image whose position between the loudspeakers is determined by the difference in the time of arrival and intensity of the two sounds.
2) Where the interval between the sounds is between approximately 3 and 50 milliseconds, the

sound first to arrive determines the direction; the delayed sound influences the loudness, however, and also the quality of the sound, inasmuch as it created a more spatial impression.

3) Where the interval between the sounds is greater than 50 milliseconds, the sound last to arrive is generally heard as a troublesome echo, unless it is at least 10 dB weaker than the preceding sound.

The first and second cases apply to sound reproduction and to the performance of music in an acoustically suitable auditorium. The third case applies to acoustically unsuitable auditoriums, e.g. where there are "flutter echos" between parallel walls and troublesome reflections from the rear wall. In electro-acoustical installations these conditions should be avoided at all costs by appropriate arrangement of the loudspeakers.

Auditorium acoustics

The correct application of electro-acoustical techniques implies taking into account not only the properties of hearing but also the behaviour of sound in the open air and in enclosures.

We have seen that the listeners in a hall receive the sound only to a minor extent from the source ("direct sound") and for the most part via reflections from the walls ("indirect sound"). Consequently speech and music sound much louder in an enclosed space than in the open air, where the virtual absence of reflections means that only direct sound is received.

Direct sound is characteristic of the sound source itself. It represents the information conveyed and the artistic merit of the performance. By virtue of his aural sense of direction the listener is able to perceive in the direct sound the spatial distribution of an orchestra, the movement of actors over the stage, and so on. It follows, then, that faithful sound reproduction requires that the loudspeakers should radiate the direct sound with its original spectrum, its full dynamic range and stereophonically.

Indirect sound, although of course it originates from the same source, is primarily characteristic of the acoustic properties of the auditorium. It differs from direct sound in three ways.

In the first place indirect sound does not issue from one specific direction but from all directions in the auditorium. Unlike direct sound which is localized, indirect sound is therefore diffuse, and becomes all the more so the more effectively the walls disseminate the sound in all directions (i.e. reflect it diffusely) and the less they absorb it. In order to reflect sound diffusely the walls must be rough. The roughness should be considered in relation to the wavelengths of the sound. These vary from a few metres for the low tones to a few centimetres for the high tones. From the viewpoint of diffuseness the old concert halls with their wealth of ornamentation are more favourable than modern concert halls the walls of which are generally much plainer. It is particularly unfavourable if the sound is converged upon certain points in the auditorium in consequence of the shape of the walls. This can give rise to annoying echos.

Since the indirect sound is diffuse its intensity will be roughly the same everywhere in the auditorium. The intensity of direct sound, on the other hand, is inversely proportional to the square of the distance from the sound source. The proportional intensities of the direct and indirect sound gives the listener an indication of his distance from the source.

The second difference between the two kinds of sound is that, in travelling to the listener via the walls, the indirect sound always arrives later than the direct sound. This delay is relatively slight as far as the reflections from the rear wall of the stage or platform and from the floor are concerned; these reflections come from virtually the same direction as the direct sound. The reflections from other areas will be more delayed the larger is the auditorium. As explained above, a very slight delay in reflected sound is sufficient to eliminate its influence on the directional perception of the direct sound. Owing to the delay the perception of the direct and the indirect sound differs, and the listener perceives in the latter a greater or lesser diffuseness.

The third difference between direct and indirect sound is that, when the source stops radiating, the direct sound ceases at virtually the same instant, whereas the indirect sound persists for a time that depends on the degree to which the sound is absorbed every time it strikes a wall. Apart from being absorbed in the walls, the sound is attenuated — the high frequencies more than the low — on its way through the air, particularly as a result of atmospheric impurities (moisture, carbon dioxide, smoke). The less the absorption the greater will be the intensity and diffuseness of the sound and the longer will it take before it dies out.

These related properties are characterized by the reverberation time of an enclosure, which is defined as the period of time required for the sound to decrease, after the source is stopped, to one millionth of its initial intensity, i.e. by 60 dB; in practice this amounts to the time taken for the sound to become inaudible. The reverberation time is

found to be proportional to the volume of the enclosure and inversely proportional to the total equivalent absorption (Sabine's law) [8]). The unit of equivalent absorption is the "sabin" equal to the absorption of one square foot of a surface which absorbs *all* the incident sound energy. In the metric system this is given in the number of m^2 "open window"; a surface of 2 m^2 having an absorption coefficient of 0.1 contributes 0.2 m^2 "open window" to the equivalent absorption.

In general the reverberation time increases with the size of the enclosure, since the volume increases more rapidly than the surface of the walls. Measurements carried out in numerous auditoria with good acoustic qualities have provided sufficient data to make it possible to determine the optimum reverberation time for enclosures of various volumes and intended for different purposes (*fig. 6*).

Since the absorption coefficients of the various materials used for covering the walls are functions of frequency, the reverberation time of an auditorium will vary with the frequency of the sound in a way that depends on the materials used. Every auditorium, therefore, lends a distinct timbre to the indirect sound. In this respect there is a great difference between, for example, wooden and stone walls. In a hall with a glass roof or with large windows the reverberation time is short for the low notes owing to the fact that the glass transmits the low notes to a much greater extent than the high. *Fig. 7* shows a plot of reverberation time as a function of frequency for various concert halls. In general the reverberation time decreases towards the higher frequencies, which undergo more absorption in conventional wall materials and are moreover increasingly damped by the air. If *the* reverberation time of an auditorium is quoted, it usually refers to the reverberation time for a frequency of 500 cycles per second.

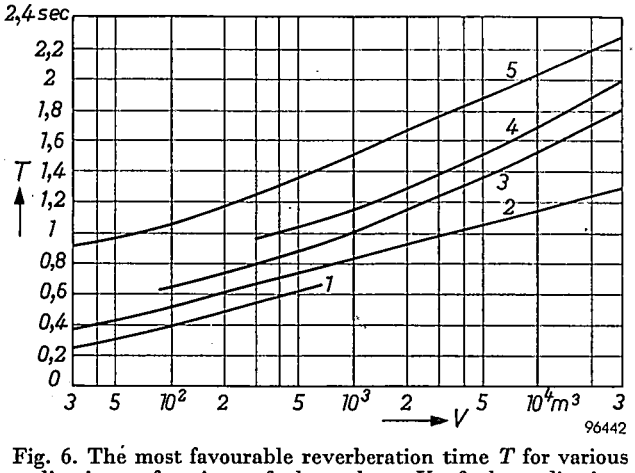

Fig. 6. The most favourable reverberation time T for various auditoria as functions of the volume V of the auditorium (taken from L. L. Beranek, Acoustics, McGraw-Hill, New York 1954). Curve *1*: broadcasting studios for speech. Curve *2*: meeting halls, cinemas. Curve *3*: broadcasting studios for music, opera house auditoria. Curve *4*: concert halls, Protestant churches, synagogues. Curve *5*: Catholic churches, auditoria for organ recitals.

[8]) See e.g. A. Th. van Urk, Auditorium acoustics and reverberation, Philips tech. Rev. **3**, 65-73 .1938.

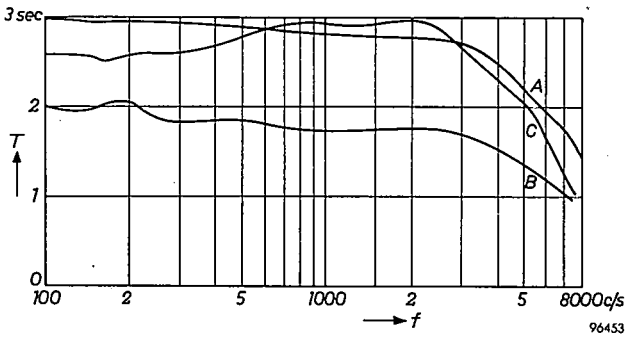

Fig. 7. Reverberation time T as a function of frequency f for various concert halls, after measurements by W. Tak. Curve *A*: Grand Hall of the Amsterdam Concertgebouw. Curve *B*: Philharmonic Hall, Liverpool. Curve *C*: St. Andrew's Grand Hall, Glasgow.

The audience in an enclosure is reponsible for a great deal of sound absorption. To prevent the acoustics depending unduly upon the size of the audience, efforts are made to cover the seats in such a way that, whether occupied or not, they present approximately the same absorption.

Auditorium acoustics for speech and music

The acoustic properties required of an auditorium for speech and for music are quite different.

Speech acoustics require the loudness reinforcement due to the indirect sound but not the reverberation, since this makes the speech less intelligible. As mentioned, the indirect sound arriving within about 50 milliseconds after the direct sound contributes usefully to the loudness and affects neither the impression of direction nor the intelligibility. Sound delayed by more than 50 milliseconds, however, reduces intelligibility in that it overlaps the sounds that follow. To be no longer troublesome the sound delayed more than 50 milliseconds must be made about 10 dB weaker. Theatres and lecture halls are therefore designed in such a way that the reflections arriving with a delay of less than 50 milliseconds are as far as possible directed towards the audience, whilst efforts are made to damp the more delayed reflections by providing the appropriate parts of the walls with absorbent material. For example, the lower part of the rear wall in a theatre will be made acoustically hard so that the audience at the back of the theatre will receive additional useful sound. The upper part of the rear

wall, however, will be covered with absorbent material to prevent long-delayed reflections from arriving at the front of the theatre and on the stage. A good theatre auditorium, in which the reflections are properly directed on the audience, has a fairly short reverberation time (0.7 to 1.0 second) and little diffuseness.

In a concert hall the diffuseness and the reverberation are essential to give "body" to the music. A symphony orchestra requires a large hall and a reverberation time of 1.8 to 2.5 seconds to be heard at its best. A church organ requires an even greater space and an even longer reverberation time.

The above aspects of auditorium acoustics, on which electro-acoustical control is based, may be summarized as follows:

1) There is a fundamental difference between direct and indirect sound. Direct sound provides the stereophonic impression of what is taking place on the stage or orchestral platform; it gives "definition" to the sound. Indirect sound, with its timbre, diffuseness and reverberation, is characteristic of the auditorium; it invests the sound with spaciousness and gives fullness or body to music, the more so the greater the degree of diffuseness. Where the indirect sound is delayed more than 50 milliseconds, however, it adversely affects the intelligibility of speech.
2) The delay of the indirect sound creates an impression of the size of the auditorium.
3) The relation between the intensities of direct and indirect sound determines the impression of distance.

Electro-acoustical control of auditorium acoustics

The natural direct and indirect sounds heard in an auditorium are correlated by the properties of the auditorium. The possibility of controlling the acoustics of an auditorium results from the fact that the direct and indirect sound can be separately produced and controlled by electro-acoustical means. It is therefore a principle in modern acoustic installations to produce the direct and indirect sound separately through individual groups of loudspeakers.

Direct sound

For producing almost pure direct sound, loudspeakers are used that beam their sound in the direction of the audience, so that as little as possible is incident on the walls. The gain in the ratio of direct to indirect sound obtained by beaming can be demonstrated by the following numerical example.

Consider a large auditorium with acoustically hard walls and a floor sloping up towards the rear, and imagine a speaker in this auditorium who sees his audience within a horizontal angle of 90° and a vertical angle of 15°.

For the notes in the low and medium frequency ranges the speaker can be regarded as a virtually spherical radiator, radiating sound with equal intensity in all directions. A simple calculation shows that the solid angle within which he sees the audience covers only 1/30th of the total solid angle of 4π steradians around the speaker. Thus only 1/30th of the radiated sound reaches the audience directly and 29/30th strikes the walls, which reflect it for the most part as disturbing, reverberant sound. The ratio of direct to indirect sound is thus about 1/30 : 1. Consequently the speaker will be understood well only in the front rows of the auditorium; towards the rear the intelligibility decreases rapidly (*fig. 8a*).

Now imagine the speaker to be replaced by an ideally beamed loudspeaker, i.e. one which exactly comprises the audience within its sharply defined radiating angle. The entire radiated sound will now reach the audience in the form of direct sound. The clothing worn by the audience and the unoccupied, suitably covered seats absorb about 80% of the incident sound (except for the very low notes, to be dealt with presently). The reflected fraction, about 20%, impinges on the walls and is responsible for a certain intensity of indirect, reverberant sound. The ratio of direct to indirect sound is now approximately 5 : 1, that is about 150 times greater than in the first case considered. The direct sound now predominates over the indirect sound right to the back of the hall, and therefore the speech is everywhere perfectly intelligible (fig. 8*b*).

In reality the speaker and the beamed loudspeaker are usually both present in the auditorium, the loudspeaker being used to reinforce the speech which is spoken at a normal level as if no sound installation were there. The indirect sound due to the speaker himself is then, of course, just as loud as it would be if no sound installation were present. As we have seen above, the direct sound from the speaker can be relayed by the loudspeaker amplified 150-fold, before the indirect sound significantly increases; the above-mentioned advantage of beaming can thus in practice be realized almost to the full. In practice a much smaller amplification is found sufficient, particularly if the beam — whose intensity gradually decreases from the centre towards the edges — is directed mainly towards the rear half of the auditorium (fig. 8*b*). The ratio between the

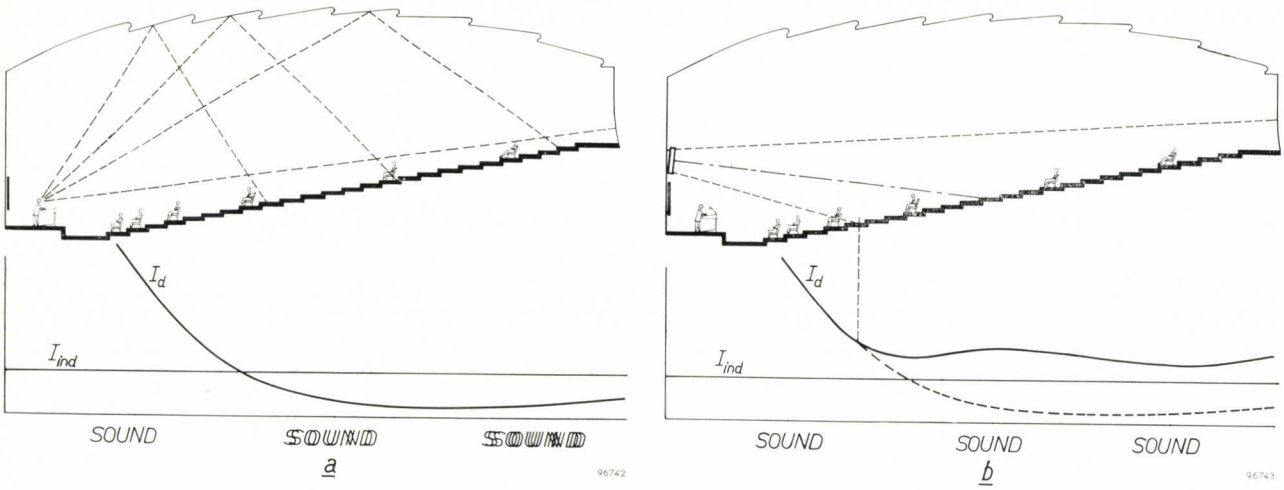

Fig. 8. *a*) A speaker in a large hall having acoustically hard walls (long reverberation time) can be understood by the audience near the front, but towards the rear the intelligibilty is spoiled by the disproportionately strong indirect sound (see the curves showing the sound intensities I_d and I_{ind} of the direct and indirect sound, respectively, as a function of the distance to the speaker). *b*) By means of a group of loudspeakers which direct the sound mainly on to the rear part of the hall, I_d can be made strong enough in proportion to I_{ind} to make the speech perfectly intelligible to the whole audience.

intensities of direct and indirect sound can now be virtually the same at all positions in the auditorium and sufficient for good intelligibility, without the audience being aware that they are listening to the loudspeaker. The impression of hearing the speaker directly can be reinforced if the loudspeaker, or loudspeakers, be so arranged that the radiated sound reaches the audience 10 to 20 milliseconds later than the direct sound from the speaker. The impression of direction is just as unaffected under these conditions as it is by the "useful" reflections of less than 50 milliseconds delay in a good auditorium.

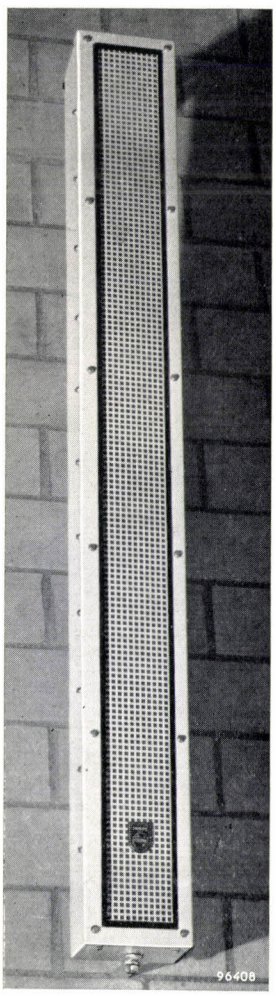

Fig. 9. A loudspeaker column.

It is well known that a beam of sound having a large horizontal and a small vertical radiating angle can be obtained by means of a loudspeaker column (or "sound column"), consisting of several loudspeakers mounted one above the other and all operating in phase (*fig. 9*).

The beaming action of a loudspeaker column is based on interference effects between the various loudspeakers. Consider a vertical column and a listener situated in the horizontal median plane of the column at a distance which is large with respect to the length of the column. The sound waves from the various loudspeakers in the column will reach the listener virtually in phase and thus augment each other. Let the column contain n loudspeakers, then the sound pressure and the sound intensity reaching the listener will be respectively n and n^2 times greater than from a single loudspeaker in the column. Since a single loudspeaker is fed with $1/n$ of the power supplied to the whole column, the sound intensity in the beam radiated by the column is n times greater than that of a single loudspeaker fed with the same total electric power.

If the listener moves his position up or down, he is no longer at an equal distance from the individual loudspeakers. He no longer receives all their sound waves in phase; the augmenting effect is therefore diminished and the sound intensity decreases. If his position is so far above or below the horizontal median plane that the distances between him and the top and bottom loudspeakers differ exactly by the wavelength λ (we assume that the loudspeakers radiate only one note), then each loudspeaker above the median plane will have a counterpart half the column length lower whose sound waves arrive at the listener exactly in anti-phase. No sound is therefore radiated in directions where this is the case. The same situation is found where the listener is so far outside the median plane that the distances between him and the top and bottom loudspeakers differ by 2λ, 3λ, and so on.

Between these regions of zero intensity there are regions of maximum intensity (*fig. 10*) which however become progressively smaller than that in the median plane; only in this plane is the sound from all the loudspeakers received in phase. Let the sound intensity in the median plane (the zero-order maximum) be I_0, then the intensity in the k^{th} maximum is:

$$I_k = \left[\frac{1}{(k+\frac{1}{2})\pi}\right]^2 I_0 .$$

The sound radiation can be said to be largely concentrated within the zero-order region. This main lobe covers an angle $2\varphi_0$ given by

$$\sin \varphi_0 = \frac{\lambda}{L},$$

where L is the length of the column. For small values of φ_0 the radiating angle can be written:

$$2\varphi_0 = \frac{2\lambda}{L}.$$

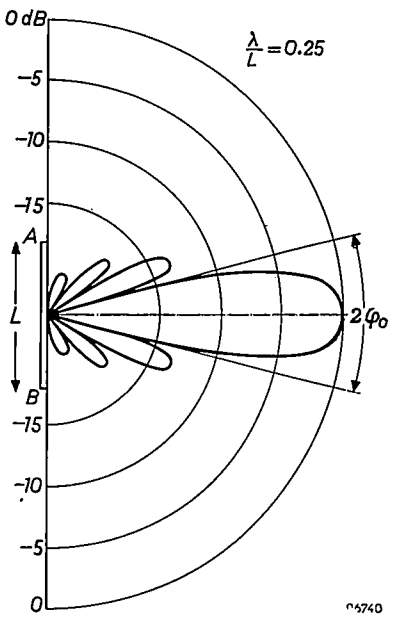

Fig. 10. Directional characteristic of a loudspeaker column AB in the vertical plane of symmetry at a given frequency. Virtually all the energy is radiated in the main lobe, the angle $2\varphi_0$ being smaller the higher the frequency and the longer the column.

The beaming effect of a loudspeaker column in the vertical plane is sharper the longer the column and the shorter the wavelength of the sound (i.e. the higher the frequency). For a column two metres in length the radiating angle at 300 c/s is 68°, and at 3000 c/s only 6.4°. To comprise as many listeners as possible within the narrow beam of the high notes it is therefore necessary to arrange the column so that the beam passes closely over the listeners' heads.

The beaming effect of the column in the horizontal plane does not differ from that of an individual loudspeaker. A single loudspeaker also tends to concentrate the high notes increasingly around the principal axis. Horizontal beaming is usually undesirable since it prevents the proper distribution of the high notes in an auditorium, and it is precisely the high notes that are essential to good intelligibility. To avoid beaming in the horizontal plane it is advisable in the first place to use twin-cone loudspeakers. The response curve of these loudspeakers extends to about 18 kc/s, i.e. to the highest audio frequencies, and the high frequencies are beamed much less sharply than by single-cone loudspeakers [9]). Secondly, the loudspeakers of the column should be mounted with their axes not parallel but with slight angular displacements with respect to each other so that the individual high-note beams uniformly fill the total beam. For the tones in the low and medium ranges the loudspeakers then form a long column with a pronounced directional character, whereas for the higher notes the effective part of the column tends to become more and more limited to those loudspeakers pointing in the listeners' direction; for the very high notes there is only one effective loudspeaker for each point of the auditorium. The reduction of the effective part of the column with increasing frequency thus keeps pace more or less with the shortening wavelengths, resulting in a fairly constant radiating angle.

Below about 300 c/s the directional effect even of a long column is inadequate, and moreover the sound undergoes less absorption by the audience. In this frequency range, then, the indirect, reverberant sound tends to increase. To avoid this it is necessary to attenuate the reproduced low notes by means of an electric filter and/or by fixing the resonance frequency of the loudspeakers in the region of 300 c/s (below resonance the radiated power drops rapidly as the frequency decreases). This relatively high resonance frequency can be obtained either by using a sufficiently small cone or by introducing a small enclosed volume of air behind the cone. The latter method has the advantage of reducing non-linear distortion [10]), a point of particular importance if the loudspeakers have to operate at full power, which is often necessary out of doors. The suppression of the sound spectrum below 300 c/s does not make speech sound any less natural; on the contrary, it restores the balance in that it compensates for the reduced damping of the sound in the auditorium at lower frequencies.

If the column is built up of small loudspeaker boxes, capable of being independently aimed, the column can be of simple construction yet completely adapted to the requirements of the auditorium. In the Palais de Chaillot, columns of this kind are mounted at either side of the stage (*fig. 11* and *fig. 12*). The columns are used for stereophonic speech reinforcement for stage plays and for relaying stereophonic sound effects pre-recorded on twin-track magnetic tape (see part II).

[9]) J. J. Schurink, The twin-cone moving-coil loudspeaker, Philips tech. Rev. **16**, 241-249, 1954/55, in particular figs. 9 and 10.

[10]) G. J. Bleeksma and J. J. Schurink, A loudspeaker installation for high-fidelity reproduction in the home, Philips tech. Rev. **18**, 304-315, 1956/57, in particular p. 310-311.

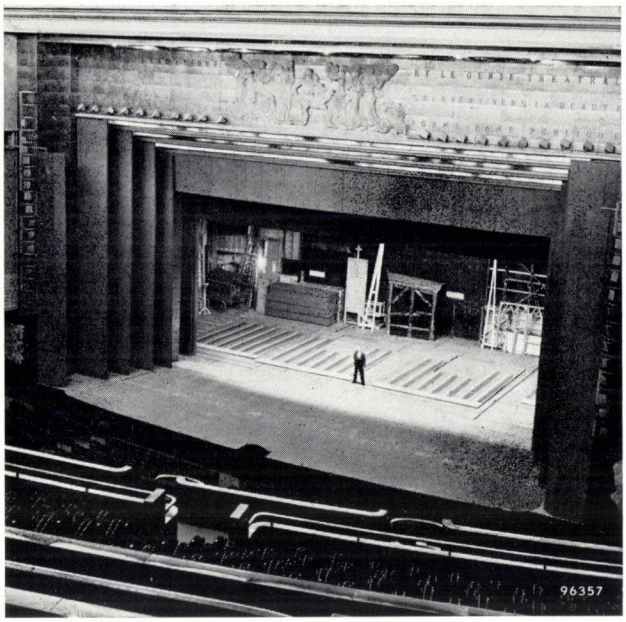

Fig. 11. The stage in the Palais de Chaillot, Paris. Loudspeaker columns for reinforcing the direct sound can be seen on the left and right of the stage (see also fig. 12). Loudspeakers for indirect (diffuse) sound are mounted above the stage.

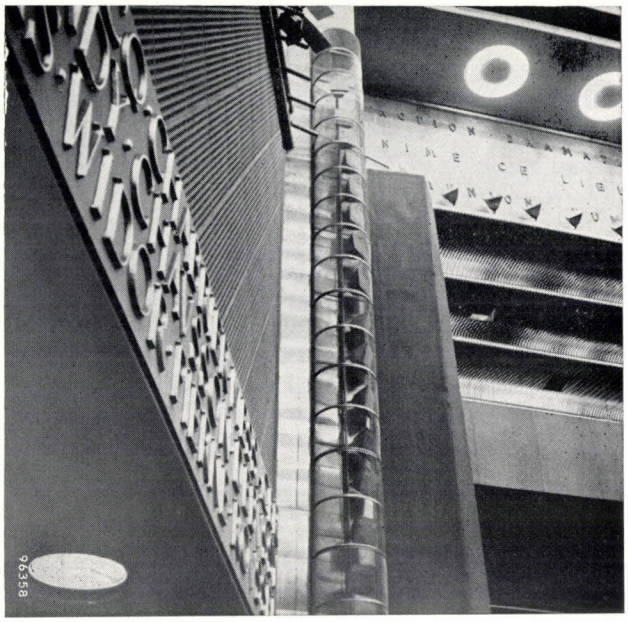

Fig. 12. One of the loudspeaker columns shown in fig. 11. The constituent loudspeakers point in different directions in order to radiate the high tones uniformly throughout the auditorium.

Beamed loudspeakers are used not only in enclosures but also in the open air. A striking example is shown in *fig. 13*. In an open-air sound reinforcement system beamed loudspeakers serve a dual function. In the first place the radiated sound is concentrated in the direction of the listeners, which makes it possible to limit the power of the amplifiers and loudspeakers required. In the second place less nuisance is caused in the surroundings, and the reproduction is not spoiled by reflections from nearby buildings. Besides columns of cone-type loudspeakers, which radiate mainly in a flat lobe, use is also made of individual horn-type loudspeakers, which radiate the sound within a conical region about the axis. The radiating angle of the cone is practically the same as that of a loudspeaker column whose length is equal to the diameter of the mouth of the horn. Horn loudspeakers combine a high efficiency with excellent weather-resistant properties. For the reproduction of music, however, their drawback is that the horn cuts off low notes below a certain frequency which is determined by the flare of the horn. If the cut-off frequency is not to be too high the cross-sectional area of the horn should increase very gradually, but in that case it would become impracticably long. For this reason considerable use is made of folded horns (*fig. 14*). For outdoor purposes, especially where sound of considerable intensity is required to cover a large area, as on airfield runways and in dock installations, columns of horn loudspeakers are often

Fig. 13. Evangelical Church Congress, held on the Rebstock airfield near Frankfurt am Main (1956). In the vertical beam of the 40-metre high Cross, loudspeakers were mounted to form a sound column 30 metres long. The speaker on the platform could be clearly understood all over the ground, covering some 50 acres and on which a crowd of over 300 000 was assembled. At the end of the congress the installation was used for controlling the traffic.

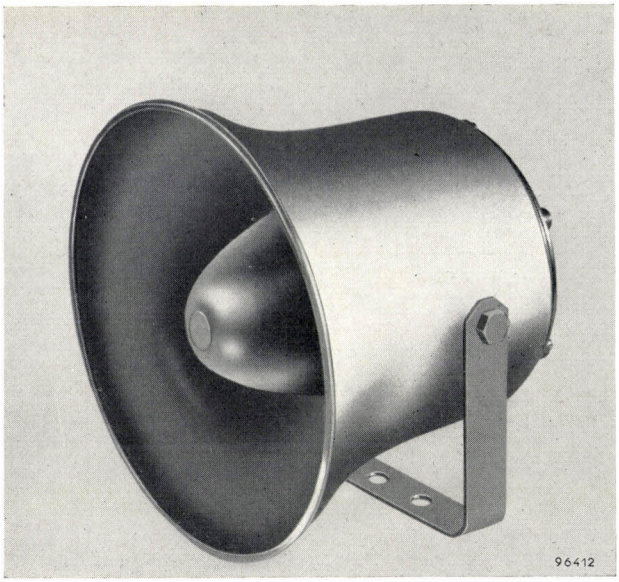

Fig. 14. Folded-horn loudspeaker.

employed which combine the advantages of the horn with additional beaming in the vertical plane.

A special form of horn loudspeaker is the multi-cellular type (*fig. 15*), which is used in cinemas for high-note distribution. The beams from the individual cells uniformly fill a wide solid angle, thus providing even distribution of the high notes.

In some cases, a central loudspeaker group for beaming direct sound is inadequate. Some examples are the following.

1) In the open air, *a*) when the contour of the ground is awkward, *b*) when it is windy, and the sound is, as it were, blown away, and *c*) when a temperature gradient exists; this phenomenon may bend the beam so far up or down that it no longer reaches the listeners (*fig. 16*).
2) In those theatres where the sound from the loudspeaker columns beside the stage does not adequately penetrate to the boxes or to the low space under the balcony.
3) In enclosures such as large churches and factory workshops where there are relatively few listeners, so that even with a highly directional loudspeaker group too much sound still strikes reflecting surfaces, thus producing excessive reverberation.

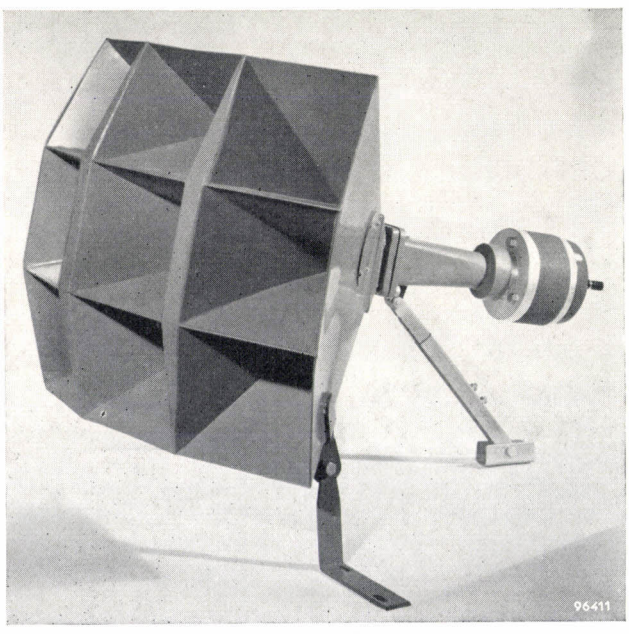

Fig. 15. Multi-cellular horn, much used in cinemas for uniformly radiating the high notes.

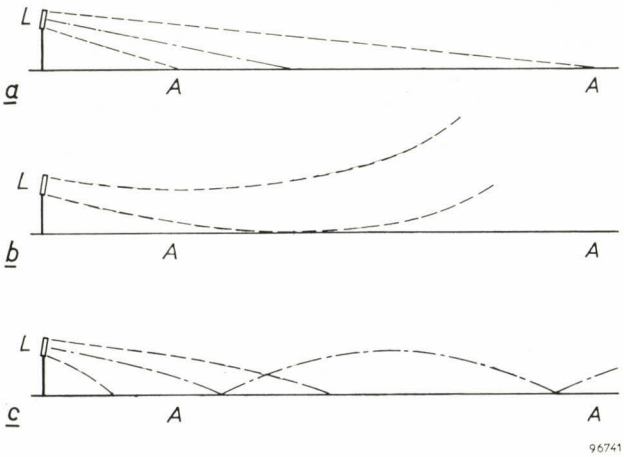

Fig. 16. Effect of a temperature gradient on the direction of sound. *a*) No temperature gradient. The sound from the loudspeaker column *L* is directed on to the audience *A*-*A*. *b*) The temperature drops with increasing height. Since the velocity of sound in warm air is greater than in cold air, the beam is refracted upwards and reaches only part of the audience. *c*) The temperature rises with increasing height. The beam is refracted downwards and only reaches the audience at the front. If the ground reflects strongly, the beam is again deflected upwards and bent downwards further on; in such conditions the sound has an exceptionally long range.

The solution in such cases is to install, instead of one central loudspeaker group, a larger number of loudspeakers with smaller fields of coverage, distributed according to the circumstances. The loudspeakers not required for certain occasions should preferably be switched off so as not to cause more reverberation than is unavoidable.

Where the fields of coverage of the loudspeakers coincide they may interfere with each other at places where they are not only almost equally loud but moreover arrive with a time difference of more than 50 milliseconds. There is a particular danger of this happening when dispersed loudspeaker columns are in use. The difficulty can be overcome by connecting the loudspeakers via a time-delay system (see below) which delays the signal to each loudspeaker to an extent corresponding to the air propagation time from the source to that loudspeaker (*fig. 17*). *Fig. 18* shows a large open-air installation in

which this principle was applied. The same method is also used in the "Volkswagen" factory public address system, to be described in part II of this article.

It is sometimes advantageous to make the delays 10 to 20 milliseconds longer than corresponds to the position of the loudspeakers. In this case the impression of direction is determined, as we have seen, by the sound first to arrive — even when it is up to about 10 dB weaker than the sound from the nearest loudspeaker. In this way the natural stereophonic effect of speech (whether directly from the stage or from the stereophonic loudspeaker columns beside the stage) is preserved for the audience at the rear, who hear the sound principally via the delayed loudspeakers.

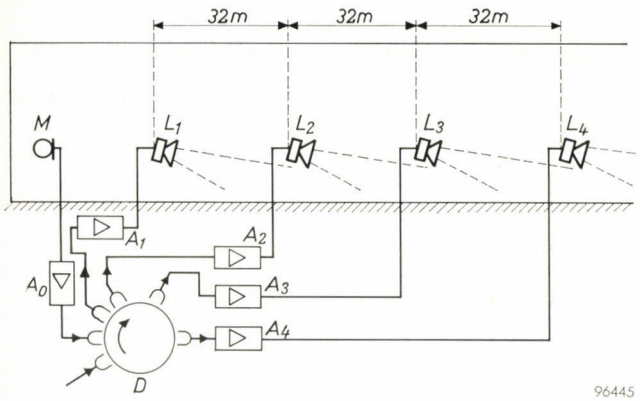

Fig. 17. Decentralized arrangement of loudspeakers for making speech intelligible in a long factory workshop with hard walls. M microphone. L_1, L_2, L_3 and L_4 are loudspeaker columns each of which cover e.g. a distance of 32 metres, corresponding to a sound transit time of 100 milliseconds. To prevent the loudspeakers interfering with each other, the electrical signal for L_2 is delayed 100 milliseconds with respect to that for L_1, the signal for L_3 100 milliseconds with respect to L_2 and so on. D is the delay system. $A_0 \ldots A_4$ are amplifiers.

Indirect sound

If an auditorium whose reverberation time is too short is to be made suitable for music, it is necessary to augment the indirect sound. The problem here is that the natural indirect sound is composed of an enormous number of reflections from all parts of the walls, whereas with sound produced electroacoustically one is naturally limited to a finite number of loudspeakers.

The solution of this problem by means of *ambiophony* [11]) has already been described in this

[11]) A new term introduced to replace the formerly used "stereo-reverberation". It appears that the latter is sometimes confused with stereophony — often abbreviated to stereo. The risk of confusion is all the greater since the advent of the stereophonic gramophone record which is making stereophony — or stereo — familiar to the general public. It is hoped that the introduction of the term *ambiophony* will put an end to this confusion.

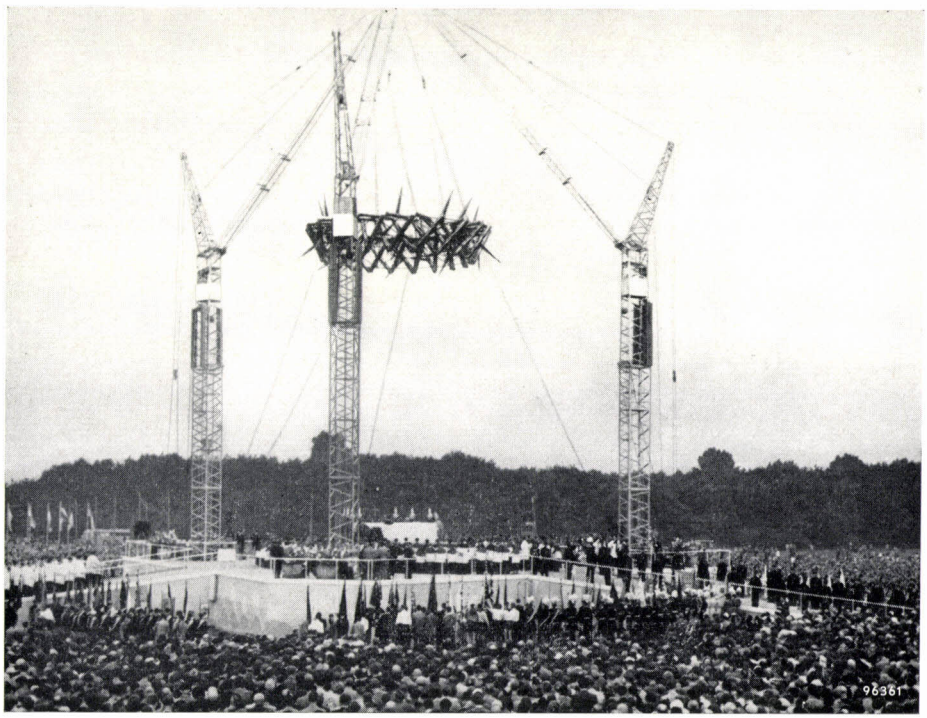

Fig. 18. Catholic Church Congress held in Cologne (1956) and attended by some 800 000 persons. Loudspeakers mounted in the symbol of the Crown of Thorns radiated sound to the distant parts of the ground. The regions nearer to the platform were covered by nine loudspeaker columns, mounted in the steel masts. To compensate for the difference in arrival time between the sound from the loudspeakers in the symbolic Crown and the sound from the columns, the signal through the columns was delayed such that both sounds reached the audience at the same time.

review [3]) and elsewhere [12]). It will therefore suffice here to briefly recapitulate the essentials of an ambiophonic installation. Above the orchestra a microphone *M* is suspended (*fig. 19*), the signal from which is recorded by a magnetic recording

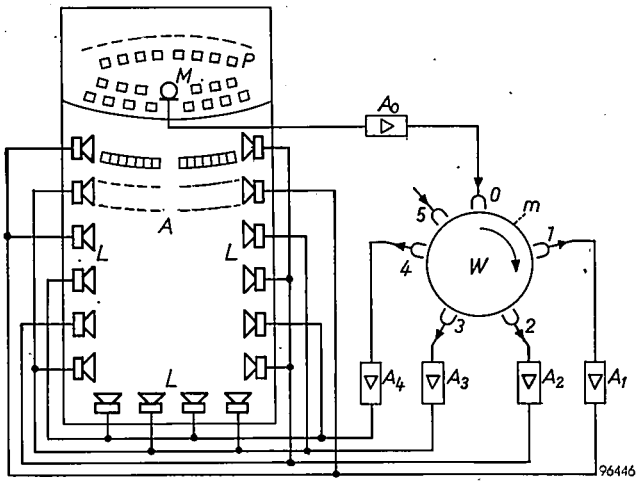

Fig. 19. Installation for ambiophony. *A* auditorium. *P* platform. *M* microphone. *W* delay wheel, coated on the edge with magnetic material *m* for magnetic recording. *0* recording head. *1* . . . *4* playback heads. *5* erasing head. $A_0 \ldots A_4$ amplifiers. *L* loudspeakers. Electrical feedback (not shown) can be applied from playback heads to the recording head.

head *0* situated at the periphery of a rotating wheel *W*, the delay wheel. The recording successively passes four playback heads *1* . . . *4* and an erasing head *5*; the latter ensures that the magnetic layer *m* is blank on returning to the recording head. The signals induced in the playback heads are delayed with respect to the microphone signal by varying degrees, depending on the speed of the wheel and on the distance, measured on the periphery, between the recording head and the playback head in question. Each of the playback heads is connected via its own amplifier to a group of loudspeakers appropriately disposed around the auditorium. The function of the loudspeakers is to radiate *diffuse* sound. To this end they are arranged around the auditorium in such a way that as little as possible of their energy is directly radiated on to the audience. The required effect can be achieved by giving each of these groups the correct intensity and timbre and the appropriate delay, and by applying electrical feedback from the playback heads to the recording head. The diffuse and delayed sound thus produced supplements the inadequate indirect sound from the walls of the auditorium. The sound can be produced for the most part by loudspeakers without the listeners being aware of it. The adjustment of the equipment is fairly critical; exaggeration detracts from the naturalness and betrays the presence of the installation. Experience has shown that, provided the system is properly operated, ambiophony appreciably improves the quality of a performance, and that actors and musicians of repute welcome its help.

An ambiophonic installation can also serve to suggest to the listeners that they are seated in a hall of greater size. The caption to *fig. 20* explains the method of calculating the delays to be applied to the various loudspeakers for this purpose.

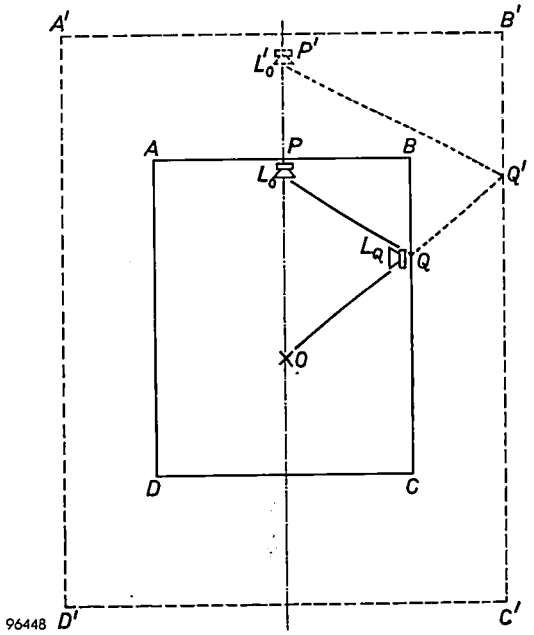

Fig. 20. Method of calculating by how much an arbitrary loudspeaker L_Q at a given position on the auditorium wall *ABCD* should be delayed in an ambiophonic installation in order 1) for an observer *O* to receive an impression of the true size of the hall, and 2) to receive the impression of being in a large enclosure (*A'B'C'D'*).

1) The loudspeaker L_Q must simulate a reflection at *Q* of sound emanating from the source L_0 at *P*. The signal for L_Q must be delayed by a time corresponding to the path *PQ*, i.e. by

$$\Delta t = \frac{PQ}{c},$$

where *c* is the velocity of sound.

2) To create the illusion of a larger auditorium, L_Q must give the impression that sound originating from an imaginary source L_0' at P' is reflected from the imaginary wall $B'C'$ at point Q'. The delay required for L_Q is now determined by the path length $P'Q' + Q'Q$, less the length PP' (the actual source still being at *P*). Hence:

$$\Delta t = \frac{P'Q' + Q'Q - PP'}{c}.$$

By repeating the construction for various points *Q*, delays can be found that should be applied to the loudspeakers L_Q around the auditorium in order to suggest the primary reflections in the simulated larger auditorium. Furthermore, to simulate the multiple reflections, other loudspeakers are needed between these loudspeakers and with greater delays.

The results of the construction depend little on the position of the point *O*.

[12]) See contribution by R. Vermeulen in the book Musik, Raumgestaltung, Elektroakustik, edited by W. Meyer-Eppler, Arsviva Verlag (H. Scherchen), Mainz 1955; see also D. Kleis, Experimente zur Verbesserung der Raumwirkung von Schall, Elektron. Rdsch. **9**, 64-68, 1955.

The lack of good musical acoustics is particularly felt in an open-air concert. The absence of wall reflections reduces the loudness and the music lacks "body", so that an outdoor performance by a first-class orchestra is often a disappointment to the listeners. These drawbacks can be overcome by supporting the performance electro-acoustically (see *fig. 21*). The direct sound can be brought to the required level by amplifying the orchestral music stereophonically and relaying through loudspeaker columns beside or above the orchestral platform. Moreover, by the addition of diffuse and delayed sound the music can be given more body, without diminishing in any way the pleasant atmosphere peculiar to a concert in the open air. The aim in such cases should be solely to enrich the sound of the music and not to emulate the acoustics of a concert hall. Since reverberation is essentially incompatible with an open-air performance, no feedback in the delay installation is normally applied in this case.

A delay wheel is also employed for compensating differences in the transit time of direct sound, as discussed above (figs. 17 and 18).

A delay wheel in its present-day form is shown in *fig. 22*; some particulars are described in the caption. *Fig. 23* shows a photograph of the complete ambiophonic installation, type EL 6910.

An auditorium provided with both installations — one for reinforcing the direct sound and one for adding ambiophony — is entirely independent of its original acoustics. *The sound installations are capable within wide limits of giving the auditorium any acoustic properties that may be required.* By appropriately selecting the delay times of the indirect sound and the ratio of direct to indirect sound it is possible to adapt to the circumstances both the apparent size of the hall and the apparent distance of the sound source from the listeners, i.e. the "relief" or auditory perspective of the auditorium. Thus the conditions most favourable for stage plays as well as for music can be created in one and the same hall. Moreover, by controlling the timbre of the indirect sound, it is possible to suggest different wall textures (stone, wood, etc.).

Microphones

Like the arrangement of loudspeakers, the positioning of the microphones constitutes a problem of acoustic adaptation that cannot be regarded separately from the auditorium. Where the microphones are used for making magnetic tape recordings, intended to be played back during the performance, or where they are situated in a separate room from which the music is to be relayed to the

Fig. 21. Open-air concert given by the Brabant Chamber Orchestra, conducted by Evert van Tright, on the square in front of the County Hall in 's-Hertogenbosch (June and July 1958). Above the platform, loudpeaker columns are mounted for stereophonically reinforcing the direct sound. Other loudspeakers are mounted on the façade of the building and in the trees for adding diffuse and delayed sound. With this arrangement the music was given a noticeably richer tone without simulating the acoustics of a concert hall and without detracting from the pleasant atmosphere of an open-air concert.

N.V. PHILIPS' GLOEILAMPENFABRIEKEN

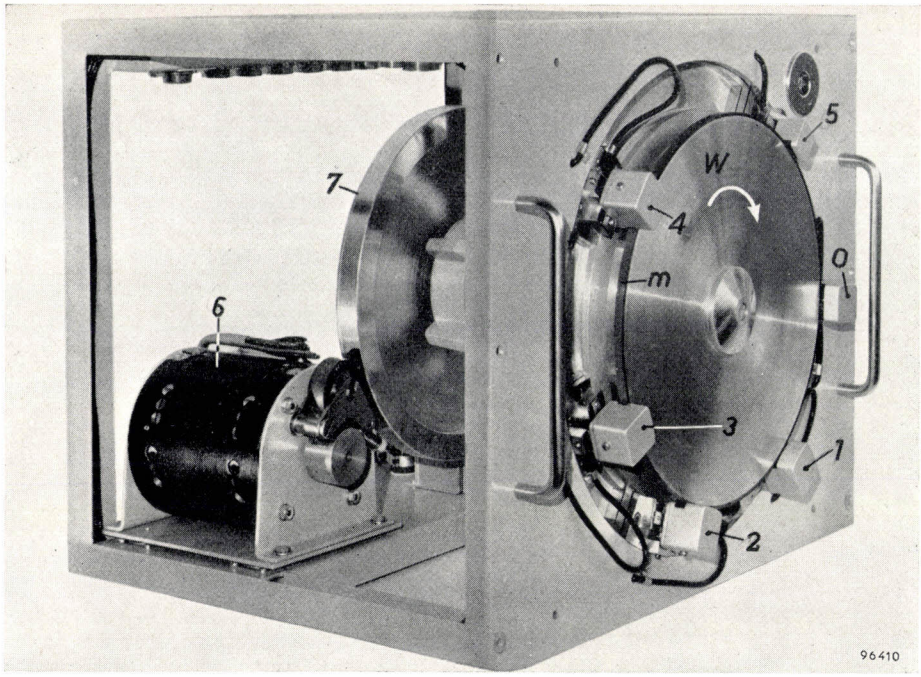

Fig. 22. Delay wheel *W* with magnetically coated rim *m*, recording head *0*, playback heads *1*, *2*, *3* and *4*, erasing head *5*, drive motor *6* and flywheel *7*. This unit is a component of the ambiophonic installation EL 6910 (see fig. 23).

The maximum delay for the fourth playback head is either 0.25 or 0.5 seconds, depending on whether the peripheral speed of the wheel is 3 or 1.5 m/sec. These two speeds are obtained by changing the number of effective poles of the drive motor. Between the magnetic layer and the various heads there is an air gap of approximately 20 microns, so that there is no mechanical contact between the layer and the heads, giving the wheel an almost unlimited useful life. The eccentricity of the wheel is less than 1 micron, the non-uniformity in the speed less than 0.01%.

auditorium, they can be arranged in accordance with conventional studio technique. Care should be taken to ensure that the microphones pick up primarily direct sound and as little as possible of reverberant sound and noise. The latter are much more perceptible when reproduced by a loudspeaker than when they are heard directly, for in the former case they cannot be dissociated by binaural location from the recorded direct sound. (For this reason broadcasting studios are always damped more than auditoria used for public performances.)

The microphones situated in the auditorium pick up in principle not only the sound from the stage or the platform but also the sound from the loudspeakers, the noise of the audience and the reverberation of the auditorium. If the microphones pick up the sound from loudspeakers to which they are themselves connected, the result is acoustic feedback. This is most pronounced for those frequencies of the sound spectrum that arrive at the microphone in a certain phase. The consequence is that notes of these frequencies receive additional amplification and hence a longer reverberation time. This preference for certain frequencies and the persistence of the associated notes are particularly troublesome effects which immediately betray the electro-acous-

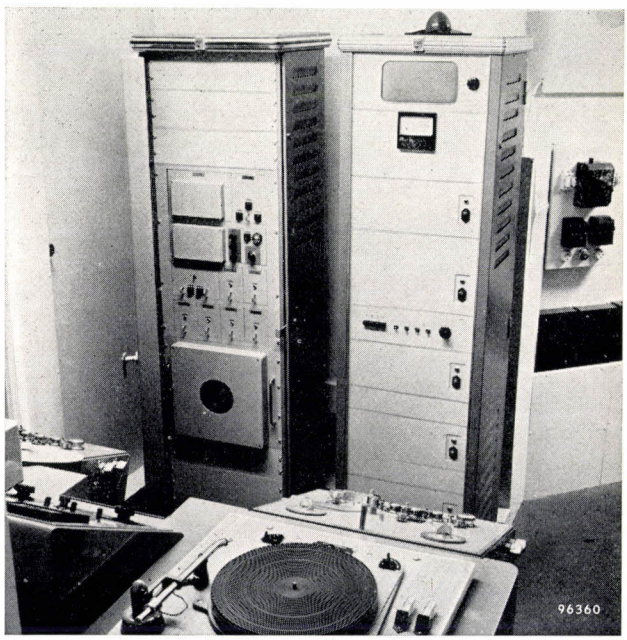

Fig. 23. Ambiophonic installation EL 6910 (left background) in the acoustic control room in the Palais de Chaillot. The reverberation time, and in each channel the loudness and timbre of the sound, can be adjusted either on the apparatus itself or remotely from a central mixing and control desk. The amplifiers are fitted with "Special Quality" tubes and have a frequency characteristic which is flat to within 1 dB from 160 to 12 000 c/s for 3 m/sec peripheral speed of the delay wheel and from 80 to 8000 c/s for 1.5 m/sec.

tical nature of the sound and adversely affect its quality. These effects are all the more troublesome the higher the amplification, which makes certain notes progressively more pronounced and more persistent. If the amplification exceeds a certain limit, the most pronounced preferred tone will not decay at all, and the installation will "howl". The occurrence of this in practice is obviously due to a gross error of operation. The undue persistence of certain notes is one of the most frequent complaints made about sound installations. In a well-designed system it is an unmistakable sign that the volume is turned up too high, another result of which, as already mentioned, is the exaggerated reproduction of the low notes.

The problem of avoiding acoustic feedback in theatre installations is made more difficult by the necessity to install the microphones unobtrusively or even out of sight. This means that the distance from the microphones to the artist on the stage or to the orchestra must always be fairly considerable. The only solution is to use microphones with marked directional characteristics.

The usefulness of a microphone in this respect is expressed by the ratio of its response in the preferred direction to the integrated omni-directional response, the front-to-random ratio. This ratio, then, is 0 dB for omni-directional microphones; for cardioid and ribbon microphones it is 5 dB, and for hypercardioid types 6 dB (see *table*).

To obtain a still better ratio, microphones can be grouped together to form a so-called "line" microphone [13]). The directivity pattern of a line microphone is identical to that of the radiation pattern of a loudspeaker column. The preferred directions lie mainly within a flat disc-shaped lobe lying symmetrically about the median plane of the line and subtending an angle which decreases with increasing length of the line and with increasing sound frequency.

Another solution is to use a "higher-order gradient microphone", which consists of two microphones mounted closely together with their diaphragms parallel, and connected in anti-phase. This leads to a more pronounced directional effect, although at the expense of the low-tone response. As we have seen, however, the latter may often be an advantage rather than a drawback.

The use of microphones sharply directed on to the stage not only reduces acoustic feedback but also the noise and reverberation picked up from the auditorium.

The best place to set up the microphones is often the front edge of the stage. Since the microphones cannot be approached closer than about 5 feet, the artists have considerable freedom of movement, without this giving rise to any noticeable intensity differences in the sound from the loudspeakers. This does much to help create a natural impression.

The microphone arrangement which, having regard to the above considerations, is best suited to give uniform pick-up (whether stereophonic or not) of the sound from stage, platform or orchestral pit, must of course be decided according to the given conditions. In part II of this article we shall discuss at greater length the arrangements in a number of sound installations.

Type of microphone	Polar diagram	Front-to-random ratio
Omnidirectional	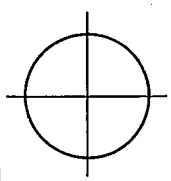	0 dB
Cardioid	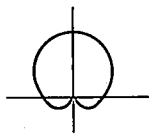	5 dB
Hypercardioid	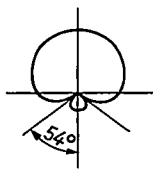	6 dB
Ribbon	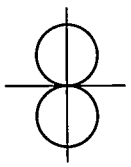	5 dB

Summary. Modern acoustical engineering is based on the properties of hearing and the acoustic properties of auditoriums. Both these subjects are briefly discussed. Many auditoriums are acoustically unsuited to the purpose for which they are to be used. Frequently, too, conflicting demands are made on the acoustics of an auditorium, for example when a hall is required to serve both for theatrical performances and for concerts. In such cases the solution is to install two electro-acoustical systems which together make it possible to exercise complete control over the auditorium acoustics. The one system serves for stereophonically reinforcing the direct sound, which is directed towards the audience by directional loudspeakers. The other system serves for introducing indirect, diffuse sound (ambiophony). By controlling the reverberation time of the indirect sound, an impression of spaciousness can be suggested. Theatrical performances can be additionally supported by means of "panoramic sound" (e.g. effect sounds from around or above the auditorium). Sound systems for large open-air meetings and outdoor concerts are also discussed. The author concludes with some comments on the arrangement of microphones.

[13]) Philips tech. Rev. **17**, 262, 1955/56, figs. 5 and 6.

COLOUR TELEVISION IN MEDICAL TEACHING

621.397.3:378.4:61

How to demonstrate surgical operations in such a way that they can be followed closely by large numbers of students is a problem of some antiquity in medical teaching. A significant step was taken towards its solution when advances in television engineering made it possible to project bright pictures of considerable dimensions. When the Philips projection system [1]) was introduced, its utility for medical teaching was quickly recognized. The system was demonstrated in the University Hospital at Leyden in February 1949, when an operation was followed on the television projection screen by more than 200 spectators [2]).

With the advent of colour television it has become possible to add colour information to the projected picture. The fact that this helps the spectators to understand what they see is illustrated in *fig. 1*, which shows the same surgical object in black-and-white and in colour.

Another important development in the last ten years has been the improvement of the variable-focus lens, or "zoom" lens. With this instrument the size of the field of view can be continuously varied, so that both general views and close-ups can be televised without shifting the camera.

These considerations induced the University of Marseilles to acquire for its Faculty of Medicine a closed-circuit colour-television system capable of projecting a very large picture (2.70 × 3.60 m). The installation, which was put into operation in October 1958, is briefly described below.

A diagram of the layout is given in *fig. 2*. In the operating theatre A the television camera is attached to the lamp above the operating table (see also *fig. 3*). The camera "sees" the brightly lit object (luminous intensity 20 000 to 30 000 lux) reflected in a flat mirror, which is mounted obliquely on the lamp and so coupled to it that if the lamp is turned the camera continues to see the illuminated field (fig. 2).

The camera contains three photoconductive

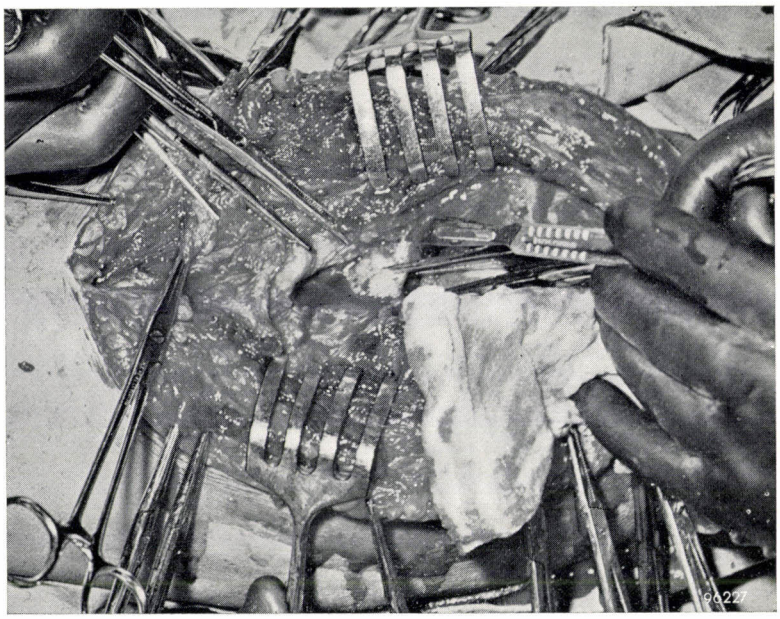

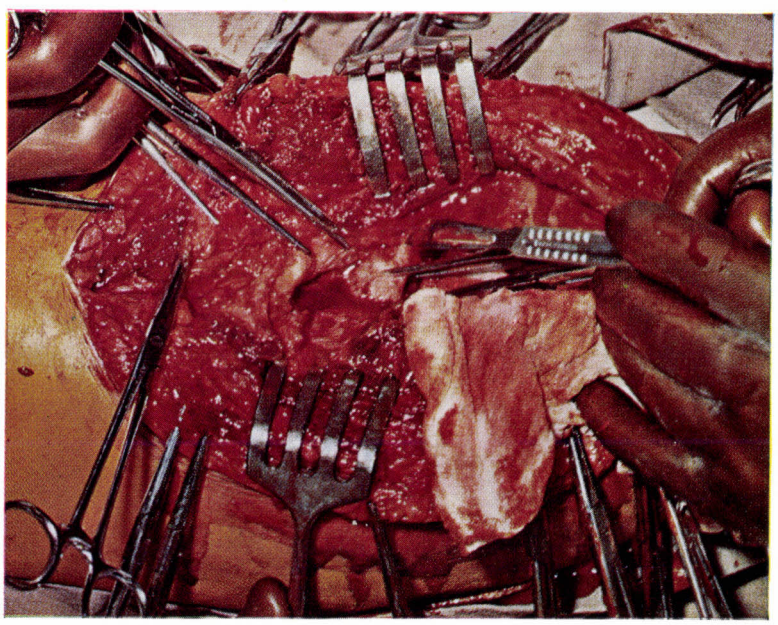

Fig. 1. A coloured picture of a surgical object shows details far more clearly than a monochrome one.

[1]) H. Rinia, J. de Gier and P. M. van Alphen, Home projection television, I. Cathode-ray tube and optical system, Proc. Inst. Rad. Engrs. **36**, 395-400, 1948.
P. M. van Alphen and H. Rinia, Projection-television receiver, I. The optical system for the projection, Philips tech. Rev. **10**, 69-78, 1948/49.

[2]) Philips tech. Rev. **11**, 42, 1949/50.

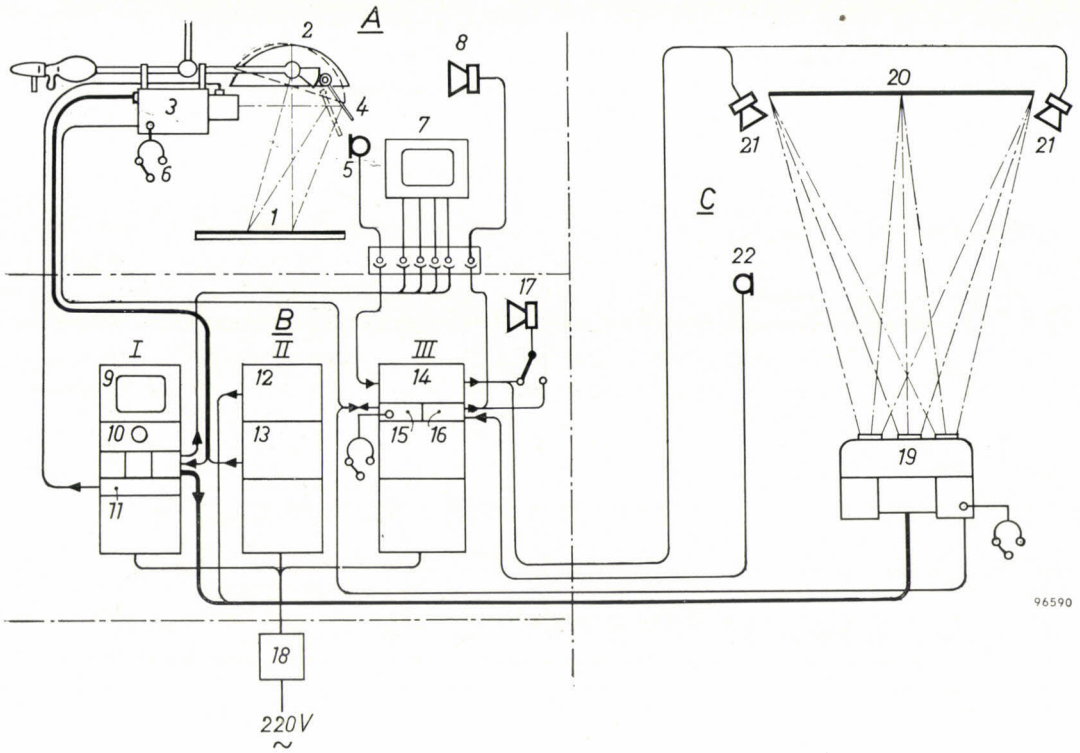

↑ Fig. 2

← Fig. 3

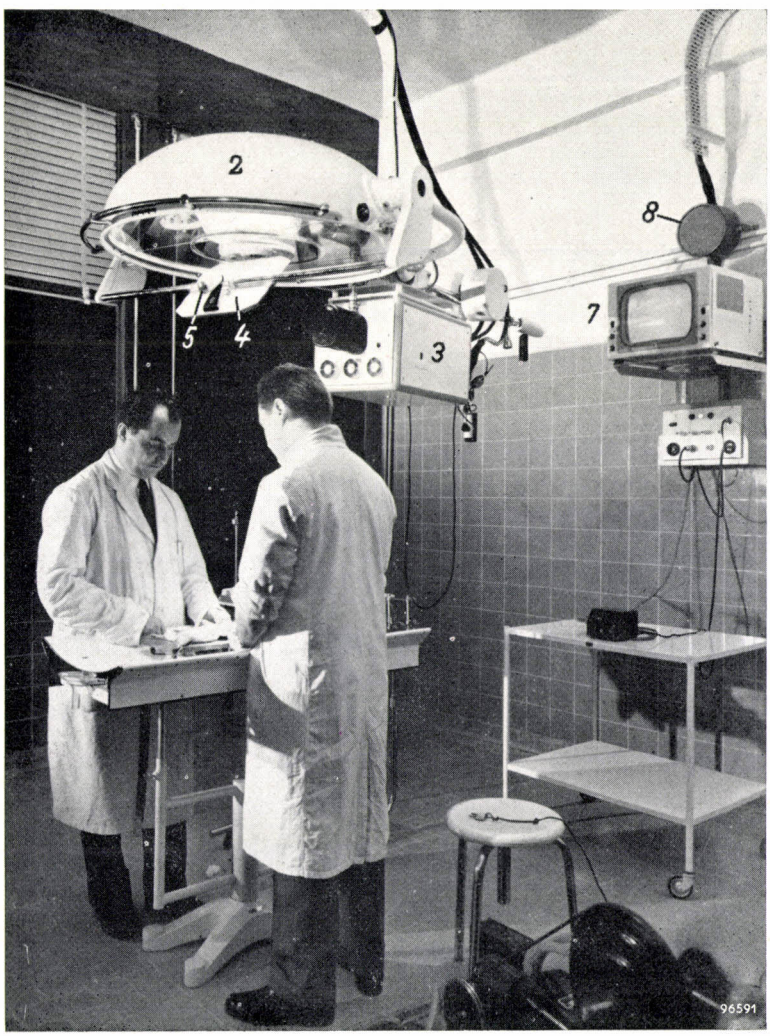

Fig. 2. Layout of the closed-circuit colour television system installed in the Department of Medicine at the University of Marseilles (the following photographs all relate to this installation).

A. Operating theatre containing operating table *1*, lamp *2*, colour-television camera *3*, mirror *4*, microphone *5*, headphone with microphone *6*, monochrome monitor *7*, loudspeaker *8*.

B. Control room containing racks *I*, *II* *III*. Rack *I* includes a monitor *9*, an oscilloscope *10* and a panel *11* containing the controls for adjusting the camera lens system (focus, focal length, aperture: these can also be controlled from the operating theatre). In Rack *II*, *12* delivers a test signal and *13* the scanning currents and correction signals for the camera. Rack *III* contains a 70 W amplifier *14* and two 2 W amplifiers *15* and *16*. Loudspeaker *17* enables the control-room operator to listen-in on both sound channels. *18* is the voltage stabilizer (5 kVA).

C. Lecture theatre with colour-television projector *19*, projection screen *20*, loudspeaker columns *21* and microphone *22*.

Fig. 3. The operating theatre. The lamp *2* (numbering as in fig. 2) and the colour camera *3* are mounted on a bracket. The lamp carries the tilted mirror *4*, to the back of which a microphone *5* is fixed. Right, the picture monitor *7* and loudspeaker *8*. None of the equipment obstructs the surgeons.

camera tubes [3]). Dichroic mirrors and filters transmit the red, green and blue components of the incident light to their respective camera tubes [4]). The lens system ("Pan Cinor", made by S.O.M. Berthiot) has a continuously variable focal length of 42 to 170 mm, corresponding to a field of view of 30 to 7.5 cm diameter on the operating table. Focussing, zooming (changing the focal length) and adjustment of the diaphragm of the lens is done by remote control either from the operating theatre or from the control room. A feature of the lens system is that there is enough space between the last lens and the camera tubes for the dichroic mirrors and filters.

The operating theatre further contains a monochrome picture monitor (this could also be a colour picture monitor), on which the three primary-colour pictures can be checked separately or in combination.

As fig. 3 shows, none of the parts of the installation obstruct the surgeons.

The three primary-colour signals are transmitted by cable via the control room — which we shall discuss presently — to the lecture theatre (*C* in fig. 2). The projection system installed here (*figs. 4* and *5*) is of a type already dealt with at length in this Review [5]). It consists of three primary-colour projectors side by side, each incorporating a Schmidt optical system and a projection tube giving red, green and blue light, respectively. As described in

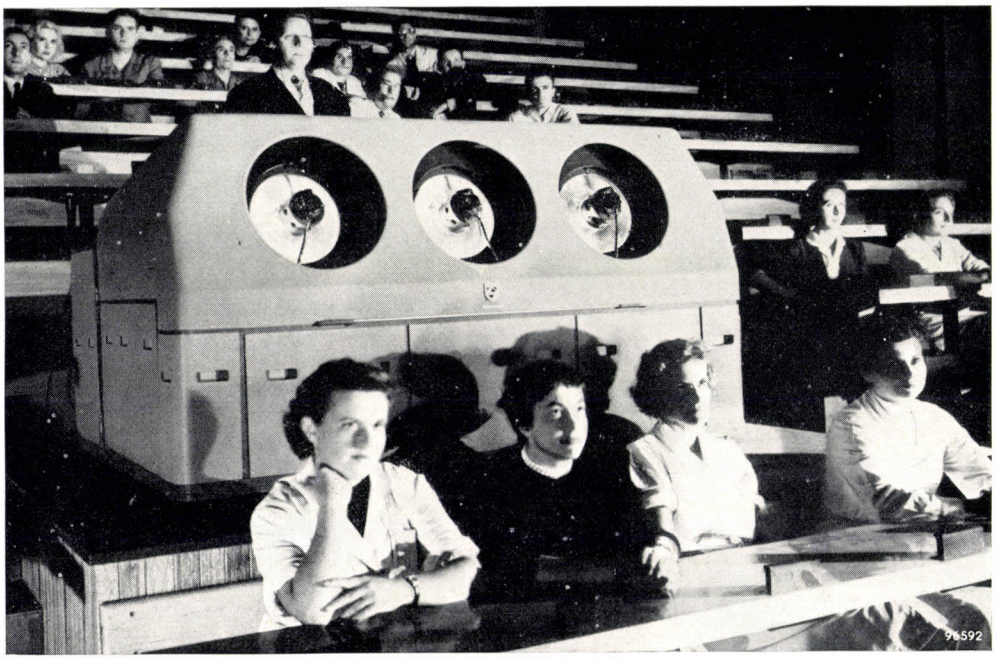

Fig. 4. The colour-television projector in the lecture theatre. The primary-colour projectors (red, green, blue) are mounted side by side [5]).

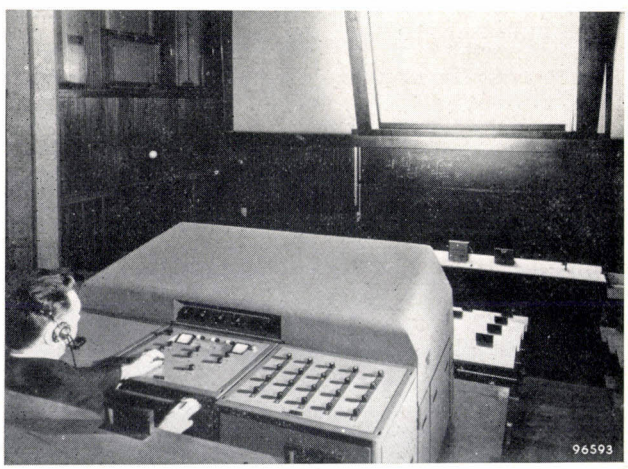

Fig. 5. The control desk for the colour-television projector. The picture on the screen measures 2.70 × 3.60 m and has a highlight luminance of 14 cd/m².

[3]) P. K. Weimer, S. V. Forgue and R. R. Goodrich, The Vidicon photoconductive camera tube, R. C. A. Rev. **12**, 306-313, 1951. L. Heijne, P. Schagen and H. Bruining, An experimental photoconductive camera tube for television, Philips tech. Rev. **16**, 23-25, 1954/55.

[4]) P. M. van Alphen, Applications of the interference of light in thin films, Philips tech. Rev. **19**, 59-67, 1957/58 (No. 2); see especially p. 65 et seq.

[5]) T. Poorter and F. W. de Vrijer, The projection of colour-television pictures, Philips tech. Rev. **19**, 338-355, 1957/58 (No. 12); see especially figs. 20, 21 and 22.

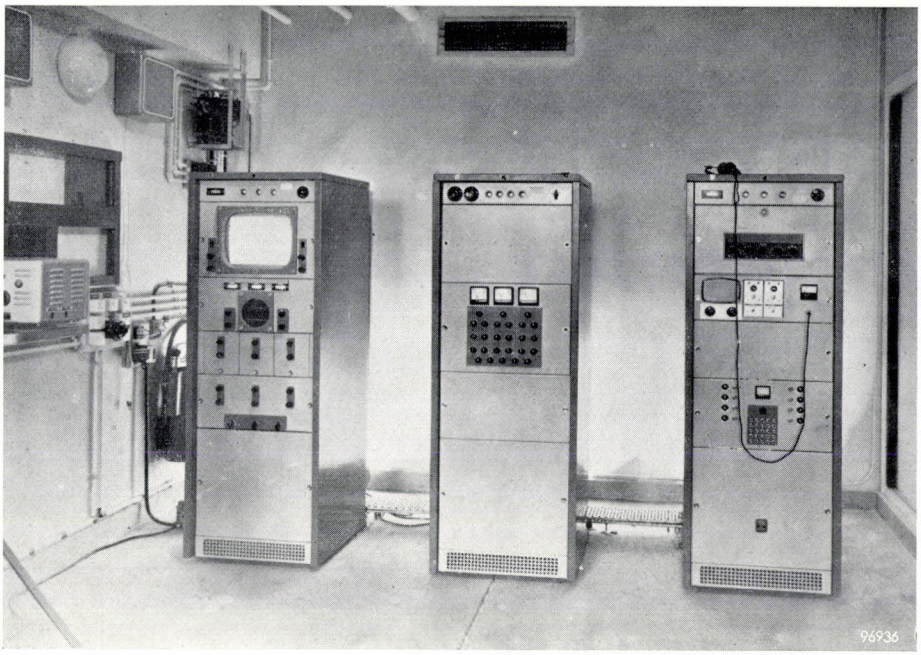

Fig. 6. The three racks in the control room (cf. fig. 2). The wall on the left is the rear wall of the lecture theatre. The operator can see the projected picture through the window.

article [5]), the three primary-colour images are brought into superposition on the projection screen partly by mechanical means (the outside projectors are pointed slightly inwards) and partly by electrical means (correction signals are added to the scanning currents). Effective measures are taken to provide protection against the X-rays generated in the projection tubes, which operate at 50 kV.

The picture on the screen (fig. 5) — beaded screen with a gain factor of about 2.5 — measures 2.70 × 3.60 m and has a highlight luminance of 14 cd/m². When the smallest field of view is used the projected image of a 7.5 cm object fills the whole screen height; this represents a linear magnification of about 36×. The size, definition, brightness and contrast of the projected picture are such that each spectator in the 300-seat lecture theatre can follow every detail of the operation. The result would still be amply satisfactory in a lecture theatre seating 500.

The control room (*B* in fig. 2) is equipped with three racks as shown in *fig. 6*. Rack *I* contains a picture monitor similar to that in the operating theatre, and an oscilloscope for checking the amplitude and waveform of the three primary-colour signals.

Rack *II* supplies the scanning currents and correction signals for the camera tubes (the picture is scanned on the 625 line system). This rack also contains the circuits generating the synchronizing signals for the camera and the colour projector, and a test signal for checking the colour projector distinct from the camera.

Rack *III* contains the amplifiers for the sound installation, viz. one 70 W amplifier and two 2W amplifiers. The first operates two loudspeaker columns, which are mounted at either side of the projection screen, and over which the commentary from the operating room is given. A limiter circuit in the amplifier prevents distortion if the speaker should approach too close to the microphone (which is attached to the back of the mirror); this allows the speaker appreciable freedom of movement in relation to the microphone. One of the 2W amplifiers serves the intercommunication system of headphones and microphones between the operating theatre, the control room and the projectionist. The other 2W amplifier connects a microphone in the lecture theatre to a loudspeaker in the operating theatre. A loudspeaker in the control room enables the operator stationed there to listen-in on this channel as well as on the 70W-amplifier channel.

The whole installation is powered from the mains via a 5 kVA voltage stablizer.

It is evident that the usefulness of this installation is not confined to instruction in surgery. Dentistry, anatomy, autopsies, sterilization technique, etc., can similarly be demonstrated to large audiences, not only for the teaching of medical students but also for the training courses provided in hospitals for the nursing staff.

W. A. HOLM and F. H. J. van der POEL.

AN APPARATUS FOR CINEFLUOROGRAPHY WITH AN 11-INCH X-RAY IMAGE INTENSIFIER

by J. J. C. HARDENBERG.

621.386.17:621.386.832.032.217.2:616-073.75

The radiograph (or X-ray photograph) owes its importance in medical diagnostic practice to the wealth of anatomical information it provides on the state or location of tissues and organs in the human body and on their pathological disorders. Cinefluorography (or X-ray cinematography), which has become practicable since the advent of the image intensifier, goes a step further inasmuch as it records the normal or abnormal behaviour of the organs while they are performing their function. Films made in this way yield valuable physiological information for diagnostic and instructional purposes.

The apparatus described below, with its large image field, makes it possible to examine cinematographically the large organs, such as the heart, the stomach and the lungs.

Members of various departments of the Philips factories have contributed to the development of this equipment, in particular J. R. Boerman, J. H. J. Maartens and J. H. A. Moubis of the Electron Tubes Division, and P. J. M. Botden, J. Fransen and A. Verboon of the X-ray and Medical Apparatus Division.

In medical X-ray examinations the technique of serial (spot-film) radiography occupies an important place. The movements of the organs to be examined, e.g. the gastro-intestinal organs, made visible by a contrast medium administered to the patient, are observed on the fluoroscopic screen and a radiograph is taken at the instant a diagnostically significant phase is seen to appear.

Where the movements of the object are rapid (as, for example, the deglutition of the oesophagus, the pulsation of blood-vessel walls, the peristalsis of the duodenum) it is necessary to take a number of spot-film radiographs in quick succession. Keeping to the method of direct radiography this has been effected by means of a mechanical device which changes the film approximately 10 times per second. A more elegant solution is that offered by fluorography, whereby photographs of reduced size are taken of the fluoroscopic image, the sequence of photographs being recorded on a rapidly transported roll of film of e.g. 70 mm width [1]). A series of such photographs offers for a diagnosis not only the anatomical information given by a single radiograph but also physiological information, inasmuch as the movement of an organ can be reconstructed by measuring geometrical changes (in particular the displacement of the contrast medium) in the successive photographs.

It would seem but a small step from this to X-ray cinematography or cinefluorography, i.e. to provide a permanent film record which, when cinematographically projected, gives a direct representation of the movement of the examined object. Compared with the original observation of the moving image on the fluoroscopic screen a cinefluorographic record has important advantages: the doctor is able to study a phenomenon at leisure over and over again, at a favourable luminance level and, if desired, together with colleagues or students; the film constitutes a documentary support for a diagnosis based on physiological abnormalities; and it is possible to follow details of a phenomenon more closely by slow-motion projection (or, rather, by making the exposure at increased frame-speed).

Though it would seem but a small step, in reality it presented almost insurmountable difficulties. To obtain the advantages mentioned it is usually necessary to make substantially more than ten exposures per second, and to do so continuously for a relatively long time, e.g. for half a minute. Since a fairly large quantity of radiation is required to take a single radiograph of organs such as the stomach, heart or lungs by the orthodox techniques, the making of a film entailed exposing the patient to an accumulated dose that could scarcely be justified. Moreover, it meant subjecting the X-ray tube to an extremely heavy load. The high dose of radiation required was due in part to the fact that to make such films the fluorographic method mentioned above, i.e. photography of the fluorescent screen was the only available method. The limited solid angle subtended by the light rays entering the camera, even with mirror cameras of very high light-gathering power, makes the situation about five times less favourable than with the same number of contact radiographs.

It is evidence of the importance attached to X-ray cinematography that, in spite of these drawbacks,

[1]) See e.g. W. Hondius Boldingh, Mirror cameras for general X-ray diagnostics, Philips tech. Rev. **15**, 58-65, 1953/54.

experiments in this field [2]) have been carried out for many years in a number of countries. Its application, however, was restricted to cases where the exposure of the patient to a very considerable dose of radiation could be regarded as the lesser of two evils. To obtain the necessary intensity of radiation from the X-ray tube, ingenious but intricate devices were evolved (e.g. rapid switching of the high tension on the tube in order to minimize unnecessary generation of heat at the anode).

One of the greatest advantages resulting from the development of X-ray image-intensifiers is that it enabled the problem of cinefluorography to be tackled afresh and with considerable success. The primary fluoroscopic image is transformed by the image intensifier into an image of many times higher luminance. For the purposes of fluorography or cinefluorography much weaker primary images can therefore be used, and hence the X-ray intensity drastically reduced.

This possibility has been discussed in earlier articles in this journal and elsewhere on the applications of the first X-ray image intensifier developed by Philips [3])[4]). This has an image field of 5″ (12.5 cm) diameter and gives a luminance intensification of 1000× or more. For cinefluorography with this image intensifier, use was initially made of a suitably adapted commercial 35 mm cinecamera. Later, 16 mm cameras were employed for the same purpose [5]). We shall return presently to the relative merits of 16 mm and 35 mm film for cinefluorography.

The apparatus referred to proved of great value for many examinations in X-ray diagnosis. From the very beginning, however, the relatively small field of view limited the usefulness of the apparatus. For filming the large organs, such as the heart and lungs, a larger field is necessary. To meet this need, Philips have developed in recent years an apparatus specially designed for cinefluorography, which employs a large image intensifier having an image field of *11″ (28 cm) diameter*. Various publications have already appeared on the medical application of this apparatus [6]). In this article we shall deal with the more important technical details.

Like the smaller version earlier described, the new image intensifier is of the electronic type; it consists of an evacuated tube in which the fluorescent X-ray image is converted into an electronic image. Although it is possible in principle to make intensifiers of this type for even larger image fields, e.g. for a field of 12″×16″ (30×40 cm) covering the whole thorax and capable of being used for normal fluoroscopic screens, we have not gone farther than the said diameter of 11 inches for fabrication reasons and also in order to avoid an unwieldy size of tube. (Recently an image intensifier of intermediate size, 9″, has been added to our range of current types.)

In this connection it is obvious to think of using solid-state image intensifiers (e.g. the "amplificon") whose operation depend on the phenomenon of electroluminescence and of which some basic forms have been described in an earlier article in this Review [7]). Work on the development of such devices is in progress in various parts of the world, but it will probably be many years before their principal limitation is overcome, namely their excessive inertia, which makes them at present unsuitable for cinefluorography.

Description of the apparatus

We shall begin by reviewing the installation, after which we shall discuss the principal parameters and the construction of the main components.

In the first place the apparatus contains the above-mentioned 11-inch image intensifier and a cine-camera fitted with a Schmidt mirror system of great speed. The image intensifier and the mirror camera are optically matched and contained in a cylindrical housing. In *fig. 1* this can be seen at the right, mounted on a stand. The patient is shown in this photograph positioned on a "Müller" UGX universal stand [8]). A "ring stand" specially developed for the cinefluorographic equipment is discussed at the end of this article. The X-ray tube is on the left in fig. 1, and behind it the high-tension generator. The control desk, which contains some special features for cinefluorography, is not shown.

---

[2]) For the history of cinefluorography see the papers presented by F. Dessauer, R. Janker, R. Reynolds and H. van de Maele at the X-ray Congress held at Vienna in September 1936 (Fortschr. Geb. Röntgenstr. **56**, 126-142, 1937). The first paper deals, among other things, with the work of P.H. Eijckman, the Dutch pioneer of cineradiography, who made "synthetic" X-ray films ar early as 1903, and genuine X-ray films in cooperation with others in the years from 1908 to 1915. See also:
R. Janker, Roentgen cinematography, Amer. J. Roentgenology **36**, 384-390, 1936.
G. H. Ramsey, J. S. Watson, J. B. Steinhausen, J. J. Thompson, F. Dreisinger and S. Weinberg, Cinefluorography: a progress report on technical problems, dosage factors and clinical impressions, Radiology **52**, 684-690, 1949.
R. Janker, Apparatur und Technik der Röntgenkinematographie zur Darstellung der Herzbinnenräume und der grossen Gefässe (Angiokardio-Kinematographie), Fortschr. Geb. Röntgenstr. **72**, 513-520, 1950.

[3]) M. C. Teves and T. Tol, Electronic intensification of fluoroscopic images, Philips tech. Rev. **14**, 33-43, 1952/53.

[4]) J. Feddema, Medical aspects of the image intensifier, Philips tech. Rev. **17**, 88-93, 1955/56.

[5]) See e.g. L. B. Lusted and E. R. Miller, Progress in indirect cineroentgenography, Amer. J. Roentgenology **75**, 56-62, 1956; G. M. Ardran and D. G. Wyatt, A portable X-ray cinecamera, Brit. J. Radiol. **30**, 52-54, 1957 (No. 1).

[6]) R. Janker, Medicamundi **2**, 38, 1956 (No. 2) and Röntgen-Blätter **10**, 289, 1957.
G. J. van der Plaats, Fortschr. Geb. Röntgenstr. **86**, 1957, Beiheft, p. 54.

[7]) G. Diemer, H. A. Klasens and P. Zalm, Electroluminescence and image intensification, Philips tech. Rev. **19**, 1-11, 1957/58.

[8]) H. Verse and K. Weigel, A novel type of diagnostic X-ray unit, Philips tech. Rev. **17**, 138-145, 1955/56.

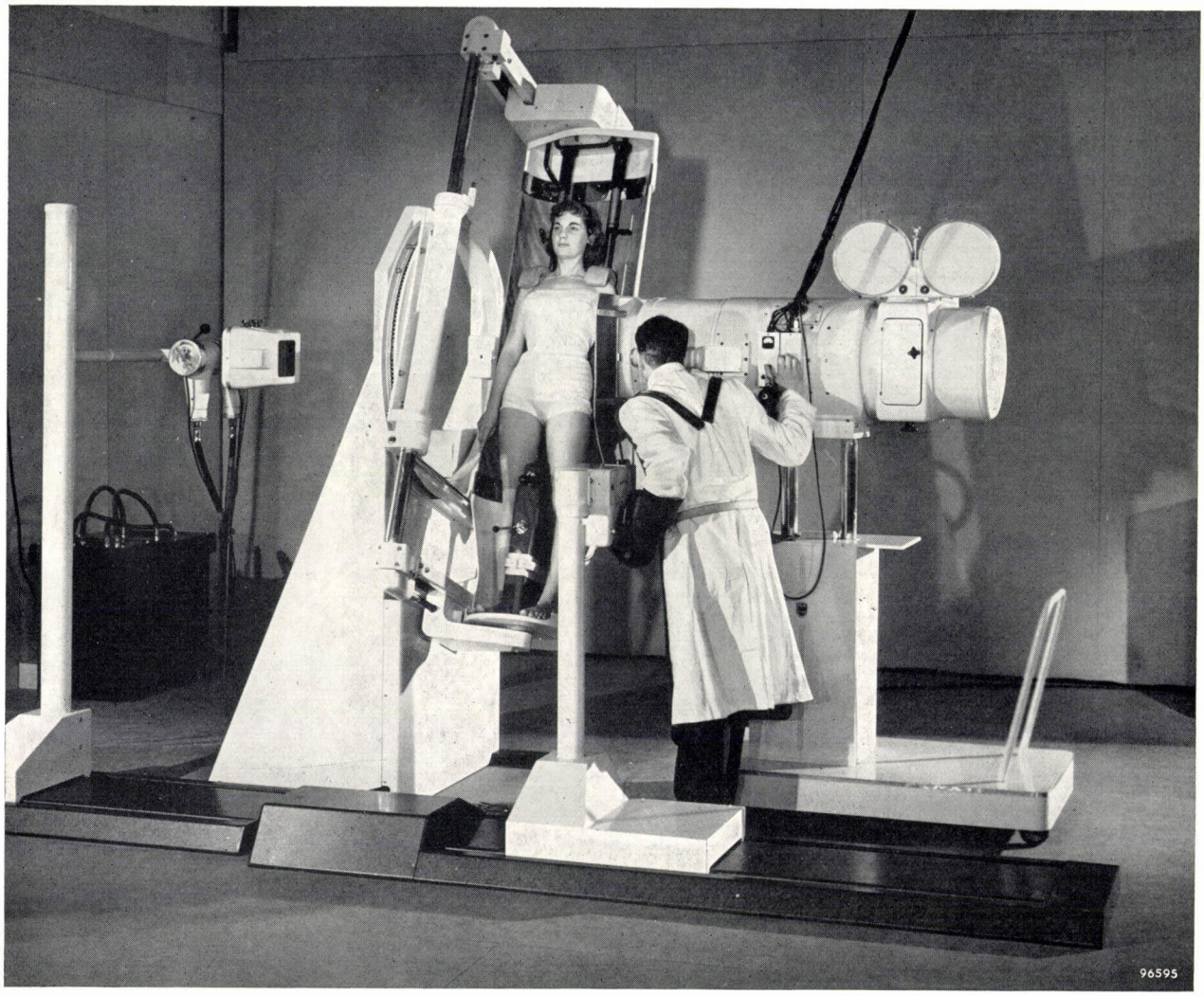

Fig. 1. Apparatus for cinefluorography with the 11-inch image intensifier. The patient is positioned here in a "Müller" UGX universal stand.

The 11-inch image intensifier gives a luminance intensification of at least 100×. The intensified image on the viewing screen can be viewed by two observers simultaneously through two optical systems mounted on the camera housing. These viewing systems are arranged in such a way that the patient remains within reach of the observer. At any appropriate moment during the fluoroscopic examination the radiologist can start filming by depressing a push-button (delay time only 0.2 sec). While filming he continues to watch the fluoroscopic image. This is of great practical importance, for one reason because the radiologist may wish to cause the patient to make or undergo various movements while the film is being made, the results of which he can now check on the viewing screen. With the aid of a photoelectric exposure meter the average photographic density (blackening) of the film can, if required, be kept constant irrespective of differences in X-ray absorption resulting from the movement or turning of the patient. A "heat integrator" can be incorporated in the X-ray apparatus to prevent excessive heating of the tube anode by unduly prolonged and heavy loading.

Films can be taken at a frame frequency ranging from 6 to 48 frames per second, adjustable in six steps. The film spools, visible above the camera housing in fig. 1, can accommodate 300 metres of film. The X-ray tube is operated for cinefluorography at a voltage between 50 and about 125 kV, as is usual in diagnostic practice; the tube current as a rule need not be higher than 20 mA.

Choice of picture size and splitting of the reduction factor

The situation of cinefluorography before the advent of the image intensifier is characterized by the fact that protagonists of this practice designed

70 mm cameras for the purpose [9]). Lack of light made it necessary to use an extremely sensitive and therefore coarse-grained film. For this reason a relatively large film size was important if detail perceptibility was not to suffer unduly from the graininess of the film. This applied particularly to the viewing of separate frames of the film strip, in which case no use is made of the property of the eye to integrate over a time of about 0.2 sec., i.e. over a number of successive frames. The advantage of 70 mm film in this respect was found to outweigh its drawbacks, namely that it called for a costly special optical system and that a 70 mm film cannot be directly projected with the standard projectors designed for 35 mm or 16 mm film. For the present apparatus, in which the light problem is much less acute and thus allows the use of finer-grained types of film, only the 35 mm and 16 mm sizes entered into consideration in view of the desirability of projecting the films with standard projectors. As regards the choice between 35 mm and 16 mm, the 16 mm size is attractive in that the films can be projected with amateur equipment, which is cheaper and in most countries is not subject to restrictive regulations. However, to reproduce all the information contained on the 11 inch screen the 16 mm film would have to be so fine-grained that it would be too insensitive for most diagnostic problems. For this reason we decided to adopt the 35 mm size.

The film gate in a standard 35 mm projector measures about 15×21 mm. The round image-field of the 28 cm image intensifier can therefore be reproduced, without significant losses, with a diameter of 18 mm. Thus, the image must be reduced in all by 15.5 times. The reduction is effected in two steps: the image intensifier produces on the viewing screen a reduced image of the primary fluoroscopic image (reduction factor r_1), and the cinecamera projects a reduced image of the viewing screen on to the film (reduction factor r_2). The condition $r_1 \times r_2 = 15.5$ leaves the choice of the ratio of the two reduction factors still open (distribution of the total reduction over image intensifier and camera).

It is useful to make the reduction factor r_1 of the image intensifier as large as possible, because the luminance intensification relies to a large extent on the electron-optical reduction [10]), and this is proportional to r_1^2. The resolving power of the electron-optical image projection and of the viewing screen would impose the only limitation on r_1, except that the cine-camera, whose reduction factor r_2 must be decreased as r_1 is increased, also imposes limitations.

As mentioned, the camera contains a Schmidt mirror optical system; the system used is of the type earlier developed for single-exposure fluorography [1]). It contains a mirror of 33 cm diameter and a correction plate of $D = 20.5$ cm diameter (diaphragm); the focal length f of the system is 17 cm. There are two reasons why it is useful to have the smallest possible reduction factor for such a system. In the first place it shortens the object-distance $v = (r_2 + 1)f$, which is responsible for most of the total length of the apparatus; see *fig. 2*. (The length of the image intensifier is only slightly altered by variation of the factor r_1.) In the second place, a smaller

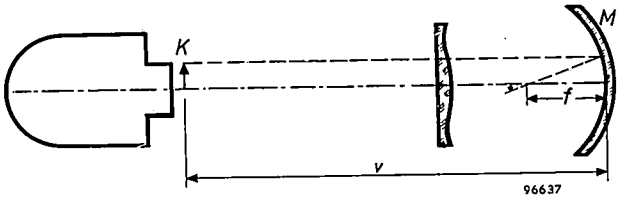

Fig. 2. Sketch showing the relative positions of image intensifier and mirror camera. The total length of the apparatus is largely governed by the object distance v (from viewing screen K to mirror M).

reduction factor means a larger aperture ratio $1 : N$ of the mirror system. This aperture ratio, which primarily determines the speed of the camera [11]), may be formulated generally as:

$$1 : N = \frac{D}{f} \frac{r_2}{r_2 - 1}. \quad \ldots . \quad (1)$$

For values of r_2 equal to 10, 5 and 2.5, the factor $r_2/(r_2 - 1)$ has the values 1.1, 1.25 and 1.66, respectively.

The requirements with regard to r_1 and r_2 are thus nicely in harmony. Unfortunately, however, limitations are earlier encountered in the reduction of r_2 than in the raising of r_1. The most serious limitation consists in the fact that the reduction of r_2 brings the film holder increasingly farther away from the mirror and nearer to the correction plate. To avoid the constructional difficulties which this would entail, the lower limit of r_2 for the mirror camera has been fixed at 3.6. The reduction factor of the image intensifier is thus fixed at $r_1 \approx 4.5$ and the diameter of the viewing screen at about 60 mm.

[9]) J. S. Watson, S. Weinberg and G. H. Ramsey, A 70 mm cinefluorographic camera and its relation to detail, Radiology **59**, 858-865, 1952.
R. Janker and K. Einert, Röntgenkinematographie mit einer neu entwickelten Kamera für 70 mm breiten perforierten Film, Röntgen-Blätter 7, 51-58, 1954.

[10]) See article [3]), p. 35.

[11]) See W. Hondius Boldingh, Fluorography with the aid of a mirror system, Philips tech. Rev. **13**, 269-281, 1951/52.

Owing to the masking factor S of the mirror camera, a further reduction of r_2 would not entail much improvement in the light-gathering power of the optical system: the film holder, with the film gate, the rotary shutter and parts of the transport mechanism, inevitably intercept a part of the useful light proceeding towards the mirror, so that only a fraction S actually reaches the mirror. It can be seen from fig. 3 that this fraction is smaller the smaller the object distance, i.e. the smaller the reduction factor r_2; this partly destroys the gain in the aperture ratio.

After the above considerations it is necessary to return for a moment to the choice of a mirror system for the cine-camera. When used for fluorography, as earlier described [1]), the mirror camera is required to project the image of a large object (a standard fluoroscopic screen) on to a certain small size of film, hence with a fixed reduction factor of about 6 to 10. For this purpose mirror optical systems have almost entirely superseded lens systems, since they combine a much greater speed with good image quality and a reasonable price. In our case, where a much smaller reduction factor is possible and desirable, this advantage of the mirror system carries less weight. This remains true even when the focal length is not taken as fixed (see above) but is chosen in relation to the other considerations. Our decision in favour of the mirror system was therefore prompted mainly by other factors, such as the relative ease with which a good image quality can be obtained, the large available space for viewing systems, etc., and by the considerable experience already gained by Philips in the development of mirror cameras for fluorography.

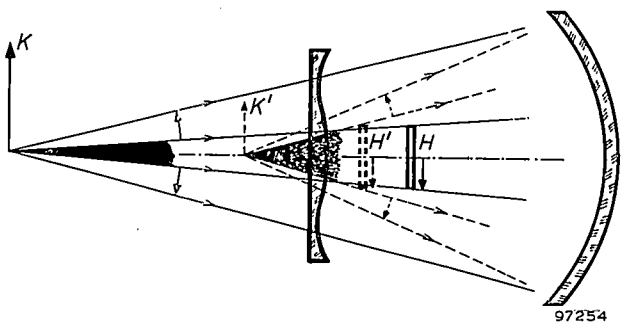

Fig. 3. For a given size of image (film size) the film holder intercepts a larger fraction of the useful beam of light the lower is the reduction factor K/H ($K'/H' < K/H$).

The 11-inch X-ray image intensifier

The operation of the 11-inch X-ray image intensifier is essentially similar to that of the smaller type earlier described [3]). We shall briefly recapitulate it with reference to the schematic cross-section shown in *fig. 4*. The X-rays transmitted by the object impinge on the primary fluorescent screen R and excite it into bluish fluorescence. The fluorescent light liberates electrons from the photocathode F, which is in contact with the fluorescent screen and is mainly sensitive to blue light. The X-ray image is thus converted into an electron image: the photoelectrons are accelerated by an electrostatic field in the evacuated tube and at the same time focused to an electron-optical image of reduced size on a fluorescent screen K (viewing screen) in the anode A. The accelerating potential between photocathode and anode is 25 kV. The focusing electrode E, to which a variable voltage of 100 to 500 V is applied, makes it possible to adjust the definition of the image (i.e. to achieve the best compromise between central and peripheral sharpness).

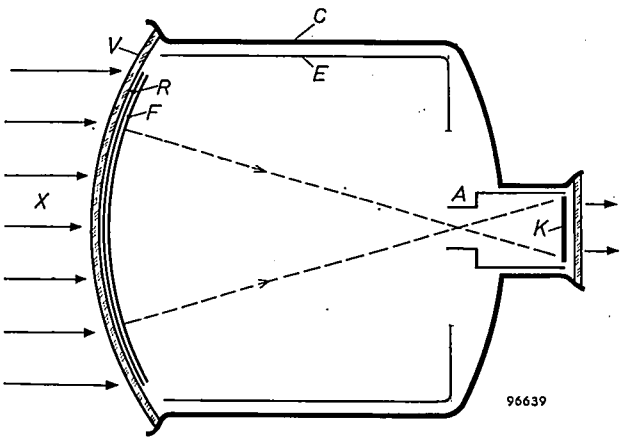

Fig. 4. Schematic cross-section of the 11-inch X-ray image intensifier. V glass window in front of primary fluorescent screen R, F photocathode, A anode, K viewing screen, E focusing electrode, C chrome-iron envelope.

The principal data of the large tube, some of which we have already mentioned above, are given in *Table I* side by side with those of the 5-inch tube. Various differences will be indicated in the following.

Table I. Particulars of the Philips 5″ and 11″ image intensifiers *).

	5″	11″
Diameter of useful image field	12.5 cm	28 cm
Electron-optical reduction factor	9.5	4.5
Luminance intensification	≧1000	≧100
Resolving power (lines/cm):		
in middle of primary fluorescent screen	30	22
at the edges of primary fluorescent screen	20	15
Smallest perceptible contrast	4%	6%

*) The large tube is a version, specially modified for cinefluorography, of an 11-inch image intensifier developed by Philips Electron Tubes Division in 1953. This tube, like its 5-inch predecessor, had a reduction factor of approx. 9.5.

Outwardly the most striking difference between the two tubes is that the large tube, because of its greater size, is made largely of metal, i.e. of chrome-iron (*fig. 5*). Experience gained with chrome-iron/glass vacuum seals in the fabrication of television picture tubes played of course an important part in the design of this tube. The X-rays enter the tube through a convex glass window with

[12]) Philips tech. Rev. 14, 281, 1952/53.

which, in this case, the primary fluorescent screen is in direct contact. Sealed into the base of the tube at the opposite end is an optically flat viewing window. The X-ray window must be thick enough to withstand atmospheric pressure and shocks, although not thicker than is strictly necessary, in order not to attenuate the X-rays excessively. For the same reason the glass chosen had to be a type containing the fewest possible elements of high atomic weight. Furthermore the composition of the glass had to be such as to ensure a good seal to chrome-iron. With the glass employed the X-ray transmission amounts to 60% for the window of the large tube and 90% for that of the small tube, both measured at a voltage of 90 kV on the X-ray tube and with a filter of 20 mm Al (approximately equivalent to the thorax).

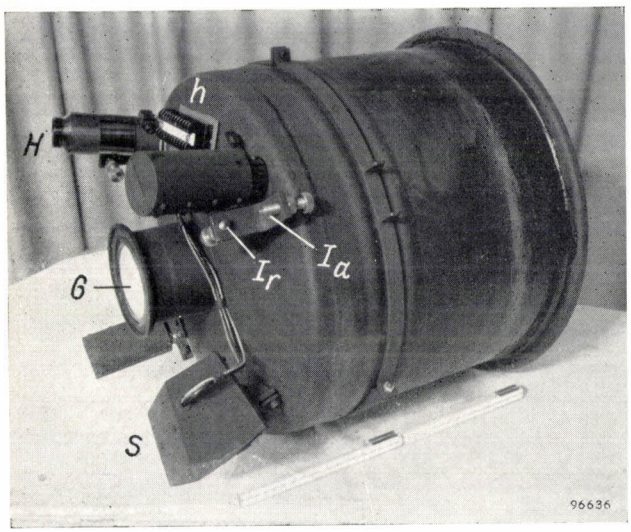

Fig. 5. The 11-inch X-ray image intensifier. *G* glass window in front of viewing screen, *H* high-tension connection (25 kV), *h* terminal block for other connections, *S* ionization gauge and pump, I_r one of the three radial adjusting screws, I_a one of the three axial adjusting screws.

In an earlier article on the 5-inch image intensifier various effects were described that cause slight blurring of the image. One cause of blurring is the X-radiation which is scattered in the window or, having passed the X-ray screen, on the tube walls. The fluorescent light, too, insofar as it is not absorbed by the photocathode, can cause image blur as a result of diffuse reflection from the tube walls. The first effect is somewhat greater in the large tube owing to the greater thickness of the X-ray window (more scattered X-radiation). Nevertheless, the total loss of contrast is not very significant, as appears from the value of 6% given in the above table for the smallest perceptible contrast (in light as well as in dark parts). The *reproduction* of the contrasts present in the X-ray image can always be appreciably improved photographically as compared with the observed image by using a high-gamma film.

A difficulty arising from making the tube largely of metal is that gases are released from the walls during the life of the tube. If their pressure exceeds a certain value, e.g. 10^{-5} mm Hg, a grey spot will develop in the centre of the viewing screen, which may prove troublesome. This is caused by ion bombardment of the centre of the photocathode, as a result of which photoelectrons are liberated and in turn accelerated towards the anode. The metal parts cannot be completely degassed during fabrication since it is not possible to raise the temperature during pumping to a high enough value. The solution found for this problem was to fit an "ion pump" to the image intensifier tube. This pump is simply an ionization gauge in which the gas molecules emerging from the tube are ionized and accumulated in an ion collector [13]). The supply voltage for this pump, approximately 2000 V, is tapped from the high-tension generator which supplies the 25 kV accelerating voltage. The ion pump also serves as a gauge to measure the pressure in the tube. The pressure indication is used for controlling a safety device, which prevents the high-tension from being switched on when the tube pressure it too high.

To avoid having to refocus the cine-camera on to the viewing screen if the tube should have to be replaced — which would be a very laborious process — the tube is provided with six adjusting screws by means of which the tube location is prefocussed during manufacture. Three screws (see fig. 5) are in the axial direction and are so adjusted that their stop faces lie in a certain plane parallel to the viewing screen, with an error of less than 0.1 mm. The housing in which the tube and camera are mounted is provided with a thrust surface perpendicular to the optical axis of the whole assembly. By means of a sprung suspension system the tube with its three stop faces is pressed against this thrust surface, so that the viewing screen lies exactly in the object plane of the mirror camera. Analogously, with three preset radial adjusting screws and a cylindrical surface in the housing, the centre of the viewing screen is correctly aligned, the deviation amounting to no more than 0.5 mm.

Cinefluorographic camera and accessories

Light-gathering power and resolving power

Some details of the optical system of the mirror camera have already been touched on in the fore-

[13]) See e.g. Philips tech. Rev. **20**, p. 145, 1958/59 (No. 6).

going, viz. the diameter of the mirror = 33 cm, diameter D of the diaphragm = 20.5 cm, focal length f = 17 cm, reduction factor r = 3.6. With these data the aperture ratio is found from equation (1) to be $1 : N = 1 : 0.60$. The effective aperture ratio is smaller, because the camera housing, the shutter etc. intercept part of the light entering the camera, amounting in our case to about 50% (masking factor 0.5). This gives:

$$1 : N_{\text{eff}} = 1 : 0.83,$$

which is an extremely high value, corresponding approximately to the highest values obtainable with mirror cameras in single-exposure fluorography.

A proper appreciation of the light-gathering power of the camera must also take into account the image quality and factors extraneous to the camera such as the properties of the X-ray screen and the film material, which partly determine the quantity of X-radiation needed for a single frame. This, after all, is the quantity which matters.

As regards image quality, a very favourable circumstance is that the optical system need only have a small field of view, namely 7°. This is due to the relatively large focal length and to the small dimensions of the viewing screen. For comparison it may be mentioned that fields of view of about 30° are needed in single-exposure fluorography. Even with the Schmidt mirror camera, which, compared with other optical systems, lends itself particularly well to the sharp focusing of large fields of view, difficulties are experienced where such large angles are concerned. For technical purposes an image of adequate sharpness, both at the edges and in the centre, can be obtained up to 25°, but at 30° some central sharpness must be sacrificed in order to improve the definition at the edges, by slightly modifying the shape and position of the correction plate. The only way to avoid this is to use more complicated optical systems, as for example a mirror camera with three correction plates instead of one, or with a correction element and a so-called conical lens [14]).

These complications, then, do not arise with the present cinefluorographic camera, and full attention could be concentrated on obtaining the sharpest possible definition in the centre of the small field of view. As a result the camera is capable of resolving some 110 lines per cm on the viewing screen.

In practice this means that the resolving power is limited not by the camera but almost invariably by the graininess of the film. With a sensitive fluorographic film (Gevaert Scopix, Agfa Fluorapid) the resolution is equivalent to about 60 lines/cm of the viewing screen. With slightly less sensitive but finer-grained emulsions, made experimentally by Gevaert, Agfa and Kodak, a resolution equivalent to 75 lines/cm has been achieved, still keeping the dose to the patient relatively low. This fine-grained film yields no advantage as far as observing a projected moving picture is concerned, because then, owing to the integrating power of the eye, a resolving power equivalent to 75 lines/cm is also obtained with coarse-grained film, and the integration with the fine-grained film offers no further improvement.

Finally, if we compare the X-ray energy needed for a single image produced by different radiographic methods, we arrive at the following ratios (these rough figures also depend to some extent on the X-ray tube voltage and on the filter employed, since the methods have different spectral sensitivities). Let the energy for a normal direct exposure be 1 (using intensifying screens of average luminous intensity), then the energy required with our cinefluorographic apparatus is 0.02 to 0.03; for cinefluorography with the 5-inch image intensifier and a tandem optical system, earlier described [15]), about 0.015 to 0.02; and for normal single-exposure fluorography about 3 to 5. (All these values presuppose the use of a scatter grid, though this will not usually be necessary with the 5-inch image intensifier.) In spite of the difference in energy, the load on the X-ray tube is virtually the same for both cinefluorographic systems, the camera for the 11-inch image intensifier having been provided with a 1.5 times larger shutter opening, viz. 270° instead of 180°. This entailed no particular problems because a Maltese cross mechanism is used for the film-transport of this camera (see below).

From the figures mentioned, and from the numerous exposure data already published (see e.g. [4])), it can be concluded that with X-ray equipment capable of sufficiently high voltages (125 kV) it is now possible to film all objects in the human body, even relatively large organs, without exposing the patient to an unjustifiably large dose of X-radiation (see *Table II*).

The viewing system

The cross-section in *fig. 6* shows the construction of the optical system by means of which two observers can view the image while the film is

[14]) A. Bouwers, Improvement of resolving power of optical systems by a new optical element, Appl. sci. Res. **3B**, 147-148, 1953.

[15]) P. M. van Alphen, Optical aids for the image intensifier, Philips tech. Rev. **17**, 77-83, 1955/56, especially p. 82.

being made. The eyepieces are mounted at opposite sides of the image intensifier close to the patient, and are so aligned that the observers have the impression of looking towards the X-ray screen (fig. 1). This positioning is made possible by deflecting the path of the rays in each viewing system by means of four plane mirrors. The observers see the image almost upright and at somewhat more than half its true size. The first mirror of both viewing systems is situated near the optical axis of the camera. These mirrors are kept small enough to lie almost entirely within the cone of the rays which are incident on the back of the film-holder, and which thus have no part in the exposure. By thus limiting the size of the mirrors the light-gathering power of the camera is unimpaired, though of course this is at the expense of the brightness of the *observed* image. This is also adversely affected by the losses due to the multiple reflections. Nevertheless the brightness obtained is more than adequate. A further contributory factor is that the viewers are designed with an exit pupil of 5 mm, which is larger than the entrance pupil of a normal adult eye.

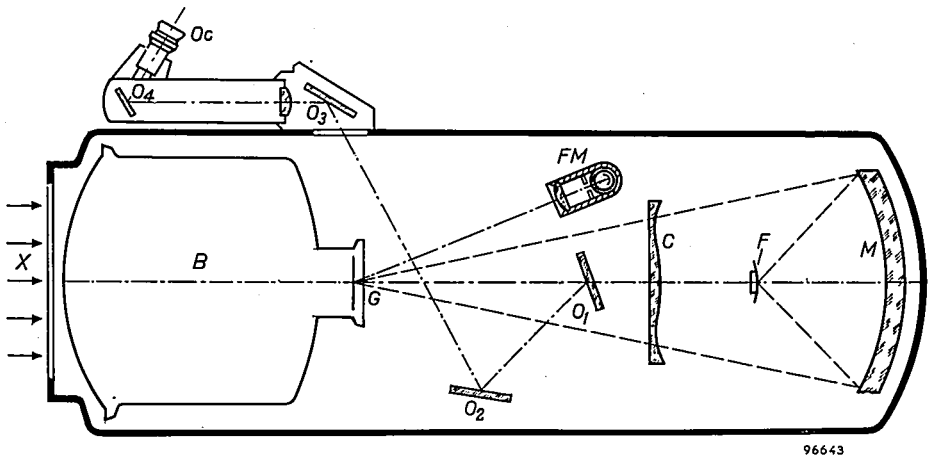

Fig. 6. Simplified horizontal section through the housing of the cinefluorographic apparatus. *X* X-rays, *B* image-intensifier tube with viewing window *G*, *M* spherical mirror and *C* correction plate of cine-camera, *F* film, O_1-O_2-O_3-O_4 mirrors and *Oc* eyepiece of viewing system (for simplicity only one of the two viewing systems is shown), *FM* photomultiplier with lens and diaphragm for measuring the luminance of the viewing screen.

Table II. Some typical operating data and patient doses for films made with the cinefluorographic apparatus, at a frame-frequency of 16 frames per sec and employing a cine-film of sensitivity comparable with 100 A.S.A. *)

Body part	Tube voltage (kV)	Tube current (mA)	Distance from focus to image intensifier (cm)	Focus-skin distance (cm)	Skin dose with 2 mm Al extra filter (r/min)
Maxilla	70	10	100	80	2.5
Cervical spine, lateral	70	6	100	80	1.5
Oesophagus, at pharynx level	80	4	100	80	1.5
Oesophagus, at thorax level	100	8	80	50	10
Stomach, antero-posterior	125	9	80	50	16
Small intestine	125	9	80	50	16
Kidneys	100	9	80	50	12

*) These exposure data are merely a rough guide, since they depend upon other factors such as object thickness, scatter grid, film-processing technique, etc.

The photometric system

The average luminance of the viewing screen of an image intensifier can, in principle, be very simply determined by measuring the current through the tube, this being a measure of the total number of photoelectrons passing from the X-ray screen to the viewing screen, and hence — for a given area of the viewing screen — a measure of the average luminance.

This method is in fact used with the 12.5 cm image intensifier. However, for the 28 cm type it is less suitable because the object under examination will often not entirely cover this larger X-ray screen. To avoid exposing the patient to unnecessary X-radiation, and also to reduce scatter, it will then sometimes be desirable to stop down the X-ray beam. In that case the area of the viewing screen over which the average brightness is to be determined will vary, thus complicating the measurement. If the X-ray beam is not stopped down the too bright or too dark peripheral parts of the screen may give misleading results when using this method of measurement.

For this reason a system was chosen whereby the luminance of the viewing screen is directly measured. Only in the central part of the screen is the luminance measured: except in very few cases, this is

always covered by the image. The system uses a photo-multiplier tube with a lens and diaphragm (see fig. 6). The lens forms an image of the viewing screen on the plane of the photocathode in the multiplier tube, and the diaphragm limits the effective image to a circle equivalent to 22 mm diameter on the viewing screen (or 10 cm on the primary fluorescent screen). This diaphragm can be changed if a different field limitation is better suited to the work on hand. A frosted glass plate in contact with the diaphragm eliminates the effect of any local differences in the sensitivity of the photocathode.

The electric signal which the photomultiplier tube delivers as a measure of the screen luminance is read on a meter. The use made of this information during the making of the film will be discussed presently.

Mechanism of the cinefluorographic camera

The films are recorded on standard perforated 35 mm film. Since the object to be filmed appears as an inverted image on the viewing screen, the film must be transported from bottom to top, instead of in the usual direction from top to bottom; when normally projected the object then appears upright.

The film mask is matched to the viewing screen: it is round and, as mentioned, has a diameter of 18 mm, which is reasonably suited to the standard dimensions, 15.2×20.9 mm, of the film mask in normal 35 mm projectors. Only 7.2% of the image is lost through projection cut-off, whilst the image is 40% larger than if the diameter 15.2 mm had been selected. This is of particular importance for the quality of the image when individual frames are examined. It is also possible in principle to enlarge the mask of a normal projector so as to lose nothing of the round image of 18 mm diameter (the frame pitch of 35 mm film is 19 mm).

The mechanism of the film-transport system is shown schematically in *fig. 7*. The sprocket (*3*) responsible for the intermittent movement of the film is actuated by a Maltese cross. Particularly at high frame-frequencies, this ensures more reliable transport of the film and causes less wear of film and moving parts than the claw mechanism usually found in cine-cameras. Moreover, with the normal (four-slot) Maltese cross the actual frame-shift period is not longer than $^1/_4$ of the total available time per frame, so that the aperture angle of the rotating shutter can be made 270° without any additional special measures. The asynchronous motor for the film transport mechanism has two speeds, and the film transport spindle is driven via a three-speed gear box, thus making it possible to obtain the six frame frequencies earlier mentioned, from 6 to 48 frames per second. The film can also be transported in reverse for subtitling and other special purposes. The shutter aperture being 270°, the exposure time varies from $^1/_8$ sec (at 6 frames per sec) to $^1/_{64}$ sec (at 48 frames per sec). The motor is kept running during the screening preparatory to cinefluorography. When the apparatus is switched over for cinefluorography, an electromagnetic clutch brings the transport spindle into motion with a delay not exceeding 0.1 sec.

As in the fluorographic mirror cameras earlier described [1]), the film is pressed against the film gate by a spherical pressure plate (*5*, fig. 7). This is necessary because in the Schmidt mirror optical system the image surface on to which a flat object is projected is spherically curved (concentrically with the mirror). Even without this condition a pressure plate would still be required, because the very large angle subtended by the mirror at the film (about 100°) necessitates extremely accurate positioning of the sensitive area of each frame — irrespective, for example, of the thickness of the film. The mechanical deformation produced by the spherical plate is easily tolerated by the film, and the image distortion after the return of the film into a flat plane is negligible. In view of the high frame-frequencies used, the spherical pressure plate cannot be designed — as it is in single-exposure cameras — to disengage the film during the transport. To ensure that the film is pulled through smoothly it is therefore necessary to pay very careful attention to the design of the pressure guides of the film gate. Moreover, with some types of film, the film gate will have to be cleaned more frequently to remove flaked emulsion than in normal cine-cameras. Little trouble will be experienced, however, if films with hardened emulsion are used.

In cinefluorography use is sometimes made of a lead shutter which is rotated in front of the X-ray tube window to protect the patient from X-radiation during the intervals in which the film is being pulled forward and hence cannot be exposed. The rotation of this lead shutter must of course be very accurately synchronized and in phase with the shutter in the cine-camera. The two shutters can be coupled for this purpose by means of a magslip or synchro: a synchro is fitted to the shaft of the asynchronous motor that drives the film and connected to another synchro on the spindle driving the lead shutter. The synchro on the motor shaft also makes it possible to run a second cine-apparatus synchronously with the first; this technique is in fact applied, for example when it is desired to make

simultaneous frontal and transversal cine-exposures of a patient.

The large spools, which hold 300 metres of film, have the advantage that the film does not have to be changed so frequently. Supply and take-up spools are driven in the usual way via a friction clutch. Moreover the supply spool is provided with an automatic run-back device, which, at the end of an exposure, takes up the loop caused by the slight over-run of the heavy supply spool. This device is necessary to avoid the risk of film breakage, particularly at a high frame-frequency (48 frames per sec): a loop in the film would allow the transport mechanism to reach full speed while the supply-spool drive was still slipping slightly, so that, at the end of the loop, the film would be jerked violently from the spool.

Since the use of large spools means that the film remains longer on the supply spool and is thus exposed in some measure to secondary X-rays, the film magazine is covered with a lead shield. This sufficiently protects the most sensitive film material against fogging, even when the X-radiation is relatively hard (generated by 125 kV).

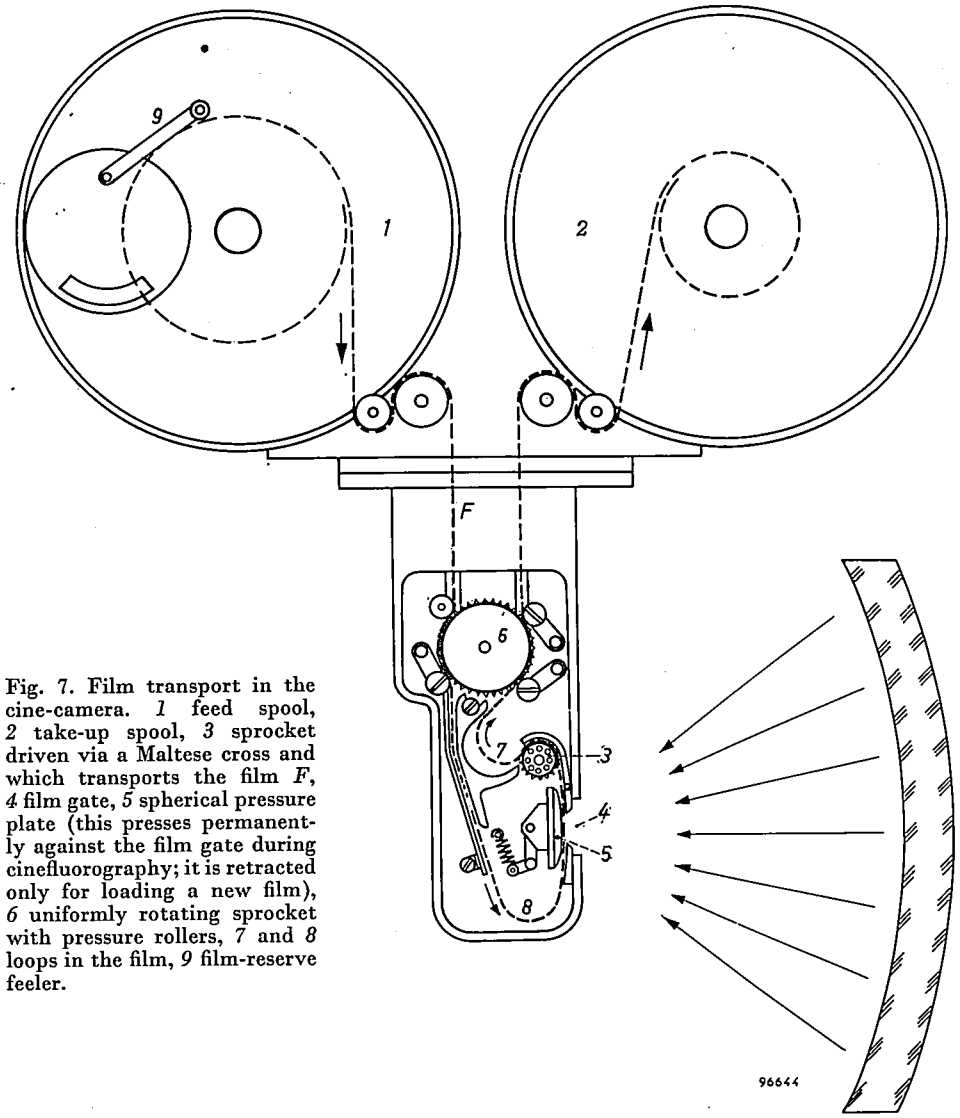

Fig. 7. Film transport in the cine-camera. *1* feed spool, *2* take-up spool, *3* sprocket driven via a Maltese cross and which transports the film *F*, *4* film gate, *5* spherical pressure plate (this presses permanently against the film gate during cinefluorography; it is retracted only for loading a new film), *6* uniformly rotating sprocket with pressure rollers, *7* and *8* loops in the film, *9* film-reserve feeler.

Special features of the X-ray equipment

In the installation here described the power supply for the X-ray tube is required to meet demands entirely different from those imposed in normal X-ray diagnosis. Although the tube tensions are the same (up to about 125 kV), the tube currents needed are much lower, usually being not more than 20 mA against 100 to 500 mA in normal diagnosis, whereas the total exposure times are very much longer, e.g. 10 to 100 seconds against the normal $^1/_{100}$ to a few seconds. The longer exposure times make it necessary to take careful account of the maximum permissible load on the X-ray tube, the limit in this case being set not by the temperature

of the focal spot but by the temperature of the anode as a whole (except when a very small focus is used, e.g. 0.3 mm). In order to film as long as possible without approaching this load limit it is as well to operate the X-ray tube on direct voltage (for example by smoothing with capacitors the rectified voltage from the high-tension generator). For a given total quantity of X-radiation the required electrical energy, and hence the heat generated in the anode, is then as low as possible. Furthermore the use of direct voltage obviates stroboscopic effects even with varying frame frequencies, whereas with a pulsating supply it would be necessary to adopt complicated measures to counteract such effects, particularly at 48 frames per second.

The time switch employed in X-ray diagnostic apparatus for presetting the duration of the load on the tube (and hence the exposure time) is not needed for the cine-apparatus. The switch used for starting the film transport also switches on the X-ray tube for as long as the film is running. To be more exact, it brings the tube load up to the required value, for the X-ray tube will generally be operating at a low current, about 1 mA, before filming starts, in order that the radiologist can adjust the X-ray image and ascertain fluoroscopically the suitable moment to begin filming. Thereupon the tube current must be raised from the fluoroscopic value to the correct value for filming as rapidly as possible. A limit is set here by the thermal inertia of the filament in the X-ray tube, but the density stabilizer, which we shall now discuss, limits the transition time to an average of 0.1 sec.

The above-described photoelectric luminance meter, which is mounted in the camera housing, delivers an electrical signal which can be read from a meter on the control desk. This reading, taken in conjunction with the sensitivity of the film and the frame-frequency in use, makes it possible to adjust the required tube current (and if necessary the tube voltage) before beginning the actual examination. Moreover, a facility is provided for coupling the circuit of the luminance meter to the filament cur-

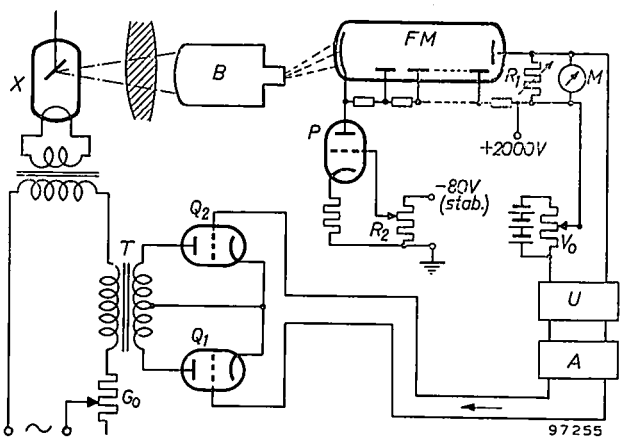

Fig. 8. Circuit diagram of density stabilizer. The filament voltage of the X-ray tube X is supplied via the primary of a transformer T, whose secondary is loaded by the triodes Q_1 and Q_2 which together constitute a variable impedance. The grid voltage on the triodes thus influences the impedance of the primary of T in the filament circuit of the X-ray tube. The output signal of the photomultiplier FM, which faces the viewing screen of the image-intensifier tube B, controls the grid voltage of Q_1 and Q_2 — and hence the current through the X-ray tube — in such a way that the deflection of the meter M, which is a measure of the observed luminance of the viewing screen, remains virtually constant. For this purpose the direct voltage produced by the photo-current across R_1 is compared with the very constant voltage V_0, and the difference (after conversion to alternating voltage in U and amplification in A) is applied to the grids of Q_1, Q_2. The required degree of blackening can be preset by adjusting the reading of M to the desired value (e.g. in the middle of the scale), by adjusting V_0.

Variation of R_1 thus means that the mean blackening is stabilized at different *viewing-screen luminances*, and a similar effect is produced by variation of R_2, which changes the supply voltage (stabilized by triode P) to the photomultiplier tube. The constant reading of M can now be made to correspond to a certain required *film-blackening* by adjusting R_1 in accordance with the frame-frequency selected (control range 1 : 8) and by adjusting R_2 to accord with the film sensitivity (control range 1 : 10).

G_0 can be adjusted to limit to a specified value (55 to 60 mA) the maximum filament current for the X-ray tube (which occurs, for example, if the image intensifier is inadversely switched off). The filament current can be regulated between about 0.3 and 50 mA.

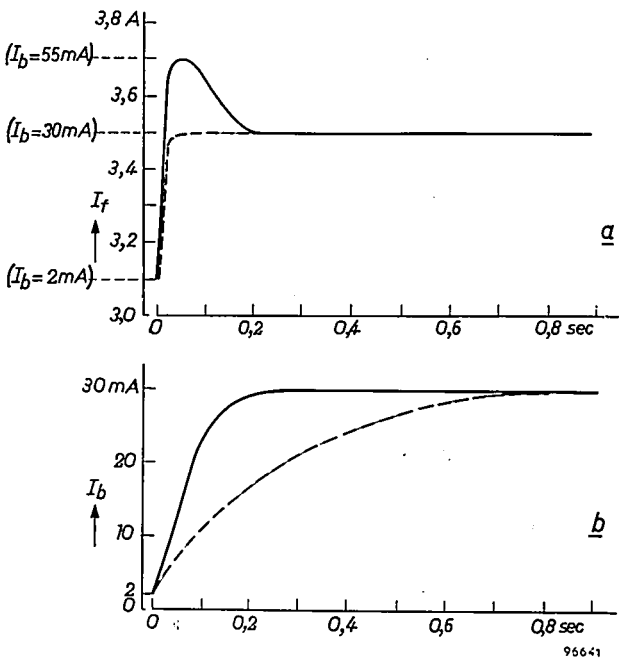

Fig. 9. *a*) Filament current I_f, *b*) tube current I_b of X-ray tube as functions of time after switching over from fluoroscopy to cinefluorography. If I_f were simply raised from the fluoroscopic value 3.1 A to the new value required, e.g. 3.5 A (for a tube current of 30 mA), then I_b would need about 0.8 sec to reach the steady value (dashed curves). The density stabilizer, however, causes the filament current initially to overshoot to the maximum possible value 3.7 A for as long as the screen luminance is still inadequate, so that the required tube current (and hence the required film blackening) is reached much earlier (solid curves). Care must of course be taken in the design of the circuit to ensure that the overshoot does not lead to oscillation.

rent circuit for the X-ray tube; the output signal from the photomultiplier then controls the tube current in such a way as to oppose variations in exposure, and hence in the average density (blackening) of the film. This density stabilization has proved to be extremely useful in cinefluorography in cases where it is important to move the patient during the film, which can give rise to considerable variations in X-ray absorption. (Sometimes automatic density regulation may be undesirable, e.g. where large shifts of the contrast medium are to be observed; for such cases manual control remains possible.) *Fig. 8* shows a simplified diagram of the stabilizer; the diagram also illustrates how changes in film sensitivity and frame-frequency are allowed for. The above-mentioned shortening of the transition time at the start of filming is due to the fact that, when the tube current suddenly has to be increased to produce a certain photographic density, the stabilizer does *not* raise the filament current immediately to the new steady value (the regulator is not "aware" of this value until the state is steady again) but raises it to a much higher value than the steady one for as long as the luminance on the viewing screen is still inadequate. This is explained in *fig. 9*.

A feature of cinefluorography that is unusual compared to normal cinematography is that the radiologist does not usually fix the length of the film beforehand, but lets it depend on what he observes through the viewing system while the film is being made. This implies that measures must be taken to avoid exceeding the permissible duration of the load corresponding to the selected values of tube voltage and current. The situation is made more complicated by the fact that the tube current, as we have seen, does not always remain constant during filming; moreover the film may be preceded by a period of screening, or periods of screening and filming may follow one upon the other, possibly punctuated by intervals of rest. It is then very difficult to apply the normal nomogram used by radiologists which gives the permissible combinations of voltage, current and loading time for given conditions of operation and cooling. We have therefore designed a kind of analogue computer (a "heat integrator") which, during operation, continuously integrates the electrical energy from the current and voltage in a way that takes account of the heating effect of each period of energy dissipation in the anode and also of the cooling during the intervals of rest and during operation (cooling by anode radiation). The principle of the circuit is explained in *fig. 10*. The result of the integration is read on a meter; the reading, which is now a direct measure of the anode temperature, can be compared with the maximum permissible total load (the maximum temperature) marked on the scale of the meter, thus providing a continuous indication of how far it is still possible to go. When the maximum load is reached the high tension is automatically switched off, so that the apparatus can be operated for as long as possible without the risk of inadvertently overloading the X-ray tube.

In addition to the stabilization of the film density and the safeguarding of the X-ray tube, a facility will in many cases be required for directly checking on the dose of radiation received by the patient during cinefluorography. For this purpose an ioniza-

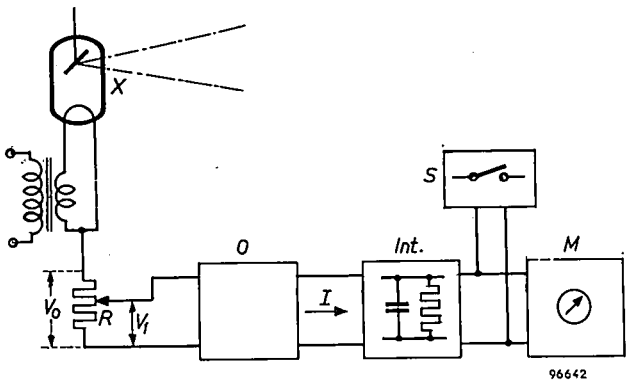

Fig. 10. Block diagram of the heat-integrater computer for safeguarding the X-ray tube against overloading. The voltage V_0 across the resistor R is proportional to the tube current. From V_0 a fraction $V_1 = aV_0$ is tapped off by the sliding contact on R. The sliding contact is coupled to the knob for controlling the tube voltage such that a is proportional to the latter. Thus, at any given instant, V_1 is a measure of the power dissipated at the tube anode.

The integration of this power is based on the fact that the supply and simultaneous dissipation of energy at the anode can be represented approximately by the charging of a leaky capacitor (i.e. with a resistor shunted across it). For this purpose the voltage V_1 is converted in circuit O into a charging current I, which is fed to an RC circuit denoted by "*Int*". When the capacitor is charged up to a predetermined value, read on the meter M — the "switch-off voltage" — the anode has then accumulated the maximum permissible quantity of heat; filming is then automatically stopped by switch S.

The circuit O is so designed that the charging current I varies according to a certain function of V_1. This function is found by selecting the current I for each value of V_1 (considered constant) such that the capacitor, starting at zero voltage, reaches the "switch-off" value after a period that corresponds exactly to the maximum loading time (found from the tube nomogram) associated with the relevant power (corresponding to V_1). Tests have shown that, even with varying power and intervals of rest, the total time taken to reach the switch-off voltage is correct to within a close approximation.

Since the tube nomogram applies to a particular size of tube focus, two individual circuits O have been designed on the basis of the nomogram data for two different foci. If the tube load is switched over from one focus to another, the correct circuit O automatically comes into operation (and the switch S is automatically set to the switch-off voltage applicable to that focus).

The switch S prevents further loading of the X-ray tube until the voltage on capacitor C has dropped to 80% of the switch-off value.

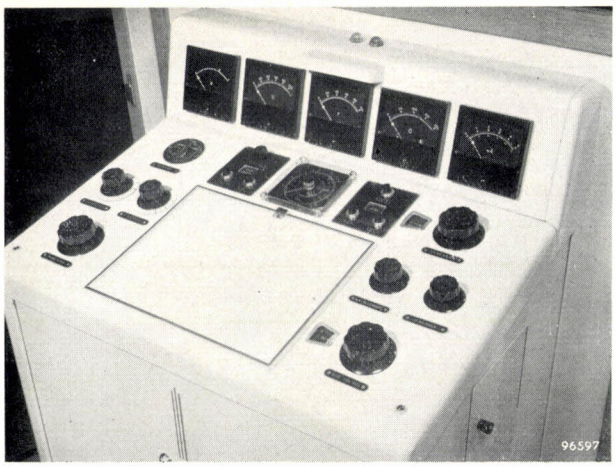

Fig. 11. Control desk for the cinefluorographic apparatus. The five meters, from right to left, indicate: the tube current, the film blackening to which the stabilizer is preset, the cumulative dose received by the patient, the cumulative load on the tube anode, and the supply voltage for the whole equipment. This voltage is corrected to the nominal value with the large knob bottom left. The two knobs above this serve to adjust the density stabilizer to the appropriate frame-frequency and film sensitivity. A clock under the meter in the middle indicates the filming time. The knob bottom right controls the tube voltage, the two above it control the tube current for fluoroscopy and cinefluorography, respectively, and the knob top right is the focus selector.

tion chamber can be placed in the X-ray beam, and the ionization current integrated by an amplifier circuit. The result of the integration, which is a

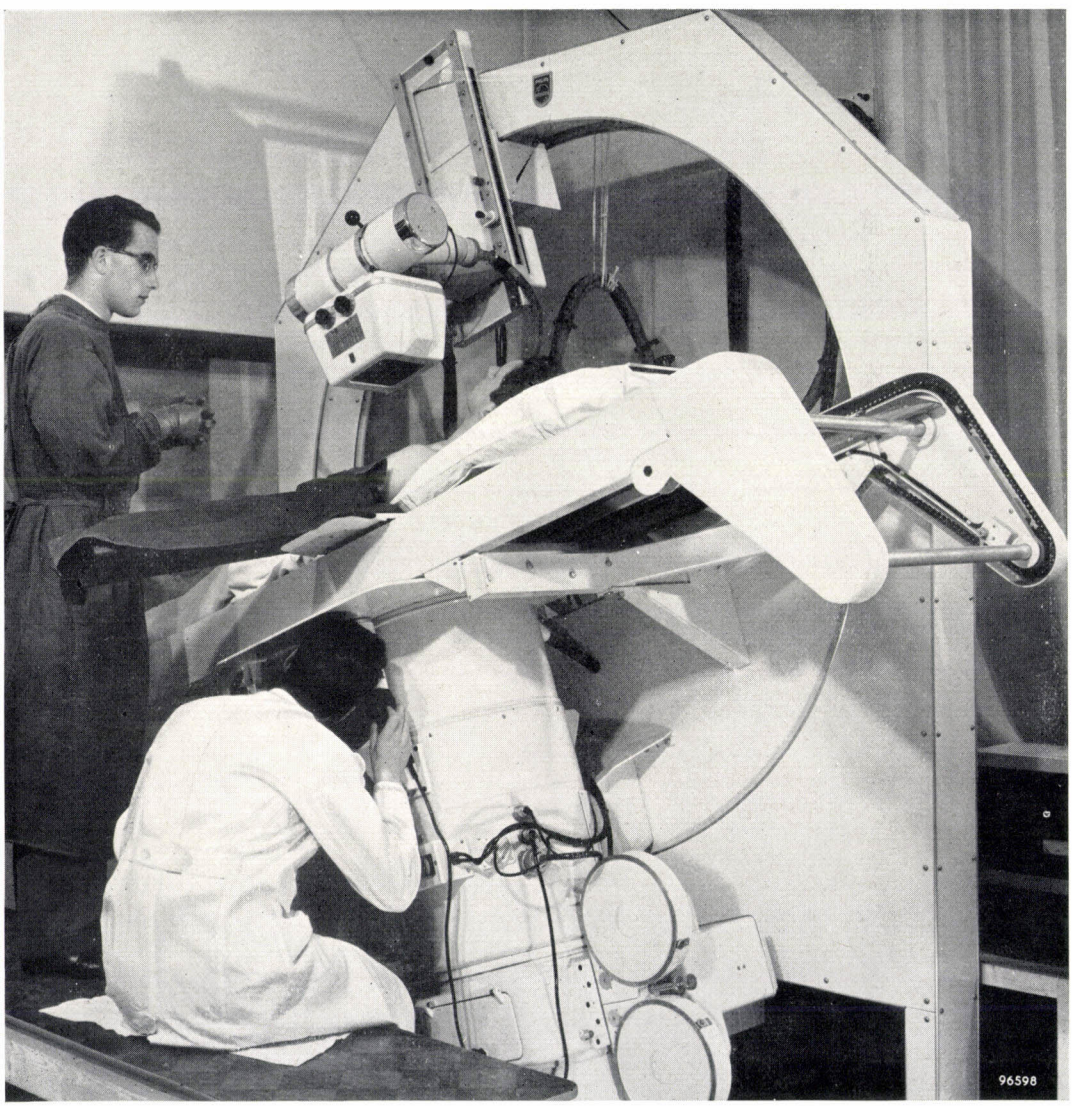

Fig. 12. "Ring stand" for cinefluorography. The X-ray tube (top) and the cinefluorographic equipment (below) are mounted on the ring such that the X-ray beam traverses a diameter of the ring. The part of the patient's body to be filmed lies virtually in the centre of rotation. Rotation of the ring tilts the patient into any desired position without altering his positioning in relation to the X-ray beam.

measure of the total dose in röntgens delivered by the tube at a particular distance, can be read from a meter on the control desk. At the same time the clock on the control desk indicates the total filming time.

The meters mentioned can be seen in *fig. 11*, which shows a photograph of the control desk for the cinefluorographic apparatus. The X-ray tube and the high-tension generator can also be connected to a normal control desk, so that they can be used without the cine-camera for the purposes of conventional X-ray diagnosis.

graphy. The simplicity of the UGX stand was obtained, however, by abandoning a conventional and widely used method of examination, namely the method of vertically irradiating a patient lying on his back, while possibly tilting the patient together with the X-ray beam about a horizontal transverse axis. To provide the radiologist with this facility, which is essential in certain diagnostic methods such as angiocardiography (examination of the heart vessels), a special stand has been designed for the 11-inch image-intensifier cinefluorographic equipment, based on the work of Janker [6]). It consists of

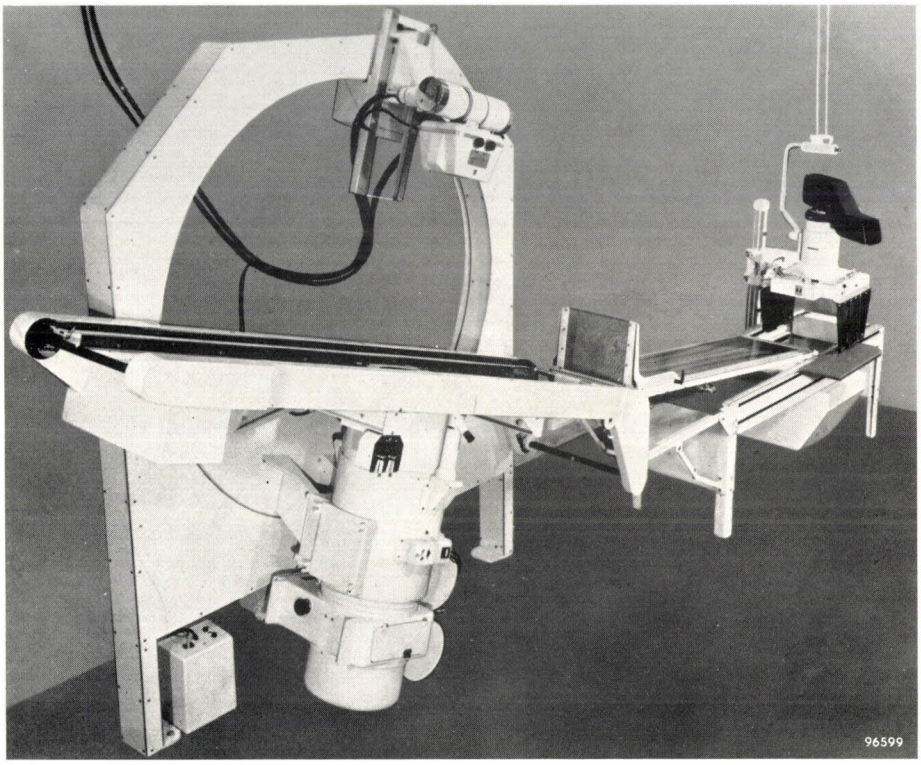

Fig. 13. Set-up for angiocardiography. For this examination a catheter is first introduced into or near the patient's heart via a vein. The introduction of the catheter is supervised by means of a 12.5 cm image intensifier, seen mounted above the catheterization table. The patient, with the catheter in position, is then conveyed to the "ring stand" by simply drawing the table top on which he is lying from the one stand to the other. The table top runs in U-channels with the aid of a chain drive.

Application of the apparatus

The considerable size and weight of the combination of the 11-inch image intensifier with a cine-camera make it impossible to mount this equipment on one of the normal stands used in X-ray diagnosis. A simple solution to this problem is offered by the "Müller" UGX stand (fig. 1), earlier described in this journal, and which was designed especially to meet the requirements imposed by the growing bulk of the viewing systems and attachments now coming increasingly into use [8]). This stand is indeed highly suited to many applications of cinefluoro-

a fixed frame containing a vertically mounted ring which rotates in its own plane. The frame is very rigidly mounted on base plates and supported on one side by two wall brackets. The ring carries the X-ray tube and the cine-apparatus, with the optical axis lying along a diameter of the ring, and between them is mounted the examination table; see *fig. 12*. The X-ray tube can be shifted along the ring diameter to vary the focus-screen distance. The centre of rotation of the ring is at a height of 165 cm above the base plates. Thus, the table and the cine-apparatus remain clear of the floor during

rotation; otherwise it would be necessary to have a hole cut in the floor, which would be a nuisance as well as dangerous to the operating personnel. The table-top lies 15 cm away from the centre of rotation, so that the part of the patient to be filmed, e.g. the heart, lies practically at the centre of rotation. Apparatus not attached to the ring and used for lateral exposures (along the axis of the ring) does not therefore have to be moved when the ring is rotated. In order to position the patient with respect to the X-ray beam, the table-top itself can be moved in its own plane over 100 cm longitudinally and over 10 cm transversely. For this purpose the table-top slides on runner guides in the table frame, while the latter runs on rollers over two cross-bars fixed to the ring.

Special provision is made for angiocardiography. As a rule, this examination is preceded by a heart catheterization, which is carried out on a table designed for the purpose. To facilitate the conveyance of the patient from the catheterization table to the ring stand, we have designed the stand such that the table-top on which the patient lies can simply be drawn from the one table on to the other. *Fig. 13* shows how this is done, and also gives an impression of the apparatus involved in an angiocardiographic examination. In these examinations, which are now carried out in many parts of the world, cinefluorography has proved to be a very valuable technique. Full advantage can be taken here, too, of the feature of our cine-apparatus which allows two persons — the radiologist and cardiologist, or perhaps a trainee radiologist — to observe the X-ray image at the same time.

Summary. Since the image intensifier greatly reduces the dose of X-rays administered to the patient, its use for the purposes of cinefluorography is obviously indicated. The earlier described 5-inch image intensifier is already widely used in this way. A larger image intensifier has since been developed having a screen of 11 inch diameter, a reduction factor of 4.5 and a luminance intensification of approx. 100×, which makes it possible to examine cinematographically such large organs as the heart and lungs. In conjunction with this image intensifier, the construction and properties of which are discussed in this article, a special cinefluorographic apparatus has been designed, comprising a 35 mm mirror cine-camera (effective aperture ratio 1:0.83), an optical viewing system allowing two observers to watch the image during cinefluorography, and a luminance meter to regulate the average photographic density of the film or, if required, automatically keep it constant. The power supply for the X-ray tube contains a heat integrater, which safeguards the anode against overheating as a result of prolonged and severe loading. The cinefluorography apparatus, the X-ray tube and the examination table can be mounted on a "ring stand", which enables the patient to be tilted during the examination without shifting his position with respect to the X-ray beam. In conclusion the author discusses the application of the apparatus to angiocardiography.

MANUFACTURE OF FLUORESCENT LAMPS

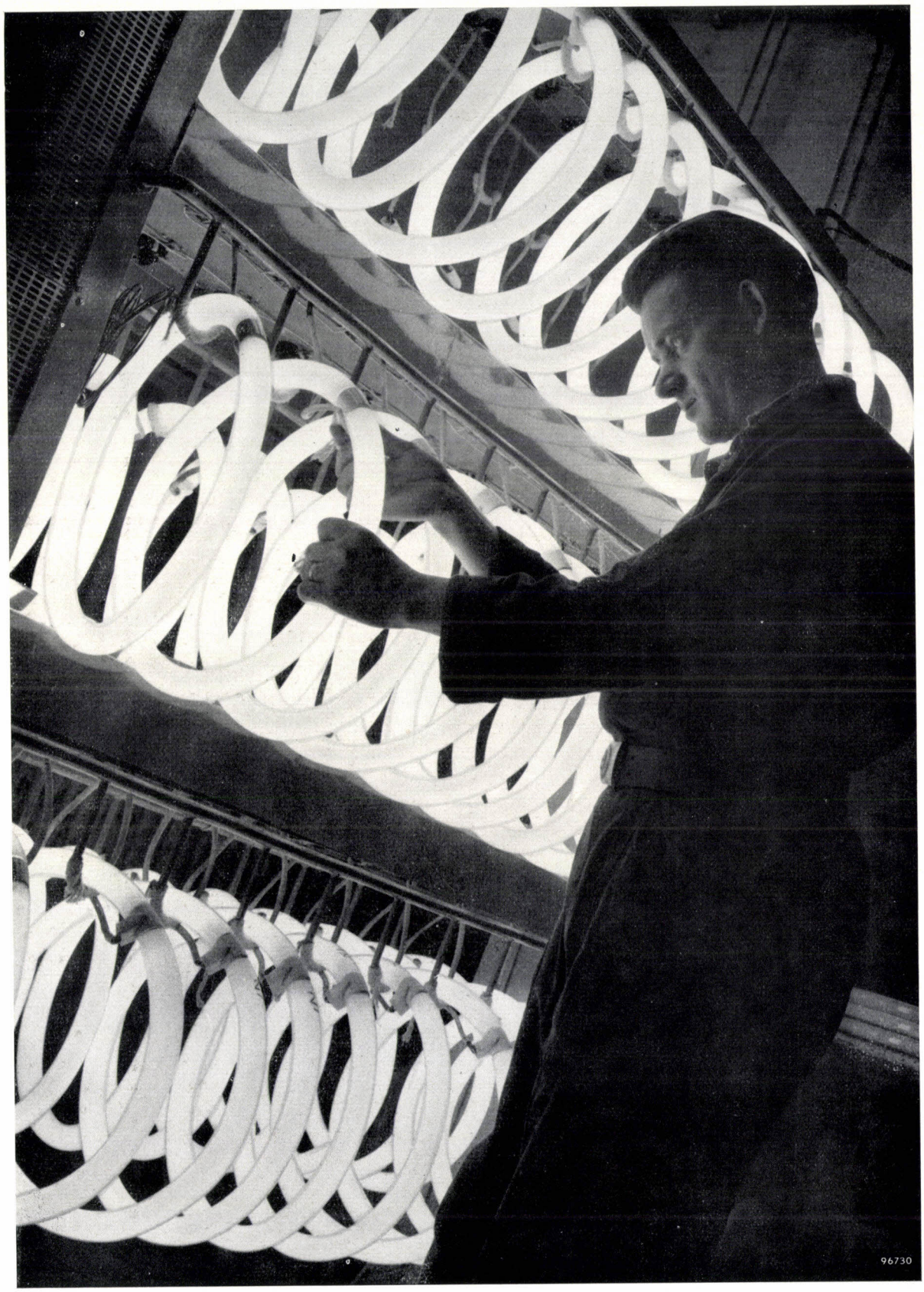

Aging and final checks of fluorescent lamps, type "TL" E, in the Philips Works at Roosendaal, Holland.

ABSTRACTS OF RECENT SCIENTIFIC PUBLICATIONS BY THE STAFF OF N.V. PHILIPS' GLOEILAMPENFABRIEKEN

Reprints of these papers not marked with an asterisk * can be obtained free of charge upon application to the Philips Research Laboratories, Eindhoven, Netherlands.

2610: H. A. Klasens: Elektrolumineszenz von suspendierten Sulfidphosphoren (Halbleiter und Phosphore, Internat. colloq. Garmisch-Partenkirchen 1956, edited by M. Schön and H. Welker, published by Vieweg & Sohn, Brunswick, 1958, pp. 247-262). (Electroluminescence of embedded sulphide phosphors; in German.)

Many sulphide phosphors, embedded in a suitable binder, fluoresce when subjected to an alternating electric field (electroluminescence: Destriau effect). An attempt is made to develop a picture of the mechanism of electroluminescence that admits a satisfactory explanation of the many observed phenomena.

2611: W. Hoogenstraaten: Der nicht-elektronische Energietransport in Phosphoren (Halbleiter und Phosphore, Internat. colloq. Garmisch-Partenkirchen 1956, edited by M. Schön and H. Welker, published by Vieweg & Sohn, Brunswick 1958, pp. 285-305). (Non-electronic energy transport in phosphors; in German.)

Various mechanisms have been proposed to explain sensitization of fluorescence in inorganic phosphors. From a discussion of these mechanisms it follows that only two of them, viz. energy transfer by metastable excitons of the base lattice and resonance transfer between sensitizers (S) and activators (A), are not in contradiction with the qualitative behaviour of these phosphors. The quantum-mechanical theory of resonance transfer by dipole-dipole, dipole-quadrupole and exchange interaction is discussed in some detail. The phenomenological theories connected with the above transfer mechanisms are compared with the experimental results on the relative efficiencies of S- and A-fluorescence as a function of the concentrations of S and A. From this comparison it appears that resonance transfer from sensitizer to activator, either directly or via other sensitizers, is the most probable mechanism of sensitized fluorescence. Finally, a short account of host-sensitization is given.

2612: J. S. van Wieringen: Paramagnetic resonance in single crystals of SiC doped with N, P, B or Al (Halbleiter und Phosphore, Internat. colloq. Garmisch-Partenkirchen 1956, edited by M. Schön and H. Welker, published by Vieweg & Sohn, Brunswick 1958, pp. 367-370).

Both n- and p-type SiC show paramagnetic resonance at liquid-nitrogen temperature, caused by electrons and holes respectively. The electron centre is located near one or more nitrogen nuclei and is isotropic. The hole centre shows anisotropic behaviour.

2613: P. Penning: Generation of imperfections by thermal stress (Halbleiter und Phosphore, Internat. colloq. Garmisch-Partenkirchen 1956, edited by M. Schön and H. Welker, published by Vieweg & Sohn, Brunswick 1958, pp. 482-485).

Further considerations on the generation of dislocations during the growth of germanium crystals from the melt. (See also these Abstracts No. **R 338** and Philips tech. Rev. **19**, 357-364, 1957/58, No. 12.)

2614: J. A. Lely and F. A. Kröger: Optical properties of pure and doped SiC (Halbleiter und Phosphore, Internat. colloq. Garmisch-Partenkirchen 1956, edited by M. Schön and H. Welker, published by Vieweg & Sohn, Brunswick 1958, pp. 514-524).

Absorption spectra of SiC, pure and doped with N or Al have been measured. Hexagonal SiC has an absorption edge at $\sim$ 4000 Å, cubic SiC at 4400 Å. Incorporation of N in hexagonal SiC gives rise to absorption bands in the blue and red, causing a green transmission colour. Incorporation of Al gives rise to absorption bands in the green and red, causing a blue transmission colour. Various luminescence bands have been observed. In the infra-red, SiC shows strong absorption in bands from 6-13 μ. Analysis of the infra-red reflection spectrum shows that the wave-numbers of the transverse and longitudinal vibrations of the optical branch are $\nu_t = 800$ cm^{-1}, $\nu_l = 975$ cm^{-1}.

2615: J. A. Lely and F. A. Kröger: Electrical properties of hexogonal SiC doped with N, B or Al (Halbleiter und Phosphore, Internat. colloq. Garmisch-Partenkirchen 1956, edited by M. Schön and H. Welker, published by Vieweg & Sohn, Brunswick 1958, pp. 525-533).

Measurements of the Hall effect and of conducti-

vity as a function of temperature have been carried out for SiC doped with nitrogen, boron or aluminium. Analysis of the experimental data leads to the following results: 1) The depth of N donor levels below the conduction band $\varepsilon_D = 0.06\text{-}0.085$ eV. 2) The separation of Al and B acceptor levels from the valence band $\varepsilon_A = 0.275$ eV. 3) Lattice scattering causes the mobility to decrease with temperature according to $\mu_H = aT^{-b}$ with $b = 1.5\text{-}1.8$ for electrons and $b = 2.2\text{-}3.0$ for holes. 4) The effective mass ratio for electrons in the conduction band is approximately $(m^*/m)_n = 0.6$. An estimate based on the mobility ratio for electrons and holes leads to an effective mass ratio for holes in the valence band of $(m^*/m)_p \approx 1.2$.

2616: W. van Gool: Fluoreszenz und Photoleitfähigkeit in Zink-Kadmium-Sulfiden aktiviert mit Silber (Halbleiter und Phosphore, Internat. colloq. Garmisch-Partenkirchen 1956, edited by M. Schön and H. Welker, published by Vieweg & Sohn, Brunswick 1958, pp. 602-609). (Fluorescence and photoconductivity in zinc-cadmium sulphides activated with silver; in German.)

Some phosphors were made from CdS activated with Ag-Ga and Ag-Cl. These phosphors show two fluorescence bands at low temperatures, viz. 6200 Å and 7300 Å. The 6200 Å emission has only been found when the activator concentration (Ag) surpasses the coactivator concentration (Cl or Ga). By making a series of mixed crystals (Zn,Cd)S it can be shown that the 7300 Å emission corresponds to the 4500 Å emission in ZnS (sphalerite) and therefore to the normal silver centre (Ag^+ at a lattice site). The 6200 Å emission in CdS is connected with 3950 Å (sphalerite) or 3850 Å (wurtzite) in ZnS. The experimental conditions necessary to obtain the short-wave emission (Ag > Ga) indicate that the short-wave fluorescence centre is formed by interstitial silver, by a sulphur vacancy or by an association containing at least one of these defects. It is also clear that the inversion of the normal band model, as has been proposed by Lambe and Klick, may be possible for the short-wave centre (6200 Å in CdS, 3950 Å in ZnS); there are no indications, however, that the band model of the normal silver centre (7300 Å in CdS, 4500 Å in ZnS) ought to be changed.

2617: P. Penning: Coefficient for self-diffusion determined from the rate of precipitation of Cu in Ge (Phys. Rev. **110**, 586-587, 1958, No. 2).

From data published by Tweet on the rate of copper precipitation in Ge during annealing, and its dependence on the dislocation density, it is shown that the coefficient of self-diffusion of germanium can be derived. The results agree closely with measurements made with radio-germanium, indicating firstly the validity of the vacancy-mechanism assumption, and secondly that etch-pit counts give an accurate measure of the density of dislocations that absorb vacancies.

2618: J. S. C. Wessels: Studies on photosynthetic phosphorylation, II. Photosynthetic phosphorylation under aerobic conditions (Biochim. biophys. Acta **29**, 113-123, 1958, No. 1).

The aerobic photochemical esterification of inorganic phosphate to adenosine triphosphate has been investigated. Evidence is presented in support of the conclusion that under aerobic conditions, in contrast to anaerobic phosphorylation, vitamin K_3 and flavin mononucleotide are interchangeable and are not involved in separate pathways for photosynthetic phosphorylation. A tentative scheme for the generation of adenosine triphosphate in chloroplasts is given and discussed in relation to the effect of various inhibitors on phosphorylation. (See also these Abstracts No. **2509**.)

2619: R. Dijkstra and J. de Jonge: The chemical effect of light on sodium p-methoxybenzenediazosulphonate (Rec. Trav. chim. Pays-Bas **77**, 538-554, 1958, No. 6).

It is deduced from kinetic measurements that irradiation of an aqueous solution of p-methoxybenzenediazosulphonate with ultra-violet light causes a dissociation of the sulphonate ion to form a p-methoxybenzenediazonium ion and a sulphite ion. The ions produced photochemically slowly recombine in the dark to form back the original sulphonate ion. The reactions may be represented by the scheme:

$$CH_3O.C_6H_4.N{=}N{-}SO_3^{(-)} \underset{\text{(light)}}{\overset{\text{(dark)}}{\rightleftarrows}} CH_3O.C_6H_4.N_2^{(+)} + SO_3^{(--)}.$$

The occurence of a labile or cis-diazosulphonate can almost certainly be excluded.

Fig. 1. Map of the Nieuwe Waterweg, which connects the Hook of Holland with Rotterdam, showing the seven radar stations and the areas normally scanned by each. Displays appearing on one of the two screens of each station are also shown.

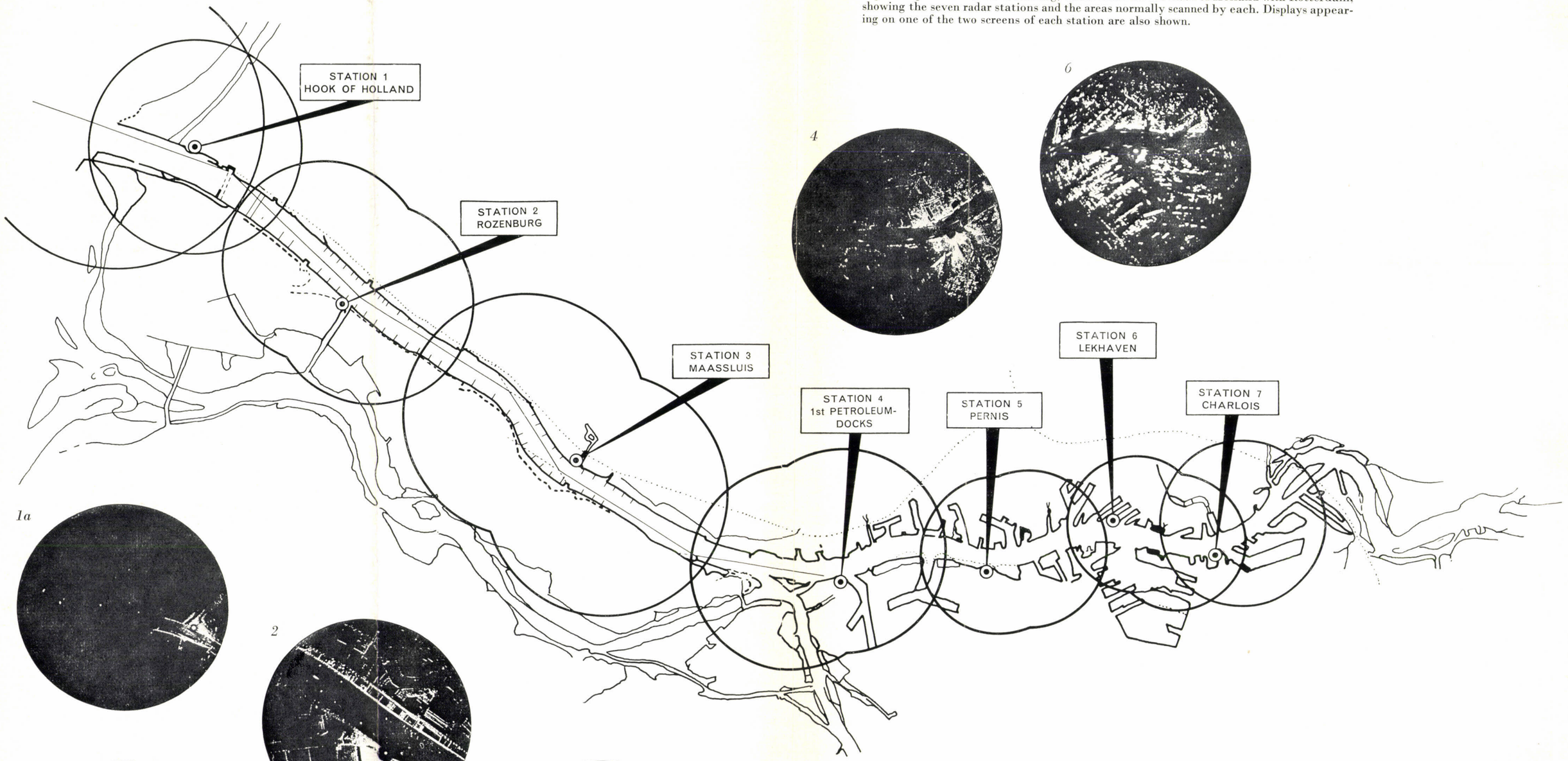

VOLUME 20, 1958/59, No. 12 pp. 349-388 Published 12th November 1959

Philips Technical Review

DEALING WITH TECHNICAL PROBLEMS
RELATING TO THE PRODUCTS, PROCESSES AND INVESTIGATIONS OF
THE PHILIPS INDUSTRIES

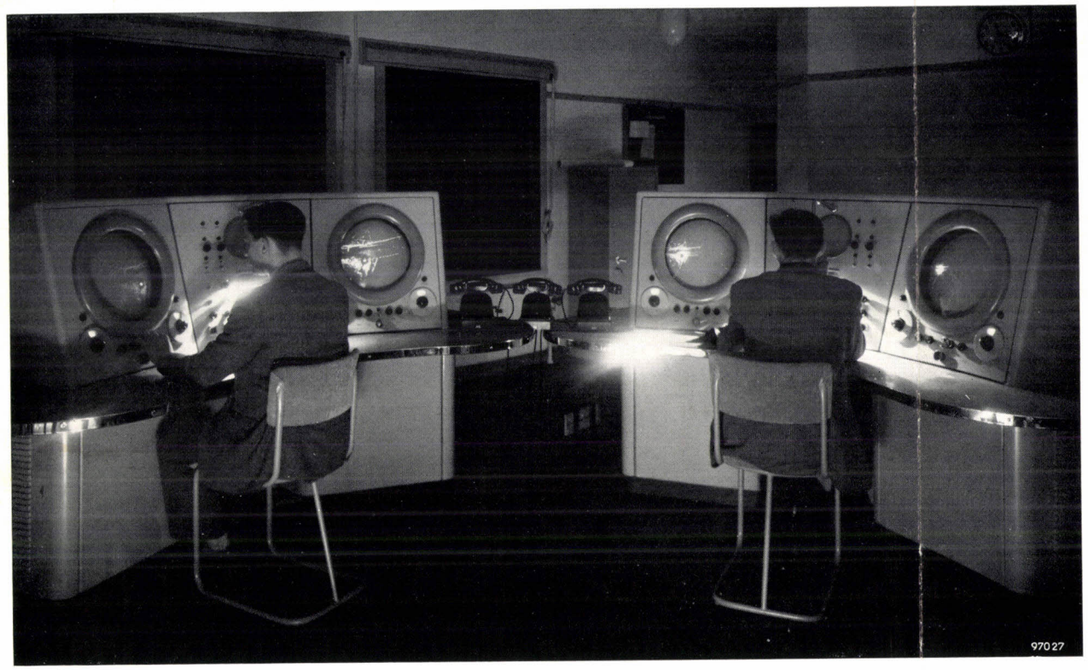

THE PORT OF ROTTERDAM RADAR SYSTEM

621.396.967

Seven radar stations spaced along the thirty odd kilometres of the Nieuwe Waterweg, a channel running from Rotterdam to the North Sea, were put into operation on the 30th November 1956. On 1st January 1958, after trials for establishing operational procedures and familiarizing personnel with the routine, the service was made available to shipping. The installation has enhanced the efficiency of the port of Rotterdam considerably. Ships can now be guided along the waterway in conditions of visibility such as would formerly have paralysed all movement.

The radar service was called upon for assistance as long ago as July 1957, before it had officially come into operation. The 30 000 ton Nieuw-Amsterdam had entered the Nieuwe Waterweg under excellent weather conditions, but halfway between the Hook of Holland and Rotterdam she ran into a fogbank that had suddenly formed. With the radar assistance the ship was able to reach harbour safely.

Port radar as an aid to navigation was not new in 1956. The port of Liverpool has been equipped with a shore radar station since 1948, and an installation at IJmuiden has been in operation since 1951 [1]). At Rotterdam, however, the situation is much more complicated, because ships are continually obliged to alter course on the winding tidal river. The Rotterdam port authorities had applied for advice on the technical aspects of

---

[1]) A short description of Philips harbour radar equipment, type SHR 101, Comm. News **13**, 147-148, 1953.
Radar station at IJmuiden (Holland), Philips tech. Rev. **14**, 95, 1952/53.

the problem to the Netherlands Radar Research Establishment at Noordwijk-on-Sea. In 1953, after extensive tests with mobile radar posts, a final report was drawn up which contained full technical specifications for suitable radar equipment, working on wavelengths in the 3 cm band. The N.V. Philips' Telecommunicatie-Industrie at Hilversum were entrusted with the development and delivery of equipment in accordance with the specifications, part of the apparatus developed by Philips being manufactured by the N.V. Van der Heem in The Hague. A brief description of this radar installation [2]) now follows.

It will be seen from the map in *fig. 1* that the seven stations sweep the whole of the Nieuwe Waterweg plus the Rotterdam harbour area, Station *1* at the Hook of Holland also covering the sea approaches to the Waterweg. In normal circumstances shipping proceeding along the Nieuwe Waterweg follows "leading-lines", as is the case in many inland waterways; these are lines connecting fixed beacons that are illuminated at night. The leading-lines of the Nieuwe Waterweg are shown in fig. 1.

If because of fog or for some other reason visibility becomes so bad that the beacons (and other landmarks) cease to be visible, it is the business of the radar service to provide pilots with the information they require. A pilot will want to know the distance of the ship from a certain leading-line and its distance from and bearing with respect to features such as harbour entrances, the points where successive leading-lines intersect, and so on. The employment of the "Raplot" system developed by the Netherlands Radar Research Establishment allows information of this kind to be supplied with a high degree of accuracy.

Under this system it is possible to superimpose on the P.P.I. display (Plan Position Indicator) one of two kinds of reference lines. This puts the operator in a position to supply the ship directly with data about its position in relation to features relevant to navigation — the entrance to the harbour at the Hook of Holland, for example.

Both kinds of reference lines are generated electronically, and the operator can place their origins anywhere within a circle concentric with the screen and having two-thirds the screen radius. One of the reference lines is a "cursor line"; the echo of some prominent fixed point is chosen as the origin for the cursor line. By turning a knob, the operator can rotate the cursor line about this origin and, with the aid of a second knob, move an electronic marker along it. Having brought the marker

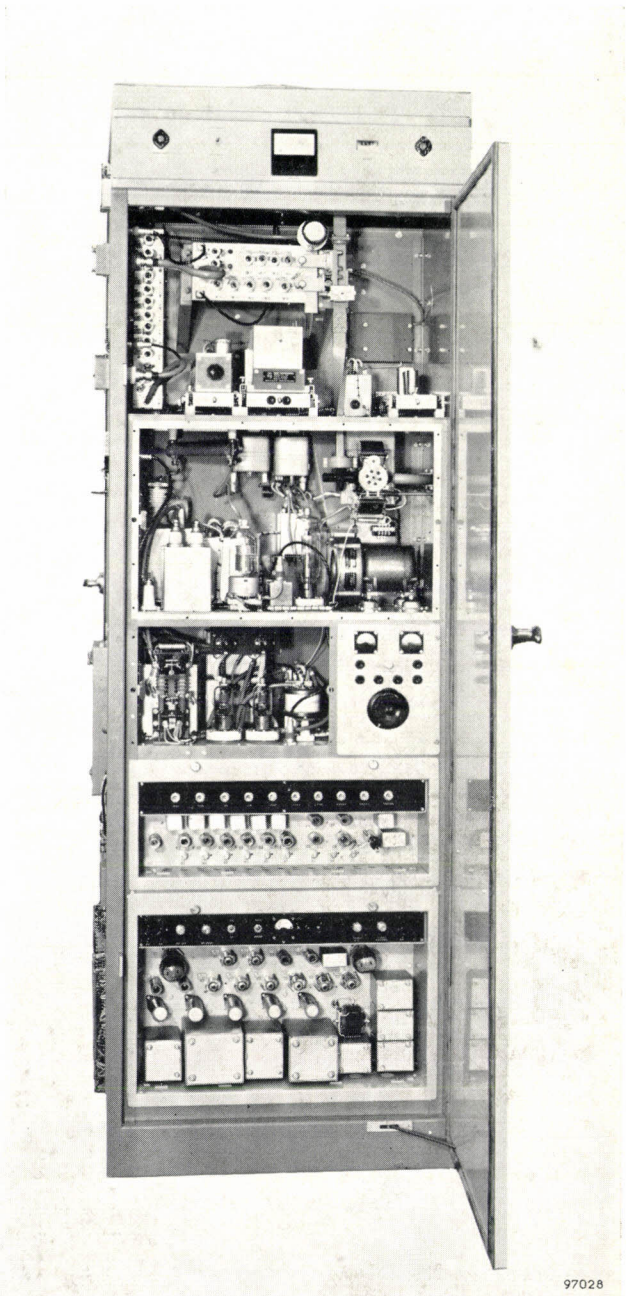

Fig. 2. Radar transceiver in standard cabinet. Technical data:

Modulator/transmitter:

Local oscillator	tunable magnetron, type 2 J 51
Frequency range	8.9 to 9.2 Gc/s
Maximum power in pulse	approx. 30 kW
Pulse duration	approx. 0.1 microsecond
Repetition frequency	2777 pulses per second (crystal-controlled)

Receiver:

Intermediate frequency	30 Mc/s
Intermediate-frequency bandwidth	18 Mc/s at −3 dB level
Adjustment of klystron frequency	manual or automatic

[2]) A more detailed description may be found in B. H. G. Prins and J. M. G. Seppen, The Rotterdam harbour radar system, Philips Telecomm. Rev. **20**, 16-30, 1958 (No. 1).

into position on the echo of a given object (the ship), he can read off on the knob dials the bearing and distance of the object with respect to the chosen origin of the cursor line. All this takes no more than a few seconds. The readings are equally accurate for an eccentric and a centric display (see below).

The other kind of reference lines are fixed lines which may, for example, represent the leading-lines referred to above or the central axis of a harbour entrance. They allow the radar operator to supply ships with information closely corresponding to that used in normal navigation. These lines appear on the screen as a chain of short dashes enabling distances to be estimated quickly and accurately, the length of one dash plus one interval being equivalent to 100 m. Examples of these broken reference lines may be seen in the screen display under Station *3* in fig. 1; in this particular case they represent leading-lines.

Distances between the ship and points on the screen can be determined down to 20 m plus 0.5% of the value indicated. Bearings are given with an error of less than 0.5°.

As will be seen from fig. 1, the ground covered by most of the stations consists of two overlapping circular areas. At the stations themselves there is a control desk with two P.P.I. screens, on each of which one of the circular areas is displayed. Since the station is not located at the centre of either circle, some means must be available for providing an eccentric displacement of the displayed picture. This is done by passing adjustable bias currents through the scanning coils of the cathode-ray tubes. It is possible in this way to adjust eccentricity in any desired direction up to a maximum displacement of two-thirds the screen radius.

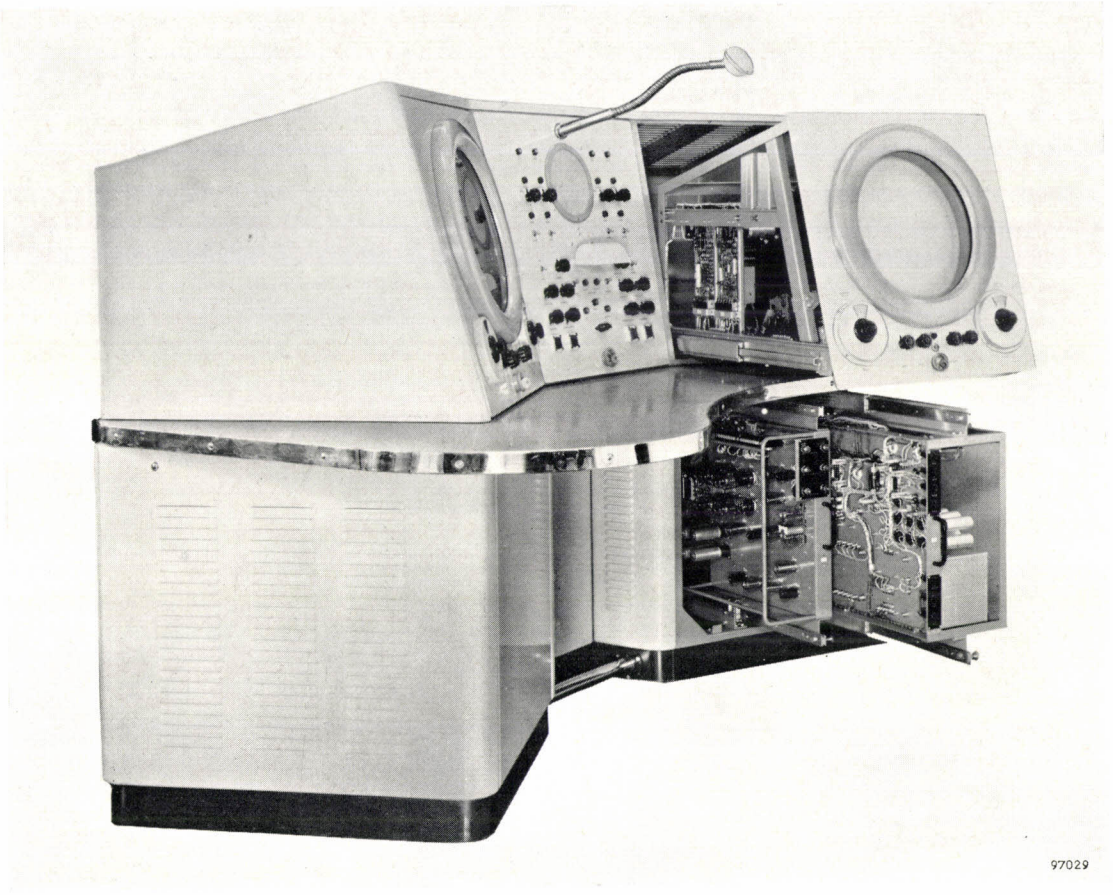

Fig. 3. A control desk with two P.P.I. screens (diam. 38 cm). All units comprising the equipment slide forward for inspection.

The scale of the display on each screen is adjustable, allowing a larger or smaller area to be covered as desired. At Stations *2* to *7* inclusive, coverage is continuously adjustable from a circular area of radius 2000 m to one of radius 5000 m. In normal circumstances both screens at each station display the smallest areas, all of these together giving coverage for the whole of the Waterweg, as in fig. 1. The areas covered by individual stations can be enlarged in such a way

as to restore complete coverage if one station goes out of action.

If a breakdown disrupts one of the displays, the other screen is switched over from small-area to large-area coverage and simultaneously recentred. In this way the whole of the area to be covered by the station is again visible. Normally two screens are in use, therefore, but each serves as a standby for the other. The radar transceivers themselves are duplicated, likewise to ensure continuity of the service.

In the Hook of Holland station there are two control desks instead of one, each having two screens (see *title photograph*). One desk covers the estuary and the port entrance, the other the approach area and a sea area extending beyond the cruising stations of the two pilot vessels. The radii of the circular areas appearing on the four screens can be adjusted as follows:

Desk 1 { screen 1: 5000-7500 m and 2000-5000 m
screen 2: 2000-5000 m and 2000-5000 m

Desk 2 { screen 1: 5000-7500 m and 2000-5000 m
screen 2: 5000-7500 m and 12 000-16 000 m.

A further feature of the Rotterdam radar service is that pilots are supplied with small transceivers enabling them to maintain contact with the radar stations by radiotelephony. The seven radar stations have their own transmitting and receiving frequencies in the 160 Mc/s band. As the ship proceeds up the Nieuwe Waterweg, the pilot is passed on from one station to the next.

Fig. 2 shows a radar transceiver built into a standardized steel cabinet. A control desk with two P.P.I. screens (diam. 38 cm) is shown in *fig. 3*. Some technical details are given in the captions to the photographs.

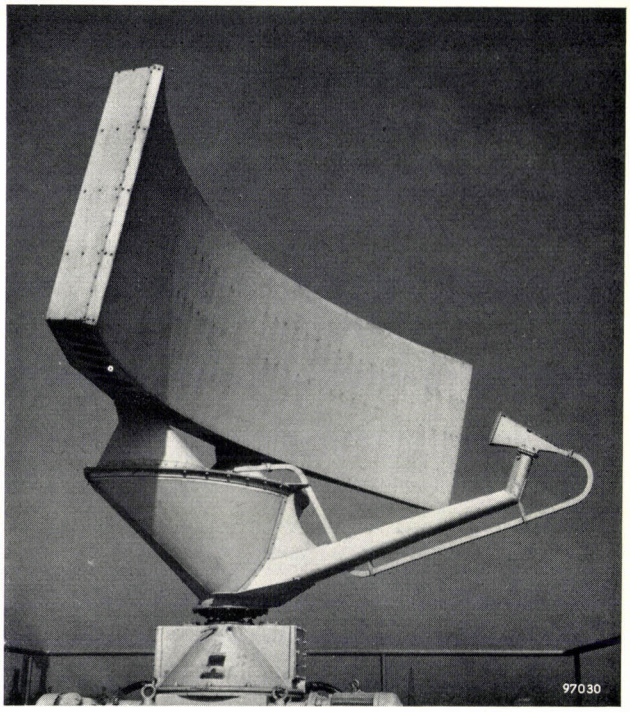

Fig. 4. Rotating aerial assembly used in the Rotterdam radar system.

The aerials, one of which is shown in *fig. 4*, are cylindrically parabolic in shape and make 18 revolutions per minute. The beam radiated has a main lobe with a 3 dB width of 0.7° in the horizontal plane and of about 17° in the vertical plane (these figures thus refer to the angles at which the radiation is 3 dB weaker than in the axial direction). In the side lobes of the radiation pattern the field is at least 27 dB weaker than in the main lobe.

B. H. G. PRINS *) and J. M. G. SEPPEN *).

*) N.V. Philips' Telecommunicatie-Industrie, Hilversum.

TOPOTACTICALLY CRYSTAL-ORIENTED FERROMAGNETICS

538.221:621.318

In recent years a group of compounds possessing hexagonal crystal structure has been added to the ceramic magnetic materials. They are compounds of Fe_2O_3 with BaO and MeO (Me represents one of the divalent metals Mn, Fe, Co, Ni, Zn or Mg). The individual crystals of many of these compounds exhibit marked magnetic anisotropy; in some the magnetization shows a strong preference for orientation in the direction of the *c*-axis (the hexagonal axis), in other compounds the preference is for an arbitrary direction perpendicular to the *c*-axis. In the first case the material is said to have a preferred *direction* of magnetization, in the second case a preferred *plane*. Materials of the first kind are particularly suitable for making permanent magnets (one example is ferroxdure [1])). Materials of the second kind are magnetically soft and particularly suitable for use at high frequencies (one example is ferroxplana [2]), suitable for frequencies up to about 1000 Mc/s).

To derive full benefit from the magnetic anisotropy it is desirable in both cases that the *c*-axes of the crystallites in the polycrystalline material, obtained by sintering, should all be parallel. Such a "crystal-oriented" material — which thus possesses a texture — shows the same magnetic anisotropy as its constituent crystallites; the sintered non-oriented material, on the other hand, is isotropic. The advantage of crystal-orientation is evident from the fact that the $(BH)_{max}$ product of crystal-oriented ferroxdure, for example, can be about 3.5 times higher than that of non-oriented ferroxdure [3]). In the case of ferroxplana, crystal-orientation can make the permeability about 3 times as large [4]).

At the Research Laboratories at Eindhoven a new method for making these crystal-oriented materials has been evolved. Before describing it, we shall give a brief outline of the method used hitherto [5]).

A powder of the material to be oriented, so fine that each grain consists of one crystal, is mixed with a liquid. A paste or thick suspension is thus produced in which the crystals are easily able to rotate. To align crystals that have a preferred *direction*, the suspension is introduced into a static magnetic field; for preferred-*plane* orientation a rotating field is used (*fig. 1a* and *b*). The crystal-orientation so obtained is made fast by compressing the suspension into a pellet of the desired form. Upon subsequent firing for a few hours at 1100 to 1300 °C the crystals become sintered together, in which process the orientation is preserved and sometimes even improved.

We shall discuss the new method with the aid of an example. From a suspension consisting of a mixture (not a compound) of 1 mole $BaFe_{12}O_{19}$ (ferroxdure), 2 mole CoO and 2 mole Fe_2O_3, a pellet is pressed whilst a static magnetic field is applied. This causes the alignment of the strongly anisotropic ferroxdure crystals, but not of the non-magnetic CoO and Fe_2O_3 crystals. When the pellet is fired for some hours at 1250 °C, the following reaction takes place:

$$BaFe_{12}O_{19}\uparrow + 2CoO + 2Fe_2O_3 \rightarrow BaCo_2Fe_{16}O_{27}\perp .$$

(The signs $\uparrow$ and $\perp$ indicate respectively a preferred direction and a preferred plane.) In this way we obtain a sintered aggregate of hexagonal crystals of the compound $BaCo_2Fe_{16}O_{27}$. The important thing is that the *c*-axes of these new crystals show the

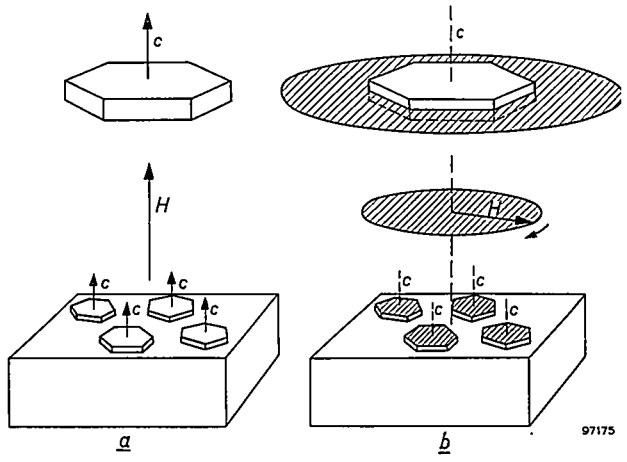

Fig. 1. Method of orienting the grains of hexagonal ceramic magnetic materials by means of a magnetic field. Each grain consists of one crystal in the form of a platelet. In (*a*) the *c*-axis (hexagonal axis), which is perpendicular to the platelet, is a preferred direction of magnetization. When a static magnetic field *H* is applied, the *c*-axes align themselves parallel with this field. In (*b*) the plane perpendicular to the *c*-axis is a preferred plane of magnetization. In this case, when a rotating field is applied, the *c*-axes align themselves perpendicular to the plane in which the field rotates.

1) J. J. Went, G. W. Rathenau, E. W. Gorter and G. W. van Oosterhout, Ferroxdure, a class of new permanent-magnet materials, Philips tech. Rev. **13**, 194-208, 1951/52.
2) G. H. Jonker, H. P. J. Wijn and P. B. Braun, Ferroxplana, hexagonal ferromagnetic iron-oxide compounds for very high frequencies, Philips tech. Rev. **18**, 145-154, 1956/57.
3) A. L. Stuijts, G. W. Rathenau and G. H. Weber, Ferroxdure II and III, anisotropic permanent-magnet materials, Philips tech. Rev. **16**, 141-147, 1954/55.
4) A. L. Stuijts and H. P. J. Wijn, Crystal-oriented ferroxplana, Philips tech. Rev. **19**, 209-217, 1957/58.
5) See also articles [3]) and [4]).

same orientation as the *c*-axes of the ferroxdure crystals, which disappeared during the reaction (*fig. 2*). We thus have the phenomenon that in a chemical reaction between solids the crystal-orientation of the reaction product is correlated with that of one of the initial substances [6]). To denote this phenomenon we have coined the term *topotaxy* [7]).

The fact that a topotactical reaction can indeed produce a well-oriented product is shown by X-ray diffraction patterns such as that in *fig. 3*. Not all topotactical reactions are as favourable as this however; there are examples in which the end product shows a poor orientation. The results will shortly be published of an investigation into the various factors that determine whether the end product of a topotactical reaction will be well-oriented or not.

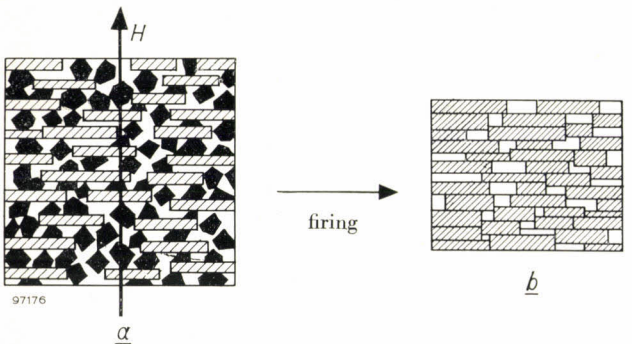

Fig. 2. Crystal-orientation of a magnetic oxide by means of a topotactical reaction. The initial mixture (*a*) contains a component consisting of crystallites of an oxide possessing strong magnetic anisotropy (hatched). This component is oriented by a magnetic field *H* and thus obtains a texture. The orientation of the other components (black) is not affected by the field. After firing (not in a field) a chemically different substance is produced (*b*, dense hatching) which exhibits the same texture as the oriented component in the initial material.

The topotactical reactions thus far investigated involve mainly compounds characterized in the composition diagram as shown in *fig. 4* by the points **M**, Me_2W, Me_2Y and Me_2Z, where **M** is an abbreviation for $BaFe_{12}O_{19}$ (ferroxdure), Me_2W for $BaMe_2Fe_{16}O_{27}$, Me_2Y for $Ba_2Me_2Fe_{12}O_{22}$ and Me_2Z for $Ba_3Me_2Fe_{24}O_{41}$. The reaction in our example is written in this notation as:

$$\mathbf{M}\uparrow + 2CoO + 2Fe_2O_3 \rightarrow Co_2\mathbf{W}\perp .$$

[6]) Research into the possibility of preparing materials in the manner described was prompted by the results of provisional experiments carried out by G. H. Jonker of this laboratory.

[7]) For further particulars regarding the choice of this name and its relation to "epitaxy" see: F. K. Lotgering, Topotactical reactions with ferrimagnetic oxides having hexagonal crystal structures, I, J. inorg. nucl. Chem. **9**, 113-123, 1959 (No. 2).

Compounds of the type Me_2Y and Me_2Z can be prepared in a similar manner.

Among the new possibilities opened up by topotaxy, the first to be mentioned is that a crystal-oriented material having a preferred *plane* of magnetization can now be made with the aid of a static magnetic field, which of course is easier to

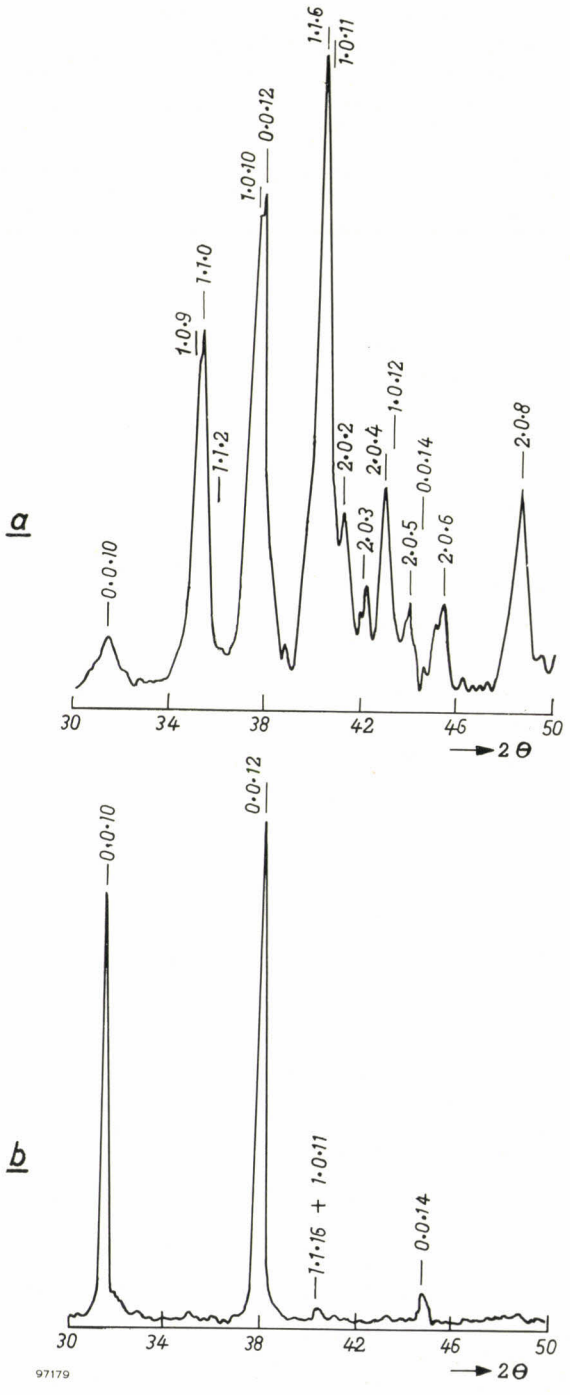

Fig. 3. *a*) X-ray diffraction diagram of non-oriented ZnCo**W** (abbreviation for $BaZnCoFe_{16}O_{27}$; see diagram in fig. 4). *b*) Diagram of oriented ZnCo**W**, prepared in accordance with the topotactical reaction $\mathbf{M}\uparrow + ZnO + CoO + 2Fe_2O_3 \rightarrow ZnCo\mathbf{W}\perp$. The only reflections occurring in this case are those originating from crystal planes perpendicular to the *c*-axis, showing that the material is indeed well-oriented.

set up than a rotating field. This is done by means of a topotactical reaction in which the orientable component in the starting mixture possesses a preferred *direction*. The reaction used above to explain the phenomenon of topotaxy is an example of this process.

Further, it is now possible to produce a well-oriented material which consists of crystals with insufficient magnetic anisotropy to be oriented directly by a magnetic field. One instance of this is found in the preparation of $Zn_{2-a}Co_aW$. For $a = 0$, we have Zn_2W, a substance with a distinct preferred *direction*. As a increases, i.e. as Co is substituted for Zn, the magnetic anisotropy decreases, and vanishes at $a \approx 0.65$. At higher values of a the anisotropy reappears, but now the material has a preferred *plane*. With the topotactical reaction

$$\mathbf{M}\uparrow + (2-a)\,ZnO + a\,CoO + 2\,Fe_2O_3 \rightarrow Zn_{2-a}Co_aW$$

a well-oriented product is obtained, even when $a \approx 0.65$.

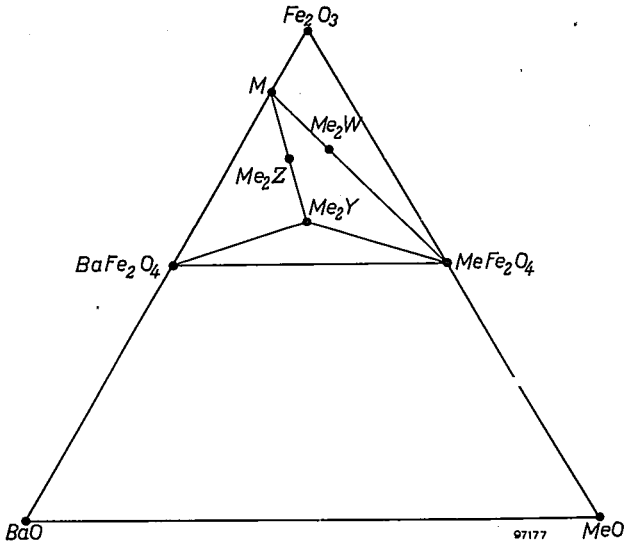

Fig. 4. Composition diagram indicating the compounds concerned in the topotactical reactions investigated here. They are the compounds **M** (i.e. $BaFe_{12}O_{19}$ = ferroxdure), Me_2W (i.e. $BaMe_2Fe_{16}O_{27}$), Me_2Y (i.e. $Ba_2Me_2Fe_{12}O_{22}$) and Me_2Z (i.e. $Ba_3Me_2Fe_{24}O_{11}$). The symbol Me represents one of the divalent elements Mn, Fe, Co, Ni, Zn or Mg or a mixture of these elements. For the compounds Me_2W, Me_2Y and Me_2Z, see the article quoted under [2]).

Other examples of topotactical reactions are given in the article quoted under [7]).

Materials having a preferred *direction* of magnetization and sufficient anisotropy for the old method can often be prepared more easily by the topotactical method. In preparing such a substance from the constituent oxides (mixed in the correct proportions) by means of a direct reaction, it is often found that after a single firing the required substance has formed only very incompletely. A repeated cycle of milling and firing is then necessary to achieve complete conversion. Frequently, however, a single firing can produce complete conversion if one of the basic substances used in the initial mixture is a substance such as **M** ($BaFe_{12}O_{19}$), which is itself a compound of two of the constituent oxides. In such a case it is possible by means of a topotactical reaction to produce in a single cycle not only a well-oriented but also a pure product. True, **M** must be available as a raw material, but this is a substance that can be produced directly in a single process from the oxides and is thus readily obtainable.

The topotactical method is at present being employed in the laboratory for preparing new materials for use in microwave directional isolators [8]). *Fig. 5* shows the hysteresis loops of such a material in the preferred direction and perpendicular thereto. These materials, which are required to have a slightly smaller anisotropy than ferroxdure, can be derived from ferroxdure by substituting Zn and Ti ions for a small fraction of the Fe ions in $BaFe_{12}O_{19}$ [9]). When these materials are prepared topotactically, they are found to be better formed and better oriented than when they are prepared from the oxides and subsequently directly oriented in a magnetic field.

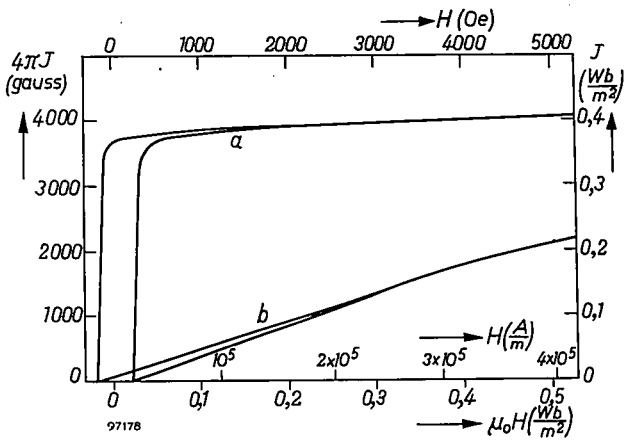

Fig. 5. Hysteresis loops of a topotactically crystal-oriented material intended for use in directional isolators, *a*) in a field *H* applied in the preferred direction, *b*) in a field perpendicular to the preferred direction.

F. K. LOTGERING.

[8]) H. G. Beljers, Ferrite isolators in the 8-9 mm wave band, Commun. Congrès internat. Circuits et Antennes Hyperfréquences, Paris 21-26 Oct. 1957, part 2 (suppl. Onde électrique **38**, No. 376 ter), pp. 647-648, Aug. 1958.

[9]) E. W. Gorter, La variation de l'énergie magnéto-cristalline de $BaFe_{12}O_{19}$, produite par la substitution de $Co^{2+} + Ti^{4+}$ à $2Fe^{3+}$, Colloque international de magnétisme, Grenoble 2-6 July 1958, published by "Centre national de la recherche scientifique", Paris 1959, pp. 303-304.

THE USE OF THERMISTORS IN THE EBULLIOSCOPIC DETERMINATION OF MOLECULAR WEIGHTS

621.317.39:536.531:541.24

Determinations of the molecular weight of chemical compounds are frequently carried out, especially in organic-chemistry laboratories. They serve primarily as a means of verifying, after completion of a synthesis, whether the compound intended has in fact been obtained. This method of verification is of particular importance in the preparation of substances that are seldom made or have never before been made, and whose physical constants are not precisely known. In the preparation of "known" substances it is more usual to measure for this purpose the melting point or the boiling point, or both, these being easier to determine than the molecular weight. In some cases both methods are combined.

The molecular weight M of a compound can be determined by making use of the phenomenon of boiling-point elevation. The boiling point of a solution differs from that of the pure solvent to an extent that depends on the concentration of solute "particles" in the solvent. If the solute is a non-dissociating substance, the "particles" are simply the molecules of the substance. If the substance does dissociate, each of the fragments acts as a "particle", and a higher boiling-point elevation is found. For *dilute* solutions the elevation Δt is proportional to the said number of particles, i.e. to the concentration of the solution. The proportionality factor, which is a characteristic of the *solvent* and which we call the molecular boiling-point elevation D, is expressed in °C per mole (gram-molecule) of solute [1]) in 100 grams of solvent (sometimes also expressed per 1000 g solvent).

Since the fraction of a gram-molecule constituted by one gram of a substance is inversely proportional to its molecular weight, we can write:

$$\Delta t = D \frac{c}{M}, \quad \ldots\ldots \quad (1)$$

where c is now the concentration of the solution in grams per 100 grams of solvent. Values of D for some widely used solutions are given in *Table I*.

In practice, M is usually determined by performing a series of measurements on increasingly concentrated solutions of the investigated substance, and a similar series on a standard substance. The standard substance used is one whose chemical properties closely resemble those of the investigated substance; moreover it is one that can be prepared in a very pure state, and of course its molecular weight is known. The boiling-point elevations found in both series of measurements are plotted versus concentration, giving a straight line for each substance, which passes through the origin, in accordance with (1). M is then found by multiplying the molecular weight of the standard substance by the ratio of the slopes of the two lines.

The reason for using this apparently cumbersome method — after all, if D is known, M could be directly calculated from the slope — is that in practice the right-hand side of equation (1) must be multiplied by an extra factor f which often differs slightly from unity. This factor is a correction for systematic errors caused partly by the apparatus and the experimental conditions (e.g. the true concentration is higher than calculated owing to part of the solvent being in vapour form) and partly by the nature of the investigated substance (e.g. unsteady boiling, which can lead to errors in the measurement of Δt). Since the value of the factor f is not always known, it is advisable to determine M from a relative measurement, i.e. from a comparison with a standard substance for which f, by virtue of the chemical similarity of the substances, may be deemed to have the same value.

Moreover, graphical treatment of the measurements offers some advantages compared with calculating M from each measurement (with the aid of (1)) and subsequently averaging the results. The graphical method not only saves much calculation, but automatically takes account of the fact that the Δt-c curves pass through the origin. It also provides a means of checking on any anomalous behaviour of the substance, such as decomposition or association of molecules, or a chemical reaction with the solvent, for in such an event the relation between Δt and c is no longer linear.

Table I. The molecular boiling-point elevation D and the boiling point of some widely used solvents (arranged in order of ascending boiling point). Water is not one of these, but is included for comparison.

Solvent	D (°C per mole in 100 g solvent)	Boiling point °C
Acetone	17	56
Chloroform	36	61
Carbon tetrachloride	50	77
Ethyl acetate	28	77
Ethanol	12	78
Benzene	25	80
Cyclohexane	28	81
Iso-octane (2,2,4-trimethyl-pentane)	40	99
Water	5.2	100

[1]) A gram-molecule always contains the same number of molecules (6.025×10^{23}, Avogadro's number).

For a substance with a molecular weight of about 250 dissolved in a solvent of $D \approx 25$, at a concentration $c = 0.4$, the boiling-point elevation Δt is found from (1) to be about 0.04 °C. To determine a molecular weight with any precision we therefore need a thermometer capable of measuring extremely small differences of temperature. For the last half century the Beckmann thermometer has been used for this purpose. This is a variable-range mercury thermometer which, with its very large bulb and exceptionally fine bore, has a scale of about 5 cm per degree, graduated to hundredths of a degree. With a magnifying glass a reading can be taken to within 0.002 °C (0.1 mm on the scale). In the above example ($\Delta t \approx 0.04$ °C) it is therefore possible to determine M to within an error of 5%. The uncertainty in the result can be much greater in measurements on substances of high molecular weight, or when it is necessary to use a solvent of lower D (not all substances dissolve in liquids having a high D; in some cases a solution, although otherwise suitable, shows a quite considerable delay in boiling). The accuracy of the temperature measurement achieved with a Beckmann thermometer thus leaves something to be desired. Another drawback is the fairly high thermal inertia of the Beckmann thermometer. Since the boiling point of a liquid depends on atmospheric pressure, this means that measurements cannot be carried out at a time when the barometer reading shows marked fluctuations. At the very small differences of boiling point to be measured here, even slight variations in atmospheric pressure can be troublesome.

This situation made it desirable to look for a more sensitive temperature-measuring instrument of lower thermal inertia. It was found that a resistance thermometer equipped with a resistance element having a negative temperature coefficient (a thermistor) was capable of meeting the requirements. The absolute value of the temperature coefficient of these elements is extremely high, which gives the thermometer the necessary sensitivity. Further, the available resistance values offer a sufficiently wide range, and finally by using a bead-type thermistor the resistance element is extremely small and thus has a low heat capacity, which favours the rapid attainment of thermal equilibrium [2]).

Very small differences in temperature, i.e. differences in the resistance of the thermistor, can be accurately measured by incorporating the thermistor in a Wheatstone bridge circuit. Starting from the balanced state of the bridge (no current through the galvanometer), a relatively small change in one of the resistances gives rise to a current, and hence a galvanometer reading, which for a small out-of-balance is proportional to the change in resistance. The galvanometer reading is thus proportional to the change in temperature [3]).

A schematic representation of an apparatus for determining boiling-point elevations, a so-called ebullioscope, is shown in *fig. 1*. The liquid under test is contained in the boiler A and is heated by an element B. The reflux condenser C minimizes the escape of vapour. The vapour bubbles rising in the liquid above B enter D and cause the liquid, mixed with vapour bubbles, to ascend in three narrow tubes E [4]). The pumped-up liquid finally flows back along the outside wall of the tube F, the return path being lengthened by the glass spiral G in order to promote good heat transfer to F. The sensitive element of the thermometer — the thermistor instead of the mercury reservoir of a Beckmann thermometer — is contained in the tube F, being immersed (to improve thermal contact) in a little silicone oil. The space between the boiler and the jacket H contains the vapour of the pure, boiling solvent. This space acts as a heat insulator. The vapour is produced by boiling in the vessel J a certain quantity of the same solvent as contained in A. The vapour is condensed in a condenser K and the condensate finally returns to J via a trap L. After the measurement the used liquids can be drained through the capillary M and the container N and by removing the stopper O.

The bridge circuit contains a second thermistor identical with the measuring thermistor (approx. 52 kΩ at 25 °C), two fixed resistors of 5100 Ω each, and two variable resistors, one of 1000 Ω and the other of 10 Ω, for balancing the bridge. The inclusion of a second, identical thermistor gives the following advantages. Since thermistors are extremely temperature-sensitive, it would be necessary,

[2]) The required sensitivity can also be obtained with a platinum resistance thermometer. However, a long length of platinum wire is then called for — the temperature coefficient of the resistance of Pt is small — which makes the thermal inertia of the instrument much higher than with a thermistor.

[3]) This proportionality applies only within a very narrow temperature range. If the temperature varies over a wider range, the resistance of a thermistor no longer changes linearly with temperature. Consequently the sensitivity of the resistance thermometer (galvanometer deflection per °C) depends on the temperature at which the measurement is made. Since we always determine M by comparison with a standard substance dissolved in the *same* solvent, this is no drawback whatsoever for the present purposes.

[4]) The principle and operation of a "vapour-bubble pump" were discussed in a recent article in this Review (see Philips tech. Rev. **20**, 177, 1958/59, No. 7).

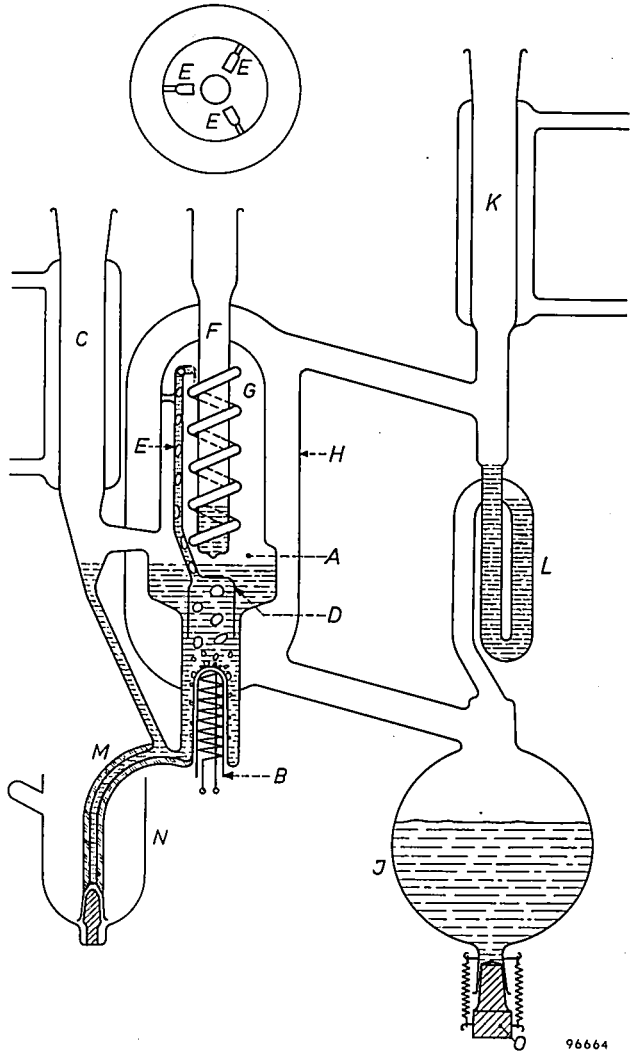

Fig. 1. Schematic representation of an ebullioscope with a vapour jacket as designed by the Central Institute for Physico-Chemical Constants (C.I.P.C.), Utrecht.

if only one were used, to alter the adjustment of the bridge considerably when changing over after a measurement with a solvent boiling at, say, 80 °C to a solvent boiling at 100 °C. By incorporating a second and identical thermistor in the circuit, and by keeping it at the boiling temperature of the pure solvent for each measurement, the circuit is always approximately balanced no matter what solvent is used. It is because of this that the potentiometers for balancing the bridge can have the small values mentioned. In the second place it is possible in this way to keep the set-up very stable in relation to variations in extraneous conditions (atmospheric pressure, room temperature, etc.). The best method of achieving this is to place the second thermistor in a separate but identical ebullioscope, the boiler of which contains the pure solvent.

Fig. 2 shows a diagram of the bridge circuit together with its power supply circuit. The set-up of the two ebullioscopes can be seen in *fig. 3*.

The application here discussed imposes very high demands on the constancy of the thermistors. The bead-thermistor thermometers mentioned (Philips B8.320.05P) have proved to be entirely satisfactory in this respect: the variation in the value of resistance was found to be smaller than 1 in 10^5, whilst the sensitivity of the circuit (galvanometer deflection per °C) seldom differed by more than $\frac{1}{2}$% from the mean value.

Before use the thermistors are artificially aged by keeping them for one day at a temperature of 150 °C; this is 50 °C higher than the highest working temperature.

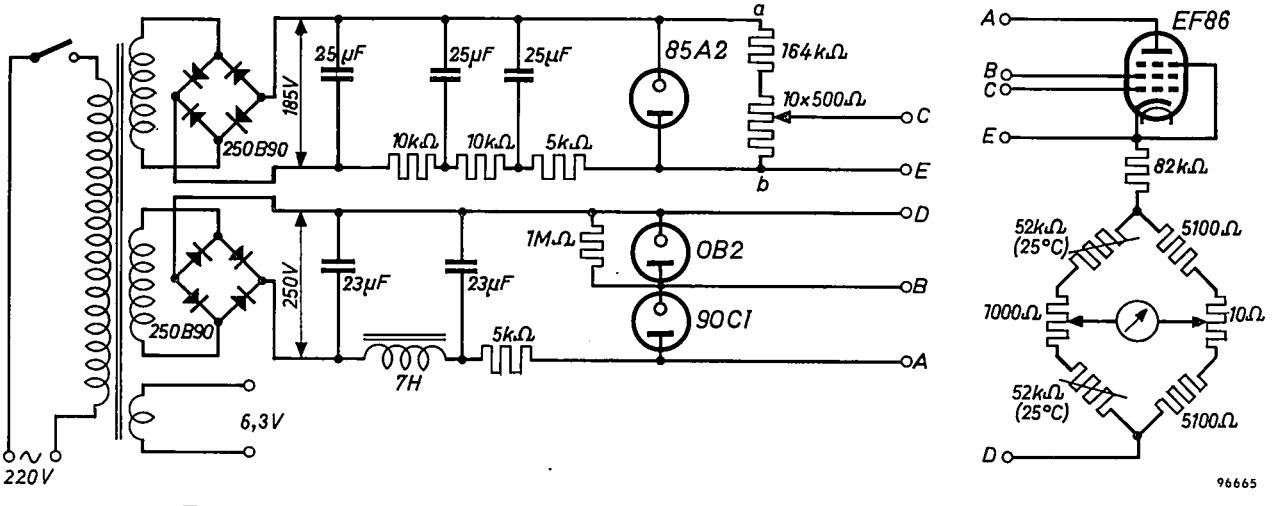

Fig. 2. Circuit of the resistance thermometer. Right, the Wheatstone bridge embodying two thermistors. Left, the power supply circuit providing the required stabilized direct voltages. The two sections are connected at the points marked *A* to *E*. A high degree of stability is provided by feeding the bridge circuit with the anode current of a pentode. This current can be varied by changing the control-grid voltage (*C-E*), which is tapped from the voltage divider *a-b* via a 9-position switch.

The thermistors are not used in the form in which they are sold; the glass tube is first shortened from 12 to 2 cm (*figs. 4* and 5). This is done in order to make it possible to keep the soldered joints between the lead-in wires and the silver wires that form the connections to the rest of the circuit at an equal and constant temperature; this is necessary to prevent the occurrence of a thermo-e.m.f. With the shortened thermistor tube the soldered joints can also be immersed in the silicone oil.

With the apparatus described it is possible to measure temperature differences with an accuracy of about 3×10^{-4} °C. This means that a molecular weight of, say, 2500 can now be determined with an accuracy of a few per cent, and molecular weights smaller than 500 with an accuracy better than 1%. Moreover, for investigations on substances of low molecular weight it is now possible to use solvents having a low molecular boiling-point elevation, and thus to perform measurements on all kinds of sub-

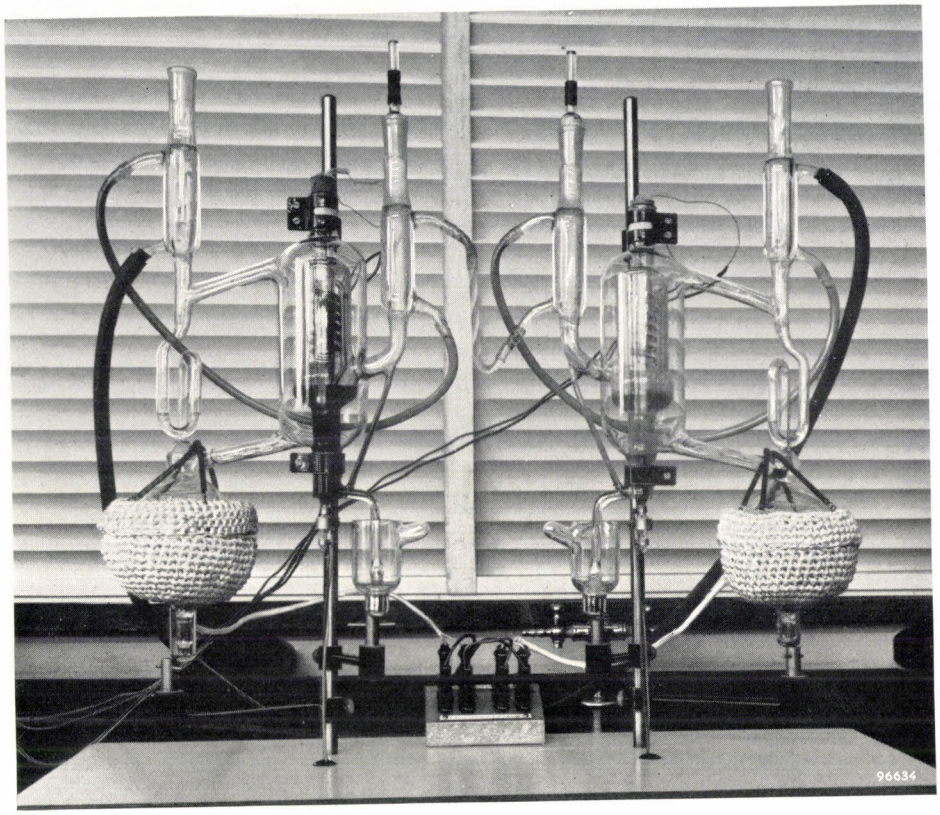

Fig. 3. Ebullioscopic apparatus embodying thermistor thermometers for the measurement of temperature differences.

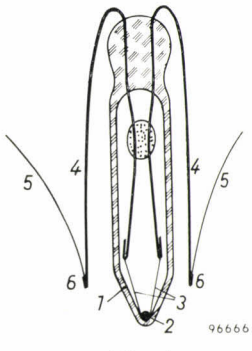

Fig. 4

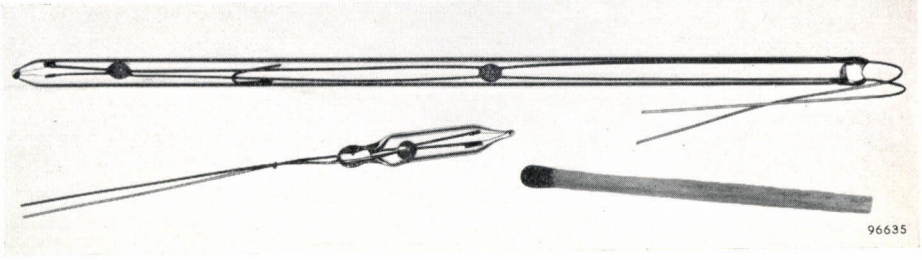

Fig. 5

Fig. 4. Schematic cross-section of the bead thermistor employed (twice actual size). *1* glass tube, *2* thermistor bead, *3* platinum wire connections to bead, *4* lead-in wires, *5* silver wires, *6* soldered joints.

Fig. 5. Thermistor suitable for ebullioscopic molecular-weight determination (below), with a Philips thermistor type B8.320.05P, from which it is made by shortening the glass tube.

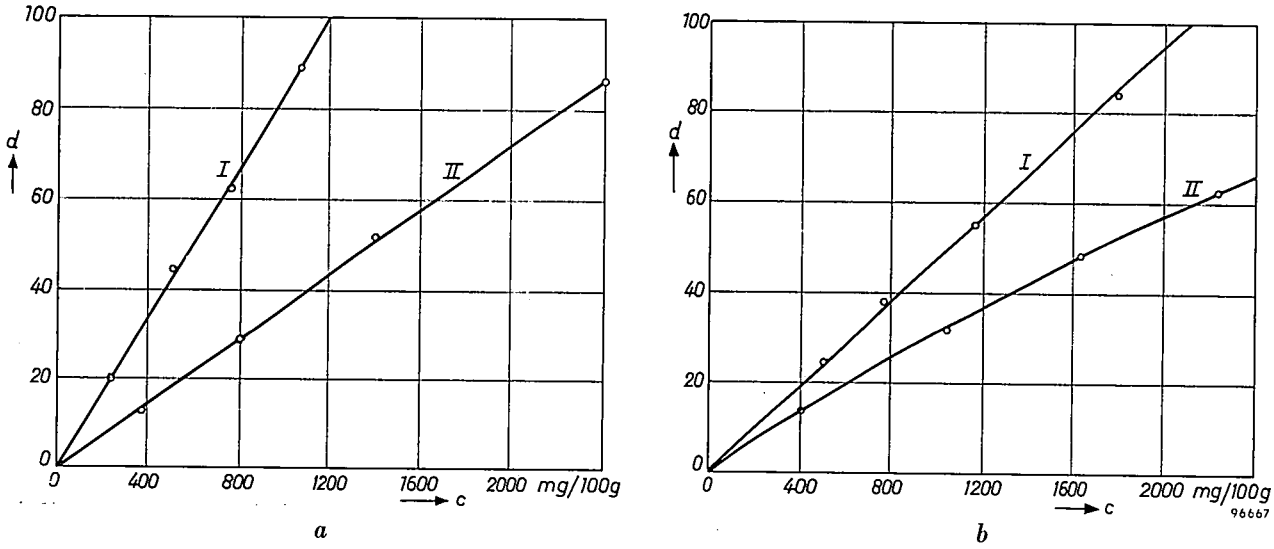

Fig. 6. *a*) The galvanometer deflection d (in arbitrary units) as a function of the concentration c of solutions of α-naphthol (standard substance, $M = 144$, curve I) and 2-diphenylacetyl-1-naphthol ($M = 338$; curve II) in benzene. Both curves are straight lines through the origin, and their slopes are inversely proportional to the molecular weights. *b*) The same for β-ionone (standard substance, $M = 192$) and β-cyclocitrylidene acetic acid ($M = 194$). The curve for the latter substance is not a straight line. A reaction apparently occurs which makes it impossible to determine the molecular weight of this substance with the aid of a solution in benzene.

stances that do not dissolve in the liquids hitherto employed.

Fig. 6 shows the results of some molecular-weight determinations by the method described above. Fig. 6*a* gives an example of linear relations between the galvanometer deflection and the concentration of the solution for the tested and for the standard substance. Fig. 6*b* represents measurements in which the linear relationship was found for the standard substance but not for the other.

J. G. van PELT *).

*) N.V. Philips-Duphar, Weesp (Netherlands).

TRANSISTOR D.C. CONVERTERS FOR FLUORESCENT-LAMP POWER SUPPLIES

by T. HEHENKAMP and J. J. WILTING.

621.314.5:621.314.7:
621.327.534.15

It has been known for some years that transistors can be used to convert direct current into alternating current with a surprisingly high efficiency. This opens up new possibilities with regard to the running of fluorescent lamps from low-voltage D.C. supplies.

Accumulators are the only source of supply available for the lighting of certain kinds of vehicles, including omnibuses and other road transport, many types of trains, and river and canal craft. The power available from accumulators is always on the low side, because the number and size of accumulators carried is determined by considerations of weight and expense. For the lighting of such vehicles it is therefore a prime condition that the installation should work with high efficiency. Now, high efficiency is one of the characteristic properties of low-pressure fluorescent lamps. It is not therefore surprising that increasing use is being made of these lamps in vehicles [1]).

Running fluorescent lamps direct from an accumulator has two disadvantages. One is of a general nature, arising whenever gas-discharge lamps are supplied from batteries. The difference between the supply voltage and the lamp voltage has to be dropped across a ballast resistor involving power losses much higher than those occasioned by the impedance that is used in an A.C. circuit. The lamp voltage is about 0.5 to 0.6 of the supply voltage. Consequently the circuit efficiency (i.e. the ratio between the power consumed by the discharge and the power taken from the battery) is no more than 50 or 60 per cent.

The second disadvantage is that fluorescent lamps are not particularly suitable for running from the 6, 12 or 24 V batteries commonly fitted in vehicles. Ignition of the short "TL" C lamps, for example, which have lengths of 38 cm and 47 cm and which were developed for train lighting [1]), calls for a battery with a rated voltage of 72 V, which is not normally available. For longer lamps, which have the advantage of higher efficiency, an even higher voltage is required.

In the many cases where the available battery voltage is too low for the fluorescent lamps it is desired to instal, some form of converter has to be used. Indeed, a converter is sometimes employed when the battery voltage *is* high enough, with a view to improving efficiency; such a device can be made to supply alternating current, and so permits ballast losses to be cut down. The alternating voltage from the converter can moreover be stepped up to 220 V, and this enables one to make use of the longer "TL" lamps, which have a higher efficiency than short ones.

Of all the various kinds of converter that will serve the purpose, the centrifugal type (mercury jet interrupter [2])) is the most commonly used. It allows the circuit efficiency to be raised to about 70%.

An important feature of devices converting D.C. into A.C. is that they allow a choice of frequency. There are various reasons for making the lamp supply frequency higher than the normal mains frequency of 50 c/s. Firstly, the efficiency of a fluorescent lamp increases with frequency — see *fig. 1*. Secondly, the higher the frequency, the smaller the ballasts can be and the lower are the losses incurred. Thirdly, increasing the frequency reduces the ripple in the luminous flux, making the light

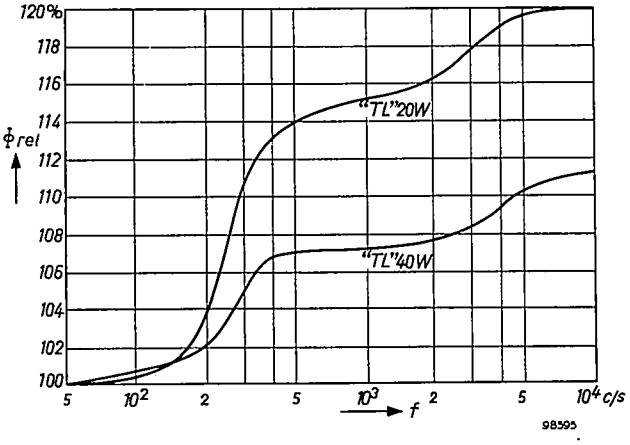

Fig. 1. Relative luminous flux Φ_{rel} from a 20 W and a 40 W "TL" lamp, as a function of the frequency f of the supply current, the power consumed by the discharge being constant. Φ_{rel} is taken to be 100% at $f = 50$ c/s.

[1]) L. P. M. ten Dam and D. Kolkman, Lighting in trains and other transport vehicles with fluorescent lamps, Philips tech. Rev. 18, 11-18, 1956/57.

[2]) See page 13 et seq. in the article cited in footnote [1]).

more restful. This is of importance in vehicles, where lighting has to satisfy more stringent requirements in this respect, owing to jolting and vibration (stroboscopic effects).

For these reasons D.C. converters are always operated at frequencies higher than 50 c/s; centrifugal converters are usually run at 100 c/s, and rotary converters of the conventional type work at 100 c/s or 150 c/s and sometimes at frequencies up to 1000 c/s. We shall presently discuss a type of converter which can be operated at still higher frequencies.

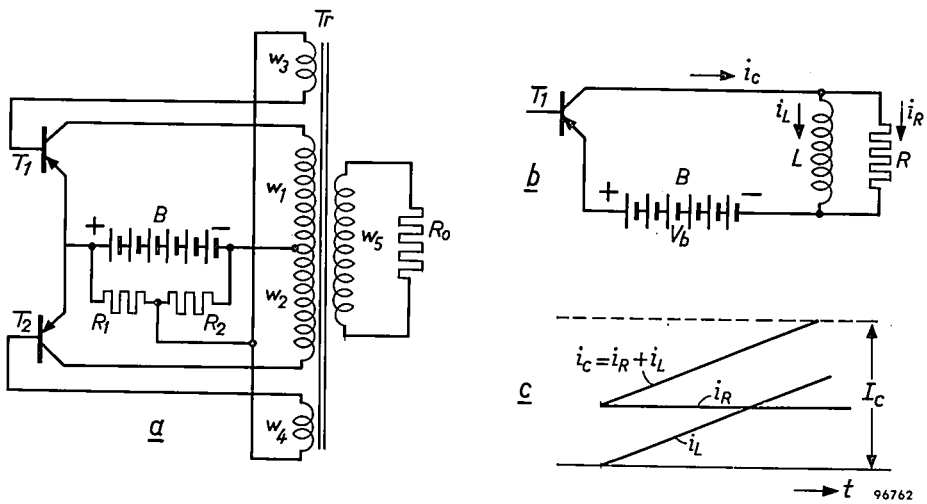

Fig. 2. *a*) Simplified circuit of a transistor D.C. converter, with load resistance R_0. *B*: supply battery. T_1, T_2: *P-N-P* type transistors. *Tr*: transformer with primary windings w_1-w_2, feedback windings w_3-w_4 and secondary winding w_5. Voltage divider R_1-R_2 gives the bases a small negative bias with respect to the emitters.
b) Windings w_1 and w_5 and the load resistance R_0 replaced by a parallel arrangement of an inductance L (the no-load inductance of w_1) and a resistance R (the resistance R_0 transferred to the primary side).
c) The collector current i_C in (*b*) may be divided into two components, a constant current $i_R = V_b/R$ and an increasing current $i_L = V_b t/L$. The current i_C stops increasing when $i_C = i_R + i_L$ has attained the value I_C.

Excellent lighting installations can be based on the principles just described, and this has in fact been widely done. Nevertheless, these installations still leave something to be desired. It would be a good thing if the rotary converters could be replaced with static devices requiring very little maintenance. Higher operating frequencies are also desirable, the main reason being that they would allow ballast size to be reduced. And, of course, a further increase in efficiency would be welcome.

New opportunities of fulfilling these desiderata have arisen in consequence of the development of the transistor and in particular of high-power types. These devices enable direct current to be converted conveniently and efficiently into alternating current at frequencies up to many kilocycles/sec [3]).

Fig. 2a shows one of the simplest arrangements for converting D.C. into A.C. with the aid of transistors, the resistance R_0 representing the load. The two transistors function as switches, not as amplifying devices. Each in turn admits current (which flows from emitter to collector, in the transistor) and the transformer delivers a voltage that is practically square in shape. The transistors can switch relatively high powers and this is due, firstly, to the fact that the voltage drop across a conducting transistor is very small and, secondly, to the fact that the leakage through a cut-off transistor is negligible, even for a high reverse voltage. Only *during* the actual switching process does a fairly heavy current through the transistors coincide with an appreciable potential difference across them, but the switching intervals only represent a small fraction of the period.

The frequency at which the circuit operates is determined by the load, the supply voltage, the transistor characteristics and the no-load inductance of the primary windings (w_1 and w_2 in fig. 2*a*) of the transformer. It has been found quite practicable to generate frequencies of several kilocycles/sec.

[3]) See for example: G. H. Royer, A switching transistor D.C. to A.C. converter having an output frequency proportional to the D.C. input voltage, Trans. Amer. Inst. Electr. Engrs. 74 I (Communication and Electronics), 322-324, 1955, and the chapter by L. H. Light entitled "Transistor D. C. converters" in "The junction transistor and its applications", edited by E. Wolfendale and published by Heywood & Co., London 1958.

A short explanation of the operation of the circuit in fig. 2*a* may be given here.

Consider the situation following an instant at which T_1 has switched into the conducting state and T_2 into the cut-off state. Current from the battery passes via the emitter and collector of T_1 and energizes w_1. The potential difference across w_1 (and w_2) is then not much less than the full battery voltage V_b, and w_3, w_4 and w_5 likewise have constant voltages across them. The windings w_3 and w_4 are so chosen that the former gives the base of T_1 a higher negative potential than that conferred on it by the voltage divider R_1-R_2, whereas w_4 gives the base of T_2 a positive potential. This is in accordance with the conducting state of T_1 and the cut-off state of T_2.

We now imagine windings w_1 and w_5 and resistance R_0 to be replaced by an inductance L (the no-load inductance of w_1) in parallel with a resistance R (being the resistance R_0 transferred to the primary side) — see fig. 2*b*. The voltage across this parallel arrangement is V_b (the drop in T_1 being disregarded). Accordingly, the collector current i_C can be split up into two components, a constant current $i_R = V_b/R$, and a current $i_L = V_b t/L$ which (provided L is constant) grows linearly with time (t). Hence the total collector current is increasing, but it cannot continue to do so indefinitely because it is subject to an upper limit I_C determined by the (constant) voltage between emitter and base. Once i_C has attained the value I_C, it cannot increase any further; nor can its component i_L. Thus di_L/dt becomes zero, which means that all the transformer voltages collapse. The disappearance of the feedback voltage across w_3 causes the base current of T_1 to diminish, i_C falls off too and the result is that the transformer windings now have voltages of the opposite sign induced in them. This cuts off T_1 and causes T_2 to become conducting, and the situation in T_2 and w_2 is the same as that which previously obtained in T_1 and w_1.

In this way the circuit alternates periodically between two states. The transformer output voltage is practically square in shape. If the brief switching interval be disregarded, one half-period is equal to the time required by i_C to grow from the value V_b/R to the value of I_C appropriate to the voltage present on the base (fig. 2*c*). This time will obviously be all the shorter, and the frequency of oscillation all the higher, according as L, R and I_C are smaller and V_b higher.

The load resistance in fig. 2*a* cannot simply be replaced by a fluorescent lamp without further ado, the main reason being the difference between the striking and operating voltages of the lamp. It might seem on the face of it that this difficulty could be avoided merely by having the unloaded transformer deliver a voltage higher than the striking voltage. However, once the lamp has ignited, the transformer has to deliver the much lower operating voltage. As far as the transformer output voltage is concerned, then, the transistors are either overloaded before the lamp strikes or underloaded afterwards. This being so, it will be advisable to take steps to bring the lamp striking and operating voltages as close to each other as possible. The following are well-known measures that can be taken to this end.

1) Heating the electrodes by means of a separate heating current. These currents can be obtained from extra transformer windings (w_6 and w_7 in *fig. 3*).
2) Fitting a conductive strip to the outside of the lamp. A higher voltage is applied to the strip than is available for the lamp itself, and for this purpose the secondary winding of the transformer is extended (w_8, fig. 3).

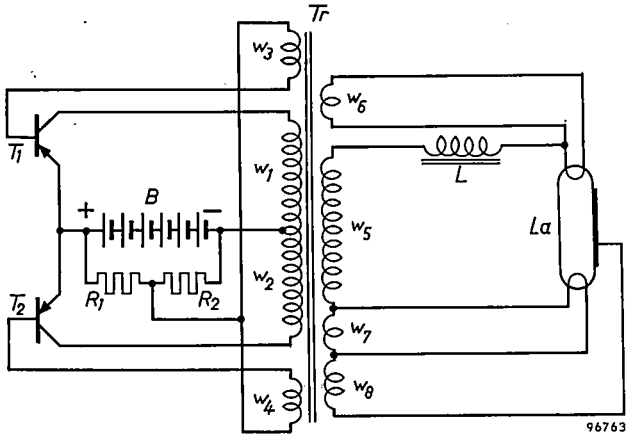

Fig. 3. Simplified circuit of a transistor converter supplying a fluorescent lamp *La*. Transformer *Tr* is somewhat more elaborate than that in fig. 2*a*, having heater windings w_6 and w_7 and a winding w_8 whose purpose is to supply a high potential to the conductive strip on the outside of the lamp. L is a choke in series with the lamp. The other letters have the same meaning as in fig. 2*a*.

In the second place, when the load resistance is replaced by a fluorescent lamp, account has to be taken of the downward sloping current/voltage characteristic of the latter. Once the lamp ignites the instantaneous value of collector current through the transistors rapidly increases, with the result that the converter starts to oscillate at a much higher frequency and becomes unstable. The remedy is to insert a choke (L in fig. 3) in series with the lamp.

The simple circuit shown in fig. 3 allows efficiencies of round about 50% to 55% to be achieved. Everywhere circuits are being developed with a view to getting higher efficiencies. Endeavours are being made to shape the current passing through the transistors during the switching intervals in such a way as to reduce losses in the transistors. *Fig. 4* shows one of the transistor converters developed at Philips. It has an efficiency of over 60%. The high frequency (several kilocycles/sec) at which it operates and the use of ferroxcube have made it possible to keep down the size of the transformer and the choke. The high frequency has the further advantage of raising the lamp efficiency to a figure considerably higher than that obtained at 50 c/s — see fig. 1,

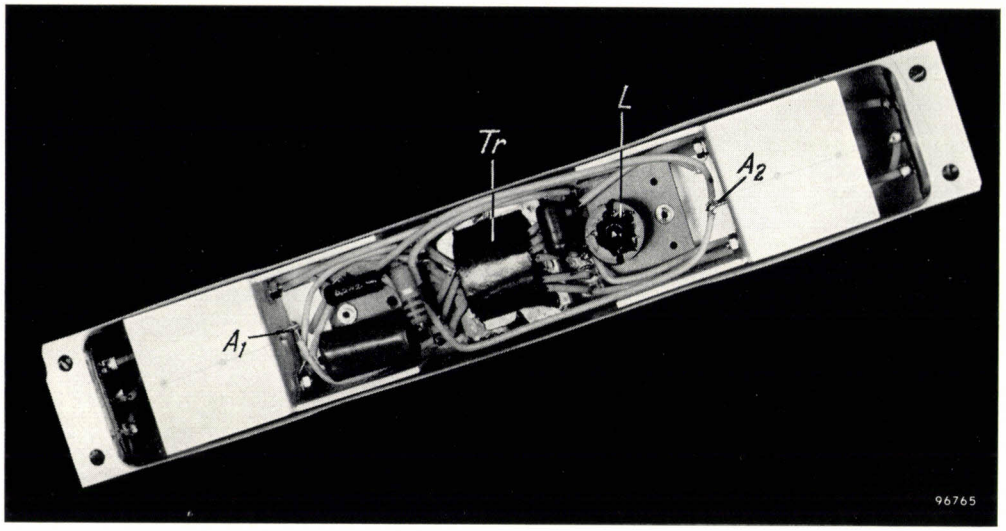

Fig. 4. One of the experimental D.C. converters. All that can be seen of the transistors is their connecting tags (A_1-A_2). Transformer *Tr* and choke *L* have ferroxcube cores.

The term "circuit efficiency" as used in this article requires some explanation.

The power input into the converter is the product of the battery voltage and the mean battery current, and is therefore easy to determine. Part of the output goes to heat the electrodes (and is therefore only indirectly useful) and the remainder is consumed by the discharge. It is clearly desirable to know what proportion of the converter output goes to the discharge, but its measurement is not easy.

A similar difficulty arises in connection with (mains) lamps in starterless circuits. A circuit used with the "TL" M lamp [4]) is given by way of example in *fig. 5*. Not one branch of the circuit carries the same current as that of the discharge, and the straightforward measurement with a wattmeter of the power supplied to the discharge is not therefore possible.

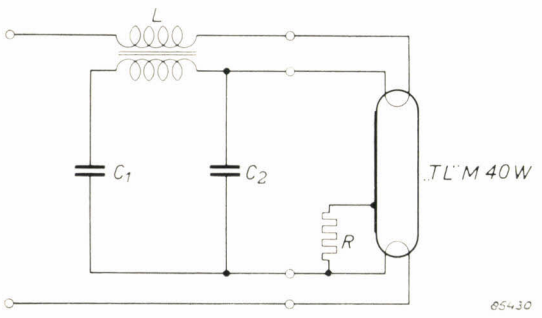

Fig. 5. Starterless circuit of "TL" M lamp — an example of a circuit in which it is difficult to measure the power actually dissipated in the discharge. (For an explanation of the circuit, reference may be made to fig. 4 in the article cited in footnote [4]).)

The following method has gained fairly wide acceptance internationally as a way of getting round the difficulty. The lamp is run from the circuit under investigation (*fig. 6a*) and a photocell connected to a millivoltmeter is set up in its vicinity. Without altering the set-up in any way, the lamp is switched over to the simple circuit shown in fig. 6*b*. The same lamp is now in series with a choke and is being supplied from a variable transformer connected to the mains (but no heating currents are now being supplied, however). The transformer is adjusted to give a current through the lamp such that the millivoltmeter deflection is the same as before. The value indicated by the wattmeter included in the second circuit is considered to be equal to the power *P* consumed by the discharge in the circuit of fig. 6*a*.

Practical considerations persuaded us to make use of this method in our development work on transistor converters for fluorescent lamps. For simplicity we have not incorporated any correction in respect of the difference in lamp efficiency; this is higher when the lamp is run from the converter than when it is supplied from the mains (the correction is dependent on the type of lamp). Hence the efficiency figures already quoted, and those that will be given below, are too high by reason of the fact that this correction has not been made, but they are too low for another reason, namely that the electrode losses are not included in *P*.

Two of the converter types that we have developed are undergoing practical trials in vehicle lighting installations. One of the installations is in a 'bus of a service operating in the vicinity of Eind-

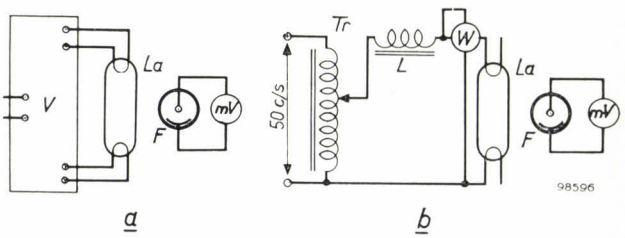

Fig. 6. *a*) *La* is a fluorescent lamp and *V* the ballast (or converter) in a circuit of a kind where direct measurement of *P*, the power dissipated in the discharge, is impracticable. *b*) Here the same lamp *La* is in series with a choke *L*, no heater currents being supplied. The wattmeter in the circuit allows *P* to be determined. It is assumed that the value indicated is valid for circuit (*a*) provided the millivoltmeter connected to photocell *F* gives the same deflection in both cases. The variable transformer *Tr* is adjusted until the photocell voltage in circuit (*b*) is equal to that obtained in circuit (*a*).

[4]) Philips tech. Rev. **17**, 291 et seq., 1955/56.

Fig. 7. Experimental installation in a carriage of the Netherlands Railways. It consists of 20 fluorescent lamps each of 20 W. Each of the lamp fittings contains a transistor converter. The supply voltage is 24 V, the frequency approx. 7 kc/s and the efficiency approx. 62%.

hoven. Five 20 W "TL" lamps of the type with a conductive strip have been installed in the 'bus, each fitting accommodating one lamp and the associated transistor converter. The battery voltage is 12 V, the converter oscillates at a frequency of about 4 kc/s and its efficiency is about 65%. The installation has been in service for over a year, giving full satisfaction.

The second installation is in a railway carriage of the Netherlands Railways (*fig.* 7). Twenty 20 W "TL" lamps, likewise with conductive strips, are mounted in fittings having contact caps of the standard type used in Dutch railway carriages. Each fitting has its transistor converter. In this case the battery voltage is 24 V, the converter works at about 7 kc/s and has an efficiency of about 62%. The installation has been in service for about six months, also without any trouble.

Experience gained from laboratory tests and from these installations shows that the transistor converter represents an excellent solution to the problem of running fluorescent lamps from low-voltage batteries. The life of the lamps has been found to exceed 7000 hours, during which time the characteristics of the transistors do not undergo any perceptible change. The efficiency of the circuit surpasses that of many rotary converters but is somewhat less than that obtainable (70%) from mercury jet converters. However, it is likely that the static converters will soon be freed from this slight drawback. An efficiency of over 80% has been attained with new circuits that are still undergoing development.

Summary. Description of experimental transistor converters which convert D. C. into A. C. with output powers up to about 20 W. The particular application concerned here is to furnish an A.C. supply for fluorescent lamps in circumstances where efficient lighting is desired but where the only source of electricity available is a low-voltage accumulator of limited capacity. The converters operate at frequencies of several kilocycles/sec; the advantages of the high frequency are that the lamp efficiency is raised to a figure about 20% higher than that obtained at 50 c/s, the ripple in the light given becomes so slight as to be imperceptible, and the bulk of the converter and ballast can be kept down. Trial installations in a train and a 'bus, working with efficiencies between 62% and 65%, have given satisfactory results. An efficiency of over 80% has been obtained from more recent circuits.

ABSTRACTS OF RECENT SCIENTIFIC PUBLICATIONS BY THE STAFF OF N.V. PHILIPS' GLOEILAMPENFABRIEKEN

Reprints of these papers not marked with an asterisk * can be obtained free of charge upon application to the Philips Research Laboratories, Eindhoven, Netherlands.

2620: R. Vermeulen: Stereo-reverberation (J. Audio Engng. Soc. **6**, 124-130, 1958, No. 2).

The quality of reproduced music depends not only on the true reproduction of the complete spectrum and the absence of spurious sounds (noise and distortion products), but also on the distribution of the sound over the listening room. Stereophonic reproduction can simulate the directions of the direct sound and thus can imitate, for instance, an orchestra in a satisfactory manner. This is not sufficient, as the room acoustics of the concert hall are essential. The diffuse character of the reverberated sound cannot be reproduced by a single loudspeaker or group of loudspeakers, and only in a limited way by stereophony. It can, however, be reconstructed, even from a single channel, by "ambiophony", i.e. by feeding several loudspeakers distributed over the hall, with different and aleatory delays, repeated many times at decreasing levels. See also Philips tech. Rev. **17**, 258-266, 1955/56; **20**, 309-326, 1958/59 (No. 11), and **21**, No. 2, to appear shortly.

2621: A. A. Kruithof: Die Lichtausbeute von Niederdruck-Leuchtstofflampen (Elektrizitätsverwertung **33**, 23-28, 1958, No. 2). (The luminous efficiency of low-pressure fluorescent lamps; in German.)

Although in an industrial community the absolute value of the energy consumed for lighting is relatively small compared with the energy converted into heat and mechanical energy, it is nevertheless important to increase the efficacy both of existing light sources and (especially) of new light sources. The author considers the mechanism of light production in low-pressure fluorescent lamps and distinguishes between two somewhat opposed criteria as regards the efficacy: these are the attainment of the highest possible luminous efficiency and the attainment of the best colour rendering properties (nearest approximation to daylight or incandescent light, etc.). See also Philips tech. Rev. **18**, 249-260, 1956/57.

2622: A. L. Zijlstra and A. M. Kruithof: L'élasticité différée d'un verre borosilicate et son influence sur la formation de contraintes dans des scellements de ce verre (Verres et Réfractaires **12**, 127-141, 1958, No. 3). (Delayed elasticity in a borosilicate glass and its effect on the formation of stresses in seals of that glass; in French.)

After an introduction to delayed elastic effects such as observed in glass, particularly in the transformation range, the writers describe in detail the delayed elasticity occurring in a borosilicate glass. The maximum deformation due to delayed elasticity can be 70 times that of instantaneous elasticity. The possibility of "freezing-in" an amount of the delayed elastic deformation is examined. This frozen-in delayed elasticity plays an important role in the formation of stresses in glass seals and it gives rise to smaller or larger deviations from the results obtained by the formulae that Hull and Burger have established in respect of stresses in glass-to-metal bead seals. For some bead seals of borosilicate glass, the effect of delayed elasticity on the formation of stresses has been stated. A method is discussed which makes it nevertheless possible to calculate these stresses by giving the formulae of Hull and Burger a more general form; this method takes into account the effect of delayed elasticity.

2623: J. Rodrigues de Miranda: Push-pull amplifiers drive speaker directly (Electronics **31**, No. 29, 76-79, 18 July 1958).

A single-ended push-pull output of a 10-watt amplifier directly feeds the voice coil of a loudspeaker making an output transformer unnecessary. The first pre-amplifying stage has positive feedback to the point of oscillation, while the first amplifier and output stages have negative feedback. The resulting circuit is stable, has low distortion, flat response and only a few degrees phase shift over the audio range. See also Philips tech. Rev. **19**, 41-49, 1957/58 (No. 2).

2624: K. Compaan and Y. Haven: Correlation factors for diffusion in solids, II. Indirect interstitial mechanism (Trans. Faraday Soc. **54**, 1498-1508, 1958, No. 10).

The relation between diffusivity D and conductivity σ of ions (N per cm^3, charge e) in ionic crystals is given by a relation of the type $D = f\sigma kT/Ne^2$, where f accounts for the correlation between the directions of successive steps of an atom. In this

paper the value of f is calculated for the indirect interstitial mechanism of transport in a few types of ionic crystals. The method of calculation is described.

2625: Y. Haven and J. H. van Santen: Dielectric relaxation of lattice defects in crystals (Suppl. to Nuovo Cimento **7** (series X), 605-611, 1958, No. 2).

Relaxation phenomena due to lattice defects in crystals can be discussed with group-theoretical methods, if so-called relaxational modes are introduced. As an example the dielectric relaxation of NaCl containing small amounts of $CaCl_2$ is discussed and compared with mechanical relaxation. See also Philips tech. Rev. **20**, 69-79, 1958/59 (No. 2/3).

2626: H. G. van Bueren, J. Hornstra and P. Penning: Dislocations in germanium and silicon (Suppl. to Nuovo Cimento **7** (series X), 646-660, 1958, No. 2).

This paper describes some recent work in Eindhoven on the subject of dislocations in the diamond structure and on the plastic deformation of its most important representative — germanium. Three topics are discussed: the nature of dislocations in germanium and silicon, the formation of dislocations by thermal stresses, and certain general aspects of the plastic deformation of germanium. See also Philips tech. Rev. **19**, 357-364, 1957/58 (No. 12).

2627: E. G. Dorgelo: Über die Verwendung von Oszillatortrioden in HF-Generatoren mit wechselnder Belastung (Elektron. Rundschau **12**, 241-247, 1958, No. 7). (On the use of oscillator triodes in H.F. generators with varying load resistance; in German.)

This article discusses a problem that arises when the load of an oscillating triode varies. The working line (the locus of all grid voltage - anode voltage combinations occurring in one period) is then displaced with respect to the characteristics, and it is interesting to examine how the H.F. power then changes. From an analysis in which the characteristics are idealized to make them mathematically definable, it is deduced what measures should be taken in the design of a tube to ensure that the delivered power varies as little as possible as a result of load changes. As an example of a "constant power" valve, the triode TB 5/2500 is mentioned. See also Philips tech. Rev. **20**, 299-304, 1958/59 (No. 10).

2628: U. Enz: Relation between disaccommodation and magnetic properties of manganese-ferrous ferrite (Physica **24**, 609-624, 1958, No. 7).

Initial permeability, crystalline anisotropy and magnetostriction have been measured on a single crystal of manganese-ferrous ferrite. The initial permeability shows a high disaccommodation, i.e. a decrease with time. This decrease can be as high as 95% of the value immediately after demagnetization. Disaccommodation is a time-dependent blocking of domain walls, the cause of which is supposed to be a transition of electrons between different ions. The blocked walls cause constricted minor hysteresis loops which indeed have been found. Manganese-ferrous ferrites have in general an extra peak of the permeability as a function of temperature, not hitherto explained. It is shown that this is an effect of disaccommodation.

2629: M. Koedam: Sputtering of a polycrystalline silver surface bombarded with monoenergetic argon ions of low energy (40-240 eV) (Physica **24**, 692-694, 1958, No. 8).

Experimental investigation of the yield of silver atoms sputtered from an electrode bombarded with Ar^+ ions. The sputtering yield is a monotonic function of the ion energy for ion energies of 40-240 eV, showing no threshold value within this range. Extrapolation to 300 eV gives a yield of 2.3 which agrees reasonably well with Keywell's value of 3.0. Similar results have been obtained with Kr^+ ions on Ag.

2630: G. Diemer and A. J. van der Houven van Oordt: Nature of blue edge emission in CdS (Physica **24**, 707-708, 1958, No. 8).

Report of measurements of the intensity dependence of blue emission lines from CdS under excitation from a filtered mercury lamp. For excitation in the region of 4000 Å the fluorescent intensity does not depend significantly on the wavelength. The fluorescent intensity depends on the excitation intensity according to about the 1.5-th power of the latter. From these and previous results the following conclusions can be drawn: 1) Free charge-carrier concentrations must play a role in determining the non-monomolecular recombination law. 2) The green emission can neither be a direct exciton annihilation nor an annihilation of free electron-hole pairs via an exciton state. 3) The blue emission could be due to the recombination of a free electron-hole pair via an exciton state. 4) It is improbable that excitons are generated directly by the exciting quanta (Hg lines in the region of 4000 Å). Free charge-carriers, however, will be formed easily.

2631: W. J. Oosterkamp: Further instrumental developments in cineradiography (Brit. J. Radiol. **31**, 507-510, 1958; No. 369).

Brief description of a cinefluorographic unit based

on the Philips 11″ image intensifier tube (for a full description see Philips tech. Rev. **20**, 331-345, 1958/59, No. 11), and a more detailed discussion of "electronic image harmonization", a method of increasing boundary contrast but reducing the contrast range in copies of radiographic films.

2632: H. C. Hamaker: Statistiek en experiment (Statistica neerl. **12**, 119-130, 1958, No. 3). (Statistics and experimentation; in Dutch.)

After a brief survey of the general importance of the statistical design of experiments, two particular examples are discussed in detail, one dealing with a series of 7 simple experiments on the proper conditions for the production of swaged joints, the other being a $3 \times 3 \times 3$ experiment on emission in radio valves. These examples provide illustrative material for some problems of a general nature, to which little attention is paid in textbooks on the subject. One of the secrets of successful experimentation lies in making a proper choice of those factors which should go into an experiment. A series of simple two — or three — factor experiments is often better than one complex design. Analysis of variance is not always needed; frequently too, textbook methods of analysis do not apply and the experimenter should be trained in recognizing such situations. The paper ends with some general conclusions concerning the present and future status of statistics as an integral part of experimental science.

2633: M. J. Sparnaay: Measurements of attractive forces between flat plates (Physica **24**, 751-764, 1958, No. 9).

Results of experiments concerning attractive forces between flat metal plates, and a description of the apparatus used, are given. The observed attractions do not contradict Casimir's theoretical prediction. An explanation of results of earlier measurements made by the author on the attraction between clean, and also between silvered glass and quartz plates, all done in an ionized atmosphere, is suggested. These results were due to differences in the surface potentials of the opposing plates.

2634: J. C. van Vessem: The transistor, seen from within (T. Ned. Radiogenootschap **23**, 177-194, 1958, No. 4).

After the first few hectic years of transistor development, the alloy technique has found the most widespread use in transistor production. The natural limits of this "classical" process are discussed in relation to audio, R.F. and power application. The author describes the later improvements upon this technique resulting from the introduction of other methods, and devotes special attention to transistors for higher frequencies and high power. A review is also given of the relationship between physical design parameters and electrical parameters.

2635: J. H. Stuy: The nucleic acids of Bacillus cereus (J. Bacteriol. **76**, 179-184, 1958, No. 2).

The ribonucleic acid and deoxyribonucleic acid contents of four strains of Bacillus cereus and of various stages in the life cycle of B. cereus strain p2 have been determined chromatographically. The base composition of both nucleic acids was the same for all cells investigated. The results were in agreement with those obtained by means of the orcinol and diphenylamine reactions. During spore germination there was no formation of the nucleic acids. Synthesis of these acids, and of other cell materials as well, began upon incubation of the germinated spores in a growth medium.

2636: H. F. L. Schöler and J. H. Gaarenstroom: The effect of BZ 55 on the pancreatic islets (Acta endocrinol. **29**, 147-159, 1958, No. 1).

In normal subjects and in experimental animals BZ 55 lowers the blood sugar level (Achelis et al., 1955, and many others) and is therefore used for this purpose in diabetes. There is no agreement as to the mechanism of action of BZ 55. In the hope of throwing more light on this mechanism, the effect of prolonged treatment with BZ 55 on the blood sugar level and the histology of the pancreas was investigated. For comparison other substances were used which are known 1) to damage the β-cells of the islets of Langerhans, 2) to inactivate the β-cells and 3) to stimulate the β-cells.

2637: H. Bremmer: Applications of operational calculus to ground-wave propagation, particularly for long waves (I.R.E. Trans. **AP-6**, 267-272, 1958, No. 3).

All results of conventional approximative diffraction theory dealing with the propagation of radio waves around a smooth spherical earth (surrounded by a homogeneous atmosphere) can be derived from a one-dimensional integral equation originally discussed by Hufford. This equation can be solved with the aid of operational calculus which leads, first of all, to the well-known residue series. In this treatment the Sommerfeld theory for a flat earth appears at once as a limiting case; moreover, analytic expressions for correction terms accounting for the finite value of the earth's radius are easily determined. Finally, the equation in question can also be used for the extension to inhomogeneous soil conditions, without neglecting the earth's curvature.

SUBJECT INDEX, VOLUMES 11-20

Figures in bold type indicate the volume number, and those in ordinary type the page number. For subjects dealt with in volumes **6-10** the reader should refer to the index published in volume **15** (1953/54), and for subjects in volumes **1-5** to the index in volume **10** (1948/49).

Acaricides **16**,353 **17**,146 **19**,165

Accelerators for elementary particles:
- betatrons **11**, 65
- Cosmotron (ferroxcube core) **15**, 73
- neutron generator **17**,109
- see further:
  - **Cascade generators**
  - **Cyclotron**
  - **Linear electron accelerators**

Acoustics, ambiophony (stereo-reverberation) **17**,258 **20**,309
Aerials, see **Radio receivers**
Aging of iron and steel, see **Steel**

Agrobiological research:
- laboratory for — **16**,353
- control of animal pests . . . **17**,146
- fungicides **17**,222
- growth substances in plants **17**,294
- pesticides, formulation of . **19**,165

Aircraft and lightning **16**,296
Air engine, see **Hot-gas engine**

Airfield beaconing:
- design and light sources . . **16**,273
- supply units **17**, 10

Air fractionating column **20**,177
Air liquefier, see **Gas refrigerating machine**
Alkali halides, lattice imperfections studied on **20**, 69
Alloys, see **Metals**
Ambiophony (stereo-reverberation) **17**,258 **20**,309
Amplificon **19**, 1

Amplifiers:
- repeaters for carrier telephony **14**,147 **16**,287
- pre-amplifier for pick-up (AG 9005) **18**,238
- single-ended push-pull output — **19**, 41
- wide-band — for 4000 Mc/s (with EC 57) **19**,145
- see also:
  - **Cathode-ray oscillographs**
  - **Noise**
  - **Oscillators**
  - **Radio receivers**
  - **Television receivers**
  - **Voltmeters, electronic**

Analogue equipments:
- electrolytic tank for study of thermal-conductivity problems **18**, 52
- see further **Control of industrial processes** and **Rubber membrane analogue**

Analysis:
- gas — with omegatron . . . **19**,218
- lead in air **11**,215
- mercury in air **11**, 91
- polarograph, direct-reading . **14**,257
- **spectrochemical —:**
  - with a Geiger counter (lead estimation) . . . **11**,215
  - optical **12**,337
  - with X-rays **17**,269

Antennae, see **Radio receivers, aerials**
Arc welding, see **Welding**
Auditorium acoustics **17**,258 **20**,309
Automatic control, see **Control of industrial processes**
Automatic potentiometer (PR 1000, PR 2000) **15**,189
Automobile headlamps, see **Car headlamps**

Bacteria, inactivation by UV . . **12**,111

Ballasts for gas-discharge lamps:
- life of transformers and chokes **20**, 59
- life of capacitors **20**,162
- noise emission of — **18**,110
- small — (in polyester resin) **18**,279

Barium getter films **19**,290
Barium titanate, see **Titanates**
Batteries, emergency supply systems with **11**,253

Beacons:
- light —, see **Airfield beaconing**
- radio —, magnetron for . . **14**, 87

Beam transmitters:
- with double FM **17**,317
- frequency stabilization for — **17**,334
- multiplex-pulse modulation . **11**,133
- **transmitting valves for —:**
  - disc-seal triodes . . . **18**,317 **20**,225
  - multi-reflex klystron . . **17**,328
- wide-band amplifier using EC 57 triode **19**,145

Beamed light sources, automatic plotting of isocandela diagrams **20**,288
Bend tests, machine for **17**,246
Beta radiation, measurement of weak **20**,170
Betatrons **11**, 65
Binaural hearing, see **Stereophony**
Braking device for X-ray apparatus **11**, 50
"Brightness engineering" **12**,200

Brussels Exhibition (Expo) 1958:
- Philips pavilion **20**, 2 **20**, 9 **20**, 17 **20**, 27
- "Electronic Poem" **20**, 37

Cadmium-sulphide photo-resistors **20**,277
Camera tubes for TV, see **Television camera tubes**

Capacitors:
- extruded — **13**,145
- life in ballasts **20**,162
- materials with high ε . . . **17**,129
- precision variable — **20**,234

Car headlamps:
- comparison of American and European systems **12**,305
- with an asymmetric dipped beam **16**,351

Carrier telephony:
- **over coaxial cables:**
  - general problems . . . **14**,141
  - through-supergroup filter **13**,223
- feedback amplifiers **16**,287
- see also **Beam transmitters**

Cascade generators:
- h.f. filament supply for — . **11**,123
- for TV receivers (50 kV) . . **14**, 21
- for fast neutrons (1 MV) . . **17**,109

Casting:
- vacuum — **15**,114
- modern techniques (lost-wax method) **15**,133

Cathodes, see:
- **Dispenser cathodes**
- **Oxide cathode**
- Thoriated-tungsten cathodes

Cathode-ray oscillographs:
- small type (GM 5655) . . . **11**,111
- stroboscopic — for h.f. . . **12**, 52 **12**, 73
- pre-amplifier for — (GM 4574) **15**,169

Cathode-ray tubes:
- efficiency of fluorescence . . **15**, 63
- for flying-spot scanning (MC 13-16) **15**,233
- low-voltage — **19**,159
- rectangular — of high aspect ratio **18**,298
- secondary emission from the screen **16**, 26
- sedimentation of screens . . **16**,232
- see also **Television picture-tubes** and **Television receivers**

Ceramic materials, see:
- **Ferroxcube**
- **Ferroxdure**
- **Ferroxplana**
- **Titanates**

Characteristic plotter for receiver valves **12**,283
Cheater circuits for testing of thyratrons **16**, 43
Chladni's figures on vibrating capacitor **19**, 84
Chokes, life in ballasts **20**, 59
Chromaticity diagram **12**,137

Cinefluorography:
- with 5 inch (12.5 cm) tube . . **17**, 89
- with 11 inch (28 cm) tube . . **20**,331

Cinema projection, see **Film projection**
Cleating, improved method . . . **19**,268
Clinical thermometer **17**,255

Cold-cathode tubes:
for telephony (types Z 500 T, Z 501 T) 15,265
theory; — for stabilization (Z 800 U) and for pulse-rate measurements (Z 801 U) . 18,128
Colour rendering of "TL" lamps 18,249
Colour triangle 12,137
"Compactix" X-ray equipment . 11,193

Complex voltage ratios:
measurement up to 100 Mc/s 14,102
cathode-ray display 18,380

Computer:
count-rate — 17,249
random-access magnetic-core memories for electronic — 20,193
Condensers, see **Capacitors**
Contact arc welding, automatic . 13,247
Contact microradiography . . 17, 45; 19,221
Contact therapy 13, 75
Contrasts, perception of 11,333

Control of industrial processes:
general considerations . . . 12,221
electro-analogue for studying regulating systems . 12,257; 12,319
electronic controls 17, 21
automatic potentiometer . . 15,189
Controlled valency 13, 90
Converters, see **D.C.-A.C. converters**
Copper, etching of 15,238
Cosmotron, ferroxcube core . . . 15, 73

Counters:
with cold-cathode tubes . . 15,269
with decade scaler tubes (E 1 T) 14,313; 16,360
with Geiger-Müller tube (battery-operated) 14,369
monitor for radioactive contamination 16,201
scintillation —, q.v.
see also **Counter tubes**

Counter tubes:
decade scaler tube (E 1 T) . 14,313
Geiger-Müller —:
application in optical-spectrochem. analysis 11,215
with halogen filling . . 13,282
ring of — for thyroid examination 18, 87
for X-ray analysis . . . 18,262
guard counter for weak beta radiation 20,170
scintillation counters, q.v.
X-ray intensity measurement with —:
count-rate computer . . 17,249
design and properties of counter tubes 18,262
diffractometer 16,123
methods 17,206
proportional counter tube for X-rays . . 11,354; 18,264
X-ray spectrochemical analysis 17,269
see also **Counters**
Crackle-free potentiometer . . . 20,283

Crystals:
piezo-electricity in — . . . 11,151
topotactical growth 20,354
see further:
Lattice defects
Quartz
X-ray diffraction analysis

Cyclotron:
theory of synchro— 12, 65
synchro— at Amsterdam:
general construction . . 12,241
oscillator and modulator 12,247
electromagnet 12,349
further constructional details 14,263
vibrating capacitor for CERN synchro— 19, 84

Damping, internal, in iron and steel 13,172
Darkroom lighting 11, 53
Daylight, effect on Poinsettia and Populus of hours of 14,175
Dazzle of lighting fittings 12,200

D.C.-A.C. converters:
centrifugal (mercury jet) — 18, 13
transistor — 20,362
vibrator — 16,118
Deaf-mute children, musical instrument for 18,276
Decade scaler tube, see **Counters**
Deformation of metals 15,246; 15,286; 16,341
De-ionization of gas-filled valves 12,178
Delta modulation 13,237
Diagnostics, see **X-ray diagnostics**

Diamond:
— dies 16, 91
styli for gramophone pick-ups 19,324
Dichroic mirrors 19, 59

Dielectric constant:
of ferrites 13,192; 15, 79
materials with high — . . . 17,129
measurement at 3000 Mc/s . 13, 61

Dielectric losses:
in glass 13,360
power-factor measurement at 3000 Mc/s 13, 61
Directional hearing, see **Stereophony**
Directional isolator 18,158
Discharge tubes, see **Cold-cathode tubes** and **Thyratrons**
Disc-seal triodes, see **Electron tubes**

Dislocations:
properties 15,246
role of — in plastic deformation 15,286
generation of — by thermal stresses 19,357

Dispenser cathodes:
L-cathode:
fundamentals and construction 11,341
under pulsed operation . 13,337
applications:
disc-seal triodes . . 18,317; 20,225
image iconoscope . 13,119
magnetrons . . . 14, 56
fabrication and properties . 19,177
pressed cathode 19,179
impregnated cathode . . . 19,186
machining of tungsten for impregnated cathodes . . 17, 97
Displacement pick-up 17, 63

Dosimetry:
pocket dosemeter for X-radiation and gamma radiation 16,134
of very weak X-radiation . . 19,264
Drawn products, composite . . . 13,145

Electric fencing 13,328
Electro-analogue equipment . 12,257; 12,319
Electroluminescence 19, 1
Electrolytic tank for study of thermal-conductivity problems 18, 52
Electron emission, secondary, see **Secondary emission**
Electron gun for picture-tubes . 18, 73
Electron lenses, measurement of field in magnetic 15, 52

Electron microscope:
for 100 kV 12, 33
of simplified construction (EM 75 kV) 17, 47
emission —:
demonstration austenite pearlite transformation 16,337
construction 18, 1
— photographs:
asbestos 14, 79
bacteria 12,318; 14, 20
ferroxdure 18,237
magnesium oxide . . . 12, 45
"Ticonal" G 19, 11
viruses 13, 45; 14, 16; 14, 18; 14, 19
zinc oxide 11,361
plant diseases, investigation with — 14, 13
ultramicrotome for — specimens 17,178

Electron trajectories:
in space-charge field 14,336
in X-ray tubes 20,291

Electron tubes:
general survey 14,117
automatic plotting of characteristics 12,283
for decimetre waves (triodes EC 80 and EC 81) 11, 79
disc-seal triodes for centimetre waves:
EC 57 18,317
EC 59 20,225
see also **Amplifiers**
noise in —, see **Noise**
professional — 18,181
with ribbon-shaped electron beam 13, 82; 14,313
sub-miniature valves:
construction 18,217
tungsten wire for — . . 18,222
applications 15, 46; 15,170; 15,283
switching tubes 13, 49; 13, 82
X-radiography of — 12,207
see further:
Cathode-ray tubes
Cold-cathode tubes
Counter tubes
Television camera tubes
Television picture-tubes
Thyratrons
Transmitting valves

Electronic control of industrial processes 17, 21
Electronic games 17,362
Electronic music, see **Music**
"Electronic Poem" (Brussels Expo 1958) 20, 37
Electronic potentiometer 15,189
Electrophoresis 12,293
Electroscope 16,134

Entropy:
concept of — 16,258
examples and applications 16,298, 16,321
— and information 18,201
Etching of copper 15,238
Expo, see **Brussels Exhibition (Expo) 1958**
"Expressor" system for the transmission of music 11,281
Extrusion products, composite . 13,145
Eye, photography of the 15,342

Faraday effect:
application in unidirectional waveguides 18,158
observation of Weiss domains by means of — 19,286
Feedback amplifier for carrier telephony 14,147, 16,287
Fencing, electric 13,328

Ferrites:
dimensional effect in — . . 13,192, 15, 79
ferromagnetic resonance, see Gyromagnetic resonance
ferroxcube, q.v.
ferroxdure, q.v.
ferroxplana, q.v.
with rectangular hysteresis loop:
theory and properties . 16, 49
switching time 18,336
application for magnetic core memories 20,193
Ferroceptor 16,186
Ferro-electricity, see **Titanates**
Ferromagnetic resonance, see Gyromagnetic resonance

Ferroxcube:
magnetic and electric properties 13,181
measurement of properties . 14,245
applications:
general review; loading coils, band filters . . . 13,301
amplitude modulation of centimetre waves . . . 18, 82
core for Cosmotron . . 15, 73
inductive aerial 16,186
magnetic-core memories 20,193
piezomagnetic vibrators 18,285
pulse transformer . . . 19, 28
in unidirectional waveguides 18,158
see also **Ferrites**

Ferroxdure:
development and properties . 13,194
crystal-oriented — (ferroxdure II and III) 16,141
comparison with other materials 18,358
electron-microscope photograph 18,237
topotaxy with — 20,354
Weiss domains, observation 19,286
applications:
focusing of TV picture-tubes 15,214
magnetodynamic gramophone pick-up . . . 18,101
pulse transformer . . . 19, 28

Ferroxplana:
development and properties 18,145
crystal-oriented — 19,209
topotactically oriented — . 20,354

Filament lamps:
additives in tungsten for filaments 19,109
car headlamps 12,305, 16,351
mirror-condenser lamp for 8 mm projectors 19,233

Film projection:
professional 16 mm projector 16,158
projector for 70 mm and 35 mm films ("Todd-A.O.") 17,299
mirror-condenser lamp for 8 mm — 19,233

Filters, electric:
with ferroxcube cores . . . 13,301
through-supergroup filter . 13,223

Flash-bulbs (type "Photoflux"):
ignition with capacitor . . . 16,333
improved types 12,185
specific light output (PF 3) 15,317
with simplified cap 16, 88

Flash-tubes, electronic:
design and properties . . . 16, 13
for ophthalmic photography 15,342
Flicker of TV pictures 13, 55
Flower bulbs (virus diseases) . . 14, 13
Fluctuations, see **Noise**

Fluorescence:
afterglow:
in image converter (ME 1201) 14,213
in flying-spot scanner (MC 13-16) 15,221
in line converter 15,297
efficiency of — in cathode-ray tubes 15, 63
electroluminescence 19, 1
halophosphates for "TL" lamps 13,346
influence of temperature . . 12, 6
saturation of — in TV picture-tubes 12,120
zinc-sulphide phosphors, controlled valency 13, 90
applications:
high-pressure mercury lamp with fluorescent bulb (HPL) 13,109
painting with fluorescent paints 11, 16

Fluorescent lamps:
ballasts, q.v.
colour rendering of — ("TL" de Luxe) 18,249
control of luminous intensity 12, 83
with directional light distribution ("TL" F) 17,198
double-flux "TL" lamp . . . 19,333
equivalent circuit 15,161
radio interference from — . 20,135
in series with filament lamp ("TL" S) 12,129
in a starterless circuit ("TL" M) 17,288, 18, 17
in vehicles:
"TL" C 18, 11
supply with centrifugal converter 18, 13
supply with transistor converter 20,362
see also **Lighting**
Flying-spot scanner, see **Television, flying-spot scanner**
Flywheel synchronization in TV receivers 13,312
Focusing of picture-tubes (ferroxdure) 15,214
Focusing of X-ray tubes 20,291
Foucault pendulum for United Nations 19,236
"Frena" and "Frenac" 19, 73
Frequency-drift meter 12,193
Frequency modulation, see **Beam transmitters** and **Radio receivers**
Frequency stabilization (IGO) . 14,130
Friction, internal, in iron and steel 13,172
Fungicides 16,353, 17,222, 19,165

Gamma radiation:
pocket dosemeter 16,134
monitor for nuclear reactor . 19,278
reduction of — background . 20,170
scintillation counter . . . 20,209, 20,263
Gas binders, see **Getters**

Gas-discharge lamps:
ballasts for —, q.v.
equivalent circuit 15,161
see further:
Flash-tubes, electronic
Fluorescent lamps
Mercury-vapour lamps
Gas-discharge tubes, see **Cold-cathode tubes** and **Thyratrons**

Gas refrigerating machine:
fundamentals 16, 69
construction 16,105
use with air fractionating column 20,177
Geiger-Müller tubes, see **Counter tubes**

Germanium:
— diodes:
theory and construction 16,213
application of point-contact Ge diodes . . 16,225
dislocations in — 19,357
— transistors, see **Transistors**

Getters:
barium films 19,290
zirconium — in transmitting valves 14,226

Glass:
structure 13,293
dielectric losses 13,360
stress investigation 14,290
"iron" —, for sealing to steel 14,281
sealing of window and cone of picture-tubes 19,318
Glazes, gloss point 17,153

Gramophones:
new developments (microgroove) 13,134
fabrication of records . . . 17,101

sapphire and diamond styli for pick-ups 19,324
high notes, reproduction . . 18, 89
magnetodynamic pick-up . . 18,101, 18,173
Greenhouse with artificial light . 12, 1
Grid emission of various materials 19,123, 20,269
Group-delay measurement in networks 15,307
Growth substances in plants . . 17,294
Guard counter 20,170

Gyrator:
a new network element . . 18,120
realization for microwaves . 18,158, 11,313
Gyromagnetic resonance (ferromagnetic resonance) . . . 18, 82, 18,158, 19,304

Hall effect, measurement 20,220

Harbour radar:
IJmuiden 14, 95
Rotterdam 20,349
Hardening of metals (oxidation hardening) 14,203

Hearing-aids:
using sub-miniature valves . 15, 37
using transistors 17,315, 19,130
Heat conduction, study with electrolytic tank 18, 52
Herbicides 16,353, 17,294, 19,165

High-frequency heating:
inductive —, method and applications 11,165
capacitive —, method and applications 11,232
inductive —, with hydrogen thyratrons 20,101
transmitting valves for — . 20,299
High-tension generators, see **Cascade generators**

Hot-gas engine:
measurement of temperature fluctuations 13,104
new construction with rhombic drive mechanism . . . 20,245
Hypar (hyperbolic paraboloid) shells, see **Brussels Exhibition (Expo) 1958**, Philips pavilion

Hysteresis loop:
automatic recording 16, 79
ferrites with rectangular —, see **Ferrites**

IGO frequency stabilization . . 14,130
Illumination, see **Lighting**
Image converter for ultra-rapid photography (ME 1201) . . . 14,213
Image iconoscope 13,119, 14,327, 17,189

Image intensifier:
X-ray —, see **X-ray image intensifier**
based on electroluminescence (amplificon) 19, 1
Impact strength of iron and steel 11,303
Impedance measurements using transmission line 16,309

Impurities in metals:
effects of — 16,341
in iron and steel, see **Steel**
in tungsten 19,109
Incandescent lamps, see **Filament lamps**
Indentation meter for paints . . 13,352
Influenza vaccine, manufacture . 12,273
Information theory and entropy 18,201
Insecticides 16,353, 17,146, 19,165
Intensification of X-ray images, see **X-ray image intensifier**
Interference of light in thin films 19, 59
Internal friction in iron and steel 13,172
Investment casting 15,133

Ion burn:
in image iconoscope . . . 14,327
in TV picture-tubes . . . 14,364, 15,258, 16, 27
Ion-trap magnet 15,258

Ionization manometer:
simple — 17,121
used as a pump 20,145
Ionospheric sounder 13,152
Iron, see **Steel**
Iron-detector 15, 97
Isocandela diagrams, automatic plotting 20,288
Isolators, directional 18,158
Isotopes, see **Radio-isotopes**

Junction transistors, see **Transistors**

Klystrons:
for 100-1000 W continuous output 13,209
multi-reflex — 17,328
reflex — for 4 mm waves . . 18, 51
low-noise high-power — . . 18,361

Laboratory, see **Research at Philips**
Lacquers, indentation meter . . 13,352
Lamps, see:
Airfield beaconing
Filament lamps
Flash-bulbs
Flash-tubes, electronic
Fluorescent lamps
Lighting
Mercury-vapour lamps

Lamp fittings:
permissible brightness . . . 12,200
measurement of light distribution 14,200
Lapping (grinding) of quartz oscillator crystals 12,166
Lathe headstock, high-precision 19, 68

Lattice defects:
general review 15,105
— and plastic deformation of metals 15,246, 15,286
interaction with foreign atoms 16,341
in alkali halides 20, 69
generation of dislocations . 19,357
L-cathode, see **Dispenser cathodes**

Lead estimation in air 11,215
Leak-tracing with Penning gauge 11,116
Levitation by magnetic fields . . 18,125
Light, units 17, 77
Light amplifier (amplificon) . . 19, 1
Light sources, see Lamps

Lighting:
comfortable — 14, 69
fittings, brightness of . . . 12,200
isocandela diagrams, automatic plotting 20,288
light distribution, general measuring apparatus . . . 14,200
linear light sources, distribution of illumination on a plane 12, 60
of Dutch National War Memorial, Amsterdam . . 18,300
open-air laboratory for road lighting 19,202
in vehicles 18, 11, 20,358
Lightning and aircraft 16,296
Line converter 15,297
Line spectra, light sources for . . 11,299

Linear electron accelerators:
fundamentals 14, 1
for 15 MeV (Harwell) . . 14,235, 15, 1
neutron spectrometer, use with — 15,325
application for X-ray therapy 17, 31
Linear light sources, distribution of illumination on a plane . . . 12, 60
Loading coils with ferroxcube cores 13,306

Losses:
dielectric — in glass 13,360
power-factor measurement at 3000 Mc/s 13, 61
— in ferroxcube 13,181, 13,301, 14,245
Lost-wax casting 15,133

Loudspeakers:
high-resistance — 19, 42
— installation for high-fidelity reproduction 18,304
public-address — 20,309
twin-cone — 16,241
Luminescence, see **Fluorescence** and **Fluorescent lamps**

Magic-eye indicator tube (E 82 M) 18,243
Magnadur, see **Ferroxdure**

Magnets, permanent:
comparison of various materials 18,358
for TV-tube focusing . . . 15,214
ion-trap magnet 15,258
Magnetic-core memories 20,193
Magnetic fields, measurement of 15, 49
Magnetic levitation 18,125

Magnetic materials:
automatic recording of hysteresis loops 16, 79
comparison of — 18,358
see further:
Ferrites
Ferroxcube
Ferroxdure
Ferroxplana
"Ticonal"

Magnetic recording:
description of equipment . . 14,181
recording and reproducing process 15, 84
for programme control . . . 20, 45
Magnetodynamic pick-up . . 18,101 18,173
Magnetostrictive vibrators, see **Piezomagnetic vibrators**

Magnetrons:
theory and construction . . 14, 44
for beacons ($\lambda = 3$ cm) . . 14, 87
Mains-voltage stabilizers . . . 17, 1
Manometer, Penning 11,116

Mechanical stresses:
in glass 14,290
measurement with the aid of strain gauges. 11, 23

Mechanical tests:
bend test apparatus 17,246
indentation meter for paints 13,352
roughness meter 14, 80
Memories, magnetic-core 20,193
Mercury estimation in air . . . 11, 91

Mercury-vapour lamps:
high-pressure —:
review of development . 18,167
with fluorescent bulb (HPL) 13,109
application of HPK lamp for floodlighting . . . 18,300
low-pressure fluorescent —, see **Fluorescent lamps**
for photo-copying processes 13,323

Metals:
aging phenomena 13,165 14, 60
casting in vacuo 15,114
etching of copper 15,238
hardening 14,203
impurities, influence of . . 16,341
iron and steel, see **Steel**
oxidation hardening 14,208
oxidation resistance 12,213
plastic deformation and lattice defects 15,246 15,286
precision casting (e.g. special alloys) 15,133
pure —, preparation 11,241
steel, q.v.
tungsten, q.v.
Metal-detectors 15, 97

Meteorology:
radio sonde 16,148
radar sonde 19,258
Microphones, placing of . . . 17,262 20,324
Microradiography 17, 45 19,221
Microtome, ultra- 17,178
Millivoltmeters, electronic, see **Voltmeters, electronic**
Mirrors, dichroic 19, 59
Mirror cameras, see **Schmidt optical system**
Mirror-condenser lamp for 8 mm projectors 19,233
Mobile transmitters, valves for . 12,157
Models, radio-controlled 15,281

Modulation:
amplitude — of centimetre waves by means of ferroxcube 18, 82
in carrier telephony 14,141
delta — 13,237
"Frena" and "Frenac" . . . 19, 73
frequency —, see **Beam transmitters and Radio receivers**
multiplex-pulse — 11,133
Molecular-weight determination . 20,357
Monitoring, see **Radiation monitoring**
Monochromatic light sources . . 11,299
"Müller" UGX unit 17,138
Multiplex-pulse modulation . . . 11,133
Multiplier tubes, see **Photomultipliers**
Multi-reflex klystron 17,328

Music:
ambiophony (stereo-reverberation) 17,258 20,309
calibration of tuning forks . 12,228
electronic —:
Philips pavilion Brussels (Varèse) 20, 43
technical aids; composition (Badings) 19,191
various instruments . . 17,363
instrument for deaf-mute children 18,276
long-playing records 13,134
reverberation, stereo- (ambiophony) 17,258 20,309
transmission by "Expressor" system 11,281
see further **Stereophony**

Negative feedback in telephone cable repeaters 14,147 16,287

Networks:
filters, q.v.
measurement of group delay in — 15,307
unit function response of — 12,233
Neutron flux, measuring methods 19,249 19,273
Neutron generator 17,109
Neutron time-of-flight spectrometer. 15,325
Nitrogen, liquid, production from air 20,177

Noise:
general survey 20, 50
in diodes at very high freq. 14,153
in triodes at very high freq. 14,236
— diode for ultra-high freq. 20,108
— figure indicator 18,141
— measurement on klystron 18,362
receiver with very low — level (radio-astronomy) . . 17,351
of a scintillation counter . 20,216 20,263
speech transmission at high — levels ("Frena", "Frenac") 19, 73
in X-ray image intensifier 14, 39 17, 72
NTC resistors, see **Thermistor applications**
Nuclear reactions for production of radio-isotopes 16, 1
Nuclear reactor (swimming-pool type), monitoring equipment 19,245 19,273
Nuclear resonance method for measuring magnetic fields . . . 15, 55
Nuclides, radioactive, see **Radio-isotopes**

Omegatron 19,218
Ophthalmic photography . . . 15,342

Oscillators:
with constant output voltage 14,304
frequency drift of —, measurement 12,193
LC —, mechanism of synchronization 14,292
pulse-synchronized — (IGO) 14,130
quartz oscillator crystals, q.v.
RC —, 20-250 000 c/s (GM 2317) 15,240
TV signal generator (GM 2887) 15,205
travelling-wave — 11,221
Oscillographs, see **Cathode-ray oscillographs**
Oscilloscope tubes, see **Cathode-ray tubes**
Oxidation, acceleration in presence of foreign oxides (e.g. MoO_3) 12,213
Oxidation hardening of metals . 14,203

Oxide cathode:
theory of conduction 11,271
pulsed operation 13,337

Paints, indentation meter for . . 13,352
Painting with fluorescent paints 11, 16
Paramagnetic resonance 19,301
Pavilion of Philips at Brussels Expo, see **Brussels Exhibition (Expo) 1958**
Peltier effect in resistance welding 20,188
Pendulum, Foucault 19,236
Penning vacuum gauge 11,116

Perception:
of contrasts 11,333
luminous frame around TV screen 19,156
of small object detail in X-ray diagnostics 17, 71
Permanent magnets, see **Magnets, permanent** and **Magnetic materials**
Pest control / Pesticides — see **Agrobiological research**
Phase difference, measurement up to 100 Mc/s 14,102
Phase response, measurement of group delay 15,307
"Philishave" 12, 27
Phosphors, see **Fluorescence**
Photoconductive TV camera tube 16, 23
Photo-copying processes, mercury lamps for 13,323

Photo-electric cells:
CdS photo-resistors 20,277
photo-transistor:
pyrometer 20, 89
relay 19,280
see also **Photomultipliers**
"Photoflux" lamp, see **Flash-bulbs**
Photographic reproduction, mercury lamps for 13,323

Photography:
darkroom lighting 11, 53
flash-bulbs, q.v.
flash-tubes, q.v.
ophthalmic 15,342
positioning of light sources . 12,145
ultra rapid — (10^{-7} sec) with image converter . . . 14,213
Photometry at low luminances . 15,182

Photomultipliers:
for flying-spot scanner . . . 15,221
for scintillation counting . 16,250, 20,209, 20,263
stroboscopic operation of — 19, 50
Photo-printing and copying, mercury lamps for 13,323
Photo-resistors, CdS 20,277
Photosynthesis 14,298
Phytopharmaceutical research, see **Agrobiological research**
Pick-up, displacement 17, 63
Pick-up, magnetodynamic . . 18,101, 18,173
Pick-up, vibration 17, 61
Pick-up tubes for TV, see **Television camera tubes**
Picture-tubes, see **Television picture-tubes**

Piezo-electricity:
materials exhibiting — . . 11,145
detection of — 11,151

Piezomagnetic vibrators:
ferroxcube for — 18,285
application 18,325, 18,368

Plants, effects of light:
general survey 11, 43
experimental greenhouse . . 12, 1
hours of daylight 14,175

Plant diseases:
investigation with electron microscope 14, 13
see also **Agrobiological research**
Plastic deformation of metals . 15,246, 15,286

Plastics:
in the radio and electrical industries 11, 33
polyvinyl chloride for wire insulation 12, 97
Polarograph, direct-reading . . . 14,257
Polyvinyl chloride ("Podur") for wire insulation 12, 97

Potentiometers:
automatic (PR 1000, PR 2000) 15,189
crackle-free 20,283
Precision casting 15,133
Precision lathe headstock . . . 19, 68
Precision variable capacitors . . 20,234
Preservation charge 11,253
Printed wiring in radio sets . . . 20,113
Process control, see **Control of industrial processes**
Projection of films, see **Film projection**
Projection television, see **Television projection, large screen**
Proportional counter, see **Counter tubes**
Proton resonance, measurement of magnetic fields with 15, 55
Pulse modulation, multiplex- . . 11,133

Pulse transformer:
for control of fluorescent lamps 12, 90
for radar transmitter 19, 28
Pyrometer using photo-transistor 20, 89

Quartz:
piezo-electric property . . . 11,145
— **oscillator crystals:**
cutting 11,323
control of cutting angles by X-ray diffraction . 11,351
lapping and frequency adjustment 12,166

Radar:
pulse transformer for radar transmitter 19, 28
— sonde 19,258
— station at IJmuiden . . . 14, 95
— system for Rotterdam . . 20,349

Radiation monitoring:
with battery-operated Geiger-Müller counter 14,369
with pocket dosemeter . . . 16,134
of hands, feet and clothing . 16,201
in nuclear reactor 19,245, 19,273
see also **Counter tubes**

Radio-astronomy:
radiation from interstellar hydrogen (21 cm) 17,305
design of receiver for hydrogen radiation 17,351
Radio-controlled models 15,281
Radio interference from fluorescent lamps 20,135

Radio-isotopes:
measurement of weak beta activity 20,170
production methods 16, 1
monitor for radioactive contamination 16,201
radioactive iodine in thyroid gland 18, 87
— as X-ray sources 18,229

Radio propagation:
influence of ionosphere on — 13,152
— through the troposphere 15,148, 15,175

Radio receivers:
aerials:
FM 17,348
inductive 16,181
reflection and impedance measurements using a long transmission line . 16,309
detector tube for FM (EQ 80) 11, 1
FM section of — 17,342
printed wiring 20,113
ratio detector for FM . . . 17,345
transistor — powered by a thermopile 18,155
see also:
Electron tubes
Loudspeakers
Noise
Oscillators
Radio sonde 16,148
Radio valves, see **Electron tubes**
RC oscillator for 20-250 000 c/s (GM 2317) 15,240
Receiver valves, see **Electron tubes**

Rectifiers:
de-ionization time of gas-filled tubes 12,178
germanium diodes 16,213, 16,225
see further:
Cascade generators
Thyratrons
Voltage stabilization
Reflection measurements using transmission line 16,309
Reflex klystrons, see **Klystrons**
Refrigerating machine, see **Gas refrigerating machine**
Relay tubes, see **Cold-cathode tubes and Thyratrons**
Remote control of models . . . 15,281
Repeaters for carrier telephony 14,147, 16,287

Research at Philips:
history, 1891-1951 . . . . . 13, 3
40th anniversary Research Laboratory 17,362
Research, science and industry . 20, 85
Resins, see **Plastics**
Resistance welding, influence of Peltier effect in 20,188
Resistivity of semiconductors, measurement 20,220
Road lighting, open-air laboratory for 19,202
"Rotalix" X-ray tube O-55 . . . 13, 71
Roughness meter 14, 80

Rubber membrane analogue:
for waveguides 11,156
for electron trajectories in space-charge fields 14,336

Sampling:
lot inspection by — 11,176
— inspection plans 11,260
practical application, methods 11,362
Sapphire styli for gramophone pick-ups 19,324
Scalers, see **Counters and Counter tubes**
"Scenioscope", TV camera tube 17,189

Schmidt optical system:
for projection TV 15, 27, 19,338
for lung examination with X-ray fluorography 13,269
for general X-ray diagnostics 16, 58
for X-ray cinefluorography . 20,331
Science and industry 20, 85

Scintillation counter:
fundamentals 20,209
signal-to-noise ratio and dead time 20,263
X-ray intensity measurement 18,266

Secondary emission:
from fluorescent screens . . 16, 26
in TV camera tubes . . . 13,119, 17,189
application in switching tubes 13, 49, 13, 82

Semiconductors:
controlled valency 13, 90
photoconductive camera tube 16, 23
electroluminescence 19, 1
measurement of resistivity and Hall coefficient 20,220
CdS photo-resistors 20,277
see also:
Germanium
Thermistors
Transistors

Series connection of lamps (airfield beaconing) 17, 10
Shaving, investigation of electrical 12, 25
Short waves, see Ultra-high frequencies

Signal generators:
RC —, 20-250 000 c/s (GM 2317) 15,240
TV — (GM 2887) 15,205
Signalling in electronic telephone exchange 15,265
Single-ended push-pull circuit . . 19, 41
Solderability of wire 20,158
Sonde, radar 19,258
Sonde, radio 16,148

Sound:
modern acoustical techniques 20,309
ambiophony (stereo-reverberation) 17,258; 20,309
see further:
Gramophones
Hearing aids
Loudspeakers
Magnetic recording
Music
Stereophony
Spectrochemical analysis, see **Analysis**
Spectroscopy, time-resolved . . 19, 50
Springs, instability of 11,245
Stabilization of frequency in beam transmitter 17,334
Stabilization of voltage, see **Voltage stabilization**
Stars, variable, TV technique for discovery of 19,140

Steel:
hardening 14,206
influence of impurities on impact strength 11,303
influence of impurities on internal friction 13,172
quench aging 13,165
strain aging 14, 60
Step-function response of networks 12,233

Stereophony:
cinema interval music . . . 11,129
comparison between reproduced and "live" music . . 17,171
application in theatres . . . 20,309
Stereo-reverberation (ambiophony) 17,258; 20,309
Strain gauges 11, 23
Stresses in glass 14,290
Structure investigations, see **X-ray diffraction**
Stud welding 17, 37
Sub-miniature valves, see **Electron tubes**
"Symmetrix" X-ray diagnostic table 17,112
Synchrocyclotron, see **Cyclotron**

Synchronization:
of *LC* oscillators 14,292
pulse — (IGO) 14,130
of TV receivers 13,312

Tap, high-vacuum 17,184
Tape recorders, see **Magnetic recording**
"Tedion" V 18 . . . . . 17,152; 19,165

Telephony:
beam transmitters, q.v.
carrier —, q.v.
delta modulation 13,237
electronic exchange 15,265
emergency supply systems with batteries 11,253
at high noise levels ("Frena", "Frenac") 19, 73
loading coils with ferroxcube core 13,306
mobile installations 12,157
private branch exchange UB 49 . . . . . 18, 19
uniselector U 45a 18, 19; 18,349

Television camera tubes:
image iconoscope 13,119; 14,327
image iconoscope with glass target ("Scenioscope") . . 17,189
photoconductive — 16, 23

Television, colour:
fundamentals 19, 86
dichroic mirrors 19, 59
projection (e.g. on 2.25 × 3 m) 19,338
for medical teaching 20,327

Television, flying-spot scanner:
design, circuits 15,221
cathode-ray tube (MC 13-16) for — 15,233
for 35 mm film 18,193
application for the discovery of variable stars 19,140

Television picture-tubes:
saturation of fluorescence . 12,120
secondary emission from the screen 16, 26
sedimentation of screens . . 16,232
steel-cone — 14,281
sealing of window and cone 19,318
bent-neck — 14,361
focusing with ferroxdure . . 15,214
ion-trap magnet 15,258
pentode gun 18, 73
for projection (MW 13-16) . 15, 28
photographs of implosion . 18,260

Television projection, large screen:
general description 15, 27
high-tension generators . . 14, 21
for medical teaching 11, 42; 20,327
see also **Television, colour**

Television receivers:
flicker in — 13, 55
flywheel synchronization . . 13,312
for four standards 17,161
group-delay measurement . 15,307
luminous frame around the screen 19,156
phase linearity of — 18, 33
signal generator (GM 2887) 15,205
visual acuity 16,172
dosimetry of weak X-radiation in — 19,264

Television standards:
considerations on the different — 16,195
line converter 15,297

Television transmitters:
100 kW output stage . . . 14,345
West-European network . . 14,358

Temperature measurement:
clinical thermometer 17,255
fluctuating gas temperatures 13,104
with autom. potentiometer . 15,189
of solutions, to determine molecular weights 20,353
Tetrodes for mobile transmitters 12,157
Thermal conductivity, electrolytic tank for study of 18, 52

Thermistor applications:
clinical thermometer 17,255
determination of molecular weights 20,357
in transistor circuits 18,240; 20,132
voltage stabilizer 17, 1
Thermopile-powered transistor radio receiver 18,155
Thoriated-tungsten cathodes in transmitting valves 14,226; 19,118; 20,301
Through-supergroup filter . . . 13,223

Thyratrons:
for control of light flux from fluorescent lamps 12, 83
de-ionization time, measurement 12,178
hydrogen — for induction heating 20,101
PL 10 13,331
testing by measurement of grid current 16, 43
life testing (MT 5544 and MT 5545) 16, 98
Thyroid gland, measurement of radioactive iodine in 18, 87

"Ticonal":
ion-trap magnet 15,258
electron-microscope photographs of — G 19, 11
comparison of magnetic materials (e.g. — XX) 18,358
Time-of-flight spectrometer . . . 15,325

Titanates:
piezo-electric behaviour . . 11,145
ferro-electricity 11,183
application in capacitors . . 17,129
"TL" lamps, see **Fluorescent lamps**
"Todd-A.O." film projector . . . 17,299
Tone generator, *RC* (GM 2317) 15,240
Topotaxy 20,354
Tracers, see **Radio-isotopes**
Transducers 15,189; 17, 61; 17, 63
Transformers, life in ballasts . . 20, 59

Transistors:
simple theory 17,233
at high current densities . . 18, 61
testing apparatus 13,254
as network element at low frequencies 19, 15; 19, 98; 20,122
applications:
D.C.-A.C. converter for "TL" lamp supply . . 20,362
hearing aid 17,315; 19,130
light-relay 19,280
pre-amplifier for magnetodynamic pick-up . 18,238
pyrometer using phototransistor 20, 89
radio receiver powered by thermopile 18,155

Transmission time in networks, measurement 15,307

Transmitters:
- mobile — 12,157
- TV —, 100 kW output stage 14,345
- West-European TV network 14,358
- see further **Beam transmitters** and **Modulation**

Transmitting valves:
- with a thoriated-tungsten cathode (types TBL 12/100 and TBW 12/100) 14,226
- for h.f. heating and generation of ultrasonic energy . 20,299
- grid emission of various materials 19,123; 20,269
- **for ultra-high frequencies:**
  - for mobile equipment (types QQE 06/40 and QQC 04/15) 12,157
  - triode up to 900 Mc/s (type TBL 2/300) . . 19,118
- see further:
  - **Electron tubes**
  - **Klystrons**
  - **Magnetrons**

Travelling-wave oscillator . . . 11,221
Triodes, see **Electron tubes** and **Transmitting valves**
Triode oscillator, see **Oscillators**
Troposphere, radio propagation through 15,148; 15,175
Tubes, see **Electron tubes**
Tuberculosis detection, see **X-ray fluorography**
Tulips, broken (virus-diseased) . 14, 13

Tungsten:
- machining technique 17, 97
- — wire for small radio valves 18,222
- function of additives in — . 19,109

Tuning forks, calibration 12,228
Tuning indicator tube (E 82 M) 18,243
Turbines, continuous monitoring of 17, 59

Ultra-high frequencies, see:
- **Beam transmitters**
- **Electron tubes**
- **Noise**
- **Radio receivers**
- **Transmitting valves**
- **Velocity-modulation tubes**

Ultramicrotome 17,178

Ultrasonics:
- ferroxcube for piezomagnetic vibrators 18,285
- machining with — (50 W and 2 kW drills) 18,325; 18,368
- transmitting valves for — . 20,299

Ultra-violet irradiation for sterilization of bacteria 12,111
Unilines 18,158
Uniselector for telephone exchanges (U 45a) 18,349
Unit function response in network testing 12,233

Vacuum technique:
- Penning vacuum gauge . . . 11,116
- melting of metals in vacuo 11,241; 15,114
- tap with short outgassing time 17,184
- ionization gauge 17,121; 20,153
- ultra-high vacua 20,145

Valency, controlled 13, 90
Valves, see **Electron tubes**
Valve voltmeter, see **Voltmeters, electronic**
Variable capacitors, precision . . 20,234

Velocity-modulation tubes:
- travelling-wave tube (helix resonator) 11,221
- see further **Klystrons**

Vibrations, mechanical, investigation with strain gauges 11, 23
Vibration pick-up, electrodynamic (PR 9260) 17, 61
Vibrator, D.C.-A.C. converter . . 16,118

Viruses:
- investigation with electron microscope 14, 13
- manufacture of influenza vaccine 12,273
- influenza —, photograph . . 13, 45

Visibility, see **Perception**
Visual acuity in connection with TV 16,172
Voltage ratios, see **Complex voltage ratios**

Voltage stabilization:
- battery preservation rectifier with electronic — 11,253
- for emission electron microscope (45 kV) 18, 1
- mains — 17, 1
- 5 kV stabilized rectifier . . . 14,190

Voltmeters, electronic:
- for 1-30 000 kc/s (GM 6006) 11,206
- D.C. — (GM 6010) 16,117
- calibration of — 14,308
- pre-amplifier (GM 4574) . . 15,169

Waveguides:
- rubber-membrane model . . 11,156
- measurement of standing-wave ratio in — 12, 15
- corrugated — for linear accelerators 14, 1; 15, 1
- unidirectional — 18,158

Weed control, see **Herbicides**
Weiss domains, observation of . 19,286

Welding:
- contact arc —, automatic . 13,247
- droplet size measurement, cinematographic 15,122
- enclosed — 20, 94
- low-hydrogen welding rods . 14, 96
- Peltier effect in resistance — 20,188
- porosity, general causes . . 11,101
- protection against dangerous voltages 15,199
- stud — 17, 37

Wire:
- "Podur" insulation 12, 97
- solderability of — 20,158
- surface cracks, detection . . 11, 12
- thin tungsten — 18,222

Wire capacitors 13,145
Wolfram, see **Tungsten**

X-ray diagnostics:
- testing with phantoms . . . 11,291
- "Symmetrix" table 17,112
- "Müller" UGX unit 17,138
- with image intensifier . . . 17, 88
- see also **X-ray fluorography**

X-ray diffraction:
- orientation of quartz oscillator crystals 11,351
- collimator for X-ray beams 13, 96
- counter-tube diffractometer 16,123
- see further **Counter tubes, X-ray intensity measurement with**

X-ray fluorography:
- mirror camera for mass chest survey 13,269
- mirror cameras for general diagnostics 16, 58
- braking device for mass chest survey equipment 11, 50

X-ray image intensifier:
- design of 5 inch (12.5 cm) tube 14, 33; 17, 69
- industrial radiology with — 17, 93
- medical aspects 17, 88
- optical aids for — 17, 77
- perception of object detail . 17, 71
- periscope optical system, — fitted with 17, 84
- cinefluorography with 5″ (12.5 cm) tube 17, 89
- cinefluorography with 11″ (28 cm) tube 20,331

X-ray therapy:
- "Compactix" equipment (for 200 kV_{max}) 11,193
- contact — 13, 75
- midget (KT) apparatus . . 14,165
- with moving tube (TU 1) . . 16, 33
- linear electron accelerators for — 17, 31

X-ray tubes:
- "Rotalix" O-55 for A.C. . . 13, 71
- contact-therapy tube . . . 13, 75
- endotherapy tube 13, 77
- diffraction tube for 10 kW . 19,314
- distant-focus — 20,291
- investigation of heat conduction in anode 18, 52
- for microradiography . . 17, 45; 19,224
- midget (KT) tube 14,165

X-rays, miscellaneous:
- cinefluorography, see **X-ray image intensifier**
- collimator for X-ray beams . 13, 96
- dosimetry of very weak radiation 19,264
- examination of electron tubes 12,207
- fluorescence analysis 17,269
- intensity measurement with counter tubes, see **Counter tubes, X-ray intensity measurement with**
- microradiography 17, 45; 19,221
- pocket dosemeter 16,134
- radioactive nuclides as X-ray sources 18,229
- spectrochemical analysis . . 17,269

Zirconium as getter in transmitting valves 14,226

AUTHOR INDEX, VOLUMES 11-20

Figures in bold type indicate the volume number, and those in ordinary type the page number. Articles marked with an asterisk * are short communications. It should be noted that ij occurring in Dutch names has in the alphabetical order been identified with y. For articles published in volumes **6-10** the reader should refer to the index published in volume **15** (1953/54), and for articles in volumes **1-5** to the index in volume **10** (1948/49).

Addink, C. C. J.
Precise calibration of tuning forks **12**,228
* An electrical clinical thermometer **17**,255
Addink, N. W. H. and W. de Groot
Spectrochemical analysis **12**,337
Alma, G., G. Diemer and H. Groendijk
A rubber membrane model for tracing electron paths in space-charge fields **14**,336
Almer, F. H. R. and P. G. van Zanten
* An experimental pyrometer using a phototransistor and designed for radio-tube inspection **20**, 89
Alons, L.
New developments in the gramophone world . . . **13**,134
Alphen, P. M. van
The application of the X-ray image intensifier, III. Optical aids for the image intensifier **17**, 77
Applications of the interference of light in thin films **19**, 59
— and M. Bierman
* A mirror-condenser lamp for 8 mm projectors . . . **19**,233
Arbelet, G., H. J. Lindenhovius and J. C. van der Breggen
A millivoltmeter for the frequency range from 1000 to 30×10^6 c/s **11**,206
Arfin, B. and G. A. Espersen
A 3 cm magnetron for beacons **14**, 87
Aschen, R. and P. Gaillard
A simple ionosphere sounder **13**,152
Aten, A. H. W. and J. Halberstadt
The production of radio-isotopes **16**, 1
Baas, G.
* Demonstration of the austenite-pearlite transformation by means of the emission electron microscope **16**,337
— and G. W. Rathenau
An emission electron microscope for research at high temperatures **18**, 1
Badings, H. and J. W. de Bruyn
Electronic music **19**,191
Bähler, W.
* Automatic recording of luminous intensity diagrams **20**,288
Balder, J. J.
* A luminous frame around the television screen . . . **19**,156
— and M. H. A. van de Weijer
The "TL" F lamp, a tubular fluorescent lamp with a directional light distribution **17**,198
Balder, T. C.
* Influence of the Peltier effect in resistance welding . **20**,188
Bandringa, M. and A. Venema
The production and measurement of ultra-high vacua **20**,145
Bareford, C. F. and M. G. Kelliher
The 15 MeV linear electron accelerator for Harwell **15**, 1
A. Choice of parameters and general design . . . **15**, 2
B. Detailed description of main components and circuits **15**, 10
C. Testing and performance **15**, 22
Barneveld, E. J. van
Fast counter circuits with decade scaler tubes . . . **16**,360
Basel, C. von, H. J. Lindenhovius and G. W. van Santen
Electronic equipment for the continuous monitoring of turbines **17**, 59
Bayfield, W. A., A. Nemet and R. B. Stephens
A radioactive-contamination monitor for the hands, feet and clothing **16**,201
Beek, R. van and W. W. Boelens
Printed wiring in radio sets **20**,113
Beekman, W. J. H., A. Verhoeff and H. W. van der Voorn
* An X-ray diffraction tube with rotating anode for 10 kW continuous loading **19**,314
Beljers, H. G.
Three methods of measuring magnetic fields, III. Measurement by the proton resonance method **15**, 55
Amplitude modulation of centimetre waves by means of ferroxcube **18**, 82
The application of ferroxcube in unidirectional waveguides and its bearing on the principle of reciprocity **18**,158
— and J. L. Snoek
Gyromagnetic phenomena occurring with ferrites . **11**,313
Bergen, J. A. van, W. P. van den Blink and H. Bienfait
Automatic welding with contact electrodes **13**,247
Berkhout, H. L.
A television receiver suitable for four standards . . **17**,161
Beun, M., J. P. Beijersbergen and J. te Winkel
The junction transistor as a network element at low frequencies,
I. Characteristics and h parameters **19**, 15
II. Equivalent circuits and dependence of the h parameters on operating point **19**, 98
III. Stabilization of the operating point, in particular with regard to temperature changes **20**,122
Beijersbergen, J. P., M. Beun and J. te Winkel
The junction transistor as a network element at low frequencies,
I. Characteristics and h parameters **19**, 15
II. Equivalent circuits and dependence of the h parameters on operating point **19**, 98
III. Stabilization of the operating point, in particular with regard to temperature changes **20**,122
Bienfait, H., W. P. van den Blink and J. A. van Bergen
Automatic welding with contact electrodes **13**,247
Bierman, A. and H. A. Oele
Betatrons with and without iron yoke **11**, 65
Bierman, M. and P. M. van Alphen
* A mirror-condenser lamp for 8 mm projectors . . . **19**,233
Biermasz, A. L. and H. Hoekstra
The measurement of changes in length with the aid of strain gauges **11**, 23
— and A. J. Michels
An electronic D.C. millivoltmeter **16**,117
Blackler, F. G.
* Rectangular cathode-ray tubes of high aspect ratio **18**,298
Blasberg, E. and A. de Groot
Metal-detectors **15**, 97
Bleeksma, G. J. and J. J. Schurink
A loudspeaker installation for high-fidelity reproduction in the home **18**.304
Blink, W. P. van den, H. Bienfait and J. A. van Bergen
Automatic welding with contact electrodes **13**,247
—, E. H. Ettema and P. C. van der Willigen
Stud welding with welding cartridges **17**, 37
Bloemen, J. P. de Visser van, see **Visser van Bloemen, J. P. de**
Blok, H. and J. J. Rietveld
Inductive aerials in modern broadcast receivers,
I. Brief history and general description **16**,181
II. Technical aspects of inductive aerials **16**,188
Blom, P.
An electronic hearing-aid **15**, 37
* A transistor hearing-aid **17**,315
— and P. Boxman
A transistor hearing-aid **19**,130
Boelens, W. W.
An instrument for recording the frequency drift of an oscillator **12**,193
— and R. van Beek
Printed wiring in radio sets **20**,113
Boer, F. de and H. Emmens
Sedimentation of fluorescent screens in cathode-ray tubes **16**,232
— and W. F. Nienhuis
Low-voltage oscilloscope tubes **19**,159
Boer, H. J. de and A. van Weel
An instrument for measuring group delay **15**,307

Boer, J. B. de
Light-beacons to aid landing aircraft 16,273
* The "Duplo" car headlamp bulb with an asymmetric dipped beam 16,351
— and M. Rutgers van der Loeff
* Floodlighting of the Dutch National War Memorial in Amsterdam 18,300
— and D. Vermeulen
The permissible brightness of lamp fittings 12,200
Motorcar headlights 12,305
Boerdijk, A. H.
* Levitation by static magnetic fields 18,125
Boerman, J. R., P. Schagen, J. H. J. Maartens and T. W. van Rijssel
The "Scenioscope", a new television camera tube . 17,189
Boldingh, W. Hondius, see **Hondius Boldingh, W.**
Bollée, B.
* Chladni's figures on the vibrating capacitor of a synchrocyclotron 19, 84
Boort, H. J. J. van, M. Klerk and A. A. Kruithof
Radio interference from fluorescent lamps 20,135
— and D. Kolkman
The double-flux "TL" lamp, a fluorescent lamp of high output per unit length 19,333
Borgman, J.
* An application of television for the discovery of variable stars 19,140
Botden, P. J. M. and B. Combée
Special X-ray tubes 13, 71
—, B. Combée and J. Houtman
An experimental X-ray apparatus with midget X-ray tube 14,165
Bouma, A. L. and F. K. Ligtenberg
The Philips pavilion at the 1958 Brussels World Fair,
III. Model tests for proving the construction of the pavilion 20, 17
Bouwmeester, E. and N. Warmoltz
A simple and reliable ionization manometer 17,121
Boxman, P. and P. Blom
A transistor hearing-aid 19,130
Braun, P. B., G. H. Jonker and H. P. J. Wijn
Ferroxplana, hexagonal ferromagnetic iron-oxide compounds for very high frequencies 18,145
Breggen, J. C. van der, H. J. Lindenhovius and G. Arbelet
A millivoltmeter for the frequency range from 1000 to 30×10^6 c/s 11,206
Brekoo, H. P. J. and T. Douma
Heating the filaments of valves in a cascade generator by means of high-frequency current 11,123
Bremmer, H.
The troposphere as a medium for the propagation of radio waves,
I 15,148
II 15,175
Bril, A., J. de Gier and H. A. Klasens
A cathode-ray tube for flying-spot scanning 15,233
— and H. A. Klasens
The efficiency of fluorescence in cathode-ray tubes 15, 63
— and F. A. Kröger
Saturation of fluorescence in television tubes 12,120
Brockman, F. G. and M. W. Louwerse
The ferroxcube transformer core used in the Brookhaven Cosmotron 15, 73
— and W. G. Steneck
A new automatic hysteresis-curve recorder 16, 79
Brooker, M. W. and D. G. Ware
Cheater circuits for the testing of thyratrons,
I. Measurement of grid current 16, 43
II. Life testing at high commutation factors . . . 16, 98
Brown, W. B. and C. F. Hendee
Stroboscopic operation of photomultiplier tubes . . 19, 50
Bruin, S. L. de
The "Electronic Poem" performed in the Philips pavilion at the 1958 Brussels World Fair,
C. The electronic control system 20, 45
Bruining, H. and J. C. Francken
New developments in the image iconoscope 14,327
—, L. Heijne and P. Schagen
* An experimental photoconductive camera tube for television 16, 23
—, P. Schagen and J. C. Francken
The image iconoscope, a camera tube for television 13,119
Bruinsma, A. H.
Radio-controlled models 15,281
Bruyn, J. W. de and H. Badings
Electronic music 19,191
Bruijning, H. G., H. van der Heide and H. P. J. Wijn
Switching time of ferrites with rectangular hysteresis loop 18,336
— and A. Rademakers
Pre-magnetization of the core of a pulse transformer by means of ferroxdure 19, 28
Bueren, H. G. van
Lattice imperfections and plastic deformation in metals,
I. Nature and characteristics of lattice imperfections, notably dislocations 15,246
II. Behaviour of lattice imperfections during deformation 15,286
Burger, G. C. E.
Phantom tests with X-rays 11,291
Burgerjon, J. J. and F. A. Heyn
The synchrocyclotron at Amsterdam,
IV. Details of construction and ancillary equipment 14,263
Burgt, C. M. van der
Ferroxcube material for piezomagnetic vibrators . 18,285
—, M. Gevers and H. P. J. Wijn
Measuring methods for some properties of ferroxcube materials 14,245
Bye, J. A. W. van der Does de, see **Does de Bye, J. A. W. van der**
Cant, B. A.
Problems in the construction of small radio valves . 18,217
Carpentier, E. E.
An easily portable cathode-ray oscillograph 11,111
Casimir, H. B. G.
Science and industry 20, 85
Cassee, E.
A preservation rectifier with electronically stabilized charging voltage 11,253
Cayzac, J.
Automatic frequency stabilization for a beam transmitter working on centimetric waves 17,334
— and P. Périlhou
A stabilized extra-high tension rectifier for 5000 V, 50 mA 14,190
Chabot, J. J. M. Taudin, see **Taudin Chabot, J. J. M.**
Champeix, R., H. Dormont and E. Morilleau
A photomultiplier tube for scintillation counting . 16,250
Chippendale, R. A. and J. A. Jenkins
High-speed photography by means of the image converter 14,213
Chippendale, T. R.
* Linear electron accelerators for deep X-ray therapy 17, 31
Coeterier, F.
The multi-reflex klystron as a transmitting valve in beam transmitters 17,328
Combée, B.
* An X-ray tube for microradiography 17, 45
— and P. J. M. Botden
Special X-ray tubes 13, 71
—, P. J. M. Botden and J. Houtman
An experimental X-ray apparatus with midget X-ray tube 14,165
— and J. Fransen
An X-ray apparatus for therapeutic treatments . . 11,193
— and A. Recourt
A simple apparatus for contact microradiography between 1.5 and 5 kV 19,221
Constable, J. M.
An automatic braking device for X-ray apparatus . 11, 50
Coppola, P. P. and R. C. Hughes
Dispenser cathodes,
II. The pressed cathode 19,179
Daams, J. and J. Voogd
Inactivation of bacteria by ultra-violet radiation . . 12,111
Dam, L. P. M. ten and D. Kolkman
Lighting in trains and other transport vehicles with fluorescent lamps 18, 11

Dammers, B. G., P. D. van der Knaap and A. G. W. Uitjens
The electrical recording of diagrams with a calibrated system of coordinates 12,283
Deelman, H. E.
* An improved method of cleating 19,268
Defize, L. F. and P. C. van der Willigen
The determination of droplet size in arc welding by high-speed cinematography 15,122
Dell, H. A. and C. H. R. Gentry
A direct-reading precision polarograph 14,257
— and N. E. Goddard
* A radar sonde system for upper-air measurements . 19,258
Derksen, J. C. and M. Stel
Plastics and their application in the electrotechnical industry 11, 33
Diemer, G., G. Alma and H. Groendijk
A rubber membrane model for tracing electron paths in space-charge fields 14,336
—, H. A. Klasens and P. Zalm
Electroluminescence and image intensification . . 19, 1
— and K. S. Knol
A model for studying electromagnetic waves in rectangular waveguides 11,156
The noise of electronic valves at very high frequencies,
I. The diode 14,153
II. The triode 14,236
—, K. Rodenhuis and J. G. van Wijngaarden
The EC 57, a disc-seal microwave triode with L cathode 18,317
Does de Bye, J. A. W. van der
The scintillation counter 20,209
Signal-to-noise ratio and dead time of a scintillation counter 20,263
Domburg, J. and W. Six
A cold-cathode gas-discharge tube as a switching element in automatic telephony 15,265
Dorgelo, E. G.
High-power transmitting valves with thoriated-tungsten cathodes 14,226
Transmitting valves for use in industry 20,299
— and P. Zijlstra
Two transmitting valves for use in mobile installations 12,157
Dormont, H., R. Champeix and E. Morilleau
A photomultiplier tube for scintillation counting 16,250
Dorsten, A. C. van
* Lightning and aircraft 16,296
* A generator for fast neutrons 17,109
— and A. J. J. Franken
Three methods of measuring magnetic fields,
II. Measurement of the field on the axis of magnetic electron lenses 15, 52
—, H. Nieuwdorp and A. Verhoeff
The Philips 100 kV electron microscope 12, 33
— and J. B. Le Poole
The EM 75 kV, an electron microscope of simplified construction 17, 47
Douma, T. and H. P. J. Brekoo
Heating the filaments of valves in a cascade generator by means of high-frequency current 11,123
Dowling, P. H., C. F. Hendee, T. R. Kohler and W. Parrish
Counters for X-ray analysis 18,262
Ducot, C.
Beam transmitters with double frequency modulation 17,317
Duis, J. A. ten
* An apparatus for testing the solderability of wire . 20,158
Dumbrill, H. W. and J. J. C. Hardenberg
The "Symmetrix", a universal table and stand for X-ray diagnosis 17,112
Duuren, K. van
* A simple and compact arrangement for measuring the β-activity of weak radioactive samples 20,170
Duyfjes, W.
The formulation of pesticides 19,165
Duyster, H. C.
The Philips pavilion at the 1958 Brussels World Fair,
IV. Construction of the pavilion in prestressed concrete 20, 27
Dijkstra, L. J. and J. D. Fast
Internal friction in iron and steel 13,172
Edens, A. H.
A method of sealing the window and cone of television picture-tubes 19,318
Elenbaas, W.
Fifty years of the high-pressure mercury-vapour lamp 18,167
— and T. Hehenkamp
A new fluorescent lamp in a starterless circuit . . . 17,288
— and T. Holmes
An instant-starting fluorescent lamp in series with an incandescent lamp 12,129
— and K. R. Labberté
High-pressure mercury-vapour lamps for photocopying processes 13,323
—, J. L. Ouweltjes and K. R. Labberté
A new high-pressure mercury lamp with fluorescent bulb 13,109
— and J. Riemens
Light sources for line spectra 11,299
Embden, H. J. Meerkamp van, see **Meerkamp van Embden, H. J.**
Emmens, H. and F. de Boer
Sedimentation of fluorescent screens in cathode-ray tubes 16,232
Ensing, L. and H. J. J. van Eyndhoven
An oscillator with constant output voltage 14,304
— and J. M. L. Janssen
The electro-analogue, an apparatus for studying regulating systems,
I. Components and functions 12,257
II. The electrical execution 12,319
Espersen, G. A. and B. Arfin
A 3 cm magnetron for beacons 14, 87
— and R. A. La Plante
A low-noise klystron with high power output . . . 18,361
— and J. W. Rogers
Electron emission of materials for electron tubes 20,269
Esveldt, C. J., H. P. J. Wijn, E. W. Gorter and P. Geldermans
Conditions for square hysteresis loops in ferrites . 16, 49
Ettema, E. H., W. P. van den Blink and P. C. van der Willigen
Stud welding with welding cartridges 17, 37
Eyndhoven, H. J. J. van and L. Ensing
An oscillator with constant output voltage 14,304
Fast, J. D.
Causes of porosity in welds 11,101
Apparatus for preparation of metals with an exactly known content of impurities 11,241
Investigations into the impact strength of iron and steel 11,303
Aging phenomena in iron and steel after rapid cooling 13,165
Strain aging in iron and steel 14, 60
Low-hydrogen welding rods 14, 96
Entropy in science and technology,
I. The concept of entropy 16,258
II. Examples and applications 16,298
III. Examples and applications (continued) . . . 16,321
IV. Entropy and information (*by — and F. L. H. M. Stumpers*) 18,201
Foreign atoms in metals 16,341
— and L. J. Dijkstra
Internal friction in iron and steel 13,172
—, A. I. Luteijn and E. Overbosch
Preparation and casting of metals and alloys under high vacuum 15,114
— and F. L. H. M. Stumpers
Entropy in science and technology,
IV. Entropy and information 18,201
Feddema, J.
The application of the X-ray image intensifier,
V. Medical aspects of the image intensifier 17, 88
Feiner, H. and H. N. Hansen
Coaxial cable as a transmission medium for carrier telephony 14,141
Fine, S. and C. F. Hendee
Nuclear X-ray sources 18,229
Fortuin, G. J.
Visual acuity in connection with television 16,172

Foskett, R. D. and E. A. Neppiras
Ultrasonic machining,
I. Technique and equipment 18,325
II. Operating conditions and performance of ultrasonic drills 18,368
Francken, J. C. and H. Bruining
New developments in the image iconoscope 14,327
—, J. de Gier and W. F. Nienhuis
A pentode gun for television picture-tubes 18, 73
—, P. Schagen and H. Bruining
The image iconoscope, a camera tube for television 13,119
Franken, A. J. J. and A. C. van Dorsten
Three methods of measuring magnetic fields,
II. Measurement of the field on the axis of magnetic electron lenses 15, 52
Fransen, J. and B. Combée
An X-ray apparatus for therapeutic treatments . . 11,193
Fransen, J. J. B. and H. J. R. Perdijk
Barium getter films 19,290
Fry, D. W.
The linear electron accelerator 14, 1
Gaillard, P. and R. Aschen
A simple ionosphere sounder 13,152
Geels, B. H.
A private automatic branch exchange using high-speed uniselectors 18, 19
Geenen, M. J. W.
* A machine for bend tests 17,246
Gelder, Z. van and J. L. H. Jonker
New electronic tubes employed as switches in communication engineering,
I. Contact tubes 13, 49
II. Switch tubes 13, 82
Geldermans, P., H. P. J. Wijn, E. W. Gorter and C. J. Esveldt
Conditions for square hysteresis loops in ferrites . . 16, 49
Gentry, C. H. R. and H. A. Dell
A direct-reading precision polarograph 14,257
Gevers, M.
Measuring the dielectric constant and the loss angle of solids at 3000 Mc/s 13, 61
—, C. M. van der Burgt and H. P. J. Wijn
Measuring methods for some properties of ferroxcube materials 14,245
Gieles, J. P. M.
A 4000 Mc/s wide-band amplifier using a disc-seal triode 19,145
Gier, J. de, A. Bril and H. A. Klasens
A cathode-ray tube for flying-spot scanning 15,233
—, J. C. Francken and W. F. Nienhuis
A pentode gun for television picture-tubes 18, 73
—, T. Hagenberg, H. J. Meerkamp van Embden, J. A. M. Smelt, O. L. van Steenis and J. G. W. Mulder
A steel picture-tube for television reception 14,281
—, A. C. Kleisma and J. Peper
Secondary emission from the screen of a picture-tube 16, 26
Gier, N. A. de, W. van Gool and J. G. van Santen
Photo-resistors made of compressed and sintered cadmium sulphide 20,277
Goddard, N. E. and H. A. Dell
* A radar sonde system for upper-air measurements . 19,258
Gool, W. van, N. A. de Gier and J. G. van Santen
Photo-resistors made of compressed and sintered cadmium sulphide 20,277
Gorter, E. W. and J. J. Went
The magnetic and electrical properties of ferroxcube materials 13,181
—, J. J. Went, G. W. Rathenau and G. W. van Oosterhout
Ferroxdure, a class of new permanent magnet materials,
I. Most important properties of ferroxdure . . . 13,194
II. Physical background of some properties of ferroxdure 13,197
III. Saturation magnetization and crystal structure 13,203
—, H. P. J. Wijn, C. J. Esveldt and P. Geldermans
Conditions for square hysteresis loops in ferrites . 16, 49
Gradstein, S.
Positioning of the sources of light when photographing with artificial light 12,145
— and J. L. H. Jonker
Fluorescent pigments as an artistic medium 11, 16
Greefkes, J. A. and F. de Jager
"Frena", a system of speech transmission at high noise levels 19, 73
—, J. F. Schouten and F. de Jager
Delta modulation, a new modulation system for telecommunication 13,237
Groendijk, H.
* A noise diode for ultra-high frequencies 20,108
—, G. Alma and G. Diemer
A rubber membrane model for tracing electron paths in space-charge fields 14,336
Groot, A. de and E. Blasberg
Metal-detectors 15, 97
Groot, W. de
Cyclotron and synchrocyclotron 12, 65
Philips' diamond jubilee: Scientific research of Philips' Industries from 1891 to 1951 . . . . . 13, 1
Photometry at low luminance levels 15,182
— and N. W. H. Addink
Spectrochemical analysis 12,337
— and F. A. Kröger
The influence of temperature on the fluorescence of solids 12, 6
— and A. A. Kruithof
The colour triangle 12,137
Gude, H. te and E. Schaaff
* A new kind of tuning indicator tube 18,243
Haaf, F. E. L. ten, G. Klein and F. J. Schijff
Monitoring, control and safety equipment for a nuclear reactor of the swimming-pool type,
II. Further description of certain component units 19,273
Haanstra, H. B.
A simple ultramicrotome 17,178
—, J. J. de Jong and J. M. G. Smeets
* The sub-microscopic structure of "Ticonal" G magnet steel 19, 11
Haantjes, J. and C. J. van Loon
A large-screen television projector 15, 27
— and T. G. Schut
A line converter for the international exchange of television programmes 15,297
— and F. W. de Vrijer
Flicker in television pictures 13, 55
Haaijman, P. W. and J. L. H. Jonker
The wire capacitor and other composite drawn products 13,145
Hagenberg, T., J. de Gier, H. J. Meerkamp van Embden, J. A. M. Smelt, O. L. van Steenis and J. G. W. Mulder
A steel picture-tube for television reception 14,281
Halberstadt, J. and A. H. W. Aten
The production of radio-isotopes 16, 1
Hamacher, E. A. and K. Lowitzsch
The "Norelco" counting-rate computer 17,249
—, W. Parrish and K. Lowitzsch
The "Norelco" X-ray diffractometer 16,123
Hamaker, H. C.
Lot inspection by sampling 11,176
The theory of sampling inspection plans 11,260
—, J. J. M. Taudin Chabot and F. G. Willemze
The practical application of sampling inspection plans and tables 11,362
Hammerton, J. C., P. E. Trier and E. Wolfendale
A time-of-flight neutron spectrometer 15,325
Hamming, I. and J. F. T. van Heemskerck Veeckens
* An open-air laboratory for road lighting 19,202
Hansen, H. N. and H. Feiner
Coaxial cable as a transmission medium for carrier telephony 14,141
Hardenberg, J. J. C.
An apparatus for cinefluorography with an 11 inch X-ray image intensifier 20,331
— and H. W. Dumbrill
The "Symmetrix", a universal table and stand for X-ray diagnosis 17,112
Haringx, J. A.
Instability of springs 11,245
— and H. van Suchtelen
The Foucault pendulum in the United Nations building in New York 19,236

Hauer, A. and M. van Tol
A radio sonde for meteorological observations . . . 16,148
Haven, Y.
Lattice imperfections in crystals, studied on alkali halides 20, 69
Heemskerck Veeckens, J. F. T. van and I. Hamming
* An open-air laboratory for road lighting 19,202
Hehenkamp, T.
Supply units for airfield light beaconing systems . . 17, 10
* Small ballasts for fluorescent lamps 18,279
The life of ballasts for gas-discharge lamps,
I. Transformers and chokes 20, 59
II. Capacitors 20,162
— and W. Elenbaas
A new fluorescent lamp in a starterless circuit . . . 17,288
— and J. J. Wilting
Transistor D.C. converters for fluorescent-lamp power supplies 20,362
Heide, H. van der, H. G. Bruijning and H. P. J. Wijn
Switching time of ferrites with rectangular hysteresis loop 18,336
Hendee, C. F. and W. B. Brown
Stroboscopic operation of photomultiplier tubes . . 19, 50
—, P. H. Dowling, T. R. Kohler and W. Parrish
Counters for X-ray analysis 18,262
— and S. Fine
Nuclear X-ray sources 18,229
Hengel, J. van and J. Volger
* A transistor radio receiver powered by a thermopile 18,155
Hepp, G.
A battery-operated Geiger-Müller counter 14,369
Hertzberger, E. and A. J. Klein
The manufacture of virus vaccine against influenza 12,273
Hess, K. W.
Measuring the de-ionization time of gas-filled diodes and triodes 12,178
— and F. H. de Jong
Controlling the luminous intensity of fluorescent lamps with the aid of relay valves 12, 83
Heuven, E. W. van
The noise emission of ballasts for fluorescent lamps . 18,110
Heyn, F. A.
The synchrocyclotron at Amsterdam,
I. General description of the installation 12,241
II. The oscillator and the modulator 12,247
III. The electromagnet 12,349
— and J. J. Burgerjon
The synchrocyclotron at Amsterdam,
IV. Details of construction and ancillary equipment 14,263
Heijn, H. J. and N. C. de Troye
A fast method of reading magnetic-core memories . 20,193
Heijne, L., P. Schagen and H. Bruining
* An experimental photoconductive camera tube for television 16, 23
Hoekstra, H. and A. L. Biermasz
The measurement of changes in length with the aid of strain gauges 11, 23
Hoekstra, J. and J. A. W. van Laar
An indentation meter for paint 13,352
Holm, W. A. and F. H. J. van der Poel
* Colour television in medical teaching 20,327
Holmes, T. and W. Elenbaas
An instant-starting fluorescent lamp in series with an incandescent lamp 12,129
Holthoon, J. van and F. G. Peuscher
A pre-amplifier for use with electronic voltmeters and oscilloscopes 15,169
Hondius Boldingh, W.
Fluorography with the aid of a mirror system . . . 13,269
Mirror cameras for general X-ray diagnostics . . . 16, 58
Hoogenband, J. C. van den and J. Stolk
Reflection and impedance measurements by means of a long transmission line 16,309
Horseling, J.
* A high-vacuum tap with short outgassing time . . 17,184
Horst, H. L. van der and P. H. G. van Vlodrop
An experimental induction-heating generator using hydrogen thyratrons 20,101
Houtman, J., P. J. M. Botden and B. Combée
An experimental X-ray apparatus with midget X-ray tube 14,165
Huber, C. and J. Rodrigues de Miranda
A transistor pre-amplifier for the magnetodynamic pick-up 18,238
Hugenholtz, E. H.
The impulse-governed oscillator, a system for frequency stabilization 14,130
Hughes, R. C. and P. P. Coppola
Dispenser cathodes,
II. The pressed cathode 19,179
Huissoon, M.
The F.M. section of modern broadcast receivers,
II. The built-in F.M. aerial 17,348
Hurck, N. van and F. L. H. M. Stumpers
* An automatic noise-figure indicator 18,141
Ingen Schenau, B. W. van
A signal generator for the testing of television receivers 15,205
Iperen, B. B. van
The helix as resonator for generating ultra-high frequencies 11,221
Velocity-modulation valves for 100 to 1000 watts continuous output 13,209
* A reflex klystron for 4 mm waves 18, 51
Jager, F. de and J. A. Greefkes
"Frena", a system of speech transmission at high noise levels 19, 73
—, J. F. Schouten and J. A. Greefkes
Delta modulation, a new modulation system for telecommunication 13,237
Jager, J.
The application of point-contact germanium diodes 16,225
Jansen, C. G. J., R. Loosjes and H. J. Vink
Thermionic emitters under pulsed operation 13,337
Jansen, M. J., H. J. Lemmens and R. Loosjes
A new thermionic cathode for heavy loads 11,341
Janssen, J. M. L.
An experimental "stroboscopic" oscilloscope for frequencies up to about 50 Mc/s,
I. Fundamentals 12, 52
— and L. Ensing
The electro-analogue, an apparatus for studying regulating systems,
I. Components and functions 12,257
II. The electrical execution 12,319
— and A. J. Michels
An experimental "stroboscopic" oscilloscope for frequencies up to about 50 Mc/s,
II. Electrical build-up 12, 73
Jaspers, A. M. J.
* The measurement of radioactive iodine in the thyroid gland 18, 87
Jenkins, J. A. and R. A. Chippendale
High-speed photography by means of the image converter 14,213
Jensen, H. and H. Verse
The application of the X-ray image intensifier,
IV. Equipment for spot film radiography incorporating an image intensifier fitted with a periscope optical system 17, 84
Jochems, P. J. W. and F. H. Stieltjes
Apparatus for testing transistors 13,254
Jong, F. H. de and K. W. Hess
Controlling the luminous intensity of fluorescent lamps with the aid of relay valves 12, 83
— and D. W. van Rheenen
An apparatus for protection against dangerous voltages in welding equipment 15,199
— and L. W. Roosendaal
Electric fencing of grazing land 13,328
Jong, J. J. de
* A remarkable etching of copper 15,238
—, H. B. Haanstra and J. M. G. Smeets
* The sub-microscopic structure of "Ticonal" G magnet steel 19, 11
Jonker, G. H.
Capacitor materials with high dielectric constant . . 17,129
— and J. H. van Santen
The ferro-electricity of titanates 11,183
—, H. P. J. Wijn and P. B. Braun
Ferroxplana, hexagonal ferromagnetic iron-oxide compounds for very high frequencies 18,145

Jonker, J. L. H.
Electronic tubes 14,117
A short-length direct-view picture-tube 14,361
— and Z. van Gelder
New electronic tubes employed as switches in communication engineering,
I. Contact tubes 13, 49
II. Switch tubes 13, 82
— and S. Gradstein
Fluorescent pigments as an artistic medium 11, 16
— and P. W. Haaijman
The wire capacitor and other composite drawn products 13,145
— and A. J. W. M. van Overbeek
The "φ-detector", a detector valve for frequency modulation 11, 1
—, A. J. W. M. van Overbeek and K. Rodenhuis
A decade counter tube for high counting rates . . . 14,313
Jonkers, C. O. and J. W. L. Köhler
Fundamentals of the gas refrigerating machine . . 16, 69
Construction of a gas refrigerating machine 16,105
Jürgens, B. F.
Three methods of measuring magnetic fields,
I. Measurement based on the generator principle . 15, 49
Kalff, L. C.
Ways to comfortable lighting 14, 69
The "Electronic Poem" performed in the Philips pavilion at the 1958 Brussels World Fair,
A. The light effects 20, 37
Kelliher, M. G. and C. F. Bareford
The 15 MeV linear electron accelerator for Harwell . 15, 1
A. Choice of parameters and general design . . . 15, 2
B. Detailed description of main components and circuits 15, 10
C. Testing and performance 15, 22
Kerstens, J. B. S. M.
Mechanical phenomena in gramophone pick-ups at high audio frequencies 18, 89
Klasens, H. A. and A. Bril
The efficiency of fluorescence in cathode-ray tubes . 15, 63
—, A. Bril and J. de Gier
A cathode-ray tube for flying-spot scanning 15,233
—, G. Diemer and P. Zalm
Electroluminescence and image intensification . . . 19, 1
Klein, A. J. and E. Hertzberger
The manufacture of virus vaccine against influenza . 12,273
Klein, G., F. E. L. ten Haaf and F. J. Schijff
Monitoring, control and safety equipment for a nuclear reactor of the swimming-pool type,
II. Further description of certain component units 19,273
Kleis, D.
Modern acoustical engineering,
I. General principles 20,309
Kleisma, A. C., J. de Gier and J. Peper
Secondary emission from the screen of a picture-tube 16, 26
Klerk, M., H. J. J. van Boort and A. A. Kruithof
Radio interference from fluorescent lamps 20,135
Klinkhamer, J. F.
A through-supergroup filter for carrier telephone systems on coaxial cable 13,223
Knaap, P. D. van der, B. G. Dammers and A. G. W. Uitjens
The electrical recording of diagrams with a calibrated system of coordinates 12,283
Knol, K. S.
Noise 20, 50
— and G. Diemer
A model for studying electromagnetic waves in rectangular waveguides 11,156
The noise of electronic valves at very high frequencies,
I. The diode 14,153
II. The triode 14,236
Köhler, J. W. L. and C. O. Jonkers
Fundamentals of the gas refrigerating machine . . 16, 69
Construction of a gas refrigerating machine 16,105
— and J. van der Ster
A small air fractionating column used with a gas refrigerating machine for producing liquid nitrogen 20,177
Kohler, T. R., P. H. Dowling, C. F. Hendee and W. Parrish
Counters for X-ray analysis 18,262
Kolkman, D. and H. J. J. van Boort
The double-flux "TL" lamp, a fluorescent lamp of high output per unit length 19,333
— and L. P. M. ten Dam
Lighting in trains and other transport vehicles with fluorescent lamps 18, 11
Koopmans, M. J.
Fungicide research 17,222
Kooy, C.
* Direct observation of Weiss domains by means of the Faraday effect 19,286
Koppius, O. G.
An application of Geiger counter tubes for spectrochemical analysis 11,215
Kotte, J. J.
A professional cine projector for 16 mm film 16,158
* A cinema projector for 70 mm and 35 mm films . . 17,299
Kröger, F. A. and A. Bril
Saturation of fluorescence in television tubes . . . 12,120
— and W. de Groot
The influence of temperature on the fluorescence of solids 12, 6
— and E. J. W. Verwey
New views on oxidic semi-conductors and zinc-sulphide phosphors 13, 90
Kruithof, A. A., H. J. J. van Boort and M. Klerk
Radio interference from fluorescent lamps 20,135
— and W. de Groot
The colour triangle 12,137
— and J. L. Ouweltjes
Colour and colour rendering of tubular fluorescent lamps 18,249
Kruithof, A. M.
Perception of contrasts when the contours of details are blurred 11,333
Kuntke, A. H. G.
Distant-focus X-ray tubes 20,291
Laar, J. A. W. van and J. Hoekstra
An indentation meter for paint 13,352
Labberté, K. R. and W. Elenbaas
High-pressure mercury-vapour lamps for photocopying processes 13,323
—, J. L. Ouweltjes and W. Elenbaas
A new high-pressure mercury lamp with fluorescent bulb 13,109
Lang, G. and R. O. Schumacher
The application of the X-ray image intensifier,
VI. Industrial radiology with the image intensifier 17, 93
La Plante, R. A., see **Plante, R. A. La**
Leblans, L. M.
* A high-precision lathe headstock 19, 68
Lely, J. A. and T. W. van Rijssel
Collimating X-rays in beams of very small divergence and high intensity 13, 96
Lemmens, H. J., M. J. Jansen and R. Loosjes
A new thermionic cathode for heavy loads 11,341
Le Poole, J. B., see **Poole, J. B. Le**
Levi, R.
A technique for machining tungsten 17, 97
Dispenser cathodes,
III. The impregnated cathode 19,186
Ligtenberg, F. K. and A. L. Bouma
The Philips pavilion at the 1958 Brussels World Fair,
III. Model tests for proving the construction of the pavilion 20, 17
Lindenhovius, H. J., G. Arbelet and J. C. van der Breggen
A millivoltmeter for the frequency range from 1000 to 30×10^6 c/s 11,206
—, C. von Basel and G. W. van Santen
Electronic equipment for the continuous monitoring of turbines 17, 59
Loeb, J.
The distribution of illumination on a plane parallel to a tubular lamp 12, 60
Loeff, M. Rutgers van der, see **Rutgers van der Loeff, M.**
Loon, C. J. van and J. Haantjes
A large-screen television projector 15, 27

Loosjes, R., H. J. Lemmens and M. J. Jansen
A new thermionic cathode for heavy loads **11**,341
— and H. J. Vink
Conduction processes in the oxide-coated cathode . **11**,271
—, H. J. Vink and C. G. J. Jansen
Thermionic emitters under pulsed operation **13**,337
Lotgering, F. K.
* Topotactically crystal-oriented ferromagnetics . . **20**,354
Louwerse, M. W. and F. G. Brockman
The ferroxcube transformer core used in the Brookhaven Cosmotron **15**, 73
Lowitzsch, K. and E. A. Hamacher
The "Norelco" counting-rate computer **17**,249
—, W. Parrish and E. A. Hamacher
The "Norelco" X-ray diffractometer **16**,123
Luteijn, A. I., J. D. Fast and E. Overbosch
Preparation and casting of metals and alloys under high vacuum **15**,114
Maartens, J. H. J., P. Schagen, J. R. Boerman and T. W. van Rijssel
The "Scenioscope", a new television camera tube . **17**,189
Meerkamp van Embden, H. J.
Modern casting techniques **15**,133
* The evolution of the permanent magnet: a brief review **18**,358
—, J. de Gier, T. Hagenberg, J. A. M. Smelt, O. L. van Steenis and J. G. W. Mulder
A steel picture-tube for television reception **14**,281
Meltzer, J.
Research on the control of animal pests **17**,146
Meijer, R. J.
The Philips hot-gas engine with rhombic drive mechanism **20**,245
Meijering, J. L.
Hardening of metals **14**,203
— and G. W. Rathenau
The oxidation of heat-resistant alloys in the presence of foreign oxides **12**,213
— and G. D. Rieck
The function of additives in tungsten for filaments . **19**,109
Michels, A. J. and A. L. Biermasz
An electronic D.C. millivoltmeter **16**,117
— and J. M. L. Janssen
An experimental "stroboscopic" oscilloscope for frequencies up to about 50 Mc/s,
II. Electrical build-up **12**, 73
Miranda, J. Rodrigues de, see **Rodrigues de Miranda, J.**
Missel, J. C. B.
Piezo-electric materials **11**,145
Mol, E. A. J.
Wire and cable insulating materials with polyvinyl chloride as base **12**, 97
Morilleau, E., R. Champeix and H. Dormont
A photomultiplier tube for scintillation counting . **16**,250
Mulder, J. G. W., J. de Gier, T. Hagenberg, H. J. Meerkamp van Embden, J. A. M. Smelt and O. L. van Steenis
A steel picture-tube for television reception **14**,281
Muller, C. A.
A receiver for the radio waves from interstellar hydrogen,
I. The investigation of the hydrogen radiation . . **17**,305
II. Design of the receiver **17**,351
Neeteson, P. A.
Flywheel synchronization of saw-tooth generators in television receivers **13**,312
Nemet, A., R. B. Stephens and W. A. Bayfield
A radioactive-contamination monitor for the hands, feet and clothing **16**,201
Neppiras, E. A. and R. D. Foskett
Ultrasonic machining,
I. Technique and equipment **18**,325
II. Operating conditions and performance of ultrasonic drills **18**,368
Nienhuis, K. and F. M. Penning
Construction and applications of a new design of the Philips vacuum gauge **11**,116
Nienhuis, W. F. and F. de Boer
Low-voltage oscilloscope tubes **19**,159
—, J. C. Francken and J. de Gier
A pentode gun for television picture-tubes **18**, 73
Nieuwdorp, H., A. C. van Dorsten and A. Verhoeff
The Philips 100 kV electron microscope **12**, 33
Niklas, W. F.
An improved ion-trap magnet **15**,258
Oele, H. A. and A. Bierman
Betatrons with and without iron yoke **11**, 65
Ooms, J. L.
The recording and production of gramophone records **17**,101
Oosterhout, G. W. van, J. J. Went, G. W. Rathenau and E. W. Gorter
Ferroxdure, a class of new permanent magnet materials,
I. Most important properties of ferroxdure . . . **13**,194
II. Physical background of some properties of ferroxdure **13**,197
III. Saturation magnetization and crystal structure **13**,203
Oosterkamp, W. J., J. Proper and J. J. F. de Wijk
* Dosimetry of the very weak X-radiation generated in television receivers and X-ray diffraction apparatus **19**,264
— and T. Tol
The application of the X-ray image intensifier,
II. The perception of small object-detail **17**, 71
Ouweltjes, J. L.
New phosphors for fluorescent lamps **13**,346
—, W. Elenbaas and K. R. Labberté
A new high-pressure mercury lamp with fluorescent bulb **13**,109
— and A. A. Kruithof
Colour and colour rendering of tubular fluorescent lamps **18**,249
Overbeek, A. J. W. M. van and J. L. H. Jonker
The "φ-detector", a detector valve for frequency modulation **11**, 1
—, J. L. H. Jonker and K. Rodenhuis
A decade counter tube for high counting rates . . . **14**,313
Overbosch, E., J. D. Fast and A. I. Luteijn
Preparation and casting of metals and alloys under high vacuum **15**,114
Pannenborg, A. E.
A measuring arrangement for waveguides **12**, 15
Papenhuijzen, P. J.
A transmitting triode for frequencies up to 900 Mc/s **19**,118
Parrish, W.
The manufacture of quartz oscillator-plates,
I. How the required cuts are obtained **11**,323
II. Control of the cutting angles by X-ray diffraction **11**,351
III. Lapping and final frequency adjustment of the blanks **12**,166
X-ray intensity measurements with counter tubes . **17**,206
X-ray spectrochemical analysis **17**,269
—, P. H. Dowling, C. F. Hendee and T. R. Kohler
Counters for X-ray analysis **18**,262
—, E. A. Hamacher and K. Lowitzsch
The "Norelco" X-ray diffractometer **16**,123
Pauw, L. J. van der
* A method of measuring the resistivity and Hall coefficient on lamellae of arbitrary shape **20**,220
Pelt, J. G. van
* The use of thermistors in the ebullioscopic determination of molecular weights **20**,357
Penning, F. M. and K. Nienhuis
Construction and applications of a new design of the Philips vacuum gauge **11**,116
Penning, P.
The generation of dislocations by thermal stresses . **19**,357
Peper, J.
* Analysis of the gaseous contents of sealed cathode-ray tubes with the aid of the omegatron **19**,218
—, J. de Gier and A. C. Kleisma
Secondary emission from the screen of a picture-tube **16**, 26
Perdok, W. G. and H. van Suchtelen
An arrangement for indicating piezo-electricity of crystals **11**,151
Perdijk, H. J. R. and J. J. B. Fransen
Barium getter films **19**,290
Périlhou, P. and J. Cayzac
A stabilized extra-high tension rectifier for 5000 V, 50 mA **14**,190
Peuscher, F. G. and J. van Holthoon
A pre-amplifier for use with electronic voltmeters and oscilloscopes **15**,169

Plante, R. A. La and G. A. Espersen
A low-noise klystron with high power output . . . 18,361
Ploegsma, A. W.
* Fabrication of sapphire and diamond styli for gramophone pick-ups 19,324
Poel, F. H. J. van der
A flying-spot scanner for televising 35 mm film . . 18,193
— and W. A. Holm
* Colour television in medical teaching 20,327
— and J. J. P. Valeton
The flying-spot scanner 15,221
Poole, J. B. Le and A. C. van Dorsten
The EM 75 kV, an electron microscope of simplified construction 17, 47
Poorter, T. and F. W. de Vrijer
The projection of colour-television pictures 19,338
Prado, E. and J. D. Veegens
A sinusoidal *RC*-oscillator for measurements in the frequency range 20-250 000 c/s 15,240
Prins, B. H. G. and J. M. G. Seppen
* The port of Rotterdam radar system 20,349
Proper, J., W. J. Oosterkamp and J. J. F. de Wijk
* Dosimetry of the very weak X-radiation generated in television receivers and X-ray diffraction apparatus 19,264
Quant, H. de and P. Zijp
The F.M. section of modern broadcast receivers, I. Circuitry and structural design 17,342
Rademakers, A. and H. G. Bruijning
Pre-magnetization of the core of a pulse transformer by means of ferroxdure 19, 28
Rathenau, G. W.
Imperfections in matter 15,105
— and G. Baas
An emission electron microscope for research at high temperatures 18, 1
— and J. L. Meijering
The oxidation of heat-resistant alloys in the presence of foreign oxides 12,213
—, A. L. Stuijts and G. H. Weber
Ferroxdure II and III, anisotropic permanent-magnet materials 16,141
—, J. J. Went, E. W. Gorter and G. W. van Oosterhout
Ferroxdure, a class of new permanent magnet materials,
I. Most important properties of ferroxdure . . . 13,194
II. Physical background of some properties of ferroxdure 13,197
III. Saturation magnetization and crystal structure 13,203
Recourt, A. and B. Combée
A simple apparatus for contact microradiography between 1.5 and 5 kV 19,221
Reiniger, F.
The study of thermal conductivity problems by means of the electrolytic tank 18, 52
Remedi, G.
Science goes to the fair 17,362
Rheenen, D. W. van and F. H. de Jong
An apparatus for protection against dangerous voltages in welding equipment 15,199
Rieck, G. D.
Dark-room lighting 11, 53
— and J. L. Meijering
The function of additives in tungsten for filaments . 19,109
— and L. H. Verbeek
The "Photoflux" series of flash-bulbs 12,185
Riemens, J. and W. Elenbaas
Light sources for line spectra 11,299
Rietveld, J. J. and H. Blok
Inductive aerials in modern broadcast receivers,
I. Brief history and general description 16,181
II. Technical aspects of inductive aerials 16,188
Robinson, N. W.
Electronic flash-tubes 16, 13
Rodenhuis, K.
Two triodes for reception of decimetric waves . . . 11, 79
—, G. Diemer and J. G. van Wijngaarden
The EC 57, a disc-seal microwave triode with L cathode 18,317
—, A. J. W. M. van Overbeek and J. L. H. Jonker
A decade counter tube for high counting rates . . . 14,313
—, H. Santing and H. J. M. van Tol
The life and reliability of valves 18,181
Rodrigues de Miranda, J.
Audio amplifiers with single-ended push-pull output 19, 41
— and C. Huber
A transistor pre-amplifier for the magnetodynamic pick-up 18,238
Rogers, J. W. and G. A. Espersen
Electron emission of materials for electron tubes 20,269
Roosdorp, H. J.
On the regulation of industrial processes 12,221
An automatic recording potentiometer for industrial use 15,189
Electronic control of industrial processes 17, 21
Roosendaal, L. W. and F. H. de Jong
Electric fencing of grazing land 13,328
Rutgers van der Loeff, M. and J. B. de Boer
* Floodlighting of the Dutch National War Memorial in Amsterdam 18,300
Rijssel, T. W. van and J. A. Lely
Collimating X-rays in beams of very small divergence and high intensity 13, 96
—, P. Schagen, J. R. Boerman and J. H. J. Maartens
The "Scenioscope", a new television camera tube . 17,189
Santen, G. W. van
An electrical roughness tester for the workshop . . 14, 80
—, C. von Basel and H. J. Lindenhovius
Electronic equipment for the continuous monitoring of turbines 17, 59
Santen, J. G. van, N. A. de Gier and W. van Gool
Photo-resistors made of compressed and sintered cadmium sulphide 20,277
Santen, J. H. van and G. H. Jonker
The ferro-electricity of titanates 11,183
Santing, H., K. Rodenhuis and H. J. M. van Tol
The life and reliability of valves 18,181
Schaaff, E. and H. te Gude
* A new kind of tuning indicator tube 18,243
Schagen, M. J. van
* Cathode-ray display of complex quantities at varying frequencies 18,380
Schagen, P., J. R. Boerman, J. H. J. Maartens and T. W. van Rijssel
The "Scenioscope", a new television camera tube . 17,189
—, H. Bruining and J. C. Francken
The image iconoscope, a camera tube for television . 13,119
—, L. Heijne and H. Bruining
* An experimental photoconductive camera tube for television 16, 23
Schampers, P. P. M. and N. Warmoltz
A pocket dosemeter, with built-in charger, for X-radiation and gamma radiation 16,134
Schenau, B. W. van Ingen, see **Ingen Schenau, B. W. van**
Schouten, J. F., F. de Jager and J. A. Greefkes
Delta modulation, a new modulation system for telecommunication 13,237
Schultink, L., H. L. Spier and A. J. van der Wagt
The wear of diamond dies 16, 91
— and P. G. van Zanten
Thin tungsten wire for small radio valves 18,222
Schultz, B. H.
Measuring rapidly fluctuating gas temperatures . . 13,104
Schumacher, R. O. and G. Lang
The application of the X-ray image intensifier, VI. Industrial radiology with the image intensifier 17, 93
Schurink, J. J.
The twin-cone moving-coil loudspeaker 16,241
— and G. J. Bleeksma
A loudspeaker installation for high-fidelity reproduction in the home 18,304
Schut, T. G. and J. Haantjes
A line converter for the international exchange of television programmes 15,297
Schwab, V. V. and J. G. van Wijngaarden
The EC 59, a transmitting triode with 10 W output at 4000 Mc/s 20,225
Schijff, F. J., F. E. L. ten Haaf and G. Klein
Monitoring, control and safety equipment for a nuclear reactor of the swimming-pool type,
II. Further description of certain component units 19,273

Seppen, J. M. G. and B. H. G. Prins
* The port of Rotterdam radar system 20,349
Six, W.
Some applications of ferroxcube 13,301
— and J. Domburg
A cold-cathode gas-discharge tube as a switching element in automatic telephony 15,265
Slogteren, E. van
The role of the electron microscope in the investigation of plant diseases 14, 13
Slooten, J. van
Experimental testing of electrical networks by means of the unit function response 12,233
Mechanism of the synchronization of *LC*-oscillators . 14,292
Smeets, J. M. G., H. B. Haanstra and J. J. de Jong
* The sub-microscopic structure of "Ticonal" G-magnet steel 19, 11
Smelt, J. A. M., J. de Gier, T. Hagenberg, H. J. Meerkamp van Embden, O. L. van Steenis and J. G. W. Mulder
A steel picture-tube for television reception 14,281
Snel, D. A.
Magnetic sound recording equipment 14,181
Snoek, J. L. and H. G. Beljers
Gyromagnetic phenomena occurring with ferrites . 11,313
Spier, H. L., L. Schultink and A. J. van der Wagt
The wear of diamond dies 16, 91
Staal, C. J. H. A.
An installation for multiplex-pulse modulation . . . 11,133
Steenis, O. L. van, J. de Gier, T. Hagenberg, H. J. Meerkamp van Embden, J. A. M. Smelt and J. G. W. Mulder
A steel picture-tube for television reception 14,281
Stel, M. and J. C. Derksen
Plastics and their application in the electrotechnical industry 11, 33
— and E. C. Witsenburg
Heating by means of high-frequency fields, II. Capacitive heating 11,232
Steneck, W. G. and F. G. Brockman
A new automatic hysteresis-curve recorder 16, 79
Stephens, R. B.
Mains-voltage stabilizers 17, 1
—, A. Nemet and W. A. Bayfield
A radioactive-contamination monitor for the hands, feet and clothing 16,201
Ster, J. van der and J. W. L. Köhler
A small air fractionating column used with a gas refrigerating machine for producing liquid nitrogen 20,177
Stevels, J. M.
The structure of glass 13,293
Dielectric losses in glass 13,360
Stieltjes, F. H. and P. J. W. Jochems
Apparatus for testing transistors 13,254
— and L. J. Tummers
Simple theory of the junction transistor 17,233
Behaviour of the transistor at high current densities 18, 61
Stolk, J. and J. C. van den Hoogenband
Reflection and impedance measurements by means of a long transmission line 16,309
Stumpers, F. L. H. M. and J. D. Fast
Entropy in science and technology, IV. Entropy and information 18,201
— and N. van Hurck
* An automatic noise-figure indicator 18,141
Stuijts, A. L., G. W. Rathenau and G. H. Weber
Ferroxdure II and III, anisotropic permanent-magnet materials 16,141
— and H. P. J. Wijn
Crystal-oriented ferroxplana 19,209
Suchtelen, H. van and J. A. Haringx
The Foucault pendulum in the United Nations building in New York 19,236
— and W. G. Perdok
An arrangement for indicating piezo-electricity of crystals 11,151
—, N. Warmoltz and G. L. Wiggerink
A method for determining the mercury content of air 11, 91
Tak, W.
The "Electronic Poem" performed in the Philips pavilion at the 1958 Brussels World Fair, B. The sound effects 20, 43
Taudin Chabot, J. J. M., H. C. Hamaker and F. G. Willemze
The practical application of sampling inspection plans and tables 11,362
Tellegen, B. D. H.
The gyrator, an electric network element 18,120
Teves, M. C.
The application of the X-ray image intensifier, I. General survey 17, 69
— and T. Tol
Electronic intensification of fluoroscopic images . . 14, 33
Thirup, G.
An instrument for measuring complex voltage ratios in the frequency range 1-100 Mc/s 14,102
Tol, H. J. M. van, K. Rodenhuis and H. Santing
The life and reliability of valves 18,181
Tol, M. van
Monitoring, control and safety equipment for a nuclear reactor of the swimming-pool type, I. General description 19,245
— and A. Hauer
A radio sonde for meteorological observations . . . 16,148
Tol, T. and W. J. Oosterkamp
The application of the X-ray image intensifier, II. The perception of small object-detail 17, 71
— and M. C. Teves
Electronic intensification of fluoroscopic images . . 14, 33
Tosswill, C. H.
Cold-cathode trigger tubes 18,128
Trier, P. E., J. C. Hammerton and E. Wolfendale
A time-of-flight neutron spectrometer 15,325
Troelstra, S. A.
Applying coatings by electrophoresis 12,293
Troye, N. C. de and H. J. Heijn
A fast method of reading magnetic-core memories . 20,193
Tummers, L. J. and F. H. Stieltjes
Simple theory of the junction transistor 17,233
Behaviour of the transistor at high current densities 18, 61
Turnbull, A. A.
Precision variable capacitors 20,234
Uitjens, A. G. W., B. G. Dammers and P. D. van der Knaap
The electrical recording of diagrams with a calibrated system of coordinates 12,283
Unk, J. M.
A high-speed uniselector for automatic telephone exchanges 18,349
Urk, A. T. van
On electrical shaving 12, 25
Valeton, J. J. P.
High-tension generators for large-picture projection television 14, 21
— and F. H. J. van der Poel
The flying-spot scanner 15,221
Veeckens, J. F. T. van Heemskerck, see **Heemskerck Veeckens, J. F. T. van**
Veegens, J. D. and E. Prado
A sinusoidal *RC*-oscillator for measurements in the frequency range 20-250 000 c/s 15,240
Veen, R. van der
Influence of light upon plants 11, 43
A small greenhouse with artificial lighting for studying plant growth under reproducible conditions 12, 1
Some of the effects of the relative length of day on Poinsettia and Populus 14,175
Photosynthesis 14,298
"Boekesteyn", the agrobiological laboratory of N.V. Philips-Roxane 16,353
Growth substances in plants 17,294
Venema, A.
Dispenser cathodes, I. Introduction 19,177
— and M. Bandringa
The production and measurement of ultra-high vacua 20,145

Verbeek, L. H.
The specific light output of "Photoflux" flash-bulbs **15,317**
— and G. D. Rieck
The "Photoflux" series of flash-bulbs **12,185**
Verhoef, J. A.
The focusing of television picture-tubes with ferroxdure magnets **15,214**
Verhoeff, A., A. C. van Dorsten and H. Nieuwdorp
The Philips 100 kV electron microscope **12, 33**
—, W. J. H. Beekman and H. W. van der Voorn
* An X-ray diffraction tube with rotating anode for 10 kW continuous loading **19,314**
Vermeulen, D. and J. B. de Boer
The permissible brightness of lamp fittings **12,200**
Motorcar headlights **12,305**
Vermeulen, R.
A comparison between reproduced and "live" music **17,171**
Stereo-reverberation **17,258**
* A musical instrument for deaf-mute children . . . **18,276**
— and W. K. Westmijze
The "Expressor" system for transmission of music . **11,281**
Verse, H.
A universal apparatus for X-ray therapy with moving-field irradiation **16, 33**
— and H. Jensen
The application of the X-ray image intensifier,
IV. Equipment for spot film radiography incorporating an image intensifier fitted with a periscope optical system **17, 84**
— and K. Weigel
A novel type of diagnostic X-ray unit **17,138**
Verweel, J.
Magnetrons **14, 44**
Verwey, E. J. W. and F. A. Kröger
New views on oxidic semi-conductors and zinc-sulphide phosphors **13, 90**
Vessem, J. C. van
The theory and construction of germanium diodes . **16,213**
Vink, H. J. and R. Loosjes
Conduction processes in the oxide-coated cathode . **11,271**
—, R. Loosjes and C. G. J. Jansen
Thermionic emitters under pulsed operation **13,337**
Visser van Bloemen, J. P. de
* Stereophonic music in the cinema **11,129**
Vlodrop, P. H. G. van and H. L. van der Horst
An experimental induction-heating generator using hydrogen thyratrons **20,101**
Volger, J. and J. van Hengel
* A transistor radio receiver powered by a thermopile **18,155**
Voogd, J. and J. Daams
Inactivation of bacteria by ultra-violet radiation . **12,111**
Voorn, H. W. van der, W. J. H. Beekman and A. Verhoeff
* An X-ray diffraction tube with rotating anode for 10 kW continuous loading **19,314**
Vreedenburgh, C. G. J.
The Philips pavilion at the 1958 Brussels World Fair,
II. The hyperbolic-paraboloidal shell and its mechanical properties **20, 9**
Vriend, J. A. de
Ignition of "Photoflux" flash-bulbs with the aid of a capacitor **16,333**
Vries, R. W. P. de
The gloss point of glazes **17,153**
Vrijer, F. W. de
Fundamentals of colour television **19, 86**
— and J. Haantjes
Flicker in television pictures **13, 55**
— and T. Poorter
The projection of colour-television pictures **19,338**
Wagt, A. J. van der, L. Schultink and H. L. Spier
The wear of diamond dies **16, 91**
Ware, D. G. and M. W. Brooker
Cheater circuits for the testing of thyratrons,
I. Measurement of grid current **16, 43**
II. Life testing at high commutation factors . . . **16, 98**
Warmoltz, N.
Geiger-Müller counters **13,282**
— and E. Bouwmeester
A simple and reliable ionization manometer **17,121**
— and P. P. M. Schampers
A pocket dosemeter, with built-in charger, for X-radiation and gamma radiation **16,134**
—, H. van Suchtelen and G. L. Wiggerink
A method for determining the mercury content of air **11, 91**
— and J. E. Winkelman
Photography of the eye with the aid of electronic flash-tubes **15,342**
Weber, G. H., A. L. Stuijts and G. W. Rathenau
Ferroxdure II and III, anisotropic permanent-magnet materials **16,141**
Weel, A. van
Phase linearity of television receivers **18, 33**
— and H. J. de Boer
An instrument for measuring group delay **15,307**
Weigel, K. and H. Verse
A novel type of diagnostic X-ray unit **17,138**
Went, J. J. and E. W. Gorter
The magnetic and electrical properties of ferroxcube materials **13,181**
—, G. W. Rathenau, E. W. Gorter and G. W. van Oosterhout
Ferroxdure, a class of new permanent magnet materials,
I. Most important properties of ferroxdure . . . **13,194**
II. Physical background of some properties of ferroxdure **13,197**
III. Saturation magnetization and crystal structure **13,203**
Werner, W.
The different television standards considered from the point of view of receiver design **16,195**
Westmijze, W. K.
The principle of the magnetic recording and reproduction of sound **15, 84**
— and R. Vermeulen
The "Expressor" system for transmission of music . **11,281**
Westra, R.
* A "Photoflux" flash-bulb with simplified cap . . . **16, 88**
Weijer, M. H. A. van de and J. J. Balder
The "TL" F lamp, a tubular fluorescent lamp with a directional light distribution **17,198**
Wieringen, J. S. van
Paramagnetic resonance **19,301**
Wiggerink, G. L., H. van Suchtelen and N. Warmoltz
A method for determining the mercury content of air **11, 91**
Willemze, F. G., H. C. Hamaker and J. J. M. Taudin Chabot
The practical application of sampling inspection plans and tables **11,362**
Willigen, P. C. van der, W. P. van den Blink and E. H. Ettema
Stud welding with welding cartridges **17, 37**
— and L. F. Defize
The determination of droplet size in arc welding by high-speed cinematography **15,122**
Wilting, J. J. and T. Hehenkamp
Transistor D.C. converters for fluorescent-lamp power supplies **20,362**
Winkel, J. te
Feedback amplifiers for carrier telephone systems . **16,287**
—, J. P. Beijersbergen and M. Beun
The junction transistor as a network element at low frequencies,
I. Characteristics and h parameters **19, 15**
II. Equivalent circuits and dependence of the h parameters on operating point **19, 98**
III. Stabilization of the operating point, in particular with regard to temperature changes **20,122**
Winkelman, J. E. and N. Warmoltz
Photography of the eye with the aid of electronic flash-tubes **15,342**
Wit, L. de
* Apparatus for measuring light distributions **14,200**
Witsenburg, E. C.
Heating by means of high-frequency fields,
I. Induction heating **11,165**
— and M. Stel
Heating by means of high-frequency fields,
II. Capacitive heating **11,232**

Wittenberg, N.
A magnetodynamic gramophone pick-up,
I. Construction **18**,101
II. Frequency characteristics **18**,173
Wolfendale, E., P. E. Trier and J. C. Hammerton
A time-of-flight neutron spectrometer **15**,325
Wijk, J. J. F. de, W. J. Oosterkamp and J. Proper
* Dosimetry of the very weak X-radiation generated in television receivers and X-ray diffraction apparatus **19**,264
Wijlen, H. B. van
* Radiographic examination of electronic valves . . **12**,207
Wijn, H. P. J., C. M. van der Burgt and M. Gevers
Measuring methods for some properties of ferroxcube materials **14**,245
—, E. W. Gorter, C. J. Esveldt and P. Geldermans
Conditions for square hysteresis loops in ferrites . . **16**, 49
—, H. van der Heide and H. G. Bruijning
Switching time of ferrites with rectangular hysteresis loop **18**,336
—, G. H. Jonker and P. B. Braun
Ferroxplana, hexagonal ferromagnetic iron-oxide compounds for very high frequencies **18**,145
— and A. L. Stuijts
Crystal-oriented ferroxplana **19**,209
Wijngaarden, J. G. van, G. Diemer and K. Rodenhuis
The EC 57, a disc-seal microwave triode with L cathode **18**,317
— and V. V. Schwab
The EC 59, a transmitting triode with 10 W output at 4000 Mc/s **20**,225
Xenakis, Y.
The Philips pavilion at the 1958 Brussels World Fair, I. The architectural design of Le Corbusier and Xenakis **20**, 2
Zaayer, D.
An experimental 100 kW television output stage . **14**,345
Zalm, P., G. Diemer and H. A. Klasens
Electroluminescence and image intensification . . **19**, 1
Zanten, P. G. van and F. H. R. Almer
* An experimental pyrometer using a phototransistor and designed for radio-tube inspection **20**, 89
— and L. Schultink
Thin tungsten wire for small radio valves **18**,222
Zoethout, G.
* Enclosed welding of rail sections **20**, 94
Zwikker, C.
The equivalent circuit of a gas-discharge lamp . . . **15**,161
Zijlstra, P.
An apparatus for detecting superficial cracks in wires **11**, 12
— and E. G. Dorgelo
Two transmitting valves for use in mobile installations **12**,157
Zijp, P. and H. de Quant
The F.M. section of modern broadcast receivers, I. Circuitry and structural design **17**,342